Application of FLAC in Bearing Capacity Analyses of Layered Clays

by

Vivek Bhardwaj

A Thesis Submitted to The Faculty of Graduate Studies

In Partial Fulfillment of the Requirements for the

Degree of

Master of Science

Department of Civil Engineering

University of Manitoba

Winnipeg, Manitoba, Canada

To my loving family and teachers

Acknowledgements

I would like to extend my sincere gratitude to my advisor Dr. Brian Stimpson for his excellent supervision of my research project. I sincerely thank him for believing in me and for his kindness and support throughout the research.

The financial support from the NSERC is greatly appreciated.

I would also like to thank Dr. James Blatz and Dr. Marolo Alfaro for their useful advice from time to time on the research.

Abstract

Understanding the bearing response of the footings on layered soils has always been a challenge for researchers. Due to the limitations of analytical and empirical solutions it had been difficult to understand the true bearing behavior. Some researchers have tried solving this problem by numerical analysis and have found some success. In this study the numerical analysis approach has been applied using a commercial tool FLAC (Fast Lagrangian Analysis of Continua) to study the bearing response of surface footings on layered clays. First, small deformation analyses were taken up to study the undrained bearing response of strip and circular footings resting on a horizontally layered strong over a soft clay foundation, and then over soft over strong clay foundation. In the end application of large strain mode of FLAC was explored to investigate the large deformation behavior of the strip footing resting on the surface of a strong over soft clay foundation. All models were run by applying velocity loading and a elastic-perfectly plastic Tresca yield criterion has been used.

The results are compared with published Finite Element Method (FEM) results, and with analytical, empirical and semi-empirical solutions. It was found that bearing capacity results from the present small-strain FLAC analyses agree well with the FEM results. However, these results in most of the cases tend to differ (as much as 49% for certain layered clay foundations) from those predicted with analytical, empirical and semi-empirical solutions, mainly due to the assumptions made in these solutions. Since no such assumptions are made in the present FLAC analyses, the results and the methodology of this thesis can be applied to predict the bearing capacity of the practical problems. Application of the large-strain mode of FLAC to study the large deformation of shallow foundations has pointed out a limitation of FLAC in completing such analyses. However, it is observed from the early trends of these analyses that whereas the small deformation analysis may under estimate the ultimate bearing capacity for certain cases of layered foundations where the upper clay is moderately stiffer than the lower clay layer, it might also over predict the ultimate bearing capacity for other cases when the upper clay is very stiff in comparison to the lower clay layer.

Table of Contents

List of Tables

List of Figures

List of Copyrighted Material for which Permission was Obtained

Title of copyrighted item	Source	Page no in thesis
Table 2.1	Reprinted from Table 3.6, Vesic (1975), with permission from Springer Science and Business Media	9
Figure 2.3	Reprinted from Figure 3.28a,& 3.28b, Vesic (1975), with permission from Springer Science and Business Media	10
Subsection 2.1.3	Equations reproduced from page 210, Bowles (1996), with permission from the Mc-Graw Hill, Companies, Inc.	11
Figure 2.4 & 2.5	Reprinted from Figure 6.34, & 6.35, Chen (1975), with permission from Elsevier	15 & 16
Figure 2.6 & 2.7	Reprinted from Figure 6, & 9, Florkiewicz (1989), with permission from NRC Research Press	17 & 18
Figure 2.8(a) & 2.8(b)	Reprinted from Fig. 5a, & 13, Wang and Carter (2001), with permission from Wang, C., Carter, J. P., and the University of Sydney	22
Figure 2.9	Reprinted from Figure 1, Georgiadis and Michalopoulos (1985), with permission from American Society of Civil Engineers	24

List of Symbols

γ unit weight of soil

ν Poisson's ratio

ϕ angle of friction of the soil

B width of the strip footing

c cohesion of soil

c_1 cohesion or shear strength of top clay layer

c_2 cohesion or shear strength of bottom clay layer

D diameter of the circular footing

D_f depth of the foundation

G_1 shear modulus of top clay layer

G_2 shear modulus of bottom clay layer

H depth of the top clay layer

I_r rigidity index

N_c, N_q, N_γ bearing capacity factors or coefficients

q_u ultimate bearing pressure

${N_c}^*$ modified bearing capacity factor

Chapter 1

Introduction

Classical solutions for undrained bearing capacity in clays assume that the foundation soil is isotropic and homogeneous, that its thickness is large relative to the width of the footing , and that deformations are small. However, it is possible to encounter layers of different stiffnesses within the zone of influence of a foundation e.g., Winnipeg lacustrine clays or offshore foundations which have large physical dimensions, and where potential failure surface may extend a significant distance below the surface of the soil. All soil layers with in the failure surface can influence the bearing capacity of the foundation. Oil storage tanks founded on a thin layer of granular fill and unpaved roads built on soft clays are some of the other examples.

This problem has attracted the attention of many researchers. Various techniques: experimental, analytical, and numerical, have been applied to understand the failure mechanism and to calculate the bearing capacity. Some of these methods are explained in the later part of this thesis. Numerical analysis has been the most popular approach for the last two decades, and finite difference and finite element are the two numerical methods primarily used for solving this type of problem. Burd and Frydman (1997) have shown that if appropriate care is taken in the numerical modeling both of these methods give similar results. Encouraged with these results, Fast Lagrangian Analysis of Continua (FLAC), a two dimensional finite difference numerical code has been used in this thesis for studying the bearing response of continuous and circular footings on layered soils. The findings of Burd and Frydman (1997) are limited only to small deformation. Since FLAC is capable of performing small-strain as well as large-strain analysis, the applicability of FLAC to both small as well as large deformation analysis has been explored. If this application of FLAC was successful it was also the intention of this research to study the influence on pile driving of a stiffer layer embedded between two soft layers. Off-shore piling operations in calcareous sands include a problem in which the pile encounters difficult driving conditions in the stiff layer, only to almost go into "free fall" after penetrating into to the softer layer beneath. Some interesting experimental studies have been done on this problem (Evans 1987), and (Houlsby et al. 1988).

The objectives of this study were:

a. Study the modes of failure of shallow foundations on layered clay soils using FLAC.

b. Compare the bearing capacity factors obtained from FLAC with those obtained by other methods in the literature.

c. Compare FLAC large deformation simulations to those obtained by finite element methods (Wang and Carter 2001).

As the research progressed, it became apparent that the large deformation mode of FLAC ran into numerical problems before significant deformations were attained. Therefore, a fourth objective developed:

d. To develop methodologies for enabling FLAC to handle large deformations without code changes.

The basic approach in the present study is to first describe the problem of footings on layered soils by reviewing the related literature. The theory and operation of FLAC is also described briefly. In the second part of the study numerical analyses are conducted to understand the failure mechanisms of strip and circular footings on layered clays, and to estimate bearing capacity using FLAC. Various models have been run by varying cohesion ratios of the top clay layer to the bottom clay layer and for different ratios of depth of top layer to breadth or diameter of the footing.

The results are verified with the existing analytical and finite element methods, and presented in the form of tables and graphs.

This thesis has been structured into five chapters and an appendix:

1. Introduction
2. Literature Review-Bearing Capacity Analysis in Layered Soils
3. Description of FLAC and its Theory
4. Influence of Footing Geometry and Soil Shear Strength on Bearing Capacity and Failure Modes of Layered Clays
5. Conclusion, and
6. Appendix A - Numerical Modelling and Discussion of Results

Chapter 2

Literature Review - Bearing Capacity Analysis in Layered Soils

There is a vast literature available on the load-bearing capacity of shallow foundations. In this chapter the literature has been reviewed briefly, focussing mainly on foundations in layered clays. The emphasis in this thesis is on numerical solutions, but since it is extremely important for any numerical solution to be acceptable it should be compared with the best available analytical or semi-empirical solutions. Some of these solutions are explained here. Whereas it is difficult to generalise, the analytical solutions may be arranged into two categories: ones which give "lower bound limit" solutions by satisfying static equilibrium and give conservative or safe bearing capacity, but may not be acceptable kinematically, others provide "upper bound limit" solution which satisfy kinematic compatibility and try to predict ultimate bearing capacity of soil.

The Terzaghi (1943) equation is based on bearing capacity theory that provides a bearing capacity formula for the centrally and vertically loaded strip foundation placed on the soil surface:

$$q_u = cN_c + \gamma D_f N_q + \frac{1}{2}\gamma B N_\gamma \tag{2.1}$$

where c= cohesion of soil, γ= unit weight of soil, D_f= depth of the foundation, B=

width of the footing, N_c, N_q, N_γ= bearing capacity coefficients which depend only on the angle of friction of the soil, ϕ, and represent the contributions of cohesion, surcharge, and self-weight of soil to the overall bearing capacity, q_u.

The ultimate bearing capacity (q_u) is a pressure which a foundation soil below and next to a footing can withstand before failing in shear. Generally, this shear failure has been defined by three failure mechanisms: (i) general shear, (ii) local shear and (iii) punching shear. These failure modes for a rigid strip footing are shown in Figure 2.1. The type of failure in which continuous failure surfaces develop between the edge of the footing and the ground surface next to it is called general shear failure. In this kind of failure mechanism, as the bearing pressure increases, a state of plastic equilibrium is first reached in the soil around the edge of the footing which with further increase in the bearing pressure spreads downwards and outwards until the state of plastic equilibrium is fully developed throughout the soil above the failure surfaces. A distinct characteristic of the general shear failure is heaving on both sides of the footing. This type of failure generally occurs in stiff or dense soils of low compressibility. A bearing pressure - settlement curve is also shown in Figure 2.1. A well defined ultimate bearing capacity can be noticed in case of general shear failure in the curve (i). The second type of failure mechanism is local shear failure. This kind of failure is characterized by large compression of the soil under the footing. However, there is a partial development of the state of plastic equilibrium. Therefore, the failure surfaces are not transmitted to the ground surface. The heaving on the sides of the footing is not that distinct and is smaller than that in the general shear failure. Local shear failure usually occurs in soft soils of high compressibility. As it can be seen from Figure 2.1. the bearing pressure - settlement curve (ii) does not have a well defined ultimate bearing pressure. The third type of failure mechanism is punching shear failure, which occurs when the soil under the footing is compressed so much that it shears vertically along the edges of the footing. A punching shear failure is also seen in the case of low compressibility soils if the foundation is deep or if a footing rests on stiff thin crust overlying a soft soil. As it can be seen from the curve (iii) in Figure 2.1, large settlement is a characteristic of punching shear failure, however ultimate bearing capacity is not well defined.

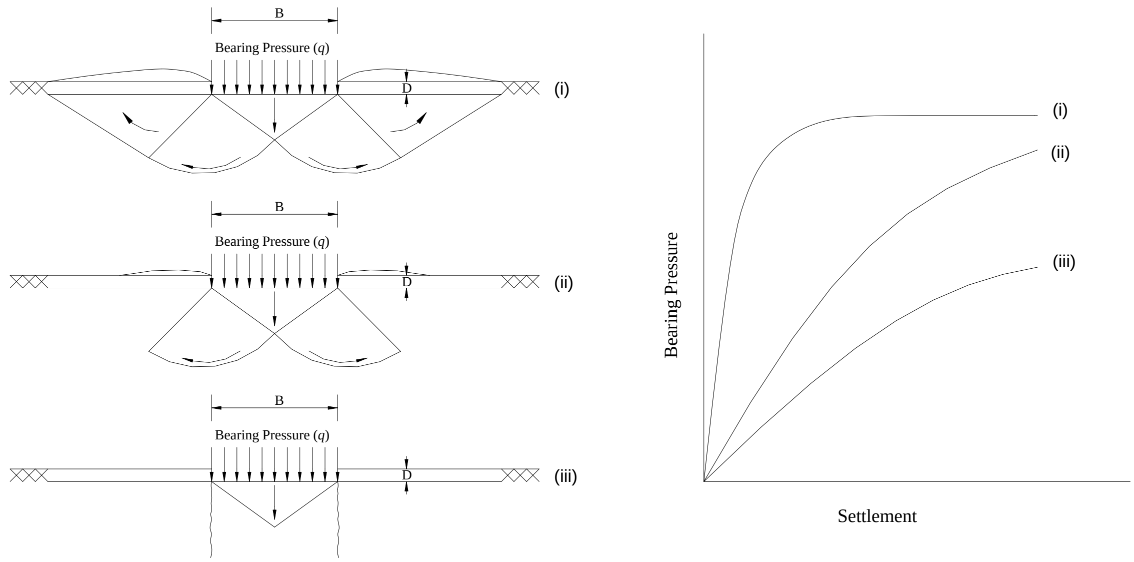

Figure 2.1: Foundation failure modes: (i) general shear, (ii) local shear, and (iii) punching shear, after (Craig 1997).

Terzaghi and Peck (1967) gave a solution to the ultimate bearing capacity of a strip footing on undrained clays ($\phi = 0$):

$$q_u = (2 + \pi)c = 5.14c$$

This solution is based on the mode of failure shown in Figure 2.2. It should be noted that surface CD and CG are circular arcs for undrained clays ($\phi = 0$) (Craig 1997).

Terzaghi's method may be very useful for finding the bearing capacity of foundations on homogeneous soils, but it may not be very effective in predicting the bearing capacity of foundations on naturally occurring layered soils, where the strength of any or all layers may influence the bearing capacity. It should also be noted that since the failure surface in the case of layered soils may pass through different layers it would be difficult to describe the overall failure modes of foundation in such case in terms of general shear, local shear or punching shear alone. The failure mode may now be a combination of different failure mechanisms in different layers. A number of

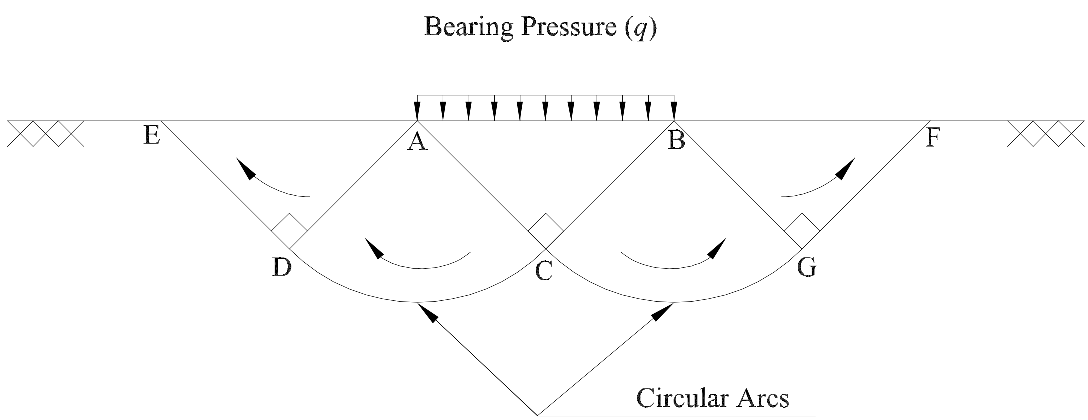

Figure 2.2: Failure mode for a rigid strip footing on an undrained clay, after (Itasca Consulting Group, Inc. 2001c).

methods have been suggested for finding the bearing capacity of layered soils. Some of these are now briefly noted:

2.1 Semi-empirical Methods

2.1.1 Brown and Meyerhof (1969) Method

Brown and Meyerhof (1969) conducted an experimental study of bearing capacity in layered clays. The ultimate bearing capacity of foundations resting on clay subsoils were investigated for the following cases:

1. Homogeneous clay

   A number of strip and circular footing tests were conducted on homogeneous clay primarily to determine the average undrained mobilized shear strength, c, in clay, and to find correction factors. The classical Prandtl solution for the ultimate bearing capacity, q_u on a rigid-plastic material is:

$$\begin{aligned} q_u &= cN_c \qquad (2.2) \\ \text{where } N_c &= 5.14 \text{ for strip footings} \\ &\quad \text{and } 6.05 \text{ for circular footings} \end{aligned}$$

The correction factors to be applied to the unconfined shear strength were calculated to be 1.10 and 1.21 for the strip and circular footings respectively.

2. Stiff clay layer overlying soft clay layer

   The ratios of top layer thickness to width or diameter of footing, H/B or $H/2R$ were varied from 0.5 to 0.3, and the strength of the the top layer was taken to be 4 times the strength of the bottom layer. It was observed from the load-settlement curves that the failure occurred at an average penetration of 16% for the strip footing and 7% for circular footing tests. The behavior of both types of footings was found to be qualitatively very similar.

   The bearing pressure at failure was defined as:

$$\begin{aligned} q_u &= c_t N_{ms} \text{ for strip footing} \qquad (2.3) \\ q_u &= c_t N_{mc} \text{ for circular footing} \qquad (2.4) \\ &\quad \text{where } N_{ms} \;\&\; N_{mc} \text{ are the modified bearing capacity factors} \qquad (2.5) \end{aligned}$$

3. Soft clay layer overlying stiff clay layer

It was found that the failure mechanism for this case was entirely different from a stiff layer overlying a soft layer. Whereas the failure in the first case occurred by footing punching through the top layer, and the full development of the bearing capacity of the bottom layer, the failure in the second case occurred mainly by squeezing of the soft layer between the footing and bottom stiff layer with some interactions between the two layers when the strength ratio c_b/c_t approaches unity. A splitting type failure of clay was also noticed below the free surface on either side of the footing.

Table 2.1: Modified Bearing Capacity Factor, N_m (Vesic 1975)

Long Rectangular Footing ($L/B \leqslant 5$)

c_2/c_1 \ B/H	2	4	6	8	10	20	∞
1.0	5.14	5.14	5.14	5.14	5.14	5.14	5.14
1.5	5.14	5.31	5.45	5.59	5.70	6.14	7.71
2	5.14	5.43	5.69	5.92	6.13	6.95	10.28
3	5.14	5.59	6.00	6.38	6.74	8.16	15.42
4	5.14	5.69	6.21	6.69	7.14	9.02	20.56
5	5.14	5.76	6.35	6.90	7.42	9.66	25.70
10	5.14	5.93	6.69	7.43	8.14	11.40	51.40
∞	5.14	6.14	7.14	8.14	9.14	14.14	∞

Square or Circular Footing ($L/B = 1$)

c_2/c_1 \ B/H	4	8	12	16	20	40	∞
1	6.17	6.17	6.17	6.17	6.17	6.17	6.17
1.5	6.17	6.34	6.49	6.63	6.76	7.25	9.25
2	6.17	6.46	6.73	6.98	7.20	8.10	12.34
3	6.17	6.63	7.05	7.45	7.82	9.36	18.51
4	6.17	6.73	7.26	7.75	8.23	10.24	24.68
5	6.17	6.80	7.40	7.97	8.51	10.88	30.85
10	6.17	6.96	7.74	8.49	9.22	12.58	61.70
∞	6.17	7.17	8.17	9.17	10.17	15.17	∞

Values of modified bearing capacity factors N_{ms} & N_{mc} can be found for different c_b/c_t ratios for different H/B ratios from charts.

2.1.2 Vesic (1975) Method

Vesic (1975) has suggested a modified bearing capacity factor for bearing capacity formulae suggested by Brown and Meyerhof (1969). This modification was based on an interpolation between rigorous solutions and the values for long rectangular and square or circular footings that have been presented in Table 2.1, and in graphical form (Figure 2.3).

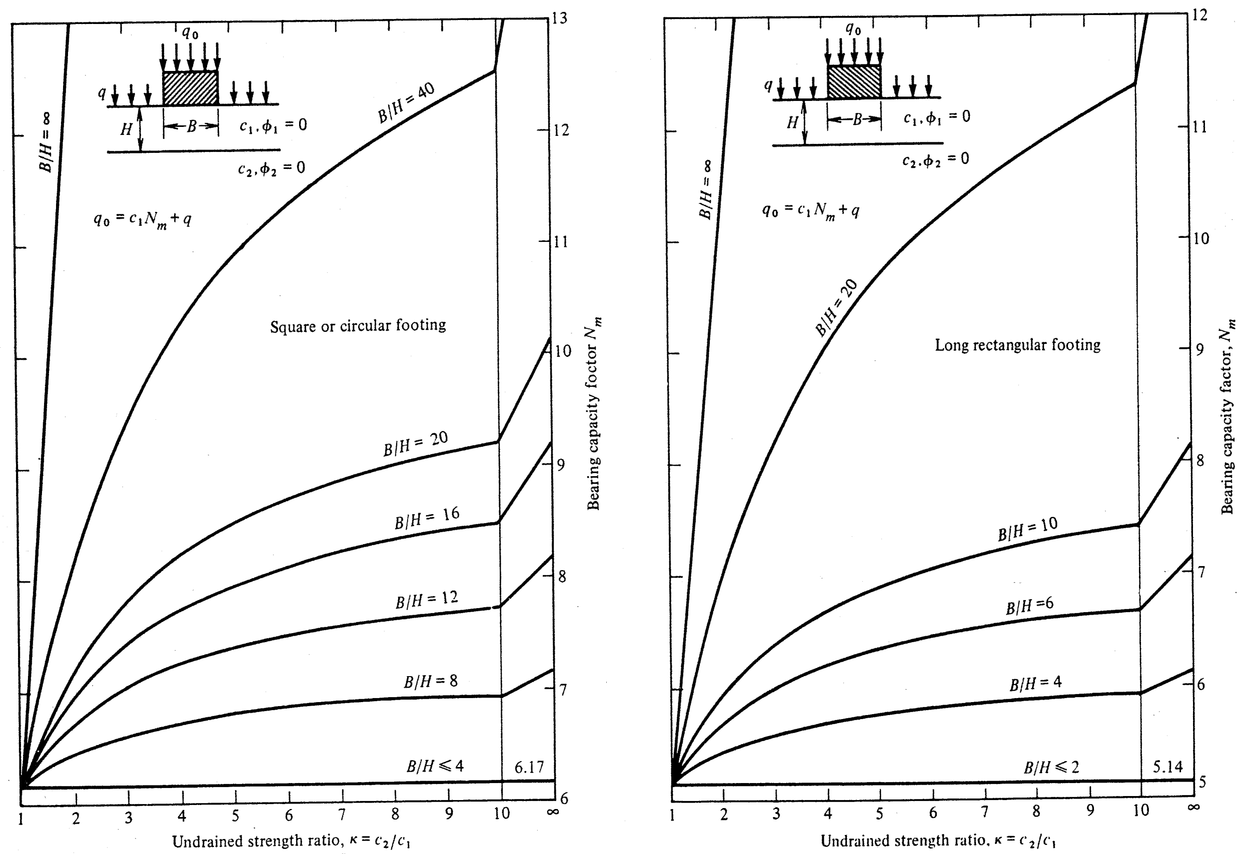

Figure 2.3: Modified bearing capacity factor for square or circular and long rectangular footings on undrained two-layer cohesive soil (Vesic 1975).

2.1.3 Bowles (1996) Method

Bowles (1996) has described a method for obtaining bearing capacity factor, $N_{c,i}$ for a footing on layered clays (all $\phi = 0$), by averaging the strength parameters This method uses bearing capacity equations given by Brown and Meyerhof (1969).

For stiff clay overlying soft clay ($C_R = \dfrac{c_2}{c_1} \leq 1$)
for a strip footing of width $= B$

$$N_{c,s} = \frac{1.5H}{B} + 5.14C_R \quad \leq 5.14 \tag{2.6}$$

and
for circular footing of diameter $= B$

$$N_{c,r} = \frac{3.0H}{B} + 6.05C_R \quad \leq 6.05 \tag{2.7}$$

The value of $N_{c,i(i=s\ or\ r)}$ is suggested to be reduced by 10% for $C_R > 0.7$.
For soft clay over stiff clay ($C_R = \dfrac{c_2}{c_1} > 1$)
for strip footing

$$N_{1,s} = 4.14 + \frac{0.5B}{d_1} \tag{2.8}$$

and

$$N_{2,s} = 4.14 + \frac{1.1B}{d_1} \tag{2.9}$$

for circular footing

$$N_{1,r} = 5.05 + \frac{0.33B}{d_1} \tag{2.10}$$

$$N_{2,r} = 5.05 + \frac{0.66B}{d_1} \tag{2.11}$$

$N_{c,i}$ is obtained by averaging the bearing capacity factors of top and bottom clay layers:

$$N_{c,i} = \frac{N_{1,i} \cdot N_{2,i}}{N_{1,i} + N_{2,i}} \cdot 2 \tag{2.12}$$

2.1.4 Meyerhof and Hanna (1978) Method

Meyerhof and Hanna (1978) developed a theory for calculating the ultimate bearing capacity of a rough footing. Different modes of failure have been compared with the results of model tests on circular and strip footings on a strong soil layer underlain by a weaker soil layer. It was assumed that failure occurs by punching shear through the top layer followed by general shear failure of bottom layer. Das (1999) has further simplified this theory for the rough continuous vertically loaded footing. The ultimate bearing capacity for a stronger clay layer overlying a weaker clay layer has been defined as:

$$\begin{aligned} q_u &= c_2 N_c + \frac{2 c_a H}{B} \\ \text{where } N_c &= 5.14 \end{aligned} \tag{2.13}$$

Equation 2.13 represents the failure mechanism of the foundation. The second term in the equation represents a punching shear failure through the strong top layer, whereas the first term defines the full general shear failure of the soft bottom layer. The term c_a in a physical sense is defined as the unit adhesion acting on the assumed punching failure plane through the top stronger soil. The values of c_a can be read for various c_2/c_1 ratios from a chart.

The modified bearing capacity factor N_c^* can be obtained from the equation 2.13 as:

$$N_c^* = \frac{q_u}{c_1} = N_c(\frac{c_2}{c_1}) + 2(\frac{c_a}{c_1})(\frac{H}{B}) \tag{2.14}$$

2.2 Limit Equilibrium

Another popular approach for estimating the bearing capacity of foundations on layered clays has been limit equilibrium methods. Some of these methods have been listed below:

2.2.1 Button (1953) Method

According to Button (1953), the ultimate bearing capacity of a long strip footing placed on a ground surface of purely cohesive soils ($\phi = 0$) can be found as:

$$q_u = c_1 N_c \tag{2.15}$$

Button used limit equilibrium for slip circle analysis. Two cases with respect to shear strength variation were considered. The values of bearing capacity factor, N_c, for constant cohesion within a layer and for variable cohesion within the top layer are presented in charts, which can be read for different values of d/b and $c_2/c_{1,}$ where d is depth of top clay layer, b is the half-width of the footing, and c_1 and c_2 are the cohesion for the top and bottom layers respectively.

2.2.2 Reddy and Srinivasan (1967) method

Reddy and Srinivasan (1967) have developed a procedure to determine variation in bearing capacity factor, N_c, in two-layered clays. In this method limit equilibrium was applied again assuming a cylindrical failure surface very similar to Button (1953). Whereas, Buttton has assumed that soil in each layer is isotropic, Reddy and Srinivasan have considered the nonhomogeneity and anisotropy of the soil in all layers. Numerical results have been presented in form of graphs for calculating bearing capacity factor, N_c, for various degrees of anisotropy.

2.3 Limit Analysis

Drucker et al. (1952) have developed upper and lower bound limit theorems for an elastic-perfectly plastic material with the associated flow rule which makes it possible to bound the true limit load or plastic limit load. Calculation of such bounds is generally known as limit analysis. Such analyses are can incorporate complex boundary conditions and soil nonhomogeneity. Some of these methods have been summarised in this section.

2.3.1 Chen and Davidson (1973) Method

Chen and Davidson (1973) have suggested an approximate solution for the two-dimensional bearing capacity problem. The soil is modelled as an elastic-perfectly plastic material satisfying the Coulomb yield condition. All displacements are assumed to be small. The upper bound theorem[1] of limit analysis was adopted for two distinct kinematically admissible velocity fields (Prandtl and Hill mechanisms). These velocity fields are defined by assigning values of angular parameters. The least upper bound solution is found numerically. The results of bearing capacity for various governing parameters have been presented in the form charts. The results have been compared favorably with other methods such as limit equilibrium methods. Although, the method was demonstrated for homogeneous soils, it has been suggested that this can also be extended to problems of layered soils.

2.3.2 Chen (1975) Method

Chen (1975) has obtained bearing capacity factors N_c for layered clays assuming a circular failure mechanism similar to Button's method (2.2.1) and is shown in Figure 2.4.

The internal and external rates of work were equated and the following expression is given to calculate the bearing capacity factor:

[1] Upper bound theorem - the rate of energy dissipation is larger than or equal to the rate of work done by external forces (gravity and footing load, here) in any kinematically admissible mechanism (Drucker et al. 1952).

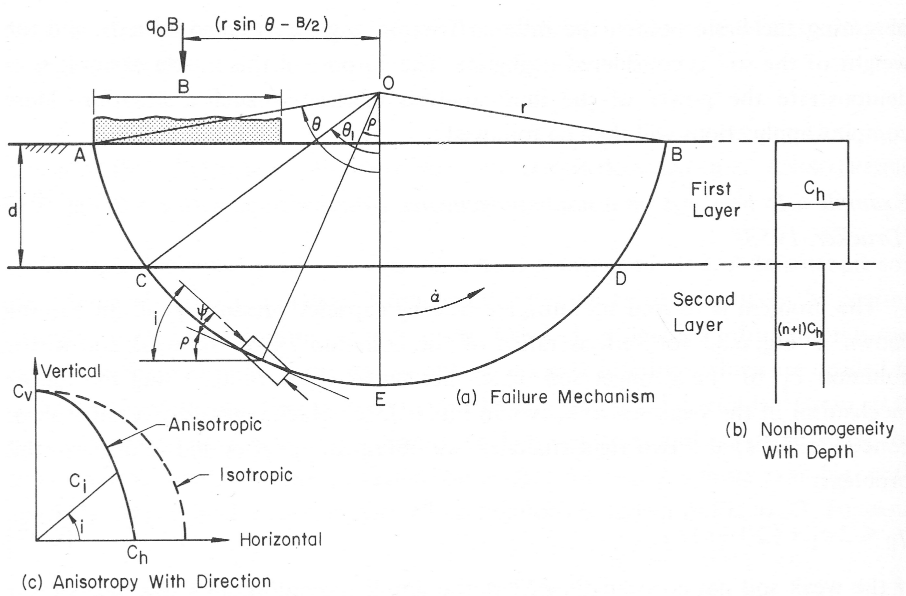

Figure 2.4: Slip circle mechanism in a two-layer clay (Chen 1975).

$$
\begin{aligned}
N_c(r,\theta) &= 2(\frac{r}{B})^2\{\frac{\theta + n\theta_i}{(r/B)\sin\theta - 1/2}\} \\
\text{where } \theta_i &= \cos^{-1}(\cos\theta + \frac{H}{r}) \\
n &= \frac{c_2}{c_1} - 1
\end{aligned}
\tag{2.16}
$$

and a least upperbound can be found by satisfying:

$$\frac{\partial N_c}{\partial \theta} = 0, \tag{2.17}$$

$$\text{and } \frac{\partial N_c}{\partial r} = 0 \tag{2.18}$$

For a homogeneous soil, 2.17 and 2.18, can be solved analytically to get $N_c = 5.53$. Bearing capacity factors for different upper layer depth to footing breadth ratios for various values of n can be read from the diagram in Figure 2.5.

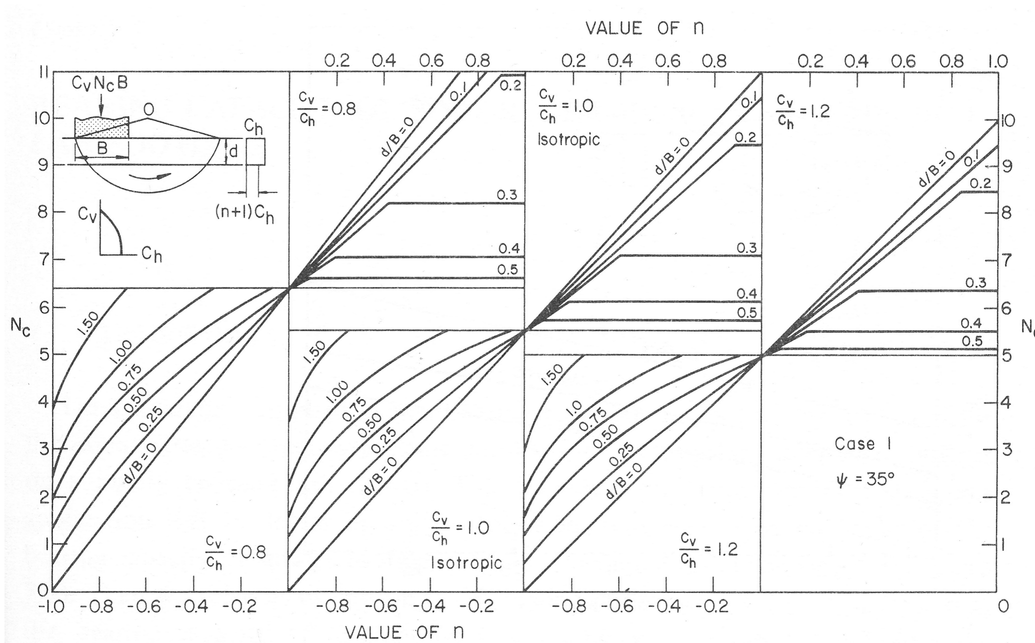

Figure 2.5: Bearing capacity factors N_c (Chen 1975).

2.3.3 Florkiewicz (1989) Method

Florkiewicz (1989) has developed a method for finding the ultimate bearing capacity of strip footings on layered soils. A kinematic limit analysis approach using the upper bound limit theorem (2.3.1) was adopted for the Mohr-Coulomb conditions. Kinematically admissible deformation patterns for layered media were applied to the rigid-motion blocks. The velocities of the individual blocks and the difference between these velocities were calculated using geometrical relations on hodographs[2]. The failure mechanism and the hodographs of the strip footing on layered soils with inclined interface are shown in Figure 2.6.

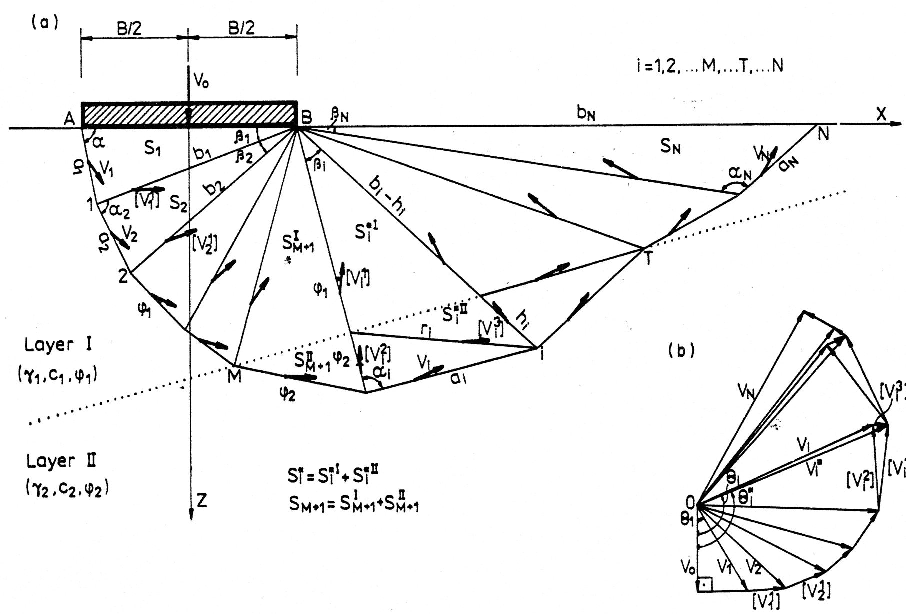

Figure 2.6: Two-layer system: (a) failure mechanism; (b) hodograph (Florkiewicz 1989).

The minimum of the upper bound limit load was computed from numerical analysis. The results for two cohesive layers, two cohesionless layers and a cohesionless layer overlying a weak cohesive layer were compared with other existing methods.

[2]Hodographs are the graphical representation of the velocity vectors where the directions are parallel to the actual velocities in the physical space and the lengths are proportional to the magnitude.

The comparison for two cohesive layers with Meyerhof and Hanna (1978) has been shown in Fig 2.7.

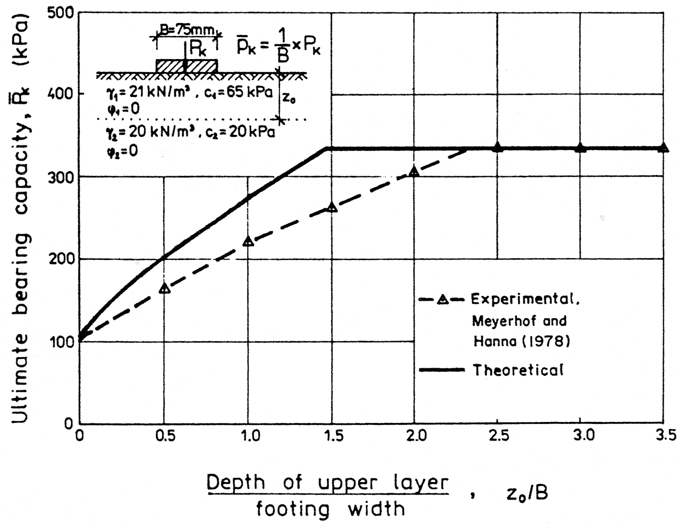

Figure 2.7: Numerical results and experimental data for two cohesive layers (Florkiewicz 1989).

Results for two-layer frictionless soils were also compared with a rotational mechanism reported by Chen (1975), and it was observed that the overestimation of the upper bound limit load was smaller with this method. One noted feature of this method is that it can be used for the inclined interface between the layered soils.

2.3.4 Michalowski and Shi (1995) Method

Michalowski and Shi (1995) have reported a limit analysis method for finding the upper bound bearing capacity of strip footings on two-layered soils. The method is quite similar to 2.3.3. Design charts are presented for a case where a layer of granular soil overlies the cohesive layer. It was suggested that the method is applicable to any combination of parameters of the two layers and hence can be used for two-layer cohesive foundation. This solution is an upper bound solution and may over estimate the bearing capacity.

2.4 Numerical Methods

The methods explained in previous sections have been used widely over the years to estimate the bearing capacity of footings on layered clays. However, these theories have their limitations and are only partially successful in explaining real failure mechanisms, mainly due to the assumptions made. Numerical methods on the other hand do not make such assumptions for the positions of the failure surface etc., but, try to simulate the insitu conditions and model the process of bearing response, and are in a better position to model the failure mechanisms. Two of the popular numerical methods for modelling the bearing capacity problem on layered soils are discrete element methods of analysis: finite element and finite difference. Some of these methods are briefly described in this section.

2.4.1 Finite Element methods

The finite element method is perhaps the most widely used method for modelling the bearing capacity problems. Some of the finite element methods have been described below:

Griffiths (1982) Analysis

Griffiths (1982) reported a finite element analysis for calculating the bearing capacity of a rough footing resting on layered clays. The analysis was performed by using a finite element program in conjunction with plasticity theory for stronger clays overlying the soft clay as well as soft clay overlying the stronger clay. The results were compared with existing analytical (2.2.1) and semi-empirical method (2.1.1) and generally a good agreement was found. This analysis has also helped in better understanding the failure mechanism.

Merifield et al. (1999) Analysis

Merifield et al. (1999) have used finite element analysis to calculate the undrained bearing capacity of a rigid surface footing resting on a two-layer clay deposit. Rigorous upper and lower bound solutions were computed using theorems of classical plasticity. The lower bound solution was obtained by modelling a statically admissible stress field, whereas the upper bound was calculated using a kinematically admissible velocity field. It was shown that the true load could be bracketed within 12%. The results were compared with existing limit analysis and empirical methods and are shown in form of tables and graphs. It was shown that limit analysis and empirical methods can either underestimate or overestimate the bearing capacity by as much as 20%.

Love et al. (1987) Analysis

Love et al. (1987) conducted a study for the effectiveness of geogrid reinforcement placed on the base of a layer of granular fill on the surface of soft clay. The problem was studied in a small-scale model test in the laboratory for a rigid footing, both for reinforced and unreinforced conditions. Even though the main objective of this study was to evaluate the effectiveness of geogrid reinforcement, yet this study can be referenced for the mechanism of failure on unreinforced layered soils. A finite element program was also developed for the investigation of this problem. This program was formulated for handling large displacements, and it was suggested that at large deformations the footing behaves as a buried footing and the larger bearing capacity factors apply in this case.

Burd and Frydman (1997) Analysis

Burd and Frydman (1997) have performed a bearing capacity analysis of a rigid surface footing resting on a sand layer overlying a clay soil for a case where the thickness of the sand layer is comparable to the width of the footing. A parametric study was carried out using both finite element and the finite difference methods. The main purpose for using two independent numerical methods was to determine the consistency and reliability of the results. The finite element analysis was performed using a program OXFEM, developed at Oxford University, (UK). The finite difference method used is described in 2.4.2 and 3.

Wang and Carter (2001) Analysis

Wang and Carter (2001) studied the bearing behavior and the failure mechanism of plane strain and circular rigid footings on two-layered undrained clays where the stronger clay overlies the softer layer. A large deformation analysis simulating the deep penetration of a footing was performed using a finite element method. This method is a modification of a method developed by Hu and Randolph (1996) which is in the class of the Arbitrary Lagrangian-Eulerian (ALE) method as suggested by Ghosh and Kikuchi (1991), and bypasses the inaccuracy due to the excessive mesh distortion in finite element large deformation methods based on Lagrangian formulation. A small deformation analysis was also conducted using the AFENA finite element method package developed by Carter and Balaam (1995). The ratios of bottom layer shear strength (c_2) to the upper layer shear strength (c_1) were varied over selected values, i.e., 0.1, 0.2, 1/3, 0.5, 2/3, 0.8 and 1. The ratio of the thickness of the top layer (H) to the footing width or diameter (B) was selected from the values of 0.25, 0.5, 1 and 2. The results were presented in the forms of graphs. It was found that the normalised load-displacement curves for large deformation analyses were very different than small deformation analyses. These results were compared with analytical values (Meyerhof 1951) for footings buried in underlying weak clay (refer Figure 2.8(a) and Figure 2.8(b)).

It was observed that as the footing penetrates, two major factors affect the bearing response; first is the movement of soil from underneath the footing to a region above the level of the footing and the second the effect of the weaker lower layer. The two effects increase with the penetration as more soil moves above the footing level and the upper layer becomes thinner. Both of these factors contribute to the bearing resistance; whereas the former tends to increase it, the latter tends to reduce it.

Effect of the self-weight was also studied, and it was found that although the self-weight does not affect the predicted bearing response in small deformation analysis, it can have significant effect in large deformation analysis. It was observed that the soil heave observed with self-weight was less than that with weightless soil.

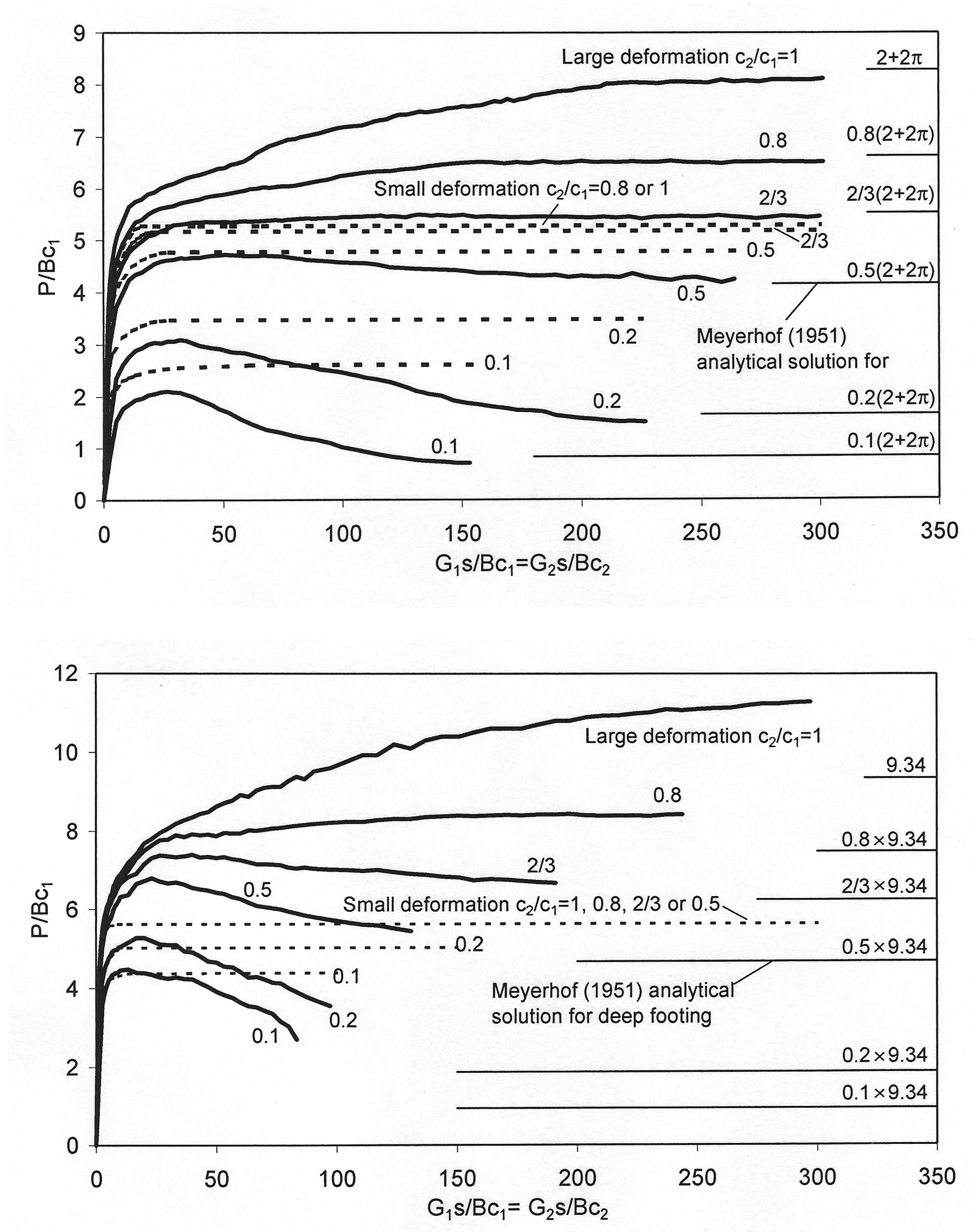

Figure 2.8: Typical normalized load-settlement curves for (a) strip footing, and (b) circular footing on homogeneous or layered clays, $H/B = 1$ (Wang and Carter 2001).

2.4.2 Finite Difference methods

There are not many finite difference methods that have been applied and documented for modelling the bearing response of the foundation on the layered soils. Burd and Frydman (1997) has carried out a study on the bearing capacity of a foundation of sand layers overlying clay soils. Although, this study was for a sand layer overlying clay which does not have a failure mechanism similar to that of a foundation of clay layers of different strengths, yet it highlights important issues related to numerical modelling of foundations on layered soils. This study has used the finite difference method (FLAC) as well as the finite element method (OXFEM) for judging consistency and reliability, and has obtained excellent agreement in results using these two different methods. This study has also given important insights into the application of FLAC in numerical modelling of foundations on layered soils. This application and the results obtained have encouraged the author to explore the use of FLAC for modelling foundation on layered clays.

2.4.3 Other Numerical Methods

Georgiadis and Michalopoulos (1985) developed a numerical method of "slip surfaces" (force equilibrium) for layered soils which is based on a similar method given by Lauritzen and Schjetne (1976) for cohesive layers with different undrained shear strengths. Georgiadis and Michalopoulos (1985) method is capable of modelling the combination of clay and sand layers both for undrained and drained conditions, and can include eccentric and inclined loads, surcharge and footing embedment. In this method a computer program was developed which determines the factor of safety against bearing capacity failure of the rectangular foundation. The results of this method when compared with those from existing semi-empirical methods (some of which are mentioned in 2.1) and the finite element analysis have demonstrated the satisfactory performance of this method, and have also shown the conservatism of the semi-empirical methods. The general failure mechanism and loadings conditions are shown in Figure 2.9.

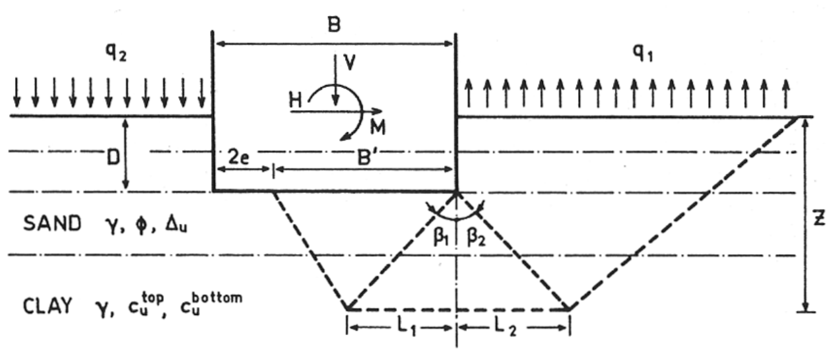

Figure 2.9: General failure mechanism and loading conditions (Georgiadis and Michalopoulos 1985).

Chapter 3

Description of FLAC and its Theory

Fast Lagrangian Analysis of Continua (FLAC) is a commercial numerical analysis program developed by Itasca Consulting Group, Inc. A brief description of FLAC is given in this chapter. The theory of FLAC is explained in detail in the manual (Itasca Consulting Group, Inc. 2001b).

3.1 Theory

FLAC is a two dimensional explicit finite difference numerical analysis program. A dynamic equation of motion is the basis of FLAC calculations. The general sequence of calculation uses the equation of motion to calculate velocities and displacements from stresses and forces. These velocities are used to calculated new strain rates and based on which new stresses are derived. One calculation loop is completed in one timestep. This calculation loop is explained in the FLAC manual by a schematic diagram similar to Figure 3.1.

FLAC can be run in two strain modes - small and large. In the explicit finite difference method in FLAC, the derivatives in the governing equations are converted into algebraic equations in terms of field variables at discrete points in space. These algebraic equations are solved at each timestep, and no global stiffness matrix is

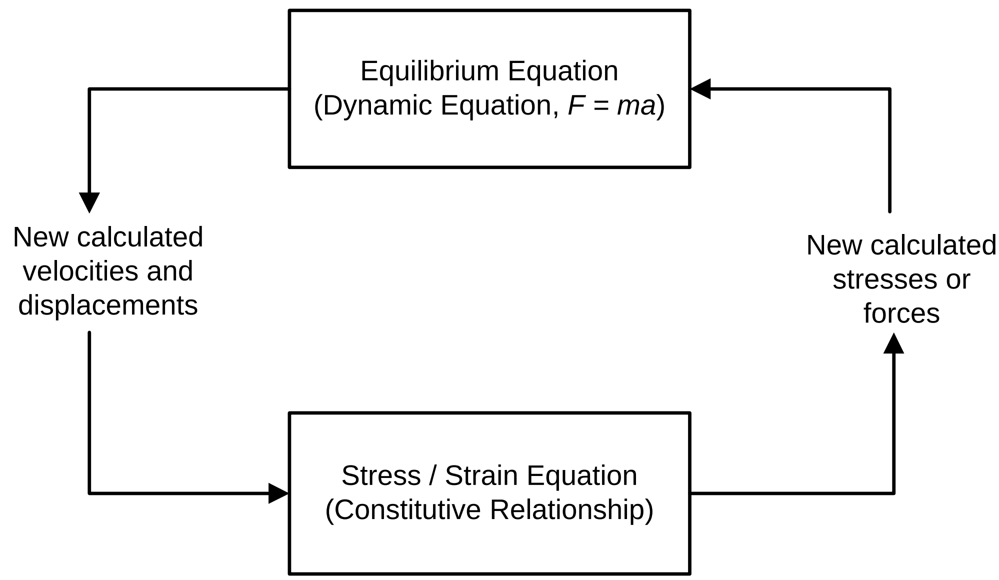

Figure 3.1: Basic FLAC Calculation Cycle (after (Itasca Consulting Group, Inc. 2001b)).

formed. Since no global stiffness matrix is formed, the coordinates of the discrete points are updated in a large-strain mode. The update is in terms of the added incremental displacements. The grid deforms with the material it represents. This is knows as "Lagrangian" formulation, which is opposite to "Eulerian" formulation in which the materials deforms but the grid remains fixed. The applicability of this large-strain feature of FLAC for the bearing capacity analyses of strip and circular footings has been explored in this thesis .

The following equation of motion and constitutive relationship are used in FLAC for a solid body problem:

$$m\frac{d\dot{u}}{dt} = F \tag{3.1}$$

where $m =$ mass of body

$\dot{u} =$ velocity

$F =$ applied force

At static equilibrium the net forces acting on a solid body and the acceleration tend to zero and $\sum F = 0$. Even though FLAC is a dynamic code, this property of law of motion is used for solving static problems in FLAC.

Considering the law of conservation of momentum and energy equation 3.1 is written as:

$$\rho \frac{\partial \dot{u}_i}{\partial t} = \frac{\partial \sigma_{ij}}{\partial x_j} + \rho g_i \tag{3.2}$$

where ρ = mass density

t = time

x_i = components of coordinate vector

g_i = components of gravitational acceleration (body forces); and

σ_{ij} = components of stress tensor

In the above equation i denotes components in Cartesian coordinate system.

The constitutive relationship or stress/ strain laws in FLAC are of the form:

$$\dot{e}_{ij} = \frac{1}{2}\left[\frac{\partial \dot{u}_i}{\partial x_j} + \frac{\partial \dot{u}_j}{\partial x_i}\right] \tag{3.3}$$

where $\dot{e}_{ij}$ = strain rate component

$\dot{u}_i$ = velocity components

The strain rate is derived from the velocity gradient by the following equation:

$$\sigma_{ij} := M(\sigma_{ij},\ \dot{e}_{ij},\ k) \tag{3.4}$$

where $M(\ )$ = constitutive law function

k = history parameter

The boundary conditions of a solid body in FLAC are either in terms of displacement or stress. Displacement conditions are specified in terms of velocities at grid points, and equation 3.1 is not used at these points.

The solid body in FLAC is modeled by a finite difference mesh consisting of quadrilateral elements. Each element in the FLAC code is subdivided into two sets of constant strain triangles[1] as shown in Figure 3.2.

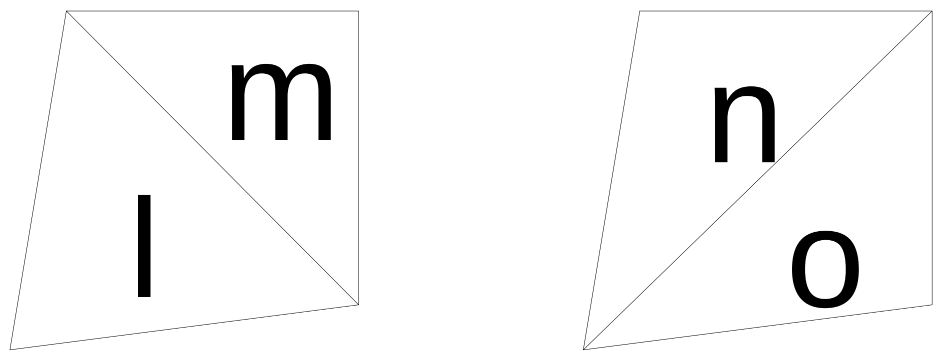

Figure 3.2: Superimposed quadrilateral elements in FLAC, after (Itasca Consulting Group, Inc. 2001b).

The deviatoric stress components for each triangle are maintained independently. The force vector at each node is the mean of the two force vectors at the two superimposed quadrilaterals. While running the calculations for particular quadrilateral, if the constituent triangle are badly deformed, i.e. the area of one triangle is much smaller than that of the other, then that quadrilateral is not considered and instead nodal forces from the other better defined/shaped quadrilateral is used. When triangle sets from both superimposed quadrilaterals exhibit excessive distortion, a "Bad Geometry" error message is displayed by FLAC and the calculations stops.

The finite difference form of equation of motion is written as

$$\dot{u}_i^{(t+\Delta/2)} = \dot{u}_i^{(t-\Delta/2)} + \sum F_i^{(t)} \frac{\Delta t}{m} \tag{3.5}$$

where F_i = nodal force vector, and

the superscripts show the time relevant variable is evaluated

[1] A constant strain triangle has three nodes and six unknown nodal displacements.

For large-strain mode, in order to evaluate the new coordinates of the gridpoint equation 3.5 is considered again

$$x_i^{(t+\Delta t)} = x_i^{(t)} + \dot{u}_i^{(t+\Delta t/2)}.\Delta t \tag{3.6}$$

The first order error term for central difference equations disappears, since both equation 3.5 and 3.6 are time - centered. The exit time for velocities at points is half a timestep from the displacements and forces.

The discretization method used in FLAC takes care of two very common problems in numerical modelling.

1) A problem of hourglass deformations, which may occur with constant-strain finite difference quadrilaterals, is avoided by the use of triangular elements.

2) Another common problem which occurs in modelling of materials undergoing yielding is the incompressibility condition of plastic flow. Plane-strain or axisymmetric geometries introduce a kinematic restraint in the out-of-plane direction, often giving rise to over-prediction of collapse load. This condition is also known as mesh locking (Nagtegaal et al. 1974). This problem is due to a condition of local mesh incompressibility which must be satisfied during flow, resulting in over constrained elements. In order to overcome this problem, the isotropic stress and strain components are kept constant over the whole quadrilateral element, while the deviatoric components are treated separately for each triangular sub-element. This procedure, referred to as mixed discretization, is described by Marti and Cundall (1982). Mixed discretization defines the two different discretizations for the isotropic and deviatoric parts of the stress and stain tensors.

3.2 Damping

Since FLAC is dynamic code it uses damping of the equation of motion to reach the static[2] or steady-state[3] solution. Two types of damping schemes are used in FLAC :

a) Local Damping

[2]Static - static equilibrium

[3]Steady state flow - e.g., plastic flow

In local damping the nodal force is proportional to the magnitude of the unbalanced force. The direction of the damping force is always in a direction of dissipation of energy.

Equation 3.5 for local damping is rewritten as

$$\dot{u}_i^{(t+\Delta/2)} = \dot{u}_i^{(t-\Delta/2)} + \sum \left[F_i^{(t)} - (F_d)_i \right] \frac{\Delta t}{m_n} \tag{3.7}$$

$$\begin{aligned} \text{where } (F_d)_i &= \alpha \left| F_i^{(t)} \right| sgn(\dot{u}_i^{(t-\Delta/2)}) \\ F_d &= \text{damping force} \\ \alpha &= \text{constant (set to 0.8)} \\ m_n &= \text{fictitious mass} \end{aligned}$$

The other scheme of damping in FLAC is:

b) Combined Damping

This type of combined damping is characterized by equation 3.7 and is activated only when velocity component changes sign. Combined damping is slow in dissipating energy and therefore local damping is used in most cases (The default damping setting in FLAC is local, but it can be changed to combined damping from GIIC menu: Setting/Mechanical. The damping values can be assigned from the menu Insitu/Initial The damping can be shut off by unchecking the "Perform Mechanical Calculations" box in the same "Mechanical Setting" dialogue box).

In FLAC for the explicit finite difference solution to be stable, the calculation timestep is chosen such that it is always smaller than some critical timestep.

$$\Delta t < \frac{\Delta x}{C} \tag{3.8}$$

where C is maximum speed of information propagation (typically p-wave speed, C_p)

$$C_p = \sqrt{\frac{K + 4G/3}{\rho}} \tag{3.9}$$

3.3 Constitutive Models

FLAC version 4.0 contains ten constitutive models. These models are categorized into three groups:

3.3.1 Null Model

Null model is used to represent excavated or removed material

3.3.2 Elastic Models

Elastic isotropic model

The material which is homogenous, isotropic, continuous material and follows linear stress-strain behavior without any hysteresis on unloading, can be described by isotropic model.

Elastic transversely isotropic model

The elastic, transversely isotropic model can model the layered elastic media having different elastic moduli in parallel and normal directions.

3.3.3 Plastic Models

Drucker-Prager Model

Soft clays with low friction angles may be modelled by the Drucker-Prager plasticity model. Its use however is recommended for comparing the results from other numerical programs.

Mohr-Coulomb Model

Mohr-Coulomb model is useful model for modelling the shear failure in soils and rocks. This model has been used for modelling all cases of foundations in undrained clays in the present study. Mohr-Coulomb model can also be used to model a Tresca material. The Tresca yield criterion is a special case of Coulomb's criterion where friction angle $\phi = 0$, and it is also identical to Von Mises' criterion for plane-strain deformation (Chen 1975).

Ubiquitous-Joint Model

It is an anisotropic plasticity model which may be used to model weak planes of a particular orientation inside the Mohr-Coulomb solids.

Strain-hardening or Strain-softening Model

This model simulates non-linear behavior of strain-hardening or softening of the Mohr-Coulomb materials.

Bilinear Strain-hardening or Strain-softening Ubiquitous-joint Model

The strain-hardening or softening of weak planes and matrices based on pre-defined variation of ubiquitous-joint model properties may be represented by this model.

Double Yield Model

This model may be used for modelling materials exhibting irreversible compaction as well as shear yielding such as in a backfill placed hydraulically or in high cemented granular materials.

Modified Cam-Clay Model

In case of materials where the change in volume has significant influence on bulk properties and shear resistance has to be considered (e.g., in soft clays); the Modified

Cam-Clay model may be used.

In addition to the above constitutive models, FLAC also has models for the creeping materials which can be invoked with a special plug in. The input parameters of all built in models can be controlled via a built-in FLAC programming language, FISH, (short for FLACish). FLAC also has an optional facility to add new user defined constitutive models written in C++. Constitutive models can also be written in FISH and can be called from an input data file.

FISH can be used to define new variables and functions. These functions may be used to extend FLAC's usefulness or add user-defined features. Some of these FISH functions have been used in the present analyses and have been described later in Appendix A.

FISH programs can be embedded in a normal FLAC input data file. The lines following the word "Define" are processed as a FISH function and the functions terminates when the word "End" is encountered. Functions may further invoke other functions. The order in which functions are defined does not matter as long as they are defined before they are used (e.g., invoked by a FLAC command). A detailed description of FISH can be found in the manual (Itasca Consulting Group, Inc. 2001a).

3.4 Grid Generation

The zones or elements in FLAC are organised in terms of rows and columns. A pair of numbers (its row and column number) represents a particular zone. Although the rows and columns of zones in a grid may look like a rectangular numerical matrix, the physical shape of the grid does not necessarily have to be rectangular. Different shapes can be created by distorting the geometries of the rows and columns (e.g., holes can be created in a grid and complex bodies can be modelled by attaching separate grids). Further the size of various zones in the FLAC grid can be changed throughout for concentrating more elements in the area of high interest (e.g. under the edge of a footing). Details of the grid generation can be found in FLAC manuals (Itasca Consulting Group, Inc. 2002c) and (Itasca Consulting Group, Inc. 2001b).

3.5 Use of FLAC

FLAC can be operated in two modes:

3.5.1 Command driven mode

In the command driven mode an input data file can be used to operate FLAC or it can be also be run interactively by typing commands. There are over 40 commands and 400 command modifiers or keywords (Itasca Consulting Group, Inc. 2002a). Depending upon the problem, a series of these commands can be inputted at the command line or an input data file consisting of various commands can be created in a text editor (e.g., Notepad). This data file can then be called into FLAC. Command driven mode can be used to create a mesh, assign material properties, choose a constitutive relationship, assign initial, and boundary conditions and define number of timesteps to get a model to a desired state of equilibrium. As discussed earlier in 3.3 special FISH functions can be written and embedded into data files.

3.5.2 Menu driven mode

FLAC can be run in a menu driven graphic user interface known as Graphical Interface for Itasca Codes (GIIC). FLAC-GIIC is point and click operation, and all commands and facilities in FLAC can be accessed from it.

Both of above modes have their own advantages. The major advantage of the command driven mode when run with a data input file is that, depending upon the feedback of initial runs, the model can be refined very easily by editing the data file in a text editor. The grid generation is easier in GIIC. Built-in grids can be brought into the model and can be modified to some extent interactively or using the programming language Java. Java can also be used to create new grids. Another advantage of menu driven mode is that the analysis results can be plotted very easily. The choice for the use of a particular mode may depend upon the individual user. In this study, the author has found that it is more efficient if both modes are used in combination according to the situation and ease.

Details of how to run FLAC can be found in the manuals - "User's Guide" and "FLAC-GIIC Reference"(Itasca Consulting Group, Inc. 2002b).

FLAC can be run in two precision versions - single and double. The single precision version is recommended for most common analyses. The double precision version runs about 2 times slower than the single precision version, and requires approximately 3 times more Random Access Memory (RAM) of a computer for a similar sized (elements) model. The precision of the results in the beginning of the present study has been tested both for single and double precision versions. Since there was no considerable difference and the completion time for an average model was in days, only single precision version has been used in the present study. The calculation time in FLAC directly depends upon the processing speed of the Central Processing Unit (CPU) in a computer. The present study was started using Pentium a III (1GHz) CPU, 256 RAM PC, and it was noticed that it takes days to run a model (model run time was found to be in general directly proportional to the number of elements in the mesh and the number of timesteps required to achieve a desired steady state equilibrium). The modelling was then switched over to a new, faster machine with Pentium IV (2.8 GHz) CPU and 1GHz of RAM, and a dramatic reduction in calculation time was observed. The details of modelling time have been presented in Appendix A.

Chapter 4

Influence of Footing Geometry and Soil Shear Strength on Bearing Capacity and Failure Modes of Layered Clays

The objectives of this study were:

a. Study the modes of failure of shallow foundations on layered clay soils using FLAC.

b. Compare the bearing capacity factors obtained from FLAC with those obtained by other methods in the literature.

c. Compare FLAC large deformation simulations to those obtained by finite element methods (Wang and Carter 2001).

As the research progressed, it became apparent that the large deformation mode of FLAC ran into numerical problems before significant deformations were attained. Therefore, a fourth objective developed:

d. To develop methodologies for enabling FLAC to handle large deformations without code changes.

All these objectives and their outcome with respect to the following special cases have been described in this chapter:

1. Strip Footing on Stiff Clay overlying Soft Clay - Small Deformation Analysis
2. Strip Footing on Soft Clay overlying Stiff Clay - Small Deformation Analysis
3. Circular Footing on Stiff Clay overlying Soft Clay - Small Deformation Analysis
4. Circular Footing on Soft Clay overlying Stiff Clay - Small Deformation Analysis
5. Strip Footing on Stiff Clay overlying Soft Clay - Large Deformation Analysis

4.1 Strip Footing on Stiff Clay Overlying Soft Clay - Small Deformation Analysis

This kind of situation can occur where a stiff crust desiccated due to weathering overlies the soft clay underneath. The bearing capacity of such foundations depends on the ratio of depth or height of upper clay layer (H) to the width of the footing (B), and the ratios of the undrained shear strengths of upper and lower clay layers. The H/B ratios considered in this study are $0.25, 0.5, 1, 2, 2.5, 3$ and 3.5. Various undrained shear strength ratios of the bottom layer (c_2) to top layer (c_1) considered in this study are $0.1, 0.2, 1/3, 0.5, 2/3, 0.8,$ and 1.

A number of different failure mechanisms occur for a rigid strip footing on a strong over soft clay system depending on the H/B and c_2/c_1 ratios. The bearing capacity depends on the steady plastic flow beneath the footing defined by different failure mechanisms. In FLAC models such failure mechanisms are described by the grid point displacement and velocity vectors, and the extent of steady-state plastic flow is represented by plasticity state indicator plots (refer A.1). As we will see later it is the nature and extent of this steady-state plastic flow which is responsible for the variation of the bearing capacity with H/B and c_2/c_1 ratios. The nature of the foundation deformation is also explained with help of a magnified grid. It should be noted that it is the height to width ratio (H/B) which influences the nature of the failure surface passing through different layers, and the relative undrained shear strength of the two layers measured in terms of c_2/c_1 ratio influences the ultimate bearing capacity of the foundation in layered clays. It is the whole process of the development of the deformation or failure and the relative shear strength which determines the ultimate bearing capacity of a foundation.

It is found in this research that when the top strong clay layer is deep enough (i.e. $H \geq 3.5B$) the failure surface is entirely contained in the top strong clay layer for all values of the c_2/c_1 ratio as shown in velocity diagrams (refer A.1.5). This depth is greater than Merifield et al. (1999) who suggested a limiting value of this ratio as $H/B = 2$, and even larger than the value of $H/B \simeq 2.5$ given by Meyerhof and Hanna (1978). For all other values of $H/B < 3.5$, depending upon the H/B and c_2/c_1 ratios, the foundation failure mechanism is general shear, local shear or full punching shear through the top layer followed by yielding of the bottom soft clay layer (refer 4.2).

For $H/B < 0.5$ full punching of the footing through the top strong clay layer occurs when the strength of the top layer is significantly more than the bottom soft layer. The bearing capacity values remain equal to the bearing capacity of the homogeneous case ($c_2/c_1 = 1$) for all ratios of $c_2/c_1 < 1$ and $H/B \geq 3.5$ (refer Table 4.8) , and less than that of the homogeneous case for $H/B \leq 0.25$ (refer Table 4.11). In general, bearing capacity values from the FLAC analysis agree very well with values from FEM analysis by Merifield et al. (1999). However, these values tend to be somewhat different than the semi-empirical values given by Meyerhof and Hanna (1978), which presume a failure surface, whereas no such assumption is made in the present FLAC analyses and the failure zone is developed incrementally as the loading is increased.

4.1.1 was considered as the base case for studying the effect of the thickness of the stronger top clay layer. The thickness is then varied first by increasing as $H > B$ ($H/B = 2, 2.5, 3, 3.5$) and then by decreasing as $H < B$ ($H/B = 0.5, 0.25$). These cases are further explained in the following subsections. The effect of the top clay thickness (H) on the ultimate bearing capacity (q_u) of the foundation is shown in form of modified bearing capacity factor (N_c^*)modified bearing capacity factor) in Figure 4.3.

4.1.1 Rigid Smooth Strip Footing on Strong over Soft Clay ($H/B = 1$)

Case 1: $c_2/c_1 = 1$ (Homogeneous clay) - Small Deformation Analysis

The failure mode for the base case of homogeneous clay is explained in the velocity vector diagram (Figure A.4), and is compared with the classical general shear failure mode. The failure modes for all cases of c_2/c_1 for $H/B = 1$ are summarised in the Table 4.2.

Besides looking at the velocity diagram it is also helpful to look at the magnified deformed grid[1] (Figure A.6), which supports and further explains the general failure mechanism interpreted by looking at the velocity vectors. The characteristic soil heaving can be clearly seen at the edge of the footing.

Another means for understanding the failure mechanism in FLAC is the plasticity indicator plot as shown in Figure A.5. For plasticity models such as Mohr-Coulomb, the FLAC code displays those zone which satisfy the yield criterion. Such indication denotes that plastic flow is occurring. Two types of failure mechanisms are indicated by the plastic state: shear failure and tensile failure. As it is explained in the FLAC manual (Itasca Consulting Group, Inc. 2001b), in the numerical implementation of the plastic models, an elastic trial (or “elastic guess”) for the stress increment is first computed from the total strain increment using the incremental form of Hooke’s law. The corresponding stresses are then evaluated. If they violate the yield criteria (i.e., the stress point representation lies above the yield function in the generalized stress space), plastic deformations take place. In this case, only the elastic part of the strain increment can contribute to the stress increment; the latter is corrected by using the plastic flow rule[2] to ensure that the stresses lie on the composite yield function. It can be see from the Figure A.5 that the plastic field is developed downwards and outwards of the footing and has reached the ground surface on the side of the footing. The depth of failure surface is less than the width of the footing (B). The depth of

[1] It should be noted here that this is a small deformation analysis i. e. the coordinates of the grid points are not updated with the footing settlement. The grid magnification shows only an estimation of the deformation of grid at the end of analysis.

[2] The flow rule specifies the direction of the plastic strain increment vector as that normal to the potential surface; it is called associated if the potential and yield functions coincide, and non-associated otherwise.

failure in this case is $0.75B$, and the horizontal extent of plastic yielding in shear is $\simeq 1.3\,\mathrm{m}$ from the centre of the footing.

As shown in Figure A.7 the contours of equal vertical stress also known as isobars can be used to demonstrate the FLAC analysis results. These contours outline the zone of influence of the footing such that the area contained in the given contour experiences stresses larger than the stress level indicated by that contour. Since this is the case of homogeneous clay foundation, The shapes of the contours are regular and smooth.

The bearing pressure versus footing penetration recorded at different time steps in the history of the model is shown in Figure A.8. The ultimate bearing pressure (q_u) for this case was found to be 103.52 kPa. The modified bearing capacity factor $N_c^* = 5.18$ which is 0.77% higher than the value given by Meyerhof and Hanna (1978), and 6.76% lower than the upper bound analysis of Chen (1975), but lies within upper and lower bound values of modified bearing capacity factor given by Merifield et al. (1999) as shown in Table 4.1.

Table 4.1: Comparison of modified Bearing Capacity Factor, N_c^* with existing values for rigid strip footing on strong over soft clay for grid 40×30, for $H/B = 1$.

Shear Strength Top Layer, (c_1)	Shear Strength Ratio, (c_2/c_1)	q_u (FLAC)	N_c^*(FLAC) = q_u(FLAC)/c_1	N_c				% Difference between N_c^*(FLAC) & N_c	
				(Merifield et al.1999)		(Meyerhof & Hanna 1978)	(Chen 1975)		
				Lowerbound	Upperbound			(Meyerhof & Hanna 1978)	(Chen 1975)
20.00	1.00	103.52	5.18	4.94	5.32	5.14	5.53	0.77	−6.76
20.00	0.80	103.51	5.18	4.87	5.30	5.14	5.53	0.77	−6.76
20.00	0.67	100.78	5.04	4.77	5.18	5.14	5.53	−1.98	−9.72
20.00	0.50	91.14	4.56	4.44	4.82	4.46	5.11	2.19	−12.06
20.00	0.33	77.05	3.85	3.89	4.24	3.47	4.52	9.87	−17.40
20.00	0.20	60.62	3.03	3.10	3.54	2.62	3.87	13.53	−27.72
20.00	0.10	41.68	2.08	–	–	1.95	2.59	6.06	−24.52

Figures 4.1 shows the comparison of modified bearing capacity factor (N_c^*) versus shear strength ratios computed from FLAC with those from literature.

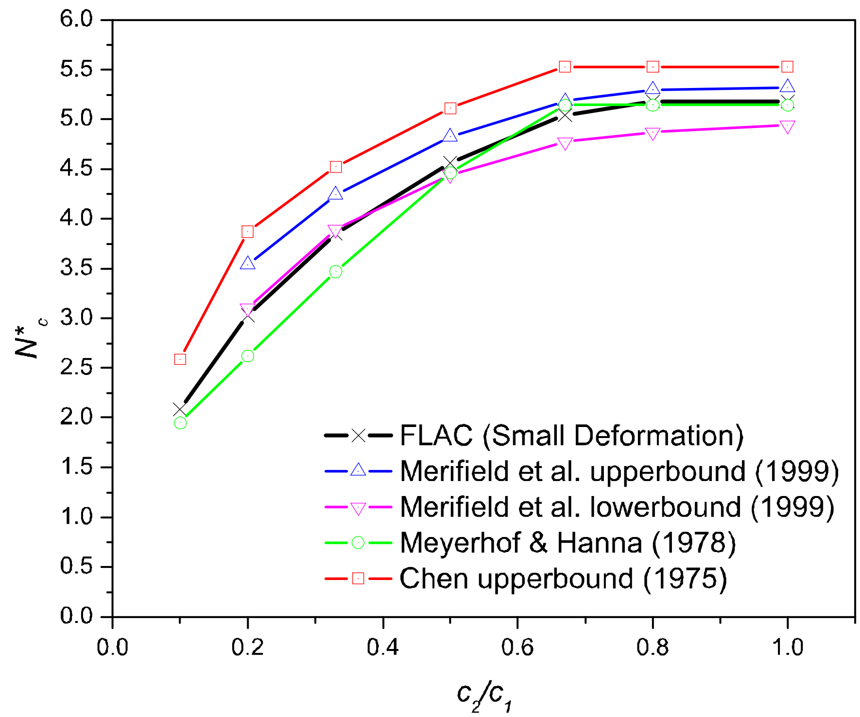

Figure 4.1: Modified bearing capacity factor (N_c^*) versus shear strength ratio (c_2/c_1) curves for a rigid smooth strip footing on strong over soft clay for 40×30 grid model, $H/B = 1$.

The normalised bearing pressure versus penetration curves for different shear strength ratios are shown in Figure 4.2.

Case 2: $c_2/c_1 = 0.8$ **- Small Deformation Analysis**

The velocity vector field shown in Figure A.9 is similar to than in Case 1.

The plasticity state indicators in Figure A.10 show that the zone of failure is starting to extend into the lower soft clay layer. The depth of the failure is found to

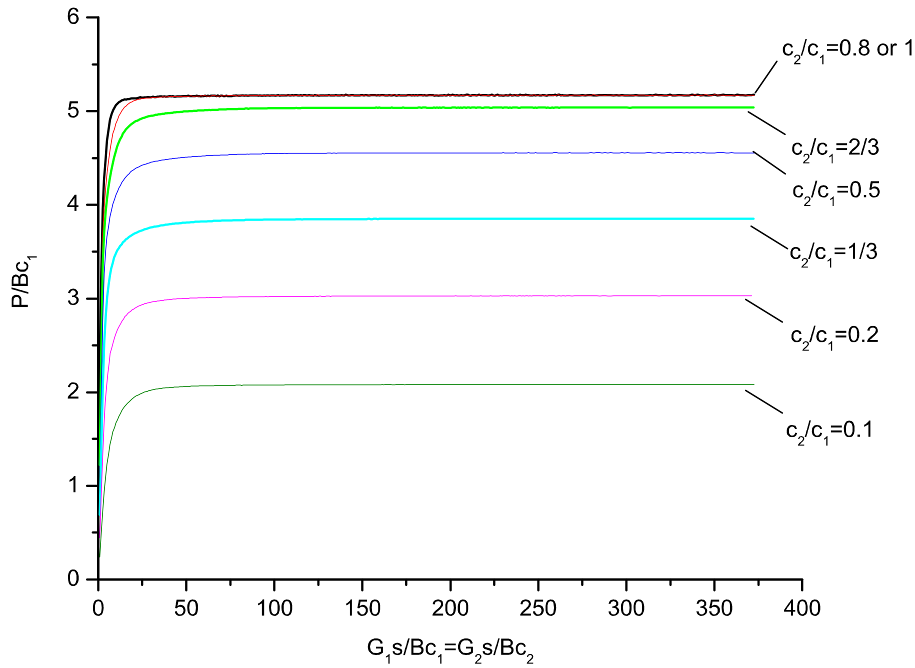

Figure 4.2: Normalised bearing pressure versus penetration curves for a rigid smooth strip footing on strong clay over soft clay for 40 × 30 grid model, $H/B = 1$.

be $\simeq B$, , and the horizontal extent of plastic yielding is $\simeq 1.4\,\mathrm{m}$ from the centre of the footing.

Figure A.11 supports a general shear type failure of the foundation with a soil heaving at the edge of the footing.

It is interpreted from the Figure A.9, A.10 and A.11 that the failure mode in this case can be defined as a general shear in top layer with some yielding and plastic flow in bottom layer.

Figure A.12 shows the equal vertical stress (σ_{yy}) contours and zone of influence of the strip footing. The zone of influence for this case was found to be about four times deeper than the width of the footing, beyond this the footing has no influence on the foundation soil. The shapes of the stress contours are regular and smooth like that in 4.1.1.

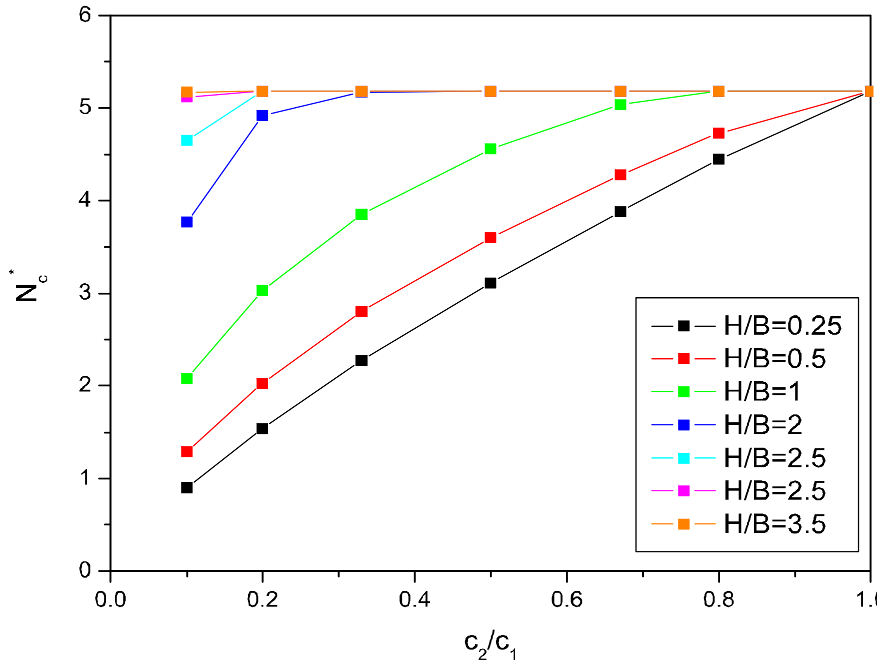

Figure 4.3: Modified bearing capacity factor (N_c^*) versus shear strength ratio (c_2/c_1) curves for a rigid smooth strip footing on strong over soft clay for 40×30 grid model, for various H/B ratios.

The bearing pressure versus footing penetration recorded at different time steps in the history of the model is shown in Figure A.13. The ultimate bearing pressure (q_u) for this case was found to be 103.51 kPa. The modified bearing capacity factor $N_c^* = 5.18$ which is 0.77% higher than the value given by Meyerhof and Hanna (1978), and 6.76% lower than the upper bound analysis of Chen (1975), but lies within upper and lower bound values of modified bearing capacity factor given by Merifield et al. (1999) as shown in Table 4.1.

Case 3: $c_2/c_1 = 2/3$ - Small Deformation Analysis

Figure A.14 starts to indicate some partial punching[3] shear failure of a foundation followed by some yielding of the bottom and top clay layers.

The plasticity state indicators in Figure A.15 show that a elastic soil wedge is trapped under the footing which is pushing into the top clay and causing the plastic flow of the soil sideways and downwards. The zone of failure extends into the soft clay layer. The depth of failure $\simeq 1.75B$, and the horizontal extent of plastic yielding is $\simeq 2.5\,\text{m}$ from the centre of the footing.

Figure A.16 shows the magnified grid which further supports the partial punching[4] shear failure of the foundation with some heave on the edge of the footing. A soil column trapped under the footing shows both downwards vertical as well as lateral movements both in top and bottom clay layers.

Figure A.17 shows the equal vertical stress (σ_{yy}) contours and zone of influence under the strip footing. The stress contours for this case was found to be extending about four times deeper than the width of the footing. The shapes of stress contours are slightly different than in the previous two cases 4.1.1, and 4.1.1 and small kinks can be noticed in the 20 kPa contours at the interface of the two clay layers. This change in shape indicates the influence of the soft bottom clay in reducing the bearing capacity of the foundation.

The bearing pressure versus footing penetration recorded at different time steps in the history of the model is shown in Figure A.18. The plastic yielding in the bottom clay reduces the ultimate bearing capacity (q_u) which was found to be 100.78 kPa in this case. The modified bearing capacity factor $N_c^* = 5.04$ which is 1.98% lower than the value given by Meyerhof and Hanna (1978), and 9.72% lower than the upper bound analysis of Chen (1975), but lies within upper and lower bound values of modified bearing capacity given by Merifield et al. (1999) as shown in Table 4.1.

[3] The punching shear failure can be interpreted by observing the magnitude of the displacement and velocity vectors. If there is distinct change in the vector magnitude under the footing this can be an indication of punching shear failure.

[4] FLAC do not allow separation of adjacent grid zones except at predefined surfaces. So the punching can only be interpreted by observing the degree of the bending of the grid zones.

Case 4: $c_2/c_1 = 0.5$ - Small Deformation Analysis

The velocity vectors shown in Figure A.19 indicate that foundation failure occurs with partial punching shear in the upper layer.

The plasticity state indicators in Figure A.20 show that the zone of failure extends into the soft clay layer. The depth of failure $\simeq 2B$, and the horizontal extent of plastic yielding in shear is $\simeq 3.25$ m from the centre of the footing.

Figure A.21 shows the magnified grid which also supports the partial punching shear failure mechanism of the foundation. There is both vertical movement as well as lateral movement of the soil wedge trapped under the footing. The soil heave near the edge of the footing is very small in comparison to Case 1 (4.1.1), Case 2 (4.1.1) and Case 3 (4.1.1).

Figure A.22 shows the equal vertical stress (σ_{yy}) contours and zone of influence under the strip footing. The vertical stress contours for this case were found to be about four times deeper than the width of the footing. The kinks in the 20 and 40 kPa contours at the interface of the two clay layers are more noticeable now, which indicates greater influence of the soft bottom clay in reducing the bearing capacity of the foundation.

The bearing pressure versus footing penetration recorded at different time steps in the history of the model is shown in Figure A.23. The ultimate bearing pressure (q_u) for this case was found to be 91.14 kPa. The reduction in bearing capacity in comparison to that in Case 1 (4.1.1), Case 2 (4.1.1) and Case 3 (4.1.1) is clearly due to the influence of the bottom soft clay layer. The modified bearing capacity factor $N_c^* = 4.56$ which is 2.19% higher than the value given by Meyerhof and Hanna (1978), and 12.06% lower than the upper bound analysis of Chen (1975), but lies within upper and lower bound values of modified bearing capacity factor given by Merifield et al. (1999) as shown in Table 4.1.

Case 5: $c_2/c_1 = 1/3$ - Small Deformation Analysis

The velocity vectors shown in Figure A.24 continues to indicate a punching shear failure of the foundation, with punching depth extending deeper into the stronger top clay layer. The top clay layer tries to restrict the upward plastic flow in the softer lower clay layer, which causes the of ground to uplift away from the edge of the footing.

The plasticity state indicators in Figure A.25 show that the zone of failure extends into the soft clay layer. The depth of failure $\simeq 2.25B$, and the horizontal extent of plastic yielding is $\simeq 3\,\text{m}$ from the centre of the footing.

Figure A.27 shows the magnified grid which further explains punching shear failure of the foundation through the stronger clay layer followed by some lateral and vertical movement of the soil in the bottom clay layer. The shape of the soil column is more like a block than a wedge now.

Figure A.26 shows the vertical stress (σ_{yy}) contours. The zone of influence of the footing for this case was found to be about six and half times deeper than its width. Due the prominent punching of footing into the top clay, the shapes of stress contours are different than those in Case (1 4.1.1), Case 2 (4.1.1), Case 3 (4.1.1).and Case 4 (4.1.1) in the bottom clay layer.

The bearing pressure versus footing penetration recorded at different time steps in the history of the model is shown in Figure A.28. The ultimate bearing capacity (q_u) for this case is reduced much more than the previous four cases due to the greater influence of the softer lower clay and was found to be 77.05 kPa. The modified bearing capacity factor $N_c^* = 3.85$ which is 9.87% higher than the value given by Meyerhof and Hanna (1978), and 17.40% lower than the upper bound analysis of Chen (1975), but agrees closely with the lower bound value of modified bearing capacity factor given by Merifield et al. (1999) as shown in Table 4.1.

Case 6: $c_2/c_1 = 0.2$ - Small Deformation Analysis

The velocity vectors shown in Figure A.29 also indicate deeper punching shear failure of the foundation, with the rigid column of the strong top clay layer punching deeper into the softer bottom clay layer. The soil under the footing moves more vertically downwards and the soil adjacent moves to fill in. There is no heave on the side of the footing, but the ground is uplifted away from the edge of the footing.

The plasticity state indicators in Figure A.30 show major yielding in the bottom soft clay layer with some minor yielding in the upper strong clay layer. The depth of failure $\simeq 2.45B$. The crust of the stronger upper clay layer restricts the upward plastic flow in the bottom layer resulting in the increase of horizontal extent of the plastic yielding. The horizontal extent of plastic yielding is $\simeq 3.5$ m from the centre of the footing.

Figure A.32 shows the magnified grid which further supports the punching shear failure of the foundation, with the rigid column of the strong top clay layer punching deeper into the softer bottom clay layer.

Figure A.31 shows the equal vertical stress (σ_{yy}) contours beneath the strip footing. The stress concentration around the edge of the footing suggests a failure mechanism in which the footing punches nearly through the top strong layer into the bottom soft layer. The zone of influence for this case was found to be about five and half times deeper than the width of the footing. The increase in the extent of influence of the stress zone also supports the mechanism of the near punching through the strong top clay layer.

The bearing pressure versus footing penetration recorded at different time steps in the history of the model is shown in Figure A.33. The ultimate bearing pressure (q_u) for this case was found to be 60.62 kPa which mainly dependents on undrained shear strength (c_2) of the bottom soft clay the top clay has a very small influence on it. The modified bearing capacity factor $N_c^* = 3.03$ which is 13.53% higher than the value given by Meyerhof and Hanna (1978), 27.72% lower than the upper bound analysis of Chen (1975), and is slightly less than the lower bound value of modified bearing capacity factor given by Merifield et al. (1999) as shown in Table 4.1.

Case 7: $c_2/c_1 = 0.1$ - Small Deformation Analysis

The velocity vectors shown in Figure A.34 continues to indicate a punching shear failure of the foundation, with deep punching in the stronger top clay layer followed by local shear failure in the softer bottom layer. The upward direction of the velocity vectors away from the footing edge indicates an uplift in the ground.

The plasticity state indicators in Figure A.25 show that the zone of failure extends into the soft clay layer. The depth of failure $\simeq 2B$. The crust of the stronger upper clay layer restricts the upward plastic flow in the bottom layer resulting in the increase of horizontal extent of the plastic yielding. The horizontal extent of plastic yielding is $\simeq 5$ m from the centre of the footing.

Figure A.37 shows the magnified grid which further supports the punching shear failure of the foundation, with punching through the stronger top clay layer followed by local shear failure in the softer bottom layer. The punching is interpreted from the bend in the grid at the interface of the two clays and is located underneath the edge of the footing.

Figure A.36 shows the equal vertical stress (σ_{yy}) contours under the strip footing. Once again the punching shear failure of the foundation is reflected by the vertical stress contours being concentrated around the edge of the footing. The influence of the bottom soft layer can be seen in the shape of 10 kPa stress contour whose shape is entirely different than the others. the The zone of influence of the footing for this case was found to be about four times deeper than the width of the footing.

The bearing pressure versus footing penetration recorded at different time steps in the history of the model is shown in Figure A.38. The ultimate bearing capacity (q_u) for this case was found to be 41.68 kPa. This reduced bearing capacity also supports the combination of failure mechanism: punching through the high shear strength (c_1) top clay layer which has almost no contribution in the bearing capacity, and local shear failure in the low shear strength (c_1) bottom clay layer which contributes mainly to the ultimate bearing capacity. The modified bearing capacity factor $N_c^* = 2.08$ which is 6.06% higher than the value given by Meyerhof and Hanna (1978), and 24.52% lower than the upper bound analysis of Chen (1975), but lies within upper and lower bound values of modified bearing capacity factor given by Merifield et al. (1999) as shown in Table 4.1.

4.1.2 Rigid Smooth Strip Footing on Strong over Soft Clay ($H/B = 2$)

Case 1 and 2: $c_2/c_1 = 1$ and 0.8 - Small Deformation Analysis

As it can be seem from Table 4.1 that the ultimate bearing capacity (q_u) values and the modified bearing capacity (N_c^*) values are the same for the Case 1 ($c_2/c_1 = 1$) and the Case 2 ($c_2/c_1 = 0.8$) for $H/B = 1$, the sensitivity of the strong over soft clay layer system is only needed to be tested for the other cases of c_2/c_1 with respect to increasing depth of the top clay layer until the top layer becomes thick enough to avoid any influence of the softer lower clay on the ultimate bearing capacity (q_u) of the foundation. The FLAC analysis results for other cases of c_2/c_1 for $H/B = 2$ are explained below, and the types of failure mechanism have been summarised in Table 4.4.

Case 3: $c_2/c_1 = 2/3$ - Small Deformation Analysis

It can be interpreted from the velocity vectors in Figure A.39 that a general shear type failure of the foundation has occurred in the stronger top clay layer. There is no sign of any plastic flow in the softer bottom clay layer.

The plasticity state indicators in Figure A.40 also show that the plastic flow and the zone of failure is contained in the strong top clay layer. The depth of failure surface $\simeq 0.9B$, and the horizontal extent of plastic yielding is $\simeq 1.1\,\text{m}$ from the centre of the footing.

Figure A.41 shows the magnified grid which further supports the general shear type failure of the foundation with some heave on the edge of the footing.

Figure A.42 shows the equal vertical stress (σ_{yy}) contours under the strip footing. The smooth shapes of the vertical stress contours show that there is no influence of the bottom soft clay layer on the bearing capacity of the foundation.

The bearing pressure versus footing penetration recorded at different time steps in the history of the model is shown in Figure A.43. The ultimate bearing pressure (q_u) for this case was found to be 103.51 kPa. The modified bearing capacity factor $N_c^* = 5.18$ which is 0.77% higher than the value given by Meyerhof and Hanna (1978), and 6.76% lower than the upper bound analysis of Chen (1975), but lies within upper and lower bound values of modified bearing capacity factor given by Merifield et al. (1999) as shown in Table 4.3.

Table 4.2: Failure modes for different shear strength ratios (c_2/c_1) for $H/B = 1$.

Shear Strength Ratio, (c_2/c_1)	Failure Modes
1.00	General shear
0.80	General shear in the top layer, some plastic yielding in the bottom layer
0.67	Local shear failure in top layer, yielding in the bottom layer
0.50	Partial punching shear failure in the top layer, local shear in the bottom layer
0.33	Partial punching shear failure in the top layer, local shear in the bottom layer
0.20	Punching shear failure in the top layer, local shear in the bottom layer
0.10	Punching shear failure in the top layer, local shear in the bottom layer

Table 4.3: Comparison of modified Bearing Capacity Factor, N_c^* with existing values for rigid strip footing on strong over soft clay for grid 40×30, for $H/B = 2$.

Shear Strength Top Layer, (c_1)	Shear Strength Ratio, (c_2/c_1)	q_u (FLAC)	N_c^*(FLAC) = q_u(FLAC)/c_1	N_c				% Difference between N_c^*(FLAC) & N_c	
				(Merifield et al.1999)		(Meyerhof & Hanna 1978)	(Chen 1975)	(Meyerhof & Hanna 1978)	(Chen 1975)
				Lowerbound	Upperbound				
20.00	1.00	103.52	5.18	4.94	5.32	5.14	5.53	0.77	−6.76
20.00	0.80	103.51	5.18	4.81	5.26	5.14	5.53	0.77	−6.76
20.00	0.67	103.51	5.18	4.81	5.26	5.14	5.53	0.77	−6.76
20.00	0.50	103.53	5.18	4.81	5.27	5.14	5.53	0.77	−6.76
20.00	0.33	103.50	5.17	4.81	5.27	5.14	5.53	0.58	−6.96
20.00	0.20	98.49	4.92	4.61	5.32	4.20	5.53	14.63	−12.40
20.00	0.10	75.32	3.77	–	–	3.39	5.53	9.97	−46.68

Figure 4.4 shows the comparison of modified bearing capacity factor (N_c^*) versus shear strength ratios computed from FLAC with those from the literature.

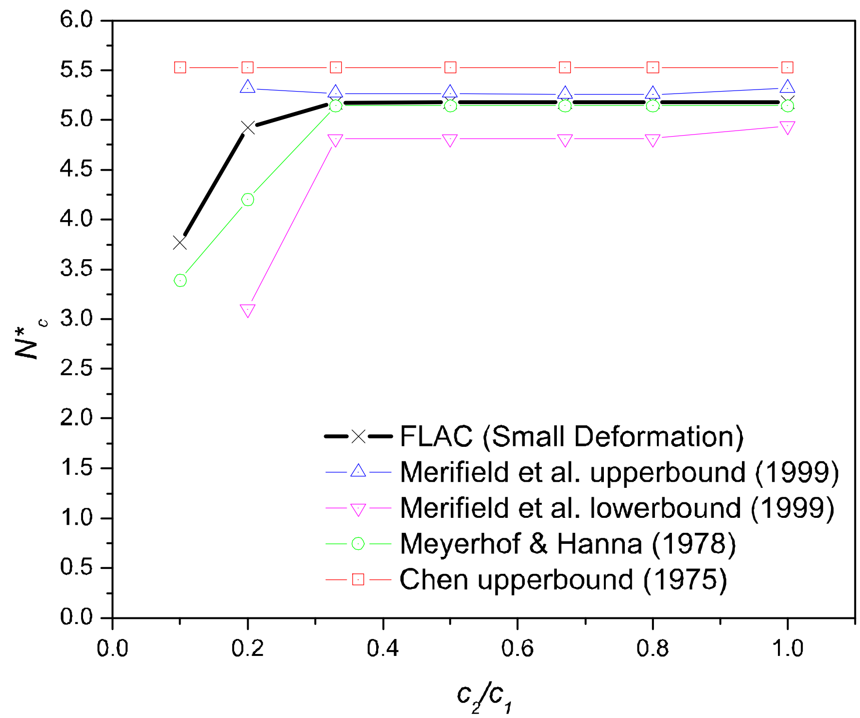

Figure 4.4: Modified bearing capacity factor (N_c^*) versus shear strength ratio (c_2/c_1) curves for a rigid smooth strip footing on strong clay over soft clay for 40 × 30 grid model, $H/B = 2$.

The normalised bearing pressure versus penetration curves for different shear strength ratios have been shown in Figure 4.5.

Case 4: $c_2/c_1 = 0.5$ - Small Deformation Analysis

The velocity vectors shown in Figure A.44 indicate that the foundation fails in general shear in the strong upper clay layer.

The plasticity state indicators in Figure A.45 show that the zone of failure is contained in the strong top clay layer. The depth of failure $\simeq 0.9B$, and the horizontal

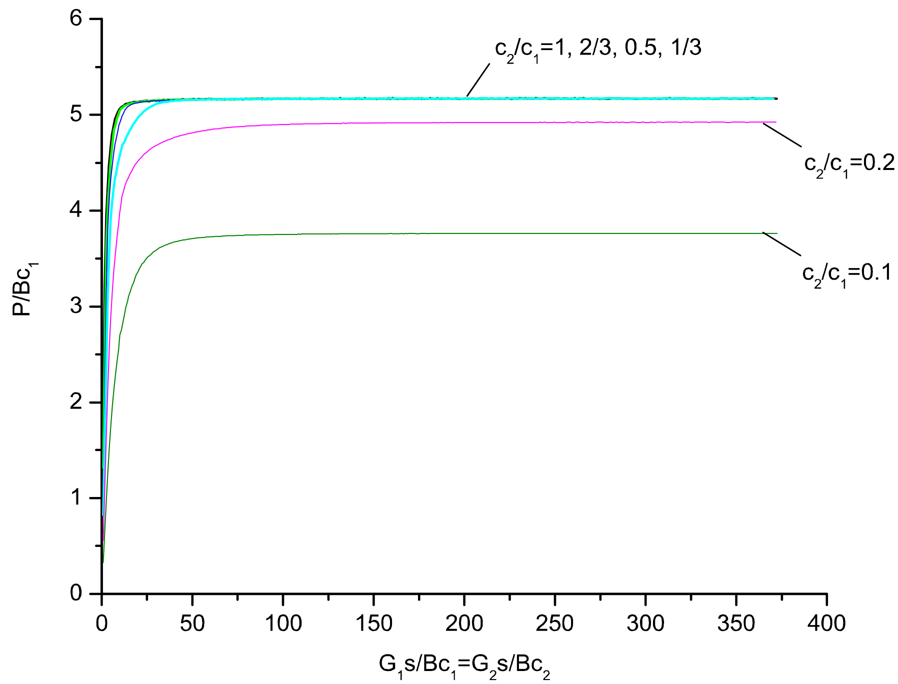

Figure 4.5: Normalised bearing pressure versus penetration curves for a rigid smooth strip footing on strong clay over soft clay for 40×30 grid model, $H/B = 2$.

extent of plastic yielding is $\simeq 1.1\,\mathrm{m}$ from the centre of the footing.

Figure A.46 shows the magnified grid that also supports the general shear type failure mechanism of the foundation. The characteristic heave of general shear type failure for a smooth footing can be clearly seen.

Figure A.47 shows the equal vertical stress (σ_{yy}) contours. The zone of influence of the footing for this case was found to be about four times deeper than the width of the footing. The shapes of stress contours are fairly smooth.

The bearing pressure versus footing penetration recorded at different time steps in the history of the model is shown in Figure A.48. The ultimate bearing pressure (q_u) for this case was found to be 103.53 kPa. The modified bearing capacity factor $N_c^* = 5.18$ which is 0.77% higher than the value given by Meyerhof and Hanna (1978),

Table 4.4: Failure modes for different shear strength ratios (c_2/c_1) for $H/B = 2$.

Shear Strength Ratio, (c_2/c_1)	Failure Modes
0.67	General shear in the top layer, no yielding in the bottom layer
0.50	General shear in the top layer, no yielding in the bottom layer
0.33	General shear in the top layer, minor yielding in the bottom layer
0.20	Partial punching shear failure in the top layer, local shear in the bottom layer
0.10	Partial punching shear failure in the top layer, local shear in the bottom layer

and 6.76% lower than the upper bound analysis of Chen (1975), but lies within upper and lower bound values of modified bearing capacity factor given by Merifield et al. (1999) as shown in Table 4.3.

Case 5: $c_2/c_1 = 1/3$ - Small Deformation Analysis

The velocity vectors shown in Figure A.49 indicate a general shear type failure of the foundation.

The plasticity state indicators in Figure A.50 show that the zone of failure is mainly contained in the stronger top clay layer, however there is some evidence of local plastic yielding in the softer bottom clay layer. The depth of failure $\simeq 0.9B$, and the horizontal extent of plastic yielding is $\simeq 1.1$ m from the centre of the footing.

Figure A.51 shows the magnified grid which further illustrates general shear type of failure.

Figure A.52 shows the equal vertical stress (σ_{yy}) contours under the strip footing. The zone of influence for this case was found to be about six and half times deeper than the width of the footing. The shapes of stress contours now changes with an evident kink in the 20 kPa contour suggesting some influence of the soft bottom clay on the bearing capacity of the foundation.

The bearing pressure versus footing penetration recorded at different time steps in the history of the model is shown in Figure A.53. Due to some influence of the soft bottom clay, the ultimate bearing capacity (q_u) is slightly reduced to 103.50 kPa.

The modified bearing capacity factor $N_c^* = 5.17$ which is 0.58% higher than the value given by Meyerhof and Hanna (1978), and 6.96% lower than the upper bound analysis of Chen (1975), but lies within the upper and lower bound values of modified bearing capacity factor given by Merifield et al. (1999) as shown in Table 4.3.

Case 6: $c_2/c_1 = 0.2$ - Small Deformation Analysis

The velocity vectors shown in Figure A.54 indicate a partial punching shear failure in the stronger upper clay layer followed by local shear type failure in the softer bottom clay layer.

The plasticity state indicators in Figure A.55 show major plastic yielding in the bottom soft clay layer with some minor plastic yielding in the upper strong clay layer. The depth of failure $\simeq 5.5B$. The crust of the stronger upper clay layer restricts the upward plastic flow in the bottom layer resulting in the increase of horizontal extent of the plastic yielding. The horizontal extent of plastic yielding is $\simeq 5.5$ m from the centre of the footing.

Figure A.56 shows the magnified grid which further supports the partial punching shear failure of the foundation, with the rigid column of the strong top clay layer punching deeper into the softer bottom clay layer.

Figure A.57 shows the equal vertical stress (σ_{yy}) contours and zone of influence under the strip footing. The 20 kPa stress contour in this case is not of regular shape and shows big change in its shape at the interface of the two clay layers. The zone of influence for this case was found to be about five and half times deeper than the width of the footing.

The bearing pressure versus footing penetration recorded at different time steps in the history of the model is shown in Figure A.58. The ultimate bearing pressure (q_u) for this case was found to be 98.49 kPa. This reduction in bearing capacity is mainly due to the greater influence of the soft bottom clay. The modified bearing capacity factor $N_c^* = 4.92$ which is 14.63% higher than the value given by Meyerhof and Hanna (1978), and 12.40% lower than the upper bound analysis of Chen (1975), but lies within the upper and lower bound values of modified bearing capacity factor given by Merifield et al. (1999) as shown in Table 4.3.

Case 7: $c_2/c_1 = 0.1$ **- Small Deformation Analysis**

The velocity vectors shown in Figure A.59 continues to indicate a punching shear failure of the foundation through the stronger top clay layer followed by local shear type failure in the softer bottom layer.

The plasticity state indicators in Figure A.60 show that the zone of failure extends into the soft clay layer. The depth of failure $\simeq 8B$. The crust of the stronger upper clay layer restricts the upward plastic flow in the bottom layer resulting in the increase of horizontal extent of the plastic yielding. The horizontal extent of plastic yielding is $\simeq 11$ m from the centre of the footing.

Figure A.61 shows the magnified grid which further supports the punching shear failure of the foundation through the stronger top clay layer followed by local shear failure in the softer bottom layer. The punching through the strong top clay layer is evident from a bend in the grid at the interface of the strong and soft clay layers and is located underneath the edge of the footing.

Figure A.62 shows the equal vertical stress (σ_{yy}) contours and zone of influence under the strip footing. The built up of stress concentration around the edge of the footing suggests a failure mechanism in which the footing punches through the top strong layer into the bottom soft layer. The zone of influence for this case was found to be about six and half times deeper than the width of the footing.

The bearing pressure versus footing penetration recorded at different time steps in the history of the model is shown in Figure A.63. The ultimate bearing pressure (q_u) for this case was found to be 75.32 kPa. This reduction in bearing capacity value supports the punching shear failure mechanism through the strong top layer which has almost no influence on the bearing capacity followed by local shear failure in the soft bottom clay which mainly contributes to the bearing capacity of the foundation. The modified bearing capacity factor $N_c^* = 3.77$ which is 9.97% higher than the value given by Meyerhof and Hanna (1978), and 46.68% lower than the upper bound analysis of Chen (1975) as shown in Table 4.3.

4.1.3 Rigid Smooth Strip Footing on Strong over Soft Clay ($H/B = 2.5$)

Case 1, 2, 3 and 4: $c_2/c_1 = 1$, 0.8, $2/3$, **and** 0.5 **- Small Deformation Analysis**

It can be seen from Table 4.3 that the value of modified bearing capacity factor (N_c^*) from FLAC analysis gives a constant value (5.18) for $c_2/c_1 = 1$, 0.8, 2/3, and 0.5. The softer bottom clay layer has no influence on the bearing capacity of the foundation for these shear strength ratios. The analysis for these cases for $H/B = 2.5$ would be same as Case 1 (Ref. 4.1.1), Case 2 (Ref. 4.1.1), Case 3 (Ref. 4.1.2) and Case 4 (Ref. 4.1.2) respectively. The FLAC analysis results for other cases of c_2/c_1 are explained below, and the types of failure mechanism have been summarised in Table 4.6.

Case 5: $c_2/c_1 = 1/3$ **- Small Deformation Analysis**

The velocity vectors shown in Figure A.64 show a general shear type failure of foundation with some soil heave on the edge of the footing.

The plasticity state indicators in Figure A.65 show that the zone of failure extends into the soft clay layer. The depth of failure $\simeq 0.9B$, and the horizontal extent of plastic yielding is $\simeq 1.25\,\text{m}$ from the centre of the footing.

Figure A.66 shows the magnified grid which further explains general shear type failure of foundation with some soil heave at the edge of the footing.

Figure A.67 shows the equal vertical stress (σ_{yy}) contours and zone of influence under the strip footing. The zone of influence for this case was found to be about six and half times deeper than the width of the footing. The shapes of stress contours are smoother than that in 4.1.2, indicating that the strong top clay layer is now thick enough to shield it against the influence of the softer bottom clay layer on the bearing capacity of the foundation.

The bearing pressure versus footing penetration recorded at different time steps in the history of the model is shown in Figure A.68. The ultimate bearing pressure (q_u) for this case was found to be 103.53 kPa. The modified bearing capacity factor $N_c^* = 5.18$ which is 0.77% higher than the value given by Meyerhof and Hanna (1978),

and 6.76% lower than the upper bound analysis of Chen (1975) as shown in Table 4.5.

Table 4.5: Comparison of modified Bearing Capacity Factor, N_c^* with existing values for rigid strip footing on strong over soft clay for grid 40×30, for $H/B = 2.5$.

Shear Strength Top Layer, (c_1)	Shear Strength Ratio, (c_2/c_1)	q_u (FLAC)	N_c^*(FLAC) = q_u(FLAC)/c_1	N_c		% Difference between N_c^*(FLAC) & N_c	
				(Meyerhof & Hanna 1978)	(Chen 1975)	(Meyerhof & Hanna 1978)	(Chen 1975)
20.00	1.00	103.52	5.18	5.14	5.53	0.77	−6.76
20.00	0.80	103.52	5.18	5.14	5.53	0.77	−6.76
20.00	0.67	103.51	5.18	5.14	5.53	0.77	−6.76
20.00	0.50	103.53	5.18	5.14	5.53	0.77	−6.76
20.00	0.33	103.53	5.18	5.14	5.53	0.77	-6.76
20.00	0.20	103.52	5.18	5.03	5.53	2.93	−6.76
20.00	0.10	92.93	4.65	4.11	5.53	11.53	−18.92

Figure 4.6 shows the comparison of modified bearing capacity factor (N_c^*) versus shear strength ratios computed from FLAC with those from the literature.

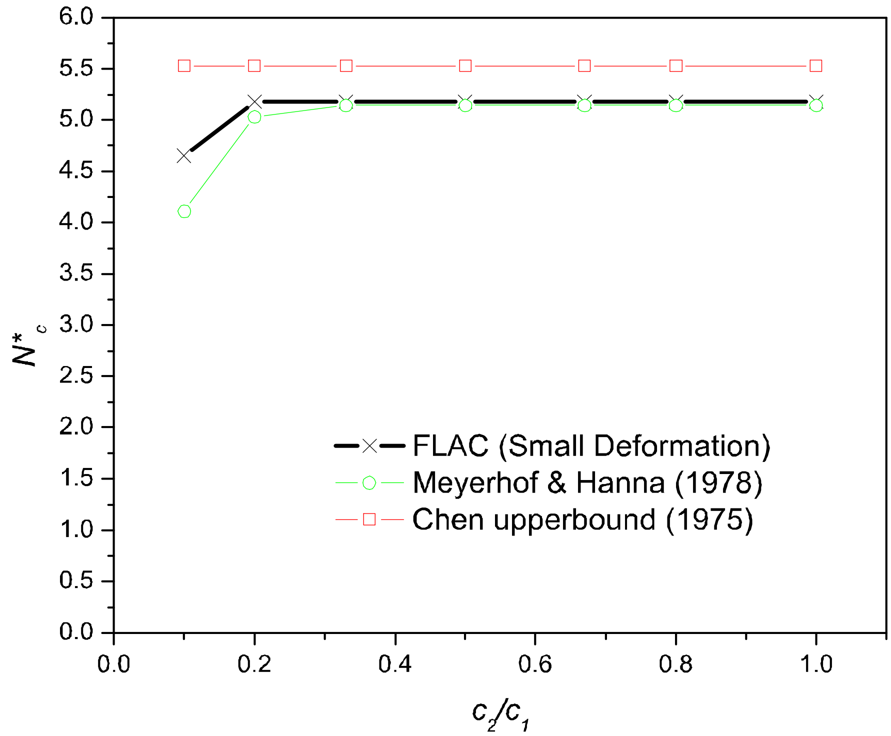

Figure 4.6: Modified bearing capacity factor (N_c^*) versus shear strength ratio (c_2/c_1) curves for a rigid smooth strip footing on strong clay over soft clay for 40×30 grid model, $H/B = 2.5$.

The normalised bearing pressure versus penetration curves for different shear strength ratios are shown in Figure 4.7.

Case 6: $c_2/c_1 = 0.2$ **- Small Deformation Analysis**

The velocity vectors shown in Figure A.69 indicate a general shear type failure of the foundation with some soil heave on the edge of the footing.

The plasticity state indicators in Figure A.70 show major plastic yielding in the

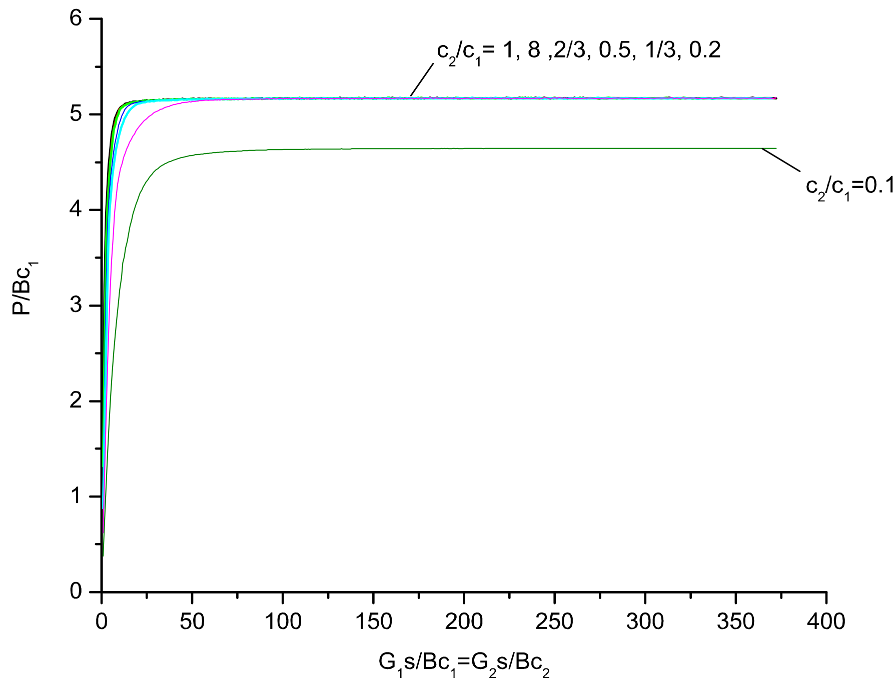

Figure 4.7: Normalised bearing pressure versus penetration curves for a rigid smooth strip footing on strong clay over soft clay for 40×30 grid model, $H/B = 2.5$.

top strong clay layer. The depth of failure $\simeq 0.9B$. The horizontal extent of plastic yielding is $\simeq 1.25\,\mathrm{m}$ from the centre of the footing.

Figure A.71 shows the magnified grid which further supports a general shear type failure of foundation with soil heaving at the edge of the footing.

Figure A.72 shows the equal vertical stress (σ_{yy}) contours and zone of influence under the strip footing. The zone of influence for this case was found to be about five and half times deeper than the width of the footing.

The bearing pressure versus footing penetration recorded at different time steps in the history of the model is shown in Figure A.73. The ultimate bearing pressure (q_u) for this case was found to be 103.52 kPa. The modified bearing capacity factor $N_c^* = 5.18$ which is 2.93% higher than the value given by Meyerhof and Hanna (1978),

Table 4.6: Failure modes for different shear strength ratios (c_2/c_1) for $H/B = 2.5$.

Shear Strength Ratio, (c_2/c_1)	Failure Modes
0.33	General shear in the top layer, no yielding in the bottom layer
0.20	General shear in the top layer, no yielding in the bottom layer
0.10	Partial punching shear failure in the top layer, local shear in the bottom layer

and 6.76% lower than the upper bound analysis of Chen (1975) as shown in Table 4.5.

Case 7: $c_2/c_1 = 0.1$ - Small Deformation Analysis

The velocity vectors shown in Figure A.74 now indicate a punching shear failure of the foundation in the stronger top clay layer followed by local shear type failure in the softer bottom layer.

The plasticity state indicators in Figure A.75 show that the zone of failure extends into the soft clay layer. The depth of failure $\simeq 1.9B$. The crust of the stronger upper clay layer restricts the upward plastic flow in the bottom layer resulting in the increase of horizontal extent of the plastic yielding. The horizontal extent of plastic yielding is $\simeq 13\,\text{m}$ from the centre of the footing.

Figure A.76 shows the magnified grid which further supports a punching shear failure of the foundation, with footing punching through the stronger top clay layer followed by local yielding in the softer bottom layer.

Figure A.77 shows the equal vertical stress (σ_{yy}) contours and zone of influence under the strip footing. There is big distortion in the shape of the 10 kPa contour at the interface of the two clay layer, which shows the influence of the soft bottom clay layer on the bearing capacity of the foundation. The zone of influence for this case was found to be about eight times deeper than the width of the footing.

The bearing pressure versus footing penetration recorded at different time steps in the history of the model is shown in Figure A.78. The ultimate bearing pressure (q_u) for this case was found to be 92.93 kPa. The modified bearing capacity factor

$N_c^* = 4.65$ which is 11.53% higher than the value given by Meyerhof and Hanna (1978), and 18.92% lower than the upper bound analysis of Chen (1975) as shown in Table 4.5.

4.1.4 Rigid Smooth Strip Footing on Strong over Soft Clay ($H/B = 3$)

Case 1, 2, 3, 4, 5 and 6: $c_2/c_1 = 1$, 0.8, 2/3, 0.5, 1/3, 0.2**- Small Deformation Analysis**

The values of modified bearing capacity factor (N_c^*) from FLAC analysis are constant (5.18) for $c_2/c_1 = 1$, 0.8, 2/3, 0.5, 1/3 and 0.2, respectively (Ref. Table 4.5), and the soft bottom layer layer has no influence on the bearing capacity of the foundation and for this thickness of the strong top clay layer ($H/B = 2.5$). Therefore analysis for these cases would be same as Case 1 (Ref. 4.1.1), Case 2 (Ref. 4.1.1), Case 3 (Ref. 4.1.2), Case 4 (Ref. 4.1.2), Case 5 (Ref. 4.1.3) and Case 6 (Ref. 4.1.3) respectively. The FLAC analysis results for $c_2/c_1 = 0.1$ are explained below.

Case 7: $c_2/c_1 = 0.1$ **- Small Deformation Analysis**

The velocity vectors shown in Figure A.79 indicate a partial punching shear failure in the stronger top clay layer followed by local yielding in the softer bottom layer.

The plasticity state indicators in Figure A.80 show that the zone of failure extends into the soft clay layer. The depth of failure $\simeq 10B$. The crust of the stronger upper clay layer restricts the upward plastic flow in the bottom layer resulting in the increase of horizontal extent of the plastic yielding. The horizontal extent of plastic yielding is $\simeq 15\,\text{m}$ from the centre of the footing.

Figure A.81 shows the magnified grid which further supports the punching shear failure of the foundation, with footing punching through the stronger top clay layer followed by local yielding in the softer bottom layer.

Figure A.82 shows the equal vertical stress (σ_{yy}) contours and zone of influence under the strip footing. The zone of influence for this case was found to be about four times deeper than the width of the footing. The shapes of the 20 kPa and 40 kPa contours are not smooth indication the influence of the softer bottom clay.

The bearing pressure versus footing penetration recorded at different time steps in the history of the model is shown in Figure A.83. The ultimate bearing pressure (q_u) for this case was found to be 102.4 kPa. The modified bearing capacity factor $N_c^* = 5.12$ which is 5.59% higher than the value given by Meyerhof and Hanna (1978), and 8.01% lower than the upper bound analysis of Chen (1975), as shown in Table 4.7.

Table 4.7: Comparison of modified Bearing Capacity Factor, N_c^* with existing values for rigid strip footing on strong over soft clay for grid 40×30, for $H/B = 3$.

Shear Strength Top Layer, (c_1)	Shear Strength Ratio, (c_2/c_1)	q_u (FLAC)	N_c^*(FLAC) = q_u(FLAC)/c_1	N_c (Meyerhof & Hanna 1978)	N_c (Chen 1975)	% Difference between N_c^*(FLAC) & N_c (Meyerhof & Hanna 1978)	% Difference between N_c^*(FLAC) & N_c (Chen 1975)
20.00	1.00	103.52	5.18	5.14	5.53	0.77	−6.76
20.00	0.80	103.52	5.18	5.14	5.53	0.77	−6.76
20.00	0.67	103.51	5.18	5.14	5.53	0.77	−6.76
20.00	0.50	103.53	5.18	5.14	5.53	0.77	−6.76
20.00	0.33	103.53	5.18	5.14	5.53	0.77	-6.76
20.00	0.20	103.52	5.18	5.14	5.53	0.77	−6.76
20.00	0.10	102.40	5.12	4.83	5.53	5.59	−8.01

Figure 4.8 shows the comparison of modified bearing capacity factor (N_c^*) versus shear strength ratios computed from FLAC with those from literature.

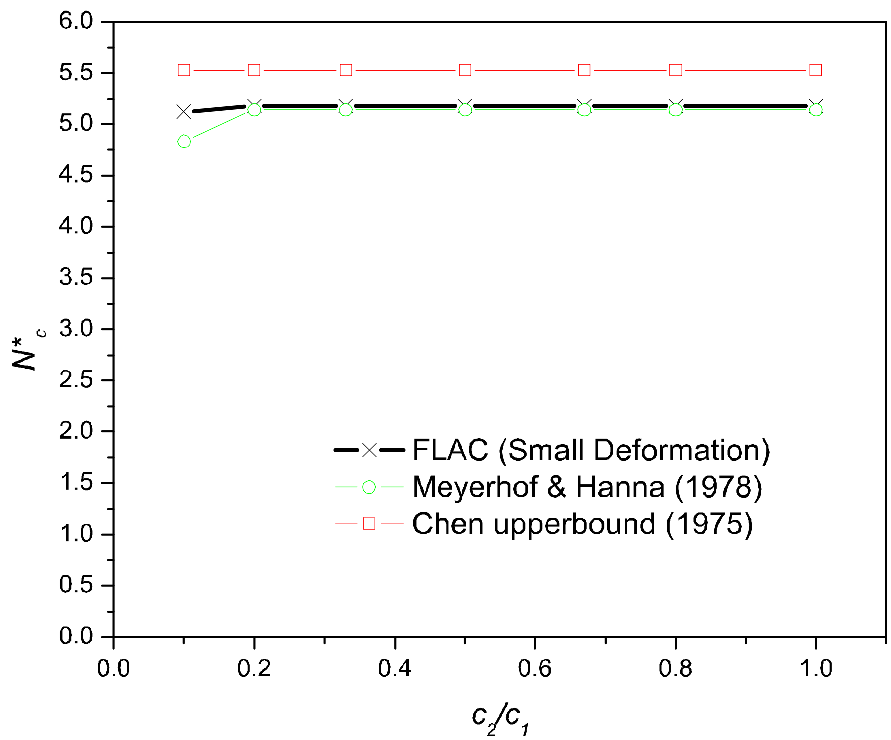

Figure 4.8: Modified bearing capacity factor (N_c^*) versus shear strength ratio (c_2/c_1) curves for a rigid smooth strip footing on strong clay over soft clay for 40×30 grid model, $H/B = 3$.

The normalised bearing pressure versus penetration curves for different shear strength ratios are shown in Figure 4.9.

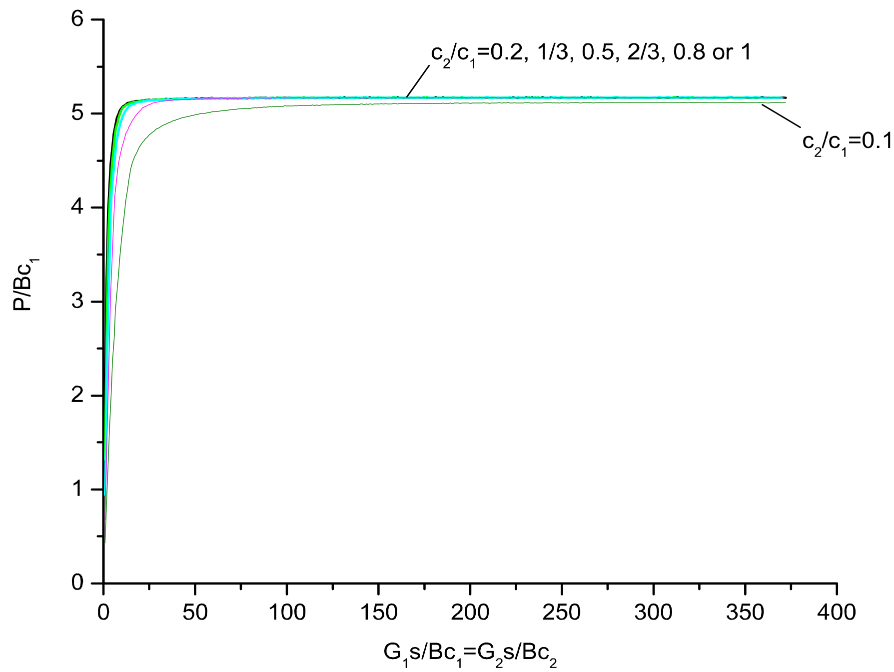

Figure 4.9: Normalised bearing pressure versus penetration curves for a rigid smooth strip footing on strong clay over soft clay for 40×30 grid model, $H/B = 3$.

4.1.5 Rigid Smooth Strip Footing on Strong over Soft Clay ($H/B = 3.5$)

Case 1, 2, 3, 4, 5 and 6: $c_2/c_1 = 1$, 0.8, 2/3, 0.5, 1/3, 0.2**- Small Deformation Analysis**

It can be seen from Table 4.3, and 4.3 that the values of modified bearing capacity factor (N_c^*) from FLAC analysis are constant (5.18) for $c_2/c_1 = 1$, 0.8, 2/3, 0.5, and for 1/3 and 0.2, respectively. Therefore analysis for these cases would be same as Case 1 (Ref. 4.1.1), Case 2 (Ref. 4.1.1), Case 3 (Ref. 4.1.2), Case 4 (Ref. 4.1.2), Case 5 (Ref. 4.1.3) and Case 6 (Ref. 4.1.3) respectively. The FLAC analysis results for other cases of c_2/c_1 are explained below.

Case 7: $c_2/c_1 = 0.1$ **- Small Deformation Analysis**

The foundation behaviour shown in Figure A.84 now shows a general shear type failure type of the foundation in the stronger top clay layer with the velocity vectors are entirely contained in top clay layer. The upward vertical direction of the velocity vectors on the side of the footing indicates a characteristic heave of the general shear type failure of the foundation for a smooth footing.

The plasticity state indicators in Figure A.85 show that the zone of failure is all contained in the strong top clay layer. The depth of failure $\simeq 0.9B$. The horizontal extent of plastic yielding is $\simeq 1.1$ m from the centre of the footing.

Figure A.87 shows the magnified grid which further supports the general shear type failure of the foundation with some soil heave at the edge of the footing.

Figure A.86 shows the equal vertical stress (σ_{yy}) contours and zone of influence under the strip footing. The zone of influence for this case was found to be about three times deeper than the width of the footing.

The bearing pressure versus footing penetration recorded at different time steps in the history of the model is shown in Figure A.88. The ultimate bearing pressure (q_u) for this case was found to be 103.49 kPa. The modified bearing capacity factor $N_c^* = 5.17$ which is 0.58% higher than the value given by Meyerhof and Hanna (1978),

but is 6.96% less than upper bound values of modified bearing capacity factor given by Chen (1975) as shown in Table 4.8.

Table 4.8: Comparison of modified Bearing Capacity Factor, N_c^* with existing values for rigid strip footing on strong over soft clay for grid 40×30, for $H/B = 3.5$.

Shear Strength Top Layer, (c_1)	Shear Strength Ratio, (c_2/c_1)	q_u (FLAC)	N_c^*(FLAC) = q_u(FLAC)/c_1	N_c		% Difference between N_c^*(FLAC) & N_c	
				(Meyerhof & Hanna 1978)	(Chen 1975)	(Meyerhof & Hanna 1978)	(Chen 1975)
20.00	1.00	103.52	5.18	5.14	5.53	0.77	−6.76
20.00	0.80	103.52	5.18	5.14	5.53	0.77	−6.76
20.00	0.67	103.51	5.18	5.14	5.53	0.77	−6.76
20.00	0.50	103.53	5.18	5.14	5.53	0.77	−6.76
20.00	0.33	103.53	5.18	5.14	5.53	0.77	-6.76
20.00	0.20	103.52	5.18	5.14	5.53	0.77	−6.76
20.00	0.10	102.40	5.17	5.14	5.53	0.58	−6.96

Figure 4.10 shows the comparison of modified bearing capacity factor (N_c^*) versus shear strength ratios computed from FLAC with those from the literature.

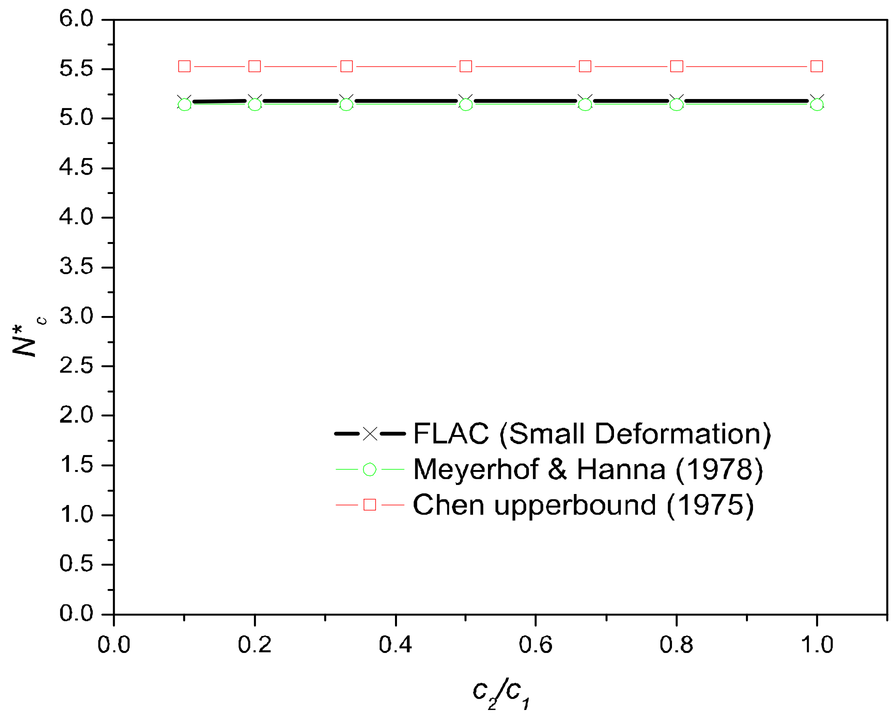

Figure 4.10: Modified bearing capacity factor (N_c^*) versus shear strength ratio (c_2/c_1) curves for a rigid smooth strip footing on strong clay over soft clay for 40×30 grid model, $H/B = 3.5$.

The normalised bearing pressure versus penetration curves for different shear strength ratios are shown in Figure 4.11.

In above cases (Ref. 4.1.1, 4.1.2, 4.1.3, 4.1.4, and 4.1.5) the limiting depth of the upper strong clay layer is being approached beyond which lower soft clay layer has no influence on the ultimate bearing capacity of the strip foundation. The following cases (Ref. 4.1.6 and 4.1.7) will show the influence of the bottom soft clay on the ultimate bearing capacity when the $H/B < 1$.

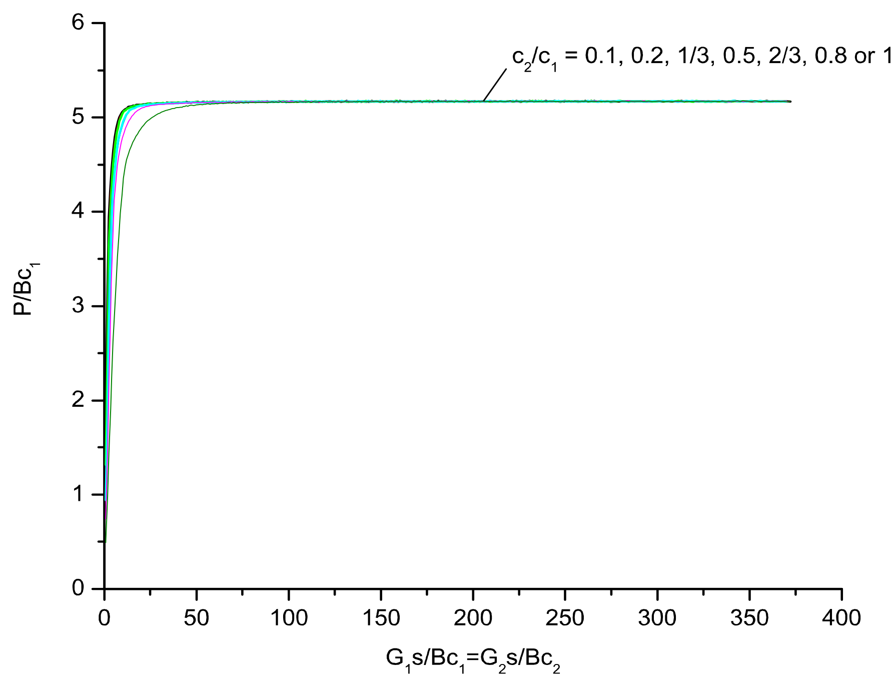

Figure 4.11: Normalised bearing pressure versus penetration curves for a rigid smooth strip footing on strong clay over soft clay for 40×30 grid model, $H/B = 3.5$.

4.1.6 Rigid Smooth Strip Footing on Strong over Soft Clay ($H/B = 0.5$)

Case 1: $c_2/c_1 = 1$ (Homogeneous clay) - Small Deformation Analysis

Since this is the case of homogeneous clay all the results will be same as Case 1 (Ref. 4.1.1). The FLAC analysis results for other cases of c_2/c_1 are explained below, and failure modes are summarised in Table 4.10.

Case 2: $c_2/c_1 = 0.8$ - Small Deformation Analysis

The velocity vectors shown in Figure A.89 show local shear type failure of the foundation in the strong top clay which spreads into the upper portion of the softer bottom clay layer.

The plasticity state indicators in Figure A.90 show that the zone of failure extends into the bottom soft clay layer. The depth of the failure is found to be $\simeq 1.2B$, , and the horizontal extent of plastic yielding is $\simeq 1.4\,\mathrm{m}$ from the centre of the footing.

Figure A.92 shows the magnified grid which further supports the local shear type failure of the foundation. There is some evidence of the grid deformation in the bottom softer clay.

Figure A.91 shows the equal vertical stress (σ_{yy}) contours and zone of influence under the strip footing. The zone of influence for this case was found to be extending about three and half times deeper than the width of the footing spreading deeper into the softer clay layer. The shapes of the stress contours are fairly smooth.

The bearing pressure versus footing penetration recorded at different time steps in the history of the model is shown in Figure A.93. The ultimate bearing pressure (q_u) for this case was found to be 94.68 kPa. The modified bearing capacity factor $N_c^* = 4.73$ which is 7.82% lower than the value given by Meyerhof and Hanna (1978), and 4.23% lower than the upper bound analysis of Chen (1975), but lies within upper and lower bound values of modified bearing capacity factor given by Merifield et al. (1999) as shown in Table 4.3.

Table 4.9: Comparison of modified Bearing Capacity Factor, N_c^* with existing values for rigid strip footing on strong over soft clay for grid 40×30, for $H/B = 0.5$.

Shear Strength Top Layer, (c_1)	Shear Strength Ratio, (c_2/c_1)	q_u (FLAC)	N_c^*(FLAC) = q_u(FLAC)/c_1	N_c				% Difference between N_c^*(FLAC) & N_c	
				(Merifield et al.1999)		(Meyerhof & Hanna 1978)	(Chen 1975)		
				Lowerbound	Upperbound			(Meyerhof & Hanna 1978)	(Chen 1975)
20.00	1.00	103.52	5.18	4.94	5.32	5.14	5.53	0.77	−6.76
20.00	0.80	94.68	4.73	4.42	4.94	5.10	5.53	−7.82	−4.23
20.00	0.67	85.62	4.28	4.07	4.48	4.41	5.53	−3.04	−5.61
20.00	0.50	72.09	3.60	3.52	3.89	3.51	5.53	2.50	−9.44
20.00	0.33	56.29	2.81	2.84	3.16	2.59	5.53	7.83	−15.66
20.00	0.20	40.69	2.03	2.16	2.44	1.82	5.53	10.34	−25.62
20.00	0.10	25.85	1.29	–	–	1.23	5.53	4.34	−48.06

Figure 4.12 shows the comparison of modified bearing capacity factor (N_c^*) versus shear strength ratios computed from FLAC with those from literature.

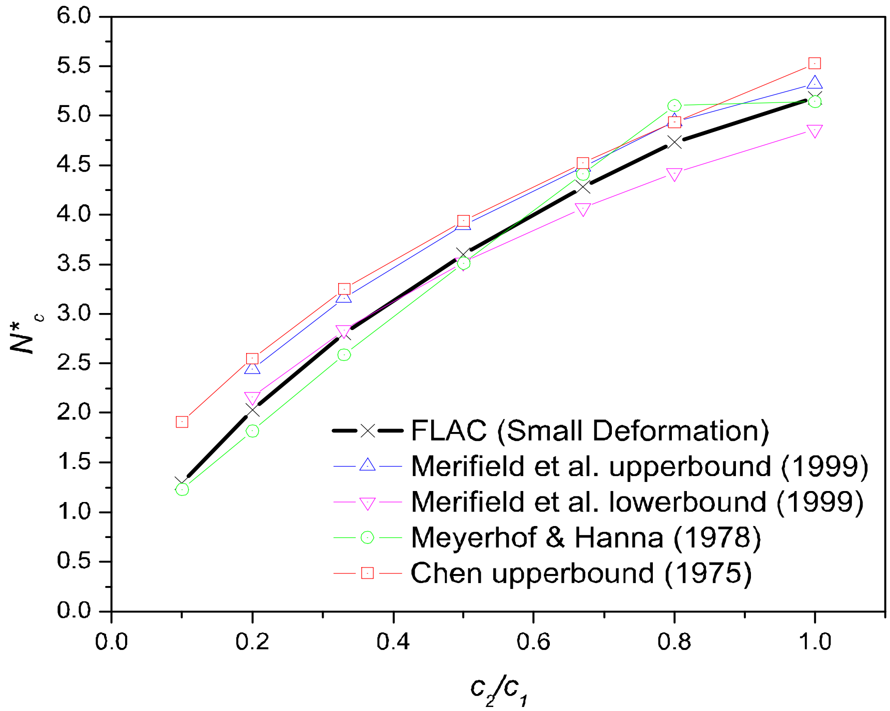

Figure 4.12: Modified bearing capacity factor (N_c^*) versus shear strength ratio (c_2/c_1) curves for rigid a smooth strip footing on strong clay over soft clay for 40×30 grid model, $H/B = 0.5$.

The normalised bearing pressure versus penetration curves for different shear strength ratios are shown in Figure 4.13.

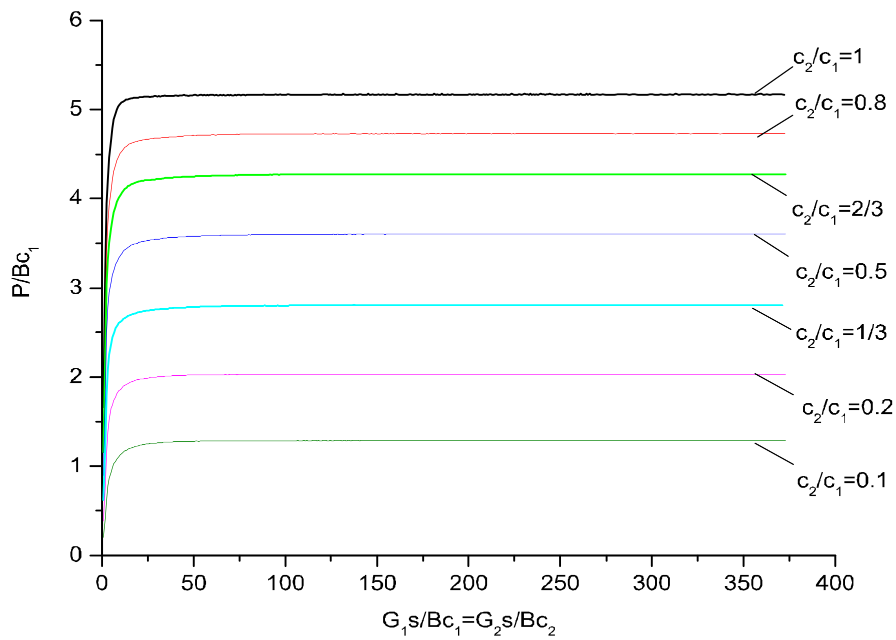

Figure 4.13: Normalised bearing pressure versus penetration curves for a rigid smooth strip footing on strong clay over soft clay for 40 × 30 grid model, $H/B = 0.5$.

Table 4.10: Failure modes for different shear strength ratios (c_2/c_1) for $H/B = 0.5$.

Shear Strength Ratio, (c_2/c_1)	Failure Modes
0.80	Local shear failure involving both top and bottom clay layers
0.67	Local shear failure involving both top and bottom clay layers
0.50	Local shear failure involving both top and bottom clay layers, increased punching in the top layer
0.33	Partial punching shear failure in the top layer, local shear in the bottom layer
0.20	Punching shear failure in the top layer, local shear in the bottom layer
0.10	Punching shear failure in the top layer, local shear in the bottom layer

Case 3: $c_2/c_1 = 2/3$ **- Small Deformation Analysis**

The velocity vectors in Figure A.94 still show local shear type failure involving both top and bottom clay layers. The partial punching shear failure is more evident in the strong top clay layer. The magnitude of the vertical velocity vector adjacent to the edge of the footing is slightly more than those at a distance from it, suggesting a smaller heave on the side of the footing.

The plasticity state indicators in Figure A.95 show that the zone of failure extends into the soft clay layer. However a very small amount of plastic yielding extends to the ground surface which again supports the local shear type failure. The depth of failure $\simeq 1.2B$, and the horizontal extent of plastic yielding is $\simeq 1.4$ m from the centre of the footing.

Figure A.97 shows the magnified grid which further supports local shear type failure of the foundation with very small heave on the edge of the footing. A soil column trapped under the footing shows both downwards vertical as well as lateral movements both in top and bottom clay layers.

Figure A.96 shows the equal vertical stress (σ_{yy}) contours and zone of influence under the strip footing. The zone of influence for this case was found to be about three and half times deeper than width of the footing. The shapes of the stress contours are fairly smooth except for some high stress contours which instead of being symmetrical about the centre of the footing are now concentrated more around the edge, supporting the partial punching in the stronger top clay layer.

The bearing pressure versus footing penetration recorded at different time steps in the history of the model is shown in Figure A.98. The ultimate bearing pressure (q_u) for this case was found to be 85.62 kPa. The modified bearing capacity factor $N_c^* = 4.28$ which is 3.04% lower than the value given by Meyerhof and Hanna (1978), and 5.61% lower than the upper bound analysis of Chen (1975), but lies within upper and lower bound values of modified bearing capacity factor given by Merifield et al. (1999) as shown in Table 4.9.

Case 4: $c_2/c_1 = 0.5$ - Small Deformation Analysis

The velocity vectors shown in Figure A.99 indicate that foundation fails in local shear type failure with partial punching shear in the strong upper layer followed by some soil flow in the softer bottom clay layer.

The plasticity state indicators in Figure A.100 show that the zone of failure extends into the soft clay layer. The depth of failure $\simeq 1.5B$, and the horizontal extent of plastic yielding is $\simeq 1.8\,\text{m}$ from the centre of the footing. The increase in the horizontal extent of the plastic yielding and its not extending to the ground surface suggests that punching has become deeper than the previous case (4.1.6) and the strong top clay crust is confining the plastic flow in soft clay.

Figure A.102 shows the magnified grid which also supports the partial punching shear failure mechanism of the foundation in the top clay layer. There is both vertical movement as well as lateral movement of the soil column trapped under the footing. There almost not soil heave near the edge of the footing now.

Figure A.101 shows the equal vertical stress (σ_{yy}) contours and zone of influence under the strip footing. The zone of influence for this case was found to be about five and half times deeper than the width of the footing. The shapes of the contours are not so regular now. The bulging of the contours at the interface of the two clay layer suggest the influence of the soft bottom clay layer. More high stress contours than that in previous case (4.1.6) are now concentrated around the edge of the footing, once again suggesting increased punching in the top clay layer.

The bearing pressure versus footing penetration recorded at different time steps in the history of the model is shown in Figure A.103. The ultimate bearing pressure (q_u) for this case was found to be 72.09 kPa. The modified bearing capacity factor $N_c^* = 3.60$ which is 2.50% higher than the value given by Meyerhof and Hanna (1978), and 9.44% lower than the upper bound analysis of Chen (1975), but lies within upper and lower bound values of modified bearing capacity factor given by Merifield et al. (1999) as shown in Table 4.9.

Case 5: $c_2/c_1 = 1/3$ - Small Deformation Analysis

The velocity vectors shown in Figure A.104 indicate a partial punching shear failure of the foundation, with punching depth extending deeper into the stronger top clay layer.

The plasticity state indicators in Figure A.105 show that the zone of failure extends into the soft clay layer. The depth of failure $\simeq 1.75B$, and the horizontal extent of plastic yielding is $\simeq 1.8\,\mathrm{m}$ from the centre of the footing. The plastic flow from the bottom clay is not reaching the ground surface, and is restricted by the strong top clay crust.

Figure A.107 shows the magnified grid which further explains partial punching shear failure of the foundation in the stronger clay layer followed by some lateral and vertical movement of the soil in the bottom clay layer. The depressed ground adjacent to the footing edge and an uplift in the ground away from the edge also supports partial punching shear failure in the top clay layer and plastic flow in the soft bottom clay layer which is now trying to lift the strong top clay up.

Figure A.106 shows the equal vertical stress (σ_{yy}) contours and zone of influence under the strip footing. The zone of influence for this case was found to be about four and half times deeper than the width of the footing. The concentration of the high stress contours around the edge of the footing also suggests the punching shear failure in the strong top clay, and the deflection of the 20 and 30 kPa contours at the interface of the two clay layers suggest the increase influence of the bottom soft clay layer.

The bearing pressure versus footing penetration recorded at different time steps in the history of the model is shown in Figure A.108. The ultimate bearing pressure (q_u) for this case was found to be 56.29 kPa. The modified bearing capacity factor $N_c^* = 2.81$ which is 7.83% higher than the value given by Meyerhof and Hanna (1978), and 15.66% lower than the upper bound analysis of Chen (1975), but agrees closely with the lower bound value of modified bearing capacity factor given by Merifield et al. (1999) as shown in Table 4.9.

Case 6: $c_2/c_1 = 0.2$ - Small Deformation Analysis

The velocity vectors shown in Figure A.109 indicate a full punching shear failure of the foundation, with the rigid column of the strong top clay layer punching deeper into the softer bottom clay layer.

The plasticity state indicators in Figure A.110 show major plastic yielding in the bottom soft clay layer with some minor yielding in the upper strong clay layer. An elastic soil column can be seen trapped under the footing, and the plastic yielding is evident underneath the footing edge again supporting the punching shear failure. The depth of failure $\simeq 1.75B$. The crust of the stronger upper clay layer restricts the upward plastic flow in the bottom layer resulting in the increase of horizontal extent of the plastic yielding. The horizontal extent of plastic yielding is $\simeq 2\,\mathrm{m}$ from the centre of the footing.

Figure A.112 shows the magnified grid which further supports the full punching shear failure of the foundation, with a column of the strong top clay layer punching deeper into the softer bottom clay layer.

Figure A.111 shows the equal vertical stress (σ_{yy}) contours and zone of influence under the strip footing. Since the failure mechanism is punching through the top layer into the bottom layer, the high stress contours are concentrated around the edge of the footing. The zone of influence for this case was found to be about three and half times deeper than the width of the footing.

The bearing pressure versus footing penetration recorded at different time steps in the history of the model is shown in Figure A.113. The ultimate bearing pressure (q_u) for this case was found to be 40.69 kPa. The modified bearing capacity factor $N_c^* = 2.03$ which is 10.34% higher than the value given by Meyerhof and Hanna (1978), and 25.62% lower than the upper bound analysis of Chen (1975), and is slightly less than the lower bound value of modified bearing capacity factor given by Merifield et al. (1999) as shown in Table 4.9.

Case 7: $c_2/c_1 = 0.1$ **- Small Deformation Analysis**

The velocity vectors shown in Figure A.114 continues to indicate a punching shear failure of the foundation, with footing punching through the stronger top clay layer followed by yielding in the softer bottom layer.

The plasticity state indicators in Figure A.115 show that the zone of failure extends into the soft clay layer. The depth of failure $\simeq 1.75B$. As in previous case (4.1.6) an elastic soil column can be seen trapped under the footing, and the plastic yielding is evident underneath the footing edge again supporting the punching shear failure. The crust of the stronger upper clay layer restricts the upward plastic flow in the bottom layer resulting in the increase of horizontal extent of the plastic yielding. The horizontal extent of plastic yielding is $\simeq 2.5$ m from the centre of the footing.

Figure A.117 shows the magnified grid which further supports the development of a punching shear failure of the foundation, with the footing punching through the stronger top clay layer followed by yielding in the softer bottom layer.

Figure A.116 shows the equal vertical stress (σ_{yy}) contours and zone of influence under the strip footing. The shapes of the stress contours are highly irregular, and the high stress contours are concentrated around the edge of the footing which supports the punching shear failure of the foundation in the top clay layer. The zone of influence for this case was found to be about two times deeper than the width of the footing.

The bearing pressure versus footing penetration recorded at different time steps in the history of the model is shown in Figure A.118. The ultimate bearing pressure (q_u) for this case was found to be 25.85 kPa. The modified bearing capacity factor $N_c^* = 1.29$ which is 4.34% higher than the value given by Meyerhof and Hanna (1978), and 48.06% lower than the upper bound analysis of Chen (1975) as shown in Table 4.9.

The normalised bearing pressure versus penetration curves for different shear strength ratios have been shown in Figure 4.13.

4.1.7 Rigid Smooth Strip Footing on Strong over Soft Clay ($H/B = 0.25$)

In this case a smooth rigid strip footing rests on the thin crust of strong clay layer lying over thicker soft clay.

Case 1: $c_2/c_1 = 1$ (Homogeneous clay) - Small Deformation Analysis

Since this is the case of homogeneous clay all the results will be same as Case 1 (Ref. 4.1.1). The FLAC analysis results for other cases of c_2/c_1 are explained below, and failure modes are summarised in Table 4.12.

Case 2: $c_2/c_1 = 0.8$ - Small Deformation Analysis

The velocity vectors shown in Figure A.119 indicate local shear type failure involving both strong top clay layer and the softer bottom clay layer with partial punching in the top clay layer.

The plasticity state indicators in Figure A.120 show that the zone of failure extends into the bottom soft clay layer. The depth of the failure is found to be $\simeq B$, , and the horizontal extent of plastic yielding is $\simeq 1.2\,\text{m}$ from the centre of the footing.

Figure A.122 shows the magnified grid which further supports the partial punching shear failure of the foundation with some soil heave at the edge of the footing. There vertical and horizontal deformation in the bottom layer is evident.

Figure A.121 shows the equal vertical stress (σ_{yy}) contours and zone of influence under the strip footing. The zone of influence for this case was found to be about four times deeper than the width of the footing. The shapes of the stress contours are fairly smooth and symmetrical about the centre of the footing except 100 kPa contour which is concentrated near the edge the footing suggesting some partial punching in the top clay layer.

The bearing pressure versus footing penetration recorded at different time steps in the history of the model is shown in Figure A.123. The ultimate bearing pressure (q_u) for this case was found to be 89.01 kPa. This decrease in the bearing capacity is due the influence of the soft bottom clay. The modified bearing capacity factor $N_c^* = 4.45$

which is 15.51% lower than the value given by Meyerhof and Hanna (1978), and 5.39% lower than the upper bound analysis of Chen (1975), but lies within upper and lower bound values of modified bearing capacity factor given by Merifield et al. (1999) as shown in Table 4.11.

Table 4.11: Comparison of modified Bearing Capacity Factor, N_c^* with existing values for rigid strip footing on strong over soft clay for grid 40×30, for $H/B = 0.25$.

Shear Strength Top Layer, (c_1)	Shear Strength Ratio, (c_2/c_1)	q_u (FLAC)	N_c^*(FLAC) = q_u(FLAC)/c_1	N_c				% Difference between N_c^*(FLAC) & N_c	
				(Merifield et al.1999)		(Meyerhof & Hanna 1978)	(Chen 1975)	(Meyerhof & Hanna 1978)	(Chen 1975)
				Lowerbound	Upperbound				
20.00	1.00	103.52	5.18	4.94	5.32	5.14	5.53	0.77	−6.76
20.00	0.80	89.01	4.45	4.10	4.60	5.14	4.69	−15.51	−5.39
20.00	0.67	77.57	3.88	3.65	4.08	4.61	4.14	−18.81	−6.70
20.00	0.50	62.13	3.11	3.01	3.34	3.42	3.40	−9.97	−9.32
20.00	0.33	45.49	2.27	2.27	3.56	2.15	2.58	5.29	−13.66
20.00	0.20	30.78	1.54	1.60	1.85	1.42	1.82	7.79	−18.18
20.00	0.10	18.09	0.90	–	–	0.87	1.34	2.89	−48.89

Figure 4.14 shows the comparison of modified bearing capacity factor (N_c^*) versus shear strength ratios computed from FLAC with those from literature.

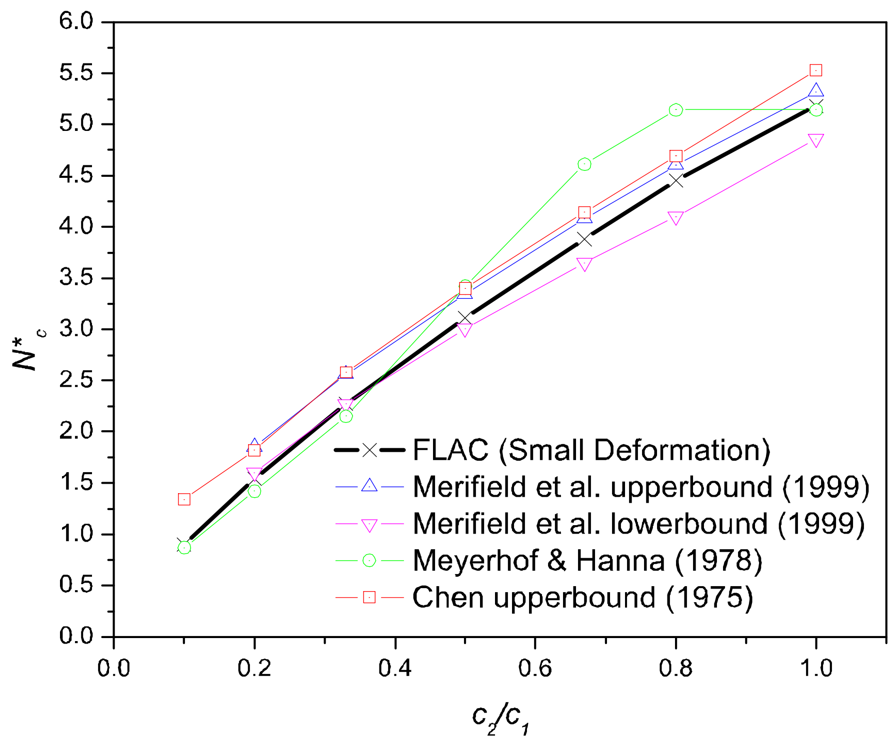

Figure 4.14: Modified bearing capacity factor (N_c^*) versus shear strength ratio (c_2/c_1) curves for a rigid smooth strip footing on strong clay over soft clay for 40×30 grid model, $H/B = 0.25$.

The normalised bearing pressure versus penetration curves for different shear strength ratios have been shown in Figure 4.15.

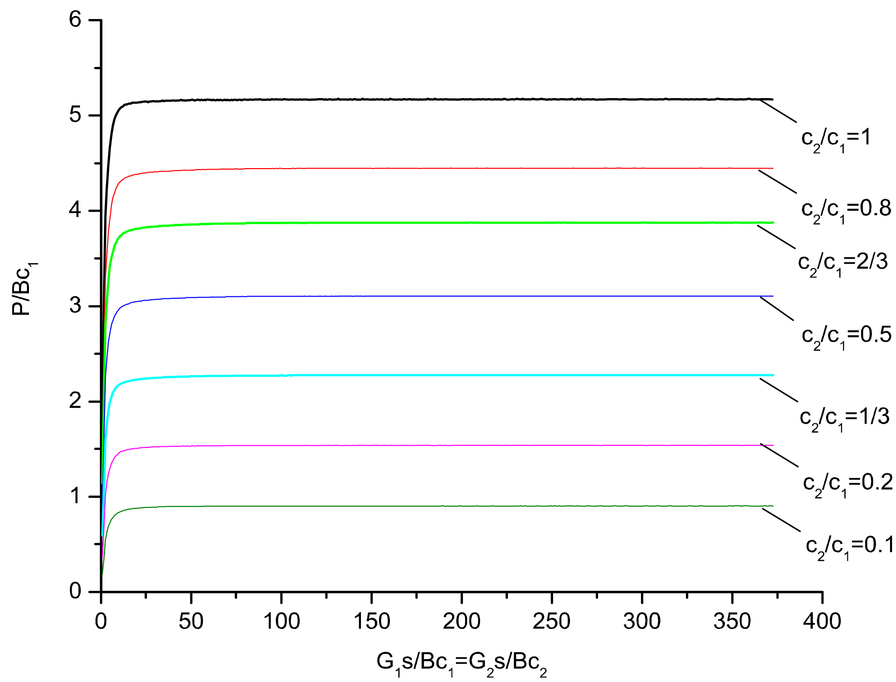

Figure 4.15: Normalised bearing pressure versus penetration curves for a rigid smooth strip footing on strong clay over soft clay for 40 × 30 grid model, $H/B = 0.25$.

Table 4.12: Failure modes for different shear strength ratios (c_2/c_1) for $H/B = 0.25$.

Shear Strength Ratio, (c_2/c_1)	Failure Modes
0.80	Local shear failure involving both top and bottom clay layers, partial punching in the top layer
0.67	Local shear failure involving both top and bottom clay layers, increased partial punching in the top layer
0.50	Punching shear failure in the top layer, local shear in the bottom layer
0.33	Punching shear failure in the top layer, local shear in the bottom layer
0.20	Punching shear failure in the top layer, local shear in the bottom layer
0.10	Punching shear failure in the top layer, local shear in the bottom layer

Case 3: $c_2/c_1 = 2/3$ - Small Deformation Analysis

The velocity vectors in Figure A.124 show a local shear type failure of the foundation with most of the velocity vectors pointing vertically downwards under the footing in the strong top layer. This is followed by plastic flow in the bottom clay layer.

The plasticity state indicators in Figure A.125 show that the zone of failure extends into the soft clay layer. The depth of failure $\simeq B$, and the horizontal extent of plastic yielding is $\simeq 1.2\,\mathrm{m}$ from the centre of the footing.

Figure A.127 shows the magnified grid which further supports the partial shear failure of the foundation with some heave on the edge of the footing. A soil column trapped under the footing shows mostly downwards vertical movements in top clay layer and both downward vertical as well as lateral movement in the bottom clay layer.

Figure A.126 shows the equal vertical stress (σ_{yy}) contours and zone of influence under the strip footing. The zone of influence for this case was found to be about four times deeper than the width of the footing. The shapes of the contours are fairly smooth and they are symmetrical about the centre of the footing except the high stress contours which are concentrated near the edge of the footing suggesting partial punching in the top clay layer.

The bearing pressure versus footing penetration recorded at different time steps in the history of the model is shown in Figure A.128. The ultimate bearing pressure (q_u) for this case was found to be 77.57 kPa. The further decrease in the bearing capacity is due to the increasing influence of the softer bottom clay layer. The modified bearing capacity factor $N_c^* = 3.88$ which is 18.81% lower than the value given by Meyerhof and Hanna (1978), and 6.70% lower than the upper bound analysis of Chen (1975) but lies within upper and lower bound values of modified bearing capacity factor given by Merifield et al. (1999) as shown in Table 4.11.

Case 4: $c_2/c_1 = 0.5$ - Small Deformation Analysis

The near vertical direction of the velocity vectors underneath the footing in the top clay layer (refer Figure A.129) now indicates that foundation failure occurs with full punching shear through the strong upper layer. This is followed by plastic flow in bottom soft layer.

The plasticity state indicators in Figure A.130 show that the zone of failure extends into the soft clay layer. The concentration of plasticity indicators underneath the edge of the footing in the strong top clay layer suggests full punching through the top clay layer. The plastic flow in the bottom soft clay layer is both vertical and horizontal but does not extend to the ground surface. The depth of failure $\simeq 1.2B$, and the horizontal extent of plastic yielding is $\simeq 1.4$ m from the centre of the footing.

The distortion of the magnified grid at the interface of the two clay layers in Figure A.132 supports the punching shear failure in the strong top clay layer. An elastic wedge of the stronger top clay can be seen trapped underneath the footing with almost no distortion in its grid. This wedge pushes into the bottom soft clay which moves vertically downwards under the footing and also away from the footing which is restricted to reach the ground by the strong top clay crust. This action in result lifts up the ground on the side of the footing.

Figure A.131 shows the equal vertical stress (σ_{yy}) contours and zone of influence under the strip footing. The zone of influence for this case was found to be about four and half times deeper than the width of the footing. The concentration of the high stress contours around the edge of the footing indicates punching shear failure in the stronger top clay. The bulging of 20 and 10 kPa contours at the interface of the two clay layers indicates the increased influence of the bottom soft clay on the bearing response of the foundation.

The bearing pressure versus footing penetration recorded at different time steps in the history of the model is shown in Figure A.133. The ultimate bearing pressure (q_u) for this case was found to be 62.13 kPa. The modified bearing capacity factor $N_c^* = 3.11$ which is 9.97% lower than the value given by Meyerhof and Hanna (1978), and 9.32% lower than the upper bound analysis of Chen (1975), but lies within upper and lower bound values of modified bearing capacity factor given by Merifield et al. (1999) as shown in Table 4.11.

Case 5: $c_2/c_1 = 1/3$ - Small Deformation Analysis

Like the previous case the downward vertical direction of the velocity vectors underneath the footing in the top clay layer (refer Figure A.134) again indicates that foundation failure occurs with full punching shear through the strong upper layer. This is followed by plastic flow in bottom soft layer.

The plasticity state indicators in Figure A.135 show that the zone of failure extends into the soft clay layer. The depth of failure $\simeq 1.2B$, and the horizontal extent of plastic yielding is $\simeq$ 1.4 m from the centre of the footing. The concentration of plasticity indicators underneath the edge of the footing in the strong top clay layer suggests full punching through the top clay layer. The plastic flow in the bottom soft clay layer is both vertical and horizontal but does not extend to the ground surface.

Figure A.137 shows the magnified grid which further explains punching shear failure of the foundation. An elastic wedge of the stronger top clay can be seen trapped underneath the footing with almost no distortion in its grid. This wedge pushes into the bottom soft clay which moves vertically downwards under the footing and also away from the footing which is restricted to reach the ground by the strong top clay crust. This action result in lifting the ground up on the side of the footing.

Figure A.136 shows the equal vertical stress (σ_{yy}) contours and zone of influence under the strip footing. The zone of influence for this case was found to be about three and half times deeper than the width of the footing. The concentration of the high stress contours around the edge of the footing supports punching shear failure in the stronger top clay. The bulging of 10 kPa contours at the interface of the footing indicates the increased influence of the bottom soft clay on the bearing response of the foundation.

The bearing pressure versus footing penetration recorded at different time steps in the history of the model is shown in Figure A.138. The ultimate bearing pressure (q_u) for this case was found to be 45.49 kPa. The modified bearing capacity factor $N_c^* = 2.27$ which is 5.29% higher than the value given by Meyerhof and Hanna (1978), and 13.66% lower than the upper bound analysis of Chen (1975), but agrees closely with the lower bound value of modified bearing capacity factor given by Merifield et al. (1999) as shown in Table 4.11.

Case 6: $c_2/c_1 = 0.2$ **- Small Deformation Analysis**

Like in the previous case the downward vertical direction of the velocity vectors underneath the footing in the top clay layer (Figure A.139) again indicates that foundation failure occurs with full punching shear through the strong upper layer. This is followed by both vertical and horizontal plastic flow in bottom soft layer.

The plasticity state indicators in Figure A.140 show that the zone of failure extends into the soft clay layer. The depth of failure $\simeq 1.5B$, and the horizontal extent of plastic yielding is $\simeq 1.6\,\mathrm{m}$ from the centre of the footing. The concentration of plasticity indicators underneath the edge of the footing in the strong top clay layer suggests full punching through the top clay layer. A void space underneath the footing showing no yielding represents the elastic column of the top strong clay trapped underneath the footing. The plastic flow in the bottom soft clay layer is both vertical and horizontal but does not extend to the ground surface.

Figure A.142 shows the magnified grid which further explains punching shear failure of the foundation through the strong clay layer. A rigid column of the stronger top clay can be seen trapped underneath the footing with almost no distortion in its grid. This column pushes into the bottom soft clay which moves vertically downwards under the footing and also away from the footing which is restricted to reach the ground by the strong top clay crust. This action result in lifting up the ground on the side of the footing.

Figure A.141 shows the equal vertical stress (σ_{yy}) contours and zone of influence under the strip footing. Since the failure mechanism is punching through the top layer into the bottom layer, the stress contour concentration is around the edge of the footing. The deflection in the shape of 10 kPa contour at the interface of the top and bottom clays shows the influence of the bottom soft clay on the bearing response of the foundation. The zone of influence for this case was found to be about two and half times deeper than the width of the footing.

The bearing pressure versus footing penetration recorded at different time steps in the history of the model is shown in Figure A.143. The ultimate bearing pressure (q_u) for this case was found to be 30.78 kPa. This decrease in the bearing capacity value also support the punching shear failure mechanism in the top clay layer with its strength not contributing much towards the bearing capacity which is now mainly governed by the shear strength of the soft bottom clay layer. The modified bearing capacity factor $N_c^* = 1.54$ which is 7.79% higher than the value given by Meyerhof and Hanna (1978), and 18.18% lower than the upper bound analysis of Chen (1975), and is slightly less than the lower bound value of modified bearing capacity factor given by Merifield et al. (1999) as shown in Table 4.11.

Case 7: $c_2/c_1 = 0.1$ - Small Deformation Analysis

In this case also the downward vertical direction of the velocity vectors underneath the footing in the top clay layer (Figure A.144) indicates that foundation failure occurs with full punching shear through the strong upper layer. This is followed by both vertical and horizontal plastic flow in bottom soft layer.

The plasticity state indicators in Figure A.145 show that the zone of failure extends into the soft clay layer. The depth of failure $\simeq 1.5B$, and the horizontal extent of plastic yielding is $\simeq$ 1.9 m from the centre of the footing. The concentration of plasticity indicators underneath the edge of the footing in the strong top clay layer suggests full punching through the top clay layer. A void space underneath the footing showing no yielding represents the elastic column of the top strong clay trapped underneath the footing which pushes into the soft clay layer. The plastic flow in the bottom soft clay layer is both vertical and horizontal but does not extend to the ground surface.

Figure A.147 shows the magnified grid which once again explains punching shear failure of the foundation through the strong clay layer. A rigid column of the stronger top clay can be seen trapped underneath the footing with no distortion in its grid. This column pushes into the bottom soft clay which moves vertically downwards under the footing and also away from the footing which is restricted to reach the ground by the strong top clay crust. This action result in uplifting the ground on the side of the footing.

Figure A.146 shows the equal vertical stress (σ_{yy}) contours and zone of influence under the strip footing. Since the failure mechanism is punching through the top layer into the bottom layer, the stress contour concentration is around the edge of the footing.

The bearing pressure versus footing penetration recorded at different time steps in the history of the model is shown in Figure A.148. The ultimate bearing pressure (q_u) for this case was found to be 18.09 kPa. This decrease in the bearing capacity value also support the punching shear failure mechanism in the top clay layer with its strength not contributing much towards the bearing capacity which is now mainly governed by the shear strength of the soft bottom clay layer. The modified bearing capacity factor $N_c^* = 0.9$ which is 2.89% higher than the value given by Meyerhof and Hanna (1978), and 48.89% lower than the upper bound analysis of Chen (1975) as shown in Table 4.11.

4.2 Strip Footing on Soft Clay Overlying Stiff Clay

This situation may occur where soft glacial lake clay overlies stiff till deposits. Plain strain analyses of a strip footing resting on the ground surface with soft clay overlying a stiff clay are described in this section. The failure mechanism in rigid strip footing on soft over strong clay system is investigated for various H/B and c_1/c_2 ratios. As it can be seen in 4.2.1 if the top strong clay layer is thick enough (i.e. $H/B > 0.5$) the failure mechanism is entirely contained in the top soft clay layer for all values of $c_1/c_2 \leq 1$, and the bearing capacity $q_u = N_c^* c_1$ where the modified bearing capacity factor $N_c^* = 5.18$. It can also be seen from 4.2.2 and 4.2.3 that for $H/B \leq 0.5$, as the H/B ratio decreases or the top soft layer becomes thinner and thinner, the bearing capacity increases as the relative strength of the bottom layer increases (Table 4.15 & 4.17). The effect of the top clay thickness (H) on the ultimate bearing capacity (q_u) of the foundation is shown in form of modified bearing capacity factor (N_c^*) in Figure 4.18.

Model Geometry

A 40×30 elements grid similar to that in 4.1 is adopted for these analyses. The model geometry is the same as shown in A.239.

4.2.1 Rigid Smooth Strip Footing on Soft over Strong Clay ($H/B = 1$)

Various undrained shear strength ratios of top layer (c_1) to bottom layer (c_2) considered are $0.1, 0.2, 1/3, 0.5, 2/3, 0.8$, and 1.

Table 4.13: Comparison of modified Bearing Capacity Factor, N_c^* with existing values for rigid strip footing on soft over strong clay for grid 40×30, for $H/B = 1$.

Shear Strength Top Layer, (c_1)	Shear Strength Ratio, (c_1/c_2)	q_u (FLAC)	N_c^*(FLAC) = q_u(FLAC)/c_1	N_c			% Difference between N_c^*(FLAC) & N_c
				(Merifield et al.1999)		(Brown & Meyerhof 1969)[5]	(Brown & Meyerhof 1969)
				Lowerbound	Upperbound		
20.00	1.00	103.56	5.18	4.94	5.32	5.14	0.77
20.00	0.80	103.54	5.18	4.94	5.30	5.14	0.77
20.00	0.67	103.54	5.18	4.94	5.30	5.14	0.77
20.00	0.50	103.53	5.18	4.94	5.30	5.14	0.77
20.00	0.33	103.54	5.18	4.94	5.30	5.14	0.77
20.00	0.20	103.55	5.18	4.94	5.30	5.14	0.77
20.00	0.10	103.56	5.18	–	–	5.14	0.77

[5] Rough footing.

Figure 4.16 shows the comparison of modified bearing capacity factor (N_c^*) versus shear strength ratios computed from FLAC with those from literature.

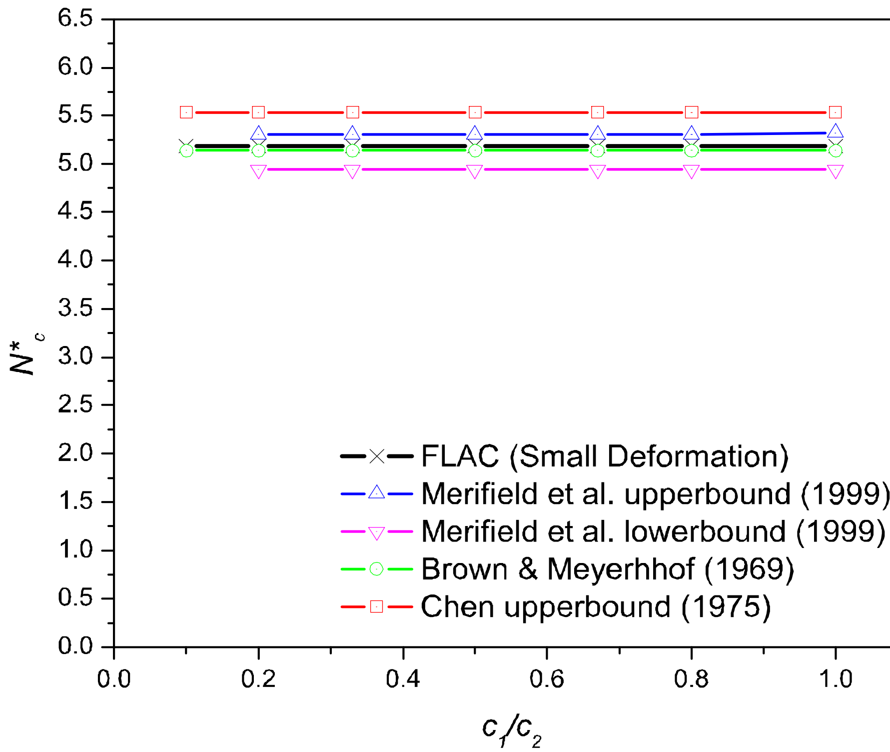

Figure 4.16: Modified bearing capacity factor (N_c^*) versus shear strength ratio (c_1/c_2) curves for a rigid smooth strip footing on soft over strong clay for 40×30 grid model, $H/B = 1$.

The normalised bearing pressure versus penetration curves for different shear strength ratios are shown in Figure 4.17.

The failure mechanisms for shear strength rations of $c_1/c_2 = 0.8, 2/3, 0.5, 1/3, 0.2$ and 0.1 are summarised in Table 4.14.

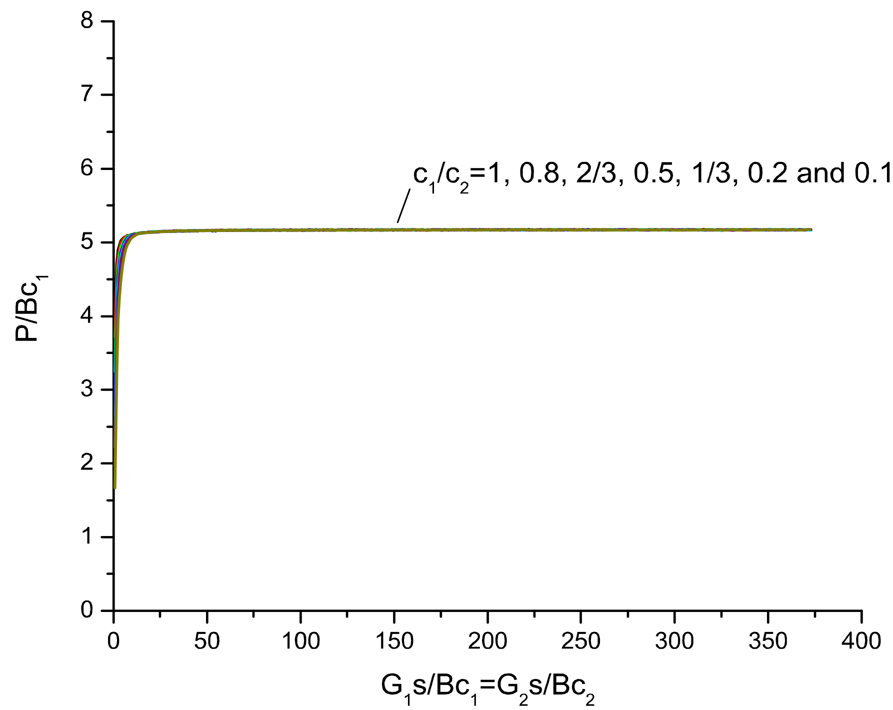

Figure 4.17: Normalised bearing pressure versus penetration curves for a rigid smooth strip footing on soft clay over strong clay for 40×30 grid model, $H/B = 1$.

Case 1: c_1/c_2 or $c_2/c_1 = 1$ (Homogeneous clay) - Small Deformation Analysis

Since this is a case of a strip footing on a homogeneous clay, the foundation behavior is the same as in Case 1 (4.1.1).

Case 2: $c_1/c_2 = 0.8$ or $c_2/c_1 = 1.25$ - Small Deformation Analysis

The velocity vectors in Figure A.149 show the plastic flow of soil. The soil underneath the footing flows away from it and indicates a general shear type failure of the foundation. The vertical direction of the vectors on the side of the footing indicates a heave in the ground.

The plasticity state indicators in Figure A.150 show the zone of failure. The

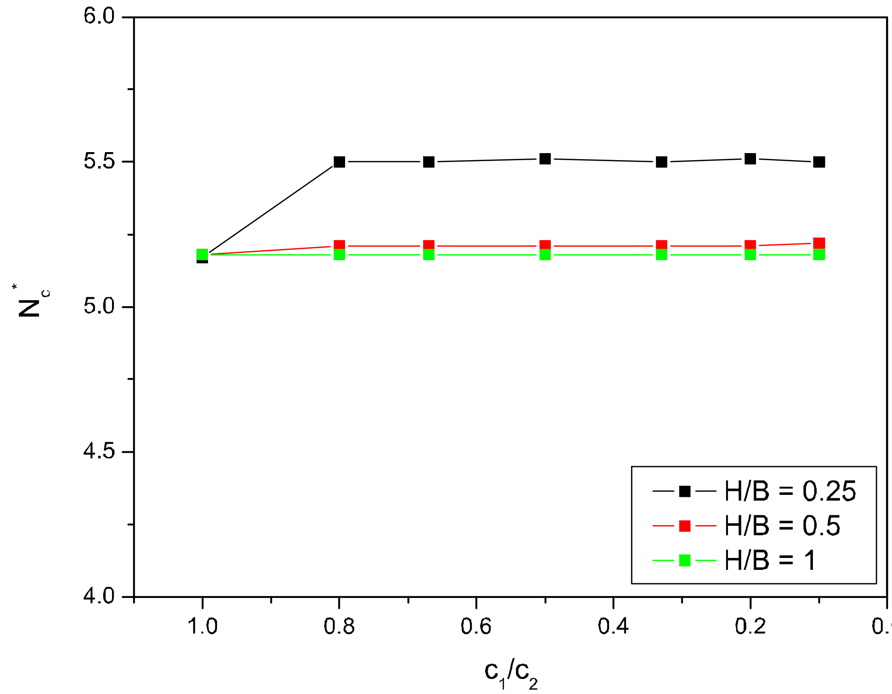

Figure 4.18: Modified bearing capacity factor (N_c^*) versus shear strength ratio (c_1/c_2) curves for a rigid smooth strip footing on soft over strong clay for 40×30 grid model, for various H/B ratios.

plastic field is developed downwards and outwards of the footing and reaches the ground surface. The depth of the failure is found to be $\simeq 0.8B$, and the horizontal extent of plastic yielding is $\simeq 1.1$ m from the centre of the footing.

Figure A.151 shows the magnified grid which further supports the general shear type failure of the foundation with soil heave on the edge of the footing. All deformation is contained in the upper clay layer.

Figure A.152 shows the equal vertical stress (σ_{yy}) contours and zone of influence under the strip footing. The zone of influence for this case was found to be $\simeq 3.5B$. The shapes of the stress contours are smooth and the contours are symmetric about the centre of the footing.

The bearing pressure versus footing penetration recorded at different time steps in

Table 4.14: Failure modes for different shear strength ratios (c_1/c_2) for $H/B = 1$.

Shear Strength Ratio, (c_1/c_2)	Failure Modes
0.80	General shear type failure
0.67	General shear type failure
0.50	General shear type failure
0.33	General shear type failure
0.20	General shear type failure
0.10	General shear type failure

the history of the model is shown in Figure A.153. The ultimate bearing pressure (q_u) for this case was found to be 103.54 kPa. The modified bearing capacity factor $N_c^* = 5.18$ from the present analysis is 0.77% higher than the value given by Brown and Meyerhof (1969), but lies within upper and lower bound values of modified bearing capacity given by Merifield et al. (1999) as shown in Table 4.13.

Case 3: $c_1/c_2 = 2/3$ **or** $c_2/c_1 = 1.5$ **- Small Deformation Analysis**

The velocity vectors in Figure A.154 again show a plastic flow which indicates a general shear type failure of the foundation.

The plasticity state indicators in Figure A.155 show that the zone of failure remains in the upper clay layer. The plastic field is developed downwards and outwards of the footing and reaches the ground surface. The depth of failure $\simeq 0.9B$, and the horizontal extent of plastic yielding is $\simeq 1.1$ m from the centre of the footing.

The magnified grid in Figure A.156 further supports the general shear type failure of the foundation with characteristic soil heave on the edge of the footing. All deformation is contained in the upper clay layer.

Figure A.157 shows the equal vertical stress (σ_{yy}) contours and zone of influence under the strip footing. The zone of influence for this case was found to be $\simeq 3.5B$. The shapes of the stress contours are smooth and the contours are symmetrical about the centre of the footing.

The bearing pressure versus footing penetration recorded at different time steps in the history of the model is shown in Figure A.158. The ultimate bearing pressure (q_u) for this case was found to be 103.54 kPa. The modified bearing capacity factor $N_c^* =$ 5.18 from the present analysis is 0.77% higher than the value given by Brown and Meyerhof (1969), but lies within upper and lower bound values of modified bearing capacity given by Merifield et al. (1999) as shown in Table 4.13.

Case 4: $c_1/c_2 = 0.5$ or $c_2/c_1 = 2$- Small Deformation Analysis

The velocity vectors shown in Figure A.19 continues to show general shear type failure of the foundation.

The plasticity state indicators in Figure A.160 show the zone of failure. The shear stress failure starts underneath the footing and spreads both downwards and away from the footing. The depth of the failure is found to be $\simeq 0.8B$, and the horizontal extent of plastic yielding is $\simeq 1.1$ m from the centre of the footing.

Figure A.161 shows the magnified grid which further supports the idea of general shear type failure of the foundation. The deformation is still contained in the upper layer there is some soil heaving at the side of the footing.

Figure A.162 shows the equal vertical stress (σ_{yy}) contours and zone of influence under the strip footing. The zone of influence for this case was found to be $\simeq 3.5B$. The shapes of the stress contours are smooth and the contours are symmetrical about the centre of the footing.

The bearing pressure versus footing penetration recorded at different time steps in the history of the model is shown in Figure A.163. The ultimate bearing pressure (q_u) for this case was found to be 103.53 kPa. The modified bearing capacity factor $N_c^* =$ 5.18 from the present analysis is 0.77% higher than the value given by Brown and Meyerhof (1969), but lies within upper and lower bound values of modified bearing capacity given by Merifield et al. (1999) as shown in Table 4.13.

Case 5: $c_1/c_2 = 1/3$ or $c_2/c_1 = 3$ - Small Deformation Analysis

The velocity vectors shown in Figure A.164 continues to show general shear type failure of the foundation.

The plasticity state indicators in Figure A.165 show the zone of failure. The shear stress of the failure of the soil starts underneath the footing and spreads downwards and away from it. The depth of the failure is found to be $\simeq 0.8B$, and the horizontal extent of plastic yielding is $\simeq 1.1\,\mathrm{m}$ from the centre of the footing.

Figure A.166 shows the magnified grid distortion in the upper softer clay layer in general shear type failure of the foundation with some soil heave at the edge of the footing.

Figure A.167 shows the equal vertical stress (σ_{yy}) contours and zone of influence under the strip footing. The zone of influence for this case was found to be $\simeq 3.5B$.

The bearing pressure versus footing penetration recorded at different time steps in the history of the model is shown in Figure A.168. The ultimate bearing pressure (q_u) for this case was found to be 103.54 kPa. The modified bearing capacity factor $N_c^* = 5.18$ from the present analysis is 0.77% higher than the value given by Brown and Meyerhof (1969), but lies within upper and lower bound values of modified bearing capacity given by Merifield et al. (1999) as shown in Table 4.13.

Case 6: $c_1/c_2 = 0.2$ or $c_2/c_1 = 5$ - Small Deformation Analysis

Figure A.169 once again shows typical plastic velocity vector flow in general shear type failure of the foundation.

The plasticity state indicators in Figure A.170 show the zone of failure with shear stress failure starting underneath the footing and then spreading downwards and away from the footing. The depth of the failure is found to be $\simeq 0.9B$, and the horizontal extent of plastic yielding is $\simeq 1.1\,\mathrm{m}$ from the centre of the footing.

Figure A.171 shows the magnified grid which further illustrates general shear type failure of the foundation with some soil heaving at the edge of the footing. The deformation is contained in the upper softer clay layer.

Figure A.172 shows the equal vertical stress (σ_{yy}) contours and zone of influence under the strip footing. The zone of influence for this case was found to be $\simeq 3.5B$.

The bearing pressure versus footing penetration recorded at different time steps in the history of the model is shown in Figure A.173. The ultimate bearing pressure (q_u)

for this case was found to be 103.55 kPa. The modified bearing capacity factor $N_c^* = 5.18$ from the present analysis is 0.77% higher than the value given by Brown and Meyerhof (1969), but lies within upper and lower bound values of modified bearing capacity given by Merifield et al. (1999) as shown in Table 4.13.

Case 7: $c_1/c_2 = 0.1$ or $c_2/c_1 = 10$ - Small Deformation Analysis

The velocity vectors shown in Figure A.174, like all cases above, continues to show general shear type failure of the foundation.

The plasticity state indicators in Figure A.165 show a typical general shear type zone of failure. The depth of the failure is found to be $\simeq 0.8B$, and the horizontal extent of plastic yielding is $\simeq 1.1$ m from the centre of the footing.

Figure A.176 shows the magnified grid which further indicates general shear type failure of the foundation with soil heave near the edge of the footing.

Figure A.177 shows the equal vertical stress (σ_{yy}) contours and zone of influence under the strip footing. The zone of influence for this case was found to be about four times deeper than the width of the footing.

The bearing pressure versus footing penetration recorded at different time steps in the history of the model is shown in Figure A.178. The ultimate bearing pressure (q_u) for this case was found to be 103.56 kPa. The modified bearing capacity factor $N_c^* = 5.18$ from the present analysis is 0.77% higher than the value given by Brown and Meyerhof (1969), but lies within upper and lower bound values of modified bearing capacity given by Merifield et al. (1999) as shown in Table 4.13.

4.2.1 was considered as the base case for studying the effect of the thickness of the soft top clay layer. Since the results of all cases above show that the bearing capacity of all c_1/c_2 ratios remains the same for $H/B = 1$, it is expected that it will remain unchanged for all $H/B \geq 1$ The thickness is then decreased as $H < B$ ($H/B = 0.5$ & 0.25).

4.2.2 Rigid Smooth Strip Footing on Soft over Strong Clay ($H/B = 0.5$)

Case 1: c_1/c_2 or $c_2/c_1 = 1$ (Homogeneous clay) - Small Deformation Analysis

Since this is the case of homogeneous clay all the results will be same as Case 1 (4.2.1). The FLAC analysis results for other cases of c_1/c_2 are explained below.

Case 2: $c_1/c_2 = 0.8$ or $c_2/c_1 = 1.25$ - Small Deformation Analysis

The velocity vectors shown in Figure A.179 show plastic flow of the soil underneath the footing moving downwards and away from the footing some what resembling to the general shear type failure of the foundation. It can be noticed that the velocity vectors tend to straighten out near the interface of softer upper and stronger bottom clays.

The plasticity state indicators in Figure A.180 show the zone of failure extends to near the top of strong clay layer. The shear stress failure of the upper softer clay starts underneath the footing and spreads downwards as well as away from the footing. The depth of failure is found to be $\simeq 0.45B$, and the horizontal extent of plastic yielding is $\simeq 0.9\,\mathrm{m}$ from the centre of the footing.

Figure A.181 shows the magnified grid which further indicates general shear type failure of the foundation with some heave at the edge of the footing. The deformation in the upper soft clay is to the top of the lower strong clay layer and shows that the contribution of the strength of the bottom strong clay is increasing the bearing capacity of the foundation.

Figure A.182 shows the equal vertical stress (σ_{yy}) contours and zone of influence under the strip footing. The zone of influence for this case was found to be $\simeq 3.5B$.

The bearing pressure versus footing penetration recorded at different time steps in the history of the model is shown in Figure A.183. The ultimate bearing pressure (q_u) for this case was found to be 104.13 kPa. The modified bearing capacity factor $N_c^* = 5.21$ which is 0.77% lower than the value given by Brown and Meyerhof (1969), but lies within upper and lower bound values of modified bearing capacity given by

Merifield et al. (1999) as shown in Table A.3.

Table 4.15: Comparison of modified Bearing Capacity Factor, N_c^* with existing values for rigid strip footing on soft clay over strong clay for grid 40×30, for $H/B = 0.5$.

Shear Strength Top Layer, (c_1)	Shear Strength Ratio, (c_1/c_2)	q_u (FLAC)	N_c^*(FLAC) = q_u(FLAC)/c_1	N_c (Merifield et al.1999) Lowerbound	N_c (Merifield et al.1999) Upperbound	N_c (Brown & Meyerhof 1969)[6]	% Difference between N_c^*(FLAC) & N_c (Brown & Meyerhof 1969)
20.00	1.00	103.56	5.18	4.86	5.32	5.14	0.77
20.00	0.80	104.13	5.21	4.86	5.31	5.25	−0.77
20.00	0.67	104.15	5.21	4.86	5.31	5.33	−2.30
20.00	0.50	104.20	5.21	4.86	5.31	5.43	−4.22
20.00	0.33	104.18	5.21	4.86	5.31	–	–
20.00	0.20	104.24	5.21	4.86	5.31	–	–
20.00	0.10	104.33	5.22	–	–	–	–

[6]Rough footing.

Figure 4.19 shows the comparison of modified bearing capacity factor (N_c^*) versus shear strength ratios computed from FLAC with those from literature.

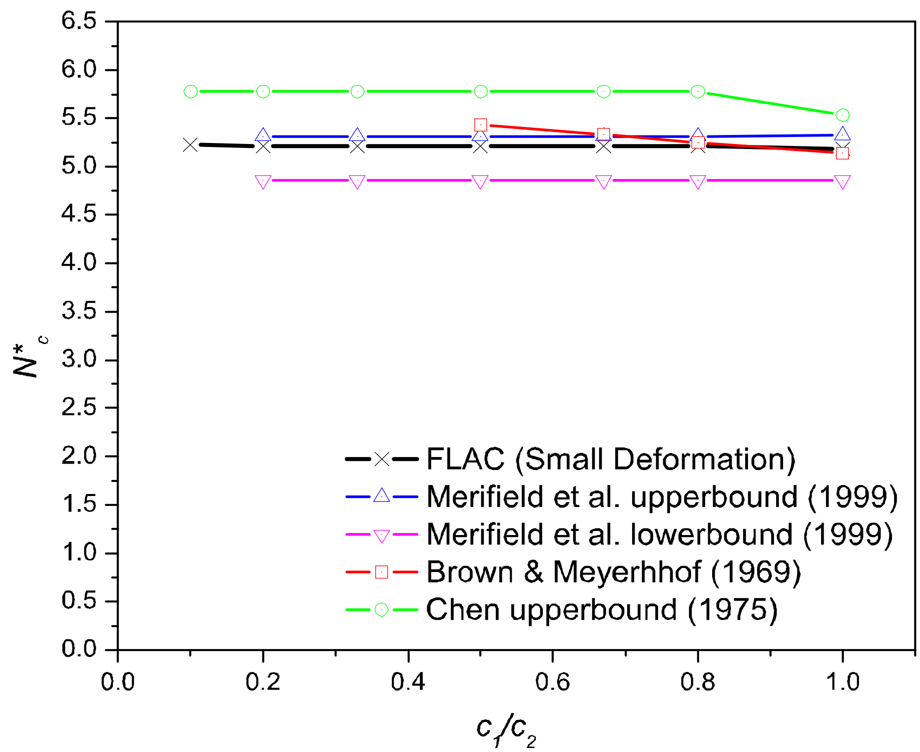

Figure 4.19: Modified bearing capacity factor (N_c^*) versus shear strength ratio (c_1/c_2) curves for a rigid smooth strip footing on soft clay over strong clay for 40×30 grid model, $H/B = 0.5$.

The normalised bearing pressure versus penetration curves for different shear strength ratios are shown in Figure 4.20.

The failure mechanisms for shear strength rations of $c_1/c_2 = 0.8, 2/3, 0.5, 1/3, 0.2$ and 0.1 are summarised in Table 4.16.

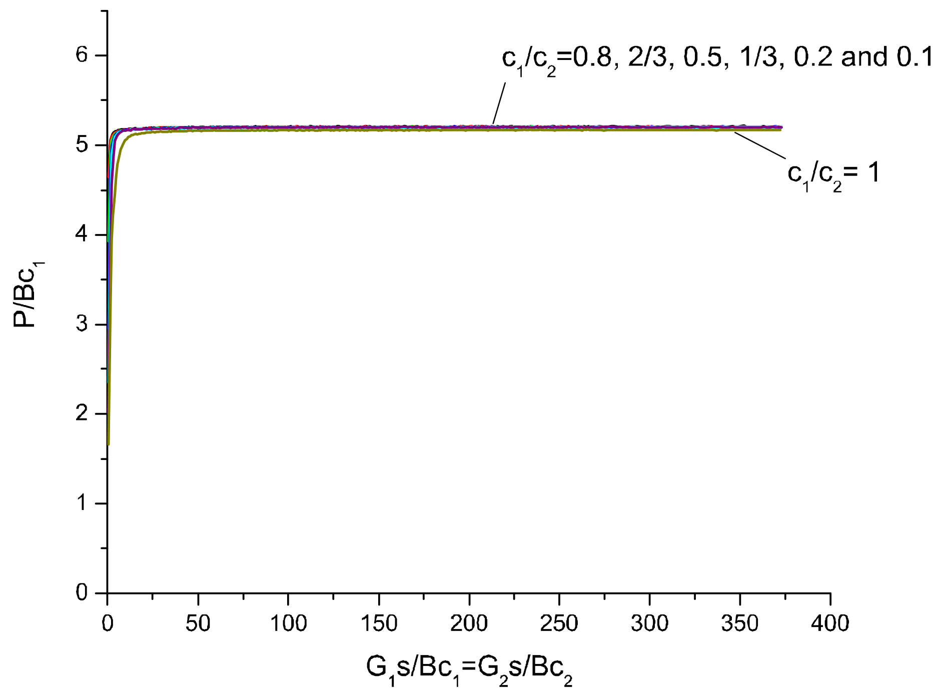

Figure 4.20: Normalised bearing pressure versus penetration curves for a rigid smooth strip footing on soft clay over strong clay for 40 × 30 grid model, $H/B = 0.5$.

Case 3: $c_1/c_2 = 2/3$ **or** $c_2/c_1 = 1.5$ **- Small Deformation Analysis**

Figure A.184 again shows general shear type failure of the foundation with plastic flow downwards and away from the footing in the upper soft clay layer. The velocity vectors straightens out as it approaches the junction of the top and bottom clay layers.

The plasticity state indicators in Figure A.185 show the zone of failure starting to extend close to bottom strong clay layer. The shear stress failure of the softer upper clay starts underneath the footing and spreads downwards and away from the footing. The depth of the failure is found to be $\simeq 0.45B$, and the horizontal extent of plastic yielding is $\simeq 0.9\,\mathrm{m}$ from the centre of the footing.

Figure A.186 shows the magnified grid which also shows general shear type failure of the foundation with some soil heaving at the edge of the footing. The deformation

Table 4.16: Failure modes for different shear strength ratios (c_1/c_2) for $H/B = 0.5$.

Shear Strength Ratio, (c_1/c_2)	Failure Modes
0.80	General shear type failure
0.67	General shear type failure
0.50	General shear type failure
0.33	General shear type failure
0.20	General shear type failure
0.10	General shear type failure

in the upper soft clay extends down to the top of the lower strong clay layer and indicates the contribution of the strength of the bottom strong clay in increasing the bearing capacity of the foundation.

Figure A.187 shows the equal vertical stress (σ_{yy}) contours and zone of influence under the strip footing. The zone of influence for this case was found to be $\simeq 3.7B$.

The bearing pressure versus footing penetration recorded at different time steps in the history of the model is shown in Figure A.188. The ultimate bearing pressure (q_u) for this case was found to be 104.15 kPa. The modified bearing capacity factor $N_c^* = 5.21$ which is 2.30% lower than the value given by Brown and Meyerhof (1969), but lies within upper and lower bound values of modified bearing capacity given by Merifield et al. (1999) as shown in Table 4.15.

Case 4: $c_1/c_2 = 0.5$ or $c_2/c_1 = 2$ - Small Deformation Analysis

The velocity vectors shown in Figure A.189 continues to indicate general shear type failure of the foundation with plastic flow in the upper soft clay layer very similar to the previous two cases.

The plasticity state indicators in Figure A.190 show the zone of failure extends deep in the soft clay layer. The depth of failure $\simeq 0.5B$, and the horizontal extent of plastic yielding is $\simeq 0.9$ m from the centre of the footing.

Figure A.191 shows the magnified grid which also shows general shear type failure of the foundation with some soil heaving at the edge of the footing. The deformation in the upper soft clay extends down to the top of the lower strong clay layer and shows that the contribution of the strength of the bottom strong clay in increasing the bearing capacity of the foundation.

Figure A.192 shows the equal vertical stress (σ_{yy}) contours and zone of influence under the strip footing. The zone of influence for this case was found to be $\simeq 3.75B$. The shapes of the stress contours are smooth and they are symmetrical about the centre of the footing.

The bearing pressure versus footing penetration recorded at different time steps in the history of the model is shown in Figure A.193. The ultimate bearing pressure (q_u) for this case was found to be 104.20 kPa. The modified bearing capacity factor $N_c^* =$ 5.21 which lies within upper and lower bound values of modified bearing capacity given by Merifield et al. (1999), but is 4.22% lower than the value given by Brown and Meyerhof (1969)as shown in Table 4.15.

Case 5: $c_1/c_2 = 1/3$ or $c_2/c_1 = 3$ - Small Deformation Analysis

The velocity vectors shown in Figure A.194 again shows general shear failure of the foundation with a plastic flow in the upper soft clay layer similar to the previous cases.

The plasticity state indicators in Figure A.195 show the zone of failure extends on top of strong clay layer. The depth of failure $\simeq 0.5B$ and the horizontal extent of plastic yielding is $\simeq 0.9$ m from the centre of the footing.

Figure A.196 shows the magnified grid which also shows general shear type failure of the foundation with some soil heaving at the edge of the footing. The grid deformation in the upper soft clay extends down to the top of the lower strong clay layer and hints the contribution of the strength of the bottom strong clay in increasing the bearing capacity of the foundation.

Figure A.197 shows the equal vertical stress (σ_{yy}) contours and zone of influence under the strip footing. The zone of influence for this case was found to be $\simeq 3.7B$.

The bearing pressure versus footing penetration recorded at different time steps in the history of the model is shown in Figure A.198. The ultimate bearing pressure (q_u)

for this case was found to be 104.18 kPa. The modified bearing capacity factor $N_c^* = 5.21$ which lies within upper and lower bound values of modified bearing capacity given by Merifield et al. (1999) as shown in Table 4.15.

Case 6: $c_1/c_2 = 0.2$ or $c_2/c_1 = 5$ - Small Deformation Analysis

The velocity vectors shown in Figure A.199 also show general shear type failure of the foundation with similar plastic flow pattern in the upper soft clay layer as in the previous cases.

The plasticity state indicators in Figure A.200 show the zone of failure extends on top of strong clay layer. The depth of failure $\simeq 0.5B$ and the horizontal extent of plastic yielding is $\simeq 0.9$ m from the centre of the footing.

Figure A.201 shows the magnified grid which further indicates the idea of a general shear type failure of the foundation.

Figure A.202 shows the equal vertical stress (σ_{yy}) contours and zone of influence under the strip footing. The zone of influence for this case was found to be $\simeq 3.7B$. The shapes of the contours are smooth and they are symmetrical about the centre of the footing.

The bearing pressure versus footing penetration recorded at different time steps in the history of the model is shown in Figure A.203. The ultimate bearing pressure (q_u) for this case was found to be 104.24 kPa. The modified bearing capacity factor $N_c^* = 5.21$ which lies within upper and lower bound values of modified bearing capacity given by Merifield et al. (1999) as shown in Table 4.15.

Case 7: $c_1/c_2 = 0.1$ or $c_2/c_1 = 10$ - Small Deformation Analysis

The velocity vectors shown in Figure A.114 continues to indicate general shear failure of the foundation with plastic flow of softer clay downwards and away from the footing in the upper soft clay layer.

The plasticity state indicators in Figure A.205 show the zone of failure extends to the top of strong clay layer. The depth of failure $\simeq 0.45B$, and the horizontal extent of plastic yielding is $\simeq 0.9$ m from the centre of the footing.

Figure A.206 shows the magnified grid which further indicates local shear failure of the foundation with some plastic flow in the upper soft clay layer. There is some soil heave near the edge of the footing.

Figure A.207 shows the equal vertical stress (σ_{yy}) contours and zone of influence under the strip footing. The zone of influence for this case was found to be about four times deeper than the width of the footing. The shapes of the contours are smooth and they are symmetrical about the centre of the footing.

The bearing pressure versus footing penetration recorded at different time steps in the history of the model is shown in Figure A.208. The ultimate bearing pressure (q_u) for this case was found to be 104.33 kPa. The modified bearing capacity factor $N_c^* = 5.22$ which lies within upper and lower bound values of modified bearing capacity given by Merifield et al. (1999) as shown in Table 4.15.

4.2.3 Rigid Smooth Strip Footing on Soft over Strong Clay ($H/B = 0.25$)

Case 1: c_1/c_2 or $c_2/c_1 = 1$ (Homogeneous clay) - Small Deformation Analysis

Since this is the case of homogeneous clay all the results will be same as Case 1 (4.2.1). The FLAC analysis results for other cases of c_2/c_1 are explained below.

Case 2: $c_1/c_2 = 0.8$ or $c_2/c_1 = 1.25$ - Small Deformation Analysis

The velocity vectors shown in Figure A.209 show a shear failure of the foundation with soft clay between the footing and the bottom stiff clay squeezing out laterally. There is also some lateral plastic flow of stronger bottom soil.

The plasticity state indicators in Figure A.210 show the zone of failure extends into the bottom strong clay layer. The depth of the failure is found to be $\simeq 0.4B$ and the horizontal extent of plastic yielding is $\simeq 0.75\,\text{m}$ from the centre of the footing. Figure A.212 shows the equal vertical stress (σ_{yy}) contours and zone of influence under the strip footing. The zone of influence for this case was found to be $\simeq 2.75$.

Figure A.211 shows the magnified grid which further indicates a shear failure of the foundation and lateral squeezing of soft clay under the footing. The squeezed out softer clay also can be seen to cause a soil heave on the side of the footing. The deformation of the grid extends into the stronger bottom clay layer.

Figure A.217 shows the equal vertical stress (σ_{yy}) contours and zone of influence under the strip footing. The zone of influence for this case was found to be about four times deeper than the width of the footing.

The bearing pressure versus footing penetration recorded at different time steps in the history of the model is shown in Figure A.213. The ultimate bearing pressure (q_u) for this case was found to be 110.07 kPa. The modified bearing capacity factor $N_c^* = 5.50$ which is 0.18% lower than the value given by Brown and Meyerhof (1969), but is 0.54% higher than the upper bound values of modified bearing capacity given by Merifield et al. (1999) as shown in Table 4.17.

Table 4.17: Comparison of modified Bearing Capacity Factor, N_c^* with existing values for rigid strip footing on soft over strong clay for grid 40×30, for $H/B = 0.25$.

Shear Strength Top Layer, (c_1)	Shear Strength Ratio, (c_1/c_2)	q_u (FLAC)	N_c^*(FLAC) = q_u(FLAC)/c_1	N_c (Merifield et al.1999) Lowerbound	N_c (Merifield et al.1999) Upperbound	N_c (Brown & Meyerhof 1969)[7]	% Difference between N_c^*(FLAC) & N_c (Brown & Meyerhof 1969)
20.00	1.00	103.56	5.18	4.86	5.32	5.14	0.77
20.00	0.80	110.07	5.50	5.11	5.48	5.52	−0.18
20.00	0.67	110.30	5.52	5.11	5.48	5.81	−5.25
20.00	0.50	110.37	5.52	5.11	5.49	6.00	−8.70
20.00	0.33	110.42	5.52	5.11	5.49	–	–
20.00	0.20	110.53	5.53	5.11	5.49	–	–
20.00	0.10	110.76	5.54	–	–	–	–

[7] Rough footing.

Figure 4.21 shows the comparison of modified bearing capacity factor (N_c^*) versus shear strength ratios computed from FLAC with those from literature.

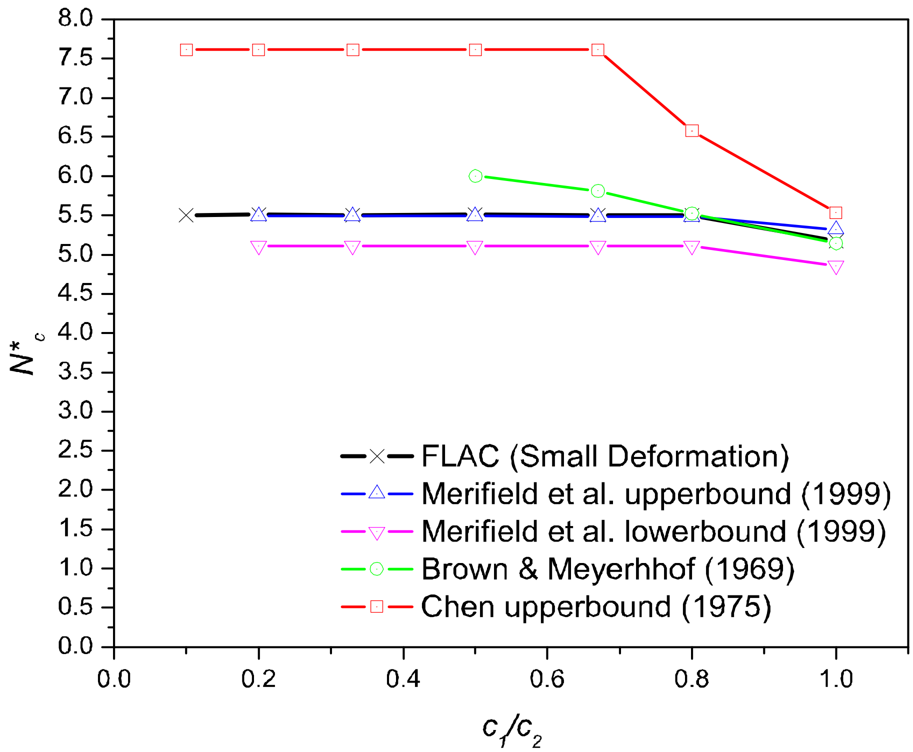

Figure 4.21: Modified bearing capacity factor (N_c^*) versus shear strength ratio (c_1/c_2) curves for a rigid smooth strip footing on soft clay over strong clay for 40×30 grid model, $H/B = 0.25$.

The normalised bearing pressure versus penetration curves for different shear strength ratios are shown in Figure 4.22.

The failure mechanisms for shear strength rations of $c_1/c_2 = 0.8, 2/3, 0.5, 1/3, 0.2$ and 0.1 are summarised in Table 4.18.

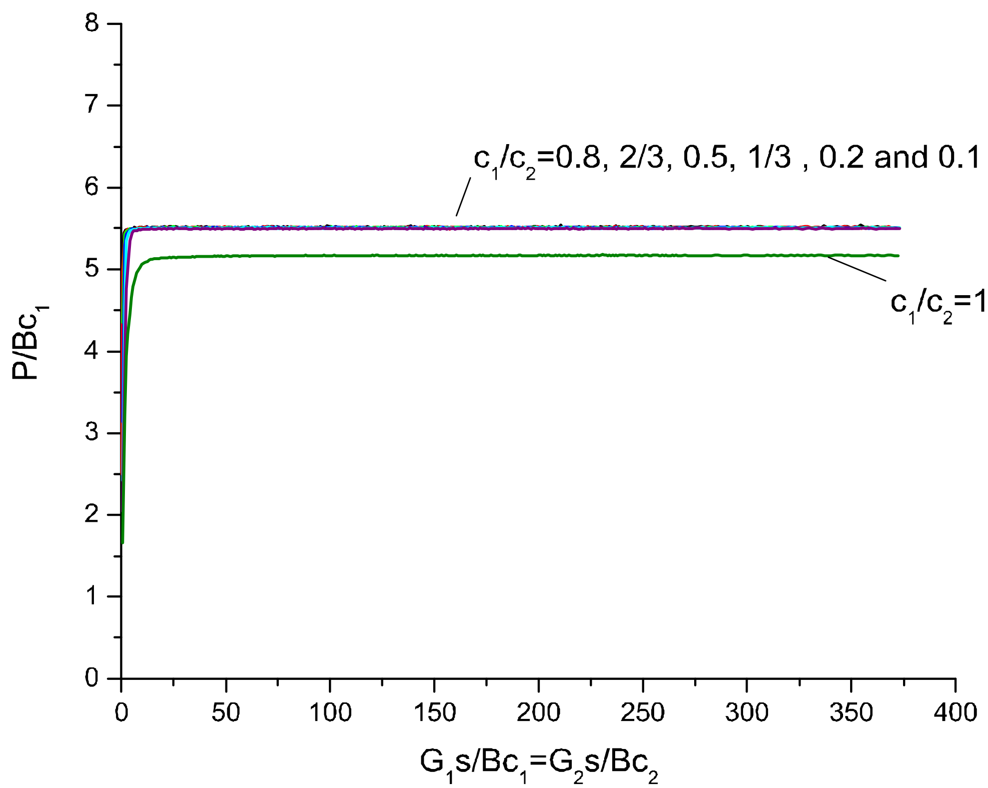

Figure 4.22: Normalised bearing pressure versus penetration curves for a rigid smooth strip footing on soft clay over strong clay for 40 × 30 grid model, $H/B = 0.25$.

Case 3: $c_1/c_2 = 2/3$ **or** $c_2/c_1 = 1.5$ **- Small Deformation Analysis**

The velocity vectors in Figure A.214 show a shear failure of the foundation with soft clay between the footing and the bottom stiff clay squeezing out laterally. Unlike the previous case the plastic flow is confined to the upper softer clay layer.

The plasticity state indicators in Figure A.215 show that the zone of failure extends deep on the top of lower stronger clay layer. The yielding in shear starts underneath the footing and spreads downwards and away. The depth of the failure is found to be $\simeq 0.25B$ and the horizontal extent of plastic yielding $\simeq 0.7\,\mathrm{m}$ from the centre of the footing.

Table 4.18: Failure modes for different shear strength ratios (c_1/c_2) for $H/B = 0.25$.

Shear Strength Ratio, (c_1/c_2)	Failure Modes
0.80	A shear failure with squeezing out of softer clay and some stronger clay
0.67	A shear failure with squeezing out of softer clay
0.50	A shear failure with squeezing out of softer clay
0.33	A shear failure with squeezing out of softer clay
0.20	A shear failure with squeezing out of softer clay
0.10	A shear failure with squeezing out of softer clay

Figure A.216 shows the magnified grid which further indicates a shear failure of the foundation with lateral squeezing of soft clay under the footing.

Figure A.217 shows the equal vertical stress (σ_{yy}) contours and zone of influence under the strip footing. The zone of influence for this case was found to be $\simeq 3B$.

The bearing pressure versus footing penetration recorded at different time steps in the history of the model is shown in Figure A.218. The ultimate bearing pressure (q_u) for this case was found to be 110.30 kPa. The modified bearing capacity factor $N_c^* = 5.52$ which is 5.25% lower than the value given by Brown and Meyerhof (1969) and is 0.72% higher than upper bound values of modified bearing capacity given by Merifield et al. (1999) as shown in Table 4.17.

Case 4: $c_1/c_2 = 0.5$ or $c_2/c_1 = 2$ - Small Deformation Analysis

The plastic flow velocity vectors shown in Figure A.219 once again suggests a shear failure of the foundation with soft clay between the footing and the bottom stiff clay squeezing out.

The plasticity state indicators in Figure A.220 show that the zone of failure extends deep into the soft clay layer. The yielding in shear starts underneath the footing and spreads away from it. The depth of failure $\simeq 0.25B$, and the horizontal extent of plastic yielding $\simeq 0.7$ m from the centre of the footing.

Figure A.221 shows the magnified grid which further indicates the idea of a lateral squeezing of soft clay under the footing. The squeezed out clay causes a heave on the side of the footing.

Figure A.222 shows the equal vertical stress (σ_{yy}) contours and zone of influence under the strip footing. The zone of influence for this case was found to be $\simeq 3B$.

The bearing pressure versus footing penetration recorded at different time steps in the history of the model is shown in Figure A.223. The ultimate bearing pressure (q_u) for this case was found to be 110.37 kPa. The modified bearing capacity factor $N_c^* = 5.52$ which is 8.70% lower than the value given by Brown and Meyerhof (1969), and is 0.54% higher than upper bound values of modified bearing capacity given by Merifield et al. (1999) as shown in Table 4.17.

Case 5: $c_1/c_2 = 1/3$ or $c_2/c_1 = 3$ - Small Deformation Analysis

The velocity vectors shown in Figure A.224 continues to indicate a shear failure of the foundation with soft clay between the footing and the bottom stiff clay is being squeezed out laterally.

The plasticity state indicators in Figure A.225 show that the zone of failure extends deep into the soft clay layer. The depth of failure $\simeq 0.25B$ and the horizontal extent of plastic yielding $\simeq 0.7$ m from the centre of the footing.

Figure A.226 shows the magnified grid which further indicates lateral squeezing of soft clay under the footing.

Figure A.227 shows the equal vertical stress (σ_{yy}) contours and zone of influence under the strip footing. The zone of influence for this case was found to be $\simeq 3B$.

The bearing pressure versus footing penetration recorded at different time steps in the history of the model is shown in Figure A.228. The ultimate bearing pressure (q_u) for this case was found to be 110.42 kPa. The modified bearing capacity factor $N_c^* = 5.52$ is 0.72% higher than upper bound values of modified bearing capacity given by Merifield et al. (1999) as shown in Table 4.17.

Case 6: $c_1/c_2 = 0.2$ or $c_2/c_1 = 5$ - Small Deformation Analysis

The velocity vectors shown in Figure A.229 once again show a shear failure of the foundation with soft clay between the footing and the bottom stiff clay is being squeezed out laterally.

The plasticity state indicators in Figure A.230 show that the zone of failure extends deep into the soft clay layer just above the top of lower strong clay layer. The depth of failure $\simeq 0.25B$ and the horizontal extent of plastic yielding $\simeq 0.7\,\text{m}$ from the centre of the footing.

Figure A.231 shows the magnified grid which further indicates a local shear failure of the foundation with soft clay between the footing and the bottom stiff clay being squeezed out laterally. There is some soil heave near the edge of the footing.

Figure A.232 shows the equal vertical stress (σ_{yy}) contours and zone of influence under the strip footing. The zone of influence for this case was found to be $\simeq 3.25B$.

The bearing pressure versus footing penetration recorded at different time steps in the history of the model is shown in Figure A.233. The ultimate bearing pressure (q_u) for this case was found to be 110.53 kPa. The modified bearing capacity factor $N_c^* = 5.53$ is 0.72% higher than upper bound values of modified bearing capacity given by Merifield et al. (1999) as shown in Table 4.17.

Case 7: $c_1/c_2 = 0.1$ or $c_2/c_1 = 10$ - Small Deformation Analysis

The velocity vectors shown in Figure A.234 continues to indicate a shear failure of the foundation with soft clay between the footing and the bottom stiff clay being squeezed out laterally.

The plasticity state indicators in Figure A.235 show that the zone of failure extends deep into the soft clay layer. The depth of failure $\simeq 2B$. The depth of failure $\simeq 0.25B$ and the horizontal extent of plastic yielding is $\simeq 0.75\,\text{m}$ from the centre of the footing.

Figure A.236 shows the magnified grid which further indicates a shear failure of the foundation with soft clay between the footing and the bottom stiff clay is being squeezed out laterally and then heaving near the edge of the footing.

Figure A.237 shows the equal vertical stress (σ_{yy}) contours and zone of influence under the strip footing. The zone of influence for this case was found to be about four times deeper than the width of the footing.

The bearing pressure versus footing penetration recorded at different time steps in the history of the model is shown in Figure A.238. The ultimate bearing pressure (q_u) for this case was found to be 110.76 kPa. The modified bearing capacity factor $N_c^* = 5.54$ as shown in Table 4.17.

4.3 Circular Footing on Stiff Clay Overlying Soft Clay

The axisymmetric analyses of a rigid smooth circular footing resting on the ground surface of stiff clay overlying a soft clay are investigated in this section. The bearing capacity and the failure mechanism for a rigid circular footing on a strong over soft clay system depends on the ratio of the depth of upper clay layer (H) to the diameter of the footing (D), and the ratios (c_2/c_1) of the undrained shear strengths of the upper and lower clay layers. The H/D ratios considered in this study are $0.25, 0.5, 1, 1.5$ and 2. The undrained shear strength ratios of the bottom layer (c_2) to top layer (c_1) considered are $0.1, 0.2, 1/3, 0.5, 2/3, 0.8$, and 1.

As in 4.1 the failure mechanisms here also are described by grid point velocity vectors and the extent of the steady-state plastic flow is represented by plasticity state indicators. The change in the nature and extent of the plastic flow helps in explaining the variation in the bearing capacity of the two layer clay foundation system for different H/D and c_2/c_1 ratios. The foundation deformation is also described with the help of magnified deformed grid.

It is observed that if the top strong clay layer is deep enough (i.e. $H \geq 2D$) the failure mechanism is entirely contained in the top strong clay layer for all values of the c_2/c_1 ratio. This depth is greater than Brown and Meyerhof (1969) who suggested the value of this ratio as $H/D = 1.5$. For all other values of $H/D < 2$, depending upon the H/D and c_2/c_1 ratios, the failure mechanism generally occurs in general shear, partial punching shear or full punching shear through the top layer followed by yielding of the bottom soft clay layer. For $H/D \leq 0.25$, full punching of the footing through the top strong clay layer occurs when the strength of the top layer is significantly greater than that of the bottom soft layer. Since FLAC does not allow the separation or slip between two elements at the attached grid points, the extent of punching has only been interpreted based on velocity vector diagrams, plasticity state indicators and to some extent by the magnified grid plots as explained below for various cases.

As it can be seen in Table 4.23 and 4.26, the bearing capacity values for all $c_2/c_1 < 1$ and $H/D \geq 2$ remain equal to the bearing capacity for homogeneous case

($c_2/c_1 = 1$), and less than that of homogeneous case for $H/D \leq 0.25$ respectively. The effect of the top clay thickness (H) on the ultimate bearing capacity (q_u) of the foundation is shown in form of modified bearing capacity factor (N_c^*) in Figure 4.25.

4.3.1 Rigid Smooth Circular Footing on Strong over Soft Clay ($H/D = 1$)

The undrained shear strength ratios of the bottom layer (c_2) to top layer (c_1) considered are $0.1, 0.2, 1/3, 0.5, 2/3, 0.8$, and 1.

Case 1: $c_2/c_1 = 1$ (Homogeneous clay) - Small Deformation Analysis

The velocity vectors shown in Figure A.241 with the plastic flow of soil underneath the footing away from the footing indicate general shear type failure of the foundation. The vertical direction of the vectors on the side of the footing indicates a heave in the ground.

The plasticity state indicators in Figure A.242 show that the shear failure of the soil starts underneath the footing and spreads downwards as well as away from the footing which is a typical indication of general shear type failure. The zone of failure lies within a depth which is less than the diameter of the footing (D). The depth of failure is $0.4D$, and the horizontal extent of plastic yielding is $\simeq 0.7$ m from the centre of the footing.

Figure A.243 shows the magnified grid[8] which supports the general shear type failure of the foundation with soil heaving at the edge of the footing.

Figure A.244 shows the equal vertical stress (σ_{yy}) contours and zone of influence under the strip footing. The zone of influence for this case was found to be $\simeq 1.4D$. It may be noticed that the stress bulbs in the case of circular footing are not as smooth as in the case of strip footing (refer 4.1). This is probably due to some numerical noise. Other reason could be the way FLAC plots stress contours through the centre

[8]It should be noted here that this is a small deformation analysis i. e. the coordinates of the grid points are not updated with the footing settlement. The grid magnification shows only an estimation of the foundation soil deformation at the end of analysis.

of a zone and not at the grid points. This can be also be noticed from the A.244 that the contours do not extend to the grid points at the boundary and terminates at the centre of the boundary zones. One way of extending the contours to the boundary is by extrapolation, which is explained in the FLAC manual (Itasca Consulting Group, Inc. 2002c). The results of least-squares fit extrapolation are shown in Case 7 (4.3.2).

The bearing pressure versus footing penetration recorded at different time steps in the history of the model is shown in Figure A.245. The ultimate bearing pressure (q_u) for this case was found to be 112.20 kPa. The modified bearing capacity factor $N_c^* = 5.61$ from the present analysis agrees with the value given by Wang and Carter (2001), but is slightly lower (1.34%) than the bearing capacity factor for a rough circular footing given by Brown and Meyerhof (1969) which is reduced by 6% for comparison with a smooth footing as suggested by Wang and Carter (2001) Table (4.19).

The ultimate bearing pressures for the various cases studied are obtained from the FLAC model history files. The modified bearing capacity factors N_c^* are calculated for the present analyses using equation A.2 and shown in Table 4.19. The comparison of modified bearing capacity factor N_c^* versus shear strength ratios computed from FLAC with those from literature is shown in Figure 4.23. The normalised bearing pressure versus penetration curves for different shear strength ratios have been shown in Figure 4.24. The failure modes for all cases of c_2/c_1 for $H/B = 1$ are summarised in the Table 4.20.

Table 4.19: Comparison of modified Bearing Capacity Factor, N_c^* with existing values for rigid circular footing on strong over soft clay for grid 40×30, for $H/D = 1$.

Shear Strength Top Layer, (c_1)	Shear Strength Ratio, (c_2/c_1)	q_u (FLAC)	N_c^*(FLAC) = q_u(FLAC)/c_1	N_c		% Difference between N_c^*(FLAC) & N_c	
				(Brown & Meyerhof 1969)[9]	(Wang & Carter 2001)	(Brown & Meyerhof 1969)	(Wang & Carter 2001)
20.00	1.00	112.20	5.61	5.69	5.61	−1.34	0.00
20.00	0.80	112.25	5.61	5.69	5.61	−1.34	−0.01
20.00	0.67	112.21	5.61	5.69	5.61	−1.34	−0.01
20.00	0.50	112.21	5.61	5.69	5.61	−1.34	−0.01
20.00	0.33	112.18	5.61	4.67	5.45	16.75	2.80
20.00	0.20	112.10	5.61	3.95	5.03	29.52	10.11
20.00	0.10	99.21	4.96	3.42	4.38	31.04	11.71

[9] Values reduced by 6% for smooth footing (Wang and Carter 2001)

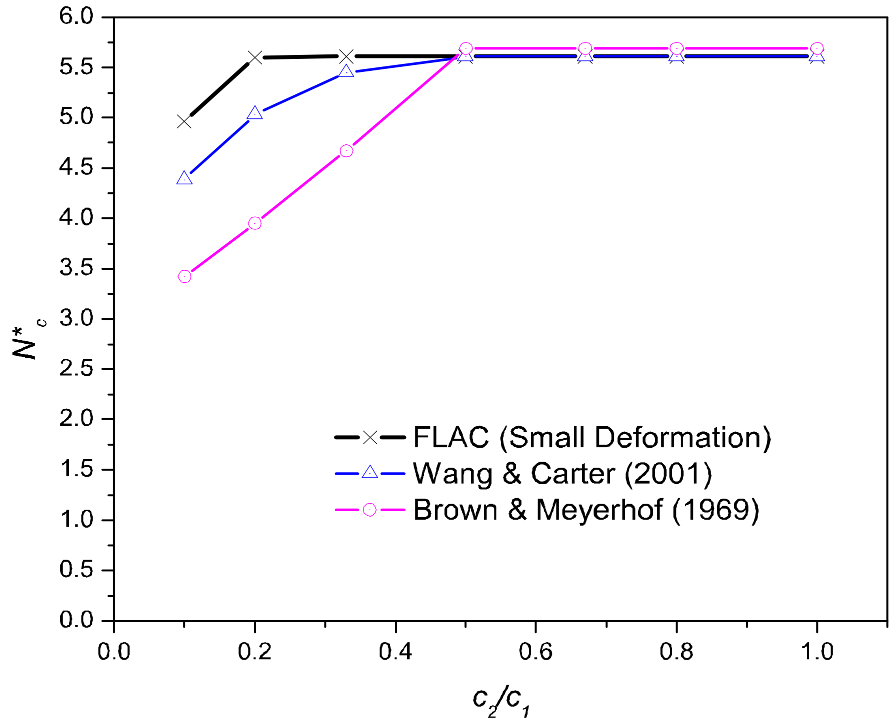

Figure 4.23: Modified bearing capacity factor (N_c^*) versus shear strength ratio (c_2/c_1) curves for a rigid smooth circular footing on strong over soft clay for 40 × 30 grid model, $H/D = 1$.

Case 2: $c_2/c_1 = 0.8$ **- Small Deformation Analysis**

The velocity vectors shown in Figure A.246 again show general shear type failure with plastic flow downwards and away from the footing.

The plasticity state indicators in Figure A.247 show the extent of failure. The nature, horizontal extent and the depth of the failure was found to be about the same as that in Case 1 (4.3.1).

Figure A.248 shows the magnified grid which further supports the general shear type failure with heave on the side of the footing.

Figure A.249 shows the equal vertical stress (σ_{yy}) contours and zone of influence

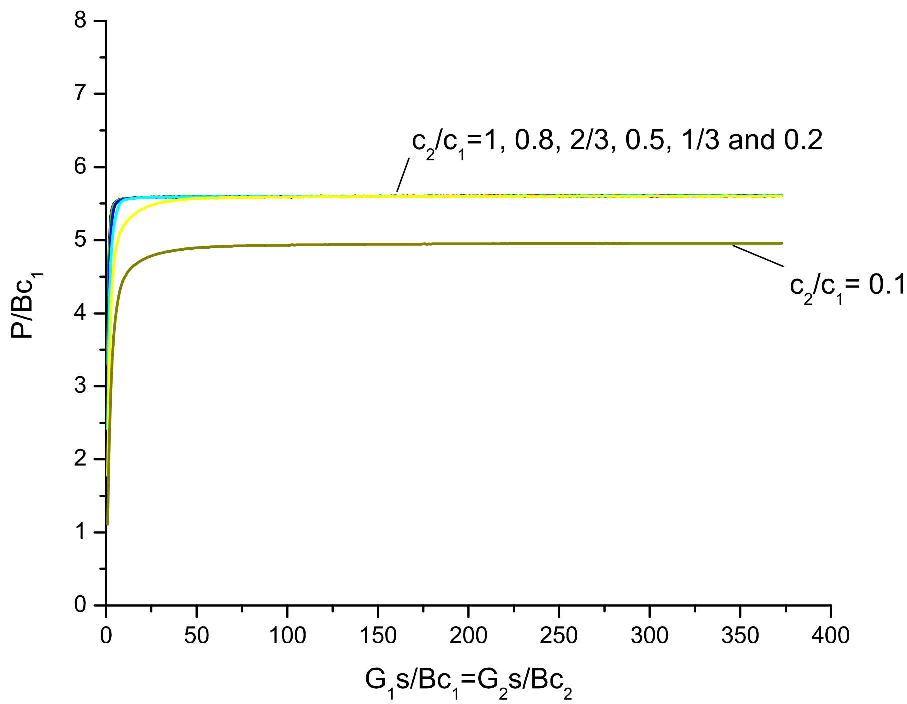

Figure 4.24: Normalised bearing pressure versus penetration curves for a rigid smooth circular footing on strong clay over soft clay for 40 × 30 grid model, $H/D = 1$.

under the circular footing. The depth zone of influence for this case was found to be same as that in Case 1 (4.3.1).

The bearing pressure versus footing penetration recorded at different time steps in the history of the model is shown in Figure A.250. The ultimate bearing pressure (q_u) for this case was found to be 112.25 kPa. The modified bearing capacity factor $N_c^* = 5.61$ from present analysis agrees with the value given by Wang and Carter (2001), but is slightly lower (1.34%) than the bearing capacity factor for rough circular footing given by Brown and Meyerhof (1969) which is reduced by 6% for comparison with a smooth footing as suggested by Wang and Carter (2001) (Table 4.19).

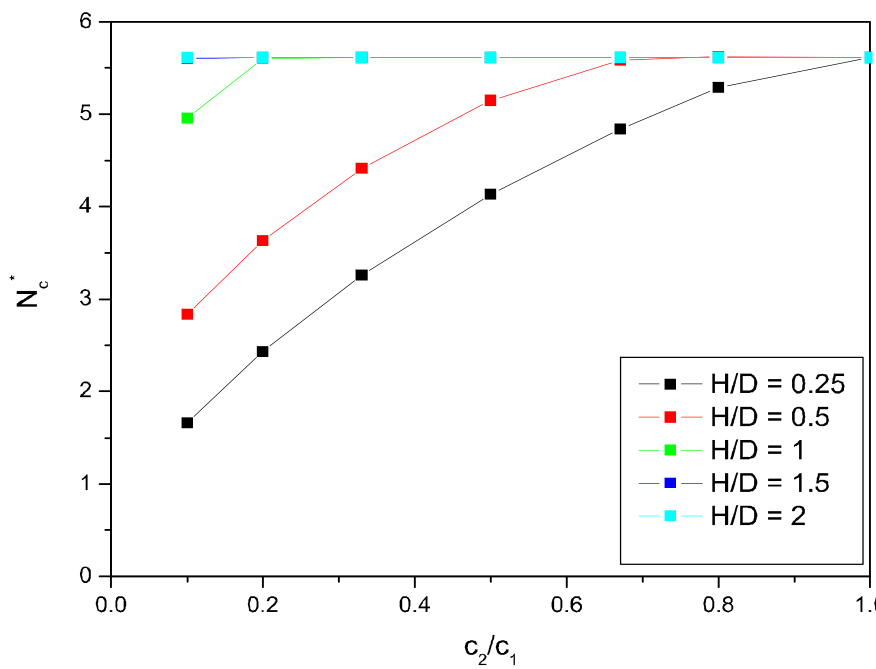

Figure 4.25: Modified bearing capacity factor (N_c^*) versus shear strength ratio (c_2/c_1) curves for a rigid smooth circular footing on strong over soft clay for 40 × 30 grid model, for various H/D ratios.

Table 4.20: Failure modes for different shear strength ratios (c_2/c_1) for $H/D = 1$.

Shear Strength Ratio, (c_2/c_1)	Failure Modes
1.00	General shear type failure
0.80	General shear type failure
0.67	General shear type failure
0.50	General shear type failure
0.33	General shear type failure
0.20	Local shear type failure involving both top and bottom layers
0.10	Punching shear failure in the top layer, local shear in the bottom layer

Case 3: $c_2/c_1 = 2/3$ - Small Deformation Analysis

Figure A.251 still shows general shear type failure of the foundation with similar plastic flow as in the previous two cases.

The zone of failure shown by the plasticity state indicators (refer Figure A.252) is similar to the previous two cases.

Figure A.253 shows the magnified grid which supports the idea of a general shear type failure with characteristic heave on the side of the footing.

Figure A.254 shows the equal vertical stress (σ_{yy}) contours and zone of influence under the circular footing. The depth of zone of influence for this case was found to be same as that in Case 1 (4.3.1) and in Case 2 (4.3.1).

The bearing pressure versus footing penetration recorded at different time steps in the history of the model is shown in Figure A.255. The ultimate bearing pressure (q_u) for this case was found to be 112.21 kPa. The modified bearing capacity factor $N_c^* = 5.61$ from present analysis agrees with the value given by Wang and Carter (2001), but is slightly lower (1.34%) than the bearing capacity factor for rough circular footing given by Brown and Meyerhof (1969) which is reduced by 6% for comparison with a smooth footing as suggested by Wang and Carter (2001) (Table 4.19).

Case 4: $c_2/c_1 = 0.5$ - Small Deformation Analysis

The velocity vectors shown in Figure A.256 once again indicate a general shear type failure of the foundation.

The plasticity state indicators in Figure A.257 show the zone of failure. The horizontal extent and the depth of the failure was found to be about the same as in Case 1 (4.3.1), Case 2 (4.3.1) and in Case 3 (4.3.1).

Figure A.258 shows the magnified grid which supports the idea of general shear type failure mechanism. The soil heave near the edge of the footing is similar to that in and Case 1 (4.1.1), Case 2 (4.1.1) and in Case 3 (4.1.1).

Figure A.259 shows the equal vertical stress (σ_{yy}) contours and zone of influence under the circular footing. The depth of the zone of influence for this case was found to be the same as that in Case 1 (4.3.1), Case 2 (4.3.1) and in Case 3 (4.3.1).

The bearing pressure versus footing penetration recorded at different time steps in the history of the model is shown in Figure A.260. The ultimate bearing pressure (q_u) for this case was found to be 112.17 kPa. The modified bearing capacity factor $N_c^* = 5.61$ from present analysis agrees with the value given by Wang and Carter (2001), but is slightly lower (1.34%) than the bearing capacity factor for a rough circular footing given by Brown and Meyerhof (1969) which is reduced by 6% for comparison with a smooth footing as suggested by Wang and Carter (2001) (Table 4.19).

Case 5: $c_2/c_1 = 1/3$ - Small Deformation Analysis

The velocity vectors shown in Figure A.261 continues to indicate a general shear failure of the foundation.

The plasticity state indicators in Figure A.262 show the zone of failure. The horizontal extent and the depth of the failure was found to be about the same as in Case 1 (4.3.1), Case 2 (4.3.1) and in Case 3 (4.3.1).

The deformed magnified grid in Figure A.263 supports general shear type failure.

Figure A.264 shows the equal vertical stress (σ_{yy}) contours and zone of influence under the circular footing. The zone of influence for this case was found to be $\simeq 0.6D$.

The shapes of stress contours are now becoming smoother than in the previous four cases.

The bearing pressure versus footing penetration recorded at different time steps in the history of the model is shown in Figure A.265. The ultimate bearing pressure (q_u) for this case was found to be 112.18 kPa. The modified bearing capacity factor $N_c^* = 5.61$ from present analysis is 2.80% higher than the value given by Wang and Carter (2001), and is 16.75% higher than the bearing capacity factor for rough circular footing given by Brown and Meyerhof (1969) which is reduced by 6% for comparison with a smooth footing as suggested by Wang and Carter (2001) (Table 4.19).

Case 6: $c_2/c_1 = 0.2$ - Small Deformation Analysis

The velocity vectors shown in Figure A.266 now indicate a local shear failure of the foundation.

The plasticity state indicators in Figure A.267 show yielding in shear both in top and bottom soft clay layers. The depth of failure $\simeq 3.5D$. The horizontal extent of plastic yielding is $\simeq 1.5$ m from the centre of the footing.

Figure A.273 shows the magnified grid which further supports the idea of some local shear failure of the foundation. The horizontal extent of soil heave from the edge of the footing is now reduced.

Figure A.269 shows the equal vertical stress (σ_{yy}) contours and zone of influence under the strip footing. The zone of influence for this case was found to be $\simeq 1.8D$. A kink visible in the 25 kPa stress contour at the interface of the two clay layers shows that the soft bottom clay layer has started to influence the bearing capacity of the foundation.

The bearing pressure versus footing penetration recorded at different time steps in the history of the model is shown in Figure A.270. The ultimate bearing pressure (q_u) for this case was found to be 112.10 kPa. The modified bearing capacity factor $N_c^* = 5.60$ from present analysis is 10.11% higher than the value given by Wang and Carter (2001), and is 29.52% higher than the bearing capacity factor for rough circular footing given by Brown and Meyerhof (1969) which is reduced by 6% for comparison with a smooth footing as suggested by Wang and Carter (2001) (Table 4.19).

Case 7: $c_2/c_1 = 0.1$ - Small Deformation Analysis

The velocity vectors shown in Figure A.271 indicate a partial punching shear failure of the foundation, the footing punches partially through the stronger top clay layer followed by some local shear type failure in the softer bottom layer.

The plasticity state indicators in Figure A.262 show that the zone of failure extends into the soft clay layer. The cluster of plasticity indicator showing yield in shear underneath the edge of the footing also supports partial punching in the stronger top clay layer. The depth of failure $\simeq 4D$. The crust of the stronger upper clay layer restricts the upward plastic flow in the bottom layer resulting in an increase of horizontal extent of the plastic yielding in shear. The horizontal extent of plastic yielding in shear is $\simeq 2.5\,\mathrm{m}$ from the centre of the footing.

Figure A.273 shows the magnified grid which further supports the idea of some partial punching shear failure of the foundation with negligible soil heave at the edge of the footing. A elastic wedge of strong clay trapped under the footing with no visible deformation is pushing into the soft clay layer.

Figure A.274 shows the equal vertical stress (σ_{yy}) contours and zone of influence under the circular footing. The zone of influence for this case was found to be $\simeq 1.2D$. Not all contours are now symmetrical about centre of the footing.

The bearing pressure versus footing penetration recorded at different time steps in the history of the model is shown in Figure A.275. The ultimate bearing pressure (q_u) for this case was found to be 99.21 kPa. The modified bearing capacity factor $N_c^* = 4.96$ from present analysis is 11.71% higher than the value given by Wang and Carter (2001), and is 31.04% higher than the the bearing capacity factor for rough circular footing given by Brown and Meyerhof (1969) which is reduced by 6% for comparison with a smooth footing as suggested by Wang and Carter (2001) (Table 4.19).

4.3.1 was considered as the base case for studying the effect of the thickness of the stronger top clay layer. The thickness is then varied first by increasing as $H > D$ ($H/D = 1.5$ and 2) and then by decreasing as $H < D$ ($H/D = 0.5, 0.25$).

4.3.2 Rigid Smooth Circular Footing on Strong over Soft Clay ($H/D = 1.5$)

Case 1, 2, 3, 4 and 5: $c_2/c_1 = 1,\ 0.8,\ 2/3,\ 0.5$ **and** $1/3$ **- Small Deformation Analysis**

It can be seen from Table 4.19 that the values of the modified bearing capacity factor (N_c^*) from FLAC analysis are constant (5.61) for $c_2/c_1 = 1,\ 0.8,\ 2/3,\ 0.5$ and $1/3$ respectively. Therefore analyses for these cases would be same as Case 1 (4.3.1), Case 2 (4.3.1), Case 3 (4.3.1), Case 4 (4.3.1), and Case 5 (4.3.1) respectively.

Case 6: $c_2/c_1 = 0.2$ **- Small Deformation Analysis**

The velocity vectors shown in Figure A.276 is a general shear type failure of the foundation followed by soil flowing downwards and away from the footing. A heave in the ground is evident from the upward vertical direction of the velocity vectors on the side of the footing.

The plasticity state indicators in Figure A.277 show that the zone of failure is now mainly confined to the upper strong clay layer. The yielding in shear in the top clay starts from under the footing and continues to spread downwards and away from the footing. The depth of failure is found to be $\simeq 0.4D$ and the horizontal extent of plastic yielding in shear is $\simeq 0.7$ m from the centre of the footing.

Figure A.283 shows the magnified grid which further supports the idea of general shear type failure of the foundation. A heave in the ground on the side of the footing is visible.

Figure A.279 shows the equal vertical stress (σ_{yy}) contours and zone of influence under the circular footing. The zone of influence for this case was found to be $\simeq 1.25D$.

The bearing pressure versus footing penetration recorded at different time steps in the history of the model is shown in Figure A.280. The ultimate bearing pressure (q_u) for this case was found to be 112.20 kPa. The modified bearing capacity factor $N_c^* = 5.61$ from present analysis is slightly higher (5.02%) than the bearing capacity factor for rough circular footing given by Brown and Meyerhof (1969) which is reduced by 6% for comparison with a smooth footing as suggested by Wang and Carter (2001) (Table 4.21).

Table 4.21: Comparison of modified Bearing Capacity Factor, N_c^* with existing values for rigid circular footing on strong over soft clay for grid 40×30, for $H/D = 1.5$.

Shear Strength Top Layer, (c_1)	Shear Strength Ratio, (c_2/c_1)	q_u (FLAC)	N_c^*(FLAC) = q_u(FLAC)/c_1	N_c (Brown & Meyerhof 1969)[10]	% Difference between N_c^*(FLAC) & N_c (Brown & Meyerhof 1969)
20.00	1.00	112.20	5.61	5.69	−1.34
20.00	0.80	112.25	5.61	5.69	−1.34
20.00	0.67	112.21	5.61	5.69	−1.34
20.00	0.50	112.21	5.61	5.69	−1.34
20.00	0.33	112.18	5.61	5.69	−1.34
20.00	0.20	112.20	5.61	5.33	5.02
20.00	0.10	112.01	5.60	4.67	16.6

[10] Values reduced by 6% for smooth footing (Wang and Carter 2001)

The normalised bearing pressure versus penetration curves for different shear strength ratios have been shown in Figure 4.26.

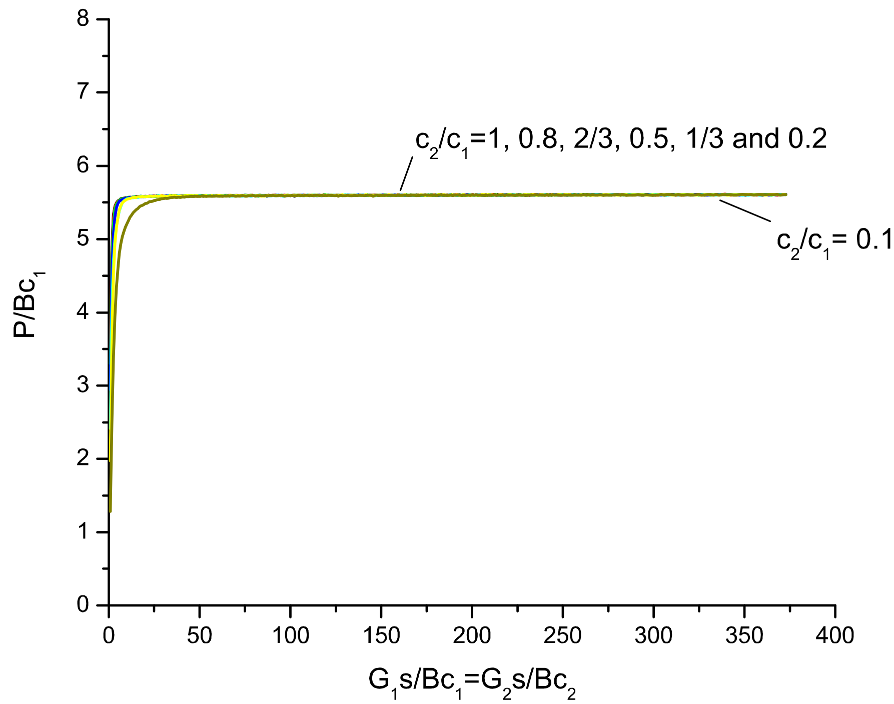

Figure 4.26: Normalised bearing pressure versus penetration curves for a rigid smooth circular footing on strong clay over soft clay for 40 × 30 grid model, $H/D = 1.5$.

Figure 4.27 shows comparison of the modified bearing capacity factor (N_c^*) versus shear strength ratios computed from FLAC with those from literature.

The failure modes for cases, $c_2/c_1 = 0.2$ and 0.1 are summarised in the Table (4.22).

Case 7: $c_2/c_1 = 0.1$ **- Small Deformation Analysis**

The velocity vectors shown in Figure A.281 now indicate a local shear failure.

The plasticity state indicators in Figure A.282 show that the zone of failure extends into the soft clay layer. The depth of failure $\simeq 4.5D$. The horizontal extent of plastic

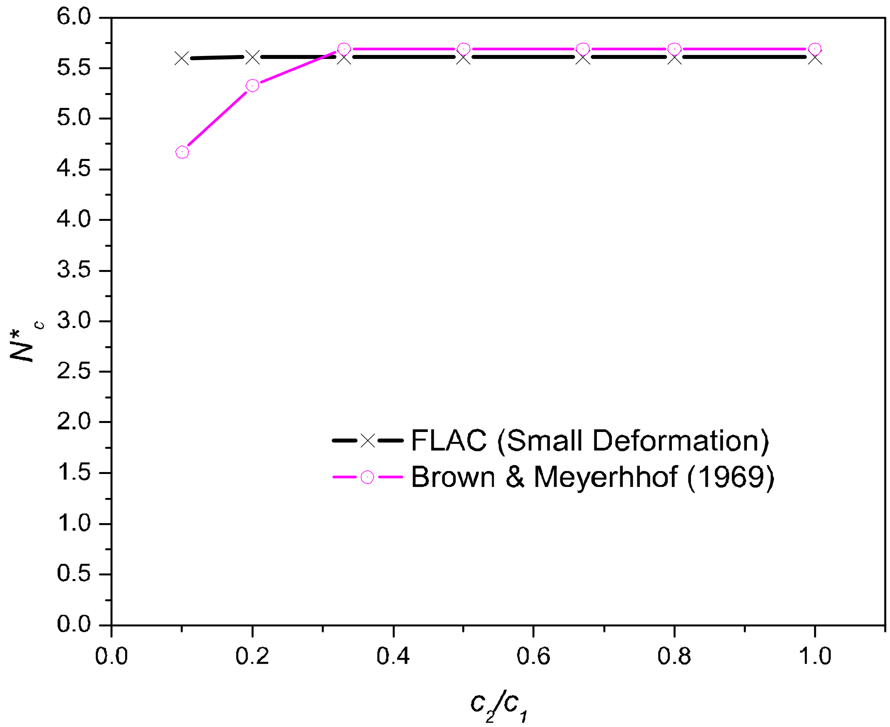

Figure 4.27: Modified bearing capacity factor (N_c^*) versus shear strength ratio (c_2/c_1) curves for a rigid smooth circular footing on strong clay over soft clay for 40×30 grid model, $H/D = 2$.

yielding in shear is $\simeq 2.5\,\mathrm{m}$ from the centre of the footing.

Figure A.283 shows the magnified grid which further supports the local shear failure of the foundation with some soil heave on the edge of the footing.

Figure A.284 shows the equal vertical stress (σ_{yy}) contours and zone of influence under the strip footing. The zone of influence for this case was found to be about 1.2 times deeper than the diameter of the footing. The extrapolation of (σ_{yy}) contours to the boundary of the model in Figure A.286 can be compared with (σ_{yy}) contours in Figure A.285.

The bearing pressure versus footing penetration recorded at different time steps in the history of the model is shown in Figure A.287. The ultimate bearing pressure

Table 4.22: Failure modes for different shear strength ratios (c_2/c_1) for $H/D = 1.5$.

Shear Strength Ratio, (c_2/c_1)	Failure Modes
0.20	General shear type failure
0.10	Local shear type failure

(q_u) for this case was found to be 112.01 kPa. The modified bearing capacity factor $N_c^* = 5.60$ from the present analysis is higher (16.6%) than the bearing capacity factor for rough circular footing given by Brown and Meyerhof (1969) which is reduced by 6% for comparison with a smooth footing as suggested by Wang and Carter (2001) (Table 4.21).

4.3.3 Rigid Smooth Circular Footing on Strong over Soft Clay ($H/D = 2$)

Case 1, 2, 3, 4, 5 and 6: $c_2/c_1 = 1$, 0.8, 2/3, 0.5, 1/3, 0.2 **- Small Deformation Analysis**

It can be seen from Table 4.21 that the values of the modified bearing capacity factor (N_c^*) from FLAC analysis are constant (5.61) for $c_2/c_1 = 1$, 0.8, 2/3, 0.5, 1/3 and 0.2 respectively. Therefore analysis for these cases would be same as Case 1 (4.3.1), Case 2 (4.3.1), Case 3 (4.3.1), Case 4 (4.3.1), Case 5 (4.3.1) and Case 6 (4.3.2) respectively.

Case 7: $c_2/c_1 = 0.1$ **- Small Deformation Analysis**

The velocity vectors shown in Figure A.288 now indicate a general shear failure of the foundation with plastic flow downwards and away from the footing. The upward vertical velocity vectors on the side of the footing represent a heave.

The plasticity state indicators in Figure A.289 show that the zone of failure is now confined in the stronger top clay layer. The plasticity indicators in shear starts from under the footing and progresses downwards and away from the footing. The depth of failure $\simeq 0.4B$. The horizontal extent of plastic yielding is $\simeq 0.75\,\mathrm{m}$ from the centre of the footing.

Figure A.290 shows the magnified grid which supports the local shear failure of the foundation with plastic flow. There is some heave on the edge of the footing.

Figure A.291 shows the equal vertical stress (σ_{yy}) contours and zone of influence under the strip footing. The zone of influence for this case was found to be $\simeq 1.2D$. The contours are symmetrical about the centre of the footing.

The bearing pressure versus footing penetration recorded at different time steps in the history of the model is shown in Figure A.292. The ultimate bearing pressure (q_u) for this case was found to be 112.23 kPa. The modified bearing capacity factor $N_c^* = 5.61$ from present analysis is lower (1.34%) than the bearing capacity factor for rough circular footing given by Brown and Meyerhof (1969) which is reduced by 6% for comparison with a smooth footing as suggested by Wang and Carter (2001)

(Table 4.23).

Table 4.23: Comparison of modified Bearing Capacity Factor, N_c^* with existing values for regid circular footing on strong over soft clay for grid 40×30, for $H/D = 2$.

Shear Strength Top Layer, (c_1)	Shear Strength Ratio, (c_2/c_1)	q_u (FLAC)	N_c^*(FLAC) = q_u(FLAC)/c_1	N_c (Brown & Meyerhof 1969)[11]	% Difference between N_c^*(FLAC) & N_c (Brown & Meyerhof 1969)
20.00	1.00	112.20	5.61	5.69	−1.34
20.00	0.80	112.25	5.61	5.69	−1.34
20.00	0.67	112.21	5.61	5.69	−1.34
20.00	0.50	112.21	5.61	5.69	−1.34
20.00	0.33	112.18	5.61	5.69	−1.34
20.00	0.20	112.20	5.61	5.69	−1.34
20.00	0.10	112.23	5.61	5.69	−1.34

[11] Values reduced by 6% for smooth footing (Wang and Carter 2001)

Figure 4.28 shows the comparison of modified bearing capacity factor (N_c^*) versus shear strength ratios computed from FLAC with those from literature.

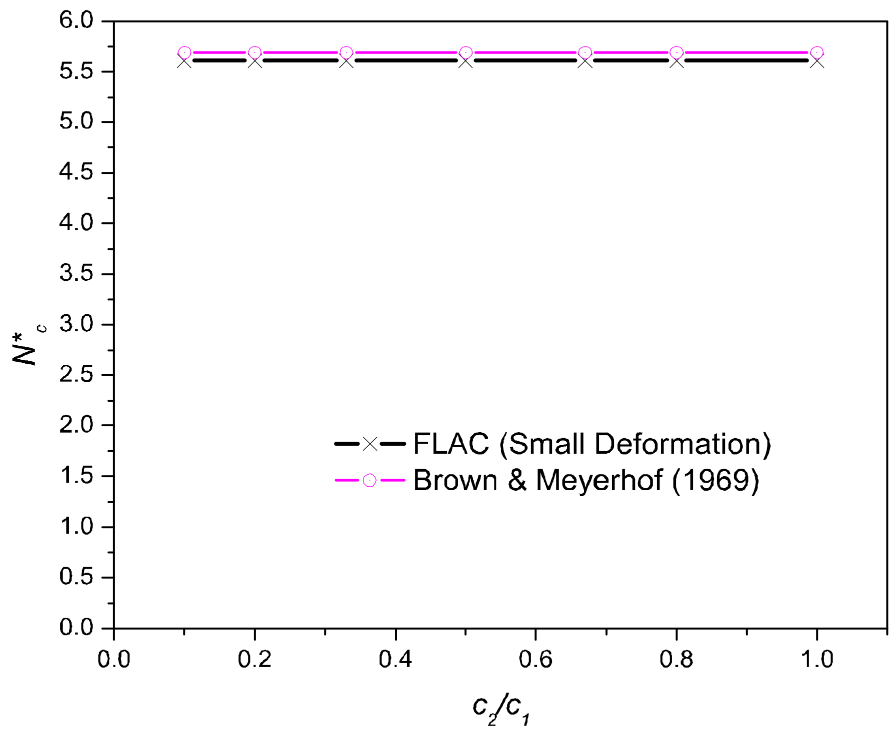

Figure 4.28: Modified bearing capacity factor (N_c^*) versus shear strength ratio (c_2/c_1) curves for a rigid smooth circular footing on strong clay over soft clay for 40×30 grid model, $H/D = 2$.

The normalised bearing pressure versus penetration curves for different shear strength ratios have been shown in Figure 4.29.

Numerical analyses in 4.3.1, 4.3.2 and 4.3.3 give the minimum depth of the upper strong clay layer beyond which the lower soft clay layer has no influence on the ultimate bearing capacity of the circular foundation for $H/D \geq 2$. The following cases (4.3.4 and 4.3.5) will show the influence of the bottom soft clay on the ultimate bearing capacity when the $H/D < 1$.

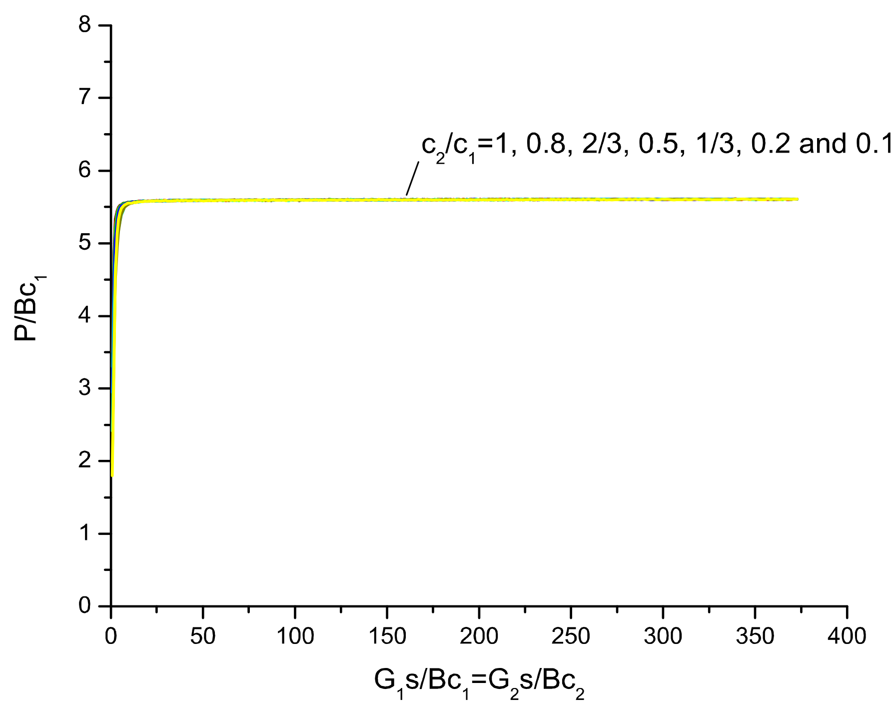

Figure 4.29: Normalised bearing pressure versus penetration curves for a rigid smooth circular footing on strong clay over soft clay for 40×30 grid model, $H/D = 2$.

4.3.4 Rigid Smooth Circular Footing on Ground Surface ($H/D = 0.5$)

Case 1: $c_2/c_1 = 1$ (Homogeneous clay) - Small Deformation Analysis

Since this is the case of homogeneous clay all the results will be same as in Case 1 (4.3.1). The FLAC analysis results for other cases of c_2/c_1 are explained below.

Case 2: $c_2/c_1 = 0.8$ - Small Deformation Analysis

The velocity vectors shown in Figure A.293 indicate a general shear type failure of the foundation involving both top and bottom clay layers.

The plasticity state indicators in Figure A.294 show that the failure zone extends into the bottom soft clay layer. The plasticity state indicators yielding in shear starts underneath the footing and progresses downwards and away from the footing representing a plastic flow of soil. The depth of the failure is found to be $\simeq 0.6D$, and the horizontal extent of plastic yielding is $\simeq 0.75$ m from the centre of the footing.

Figure A.295 shows the magnified grid which supports the idea of general shear failure of the foundation with some soil heaving at the edge of the footing.

Figure A.296 shows the equal vertical stress (σ_{yy}) contours and zone of influence under the circular footing. The zone of influence for this case was found to be about $\simeq 1.5D$. The contours are symmetrical about the centre of the footing.

The bearing pressure versus footing penetration recorded at different time steps in the history of the model is shown in Figure A.297. The ultimate bearing pressure (q_u) for this case was found to be 112.47 kPa. The modified bearing capacity factor $N_c^* = 5.62$ from present analysis agrees with the value given by Wang and Carter (2001), but is slightly lower (1.16%) than the bearing capacity factor for rough circular footing given by Brown and Meyerhof (1969) which is reduced by 6% for comparison with a smooth footing as suggested by Wang and Carter (2001) (Table 4.24).

Table 4.24: Comparison of modified Bearing Capacity Factor, N_c^* with existing values for rigid circular footing on strong over soft clay for grid 40×30, for $H/D = 0.5$.

Shear Strength Top Layer, (c_1)	Shear Strength Ratio, (c_2/c_1)	q_u (FLAC)	N_c^*(FLAC) = q_u(FLAC)/c_1	N_c		% Difference between N_c^*(FLAC) & N_c	
				(Brown & Meyerhof 1969)[12]	(Wang & Carter 2001)	(Brown & Meyerhof 1969)	(Wang & Carter 2001)
20.00	1.00	112.20	5.61	5.69	5.61	−1.34	0.00
20.00	0.80	112.47	5.62	5.69	5.61	−1.16	0.24
20.00	0.67	111.67	5.58	5.25	5.49	5.86	1.59
20.00	0.50	103.08	5.15	4.28	5.07	16.98	1.47
20.00	0.33	88.42	4.42	3.35	4.22	24.10	4.63
20.00	0.20	72.59	3.63	2.57	3.41	29.13	5.83
20.00	0.10	56.73	2.84	2.04	2.73	27.95	3.45

[12] Values reduced by 6% for smooth footing (Wang and Carter 2001)

Figure 4.30 shows the comparison of the modified bearing capacity factor (N_c^*) versus shear strength ratios computed from FLAC with those from literature.

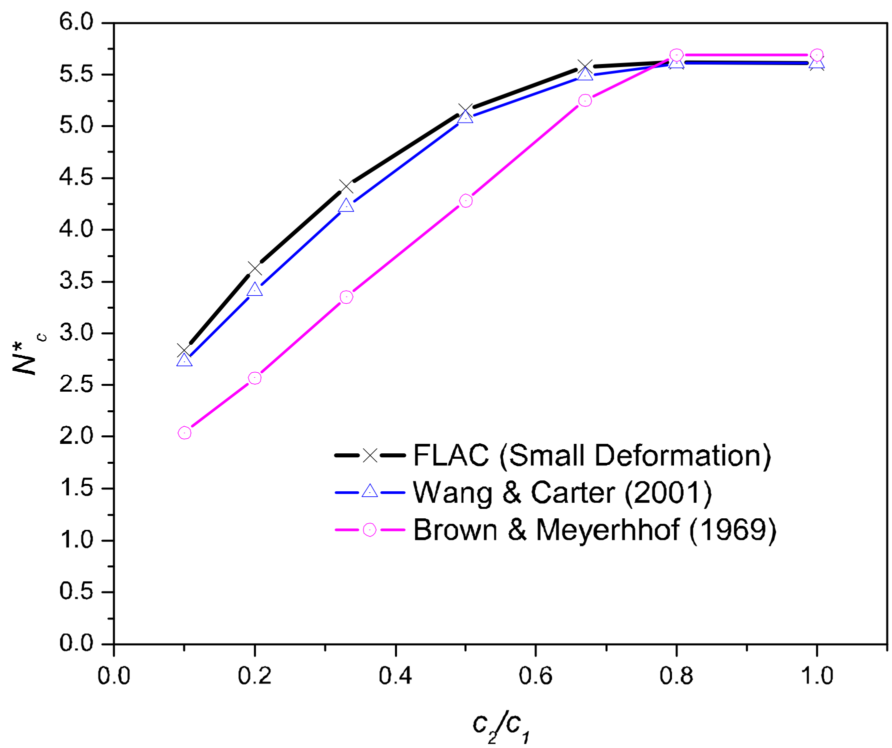

Figure 4.30: Modified bearing capacity factor (N_c^*) versus shear strength ratio (c_2/c_1) curves for a rigid smooth circular footing on strong clay over soft clay for 40×30 grid model, $H/D = 0.5$.

The normalised bearing pressure versus penetration curves for different shear strength ratios are shown in Figure 4.31.

The failure mechanisms for shear strength rations of $c_2/c_1 = 0.8, 2/3, 0.5, 1/3, 0.2$ and 0.1 are summarised in Table (4.25).

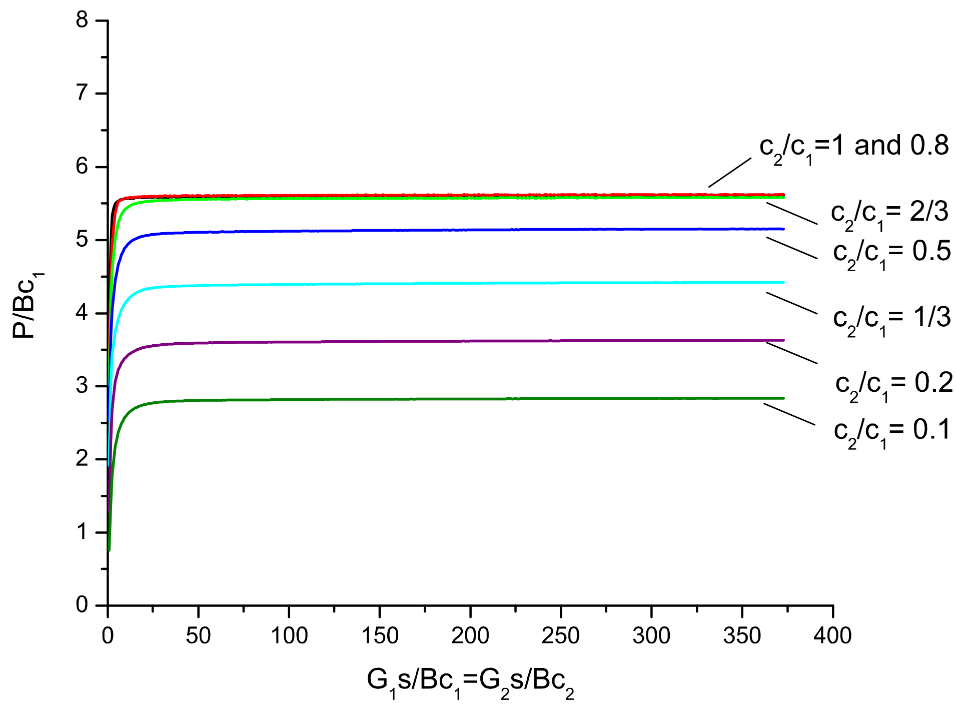

Figure 4.31: Normalised bearing pressure versus penetration curves for a rigid smooth circular footing on strong clay over soft clay for 40 × 30 grid model, $H/D = 0.5$.

Case 3: $c_2/c_1 = 2/3$ **- Small Deformation Analysis**

Figure A.298 indicates a general shear type failure of a foundation which involves both the strong upper clay layer and the soft bottom clay layer.

The plasticity state indicators in Figure A.299 show that the zone of failure extends into the soft clay layer. The plastic yielding in shear starts underneath the footing and extends both in downwards and lateral directions. The depth of failure $\simeq 0.8D$. The horizontal extent of plastic yielding is $\simeq 0.9\,\mathrm{m}$ from the centre of the footing.

Figure A.300 shows the magnified grid which further supports the idea of a general shear type failure of the foundation with some soil heaving on the side of the footing.

Figure A.301 shows the equal vertical stress (σ_{yy}) contours and zone of influence under the circular footing. The contours are symmetrical about the centre of the

Table 4.25: Failure modes for different shear strength ratios (c_2/c_1) for $H/D = 0.5$.

Shear Strength Ratio, (c_2/c_1)	Failure Modes
0.80	General shear type failure
0.67	General shear type failure
0.50	Partial punching shear type failure
0.33	Partial punching shear type failure
0.20	Full punching shear type failure through the top clay layer
0.10	Full punching shear type failure through the top clay layer

footing. The zone of influence for this case was found to be $\simeq 1.8D$.

The bearing pressure versus footing penetration recorded at different time steps in the history of the model is shown in Figure A.302. The ultimate bearing pressure (q_u) for this case was found to be 111.67 kPa. The modified bearing capacity factor $N_c^* = 5.58$ from present analysis is slightly (1.59%) higher than the value given by Wang and Carter (2001), and is 5.86% higher than the bearing capacity factor for rough circular footing given by Brown and Meyerhof (1969) which is reduced by 6% for comparison with a smooth footing as suggested by Wang and Carter (2001) (Table 4.24).

Case 4: $c_2/c_1 = 0.5$ - Small Deformation Analysis

The vertical direction of the velocity vector under most of the footing in Figure A.303 indicates that foundation failure occurs through partial punching shear in the upper layer.

The cluster of the plasticity state indicators showing yielding in shear underneath the edge of the footing also supports partial punching shear type failure mechanism accompanied by plastic flow both in top and bottom clays as shown in Figure A.304. The depth of failure is $\simeq 1.2D$. The horizontal extent of plastic yielding is $\simeq 1$ m from the centre of the footing.

An elastic wedge of top soil is trapped under the footing with no distortion in the grid (refer Figure A.305). This wedge pushes the stiff top clay layer into the softer bottom clay causing it to spread laterally The soil heave near the edge of the footing is very small in comparison to 4.3.4 and 4.3.4.

Figure A.306 shows the equal vertical stress (σ_{yy}) contours and zone of influence under the strip footing. The high stress contours are no longer symmetrical about the centre of the footing but are inclined towards the edge of the footing. This shift can be seen as partial punching of the footing. The zone of influence for this case was found to be $\simeq 2D$.

The bearing pressure versus footing penetration recorded at different time steps in the history of the model is shown in Figure A.307. The ultimate bearing pressure (q_u) for this case was found to be 103.08 kPa. The modified bearing capacity factor $N_c^* = 5.15$ from present analysis is slightly (1.47%) higher than the value given by Wang and Carter (2001), and is 16.98% higher than the bearing capacity factor for rough circular footing given by Brown and Meyerhof (1969) which is reduced by 6% for comparison with a smooth footing as suggested by Wang and Carter (2001) (Table 4.24).

Case 5: $c_2/c_1 = 1/3$ - Small Deformation Analysis

In this case the rigid smooth circular footing rests on the top strong clay surface. The velocity vectors shown in Figure A.308 continues to indicate a partial punching shear failure of the foundation, with punching depth extending deeper into the stronger top clay layer compared to 4.3.4. The plastic flow in the bottom soft layer now increases compared to 4.3.4.

The plasticity state indicators in Figure A.309 show that the zone of failure extends into the soft clay layer. The depth of failure $\simeq 2D$, and the horizontal extent of plastic yielding is $\simeq 1.25$ m from the centre of the footing. There is zone underneath the footing which does not show any kind of yielding. This zone represents an elastic wedge trapped under the footing which along with footing pushes into the soft clay causing plastic flow in it. The cluster of the indicators under the edge of the footing representing yielding in shear supports the punching shear type failure in the strong top clay.

The undeformed magnified grid underneath the footing in Figure A.310 represents the elastic wedge trapped under the footing which pushes into the soft bottom clay causing it to spread laterally. There is almost no heave on the side of the footing.

Figure A.311 shows the equal vertical stress (σ_{yy}) contours and zone of influence under the strip footing. The zone of influence for this case was found to be $\simeq 2D$. The high stress are not symmetric about the centre of the footing but tend to lean towards the edge of the footing supporting some punching in the top clay layer.

The bearing pressure versus footing penetration recorded at different time steps in the history of the model is shown in Figure A.312. The ultimate bearing pressure (q_u) for this case was found to be 88.42 kPa. The modified bearing capacity factor $N_c^* = 4.42$ from present analysis is slightly (4.63%) higher than the value given by Wang and Carter (2001), and is 24.10% higher than the bearing capacity factor for rough circular footing given by Brown and Meyerhof (1969) which is reduced by 6% for comparison with a smooth footing as suggested by Wang and Carter (2001) (Table 4.24).

Case 6: $c_2/c_1 = 0.2$ - Small Deformation Analysis

The velocity vectors shown in Figure A.313 now indicate a full punching shear failure of the foundation, with a column of the strong top clay layer trapped under the footing punching through into the softer bottom clay layer.

The plasticity state indicators in Figure A.314 show major yielding in shear in the lower soft clay layer. There is a cluster of the indicators under the edge of the footing representing yielding in shear which supports the punching shear type failure in the strong top clay. The zone underneath the footing not showing any kind of yielding is bigger than the previous case. This zone represents an elastic wedge trapped under the footing which along with footing pushes into the soft clay causing plastic flow in it. The depth of failure $\simeq 1.5D$. The horizontal extent of plastic yielding is $\simeq 1.4$ m from the centre of the footing.

An undeformed elastic column of top soil can be seen trapped underneath the footing which pushes into the softer clay layer making it move both in downwards vertical and lateral directions (refer Figure A.315). There is no soil heaving at the edge of the footing now.

Figure A.316 shows the equal vertical stress (σ_{yy}) contours and zone of influence under the strip footing. Since the failure mechanism is a punching through the top layer into the bottom layer, the high stress contours concentration is around the edge of the footing. The zone of influence for this case was found to be $\simeq 1.6D$.

The bearing pressure versus footing penetration recorded at different time steps in the history of the model is shown in Figure A.317. The ultimate bearing pressure (q_u) for this case was found to be 72.59 kPa. The modified bearing capacity factor $N_c^* = 3.63$ from present analysis is slightly (5.83%) higher than the value given by Wang and Carter (2001), and is 29.13% higher than the bearing capacity factor for rough circular footing given by Brown and Meyerhof (1969) which is reduced by 6% for comparison with a smooth footing as suggested by Wang and Carter (2001) and shown in Table 4.24.

Case 7: $c_2/c_1 = 0.1$ - Small Deformation Analysis

The velocity vectors shown in Figure A.318 continues to indicate a full punching shear failure of the foundation, with footing punching through the stronger top clay layer followed by plastic flow in the softer bottom layer.

The plasticity state indicators in Figure A.319 show that the zone of failure extends deeper into the soft clay layer. The depth of failure $\simeq 2.2D$. The horizontal extent of plastic yielding is $\simeq 1.8$ m from the centre of the footing.

The undeformed grid underneath the footing represents an elastic column of the strong top soil which punches into the softer bottom soil moving it vertically downwards and horizontally (refer Figure A.320). The bend in the grid at the interface of the two soils represents the full punching shear type failure in the top soil. There is no soil heaving at the side of the footing.

Figure A.321 shows the equal vertical stress (σ_{yy}) contours and zone of influence under the strip footing. The high stress contours concentration around the edge of the footing supports the punching shear type failure. The bulge in the 10 kPa shows the influence of the soft bottom clay. The zone of influence for this case was found to be $\simeq 1.8D$.

The bearing pressure versus footing penetration recorded at different time steps in the history of the model is shown in Figure A.322. The ultimate bearing pressure (q_u) for this case was found to be 56.73 kPa. The modified bearing capacity factor $N_c^* = 2.84$ from present analysis is slightly (3.45%) higher than the value given by Wang and Carter (2001), and is 27.95% higher than the bearing capacity factor for rough circular footing given by Brown and Meyerhof (1969) which is reduced by 6% for comparison with a smooth footing as suggested by Wang and Carter (2001) (Table 4.24).

4.3.5 Rigid Smooth Circular Footing on Strong over Soft Clay ($H/D = 0.25$)

Case 1: $c_2/c_1 = 1$ (Homogeneous clay) - Small Deformation Analysis

Since this is the case of homogeneous clay all the results will be same as in Case 1 (4.3.1). The FLAC analysis results for other cases of c_2/c_1 are explained below.

Case 2: $c_2/c_1 = 0.8$ - Small Deformation Analysis

The vertical direction of velocity vectors at most of the grid points in Figure A.323 shows compression in the strong top soil. The soil flows both vertically downwards as well as laterally outwards underneath the footing. The upwards vertical direction of the velocity vectors on the side of the footing represents the heave in the ground. The failure mechanism can be defined as partial punching shear type failure.

The plasticity state indicators in Figure A.324 show that the zone of failure extends into the bottom soft clay layer as the yielding in shear spreads from the soil underneath the footing in vertically downwards and lateral directions. The depth of the failure is found to be $\simeq 0.65D$, and the horizontal extent of plastic yielding is $\simeq 0.9\,\text{m}$ from the centre of the footing. An elastic soil zone underneath the footing supports the compression of the top soil.

Figure A.325 shows the magnified grid which further supports the idea of a partial punching shear type failure of the foundation. An undeformed grid underneath the grid represents the compression of the top strong soil. A heave is also visible on the side of the footing.

Figure A.326 shows the equal vertical stress (σ_{yy}) contours and zone of influence under the circular footing. The zone of influence for this case was found to be $\simeq 1.7D$.

The bearing pressure versus footing penetration recorded at different time steps in the history of the model is shown in Figure A.327. The ultimate bearing pressure (q_u) for this case was found to be 105.88 kPa. The modified bearing capacity factor $N_c^* = 5.29$ from present analysis is 6.39% higher than the bearing capacity factor for rough circular footing given by Brown and Meyerhof (1969) which is reduced by

6% for comparison with a smooth footing as suggested by Wang and Carter (2001) (Table 4.26).

Table 4.26: Comparison of modified Bearing Capacity Factor, N_c^* with existing values for rigid circular footing on strong over soft clay for grid 40×30, for $H/D = 0.25$.

Shear Strength Top Layer, (c_1)	Shear Strength Ratio, (c_2/c_1)	q_u (FLAC)	N_c^*(FLAC) = q_u(FLAC)/c_1	N_c (Brown & Meyerhof 1969)[13]	% Difference between N_c^*(FLAC) & N_c (Brown & Meyerhof 1969)
20.00	1.00	112.20	5.61	5.69	−1.34
20.00	0.80	105.88	5.29	4.95	6.39
20.00	0.67	96.87	4.84	4.48	7.39
20.00	0.50	82.50	4.13	3.52	14.47
20.00	0.33	65.15	3.26	2.54	21.93
20.00	0.20	48.57	2.43	1.87	22.73
20.00	0.10	33.11	1.66	1.31	20.84

[13] Values reduced by 6% for smooth footing (Wang and Carter 2001)

Figure 4.32 shows the comparison of the modified bearing capacity factor (N_c^*) versus shear strength ratios computed from FLAC with those from literature.

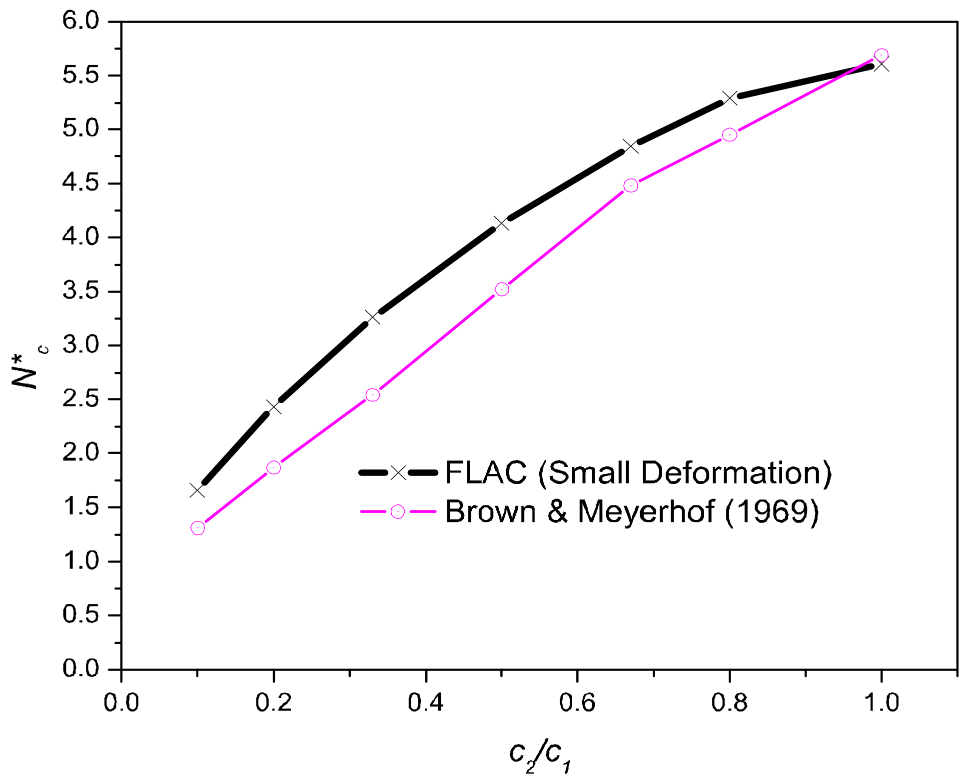

Figure 4.32: Modified bearing capacity factor (N_c^*) versus shear strength ratio (c_2/c_1) curves for a rigid smooth circular footing on strong clay over soft clay for 40×30 grid model, $H/D = 0.25$.

The normalised bearing pressure versus penetration curves for different shear strength ratios are shown in Figure 4.33.

The failure mechanisms for shear strength rations of $c_2/c_1 = 0.8, 2/3, 0.5, 1/3, 0.2$ and 0.1 are summarised in Table 4.27.

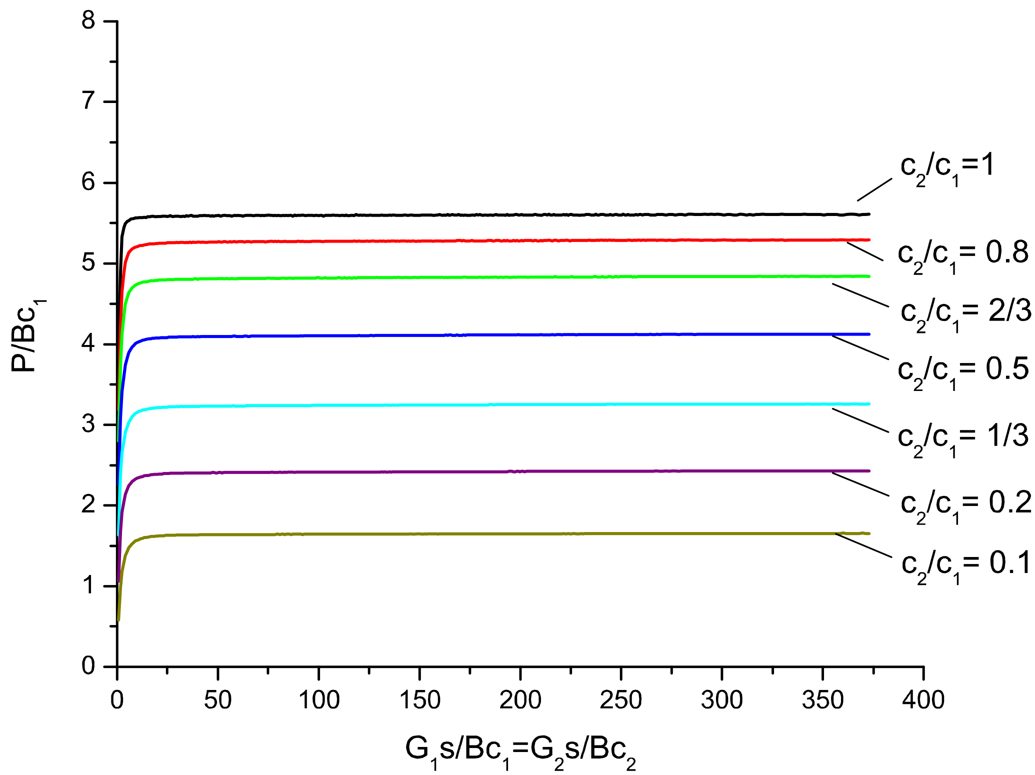

Figure 4.33: Normalised bearing pressure versus penetration curves for a rigid smooth circular footing on strong clay over soft clay for 40 × 30 grid model, $H/D = 0.25$.

Case 3: $c_2/c_1 = 2/3$ - Small Deformation Analysis

The vertical downward direction of most of the velocity vectors underneath the footing in the stronger top clay layer indicates partial punching shear type failure of the foundation (refer A.328).

The concentration of the plasticity indicators of soil yielded in shear around the edge of the footing in Figure A.329 also supports partial punching in the top clay layer. The zone of failure extends deeper into the soft clay layer. The depth of failure $\simeq 0.8D$, and the horizontal extent of plastic yielding is $\simeq 0.9\,\mathrm{m}$ from the centre of the footing.

Table 4.27: Failure modes for different shear strength ratios (c_2/c_1) for $H/D = 0.25$.

Shear Strength Ratio, (c_2/c_1)	Failure Modes
0.80	Partial punching shear type failure
0.67	Partial punching shear type failure
0.50	Full punching shear type failure through the top clay layer
0.33	Full punching shear type failure through the top clay layer
0.20	Full punching shear type failure through the top clay layer
0.10	Full punching shear type failure through the top clay layer

Figure A.330 shows the magnified grid which further supports the partial punching shear failure of the foundation. The undeformed grid under the footing represents an elastic wedge of the stiff top soil trapped underneath it. This wedge pushes into the soft soil causing both the top an bottom soil to move laterally away from the footing.

Figure A.331 shows the equal vertical stress (σ_{yy}) contours and zone of influence under the strip footing. The zone of influence for this case was found to be $\simeq 1.5D$. The higher stress contour (100 kPa) can be seen concentrating around the edge of the footing, once again suggesting some partial punching.

The bearing pressure versus footing penetration recorded at different time steps in the history of the model is shown in Figure A.332. The ultimate bearing pressure (q_u) for this case was found to be 96.87 kPa. The modified bearing capacity factor $N_c^* = 4.84$ from present analysis is 7.39% higher than the bearing capacity factor for rough circular footing given by Brown and Meyerhof (1969) which is reduced by 6% for comparison with a smooth footing as suggested by Wang and Carter (2001) (Table 4.26).

Case 4: $c_2/c_1 = 0.5$ - Small Deformation Analysis

The downwards vertical direction of almost all grid point velocity vectors underneath the footing in Figure A.333 shows increase in punching shear failure of the foundation in the stronger top clay layer.

The clustering of the most of plasticity indicators in shear around the edge of the footing supports the punching shear failure in the top clay (refer Figure A.334). The zone under the footing showing no yielding of any kind or elastic yielding in the past represents a top soil wedge trapped under the footing. The depth of failure $\simeq 0.8D$, and the horizontal extent of plastic yielding is $\simeq 0.9$ m from the centre of the footing.

Figure A.335 shows the magnified grid which also supports the idea of punching type failure mechanism of the foundation. The undeformed grid underneath the footing represents the stiff soil wedge trapped under the footing which pushes into the soft soil below moving it and the top soil laterally away from the footing. The soil heave near the edge of the footing is very small in comparison to Case 3 (4.3.5).

Figure A.336 shows the equal vertical stress (σ_{yy}) contours and zone of influence under the strip footing. The zone of influence for this case was found to be $\simeq 1.5D$. The concentration of the high stress contours around the edge of the footing once again supports the idea of punching shear failure in the top soil.

The bearing pressure versus footing penetration recorded at different time steps in the history of the model is shown in Figure A.337. The ultimate bearing pressure (q_u) for this case was found to be 82.50 kPa. The modified bearing capacity factor $N_c^* = 4.13$ from present analysis is 14.47% higher than the bearing capacity factor for rough circular footing given by Brown and Meyerhof (1969) which is reduced by 6% for comparison with a smooth footing as suggested by Wang and Carter (2001) (Table 4.26).

Case 5: $c_2/c_1 = 1/3$ - Small Deformation Analysis

The near downward vertical direction of the velocity vectors shown in Figure A.338 indicates a punching shear failure of the foundation, with punching through the stronger top clay layer.

The clustering of plasticity indicators yielded in shear around the edge of the footing in Figure A.339 supports the punching shear type failure in the strong top clay. The zone underneath the footing showing no plasticity indicators or elastic indicators represents the elastic wedge of the stiff top clay trapped under the footing which pushes into the bottom soft clay. The zone of failure extends deep into the soft clay layer. The depth of failure $\simeq D$, and the horizontal extent of plastic yielding is $\simeq 0.95$ m from the centre of the footing.

Figure A.340 shows the magnified grid which further supports punching shear failure of the foundation through the stronger clay layer followed by some lateral and vertical movement of the soil in the bottom clay layer. The undeformed grid underneath the footing represents the elastic soil wedge which pushes into the soft bottom clay.

Figure A.341 shows the equal vertical stress (σ_{yy}) contours and zone of influence under the strip footing. The zone of influence for this case was found to be $\simeq 1.75D$. Since the failure mechanism is a punching through the top layer into the bottom layer, the high stress contours concentrate around the edge of the footing. A big bulging of 10 kPa contour at the interface of the two soil layer also supports the punching shear type failure.

The bearing pressure versus footing penetration recorded at different time steps in the history of the model is shown in Figure A.138. The ultimate bearing pressure (q_u) for this case was found to be 65.15 kPa. The modified bearing capacity factor $N_c^* = 3.26$ from present analysis is 21.93% higher than the bearing capacity factor for rough circular footing given by Brown and Meyerhof (1969) which is reduced by 6% for comparison with a smooth footing as suggested by Wang and Carter (2001) (Table 4.26).

Case 6: $c_2/c_1 = 0.2$ - Small Deformation Analysis

The downwards vertical direction of velocity vectors underneath the footing in the top clay shows the punching shear failure through the strong top clay (refer Figure A.343). The direction of the velocity vectors is also vertically downwards underneath the footing in the top part of the soft clay. This shows that the elastic wedge of the top clay trapped under the footing pushes deeper into the soft clay. The lateral and vertical upward flow in the bottom soft clay tries to lift the overlying strong clay crust.

The alignment of the plasticity indicators yielded in shear under the edge of the footing in Figure A.344 also supports the idea of the footing punching through the top clay layer The zone showing no plasticity indicators or some elastic indicators of yielding in past represents the elastic column of the top clay layer trapped under the footing and pushing into the soft clay layer. The depth of failure $\simeq 1.5D$. The horizontal extent of plastic yielding is $\simeq 1.15$ m from the centre of the footing.

Figure A.345 shows the magnified grid which again indicates punching shear failure of the foundation through the stronger clay layer followed by some lateral and vertical movement of the soil in the bottom clay layer. The undeformed grid underneath the footing represents the elastic column of the strong top clay layer which pushes into the soft clay layer. It can be noticed that there is no soil heaving at the side of the footing, however the soft clay layer uniformly lifts up the strong top clay.

Figure A.346 shows the equal vertical stress (σ_{yy}) contours and zone of influence under the strip footing. Since the failure mechanism is by punching of the footing through the top layer into the bottom layer, the high stress contours concentration is around the edge of the footing. The zone of influence for this case was found to be $\simeq 1.75D$.

The bearing pressure versus footing penetration recorded at different time steps in the history of the model is shown in Figure A.347. The ultimate bearing pressure (q_u) for this case was found to be 48.57 kPa. This reduction in the bearing capacity value also explains punching shear type failure where the top clay layer has very little contribution in the bearing capacity of the foundation. The modified bearing capacity factor $N_c^* = 2.43$ from present analysis is 22.73% higher than the bearing capacity factor for rough circular footing given by Brown and Meyerhof (1969) which is reduced by 6% for comparison with a smooth footing as suggested by Wang and Carter (2001) (Table 4.26).

Case 7: $c_2/c_1 = 0.1$ - Small Deformation Analysis

The vertically downwards velocity vectors underneath the footing shown in Figure A.348 continues to indicate a punching shear failure with the footing punching through the stiff crust of the top clay layer followed by plastic flow in the bottom soft layer.

The alignment of the plasticity indicators in shear under the edge of the footing in Figure A.349 supports the full punching of the footing through the top clay layer. A zone of the plasticity indicators showing yielding in past representing the insitu conditions is an elastic column of clay layer trapped underneath the footing. The yielding in shear does not extend to the ground, the stiff top clay crust restricts it. This results in lateral spreading of yielding in soft clay layer. The depth of failure $\simeq 1.2D$. The horizontal extent of plastic yielding is $\simeq 1.4\,\mathrm{m}$ from the centre of the footing.

Figure A.350 shows the magnified grid which further supports the punching shear failure. An undeformed grid underneath the footing represents the elastic column of the strong top clay pushing deeper into the bottom clay causing it to move both vertically and laterally away from the footing. A bend in the grid at the interface of the two clay layers underneath the footing also supports the punching shear failure. It can be noticed there is no soil heave at the side of the footing, however due to the soft clay trying to flow upwards but restricted by the stiff top clay layer ends up small uniform lifting of the top clay layer.

Figure A.351 shows the equal vertical stress (σ_{yy}) contours and zone of influence under the strip footing. Most of the high stress contours concentrate around the edge of the footing, once again supporting the punching shear failure mechanism. The zone of influence for this case was found to be $\simeq 1.2D$.

The bearing pressure versus footing penetration recorded at different time steps in the history of the model is shown in Figure A.352. The ultimate bearing pressure (q_u) for this case was found to be 33.11 kPa. This reduction in the bearing capacity value is due to the punching shear failure mechanism in which the strong top clay layer has negligible contribution towards the bearing capacity value. The modified bearing capacity factor $N_c^* = 1.66$ which is 20.84% higher than the bearing capacity factor for rough circular footing given by Brown and Meyerhof (1969) which is reduced by 6% for comparison with a smooth footing as suggested by Wang and Carter (2001) (Table 4.26).

4.4 Circular Footing on Soft Clay Overlying Strong Clay

This situation may occur where soft glacial lake clay overlies stiff till deposits. An axisymmetric analyses of the circular footing resting on the ground surface of soft clay overlying a stiff clay was investigated in this section. The failure mechanism in rigid circular footing on soft over strong clay system is either a general shear failure or a failure in which soft clay is squeezed out laterally between the footing and the bottom strong clay layer. The type of failure depends on the H/D and c_1/c_2 ratios. As it can be seen in 4.4.1, if the top strong clay layer is thick enough (i.e. $H \geq 1$) the failure mechanism is entirely contained in the top soft clay layer for all value of $c_1/c_2 \leq 1$, and the bearing capacity is $q_u = N_c^* c_1$ where the modified bearing capacity factor $N_c^* = 5.61$ (Table 4.13). For $H/D < 1$, as the H/D ratio decreases or the upper soft layer becomes thinner, the bearing capacity increases (Table 4.15 & 4.17). The effect of the top clay thickness (H) on the ultimate bearing capacity (q_u) of the foundation is shown in form of modified bearing capacity factor (N_c^*) in Figure 4.36.

Model Geometry A 40×30 elements grid similar to that in 4.3 is adopted for this analysis. The model geometry is same as shown in Figure A.239.

4.4.1 Rigid Smooth Circular Footing on Soft over Strong Clay ($H/D = 1$)

Various undrained shear strength ratios of top layer (c_1) to bottom layer (c_2) considered are $0.1, 0.2, 1/3, 0.5, 2/3, 0.8$, and 1. The ultimate bearing pressures for various c_1/c_2 ratios have been obtained from the FLAC model history files. The modified bearing capacity factor N_c^* is calculated as in A.2 for the present analyses (Table 4.28).

Table 4.28: Comparison of modified Bearing Capacity Factor, N_c^* with existing values for rigid circular footing soft on over strong clay for grid 40×30, for $H/D = 1$.

Shear Strength Top Layer, (c_1)	Shear Strength Ratio, (c_1/c_2)	q_u (FLAC)	N_c^*(FLAC) = q_u(FLAC)/c_1	N_c		% Difference between N_c^*(FLAC) & N_c	
				(Brown & Meyerhof 1969)[14]	(Vesic 1975)[15]	(Brown & Meyerhof 1969)	(Vesic 1975)[16]
20.00	1.00	112.20	5.61	5.69	5.80	−1.34	−3.38
20.00	0.80	112.22	5.61	5.69	5.80	−1.34	−3.38
20.00	0.67	112.21	5.61	5.69	5.80	−1.34	−3.38
20.00	0.50	112.20	5.61	5.69	5.80	−1.34	−3.38
20.00	0.33	112.21	5.61	–	5.80	–	−3.38
20.00	0.20	112.21	5.61	–	5.80	–	−3.38
20.00	0.10	112.23	5.61	–	5.80	–	−3.38

[14] Values reduced by 6% for smooth footing (Wang and Carter 2001)
[15] Values reduced by 6% for smooth footing (Wang and Carter 2001)

Figure 4.34 shows the comparison of the modified bearing capacity factor (N_c^*) versus shear strength ratios computed from FLAC with those from literature.

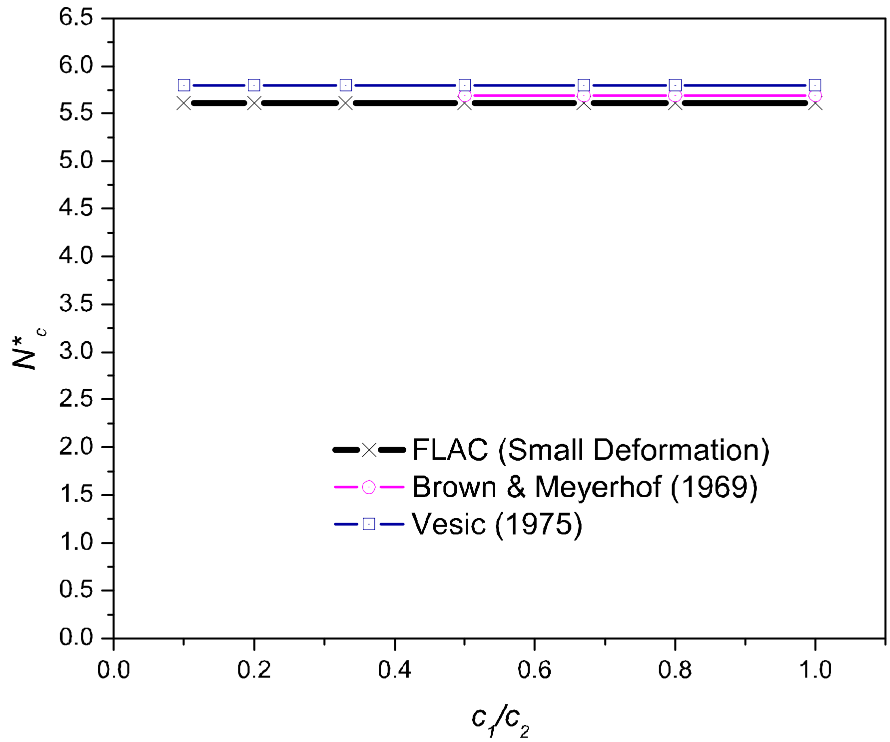

Figure 4.34: Modified bearing capacity factor (N_c^*) versus shear strength ratio (c_1/c_2) curves for a rigid smooth circular footing on soft over strong clay for 40×30 grid model, $H/D = 1$.

The normalised bearing pressure versus penetration curves for different shear strength ratios are shown in Figure 4.35.

The failure mechanisms for shear strength ratios of $c_1/c_2 = 0.8, 2/3, 0.5, 1/3, 0.2$ and 0.1 are summarised in Table 4.29.

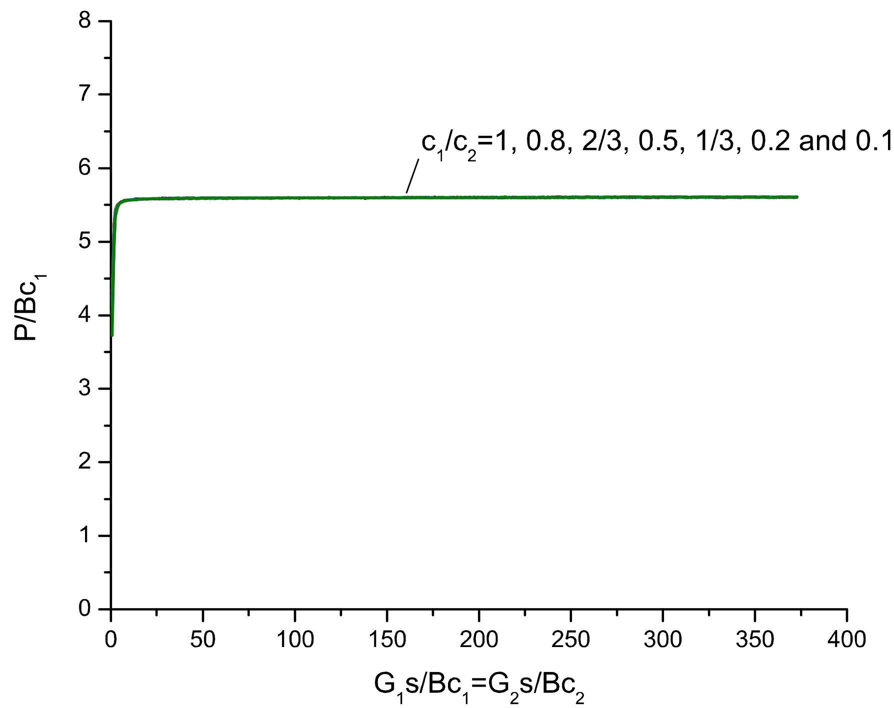

Figure 4.35: Normalised bearing pressure versus penetration curves for a rigid smooth circular footing on strong clay over strong clay for 40×30 grid model, $H/D = 1$.

Case 1: c_1/c_2 or $c_2/c_1 = 1$ (Homogeneous clay) - Small Deformation Analysis

Since this is case of circular footing resting on the homogeneous clay the behavior and the analysis results are the same as in 4.3.1.

Case 2: $c_1/c_2 = 0.8$ or $c_2/c_1 = 1.25$ - Small Deformation Analysis

The velocity vectors shown in Figure A.353 indicate a general shear type failure with plastic flow of the softer clay in the upper layer away from the centre of the foundation.

The plasticity state indicators in Figure A.354 show that the zone of failure is contained in the upper soft clay layer. The plastic yielding in shear starts underneath the footing and then spreads downwards and outwards. The yielding in tension zone

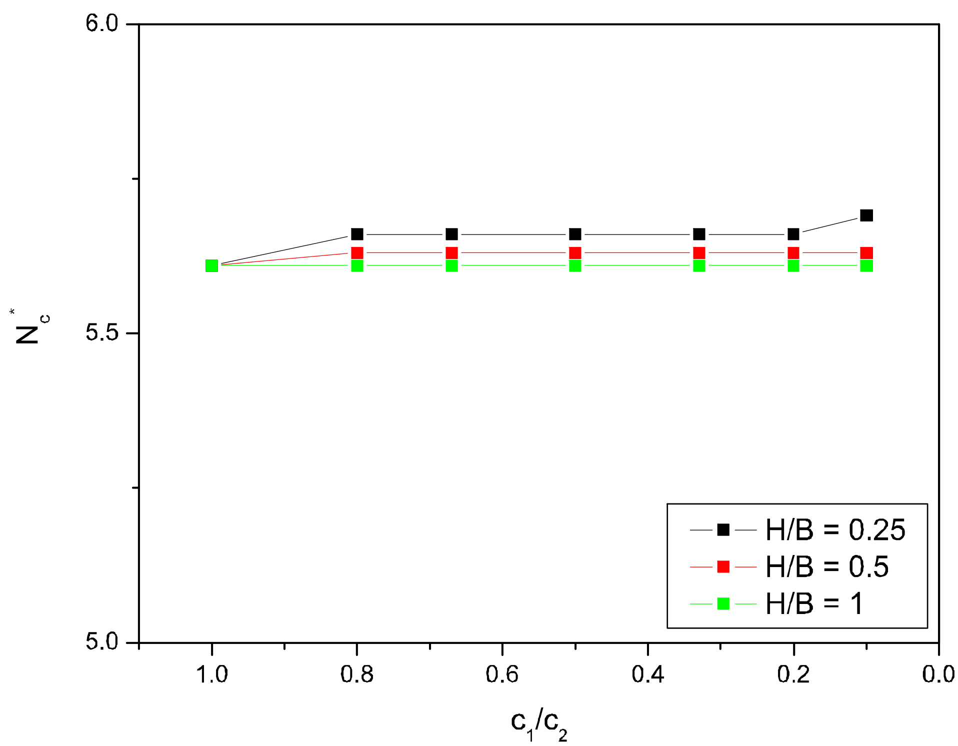

Figure 4.36: Modified bearing capacity factor (N_c^*) versus shear strength ratio (c_1/c_2) curves for a rigid smooth circular footing on soft over strong clay for 40 × 30 grid model, for various H/D ratios.

Table 4.29: Failure modes for different shear strength ratios (c_1/c_2) for $H/D = 1$.

Shear Strength Ratio, (c_1/c_2)	Failure Modes
0.80	General shear type failure
0.67	General shear type failure
0.50	General shear type failure
0.33	General shear type failure
0.20	General shear type failure
0.10	General shear type failure

next to the yielding in shear represents the heave on the side of the footing. The depth of the failure is found to be $\simeq 0.4D$, , and the horizontal extent of plastic yielding is $\simeq 0.7$ m from the centre of the footing.

Figure A.355 shows the magnified grid which further indicates a general shear type failure of the foundation with some soil heave at the side of the footing. The grid deformation is contained in the upper clay layer.

Figure A.356 shows the equal vertical stress (σ_{yy}) contours and zone of influence under the strip footing. The zone of influence for this case was found to be $\simeq 1.4D$. As in the case of stronger clay layer overlying a softer clay layer (refer 4.3) the shapes of the contours are not very smooth.

The bearing pressure versus footing penetration recorded at different time steps in the history of the model is shown in Figure A.357. The ultimate bearing pressure (q_u) for this case was found to be 112.22 kPa. The modified bearing capacity factor $N_c^* = 5.61$ which is 1.34% lower than the bearing capacity factor for rough circular footing given by Brown and Meyerhof (1969) which is reduced by 6% for comparison with a smooth footing as suggested by Wang and Carter (2001) (Table 4.28).

Case 3: $c_1/c_2 = 2/3$ or $c_2/c_1 = 1.5$ - Small Deformation Analysis

Figure A.358 again show general shear type failure with some plastic flow away from the centre of the foundation. The upwards vertical direction of the velocity vectors on the side of the footing represents the soil heave.

The plasticity state indicators in Figure A.359 show that the zone of failure is contained in the upper soft clay layer. The plastic yielding in shear starts underneath the footing and then spreads downwards and outwards. The yielding in tension zone next to the yielding in shear represents the heave on the side of the footing. The depth of the failure is found to be $\simeq 0.4D$, and the horizontal extent of plastic yielding is $\simeq 0.7$ m from the centre of the footing.

Figure A.360 shows the magnified grid which further indicates a general shear type failure of the foundation with some soil heave at the edge of the footing. The grid deformation is limited to the upper softer clay layer.

Figure A.361 shows the equal vertical stress (σ_{yy}) contours and zone of influence under the strip footing. The zone of influence for this case was found to be $\simeq 1.4D$.

The bearing pressure versus footing penetration recorded at different time steps in the history of the model is shown in Figure A.362. The ultimate bearing pressure (q_u) for this case was found to be 112.21 kPa. The modified bearing capacity factor $N_c^* = 5.61$ which is 1.34% lower than the bearing capacity factor for rough circular footing given by Brown and Meyerhof (1969) which is reduced by 6% for comparison with a smooth footing as suggested by Wang and Carter (2001) (Table 4.28).

Case 4: $c_1/c_2 = 0.5$ or $c_2/c_1 = 2$ - Small Deformation Analysis

The velocity vectors shown in Figure A.363 once again indicate general shear type failure with some plastic flow away from the centre of the foundation.

The plasticity state indicators in Figure A.364 show that the zone of failure is contained in the top soft clay layer. The plastic yielding in shear starts underneath the footing and then spreads downwards and outwards. The yielding in tension zone next to the yielding in shear represents the heave on the side of the footing. The depth of the failure is found to be $\simeq 0.4D$ and the horizontal extent of plastic yielding is $\simeq 0.75$ m from the centre of the footing.

Figure A.365 shows the magnified grid which indicates general shear type failure of the foundation with some soil heave at the edge of the footing. The grid deformation once again is contained in the softer upper clay layer.

Figure A.366 shows the equal vertical stress (σ_{yy}) contours and zone of influence under the strip footing. The zone of influence for this case was found to be $\simeq 1.4D$.

The bearing pressure versus footing penetration recorded at different time steps in the history of the model is shown in Figure A.367. The ultimate bearing pressure (q_u) for this case was found to be 112.20 kPa. The modified bearing capacity factor $N_c^* = 5.61$ which is 1.34% lower than the bearing capacity factor for rough circular footing given by Brown and Meyerhof (1969) which is reduced by 6% for comparison with a smooth footing as suggested by Wang and Carter (2001) (Table 4.28).

Case 5: $c_1/c_2 = 1/3$ or $c_2/c_1 = 3$ - Small Deformation Analysis

The velocity vectors shown in Figure A.368 continues to indicate a general shear type failure with some plastic flow away from the centre of the foundation. The upwards vertical direction of the velocity vectors on the side of the footing represents the soil heave.

The plasticity state indicators in Figure A.369 show that the zone of failure is contained in top soft clay layer. The depth of the failure is found to be $\simeq 0.4D$, and the horizontal extent of plastic yielding is $\simeq 0.7$ m from the centre of the footing.

In Figure A.370 the magnified grid further indicates a general shear type failure of the foundation with some soil heave at the edge of the footing.

Figure A.371 shows the equal vertical stress (σ_{yy}) contours and zone of influence under the strip footing. The zone of influence for this case was found to be $\simeq 1.4D$.

The bearing pressure versus footing penetration recorded at different time steps in the history of the model is shown in Figure A.372. The ultimate bearing pressure (q_u) for this case was found to be 112.21 kPa. The modified bearing capacity factor $N_c^* = 5.61$ which is 3.38% lower than the bearing capacity factor for rough circular footing given by Vesic (1975) which is reduced by 6% for comparison with a smooth footing as suggested by Wang and Carter (2001) (Table 4.28).

Case 6: $c_1/c_2 = 0.2$ **or** $c_2/c_1 = 5$ **- Small Deformation Analysis**

The velocity vectors shown in Figure A.373 also indicate general shear type failure with some plastic flow downwards and away from the centre of the foundation. The upwards vertical direction of the velocity vectors on the side of the footing represents the soil heave.

The plasticity state indicators in Figure A.374 show that the zone of failure is contained in top soft clay layer. The depth of the failure is found to be $\simeq 0.4D$, and the horizontal extent of plastic yielding is $\simeq 0.7\,\text{m}$ from the centre of the footing.

Figure A.375 shows the magnified grid which also indicates general shear type failure of the foundation with some soil heave at the edge of the footing. The grid deformation is limited to the upper softer clay layer.

Figure A.376 shows the equal vertical stress (σ_{yy}) contours and zone of influence under the strip footing. The zone of influence for this case was found to be $\simeq 1.4D$.

The bearing pressure versus footing penetration recorded at different time steps in the history of the model is shown in Figure A.377. The ultimate bearing pressure (q_u) for this case was found to be 112.21 kPa. The modified bearing capacity factor $N_c^* = 5.61$ which is 3.38% lower than the bearing capacity factor for rough circular footing given by Vesic (1975) which is reduced by 6% for comparison with a smooth footing as suggested by Wang and Carter (2001) (Table 4.28).

Case 7: $c_1/c_2 = 0.1$ **or** $c_2/c_1 = 10$ **- Small Deformation Analysis**

The velocity vectors shown in Figure A.378 like all earlier c_1/c_2 ratios, continue to show general shear type failure with some plastic flow downwards and away from the centre of the foundation.

The plasticity state indicators in Figure A.379 show that the zone of failure is contained in the upper soft clay layer. The plastic yielding in shear starts underneath the footing and then spreads downwards and outwards. The yielding in tension zone next to the yielding in shear represents the heave on the side of the footing. The depth of the failure is found to be $\simeq 0.4D$, and the horizontal extent of plastic yielding is $\simeq 0.7\,\text{m}$ from the centre of the footing.

Figure A.380 shows the magnified grid which also indicates the general shear failure of the foundation with some soil heave at the edge of the footing. The grid deformation is contained in upper softer clay layer.

Figure A.381 shows the equal vertical stress (σ_{yy}) contours and zone of influence under the strip footing. The zone of influence for this case was found to be $\simeq 1.4D$.

The bearing pressure versus footing penetration recorded at different time steps in the history of the model is shown in Figure A.382. The ultimate bearing pressure (q_u) for this case was found to be 112.23 kPa. The modified bearing capacity factor $N_c^* = 5.61$ which is 3.38% lower than the bearing capacity factor for rough circular footing given by Vesic (1975) which is reduced by 6% for comparison with a smooth footing as suggested by Wang and Carter (2001) (Table 4.28).

4.3.1 was considered as the base case for studying the effect of the thickness of the stronger top clay layer. Since the bearing capacity is unchanged and is equal to that of homogeneous case, the thickness of the top soft clay layer is then decreased as $H < D$ ($H/D = 0.5$ & 0.25).

4.4.2 Rigid Smooth Circular Footing on Soft over Strong Clay ($H/D = 0.5$)

Case 1: c_1/c_2 or $c_2/c_1 = 1$ (Homogeneous clay) - Small Deformation Analysis

Since this is the case of homogeneous clay all the results will be same as Case 1 (4.4.1). The FLAC analysis results for other cases of c_2/c_1 are explained below.

Case 2: $c_1/c_2 = 0.8$ or $c_2/c_1 = 1.25$ - Small Deformation Analysis

The velocity vectors shown in Figure A.383 indicate general shear type failure with some plastic flow away from the centre of the foundation.

The plasticity state indicators in Figure A.384 show that the zone of failure is contained in the upper soft clay layer, however it is extending deeper and is just above the bottom strong clay layer. The plastic yielding in shear starts underneath the footing and then spreads downwards and outwards. The yielding in tension zone next to the yielding in shear represents the heave on the side of the footing. The depth of the failure is found to be $\simeq 0.45D$, and the horizontal extent of plastic yielding is $\simeq 0.75\,\mathrm{m}$ from the centre of the footing.

Figure A.385 shows the magnified grid which indicates the general shear type failure of the foundation with some soil heave at the edge of the footing. The deformation is still limited to the upper softer clay layer.

Figure A.386 shows the equal vertical stress (σ_{yy}) contours and zone of influence under the strip footing. The zone of influence for this case was found to be $\simeq 1.5D$.

The bearing pressure versus footing penetration recorded at different time steps in the history of the model is shown in Figure A.387. The ultimate bearing pressure (q_u) for this case was found to be 112.52 kPa. The modified bearing capacity factor $N_c^* = 5.63$ which is 0.98% lower than the bearing capacity factor for rough circular footing given by Brown and Meyerhof (1969) which is reduced by 6% for comparison with a smooth footing as suggested by Wang and Carter (2001) (Table 4.30).

Table 4.30: Comparison of modified Bearing Capacity Factor, N_c^* with existing values for rigid circular footing on soft over strong clay for grid 40×30, for $H/D = 0.5$.

Shear Strength Top Layer, (c_1)	Shear Strength Ratio, (c_1/c_2)	q_u (FLAC)	N_c^*(FLAC) = q_u(FLAC)/c_1	N_c		% Difference between N_c^*(FLAC) & N_c	
				(Brown & Meyerhof 1969)[17]	(Vesic 1975)[18]	(Brown & Meyerhof 1969)	(Vesic 1975)[19]
20.00	1.00	112.20	5.61	5.69	5.80	−1.34	−3.38
20.00	0.80	112.52	5.63	5.69	5.80	−0.98	−3.02
20.00	0.67	112.51	5.63	5.69	5.80	−0.98	−3.02
20.00	0.50	112.52	5.63	5.69	5.80	−0.98	−3.02
20.00	0.33	112.59	5.63	–	5.80	–	−3.02
20.00	0.20	112.57	5.63	–	5.80	–	−3.02
20.00	0.10	112.55	5.63	–	5.80	–	−3.02

[16] Values reduced by 6% for smooth footing (Wang and Carter 2001)
[17] Values reduced by 6% for smooth footing (Wang and Carter 2001)

Figure 4.37 shows the comparison of modified bearing capacity factor (N_c^*) versus shear strength ratios computed from FLAC with those from literature.

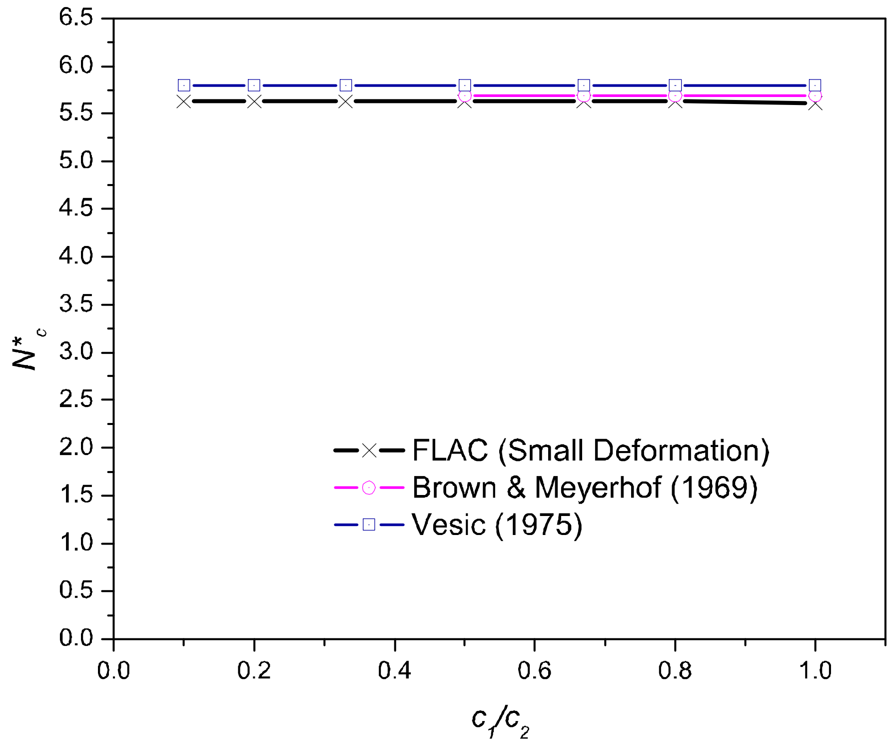

Figure 4.37: Modified bearing capacity factor (N_c^*) versus shear strength ratio (c_1/c_2) curves for a rigid smooth circular footing on soft clay over strong clay for 40×30 grid model, $H/D = 0.5$.

The normalised bearing pressure versus penetration curves for different shear strength ratios are shown in Figure 4.38.

The failure mechanisms for shear strength rations of $c_1/c_2 = 0.8, 2/3, 0.5, 1/3, 0.2$ and 0.1 are summarised in Table 4.31.

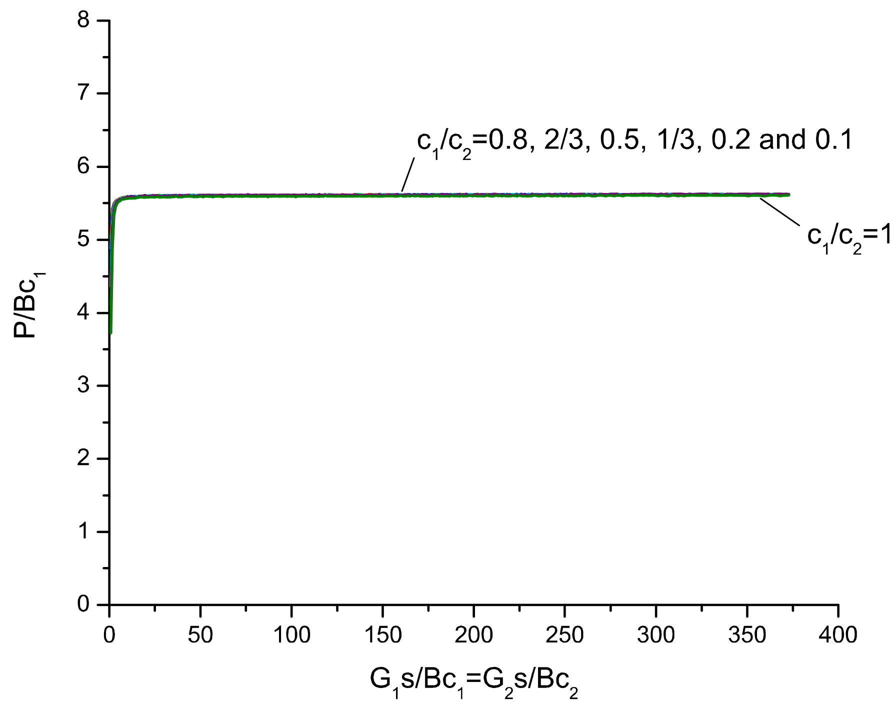

Figure 4.38: Normalised bearing pressure versus penetration curves for a rigid smooth circular footing on soft clay over strong clay for 40 $\times$ 30 grid model, $H/D = 0.5$.

Case 3: $c_1/c_2 = 2/3$ **or** $c_2/c_1 = 1.5$ **- Small Deformation Analysis**

The velocity vector field in Figure A.388 also shows a general shear type failure with some plastic flow away from the centre of the foundation. The upwards pointing velocity vectors on the side of the footing represents the soil heave.

The plasticity state indicators in Figure A.389 show that the zone of failure extends deeper into the soft clay layer. The depth of failure $\simeq 1.75B$, and the horizontal extent of plastic yielding is $\simeq 2.5\,\text{m}$ from the centre of the footing.

Figure A.390 shows the magnified grid which indicates the idea of a general shear failure of the foundation with some soil heave at the edge of the footing. The grid deformation is limited to the upper softer clay layer.

Figure A.391 shows the equal vertical stress (σ_{yy}) contours and zone of influence

Table 4.31: Failure modes for different shear strength ratios (c_1/c_2) for $H/D = 0.5$.

Shear Strength Ratio, (c_1/c_2)	Failure Modes
0.80	General shear type failure
0.67	General shear type failure
0.50	General shear type failure
0.33	General shear type failure
0.20	General shear type failure
0.10	General shear type failure

under the strip footing. The zone of influence for this case was found to be $\simeq 1.5D$.

The bearing pressure versus footing penetration recorded at different time steps in the history of the model is shown in Figure A.392. The ultimate bearing pressure (q_u) for this case was found to be 112.51 kPa. The modified bearing capacity factor $N_c^* = 5.63$ which is 0.98% lower than the bearing capacity factor for rough circular footing given by Brown and Meyerhof (1969) which is reduced by 6% for comparison with a smooth footing as suggested by Wang and Carter (2001) (Table 4.30).

Case 4: $c_1/c_2 = 0.5$ or $c_2/c_1 = 2$ - Small Deformation Analysis

The velocity vectors shown in Figure A.393 again indicate a general shear type failure with some plastic flow away from the centre of the foundation. The upwards vertical direction of the velocity vectors on the side of the footing represents soil heave.

The plasticity state indicators in Figure A.394 show that the zone of failure is contained in the upper soft clay layer. The plastic yielding in shear starts underneath the footing and then spreads downwards and outwards. The yielding in tension zone next to the yielding in shear represents the heave on the side of the footing. The depth of the failure is found to be $\simeq 0.45D$, and the horizontal extent of plastic yielding is $\simeq 0.7$ m from the centre of the footing.

Figure A.395 shows the magnified grid which indicates general shear failure of the foundation with some soil heave at the edge of the footing.

Figure A.396 shows the equal vertical stress (σ_{yy}) contours and zone of influence

under the strip footing. The zone of influence for this case was found to be $\simeq 1.5D$.

The bearing pressure versus footing penetration recorded at different time steps in the history of the model is shown in Figure A.397. The ultimate bearing pressure (q_u) for this case was found to be 112.52 kPa. The modified bearing capacity factor $N_c^* = 5.63$ which is 0.98% lower than the bearing capacity factor for rough circular footing given by Brown and Meyerhof (1969) which is reduced by 6% for comparison with a smooth footing as suggested by Wang and Carter (2001) (Table 4.30).

Case 5: $c_1/c_2 = 1/3$ or $c_2/c_1 = 3$ - Small Deformation Analysis

The velocity vectors shown in Figure A.398 continues to indicate a general shear type failure with some plastic flow away from the centre of the foundation.

The plasticity state indicators in Figure A.399 show that the zone of failure extends into the soft clay layer. The plastic yielding in shear starts underneath the footing and then spreads downwards deeper just above the top of the stronger bottom clay layer and outwards. The yielding in tension zone next to the yielding in shear represents the heave on the side of the footing. The depth of the failure is found to be $\simeq 0.45D$, and the horizontal extent of plastic yielding is $\simeq 0.7$ m from the centre of the footing.

Figure A.400 shows the magnified grid which supports the local shear failure of the foundation with some soil heave at the edge of the footing. The deformation of the grid is still contained in the top softer clay layer.

Figure A.401 shows the equal vertical stress (σ_{yy}) contours and zone of influence under the strip footing. The zone of influence for this case was found to be $\simeq 1.5D$.

The bearing pressure versus footing penetration recorded at different time steps in the history of the model is shown in Figure A.402. The ultimate bearing pressure (q_u) for this case was found to be 112.59 kPa. The modified bearing capacity factor $N_c^* = 5.63$ which is 3.02% lower than the bearing capacity factor for rough circular footing given by Vesic (1975) which is reduced by 6% for comparison with a smooth footing as suggested by Wang and Carter (2001) (Table 4.30).

Case 6: $c_1/c_2 = 0.2$ **or** $c_2/c_1 = 5$ **- Small Deformation Analysis**

The velocity vectors shown in Figure A.403 also indicate general shear type failure with some plastic flow away from the centre of the foundation.

The plasticity state indicators in Figure A.404 show that the zone of failure extends deeper into the soft clay layer reaching just above the top of stronger clay layer. The depth of the failure is found to be $\simeq 0.45D$, and the horizontal extent of plastic yielding is $\simeq 0.7$ m from the centre of the footing.

Figure A.405 shows the magnified grid which indicates the idea of a general shear failure of the foundation with some soil heave at the edge of the footing. Once again the deformation is limited to the upper softer clay layer.

Figure A.406 shows the equal vertical stress (σ_{yy}) contours and zone of influence under the strip footing. The zone of influence in this case was found to be $\simeq 1.5D$.

The bearing pressure versus footing penetration recorded at different time steps in the history of the model is shown in Figure A.407. The ultimate bearing pressure (q_u) for this case was found to be 112.57 kPa. The modified bearing capacity factor $N_c^* = 5.63$ which is 3.02% lower than the bearing capacity factor for rough circular footing given by Vesic (1975) which is reduced by 6% for comparison with a smooth footing as suggested by Wang and Carter (2001) (Table 4.30).

Case 7: $c_1/c_2 = 0.1$ **or** $c_2/c_1 = 10$ **- Small Deformation Analysis**

The velocity vector field shown in Figure A.408 continue to show a general shear type failure with some plastic flow away from the centre of the foundation. The upward direction of the velocity vectors on the side of the footing represents the soil heave.

The plasticity state indicators in Figure A.409 show that the zone of failure extends into the soft clay layer. The depth of the failure is found to be $\simeq 0.45D$, and the horizontal extent of plastic yielding is $\simeq 0.75$ m from the centre of the footing.

Figure A.410 shows the magnified grid which indicates a general shear type failure of the foundation with some soil heave at the edge of the footing.

Figure A.411 shows the equal vertical stress (σ_{yy}) contours and zone of influence under the strip footing. The zone of influence in this case was found to be $\simeq 1.5D$.

The bearing pressure versus footing penetration recorded at different time steps in the history of the model is shown in Figure A.412. The ultimate bearing pressure (q_u) for this case was found to be 112.55 kPa. The modified bearing capacity factor $N_c^* = 5.63$ which is 3.02% lower than the bearing capacity factor for rough circular footing given by Vesic (1975) which is reduced by 6% for comparison with a smooth footing as suggested by Wang and Carter (2001) (Table 4.30).

4.4.3 Rigid Smooth Circular Footing on Soft over Strong Clay ($H/D = 0.25$)

Case 1: c_1/c_2or $c_2/c_1 = 1$ (Homogeneous clay) - Small Deformation Analysis

Since this is the case of homogeneous clay all the results will be same as Case 1 (4.4.1). The FLAC analysis results for other cases of c_2/c_1 are explained below.

Case 2: $c_1/c_2 = 0.8$ or $c_2/c_1 = 1.25$ - Small Deformation Analysis

The velocity vectors shown in Figure A.413 indicate a failure of a foundation with lateral plastic flow of the soft clay under the footing similar to that when a solid is squeezed between two plates. The vertical direction of the velocity vectors on the side of the footing represents the heave squeezed out clay is causing.

The plasticity state indicators in Figure A.414 show that the zone of failures extends deep in soft clay layer, just reaching the top of the bottom strong clay layer. The depth of the failure is found to be $\simeq 0.25D$ and the horizontal extent of plastic yielding is $\simeq 0.6\,\text{m}$ from the centre of the footing.

Figure A.415 shows the magnified grid which further indicates a squeezing type of failure. The deformation in the upper soft clay layer reaches to the top of lower strong clay layer.

Figure A.416 shows the equal vertical stress (σ_{yy}) contours and zone of influence under the strip footing. The zone of influence for this case was found to be $\simeq 1.35D$.

The bearing pressure versus footing penetration recorded at different time steps in the history of the model is shown in Figure A.417. The ultimate bearing pressure (q_u) for this case was found to be 113.13 kPa. The modified bearing capacity factor $N_c^* = 5.66$ which is 2.47% lower than the bearing capacity factor for rough circular footing given by Vesic (1975) which is reduced by 6% for comparison with a smooth footing as suggested by Wang and Carter (2001) (Table 4.32).

Table 4.32: Comparison of modified Bearing Capacity Factor, N_c^* with existing values for rigid circular footing on soft over strong clay for grid 40×30, for $H/D = 0.25$.

Shear Strength Top Layer, (c_1)	Shear Strength Ratio, (c_1/c_2)	q_u (FLAC)	N_c^*(FLAC) = q_u(FLAC)/c_1	N_c (Vesic 1975)[20]	% Difference between N_c^*(FLAC) & N_c (Vesic 1975)
20.00	1.00	112.20	5.61	5.80	−3.38
20.00	0.80	113.13	5.66	5.80	−2.47
20.00	0.67	113.17	5.66	5.80	−2.47
20.00	0.50	113.19	5.66	5.80	−2.47
20.00	0.33	113.19	5.66	5.80	−2.47
20.00	0.20	113.21	5.66	5.80	−2.47
20.00	0.10	113.74	5.69	5.80	−1.93

[20] Values reduced by 6% for smooth footing (Wang and Carter 2001)

Figure 4.39 shows the comparison of the modified bearing capacity factor (N_c^*) versus shear strength ratios computed from FLAC with those from literature.

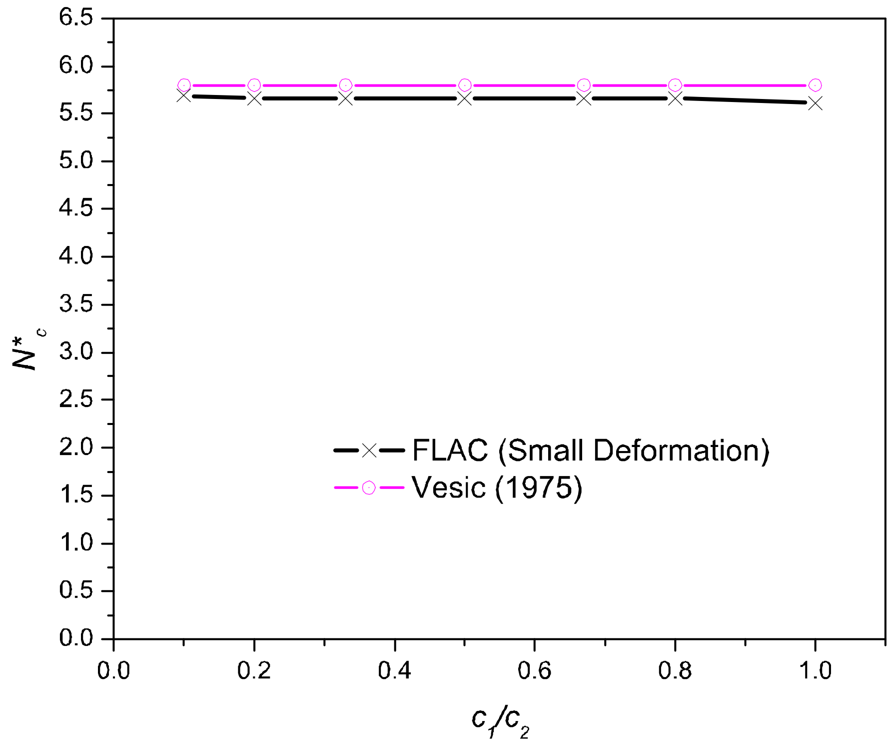

Figure 4.39: Modified bearing capacity factor (N_c^*) versus shear strength ratio (c_1/c_2) curves for a rigid smooth circular footing on soft clay over strong clay for 40×30 grid model, $H/D = 0.25$.

The normalised bearing pressure versus penetration curves for different shear strength ratios are shown in Figure 4.40.

The failure mechanisms for shear strength rations of $c_1/c_2 = 0.8, 2/3, 0.5, 1/3, 0.2$ and 0.1 are summarised in Table 4.33.

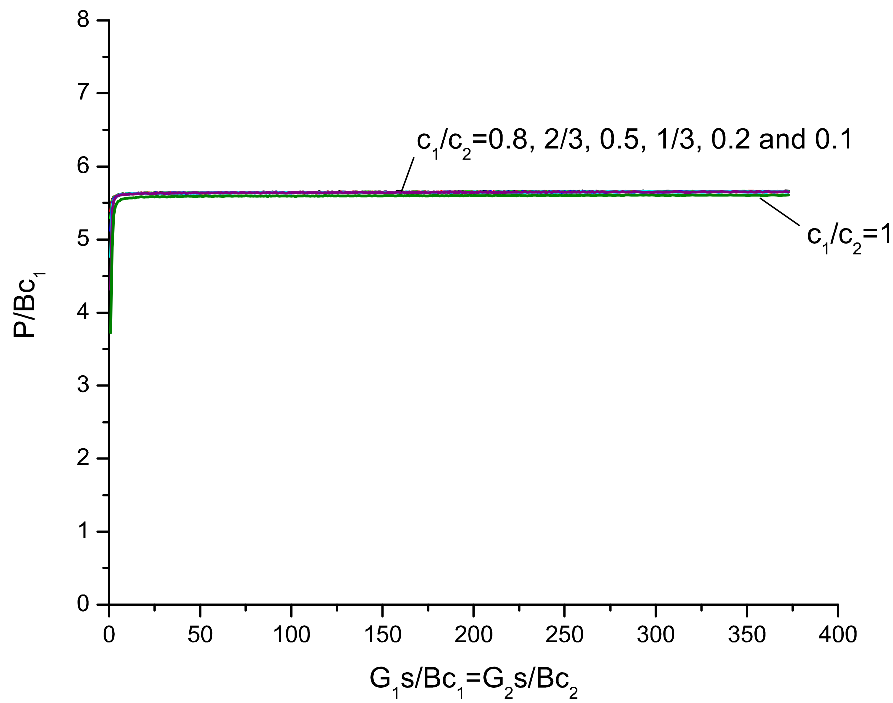

Figure 4.40: Normalised bearing pressure versus penetration curves for a rigid smooth circular footing on soft clay over strong clay for 40 × 30 grid model, $H/D = 0.25$.

Case 3: $c_1/c_2 = 2/3$ **or** $c_2/c_1 = 1.5$ **- Small Deformation Analysis**

The velocity vector field in Figure A.418 again shows a failure of a foundation by a lateral squeezing type plastic flow of the soft clay between the footing and strong bottom clay.

The plasticity state indicators in Figure A.419 show that the zone of failure extends to the strong clay layer. The depth of failure $\simeq 0.25D$ and the horizontal extent of plastic yielding is $\simeq 0.65\,\mathrm{m}$ from the centre of the footing.

Figure A.420 shows the magnified grid which further indicates squeezing type of failure in the upper clay layer.

Figure A.421 shows the equal vertical stress (σ_{yy}) contours and zone of influence under the strip footing. The zone of influence for this case was found to be $\simeq 1.35D$.

Table 4.33: Failure modes for different shear strength ratios (c_1/c_2) for $H/D = 0.25$.

Shear Strength Ratio, (c_1/c_2)	Failure Modes
0.80	A shear failure with squeezing out of softer clay
0.67	A shear failure with squeezing out of softer clay
0.50	A shear failure with squeezing out of softer clay
0.33	A shear failure with squeezing out of softer clay
0.20	A shear failure with squeezing out of softer clay
0.10	A shear failure with squeezing out of softer clay

The bearing pressure versus footing penetration recorded at different time steps in the history of the model is shown in Figure A.422. The ultimate bearing pressure (q_u) for this case was found to be 113.17 kPa. The modified bearing capacity factor $N_c^* = 5.66$ which is 2.47% lower than the bearing capacity factor for rough circular footing given by Vesic (1975) which is reduced by 6% for comparison with a smooth footing as suggested by Wang and Carter (2001) (Table 4.32).

Case 4: $c_1/c_2 = 0.5$ or $c_2/c_1 = 2$ - Small Deformation Analysis

The velocity vectors shown in Figure A.423 also show a failure of the foundation by lateral plastic flow of the soft clay under the footing.

The plasticity state indicators in Figure A.424 show that the zone of failure is contained in the upper soft clay extending to the top of lower strong clay layer. The depth of failure $\simeq 0.25D$, and the horizontal extent of plastic yielding $\simeq 0.6$ m from the centre of the footing.

Figure A.425 shows the magnified grid which further indicates a squeezing type of failure. The deformation in the upper soft clay layer reaches to the top of lower strong clay layer.

Figure A.426 shows the equal vertical stress (σ_{yy}) contours and zone of influence under the strip footing. The zone of influence for this case was found to be $\simeq 1.35D$.

The bearing pressure versus footing penetration recorded at different time steps in the history of the model is shown in Figure A.427. The ultimate bearing pressure

(q_u) for this case was found to be 113.19 kPa. The modified bearing capacity factor $N_c^* = 5.66$ which is 2.47% lower than the bearing capacity factor for rough circular footing given by Vesic (1975) which is reduced by 6% for comparison with a smooth footing as suggested by Wang and Carter (2001) (Table 4.32).

Case 5: $c_1/c_2 = 1/3$ or $c_2/c_1 = 3$ - Small Deformation Analysis

The velocity vectors shown in Figure A.428 continue to show a squeezing type of failure of the foundation.

The plasticity state indicators in Figure A.429 show that the zone of failure extends to the top of strong clay layer. The depth of failure $\simeq 0.25D$ and the horizontal extent of plastic yielding is $\simeq 0.6$ m from the centre of the footing.

Figure A.430 shows the magnified grid which further indicates the lateral plastic flow of the upper soft clay layer.

Figure A.431 shows the equal vertical stress (σ_{yy}) contours and zone of influence under the strip footing. The zone of influence for this case was found to be $\simeq 1.4D$.

The bearing pressure versus footing penetration recorded at different time steps in the history of the model is shown in Figure A.432. The ultimate bearing pressure (q_u) for this case was found to be 113.19 kPa. The modified bearing capacity factor $N_c^* = 5.66$ which is 2.47% lower than the bearing capacity factor for rough circular footing given by Vesic (1975) which is reduced by 6% for comparison with a smooth footing as suggested by Wang and Carter (2001) (Table 4.32).

Case 6: $c_1/c_2 = 0.2$ or $c_2/c_1 = 5$ - Small Deformation Analysis

The velocity vectors shown in Figure A.433 again show a failure of a foundation with a lateral squeezing type plastic flow of the soft clay between the footing and strong bottom clay.

The plasticity state indicators in Figure A.434 show that the zone of failure is contained in the upper soft clay, but extends to the top of lower strong clay layer. The depth of failure $\simeq 0.25D$ and the horizontal extent of plastic yielding is $\simeq 0.6$ m from the centre of the footing.

Figure A.435 shows the magnified grid indicates a lateral plastic flow of the upper soft clay layer.

Figure A.436 shows the equal vertical stress (σ_{yy}) contours and zone of influence under the strip footing. The zone of influence for this case was found to be $\simeq 1.4D$.

The bearing pressure versus footing penetration recorded at different time steps in the history of the model is shown in Figure A.437. The ultimate bearing pressure (q_u) for this case was found to be 113.21 kPa. The modified bearing capacity factor $N_c^* = 5.66$ which is 2.47% lower than the bearing capacity factor for rough circular footing given by Vesic (1975) which is reduced by 6% for comparison with a smooth footing as suggested by Wang and Carter (2001) (Table 4.32).

Case 7: $c_1/c_2 = 0.1$ or $c_2/c_1 = 10$ - Small Deformation Analysis

The velocity vectors shown in Figure A.438 like all above cases once again show a failure of a foundation with a lateral squeezing type plastic flow of the soft clay between the footing and strong bottom clay.

The plasticity state indicators in Figure A.439 show that the zone of failure extends to the top of strong clay layer. The depth of failure $\simeq 0.25D$, and the horizontal extent of plastic yielding is $\simeq 0.65$ m from the centre of the footing.

Figure A.440 shows the magnified grid which once again indicates the squeezing type failure of the foundation.

Figure A.441 shows the equal vertical stress (σ_{yy}) contours and zone of influence under the strip footing. The zone of influence for this case was found to be $\simeq 1.4D$.

The bearing pressure versus footing penetration recorded at different time steps in the history of the model is shown in Figure A.442. The ultimate bearing pressure (q_u) for this case was found to be 113.74 kPa. The modified bearing capacity factor $N_c^* = 5.69$ which is 1.93% lower than the bearing capacity factor for rough circular footing given by Vesic (1975) and is reduced by 6% for smooth footing as suggested by Wang and Carter (2001) (Table 4.32).

4.5 Strip Footing on Stiff Clay Overlying Soft Clay - Large Deformation Analysis

The large strain feature of FLAC (refer 3.1) is used in this section with goal of verifying the results of Wang and Carter (2001) for their large deformation analysis of a strip footing resting on strong over soft clay using finite element analysis (refer 2.4.1). The application of the Lagrangian formulation of FLAC to the shallow foundations and its inability to remesh the grid once distortion of the grid has occurred in large deformation analysis is studied and is explained in this section. An attempt is made to verify the results from FEM analysis of Wang and Carter (2001). This verification is not successful due the limitation of FLAC formulation. However, as shown in Figure 4.45 the analyses completed with combination of large strain and small strain modes are able to capture the early trend of curves from Wang and Carter (2001) and show that the bearing capacity values are of higher value in early stages of curve for $c_2/c_1 = 1$, but lower for $c_2/c_1 = 0.1$ than that predicted with the small strain analysis alone.

Model Geometry

The footing is assumed to be a rigid smooth footing. Due to the symmetry of the problem only half of the width of footing is considered and a half space model is used for the analysis. A 40×30 elements mesh and material properties similar to that for the small deformation analysis are selected for the large deformation analysis. A typical geometry of the model is shown in Figures A.239 and A.240.

4.5.1 Rigid Smooth Strip Footing on Strong over Soft Clay ($H/B = 1$)

Only two cases of undrained shear strength ratios $c_2/\ c_1 = 1$ and 0.1 are considered in this analysis to study the effectiveness of FLAC in large deformation analysis.

Case 1: $c_2/c_1 = 1$ (Homogeneous clay) - Large Deformation Analysis

Test 1: Large Strain Analysis

In the first test model mesh with material properties similar to Case 1 (4.1.1) were chosen. When the model was run in the large strain mode it ceased running after only 186620 timesteps, with "Bad Geometry" error signified as explained in 3.1. During large deformation the grid coordinates are constantly updated at every timestep and the zones in the foundation compress, stretch and rotate. In this process the zone ($i = 11, j = 30$) on the side of the footing became so distorted (Figures A.443 & A.444), that its shape exceeded the minimum undistorted area criterion (refer 3.1).

The above test showed the limitation of numerical analysis codes like FLAC based on Lagrangian formulations in handling large deformation analysis of bearing capacity of shallow foundations. In Lagrangian formulation, the grid deforms with the material as compared to the Eulerian formulation in which the material deforms but the grid remains fixed. Thus it was not possible to verify the large deformation analyses of Wang and Carter (2001) for shallow foundation by using FLAC. Wang and Carter (2001) used a special formulation (Arbitrary Lagrangian-Eularian) which is a combination of Lagrangian and Eulerian formulations and regenerates the mesh after large deformation occur and soil boundary become irregular, so as to fit the distorted boundary at regular intervals (refer 2.4.1).

Test 2: Combined Large Strain and Small Strain Analysis - Soil Not Restrained from Flowing over Footing

As observed in Test 1 (4.5.1) the FLAC code in large strain was not able to complete the run due to the "Bad Geometry" error. However, it was successful to run up to a certain stage. So, it was thought that it would be helpful to verify the initial stages if not the final results of Wang and Carter (2001). Therefore a FLAC analysis was conducted keeping model grid, geometry and properties similar to those in 4.5.1, but running it in two stages. The model was first run up to 185739 steps and then stopped before the "Bad Geometry" error could occur. In the second stage, the first stage was restored and the model was run in the small strain mode in which the grid coordinates are not updated at every timestep. The results are discussed as below:

As can be seen from Figure A.445 there is more soil heaving on the edge of the footing in comparison to that observed in 4.1.1.

Figure A.446 shows that the depth of the failure is deeper than shown in Figure A.5. However, the horizontal extent of the failure zone is similar.

The grid shown in Figure A.447 is quite different than in Figure A.6, which may be due to the large strain deformation FLAC was able to calculate in the initial stages.

The zone of influence of equal vertical stress (σ_{yy}) contours in Figure A.448 is similar to that in Figure A.7. However, the shapes of the stress contours are not as smooth due to the distortion in grid in large strains.

Figure 4.41 shows the comparison of the bearing pressure versus y - displacement curves for small strain analysis and the small strain - large strain combined analysis. As is clear from Table 4.34, and Figure 4.43, the ultimate bearing capacity $(q_u) =$ 108.14 kPa is larger than the small strain value of $(q_u) = 103.52$ kPa. However since the whole analysis cannot be completed in the large strain mode, the shape of the curve is quite different than that given by Wang and Carter (2001) as shown in Figure 2.8(a). The large strain FLAC analysis catches the early trend of the curve only, and cannot be used for bearing capacity predictions of the shallow foundations.

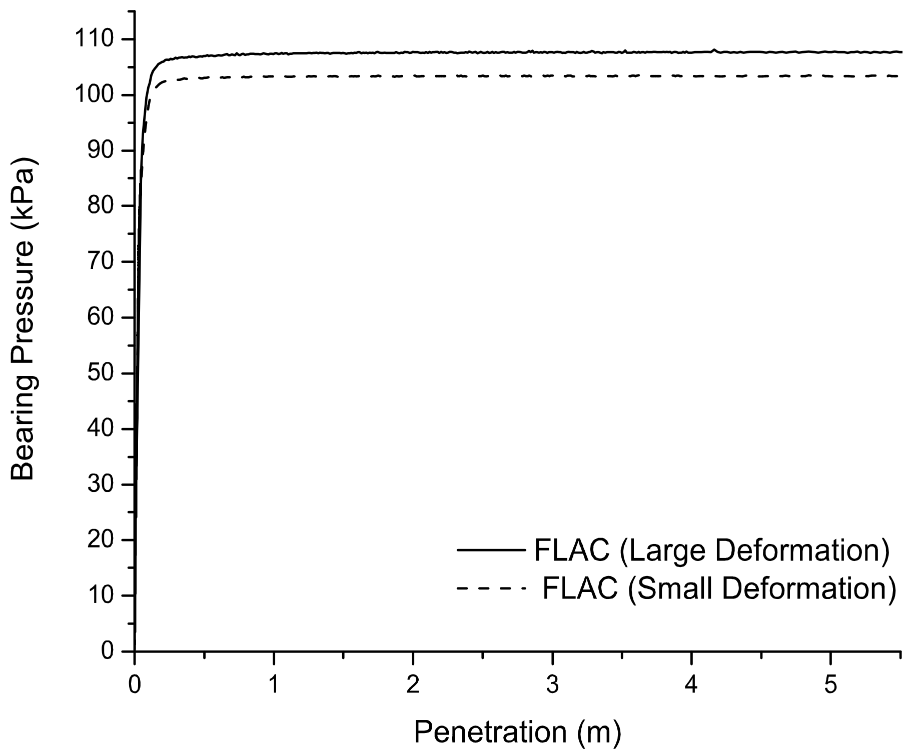

Figure 4.41: Bearing pressure versus penetration curve for combined large strain - small strain analysis of a rigid smooth strip footing on strong clay over soft clay for 40×30 grid model, $H/B = 1$, $c_2/c_1 = 1$.

Table 4.34: Ultimate Bearing Capacity , q_u of rigid strip footing on strong over soft clay for large combined strain - small strain analysis for grid 40×30, for $H/B = 1$.

Shear Strength Top Layer, (c_1)	Shear Strength Bottom Layer, (c_2)	Shear Strength Ratio, (c_2/c_1)	q_u (Small Strain) (FLAC)	q_u (Large Strain - Small Strain) (FLAC)	
				No Spill Control	Spill Control
20.00	20.00	1.00	103.52	108.14	108.21
20.00	2.00	0.10	41.68	40.80	40.72

Test 3: Combined Large Strain and Small Strain Analysis - Soil Restrained from Flowing over Footing

As it can be seen from Figure A.445 that the clay heaving at the edge of the footing tries to flow over the footing which twists the zone ($i = 11, j = 30$) causing the early stopping of analysis due to "Bad Geometry" error. If this spilling of clay could be stopped, the degeneration of the zone can be delayed, and the analysis could be taken on a little farther. In order to provide this horizontal restraint a vertical beam simulating a wall over the footing is introduced which now stops the soil spill on to the footing. The results are shown below:

The introduction of a vertical beam to simulate a wall at the edge of the footing as shown in Figure A.449 helps to avoid "Bad Geometry" error from occurring until 190054 timesteps, which is only 4315 timesteps more than in 4.5.1. This shows that degeneration of the zones can not be delayed any longer and FLAC is not able to do the large strain analysis for shallow foundations.

It is clear from Figure A.450 that the soil flow becomes more vertical at the side of the footing when the soil heave is stopped from spilling over the footing.

It can be noticed from Figure A.451 and A.446 that there is difference in horizontal extent of the plasticity indicators. The plastic yielding of the clay seems to extend vertically down below the footing rather than extending horizontally when the vertical wall is in place.

The equal vertical stress (σ_{yy}) contours in Figure A.452 have more regular shapes than in Figure A.448 and the zone of influence is a little deeper now.

As it can be seen from Table 4.34 and Figure 4.42, the ultimate bearing capacity (q_u)= 108.21 kPa is almost the same as in 4.5.1. Therefore it can be concluded that although the extent of yielding under the footing has changed when the soil spill is constrained there is negligible change in the ultimate bearing capacity (q_u) in this type of combined large strain - small strain analysis.

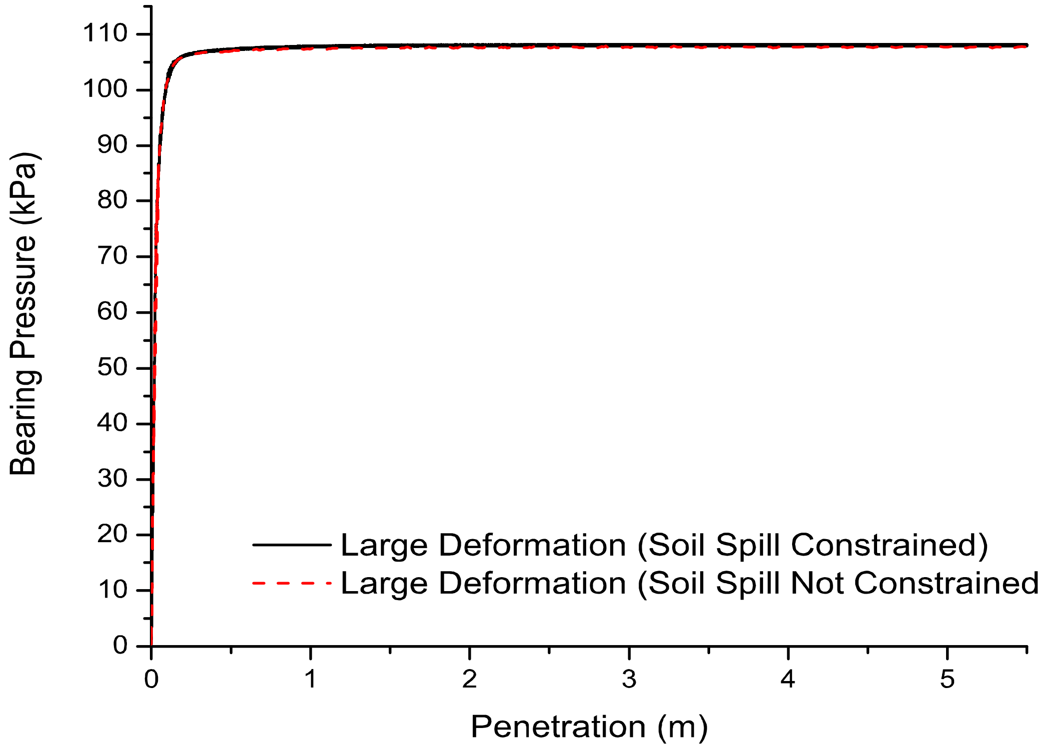

Figure 4.42: Bearing pressure versus penetration curve for combined large strain - small strain analysis of a rigid smooth strip footing on strong clay over soft clay for 40×30 grid model, $H/B = 1$, $c_2/c_1 = 1$.

Case 2: $c_2/c_1 = 0.1$ **(Homogeneous clay) - Large Deformation Analysis**

It appears from 4.5.1 and as shown in Table 4.34 that the small strain analysis predicts lower values of ultimate bearing capacity (q_u) than large strain analysis. However, this is shown by Wang and Carter (2001) in their FEM analysis (see Figure 2.8(a)) showed that for $c_2/c_1 = 0.2$ and 0.1 the small strain predicts higher values of ultimate bearing capacity (q_u) than large strain analysis. Large strain mode application of FLAC for the latter case only is explored and is described below:

Test 1: Large Strain Analysis

In the first test model mesh and properties similar to Case 1 (4.1.1) were used, but the model was run in large strain mode. It was noticed that FLAC model run, as in 4.5.1, stopped with "Bad Geometry" error after 533790 steps. In this case also zone ($i = 11, j = 30$) just on the side of footing is so distorted (see Figure A.453 and A.454) that it exceeds the minimum undistorted area criterion set in the FLAC code.

In this case too, it is not possible to verify the large deformation FEM analysis for shallow foundation by Wang and Carter (2001) with FLAC.

Test 2: Combined Large Strain and Small Strain Analysis - Soil Not Restrained from Flowing over Footing

Since FLAC model in Test 1 (4.5.1) large strain was able to run to 533790 timesteps before stopping due to the "Bad Geometry" error it could be useful to verify the initial stages Wang and Carter (2001) analysis. Therefore a FLAC analysis was conducted keeping model grid, geometry and properties similar to that in 4.5.1, but running it in two stages. The model was first run up to 533770 timesteps, well before "Bad Geometry" error could occur, and then in the second stage the first stage was restored and the model was run in the small strain mode in which the grid coordinates are not updated at every step. The results are discussed as below:

As it can be seen from Figure A.455 there is more soil heave at the edge of the footing in comparison to that in 4.1.1.

Figure A.456 shows that the depth of the failure is now deeper than shown in Figure A.35. However, the horizontal extent of the failure zone is similar.

The grid shown in Figure A.457 is quite different than in A.37 which shows the magnified and not the actual grid.

The zone of the influence of equal vertical stress (σ_{yy}) contours is similar in Figure A.458 and A.36.

Figure 4.43 shows the comparison of the bearing pressure versus y - displacement curves for small strain analysis and the small strain - large strain combined analysis.

It is clear from the Table 4.34 and Figure 4.43 that the ultimate bearing capacity $(q_u) = 40.80\,\text{kPa}$ is less than for the small strain value of $(q_u) = 41.68\,\text{kPa}$. However, since the whole analysis could not be completed in the large stain mode, the shape of the curve is quite different than that given by Wang and Carter (2001) as shown in Figure 2.8(a). This analysis only catches the early trend of the curve, and cannot be used for bearing capacity predictions.

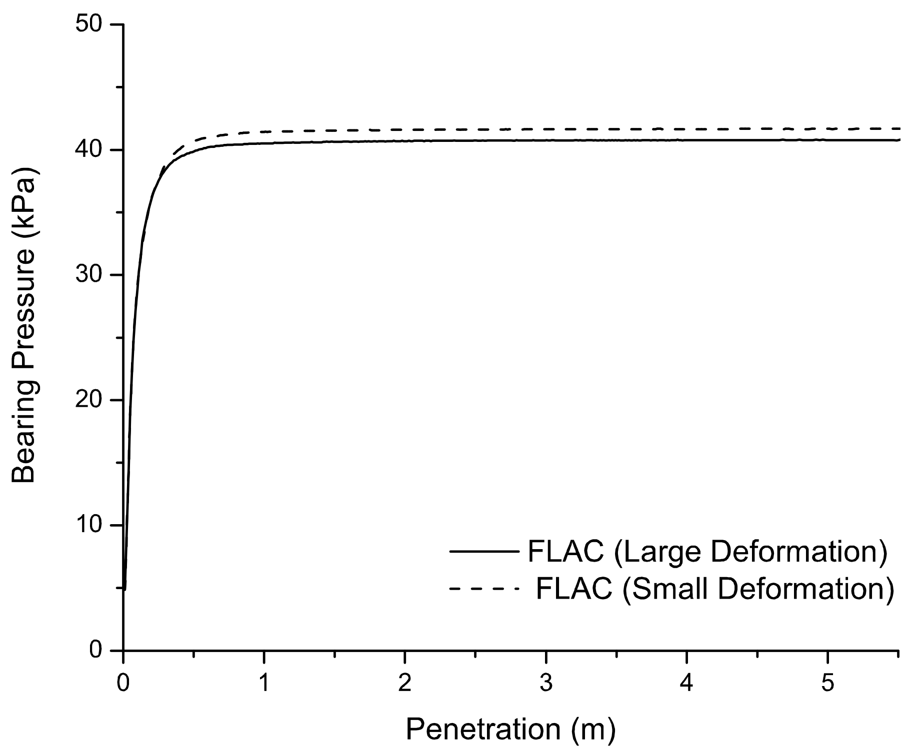

Figure 4.43: Bearing pressure versus penetration curve for combined large strain - small strain analysis of a rigid smooth strip footing on strong clay over soft clay for 40×30 grid model, $H/B = 1$, $c_2/c_1 = 0.1$.

Test 3: Combined Large Strain and Small Strain Analysis - Soil Restrained from Flowing over Footing

It can be seen from Figure A.455 that the clay heaving at the edge of the footing tries to flow over the footing which results in distorting the zone ($i = 11, j = 30$) causing the early stopping of run due to "Bad Geometry" error. If this spilling of clay could be stopped, the distortion of the zone can be delayed, and the analysis could be taken a little farther. An arrangement similar to 4.5.1 was made to restrain the soil spill with a vertical beam. The results are described below:

The introduction of a vertical beam to simulate the wall on the edge of the footing as shown in Figure A.459 helps to avoid "Bad Geometry" error from occurring until 565250 steps, which are 31480 steps more than in 4.5.1, which shows that degeneration of the zones can only be delayed but not avoided. Thus FLAC is not able to complete the large strain analysis for shallow foundations.

It is clear from Figure A.460 that the soil flow becomes more vertical at the side of the footing when the soil heave is stopped from spilling over the footing.

It can be noticed from Figure A.461 and A.456 that there is a difference in horizontal extent of the plasticity indicators. The plastic yielding of the clay seems to extend vertically down below the footing rather than extending horizontally.

The equal vertical stress (σ_{yy}) contours in Figure A.462 have more regular shapes than in Figure A.458 and the zone of influence is shallower now.

As it can be seen from Table 4.34 and Figure 4.44 the ultimate bearing capacity $(q_u) = 40.72\,\text{kPa}$ which is almost the same as in 4.5.1. Therefore, it can be concluded that although the extent of yielding under the footing has changed when the soil spill is constrained there is negligible change in the ultimate bearing capacity (q_u) in this type of combined large strain - small strain analysis.

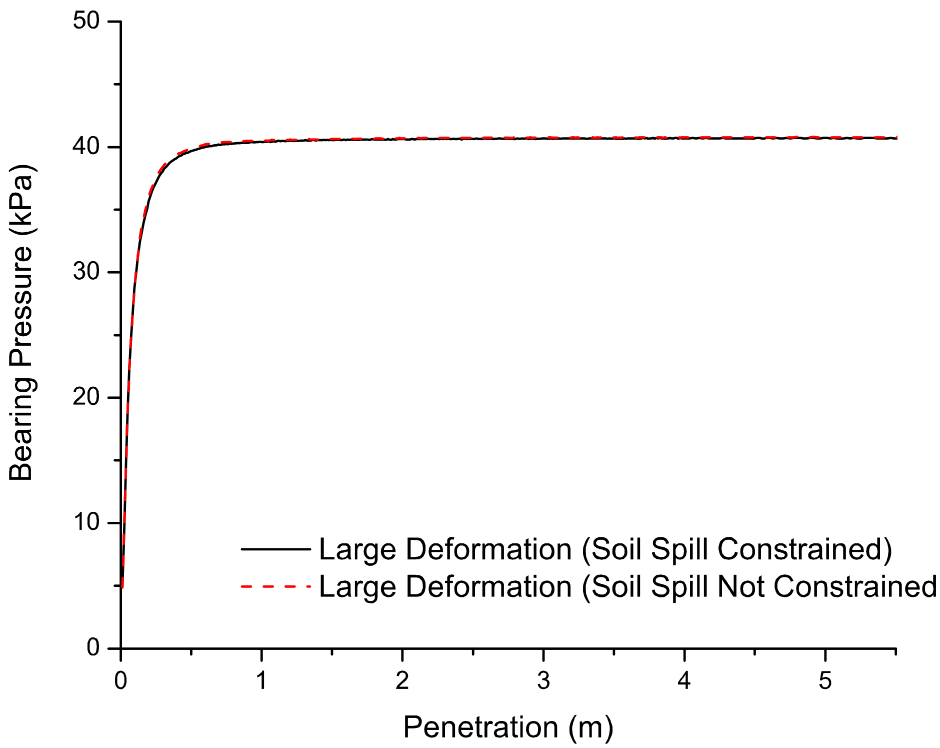

Figure 4.44: Bearing pressure versus penetration curve for combined large strain - small strain analysis of a rigid smooth strip footing on strong clay over soft clay for 40×30 grid model, $H/B = 1$, $c_2/c_1 = 0.1$.

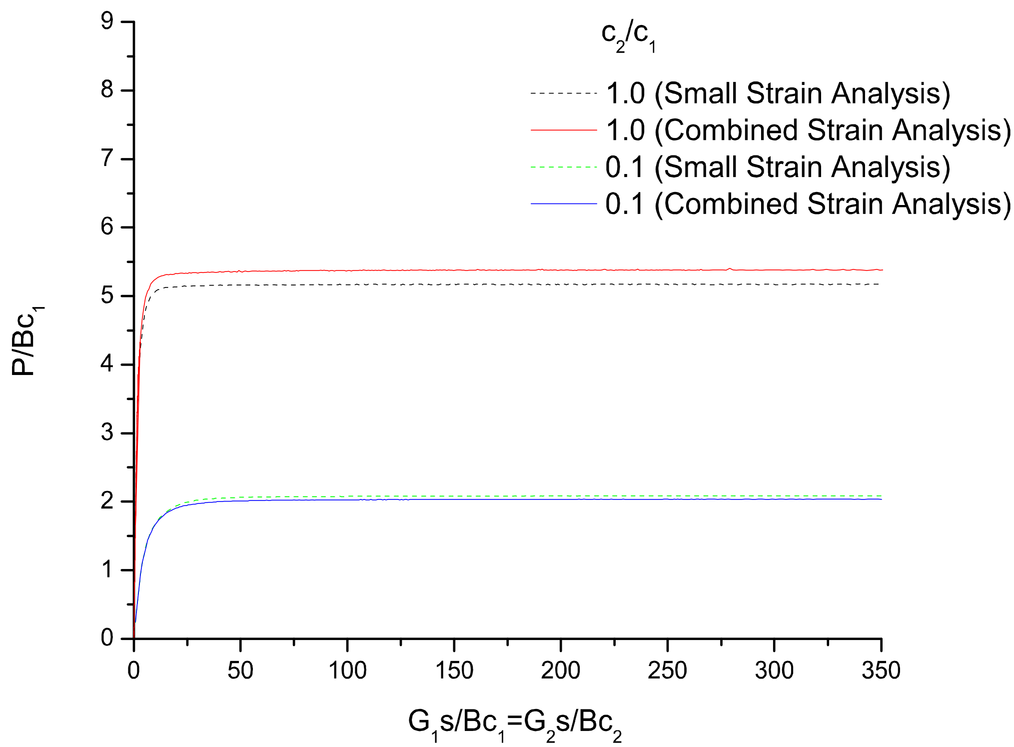

Figure 4.45: Normalised bearing pressure versus penetration curves for a rigid smooth strip footing on soft clay over strong clay for 40×30 grid model, $H/B = 1$, for Small Strain and Combined (large & small) Strain Analyses.

Chapter 5

Conclusion

The main objective of this thesis was to investigate the use of FLAC in predicting the bearing capacity of rigid smooth strip and circular surface footings resting on the surface of undrained two layer clay systems. Small deformation analyses for each type of footing were investigated when the foundation clay profile comprises strong clay overlying soft clay, and also when these footings rest on soft clay over strong clay. Various cases were studied by varying the relative undrained shear strength of the two clay layers and the thickness of the top clay layer. The application of the large strain mode of FLAC was investigated for large deformation analysis in case of a strip footing resting on strong over soft clay system. The results for the bearing capacity and the modified bearing capacity factor N_c^* are shown in form of Tables and graphs.

The following can be concluded from the present study:

Strip Footing on Strong Clay overlying Soft Clay

A number of different failure mechanisms occur for a rigid strip footing on a strong over soft clay system depending on the H/B and c_2/c_1 ratios. If the top strong clay layer is deep enough (i.e. $H \geq 3.5B$) the failure mechanism is entirely contained in the top strong clay layer for all values of the c_2/c_1 ratio. This depth is greater than Merifield et al. (1999) who suggested a limiting value of this ratio as $H/B = 2$, and even larger than the value of $H/B \simeq 2.5$ given by Meyerhof and Hanna (1978). For all other values of $H/B < 3.5$, depending upon the H/B and c_2/c_1 ratios, the failure mechanism generally occurs in general shear, local shear or full punching shear through the top layer followed by yielding of the bottom soft clay layer. For $H/B < 0.5$ full punching of the footing through the top strong clay layer occurs when the strength of the top layer is significantly more than the bottom soft layer. The bearing capacity values remain equal to the bearing capacity of the homogeneous case ($c_2/c_1 = 1$) for all ratios of $c_2/c_1 < 1$ and $H/B \geq 3.5$, and less than that of homogeneous case for $H/B \leq 0.25$. In general, bearing capacity values from the FLAC analysis agree very well with values from FEM analysis by Merifield et al. (1999). However, these values tend to be somewhat different than the semi-empirical values given by Meyerhof and Hanna (1978), which presume a failure surface, no such assumption is made in the present FLAC analyses and the failure zone is developed incrementally as the loading is increased.

Circular Footing on Strong Clay overlying Soft Clay

The failure mechanism in a rigid circular footing on strong over soft clay system occurs in general shear, local shear and punching shear, which depends on the H/D and c_2/c_1 ratios. It has been found that if the top strong clay layer is deep enough i.e. $H \geq 2D$ the failure mechanism is entirely contained in the top strong clay layer for all value of the c_2/c_1 ratio. This depth is greater than Brown and Meyerhof (1969) who suggested a value of $H/D = 1.5$. For all other values of $H/D < 2$, depending upon the H/D and c_2/c_1 ratios, the failure mechanism generally occurs in general shear, local shear, partial punching shear or full punching shear through the top layer followed by yielding of the bottom soft clay layer. For $H/D \leq 0.25$ full punching of the footing through the top strong clay layer occurs when strength of the top layer is significantly greater than the bottom soft layer. The bearing capacity values remain equal to the bearing capacity of the homogeneous case ($c_2/c_1 = 1$) for all $c_2/c_1 < 1$ and $H/D \geq 2$, and less than the bearing capacity of the homogeneous case for all $H/D \leq 0.25$ respectively. It has been observed that for $H/D = 1$, and $c_2/c_1 \geq 0.5$ the modified bearing capacity factor N_c^* values are the same as FEM values from small deformation analysis of Wang and Carter (2001), but for $c_2/c_1 < 0.5$ the values are a little higher.

One reason could be the different values of the effective radii chosen in two analyses, and the different methods used in calculating the bearing capacity. Another reason could be the difference in the FEM and FDM methods. Selection of element type in the FEM has a significant effect on the bearing capacity prediction (Wang and Carter 2001). The only element type allowed in FLAC is a constant strain triangle with two overlapping sets of such triangular elements constituting one quadrilateral zone in the FLAC mesh. For $H/D = 0.5$, and for $0.1 \leq c_2/c_1 \leq 0.8$, the FLAC analyses give modified bearing capacity factor, N_c^*, values which are a little higher than values given by Wang and Carter (2001). There are no FEM bearing capacity values published for $H/D = 0.25$ and 2. When the modified bearing capacity factor, N_c^*, values from the FLAC analyses are compared with the empirical values given by Brown and Meyerhof (1969), they are higher for $H/D = 0.25$ and $0.1 \leq c_2/c_1 \leq 0.8$, but tend to a lower value in the cases of $H/D = 1$ and $0.1 \leq c_2/c_1 \leq 0.8$.

Strip Footing on Soft Clay overlying Strong Clay

The failure mechanisms in a rigid strip footing on a soft over strong clay system are general shear or squeezing type shear failure with lateral plastic flow. If the top strong clay layer is thick enough (i.e. $H/B > 0.5$) the failure mechanism is entirely contained in the top soft clay layer for all value of $c_1/c_2 \leq 1$, and the bearing capacity $q_u = N_c^* c_1$ where the modified bearing capacity factor $N_c^* = 5.18$, For $H/B \leq 0.5$, as H/B ratio decreases or the top soft clay layer becomes thinner and thinner, the bearing capacity increases as the relative strength of the bottom layer increases. The modified bearing capacity factor N_c^* values falls in between the upper and lower bound values given by Merifield et al. (1999) for $H/B \geq 0.5$ and $c_1/c_2 < 1$. However, values from the FLAC analyses tend to be higher than those of Merifield et al. (1999) for $H/B < 0.5$ for all $c_1/c_2 < 1$.

Circular Footing on Soft Clay overlying Strong Clay

The failure mechanism for a rigid circular footing on a soft over strong clay system is either a general shear type failure or failure in which soft clay is squeezed out from beneath the footing and the bottom strong clay layer. The type of failure depends on the H/B and c_1/c_2 ratios. If the top strong clay layer is thick enough (i.e. $H \geq 1$) the failure mechanism is entirely contained in the top soft clay layer for all value of $c_1/c_2 \leq 1$, and the bearing capacity is $q_u = N_c^* c_1$ where the modified bearing capacity factor $N_c^* = 5.61$. For $H/B < 1$, as H/B ratio decreases or the top soft layer becomes thinner, the bearing capacity increases. For $H/B \leq 0.25$ the bearing capacity increases as the relative strength of the bottom layer increases. For $0.5 \leq c_1/c_2 \leq 1$ for $H/B \geq 0.5$ the modified bearing capacity factor N_c^* values are slightly lower than the values of the empirical values of Brown and Meyerhof (1969). However, for $c_1/c_2 < 0.5$ the N_c^* values for the semi-empirical formulation by Vesic (1975) are much higher.

Strip Footing on Stiff Clay Overlying Soft Clay - Large Deformation Analysis

It was observed that due to the Lagrangian formulation of FLAC and its inability to remesh the grid once distortion of the grid has occurred in large strain analysis, it is impossible to complete large deformation bearing capacity analysis for shallow foundations. Hence, results from FEM analysis of Wang and Carter (2001) could not be verified independently. However, the analyses completed with combination of large strain - small strain analysis were able to capture the early trend of curves from Wang and Carter (2001) and show that the bearing capacity values are of higher value in early stages of curve for $c_2/c_1 = 1$, but gives a lower value for $c_2/c_1 = 0.1$ than those predicted with the small strain analysis alone.

It can be concluded that the present study to explore the use of FLAC in understanding the bearing response of shallow foundations on two-layered clays have produced mixed results. The first part of the study which included the verification of the FLAC shallow foundation models on the two-layered clays were successful. However, it was not possible to verify the large deformation analyses results from published literature due to the limitation of the FLAC in dealing with this particular problem of shallow foundations in large strain mode. This limitation of FLAC in carrying out this type of analysis is built in its code which generates "Bad Geometry Error" when elements are distorted to such an extent that the area of the triangular elements with in a quadrilateral element becomes less than 20% of its total initial area. FLAC is based on the Lagrangian method, but it does not support remeshing and reassigning of boundary conditions once the mesh gets distorted to a certain level. Since FLAC is a commercial code and its source code is not open to the end users, it was not possible to make such modification in the FLAC models, so various improvisations were made in the model for extending the FLAC calculations before the analysis stops with the "Bad Geometry Error", but only limited success was achieved. Owner of FLAC, Itasca Consulting, Inc. was approached for help. The author of this thesis visited Itasca's office in Minneapolis, Minnesota, USA. The problem was discussed in detail with one of Itasca's analyst for consulting fees, but the issue could not be resolved.

In conclusion, although FLAC may be a widely used numerical modelling software, it was found that it can only be used to estimate the ultimate bearing capacity of footings on two-layered or homogeneous undrained clays in small strain mode. The large strain mode in FLAC is not capable of modelling the large deformations of foundations in layered clays, and cannot perform such analysis without any modification to its code. The main focus in numerical modelling these days is on finite element methods, and tremendous progress has been made in development and use of these methods. On the other hand the finite difference method is less popular and not many researchers have been developing or using these methods. Since FLAC is one of the best known finite difference based numerical analysis software left, it would be valuable if its owners make some modification in the code so that it can do large strain analysis for this type of problem. It is also suggested that some sort of finite difference code may be developed which incorporates the Arbitrary Lagrangian-Eulerian (ALE) for studying the large strain bearing response of foundations in layered clays.

References

Bowles, J. E. (1996). *Foundation Analysis and Design*. The McGraw-Hill Companies, Inc., New York.

Brown, J. D. and Meyerhof, G. G. (1969). "Experimental study of bearing capacity in layered clays." *Proceedings of 7th International Conference on Soil Mechanics and Foundation Engineering, Mexico*, Vol. 2. 45–51.

Burd, H. J. and Frydman, S. (1997). "Bearing capacity of plane-strain footings on layered soils." *Canadian Geotechnical Journal*, 34, 241–253.

Button, S. J. (1953). "The bearing capacity of footings on a two-layer cohesive subsoil." *Proceedings of 3rd International Conference on Soil Mechanics and Foundation Engineering, Zurich*, Vol. 1. 332–335.

Carter, J. P. and Balaam, N. (1995). *AFENA Users Manual*. Geotechnical Research Centre, The University of Sydney.

Chen, W. F. (1975). *Limit Analysis and Soil Plasticity*. Elsevier, Amsterdam, The Netherlands.

Chen, W. F. and Davidson, H. L. (1973). "Bearing capacity determination by limit analysis." *Journal of the Soil Engineering and Foundations Division, ASCE*, 99(6), 433–449.

Craig, R. F. (1997). *Soil Mechanics*. E and FN Spon, London, UK, Sixth edition.

Das, B. M. (1999). *Shallow Foundations: Bearing Capacity and Settlement*. CRC Press LLC.

Drucker, D., Prager, W., and Greenberg, H. J. (1952). "Extended limit design theorems for continuous media." *Quarterly of Applied Mathematics*, 9(4), 381–389.

Evans, K. M. (1987). "A model study of the end bearing capacity of piles in layered calcareous soils," PhD thesis, Keble College, Oxford University.

Florkiewicz, A. (1989). "Upper bound to bearing capacity of layered soils." *Canadian Geotechnical Journal*, 26, 730–736.

Frydman, S. and Burd, H. J. (1997). "Numerical studies of bearing-capacity factor N_γ." *Journal of Geotechnical and Geoenvironmental Engineering*, 123(1), 20–29.

Georgiadis, M. and Michalopoulos, A. P. (1985). "Bearing capacity of gravity bases on layered soil." *Journal of Geotechnical Engineering, ASCE*, 111(6), 712–727.

Ghosh, S. and Kikuchi, N. (1991). "An arbitrary lagrangian-eulerian finite element method for large deformation analysis of elastic-viscoplastic solid." *Computer Methods in Applied Mechanics and Engineering*, 86, 127–188.

Griffiths, D. V. (1982). "Computation of bearing capacity on layered soils." *Proceedings 4th International Conference on Numerical Methods in Geomechanics*, Vol. 1. 163–170.

Houlsby, G. T., Evans, K. M., and Sweeney, M. A. (1988). "End bearing capacity of model piles in layered carbonate soils." *Engineering for calcareous sediments*, Jewell and Andrews, eds., Balkema, Rotterdam, Boulder, Colo., 69–129.

Hu, Y. and Randolph, M. F. (1996). "A practical numerical approach for large deformation problems in soil." *International Journal for Numerical and Analytical Methods in Geomechanics*, 22, 327–350.

Itasca Consulting Group, Inc. (2001a). *FISH in FLAC - Fast Lagrangian Analysis of Continua*. Minneapolis, Minnesota, First revision, Second edition.

Itasca Consulting Group, Inc. (2001b). *Theory and Background - Fast Lagrangian Analysis of Continua*. Minneapolis, Minnesota, First revision, Second edition.

Itasca Consulting Group, Inc. (2001c). *Verification Problems - Fast Lagrangian Analysis of Continua*. Minneapolis, Minnesota, First revision, Second edition.

Itasca Consulting Group, Inc. (2002a). *Command Reference - Fast Lagrangian Analysis of Continua*. Minneapolis, Minnesota, Second revision, First edition.

Itasca Consulting Group, Inc. (2002b). *FLAC-GIIC Reference - Fast Lagrangian Analysis of Continua*. Minneapolis, Minnesota, First edition.

Itasca Consulting Group, Inc. (2002c). *User's Guide - Fast Lagrangian Analysis of Continua*. Minneapolis, Minnesota, Second revision, First edition.

Lauritzen, R. and Schjetne, K. (1976). "Stability calculations for offshore gravity structures." *Proceedings of the Eighth Offshore Technology Conference, Houston, Texas*, (OTC-2431), 75–82.

Love, J. P., Burd, H. J., Milligan, G. W. E., and Houlsby, G. T. (1987). "Analytical and model studies of reinforcement of a layer of granular fill on a soft clay and subgrade." *Canadian Geotechnical Journal*, 24, 611–622.

Marti, J. and Cundall, P. A. (1982). "Mixed discretisation procedure for accurate solution of plasticity problems." *International Journal of Numerical Methods and Analytical Methods in Geomechanics*, 6, 129–139.

Merifield, R. S., Sloan, S. W., and Yu, H. S. (1999). "Rigorous plasticity solutions for the bearing capacity of two-layered clays." *Géotechnique*, 49(4), 471–490.

Meyerhof, G. G. (1951). "The ultimate bearing capacity of foundations." *Géotechnique*, 2(4), 301–332.

Meyerhof, G. G. and Hanna, A. M. (1978). "Ultimate bearing capacity of footings over two layer foundation soils." *Canadian Geotechnical Journal*, 15, 565–572.

Michalowski, R. L. and Shi, L. (1995). "Bearing capacity of footings over two-layer foundation soils." *Journal of Geotechnical Engineering*, 121(5), 421–428.

Nagtegaal, J. C., Parks, D. M., and Price, J. R. (1974). "On numerically accurate finite element solution in the fully plastic range." *Computer Methods in Applied Mechanics and Engineering*, 4, 153–177.

Reddy, A. S. and Srinivasan, R. J. (1967). "Bearing capacity of footings on layered clays." *Journal of Soil Mechanics and Foundations Division, ASCE*, 93(2), 83–99.

Terzaghi, K. (1943). *Theoretical Soil Mechanics*. John Willey and Sons, Inc., New York, N. Y.

Terzaghi, K. and Peck, R. B. (1967). *Soil Mechanics in Engineering Practice*. John Wiley and Sons, New York, 2nd edition.

Vesic, A. S. (1975). "Bearing capacity of shallow foundations." *Foundation Engineering Handbook*, H. F. Winterkorn and H. Y. Fang, eds., Van Nostrand Reinhold Company, New York, N. Y., chapter 3, 121–147.

Wang, C. and Carter, J. P. (2001). "Deep penetration of strip and circular footings into layered clays." *Report No. R807*, Dept of Civil Engineering, University of Sydney, Australia.

Appendix A

Numerical Modelling and Discussion of Results

In this chapter numerical analysis for the bearing response of strip and circular footing on two layered clays have been described for the following cases:

1. Strip Footing on Stiff Clay overlying Soft Clay - Small Deformation Analysis
2. Circular Footing on Soft Clay overlying Stiff Clay - Small Deformation Analysis
3. Strip Footing on Soft Clay overlying Stiff Clay - Small Deformation Analysis
4. Circular Footing on Soft Clay overlying Stiff Clay - Small Deformation Analysis
5. Strip Footing on Stiff Clay overlying Soft Clay - Large Deformation Analysis

A.1 Strip Footing on Stiff Clay Overlying Soft Clay - Small Deformation Analysis

In this section plain strain FLAC numerical models for vertically loaded rigid strip footing on surface of a horizontally layered strong over soft undrained clay system have been described. The upper and lower bound bearing capacity analysis for the small deformation of the footings has been discussed. Various cases have been studied by varying the soil properties as well as the thickness of the top layer. In all the cases the soil was assumed to be an elastic-perfectly plastic Tresca material. The rigidity index (I_r) taken was $G_1/c_1 = G_2/c_2 = 67$[1], where G_1, G_2, c_1 and c_2 are the shear modulus and cohesion of the top and bottom clay layers respectively. The rigidity index (I_r) is a rational parameter for evaluation of relative compressibility of soil masses under load (Vesic 1975) The value of Poisson's ratio used was $\nu = 0.49$ which is close to 0.5 for incompressible undrained clays, and it helps in avoiding numerical difficulties (Burd and Frydman 1997). Various undrained shear strength ratios of the bottom layer (c_1) to top layer (c_2) considered were $0.1, 0.2, 1/3, 0.5, 2/3, 0.8$, and 1. The ratios of the depth (H) of top clay layer and width (B) of the footing were varied as $0.25, 0.5, 1$ and $2, 2.5, 3$ and 3.5. Since in small deformation analysis there is no change in the geometry, the ultimate bearing capacity of foundation is due to the shear strength of clay under the footing and self weight of the undrained clays does not have any influence on it (Wang and Carter 2001). All small deformation cases are performed by not considering the self-weight.

It is very important in predicting the ultimate bearing capacity of a foundation by numerical analysis that its value should be bracketed by finding the upper and lower bound values. The solution approaches a "true value" when the upper and lower limit collapse loads tend to be equal. Generally, in FEM the upper bound solution are calculated by modelling a kinematically admissible velocity field, and the lower bound solution is obtained by modelling a statically admissible field (Merifield, Sloan, and Yu 1999). In FLAC if the maximum unbalanced nodal force vector also known as "unbalanced force" is zero (elastic materials) or a constant value close to zero (plastic materials, a steady-state flow of material occurs indicating a portion or all of the model is failing) the model is in equilibrium and the solution approaches the "true value". All model runs described in this section and the subsequent sections are run keeping the unbalanced force close to 1×10^{-3} by controlling the applied velocity and damping the energy in the the model.

Model Geometry The footing is assumed to be a smooth footing. Due to the symmetry of the problem only half of the width of footing is considered, and a half

[1] This value of G/c was chosen for verifying the results with Wang and Carter (2001).

space model is used for the analysis. A typical geometry of the model is shown in FigureA.1 & A.2.

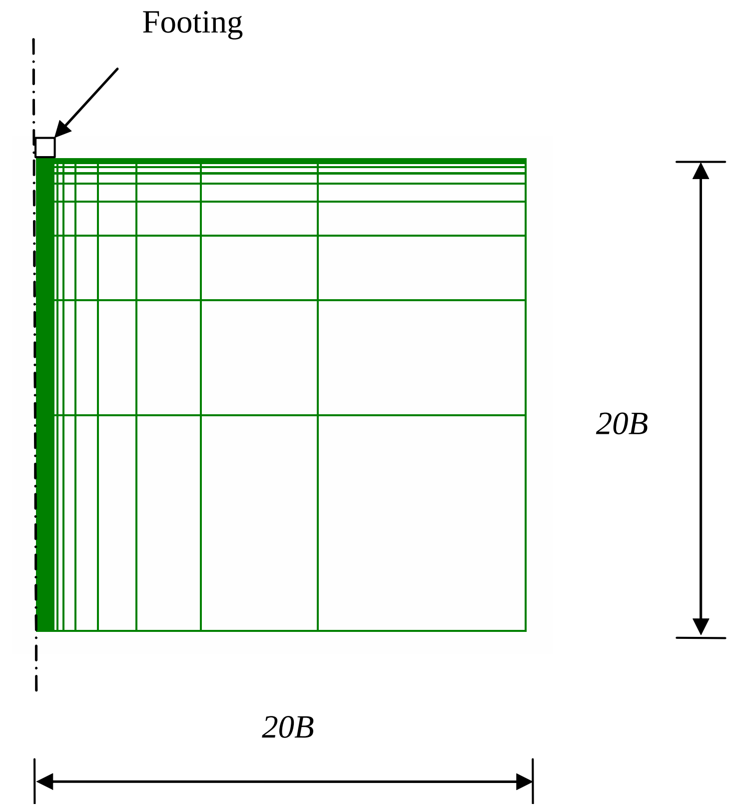

Figure A.1: Typical model geometry for 20×10 elements grid, $H/B = 1$

Width/diameter of strip/circular footing (B or D) $= 1$ m

Half width/radius of the strip/circular footing ($B/2$ or $D/2$) $= 0.5$ m

Width of the half space soil model ($20B$ or $20D$) $= 20$ m

Depth of the half space soil model ($20B$ or $20D$) $= 20$ m

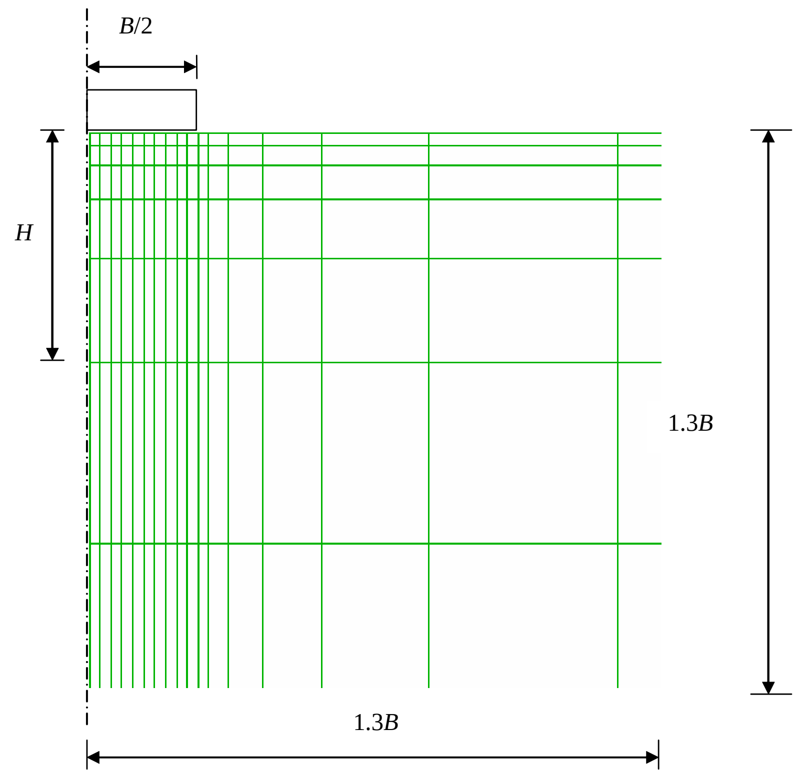

Figure A.2: Zoomed model geometry for 20 $\times$ 10 elements grid, $H/B = 1$

A.1.1 Rigid Smooth Strip Footing on Strong over Soft Clay ($H/B = 1$)

In order to make sure that the discretization errors were small in these analyses, various trials were conducted by using grids of different refinements, four grids: 20×10 (horizontal elements by vertical elements), 60×30 and 40×30 were considered for optimizing the grid density to calculate the true collapse load.

Grid 20×10 :

Various undrained shear strength ratios of the bottom layer (c_2) to top layer (c_1) considered are $0.1, 0.2, 1/3, 0.5, 2/3, 0.8$, and 1.

Case 1: $c_2/c_1 = 1$ **(Homogeneous clay) - Small Deformation Analysis**

In the beginning a relatively coarser 20×10 grid is selected. No. of elements below half-footing in this case is kept to 10 and are equisized in x-direction. A prominent difficulty in the numerical analysis of footing problem is the high stress gradients developed at the footing edge. For a footing resting on surface of a soil, major principal stress acts vertically below the footing, whereas it acts horizontally in soil adjacent to footing edge. This abrupt change in the stress directions and high strain rate at the edge of the footing causes computational difficulties. In order to make the transition of the stresses smoother, and to prevent out-of-balance forces, smaller elements are concentrated at the edge by refining the grid. The velocity field decays quite rapidly with depth, so the grid is graded in order to allow remote boundaries without the concentration of large numbers of zones. The boundaries of the grid are kept at a sufficient distance from the footing in order to ensure that the plastic zone developed in soil does not extend to the grid boundaries. Another option to make sure this does not happen, is by allowing the grid to move in a vertical direction at the vertical boundary which is equivalent of putting a roller at the boundary This approach has only been adopted in bringing the initial equilibrium[2] to the models.

[2] The model is in equilibrium when the net nodal force vector at each gridpoint is close to zero. Initial equilibrium under the given boundary and initial conditions is achieved for simulating insitu

The grid is also allowed to move vertically at the centerline of the footing.

Mohr-Coulomb constitutive soil model was chosen for all cases.

A controlled downward velocity (displacement (m) per calculation step) of 2.5×10^{-8} is applied to simulate the vertical loading of the footing. FLAC calculates the nodal forces to maintain the applied velocity and the displacement of the footing is calculated continuously as the integral of the velocity over the calculation step. The footing pressure or the bearing capacity is calculated using a FISH function **"load"** (explained later in this section) as the sum of nodal forces on the footing divided by footing half-width. The half-width is calculated by assuming that the velocity varies linearly at the last applied gridpoint to zero at the next grid point. The half-width is then:

$$B/2 = \frac{x_i + x_{i+1}}{2} \tag{A.1}$$

where x_i is the x - distance to the last applied gridpoint from the center of the footing, and x_{i+1} is to the gridpoint adjacent to it. In principle a contact stress at the edge of the footing should be zero (Frydman and Burd 1997). However, due to the singularity at the edge of the footing the bearing capacity is over predicted if the actual width of the footing is used in the calculations. The extended width calculation equation A.1 reduces this error by "extending" the edge of the footing close to the approximate position of zero stress.

A FLAC model data input file has be described below. For explanation the FLAC input data file has be divided into two stages. The objective of the first stage is to bring the model into equilibrium, and simulate insitu stresses and strains[3]. In the second stage of the data file the rigid footing is simulated by applying a constant downward initial velocity, and the stresses, strains and bearing pressure is calculated in the process of getting a final equilibrium for the model. The comments after (;) in italic fonts are the explanations for the FLAC commands and FISH functions.

stresses and strains.

[3] In purely cohesive ($\phi = 0$) undrained clays with Tresca failure criterion, the soil behavior is independent of confining insitu stresses. This step is only for the explanation of initial equilibrium stage.

Stage 1: Bringing the foundation model to initial equilibrium (Simulation of insitu stresses and strains)

title

clay foundation smooth $H/B = 1$, c_1 20, c_2 20, initial yvel $-2.5\mathrm{e}{-8}$ m/ timestep

;$x(10) = 0.5$ - *i.e.* 10 *elements below footing*

;

Part - I : Grid generation and assigning the soil model and soil properties

; Grid size 20 elements in x - direction and 10 elements in y - direction

g 20 10

; Soil model is Mohr-Coulomb

mo mo

; Generates a model geometry of $20\,\mathrm{m} \times 20\,\mathrm{m}$

gen 0,0 0,20.0 20.0,20.0 20.0,0

; Soil properties are defined as shear modulus (s), bulk modulus (b), density (d), cohesion (coh), friction (fric), $(s)/(coh) = 67$

pro s 1.34000e3 b 6.65533e4 d 2.0 coh 20 fric 0 j=6,10

pro s 1.34000e3 b 6.65533e4 d 2.0 coh 20 fric 0 j=1,5

; Generates lower clay layer, and grades the grid (uniform spacing in x - direction and variable spacing in y - direction)

gen 0,0 0,19.0 0.5,19.0 0.5,0 i=1,11 j=1,6 rat 1.0 0.5412

; Generates lower clay layer, and grades the grid in x and y - directions

gen same same 20.0,19.0 20.0,0 i=11,21 j=1,6 rat 1.7696,0.5412

; Generates upper clay layer, and grades the grid (uniform spacing in x - direction and variable spacing in y - direction)

gen 0, 19.0 0,20 0.5,20 0.5,19.0 i=1,11 j=6,11 rat 1.0,0.5767

; Generates upper clay layer, and grades the grid in x and y - directions

gen same same 20,20 20,19.0 i=11,21 j=6,11 rat 1.7696,0.5767

;

Part - II : Defining the displacement boundary conditions

fix x i=1; *Fixes x - velocity at i=1 (free to roll along y - direction)* fix x i=21; *Fixes x - velocity at i=21 (free to roll along y - direction)*

fix x y j=1; *Fixes both x & y - velocities at i=1 (no movement along x and y - directions)*

;

; **Part - III : Defining the recordings of parameters' history**

his 1 unbal; *History of unbalanced forces is recorded*

his 2 ydisp i=2 j=11; *History of y - displacement (footing penetration) is recorded under the centre of footing*

set hisfile IETest.his; *Sets history file name IETest.his for the above set of histories*

;

; **Part - IV : Calculations**

set small; *Sets small strain analysis, coordinates are not updated at each step*

solve elastic; *Calculation is performed until a steady - state solution is reached (constitutive model is changed to elastic for quick initial equilibrium)*

save IETest.sav; *Model state at initial equilibrium is saved*

;

; Stage 2: Bringing Final equilibrium to foundation model (Simulation of final stresses and strains)

res IETest.sav; *Restoration of initial equilibrium condition (insitu) stresses and strains*

;

; Part - I : Redefining boundary conditions

fix x y i=21; *Fixes x & y - velocities at i=21 for all value of j (grid points not allowed to move, simulates infinite boundary)*

fix y i=1,11 j=11; *Fixes y - velocity but frees x - velocity for the nodes under the footing (simulates smooth footing conditions)*

;The final boundary conditions are shown in Figure A.3.

; Part - II : Defining initial conditions

ini xdisp = 0*; Bringing all x-displacements to zero before starting calculations for the final equilibrium*

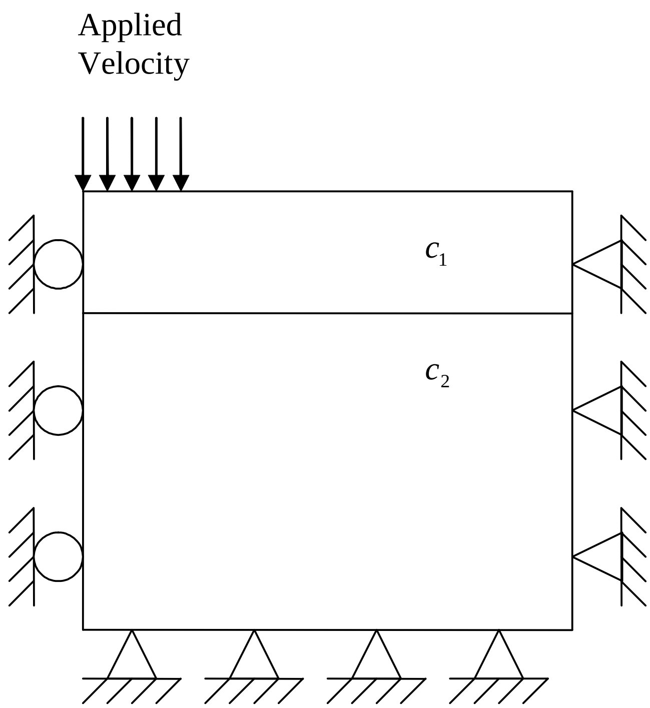

Figure A.3: Typical boundary conditions after (Itasca Consulting Group, Inc. 2001c)

ini ydisp = 0*; Bringing all y-displacements to zero before starting calculations for the final equilibrium*

ini xv=0*; Bringing all x-velocities to zero before starting calculations for the final equilibrium*

ini yv=0*; Bringing all y-velocities to zero before starting calculations for the final equilibrium*

ini yv = -2.5e-8 i=1,11 j=11; *Vertical velocity (displacement/timestep) is applied to the nodes at the base of footing, also represents a rigid boundary that moves with constant velocity for finding the collapse load of soil. This approach has two advantages 1) it is much easier to control the test and obtain a good load/displacement graph, and 2) FLAC takes a long time to converge if there is a large contrast in stiffnesses of materials (footing and soil in this case)* (Itasca Consulting Group, Inc. 2002c) *3)*

Assigning smaller initial velocity value reduces the inertial shock to the system. The oscillations in the model can further be reduced by reducing the magnitude of initial velocity. Also, the predicted bearing pressure approaches the "true" bearing pressure (where upper and lower bound tends to equal) when a low velocity is applied. However, FLAC has practical limitation in reducing the magnitude of the velocity to be applied because a) limited precision error leads to rounding errors, and b) low velocity makes the model run for longer time

;

mark i=1,11 j=11; *Marks nodes under the footing which can be seen in the model in forms of crosses*

;

; FISH function for minimizing the influence of inertial effects on the response of the model

def servo; *Servo - Control FISH function is used to minimize the influence of inertial effects on the response of the model. It is shown here how the applied velocities are adjusted as a function of the maximum unbalanced force in the model* (Itasca Consulting Group, Inc. 2001a)

```
 while_stepping
   if unbal > 0.05 then
     loop i (1,11)
     yvel(i,11) = yvel(i,11)*0.975
     if yvel(i,11) < -2.5e-7 then
        yvel(i,11) = -2.5e-7
     end_if
     if yvel(i,11) > -2.5e-9 then
        yvel(i,11) = -2.5e-9
    end_if
   end_loop
  end_if
;
 if unbal < 0.02 then
```

```
 loop i (1,11)
   yvel(i,11) = yvel(i,11)*1.025
   if yvel(i,11) < -2.5e-7 then
      yvel(i,11) = -2.5e-7
    end_if
    if yvel(i,11) > -2.5e-9 then
       yvel(i,11) = -2.5e-9
   end_if
  end_loop
end_if
end
; — comparison to analytical solution —
; FISH function for calculating footing pressure by summing up the vertical nodal loads at the base of the footing and then dividing by half-width. The width of the footing extends to one-half the zone at which the velocity jump occurs.
    sum =0.0
   loop i (1,11)
      sum = sum + yforce(i,11)
   end_loop
   load = 2.0*sum/(x(11,11)+x(12,11)); Numerical Bearing pressure
   disp = -ydisp(1,11); y - displacement of grid point i=1, j=31 under footing
end
; FISH function  for calculating the difference between analytical and numerical results
def err
   sol=5.14*20; Analytical Bearing pressure (Meyerhof and Hanna 1978)
   err=(load-sol)/sol; Numerical and analytical Bearing pressure comparison
end
;
def myclock; FISH function for calculating the total time taken for the calculations
   myclock=clock/100 ; Time in seconds since midnight
```

end

; — **parameter histories recorded** —

hist 3 load

hist 4 err

hist 5 sol

hist 6 disp

hist 7 yv i 1 j 11

hist 8 myclock

set hisfile CR1T1.his

;

set ncw=100000; *sets the write to screen during cycling to every 100,000 steps*

step 20000000; *Executes 20,000,000 steps of iterations for achieving the equilibrium*

his write 3 5 vs 6 skip 5000; *Records histories (his 3 & 5 versus his 6 after every 5000)*

save CR1.sav; *Model state at final equilibrium is saved*

Case 2: $c_2/c_1 = 0.8$ **- Small Deformation Analysis**

Keeping the top clay layer shear strength $c_1 = 20$ kPa, the bottom clay layer shear strength was reduced to $c_2 = 16$ kPa.

Case 3: $c_2/c_1 = 2/3$ **- Small Deformation Analysis**

Keeping the top clay layer shear strength $c_1 = 20$ kPa, the bottom clay layer shear strength was reduced to $c_2 = 13.333$ kPa for simulating softer clay.

Case 4: $c_2/c_1 = 0.5$ **- Small Deformation Analysis**

Keeping the top clay layer shear strength $c_1 = 20$ kPa, the bottom clay layer shear strength was reduced to $c_2 = 10$ kPa for simulating softer clay.

Case 5: $c_2/c_1 = 1/3$ - Small Deformation Analysis

Keeping the top clay layer shear strength $c_1 = 20$ kPa, the bottom clay layer shear strength was reduced to $c_2 = 6.667$ kPa for simulating softer clay.

Case 6: $c_2/c_1 = 0.2$ - Small Deformation Analysis

Keeping the top clay layer shear strength $c_1 = 20$ kPa, the bottom clay layer shear strength was reduced to $c_2 = 4$ kPa for simulating softer clay.

Case 7: $c_2/c_1 = 0.1$ - Small Deformation Analysis

Keeping the top clay layer shear strength $c_1 = 20$ kPa, the bottom clay layer shear strength was reduced to $c_2 = 2$ kPa for simulating softer clay.

The average time taken by one Grid 20×10 model to complete on Pentium 4, 1GB RAM PC was 2 h and 30 min.

Merifield et al. (1999) has suggested equation A.2 for calculating the modified bearing capacity factor N_c^* :

$$
\begin{aligned}
N_c^* &= \frac{q_u}{c_1} \qquad \text{(A.2)} \\
\text{where } q_u &= \text{Ultimate bearing pressure from numerical analysis}
\end{aligned}
$$

For the present analysis ultimate bearing pressures for above cases have been extracted from the FLAC model history files, and modified bearing capacity factor N_c^* is calculated from equation A.2. The results are shown in Table A.1.

Table A.1: Comparison of modified Bearing Capacity Factor, N_c^* with existing values for rigid strip footing on strong over soft clay for grid 20×10, for $H/B = 1$.

Shear Strength Top Layer, (c_1)	Shear Strength Ratio, (c_2/c_1)	q_u (FLAC)	N_c^*(FLAC) = q_u(FLAC)$/c_1$	N_c (Merifield et al.1999) Lowerbound	Upperbound	(Meyerhof & Hanna 1978)	(Chen 1975)	% Difference between N_c^*(FLAC) & N_c (Meyerhof & Hanna 1978)	(Chen 1975)
20.00	1.00	103.59	5.18	4.94	5.32	5.14	5.53	0.77	−6.76
20.00	0.80	103.61	5.18	4.87	5.30	5.14	5.53	0.77	−6.76
20.00	0.67	102.25	5.11	4.77	5.18	5.14	5.53	−0.59	−8.22
20.00	0.50	94.78	4.74	4.44	4.82	4.46	5.11	5.91	−7.81
20.00	0.33	81.44	4.07	3.89	4.24	3.47	4.52	14.74	−11.06
20.00	0.20	65.89	3.29	3.10	3.54	2.62	3.87	20.36	−17.63
20.00	0.10	47.24	2.36	–	–	1.95	2.59	17.37	−9.75

Grid 60×30 :

In order to study the effect of the grid density, a 60×30 elements grid was chosen which has nine time more elements than in 20×10 grid. The elements under the footing are equisized in x-direction. but spacing in y-direction increases with depth. The spacing for elements on the side of the footing increases as it moves towards the model boundaries. As it can been seen from Table A.2 that the bearing capacity values calculated from 60×30 elements grid were in general found to be to lower than that from 20×10 element grid. The difference increases as c_2/c_1 decreases. The average completion time for a 60×30 grid FLAC model was 18 h and 45 min.

Table A.2: Comparison of modified Bearing Capacity Factor, N_c^* values for coarse (20×10) grid with fine (60×30) grid, for $H/B = 1$.

Shear Strength Ratio, (c_2/c_1)	q_u(FLAC)		% Difference	$N_c^*(\text{FLAC}) = q_u(\text{FLAC})/c_1$		% Difference
	G2010	G6030		G2010	G6030	
1.00	103.59	103.79	−0.19	5.18	5.19	−0.19
0.80	103.61	103.63	−0.02	5.18	5.18	−0.02
0.67	102.25	100.57	1.65	5.11	5.03	1.65
0.50	94.78	91.06	3.93	4.74	4.55	3.93
0.33	81.44	76.97	5.48	4.07	3.85	5.48
0.20	65.89	60.55	8.11	3.29	3.03	8.11
0.10	47.24	41.68	11.78	2.36	2.08	11.78

Grid 40×30 :

Since the completion time for 60×30 grid model is a much longer than the 20×10 grid, a different approach was required which reduces the size of the grid, but at the same time does not compromise bearing capacity results. A smaller element grid (40×30) was adopted. The elements under the footing were now graded both in in x & y - directions. The spacing was kept finer near the edge of the footing, but it increases as it moves towards the centre of the footing ($-x$ - direction). No. of elements in the region outside the footing in x - direction (30) are same as that in 60×30 grid. No. of elements in the y - direction (30) are also kept same as that in 60×30 grid. The comparison between the bearing capacity results from 40×30 and 60×30 are shown in Table A.3. The modified bearing capacity values N_c^* for 40×30 are within 0.3% of that in grid 60×30 model. The average completion for 40×30 grid model was 10 h and 45 min which is 8 h less than that in 60×30 grid model. A 40×30 grid model then is used in rest of this study.

Table A.3: Comparison of modified Bearing Capacity Factor, N_c^* values for coarse (40×30) with fine (60×30), for $H/B = 1$.

Shear Strength Ratio, (c_2/c_1)	q_u(FLAC)		% Difference	N_c^*(FLAC) $= q_u$(FLAC)$/c_1$		% Difference
	G4030	G6030		G4030	G6030	
1.00	103.52	103.79	−0.27	5.18	5.19	−0.27
0.80	103.51	103.63	−0.11	5.18	5.18	−0.11
0.67	100.78	100.57	0.21	5.04	5.03	0.21
0.50	91.14	91.06	0.09	4.56	4.55	0.09
0.33	77.05	76.97	0.10	3.85	3.85	0.10
0.20	60.62	60.55	0.12	3.03	3.03	0.12
0.10	41.68	41.68	0.01	2.08	2.08	0.01

The following figures and section describe the behaviour of a rigid smooth strip footing resting on strong clay underlain by soft clay for cases as in A.1.1. These figures show the steady state model conditions at the end of analysis.

Case 1: $c_2/c_1 = 1$ (Homogeneous clay) - Small Deformation Analysis

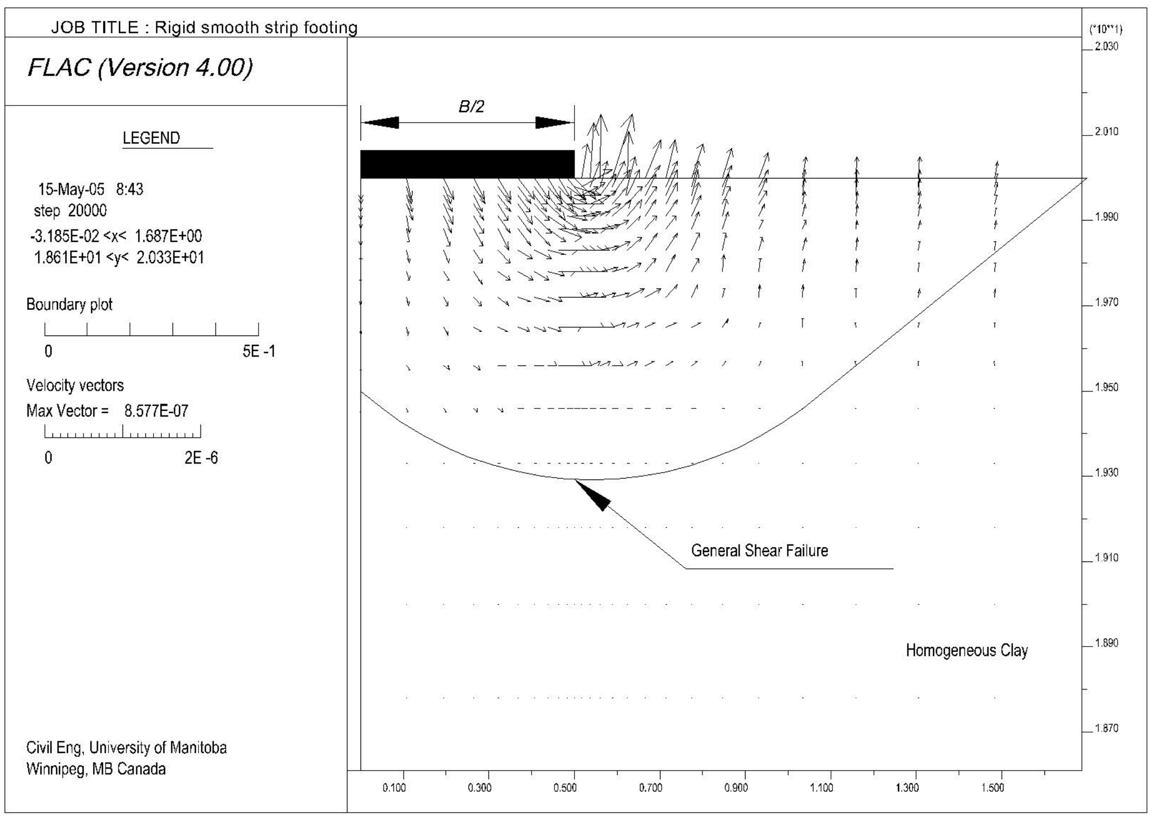

Figure A.4: Velocity vectors and general shear failure mechanism for a rigid strip footing for 40×30 grid model on homogeneous clay $H/B = 1$, $c_2/c_1 = 1$.

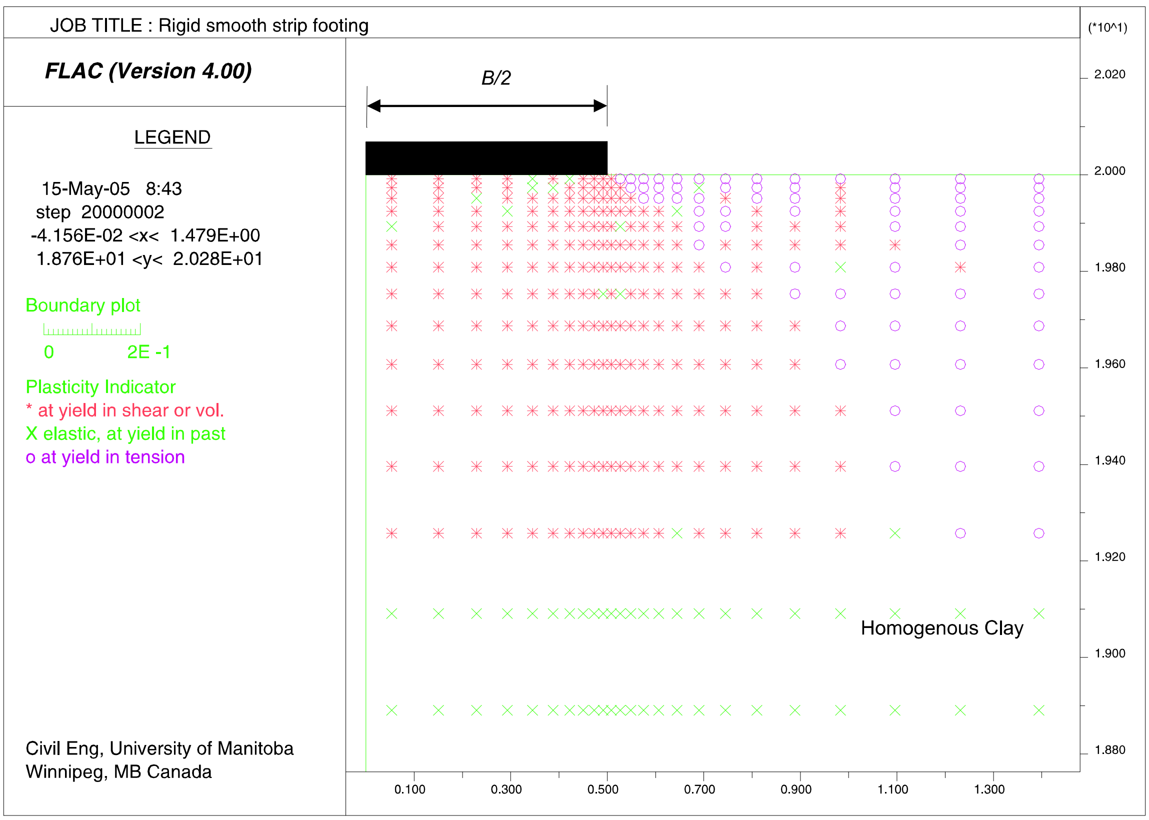

Figure A.5: Plasticity state indicators at steady state condition for a rigid smooth strip footing on strong over soft clay for 40 × 30 grid model, $H/B = 1$, $c_2/c_1 = 1$.

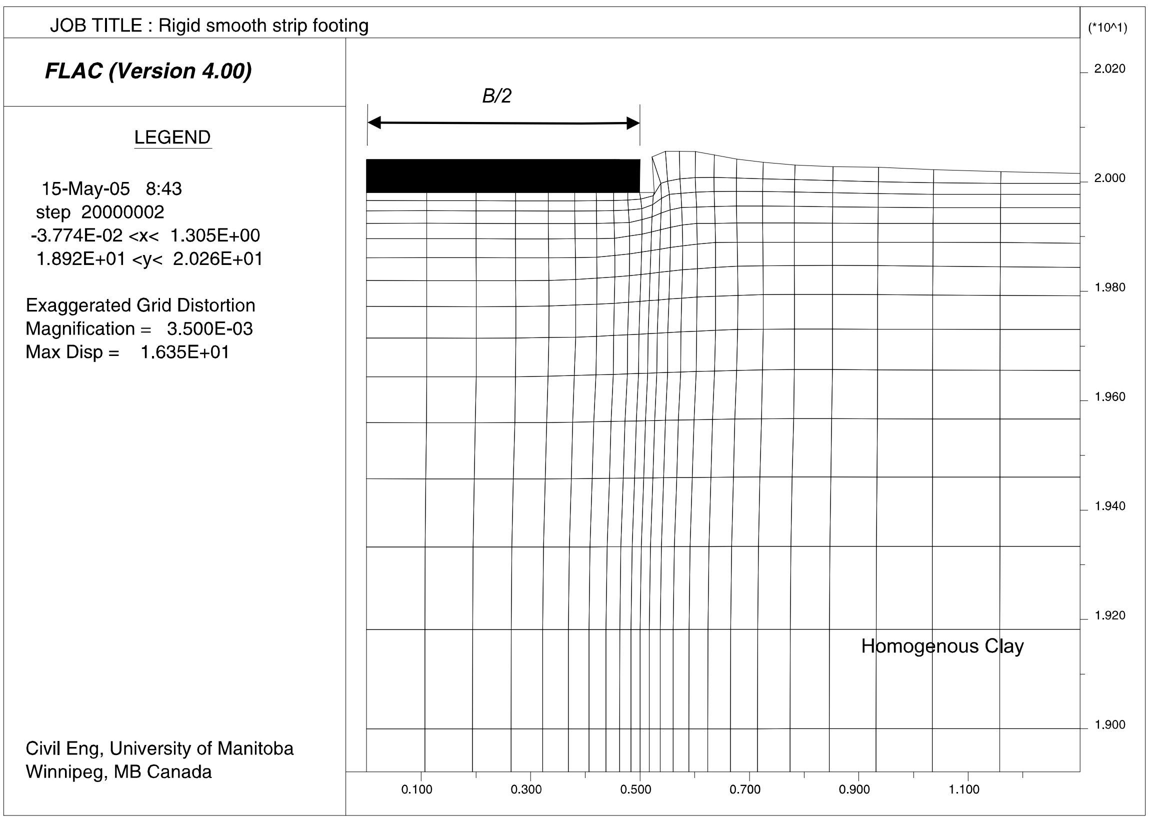

Figure A.6: Magnified grid for a rigid smooth strip footing on strong over soft clay for 40 × 30 grid model, $H/B = 1$, $c_2/c_1 = 1$.

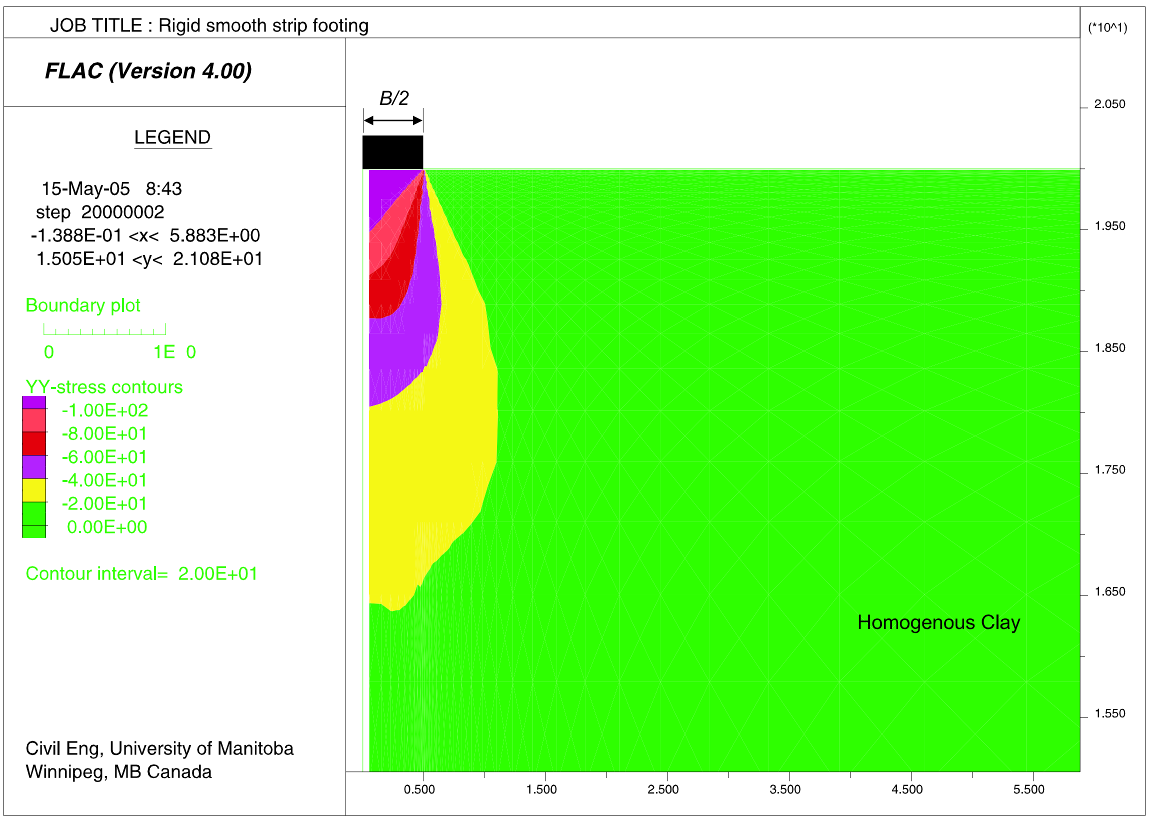

Figure A.7: Vertical stress (σ_{yy}) contours for a rigid smooth strip footing on strong over soft clay for 40×30 grid model, $H/B = 1$, $c_2/c_1 = 1$.

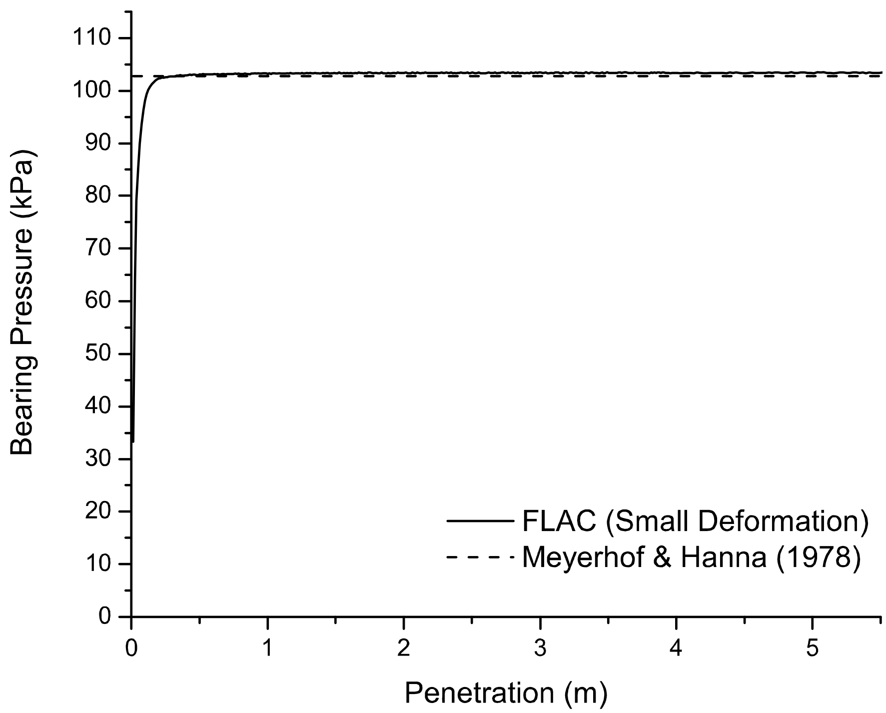

Figure A.8: Bearing pressure versus penetration curve for a rigid smooth strip footing on strong over soft clay for 40 × 30 grid model, $H/B = 1$, $c_2/c_1 = 1$.

Case 2: $c_2/c_1 = 0.8$ **- Small Deformation Analysis**

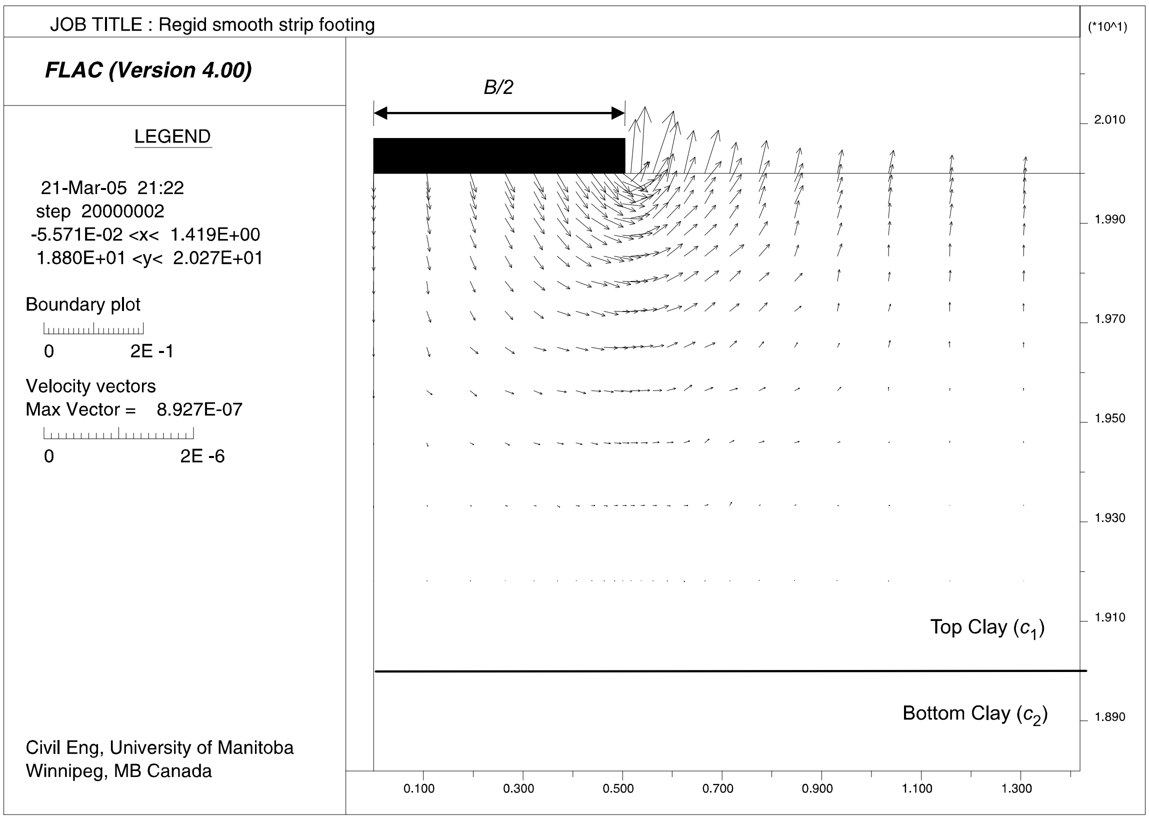

Figure A.9: Velocity vectors for a rigid strip footing on strong over soft clay for 40×30 grid model, $H/B = 1$, $c_2/c_1 = 0.8$.

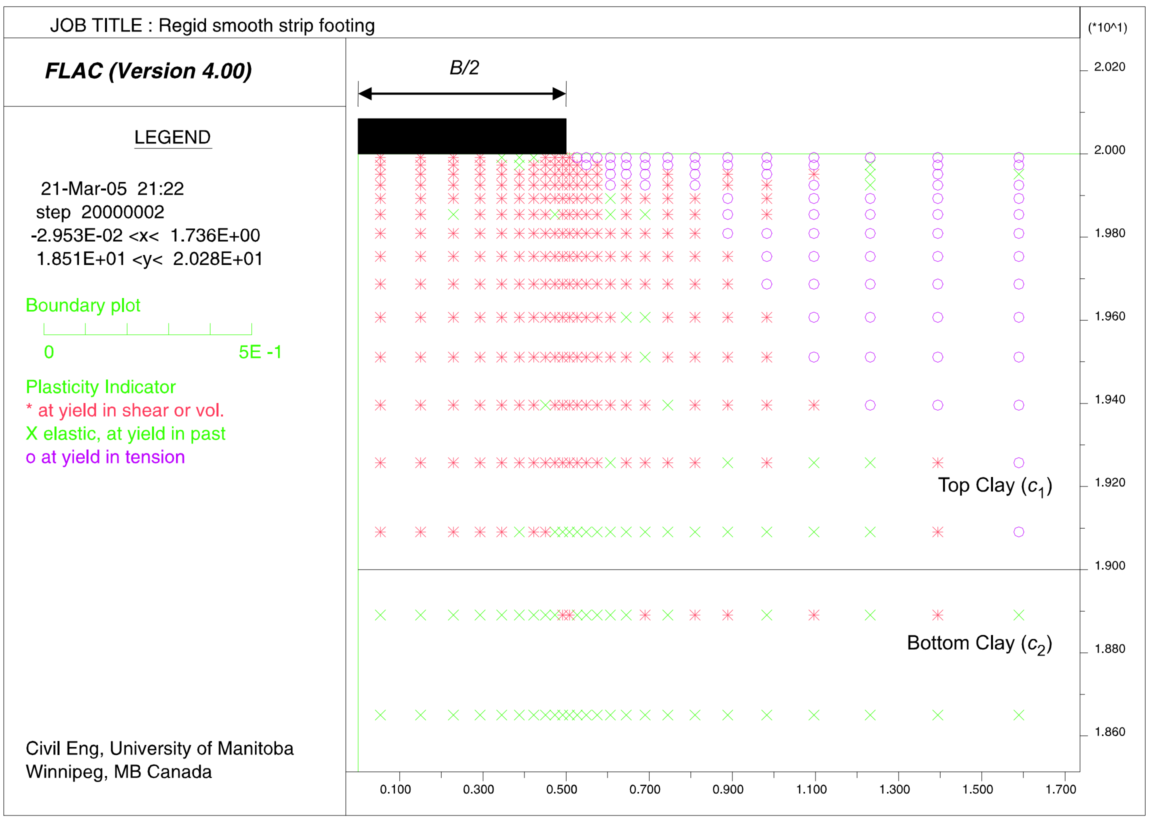

Figure A.10: Plasticity state indicators at steady state condition for a rigid smooth strip footing on strong over soft clay for 40×30 grid model, $H/B = 1$, $c_2/c_1 = 0.8$.

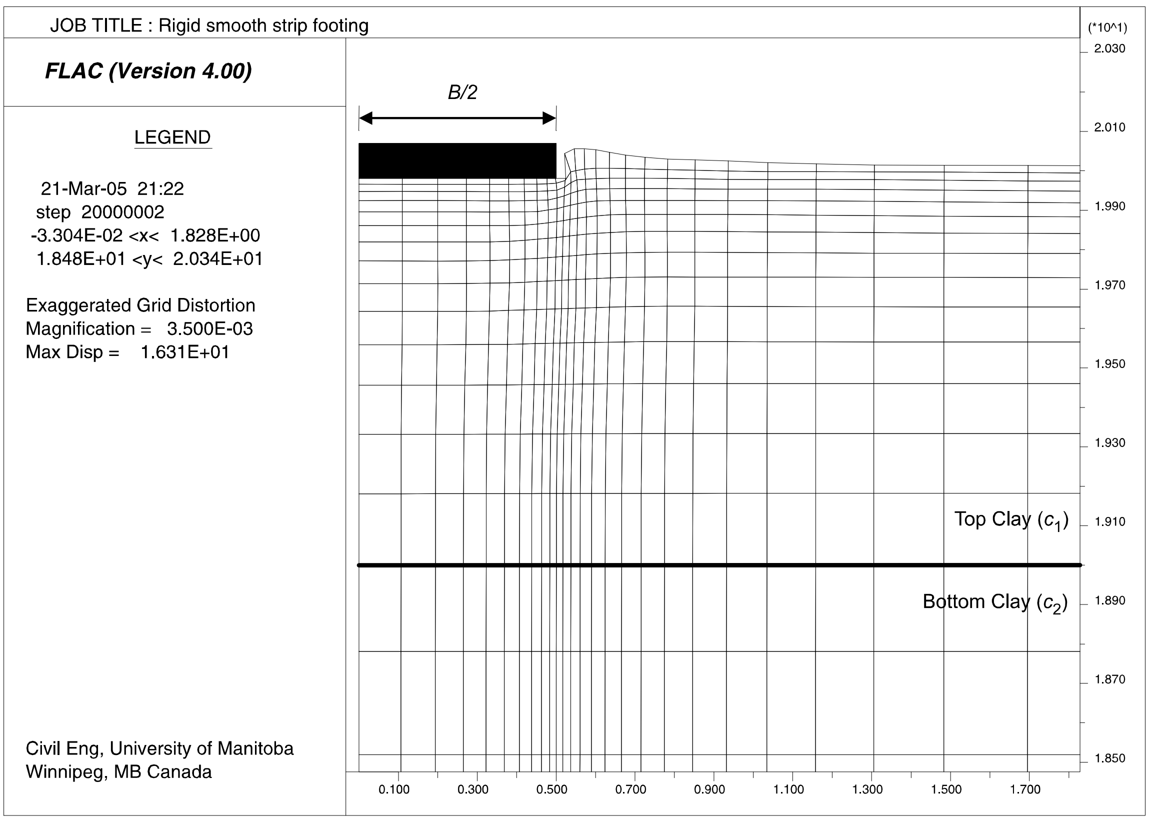

Figure A.11: Magnified grid for a rigid smooth strip footing on strong over soft clay for 40 × 30 grid model, $H/B = 1$, $c_2/c_1 = 0.8$.

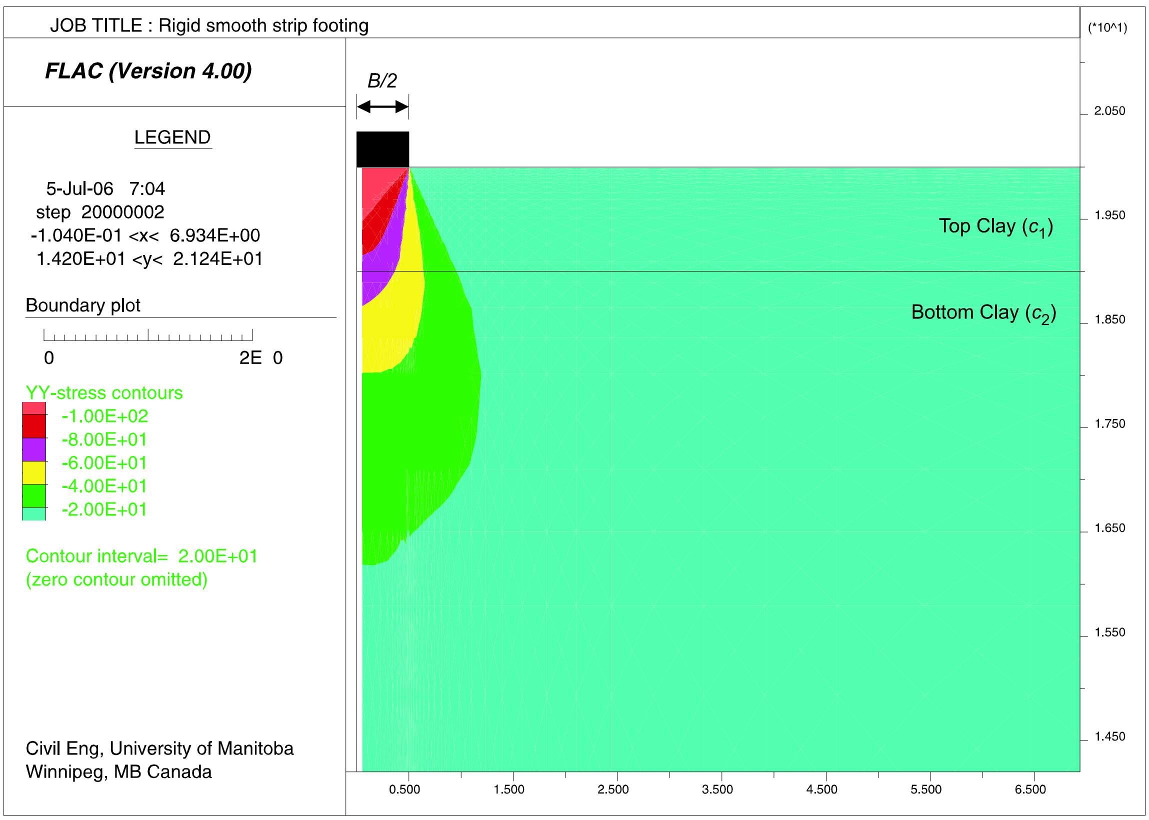

Figure A.12: Vertical stress (σ_{yy}) contours for a rigid smooth strip footing on strong over soft clay for 40×30 grid model, $H/B = 1$, $c_2/c_1 = 0.8$.

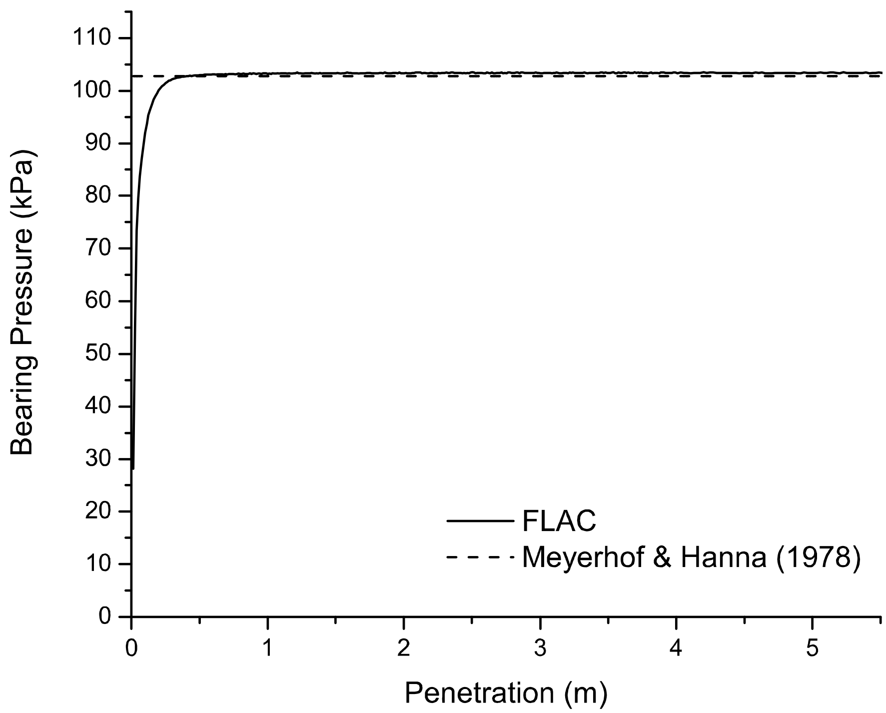

Figure A.13: Bearing pressure versus penetration curve for a rigid smooth strip footing on strong over soft clay for 40×30 grid model, $H/B = 1$, $c_2/c_1 = 0.8$.

Case 3: $c_2/c_1 = 2/3$ **- Small Deformation Analysis**

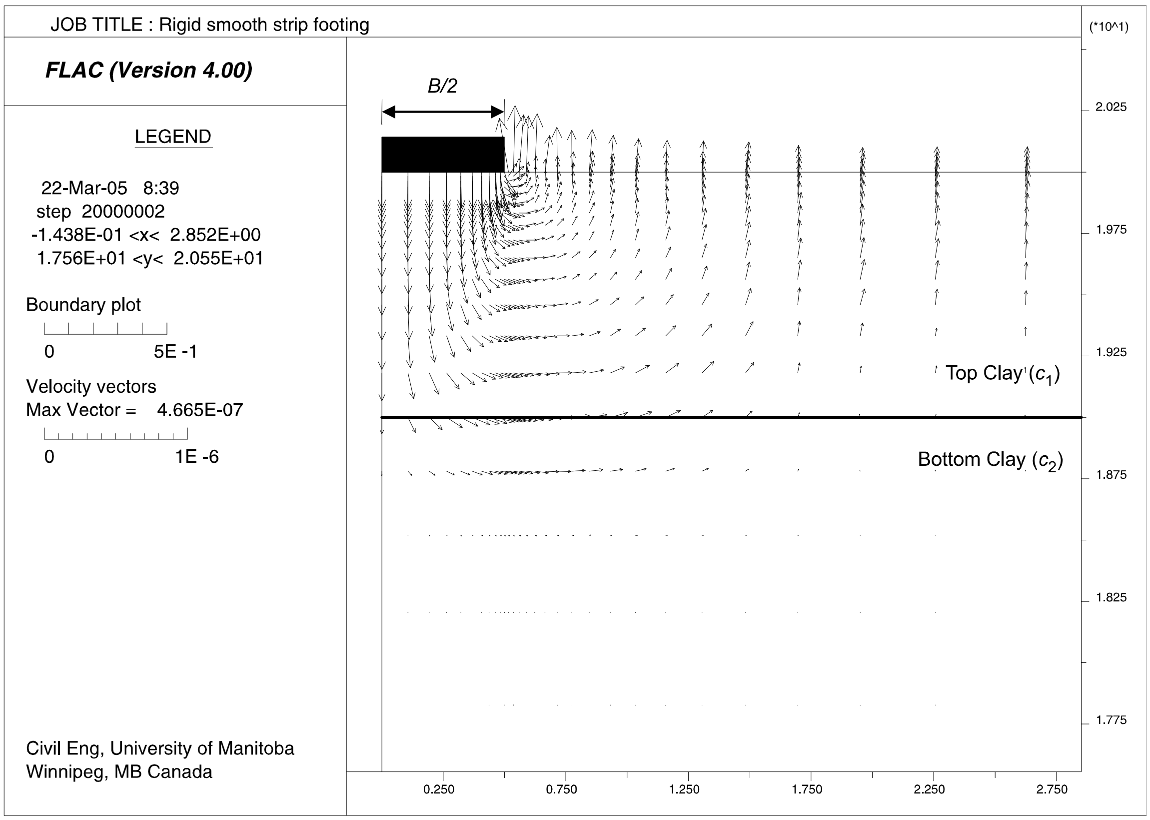

Figure A.14: Velocity vectors for a rigid smooth strip footing on strong over soft clay for 40 × 30 grid model, $H/B = 1$, $c_2/c_1 = 2/3$.

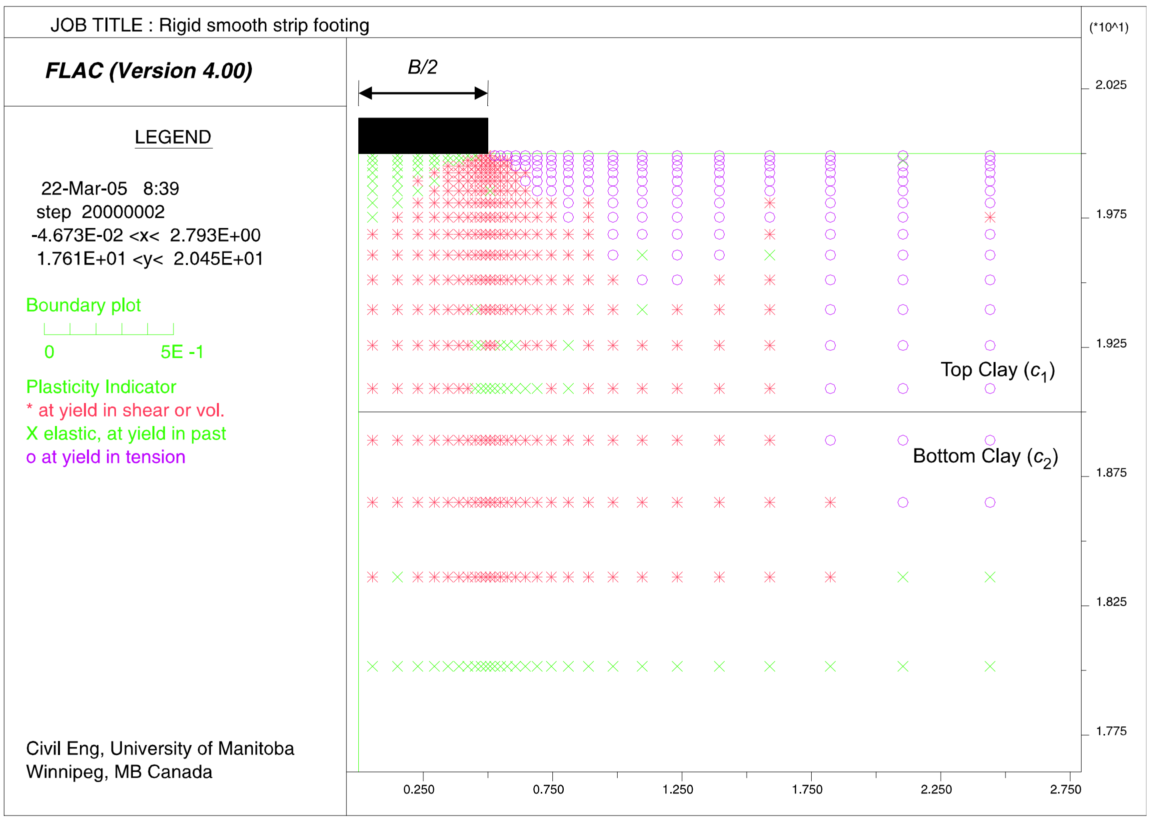

Figure A.15: Plasticity state indicators at steady state condition for a rigid smooth strip footing on strong over soft clay for 40 × 30 grid model, $H/B = 1$, $c_2/c_1 = 2/3$.

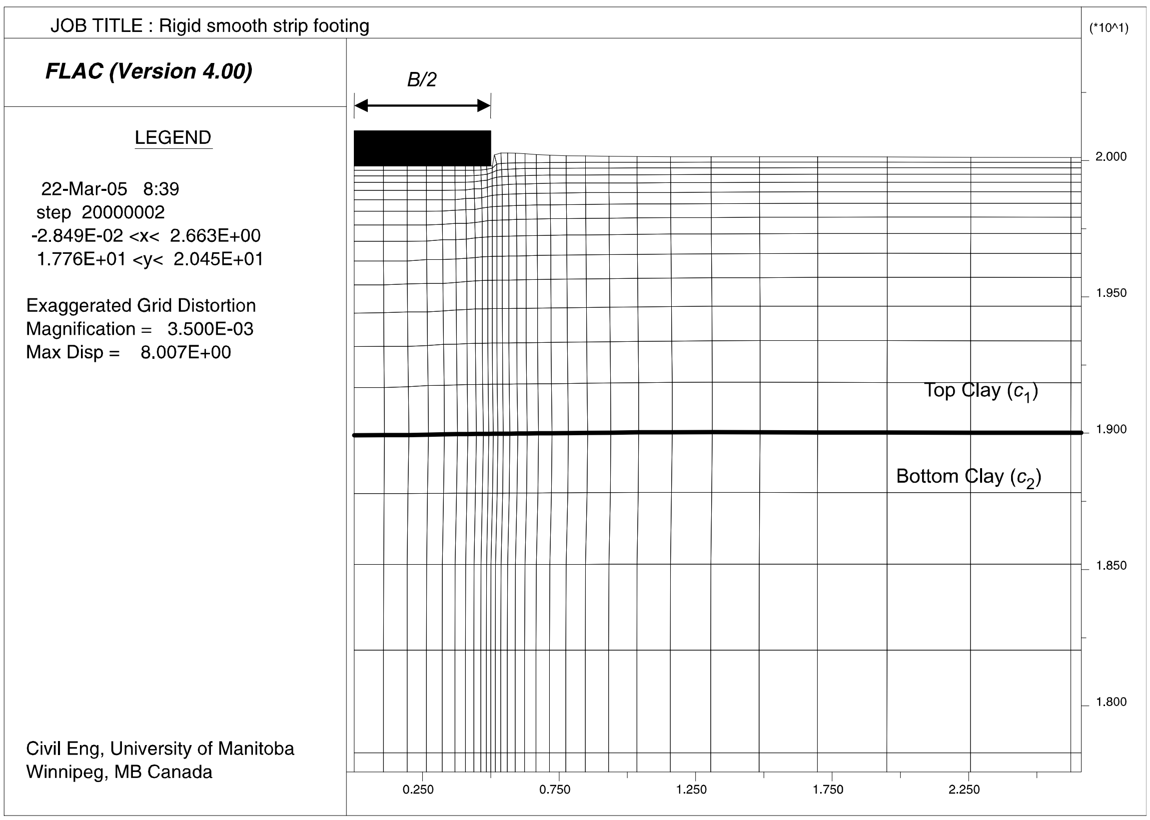

Figure A.16: Magnified grid for a rigid smooth strip footing on strong over soft clay for 40 × 30 grid model, $H/B = 1$, $c_2/c_1 = 2/3$.

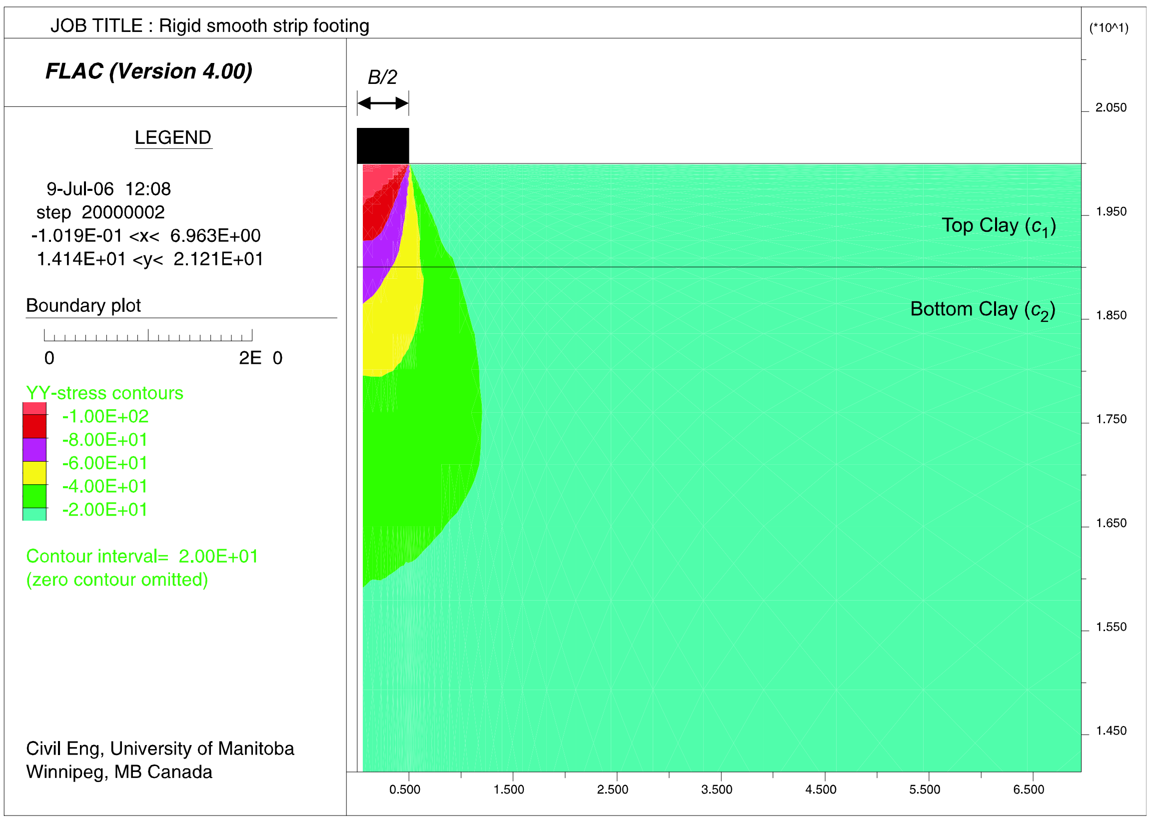

Figure A.17: Vertical stress (σ_{yy}) contours for a rigid smooth strip footing on strong over soft clay for 40×30 grid model, $H/B = 1$, $c_2/c_1 = 2/3$.

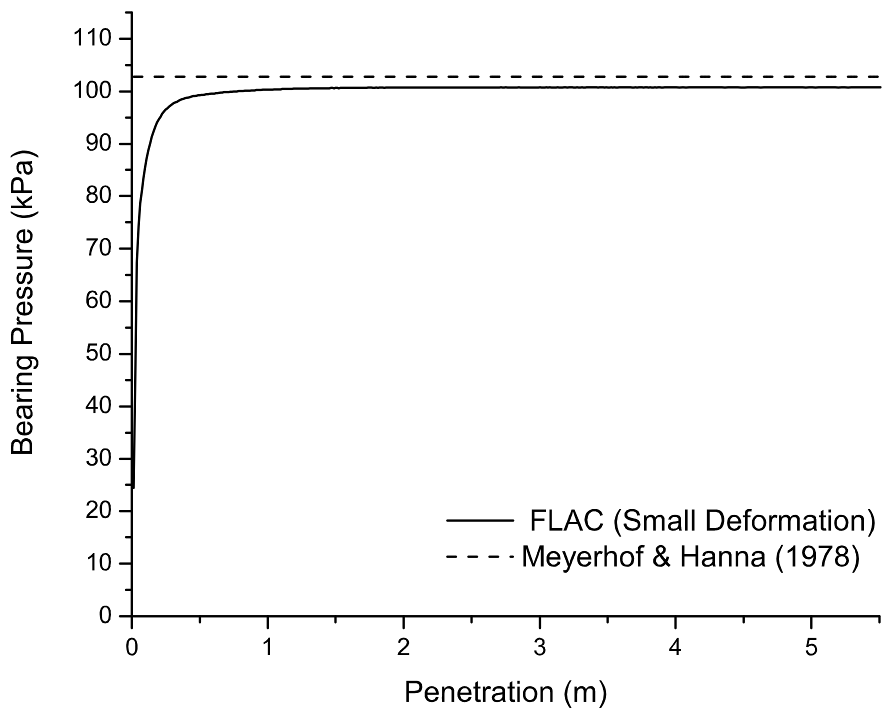

Figure A.18: Bearing pressure versus penetration curve for a rigid smooth strip footing on strong over soft clay for 40 × 30 grid model, $H/B = 1$, $c_2/c_1 = 2/3$.

Case 4: $c_2/c_1 = 0.5$ - Small Deformation Analysis

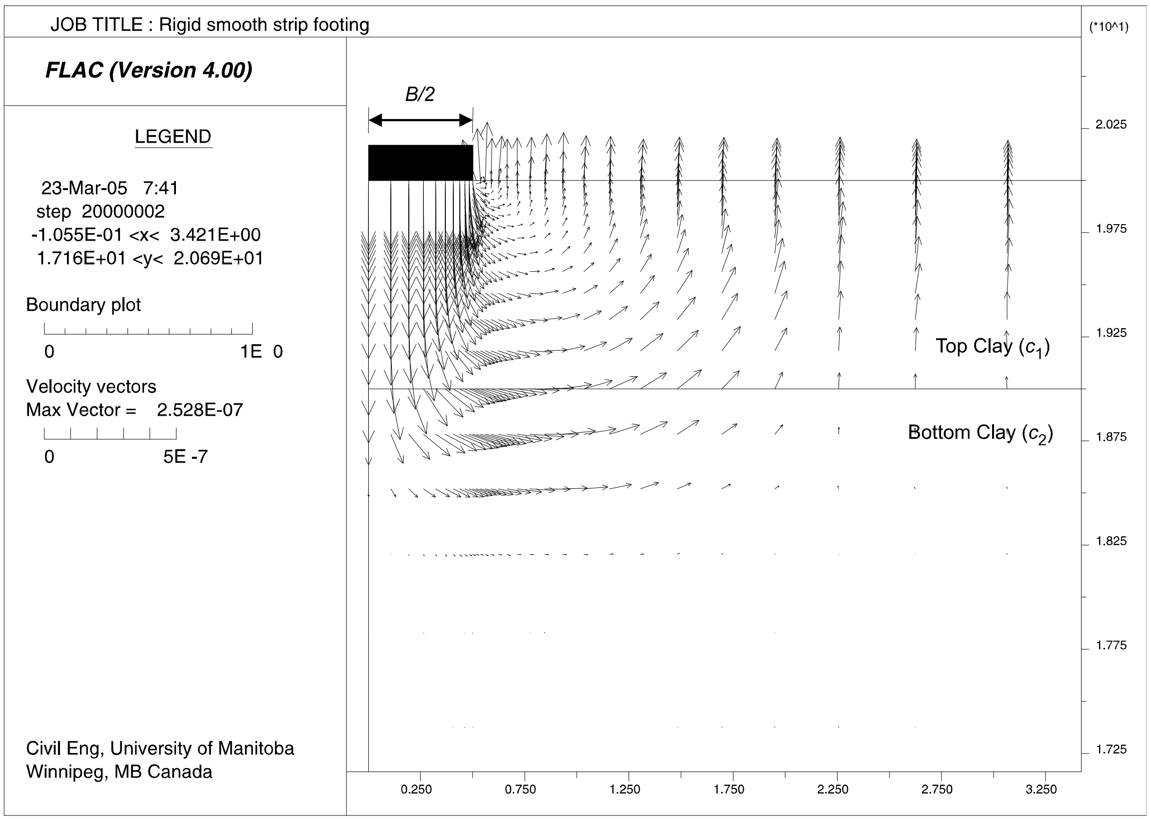

Figure A.19: Velocity vectors for rigid smooth strip footing on strong over soft clay for 40×30 grid model, $H/B = 1$, $c_2/c_1 = 0.5$.

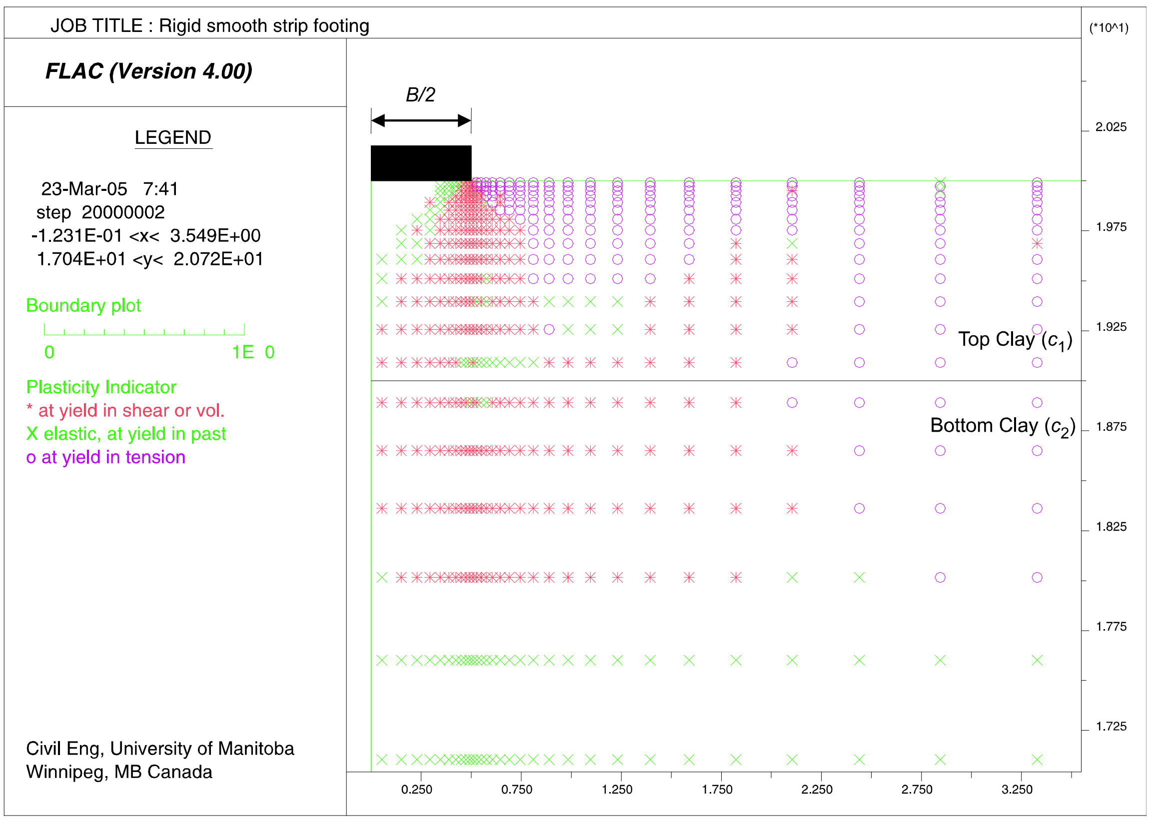

Figure A.20: Plasticity state indicators at steady state condition for a rigid smooth strip footing on strong over soft clay for 40 × 30 grid model, $H/B = 1$, $c_2/c_1 = 0.5$.

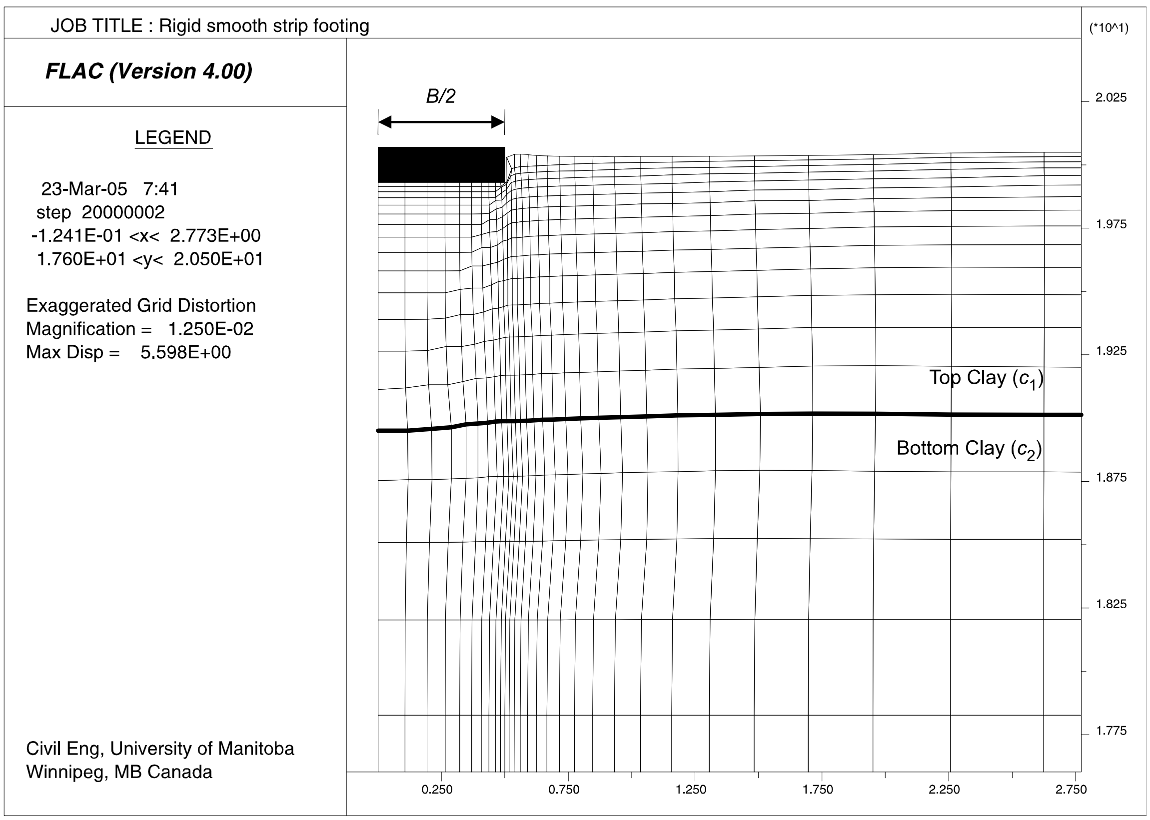

Figure A.21: Magnified grid for a rigid smooth strip footing on strong over soft clay for 40 × 30 grid model, $H/B = 1$, $c_2/c_1 = 0.5$.

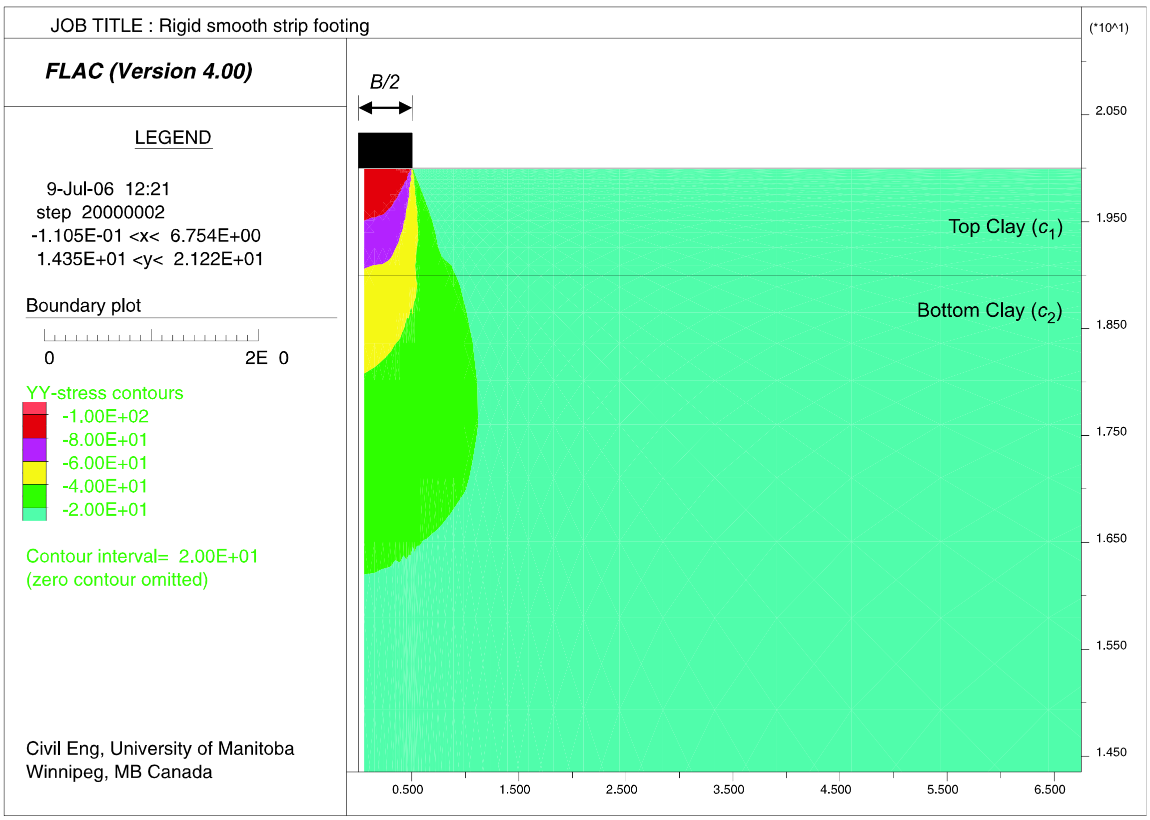

Figure A.22: Vertical stress (σ_{yy}) contours for a rigid smooth strip footing on strong over soft clay for 40 × 30 grid model, $H/B = 1$, $c_2/c_1 = 0.5$.

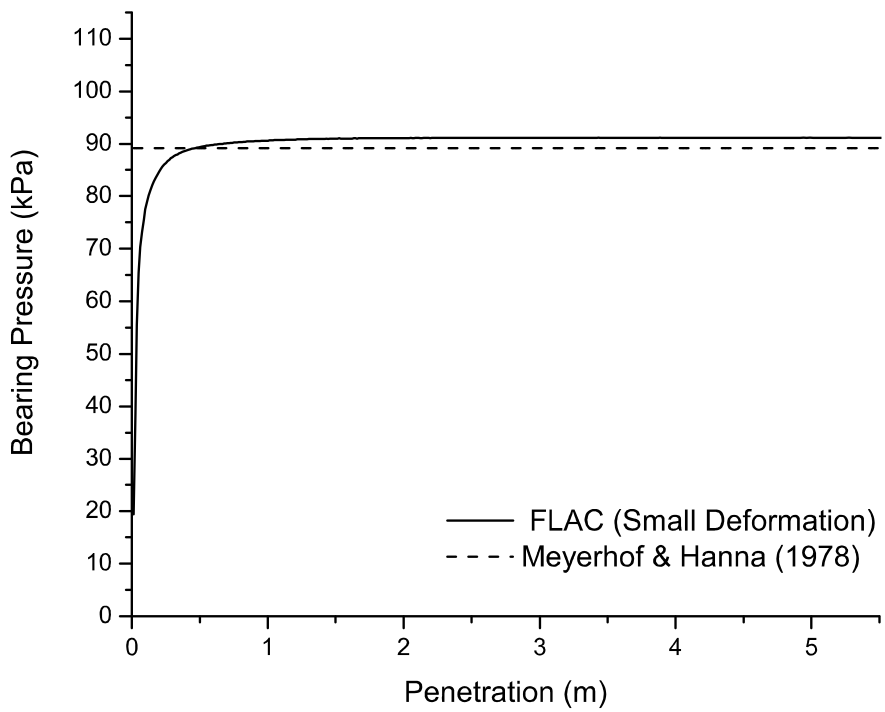

Figure A.23: Bearing pressure versus penetration curve for a rigid smooth strip footing on strong over soft clay for 40 × 30 grid model, $H/B = 1$, $c_2/c_1 = 0.5$.

Case 5: $c_2/c_1 = 1/3$ - Small Deformation Analysis

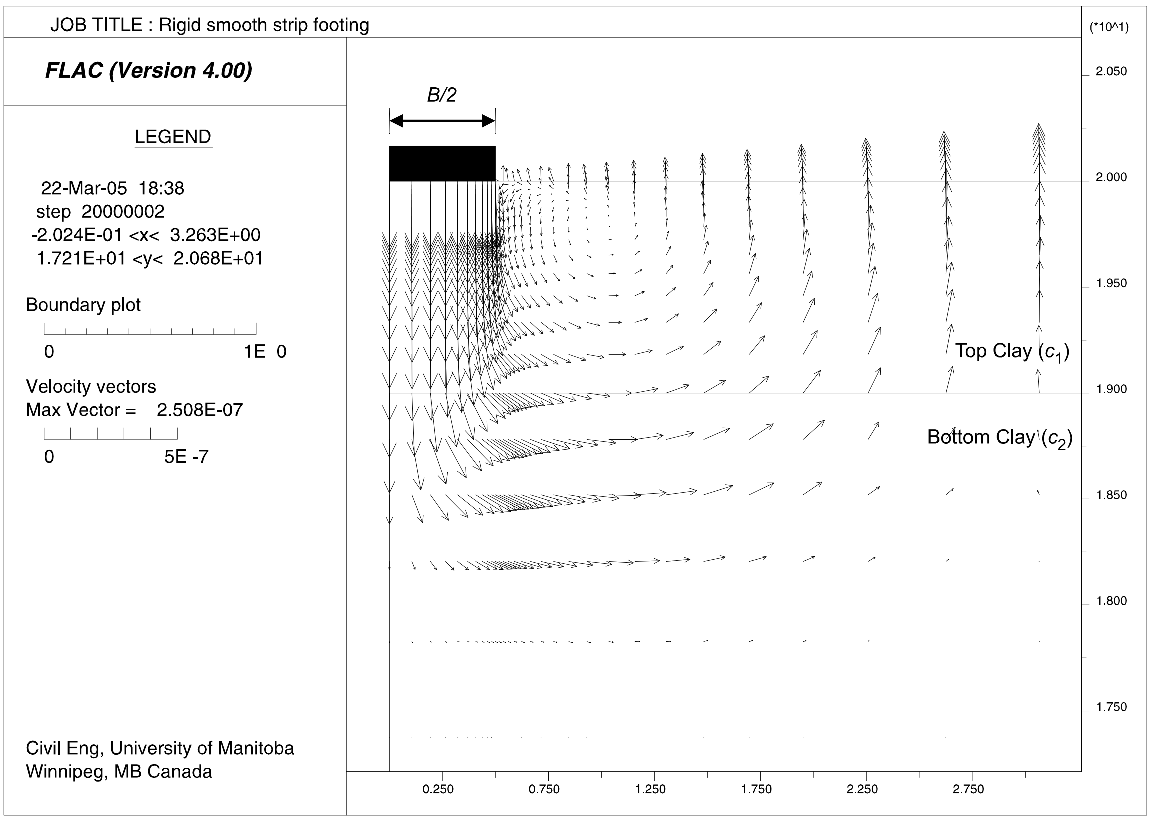

Figure A.24: Velocity vectors for a rigid smooth strip footing on strong over soft clay for 40×30 grid model, $H/B = 1$, $c_2/c_1 = 1/3$.

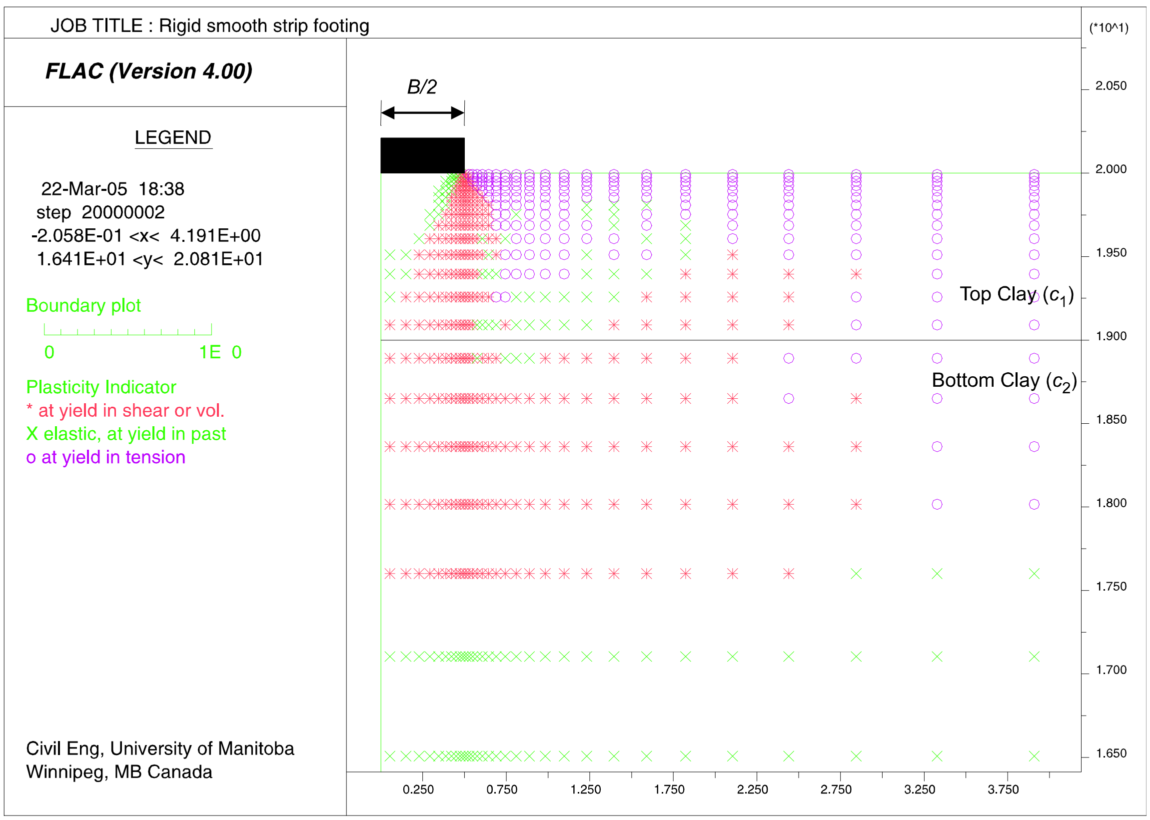

Figure A.25: Plasticity state indicators at steady state condition for a rigid smooth strip footing on strong over soft clay for 40×30 grid model, $H/B = 1$, $c_2/c_1 = 1/3$.

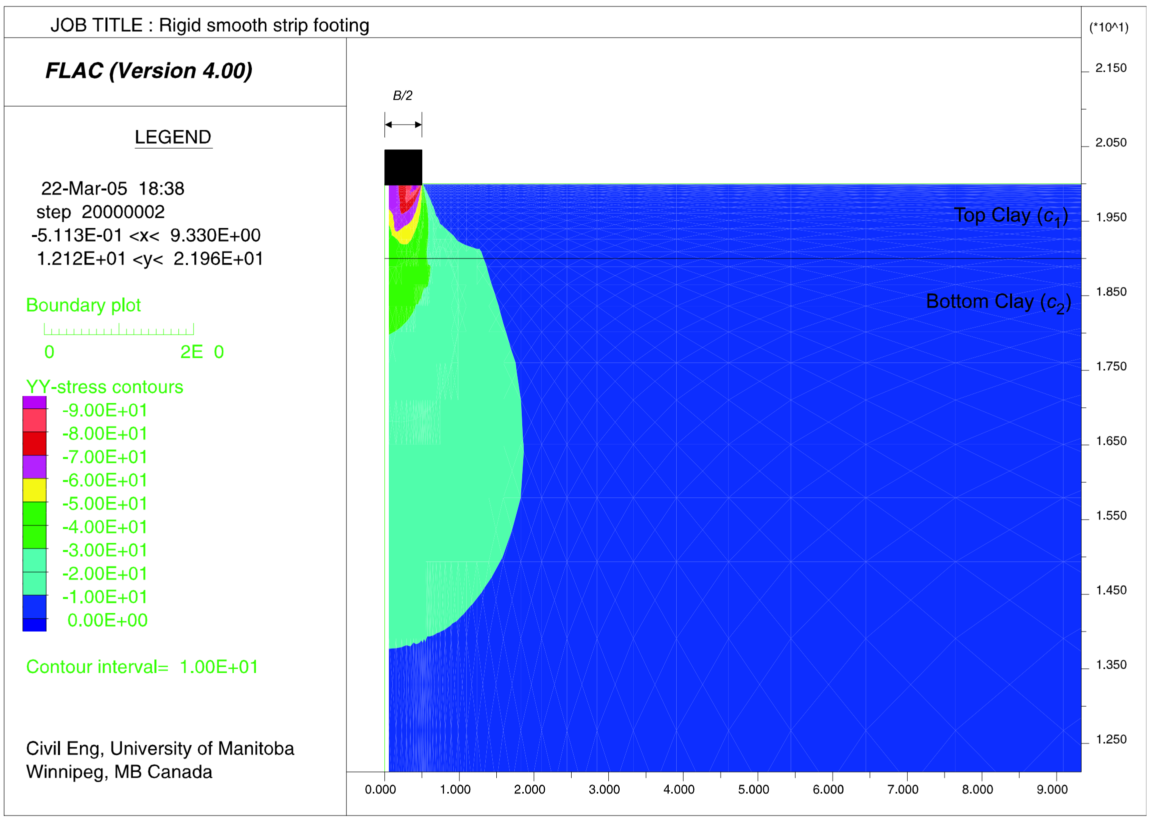

Figure A.26: Vertical stress (σ_{yy}) contours for a rigid smooth strip footing on strong over soft clay for 40 × 30 grid model, $H/B = 1$, $c_2/c_1 = 1/3$.

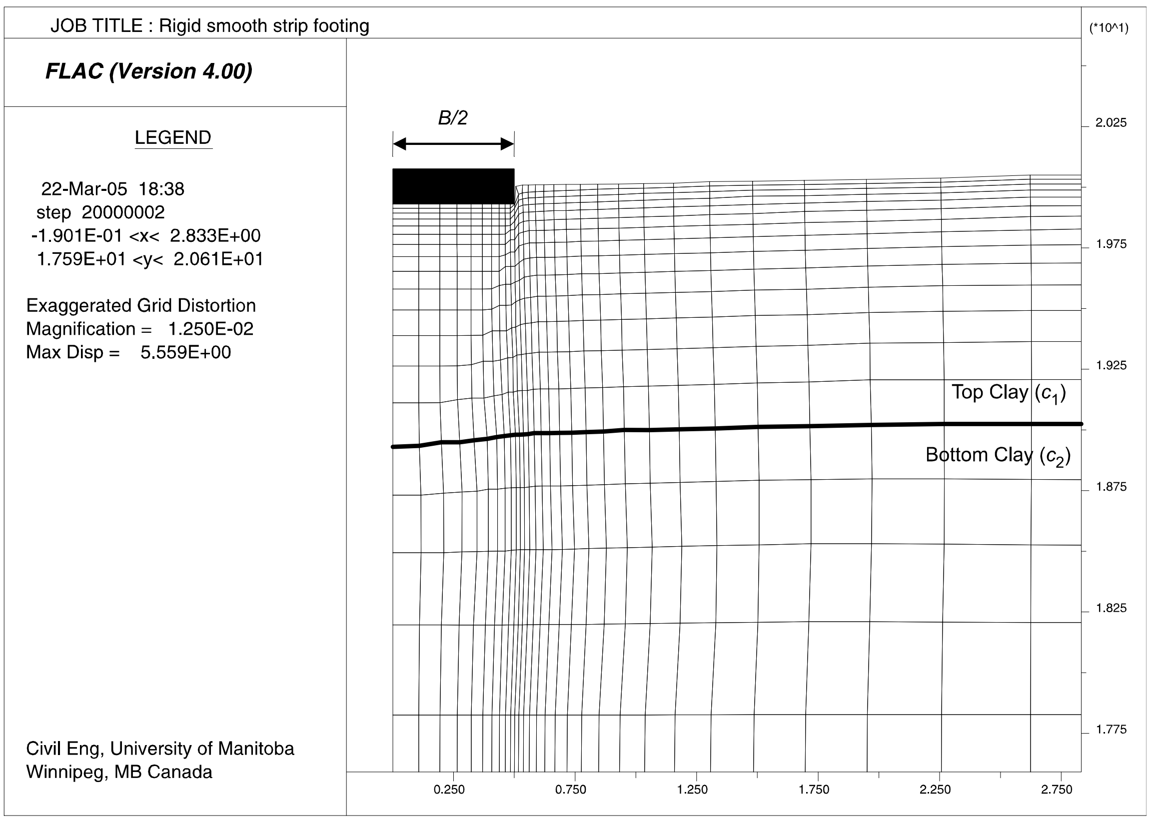

Figure A.27: Magnified grid for a rigid smooth strip footing on strong over soft clay for 40 × 30 grid model, $H/B = 1$, $c_2/c_1 = 1/3$.

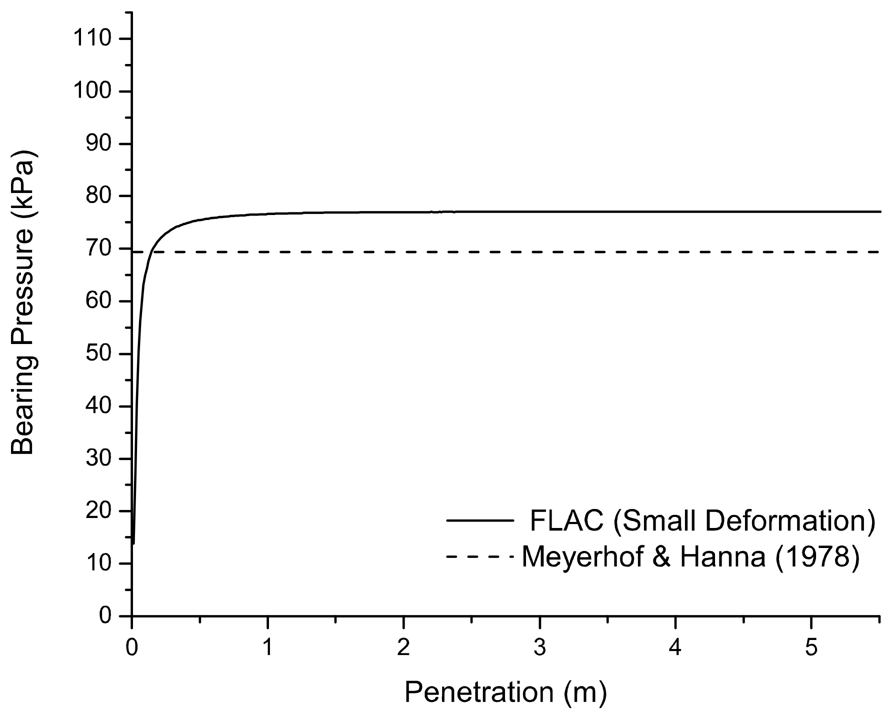

Figure A.28: Bearing pressure versus penetration curve for a rigid smooth strip footing on strong over soft clay for 40 × 30 grid model, $H/B = 1$, $c_2/c_1 = 1/3$.

Case 6: $c_2/c_1 = 0.2$ **- Small Deformation Analysis**

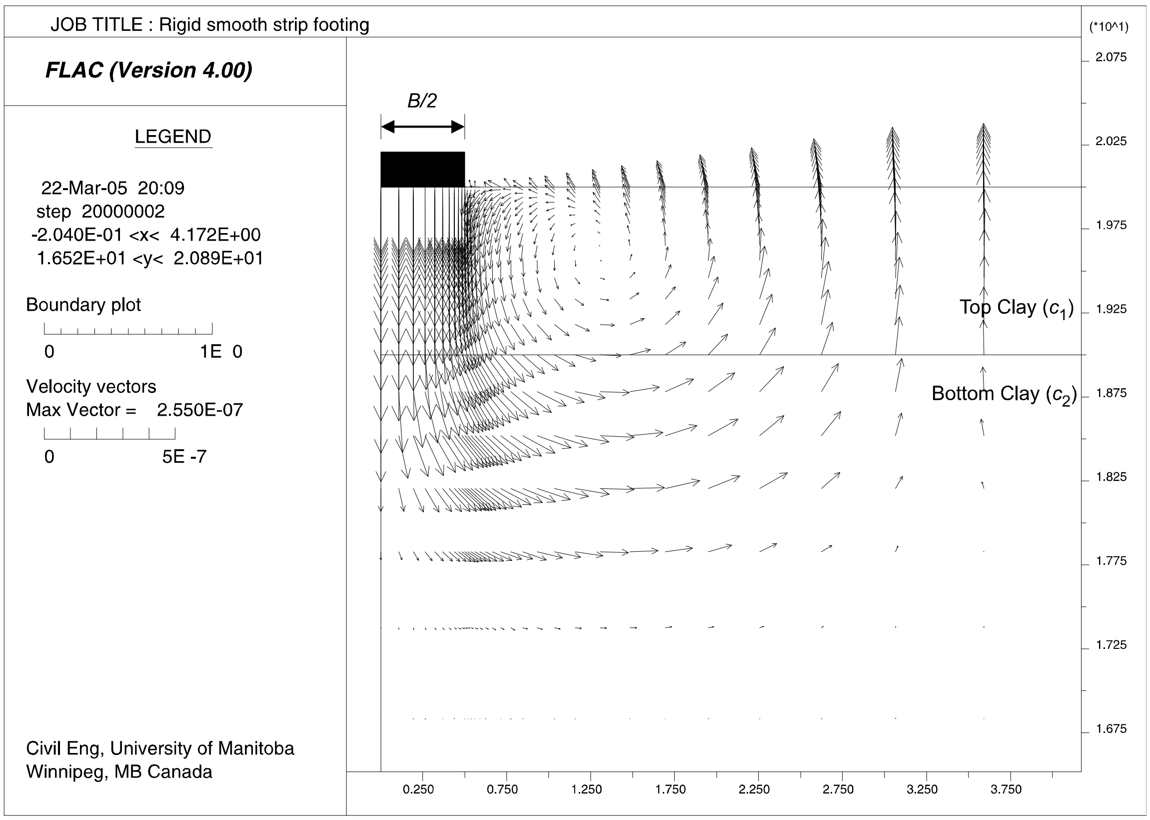

Figure A.29: Velocity vectors for a rigid smooth strip footing on strong over soft clay for 40 × 30 grid model, $H/B = 1$, $c_2/c_1 = 0.2$.

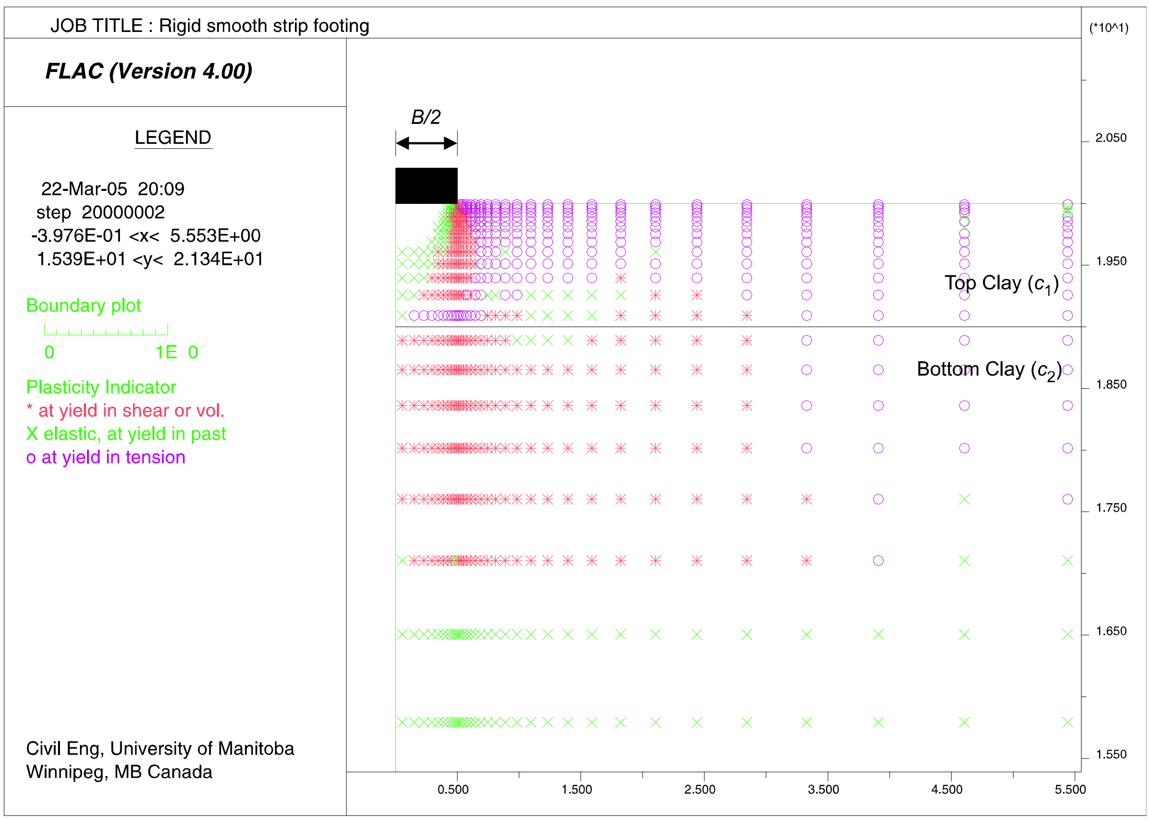

Figure A.30: Plasticity state indicators at steady state condition for a rigid smooth strip footing on strong over soft clay for 40 × 30 grid model, $H/B = 1$, $c_2/c_1 = 0.2$.

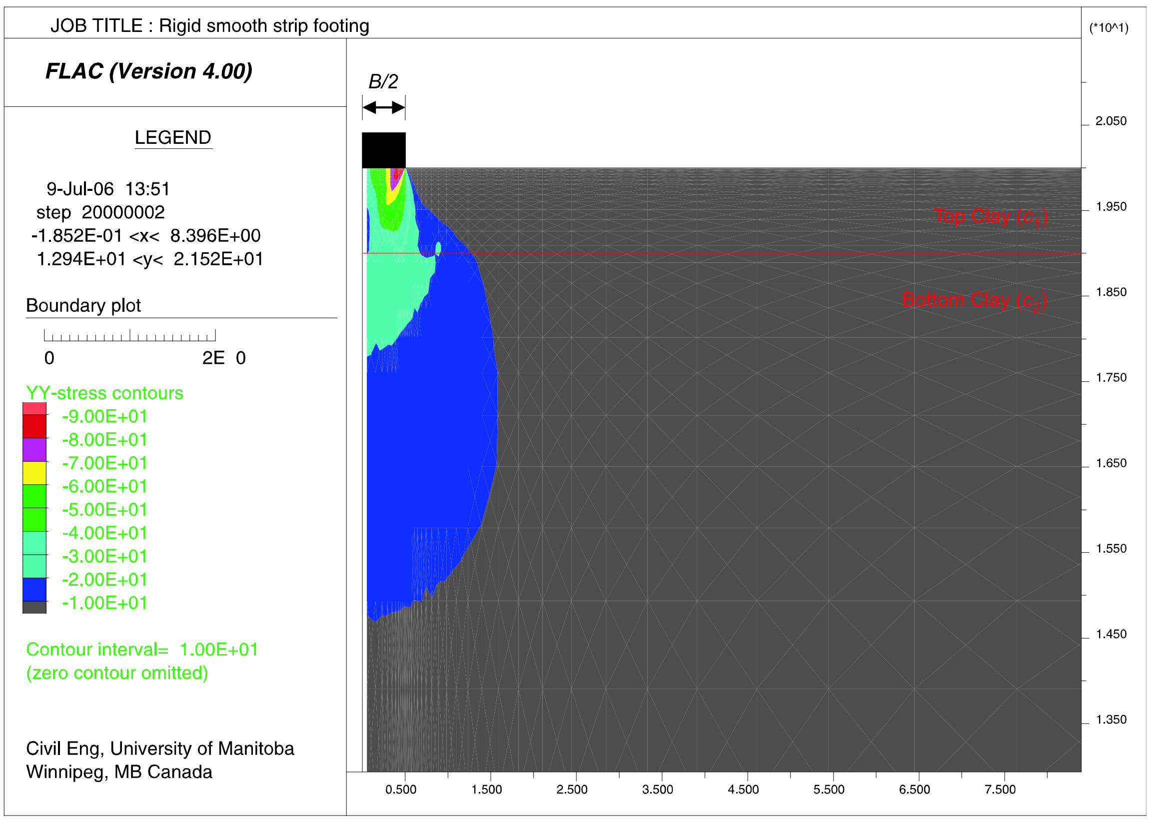

Figure A.31: Vertical stress (σ_{yy}) contours for a rigid smooth strip footing on strong over soft clay for 40×30 grid model, $H/B = 1$, $c_2/c_1 = 0.2$.

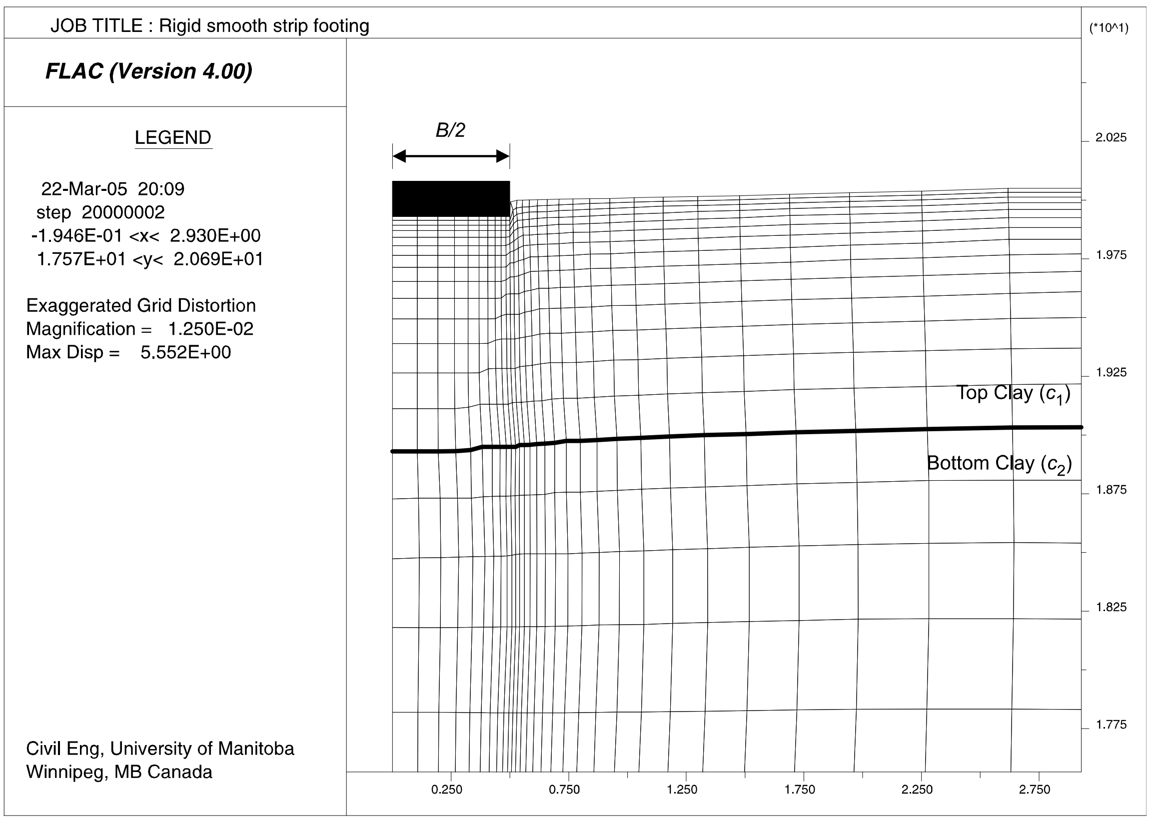

Figure A.32: Magnified grid for a rigid smooth strip footing on strong over soft clay for 40×30 grid model, $H/B = 1$, $c_2/c_1 = 0.2$.

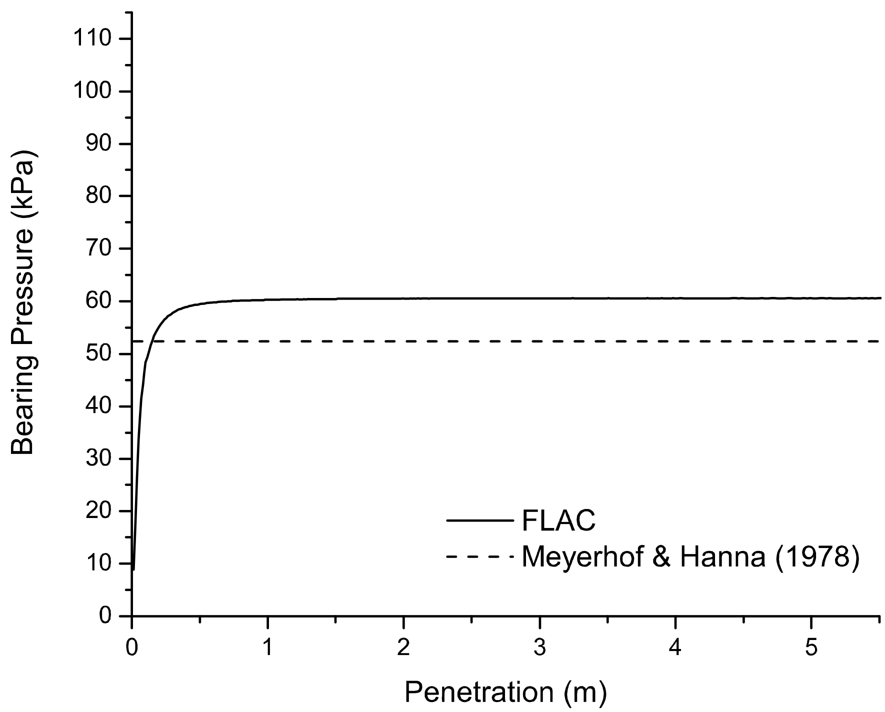

Figure A.33: Bearing pressure versus penetration curve for a rigid smooth strip footing on strong over soft clay for 40 × 30 grid model, $H/B = 1$, $c_2/c_1 = 0.2$.

Case 7: $c_2/c_1 = 0.1$ **- Small Deformation Analysis**

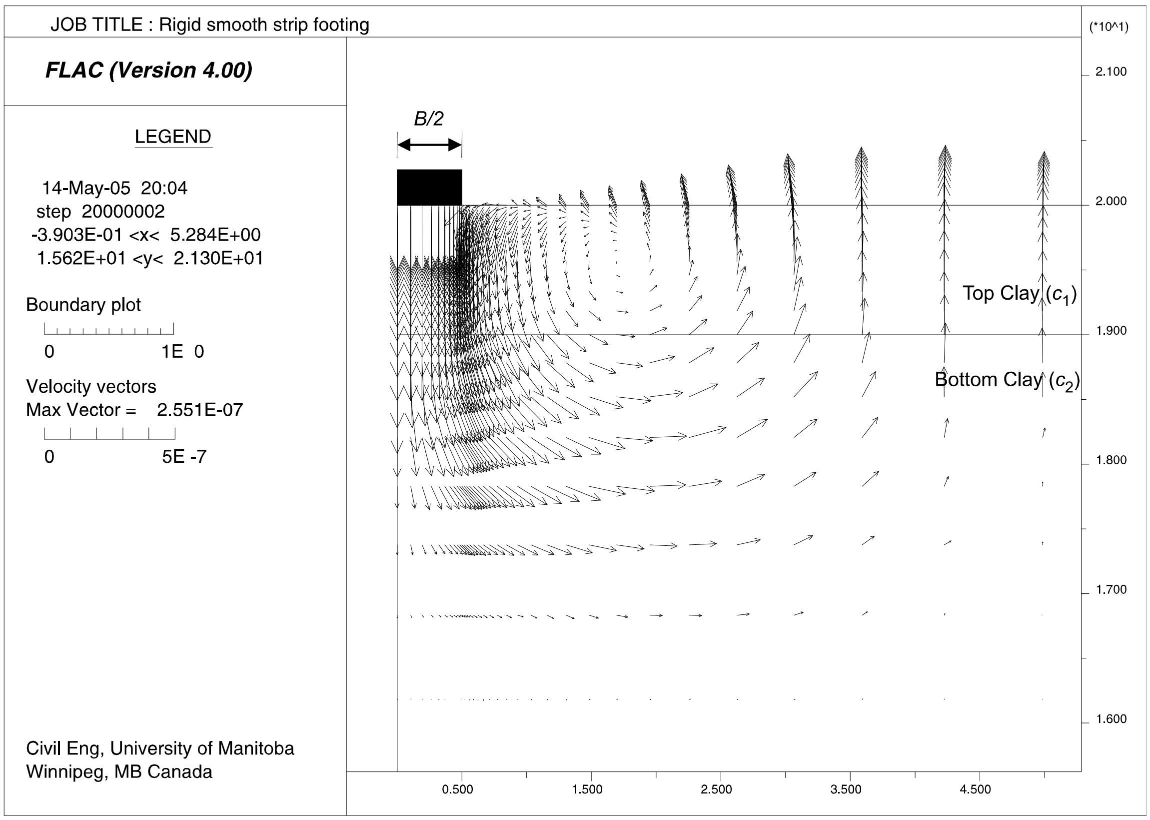

Figure A.34: Velocity vectors for a rigid smooth strip footing on strong over soft clay for 40×30 grid model, $H/B = 1$, $c_2/c_1 = 0.1$.

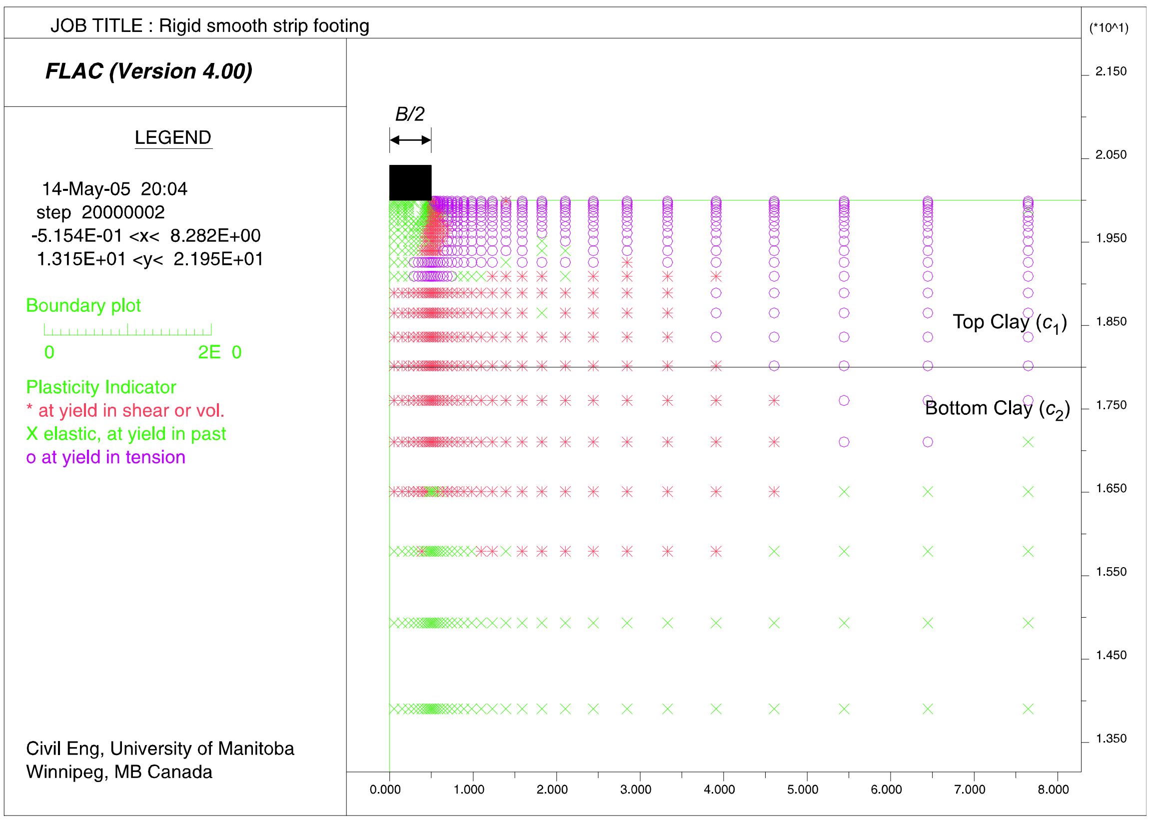

Figure A.35: Plasticity state indicators at steady state condition for a rigid smooth strip footing on strong over soft clay for 40×30 grid model, $H/B = 1$, $c_2/c_1 = 0.1$.

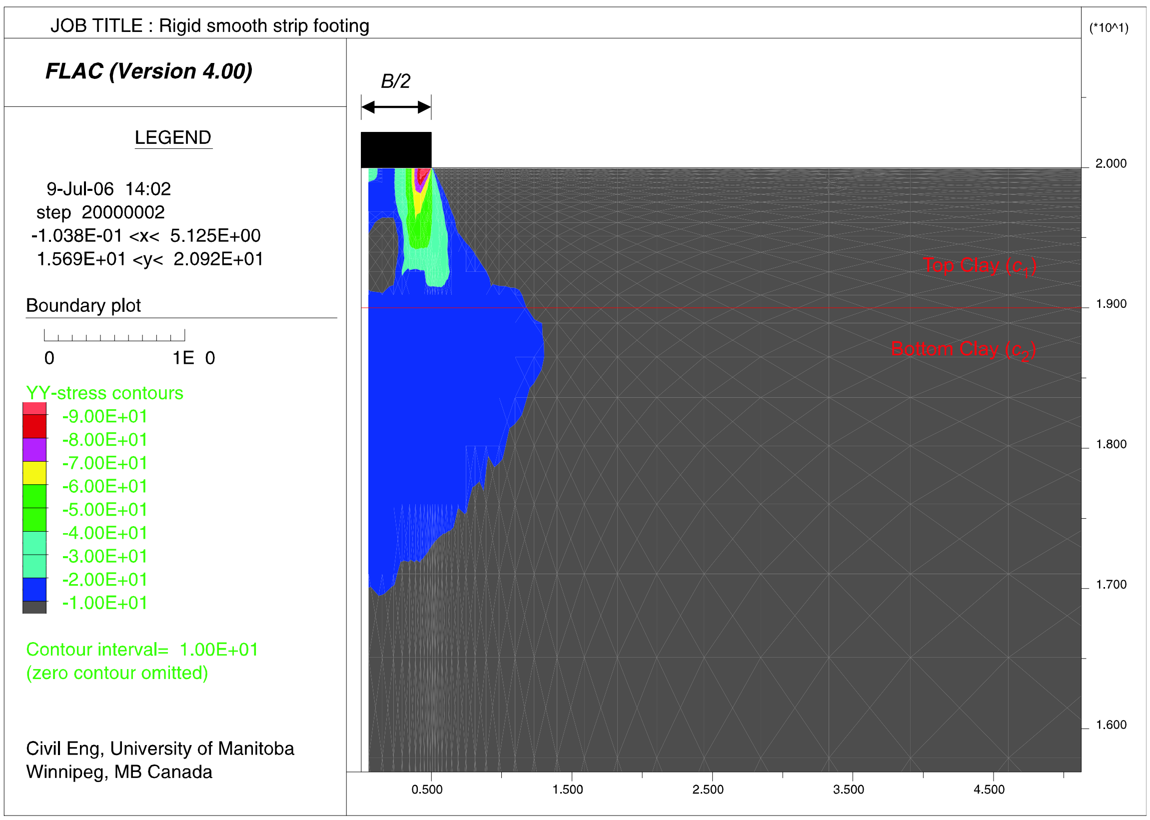

Figure A.36: Vertical stress (σ_{yy}) contours for a rigid smooth strip footing on strong over soft clay for 40×30 grid model, $H/B = 1$, $c_2/c_1 = 0.1$.

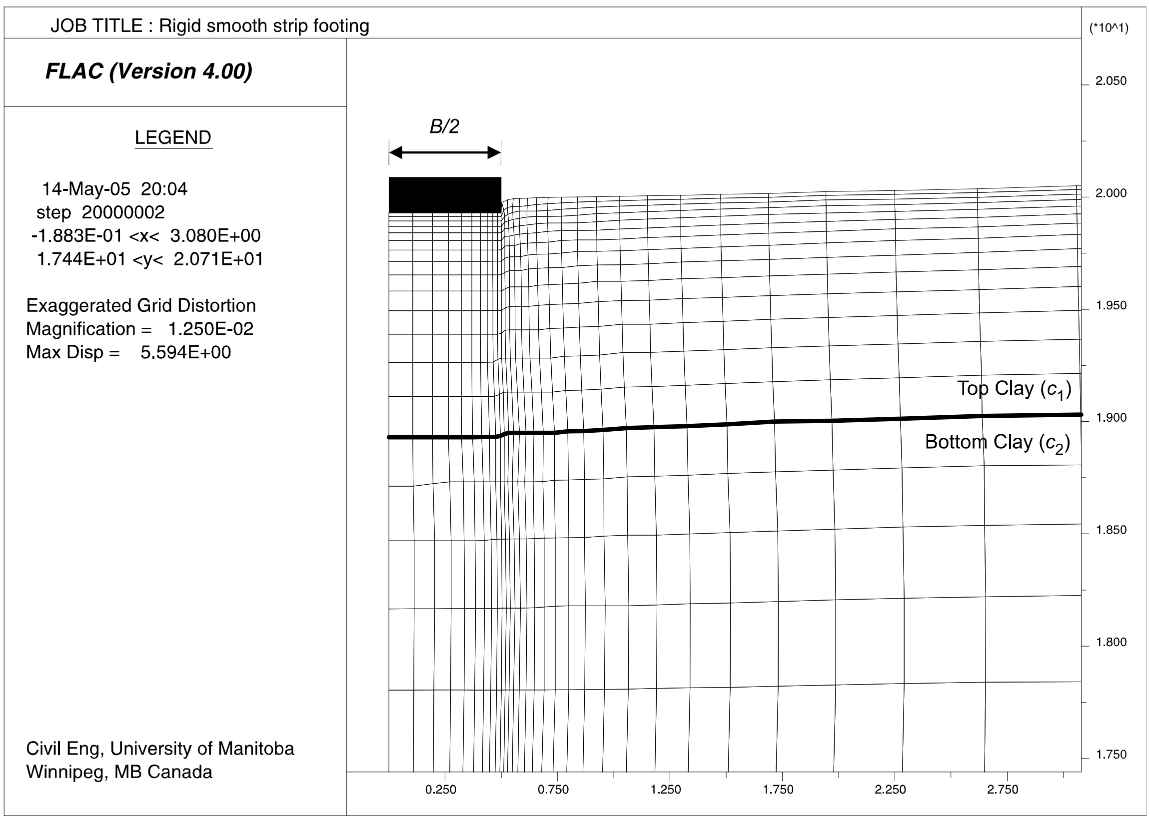

Figure A.37: Magnified grid for a rigid smooth strip footing on strong over soft clay for 40 × 30 grid model, $H/B = 1$, $c_2/c_1 = 0.1$.

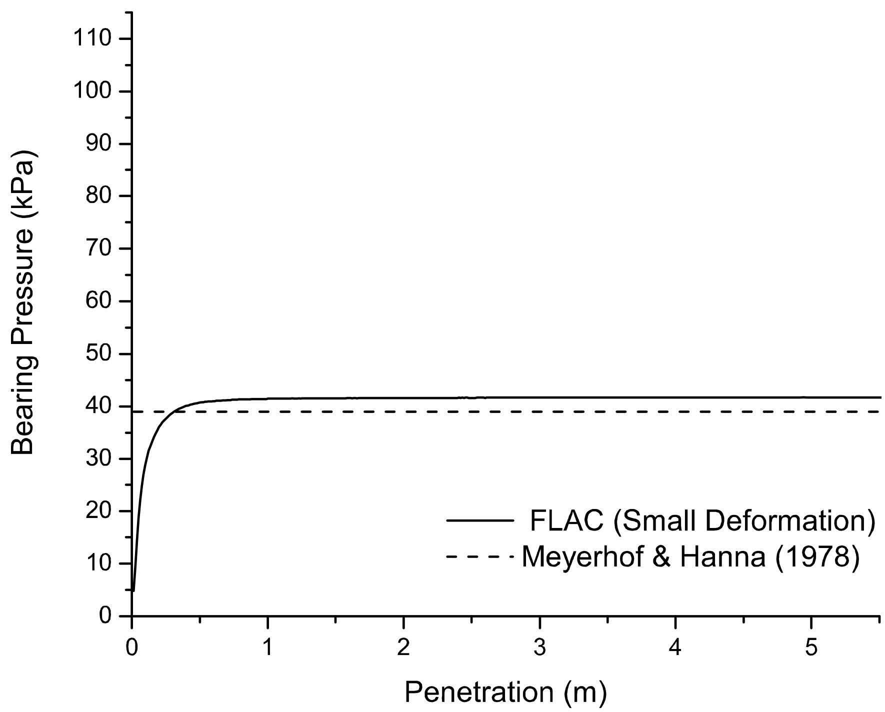

Figure A.38: Bearing pressure versus penetration curve for a rigid smooth strip footing on strong over soft clay for 40×30 grid model, $H/B = 1$, $c_2/c_1 = 0.1$.

A.1.2 Rigid Smooth Strip Footing on Strong over Soft Clay ($H/B = 2$)

Case 3: $c_2/c_1 = 2/3$ **- Small Deformation Analysis**

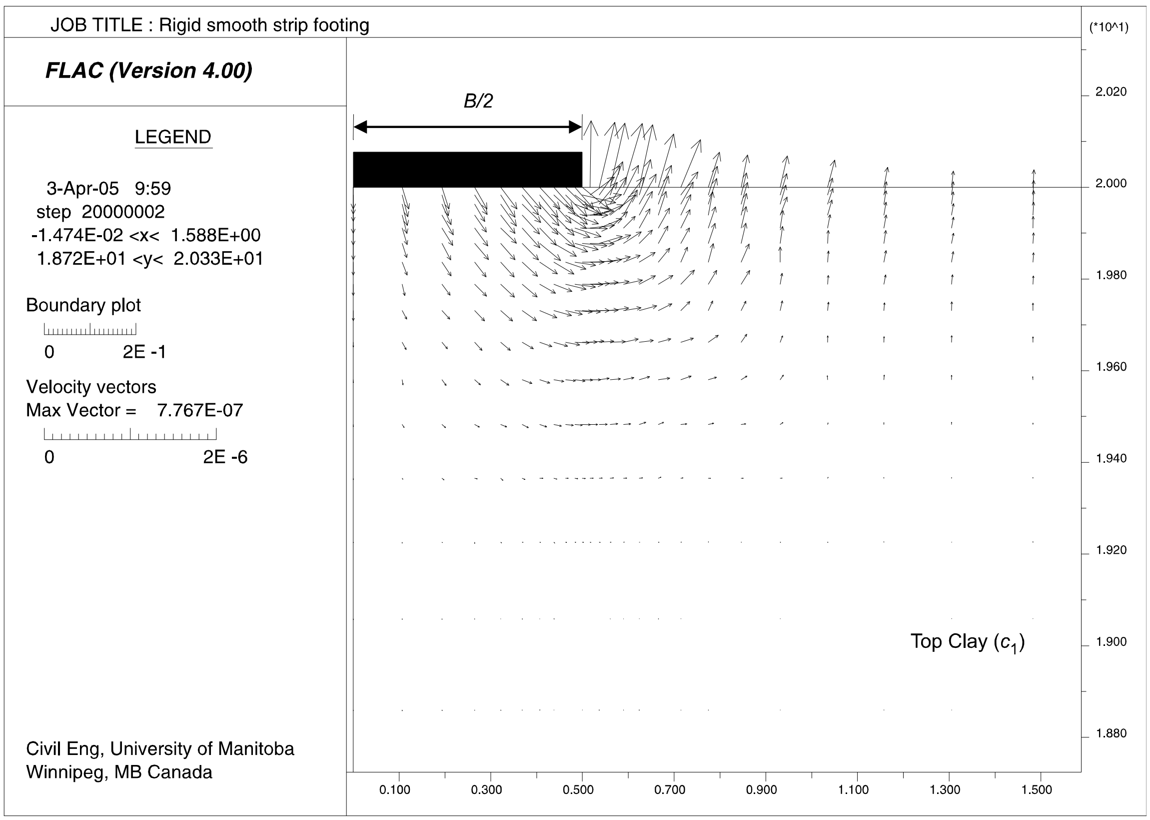

Figure A.39: Velocity vectors for a rigid smooth strip footing on strong over soft clay for 40×30 grid model, $H/B = 2$, $c_2/c_1 = 2/3$.

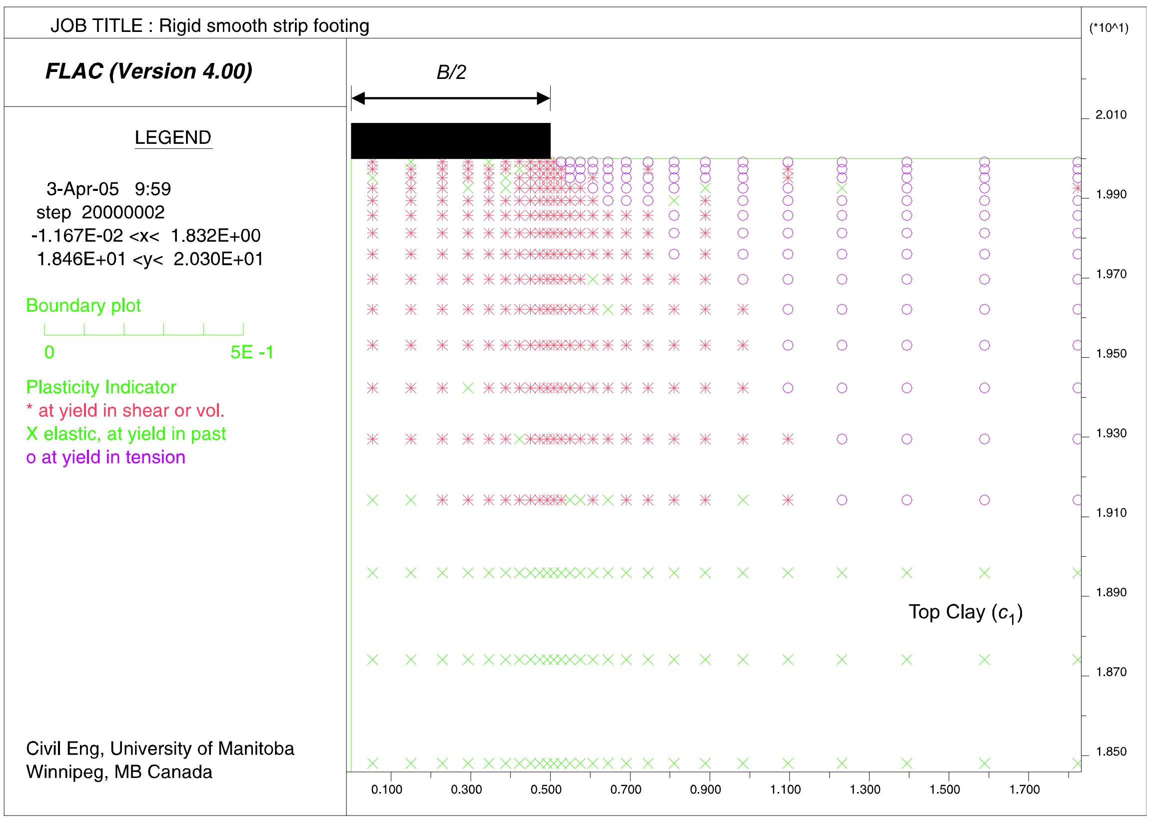

Figure A.40: Plasticity state indicators at steady state condition for a rigid smooth strip footing on strong over soft clay for 40 × 30 grid model, $H/B = 2$, $c_2/c_1 = 2/3$.

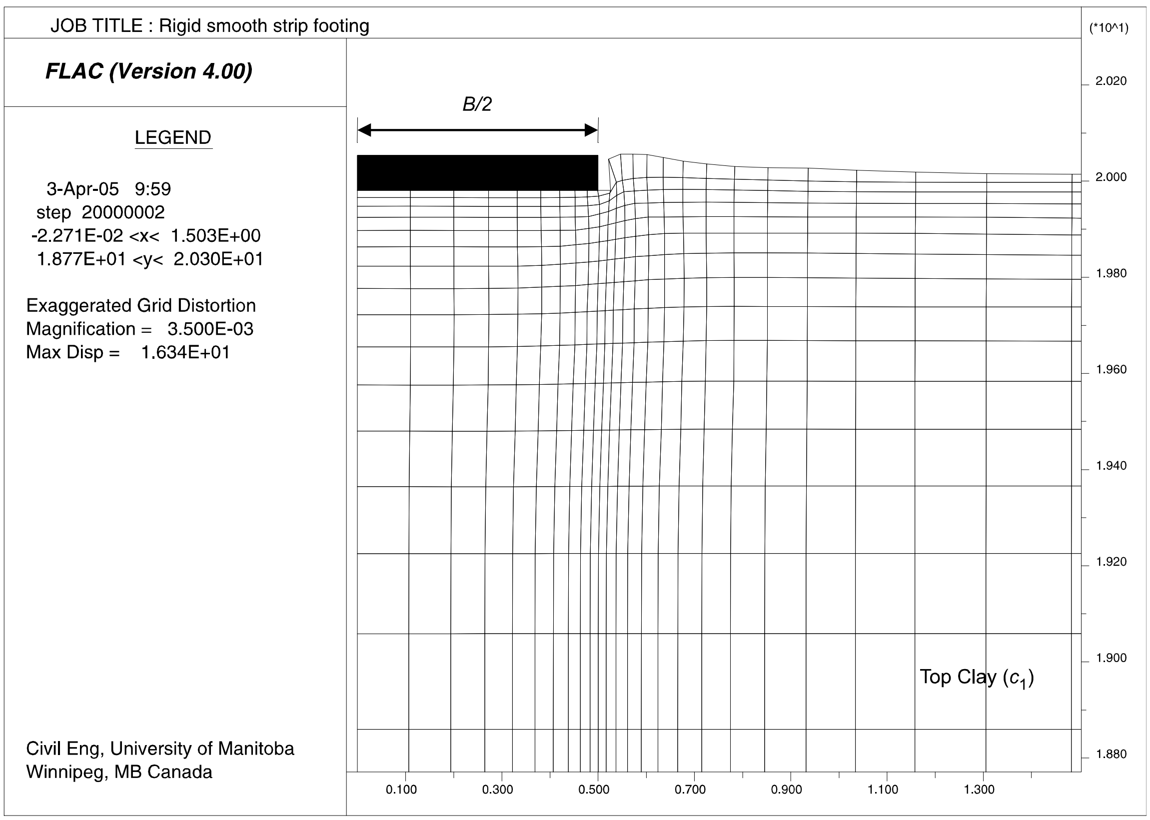

Figure A.41: Magnified grid for a rigid smooth strip footing on strong over soft clay for 40 × 30 grid model, $H/B = 2$, $c_2/c_1 = 2/3$.

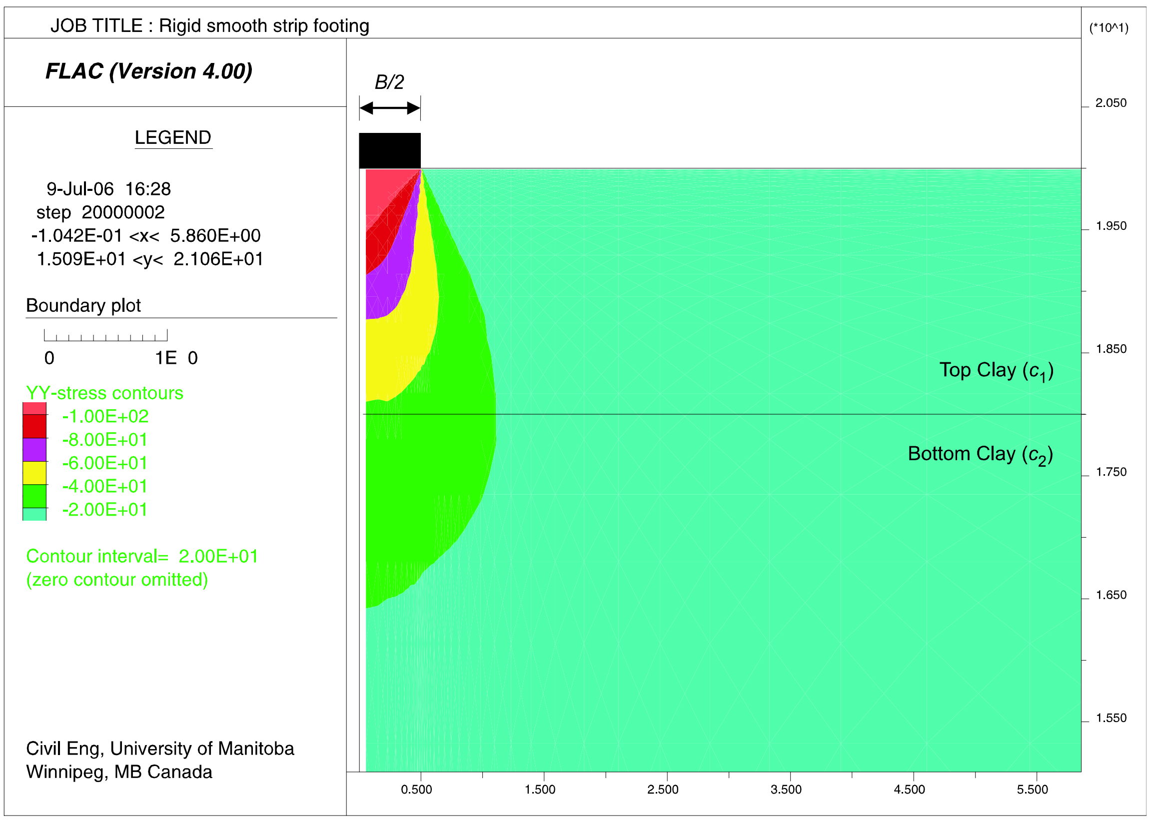

Figure A.42: Vertical stress (σ_{yy}) contours for a rigid smooth strip footing on strong over soft clay for 40×30 grid model, $H/B = 2$, $c_2/c_1 = 2/3$.

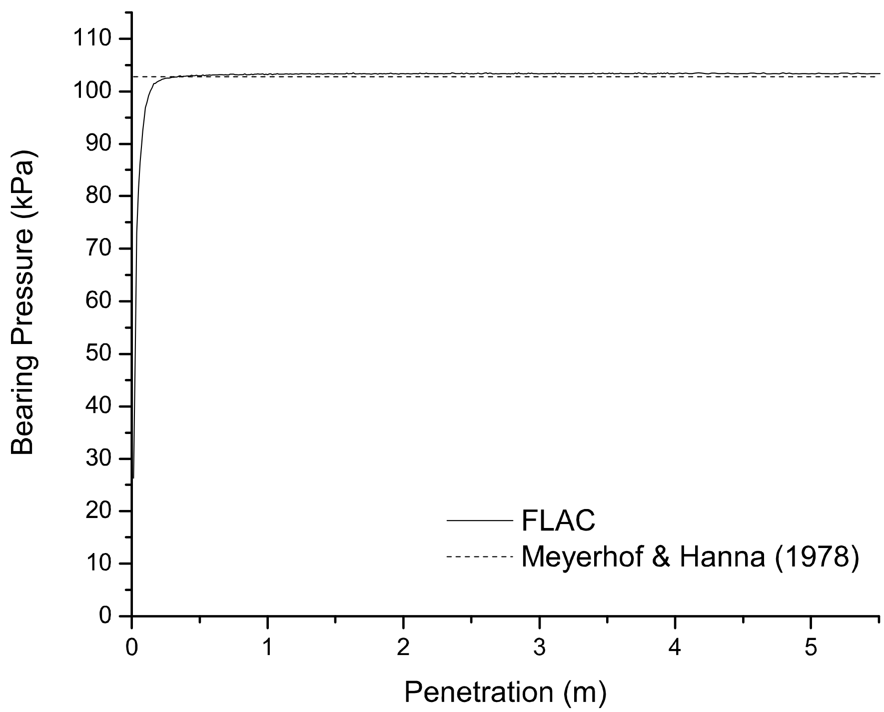

Figure A.43: Bearing pressure versus penetration curve for a rigid smooth strip footing on strong over soft clay for 40 × 30 grid model, $H/B = 2$, $c_2/c_1 = 2/3$.

Case 4: $c_2/c_1 = 0.5$ - Small Deformation Analysis

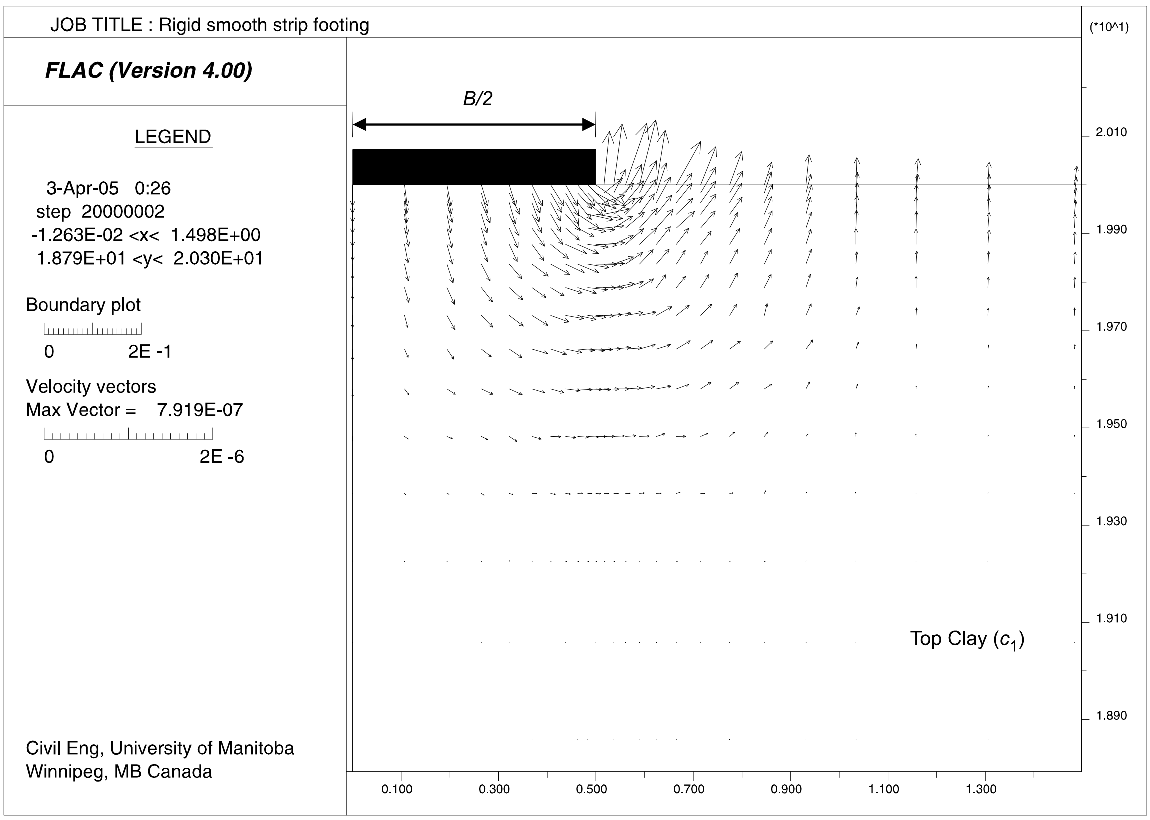

Figure A.44: Velocity vectors for a rigid smooth strip footing on strong clay over soft clay for 40×30 grid model, $H/B = 2$, $c_2/c_1 = 0.5$.

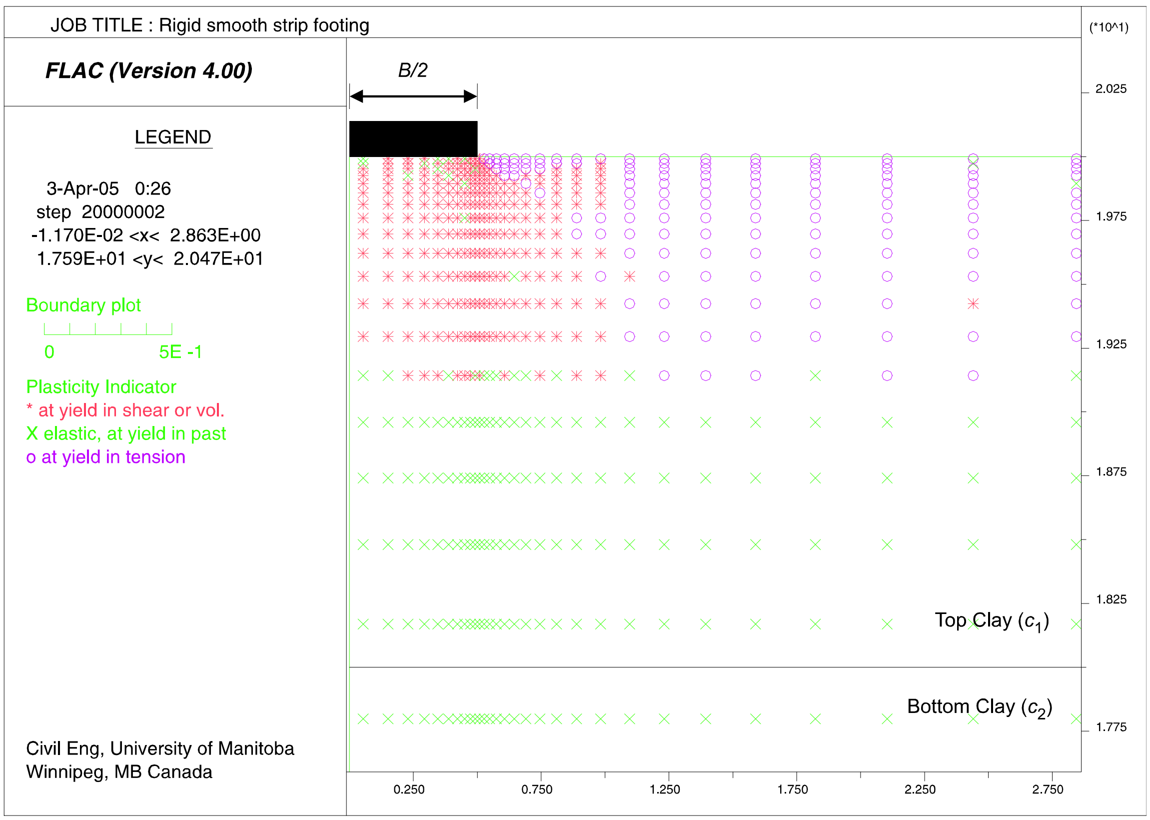

Figure A.45: Plasticity state indicators at steady state condition for a rigid smooth strip footing on strong over soft clay for 40 × 30 grid model, $H/B = 2$, $c_2/c_1 = 0.5$.

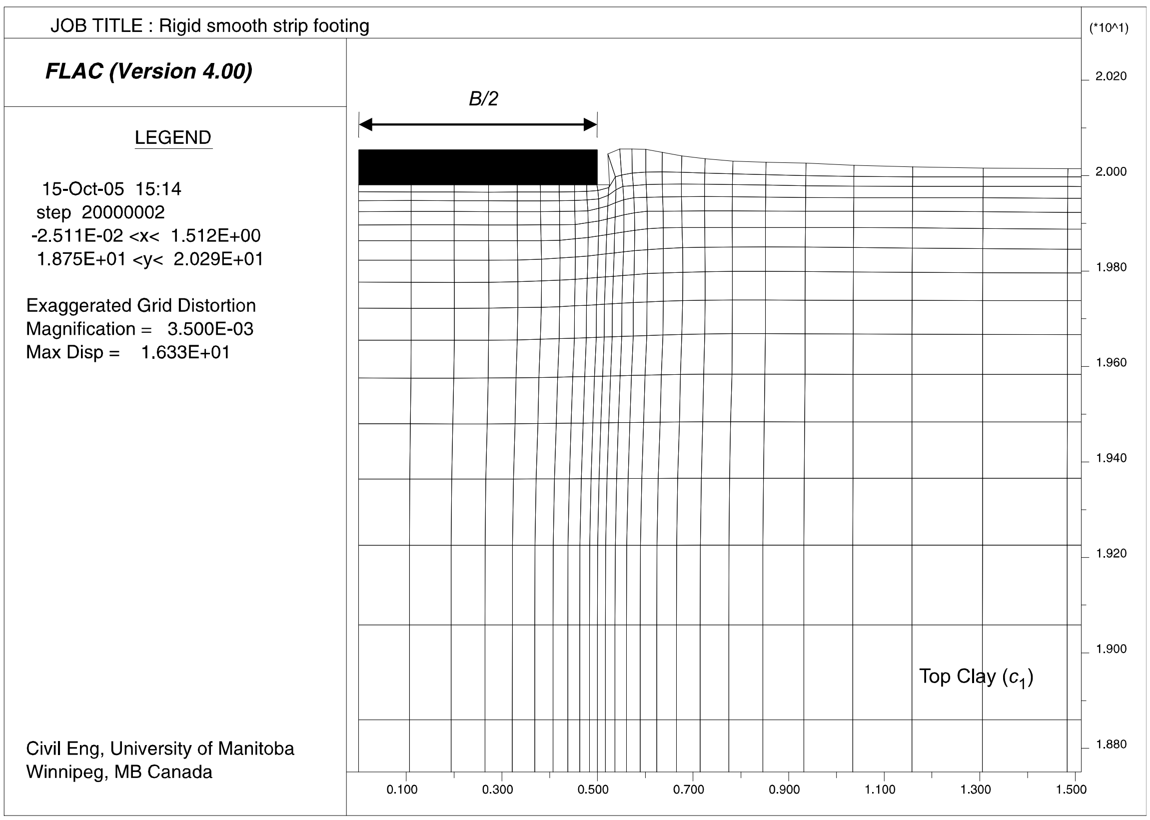

Figure A.46: Magnified grid for a rigid smooth strip footing on strong clay over soft clay for 40 × 30 grid model, $H/B = 2$, $c_2/c_1 = 0.5$.

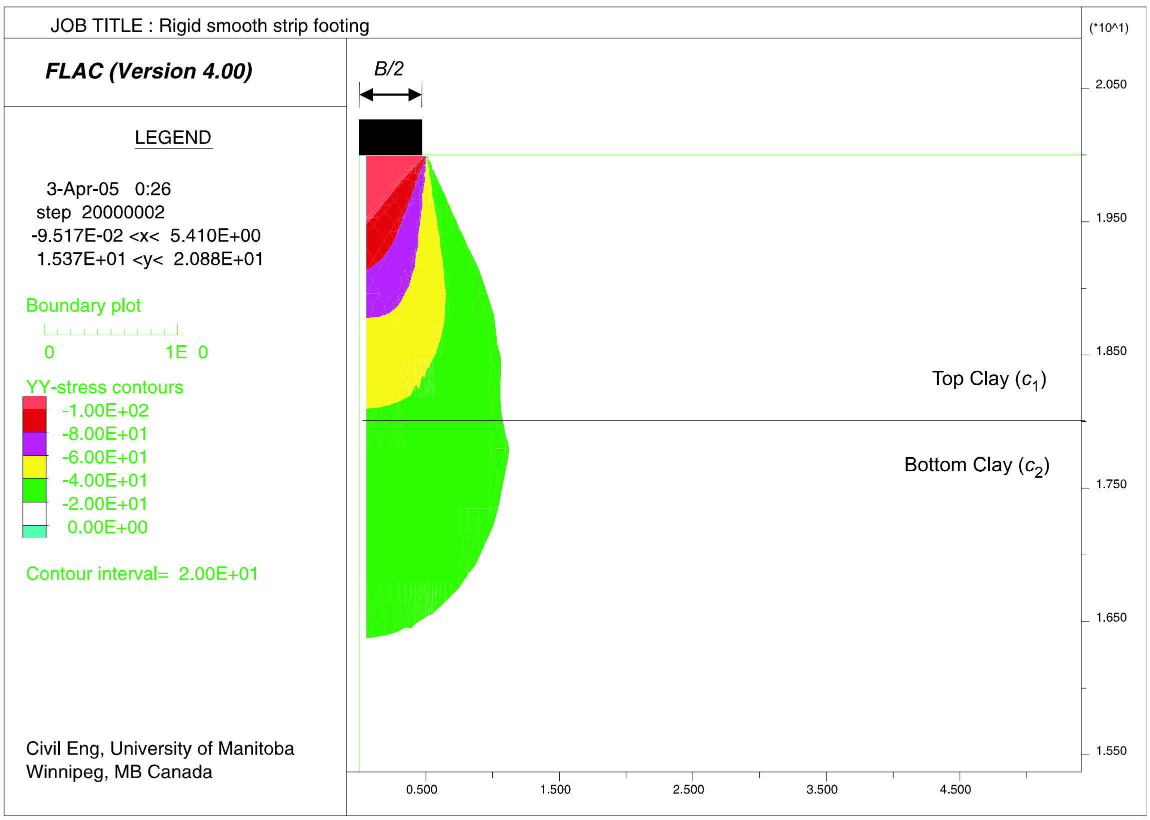

Figure A.47: Vertical stress (σ_{yy}) contours for a rigid smooth strip footing on strong clay over soft clay for 40×30 grid model, $H/B = 2$, $c_2/c_1 = 0.5$.

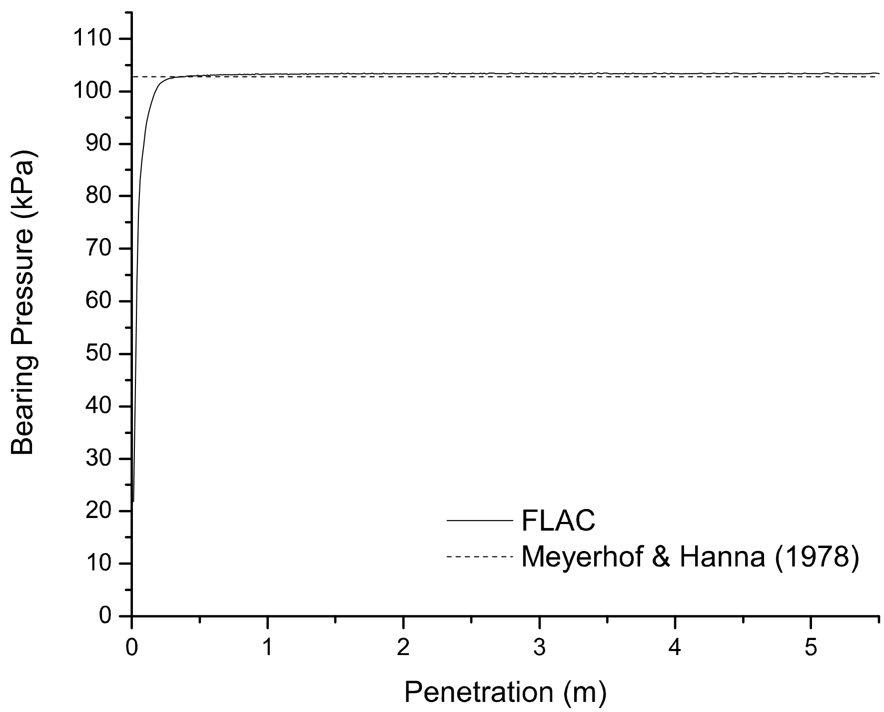

Figure A.48: Bearing pressure versus penetration curve for a rigid smooth strip footing on strong clay over soft clay for 40×30 grid model, $H/B = 2$, $c_2/c_1 = 0.5$.

Case 5: $c_2/c_1 = 1/3$ - Small Deformation Analysis

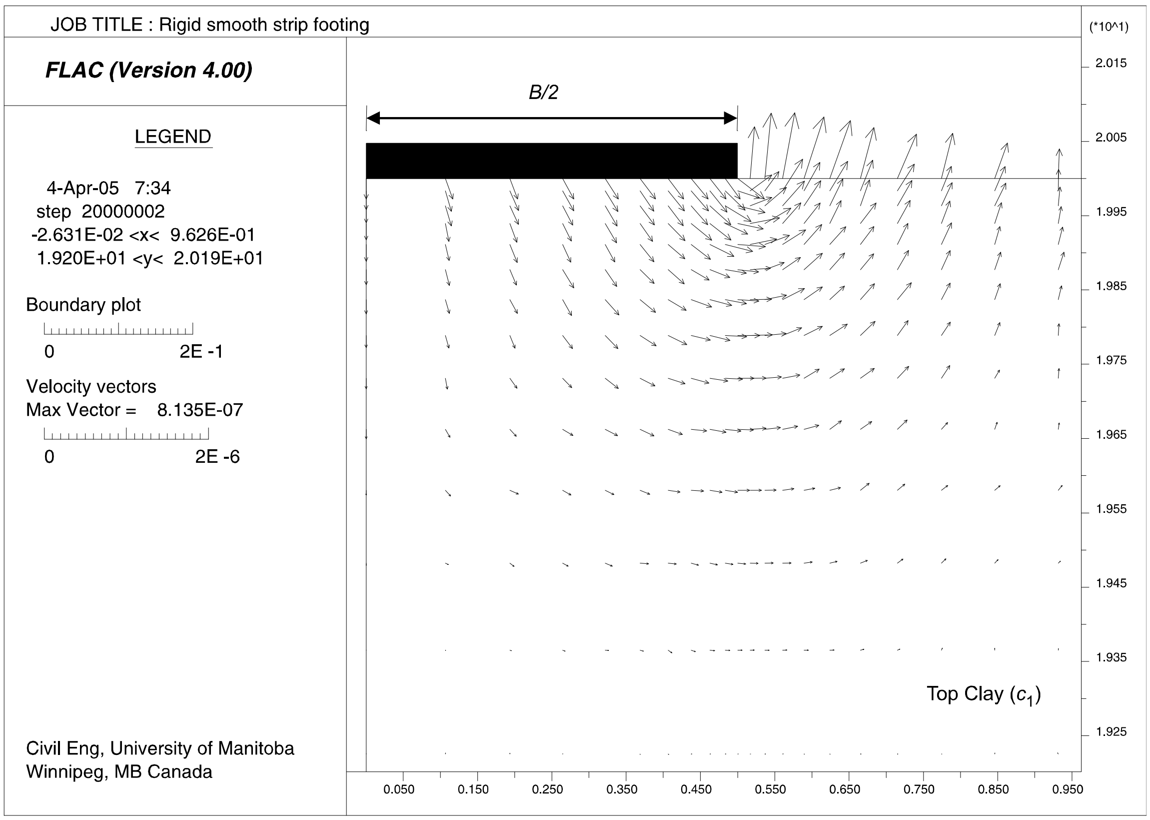

Figure A.49: Velocity vectors for a rigid smooth strip footing on strong clay over soft clay for 40×30 grid model, $H/B = 2$, $c_2/c_1 = 1/3$.

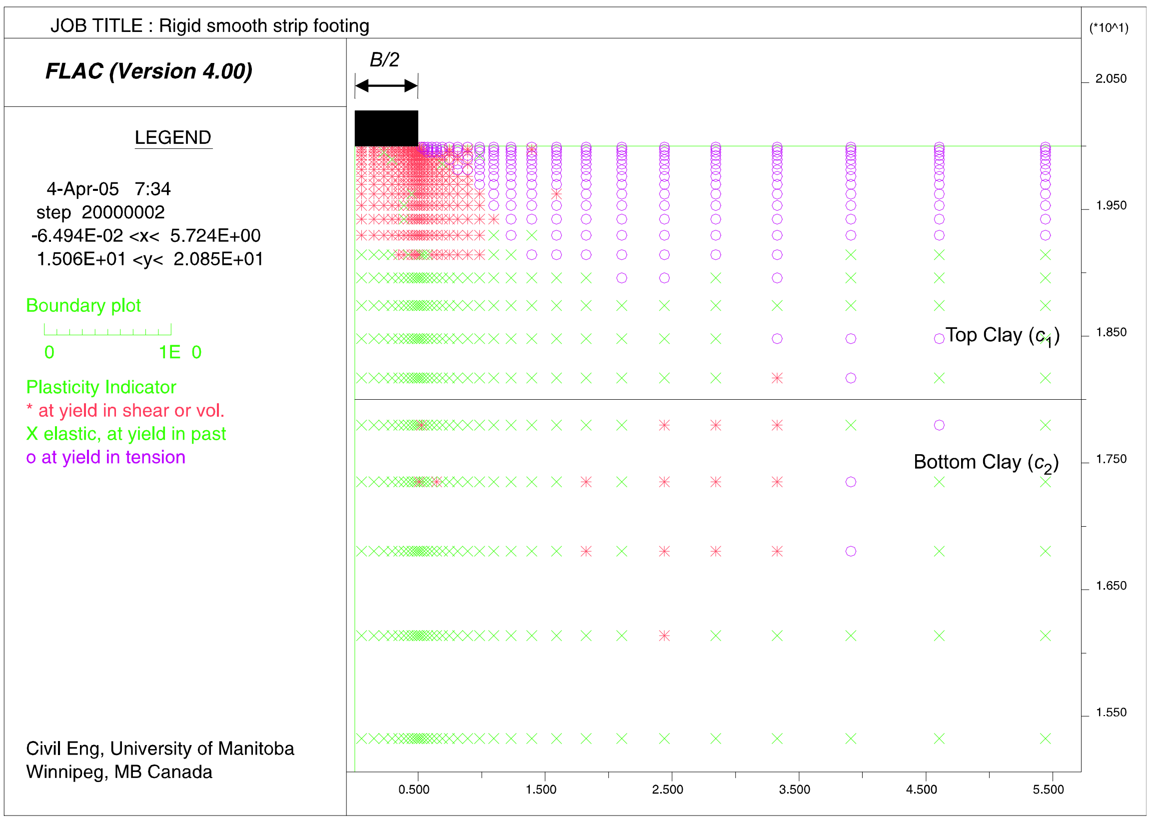

Figure A.50: Plasticity state indicators at steady state condition for a rigid smooth strip footing on strong over soft clay for 40×30 grid model, $H/B = 2$, $c_2/c_1 = 1/3$.

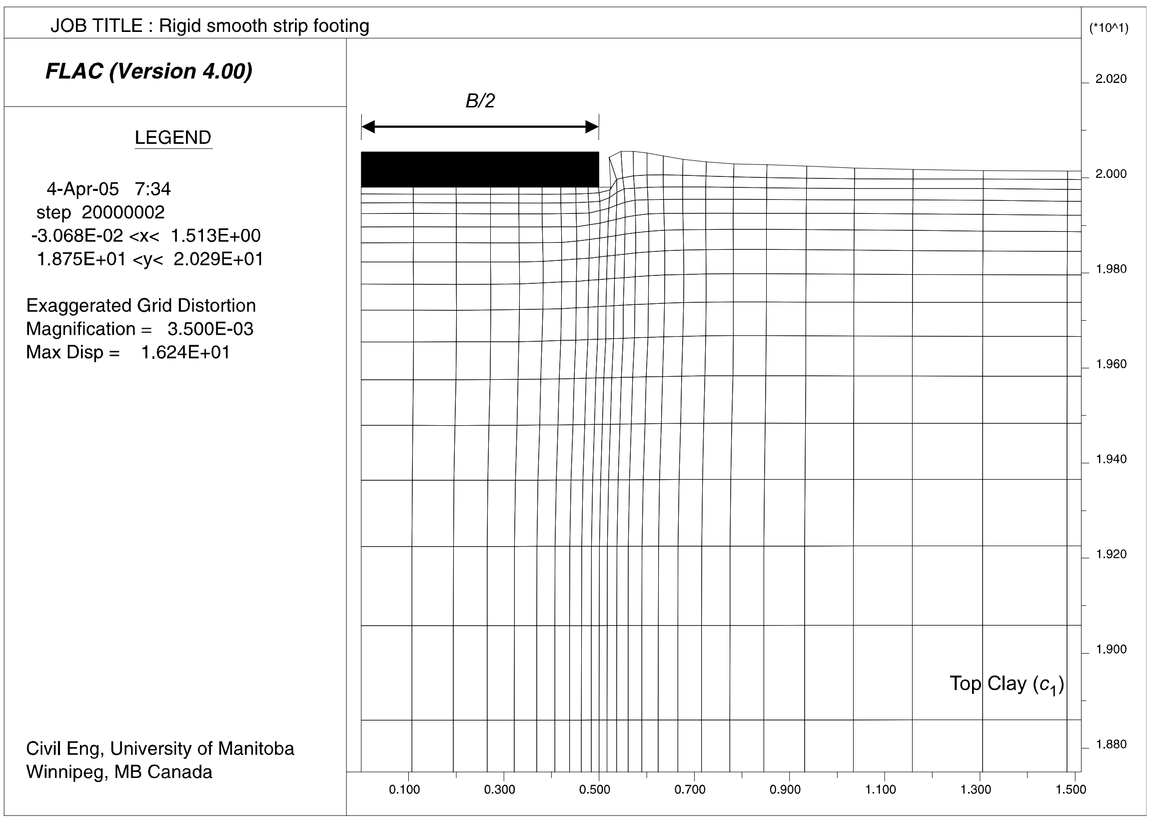

Figure A.51: Magnified grid for a rigid smooth strip footing on strong clay over soft clay for 40×30 grid model, $H/B = 2$, $c_2/c_1 = 1/3$.

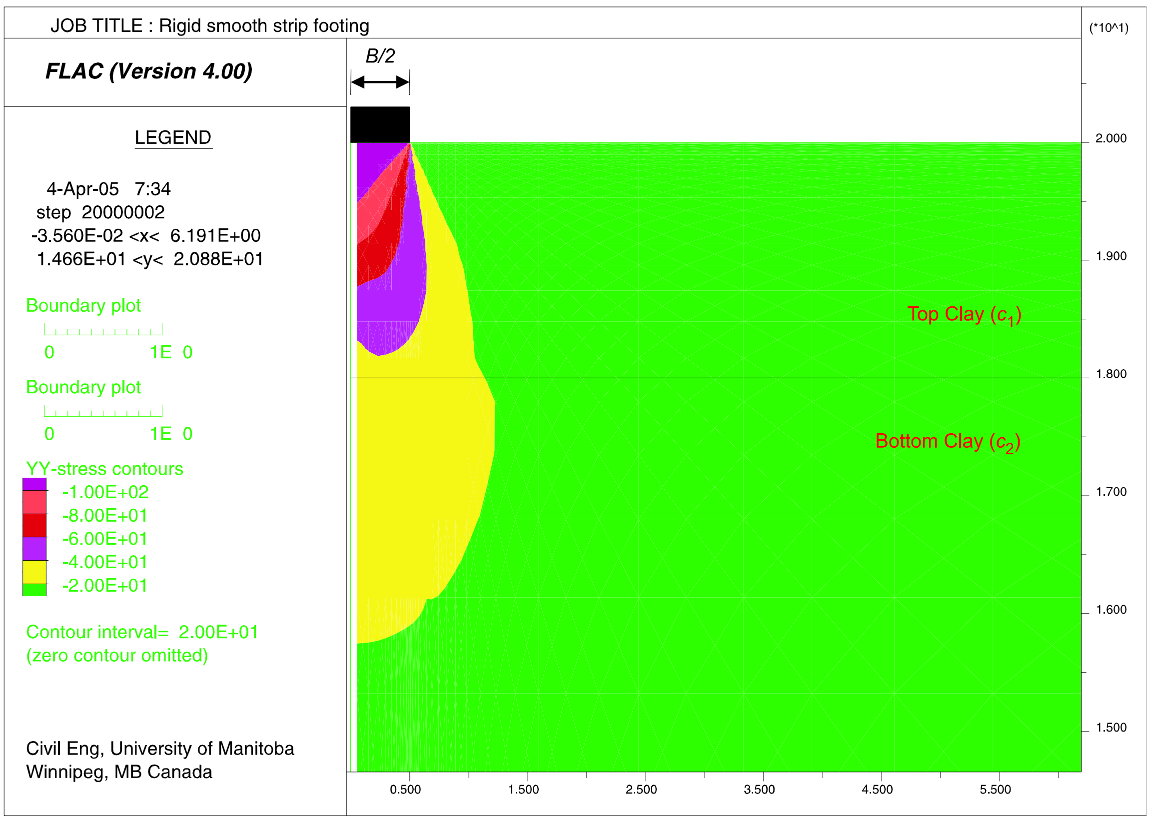

Figure A.52: Vertical stress (σ_{yy}) contours for a rigid smooth strip footing on strong clay over soft clay for 40×30 grid model, $H/B = 2$, $c_2/c_1 = 1/3$.

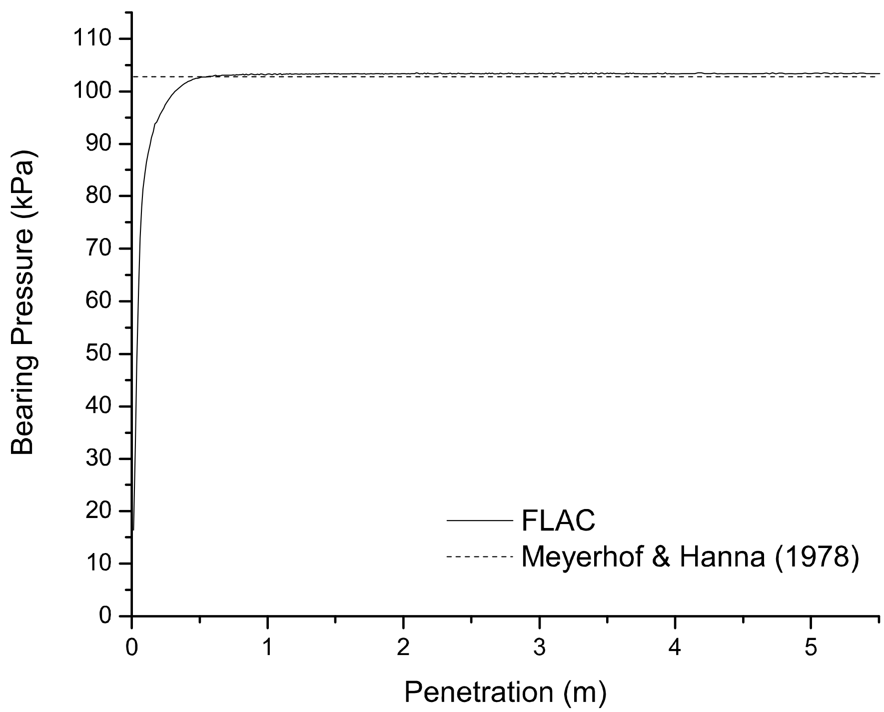

Figure A.53: Bearing pressure versus penetration curve for a rigid smooth strip footing on strong clay over soft clay for 40 × 30 grid model, $H/B = 2$, $c_2/c_1 = 1/3$.

Case 6: $c_2/c_1 = 0.2$ - Small Deformation Analysis

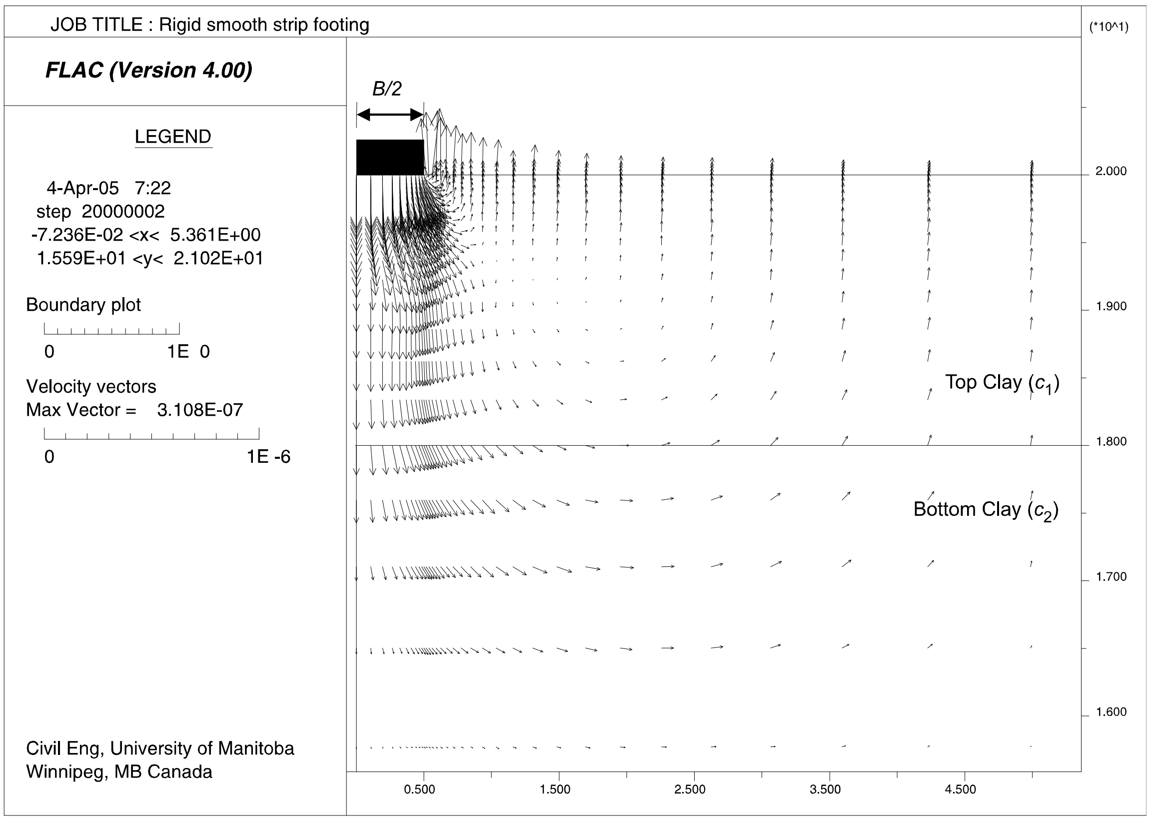

Figure A.54: Velocity vectors for a rigid smooth strip footing on strong clay over soft clay for 40×30 grid model, $H/B = 2$, $c_2/c_1 = 0.2$.

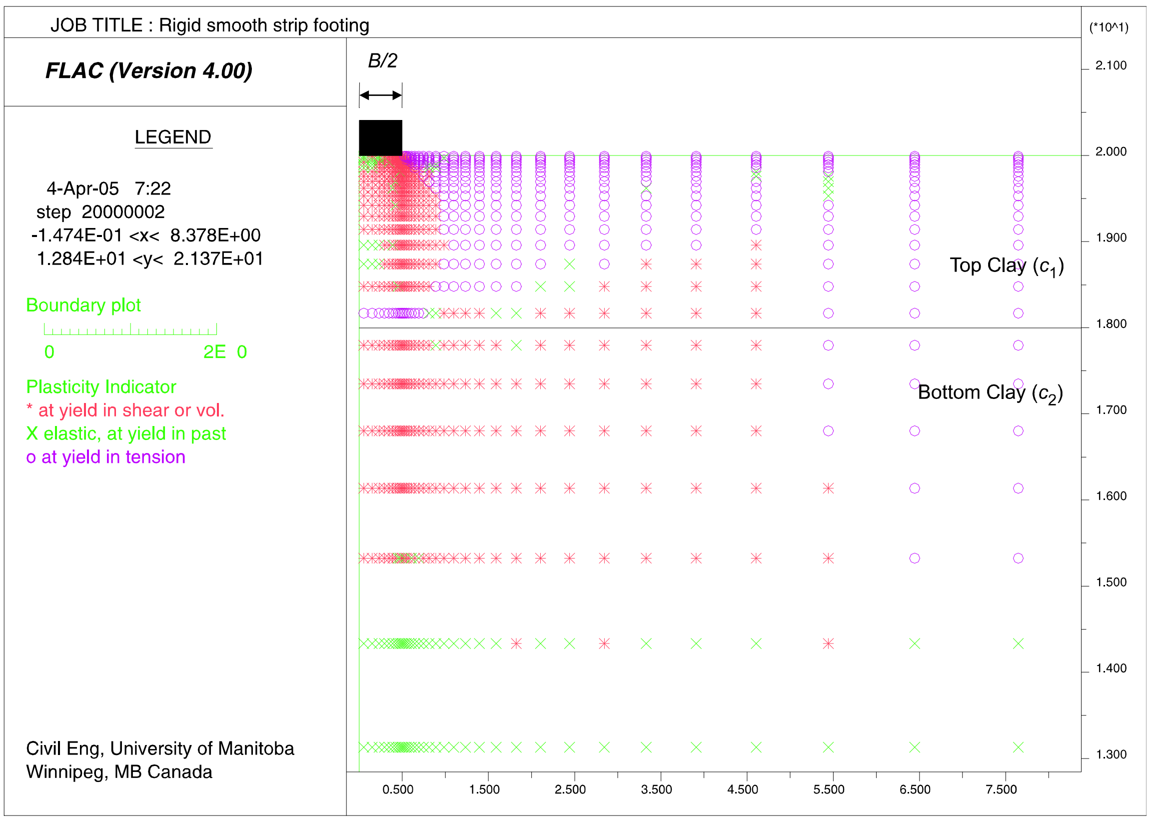

Figure A.55: Plasticity state indicators at steady state condition for a rigid smooth strip footing on strong over soft clay for 40 × 30 grid model, $H/B = 2$, $c_2/c_1 = 0.2$.

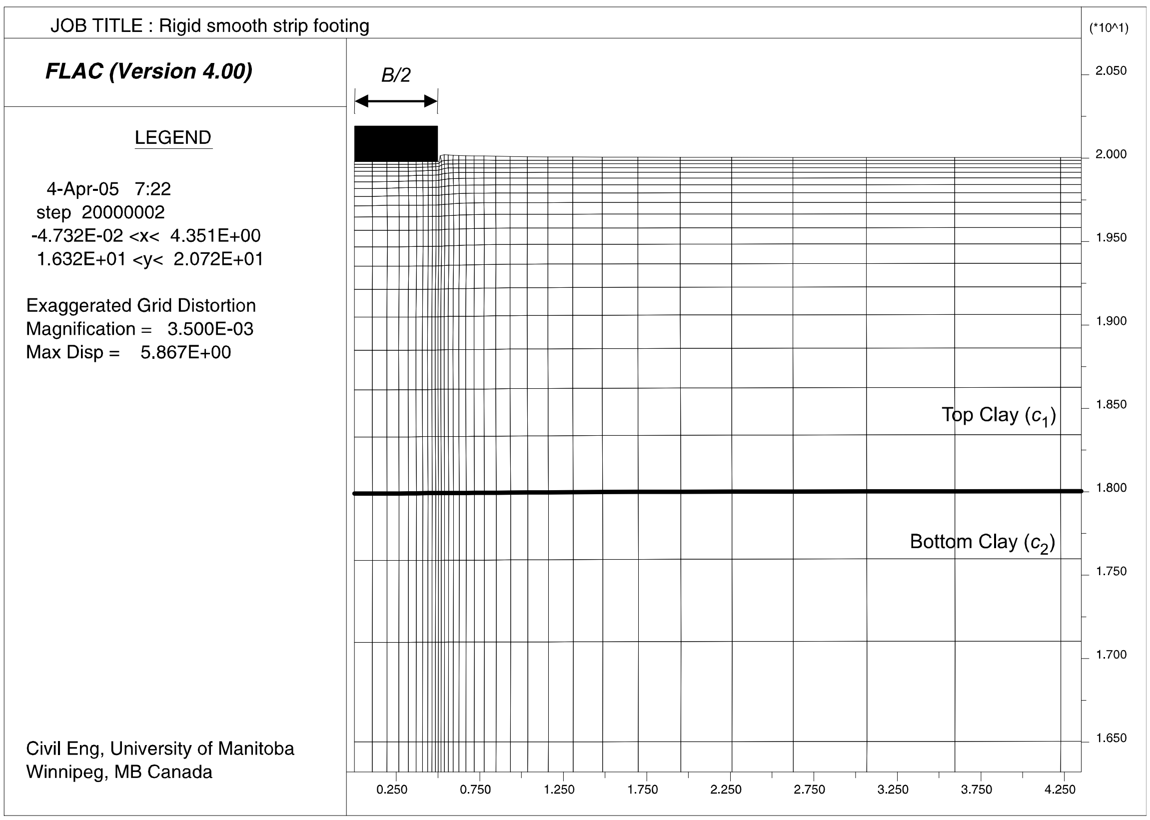

Figure A.56: Magnified grid for a rigid smooth strip footing on strong clay over soft clay for 40 × 30 grid model, $H/B = 2$, $c_2/c_1 = 0.2$.

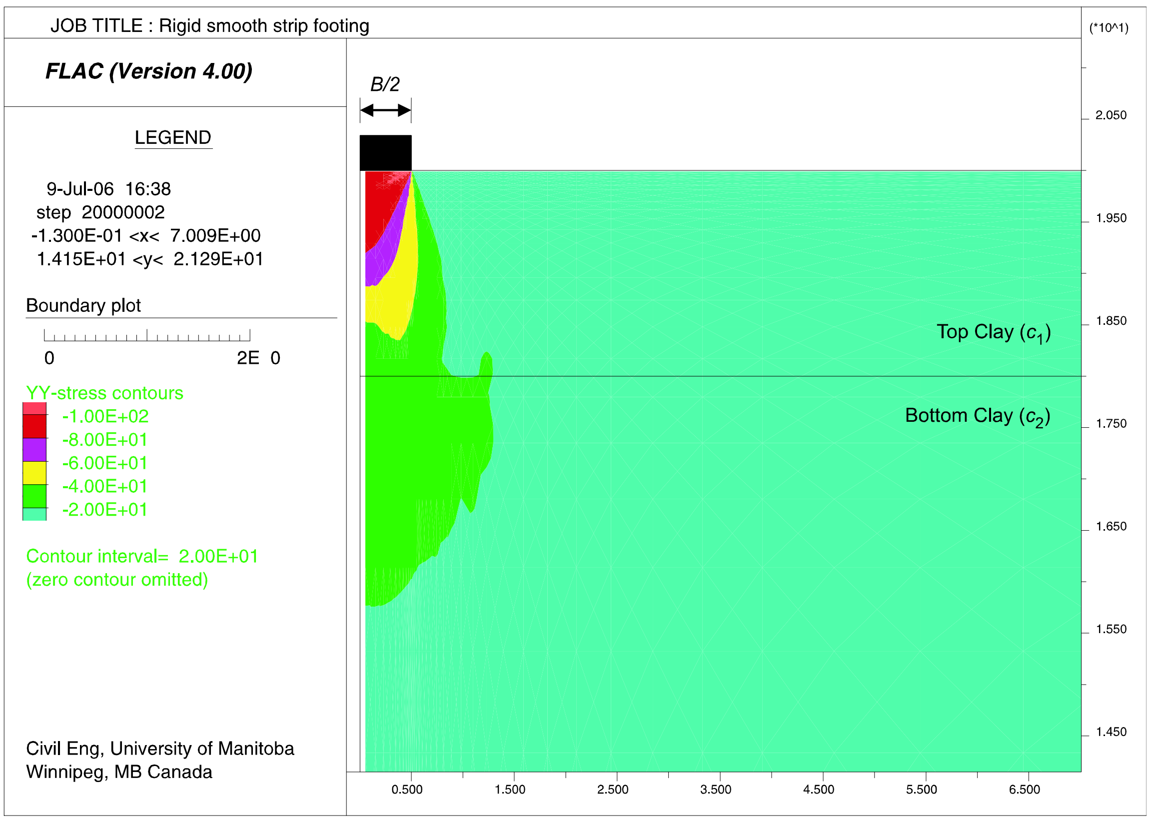

Figure A.57: Vertical stress (σ_{yy}) contours for a rigid smooth strip footing on strong clay over soft clay for 40×30 grid model, $H/B = 2$, $c_2/c_1 = 0.2$.

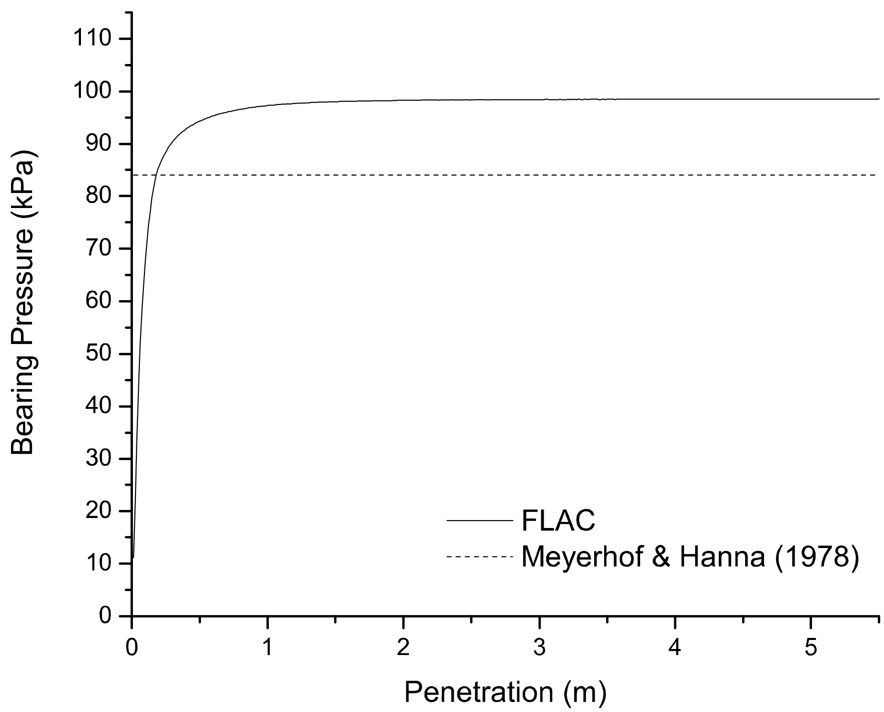

Figure A.58: Bearing pressure versus penetration curve for a rigid smooth strip footing on strong clay over soft clay for 40×30 grid model, $H/B = 2$, $c_2/c_1 = 0.2$.

Case 7: $c_2/c_1 = 0.1$ - Small Deformation Analysis

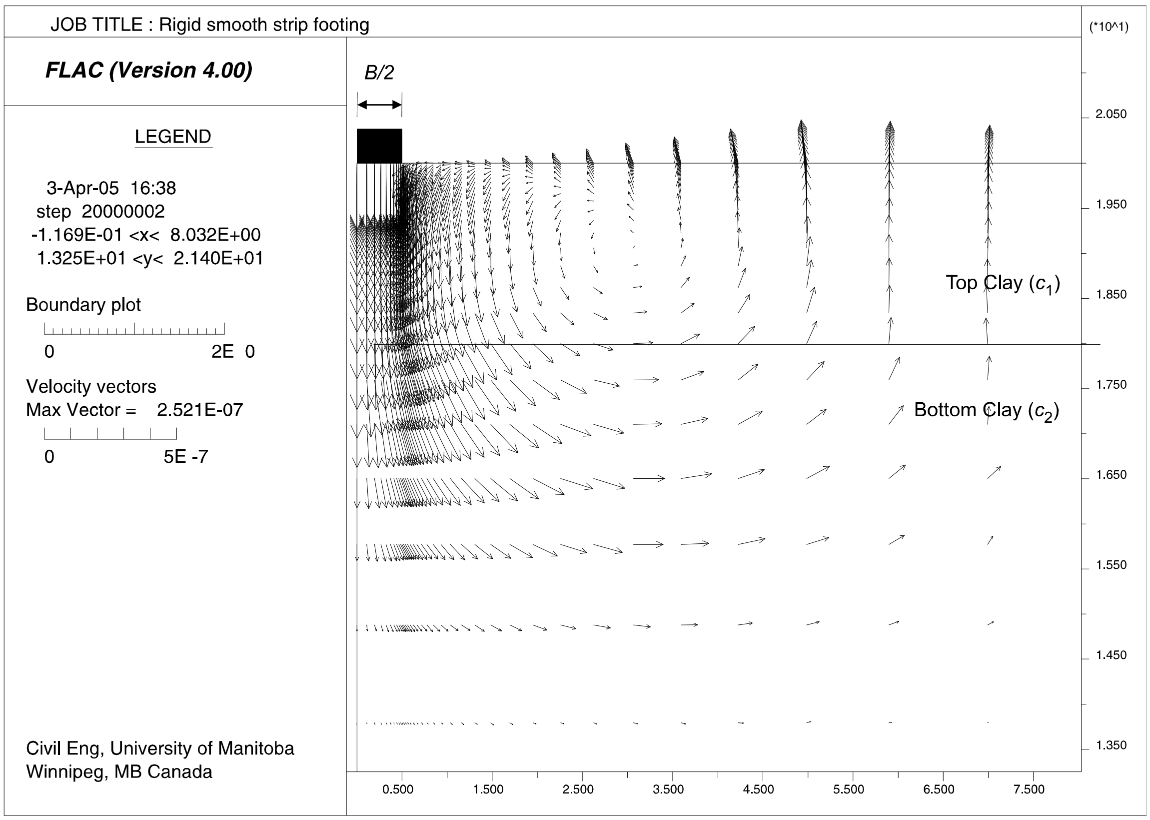

Figure A.59: Velocity vectors for a rigid smooth strip footing on strong clay over soft clay for 40×30 grid model, $H/B = 2$, $c_2/c_1 = 0.1$.

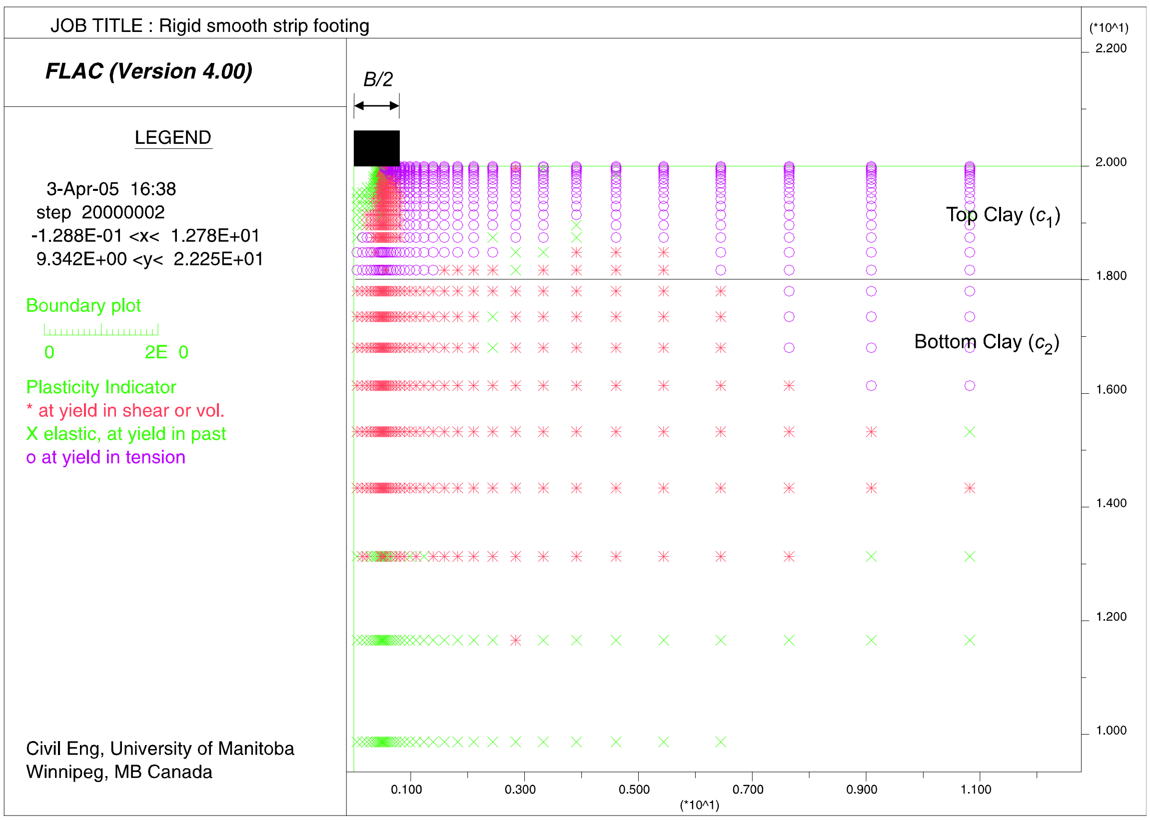

Figure A.60: Plasticity state indicators at steady state condition for a rigid smooth strip footing on strong over soft clay for 40 × 30 grid model, $H/B = 2$, $c_2/c_1 = 0.1$.

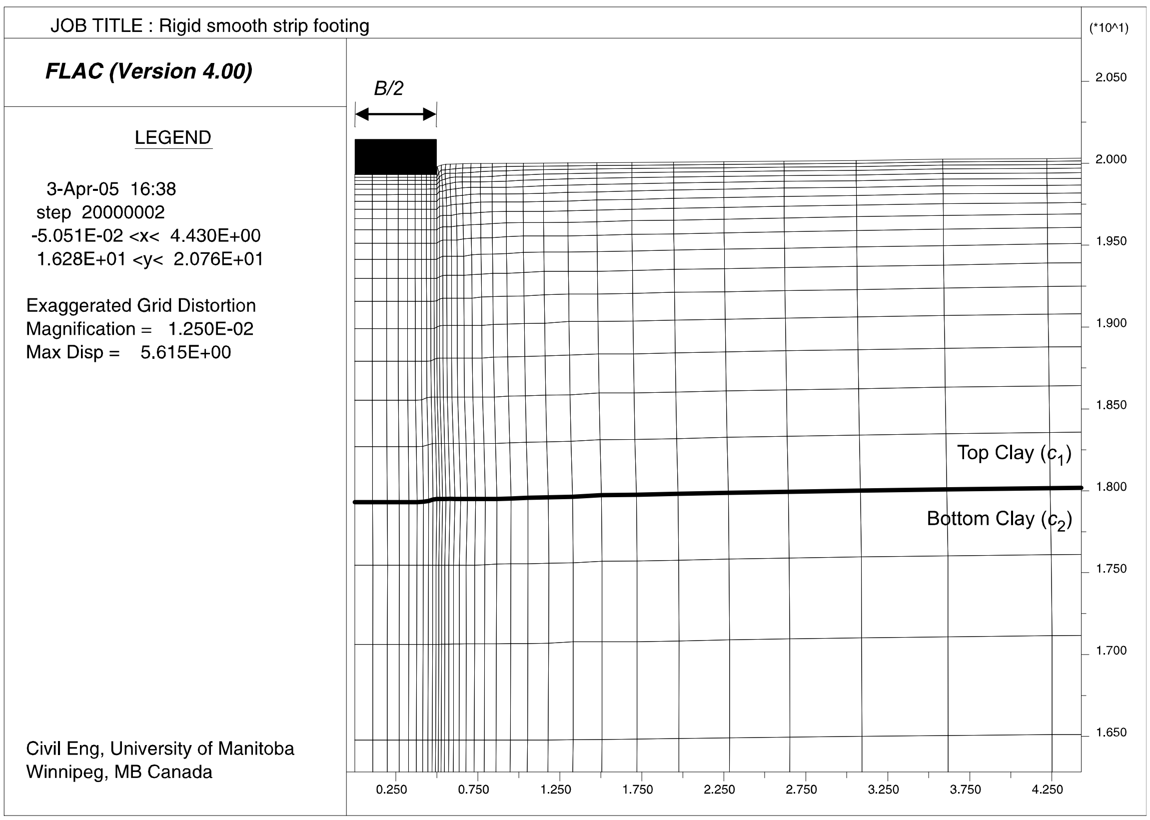

Figure A.61: Magnified grid for a rigid smooth strip footing on strong clay over soft clay for 40 × 30 grid model, $H/B = 2$, $c_2/c_1 = 0.1$.

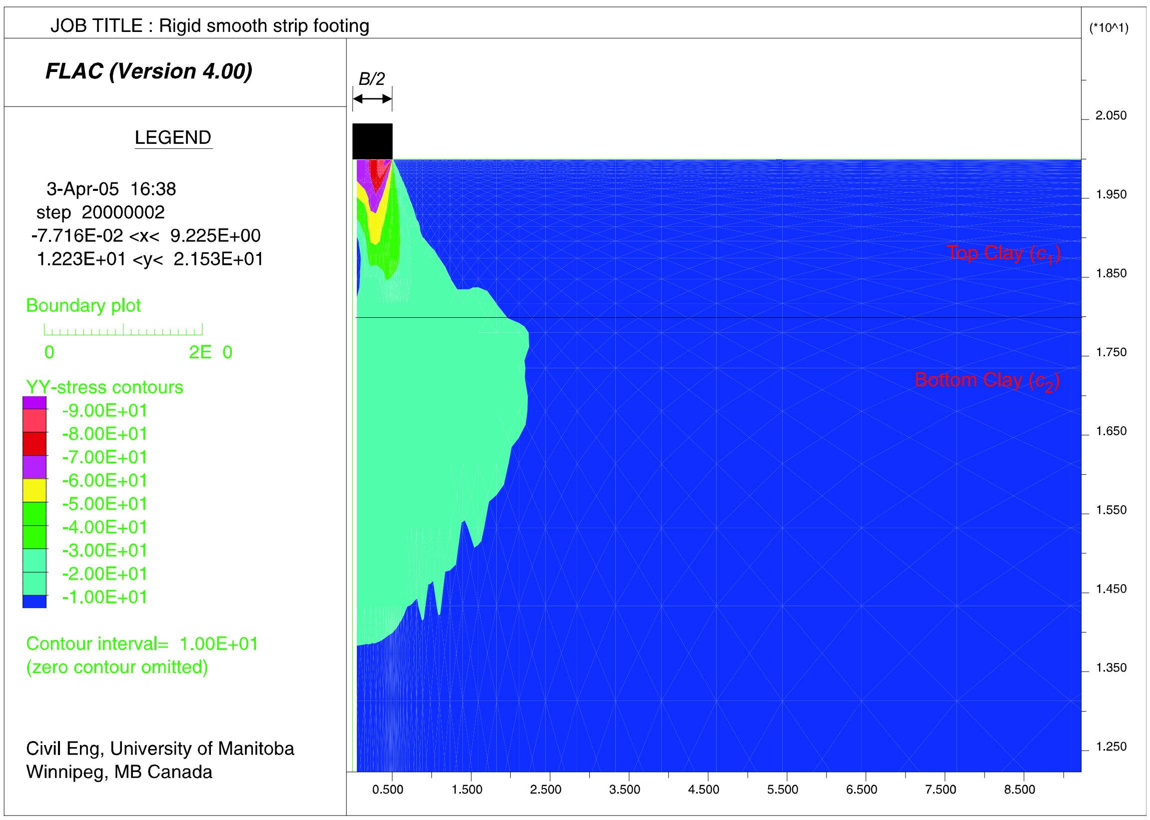

Figure A.62: Vertical stress (σ_{yy}) contours for a rigid smooth strip footing on strong clay over soft clay for 40×30 grid model, $H/B = 2$, $c_2/c_1 = 0.1$.

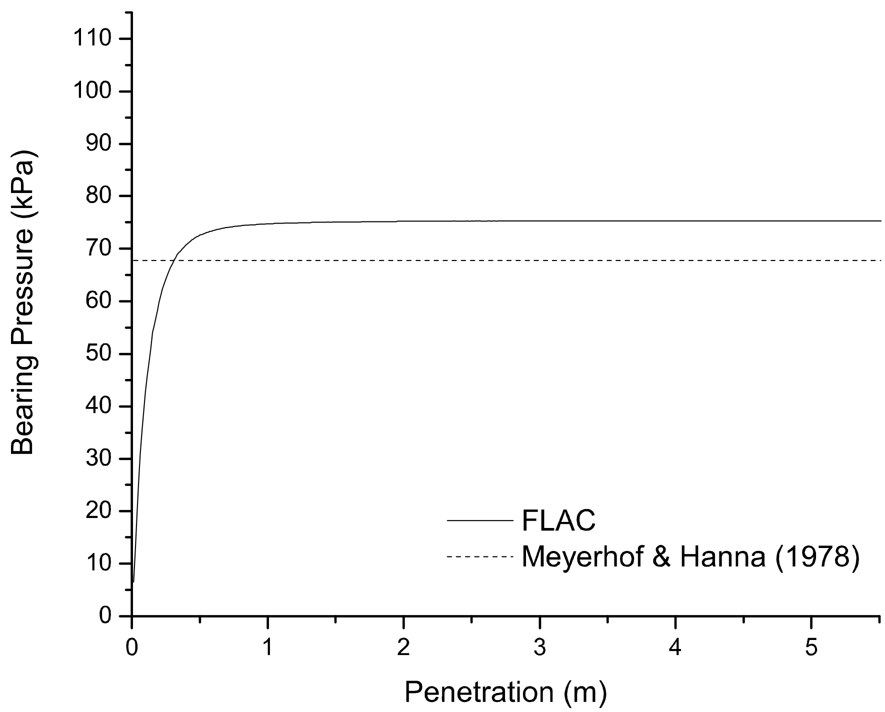

Figure A.63: Bearing pressure versus penetration curve for a rigid smooth strip footing on strong clay over soft clay for 40 × 30 grid model, $H/B = 2$, $c_2/c_1 = 0.1$.

A.1.3 Rigid Smooth Strip Footing on Strong over Soft Clay ($H/B = 2.5$)

Case 5: $c_2/c_1 = 1/3$ - Small Deformation Analysis

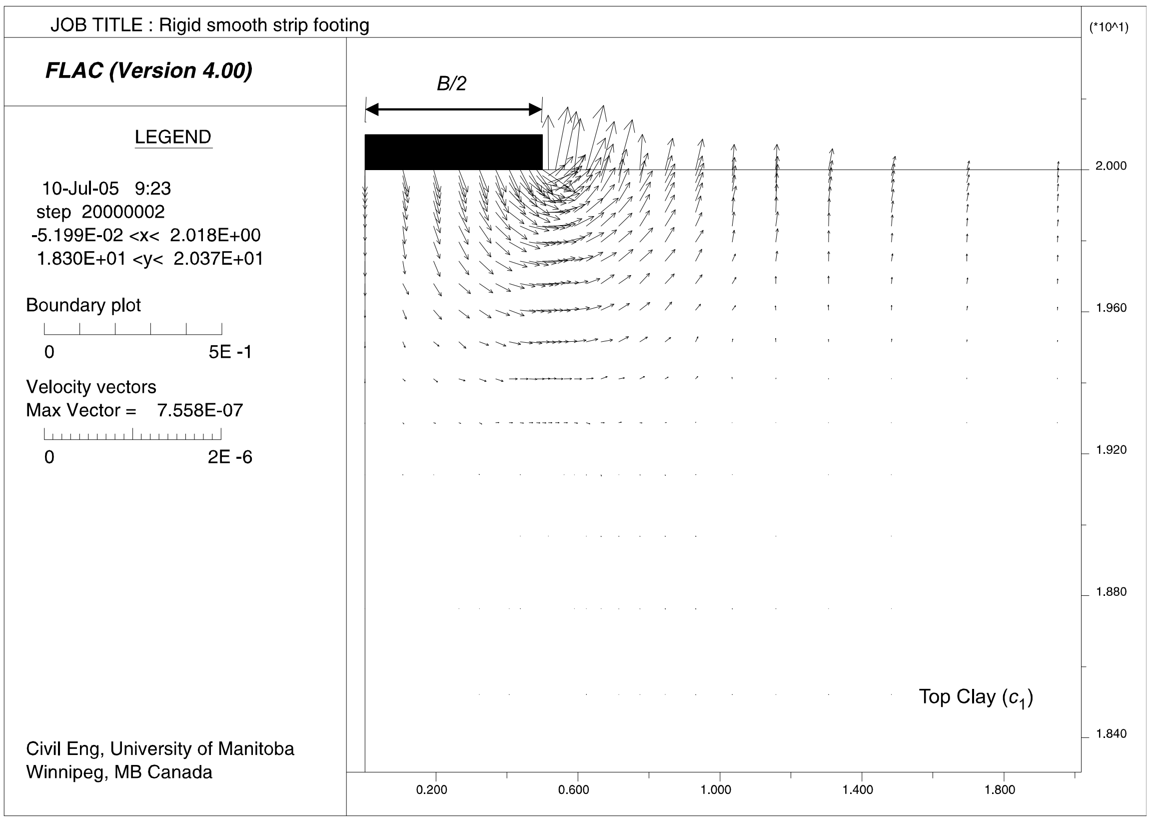

Figure A.64: Velocity vectors for a rigid smooth strip footing on strong clay over soft clay for 40 × 30 grid model, $H/B = 2.5$, $c_2/c_1 = 1/3$.

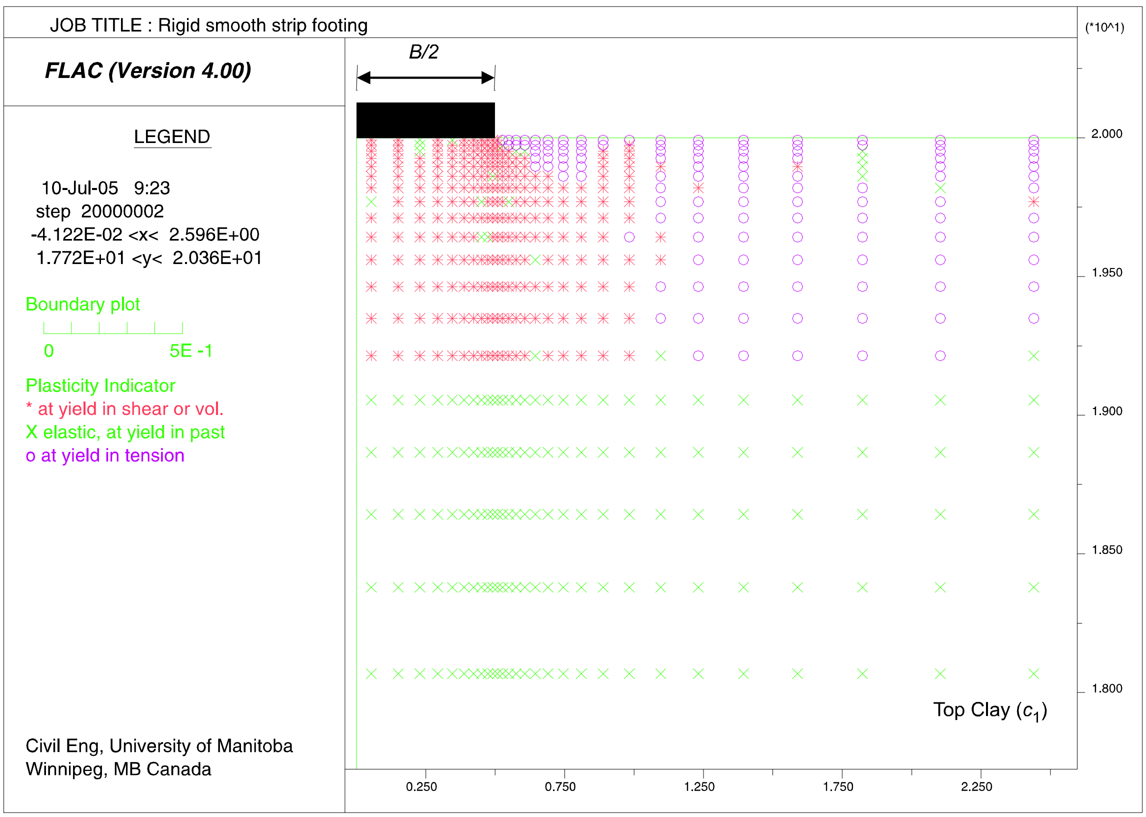

Figure A.65: Plasticity state indicators at steady state condition for a rigid smooth strip footing on strong over soft clay for 40×30 grid model, $H/B = 2.5$, $c_2/c_1 = 1/3$.

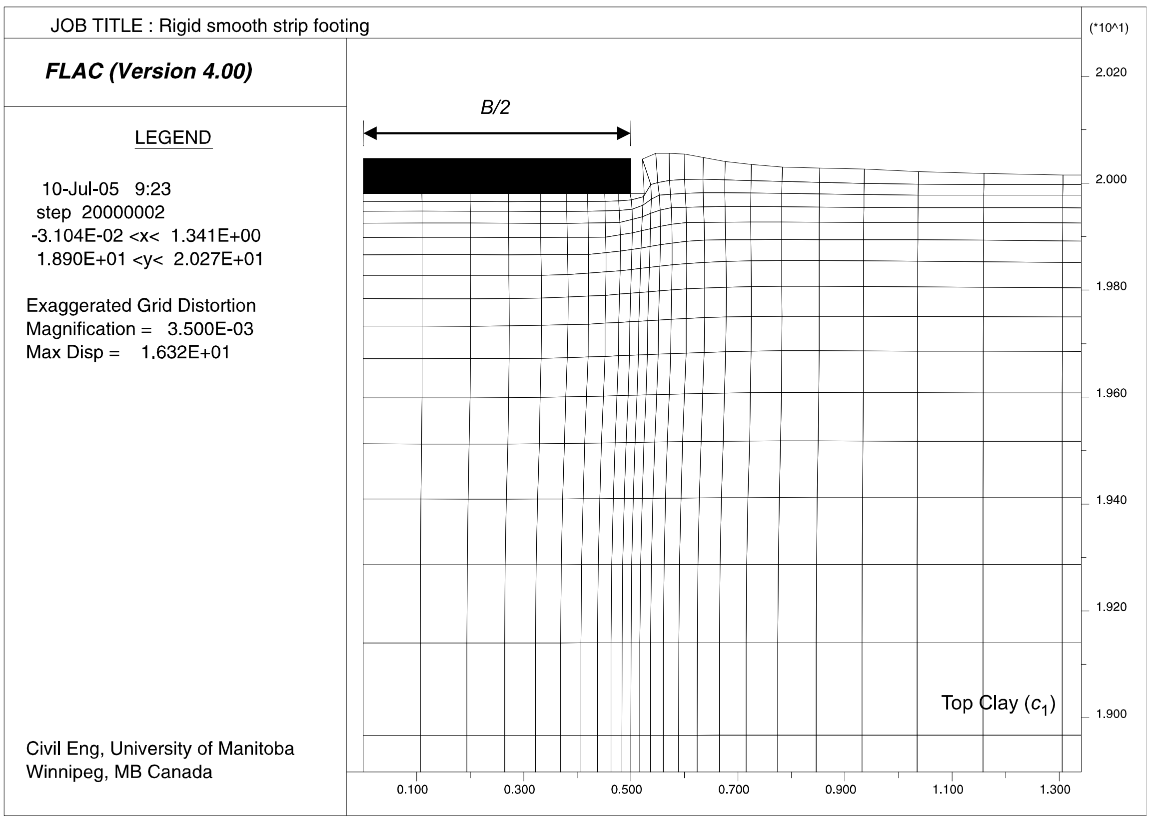

Figure A.66: Magnified grid for a rigid smooth strip footing on strong clay over soft clay for 40 × 30 grid model, $H/B = 2.5$, $c_2/c_1 = 1/3$.

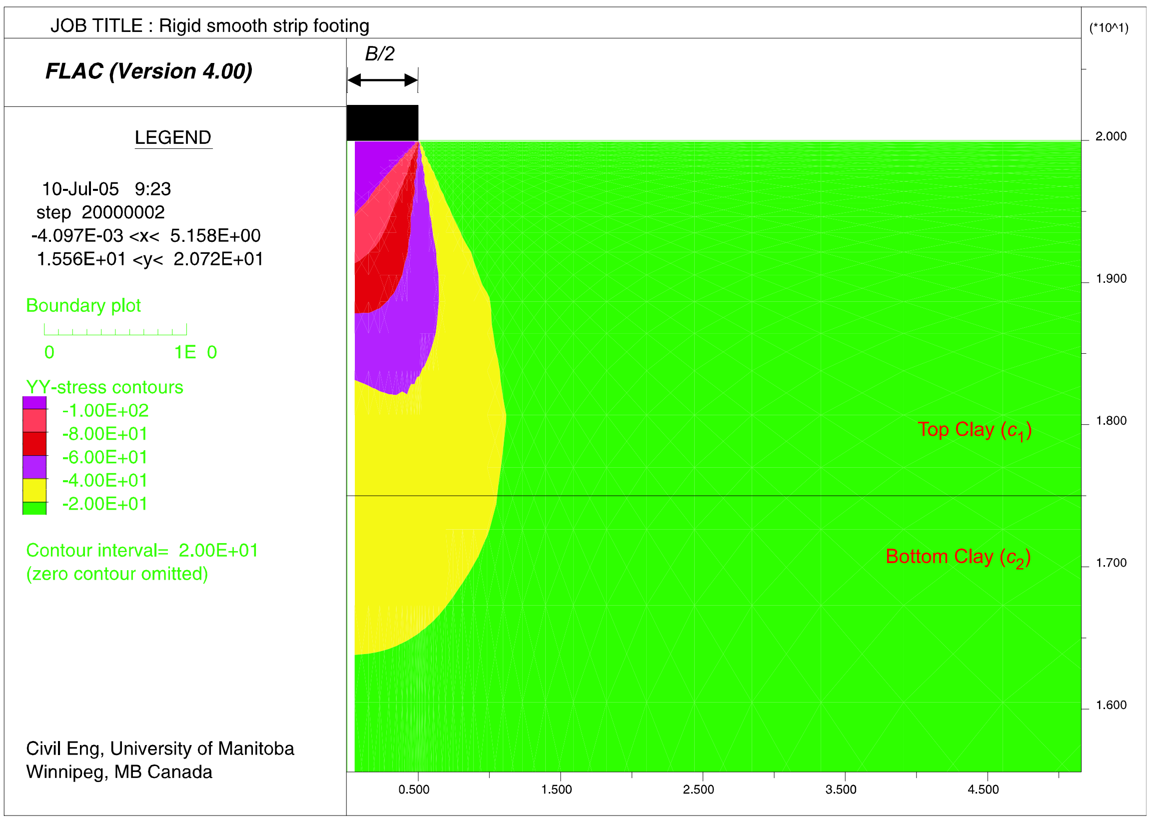

Figure A.67: Vertical stress (σ_{yy}) contours for a rigid smooth strip footing on strong clay over soft clay for 40×30 grid model, $H/B = 2.5$, $c_2/c_1 = 1/3$.

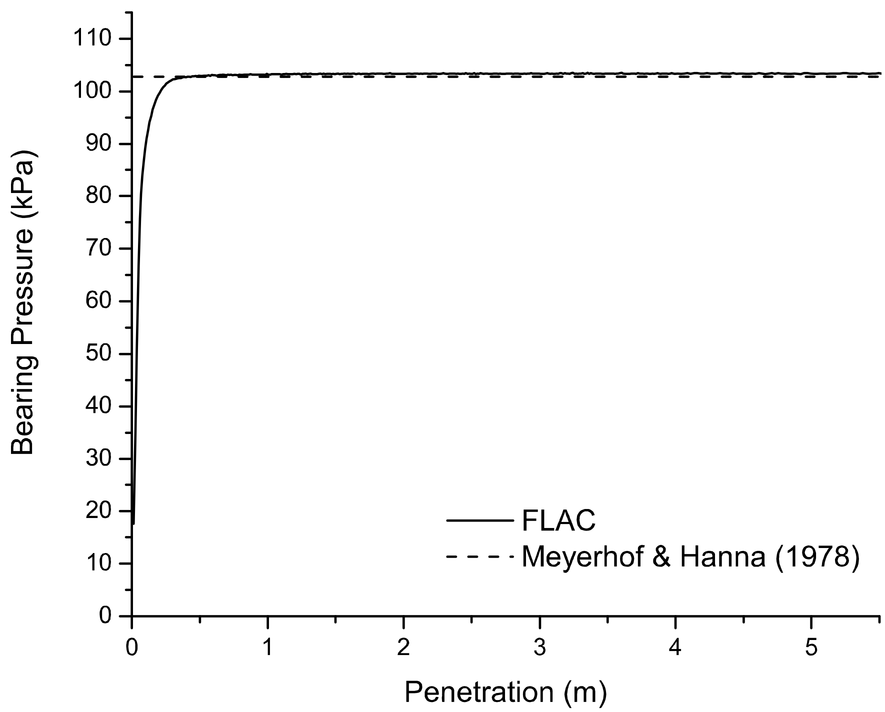

Figure A.68: Bearing pressure versus penetration curve for a rigid smooth strip footing on strong clay over soft clay for 40×30 grid model, $H/B = 2.5$, $c_2/c_1 = 1/3$.

Case 6: $c_2/c_1 = 0.2$ **- Small Deformation Analysis**

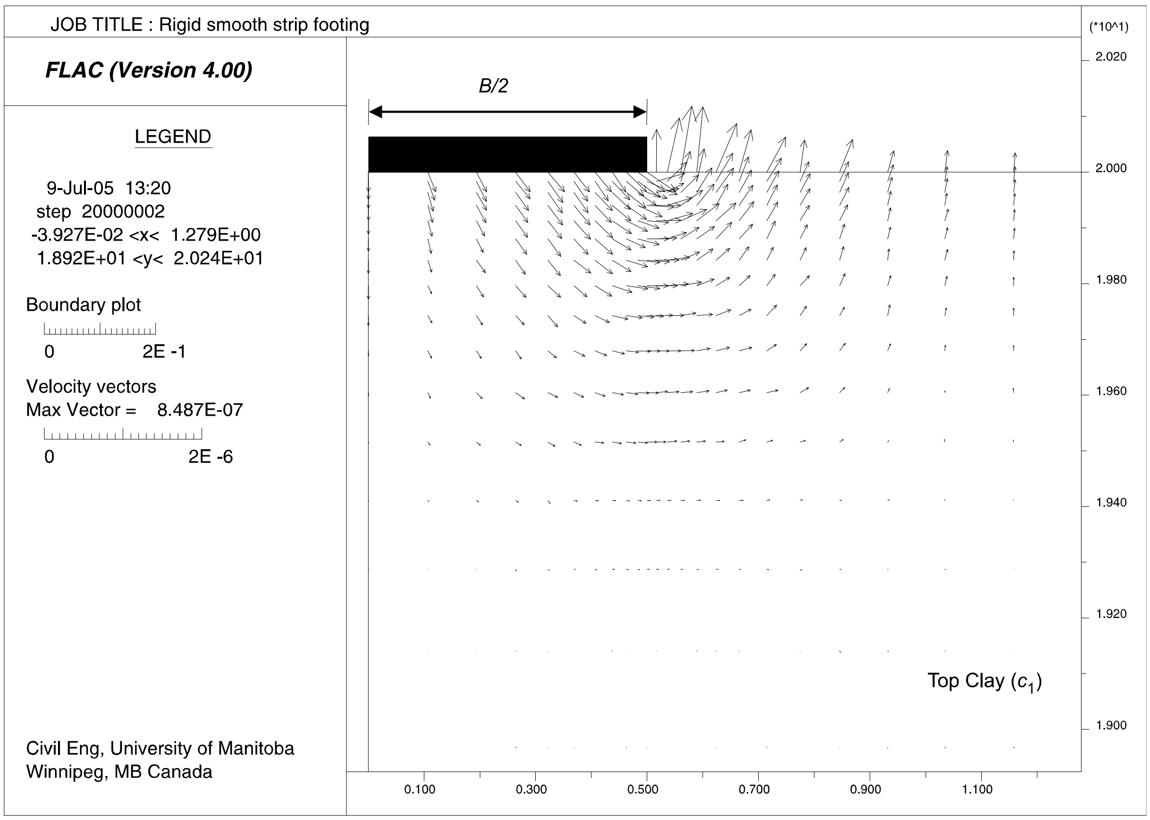

Figure A.69: Velocity vectors for a rigid smooth strip footing on strong clay over soft clay for 40×30 grid model, $H/B = 2.5$, $c_2/c_1 = 0.2$.

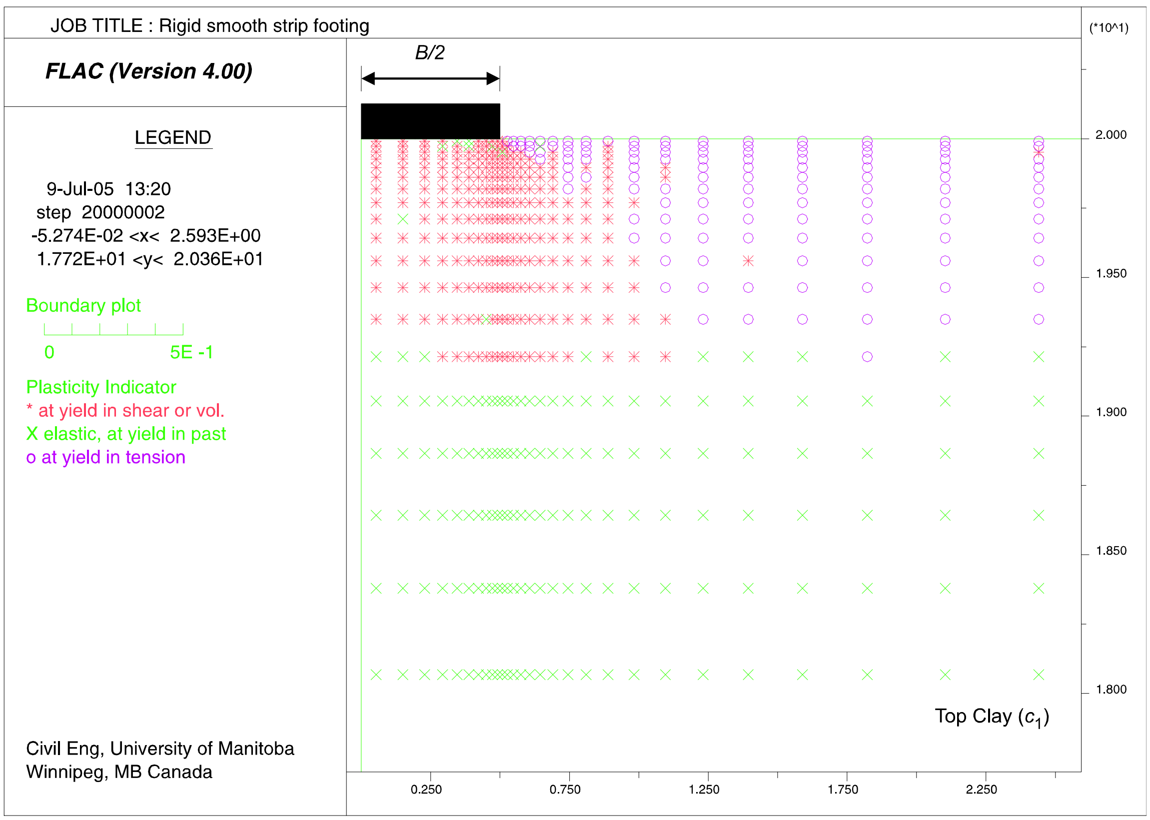

Figure A.70: Plasticity state indicators at steady state condition for a rigid smooth strip footing on strong over soft clay for 40 × 30 grid model, $H/B = 2.5$, $c_2/c_1 = 0.2$.

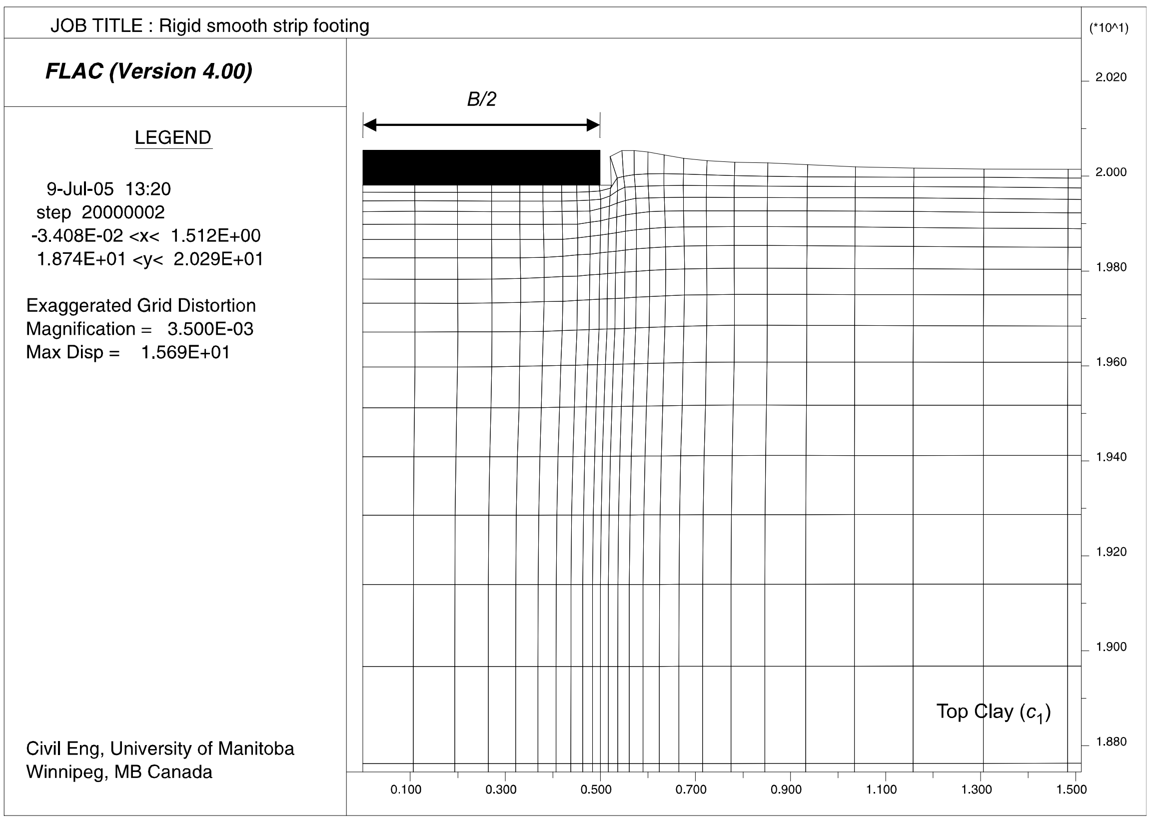

Figure A.71: Magnified grid for a rigid smooth strip footing on strong clay over soft clay for 40 × 30 grid model, $H/B = 2.5$, $c_2/c_1 = 0.2$.

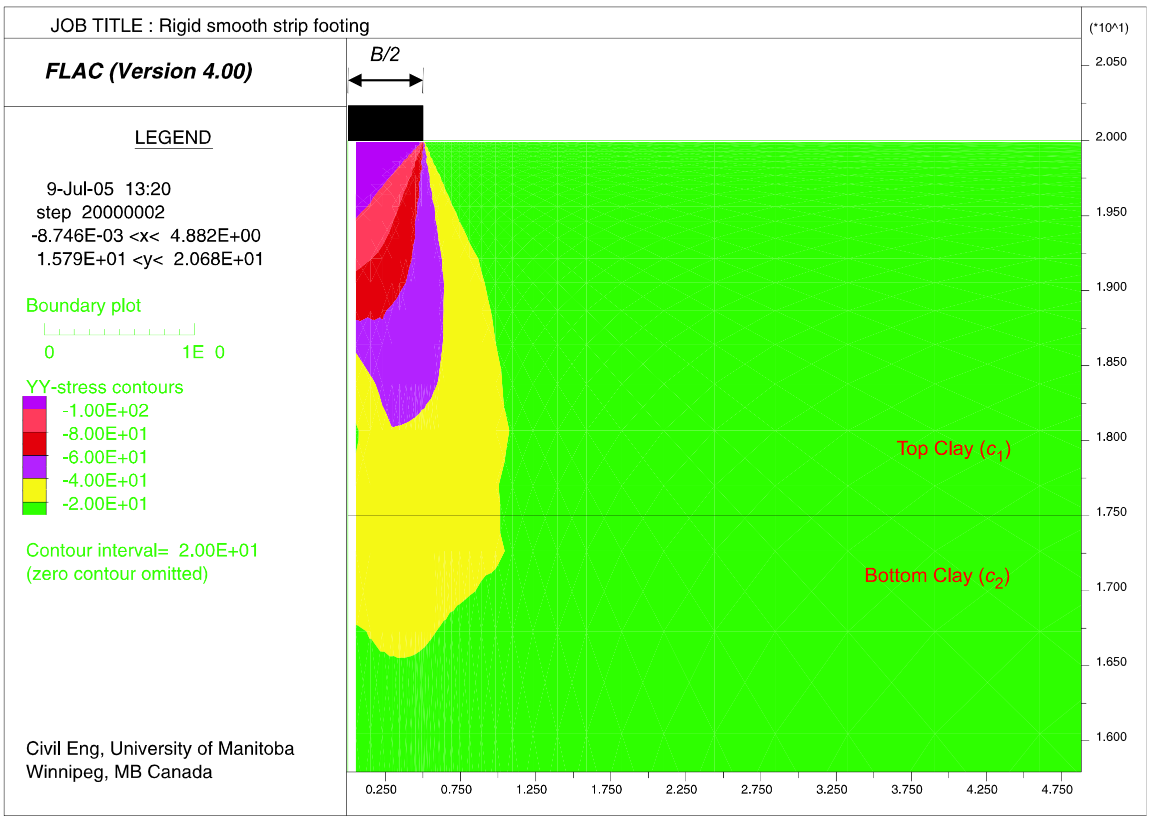

Figure A.72: Vertical stress (σ_{yy}) contours for a rigid smooth strip footing on strong clay over soft clay for 40×30 grid model, $H/B = 2.5$, $c_2/c_1 = 0.2$.

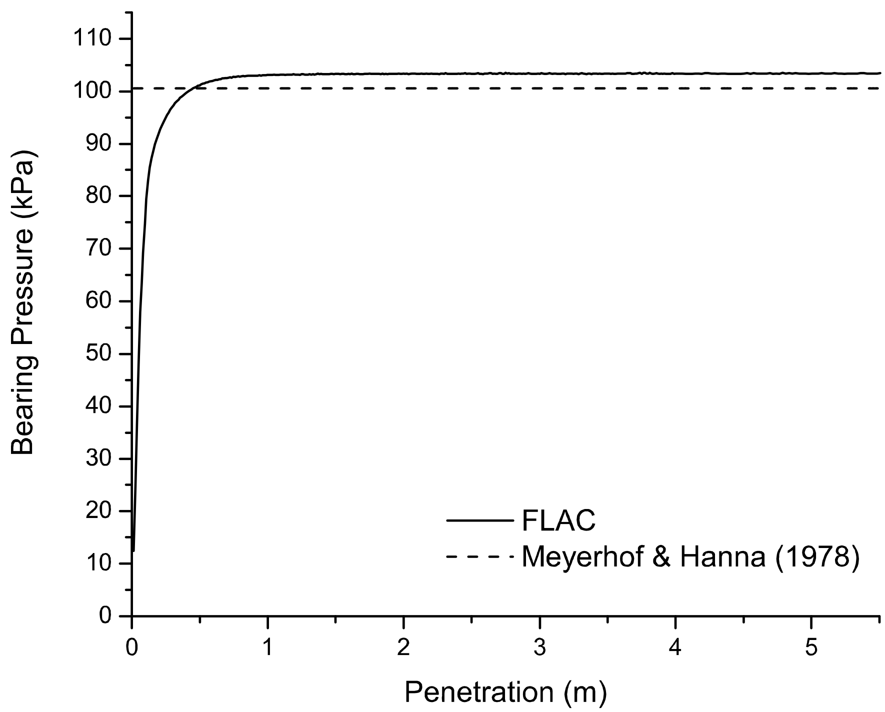

Figure A.73: Bearing pressure versus penetration curve for a rigid smooth strip footing on strong clay over soft clay for 40 × 30 grid model, $H/B = 2.5$, $c_2/c_1 = 0.2$.

Case 7: $c_2/c_1 = 0.1$ - Small Deformation Analysis

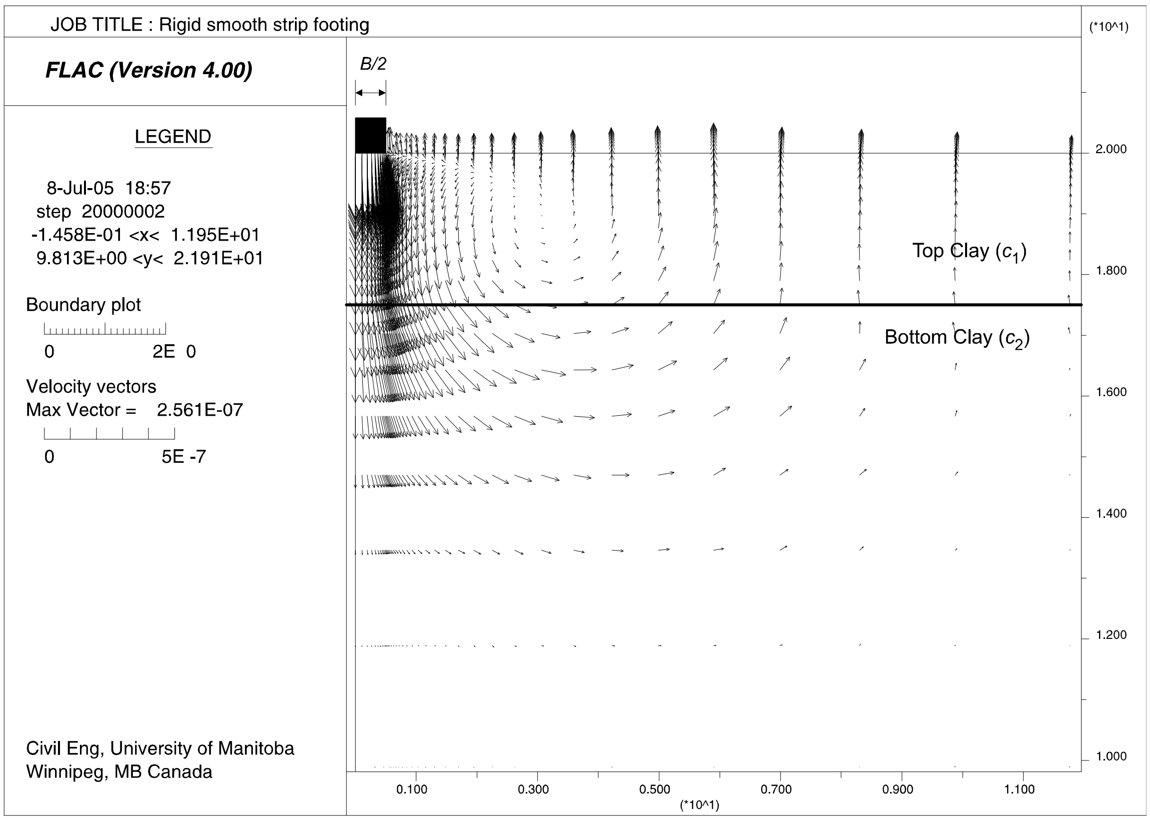

Figure A.74: Velocity vectors for a rigid smooth strip footing on strong clay over soft clay for 40×30 grid model, $H/B = 2.5$, $c_2/c_1 = 0.1$.

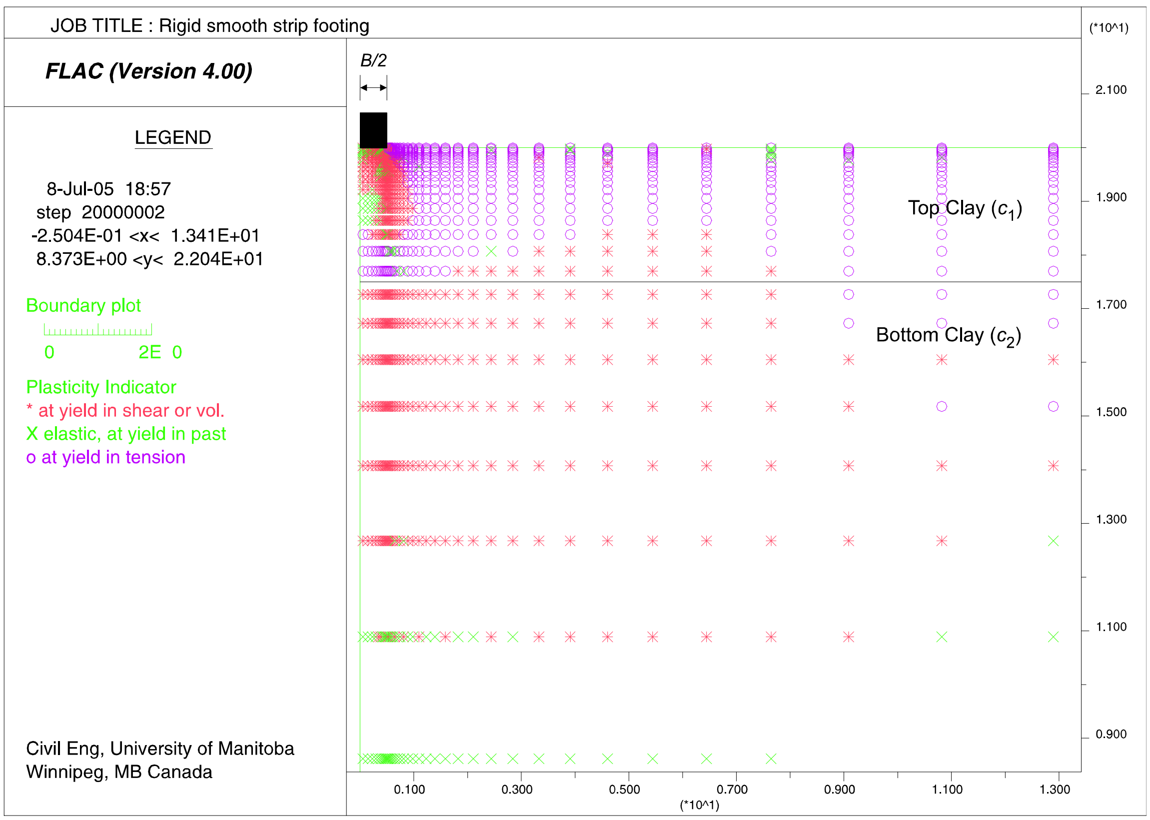

Figure A.75: Plasticity state indicators at steady state condition for a rigid smooth strip footing on strong over soft clay for 40 × 30 grid model, $H/B = 2.5$, $c_2/c_1 = 0.1$.

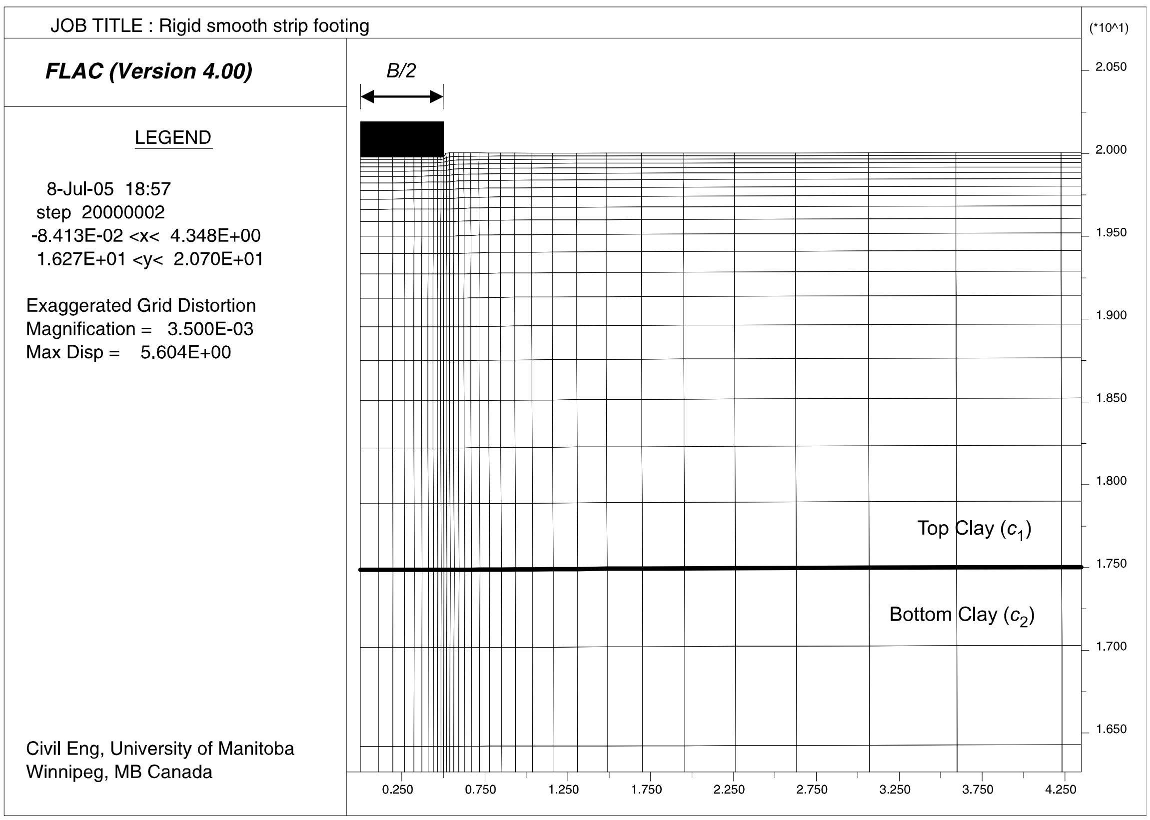

Figure A.76: Magnified grid for a rigid smooth strip footing on strong clay over soft clay for 40×30 grid model, $H/B = 2.5$, $c_2/c_1 = 0.1$.

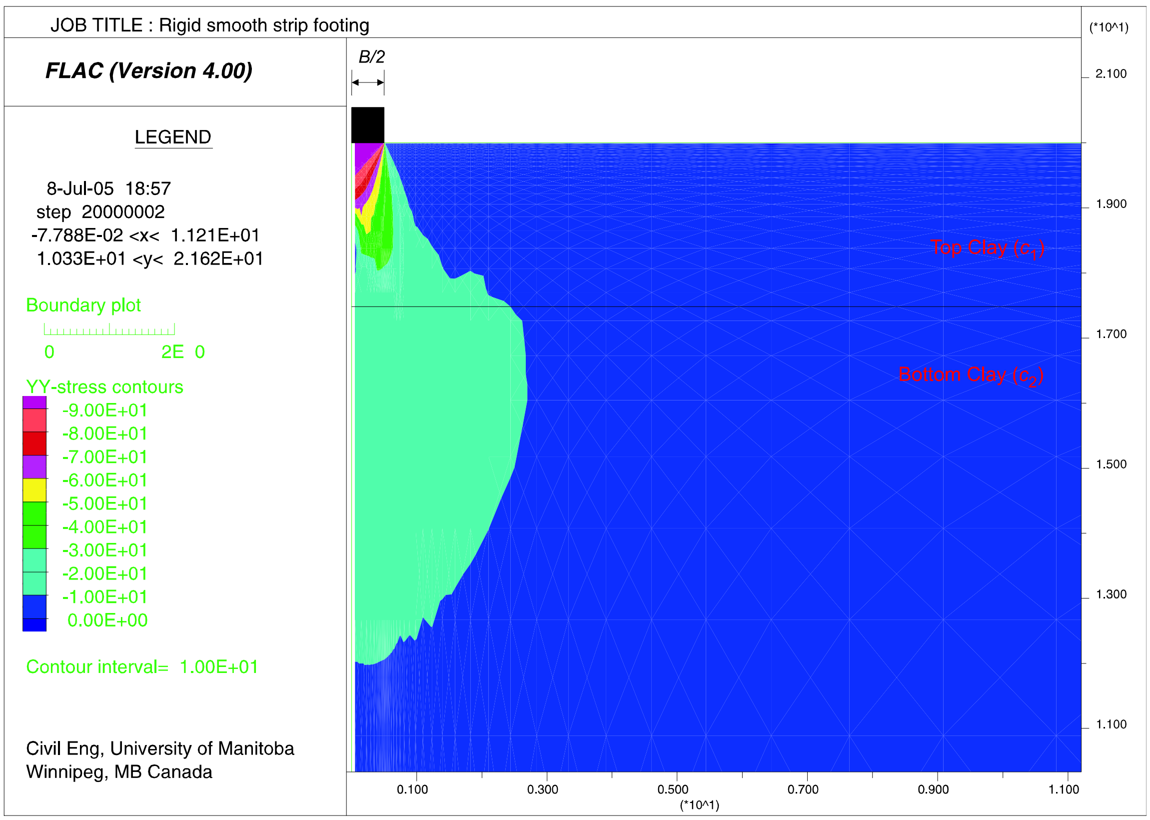

Figure A.77: Vertical stress (σ_{yy}) contours for a rigid smooth strip footing on strong clay over soft clay for 40×30 grid model, $H/B = 2.5$, $c_2/c_1 = 0.1$.

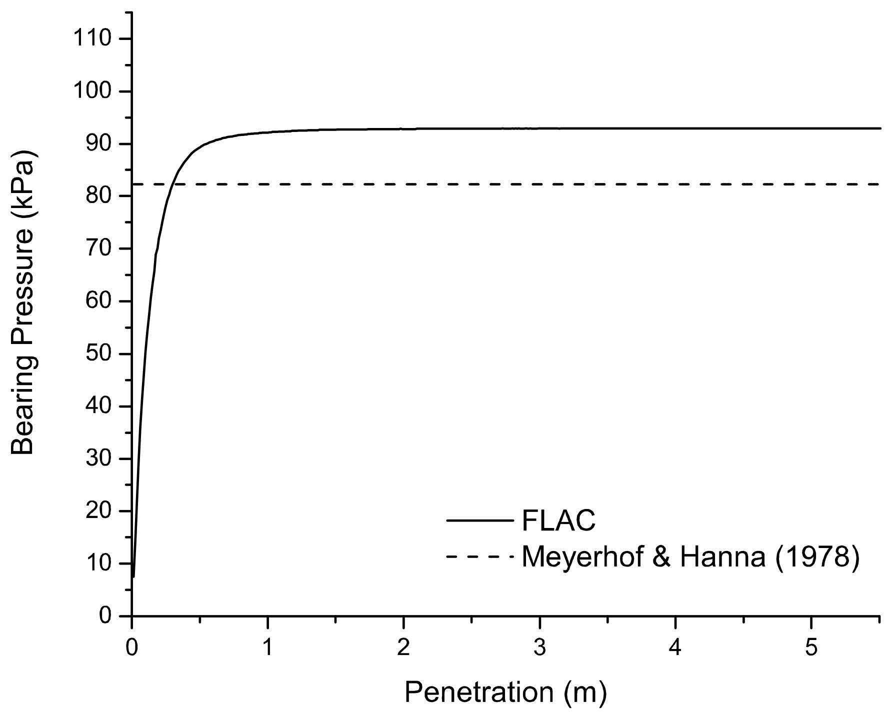

Figure A.78: Bearing pressure versus penetration curve for a rigid smooth strip footing on strong clay over soft clay for 40 × 30 grid model, $H/B = 2.5$, $c_2/c_1 = 0.1$.

A.1.4 Rigid Smooth Strip Footing on Strong over Soft Clay ($H/B = 3$)

Case 7: $c_2/c_1 = 0.1$ - Small Deformation Analysis

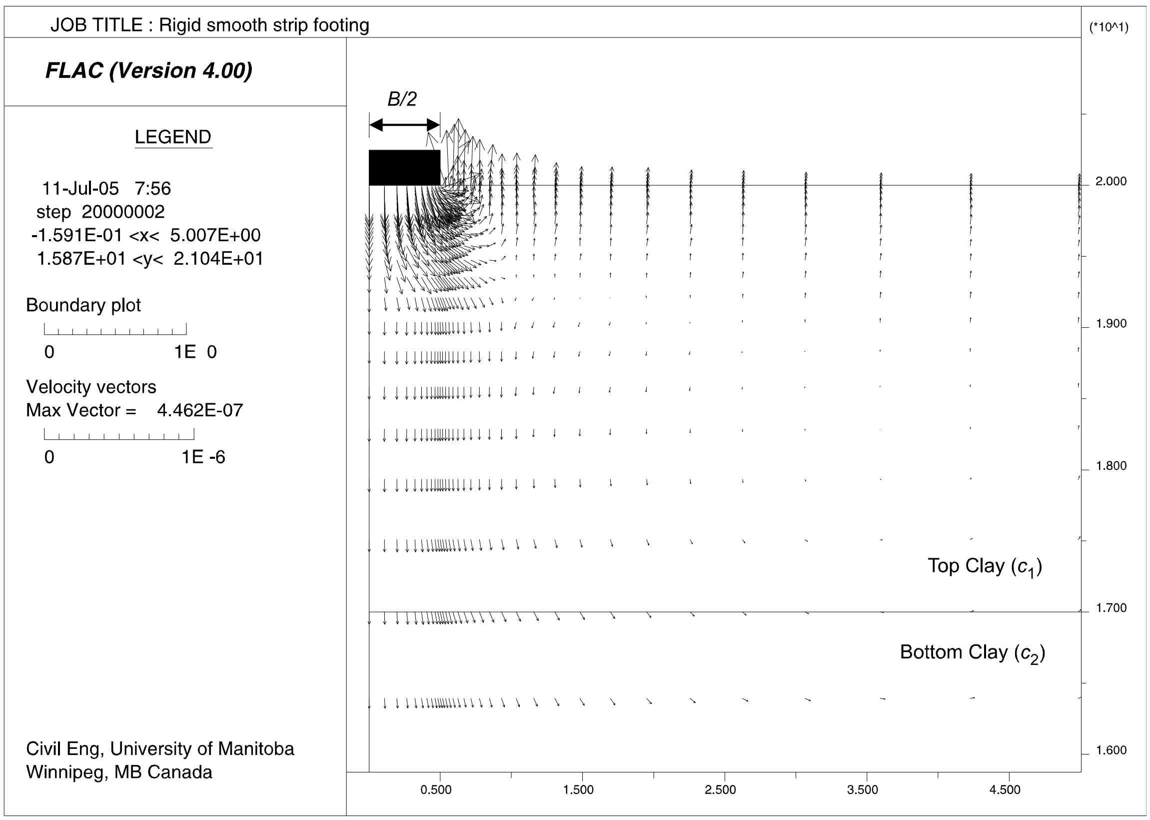

Figure A.79: Velocity vectors for a rigid smooth strip footing on strong clay over soft clay for 40 × 30 grid model, $H/B = 3$, $c_2/c_1 = 0.1$.

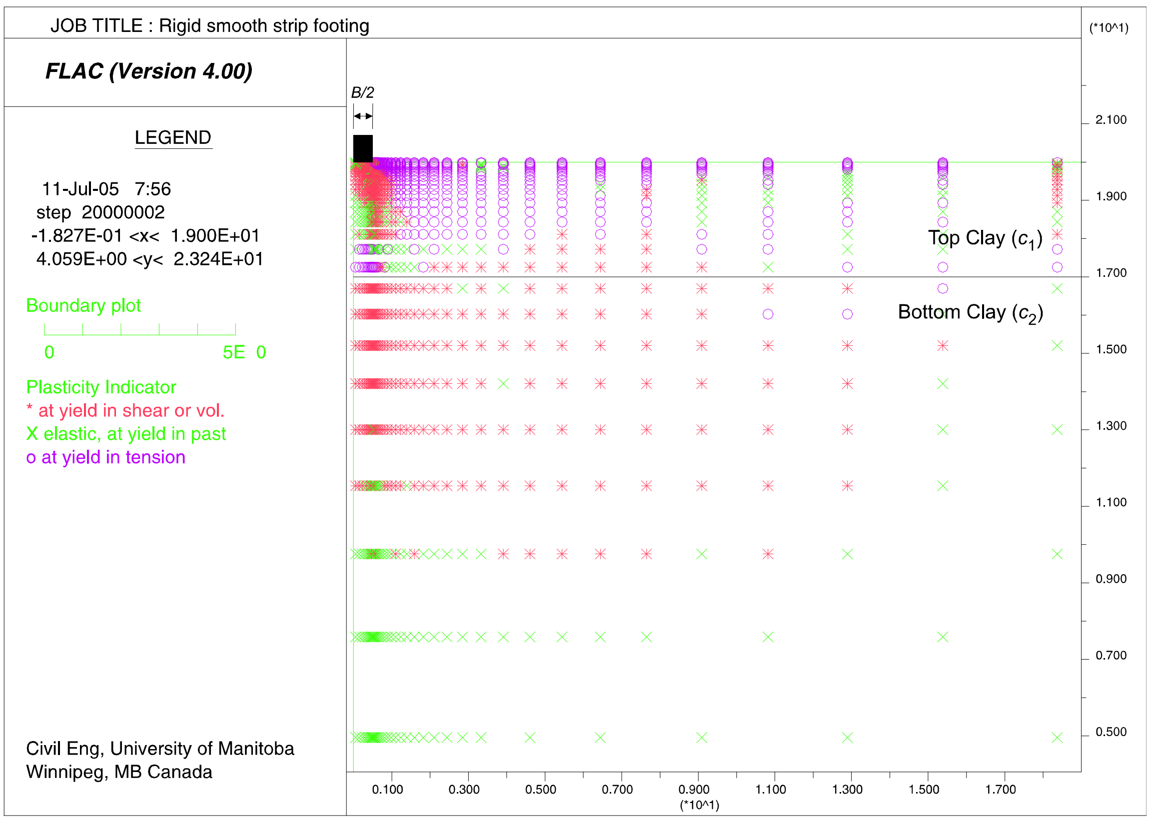

Figure A.80: Plasticity state indicators at steady state condition for a rigid smooth strip footing on strong over soft clay for 40×30 grid model, $H/B = 3$, $c_2/c_1 = 0.1$.

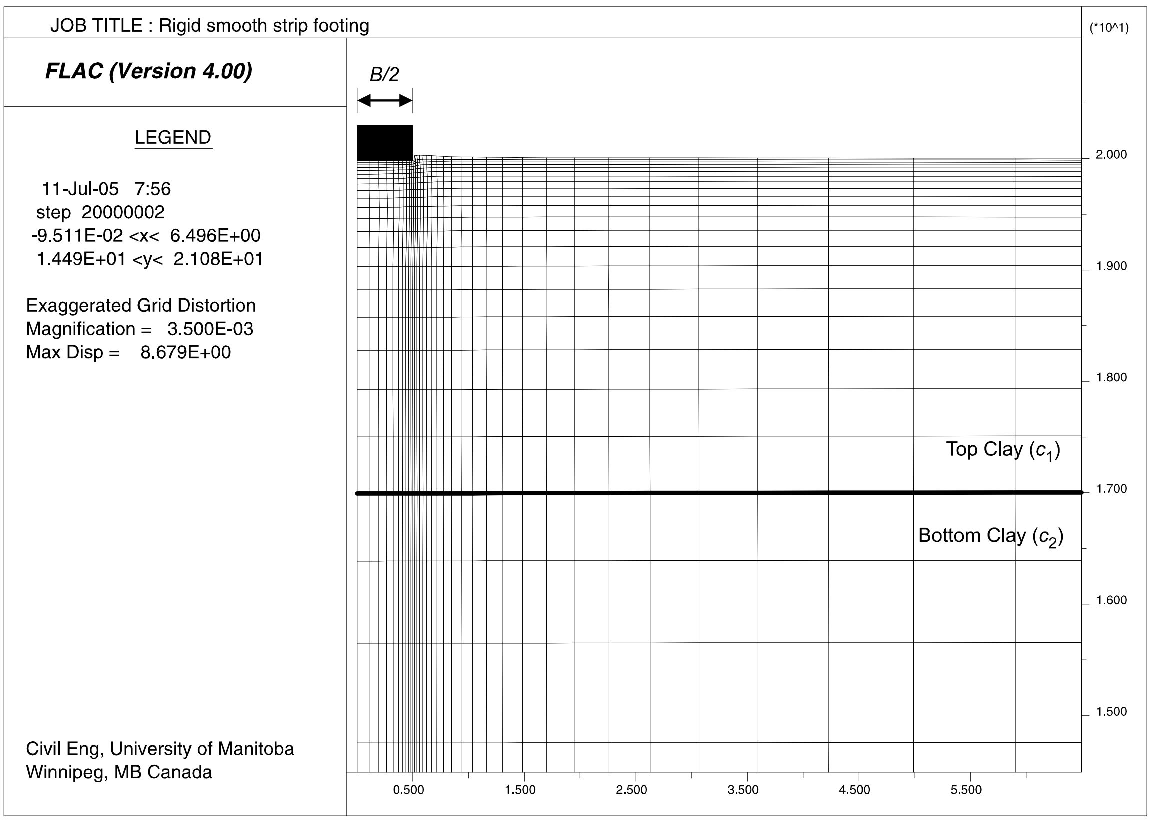

Figure A.81: Magnified grid for a rigid smooth strip footing on strong clay over soft clay for 40×30 grid model, $H/B = 3$, $c_2/c_1 = 0.1$.

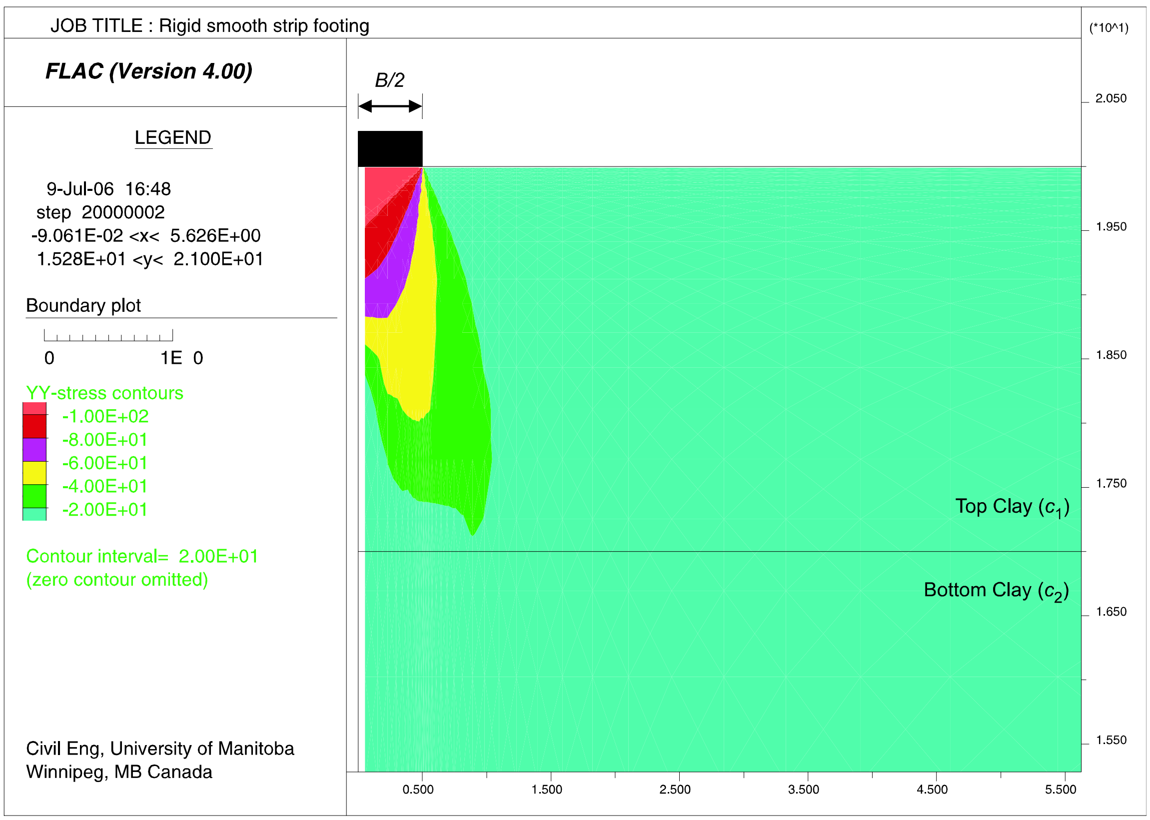

Figure A.82: Vertical stress (σ_{yy}) contours for a rigid smooth strip footing on strong clay over soft clay for 40×30 grid model, $H/B = 3$, $c_2/c_1 = 0.1$.

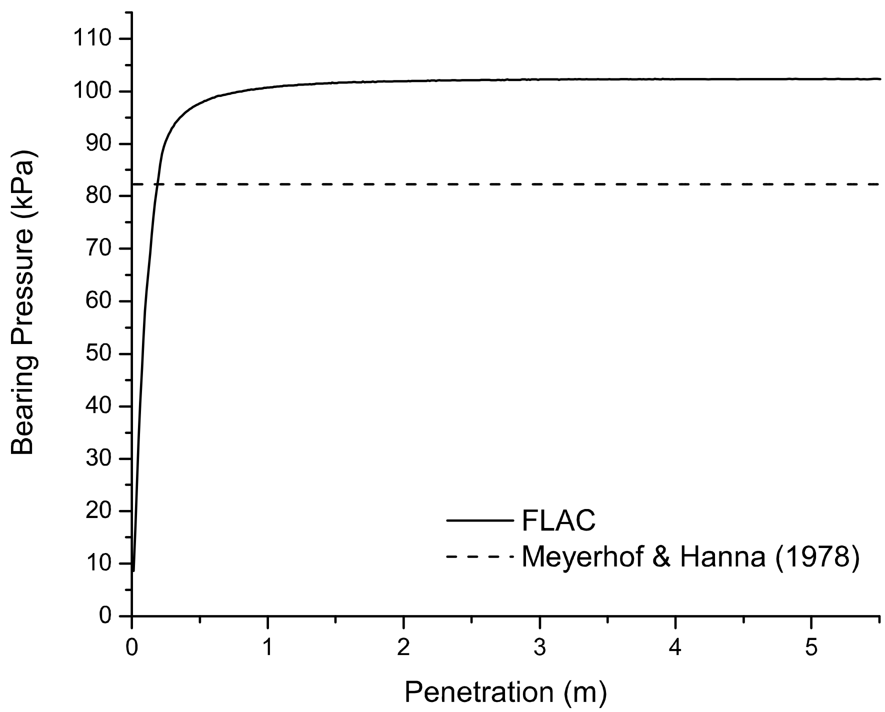

Figure A.83: Bearing pressure versus penetration curve for a rigid smooth strip footing on strong clay over soft clay for 40 × 30 grid model, $H/B = 3$, $c_2/c_1 = 0.1$

A.1.5 Rigid Smooth Strip Footing on Strong over Soft Clay ($H/B = 3.5$)

Case 7: $c_2/c_1 = 0.1$ **- Small Deformation Analysis**

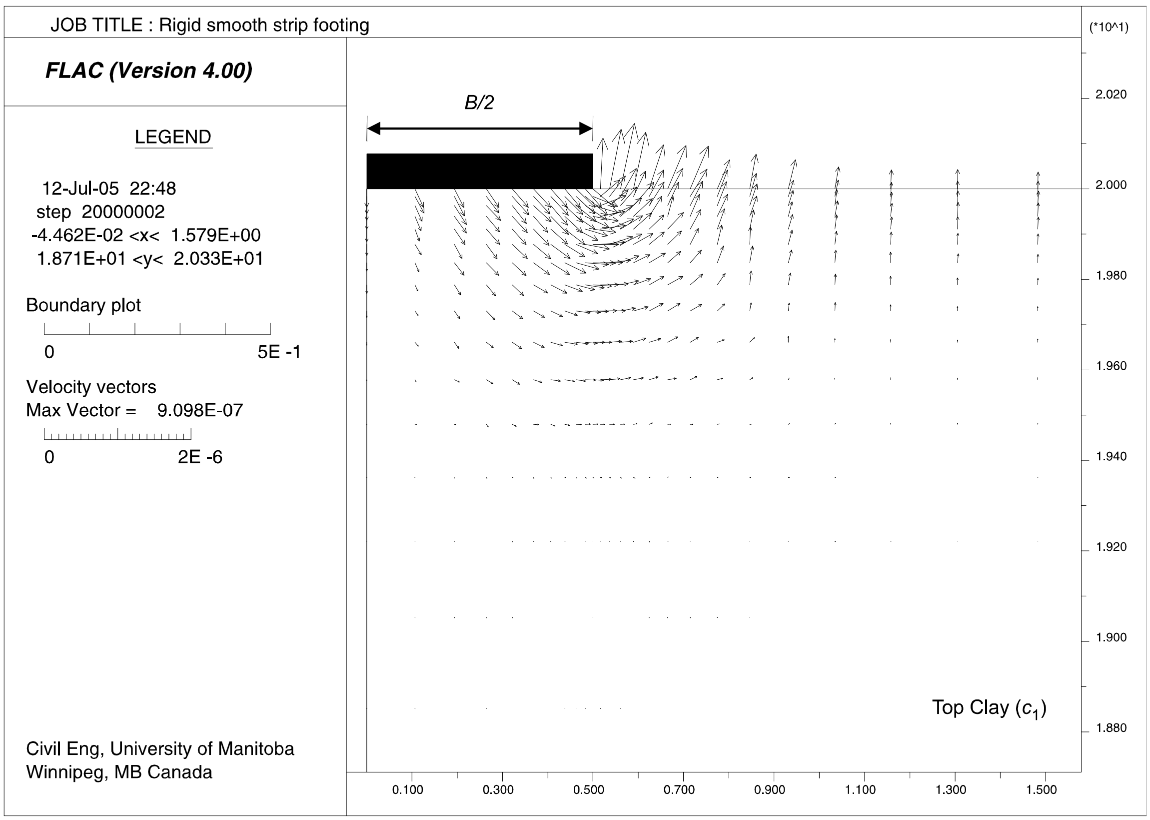

Figure A.84: Velocity vectors for a rigid smooth strip footing on strong clay over soft clay for 40×30 grid model, $H/B = 3.5$, $c_2/c_1 = 0.1$.

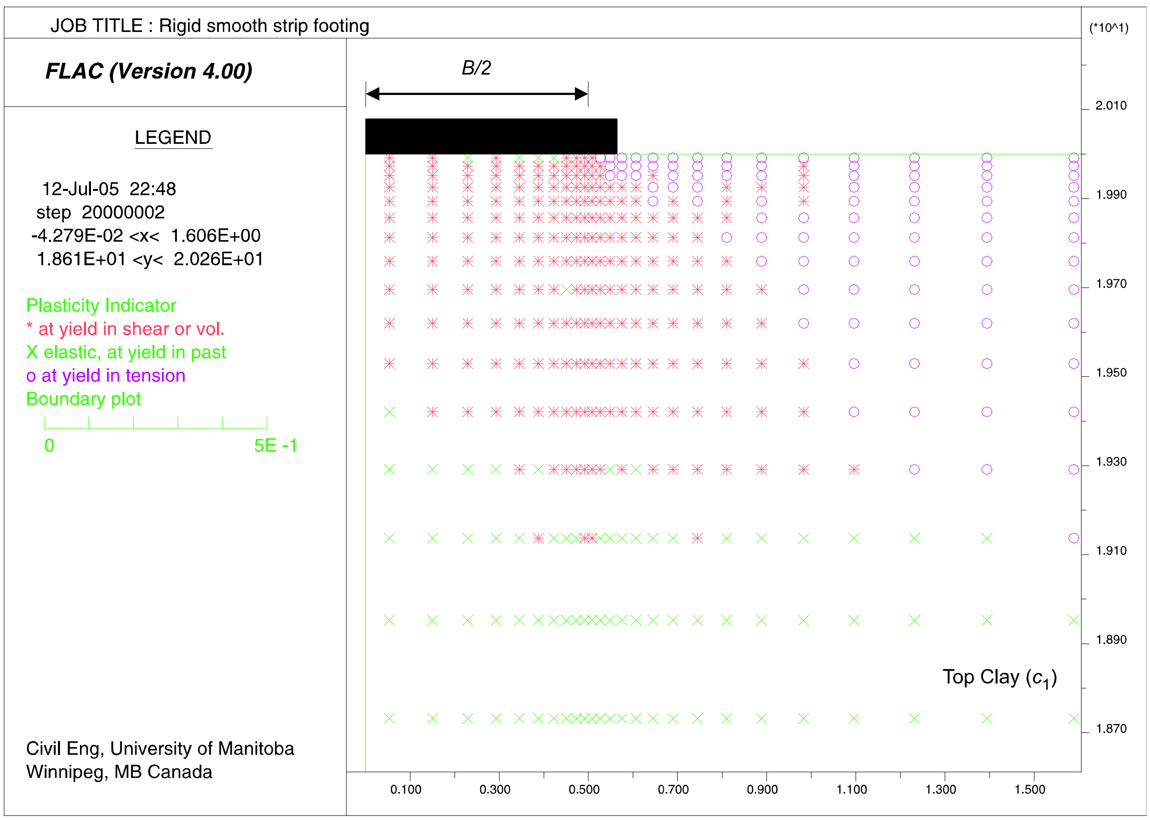

Figure A.85: Plasticity state indicators at steady state condition for a rigid smooth strip footing on strong over soft clay for 40×30 grid model, $H/B = 3.5$, $c_2/c_1 = 0.1$.

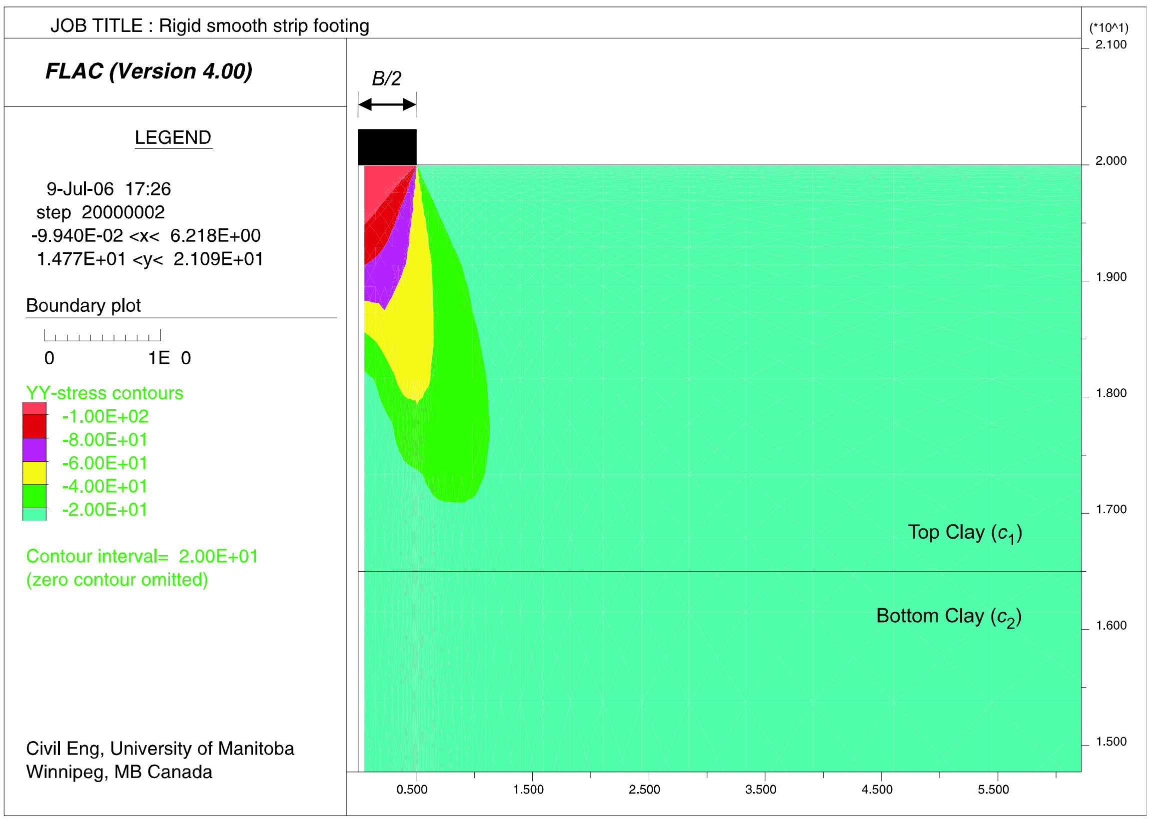

Figure A.86: Vertical stress (σ_{yy}) contours for a rigid smooth strip footing on strong clay over soft clay for 40×30 grid model, $H/B = 3.5$, $c_2/c_1 = 0.1$.

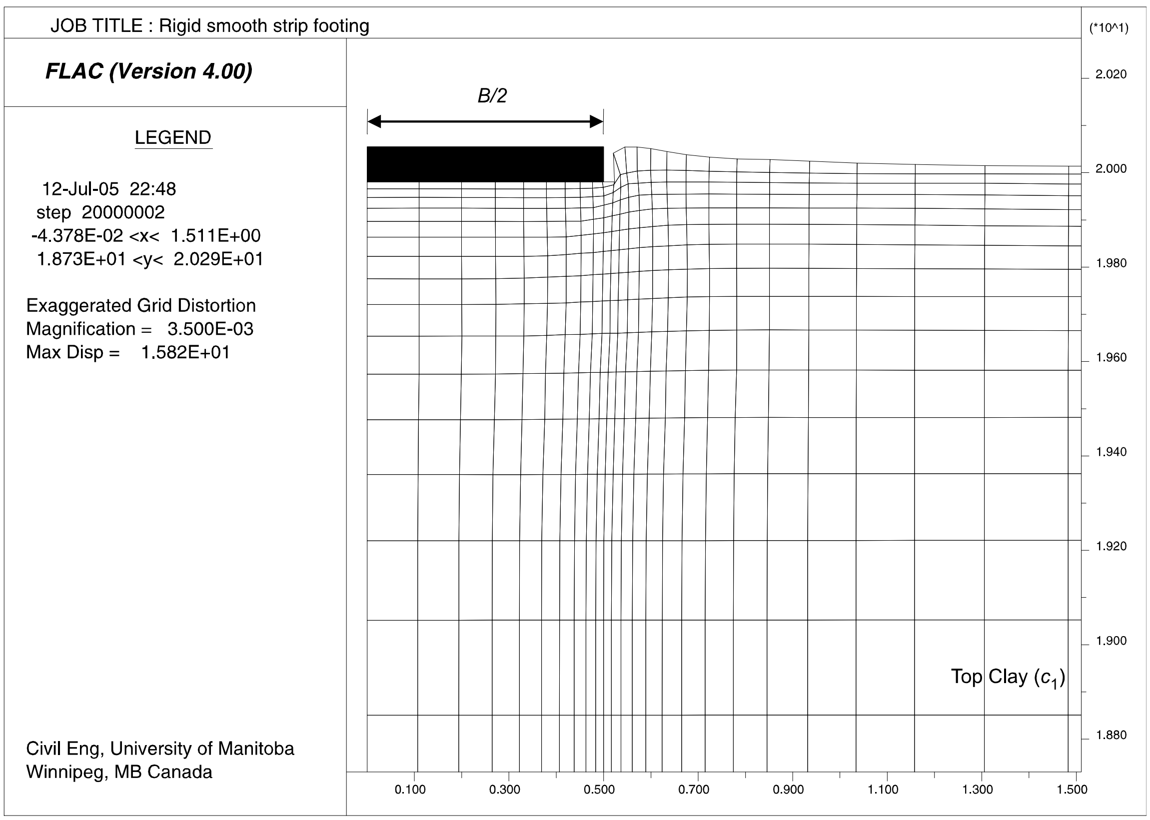

Figure A.87: Magnified grid for a rigid smooth strip footing on strong clay over soft clay for 40×30 grid model, $H/B = 3.5$, $c_2/c_1 = 0.1$.

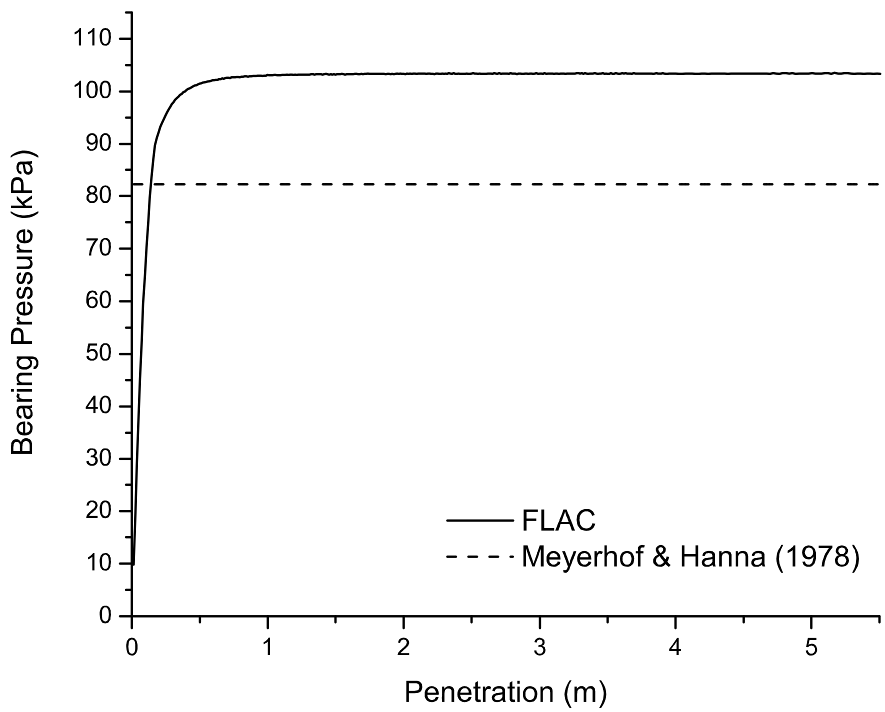

Figure A.88: Bearing pressure versus penetration curve for a rigid smooth strip footing on strong clay over soft clay for 40 × 30 grid model, $H/B = 3.5$, $c_2/c_1 = 0.1$

A.1.6 Rigid Smooth Strip Footing on Strong over Soft Clay ($H/B = 0.5$)

Case 2: $c_2/c_1 = 0.8$ **- Small Deformation Analysis**

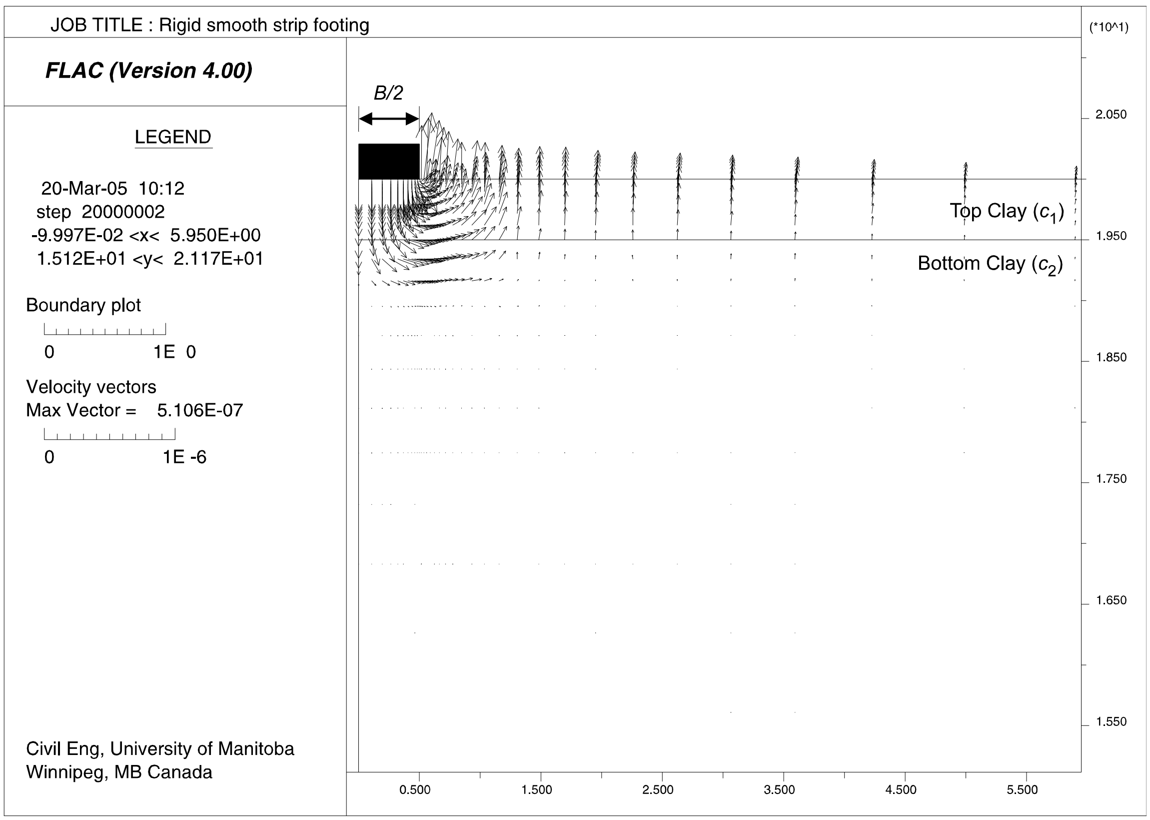

Figure A.89: Velocity vectors for a rigid strip footing on strong over soft clay for 40×30 grid model, $H/B = 0.5$, $c_2/c_1 = 0.8$.

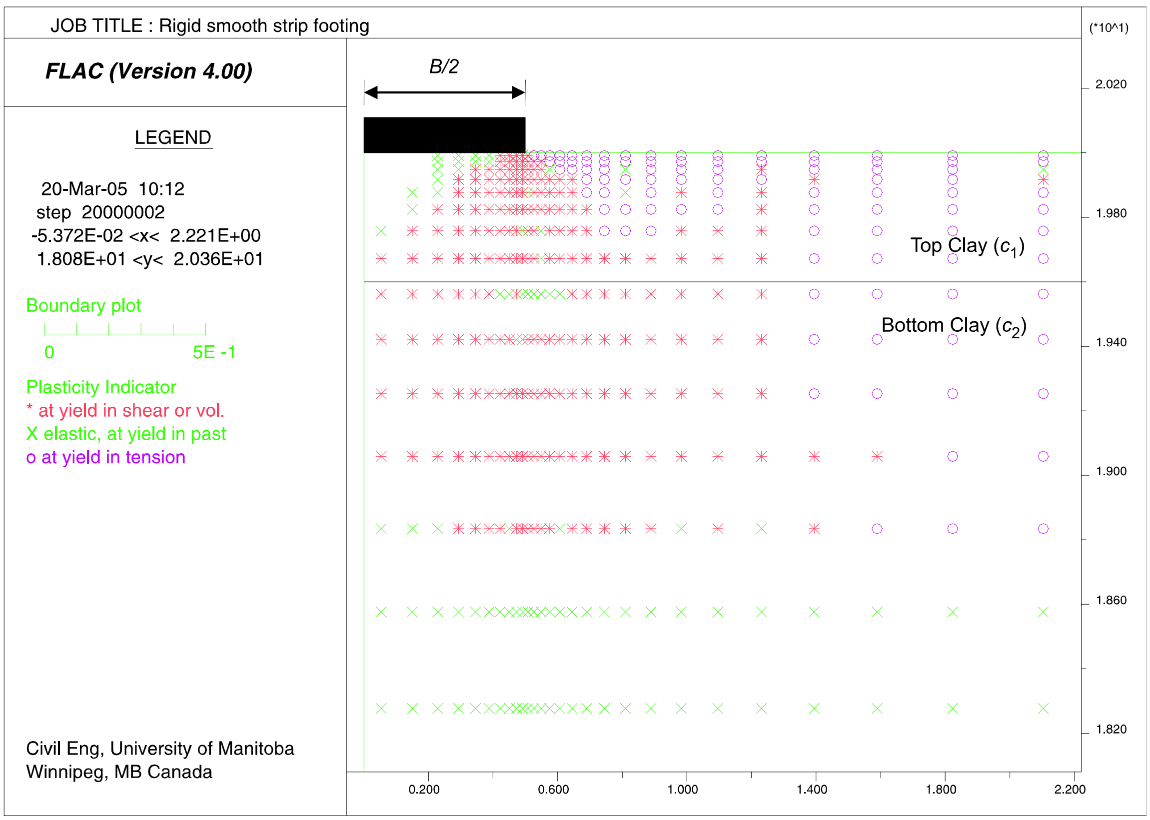

Figure A.90: Plasticity state indicators at steady state condition for a rigid smooth strip footing on strong over soft clay for 40 × 30 grid model, $H/B = 0.5$, $c_2/c_1 = 0.8$.

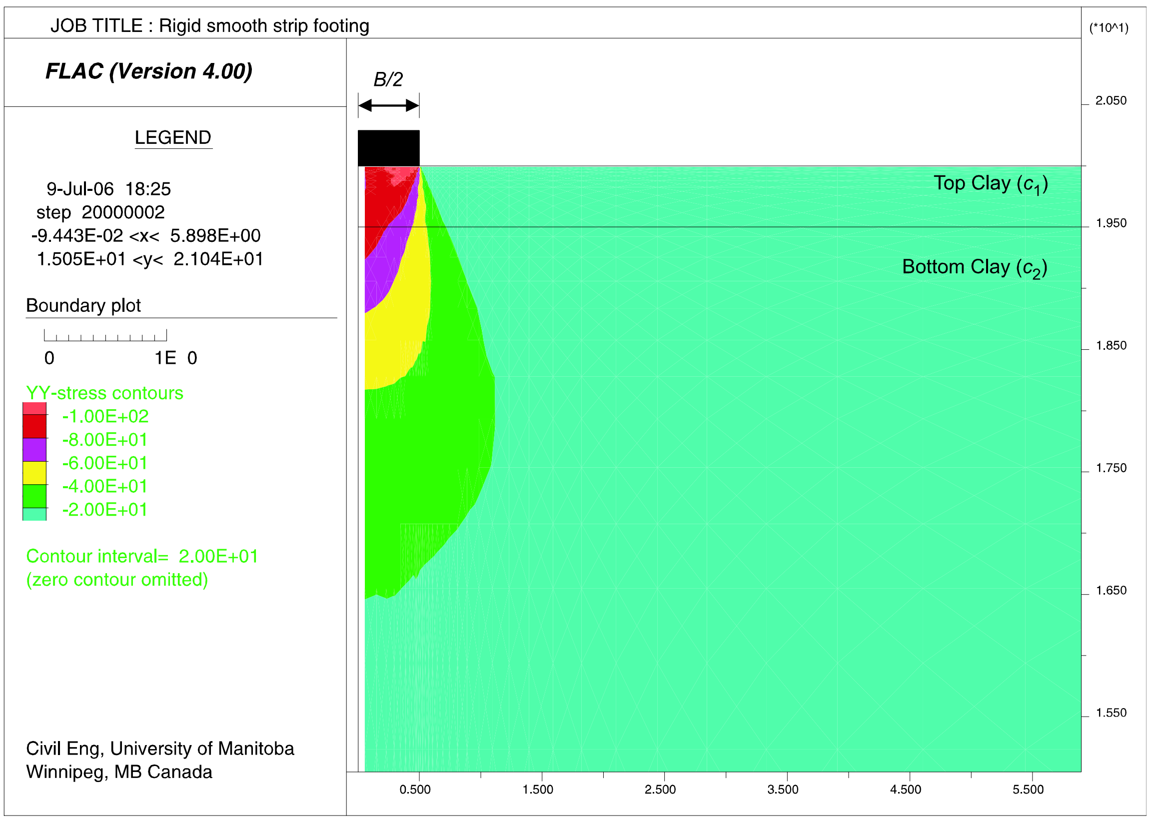

Figure A.91: Vertical stress (σ_{yy}) contours for a rigid smooth strip footing on strong over soft clay for 40×30 grid model, $H/B = 0.5$, $c_2/c_1 = 0.8$.

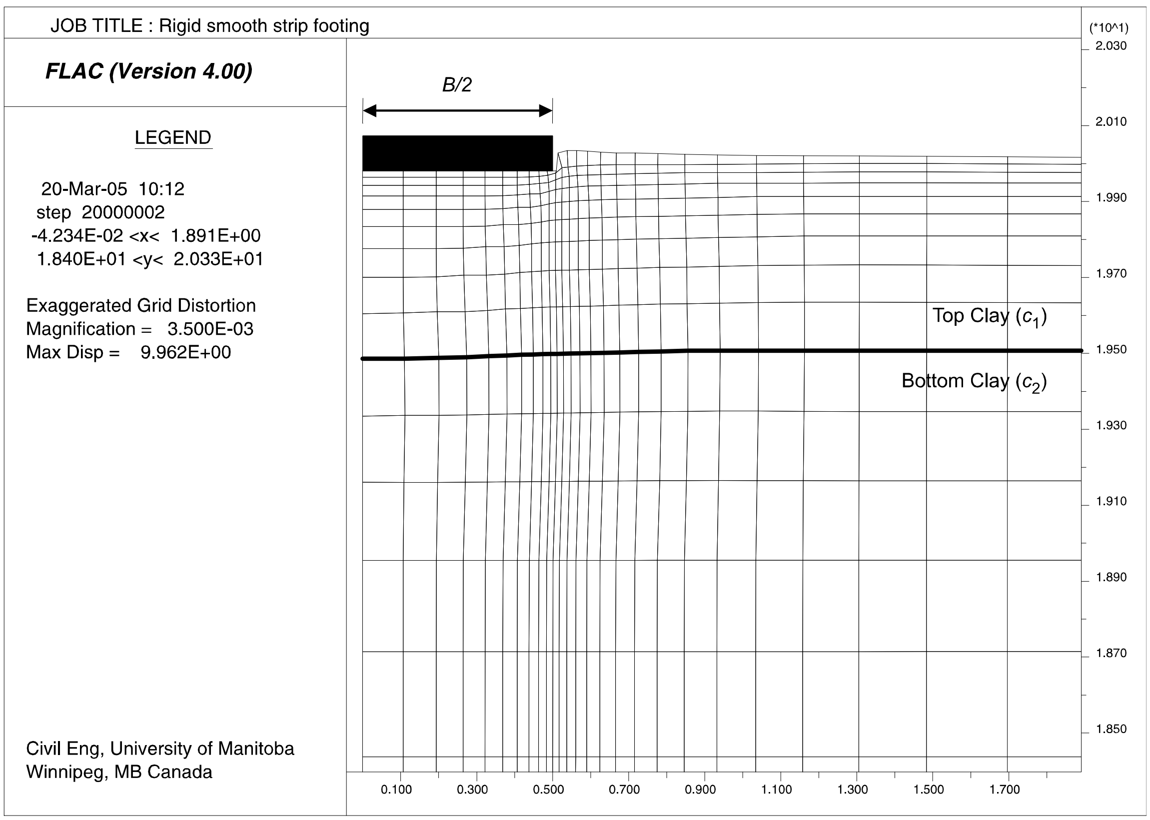

Figure A.92: Magnified grid for a rigid smooth strip footing on strong over soft clay for 40×30 grid model, $H/B = 0.5$, $c_2/c_1 = 0.8$.

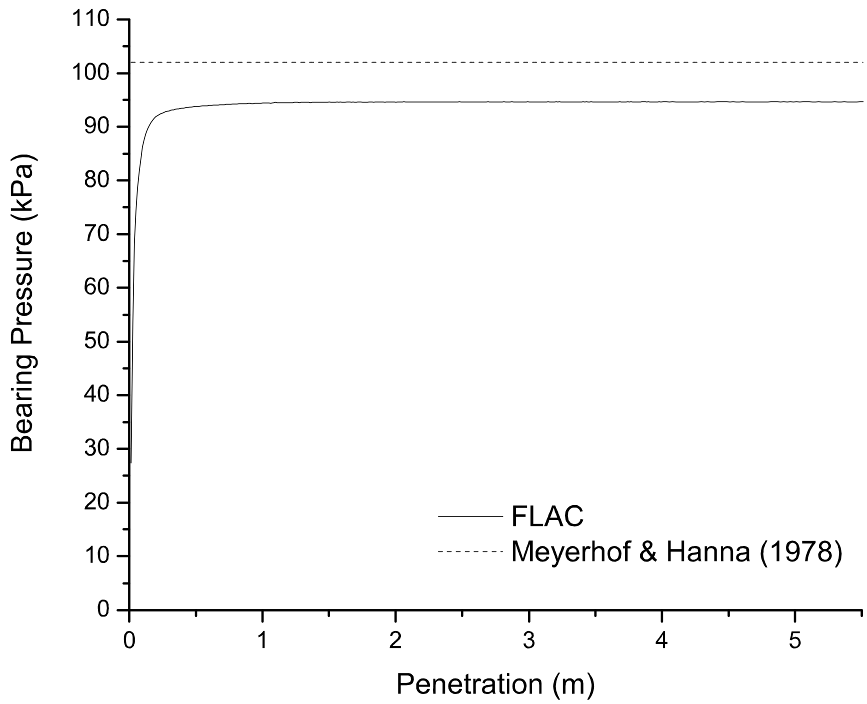

Figure A.93: Bearing pressure versus penetration curve for a rigid smooth strip footing on strong over soft clay for 40 × 30 grid model, $H/B = 0.5$, $c_2/c_1 = 0.8$.

Case 3: $c_2/c_1 = 2/3$ - Small Deformation Analysis

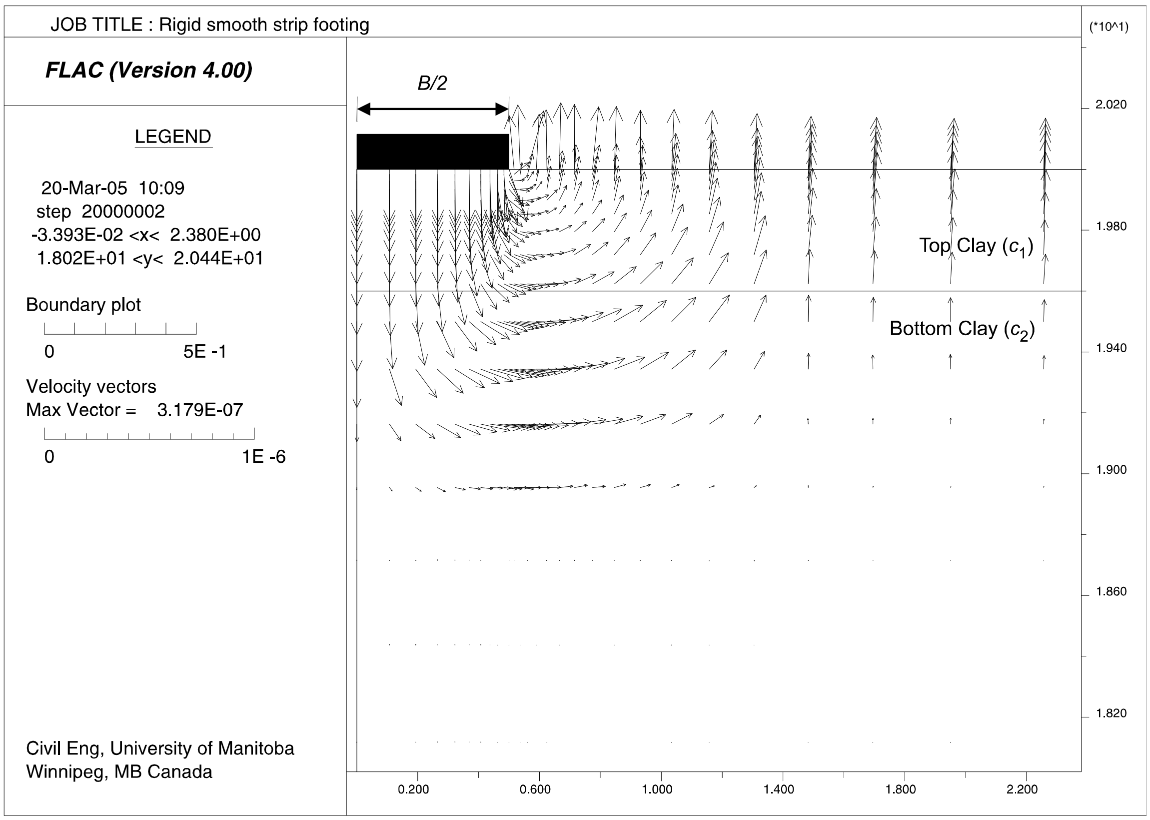

Figure A.94: Velocity vectors for a rigid smooth strip footing on strong over soft clay for 40 × 30 grid model, $H/B = 0.5$, $c_2/c_1 = 2/3$.

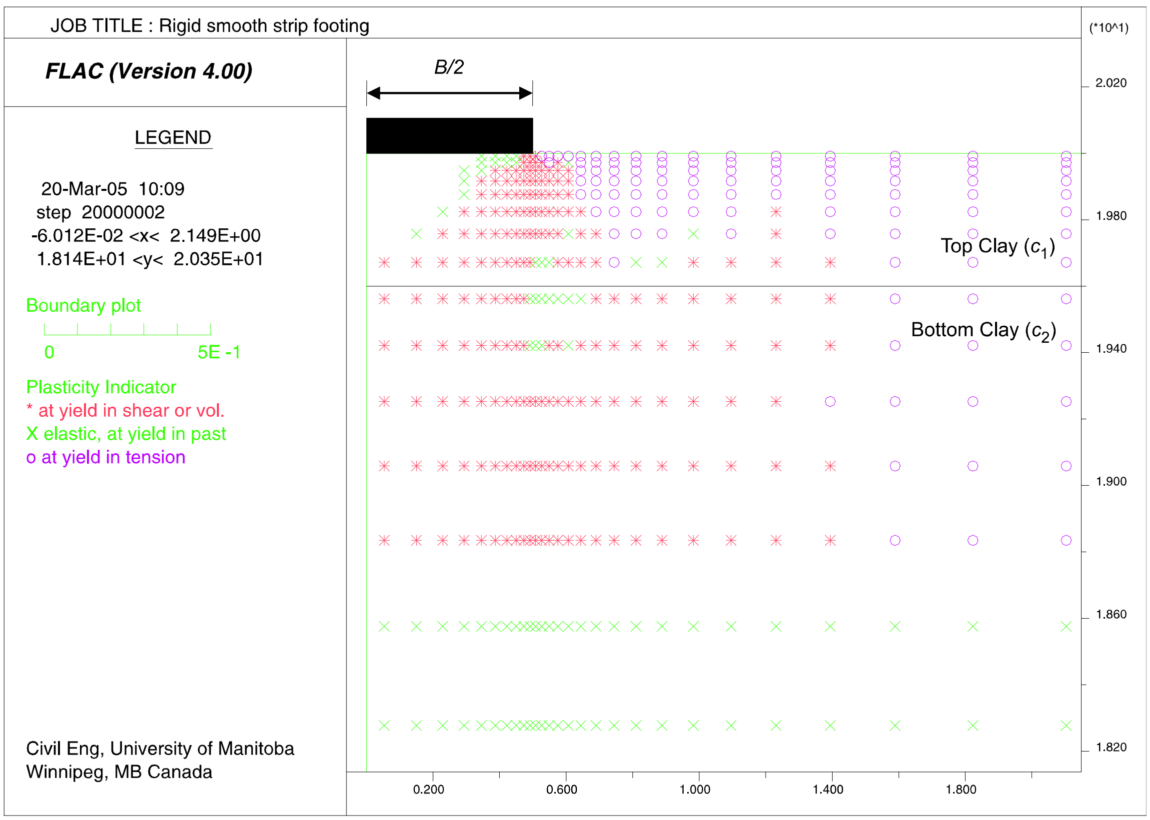

Figure A.95: Plasticity state indicators at steady state condition for a rigid smooth strip footing on strong over soft clay for 40×30 grid model, $H/B = 0.5$, $c_2/c_1 = 2/3$.

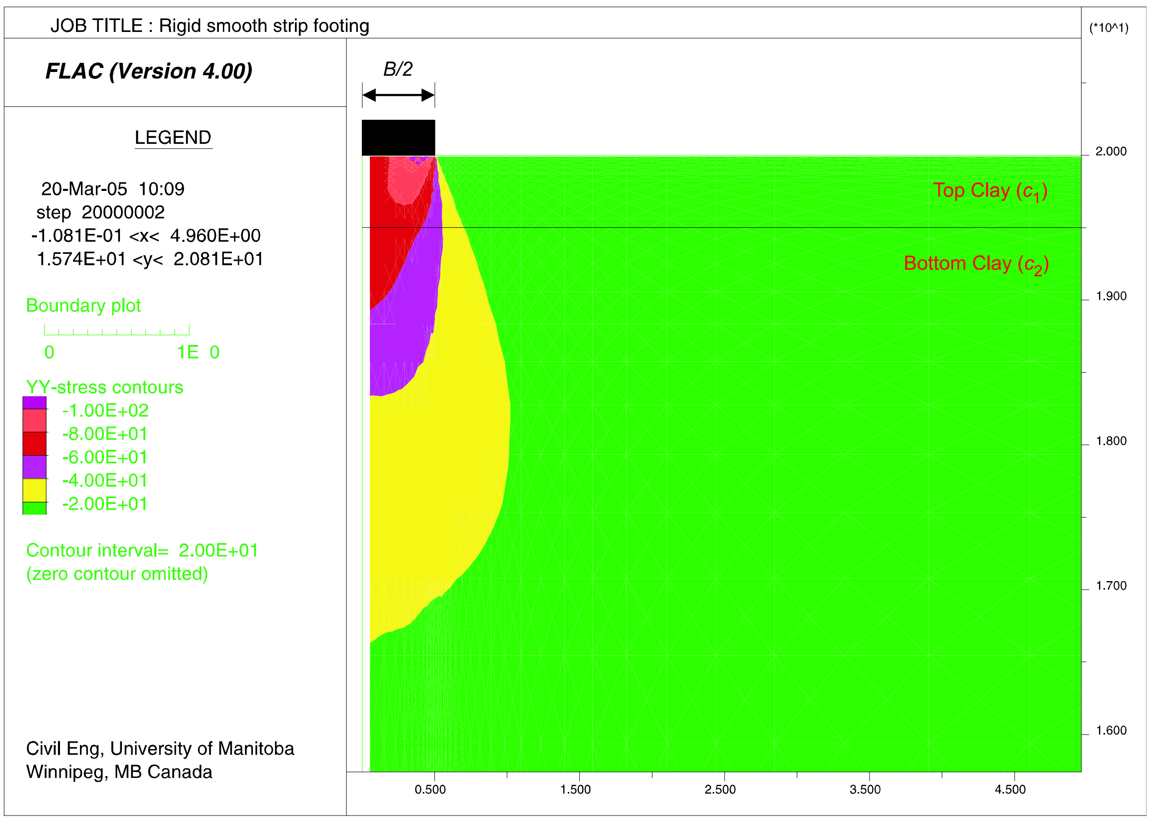

Figure A.96: Vertical stress (σ_{yy}) contours for a rigid smooth strip footing on strong over soft clay for 40×30 grid model, $H/B = 0.5$, $c_2/c_1 = 2/3$.

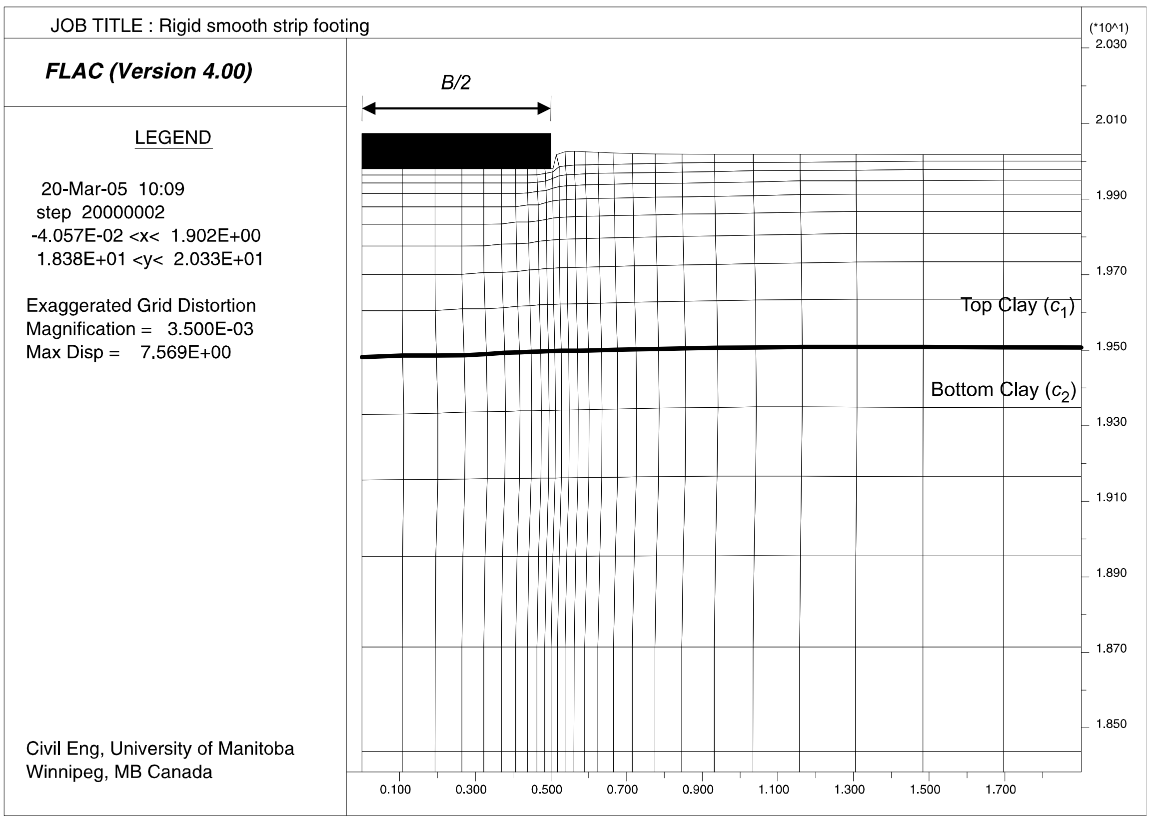

Figure A.97: Magnified grid for a rigid smooth strip footing on strong over soft clay for 40×30 grid model, $H/B = 0.5$, $c_2/c_1 = 2/3$.

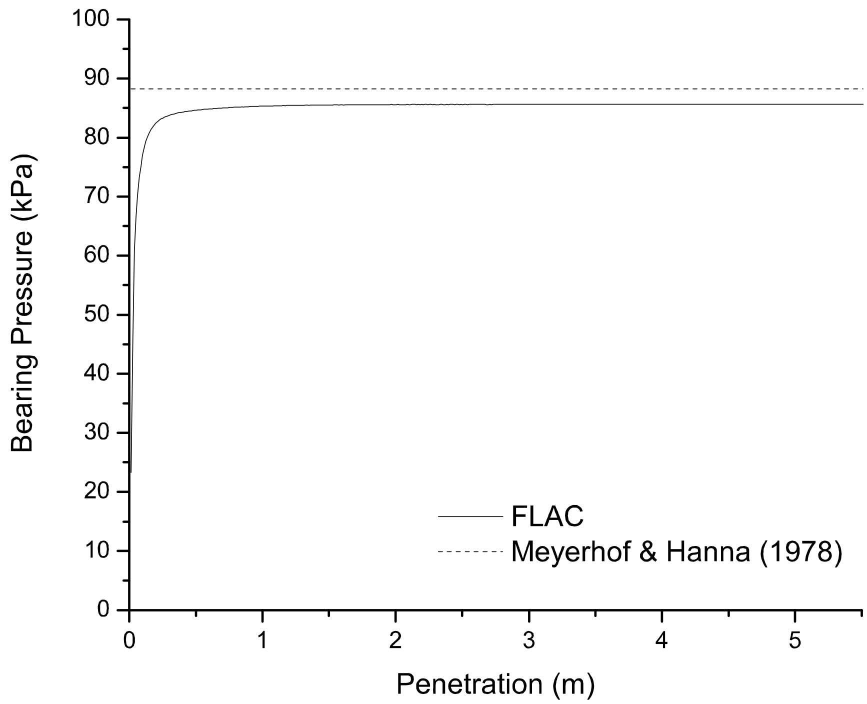

Figure A.98: Bearing pressure versus penetration curve for a rigid smooth strip footing on strong over soft clay for 40×30 grid model, $H/B = 0.5$, $c_2/c_1 = 2/3$.

Case 4: $c_2/c_1 = 0.5$ - Small Deformation Analysis

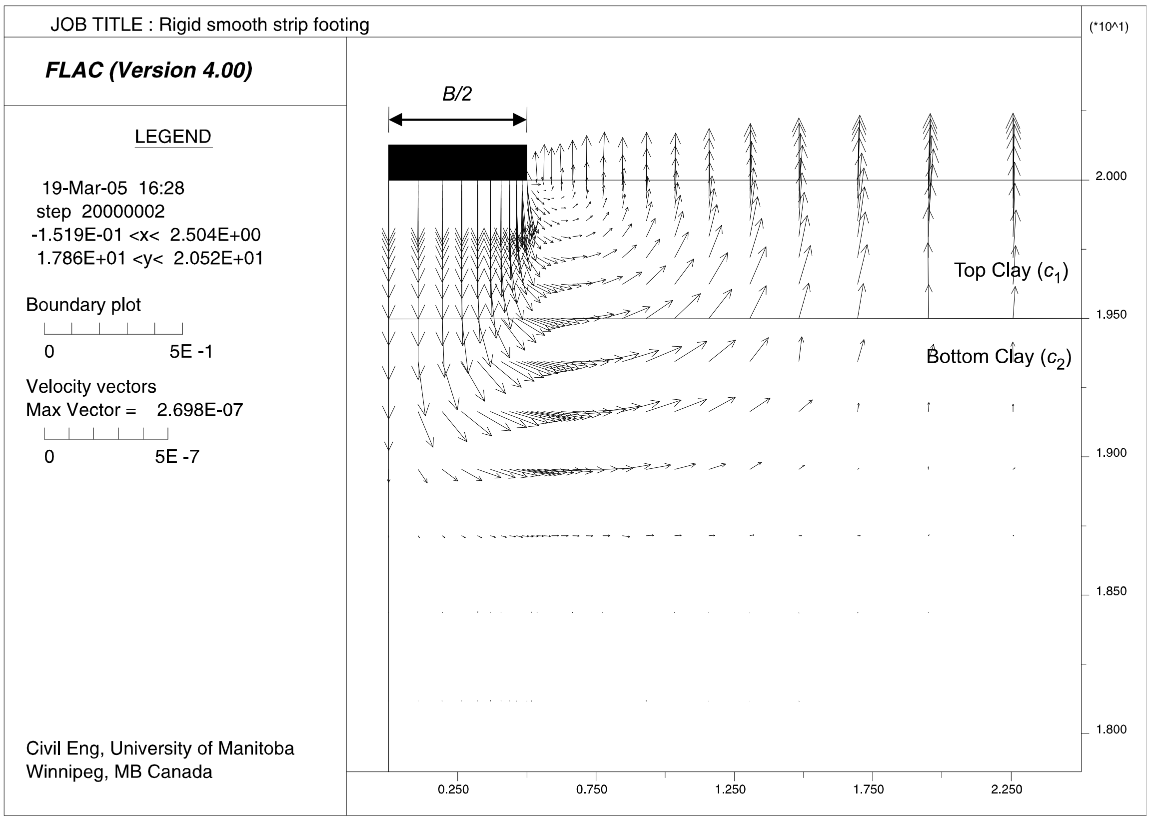

Figure A.99: Velocity vectors for a rigid smooth strip footing on strong clay over soft clay for 40×30 grid model, $H/B = 0.5$, $c_2/c_1 = 0.5$.

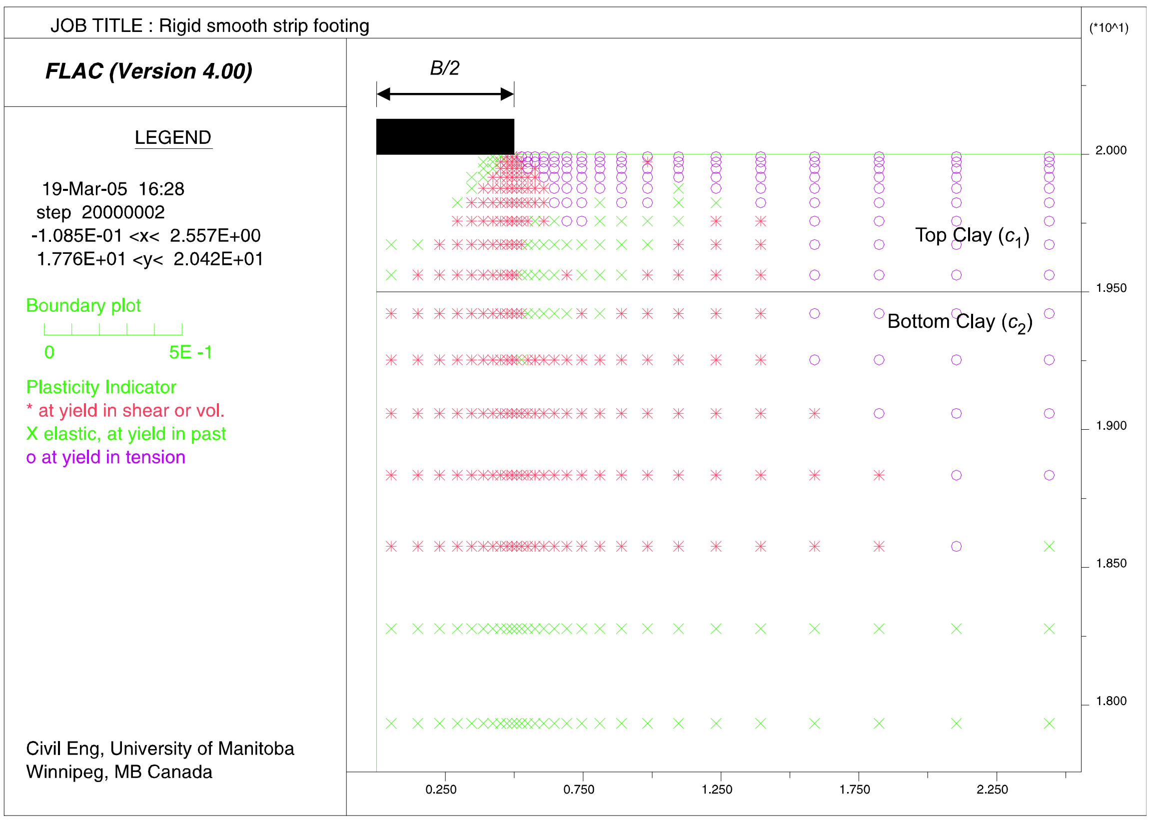

Figure A.100: Plasticity state indicators at steady state condition for a rigid smooth strip footing on strong over soft clay for 40 × 30 grid model, $H/B = 0.5$, $c_2/c_1 = 0.5$.

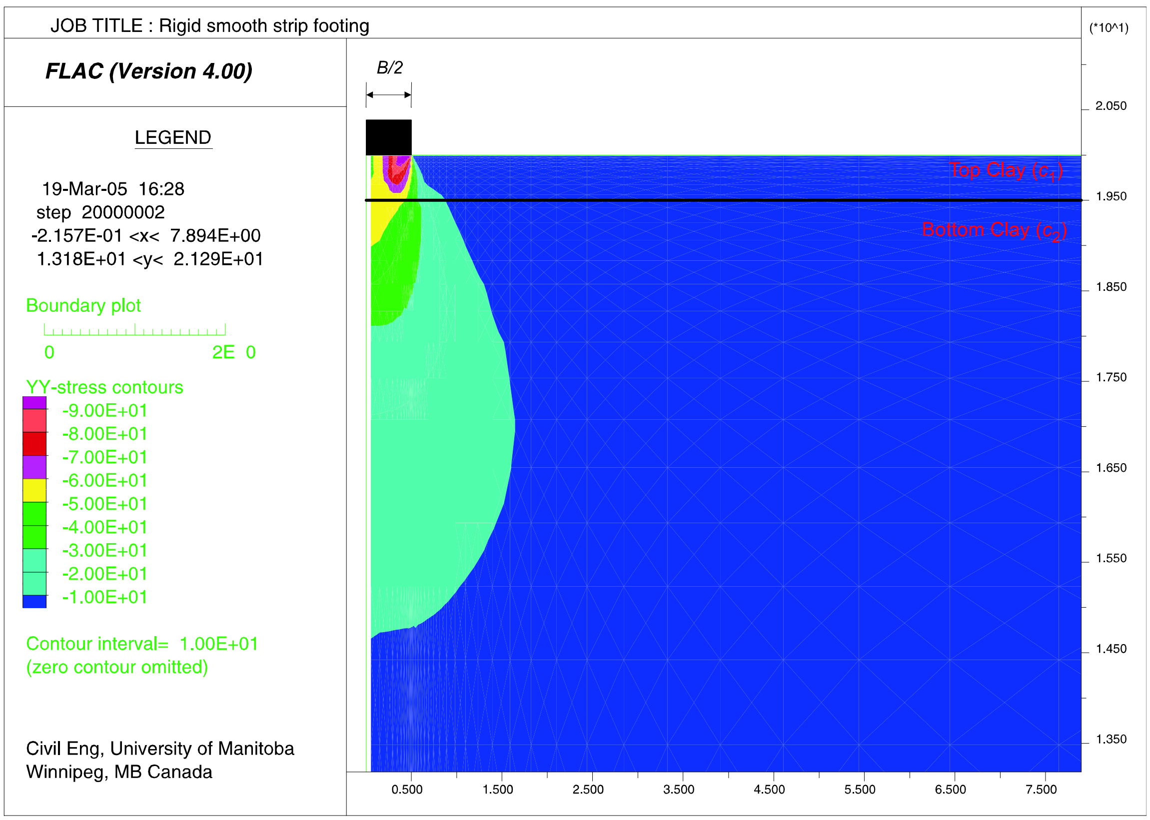

Figure A.101: Vertical stress (σ_{yy}) contours for a rigid smooth strip footing on strong clay over soft clay for 40×30 grid model, $H/B = 0.5$, $c_2/c_1 = 0.5$.

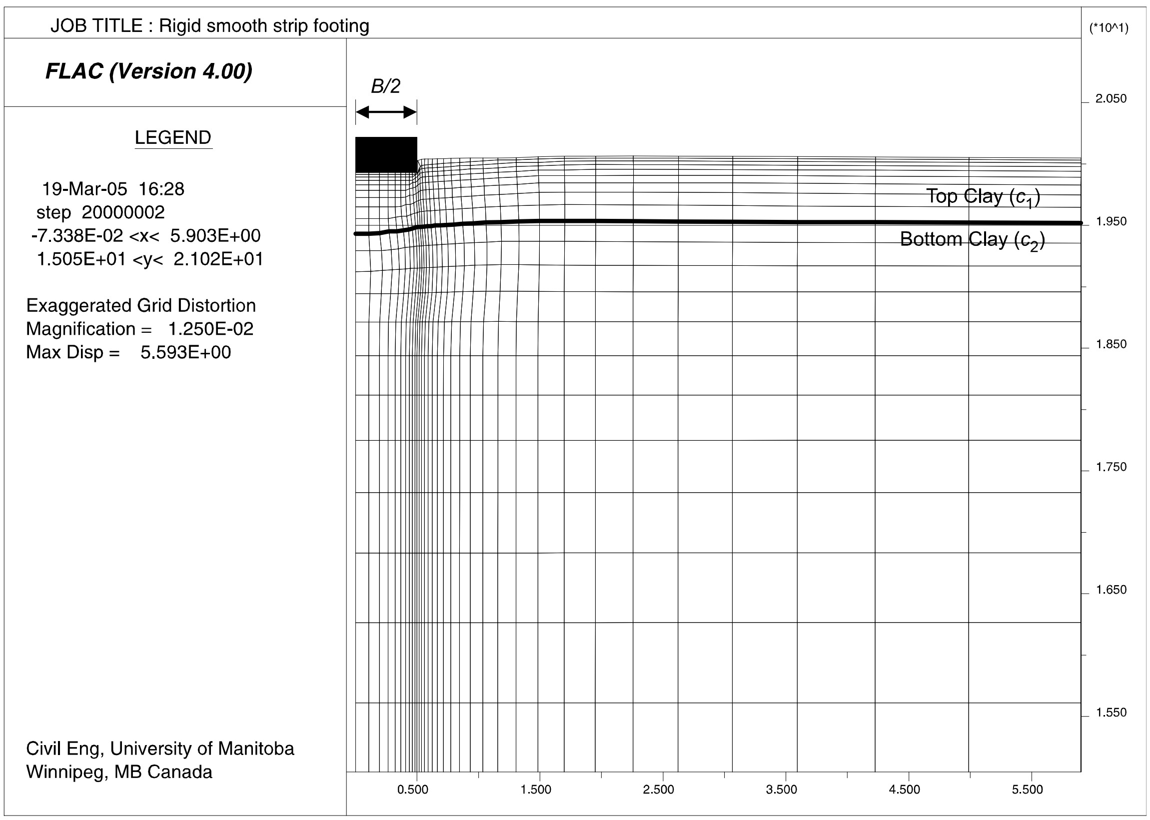

Figure A.102: Magnified grid for a rigid smooth strip footing on strong clay over soft clay for 40 × 30 grid model, $H/B = 0.5$, $c_2/c_1 = 0.5$.

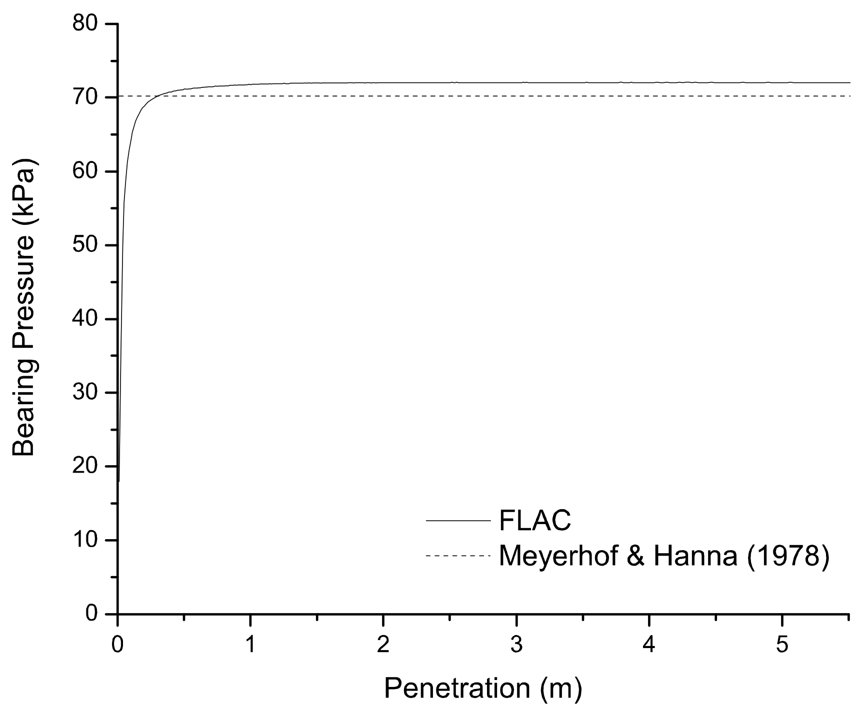

Figure A.103: Bearing pressure versus penetration curve for a rigid smooth strip footing on strong clay over soft clay for 40×30 grid model, $H/B = 0.5$, $c_2/c_1 = 0.5$.

Case 5: $c_2/c_1 = 1/3$ **- Small Deformation Analysis**

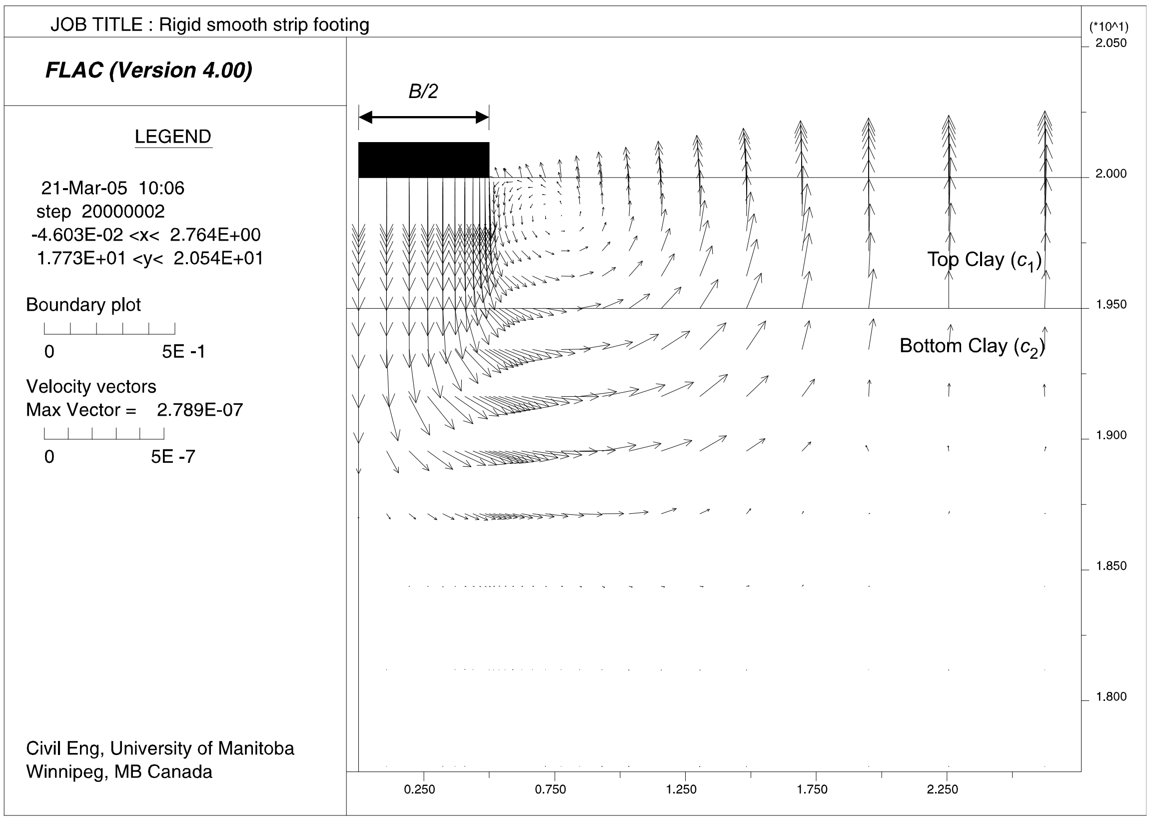

Figure A.104: Velocity vectors for a rigid smooth strip footing on strong clay over soft clay for 40×30 grid model, $H/B = 0.5$, $c_2/c_1 = 1/3$.

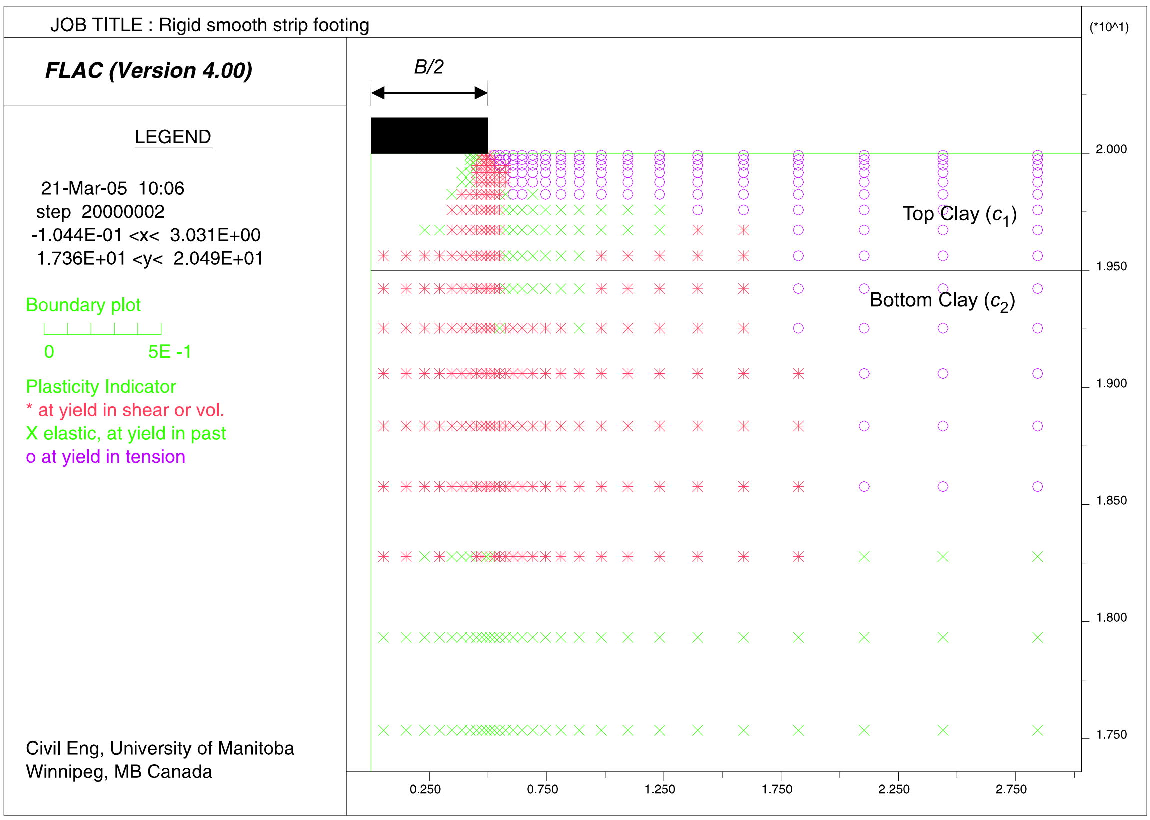

Figure A.105: Plasticity state indicators at steady state condition for a rigid smooth strip footing on strong over soft clay for 40×30 grid model, $H/B = 0.5$, $c_2/c_1 = 1/3$.

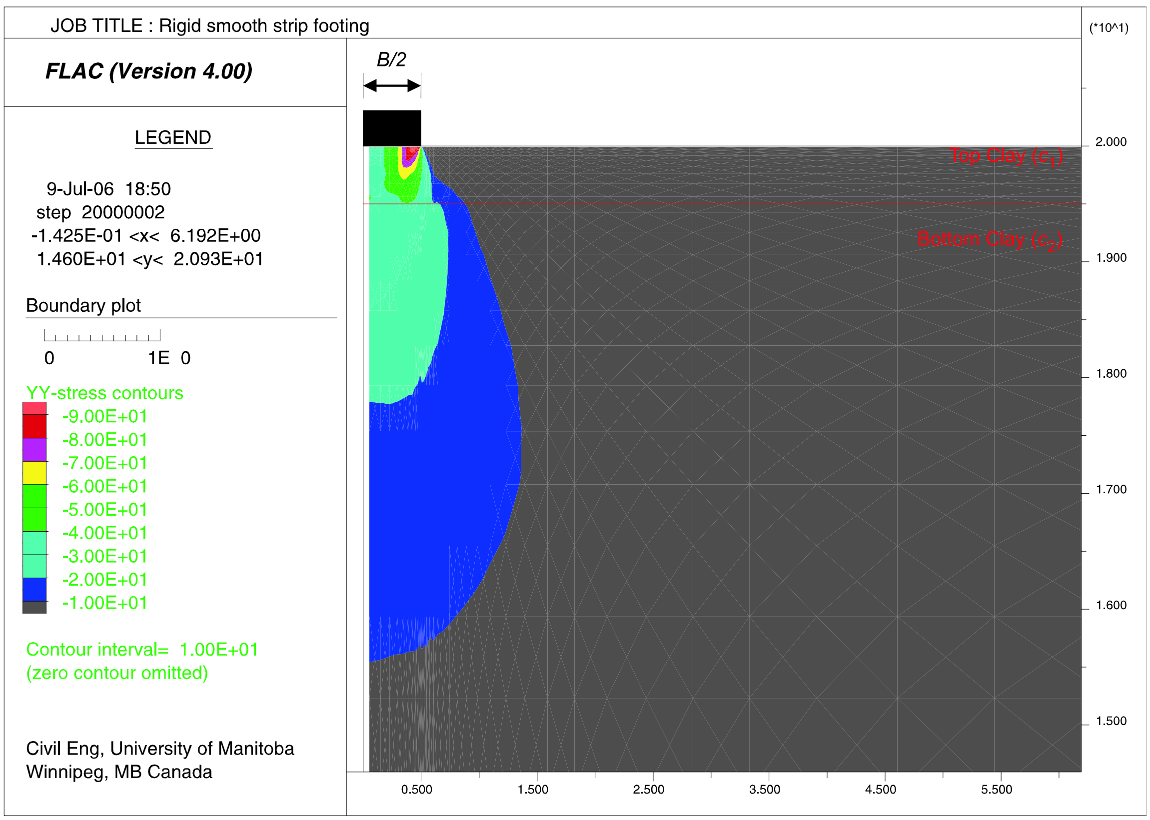

Figure A.106: Vertical stress (σ_{yy}) contours for a rigid smooth strip footing on strong clay over soft clay for 40×30 grid model, $H/B = 0.5$, $c_2/c_1 = 1/3$.

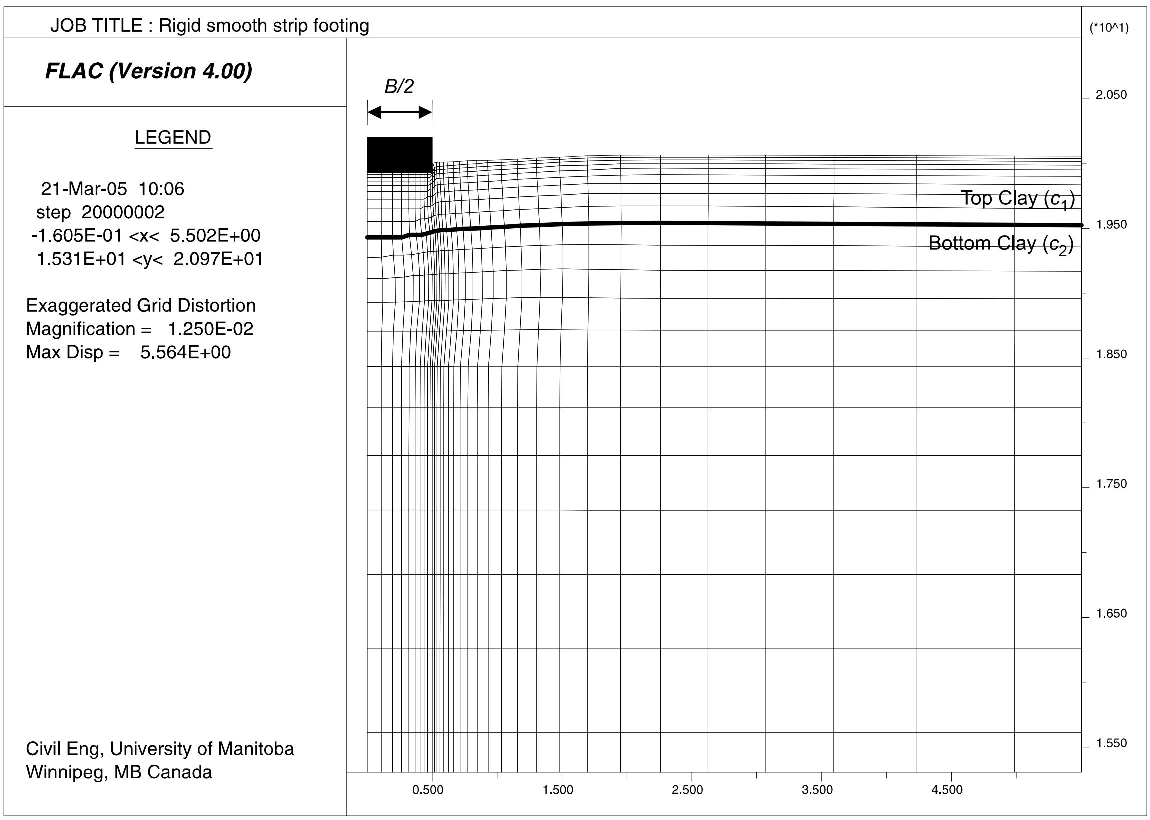

Figure A.107: Magnified grid for a rigid smooth strip footing on strong clay over soft clay for 40×30 grid model, $H/B = 0.5$, $c_2/c_1 = 1/3$.

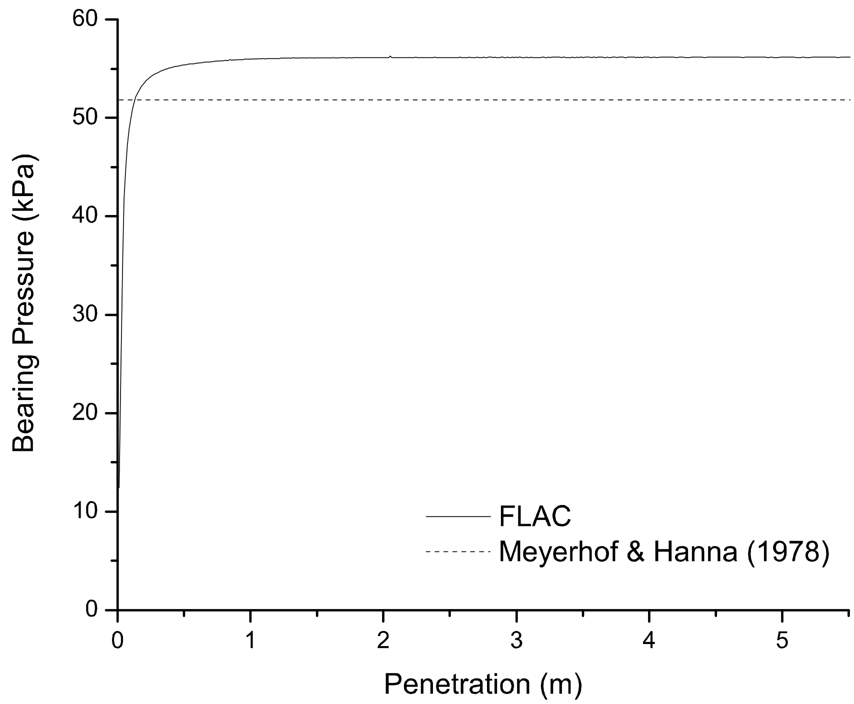

Figure A.108: Bearing pressure versus penetration curve for a rigid smooth strip footing on strong clay over soft clay for 40×30 grid model, $H/B = 0.5$, $c_2/c_1 = 1/3$.

Case 6: $c_2/c_1 = 0.2$ **- Small Deformation Analysis**

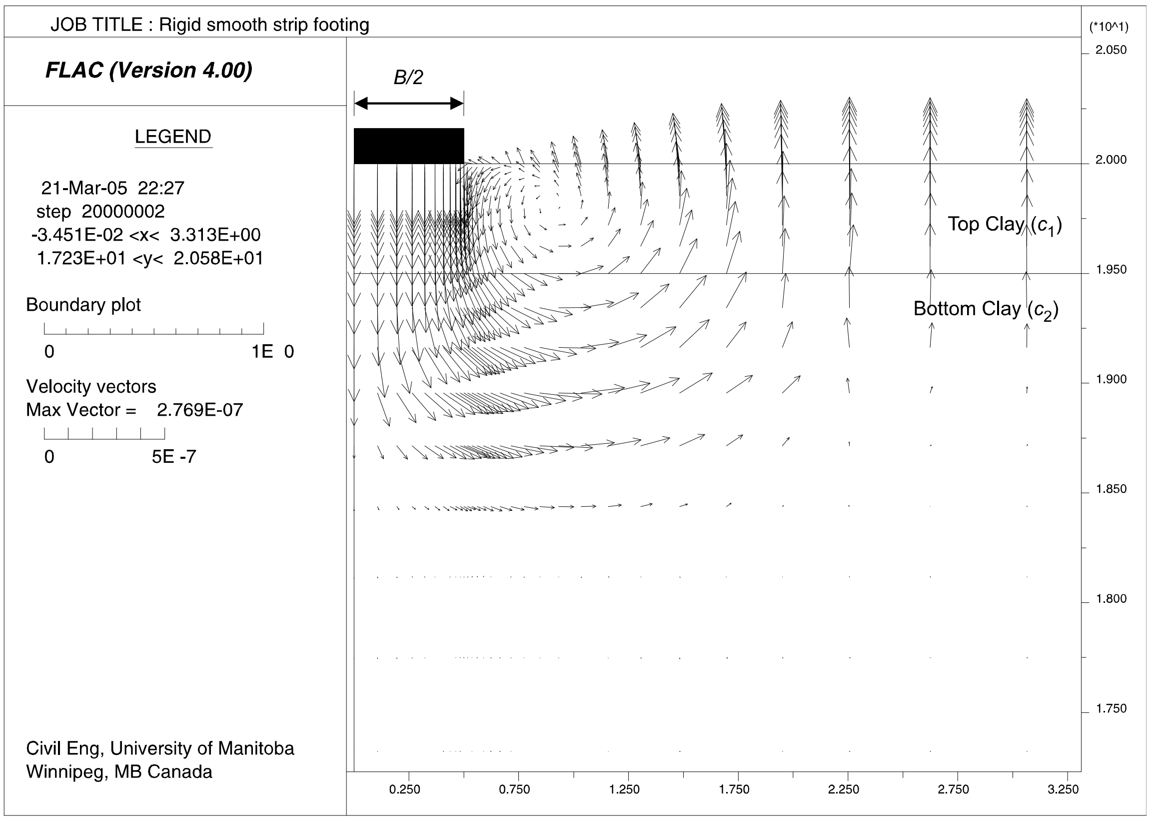

Figure A.109: Velocity vectors for a rigid smooth strip footing on strong clay over soft clay for 40×30 grid model, $H/B = 0.5$, $c_2/c_1 = 0.2$.

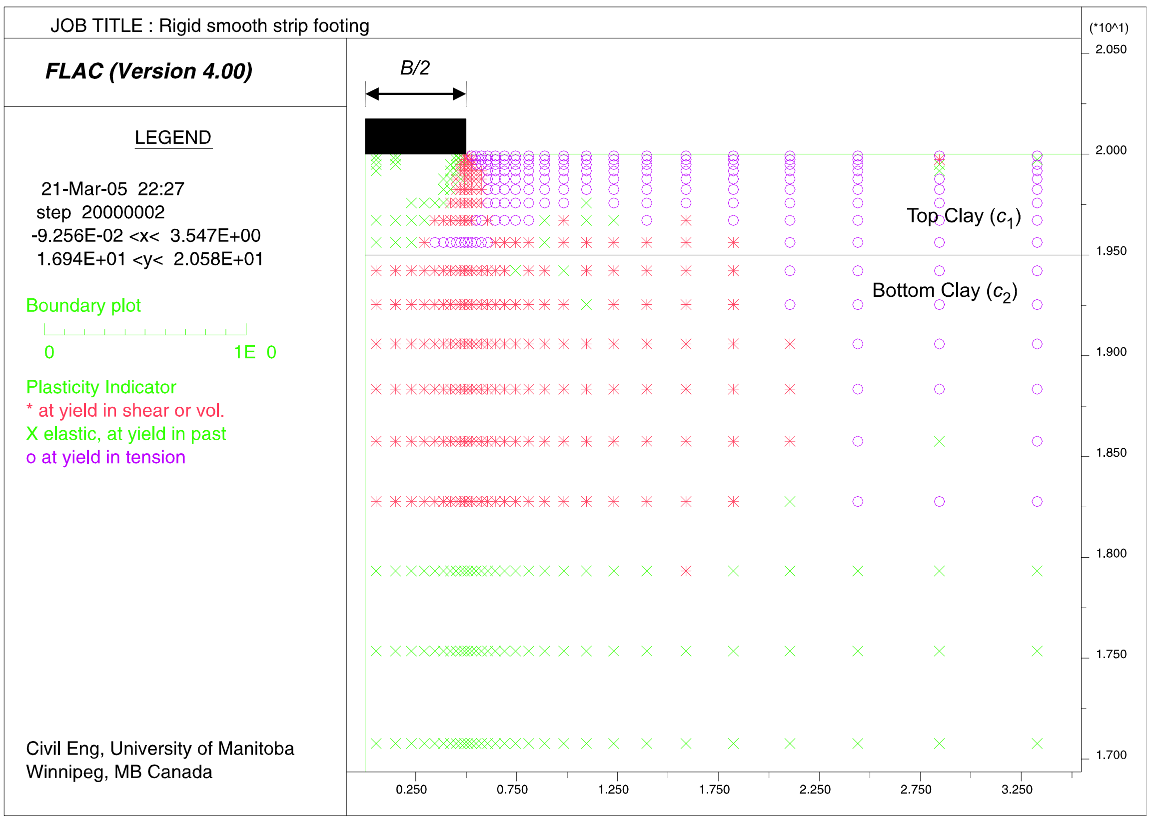

Figure A.110: Plasticity state indicators at steady state condition for a rigid smooth strip footing on strong over soft clay for 40×30 grid model, $H/B = 0.5$, $c_2/c_1 = 0.2$.

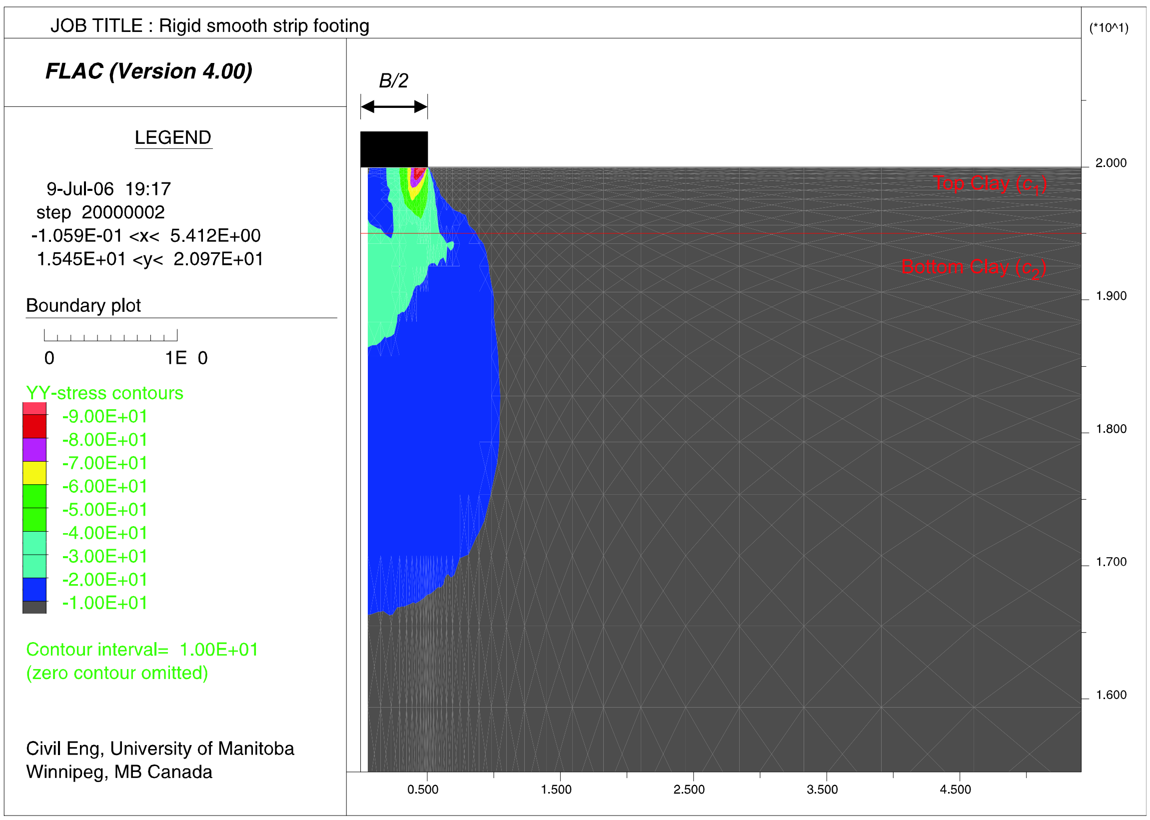

Figure A.111: Vertical stress (σ_{yy}) contours for a rigid smooth strip footing on strong clay over soft clay for 40×30 grid model, $H/B = 0.5$, $c_2/c_1 = 0.2$.

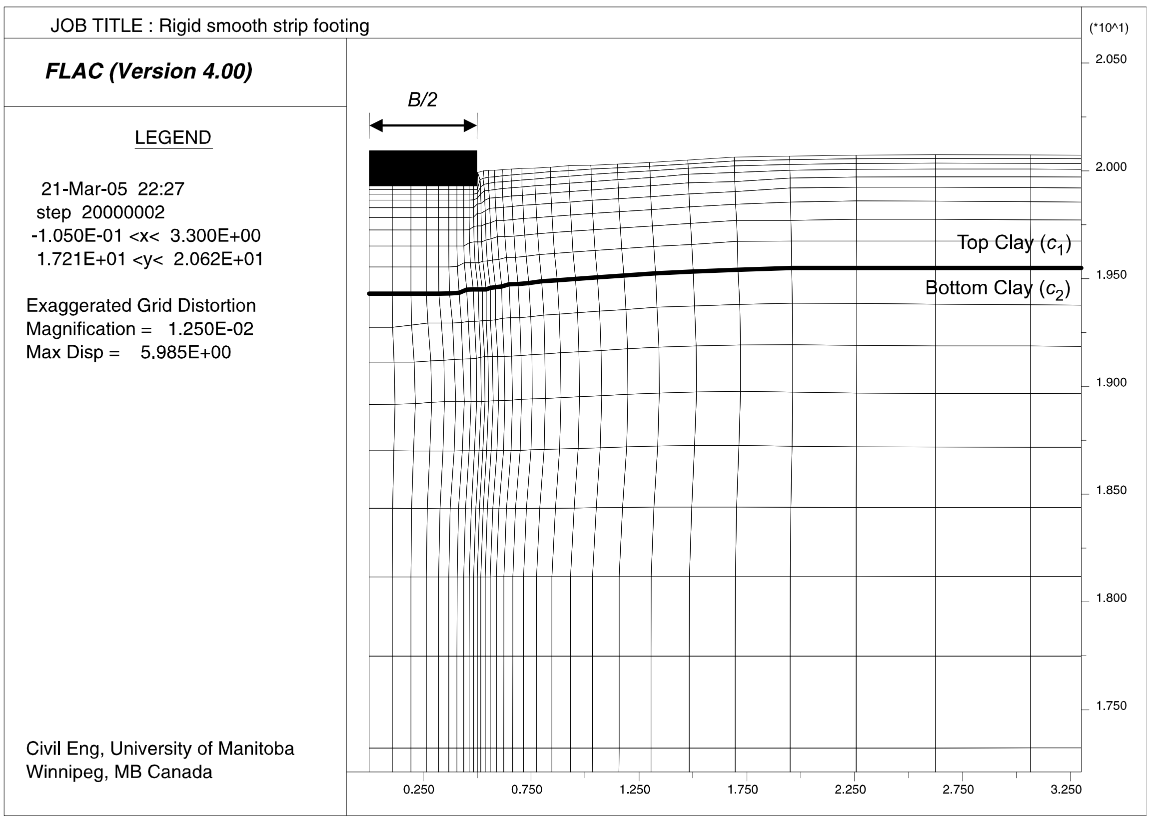

Figure A.112: Magnified grid for a rigid smooth strip footing on strong clay over soft clay for 40×30 grid model, $H/B = 0.5$, $c_2/c_1 = 0.2$.

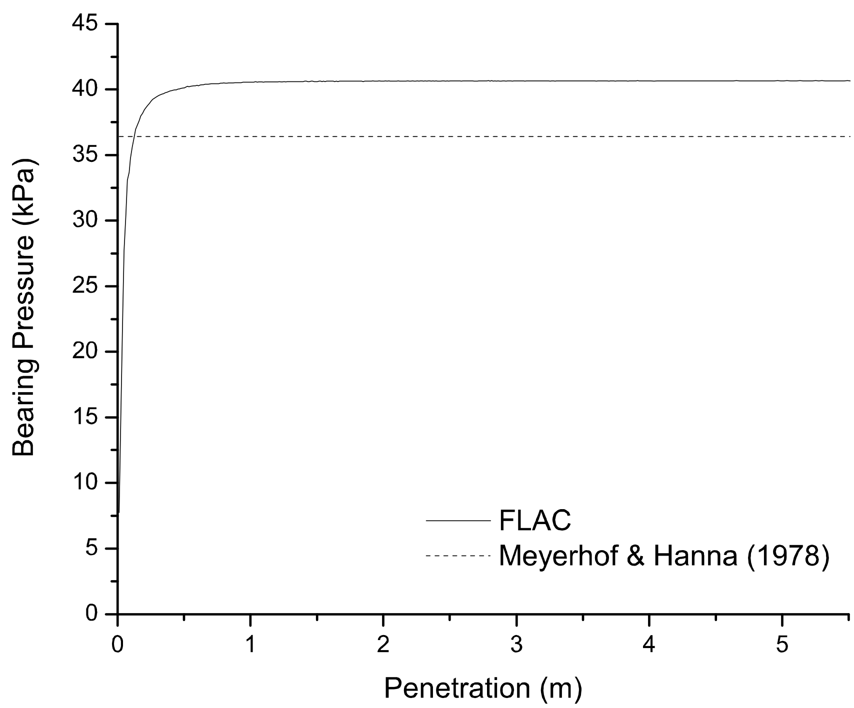

Figure A.113: Bearing pressure versus penetration curve for a rigid smooth strip footing on strong clay over soft clay for 40 × 30 grid model, $H/B = 0.5$, $c_2/c_1 = 0.2$.

Case 7: $c_2/c_1 = 0.1$ **- Small Deformation Analysis**

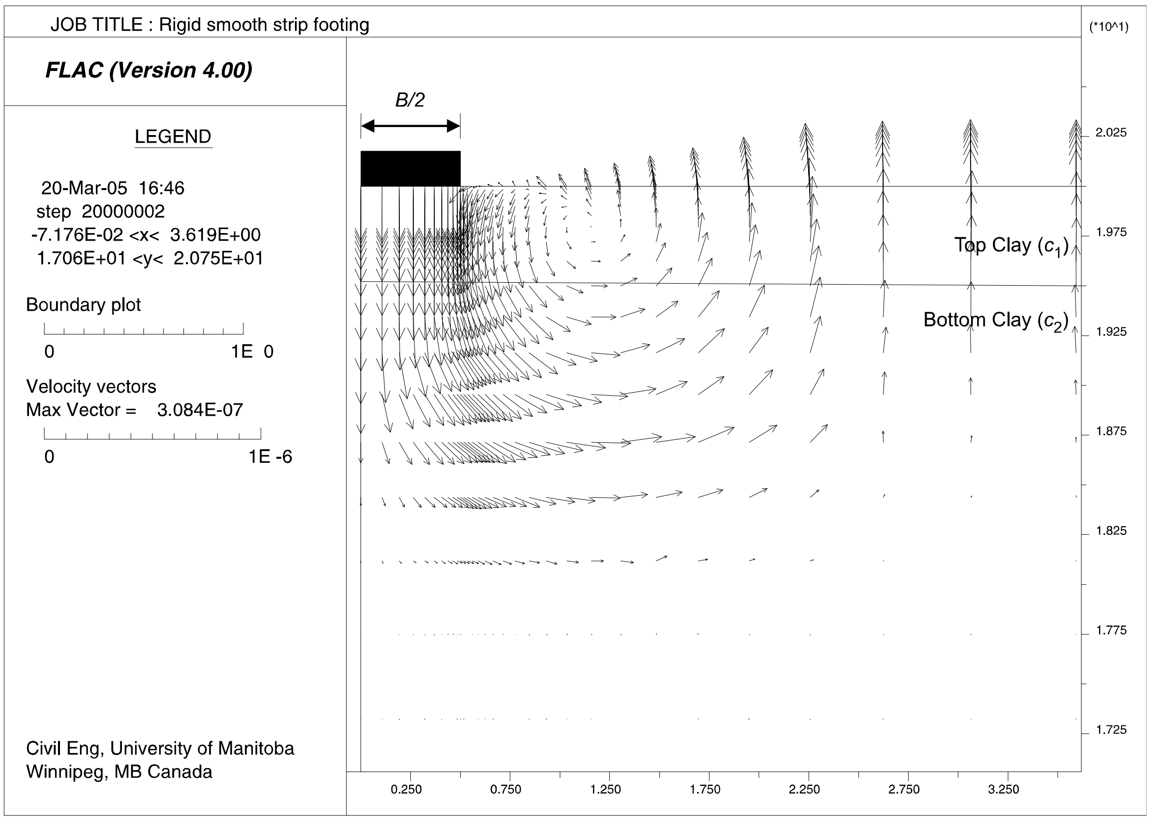

Figure A.114: Velocity vectors for a rigid smooth strip footing on strong clay over soft clay for 40 × 30 grid model, $H/B = 0.5$, $c_2/c_1 = 0.1$.

Figure A.115: Plasticity state indicators at steady state condition for a rigid smooth strip footing on strong over soft clay for 40 × 30 grid model, $H/B = 0.5$, $c_2/c_1 = 0.1$.

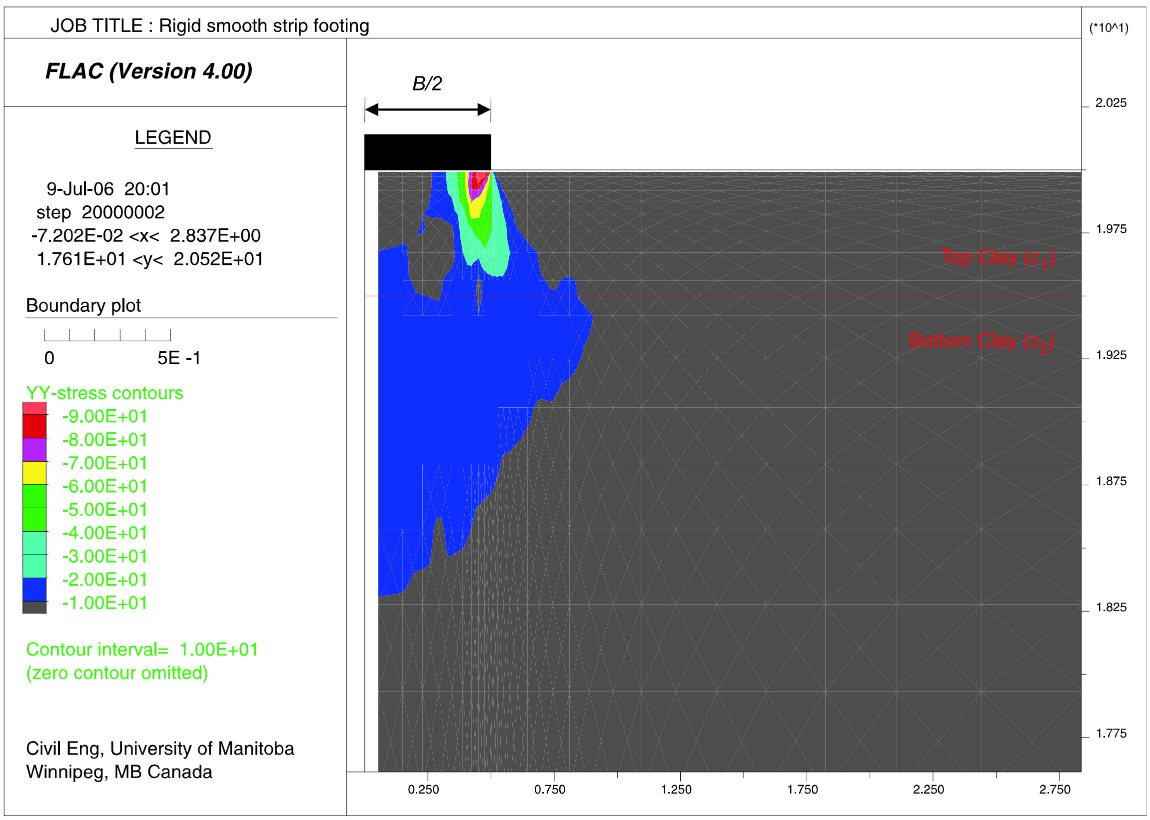

Figure A.116: Vertical stress (σ_{yy}) contours for a rigid smooth strip footing on strong clay over soft clay for 40 × 30 grid model, $H/B = 0.5$, $c_2/c_1 = 0.1$.

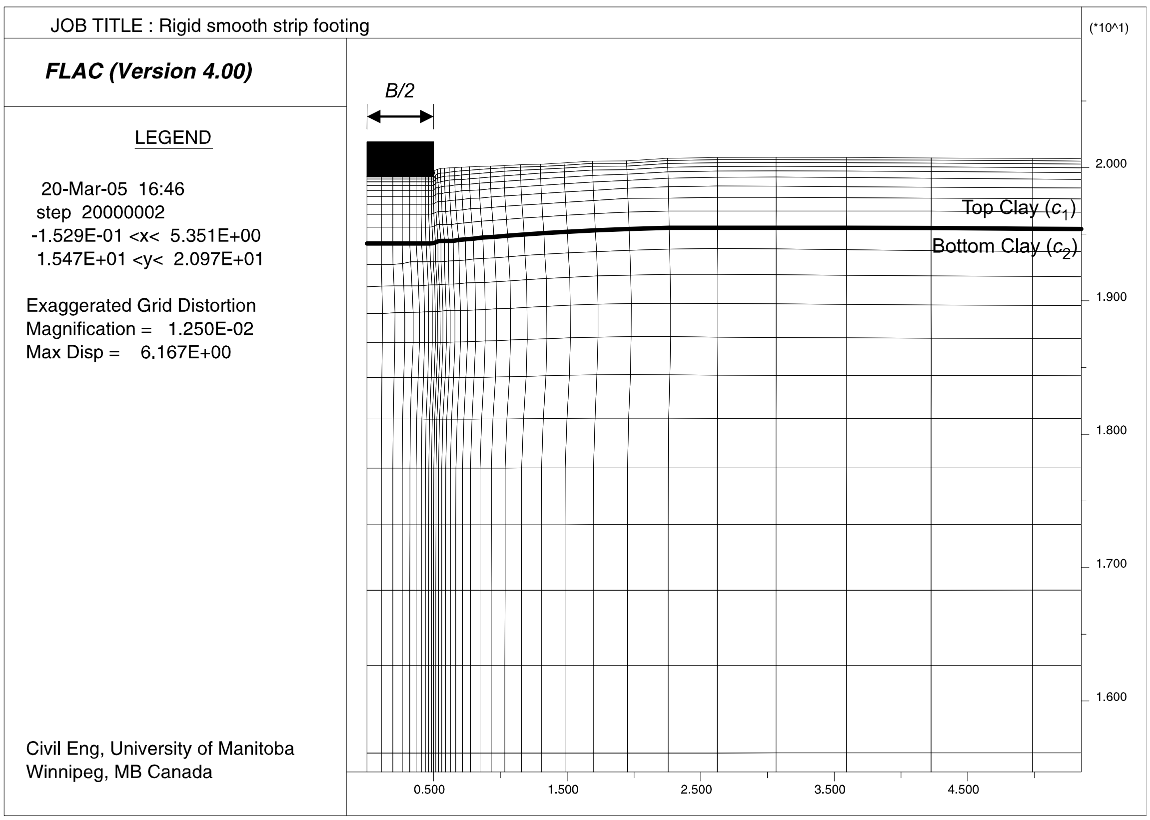

Figure A.117: Magnified grid for a rigid smooth strip footing on strong clay over soft clay for 40×30 grid model, $H/B = 0.5$, $c_2/c_1 = 0.1$.

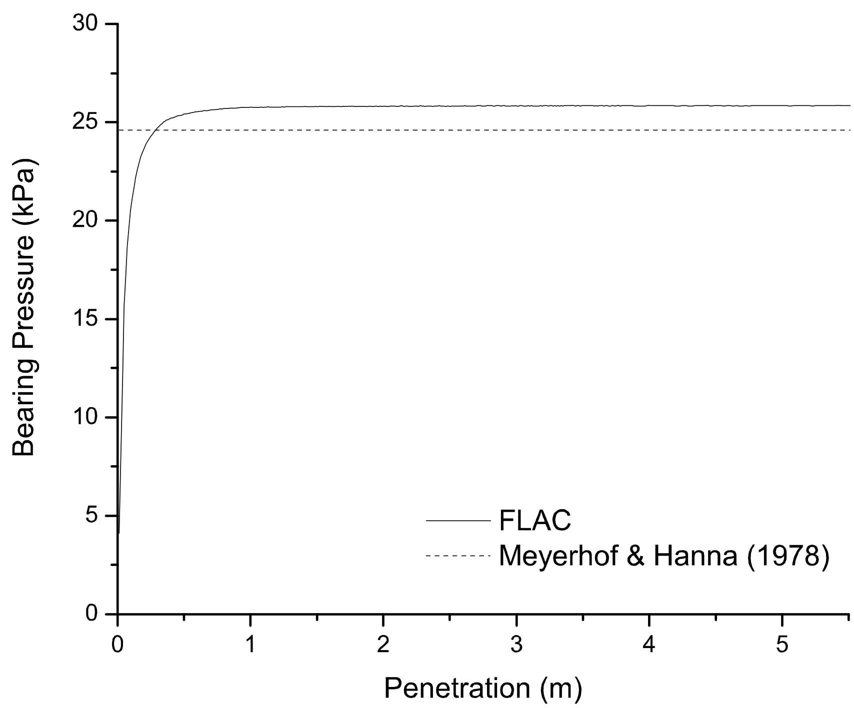

Figure A.118: Bearing pressure versus penetration curve for a rigid smooth strip footing on strong clay over soft clay for 40×30 grid model, $H/B = 0.5$, $c_2/c_1 = 0.1$.

A.1.7 Rigid Smooth Strip Footing on Strong over Soft Clay ($H/B = 0.25$)

Case 1: $c_2/c_1 = 1$ (Homogeneous clay) - Small Deformation Analysis

Since this is the case of homogeneous clay all the results will be same as Case 1 4.1.1. The FLAC analysis results for other cases of c_2/c_1 are explained below.

Case 2: $c_2/c_1 = 0.8$ - Small Deformation Analysis

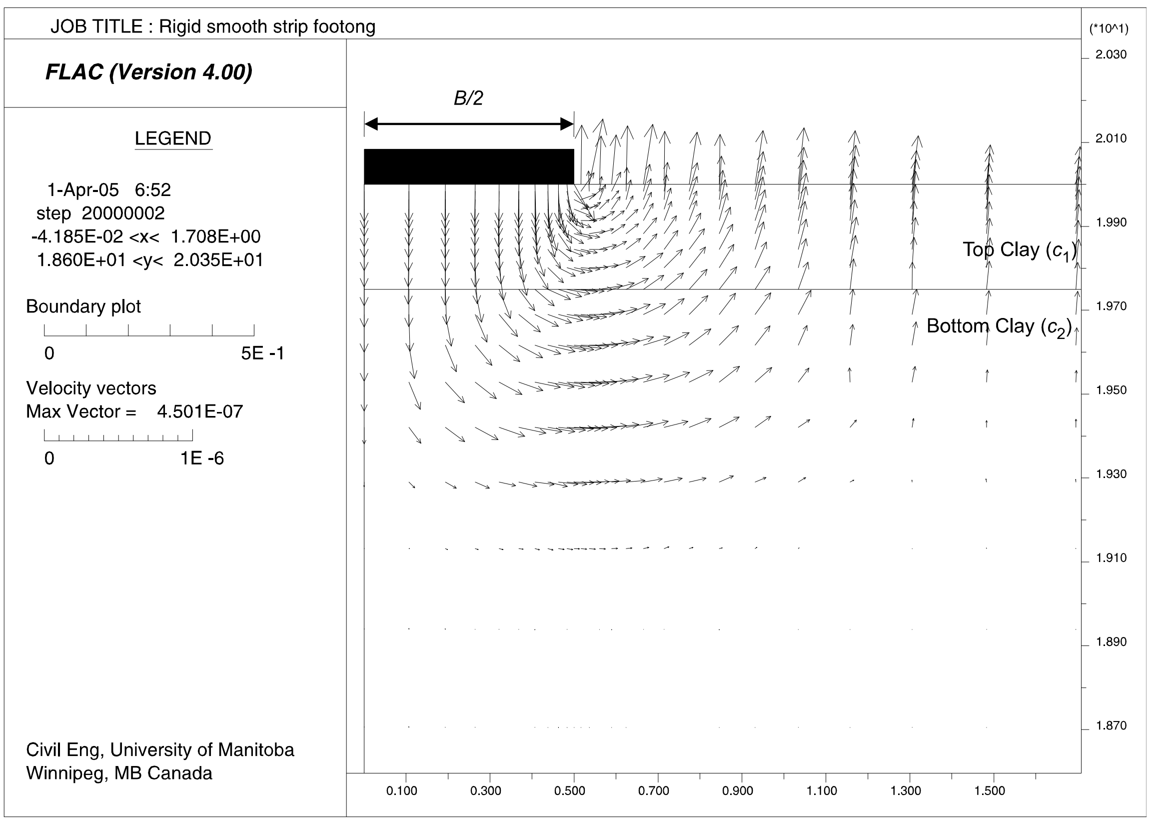

Figure A.119: Velocity vectors for a rigid strip footing on strong over soft clay for 40×30 grid model, $H/B = 0.25$, $c_2/c_1 = 0.8$.

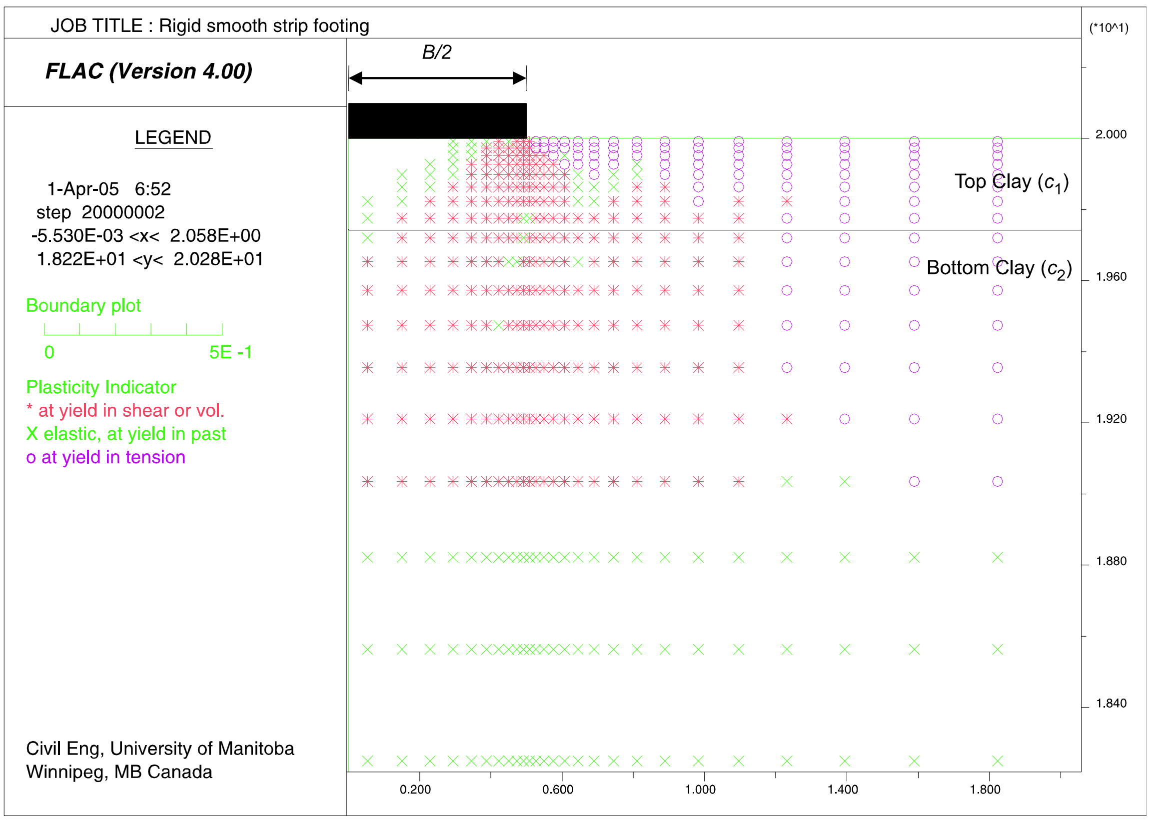

Figure A.120: Plasticity state indicators at steady state condition for a rigid smooth strip footing on strong over soft clay for 40×30 grid model, $H/B = 0.25$, $c_2/c_1 = 0.8$.

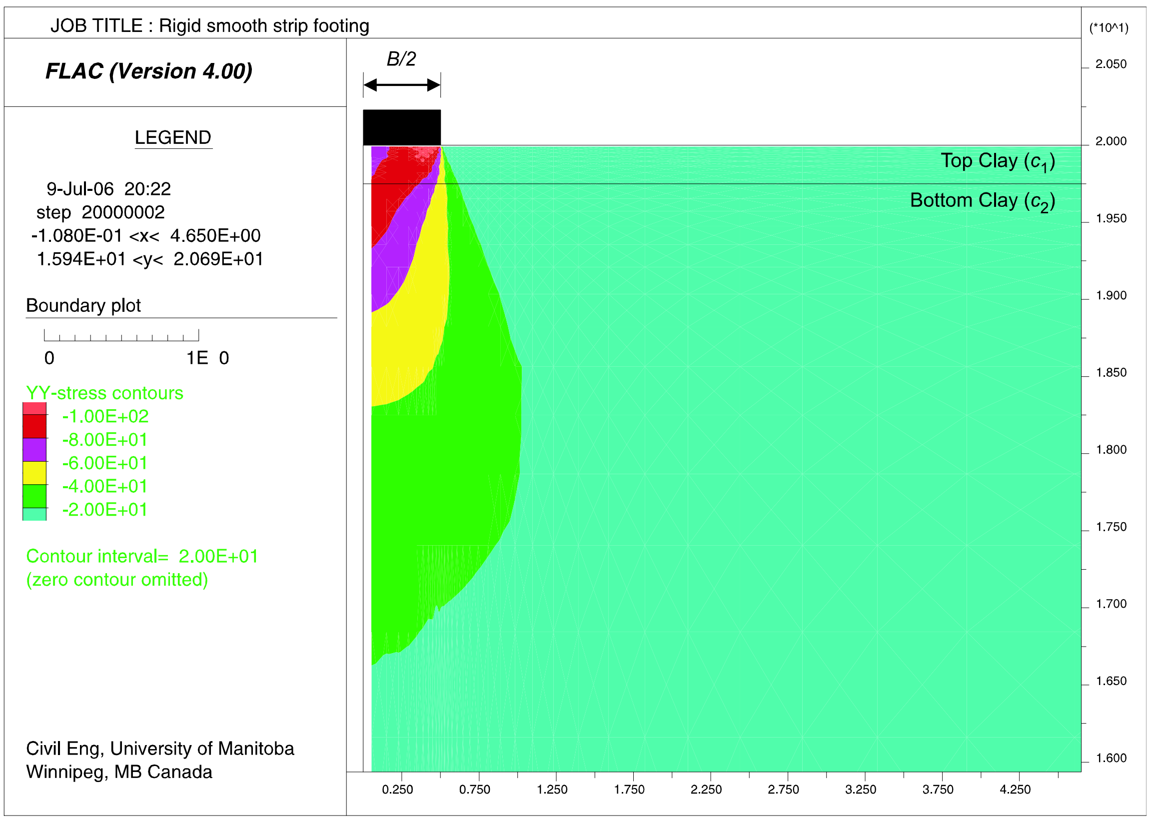

Figure A.121: Vertical stress (σ_{yy}) contours for a rigid smooth strip footing on strong over soft clay for 40×30 grid model, $H/B = 0.25$, $c_2/c_1 = 0.8$.

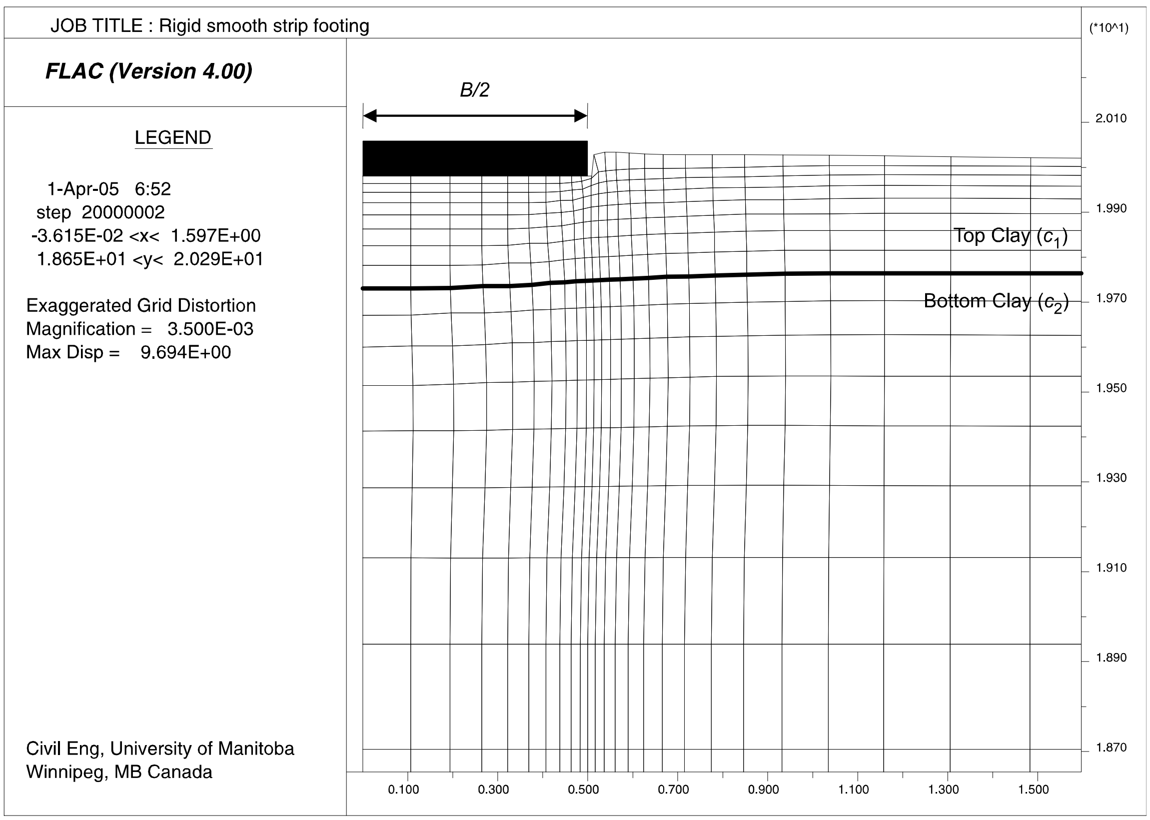

Figure A.122: Magnified grid for a rigid smooth strip footing on strong over soft clay for 40×30 grid model, $H/B = 0.25$, $c_2/c_1 = 0.8$.

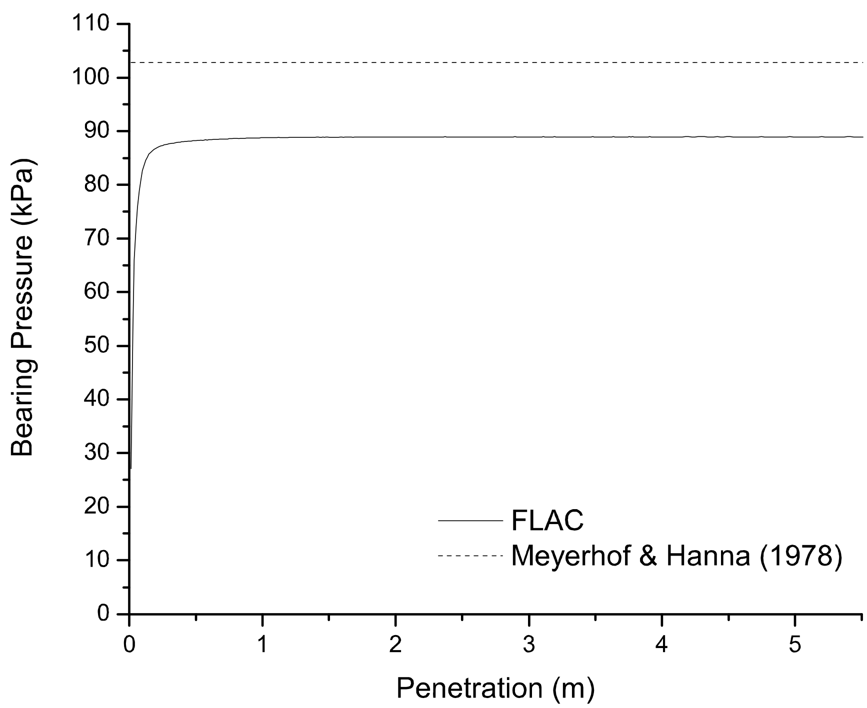

Figure A.123: Bearing pressure versus penetration curve for a rigid smooth strip footing on strong over soft clay for 40 × 30 grid model, $H/B = 0.25$, $c_2/c_1 = 0.8$.

Case 3: $c_2/c_1 = 2/3$ - Small Deformation Analysis

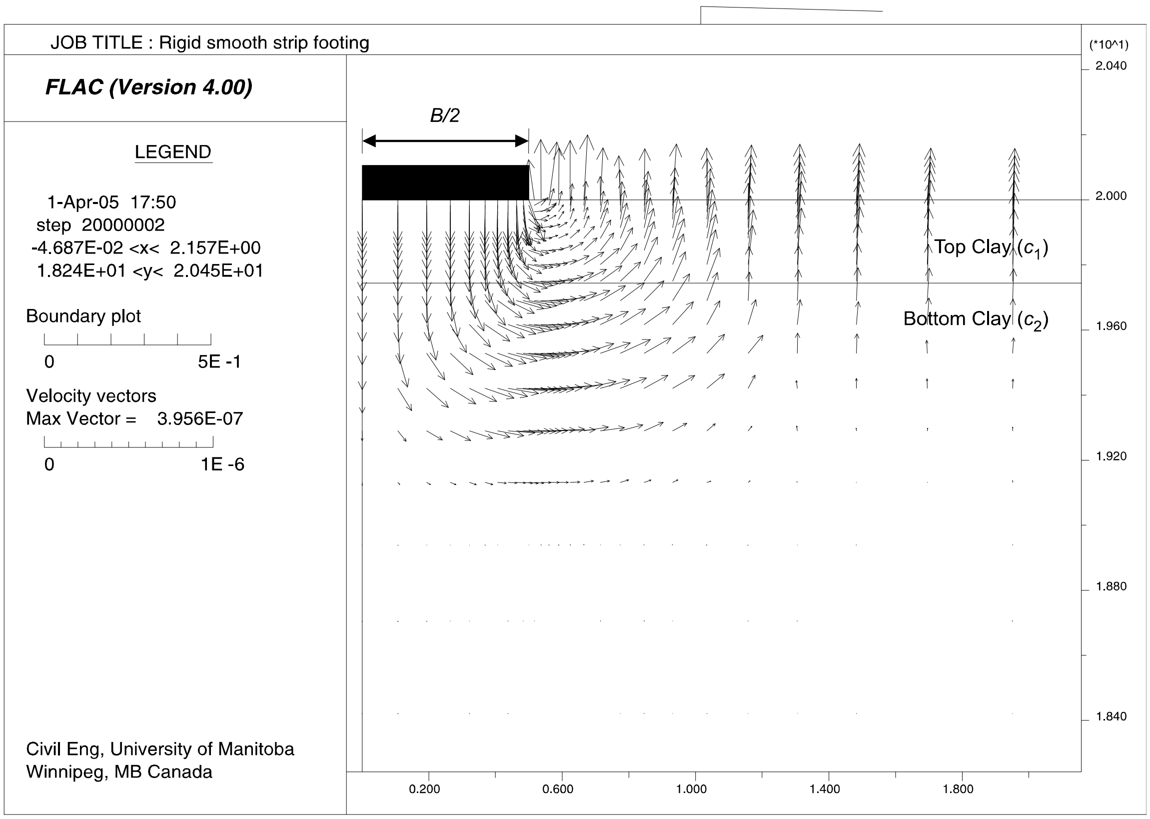

Figure A.124: Velocity vectors for a rigid smooth strip footing on strong over soft clay for 40×30 grid model, $H/B = 0.25$, $c_2/c_1 = 2/3$.

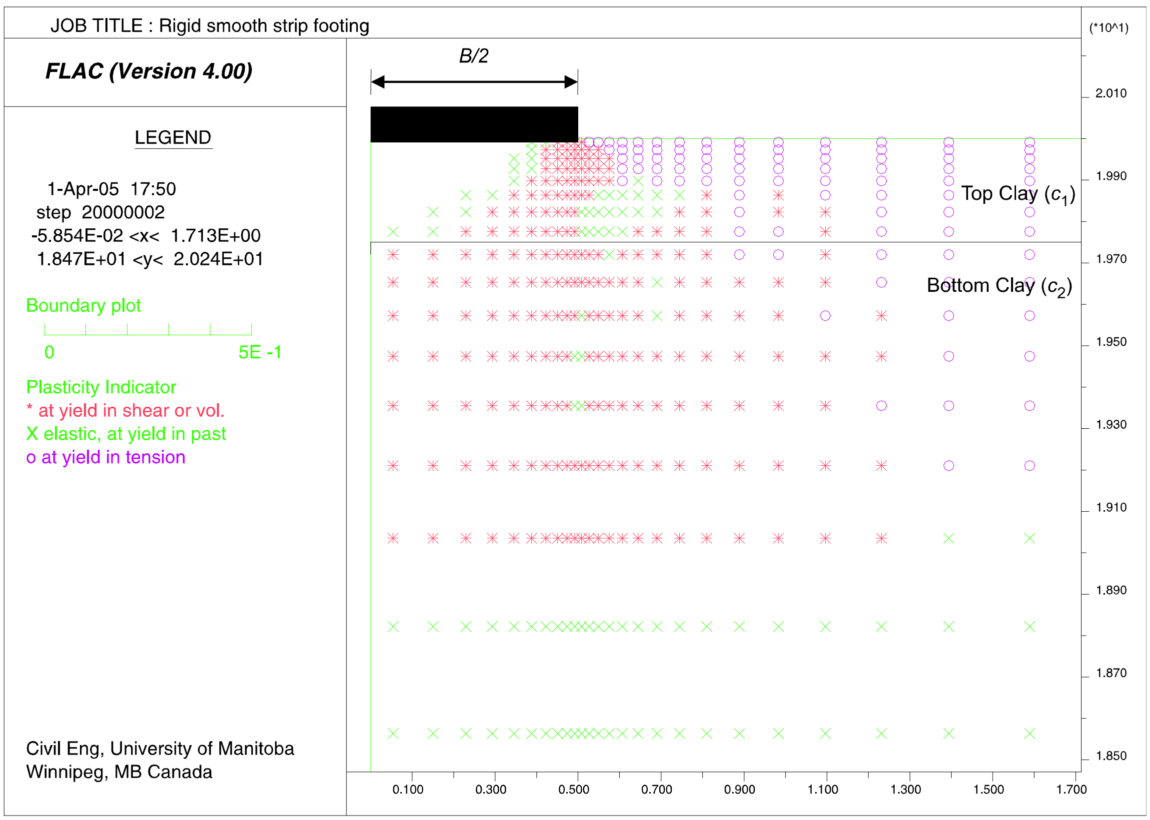

Figure A.125: Plasticity state indicators at steady state condition for a rigid smooth strip footing on strong over soft clay for 40×30 grid model, $H/B = 0.25$, $c_2/c_1 = 2/3$.

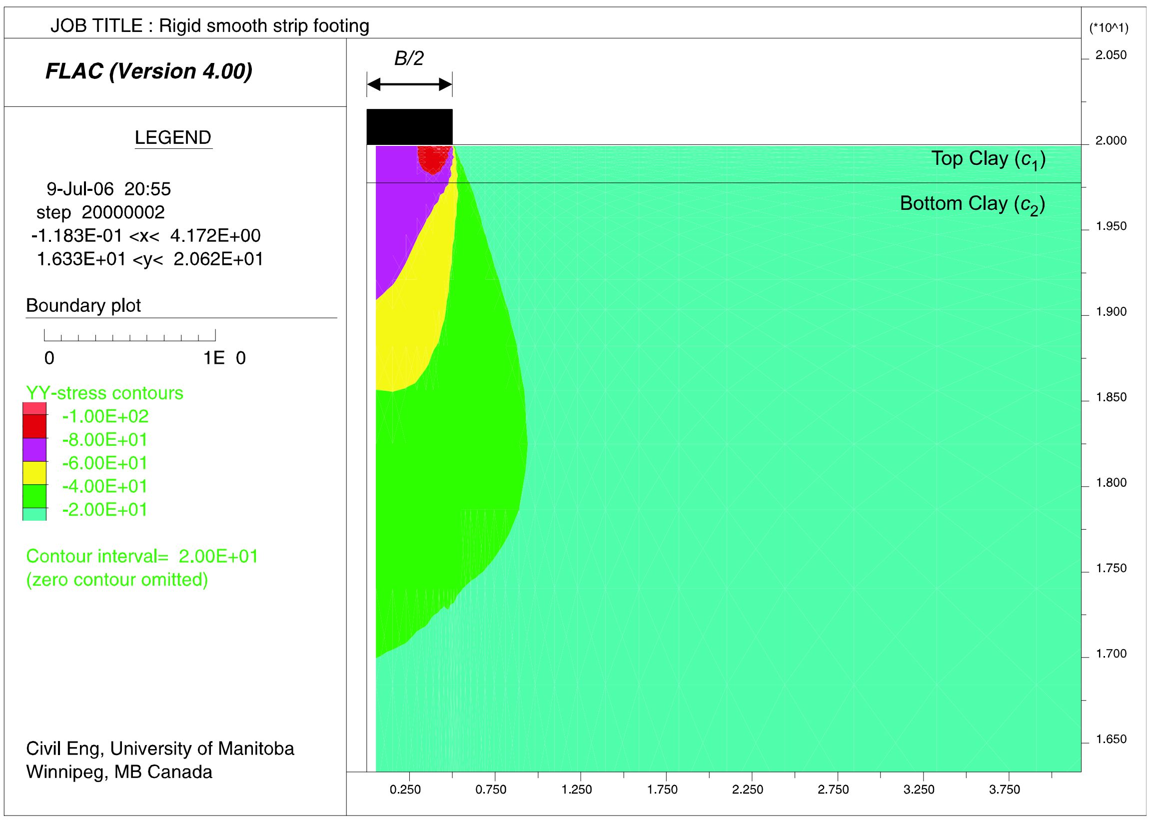

Figure A.126: Vertical stress (σ_{yy}) contours for a rigid smooth strip footing on strong over soft clay for 40×30 grid model, $H/B = 0.25$, $c_2/c_1 = 2/3$.

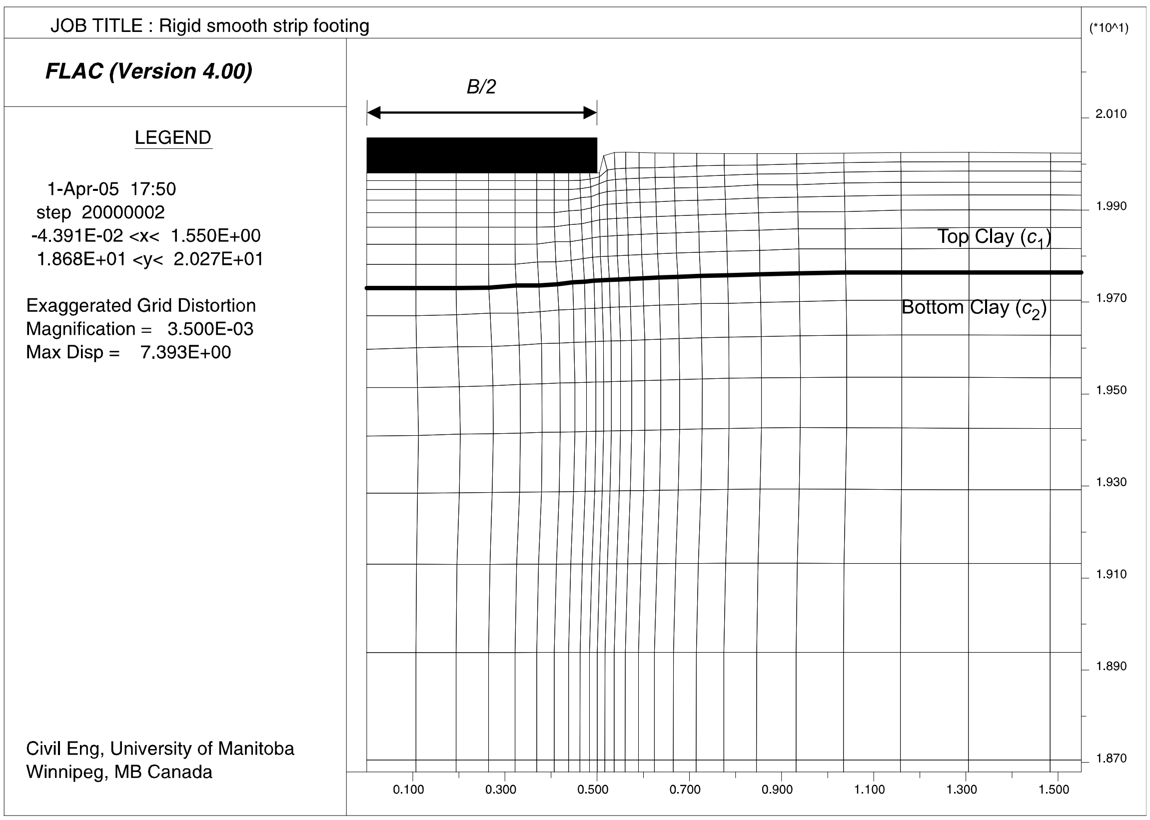

Figure A.127: Magnified grid for a rigid smooth strip footing on strong over soft clay for 40×30 grid model, $H/B = 0.25$, $c_2/c_1 = 2/3$.

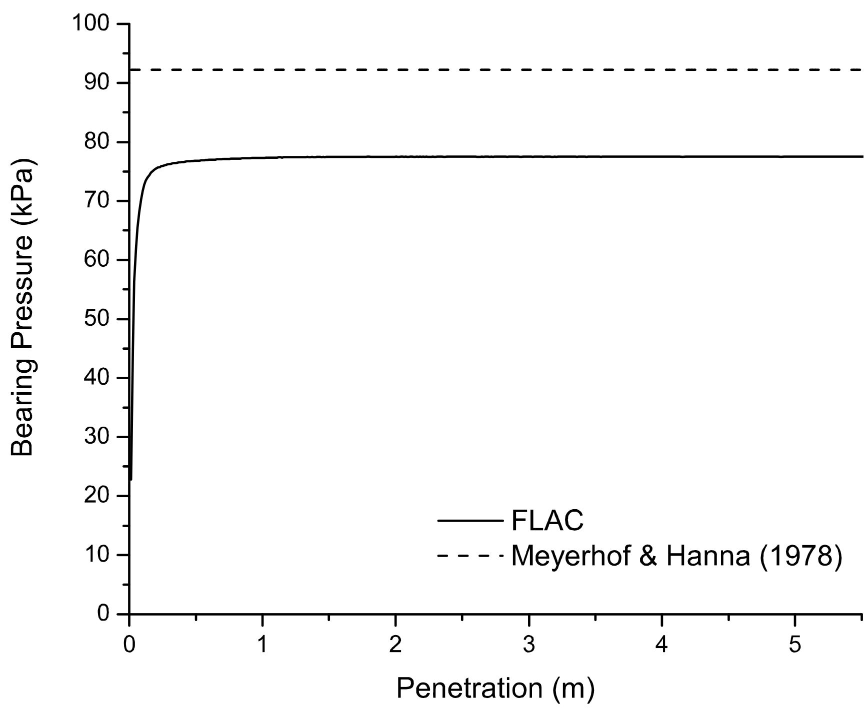

Figure A.128: Bearing pressure versus penetration curve for a rigid smooth strip footing on strong over soft clay for 40×30 grid model, $H/B = 0.25$, $c_2/c_1 = 2/3$.

Case 4: $c_2/c_1 = 0.5$ - Small Deformation Analysis

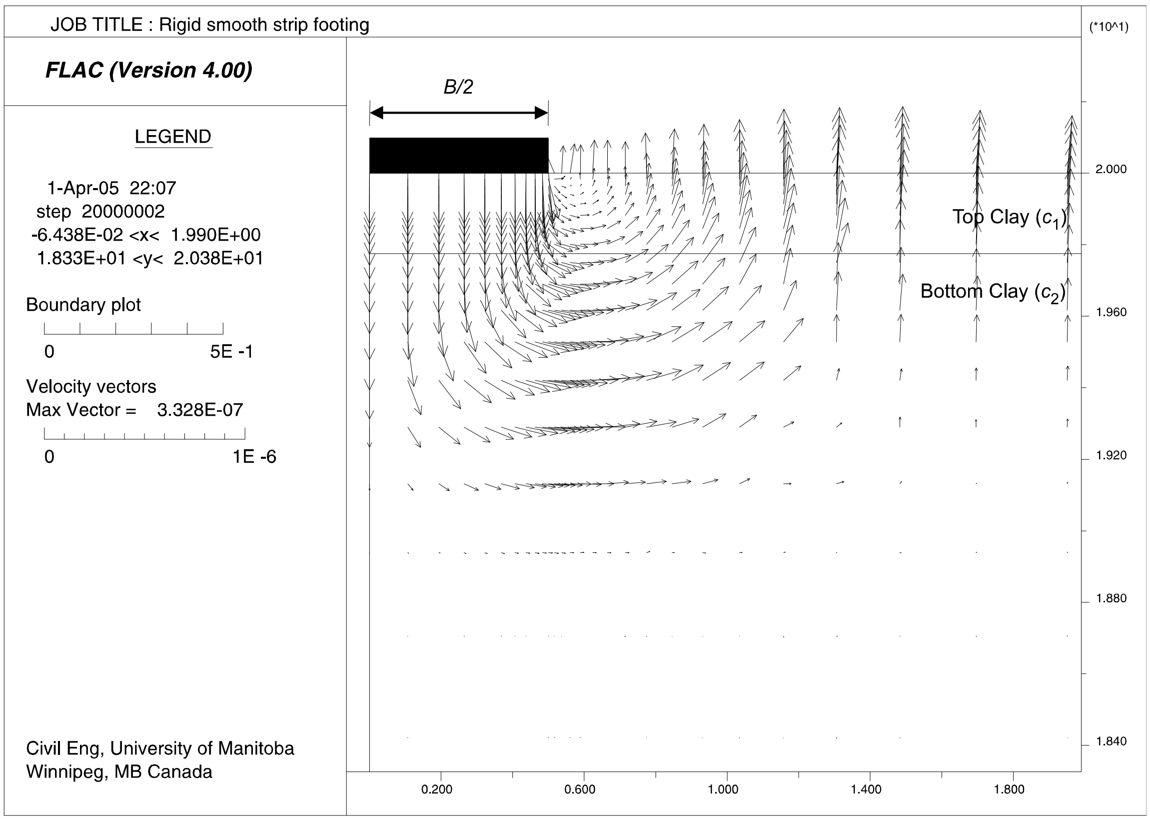

Figure A.129: Velocity vectors for a rigid smooth strip footing on strong clay over soft clay for 40×30 grid model, $H/B = 0.25$, $c_2/c_1 = 0.5$.

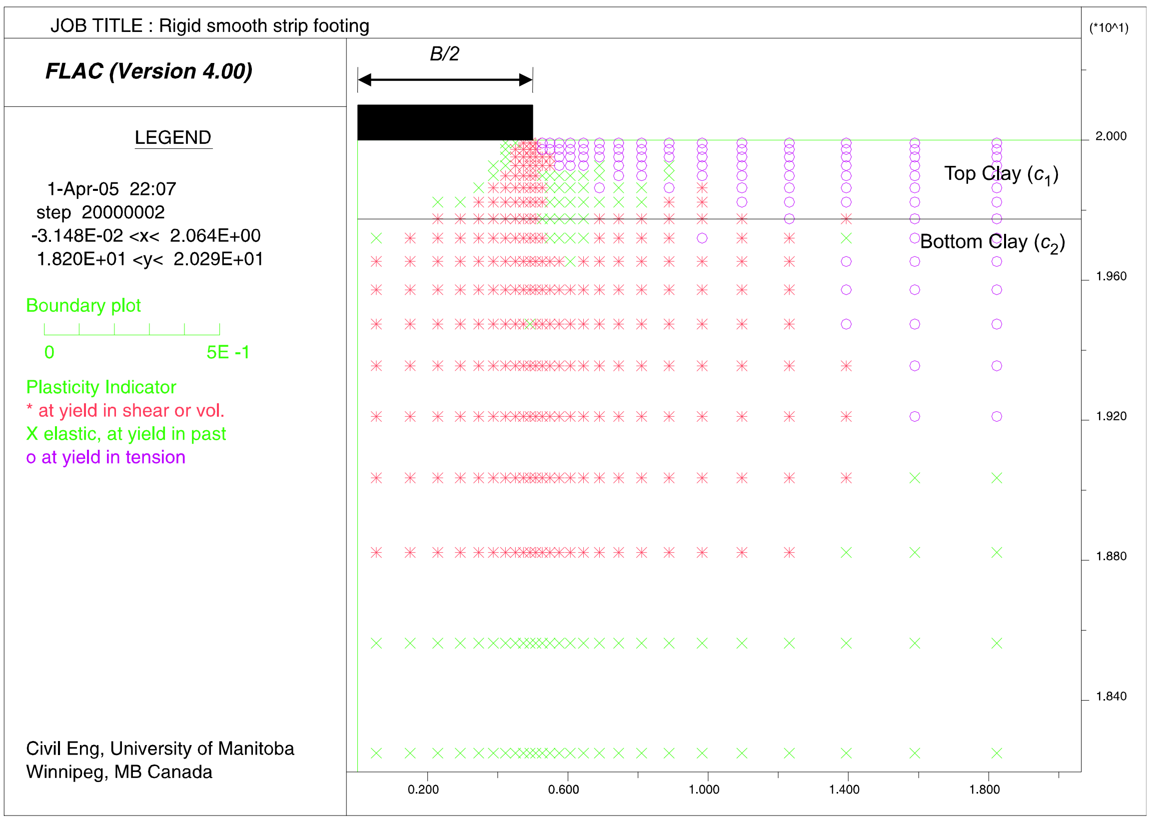

Figure A.130: Plasticity state indicators at steady state condition for a rigid smooth strip footing on strong over soft clay for 40×30 grid model, $H/B = 0.25$, $c_2/c_1 = 0.5$.

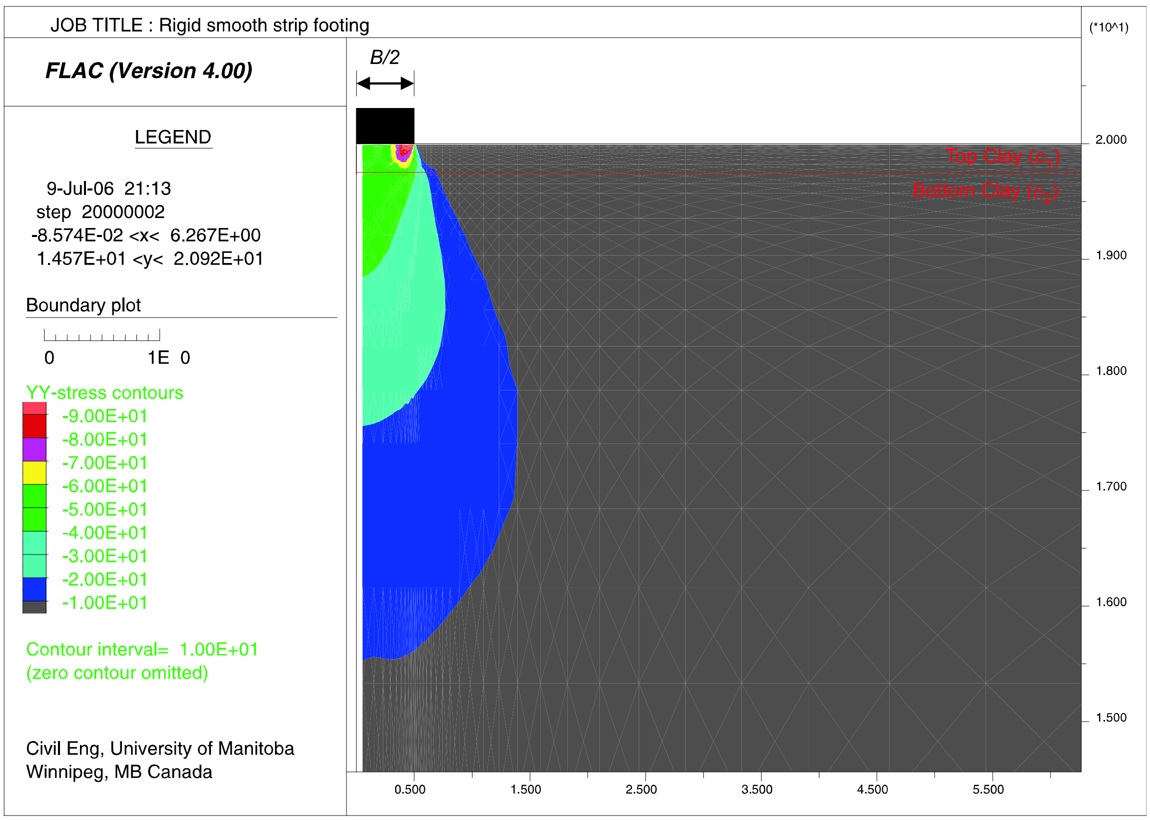

Figure A.131: Vertical stress (σ_{yy}) contours for a rigid smooth strip footing on strong clay over soft clay for 40×30 grid model, $H/B = 0.25$, $c_2/c_1 = 0.5$.

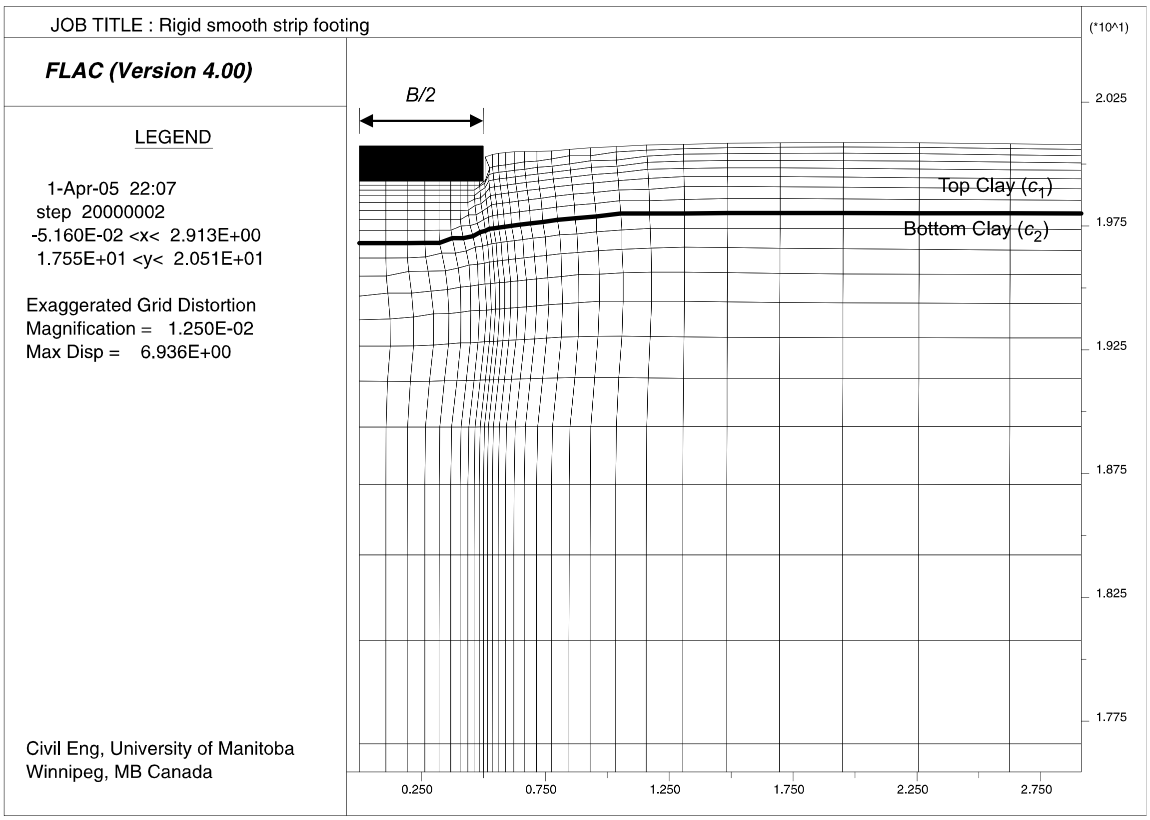

Figure A.132: Magnified grid for a rigid smooth strip footing on strong clay over soft clay for 40×30 grid model, $H/B = 0.25$, $c_2/c_1 = 0.5$.

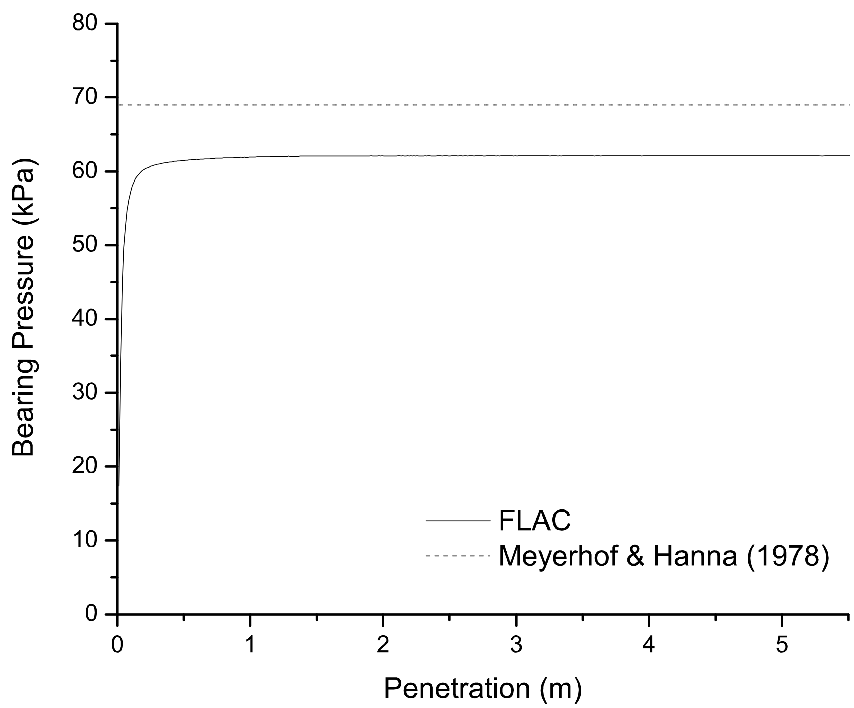

Figure A.133: Bearing pressure versus penetration curve for a rigid smooth strip footing on strong clay over soft clay for 40×30 grid model, $H/B = 0.25$, $c_2/c_1 = 0.5$.

Case 5: $c_2/c_1 = 1/3$ **- Small Deformation Analysis**

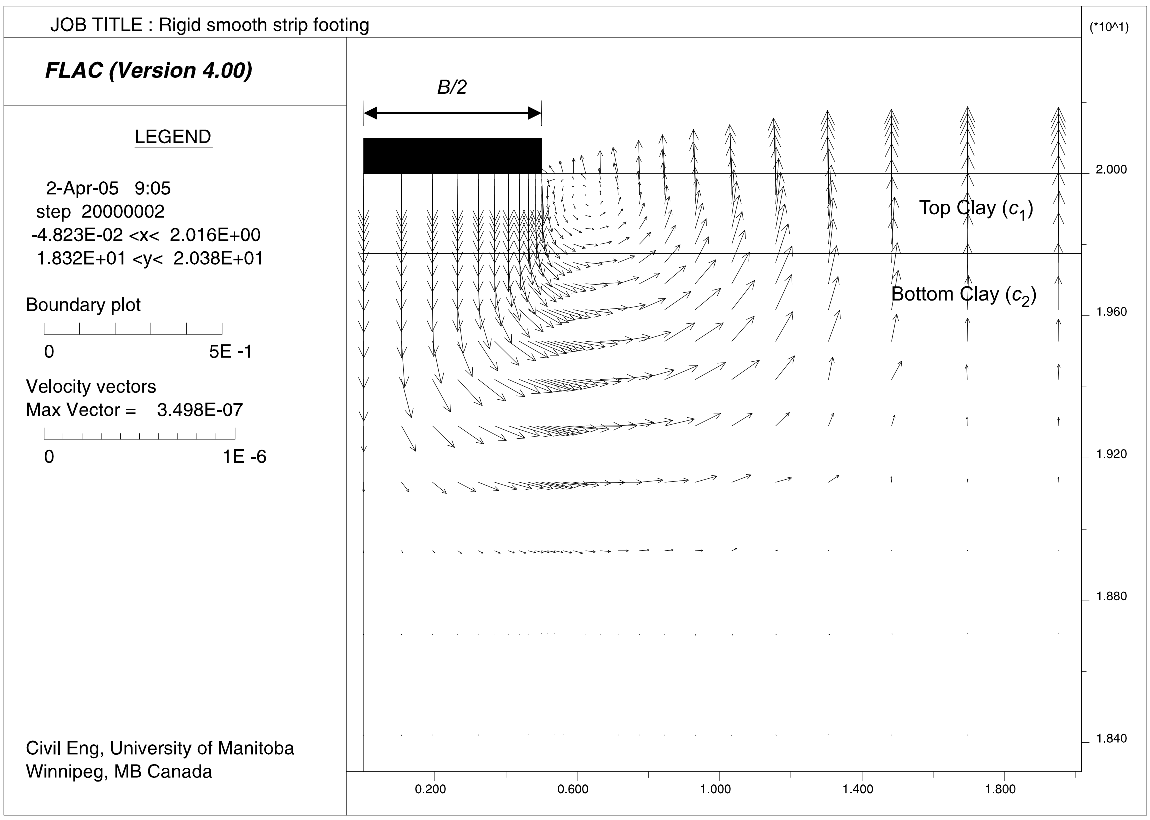

Figure A.134: Velocity vectors for a rigid smooth strip footing on strong clay over soft clay for 40 × 30 grid model, $H/B = 0.25$, $c_2/c_1 = 1/3$.

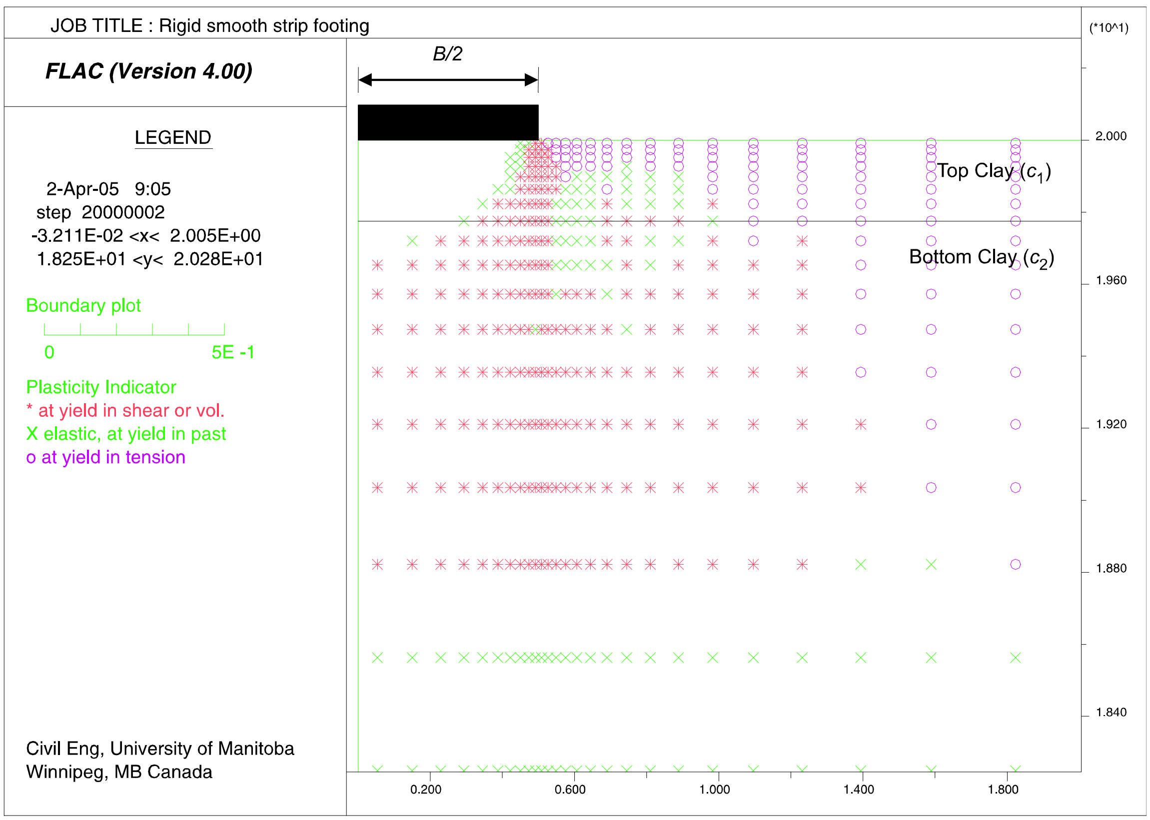

Figure A.135: Plasticity state indicators at steady state condition for a rigid smooth strip footing on strong over soft clay for 40×30 grid model, $H/B = 0.25$, $c_2/c_1 = 1/3$.

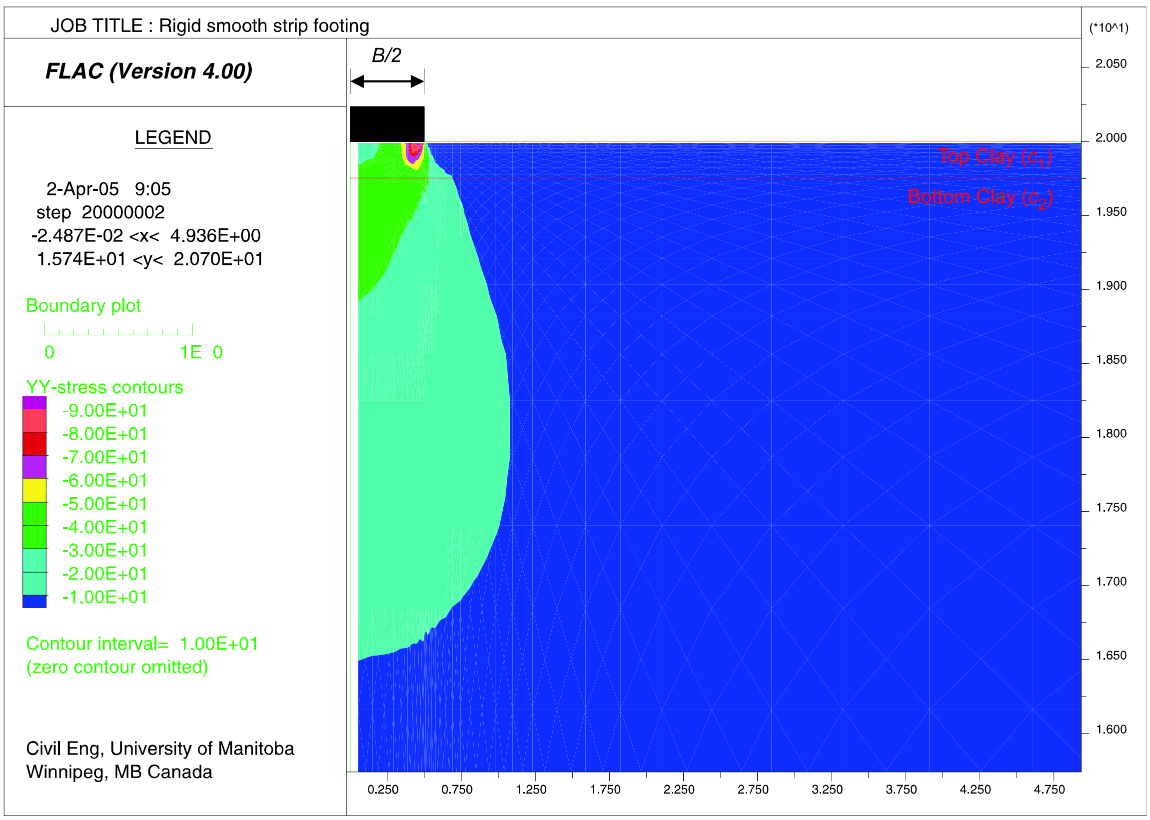

Figure A.136: Vertical stress (σ_{yy}) contours for a rigid smooth strip footing on strong clay over soft clay for 40×30 grid model, $H/B = 0.25$, $c_2/c_1 = 1/3$.

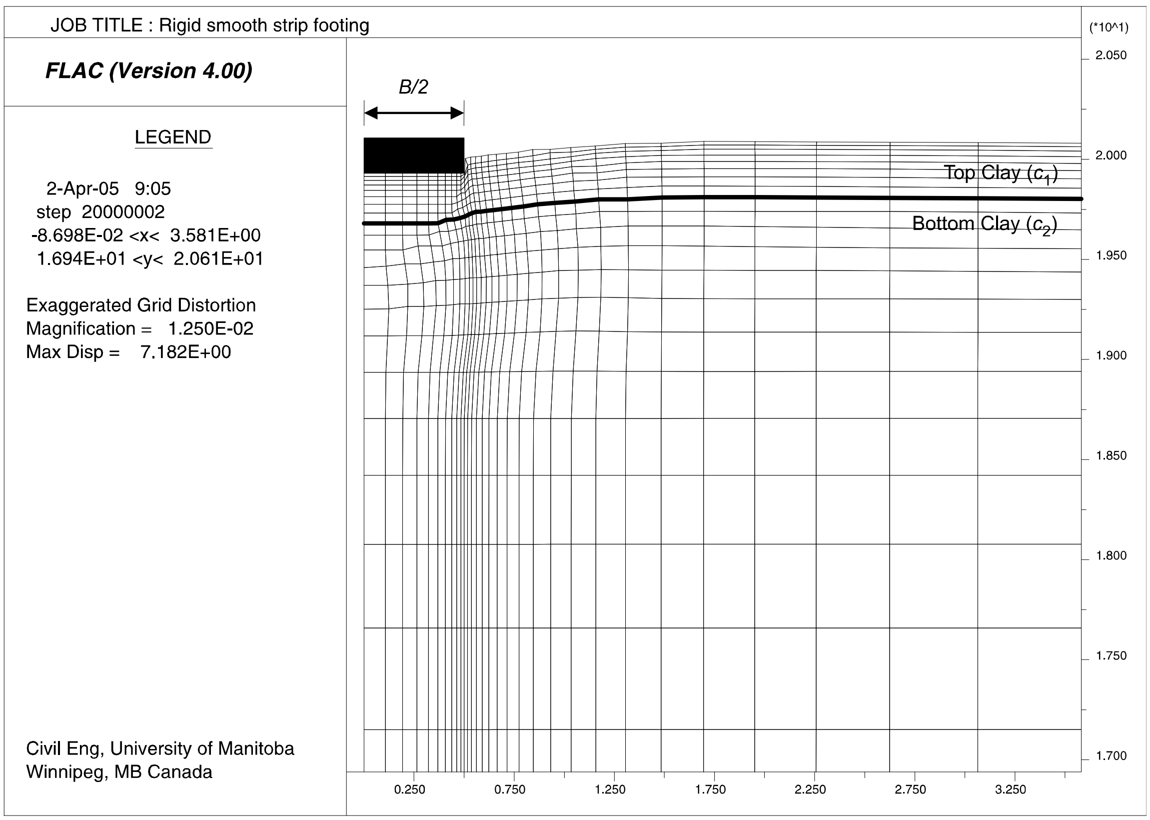

Figure A.137: Magnified grid for a rigid smooth strip footing on strong clay over soft clay for 40×30 grid model, $H/B = 0.25$, $c_2/c_1 = 1/3$.

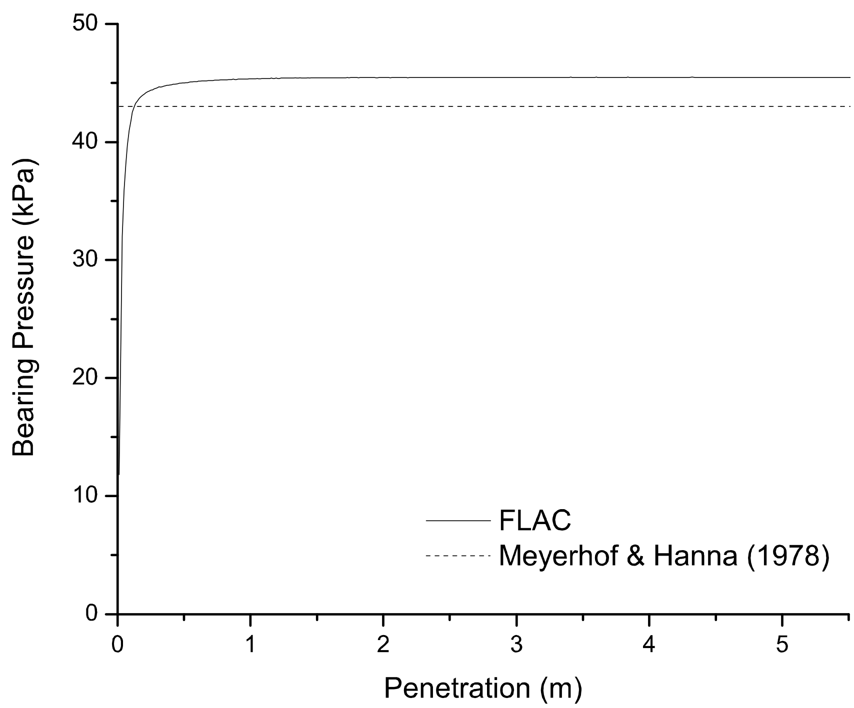

Figure A.138: Bearing pressure versus penetration curve for a rigid smooth strip footing on strong clay over soft clay for 40×30 grid model, $H/B = 0.25$, $c_2/c_1 = 1/3$.

Case 6: $c_2/c_1 = 0.2$ **- Small Deformation Analysis**

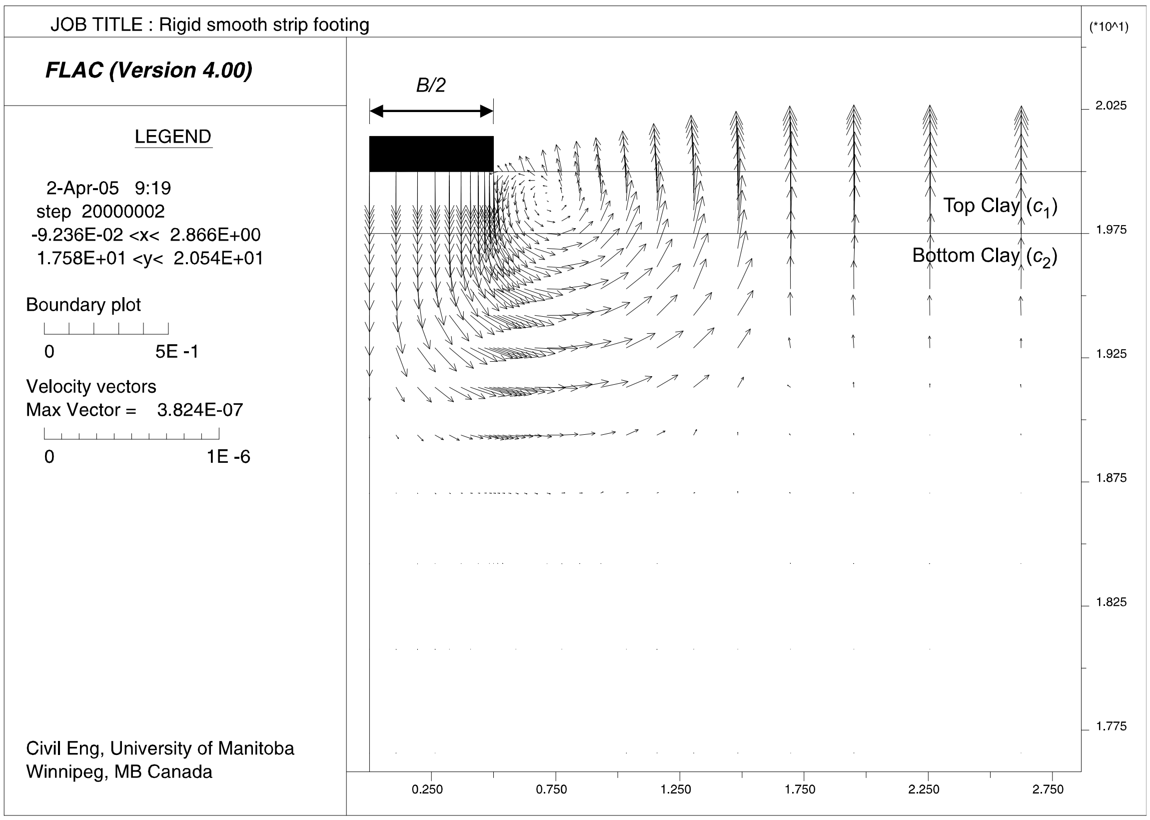

Figure A.139: Velocity vectors for a rigid smooth strip footing on strong clay over soft clay for 40×30 grid model, $H/B = 0.25$, $c_2/c_1 = 0.2$.

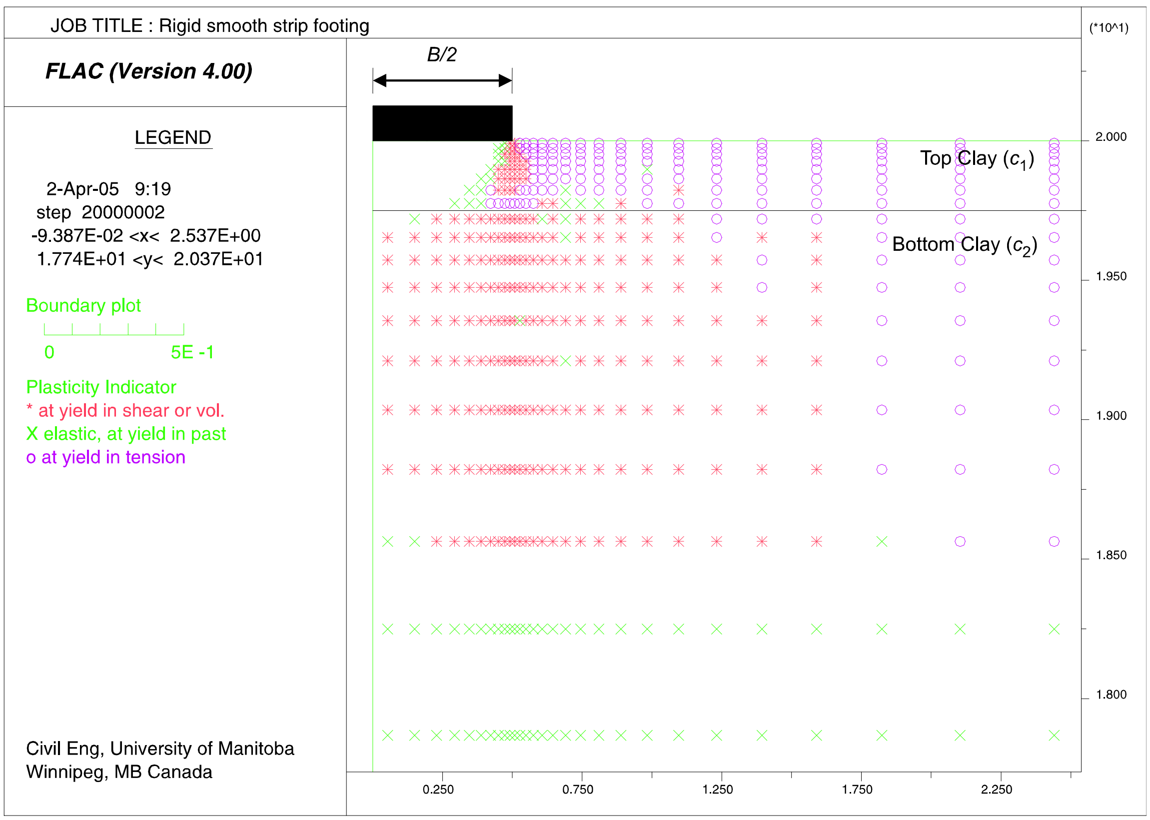

Figure A.140: Plasticity state indicators at steady state condition for a rigid smooth strip footing on strong over soft clay for 40×30 grid model, $H/B = 0.25$, $c_2/c_1 = 0.2$.

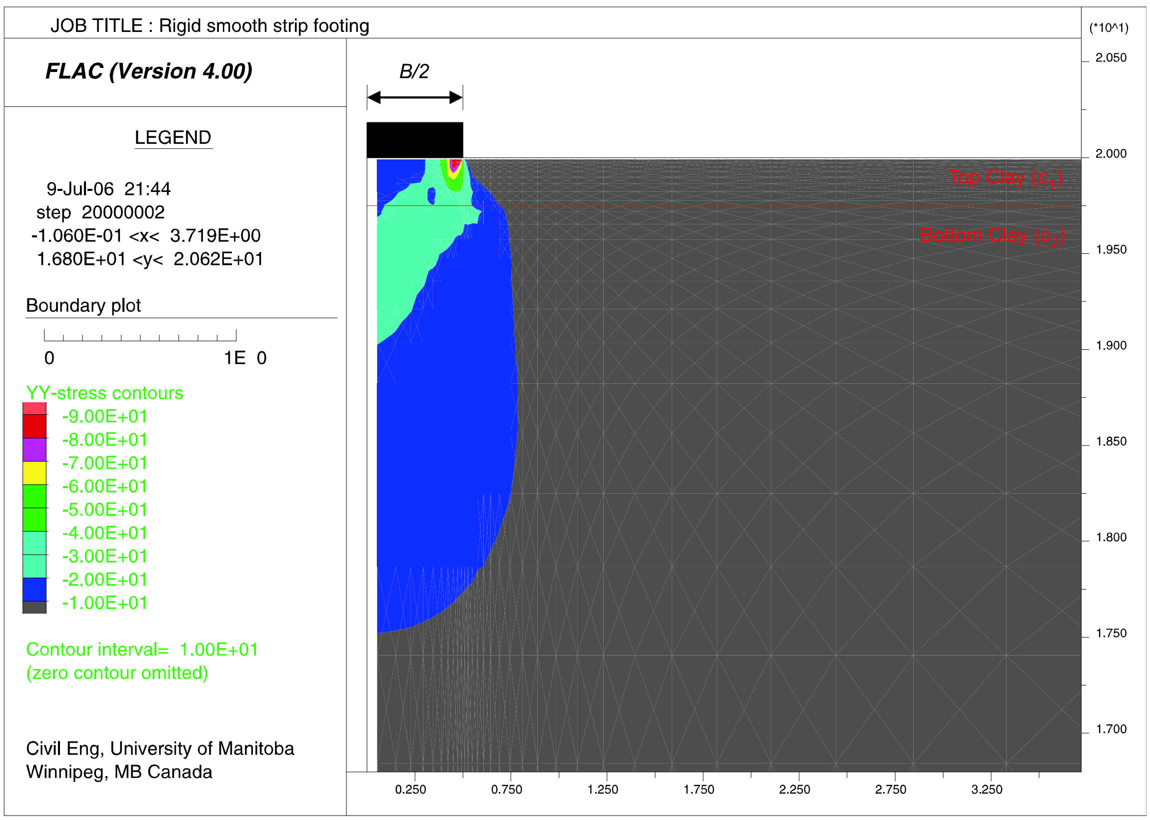

Figure A.141: Vertical stress (σ_{yy}) contours for a rigid smooth strip footing on strong clay over soft clay for 40×30 grid model, $H/B = 0.25$, $c_2/c_1 = 0.2$.

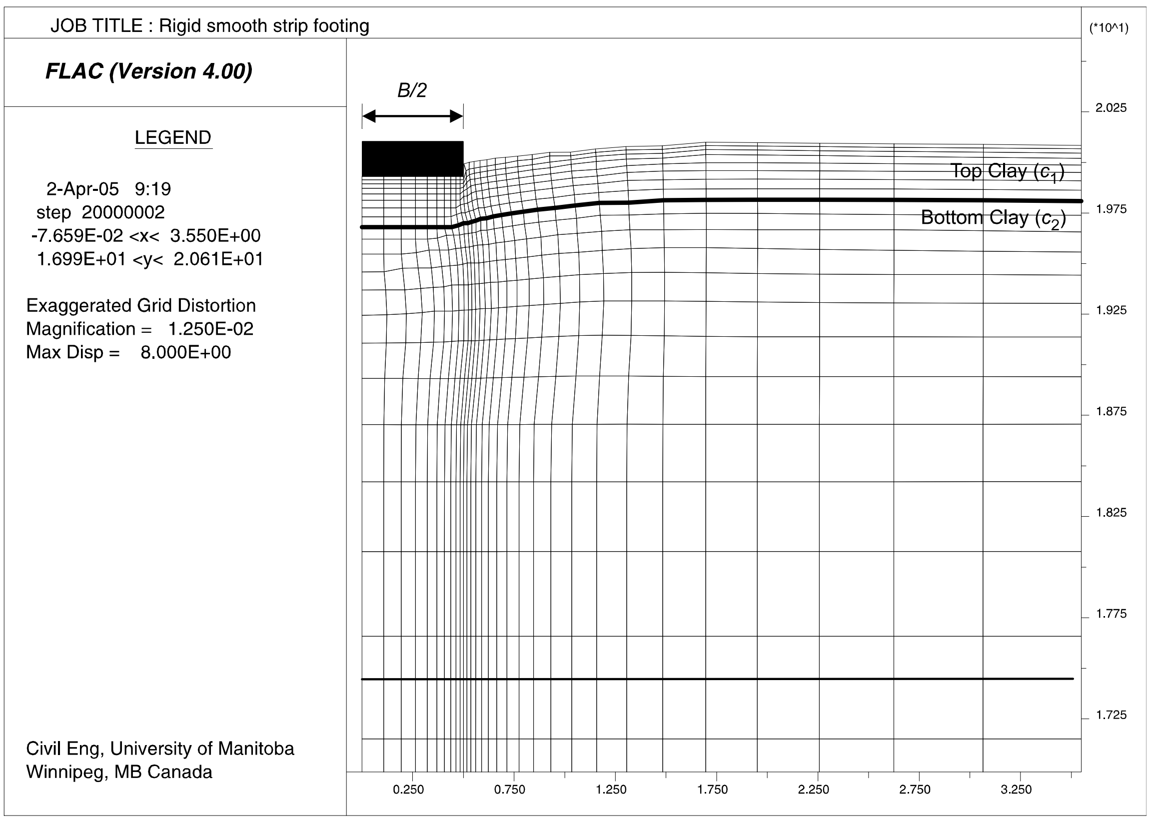

Figure A.142: Magnified grid for a rigid smooth strip footing on strong clay over soft clay for 40×30 grid model, $H/B = 0.25$, $c_2/c_1 = 0.2$.

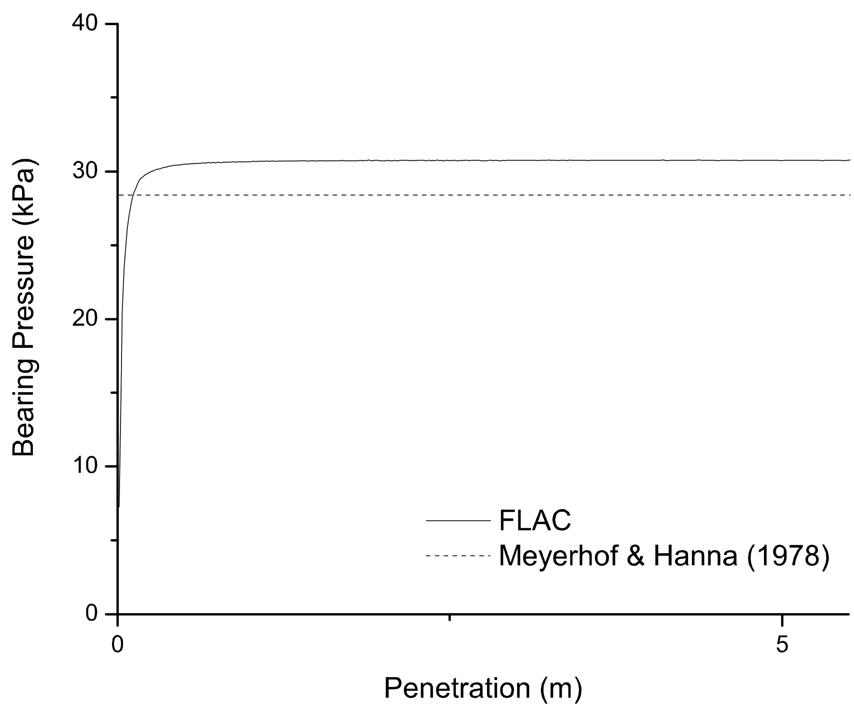

Figure A.143: Bearing pressure versus penetration curve for a rigid smooth strip footing on strong clay over soft clay for 40×30 grid model, $H/B = 0.25$, $c_2/c_1 = 0.2$.

Case 7: $c_2/c_1 = 0.1$ - Small Deformation Analysis

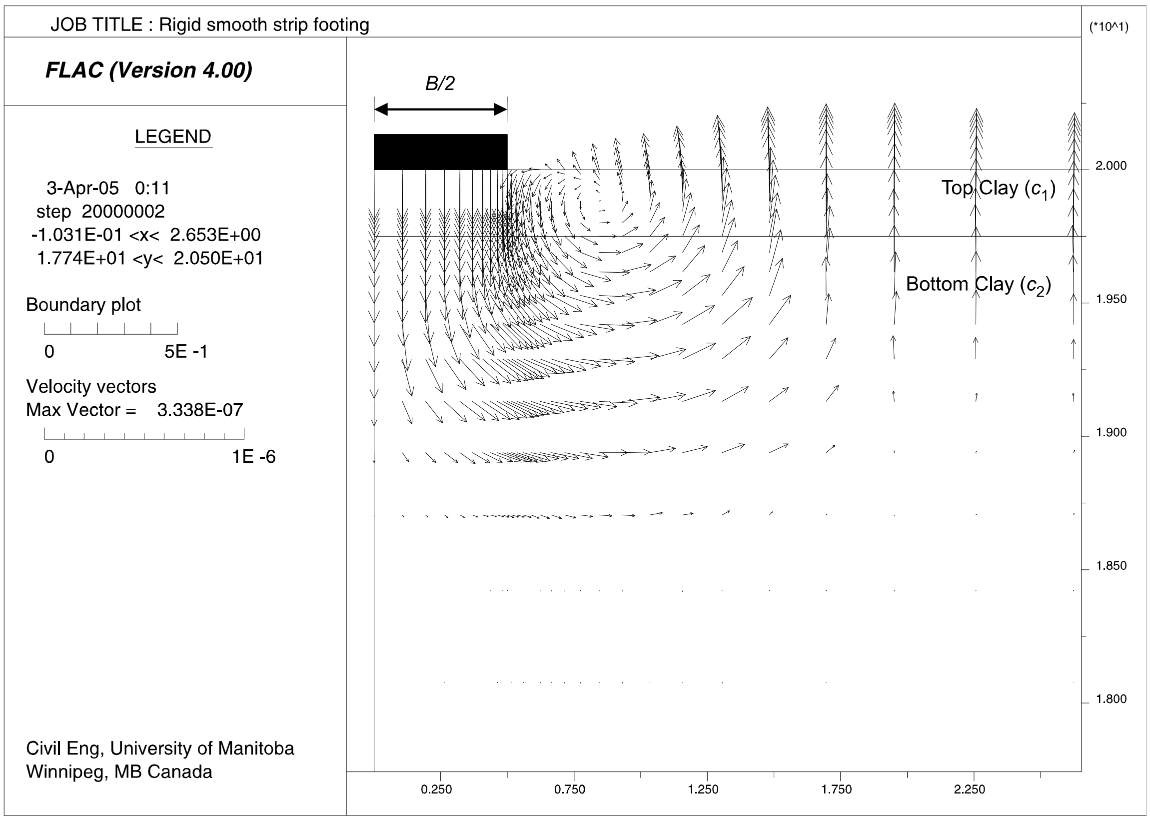

Figure A.144: Velocity vectors for a rigid smooth strip footing on strong clay over soft clay for 40×30 grid model, $H/B = 0.25$, $c_2/c_1 = 0.1$.

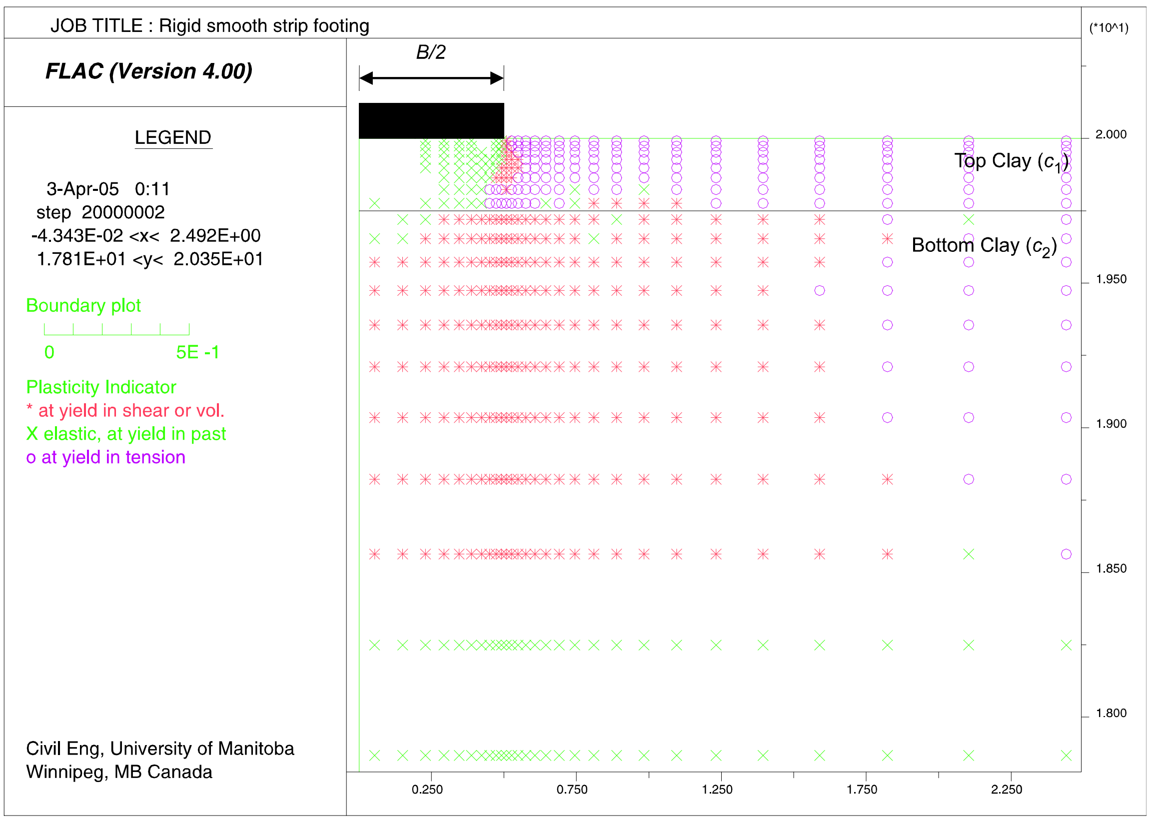

Figure A.145: Plasticity state indicators at steady state condition for a rigid smooth strip footing on strong over soft clay for 40×30 grid model, $H/B = 0.25$, $c_2/c_1 = 0.1$.

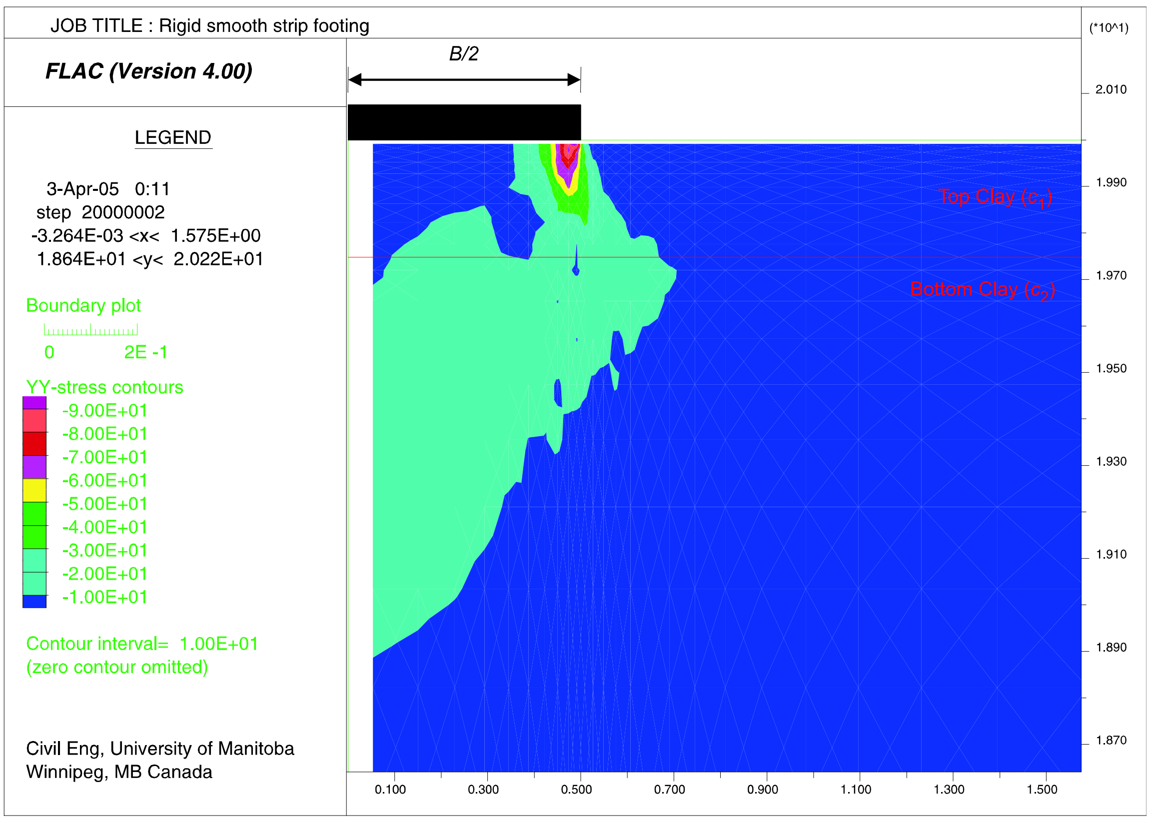

Figure A.146: Vertical stress (σ_{yy}) contours for a rigid smooth strip footing on strong clay over soft clay for 40×30 grid model, $H/B = 0.25$, $c_2/c_1 = 0.1$.

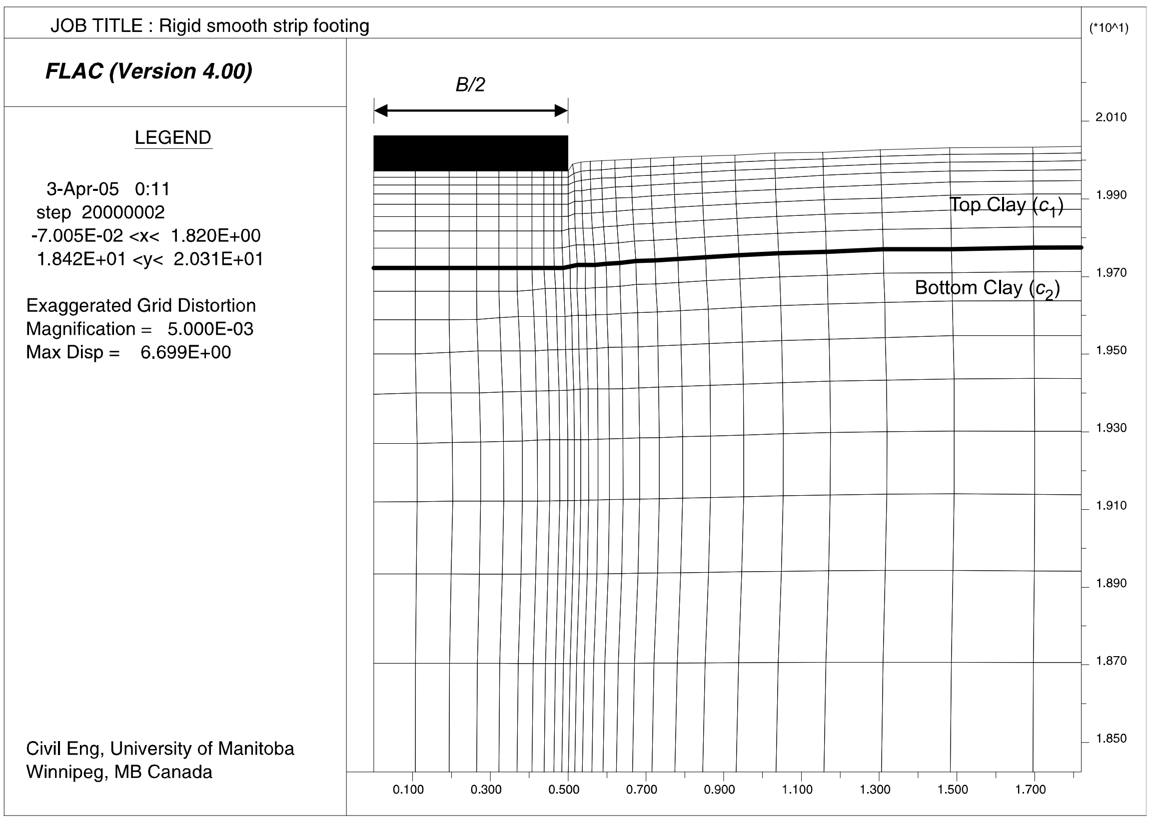

Figure A.147: Magnified grid for a rigid smooth strip footing on strong clay over soft clay for 40 × 30 grid model, $H/B = 0.25$, $c_2/c_1 = 0.1$.

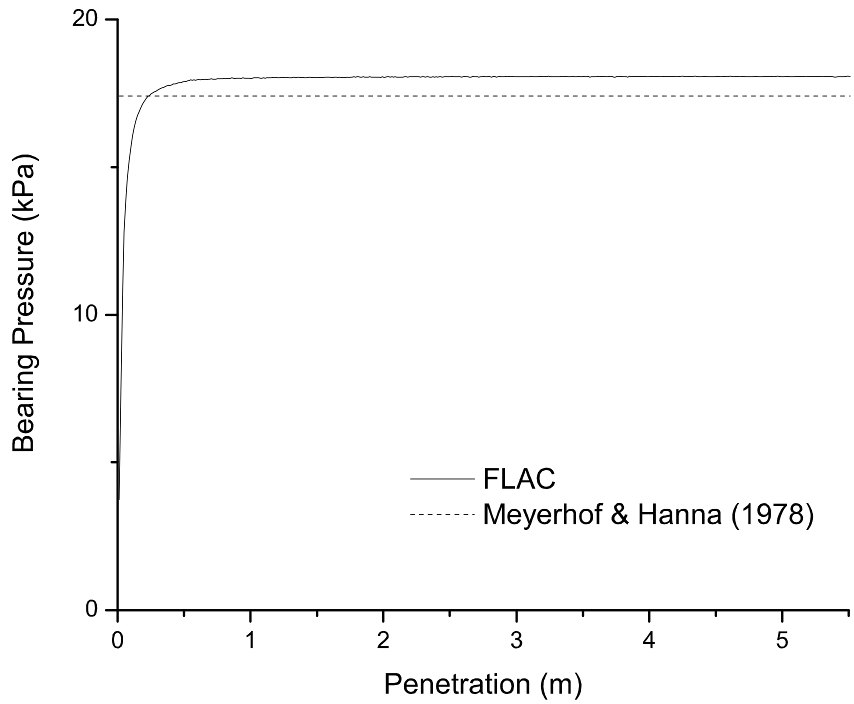

Figure A.148: Bearing pressure versus penetration curve for a rigid smooth strip footing on strong clay over soft clay for 40×30 grid model, $H/B = 0.25$, $c_2/c_1 = 0.1$.

A.2 Strip Footing on Soft Clay Overlying Stiff Clay

This situation may occur where soft glacial lake clay overlies stiff till deposits. Plain strain analyses of a strip footing resting on the ground surface with soft clay overlying a stiff clay are described in this section:

Model Geometry

A 40×30 elements grid similar to that in A.1. is adopted for these analyses. The model geometry is the same as shown in A.239

A.2.1 Rigid Smooth Strip Footing on Soft over Strong Clay ($H/B = 1$)

Case 2: $c_1/c_2 = 0.8$ **or** $c_2/c_1 = 1.25$ **- Small Deformation Analysis**

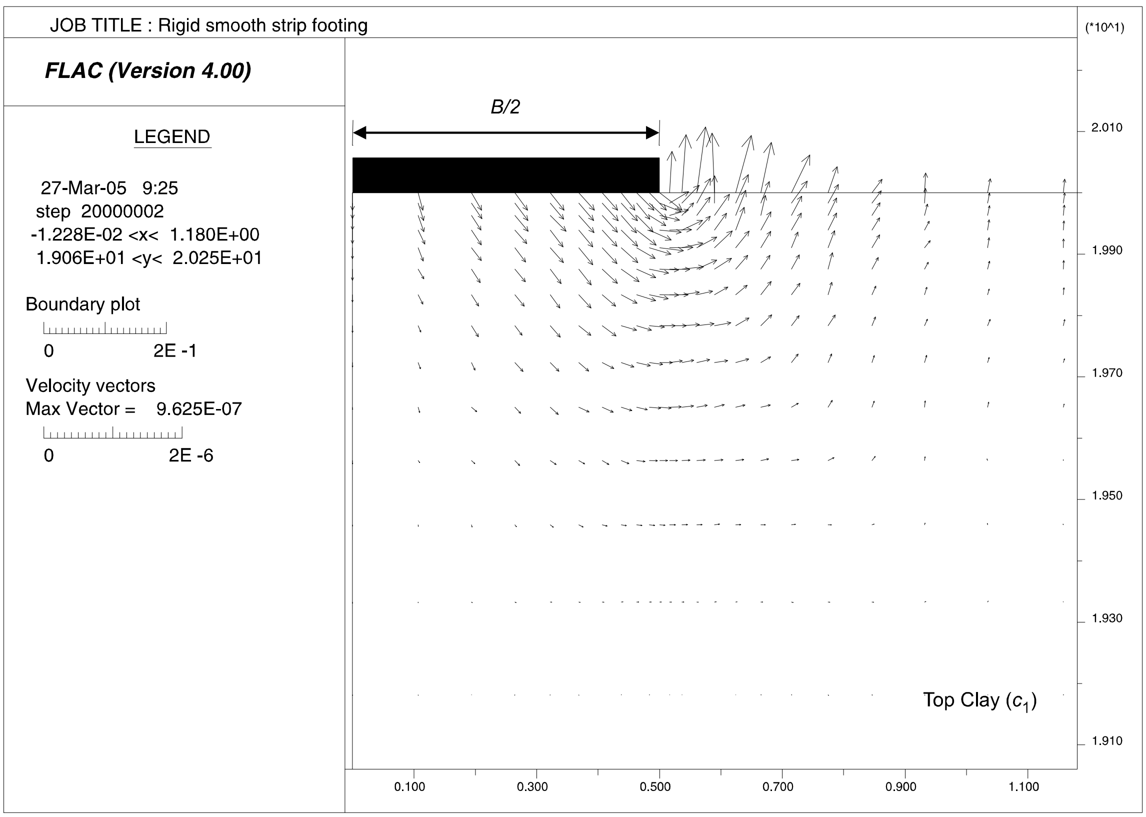

Figure A.149: Velocity vectors for a rigid strip footing on soft over strong clay for 40×30 grid model, $H/B = 1$, $c_1/c_2 = 0.8$.

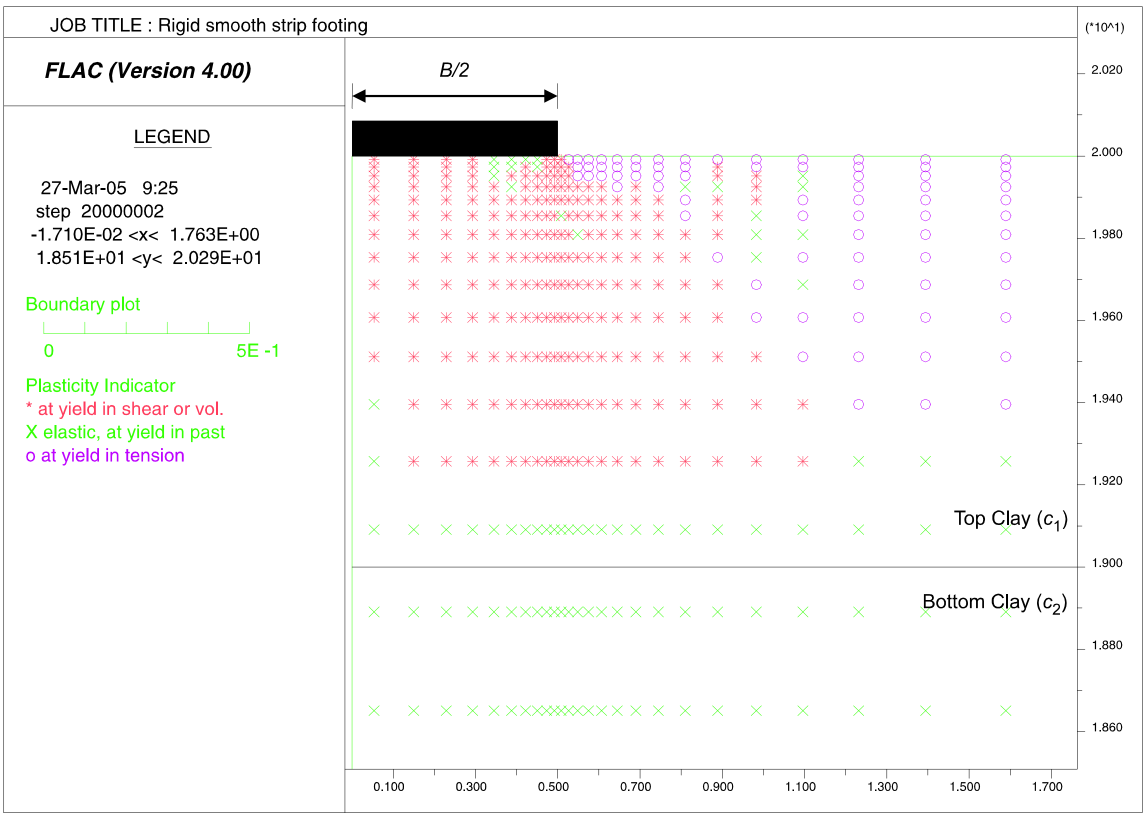

Figure A.150: Plasticity indicators for a rigid smooth strip footing on soft over strong clay for 40 × 30 grid model, $H/B = 1$, $c_1/c_2 = 0.8$.

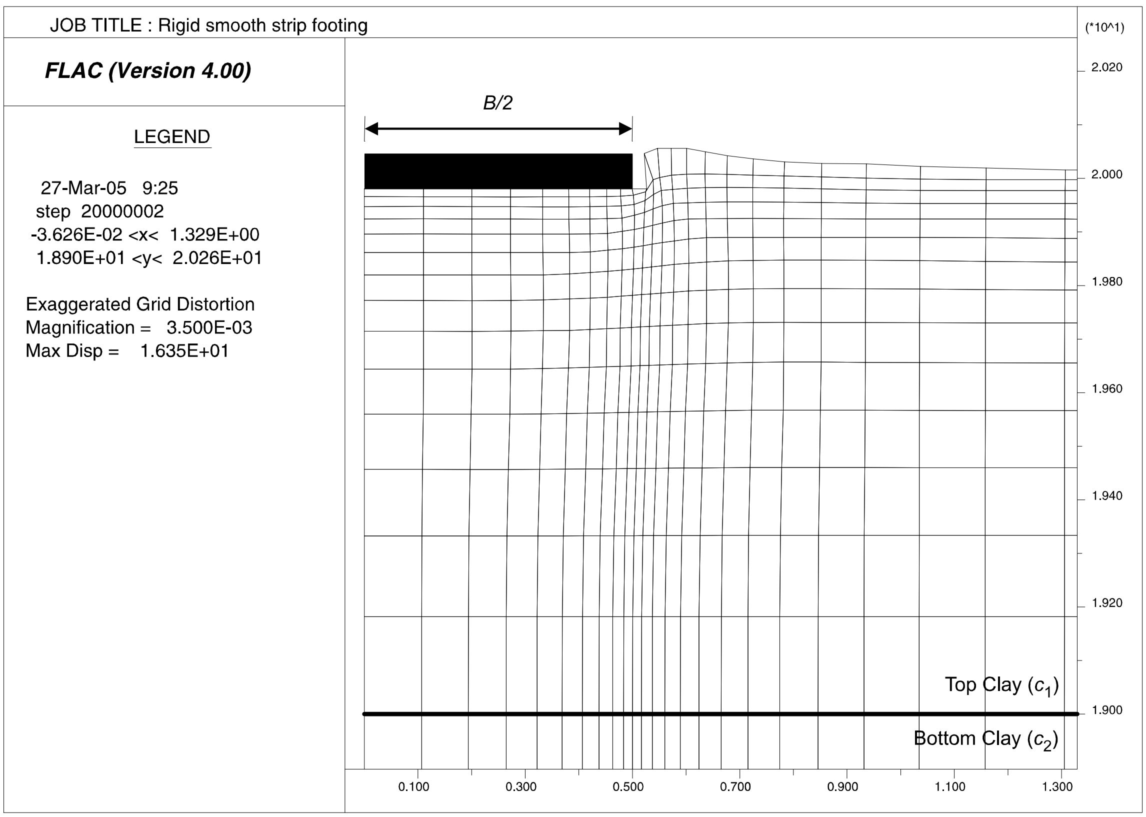

Figure A.151: Magnified grid for a rigid smooth footing on soft over strong clay for 40×30 grid model, $H/B = 1$, $c_2/c_1 = 0.8$.

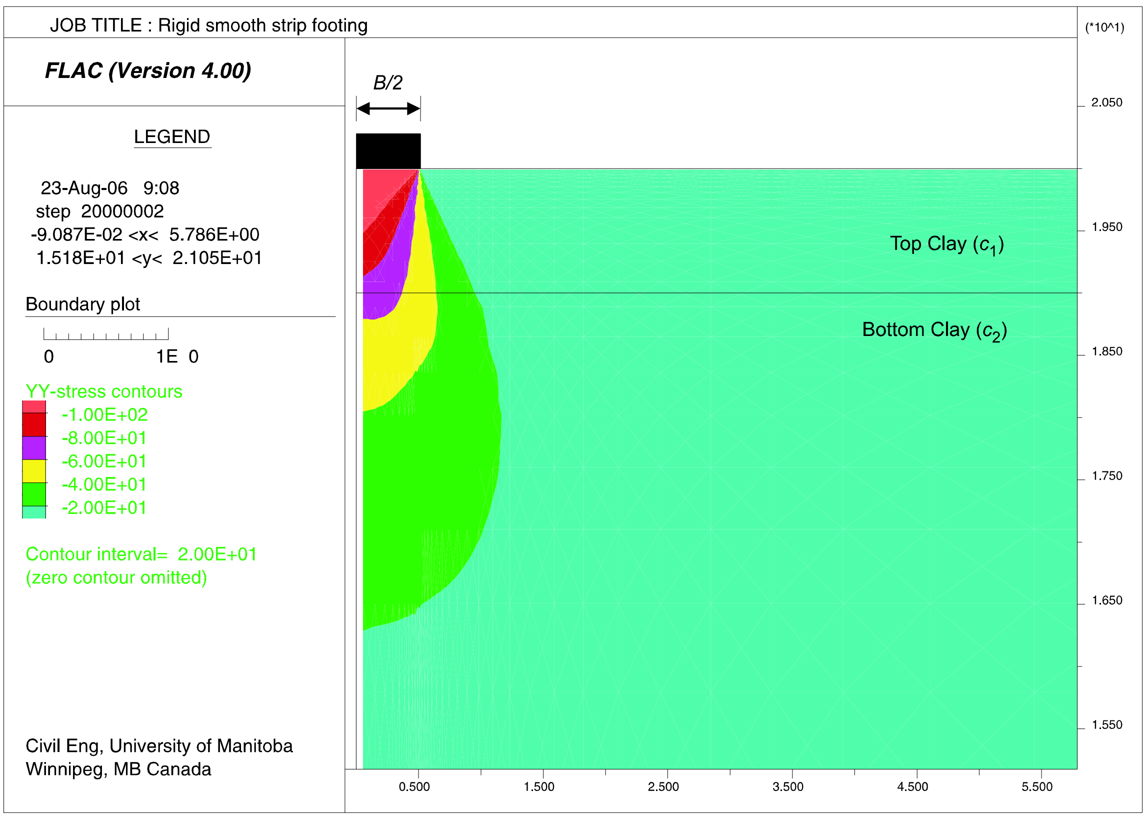

Figure A.152: Vertical stress (σ_{yy}) contours for a rigid smooth strip footing on soft over strong clay for 40×30 grid model, $H/B = 1$, $c_1/c_2 = 0.8$.

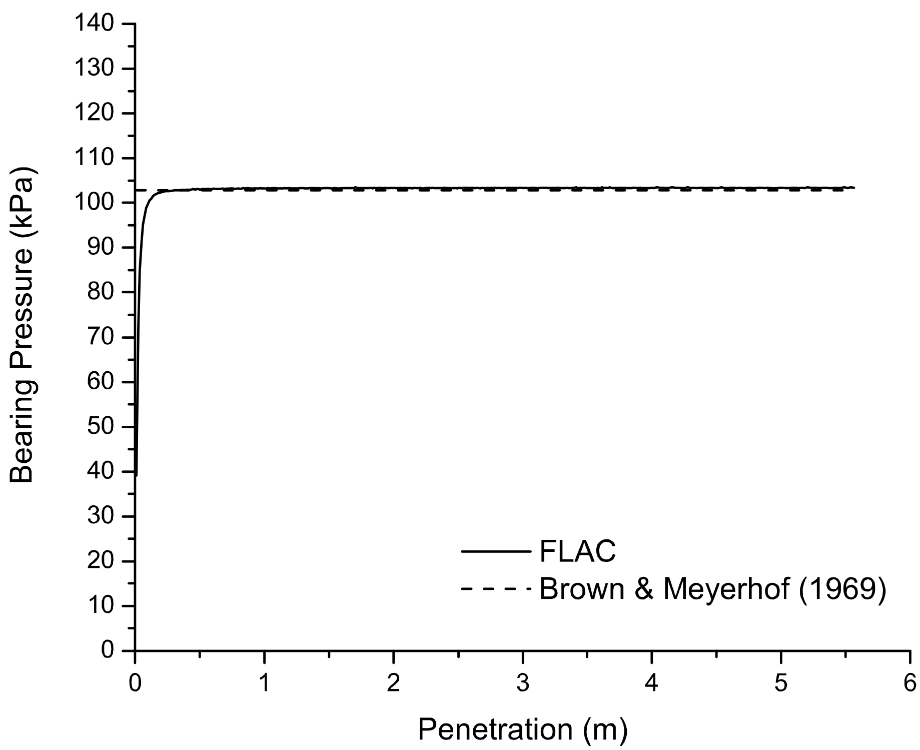

Figure A.153: Bearing pressure versus penetration curve for a rigid smooth strip footing on soft over strong clay for 40 × 30 grid model, $H/B = 1$, $c_1/c_2 = 0.8$.

Case 3: $c_1/c_2 = 2/3$ or $c_2/c_1 = 1.5$ - Small Deformation Analysis

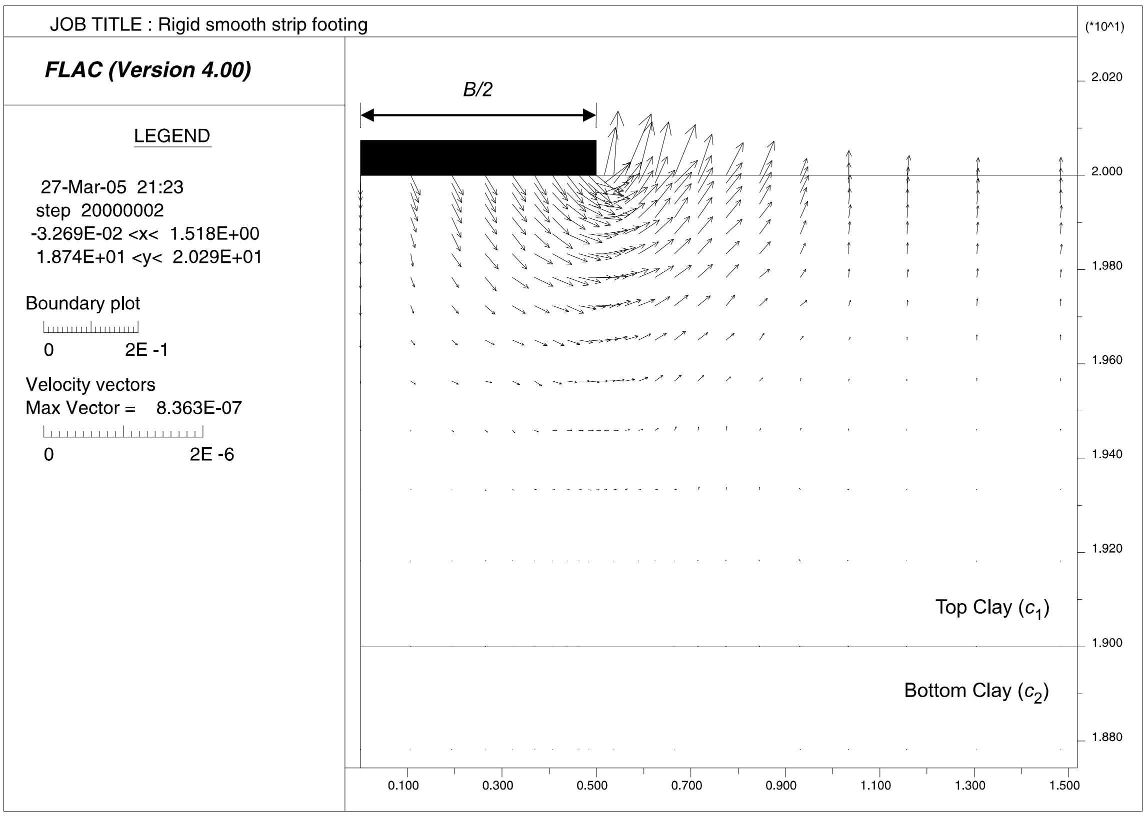

Figure A.154: Velocity vectors for a rigid smooth strip footing on soft over strong clay for 40×30 grid model, $H/B = 1$, $c_1/c_2 = 2/3$.

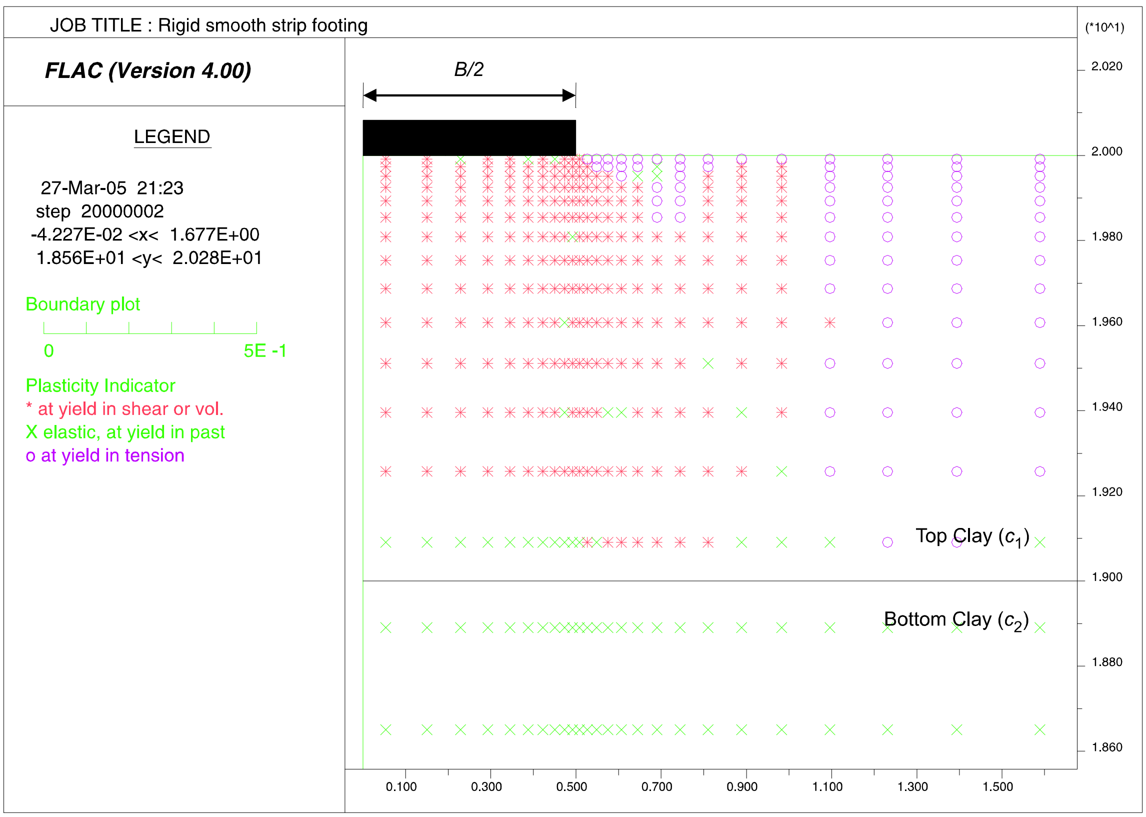

Figure A.155: Plasticity state indicators for a rigid smooth strip footing on soft over strong clay for 40×30 grid model, $H/B = 1$, $c_1/c_2 = 2/3$.

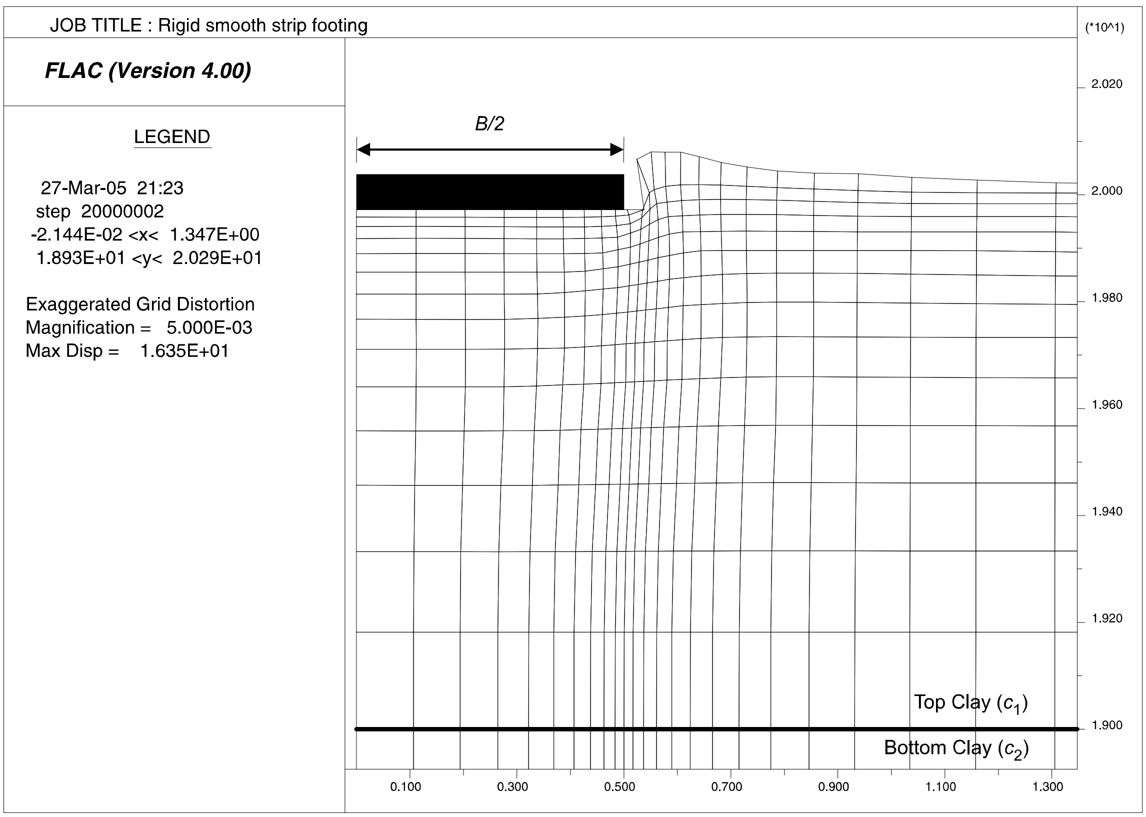

Figure A.156: Magnified grid for a rigid smooth strip footing on soft over strong clay for 40 × 30 grid model, $H/B = 1$, $c_1/c_2 = 2/3$.

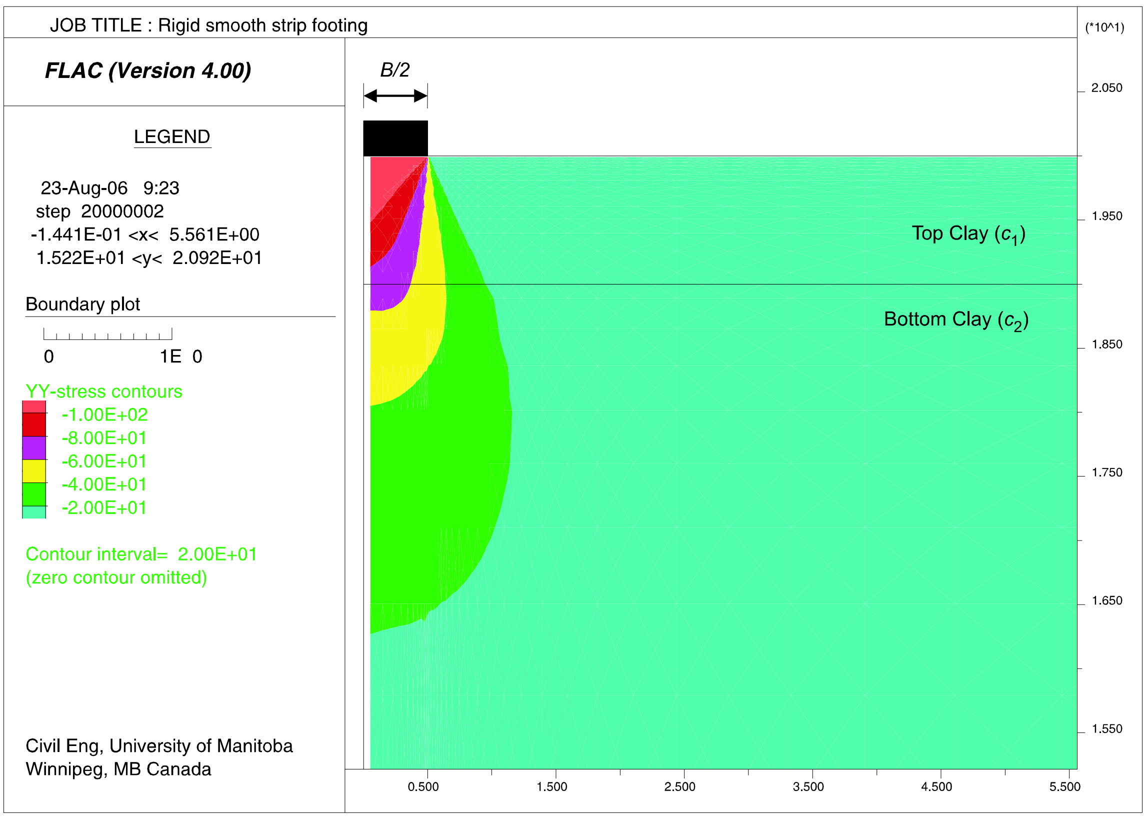

Figure A.157: Vertical stress (σ_{yy}) contours for a rigid smooth strip footing on soft over strong clay for 40×30 grid model, $H/B = 1$, $c_1/c_2 = 2/3$.

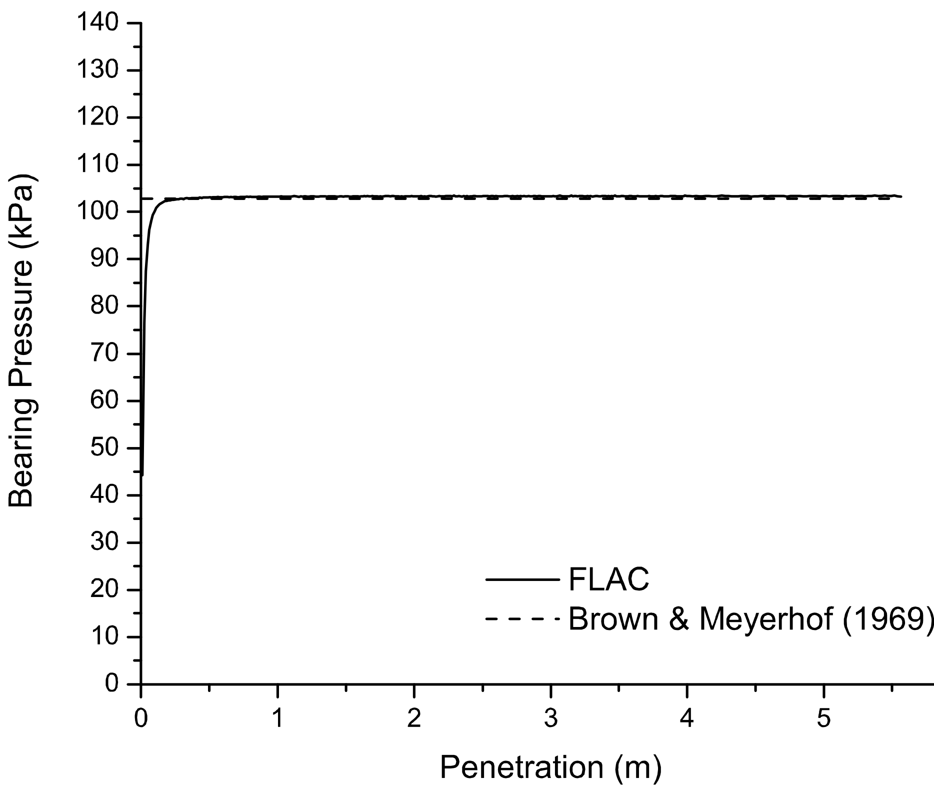

Figure A.158: Bearing pressure versus penetration curve for a rigid smooth strip footing on soft over strong clay for 40×30 grid model, $H/B = 1$, $c_1/c_2 = 2/3$.

Case 4: $c_1/c_2 = 0.5$ **or** $c_2/c_1 = 2$**- Small Deformation Analysis**

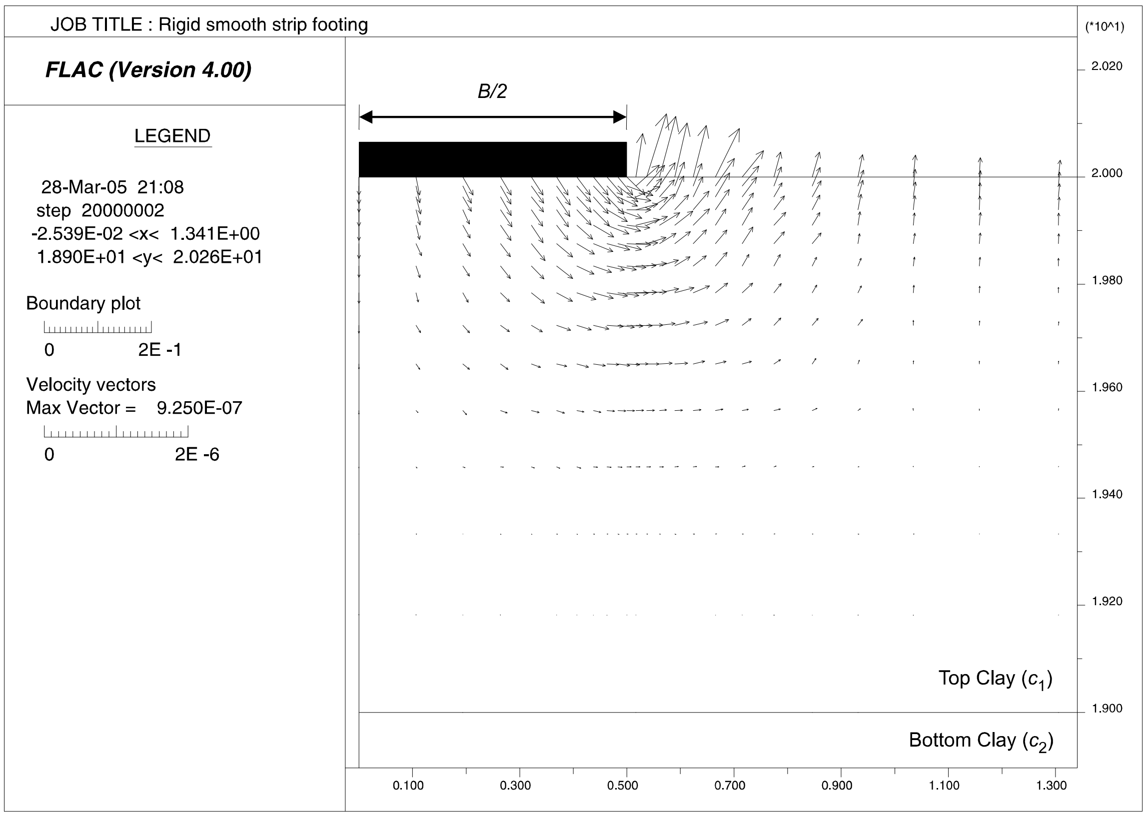

Figure A.159: Velocity vectors for a rigid smooth strip footing on soft over strong clay for 40 × 30 grid model, $H/B = 1$, $c_1/c_2 = 0.5$.

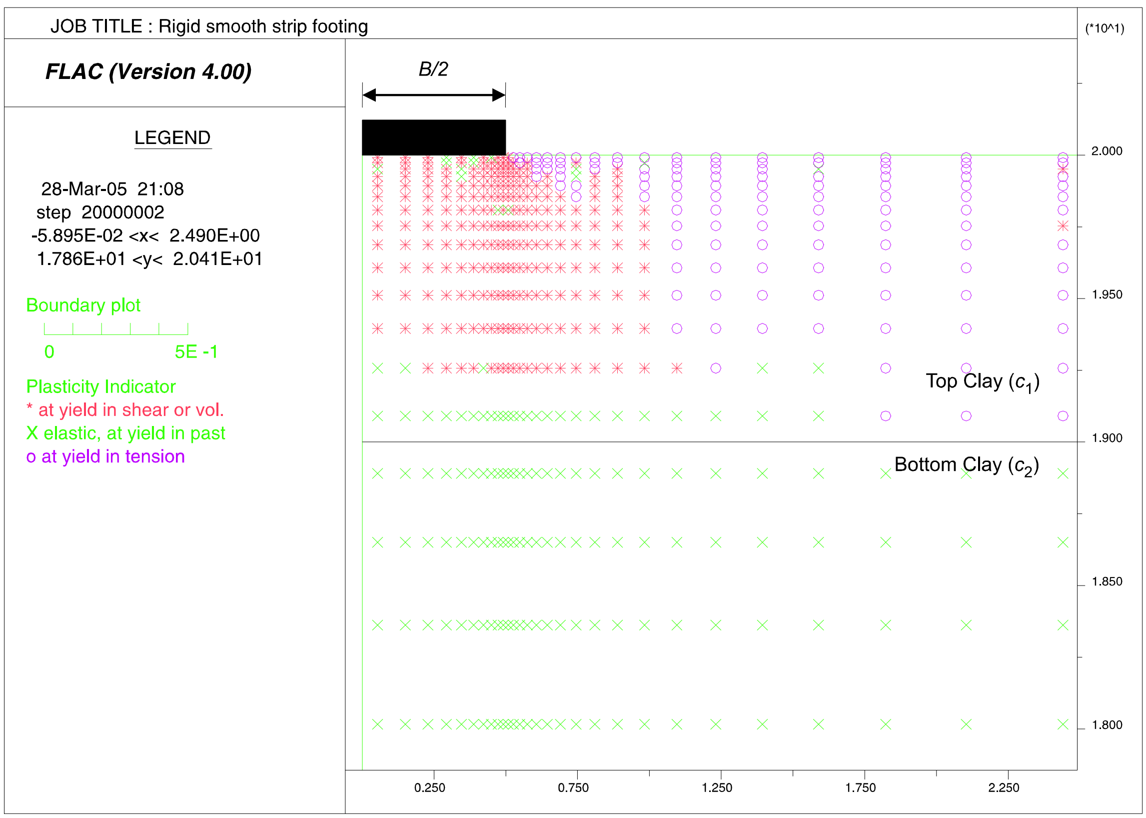

Figure A.160: Plasticity state indicators for a rigid smooth strip footing on soft over strong clay for 40 × 30 grid model, $H/B = 1$, $c_1/c_2 = 0.5$.

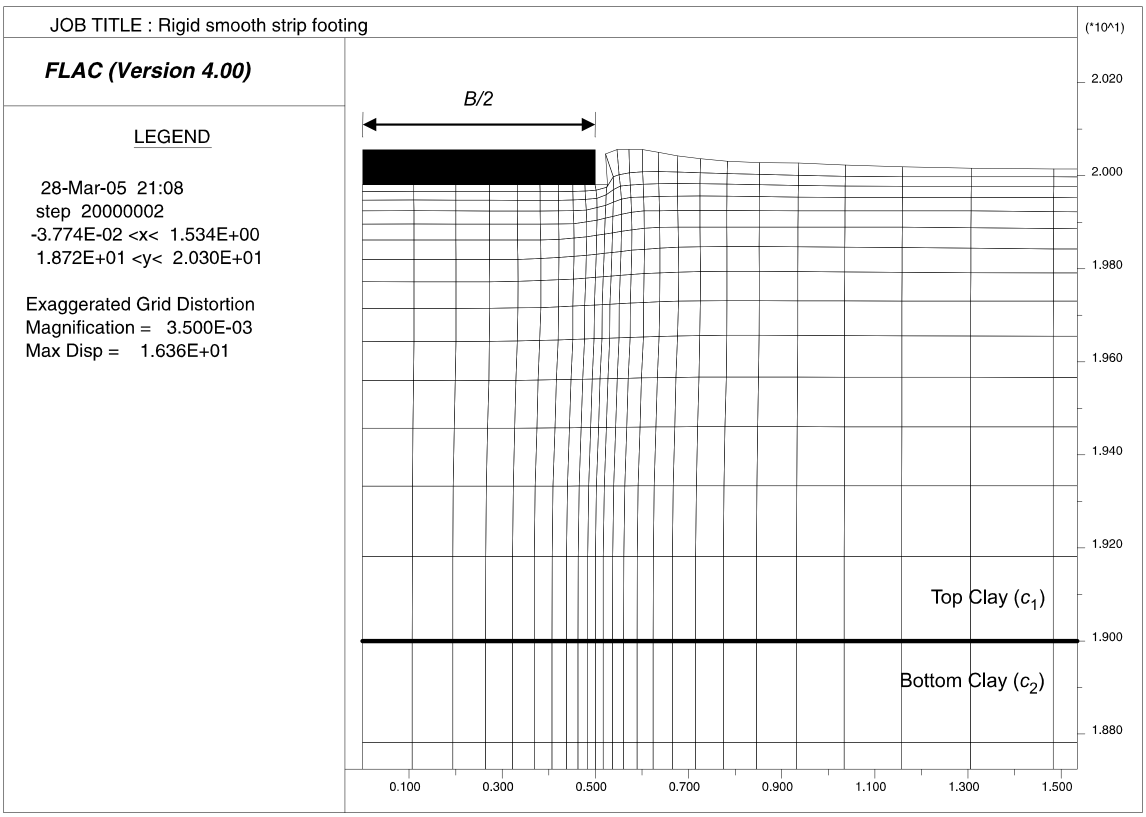

Figure A.161: Magnified grid for a rigid smooth strip footing on soft over strong clay for 40×30 grid model, $H/B = 1$, $c_1/c_2 = 0.5$.

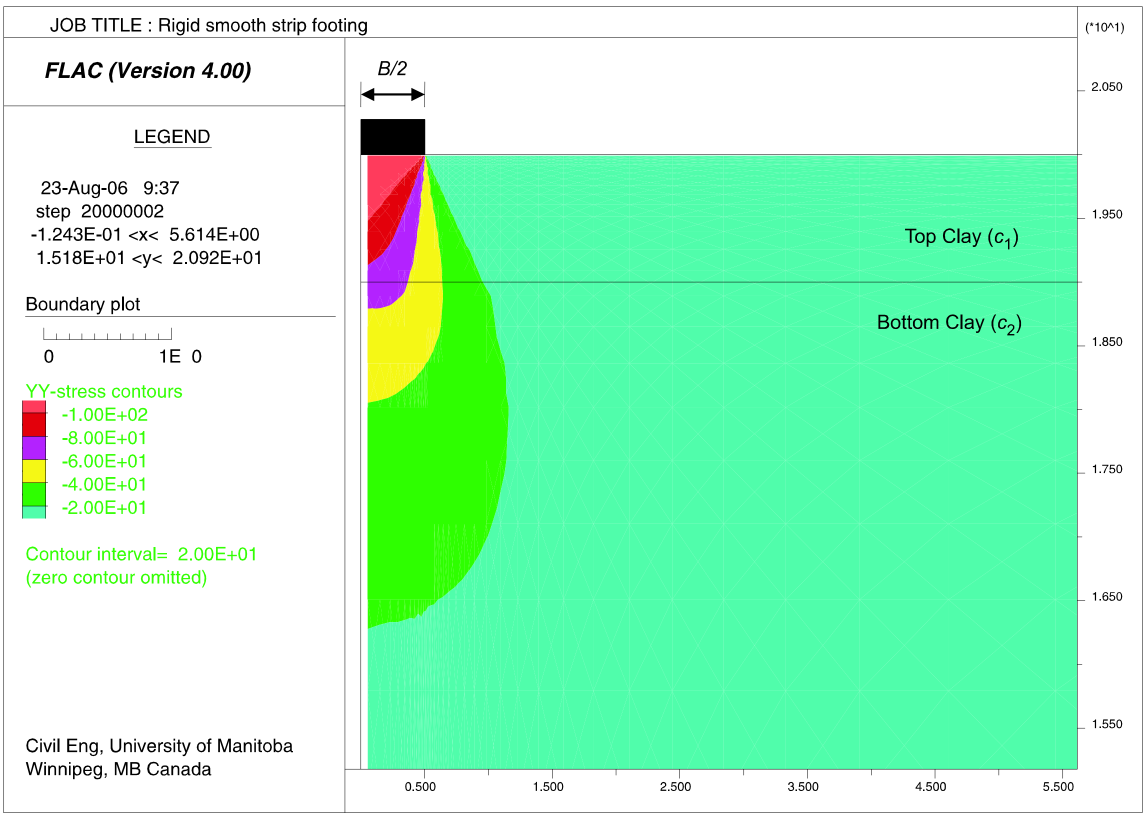

Figure A.162: Vertical stress (σ_{yy}) contours for a rigid smooth strip footing on soft over strong clay for 40×30 grid model, $H/B = 1$, $c_1/c_2 = 0.5$.

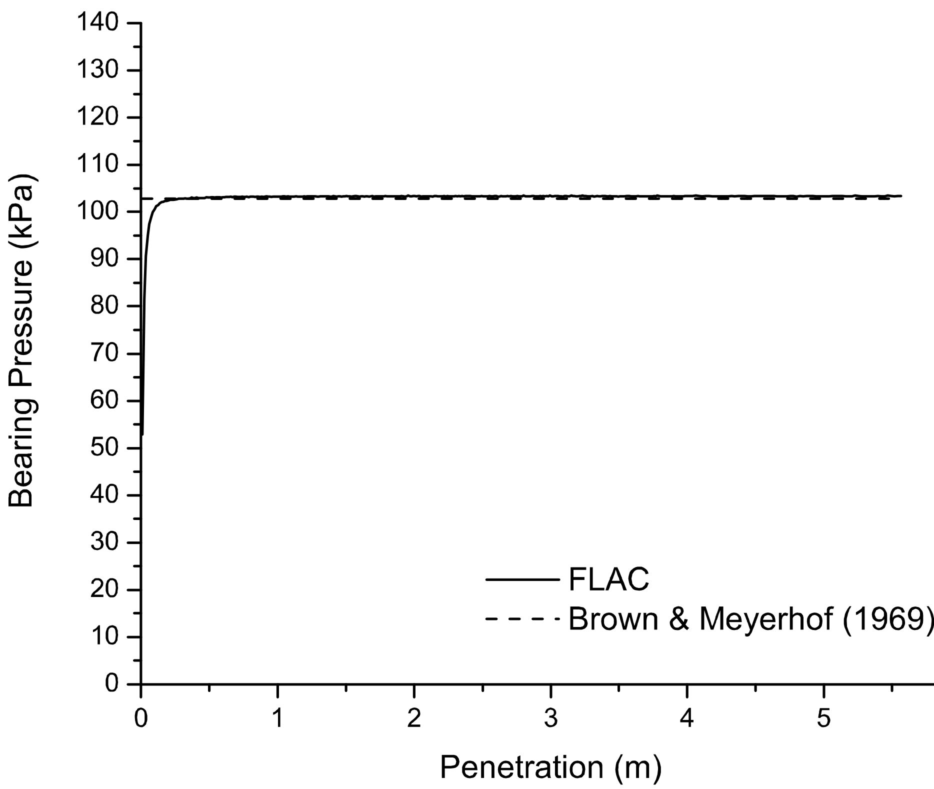

Figure A.163: Bearing pressure versus penetration curve for a rigid smooth strip footing on soft over strong clay for 40 × 30 grid model, $H/B = 1$, $c_1/c_2 = 0.5$.

Case 5: $c_1/c_2 = 1/3$ or $c_2/c_1 = 3$ - Small Deformation Analysis

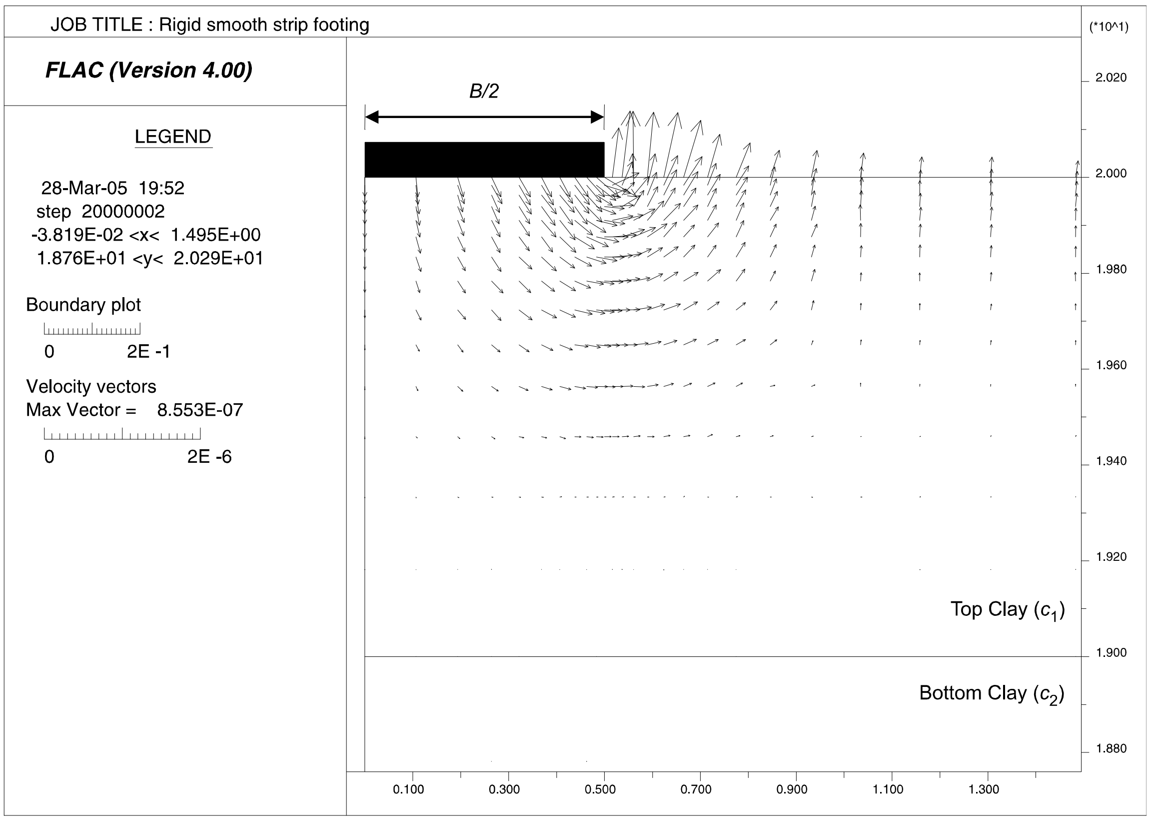

Figure A.164: Velocity vectors for a rigid smooth strip footing on soft clay over strong clay for 40×30 grid model, $H/B = 1$, $c_1/c_2 = 1/3$.

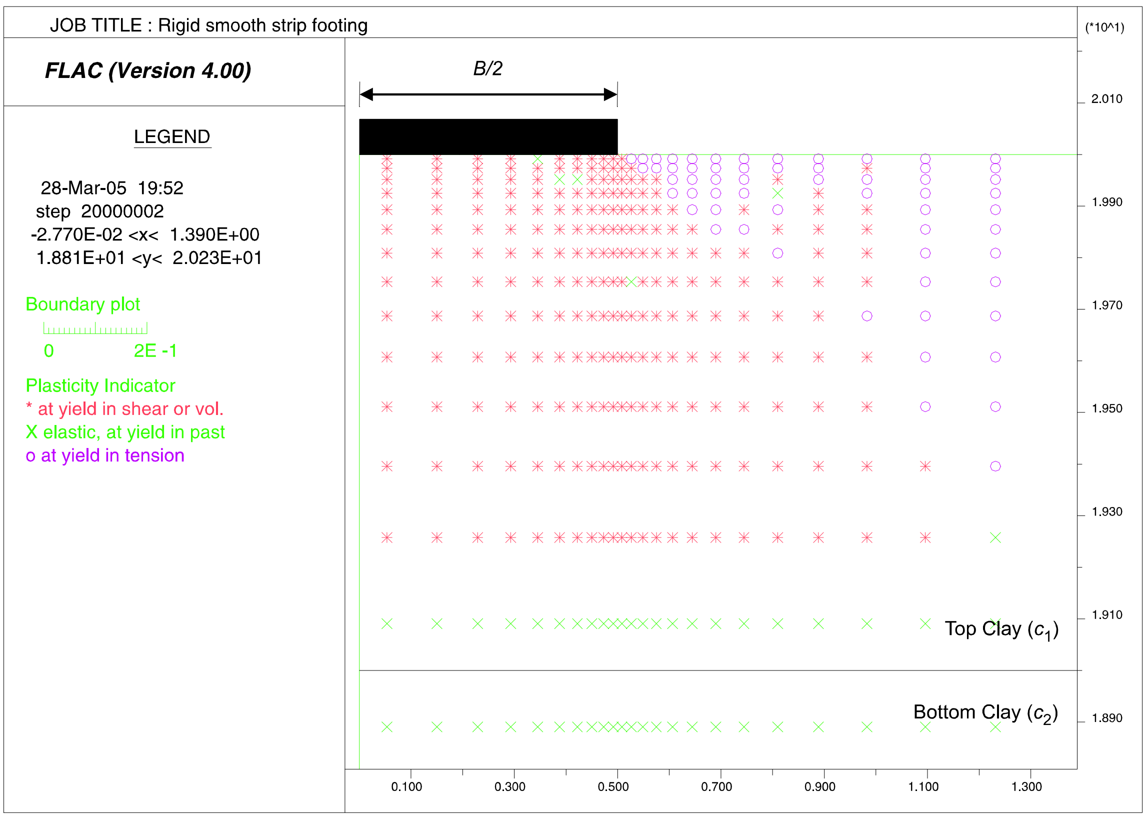

Figure A.165: Plasticity state indicators for a rigid smooth strip footing on soft over strong clay for 40 × 30 grid model, $H/B = 1$, $c_1/c_2 = 1/3$.

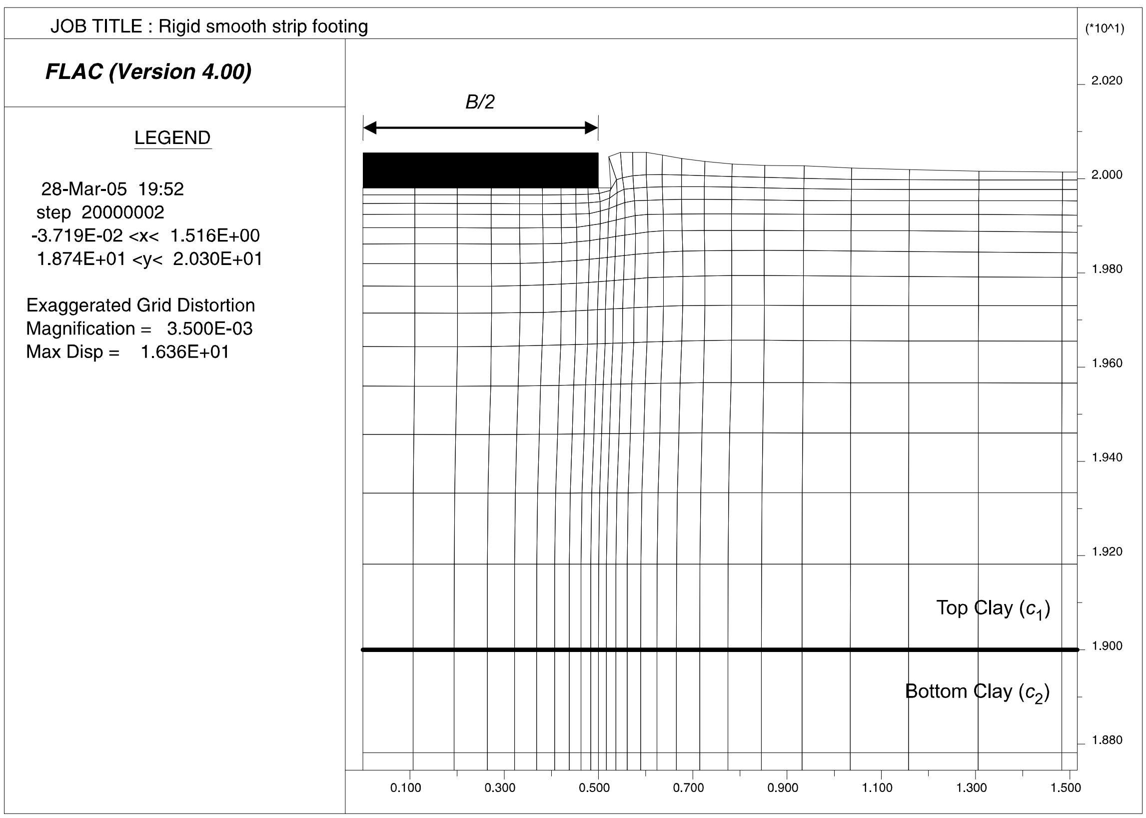

Figure A.166: Magnified grid for a rigid smooth strip footing on soft over strong clay for 40×30 grid model, $H/B = 1$, $c_1/c_2 = 1/3$.

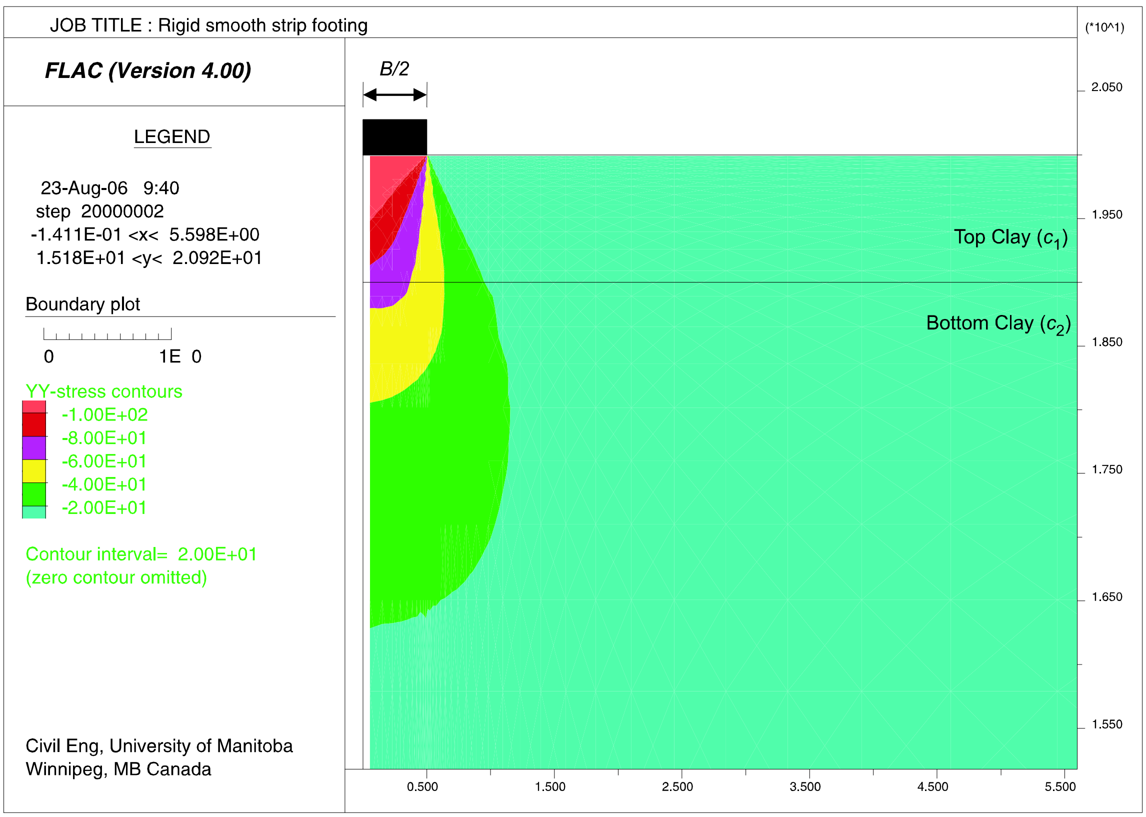

Figure A.167: Vertical stress (σ_{yy}) contours for a rigid smooth strip footing on soft over strong clay for 40×30 grid model, $H/B = 1$, $c_1/c_2 = 1/3$.

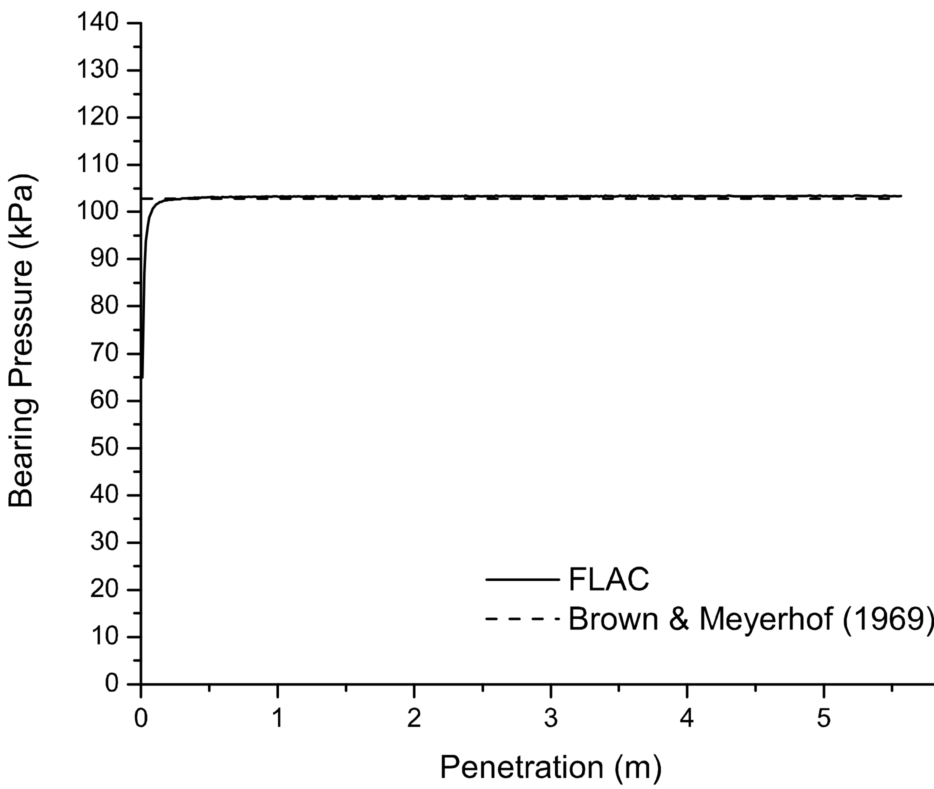

Figure A.168: Bearing pressure versus penetration curve for a rigid smooth strip footing on soft over strong clay for 40×30 grid model, $H/B = 1$, $c_1/c_2 = 1/3$.

Case 6: $c_1/c_2 = 0.2$ or $c_2/c_1 = 5$ - Small Deformation Analysis

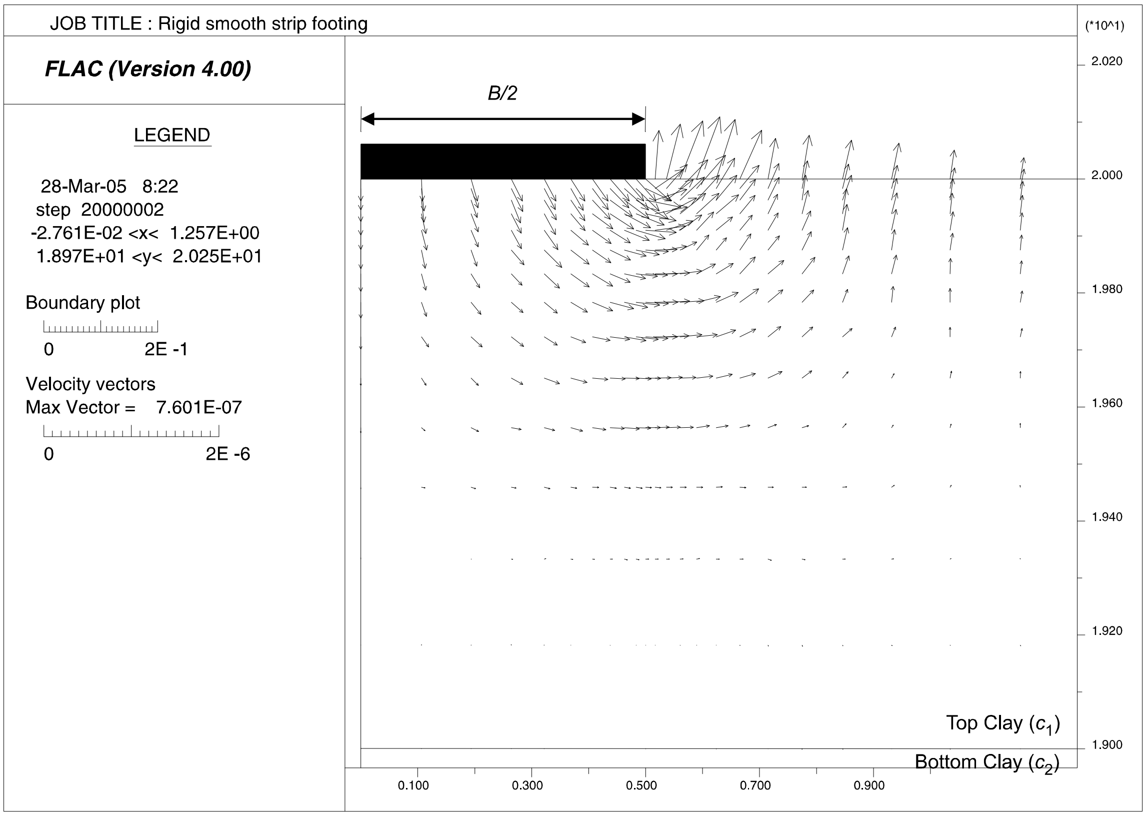

Figure A.169: Velocity vectors for a rigid smooth strip footing on soft over strong clay for 40×30 grid model, $H/B = 1$, $c_1/c_2 = 0.2$.

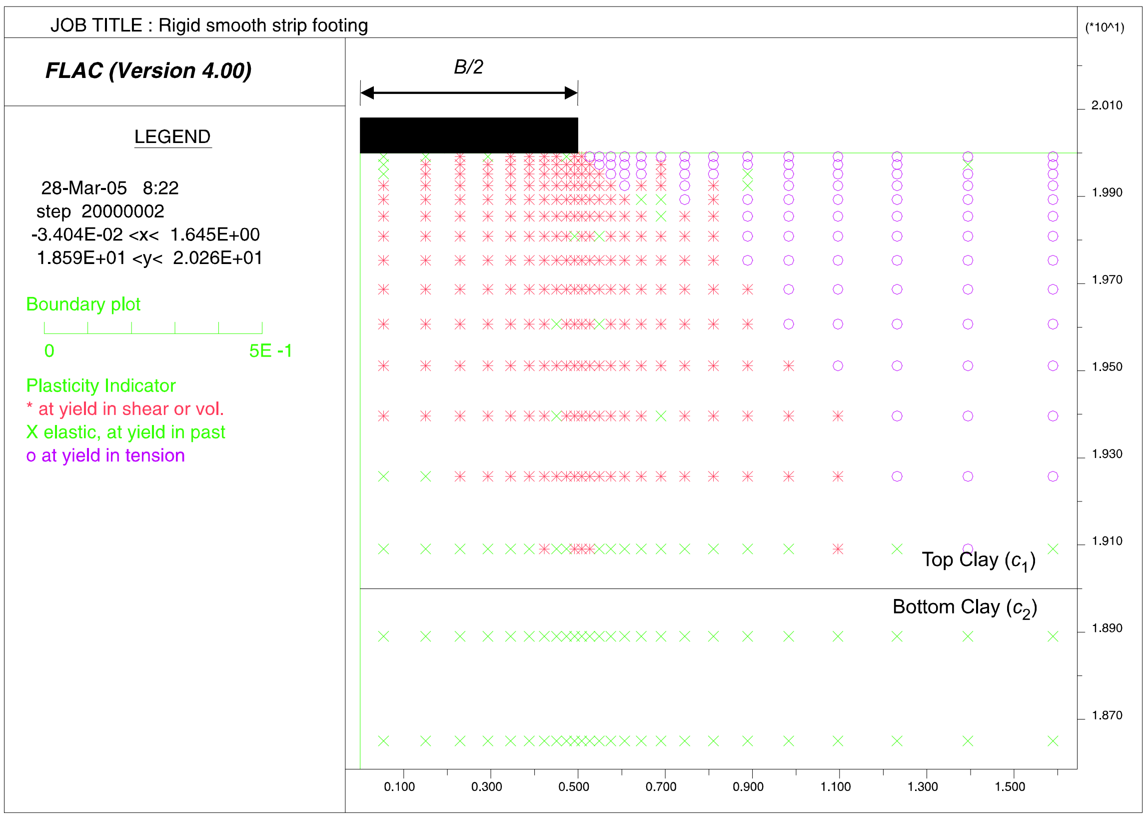

Figure A.170: Plasticity state indicators for a rigid smooth strip footing on soft over strong clay for 40 × 30 grid model, $H/B = 1$, $c_1/c_2 = 0.2$.

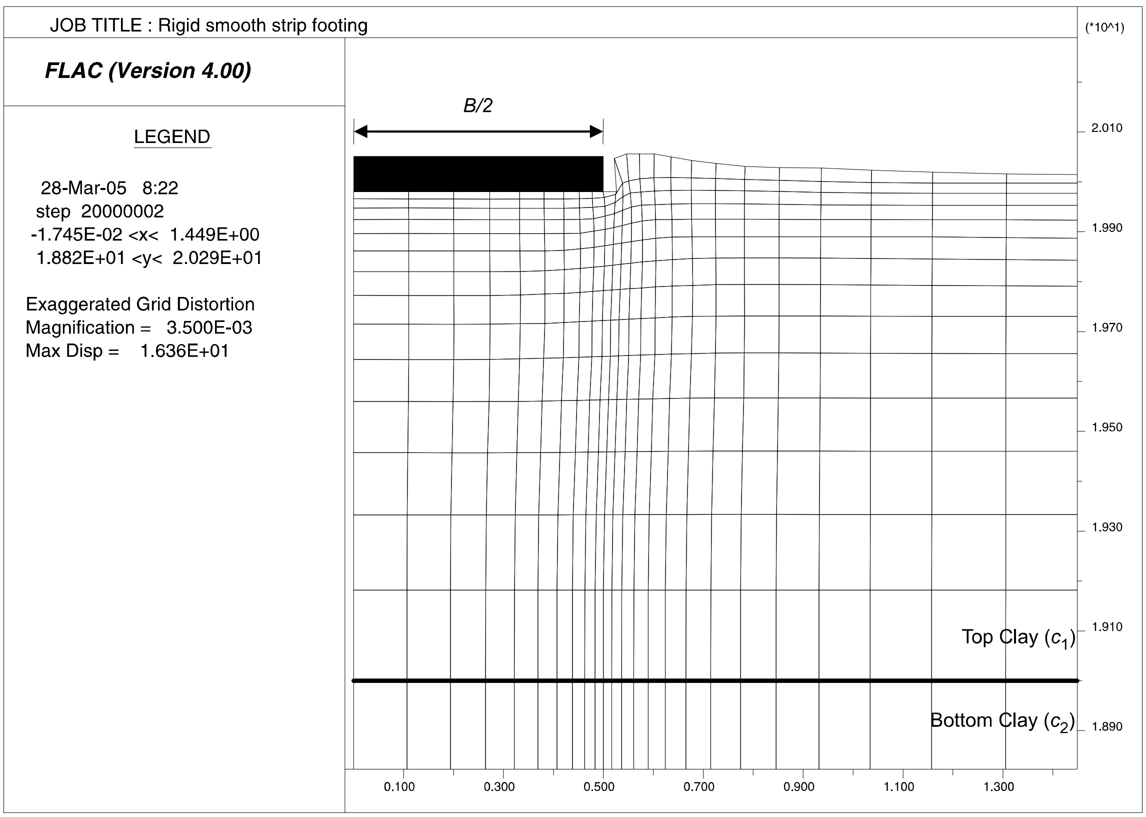

Figure A.171: Magnified grid for a rigid smooth strip footing on soft over strong clay for 40×30 grid model, $H/B = 1$, $c_1/c_2 = 0.2$.

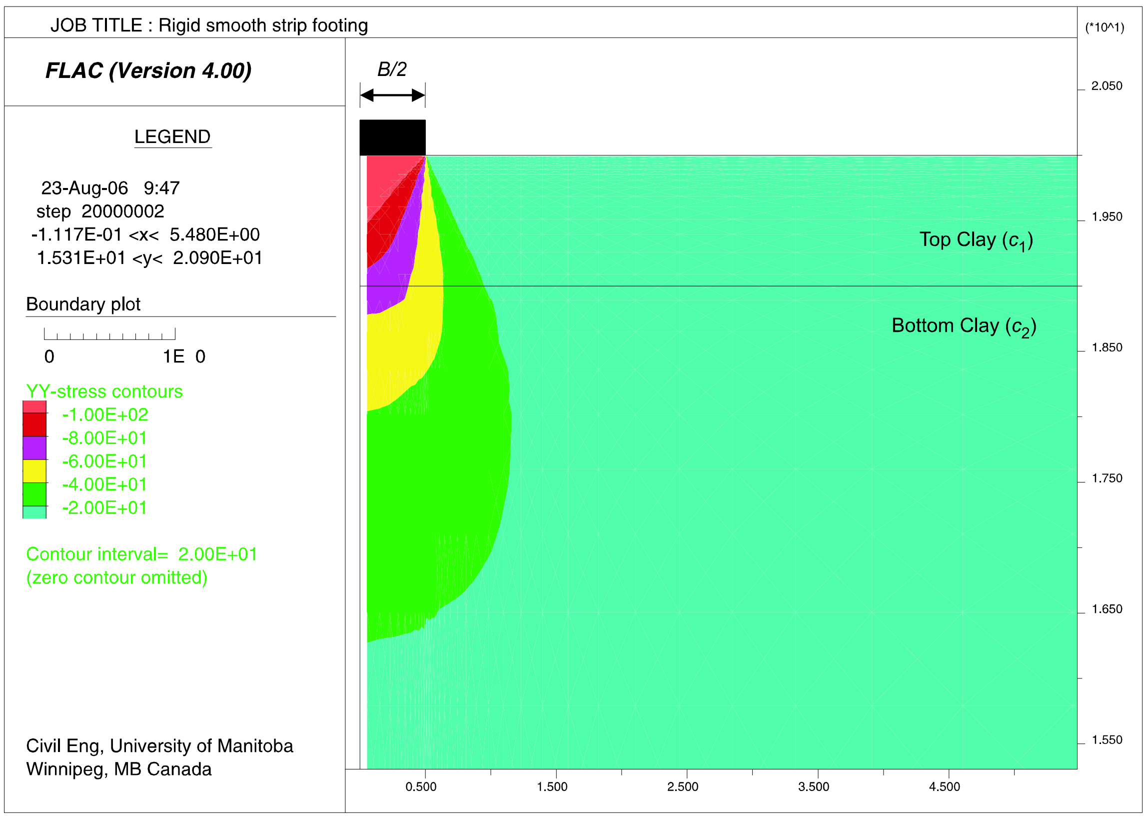

Figure A.172: Vertical stress (σ_{yy}) contours for a rigid smooth strip footing on soft over strong clay for 40×30 grid model, $H/B = 1$, $c_1/c_2 = 0.2$.

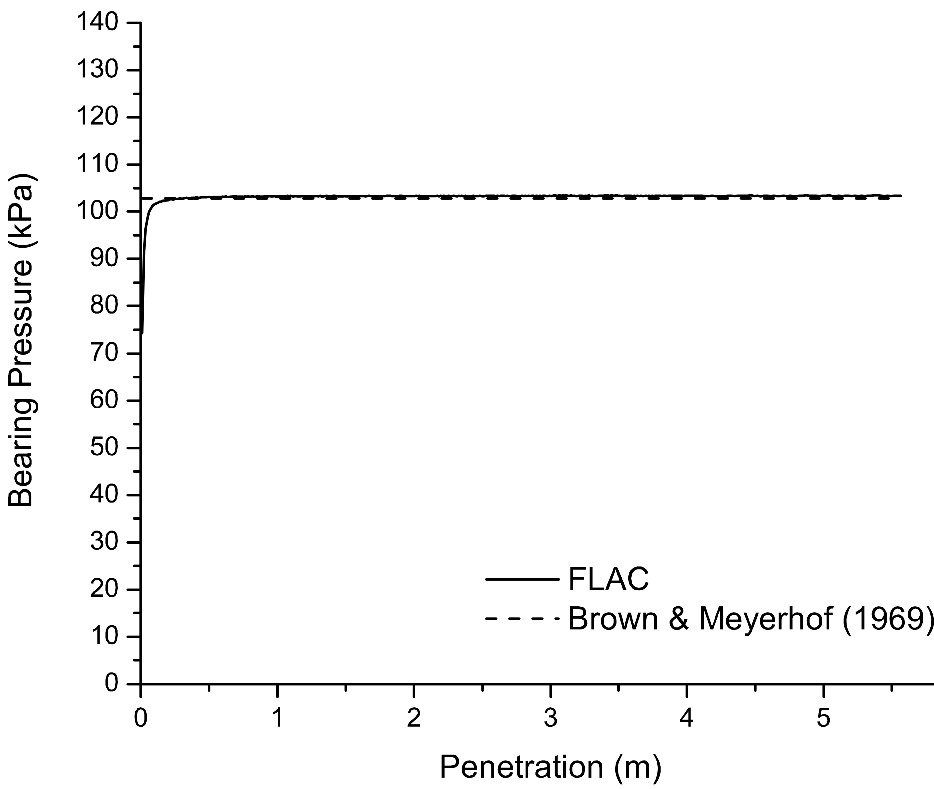

Figure A.173: Bearing pressure versus penetration curve for a rigid smooth strip footing on soft over strong clay for 40 × 30 grid model, $H/B = 1$, $c_1/c_2 = 0.2$.

Case 7: $c_1/c_2 = 0.1$ or $c_2/c_1 = 10$ - Small Deformation Analysis

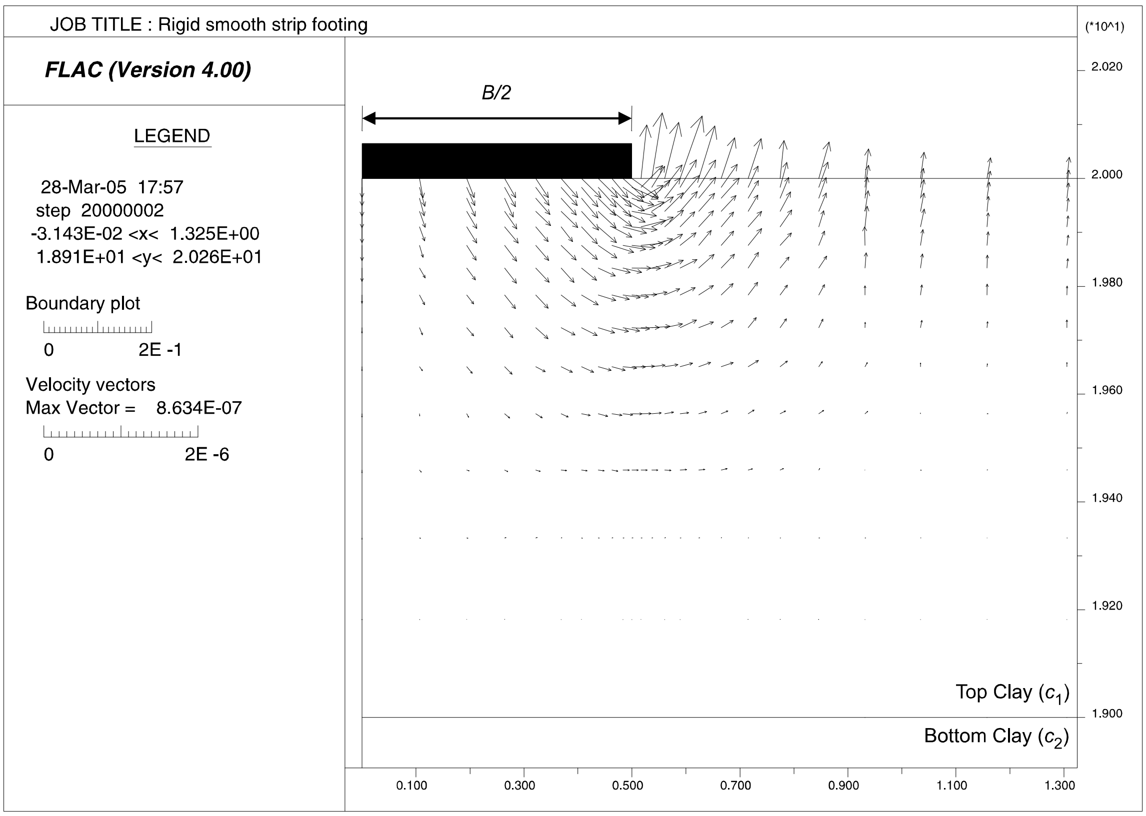

Figure A.174: Velocity vectors for a rigid smooth strip footing on soft over strong clay for 40×30 grid model, $H/B = 1$, $c_1/c_2 = 0.1$.

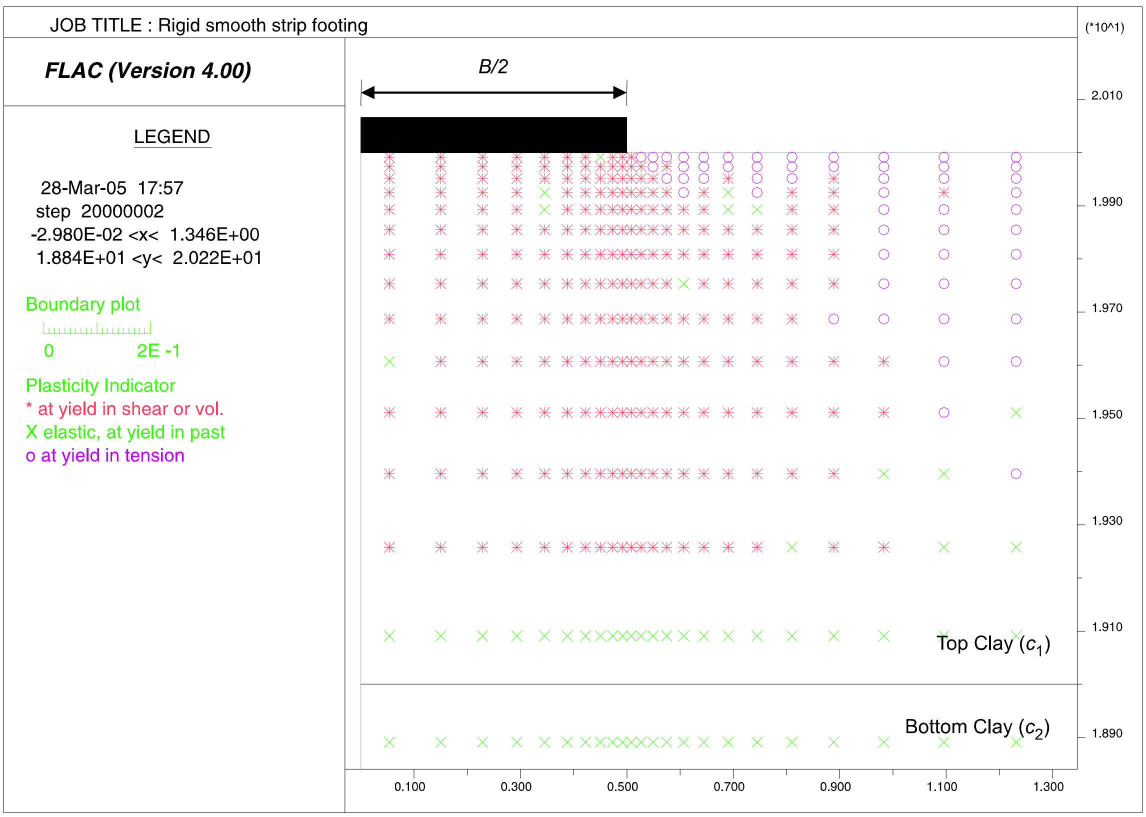

Figure A.175: Plasticity state indicators for a rigid smooth strip footing on soft over strong clay for 40×30 grid model, $H/B = 1$, $c_1/c_2 = 0.1$.

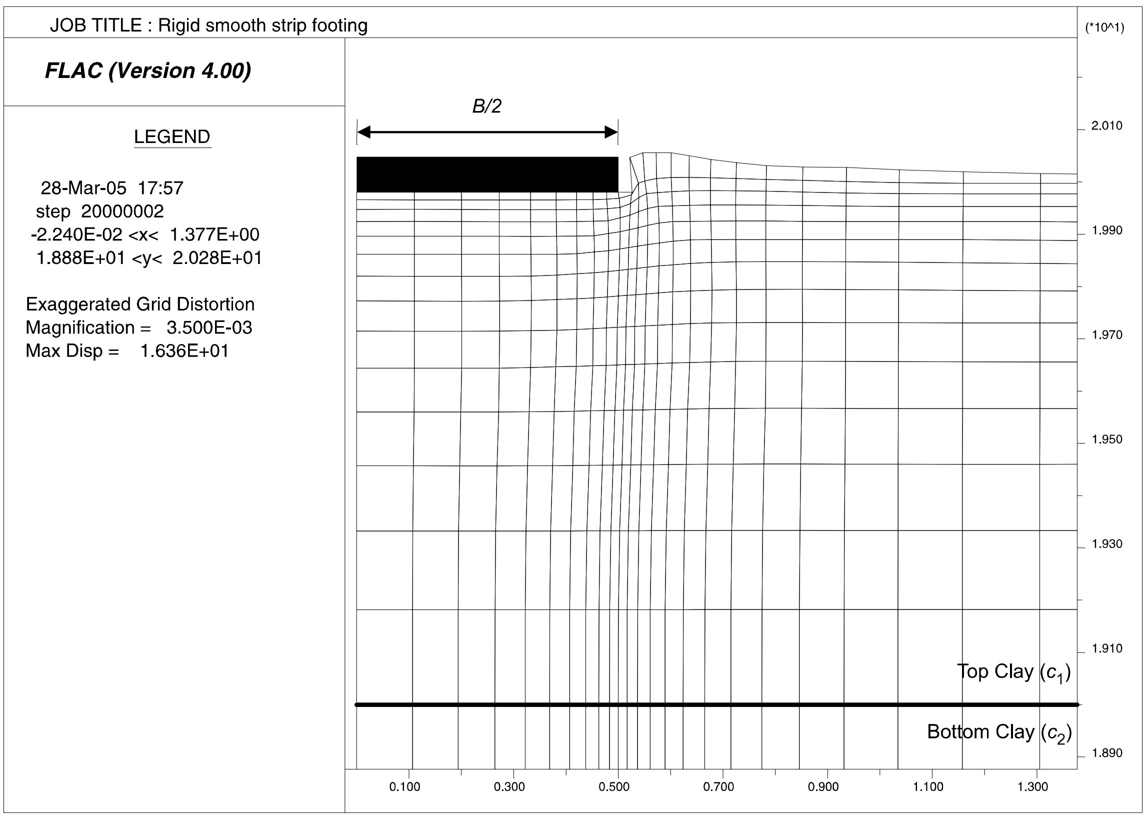

Figure A.176: Magnified grid for a rigid smooth strip footing on soft over strong clay for 40×30 grid model, $H/B = 1$, $c_1/c_2 = 0.1$.

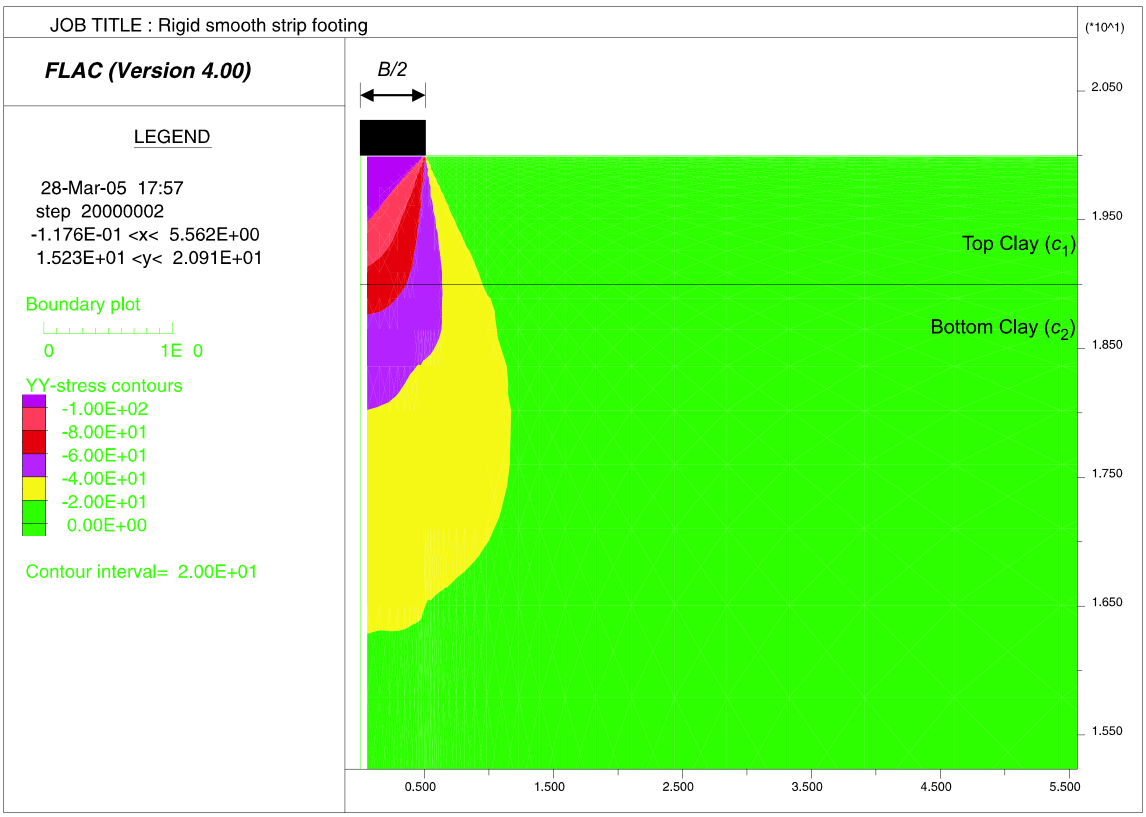

Figure A.177: Vertical stress (σ_{yy}) contours for a rigid smooth strip footing on soft over strong clay for 40×30 grid model, $H/B = 1$, $c_1/c_2 = 0.1$.

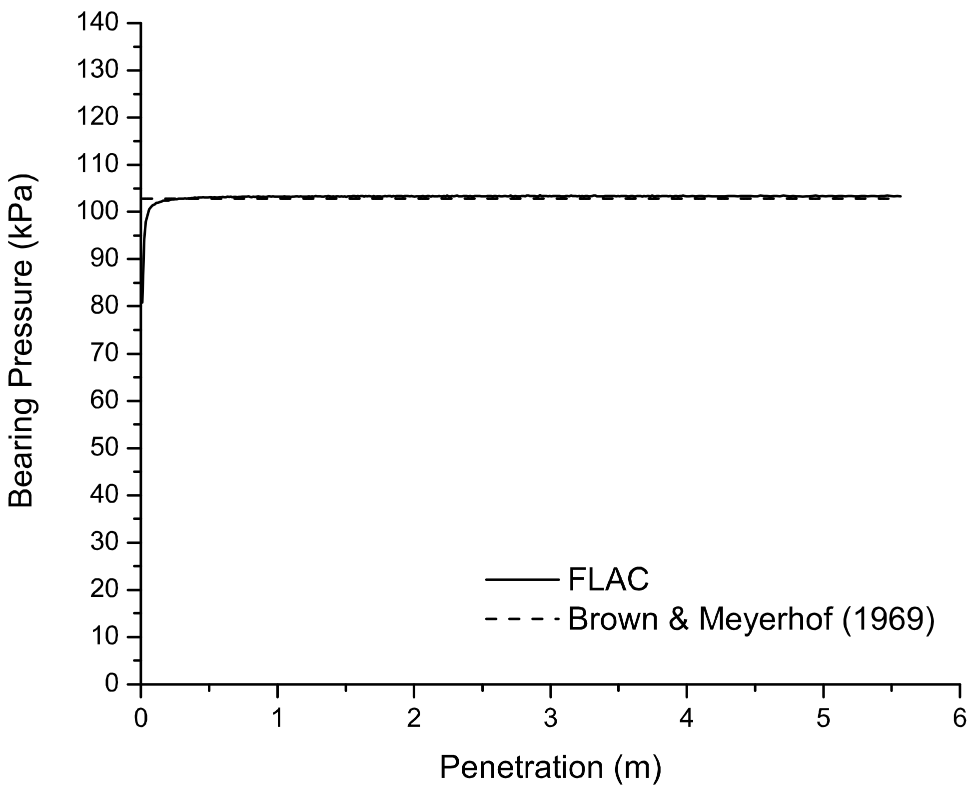

Figure A.178: Bearing pressure versus penetration curve for a rigid smooth strip footing on soft over strong clay for 40×30 grid model, $H/B = 1$, $c_1/c_2 = 0.1$.

A.2.2 Rigid Smooth Strip Footing on Soft over Strong Clay ($H/B = 0.5$)

Case 2: $c_1/c_2 = 0.8$ **or** $c_2/c_1 = 1.25$**- Small Deformation Analysis**

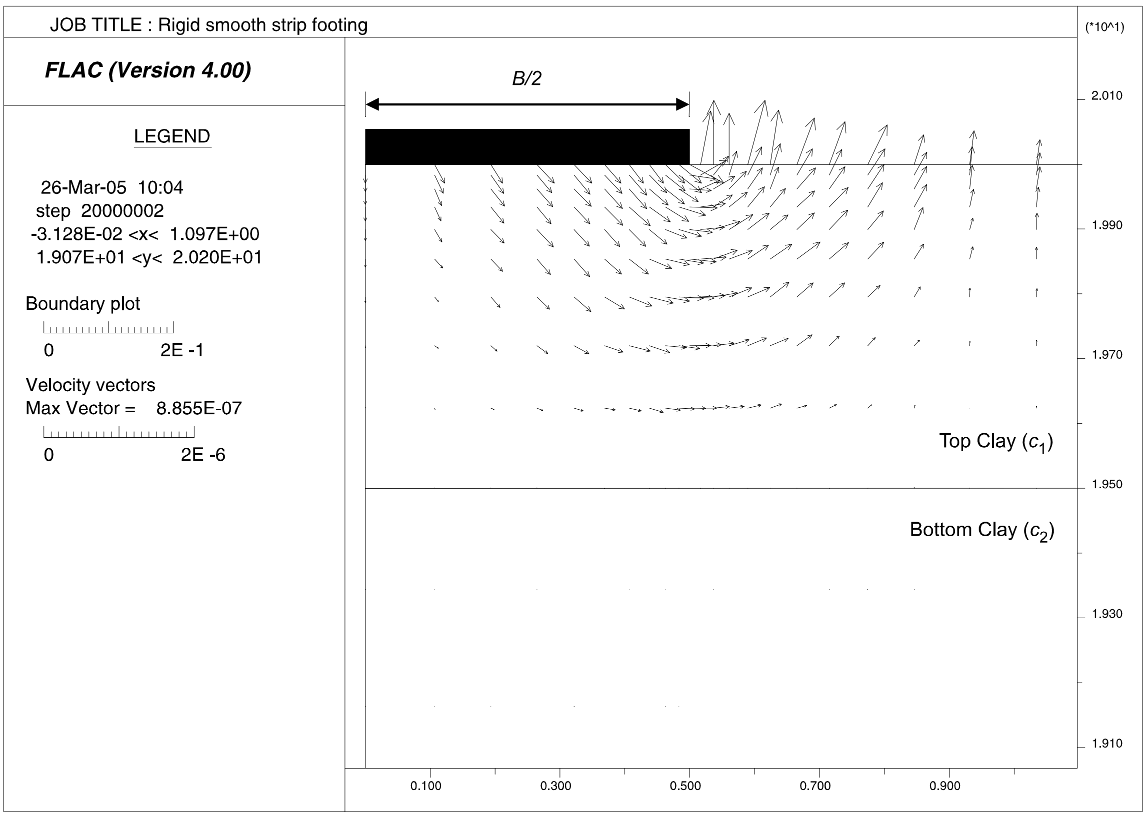

Figure A.179: Velocity vectors for a rigid strip footing on soft over strong clay for 40×30 grid model, $H/B = 0.5$, $c_1/c_2 = 0.8$.

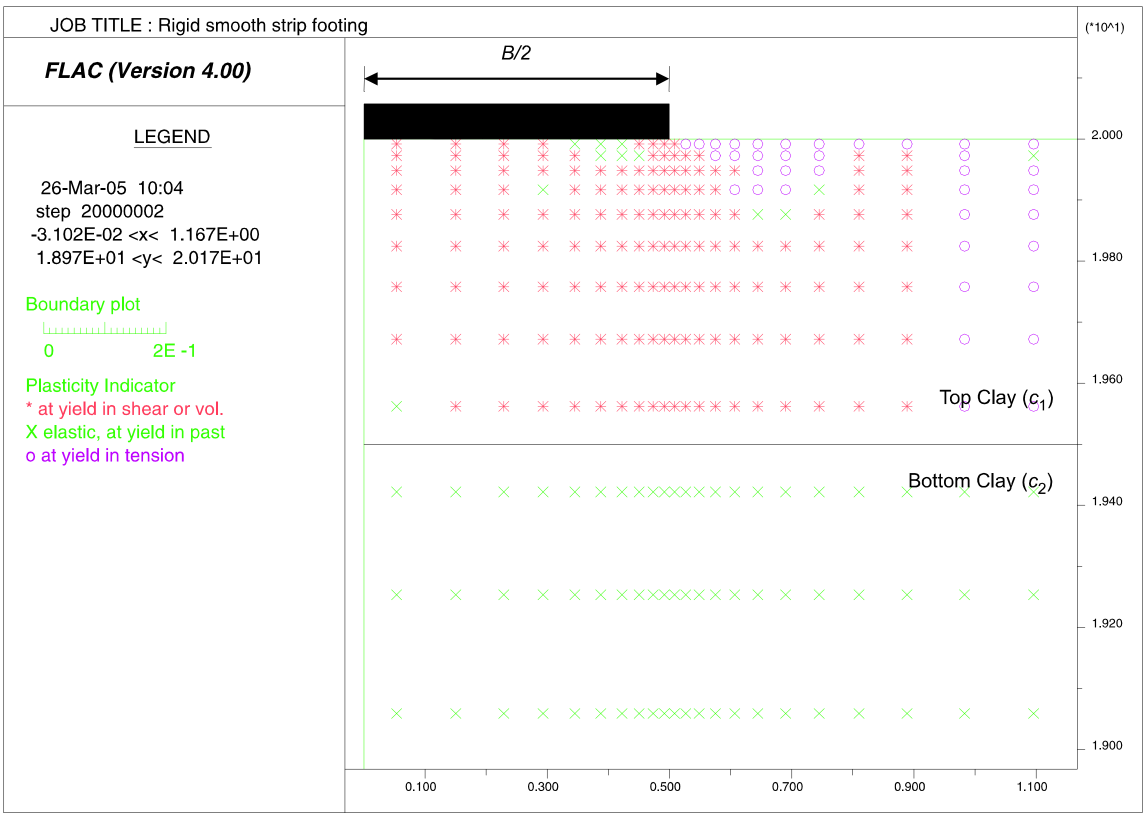

Figure A.180: Plasticity indicators for a rigid smooth strip footing on soft over strong clay for 40 × 30 grid model, $H/B = 0.5$, $c_1/c_2 = 0.8$.

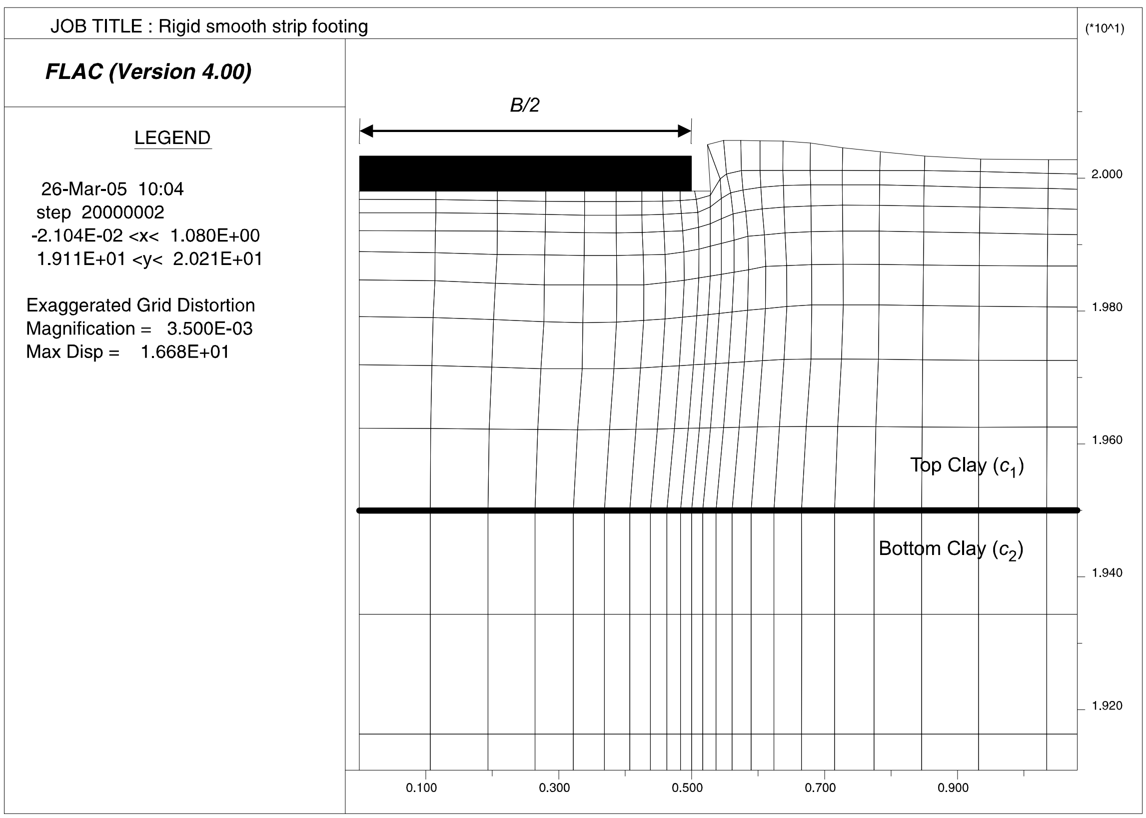

Figure A.181: Magnified grid for a rigid smooth strip footing on soft over strong clay for 40 × 30 grid model, $H/B = 0.5$, $c_1/c_2 = 0.8$.

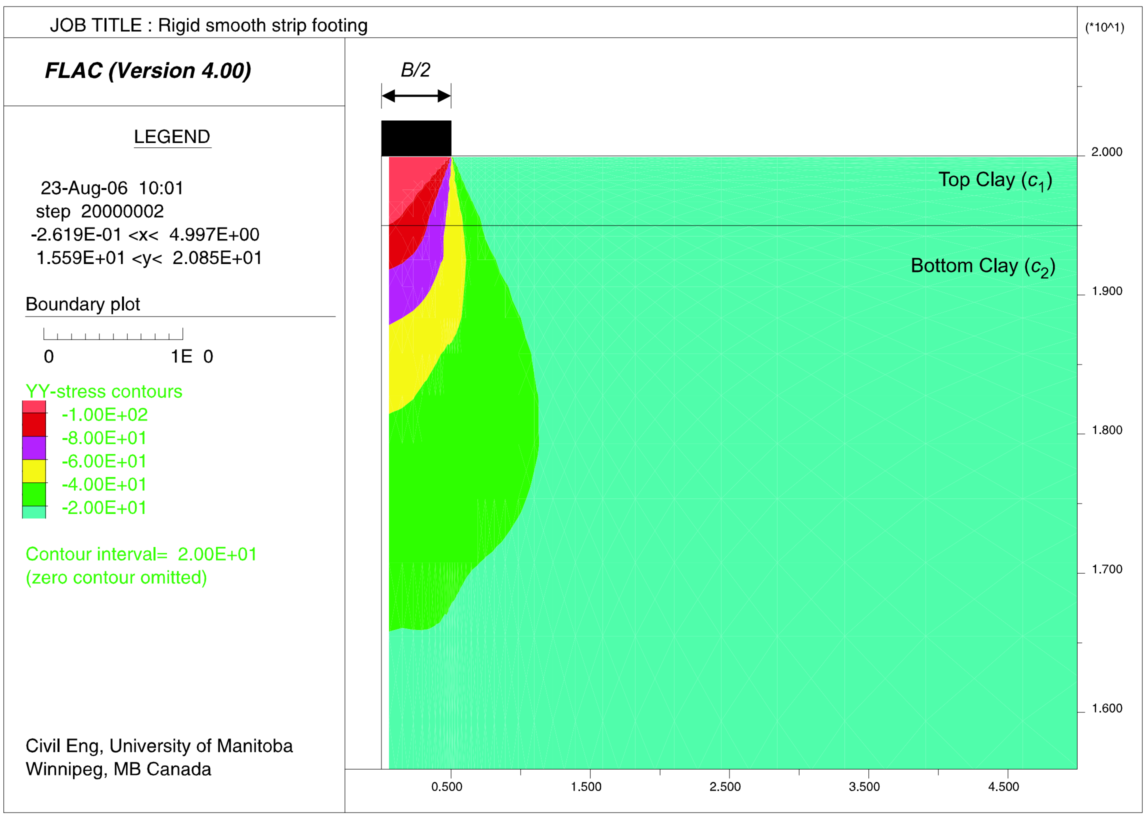

Figure A.182: Vertical stress (σ_{yy}) contours for a rigid smooth strip footing on soft over strong clay for 40×30 grid model, $H/B = 0.5$, $c_1/c_2 = 0.8$.

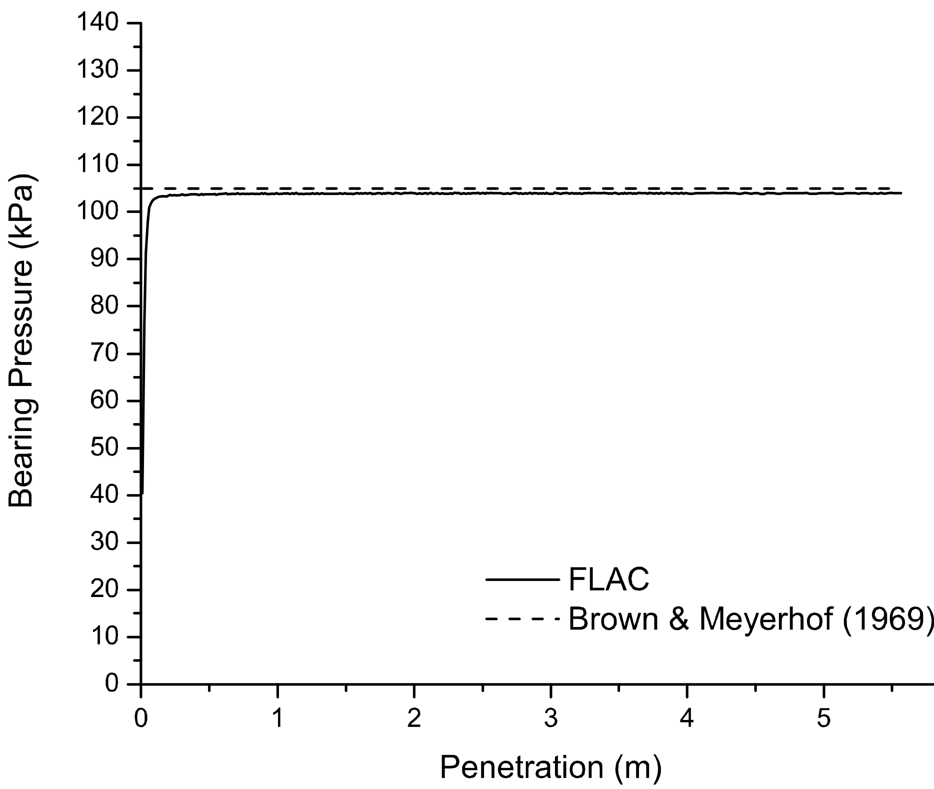

Figure A.183: Bearing pressure versus penetration curve for a rigid smooth strip footing on soft clay over strong clay for 40×30 grid model, $H/B = 0.5$, $c_1/c_2 = 0.8$.

Case 3: $c_1/c_2 = 2/3$ **or** $c_2/c_1 = 1.5$ **- Small Deformation Analysis**

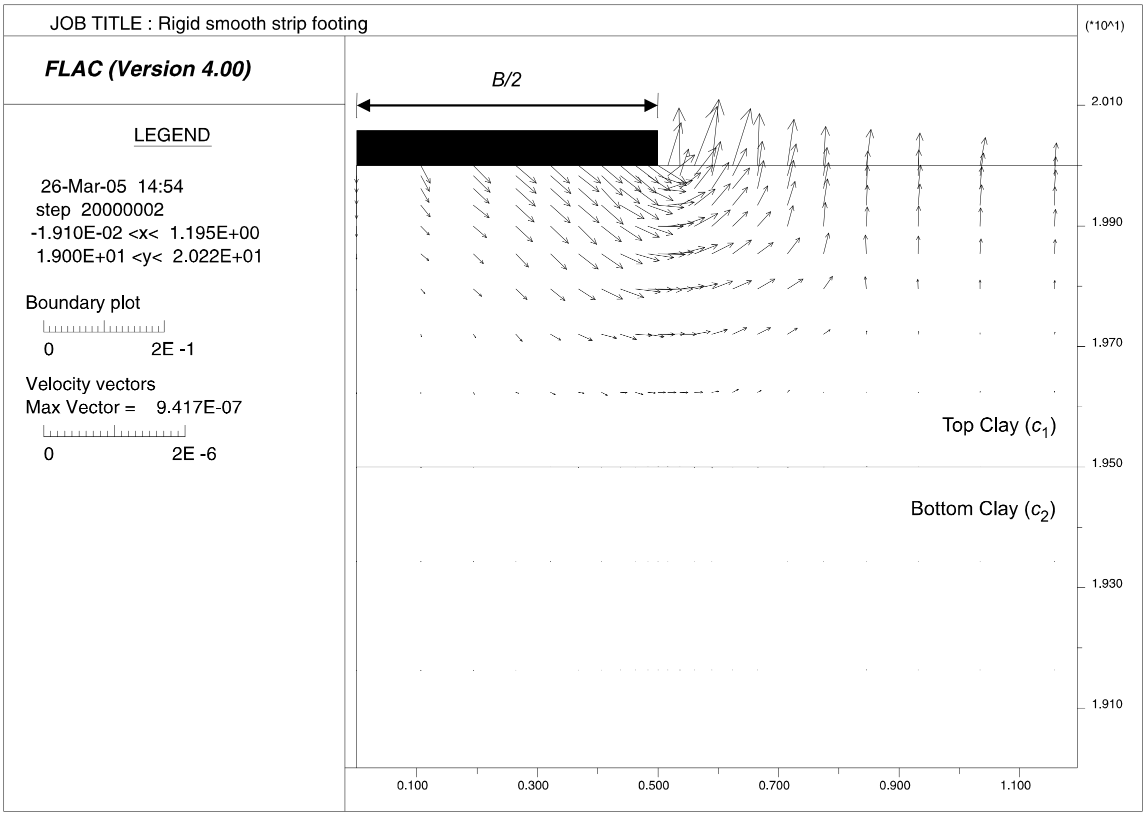

Figure A.184: Velocity vectors for a rigid smooth strip footing on soft over strong clay for 40 × 30 grid model, $H/B = 0.5$, $c_1/c_2 = 2/3$.

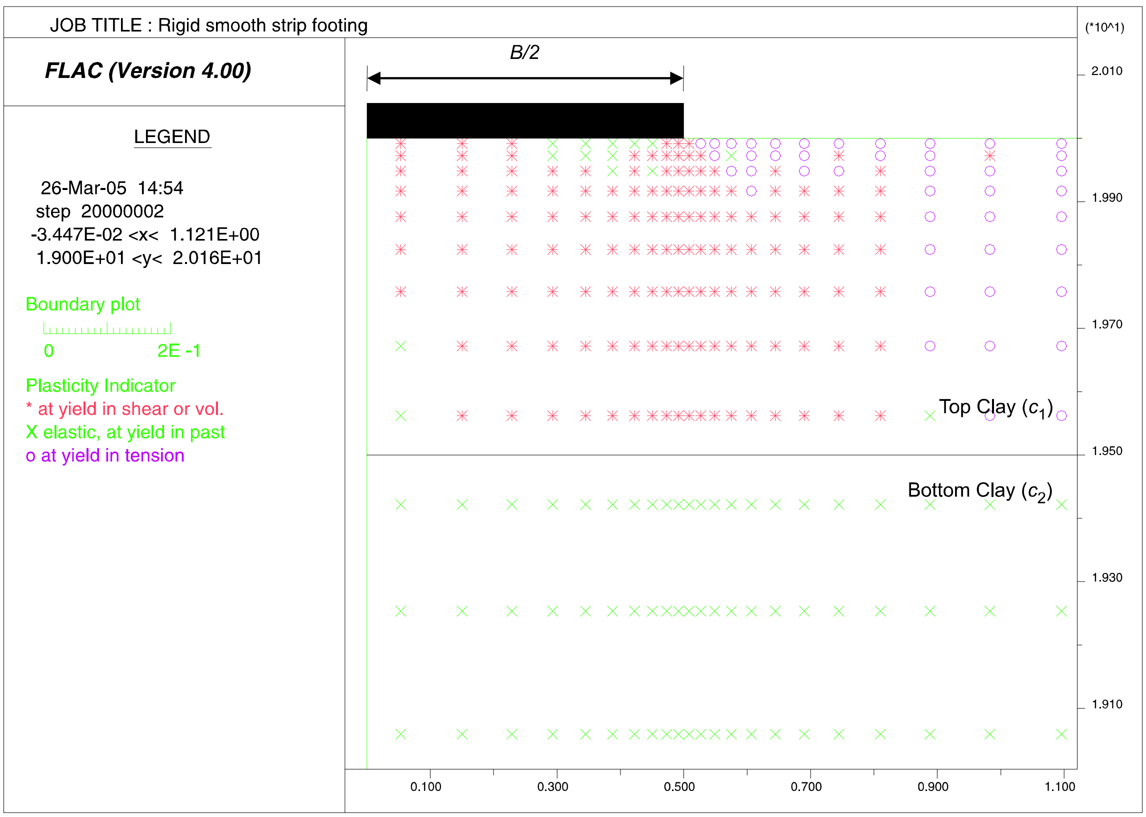

Figure A.185: Velocity vectors for a rigid smooth strip footing on strong over soft clay for 40 × 30 grid model, $H/B = 0.5$, $c_1/c_2 = 2/3$.

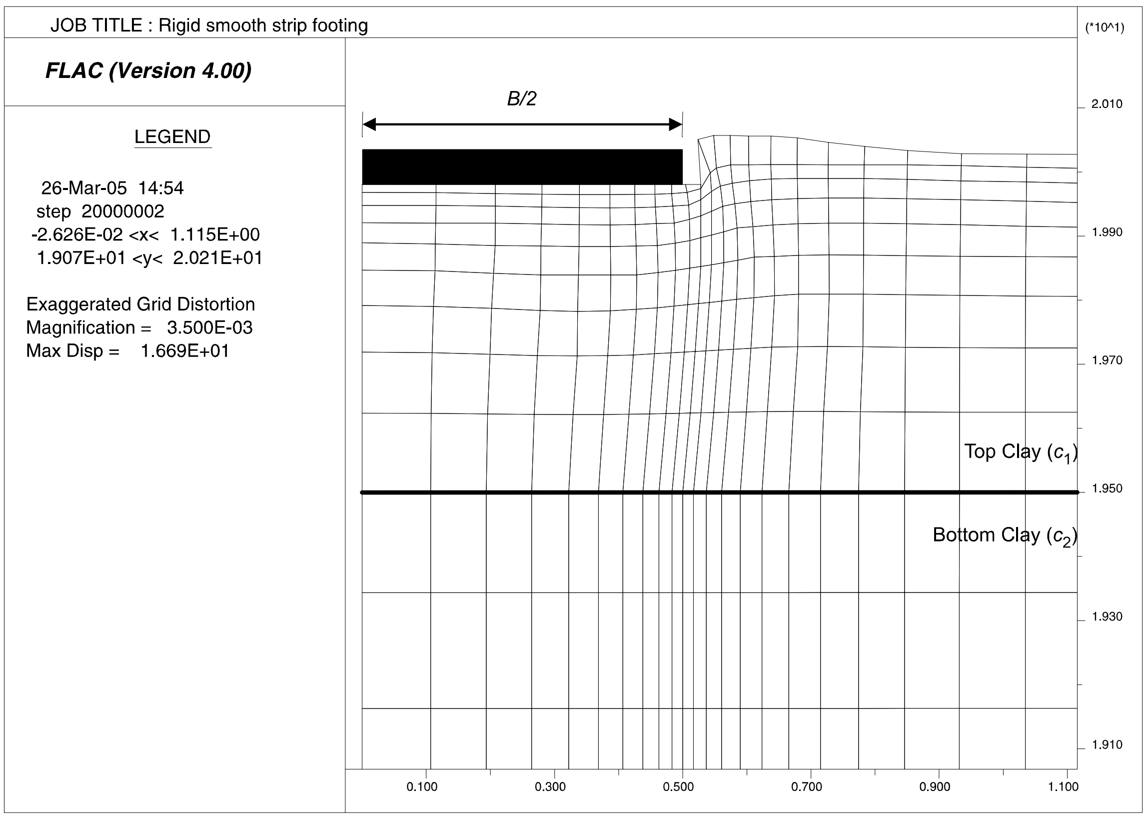

Figure A.186: Magnified grid for a rigid smooth strip footing on soft clay over strong clay for 40×30 grid model, $H/B = 0.5$, $c_1/c_2 = 2/3$.

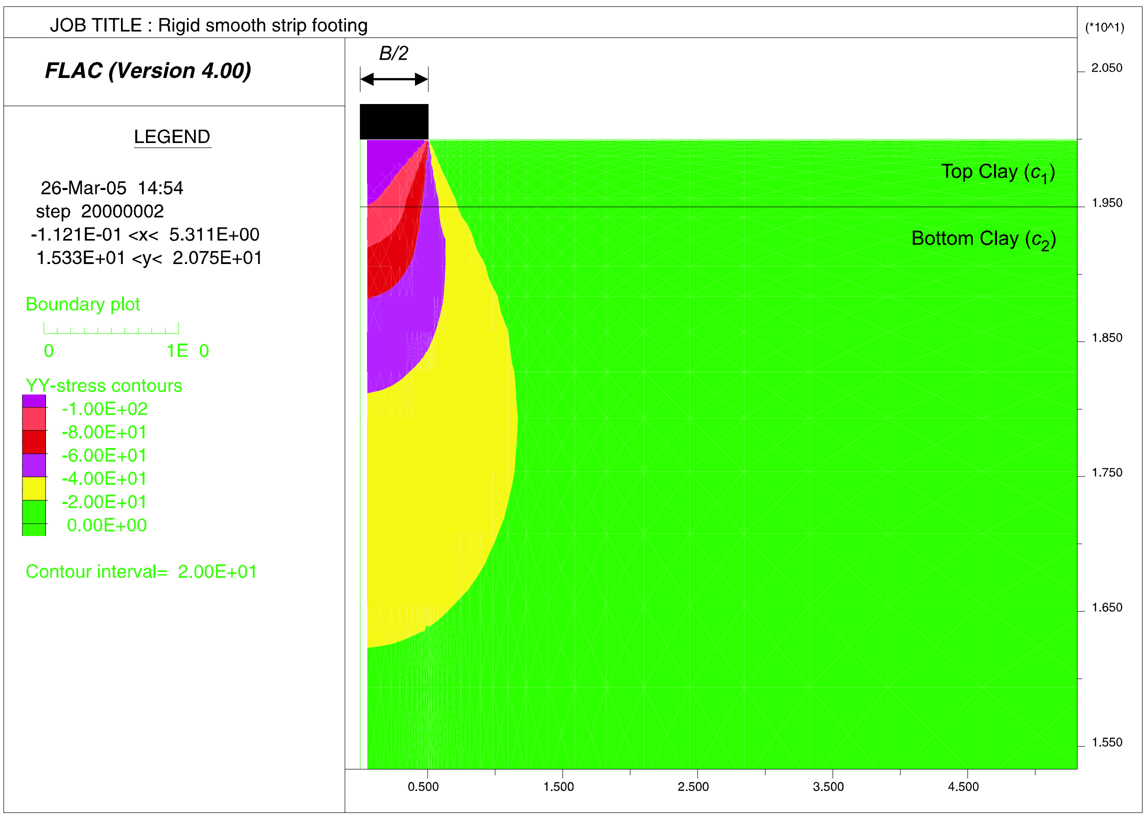

Figure A.187: Vertical stress (σ_{yy}) contours for a rigid smooth strip footing on soft over strong clay for 40×30 grid model, $H/B = 0.5$, $c_1/c_2 = 2/3$.

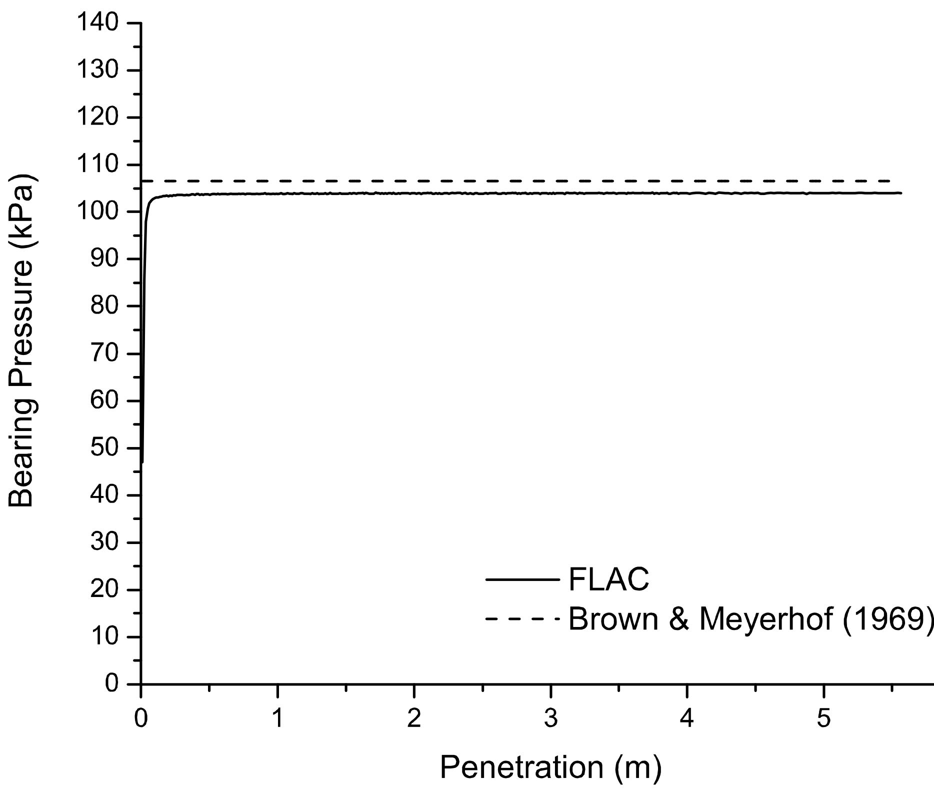

Figure A.188: Bearing pressure versus penetration curve for a rigid smooth strip footing on soft over strong clay for 40 × 30 grid model, $H/B = 0.5$, $c_1/c_2 = 2/3$.

Case 4: $c_1/c_2 = 0.5$ or $c_2/c_1 = 2$ - Small Deformation Analysis

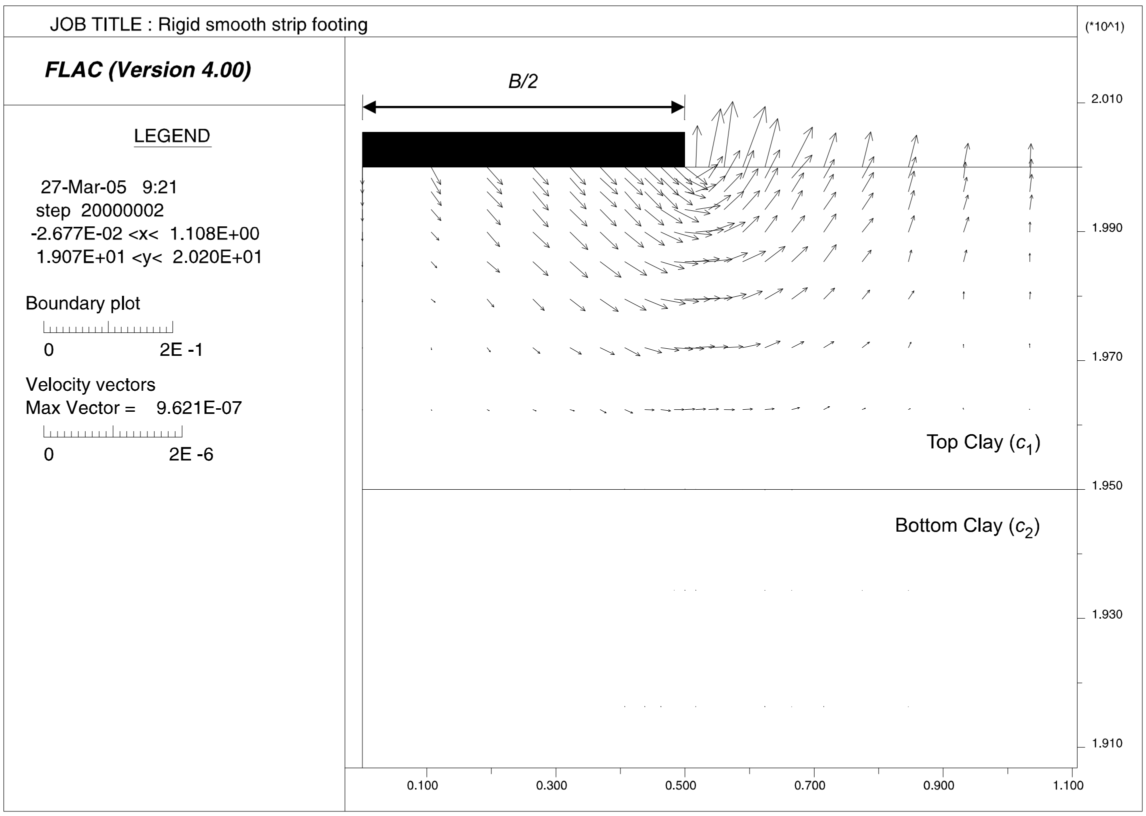

Figure A.189: Displacement vectors and x-displacement contours for a rigid strip footing on strong clay over soft clay for 40×30 grid model, $H/B = 0.5$, $c_1/c_2 = 0.5$.

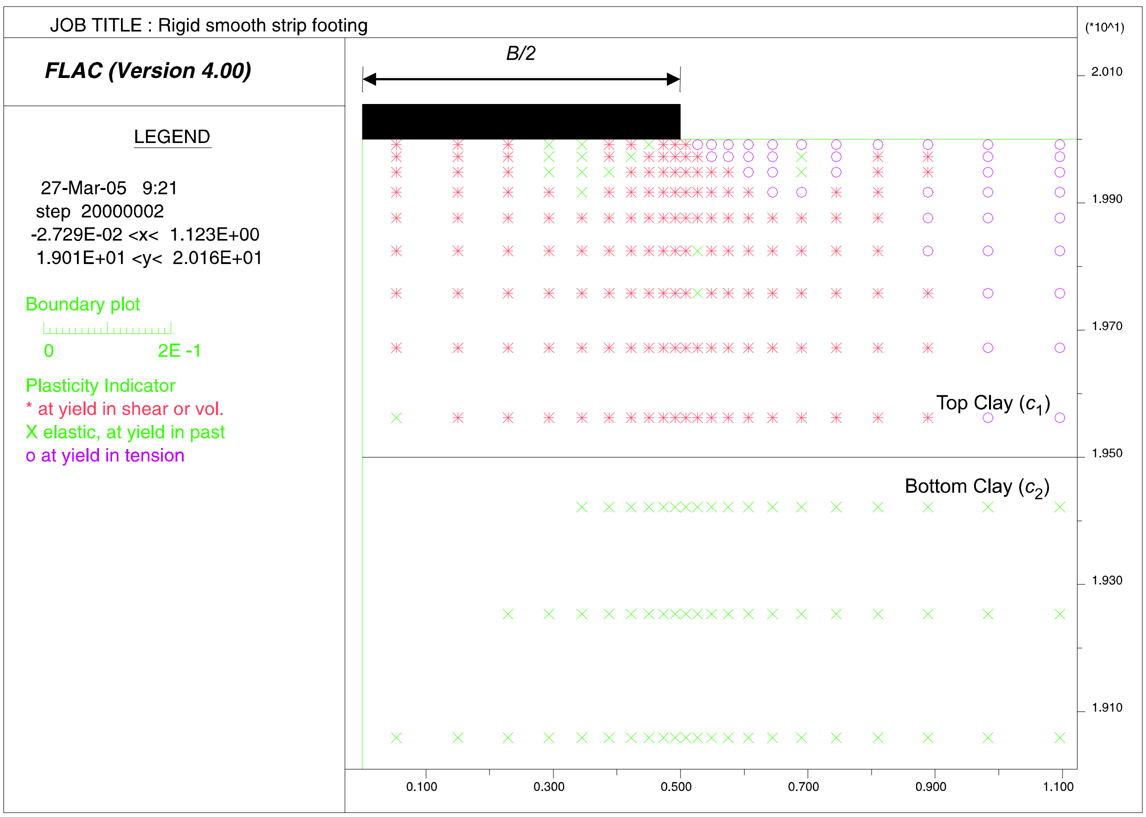

Figure A.190: Plasticity state indicators for a rigid smooth strip footing on soft clay over strong clay for 40 × 30 grid model, $H/B = 0.5$, $c_1/c_2 = 0.5$.

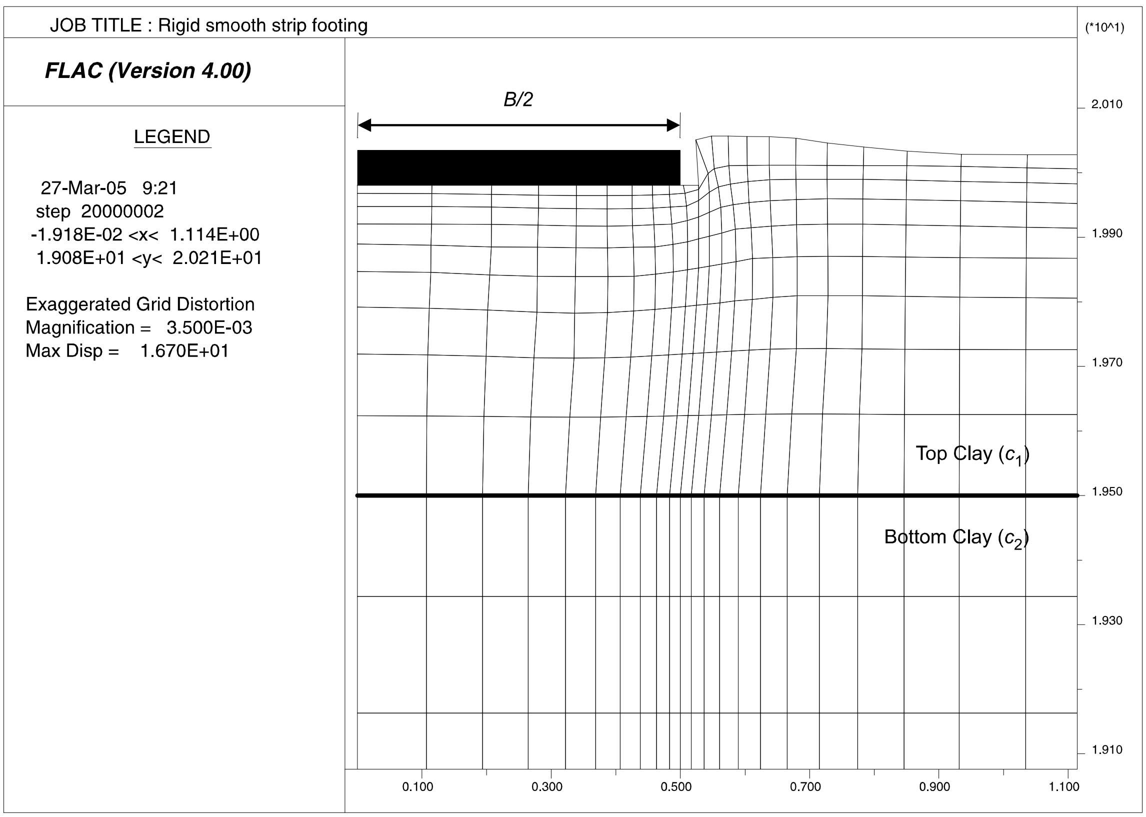

Figure A.191: Magnified grid for a rigid smooth strip footing on soft clay over strong clay for 40 × 30 grid model, $H/B = 0.5$, $c_1/c_2 = 2/3$.

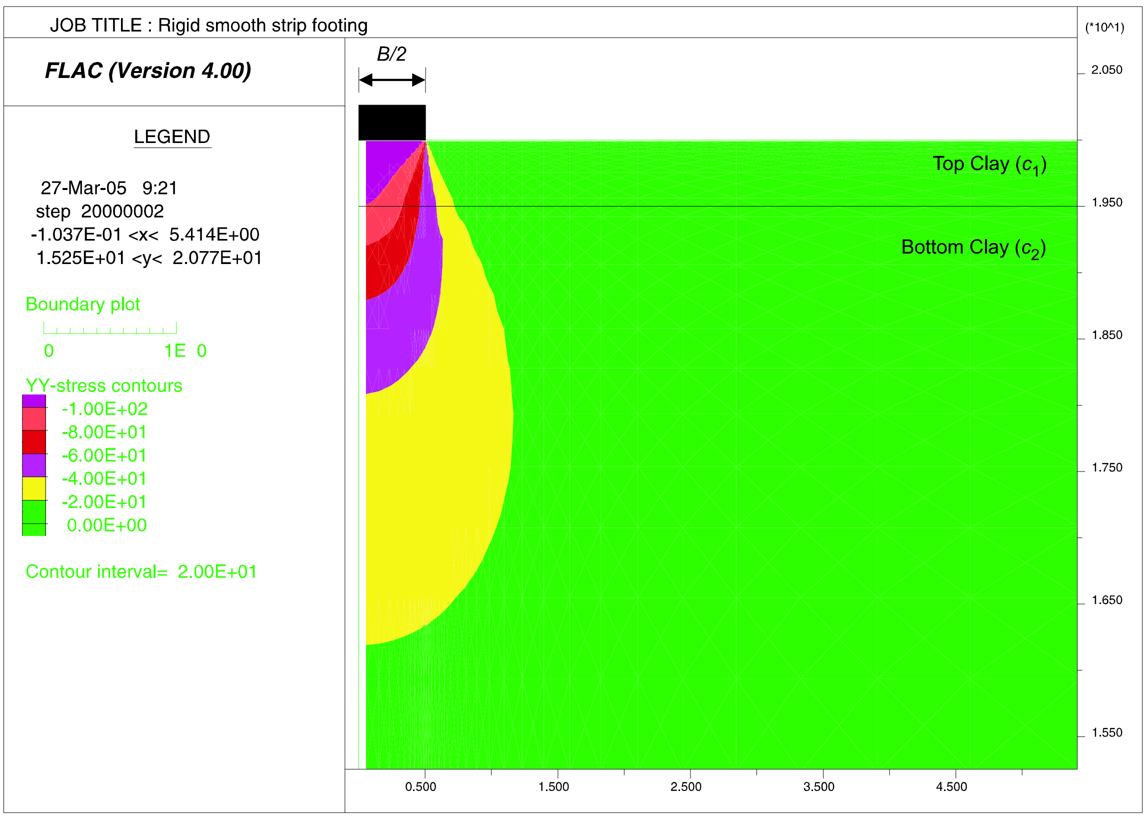

Figure A.192: Vertical stress (σ_{yy}) contours for a rigid smooth strip footing on soft clay over strong clay for 40 × 30 grid model, $H/B = 0.5$, $c_1/c_2 = 0.5$.

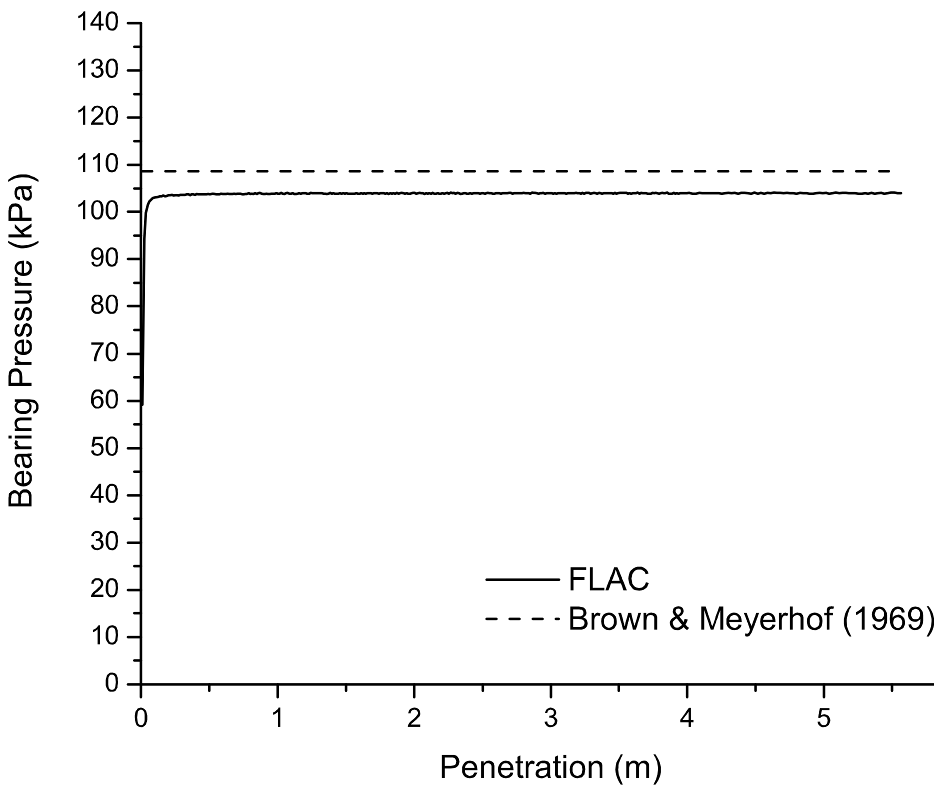

Figure A.193: Bearing pressure versus penetration curve for a rigid smooth strip footing on soft clay over strong clay for 40 × 30 grid model, $H/B = 0.5$, $c_1/c_2 = 0.5$.

Case 5: $c_1/c_2 = 1/3$ or $c_2/c_1 = 3$ - Small Deformation Analysis

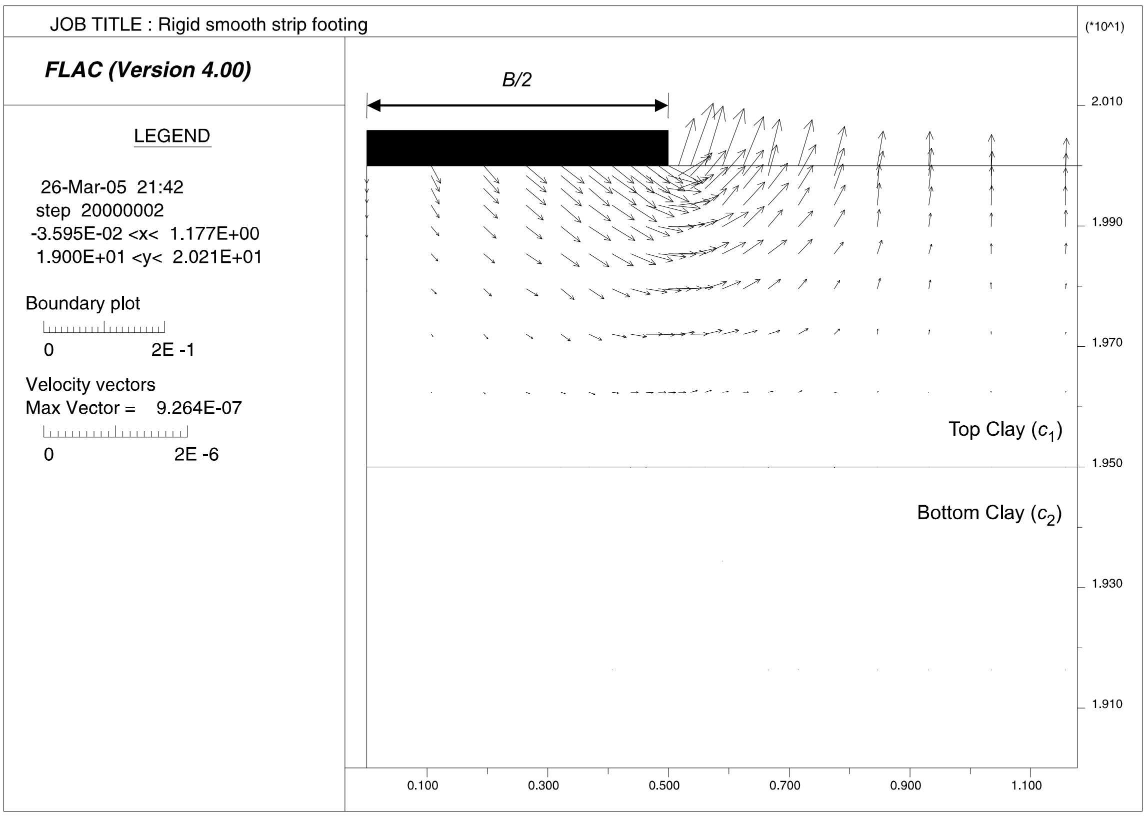

Figure A.194: Velocity vectors for a rigid smooth strip footing on soft clay over strong clay for 40×30 grid model, $H/B = 0.5$, $c_1/c_2 = 1/3$.

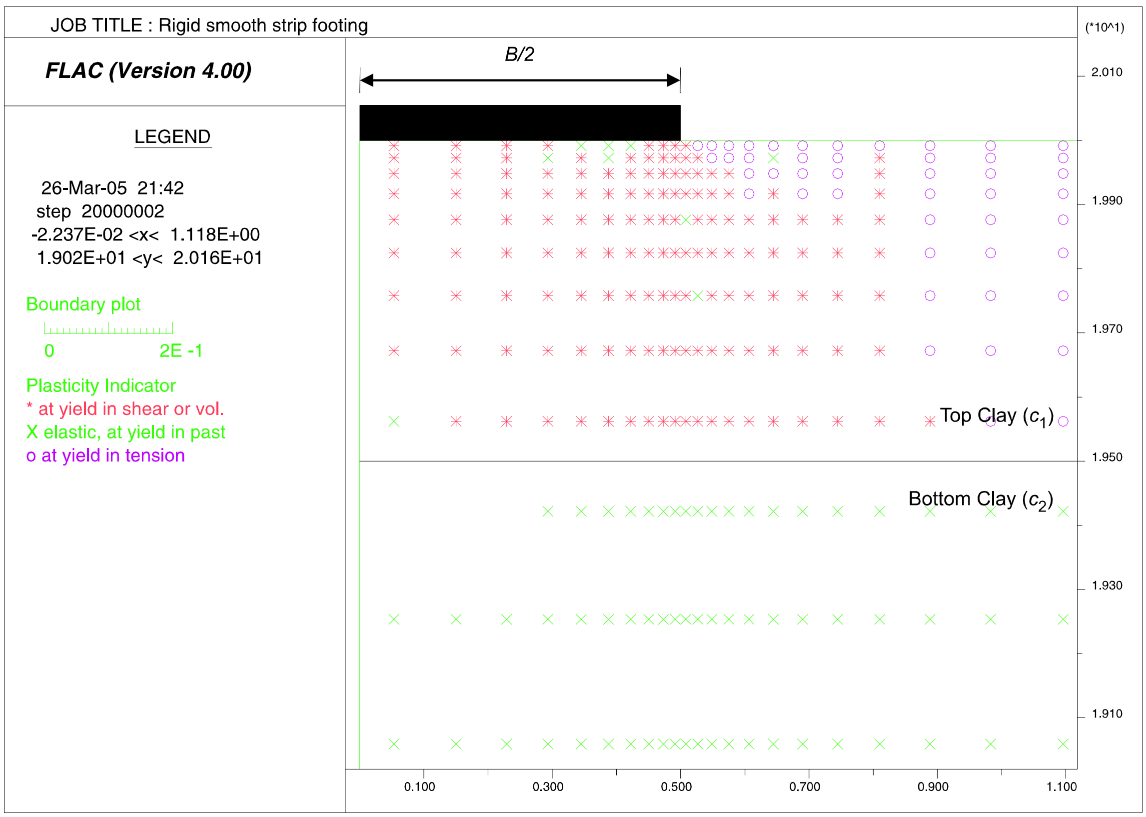

Figure A.195: Plasticity state indicators for a rigid smooth strip footing on soft clay over strong clay for 40×30 grid model, $H/B = 0.5$, $c_1/c_2 = 1/3$.

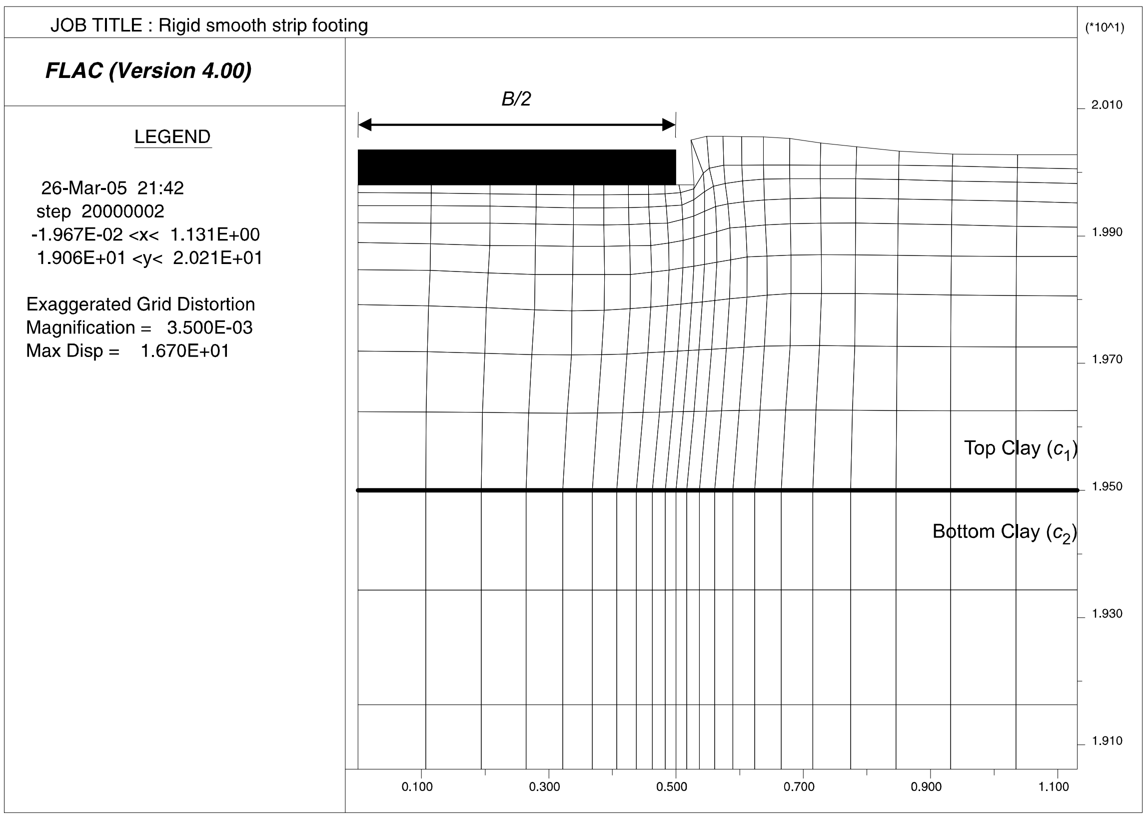

Figure A.196: Magnified grid for a rigid smooth strip footing on soft clay over strong clay for 40×30 grid model, $H/B = 0.5$, $c_1/c_2 = 1/3$.

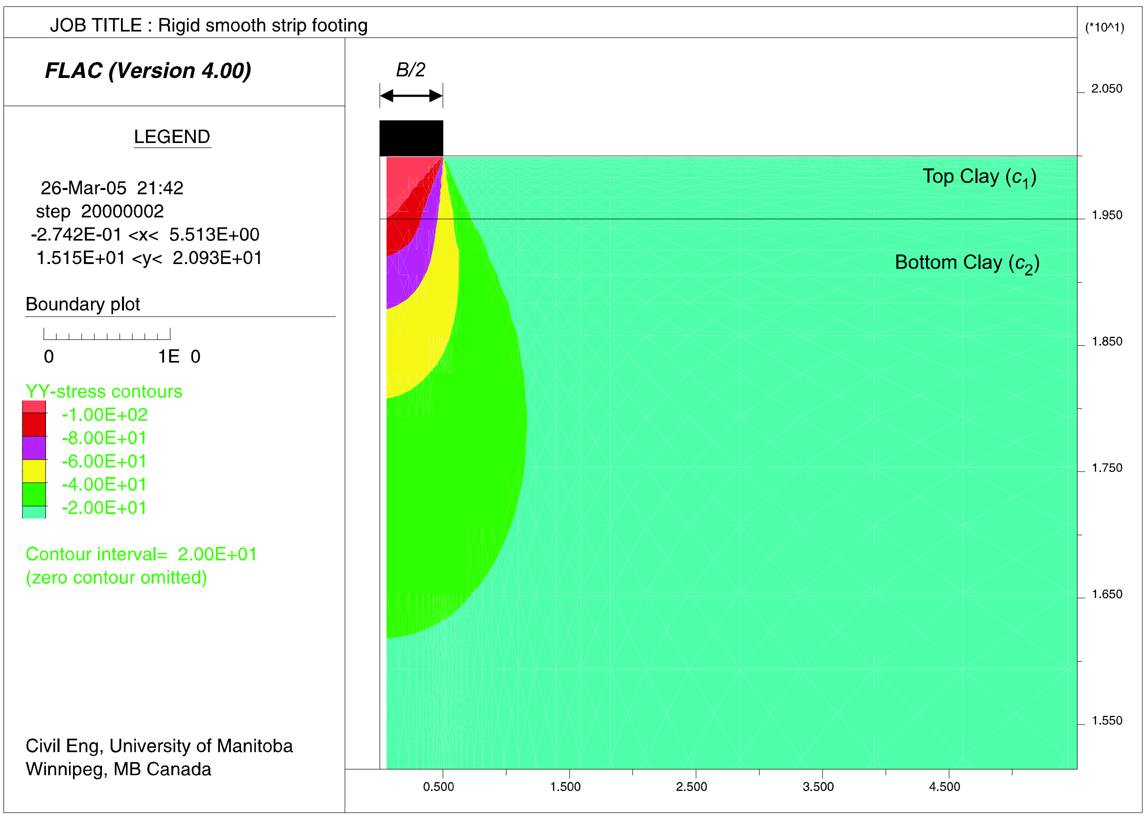

Figure A.197: Vertical stress (σ_{yy}) contours for a rigid smooth strip footing on soft clay over strong clay for 40×30 grid model, $H/B = 0.5$, $c_1/c_2 = 1/3$.

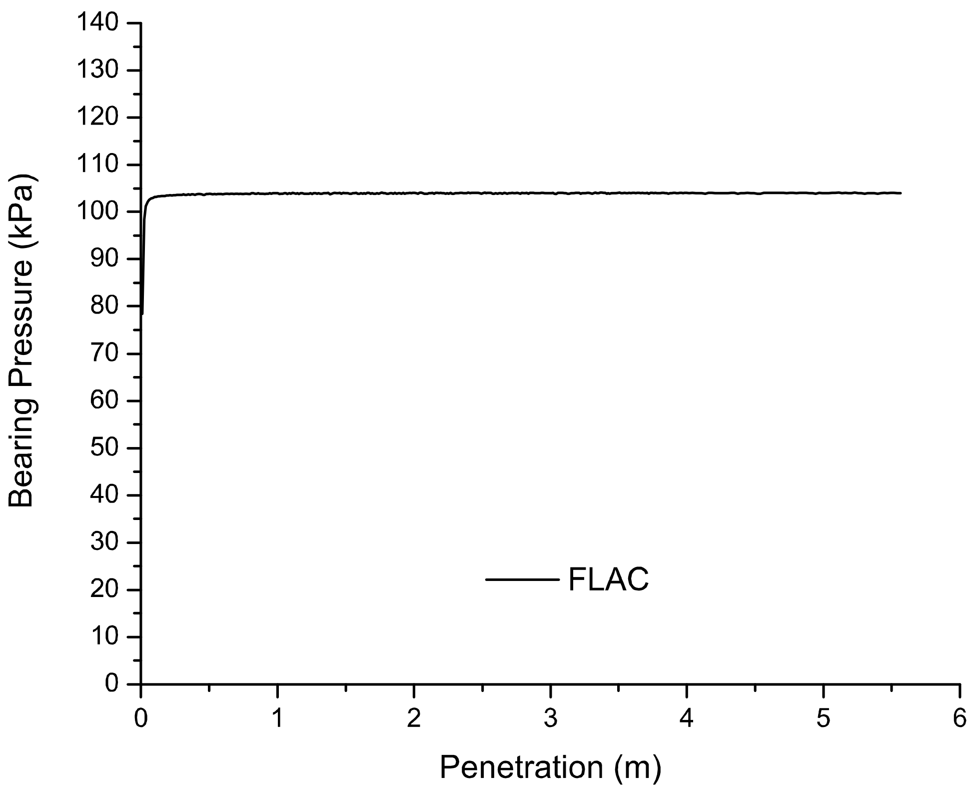

Figure A.198: Bearing pressure versus penetration curve for a rigid smooth strip footing on soft clay over strong clay for 40×30 grid model, $H/B = 0.5$, $c_1/c_2 = 1/3$.

Case 6: $c_1/c_2 = 0.2$ or $c_2/c_1 = 5$ - Small Deformation Analysis

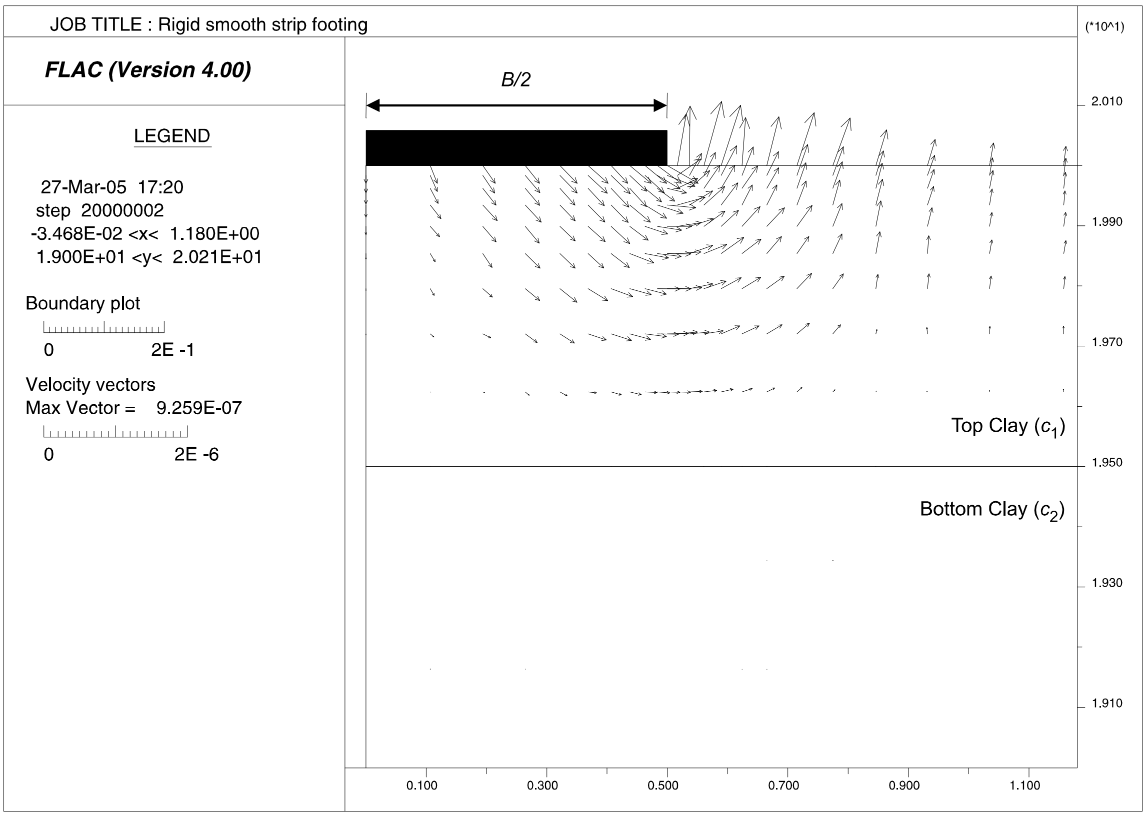

Figure A.199: Plasticity state indicators for a rigid smooth strip footing on soft clay over strong clay for 40×30 grid model, $H/B = 0.5$, $c_1/c_2 = 0.2$.

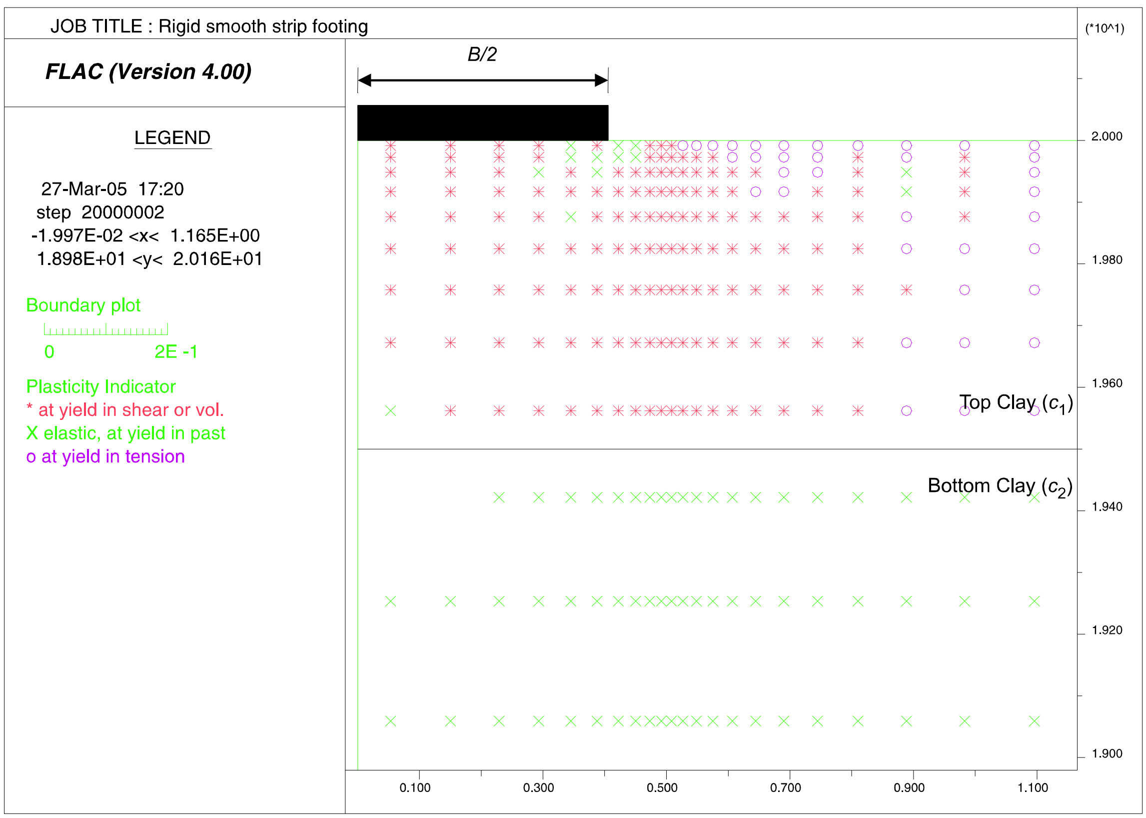

Figure A.200: Plasticity state indicators for a rigid smooth strip footing on soft clay over strong clay for 40 × 30 grid model, $H/B = 0.5$, $c_1/c_2 = 0.2$

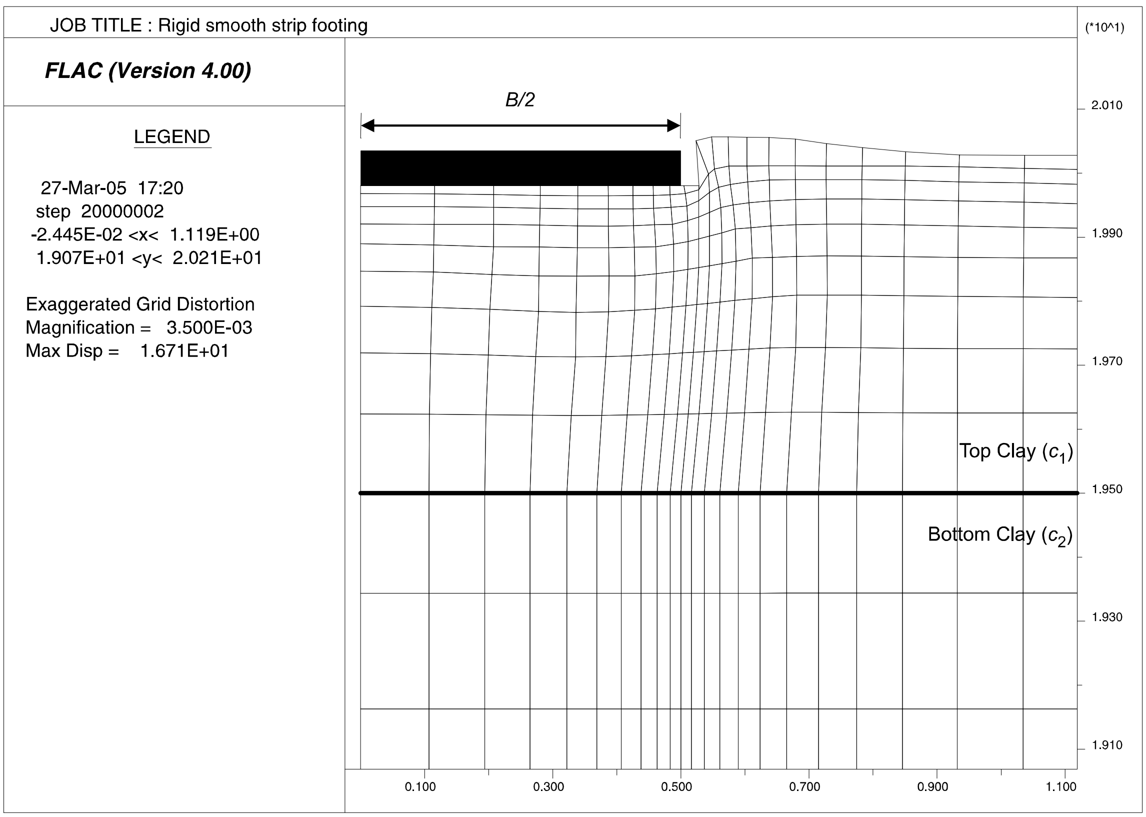

Figure A.201: Magnified grid for a rigid smooth strip footing on soft clay over strong clay for 40 × 30 grid model, $H/B = 0.5$, $c_1/c_2 = 0.2$.

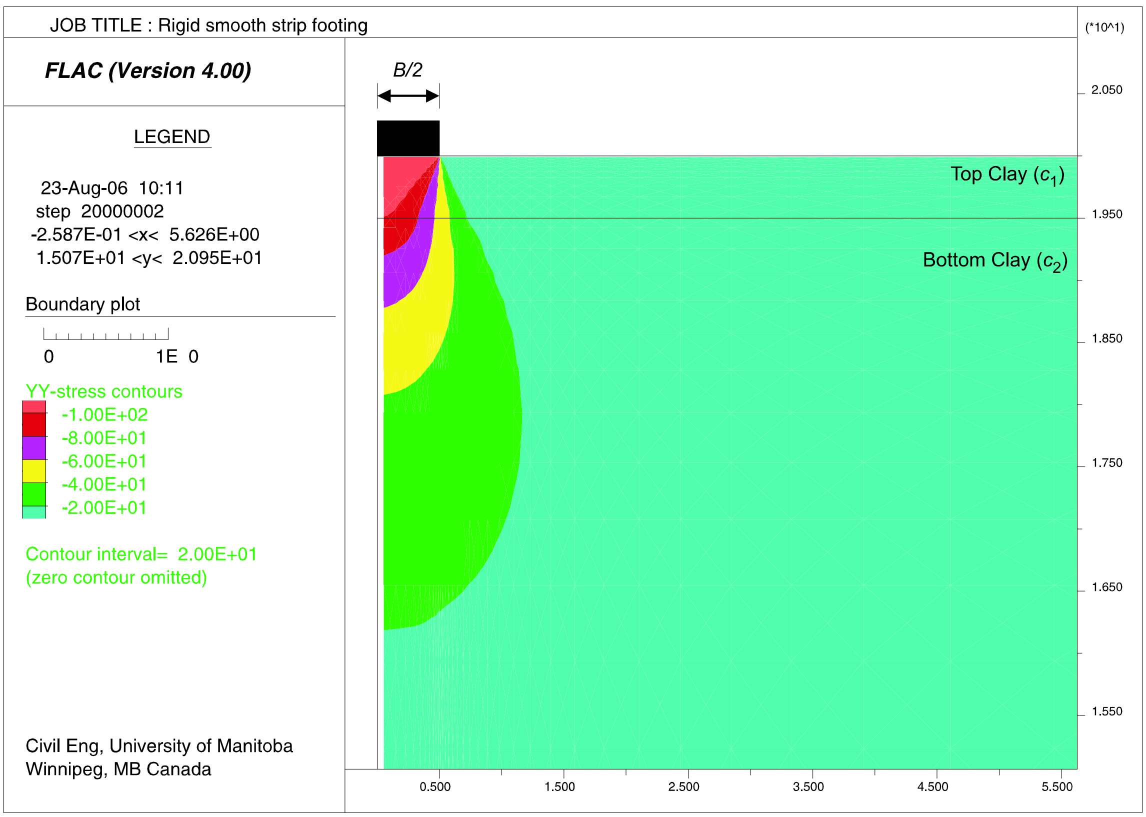

Figure A.202: Vertical stress (σ_{yy}) contours for a rigid smooth strip footing on soft clay over strong clay for 40×30 grid model, $H/B = 0.5$, $c_1/c_2 = 0.2$.

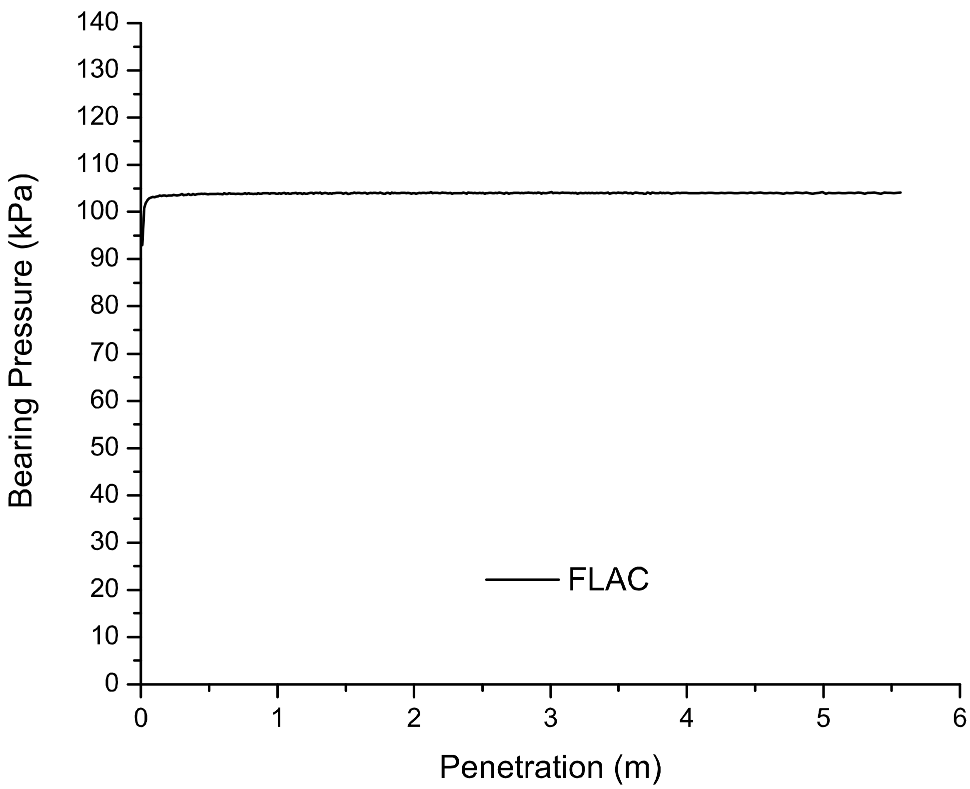

Figure A.203: Bearing pressure versus penetration curve for a rigid smooth strip footing on soft clay over strong clay for 40×30 grid model, $H/B = 0.5$, $c_1/c_2 = 0.2$.

Case 7: $c_1/c_2 = 0.1$ or $c_2/c_1 = 10$ - Small Deformation Analysis

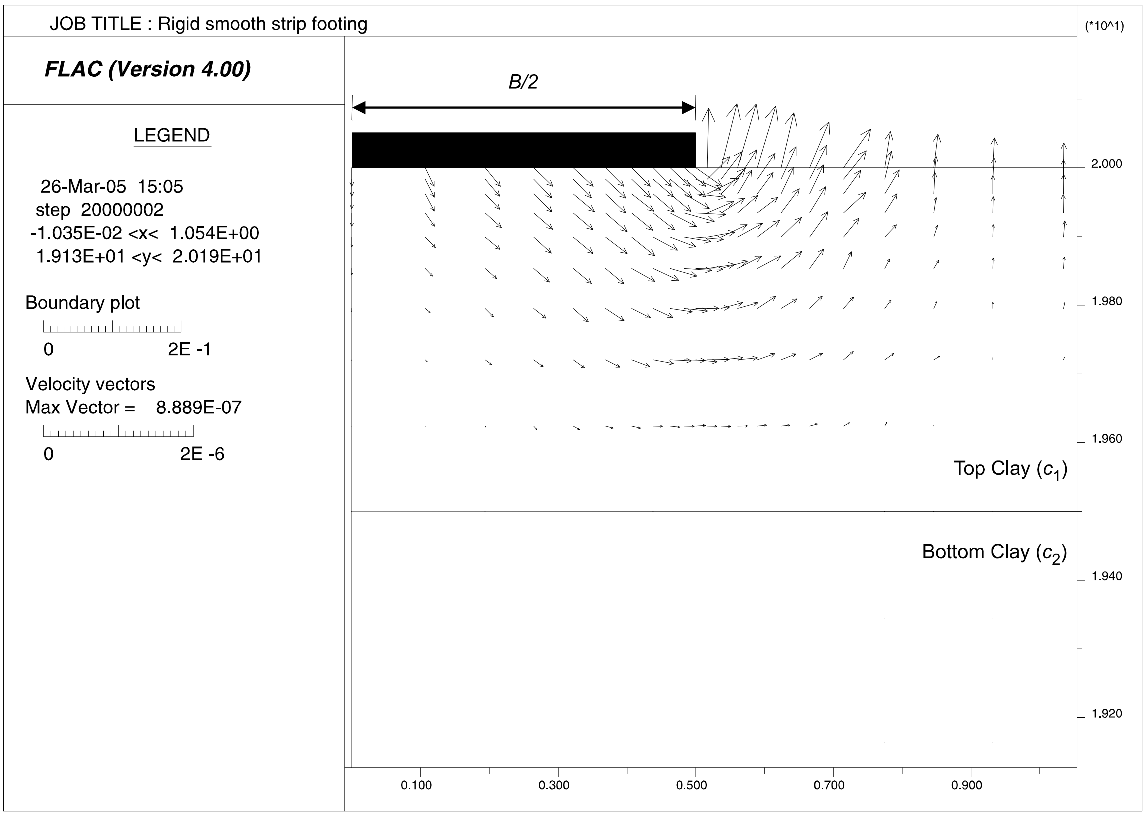

Figure A.204: Velocity vectors for a rigid smooth strip footing on soft clay over strong clay for 40×30 grid model, $H/B = 0.5$, $c_1/c_2 = 0.1$.

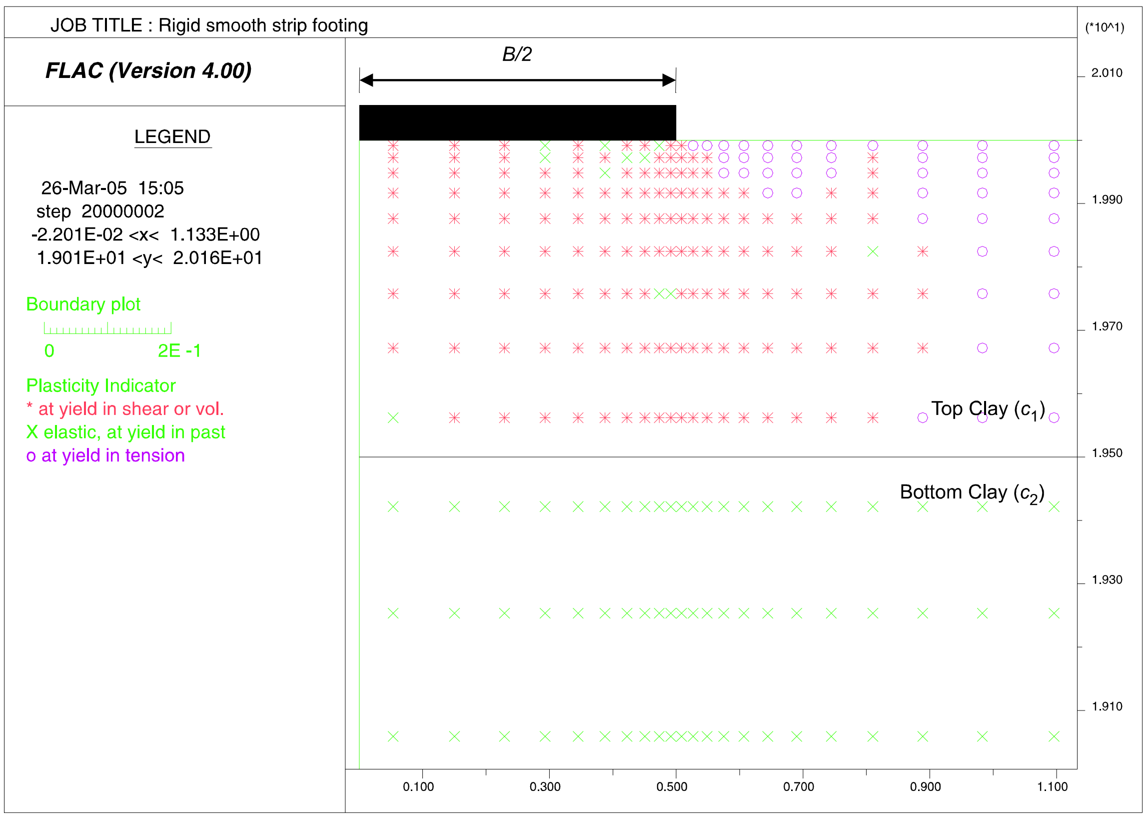

Figure A.205: Plasticity state indicators for a rigid smooth strip footing on soft clay over strong clay for 40 × 30 grid model, $H/B = 0.5$, $c_1/c_2 = 0.1$.

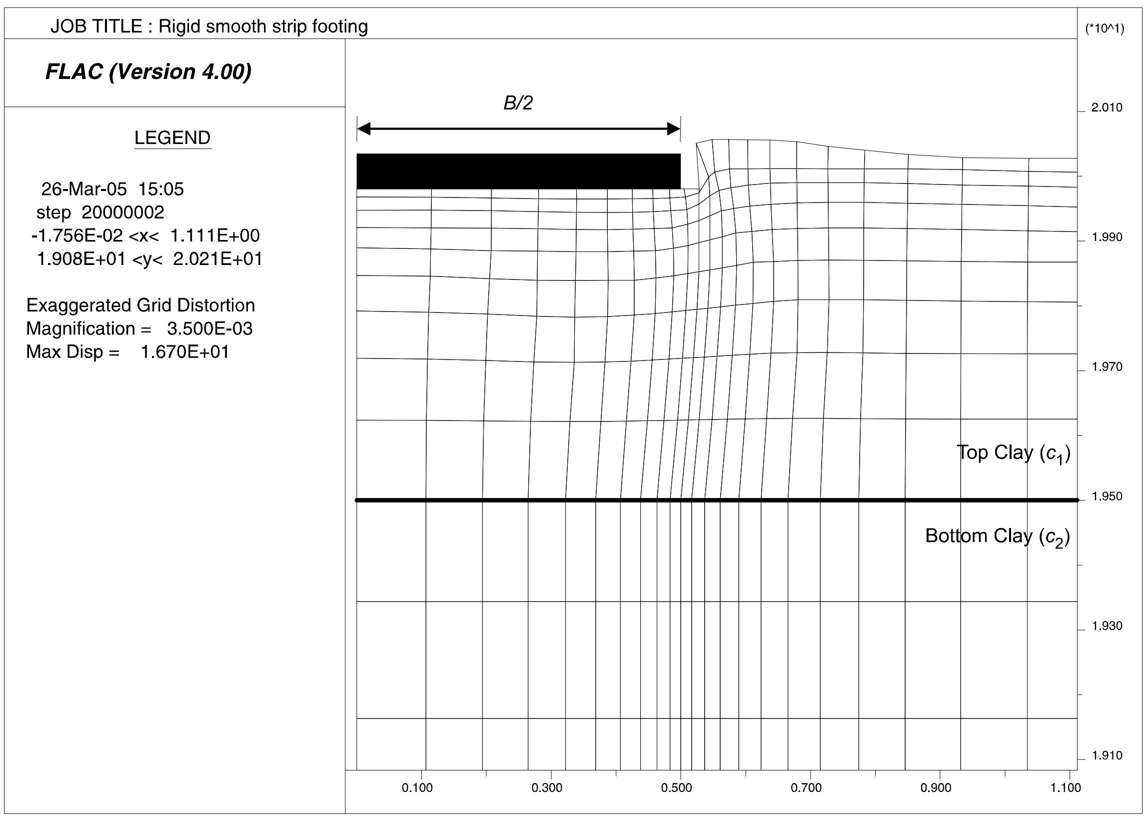

Figure A.206: Magnified grid for a rigid smooth strip footing on soft clay over strong clay for 40×30 grid model, $H/B = 0.5$, $c_1/c_2 = 0.1$.

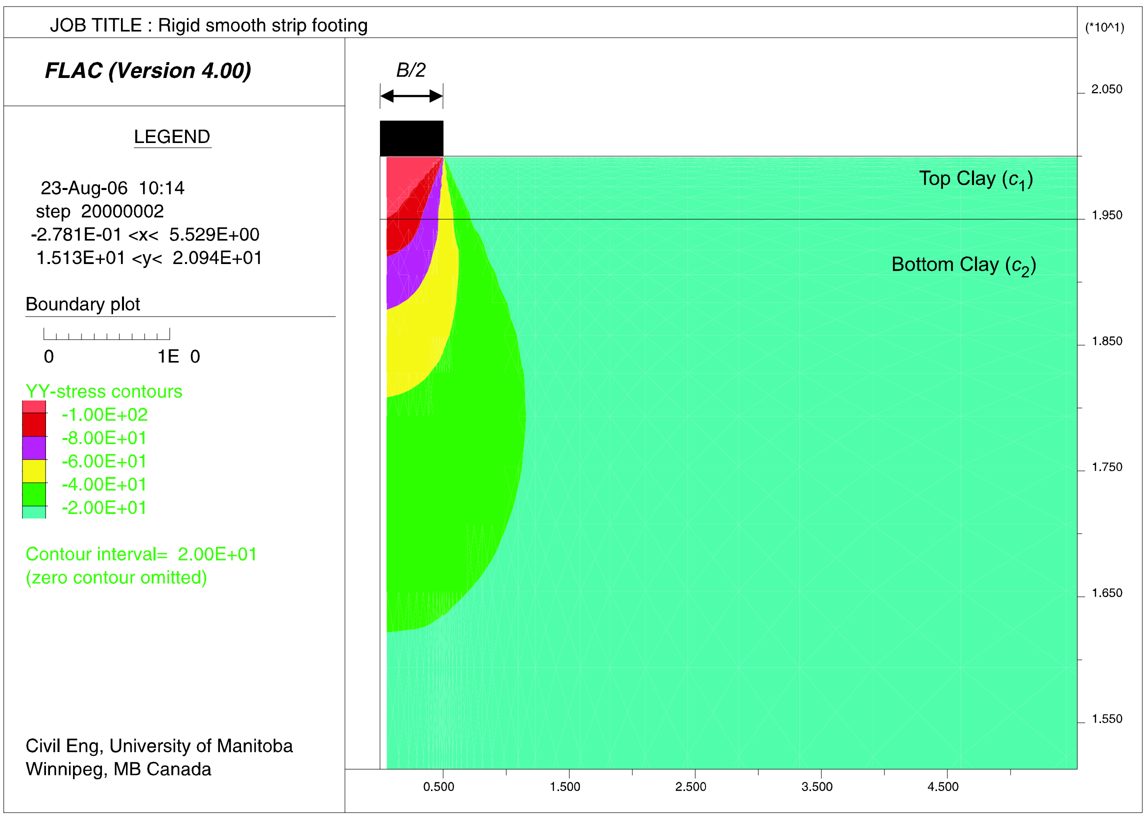

Figure A.207: Vertical stress (σ_{yy}) contours for a rigid smooth strip footing on soft clay over strong clay for 40×30 grid model, $H/B = 0.5$, $c_1/c_2 = 0.1$.

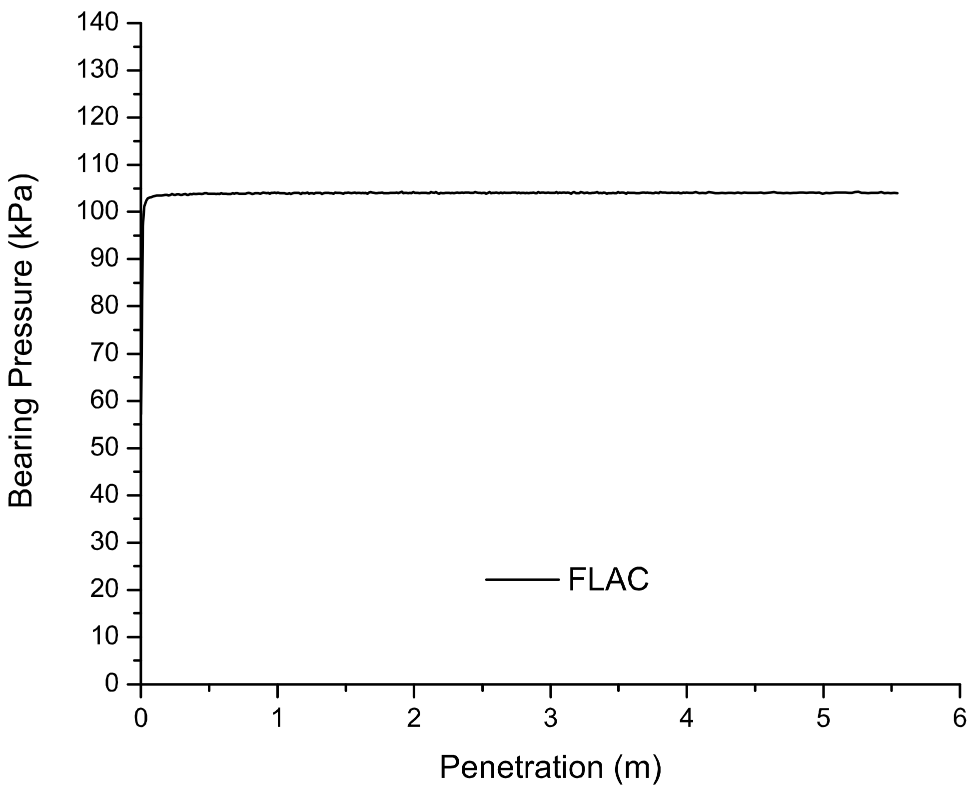

Figure A.208: Bearing pressure versus penetration curve for a rigid smooth strip footing on soft clay over strong clay for 40×30 grid model, $H/B = 0.5$, $c_1/c_2 = 0.1$.

A.2.3 Rigid Smooth Strip Footing on Soft over Strong Clay ($H/B = 0.25$)

Case 2: $c_1/c_2 = 0.8$ or $c_2/c_1 = 1.25$ - Small Deformation Analysis

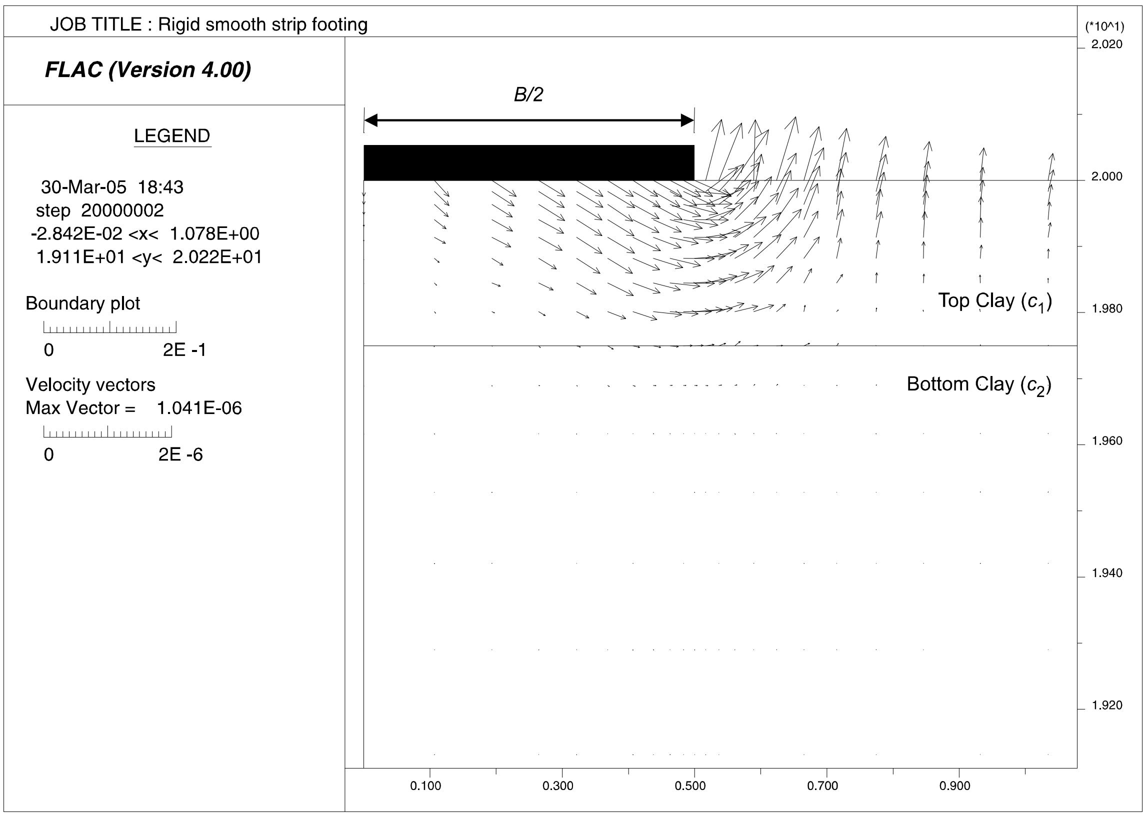

Figure A.209: Velocity vectors for a rigid strip footing on soft over strong clay for 40×30 grid model, $H/B = 0.25$, $c_1/c_2 = 0.8$.

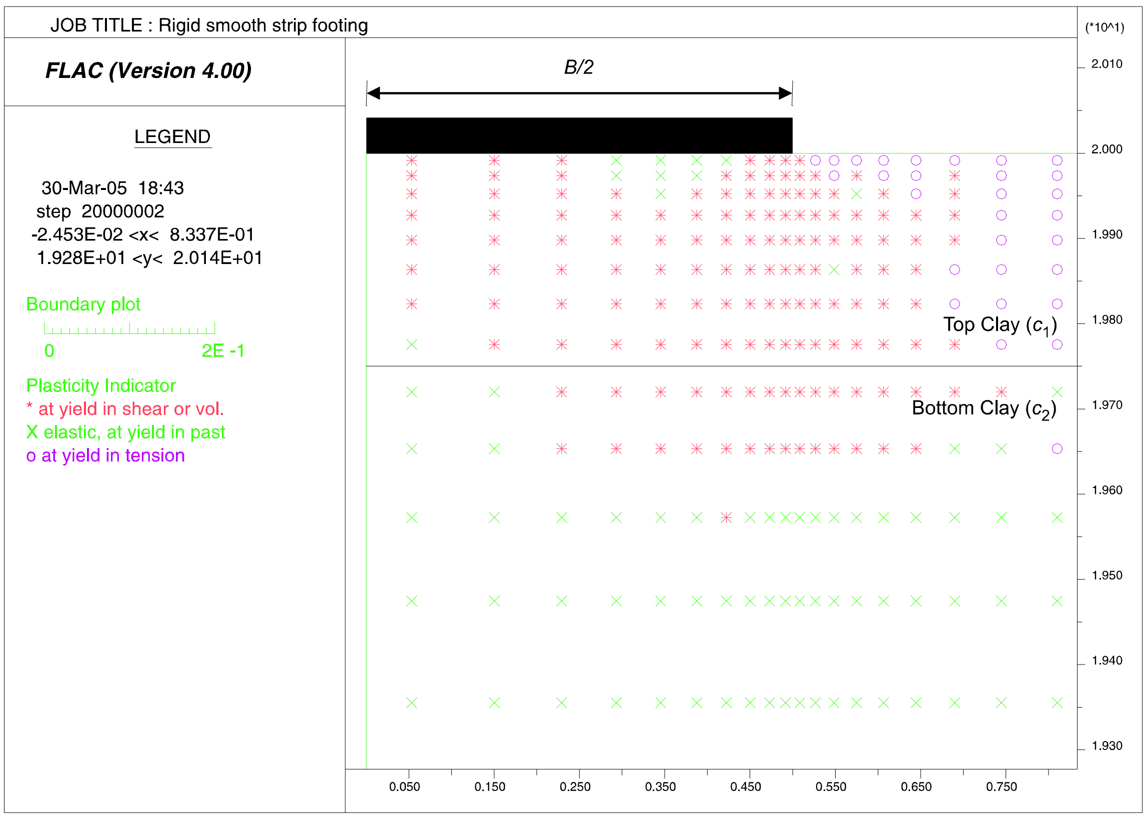

Figure A.210: Plasticity indicators for a rigid smooth strip footing on soft over strong clay for 40 × 30 grid model, $H/B = 0.25$, $c_1/c_2 = 0.8$.

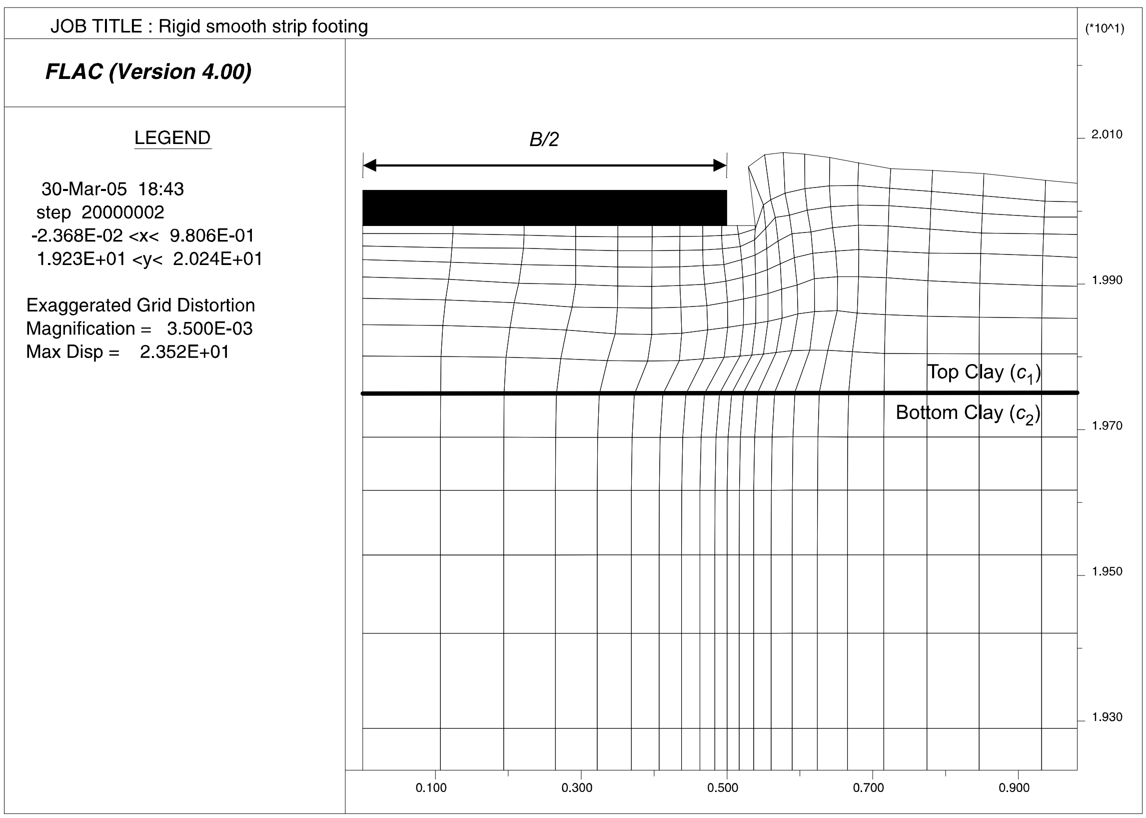

Figure A.211: Magnified grid for a rigid smooth strip footing on soft over strong clay for 40 × 30 grid model, $H/B = 0.25$, $c_1/c_2 = 0.8$.

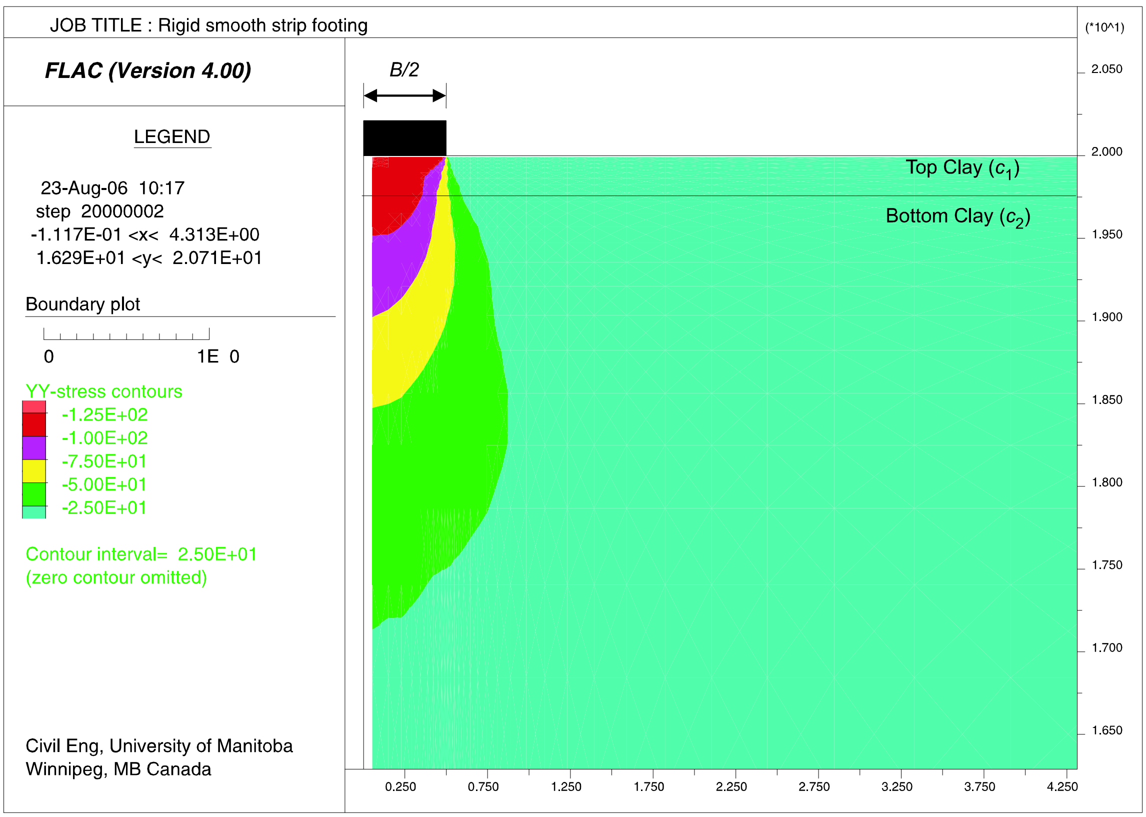

Figure A.212: Vertical stress (σ_{yy}) contours for a rigid smooth strip footing on soft over strong clay for 40×30 grid model, $H/B = 0.25$, $c_1/c_2 = 0.8$.

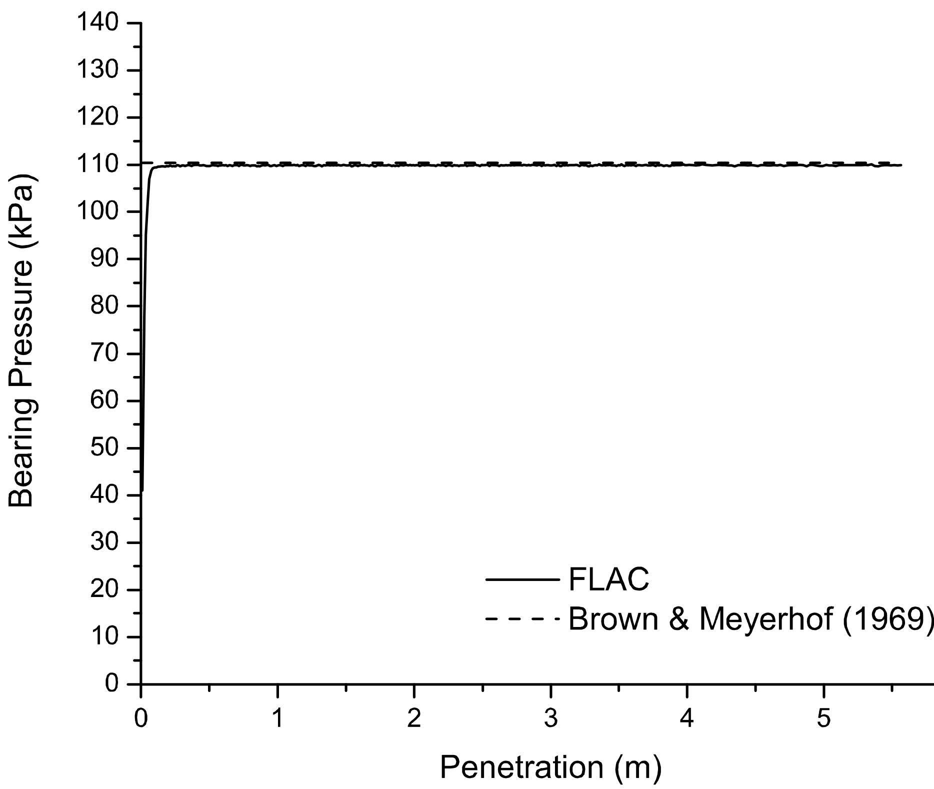

Figure A.213: Bearing pressure versus penetration curve for a rigid smooth strip footing on soft over strong clay for 40 × 30 grid model, $H/B = 0.25$, $c_1/c_2 = 0.8$.

Case 3: $c_1/c_2 = 2/3$ or $c_2/c_1 = 1.5$ - Small Deformation Analysis

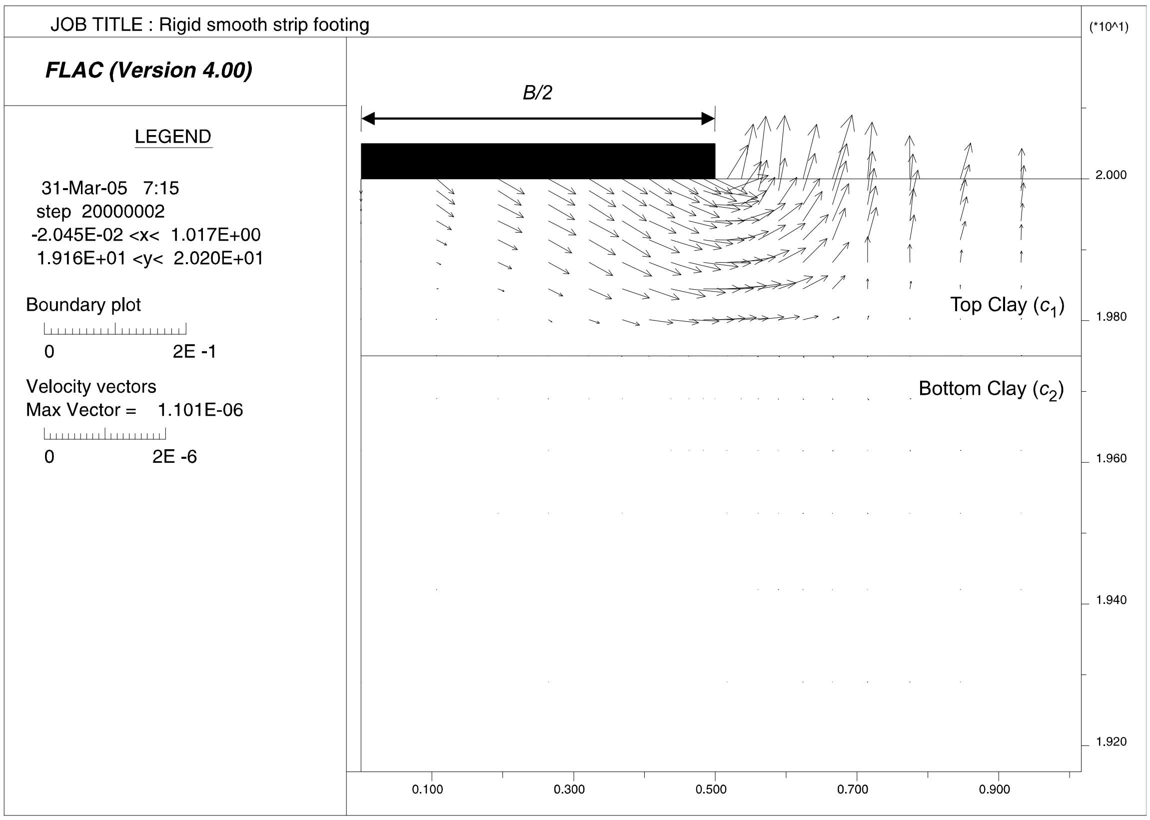

Figure A.214: Velocity vectors for a rigid smooth strip footing on soft clay over strong clay for 40 × 30 grid model, $H/B = 0.25$, $c_1/c_2 = 2/3$.

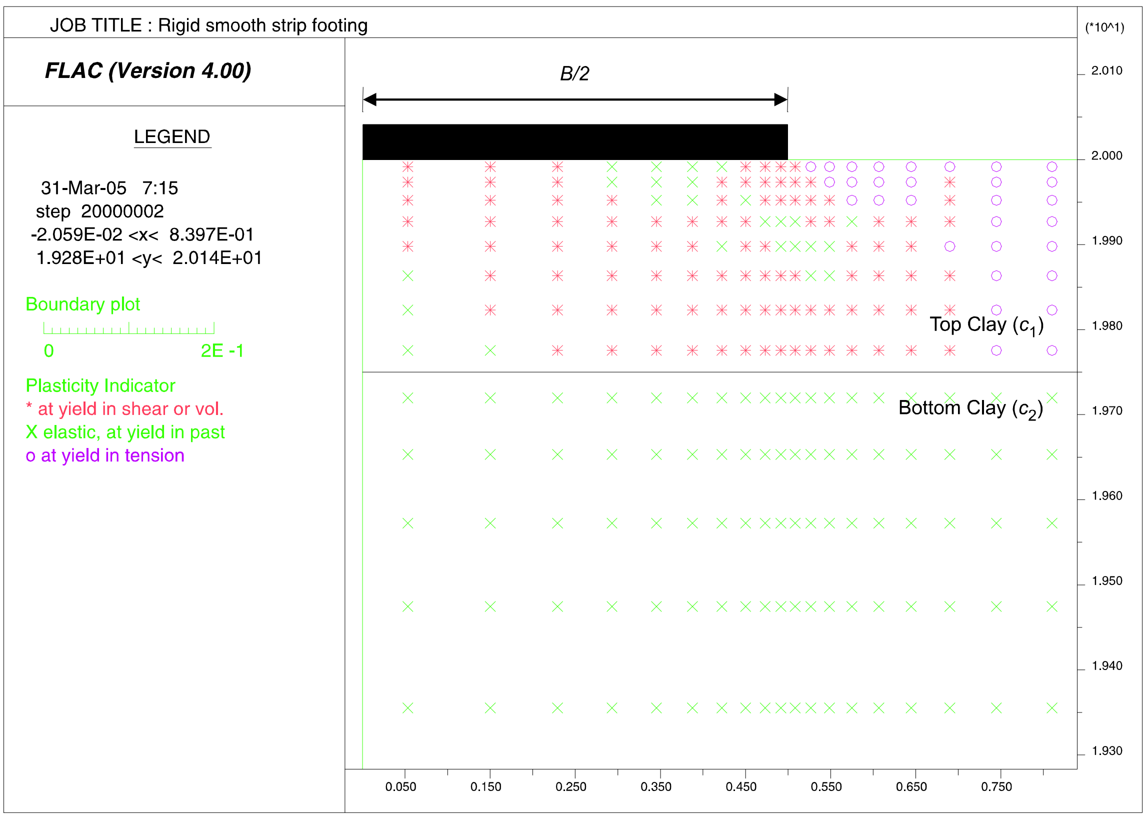

Figure A.215: Plasticity state indicators for a rigid smooth strip footing on soft over strong clay for 40 × 30 grid model, $H/B = 0.25$, $c_1/c_2 = 2/3$.

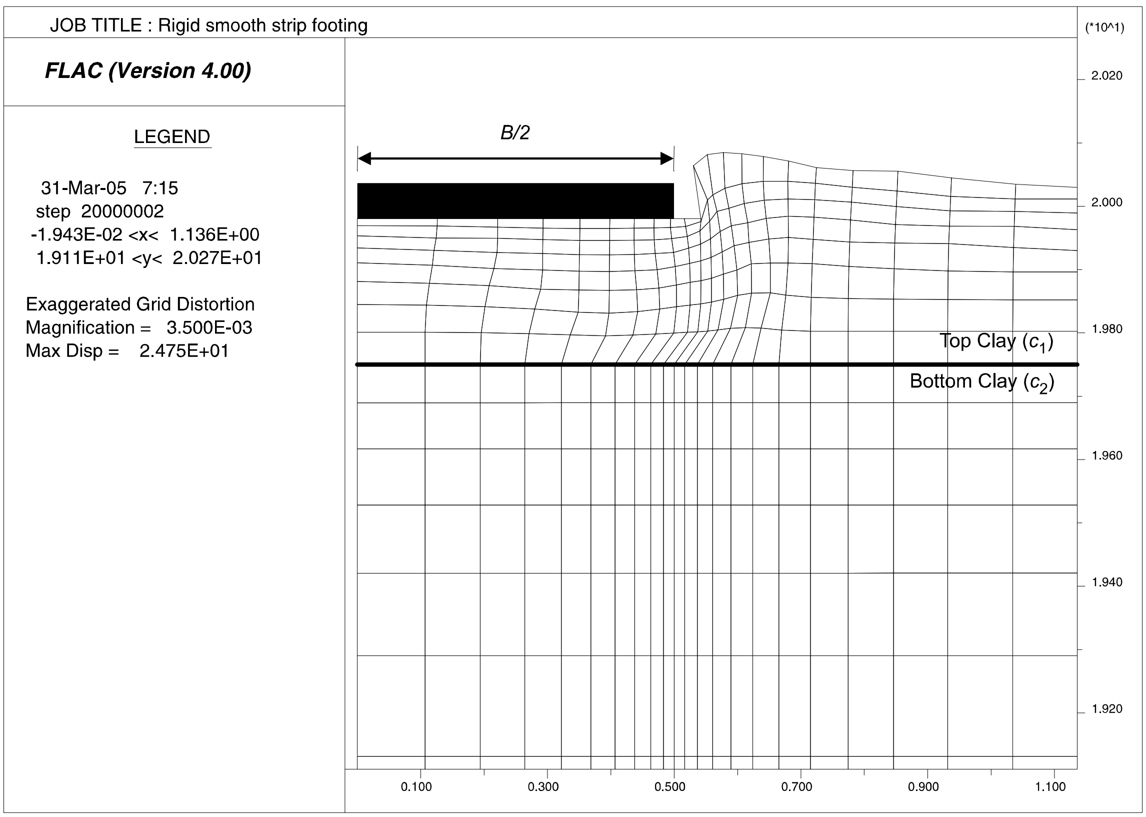

Figure A.216: Magnified grid for a rigid smooth strip footing on soft over strong clay for 40 × 30 grid model, $H/B = 0.25$, $c_1/c_2 = 2/3$.

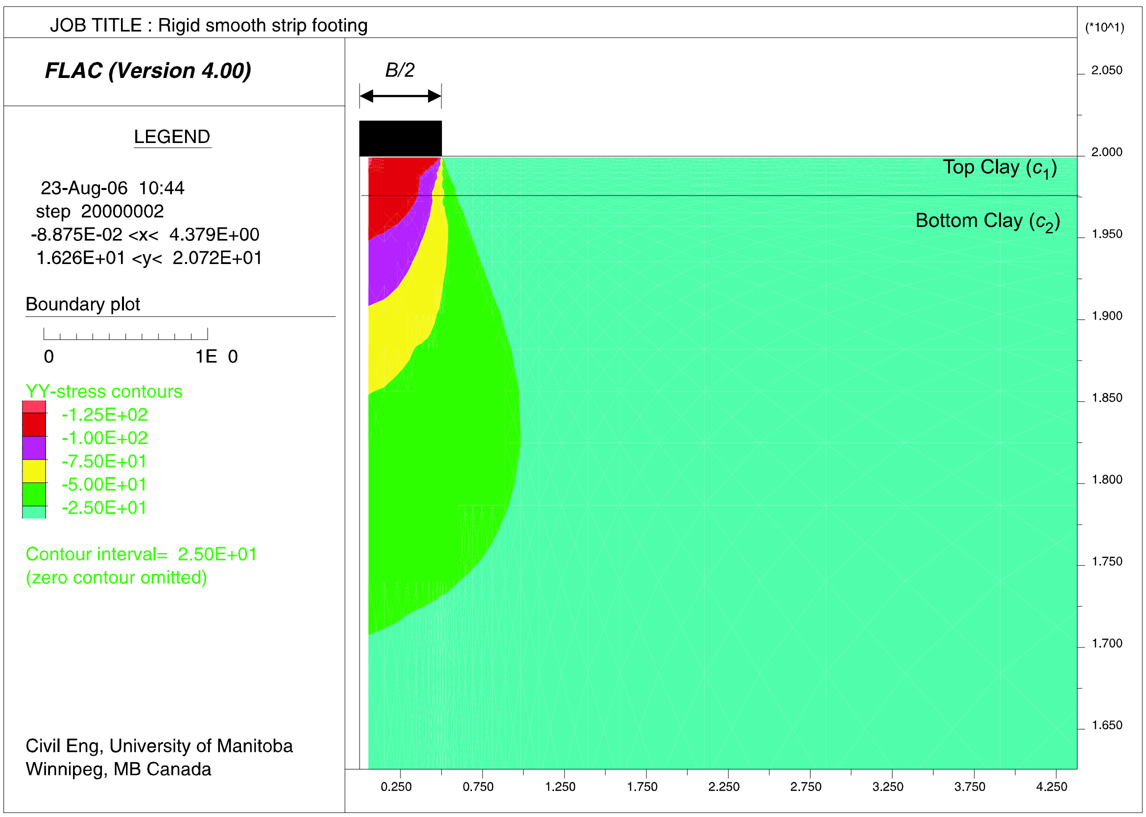

Figure A.217: Vertical stress (σ_{yy}) contours for a rigid smooth strip footing on soft over strong clay for 40×30 grid model, $H/B = 0.25$, $c_1/c_2 = 2/3$.

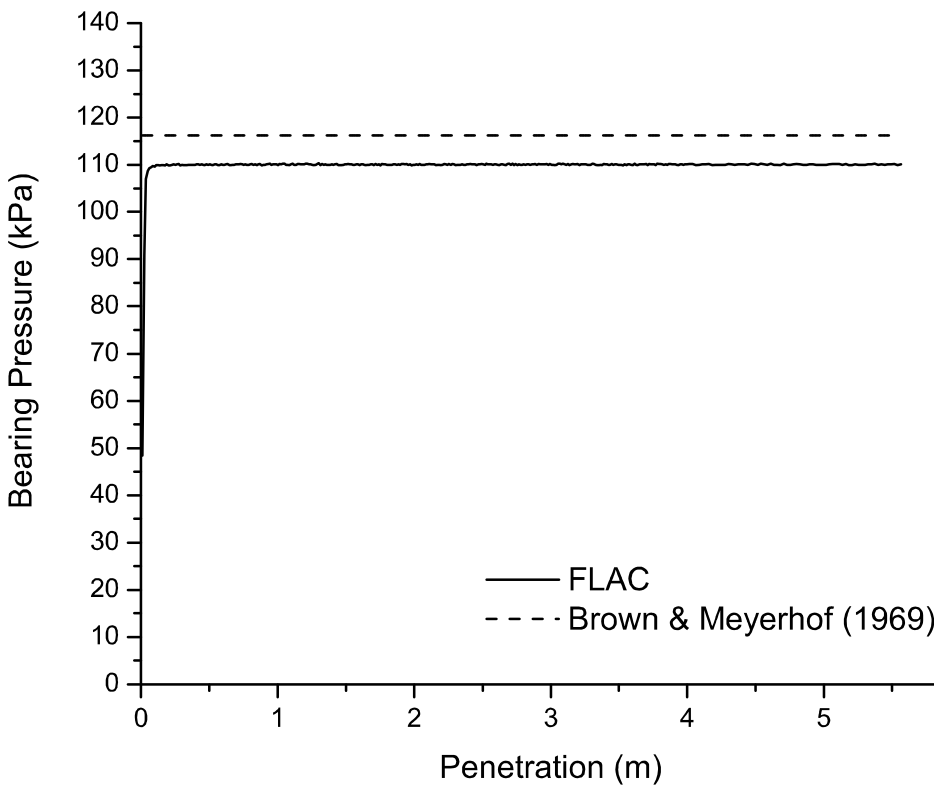

Figure A.218: Bearing pressure versus penetration curve for a rigid smooth strip footing on soft over strong clay for 40 × 30 grid model, $H/B = 0.25$, $c_1/c_2 = 2/3$.

Case 4: $c_1/c_2 = 0.5$ or $c_2/c_1 = 2$ - Small Deformation Analysis

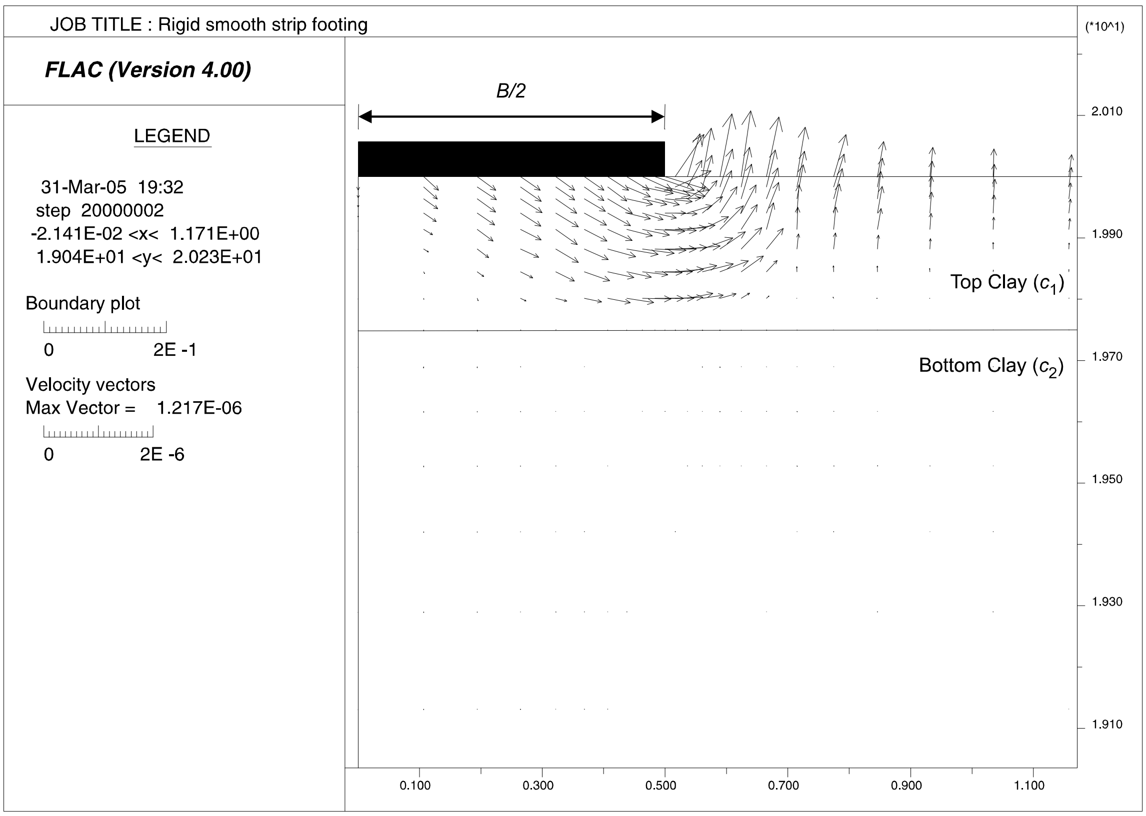

Figure A.219: Velocity vectors for a rigid smooth strip footing on soft clay over strong clay for 40×30 grid model, $H/B = 0.25$, $c_1/c_2 = 0.5$.

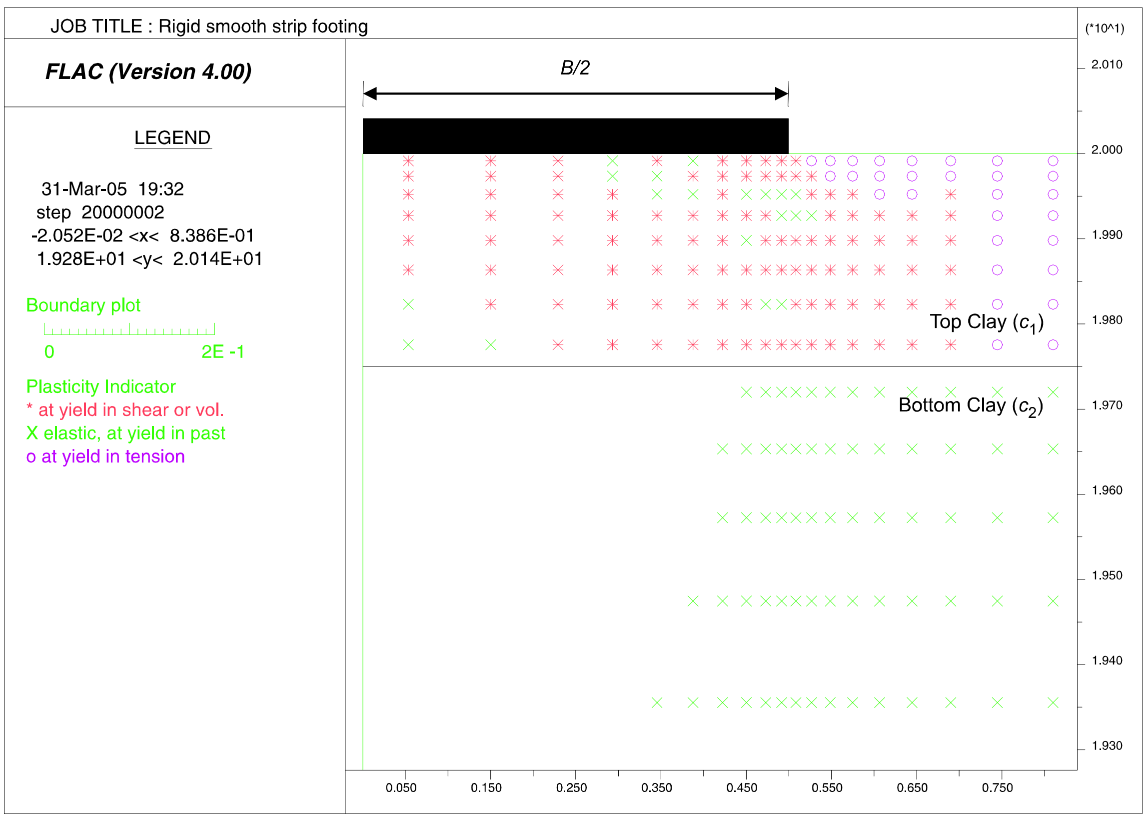

Figure A.220: Plasticity state indicators for a rigid smooth strip footing on soft clay over strong clay for 40×30 grid model, $H/B = 0.25$, $c_1/c_2 = 0.5$.

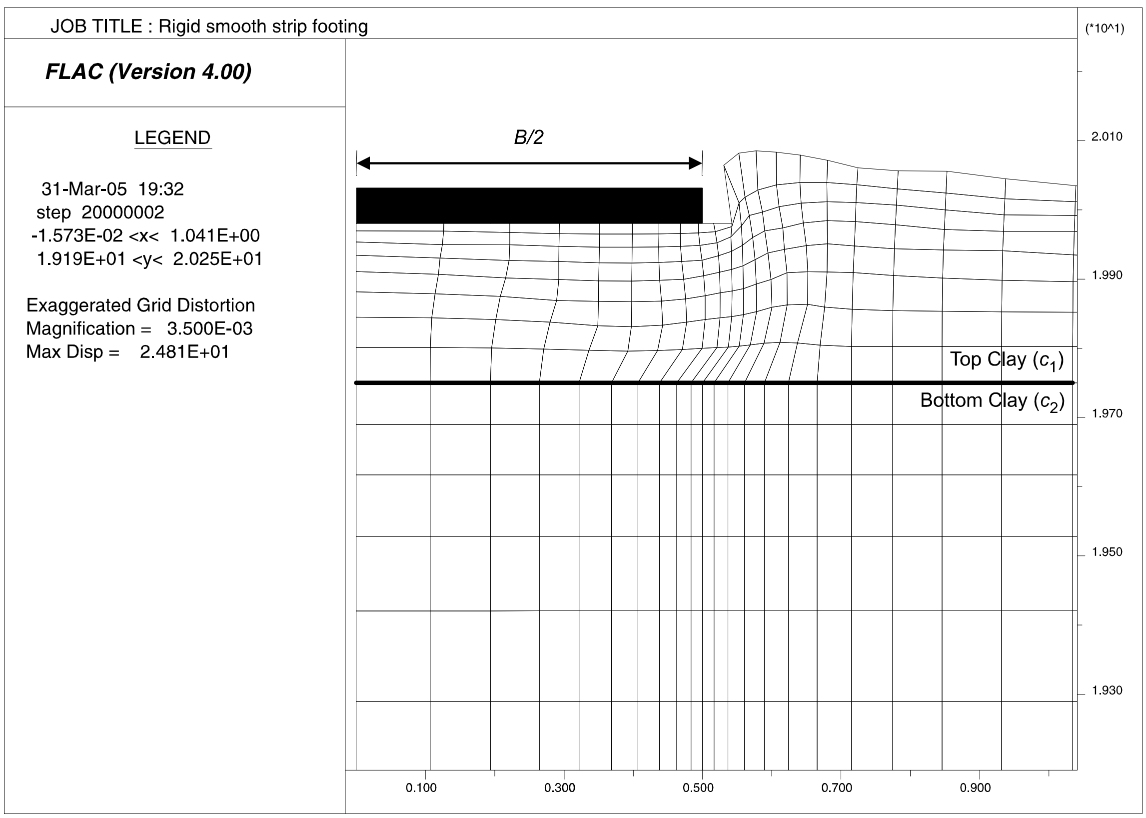

Figure A.221: Magnified grid for a rigid smooth strip footing on soft clay over strong clay for 40 × 30 grid model, $H/B = 0.25$, $c_1/c_2 = 0.5$.

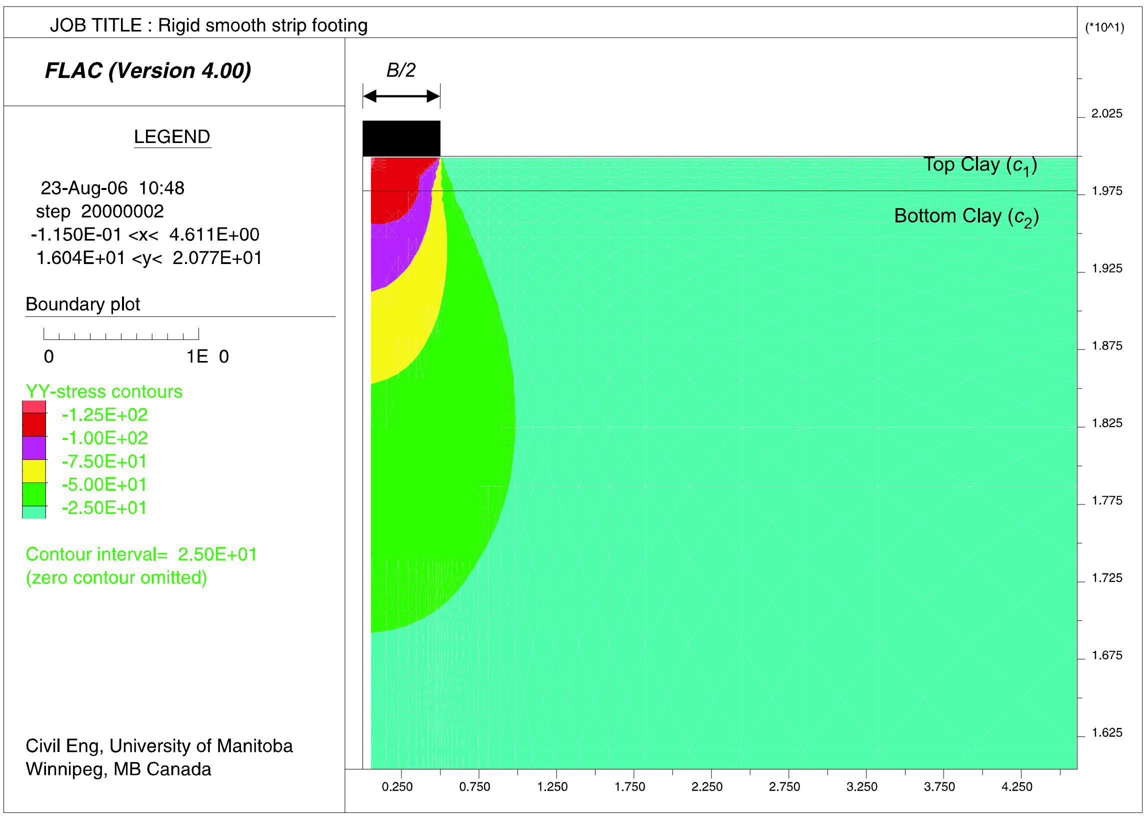

Figure A.222: Vertical stress (σ_{yy}) contours for a rigid smooth strip footing on soft clay over strong clay for 40 × 30 grid model, $H/B = 0.25$, $c_1/c_2 = 0.5$.

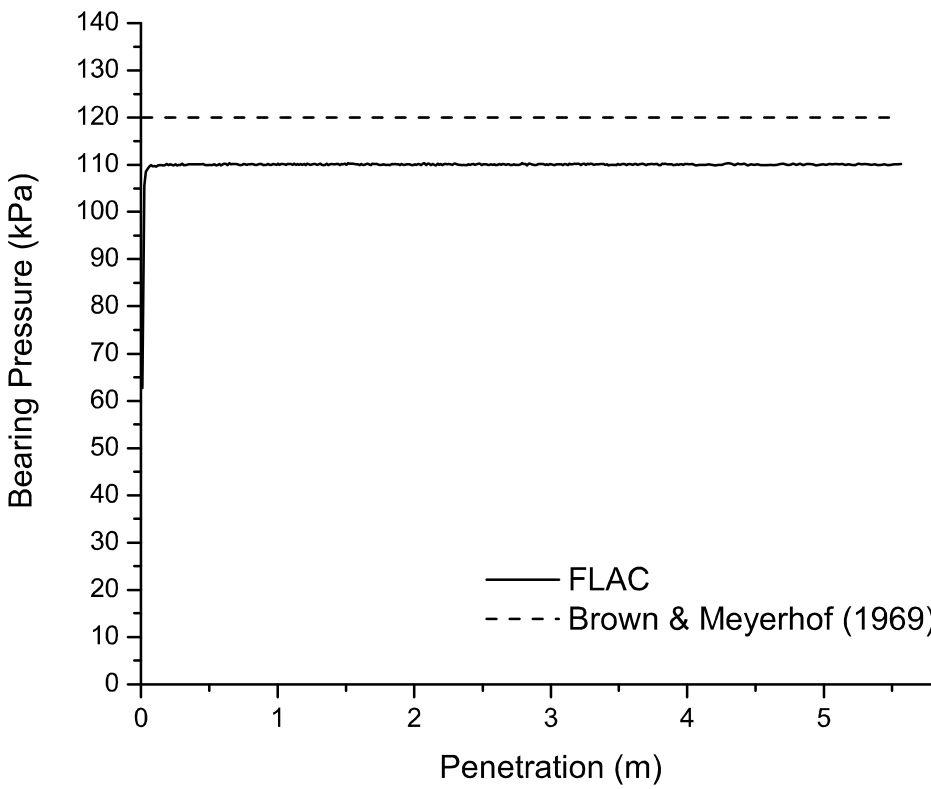

Figure A.223: Bearing pressure versus penetration curve for a rigid smooth strip footing on soft clay over strong clay for 40×30 grid model, $H/B = 0.25$, $c_1/c_2 = 0.5$.

Case 5: $c_1/c_2 = 1/3$ or $c_2/c_1 = 3$ - Small Deformation Analysis

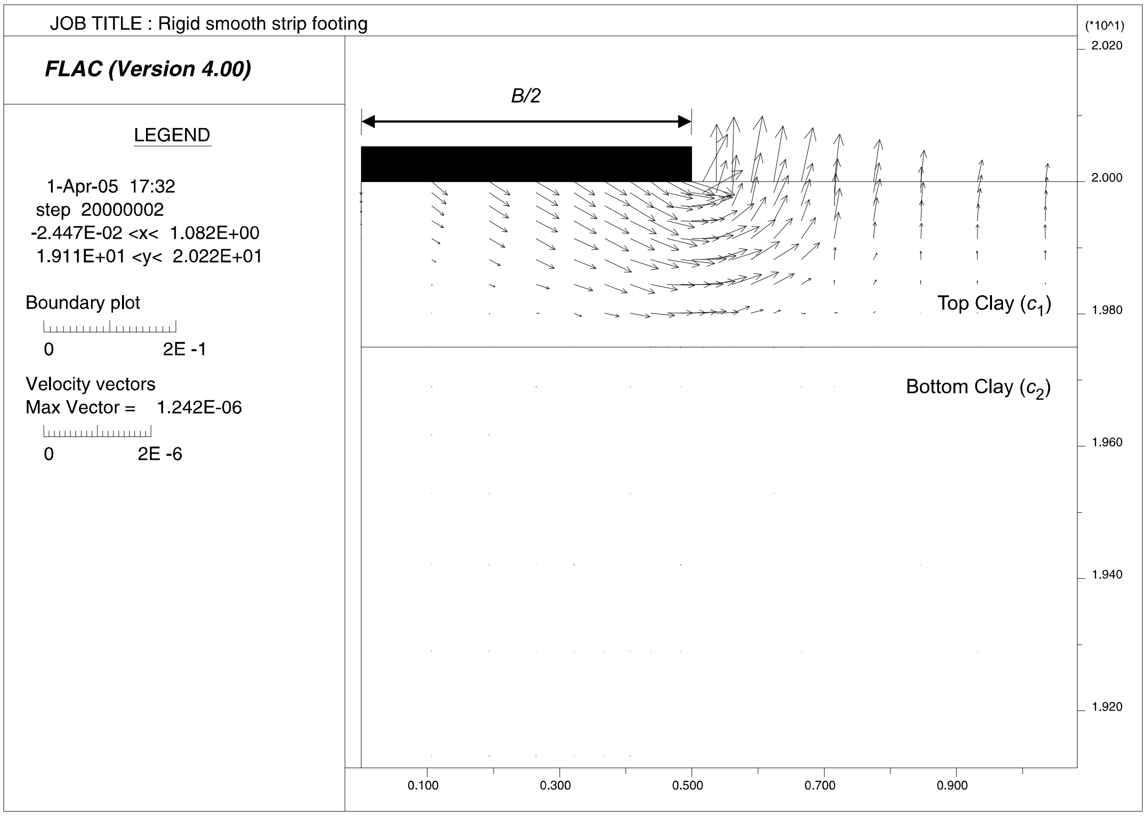

Figure A.224: Velocity vectors for a rigid smooth strip footing on soft clay over strong clay for 40×30 grid model, $H/B = 0.25$, $c_1/c_2 = 1/3$.

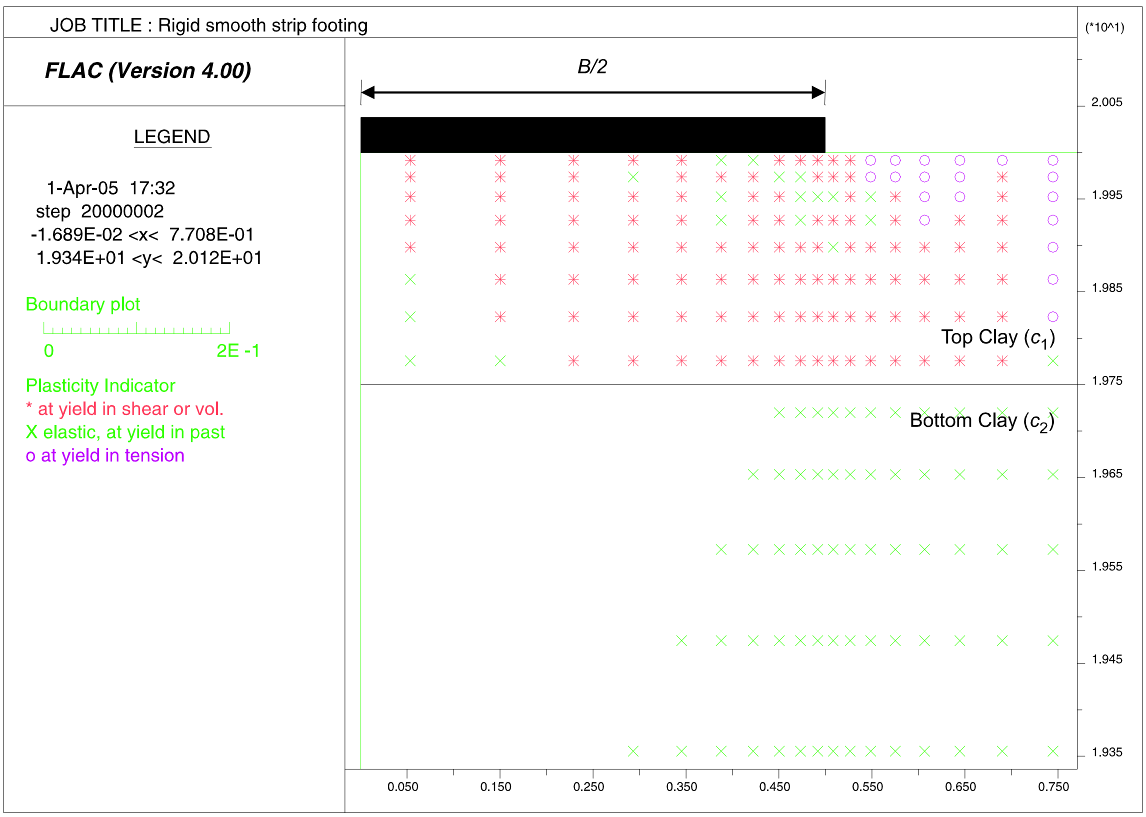

Figure A.225: Plasticity state indicators for a rigid smooth strip footing on soft clay over strongclay for 40×30 grid model, $H/B = 0.25$, $c_1/c_2 = 1/3$.

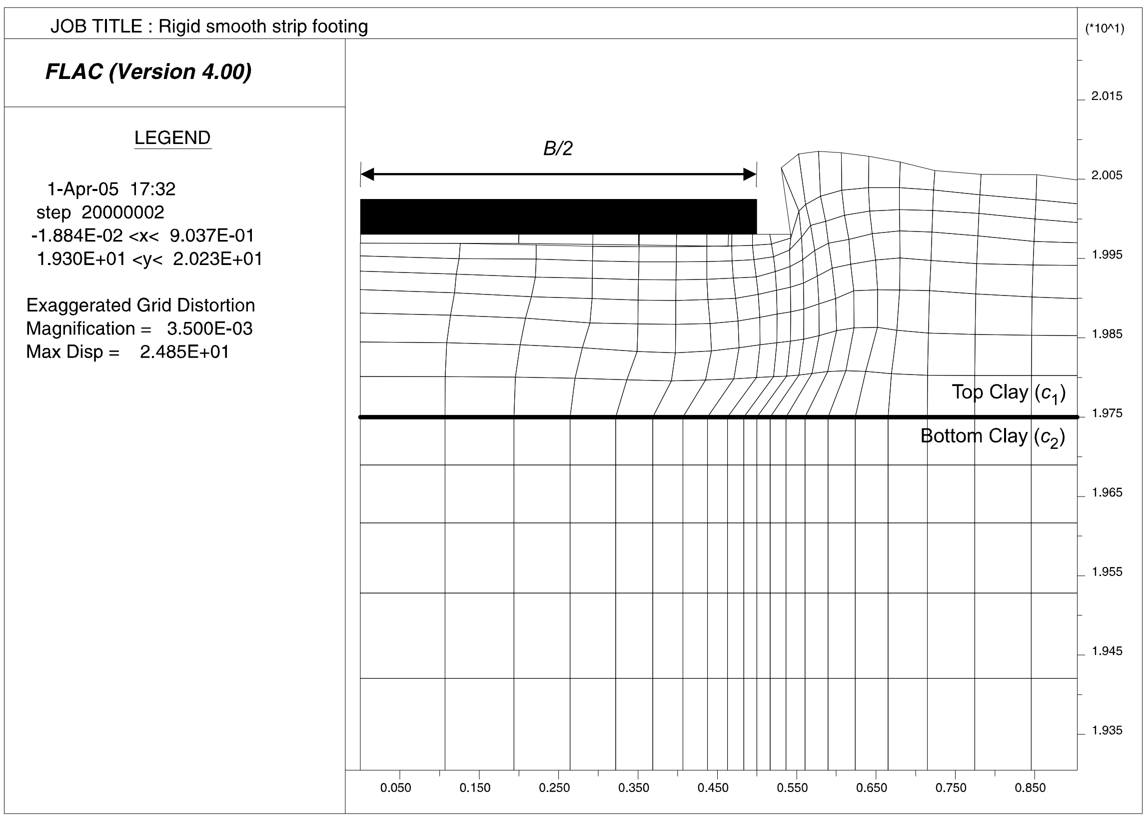

Figure A.226: Vertical stress (σ_{yy}) contours for a rigid smooth strip footing on strong clay over soft clay for 40×30 grid model, $H/B = 0.25$, $c_1/c_2 = 1/3$.

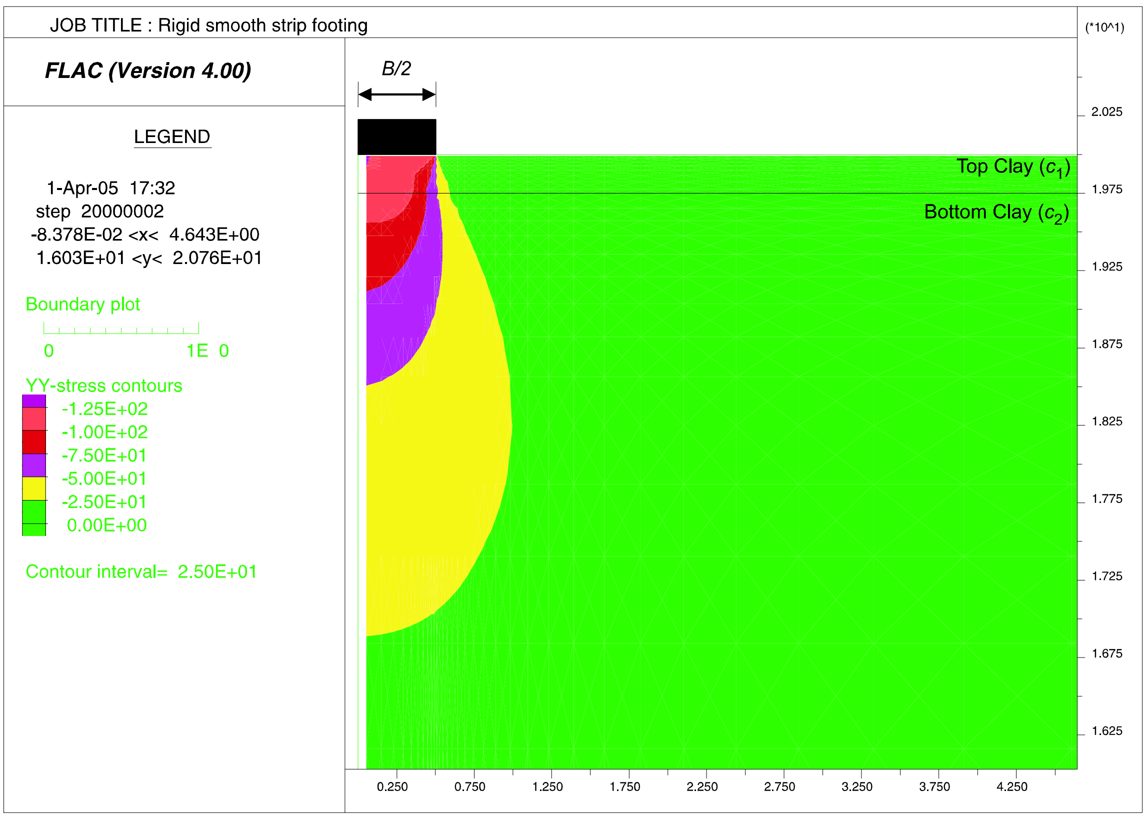

Figure A.227: Vertical stress (σ_{yy}) contours for a rigid smooth strip footing on soft clay over strong clay for 40×30 grid model, $H/B = 0.25$, $c_1/c_2 = 1/3$.

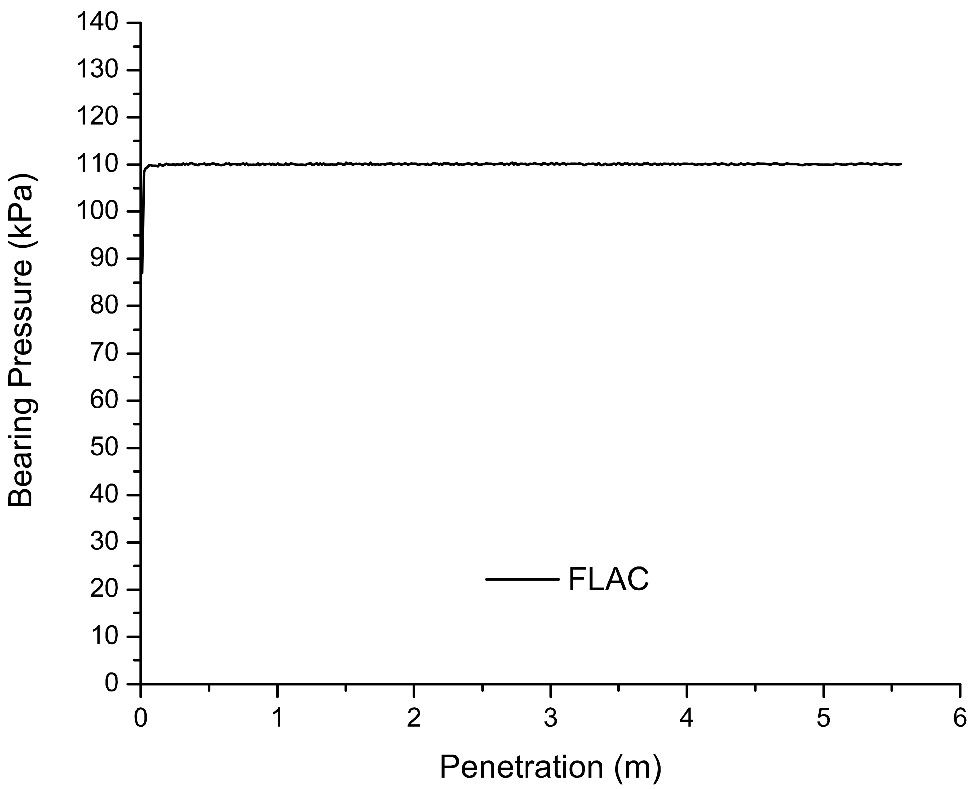

Figure A.228: Bearing pressure versus penetration curve for a rigid smooth strip footing on soft clay over strong clay for 40×30 grid model, $H/B = 0.25$, $c_1/c_2 = 1/3$.

Case 6: $c_1/c_2 = 0.2$ or $c_2/c_1 = 5$ - Small Deformation Analysis

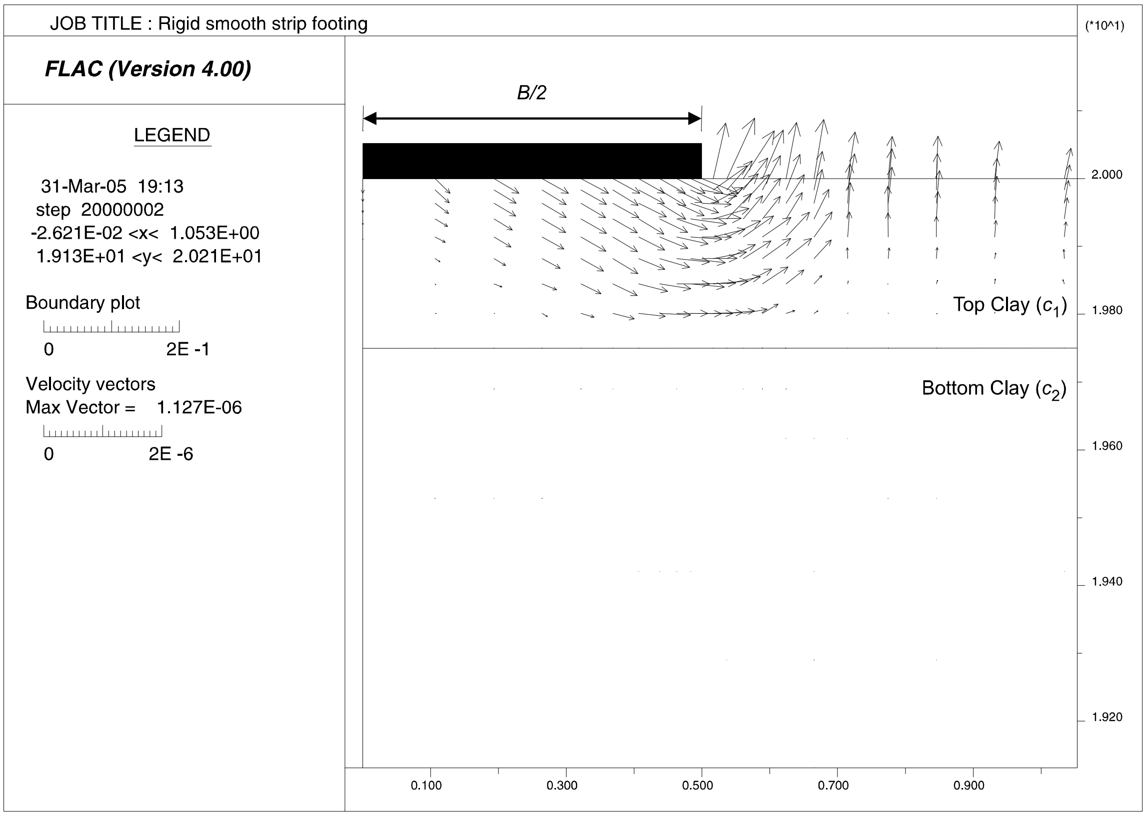

Figure A.229: Velocity vectors for a rigid smooth strip footing on soft clay over strong clay for 40×30 grid model, $H/B = 0.25$, $c_1/c_2 = 0.2$.

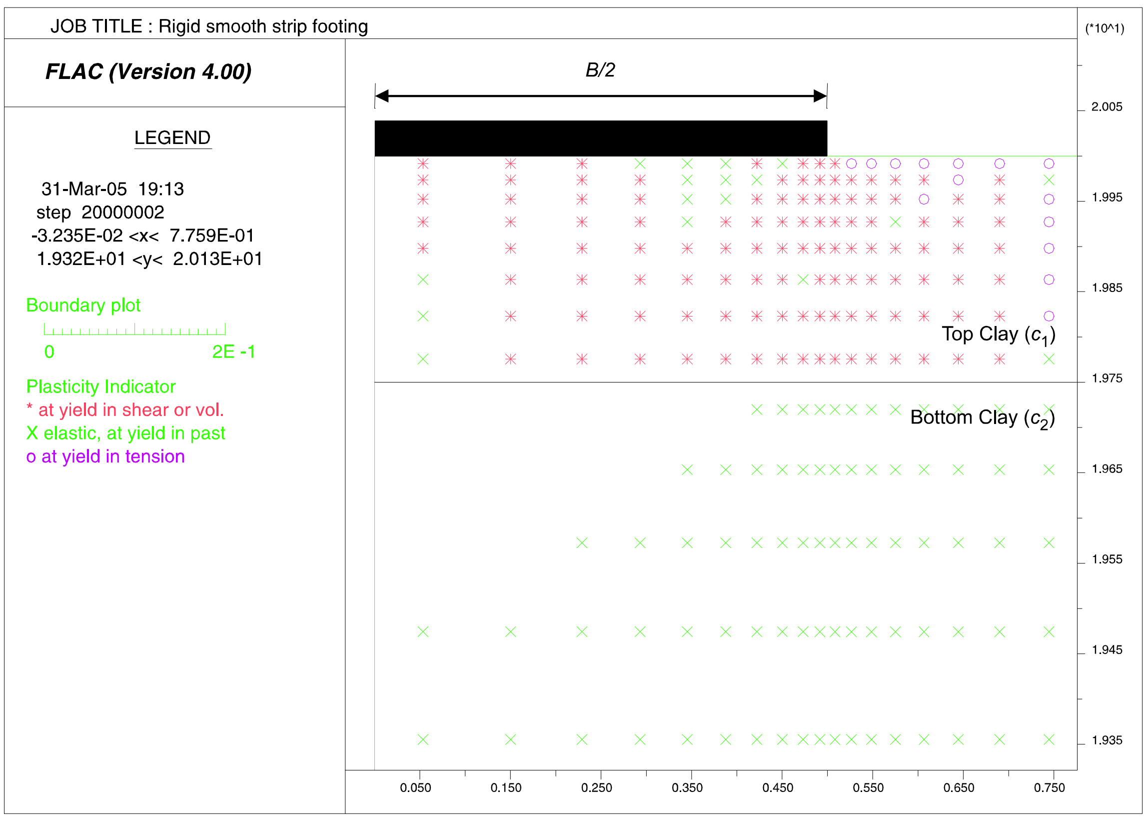

Figure A.230: Plasticity state indicators for a rigid smooth strip footing on soft clay over strong clay for 40×30 grid model, $H/B = 0.25$, $c_1/c_2 = 0.2$.

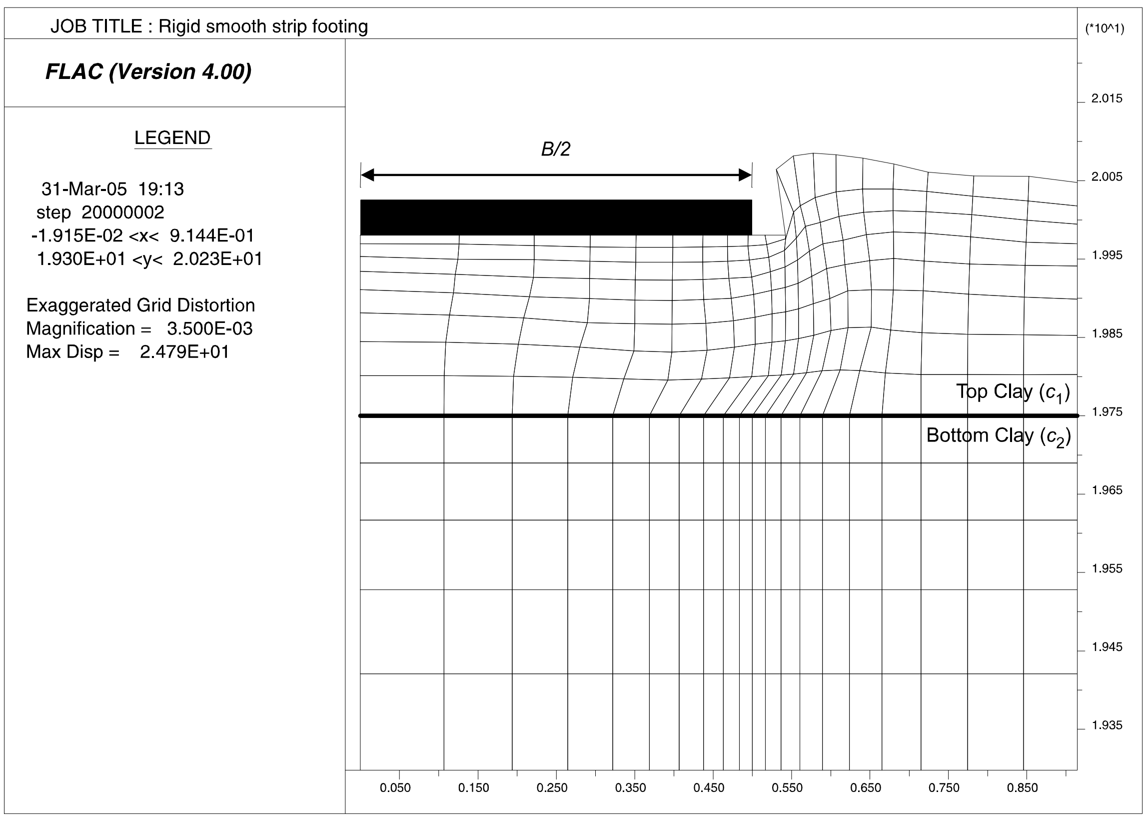

Figure A.231: Magnified grid for a rigid smooth strip footing on soft clay over strong-clay for 40 × 30 grid model, $H/B = 0.25$, $c_1/c_2 = 0.2$.

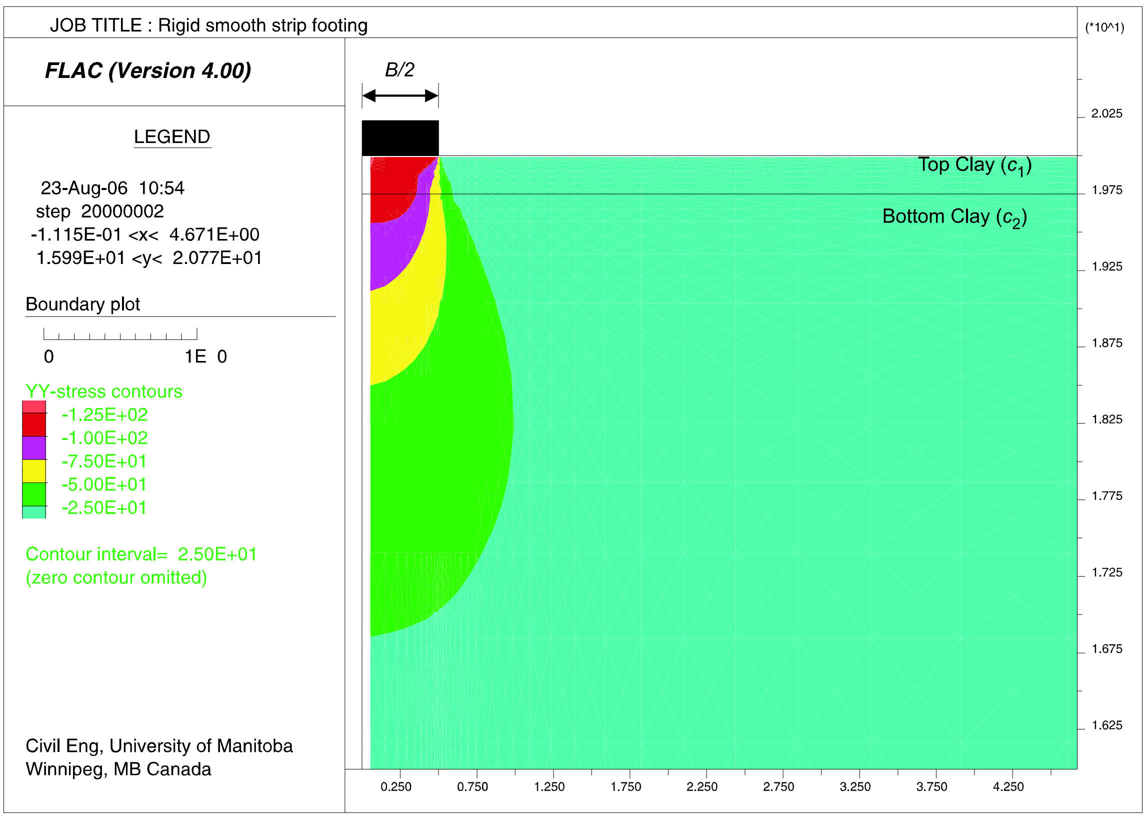

Figure A.232: Vertical stress (σ_{yy}) contours for a rigid smooth strip footing on soft clay over strong clay for 40×30 grid model, $H/B = 0.25$, $c_1/c_2 = 0.2$.

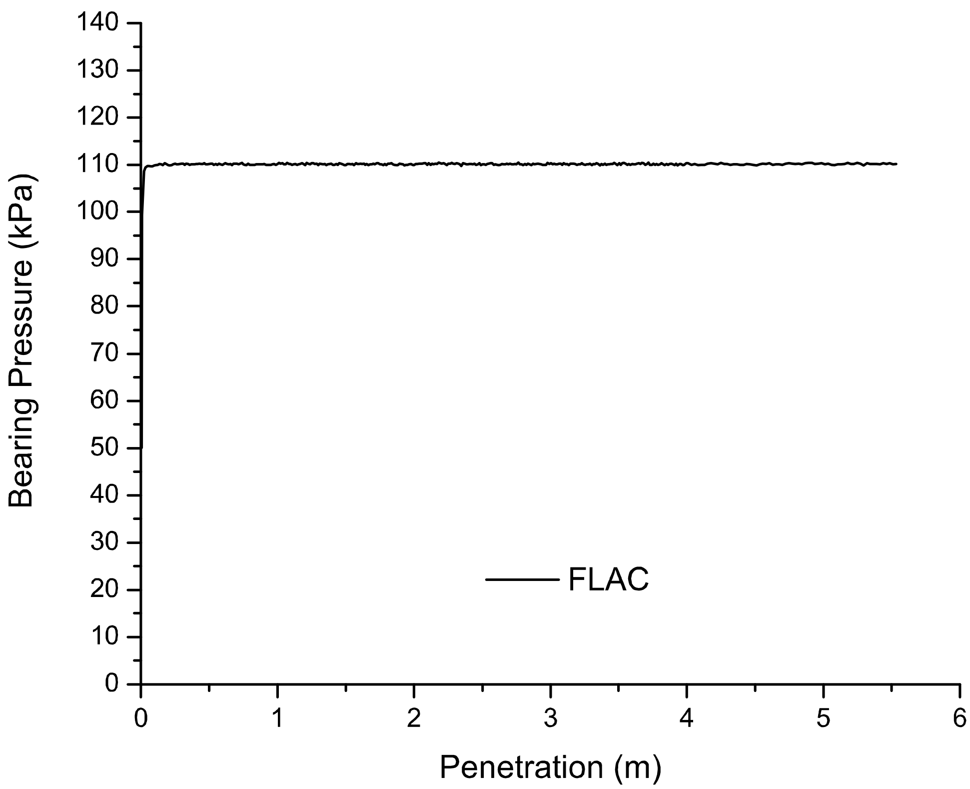

Figure A.233: Bearing pressure versus penetration curve a for rigid smooth strip footing on soft clay over strong clay for 40×30 grid model, $H/B = 0.25$, $c_1/c_2 = 0.2$.

Case 7: $c_1/c_2 = 0.1$ or $c_2/c_1 = 10$ - Small Deformation Analysis

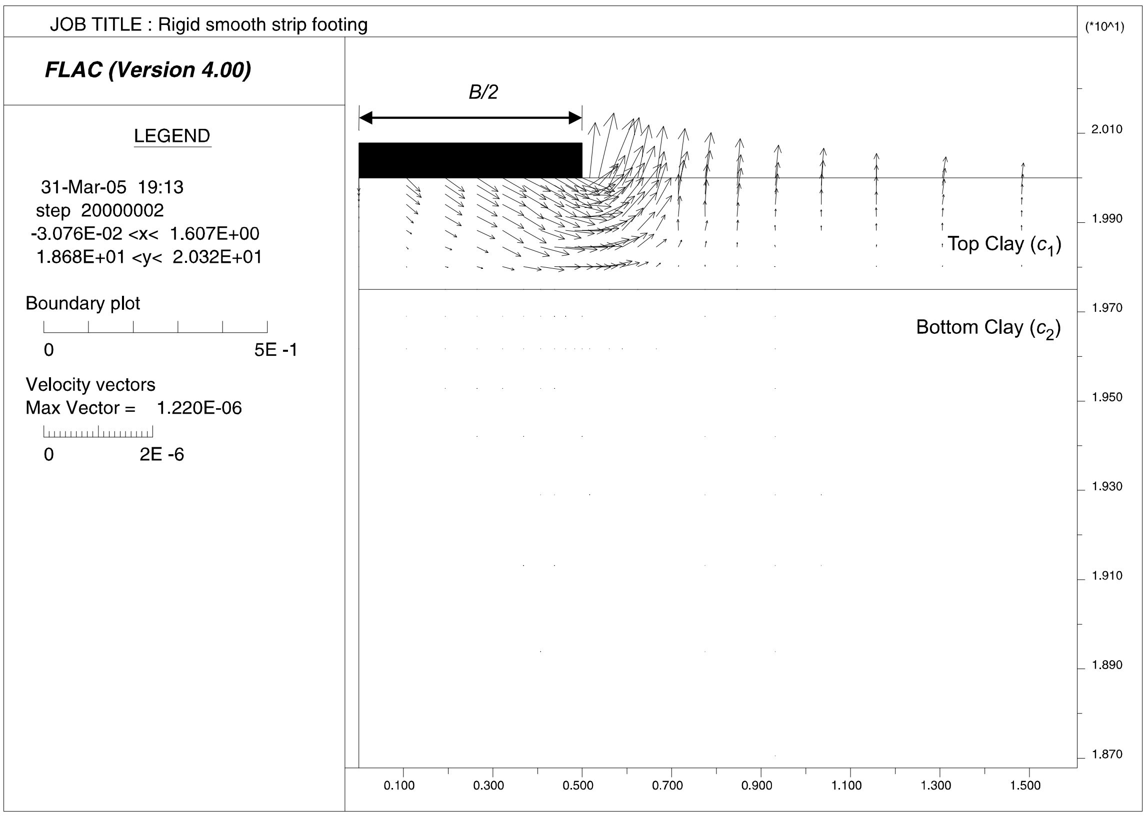

Figure A.234: Bearing pressure versus penetration curve for a rigid smooth strip footing on strong clay over soft clay for 40×30 grid model, $H/B = 0.25$, $c_1/c_2 = 0.2$.

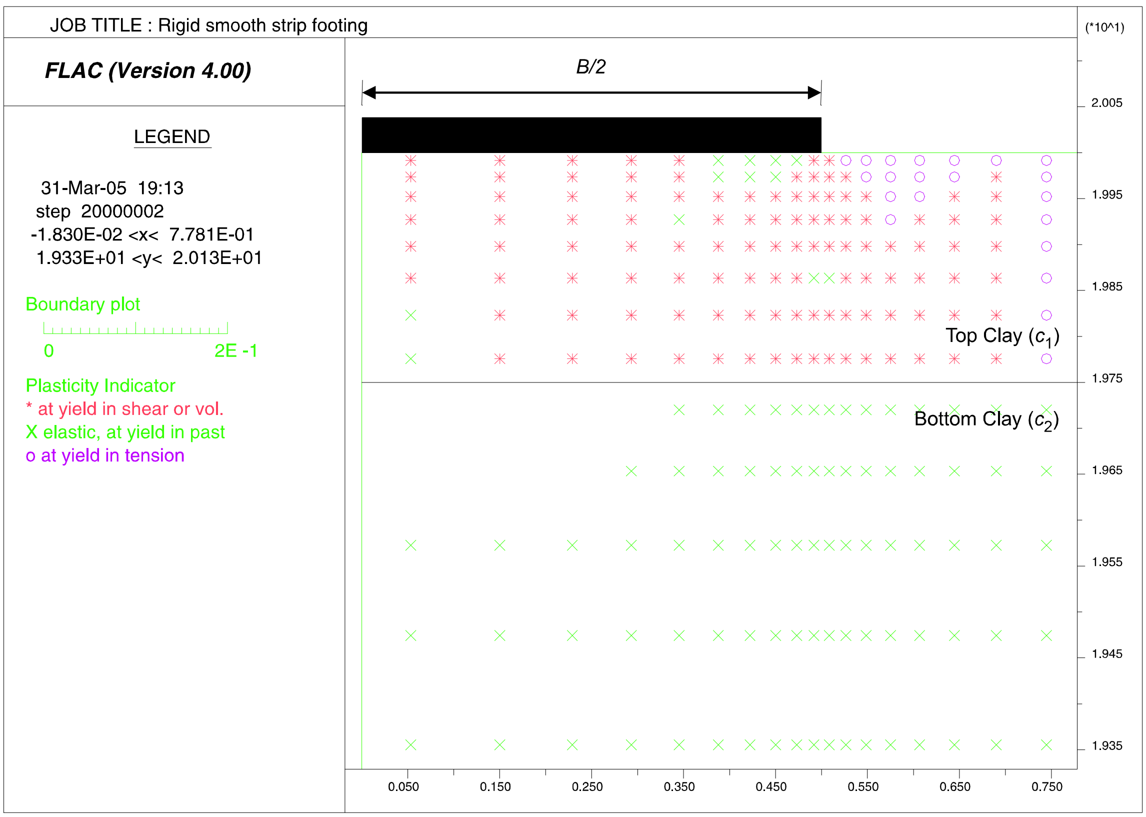

Figure A.235: Plasticity state indicators for a rigid smooth strip footing on soft clay over strong clay for 40×30 grid model, $H/B = 0.25$, $c_1/c_2 = 0.1$.

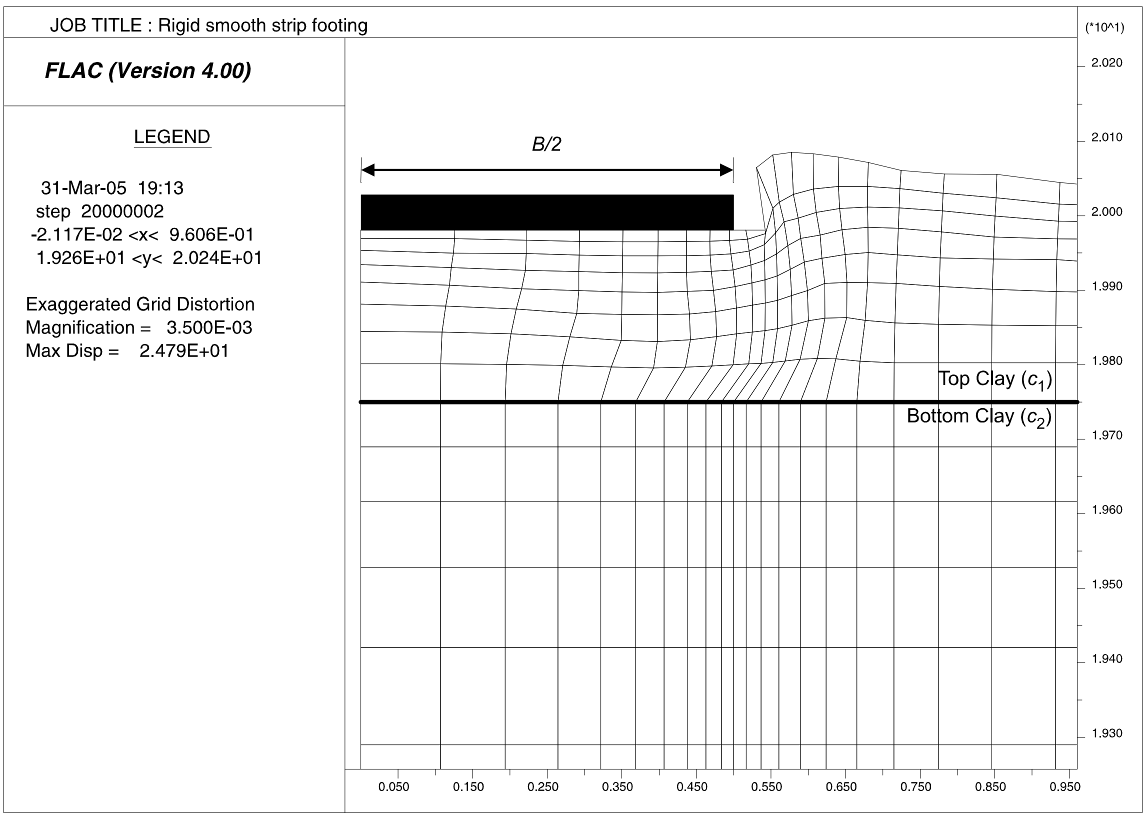

Figure A.236: Plasticity state indicators for a rigid smooth strip footing on strong clay over soft clay for 40×30 grid model, $H/B = 0.25$, $c_1/c_2 = 0.1$.

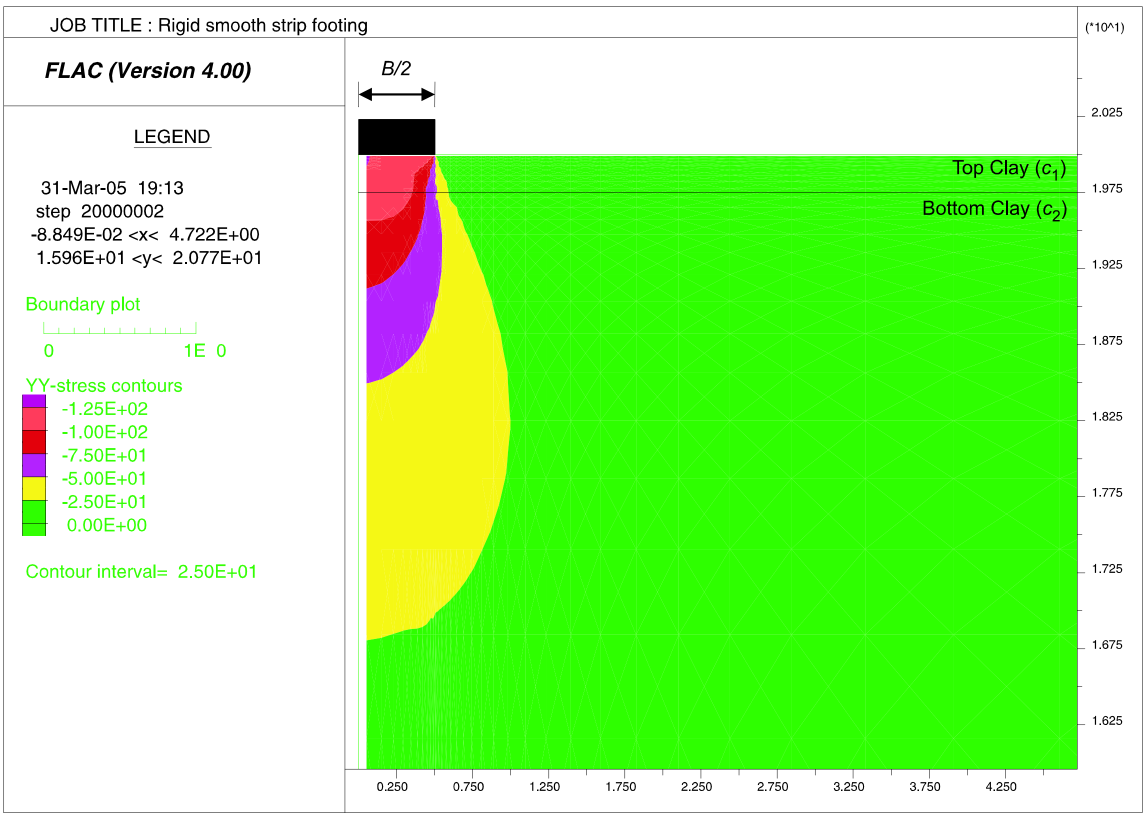

Figure A.237: Plasticity state indicators for rigid smooth strip footing on strong clay over soft clay for 40 × 30 grid model, $H/B = 0.25$, $c_1/c_2 = 0.1$.

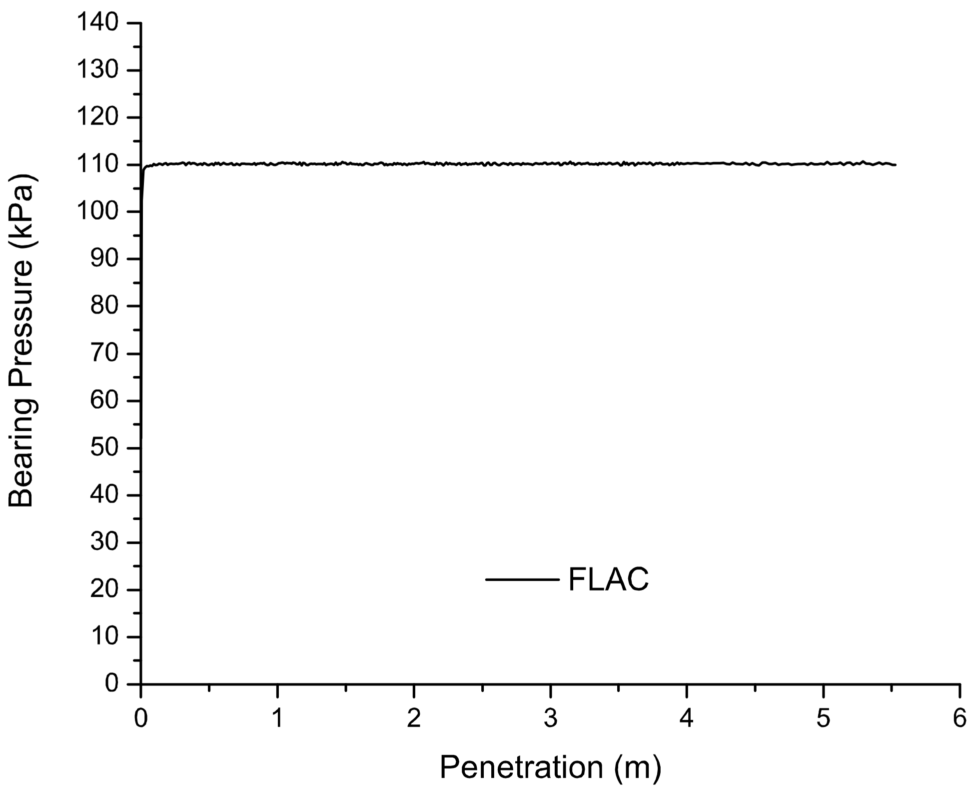

Figure A.238: Plasticity state indicators for a rigid smooth strip footing on soft clay over strong clay for 40×30 grid model, $H/B = 0.25$, $c_1/c_2 = 0.1$.

A.3 Circular Footing on Stiff Clay Overlying Soft Clay

An axisymmetric analyses of the circular footing resting on the ground surface of stiff clay overlying a soft clay is investigated in this section:

Model Geometry The circular footing is assumed to be perfectly smooth. Since the circular footing is an axisymmetric problem only a half space model is used for this analysis. The model geometry has been kept the same as that for the strip footing (4.1). The typical model geometry is shown in Figure A.239 & A.240. A 40×30 grid was selected for this analysis. There are 10 elements under the footing which are graded from the edge of the footing both in $\pm x$ - directions. The spacing was finer underneath the edge of the footing, but it becomes coarser as it moves away from the edge. There are 30 elements in x - direction in the region right of footing edge. No. of elements in the y - direction is 30.

Width/diameter of strip/circular footing (B or D) $= 1$ m
Half width/radius of the strip/circular footing ($B/2$ or $D/2$) $= 0.5$ m
Width of the half space soil model ($20B$ or $20D$) $= 20$ m
Depth of the half space soil model ($20B$ or $20D$) $= 20$ m

A.3.1 Rigid Smooth Circular Footing on Strong over Soft Clay ($H/D = 1$)

The undrained shear strength ratios of the bottom layer (c_2) to top layer (c_1) considered are $0.1, 0.2, 1/3, 0.5, 2/3, 0.8,$ and 1.

Case 1: $c_2/c_1 = 1$ (Homogeneous clay) - Small Deformation Analysis

Similar to the strip footing, the prominent difficulty in the numerical analysis of a circular footing problem by FLAC is the high stress gradients developed at the footing edge. For a footing resting on the surface of the soil, the major principal stress acts vertically below the footing, whereas it acts horizontally in the soil adjacent to footing edge. This abrupt change in the stress directions and high strain rate at the edge

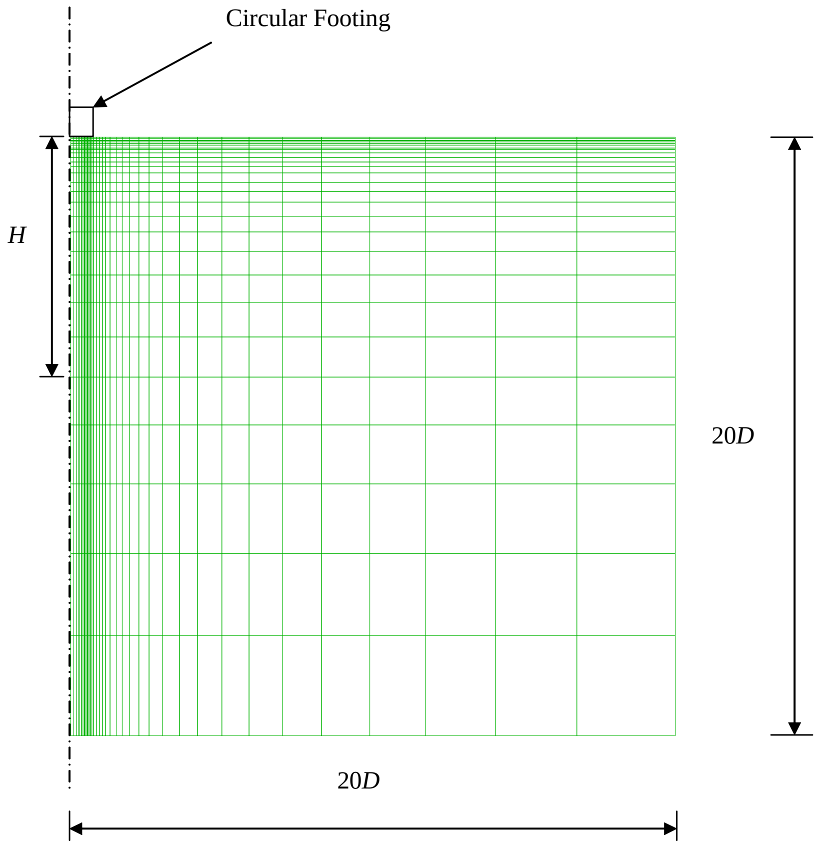

Figure A.239: Model geometry for 40×30 elements grid.

of the footing causes computational difficulties. In order to make the transition of the stresses smoother, and to prevent out-of-balance forces, smaller elements are concentrated at the edge by refining of the grid. The velocity field decays quite rapidly with depth, so the grid is graded in order to allow remote boundaries without large numbers of zones. The boundaries of the grid are kept at a sufficient distance from the footing in order to ensure that the plastic zone developed in the soil does not extend to the grid boundaries. Another option to make sure this does not happen is by allowing the grid to move in vertical direction at the vertical boundary which is equivalent to putting a roller at the boundary. This approach has only been adopted

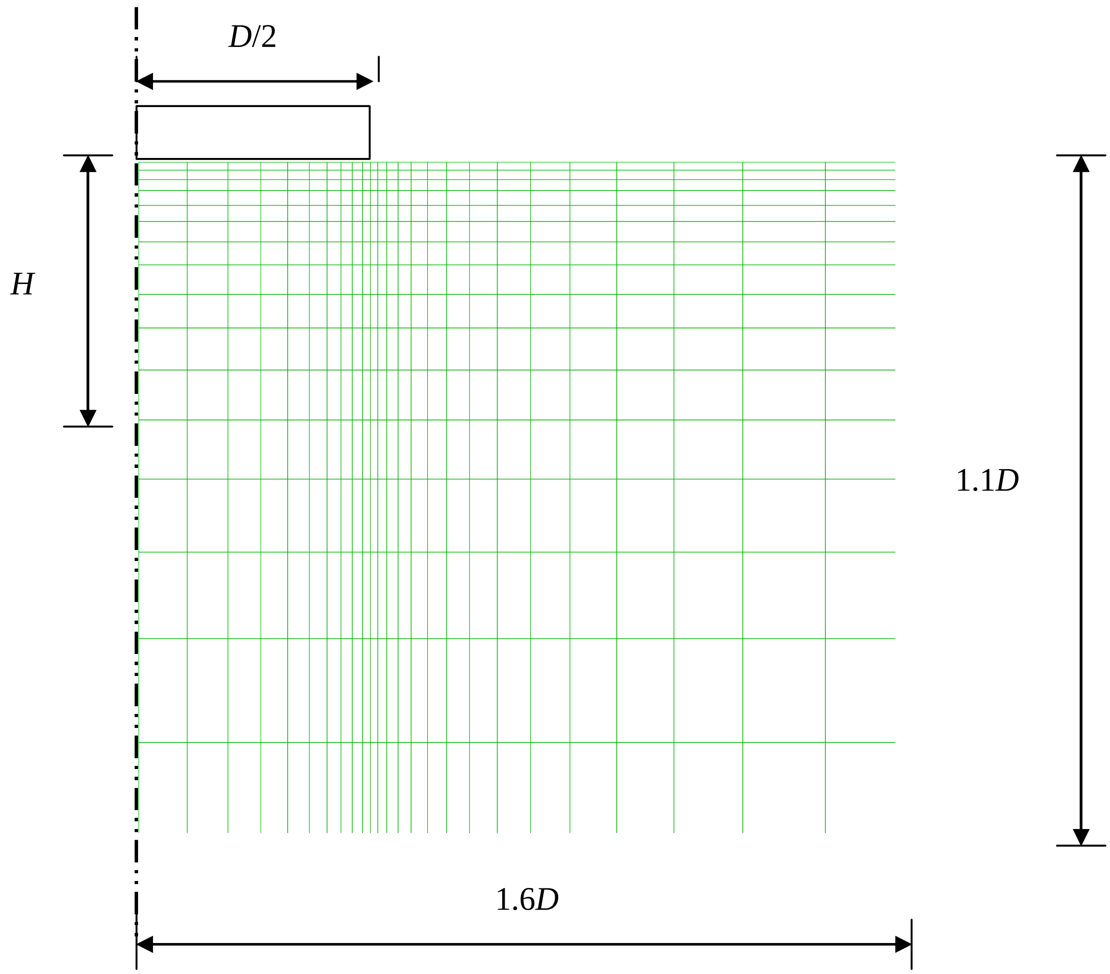

Figure A.240: Zoomed model geometry for 40 × 30 elements grid.

in bringing the initial equilibrium[4] to the models. The grid is also allowed to move vertically at the centerline of the footing.

The Mohr-Coulomb soil model was chosen for all cases.

A controlled downward velocity (displacement (m) per calculation step) of 2.5×10^{-8} is applied. FLAC calculates the nodal forces to maintain the applied velocity and the displacement of the footing is calculated continuously as the integral of the

[4]The model is in equilibrium when the net nodal force vector at each gridpoint is close to zero. Initial equilibrium under the given boundary and initial conditions is achieved for simulating insitu stresses and strains.

velocity over the calculation timestep. The footing pressure or the bearing capacity is calculated using a FISH function **"n_pres"** (explained later in this section). The footing pressure is calculated using following equation:

$$
\begin{aligned}
q &= \frac{2\pi \sum f_i^{(y)} r_i}{\pi R^2} \qquad \text{(A.3)}\\
\text{where } f_i^{(y)} &= \text{the reaction force in the } y \text{ - direction at footing gridpoint } i\\
r_i &= \text{"associated" radius at gridpoint } i\text{, and}\\
R &= \text{"effective" radius of the footing}
\end{aligned}
$$

The "associated" radius is the radial distance to each gridpoint under the footing at which velocity is applied except the gridpoint ($i = 1, j = 31$) on the axis of symmetry where the associated radius is 0.25 times the radius to gridpoint ($i = 2, j = 31$) (Itasca Consulting Group, Inc. 2001c). Due to the singularity at the edge of the footing the bearing capacity is over predicted if the actual radius of the footing is used in the bearing pressure calculations. If "effective" radius is calculated by taking the footing radius to a point midway between the last gridpoint under footing with applied velocity ($i = 11, j = 31$) and adjacent gridpoint ($i = 12, j = 31$) with no applied velocity, the footing edge is "extended" closer to the approximate position of zero stress. In this way the error in over prediction of bearing pressure is reduced.

An input data file for the FLAC analysis is described below. The data file has be divided into two stages. The objective of the first stage is to bring the model into equilibrium and to simulate insitu stresses and strains[5]. In the second stage of the data file a rigid footing is simulated by applying a constant downward velocity, and the stresses, strains and bearing pressure are calculated in the process of moving towards a final equilibrium for the model. The comments after (;) in italic fonts are the explanations for the FLAC commands and FISH functions.

Stage 1: Bringing the foundation model to initial equilibrium (Simula-

[5]In purely cohesive ($\phi = 0$) undrained clays with Tresca failure criterion, the soil behavior is independent of confining insitu stresses. This step is only for the explanation of initial equilibrium stage.

tion of insitu stresses and strains)

title

Smooth Circular Rigid Footing $H/D = 1$, $c1$ 20, $c2$ 20, initial yvel $-2.5\text{e}{-8}$ m/ timestep

;$x(10) = 0.5$ - *i.e.* 10 *elements below footing*

config ax*; axisymmetric analysis*

;

Part - I : Grid generation and assigning the soil model and soil properties

; Grid size 40 *elements in x - direction and* 30 *elements in y - direction*

g 40 30

; Soil model is Mohr-Coulomb

mo mo

; Generates a model geometry of $20\,\text{m} \times 20\,\text{m}$

gen $0, 00, 20.020.0, 20.020.0, 0$

; Soil properties are defined as shear modulus (s)*, bulk modulus* (b)*, density* (d)*, cohesion* (coh)*, friction* $(fric)$*,* $(s)/(coh) = 67$

pro s 1.34000e3 b 6.65533e4 d 2.0 coh 20 fric 0 j=17,30

pro s 1.34000e3 b 6.65533e4 d 2.0 coh 20 fric 0 j=1,16

; Generates lower clay layer, and grades the grid ,variable spacing both in x and y - direction for region under the footing

gen 0,0 0,19.0 0.5,19.0 0.5,0 i=1,11 j=1,17 rat 0.8135 0.8338

; Generates lower clay layer, and grades the grid in x and y - directions for region right side of the footing

gen same same 20.0,19.0 20.0,0 i=11,41 j=1,17 rat 1.1995 0.8338

; Generates upper clay layer, and grades the grid, variable spacing both in x and y - direction for region under the footing

gen 0, 19.0 0,20 0.5,20 0.5,19.0 i=1,11 j=17,31 rat 0.8135,0.8321

; Generates upper clay layer, and grades the grid in x and y - directions for region right side of the footing

gen same same 20,20 20,19.0 i=11,41 j=17,31 rat 1.1995 0.8321

;

Part - II : Defining the displacement boundary conditions

fix x i=1; *Fixes x - velocity at i=1 (free to roll along y - direction)*

fix x i=41; *Fixes x - velocity at i=41 (free to roll along y - direction)*

fix x y j=1; *Fixes both x & y - velocities at i=1 (no movement along x and y - directions)*

;

; **Part - III : Defining the recordings of parameters' history**

his 1 unbal; *History of unbalanced forces is recorded*

his 2 ydisp i=2 j=31; *History of y - displacement (footing penetration) is recorded under the centre of footing*

set hisfile IETest.his; *Sets history file name IETest.his for the above set of histories*

;

; **Part - IV : Calculations**

set small; *Sets small strain analysis, coordinates are not updated at each step*

solve elastic; *Calculation is performed until a steady - state solution is reached (constitutive model is changed to elastic for quick initial equilibrium)*

save IETest.sav; *Model state at initial equilibrium is saved*

;

; Stage 2: Bringing Final equilibrium to foundation model (Simulation of final stresses and strains)

res IETest.sav; *Restoration of initial equilibrium condition (insitu) stresses and strains*

;

; Part - I : Redefining boundary conditions

fix x y i=41; *Fixes x & y - velocities at i=41 for all value of j (grid points not allowed to move, simulates infinite boundary)*

fix y i=1,41 j=31; *Fixes y - velocity but frees x - velocity for the nodes under the footing (simulates smooth footing conditions)*

;The final boundary conditions are shown in Figure A.3.

; Part - II : Defining initial conditions

ini xdisp = 0*; Bringing all x-displacements to zero before starting calculations for the final equilibrium*

ini ydisp = 0*; Bringing all y-displacements to zero before starting calculations for the final equilibrium*

ini xv=0*; Bringing all x-velocities to zero before starting calculations for the final equilibrium*

ini yv=0*; Bringing all y-velocities to zero before starting calculations for the final equilibrium*

ini yv = -2.5e-8 i=1,11 j=31; *Vertical velocity (displacement/timestep) is applied to the nodes at the base of footing, also represents a rigid boundary that moves with constant velocity for finding the collapse load of soil. This approach has two advantages 1) it is much easier to control the test and obtain a good load/displacement graph, and 2) FLAC takes a long time to converge if there is large contrast in stiffnesses of materials (footing and soil in this case)* (Itasca Consulting Group, Inc. 2002c) *3) Assigning smaller initial velocity value reduces the inertial shock to the system. The oscillations in the model can further be reduced by reducing the magnitude of initial velocity. Also, the predicted bearing pressure approaches the "true" bearing pressure (where upper and lower bound tends to equal) when a low velocity is applied. However, FLAC has practical limitation in reducing the magnitude of the velocity to be applied because a) limited precision error leads to rounding errors, and b) low velocities makes the model to run for longer time*

;

mark i=1,11 j=11; *Marks nodes under the footing which can be seen in the model in forms of crosses*

;

; FISH function for minimizing the influence of inertial effects on the response of the model

def servo; *Servo - Control FISH function is used to minimize the influence of inertial effects on the response of the model. It is shown here how the applied velocities are adjusted as a function of the maximum unbalanced force in the model* (Itasca Consulting Group, Inc. 2001a)

```
 while_stepping
    if unbal > 0.05 then
      loop i (1,11)
      yvel(i,31) = yvel(i,31)*0.975
      if yvel(i,31) < -2.5e-7 then
         yvel(i,31) = -2.5e-7
      end_if
      if yvel(i,31) > -2.5e-9 then
         yvel(i,31) = -2.5e-9
     end_if
    end_loop
  end_if
;
 if unbal < 0.02 then
 loop i (1,11)
   yvel(i,31) = yvel(i,31)*1.025
   if yvel(i,31) < -2.5e-7 then
      yvel(i,31) = -2.5e-7
    end_if
    if yvel(i,31) > -2.5e-9 then
       yvel(i,31) = -2.5e-9
   end_if
  end_loop
end_if
end
; — comparison to analytical solution —
; FISH function for calculating footing pressure
def n_pres
    val = yforce(1,31)*x(2,31)*0.25
   loop i (2,11)
      val = val + yforce(i,31)*x(i,31)
```

end_loop

rad = (x(11,31)+x(12,31))*0.5; *Effective radius*

n_pres = val *2./(rad*rad); *Numerical bearing pressure*

disp = -ydisp(1,31); *y - displacement of grid point i=1, j=31 under footing*

end

; *FISH function for calculating the difference between analytical and numerical results*

def err

a_pres = 0.94*(6.05*20); *Analytical bearing pressure* (Brown and Meyerhof 1969), *value reduced for smooth footing* (Wang and Carter 2001)

err=(n_pres-a_pres)/a_pres; *Numerical and analytical Bearing pressure comparison*

end

;

def myclock; *FISH function for calculating the total time taken for the calculations*

myclock=clock/100 ; *Time in seconds since midnight*

end

; — **parameter histories recorded** —

hist 3 n_pres

hist 4 err

hist 5 a_pres

hist 6 disp

hist 7 yv i 1 j 31

hist 8 myclock

set hisfile CR1.his

;

set ncw=100000; *sets the write to screen during cycling to every 100,000 steps*

step 20000000; *Executes 20,000,000 steps of iterations for achieving the equilibrium*

his write 3 5 vs 6 skip 5000; *Records histories (his 3 & 5 versus his 6 after every 5000)* save CR1.sav; *Model state at final equilibrium is saved*

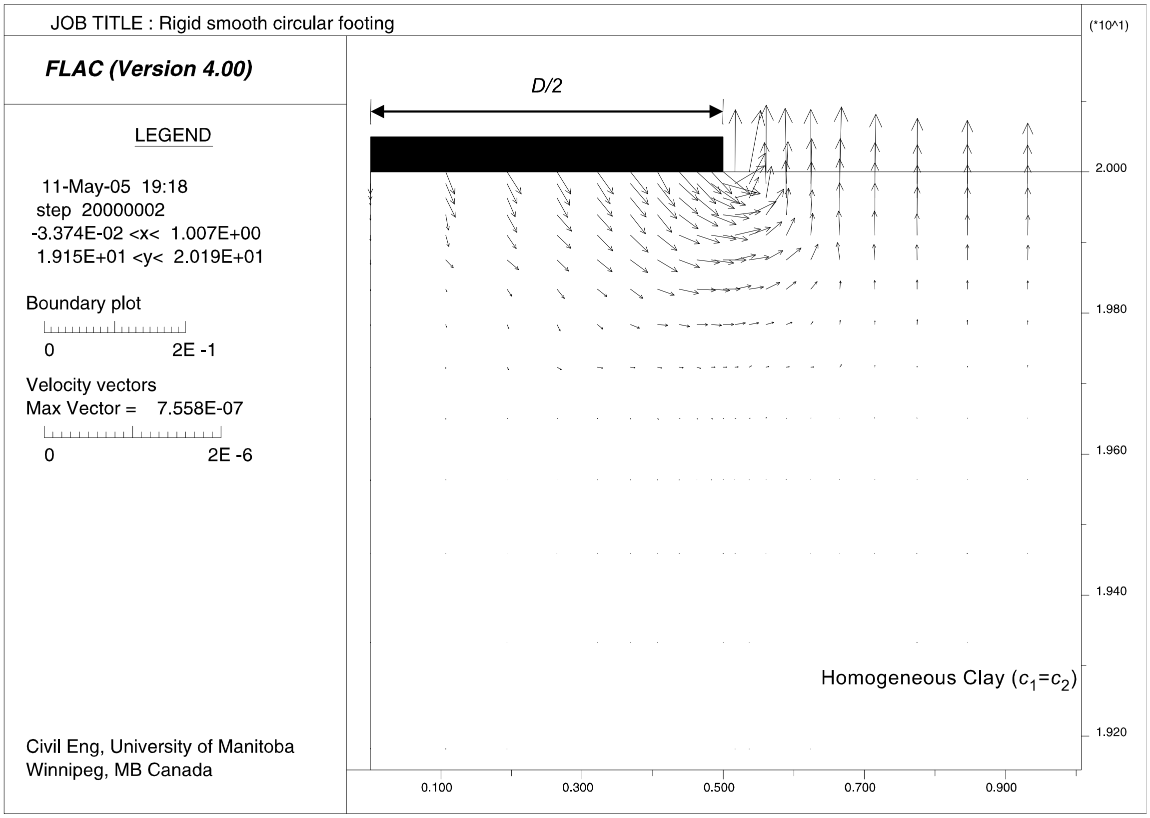

Figure A.241: Velocity vectors for a rigid smooth circular footing on strong clay over soft clay for 40×30 grid model, $H/D = 1$, $c_2/c_1 = 1$.

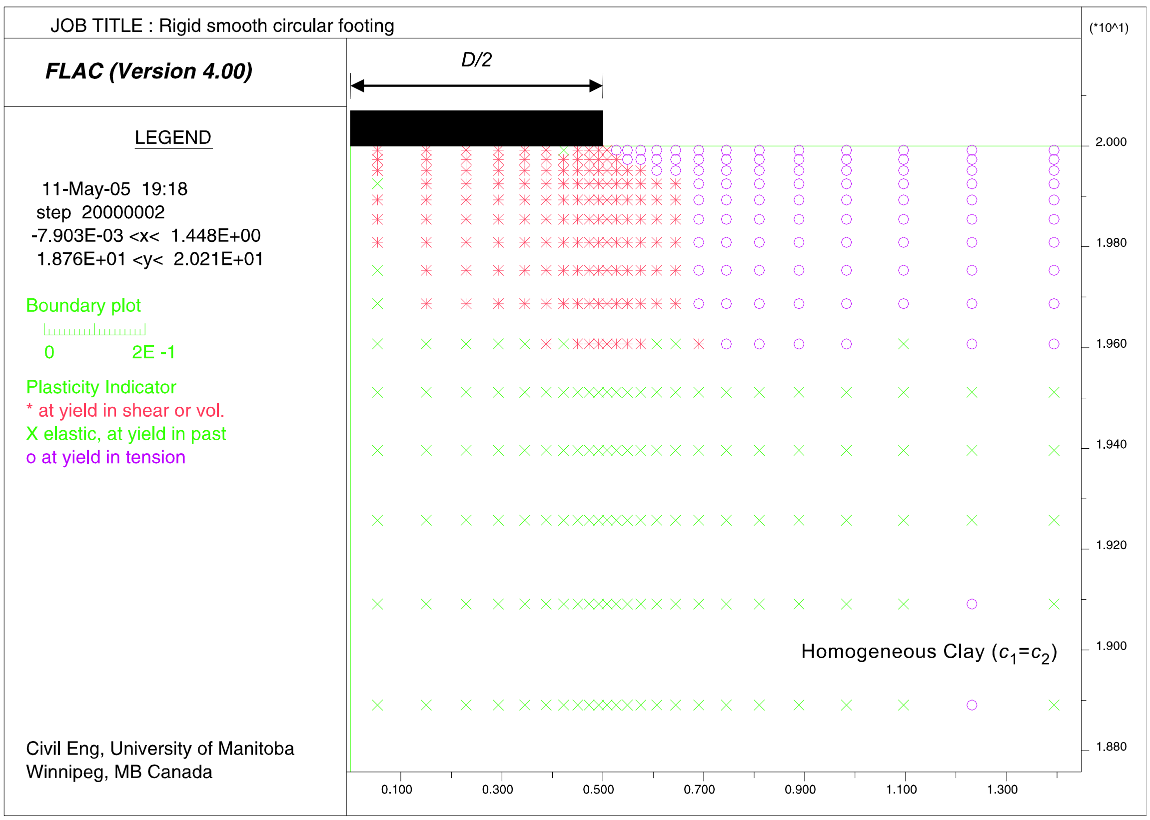

Figure A.242: Plasticity indicators for a rigid smooth circular footing on strong clay over soft clay for 40 × 30 grid model, $H/D = 1$, $c_2/c_1 = 1$.

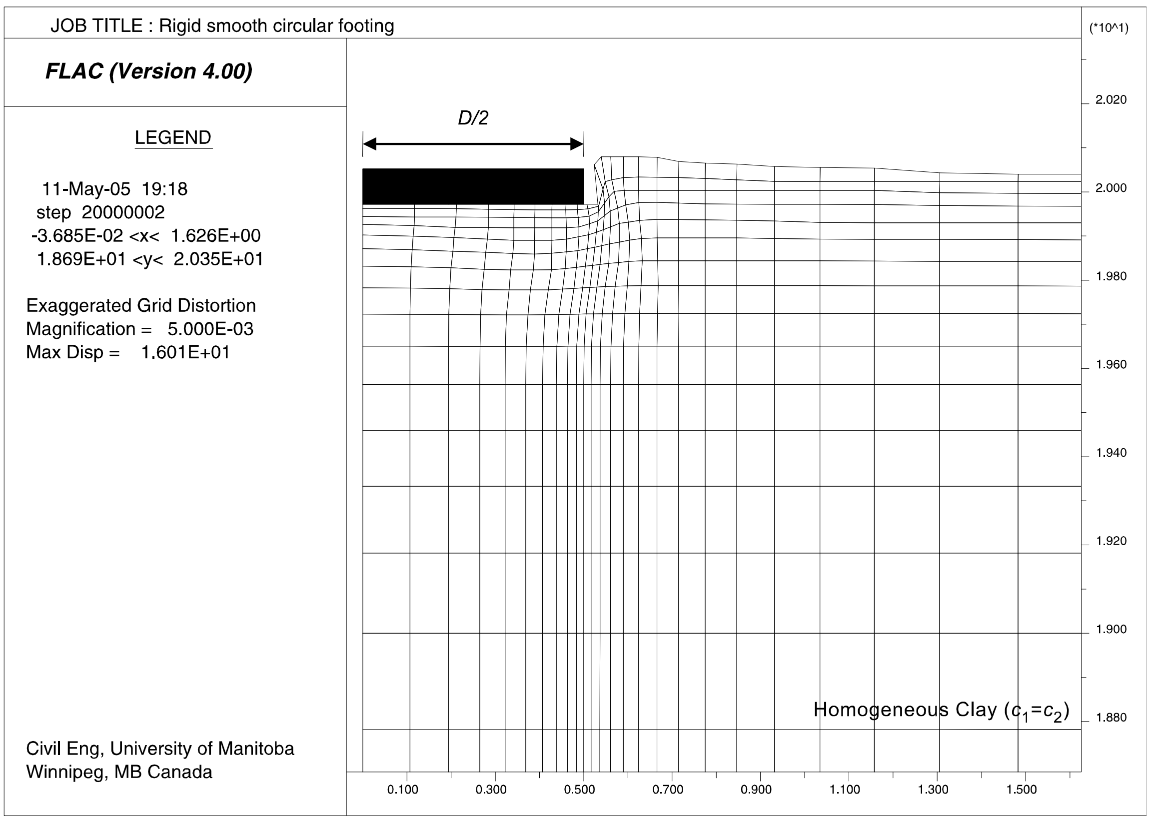

Figure A.243: Magnified grid for a rigid smooth circular footing on strong clay over soft clay for 40×30 grid model, $H/D = 1$, $c_2/c_1 = 1$.

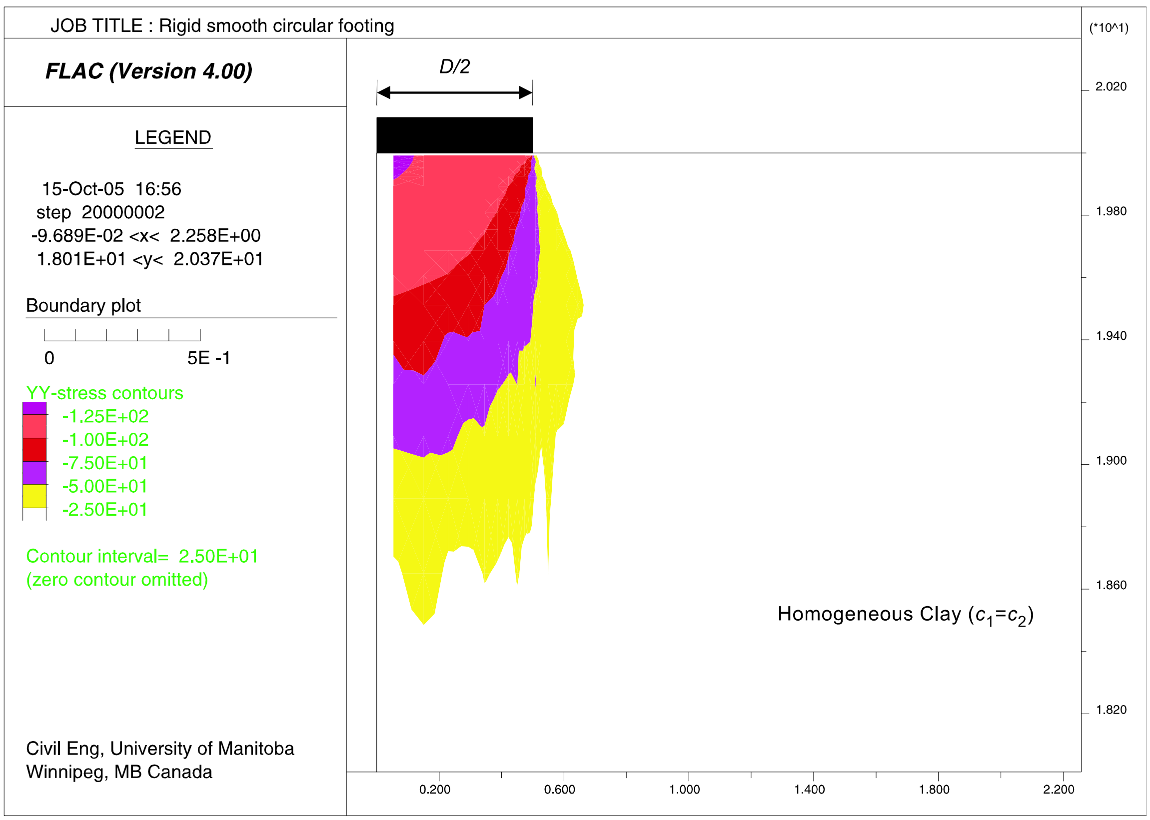

Figure A.244: Vertical stress (σ_{yy}) contours for a rigid smooth circular footing on strong clay over soft clay for 40 × 30 grid model, $H/D = 1$, $c_2/c_1 = 1$.

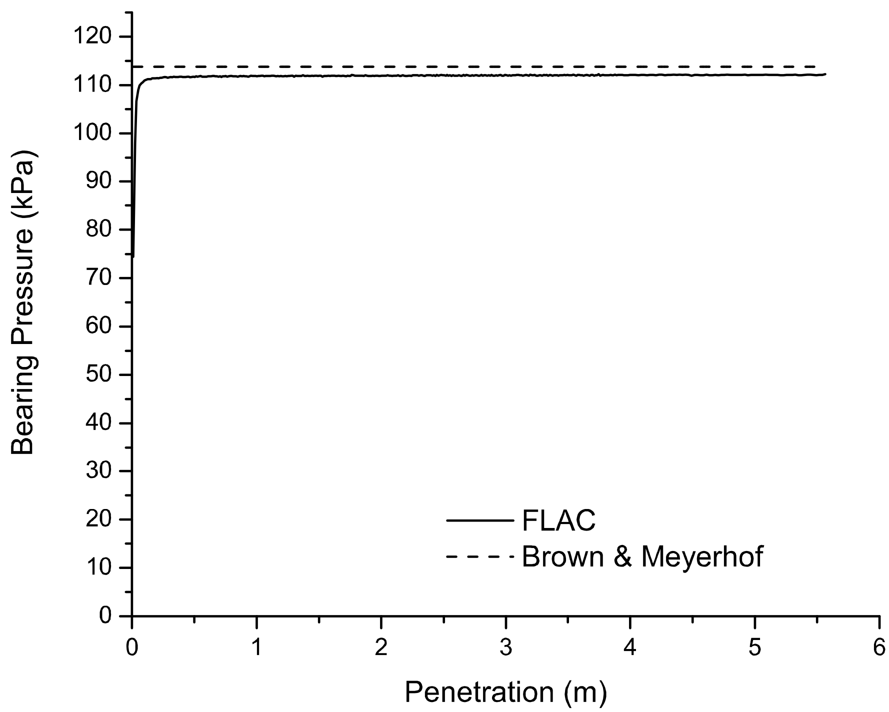

Figure A.245: Bearing pressure versus penetration curve for a rigid smooth circular footing on strong over soft clay for 40 × 30 grid model, $H/D = 1$, $c_2/c_1 = 1$.

Case 2: $c_2/c_1 = 0.8$ - Small Deformation Analysis

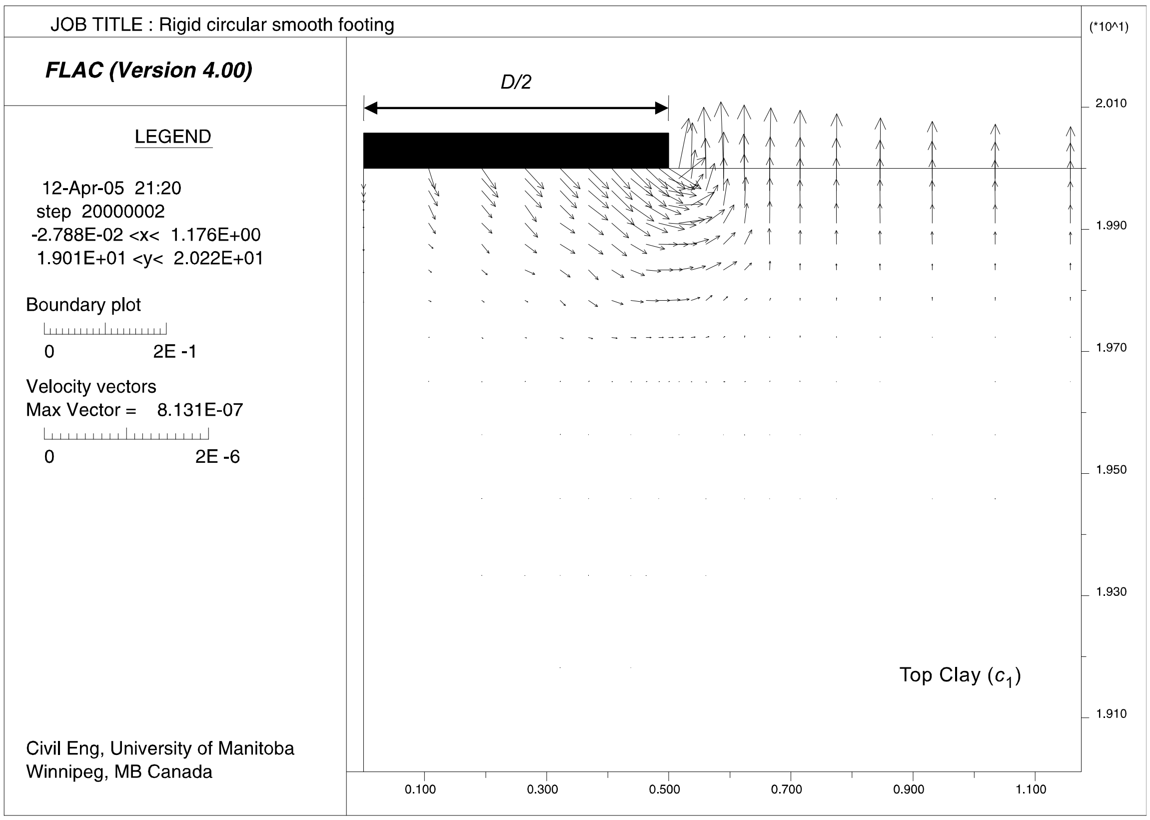

Figure A.246: Velocity vectors for a rigid circular footing on strong clay over soft clay for 40×30 grid model, $H/D = 1$, $c_2/c_1 = 0.8$.

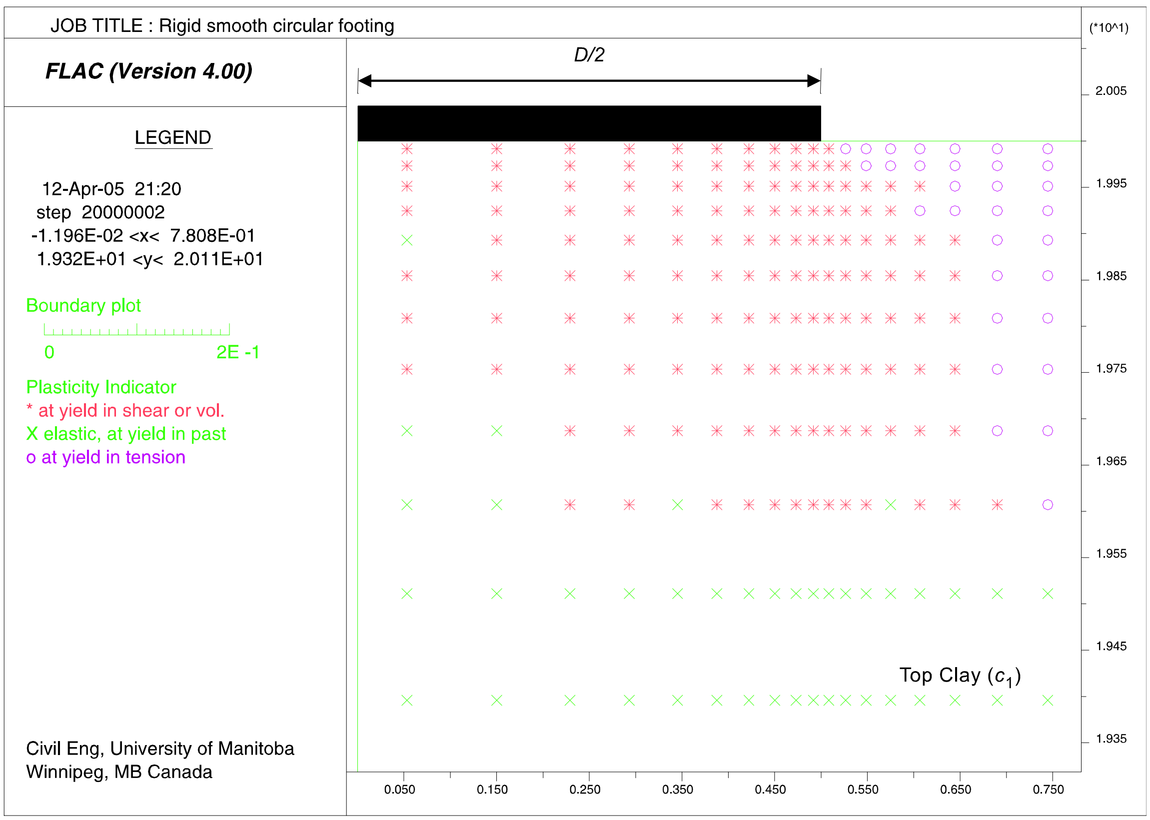

Figure A.247: Plasticity indicators for a rigid smooth circular footing on strong over soft clay for 40 × 30 grid model, $H/D = 1$, $c_2/c_1 = 0.8$.

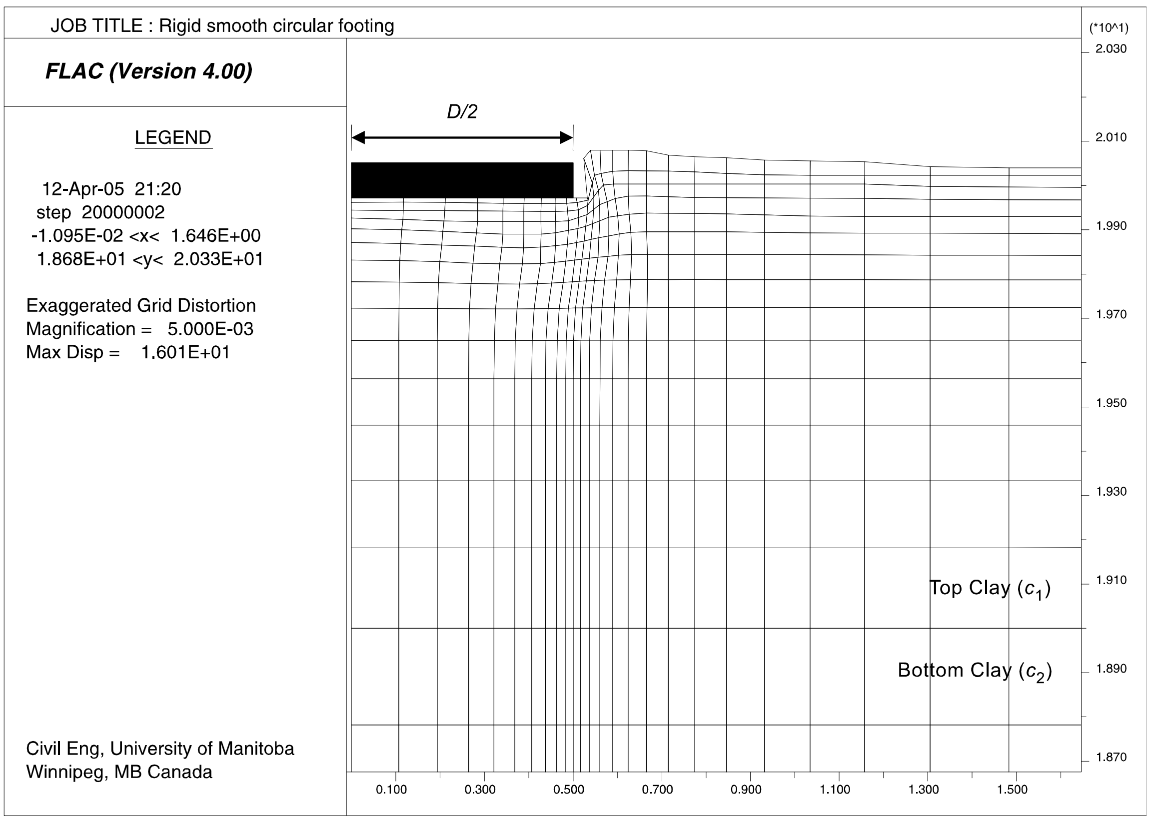

Figure A.248: Magnified grid for a rigid smooth circular footing on strong over soft clay for 40 × 30 grid model, $H/D = 1$, $c_2/c_1 = 0.8$.

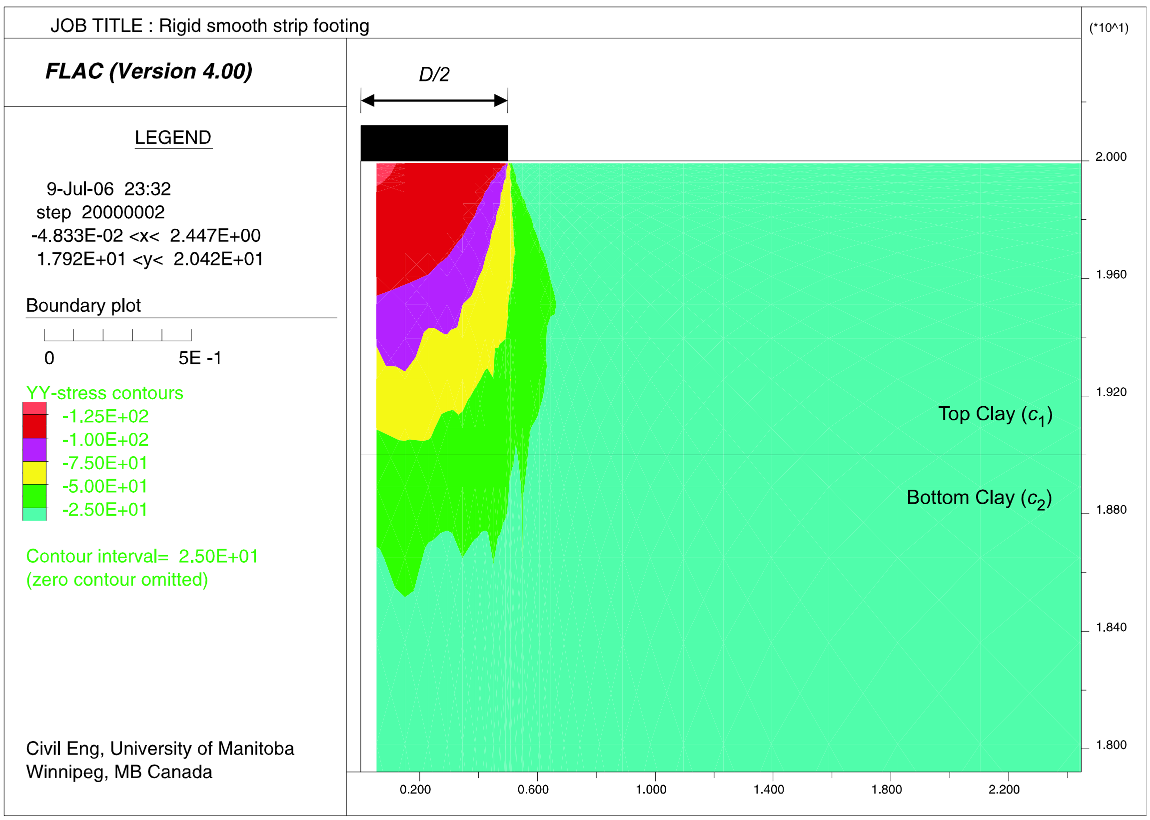

Figure A.249: Vertical stress (σ_{yy}) contours for a rigid smooth circular footing on strong over soft clay for 40 × 30 grid model, $H/D = 1$, $c_2/c_1 = 0.8$.

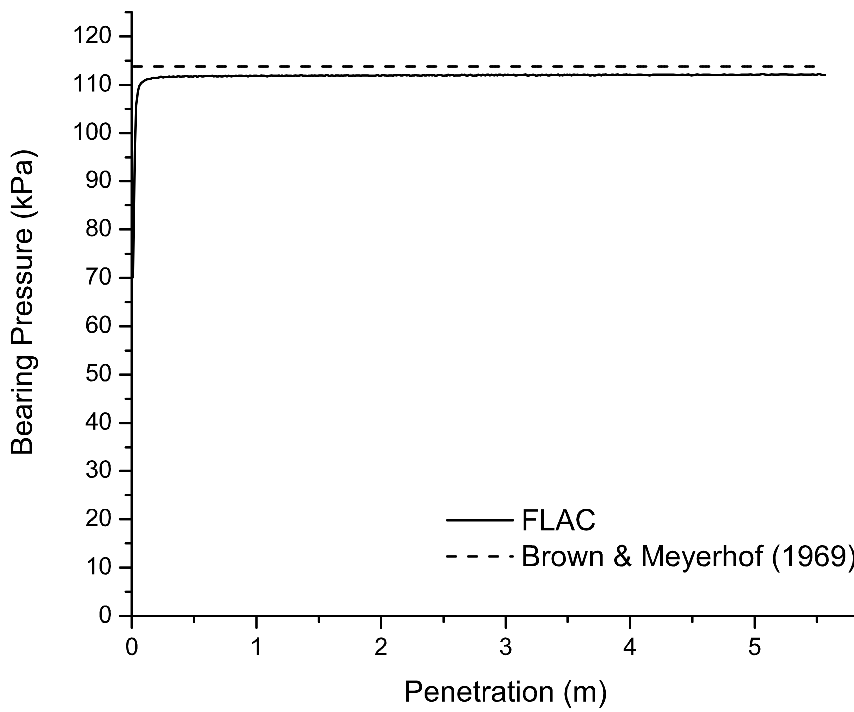

Figure A.250: Bearing pressure versus penetration curve for a rigid smooth circular footing on strong over soft clay for 40 × 30 grid model, $H/D = 1$, $c_2/c_1 = 0.8$.

Case 3: $c_2/c_1 = 2/3$ - Small Deformation Analysis

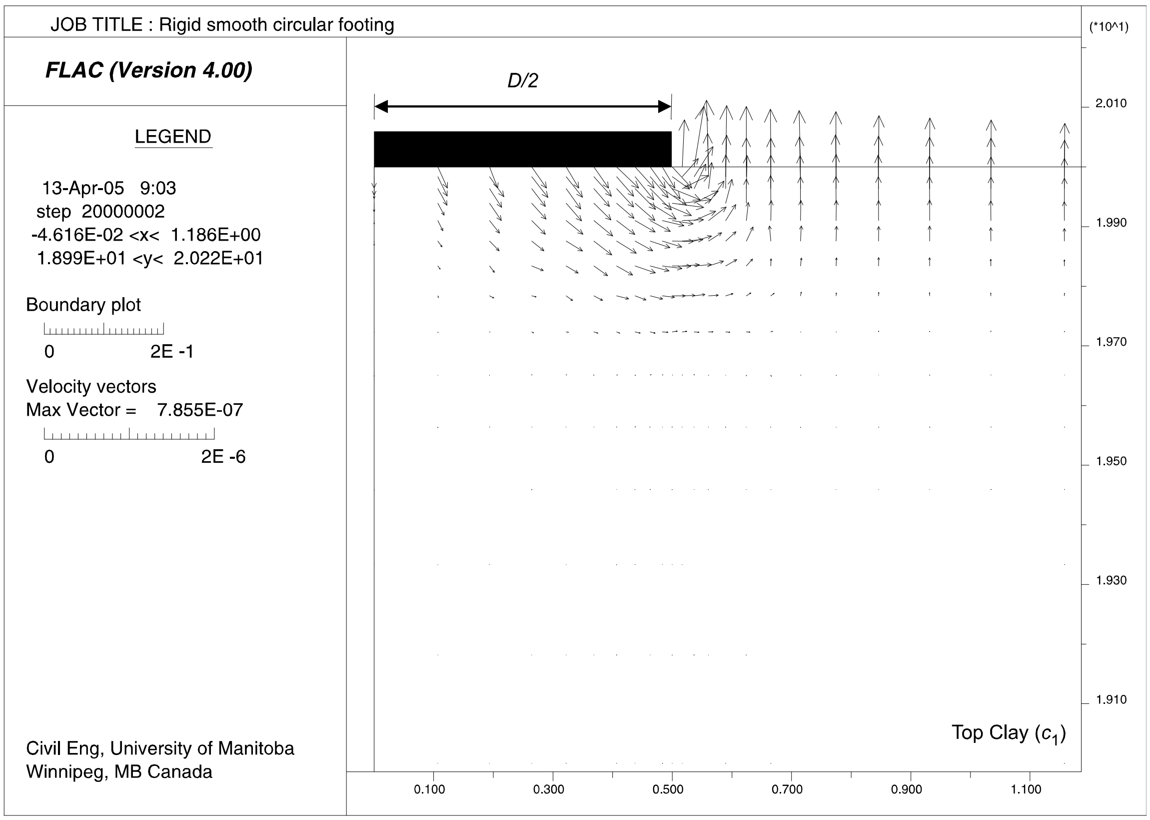

Figure A.251: Velocity vectors for a rigid smooth circular footing on strong over soft clay for 40×30 grid model, $H/D = 1$, $c_2/c_1 = 2/3$.

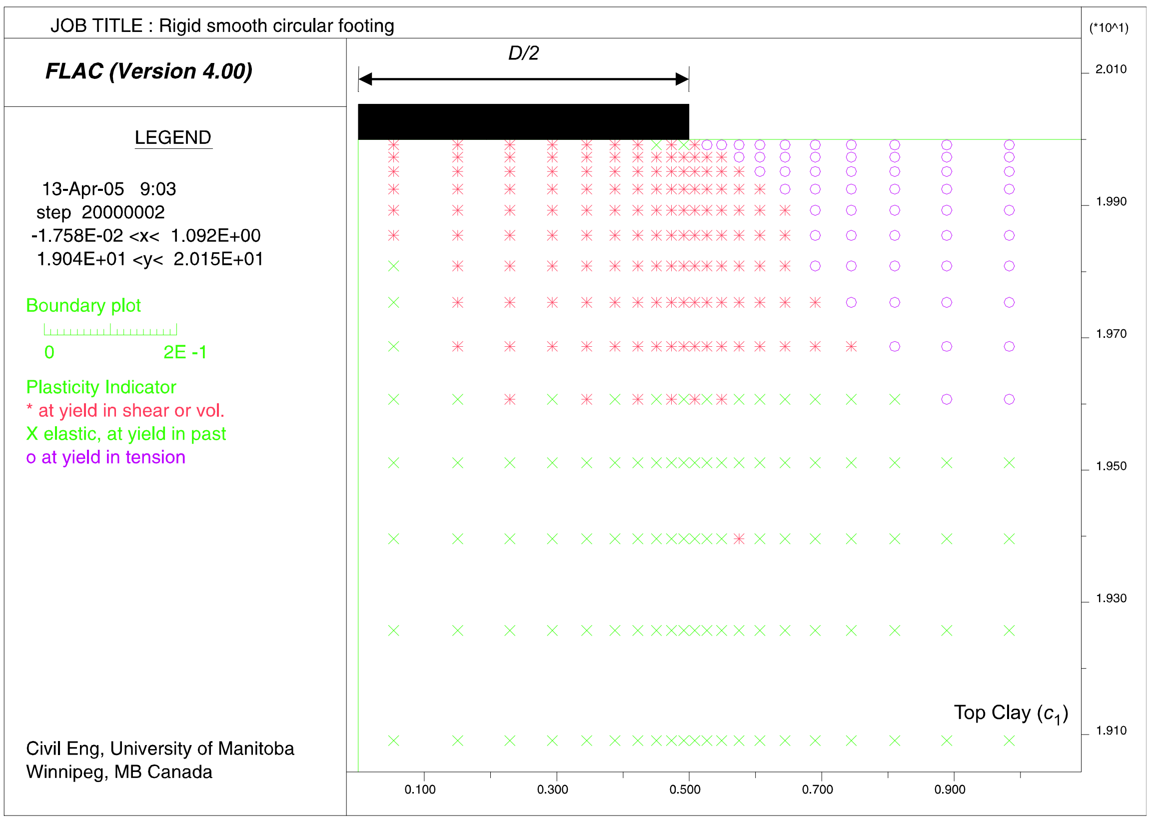

Figure A.252: Plasticity state indicators for a rigid smooth circular footing on strong over soft clay for 40×30 grid model, $H/D = 1$, $c_2/c_1 = 2/3$.

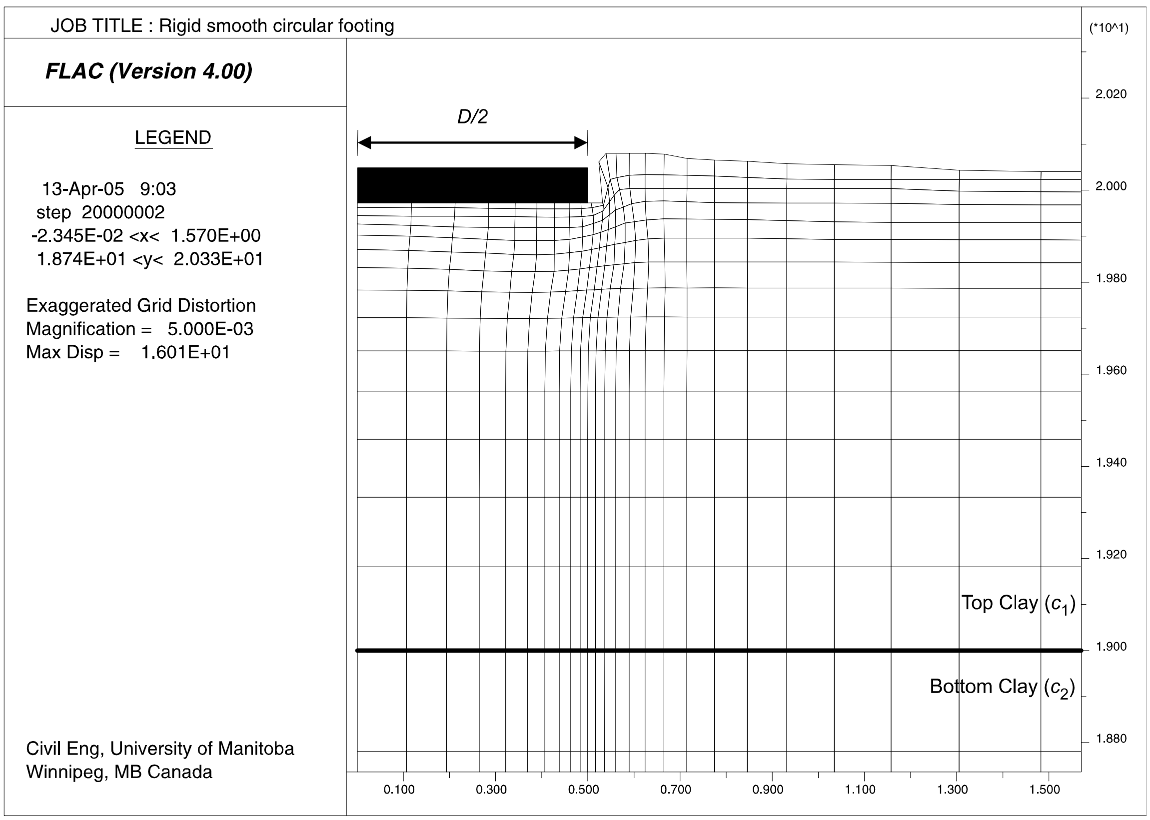

Figure A.253: Magnified grid for a rigid smooth circular footing on strong over soft clay for 40×30 grid model, $H/D = 1$, $c_2/c_1 = 2/3$.

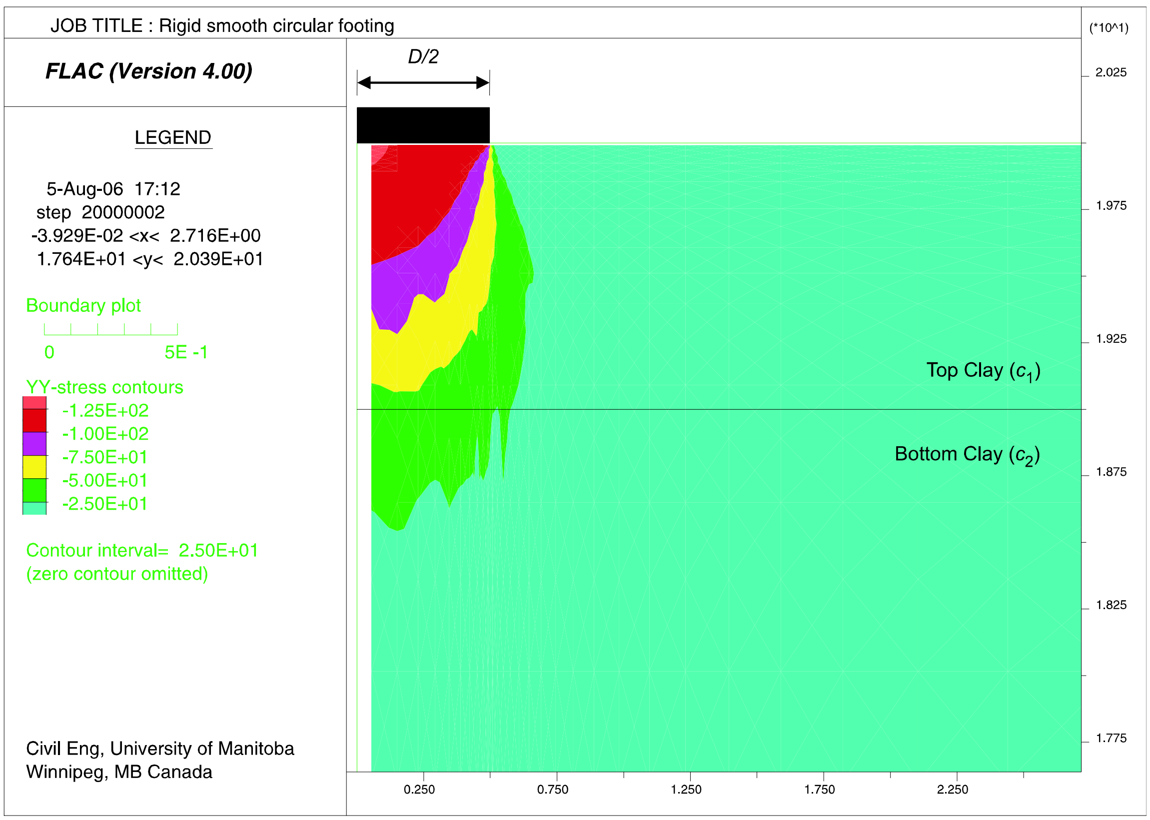

Figure A.254: Vertical stress (σ_{yy}) contours for a rigid smooth circular footing on strong over soft clay for 40 × 30 grid model, $H/D = 1$, $c_2/c_1 = 2/3$.

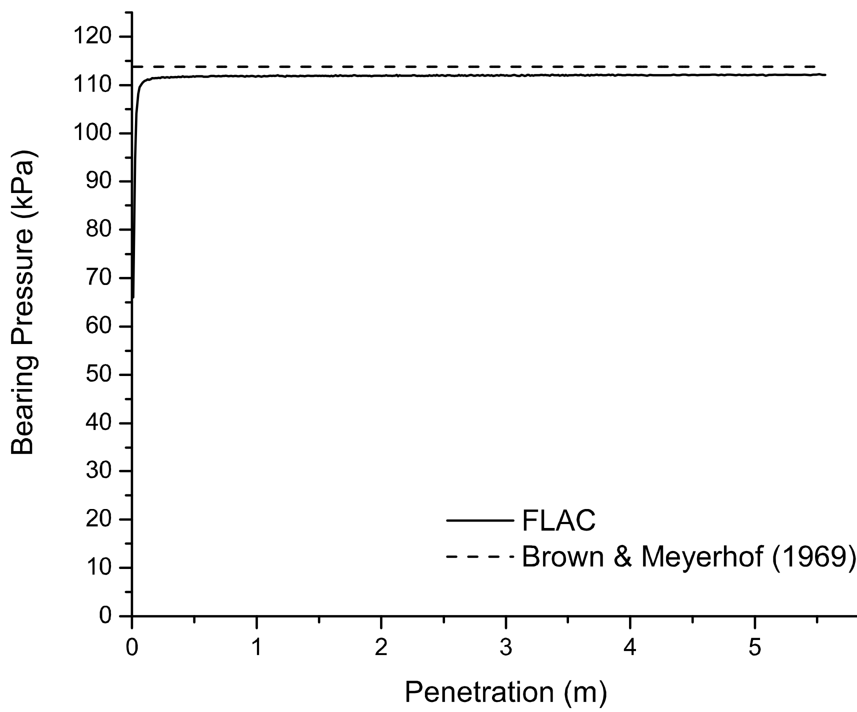

Figure A.255: Bearing pressure versus penetration curve for a rigid smooth circular footing on strong over soft clay for 40 × 30 grid model, $H/D = 1$, $c_2/c_1 = 2/3$.

Case 4: $c_2/c_1 = 0.5$ - Small Deformation Analysis

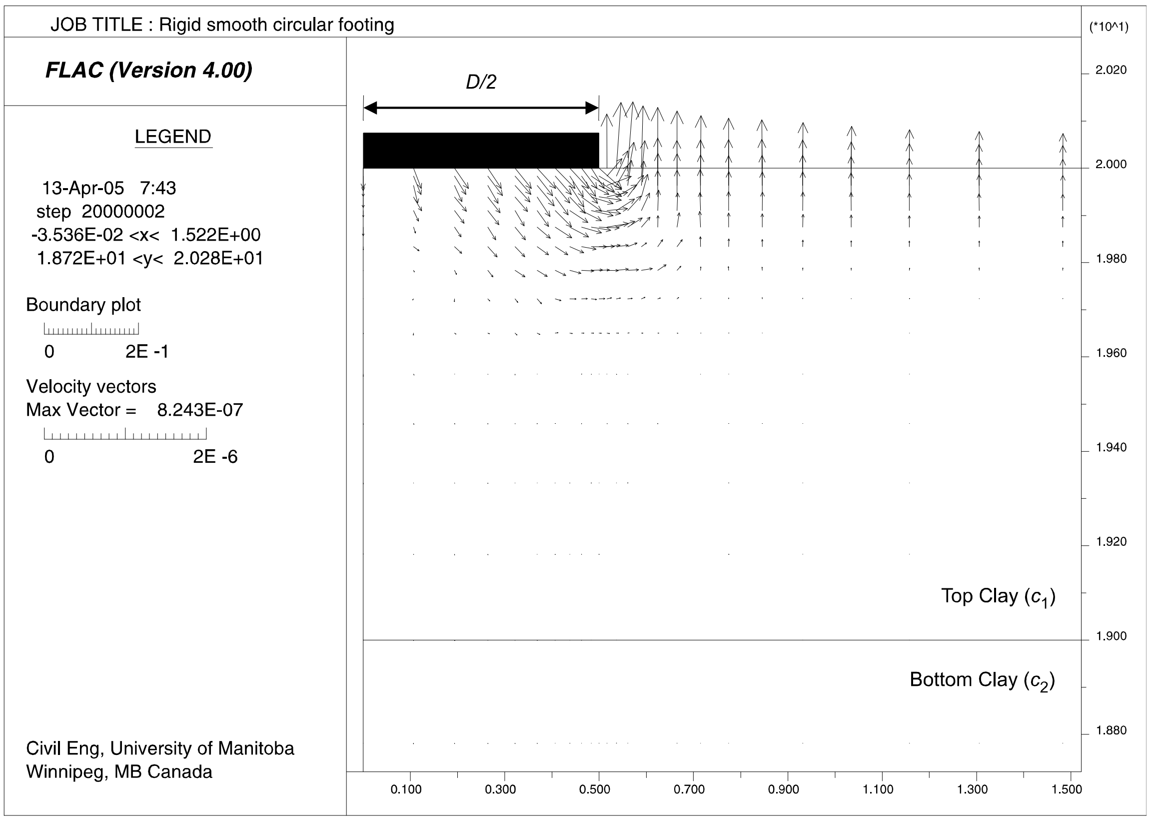

Figure A.256: Velocity vectors for a rigid smooth circular footing on strong over soft clay for 40 × 30 grid model, $H/D = 1$, $c_2/c_1 = 0.5$.

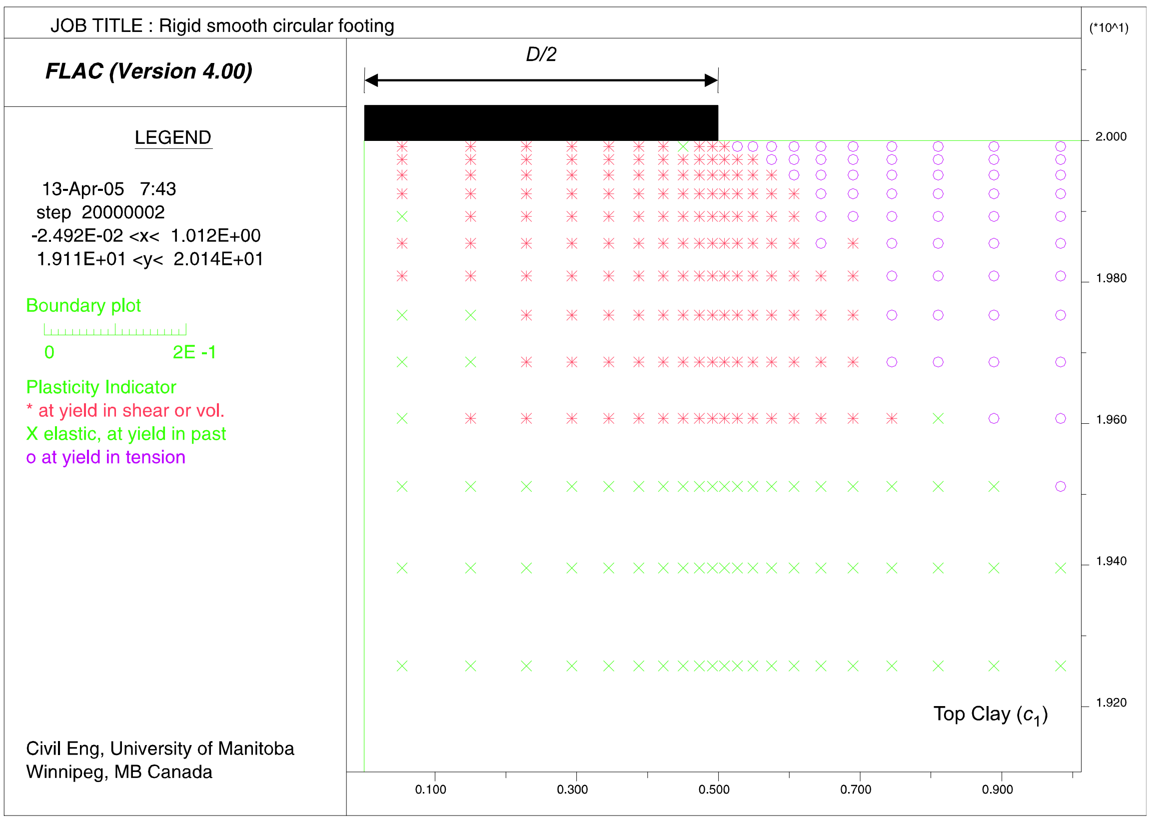

Figure A.257: Plasticity state indicators for a rigid smooth circular footing on strong over soft clay for 40×30 grid model, $H/D = 1$, $c_2/c_1 = 0.5$.

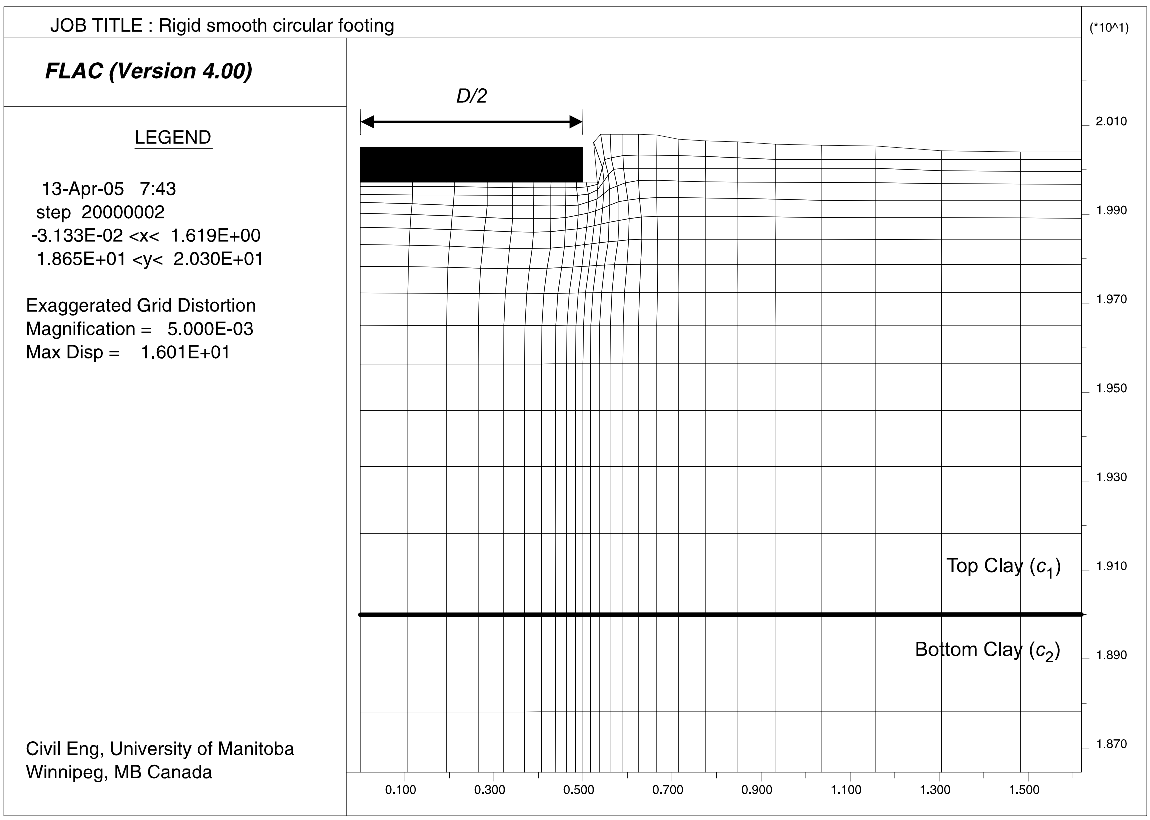

Figure A.258: Magnified grid for a rigid smooth circular footing on strong over soft clay for 40 × 30 grid model, $H/D = 1$, $c_2/c_1 = 0.5$.

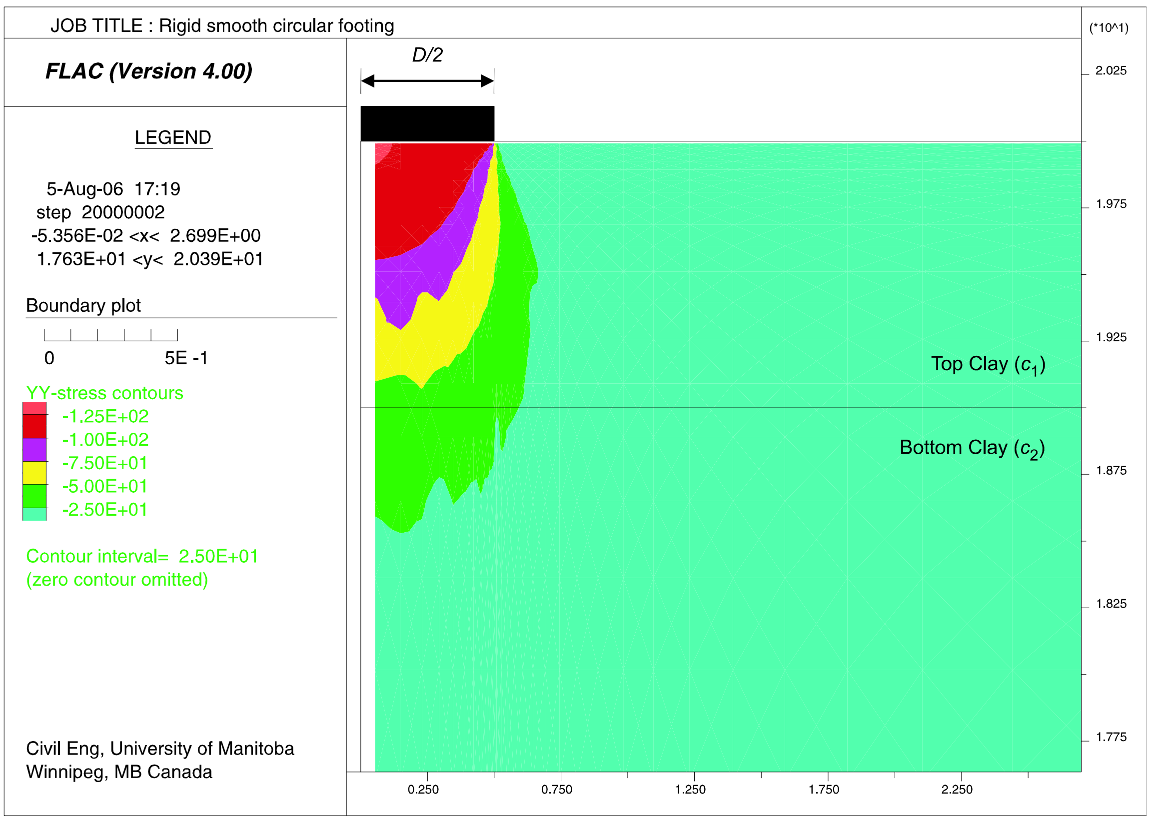

Figure A.259: Vertical stress (σ_{yy}) contours for a rigid smooth circular footing on strong over soft clay for 40 × 30 grid model, $H/D = 1$, $c_2/c_1 = 0.5$.

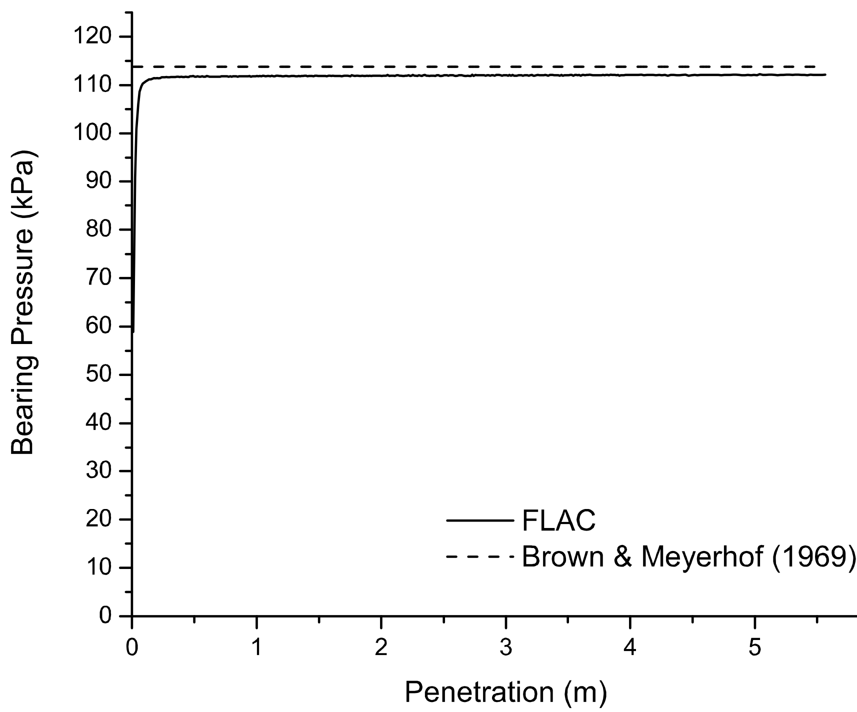

Figure A.260: Bearing pressure versus penetration curve for a rigid smooth circular footing on strong over soft clay for 40 × 30 grid model, $H/D = 1$, $c_2/c_1 = 0.5$.

Case 5: $c_2/c_1 = 1/3$ - Small Deformation Analysis

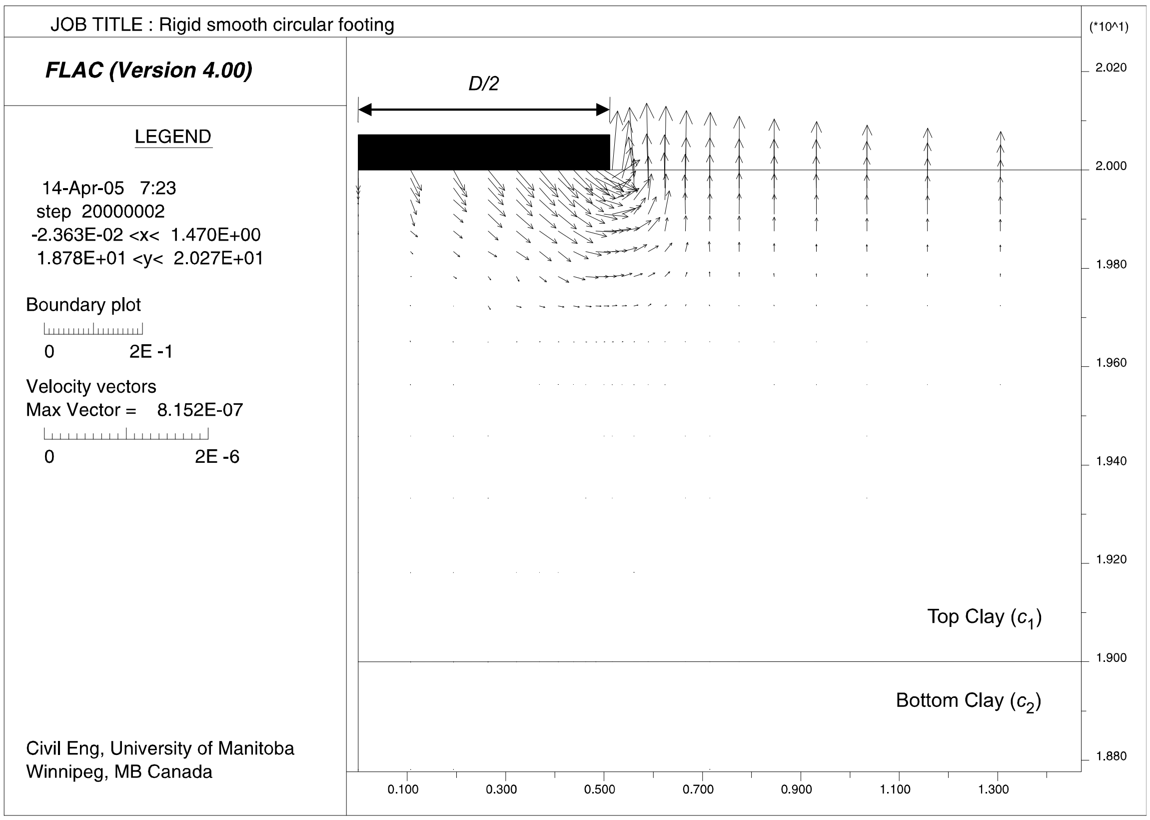

Figure A.261: Velocity vectors for a rigid smooth circular footing on strong over soft clay for 40×30 grid model, $H/D = 1$, $c_2/c_1 = 1/3$.

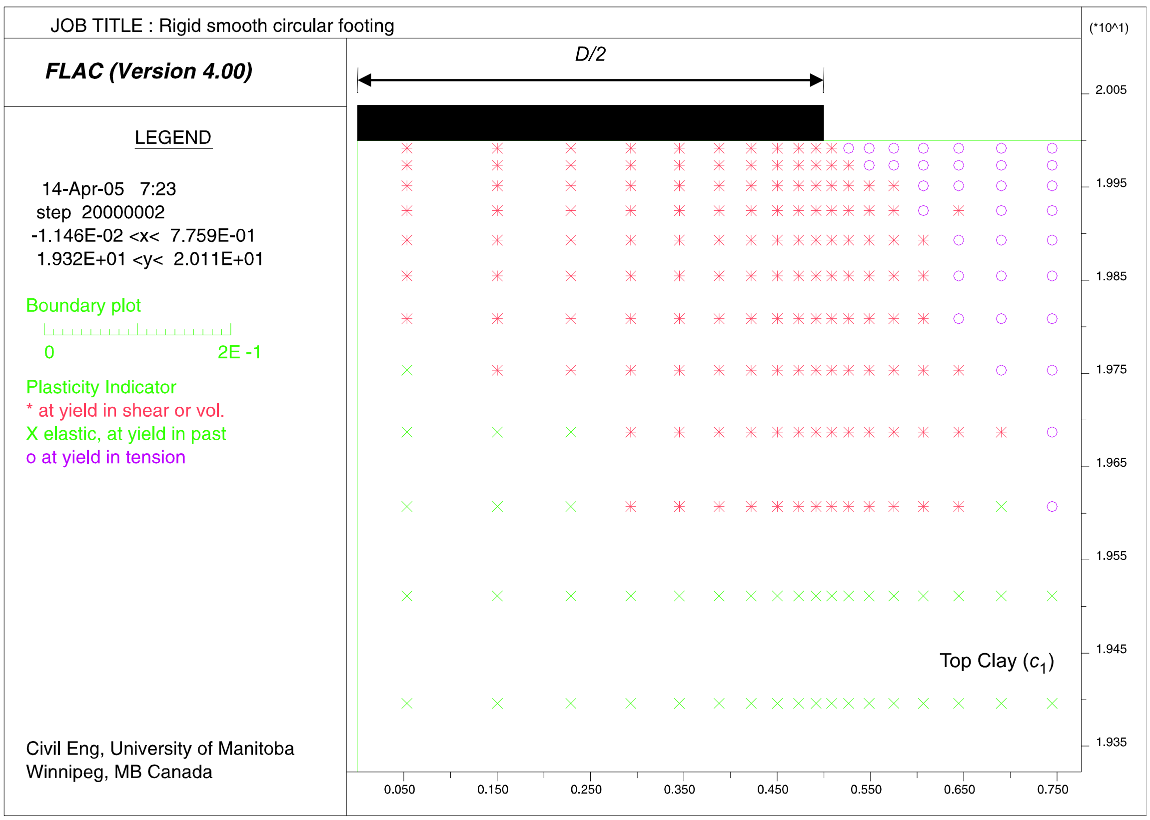

Figure A.262: Plasticity state indicators for a rigid smooth circular footing on strong over soft clay for 40 × 30 grid model, $H/D = 1$, $c_2/c_1 = 1/3$.

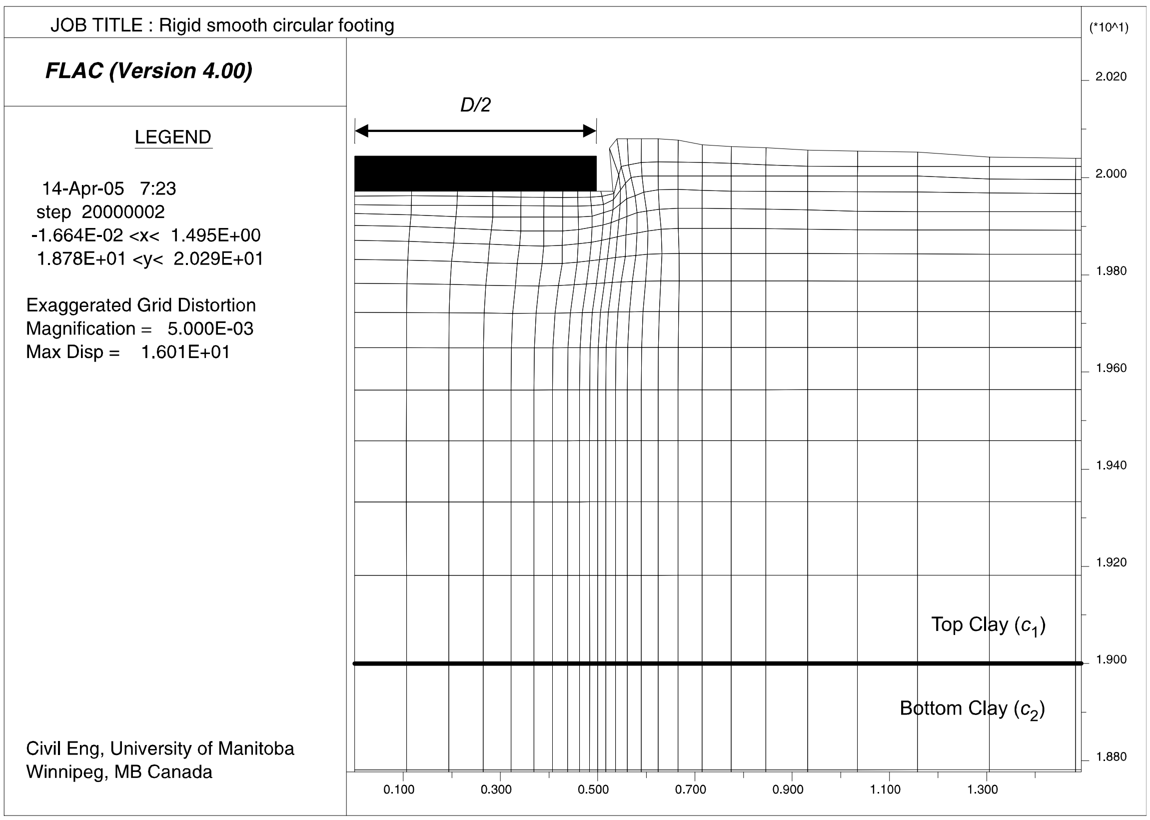

Figure A.263: Magnified grid for a rigid smooth circular footing on strong over soft clay for 40 × 30 grid model, $H/D = 1$, $c_2/c_1 = 1/3$.

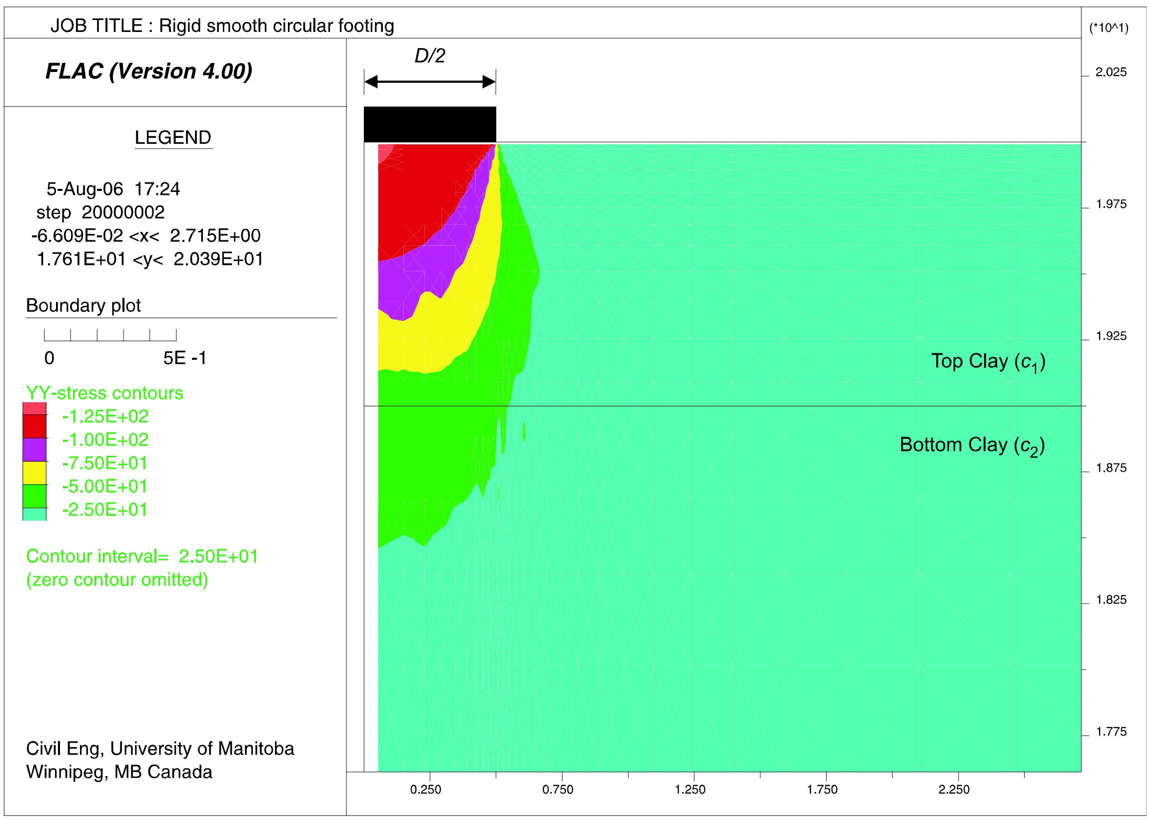

Figure A.264: Vertical stress (σ_{yy}) contours for a rigid smooth circular footing on strong over soft clay for 40 × 30 grid model, $H/B = 1$, $c_2/c_1 = 1/3$.

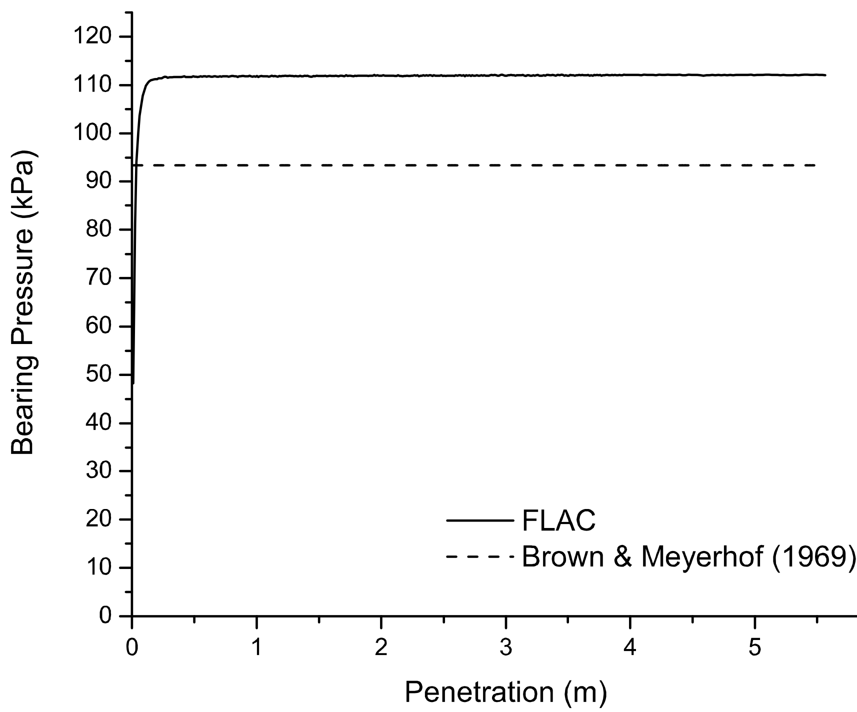

Figure A.265: Bearing pressure versus penetration curve for a rigid smooth circular footing on strong over soft clay for 40×30 grid model, $H/D = 1$, $c_2/c_1 = 1/3$.

Case 6: $c_2/c_1 = 0.2$ **- Small Deformation Analysis**

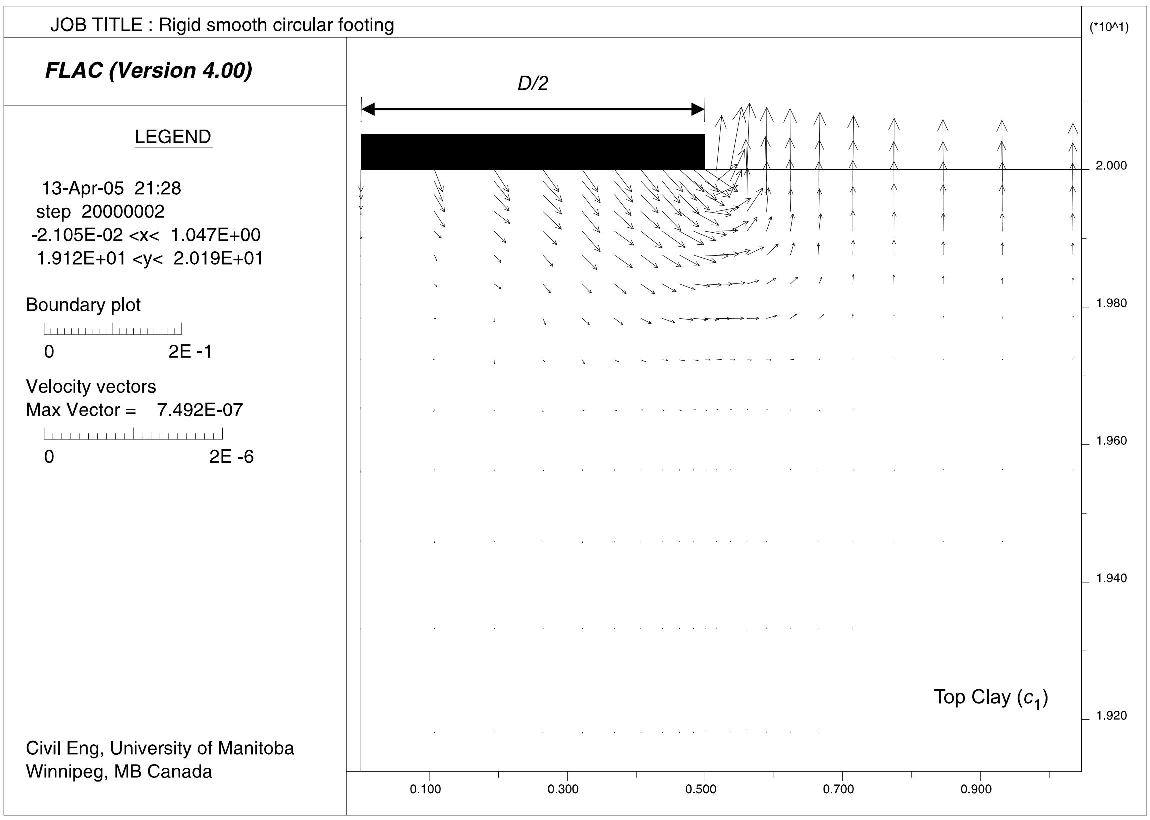

Figure A.266: Velocity vectors for a rigid smooth circular footing on strong over soft clay for 40×30 grid model, $H/D = 1$, $c_2/c_1 = 0.2$.

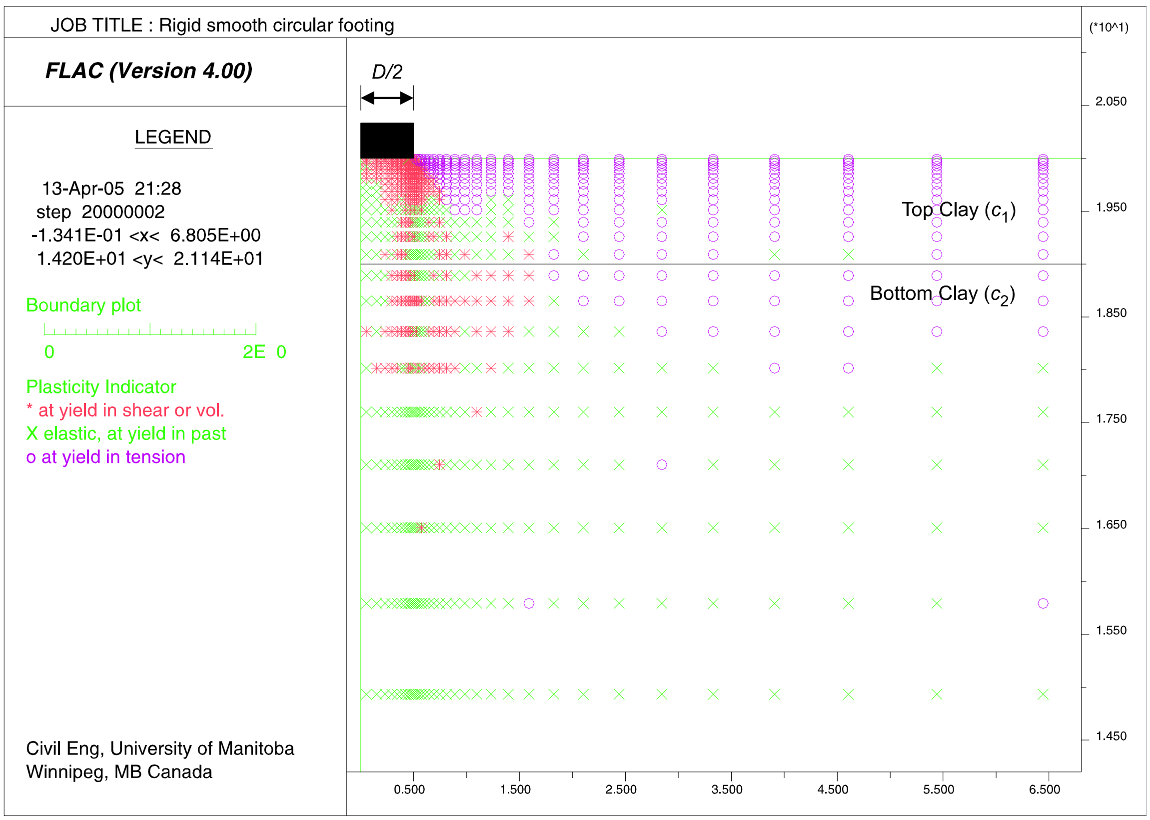

Figure A.267: Plasticity state indicators for a rigid smooth circular footing on strong over soft clay for 40×30 grid model, $H/D = 1$, $c_2/c_1 = 0.2$.

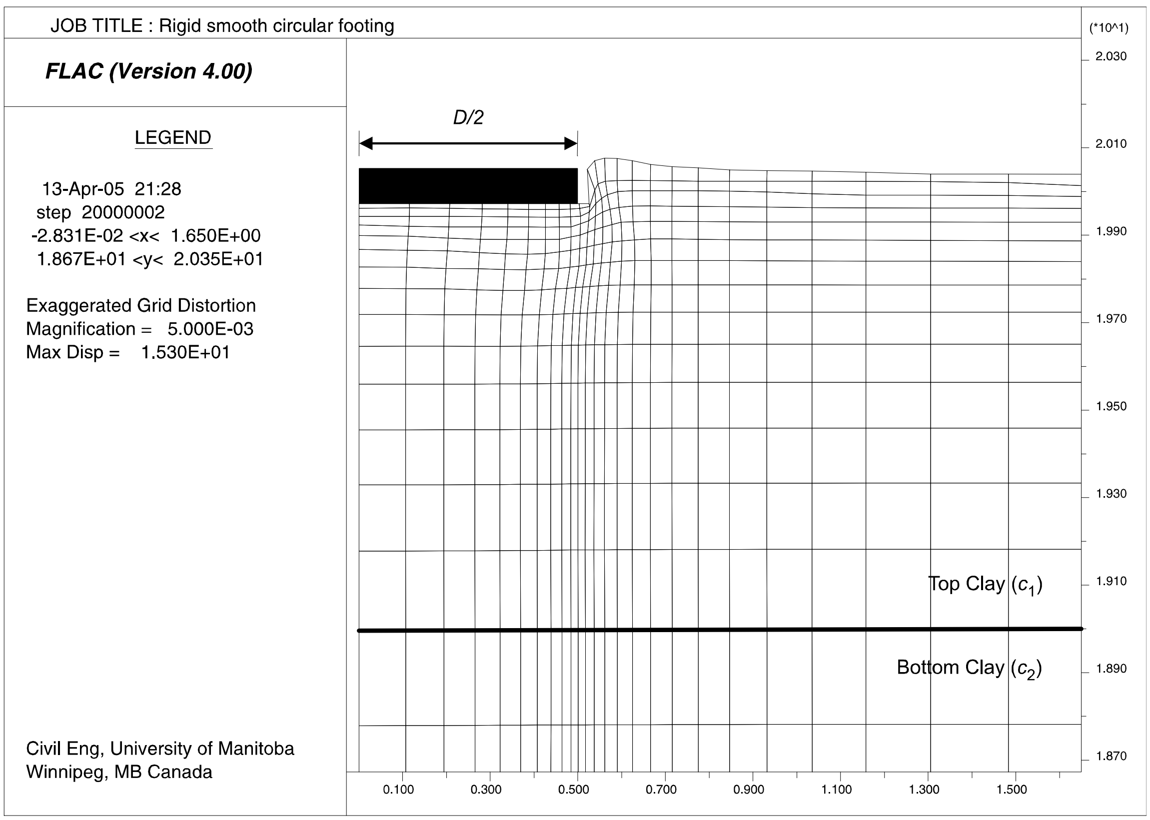

Figure A.268: Magnified grid for a rigid smooth circular footing on strong over soft clay for 40 × 30 grid model, $H/D = 1$, $c_2/c_1 = 0.2$.

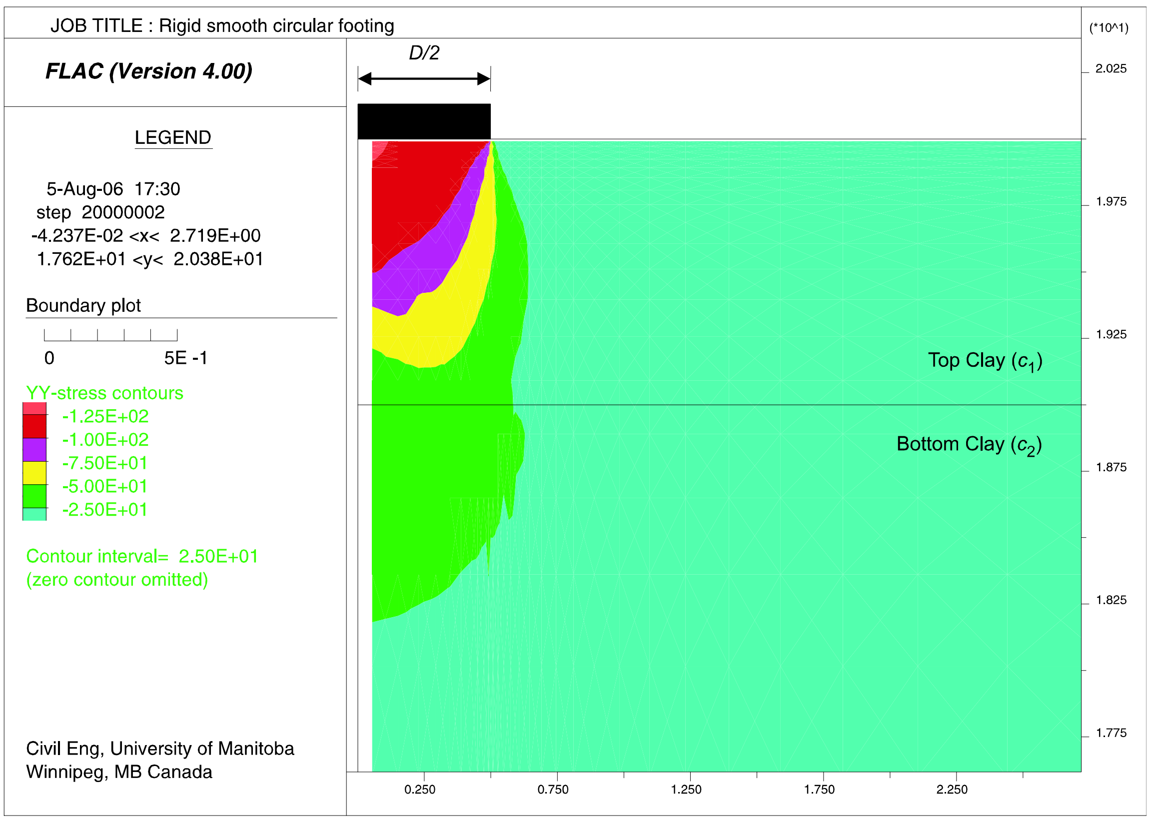

Figure A.269: Vertical stress (σ_{yy}) contours for a rigid smooth circular footing on strong over soft clay for 40×30 grid model, $H/D = 1$, $c_2/c_1 = 0.2$.

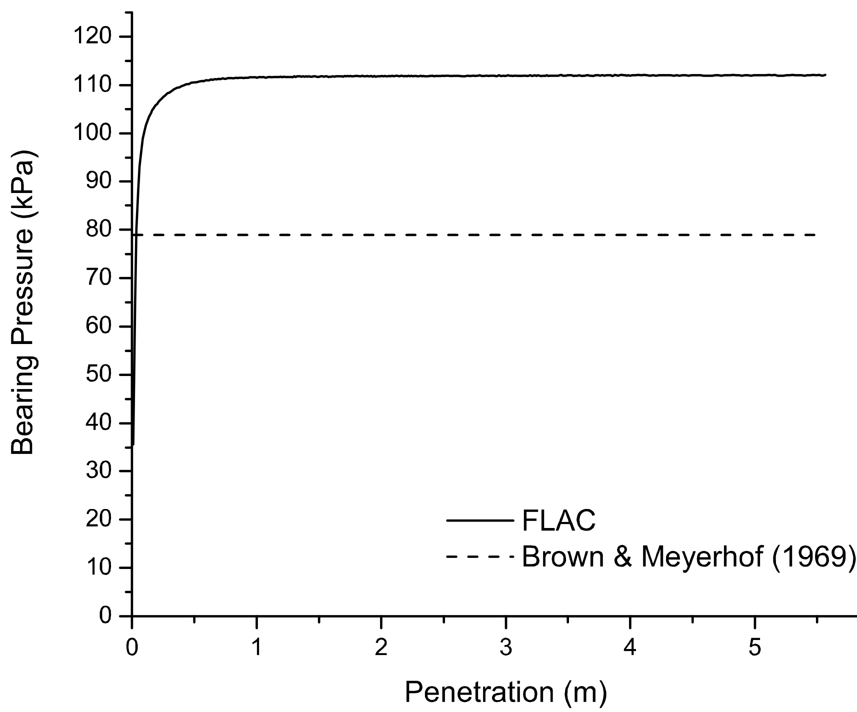

Figure A.270: Bearing pressure versus penetration curve for a rigid smooth circular footing on strong over soft clay for 40 × 30 grid model, $H/D = 1$, $c_2/c_1 = 0.2$.

Case 7: $c_2/c_1 = 0.1$ - Small Deformation Analysis

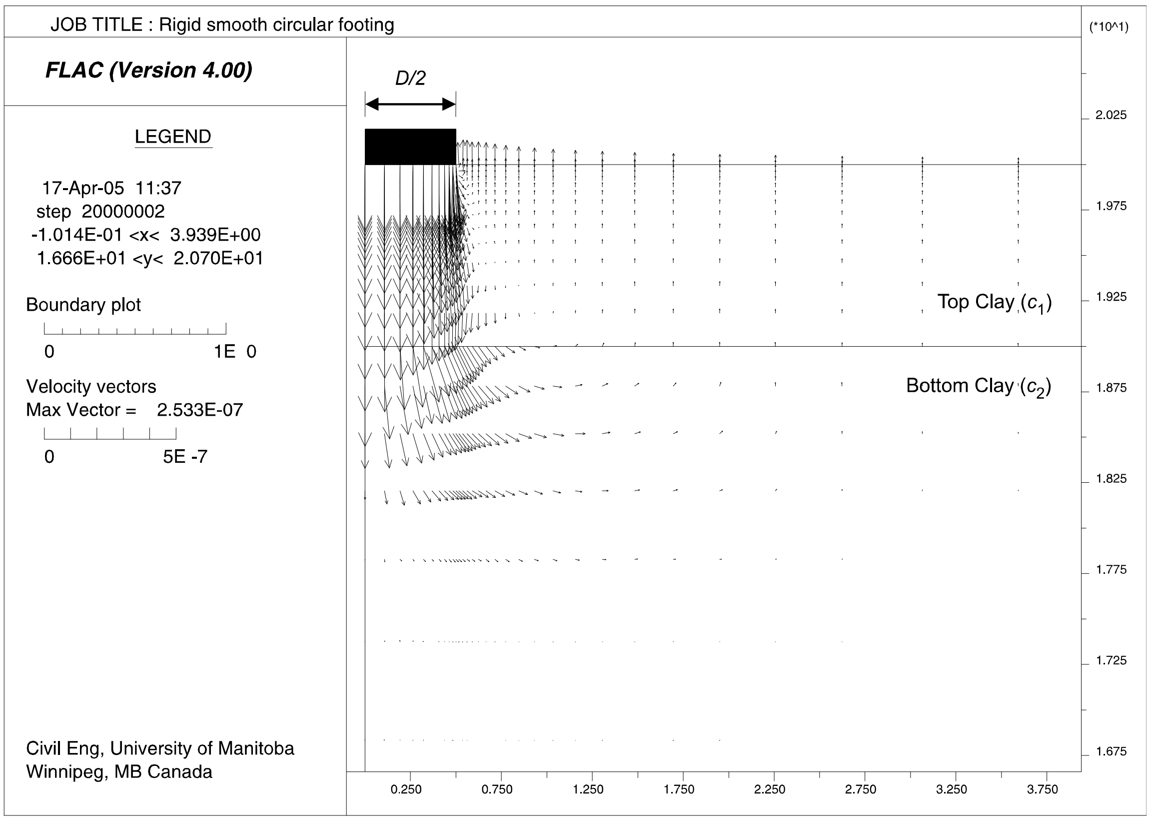

Figure A.271: Velocity vectors for a rigid smooth circular footing on strong over soft clay for 40×30 grid model, $H/D = 1$, $c_2/c_1 = 0.1$.

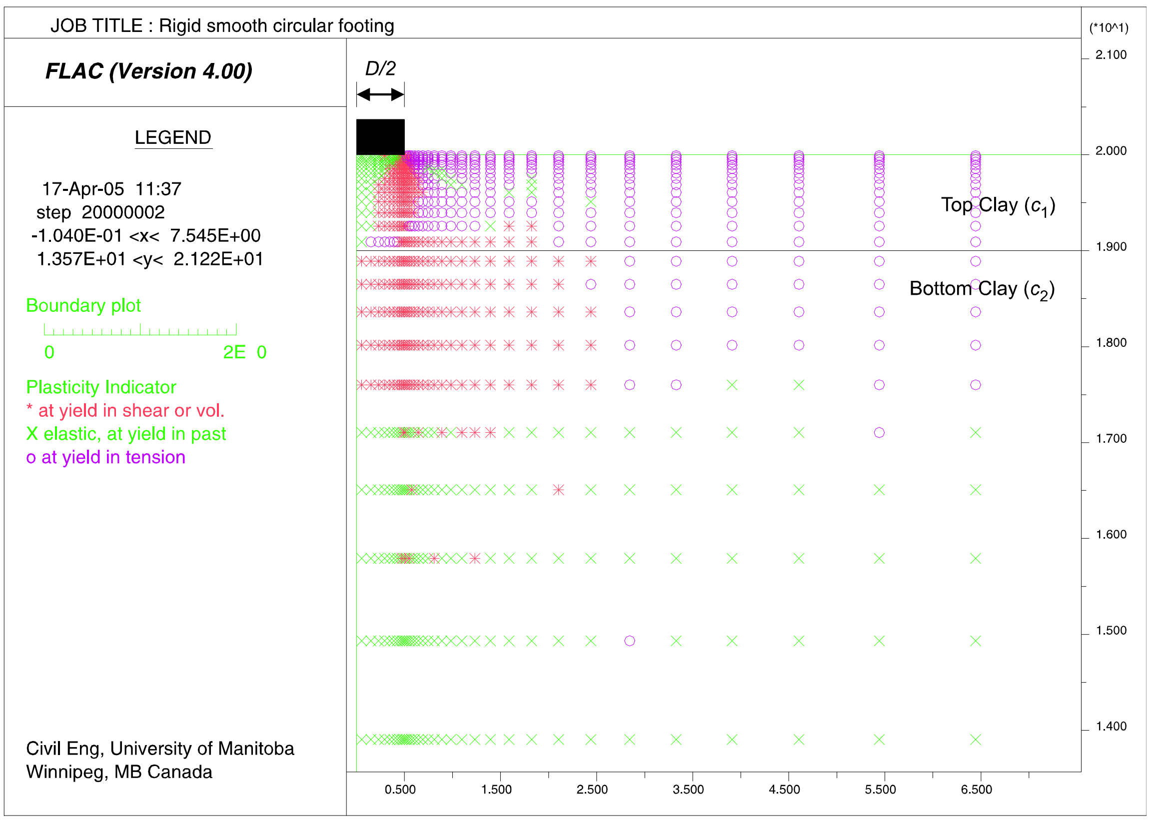

Figure A.272: Plasticity state indicators for a rigid smooth circular footing on strong over soft clay for 40 × 30 grid model, $H/D = 1$, $c_2/c_1 = 0.1$.

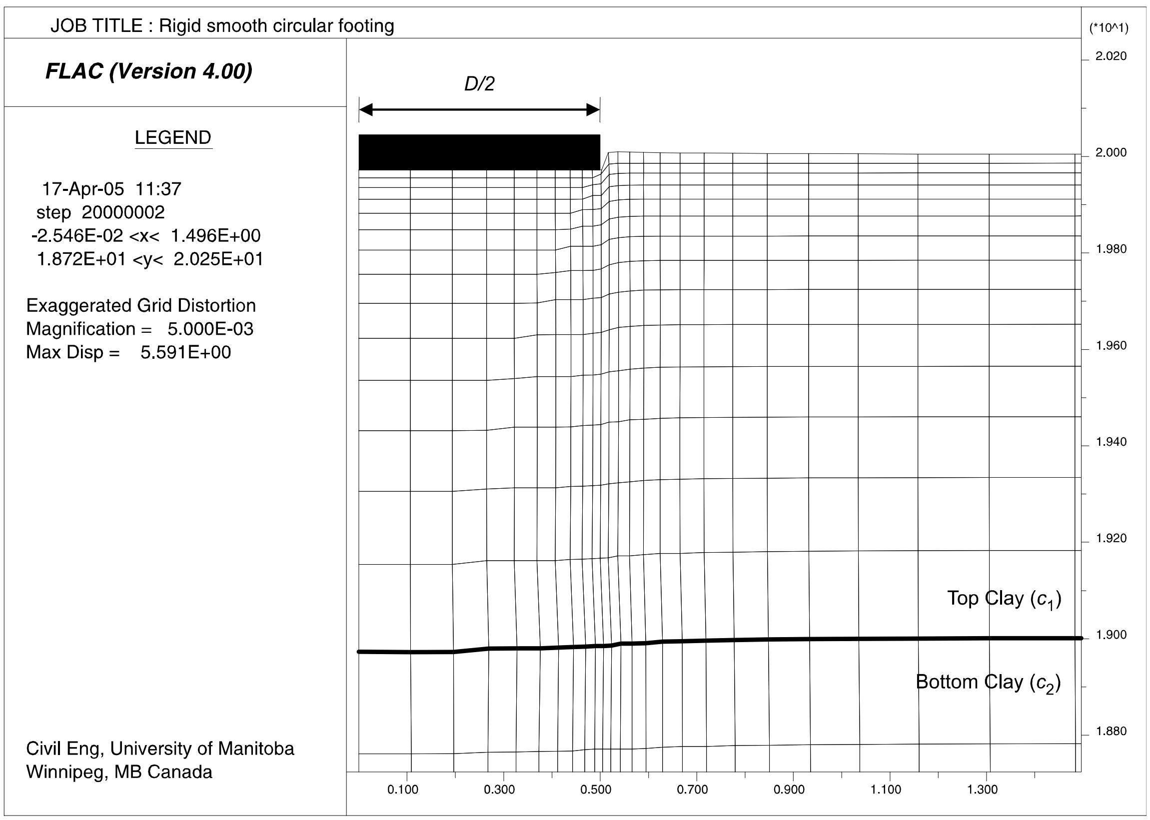

Figure A.273: Magnified grid for a rigid smooth circular footing on strong over soft clay for 40×30 grid model, $H/D = 1$, $c_2/c_1 = 0.1$.

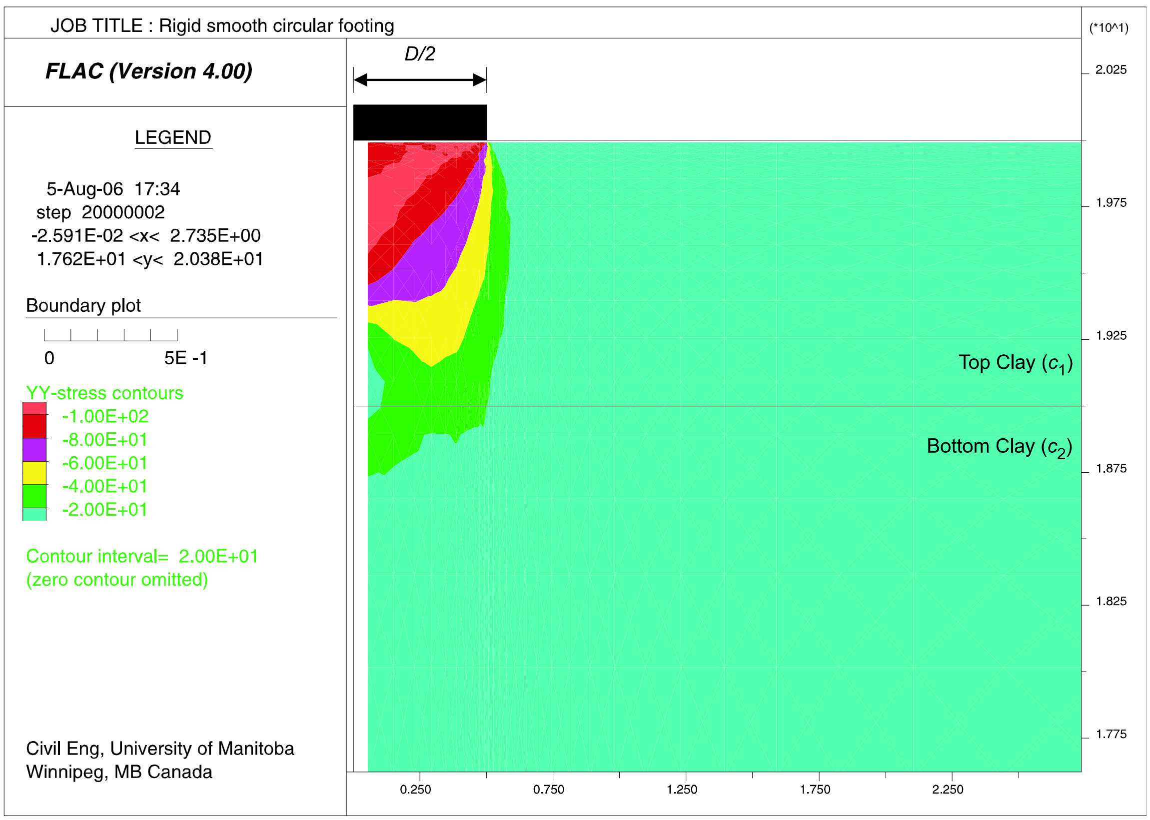

Figure A.274: Vertical stress (σ_{yy}) contours for a rigid smooth circular footing on strong over soft clay for 40×30 grid model, $H/D = 1$, $c_2/c_1 = 0.1$.

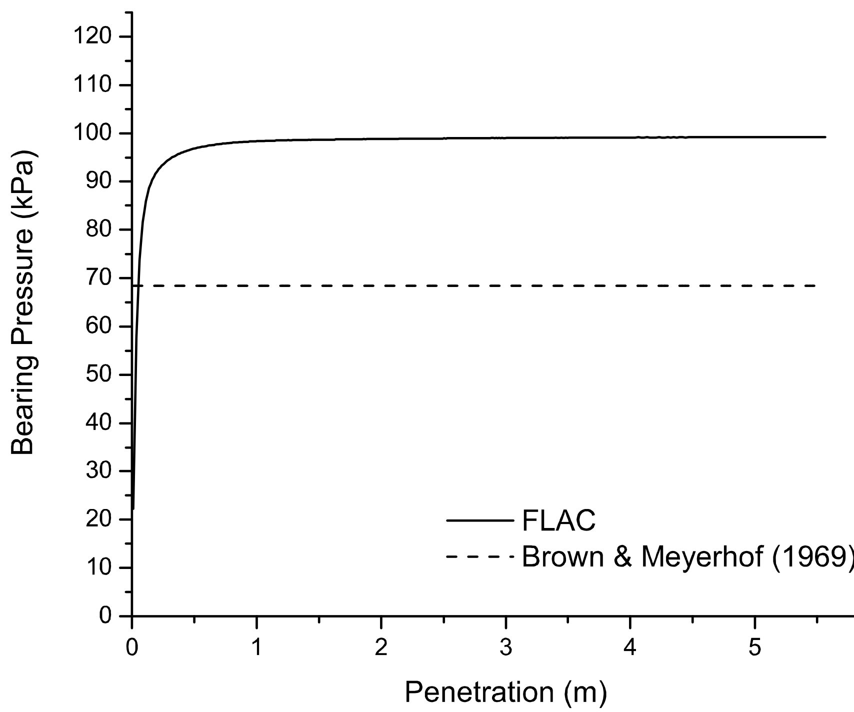

Figure A.275: Bearing pressure versus penetration curve for a rigid smooth circular footing on strong over soft clay for 40×30 grid model, $H/D = 1$, $c_2/c_1 = 0.1$.

A.3.2 Rigid Smooth Circular Footing on Strong over Soft Clay ($H/D = 1.5$)

Case 6: $c_2/c_1 = 0.2$ **- Small Deformation Analysis**

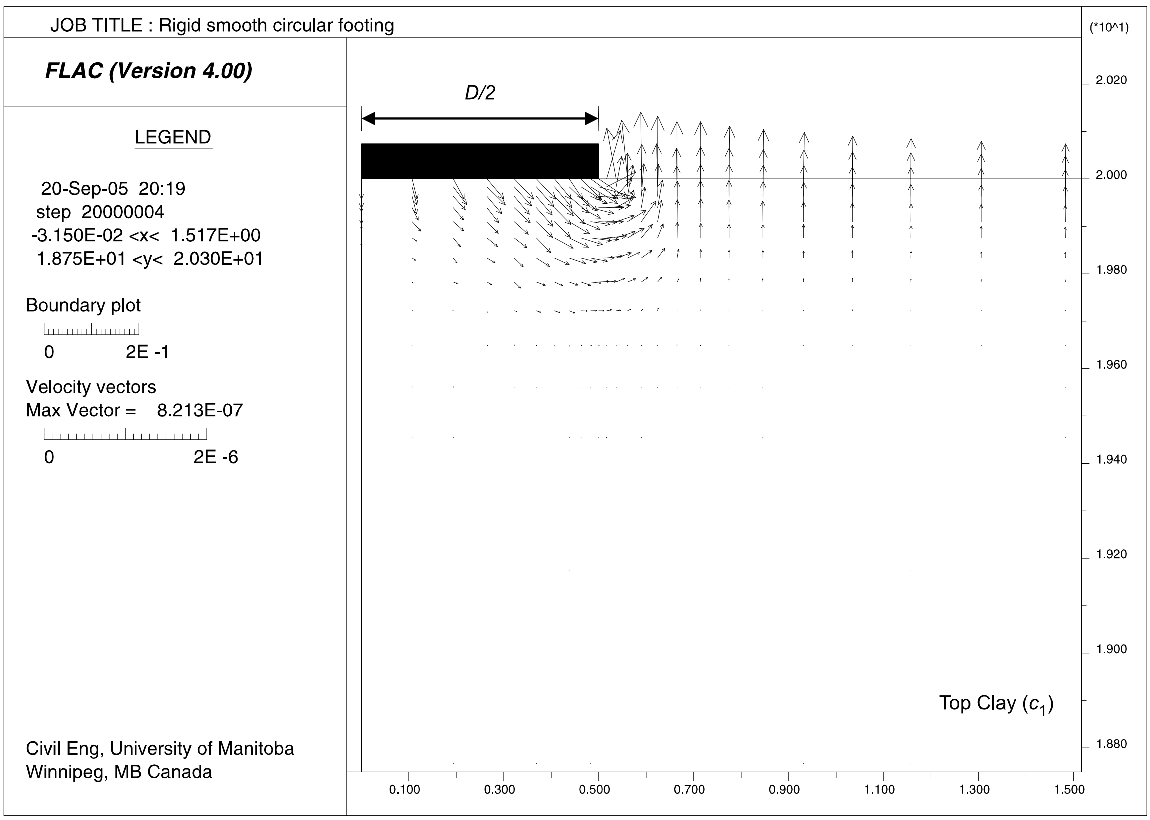

Figure A.276: Velocity vectors for a rigid smooth circular footing on strong clay over soft clay for 40 × 30 grid model, $H/D = 1.5$, $c_2/c_1 = 0.2$.

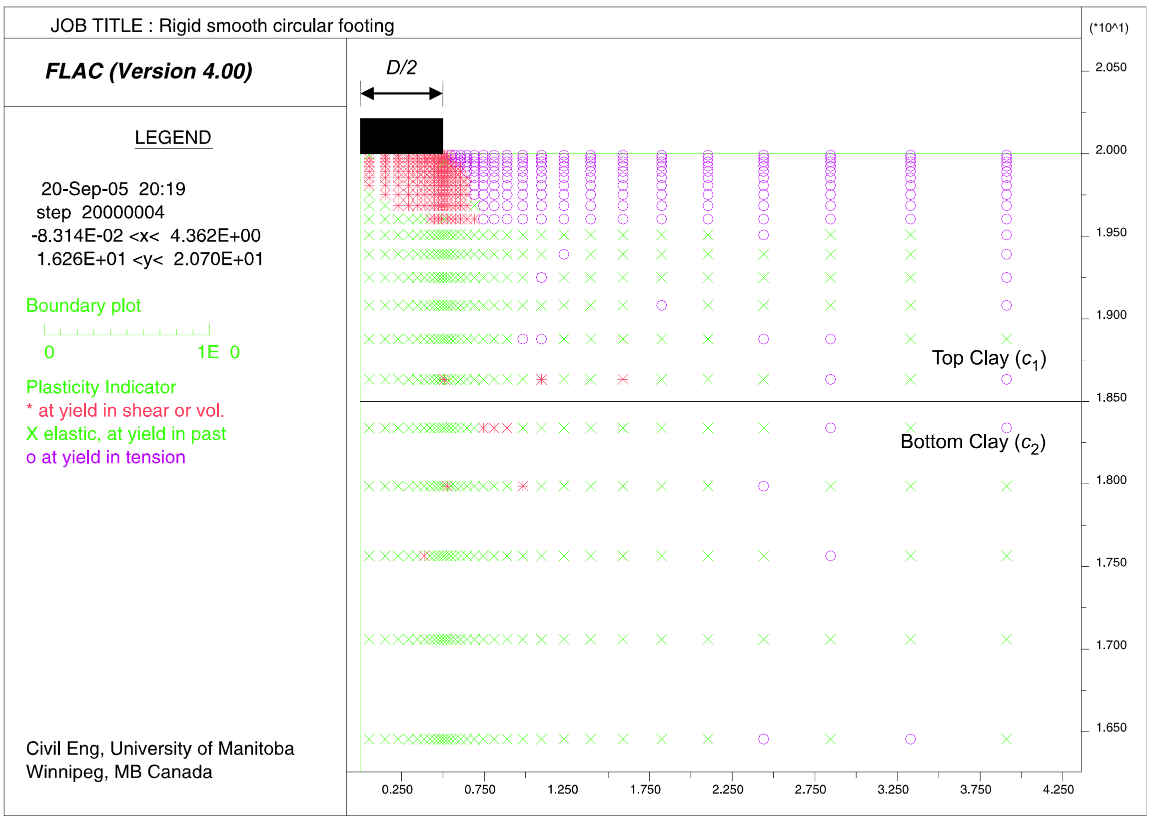

Figure A.277: Plasticity state indicators for a rigid smooth circular footing on strong clay over soft clay for 40 × 30 grid model, $H/D = 1.5$, $c_2/c_1 = 0.2$.

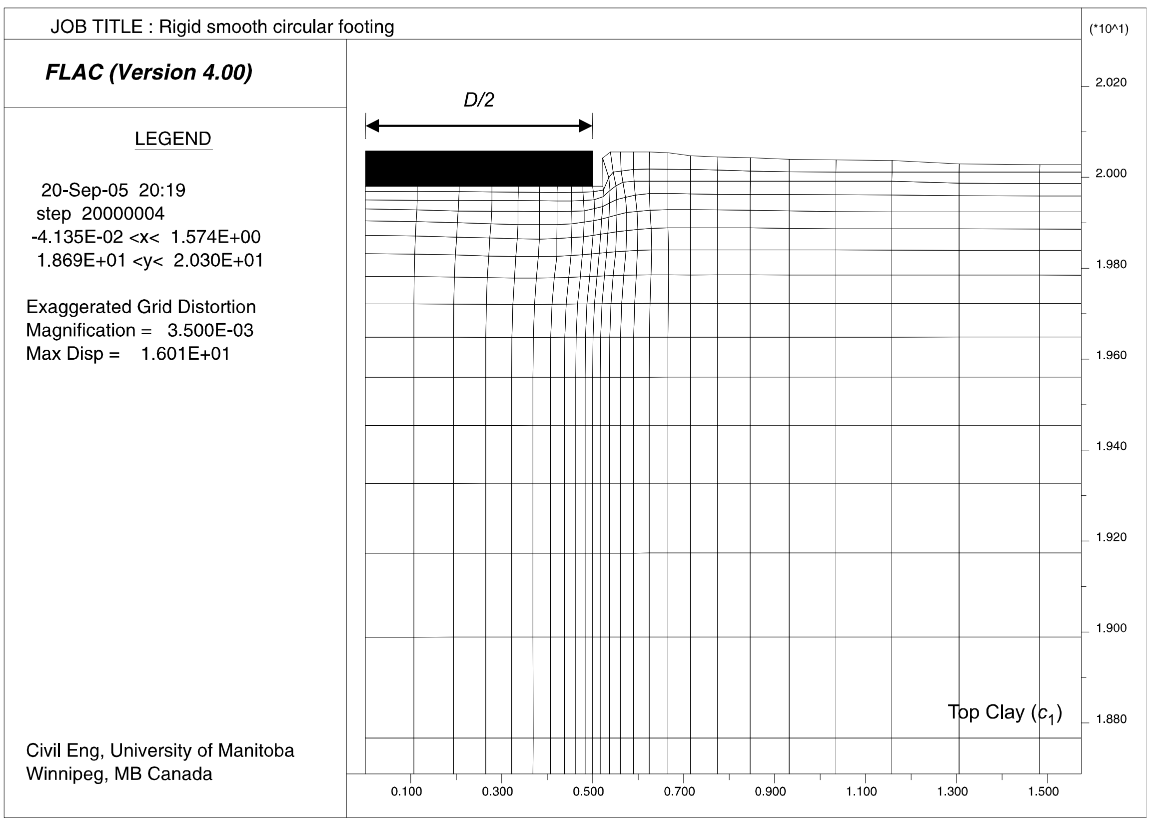

Figure A.278: Magnified grid for a rigid smooth circular footing on strong clay over soft clay for 40×30 grid model, $H/D = 1.5$, $c_2/c_1 = 0.2$.

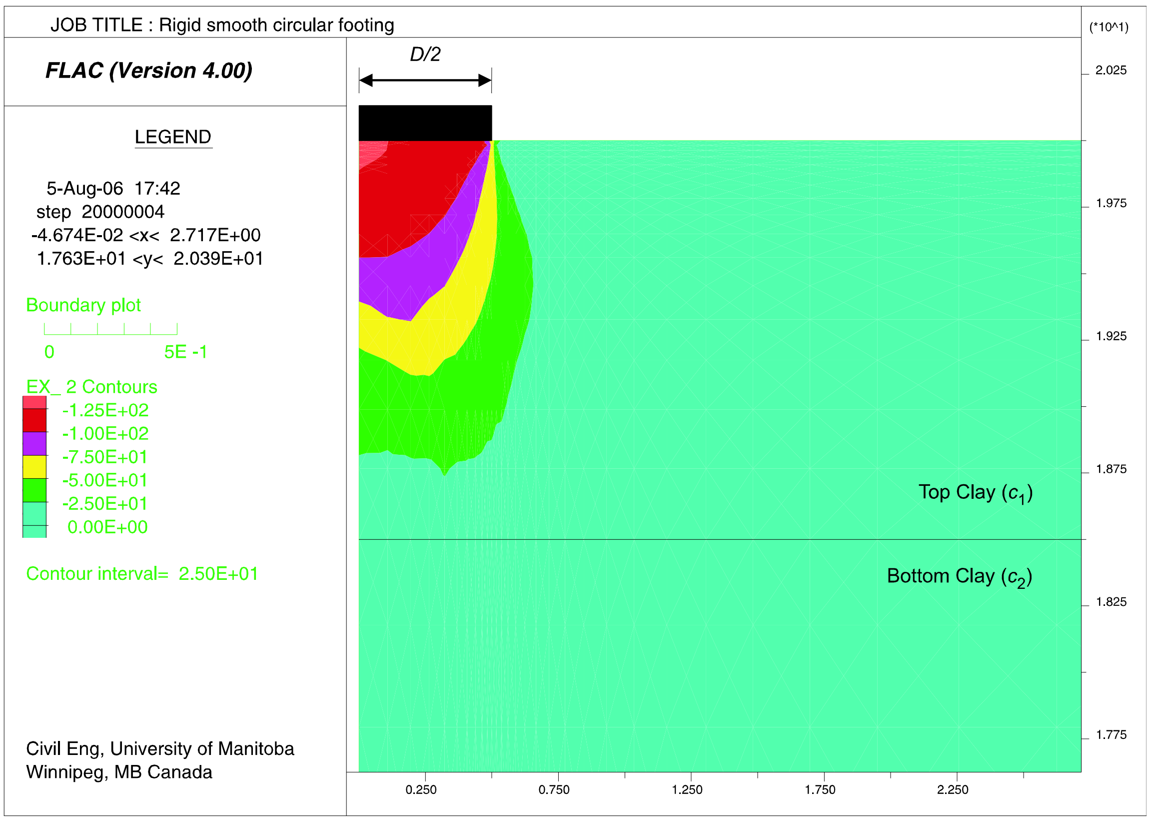

Figure A.279: Vertical stress (σ_{yy}) contours extrapolated to boundary grid points for a rigid smooth circular footing on strong clay over soft clay for 40 $\times$ 30 grid model, $H/D = 1.5$, $c_2/c_1 = 0.2$.

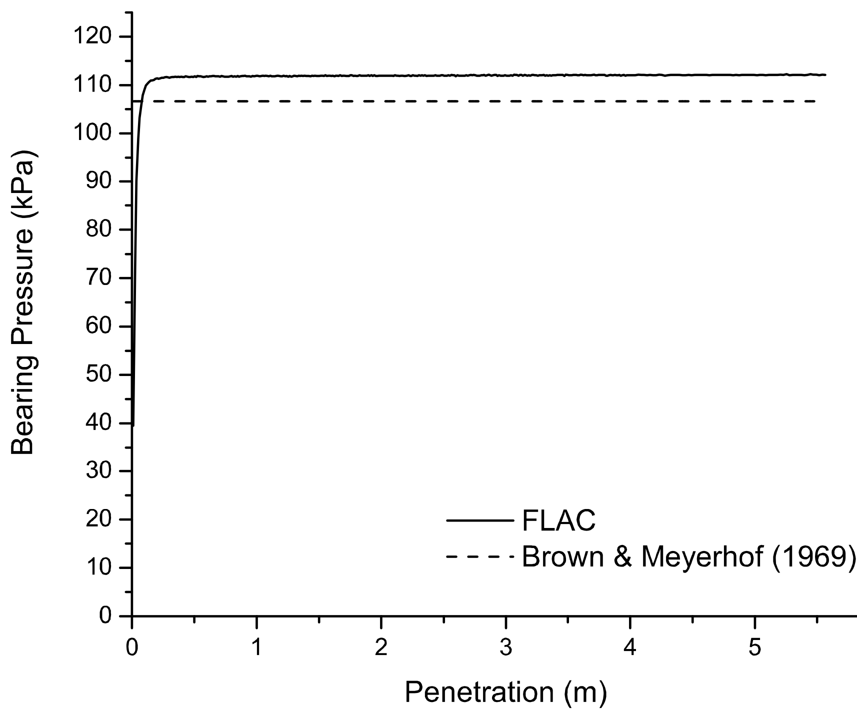

Figure A.280: Bearing pressure versus penetration curve for a rigid smooth circular footing on strong clay over soft clay for 40×30 grid model, $H/D = 1.5$, $c_2/c_1 = 0.2$.

Case 7: $c_2/c_1 = 0.1$ - Small Deformation Analysis

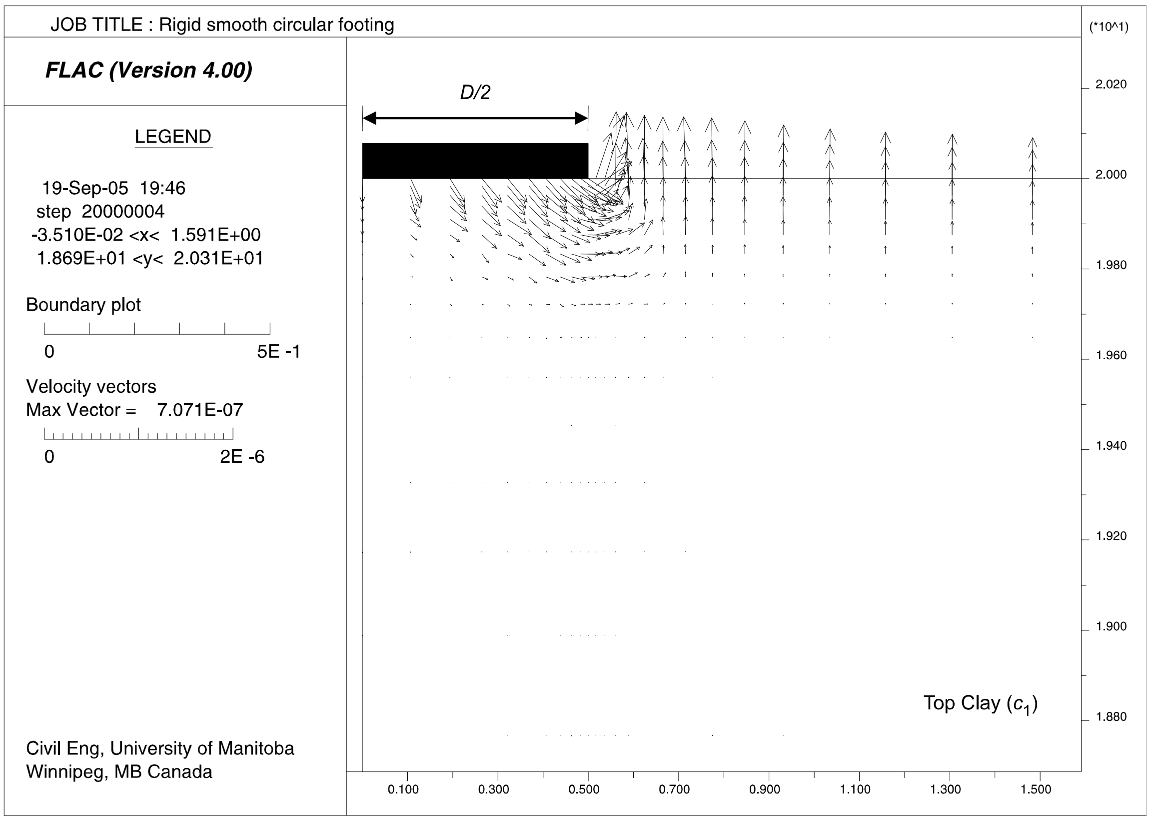

Figure A.281: Velocity vectors for a rigid smooth circular footing on strong clay over soft clay for 40×30 grid model, $H/D = 1.5$, $c_2/c_1 = 0.1$.

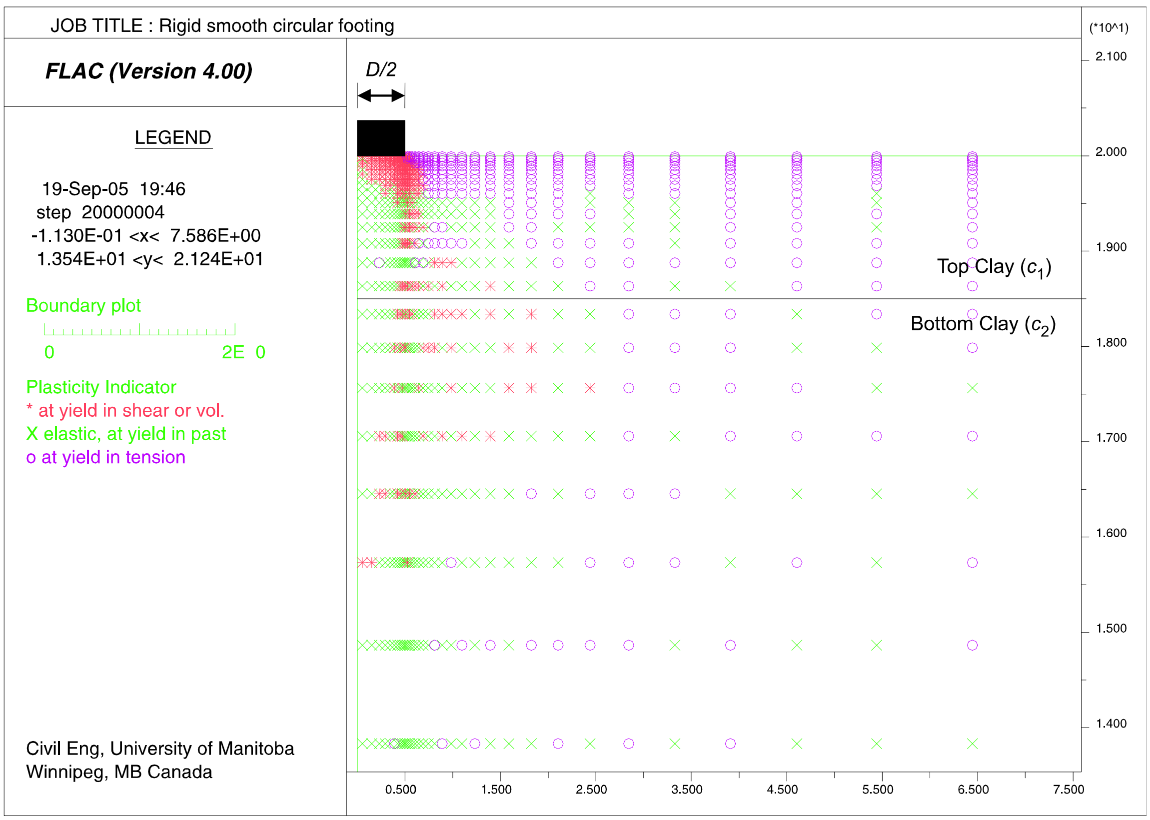

Figure A.282: Plasticity state indicators for a rigid smooth circular footing on strong clay over soft clay for 40×30 grid model, $H/D = 1.5$, $c_2/c_1 = 0.1$.

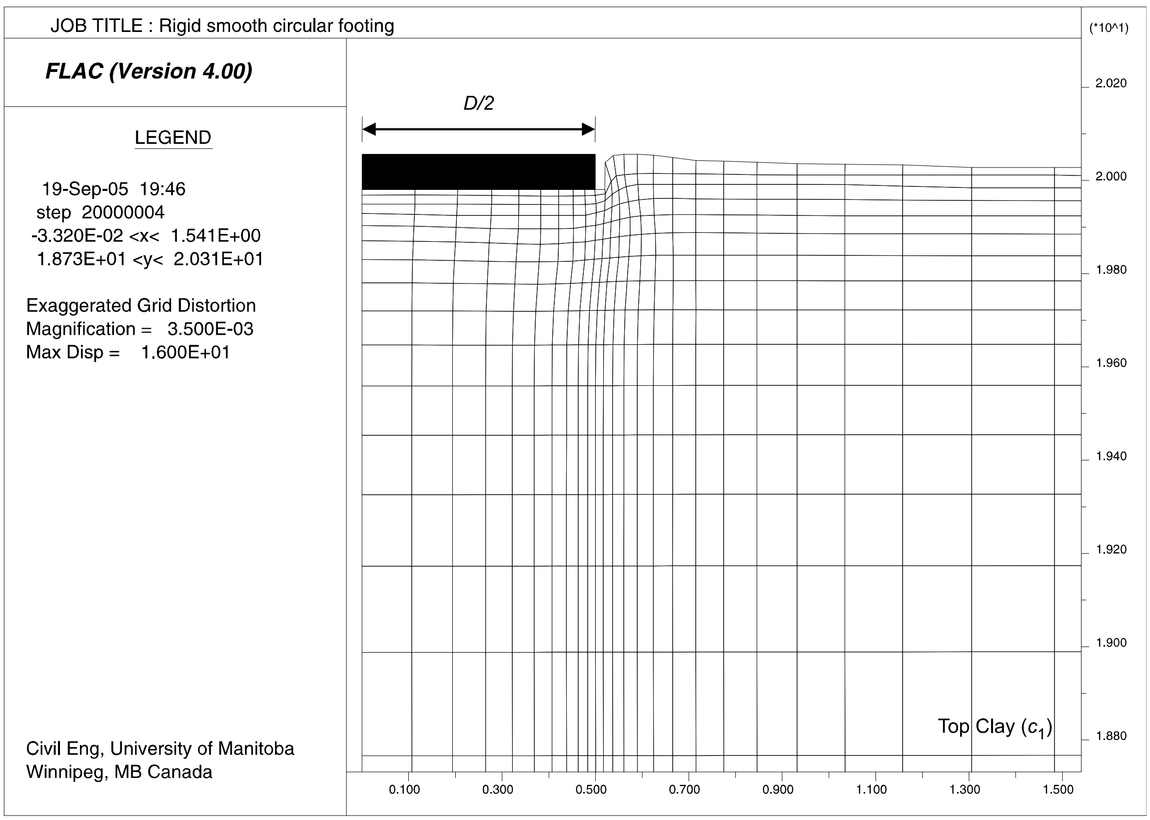

Figure A.283: Magnified grid for a rigid smooth circular footing on strong clay over soft clay for 40×30 grid model, $H/D = 1.5$, $c_2/c_1 = 0.1$.

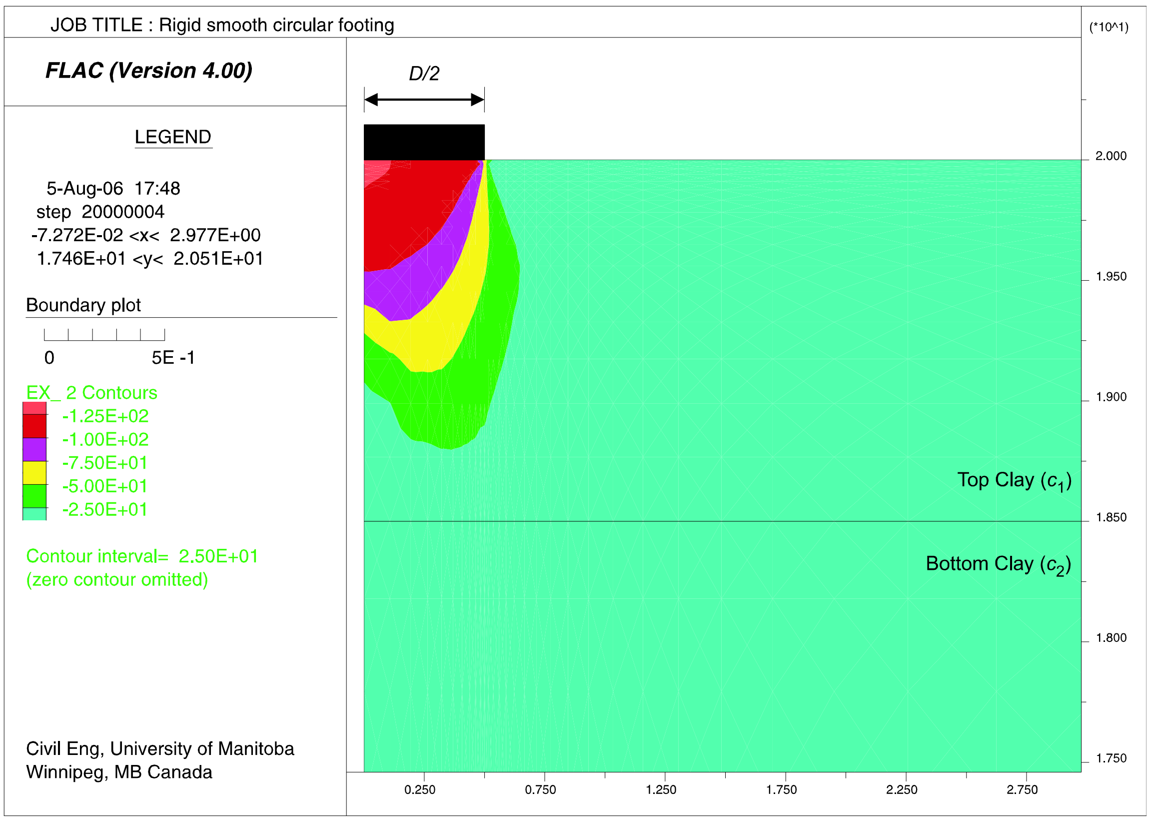

Figure A.284: Vertical stress (σ_{yy}) contours extrapolated to boundary grid points for a rigid smooth circular footing on strong clay over soft clay for 40×30 grid model, $H/D = 1.5$, $c_2/c_1 = 0.1$.

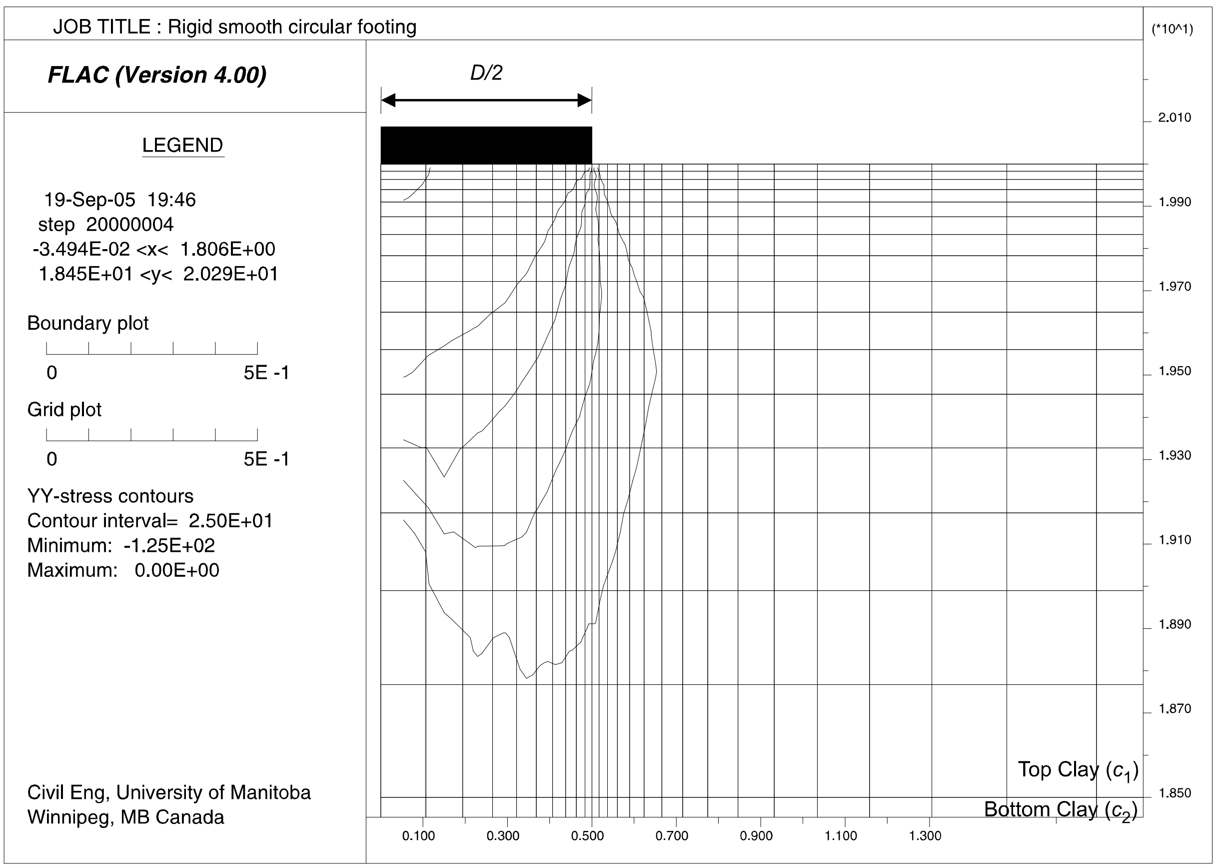

Figure A.285: Vertical stress (σ_{yy}) contours for a rigid smooth circular footing on strong clay over soft clay for 40×30 grid model, $H/D = 1.5$, $c_2/c_1 = 0.1$.

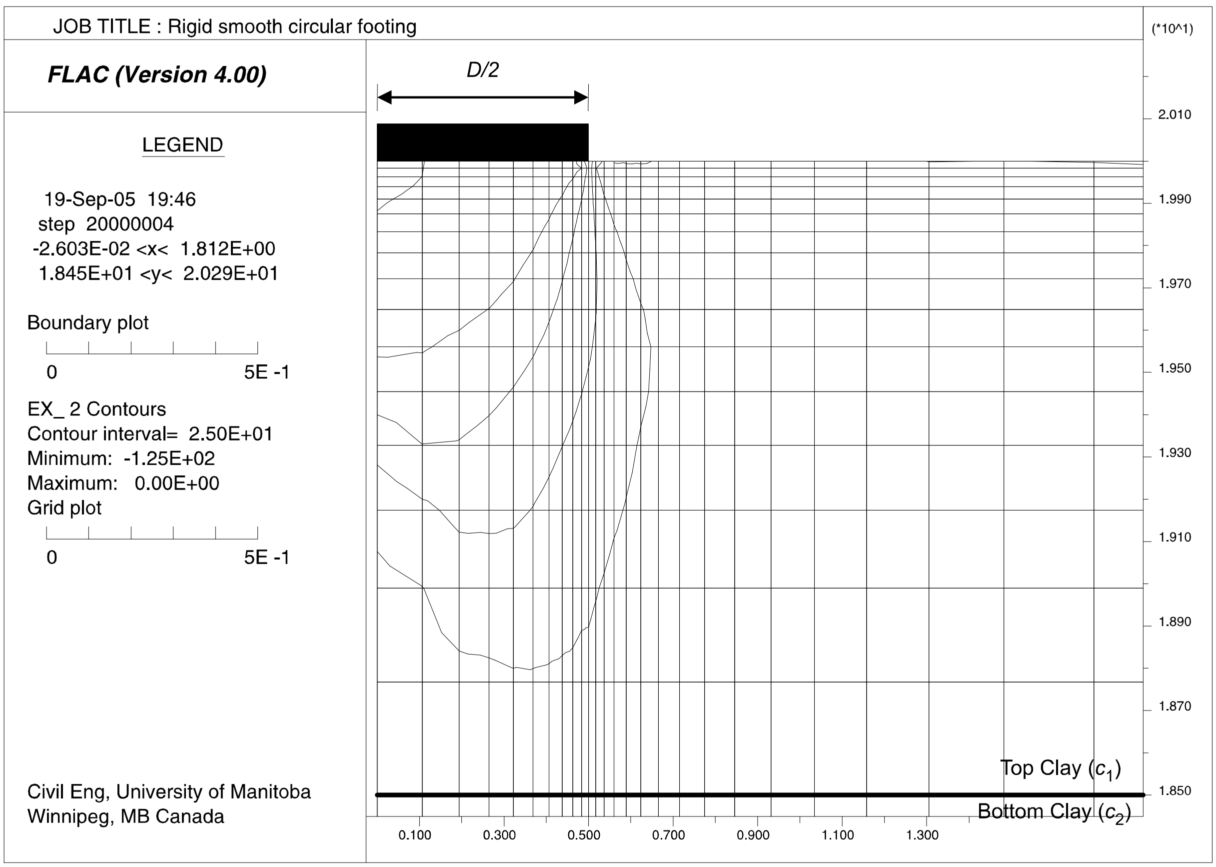

Figure A.286: Vertical stress (σ_{yy}) contours extrapolated to boundary grid points for rigid smooth circular footing on strong clay over soft clay for 40 × 30 grid model, $H/D = 1.5$, $c_2/c_1 = 0.1$.

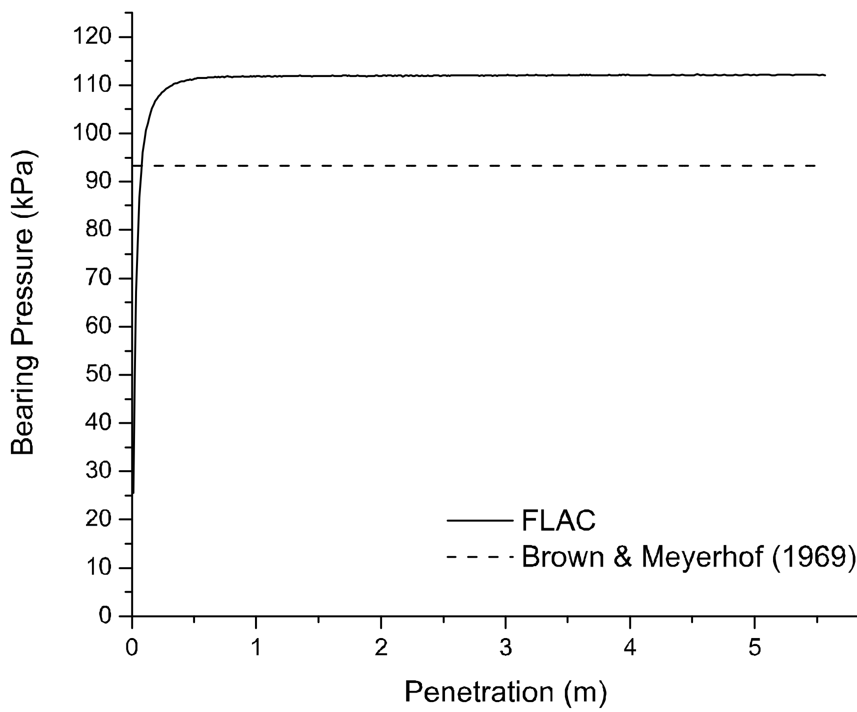

Figure A.287: Bearing pressure versus penetration curve for a rigid smooth circular footing on strong clay over soft clay for 40 × 30 grid model, $H/D = 1.5$, $c_2/c_1 = 0.1$.

A.3.3 Rigid Smooth Circular Footing on Strong over Soft Clay ($H/D = 2$)

Case 7: $c_2/c_1 = 0.1$ - Small Deformation Analysis

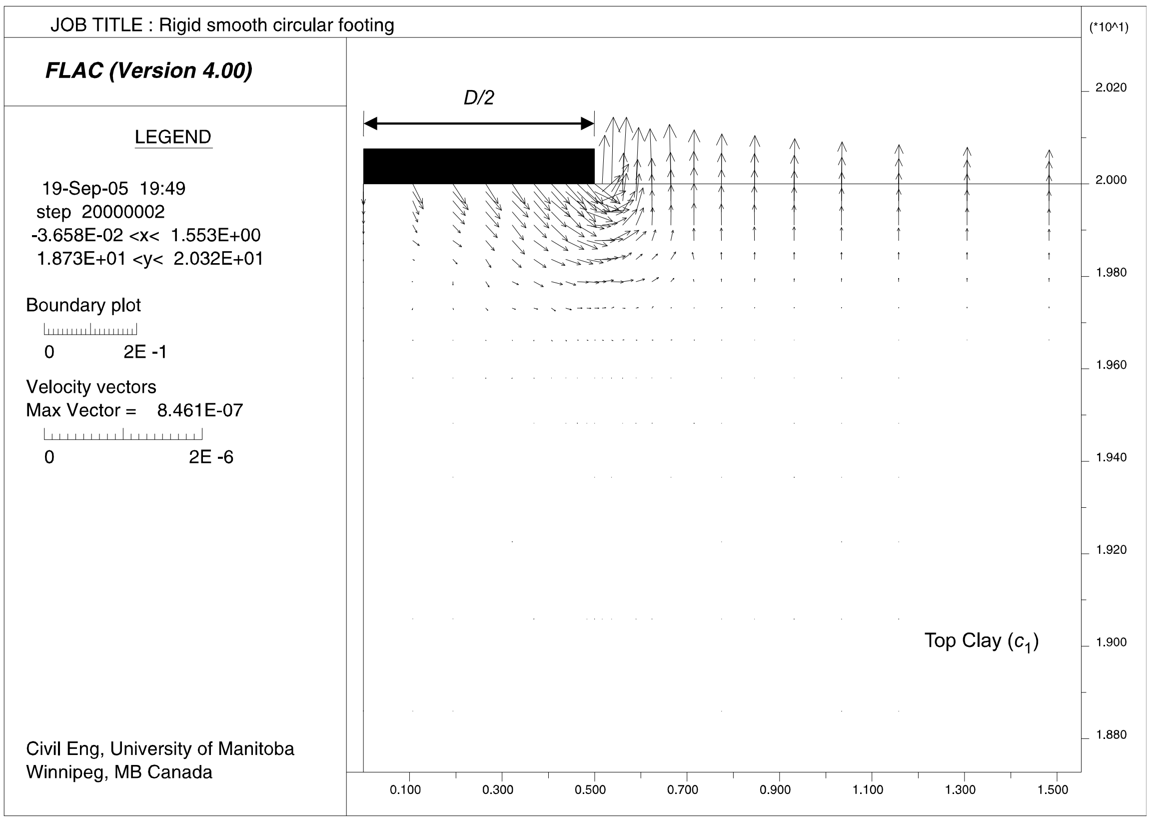

Figure A.288: Velocity vectors for a rigid smooth circular footing on strong clay over soft clay for 40×30 grid model, $H/D = 2$, $c_2/c_1 = 0.1$.

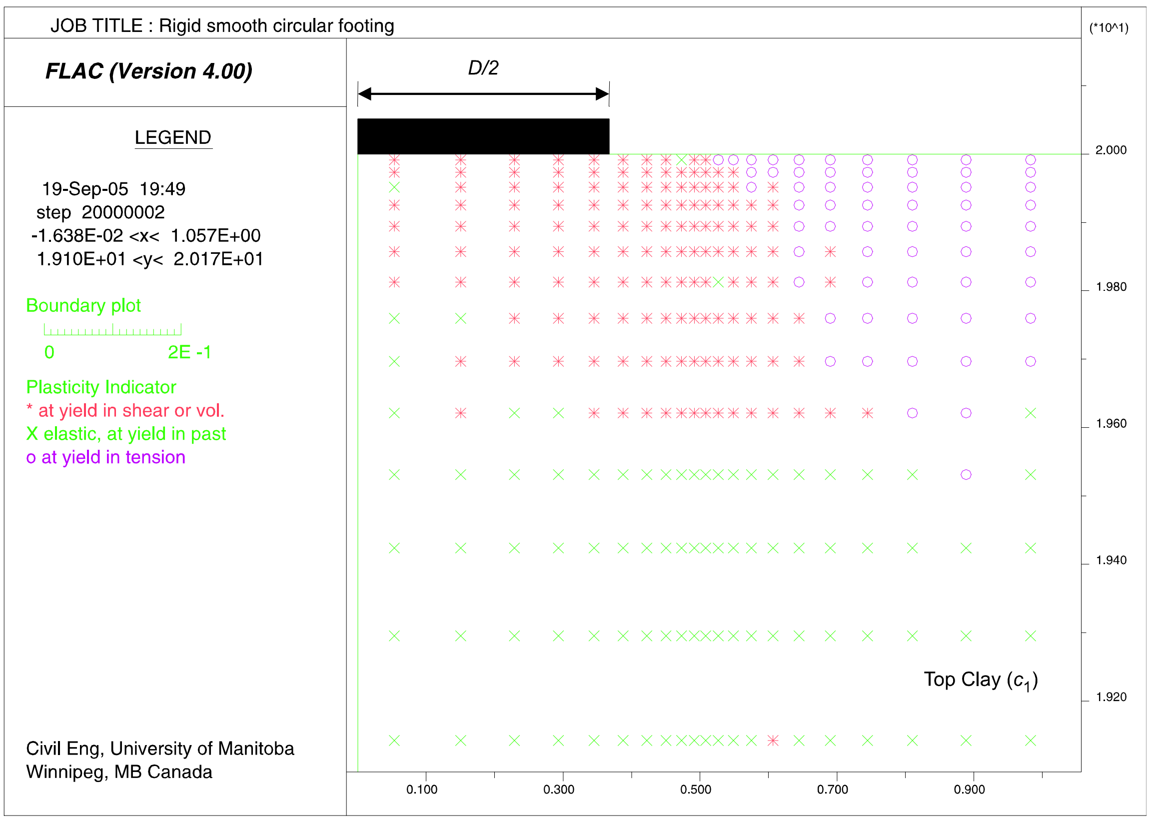

Figure A.289: Plasticity state indicators for a rigid smooth circular footing on strong clay over soft clay for 40 × 30 grid model, $H/D = 2$, $c_2/c_1 = 0.1$.

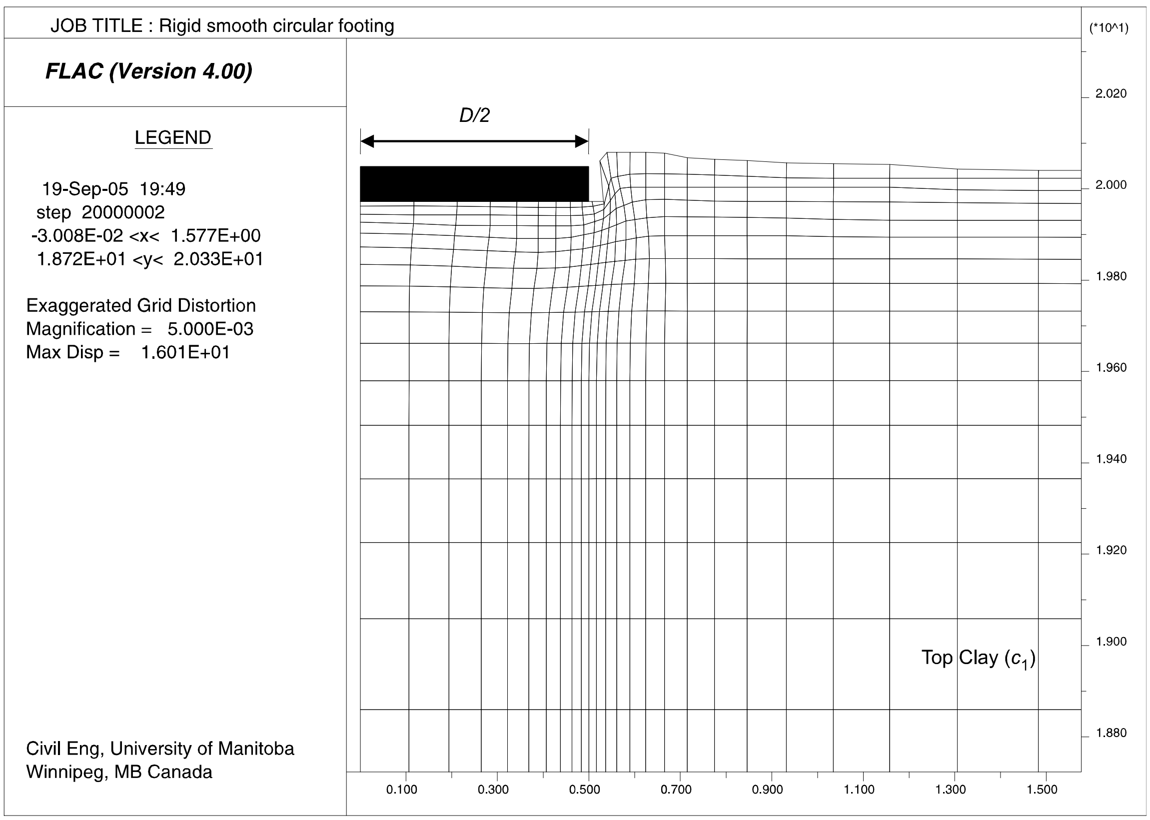

Figure A.290: Magnified grid for a rigid smooth circular footing on strong clay over soft clay for 40×30 grid model, $H/D = 2$, $c_2/c_1 = 0.1$.

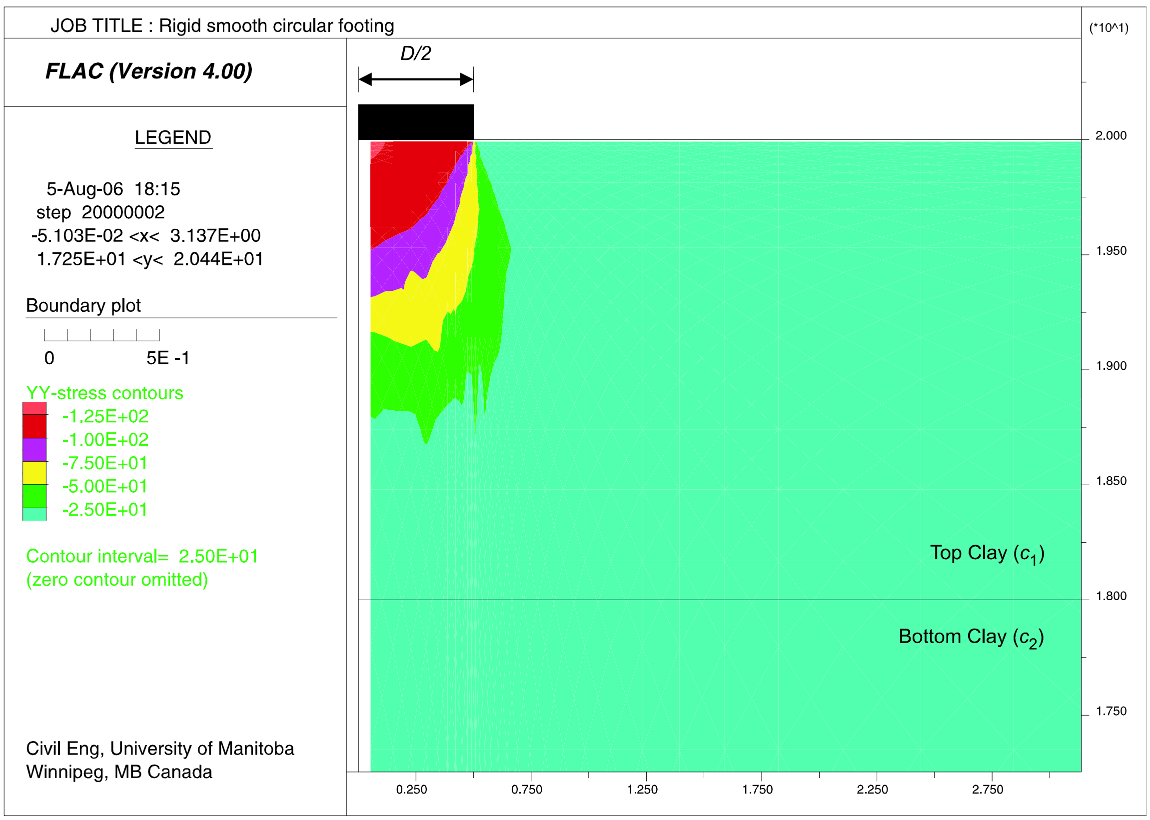

Figure A.291: Vertical stress (σ_{yy}) contours for a rigid smooth circular footing on strong clay over soft clay for 40 × 30 grid model, $H/D = 2$, $c_2/c_1 = 0.1$.

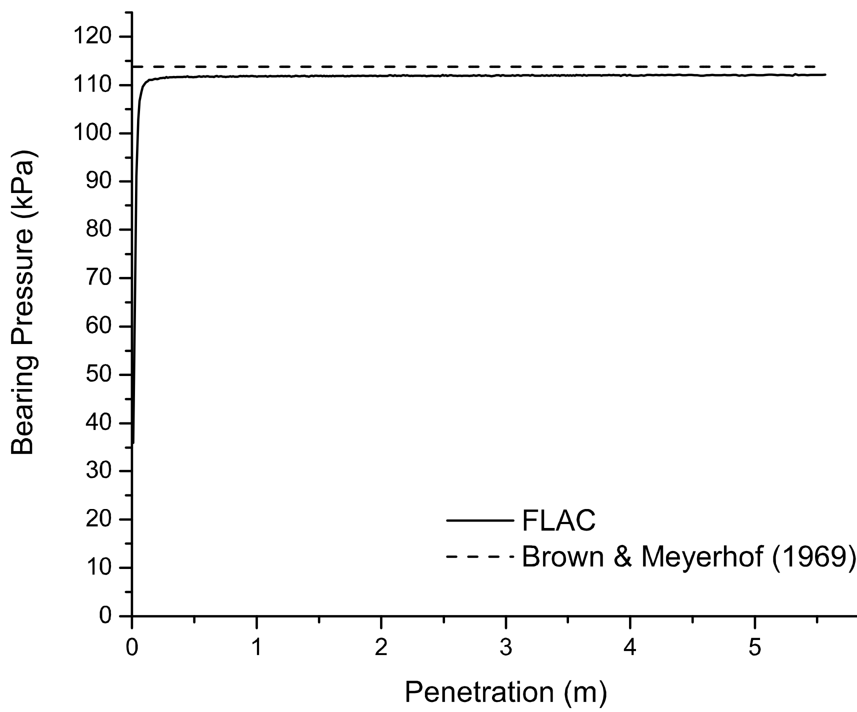

Figure A.292: Bearing pressure versus penetration curve for a rigid smooth circular footing on strong clay over soft clay for 40 × 30 grid model, $H/D = 2$, $c_2/c_1 = 0.1$.

A.3.4 Rigid Smooth Circular Footing on Ground Surface ($H/D = 0.5$)

Case 2: $c_2/c_1 = 0.8$ **- Small Deformation Analysis**

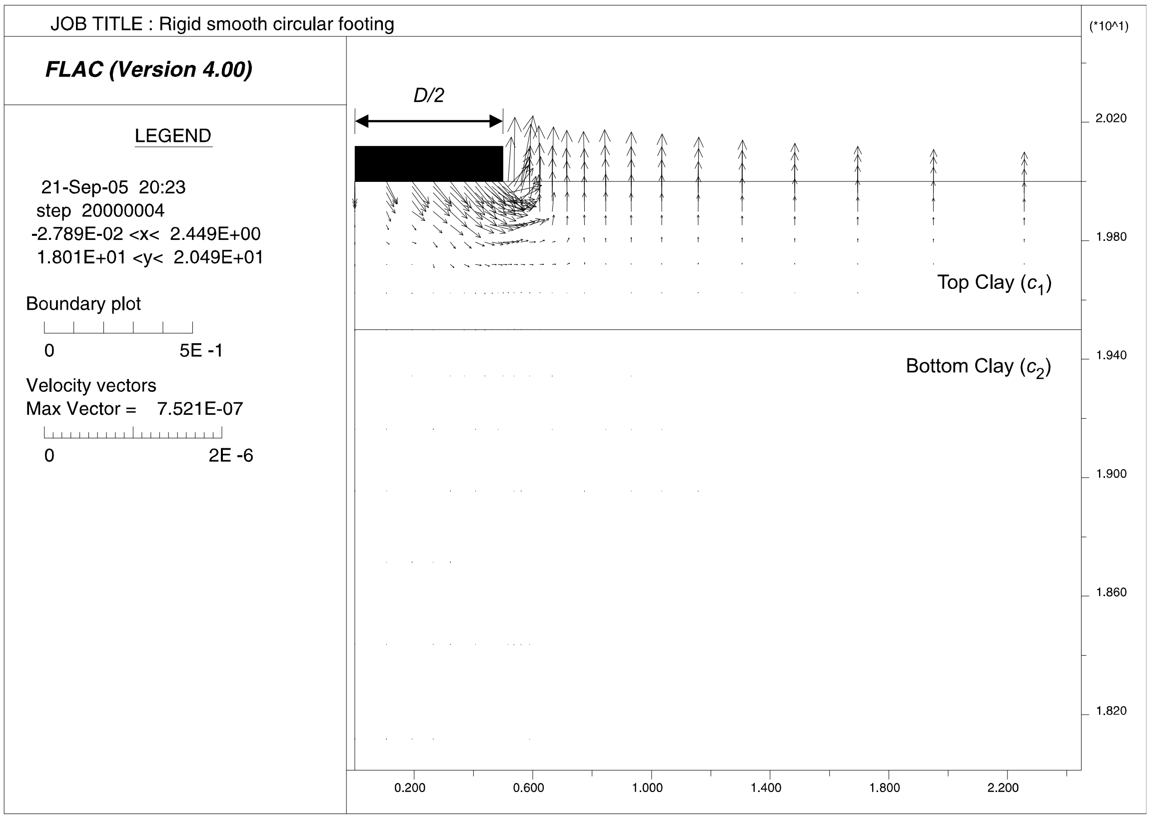

Figure A.293: Velocity vectors for a rigid circular footing on strong over soft clay for 40×30 grid model, $H/D = 0.5$, $c_2/c_1 = 0.8$.

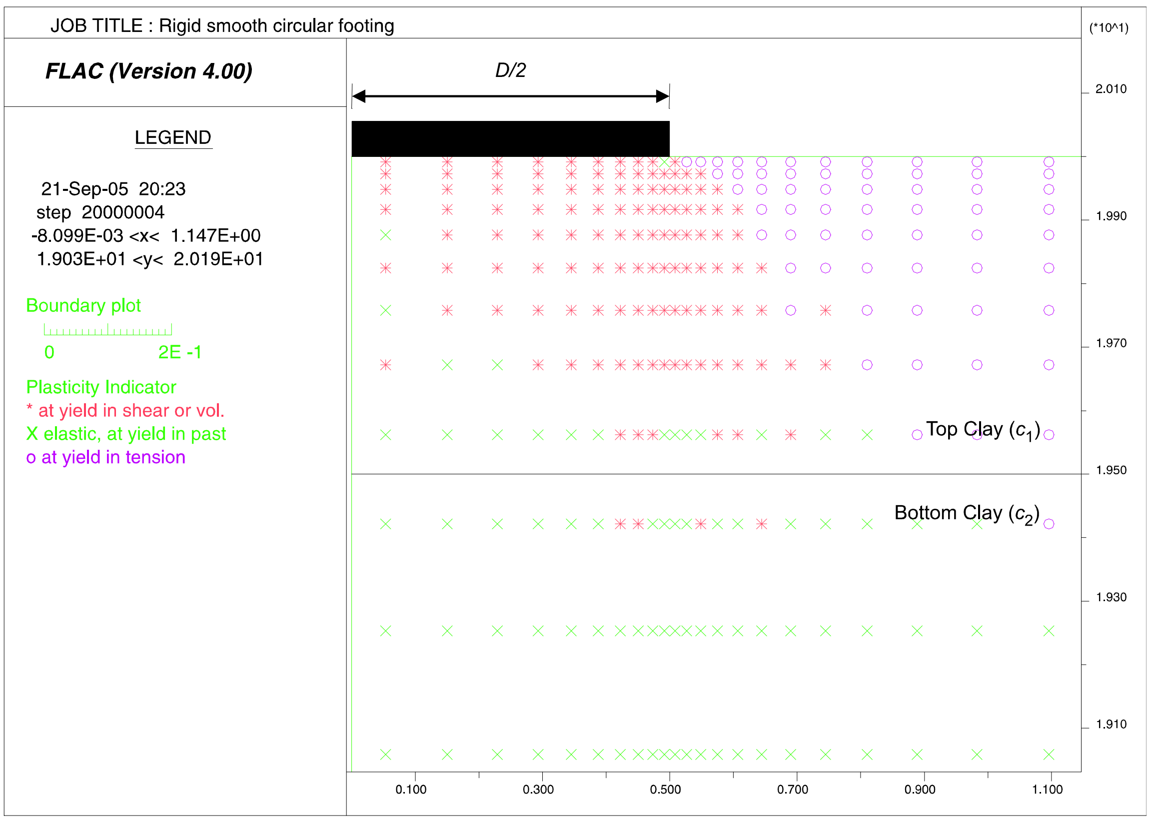

Figure A.294: Plasticity indicators for a rigid smooth circular footing on strong over soft clay for 40 × 30 grid model, $H/D = 0.5$, $c_2/c_1 = 0.8$.

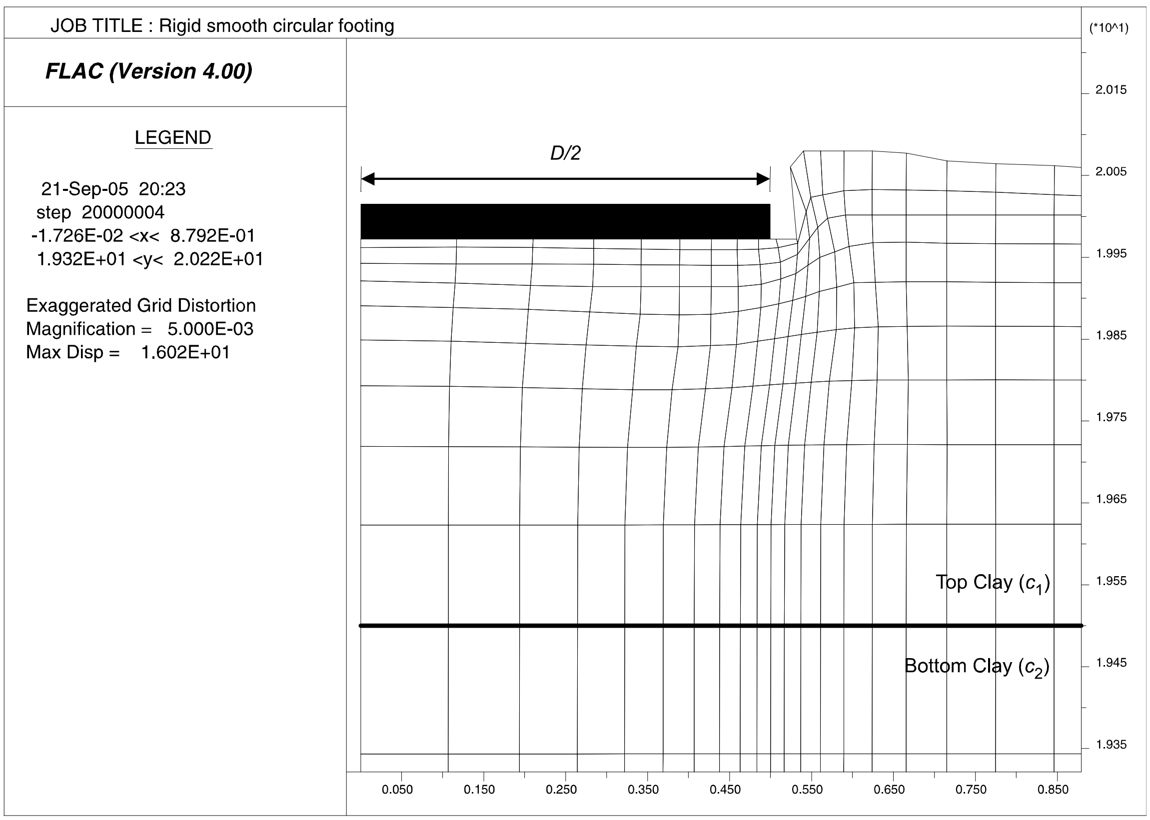

Figure A.295: Magnified grid for a rigid smooth circular footing on strong over soft clay for 40×30 grid model, $H/D = 0.5$, $c_2/c_1 = 0.8$.

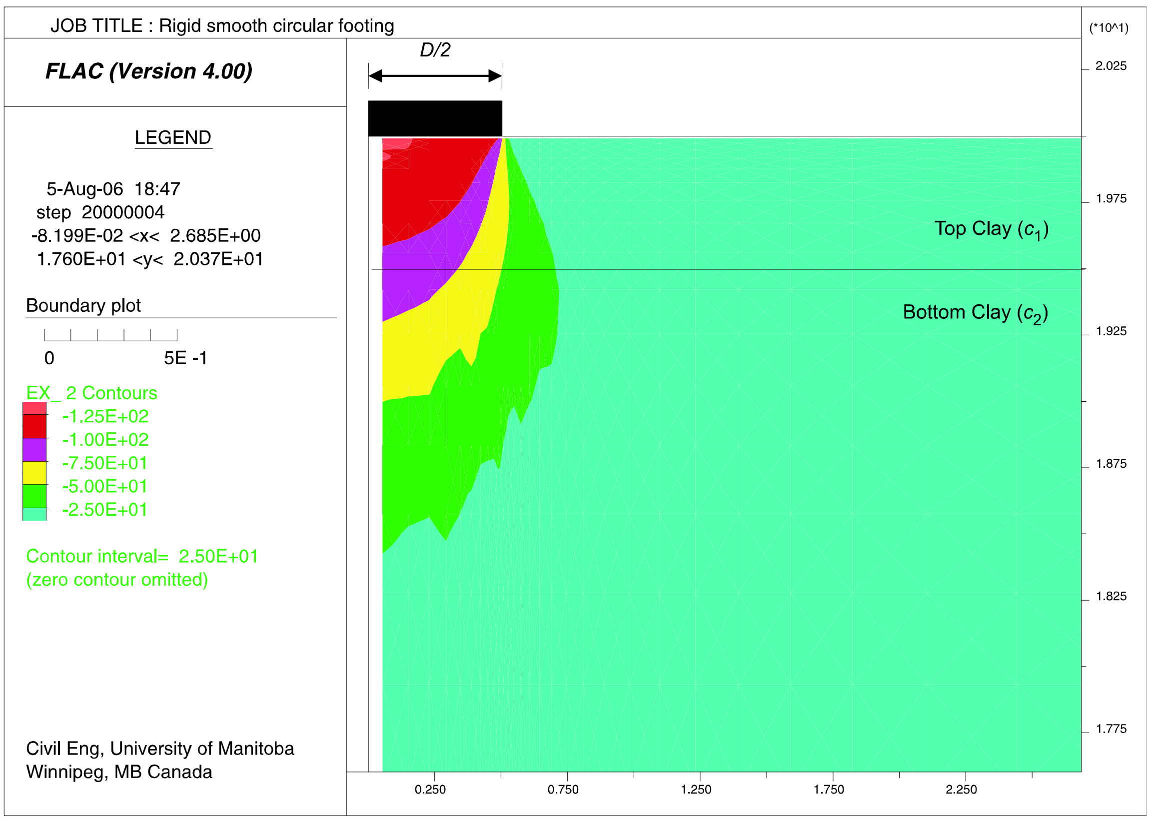

Figure A.296: Vertical stress (σ_{yy}) contours for a rigid smooth circular footing on strong over soft clay for 40×30 grid model, $H/D = 0.5$, $c_2/c_1 = 0.8$.

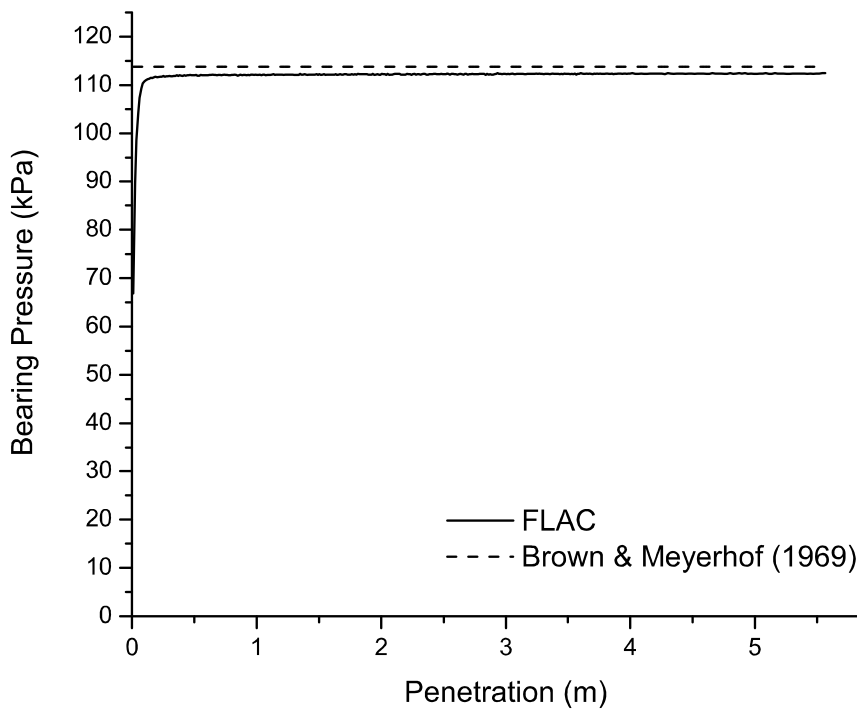

Figure A.297: Bearing pressure versus penetration curve for a rigid smooth circular footing on strong over soft clay for 40 × 30 grid model, $H/D = 0.5$, $c_2/c_1 = 0.8$.

Case 3: $c_2/c_1 = 2/3$ - Small Deformation Analysis

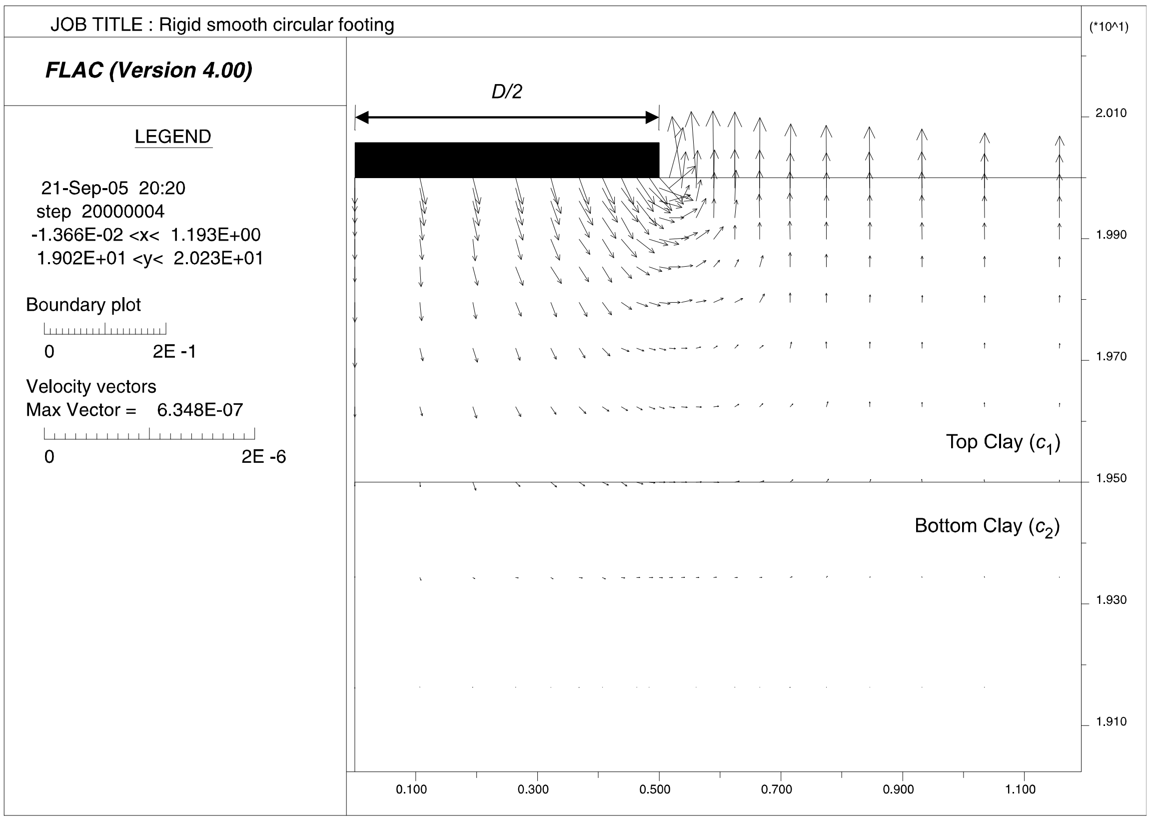

Figure A.298: Velocity vectors for a rigid smooth circular footing on strong over soft clay for 40×30 grid model, $H/D = 0.5$, $c_2/c_1 = 2/3$.

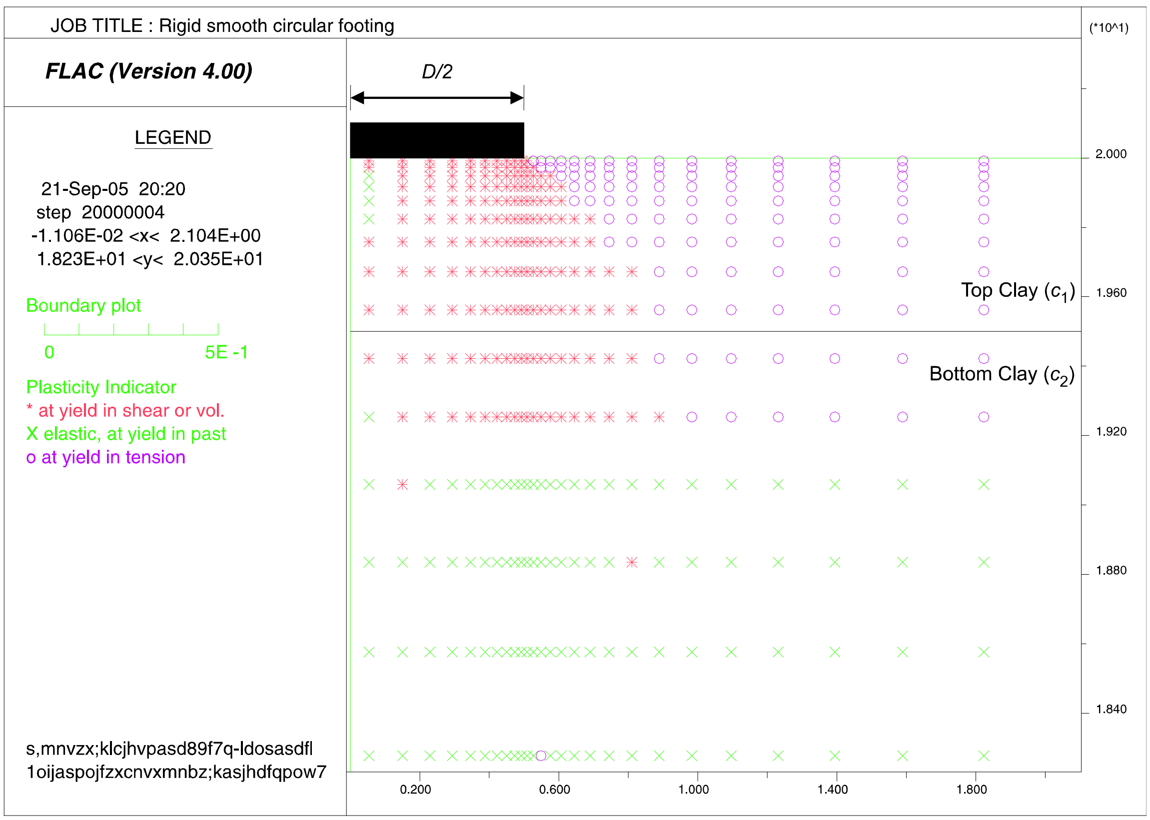

Figure A.299: Plasticity state indicators for a rigid smooth circular footing on strong over soft clay for 40×30 grid model, $H/D = 0.5$, $c_2/c_1 = 2/3$.

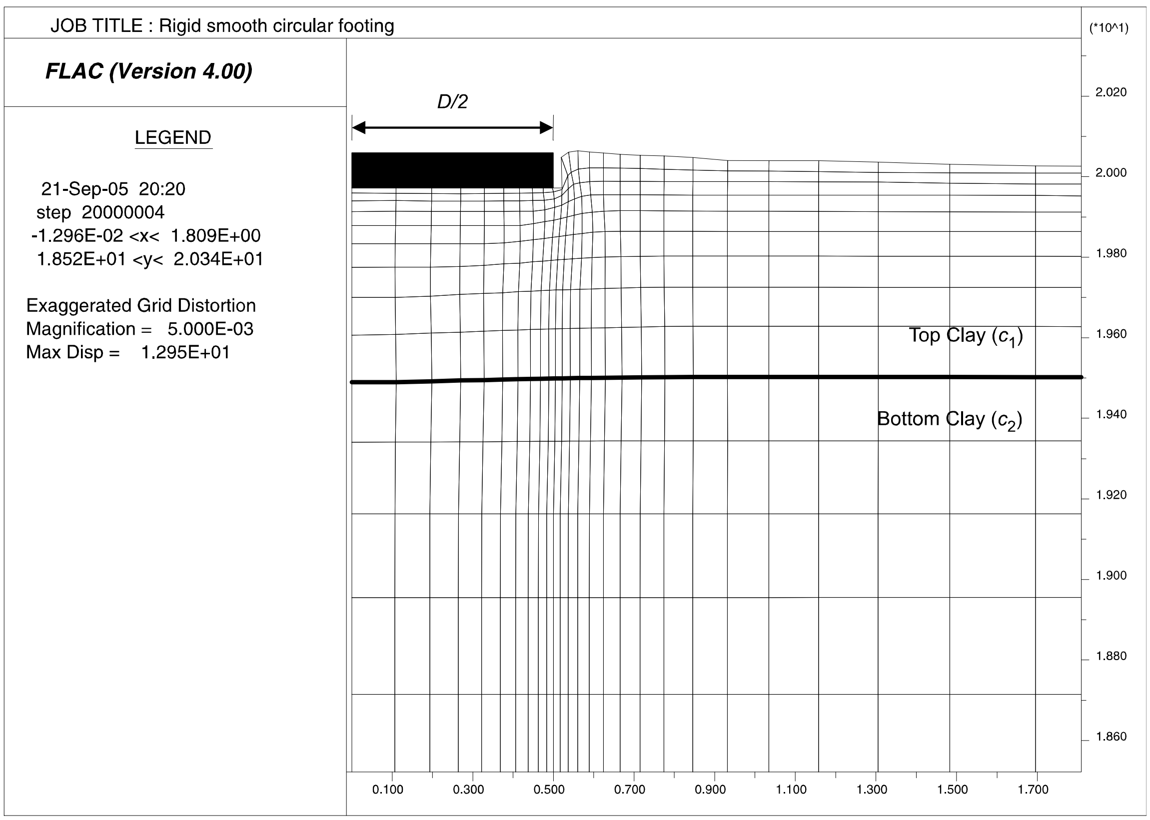

Figure A.300: Magnified grid for a rigid smooth circular footing on strong over soft clay for 40 × 30 grid model, $H/D = 0.5$, $c_2/c_1 = 2/3$.

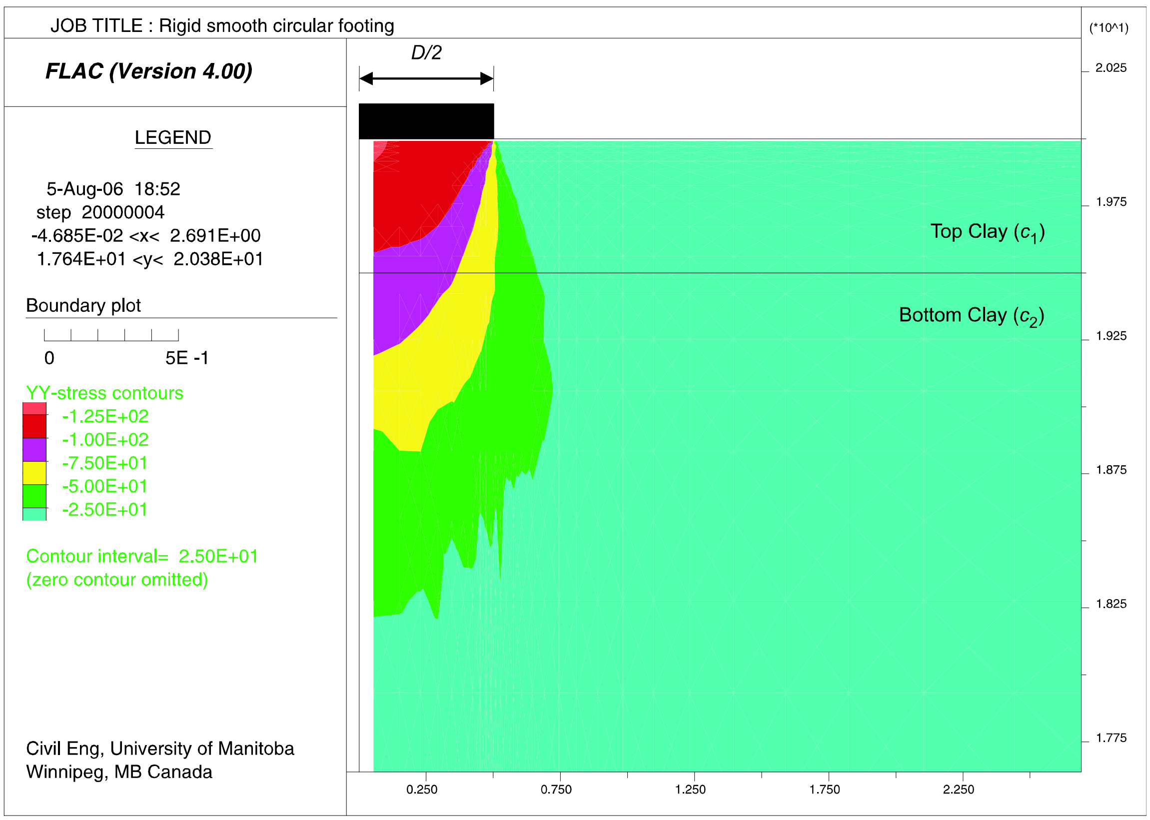

Figure A.301: Vertical stress (σ_{yy}) contours for a rigid smooth circular footing on strong over soft clay for 40 × 30 grid model, $H/D = 0.5$, $c_2/c_1 = 2/3$.

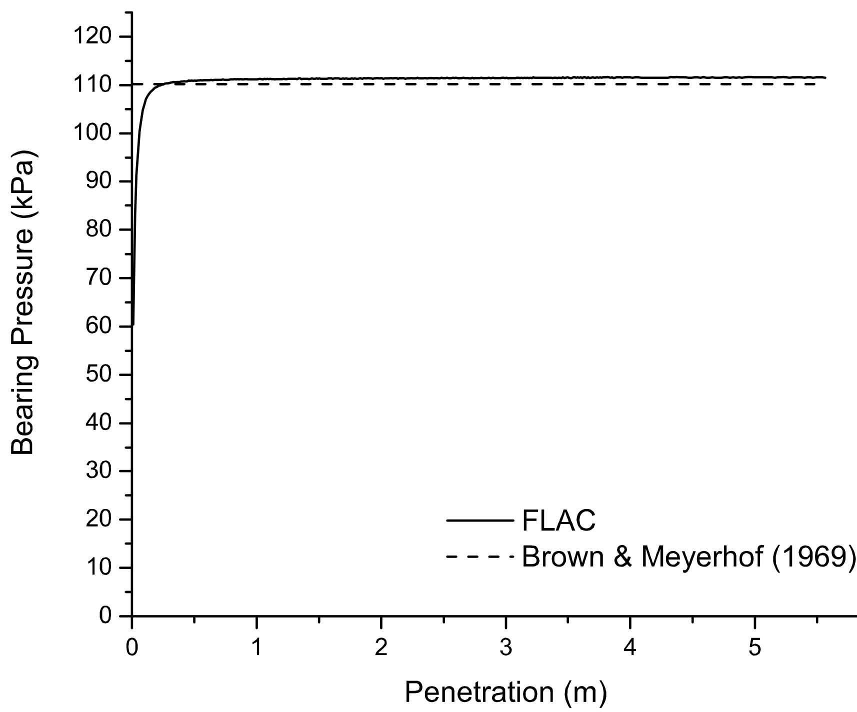

Figure A.302: Bearing pressure versus penetration curve for a rigid smooth circular footing on strong over soft clay for 40×30 grid model, $H/B = 0.5$, $c_2/c_1 = 2/3$.

Case 4: $c_2/c_1 = 0.5$ - Small Deformation Analysis

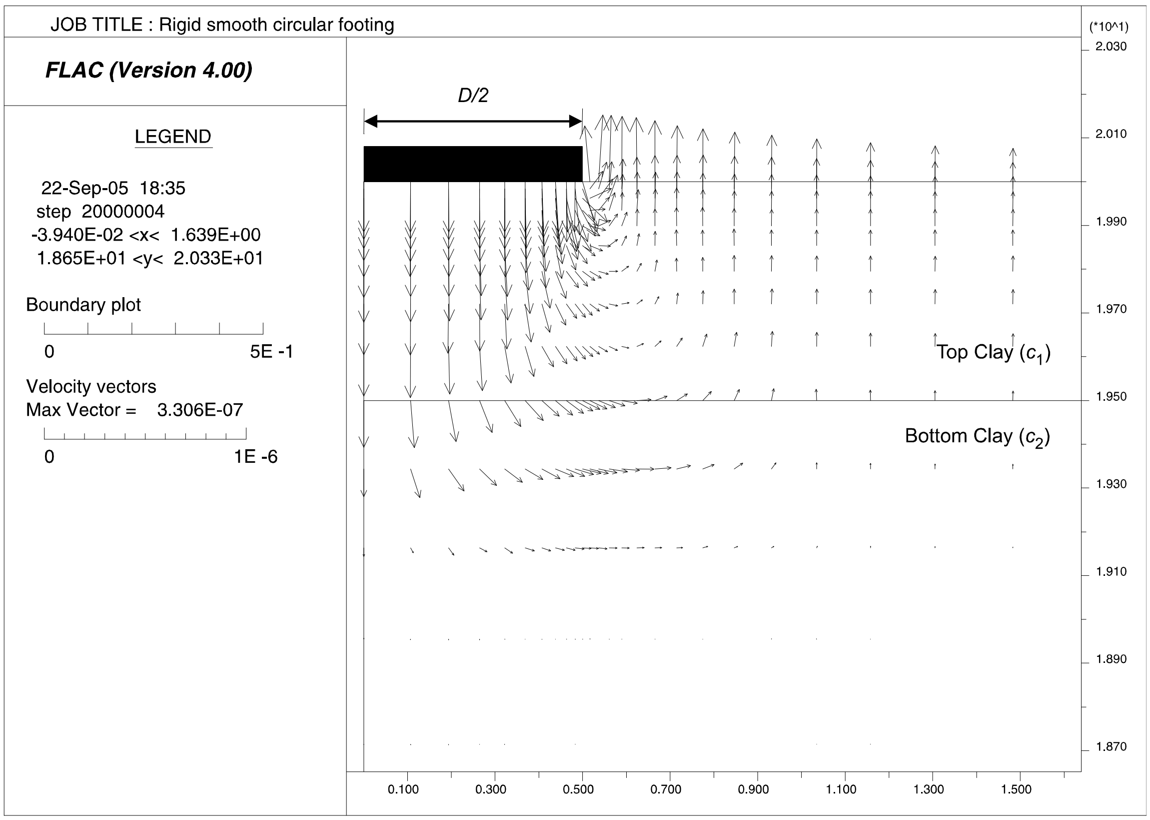

Figure A.303: Velocity vectors for a rigid smooth circular footing on strong clay over soft clay for 40×30 grid model, $H/D = 0.5$, $c_2/c_1 = 0.5$.

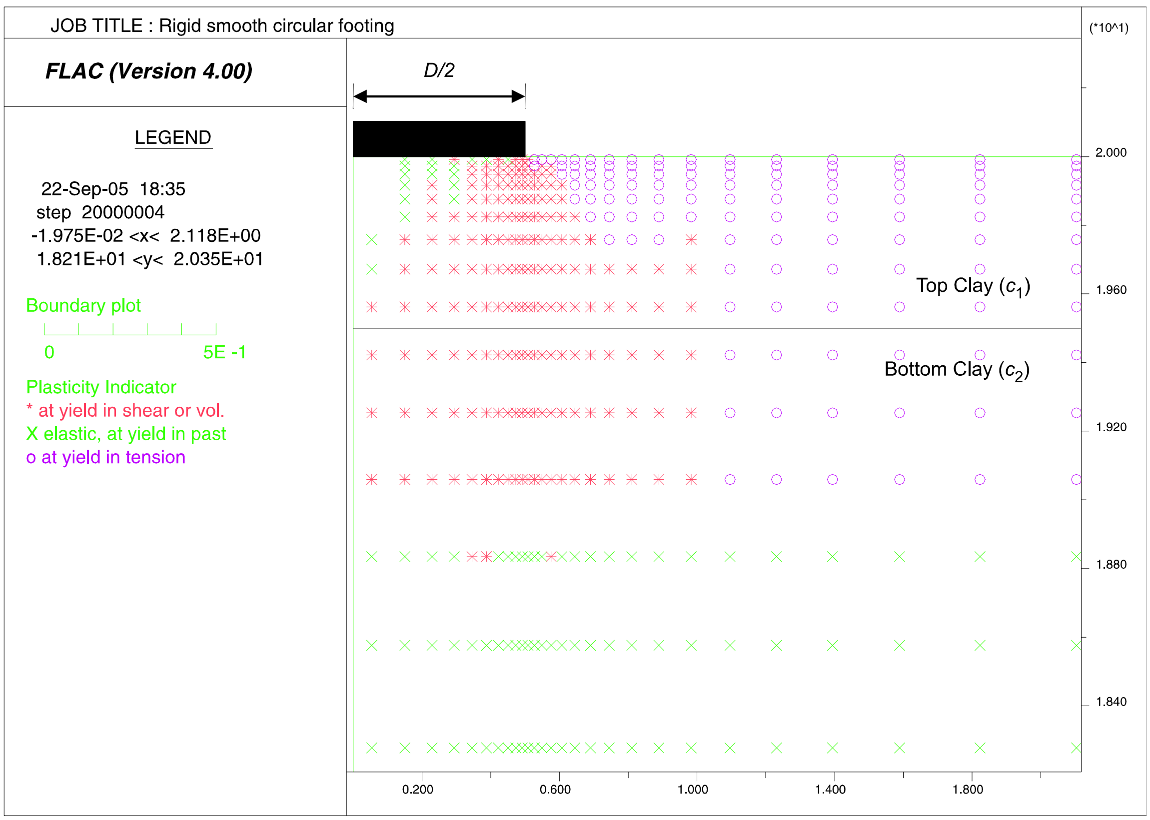

Figure A.304: Plasticity state indicators for a rigid smooth circular footing on strong clay over soft clay for 40 × 30 grid model, $H/D = 0.5$, $c_2/c_1 = 0.5$.

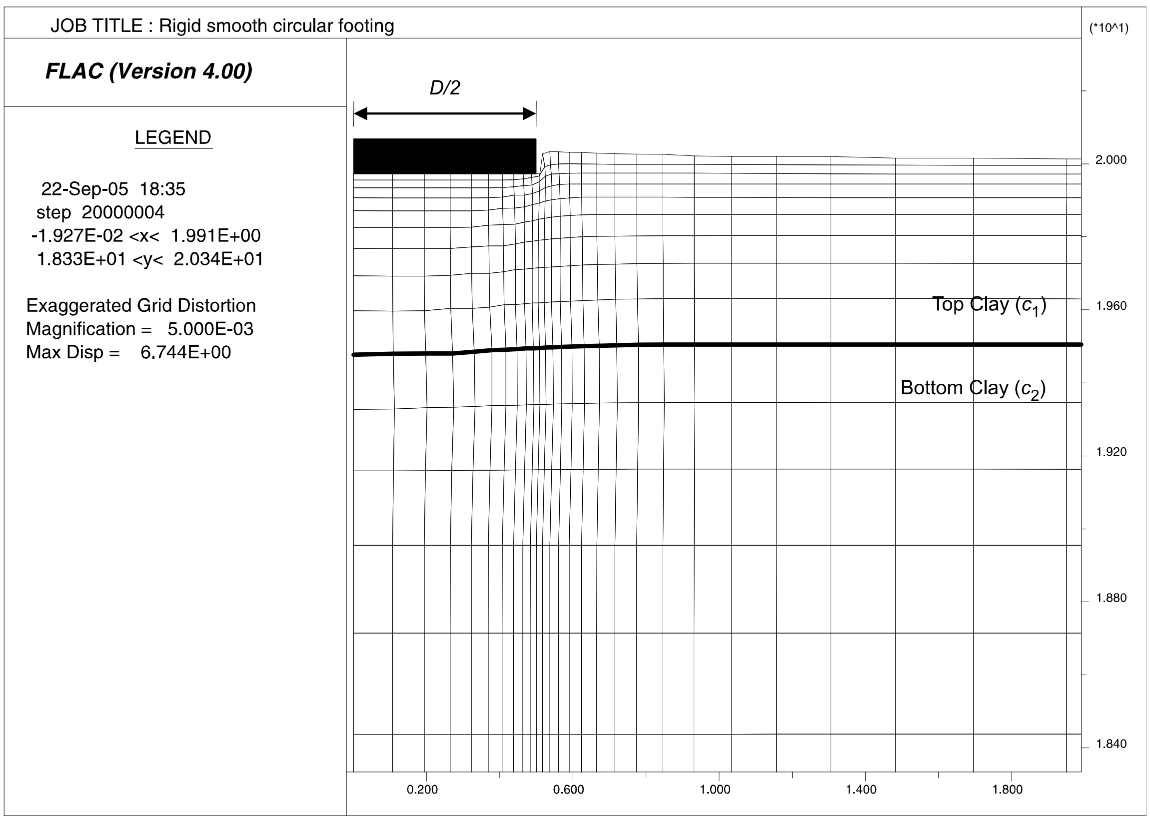

Figure A.305: Magnified grid for a rigid smooth circular footing on strong clay over soft clay for 40×30 grid model, $H/D = 0.5$, $c_2/c_1 = 0.5$.

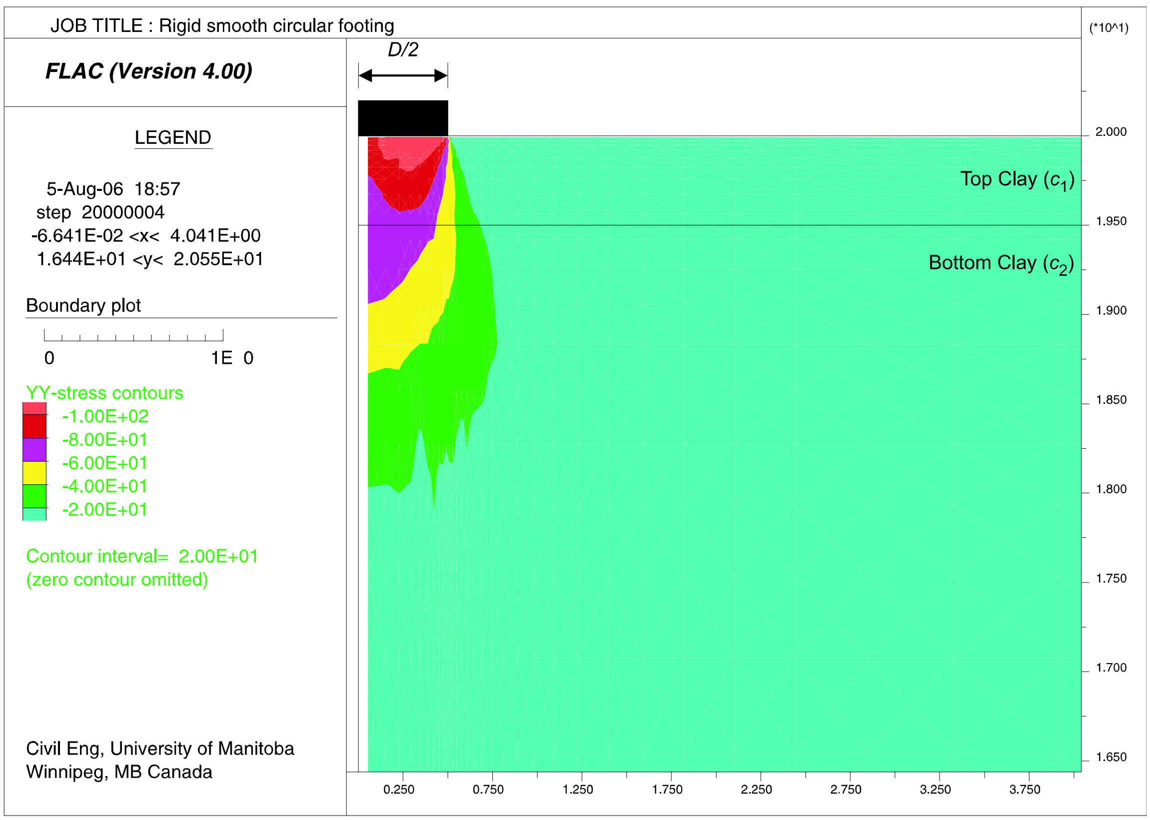

Figure A.306: Vertical stress (σ_{yy}) contours for a rigid smooth circular footing on strong clay over soft clay for 40 × 30 grid model, $H/D = 0.5$, $c_2/c_1 = 0.5$.

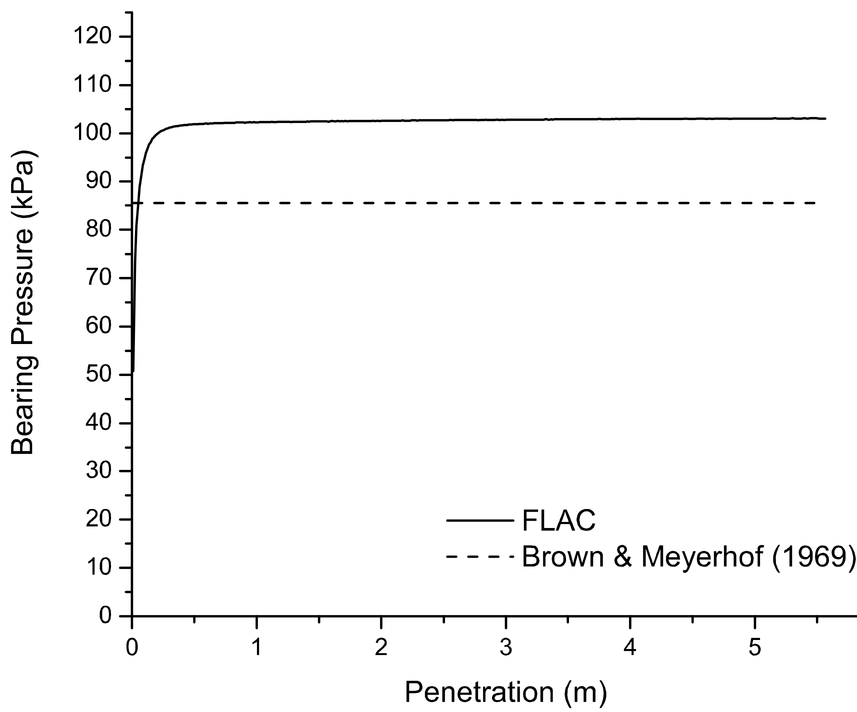

Figure A.307: Bearing pressure versus penetration curve for a rigid smooth circular footing on strong clay over soft clay for 40×30 grid model, $H/D = 0.5$, $c_2/c_1 = 0.5$.

Case 5: $c_2/c_1 = 1/3$ - Small Deformation Analysis

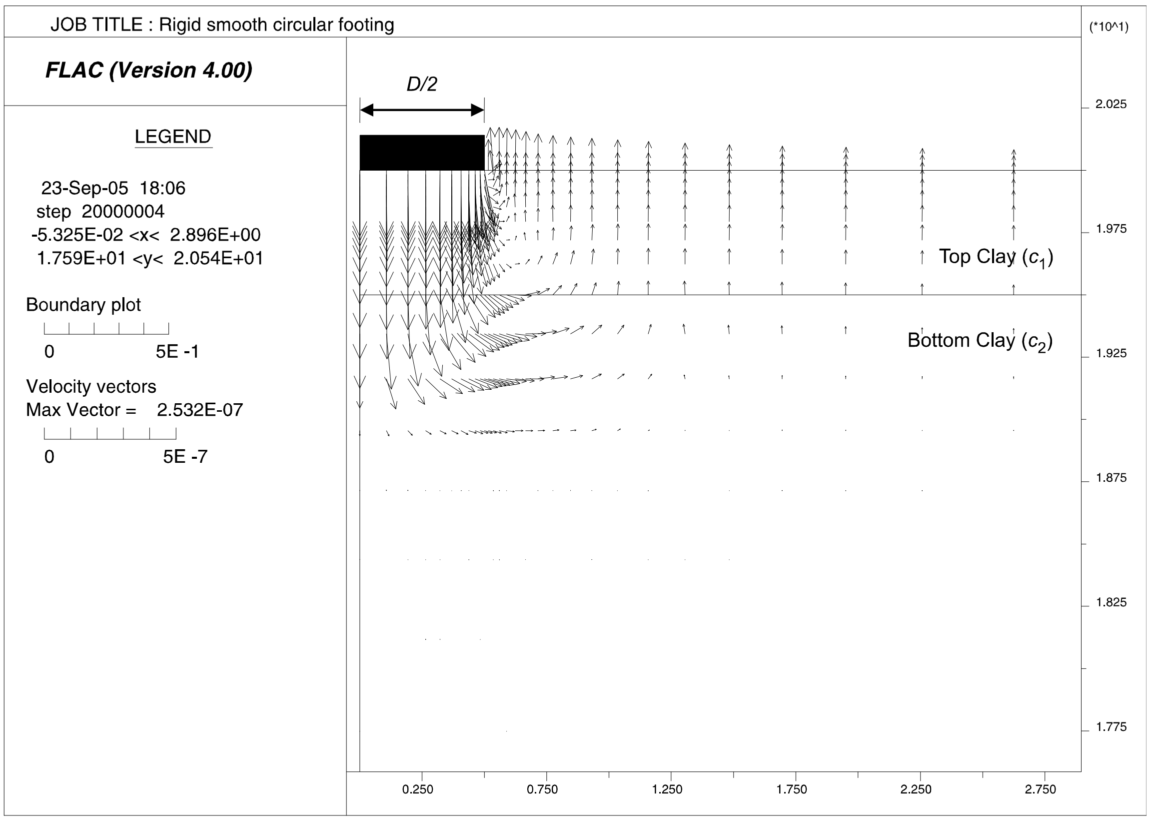

Figure A.308: Velocity vectors for a rigid smooth circular footing on strong clay over soft clay for 40×30 grid model, $H/D = 0.5$, $c_2/c_1 = 1/3$.

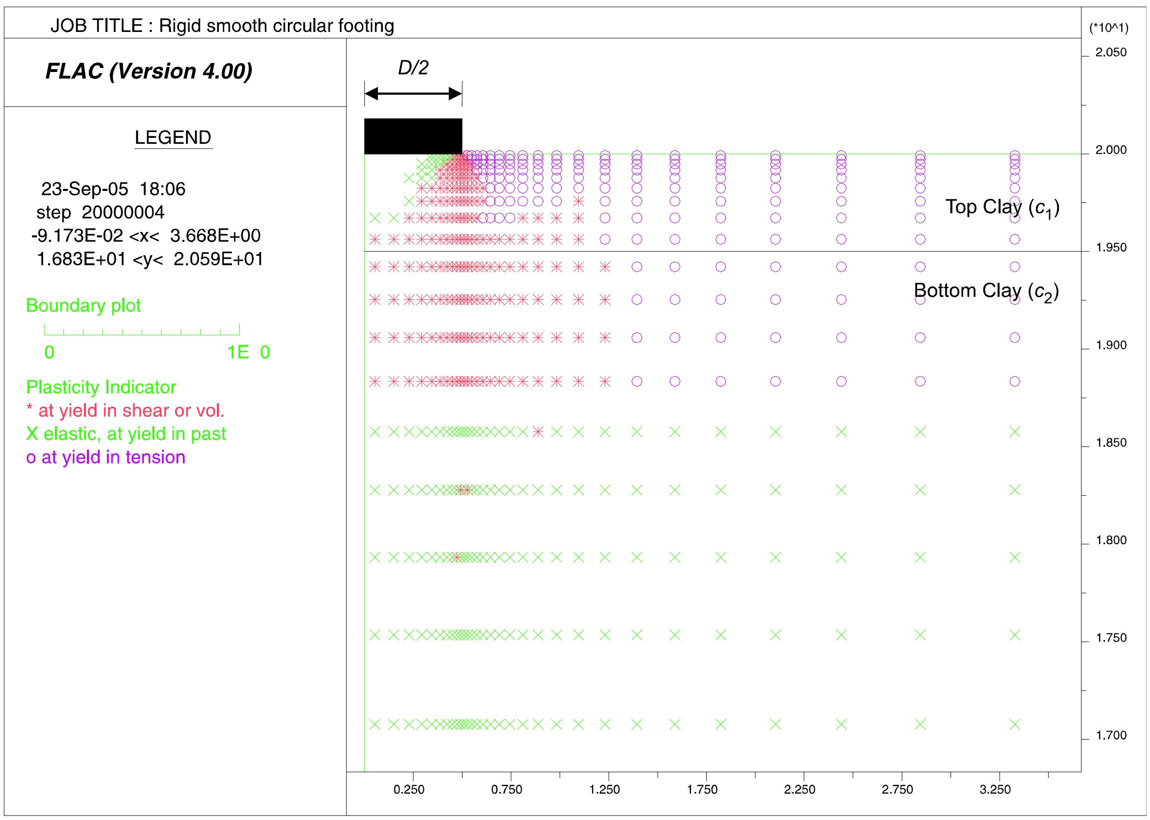

Figure A.309: Plasticity state indicators for a rigid smooth circular footing on strong clay over soft clay for 40 × 30 grid model, $H/D = 0.5$, $c_2/c_1 = 1/3$.

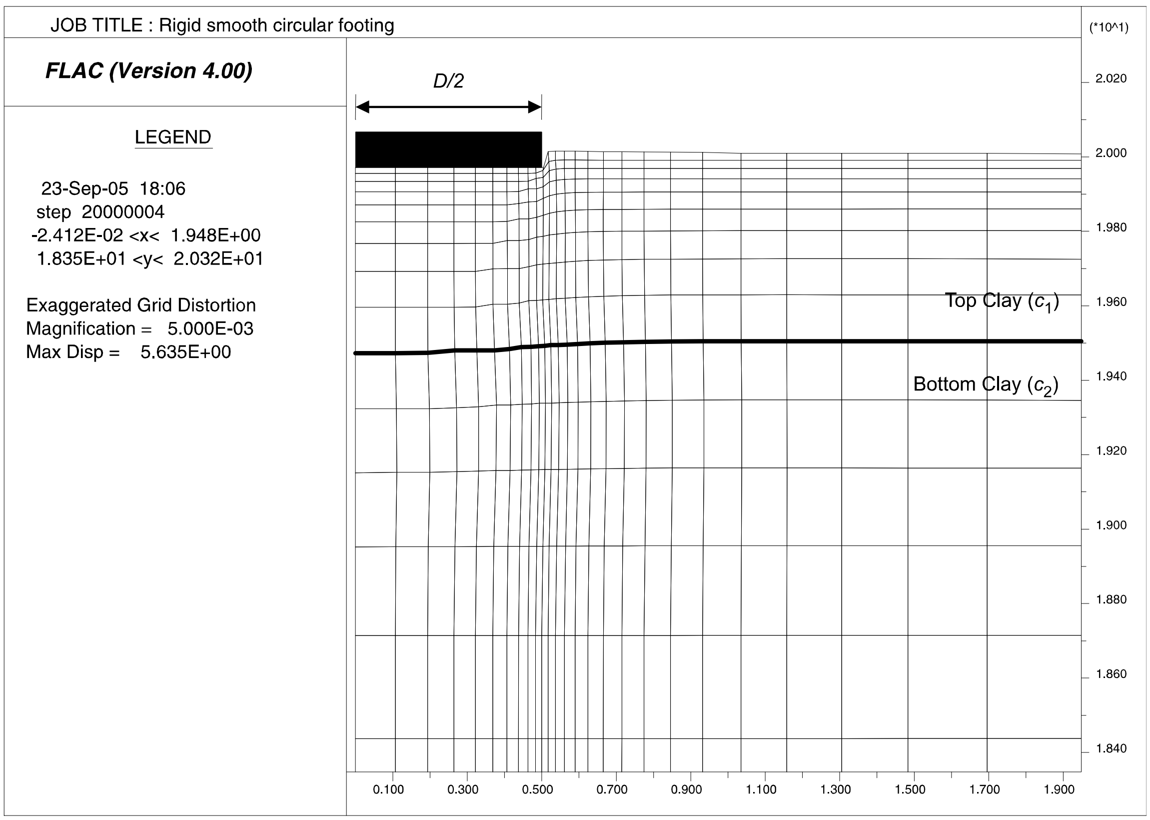

Figure A.310: Magnified grid for a rigid smooth circular footing on strong clay over soft clay for 40×30 grid model, $H/D = 0.5$, $c_2/c_1 = 1/3$.

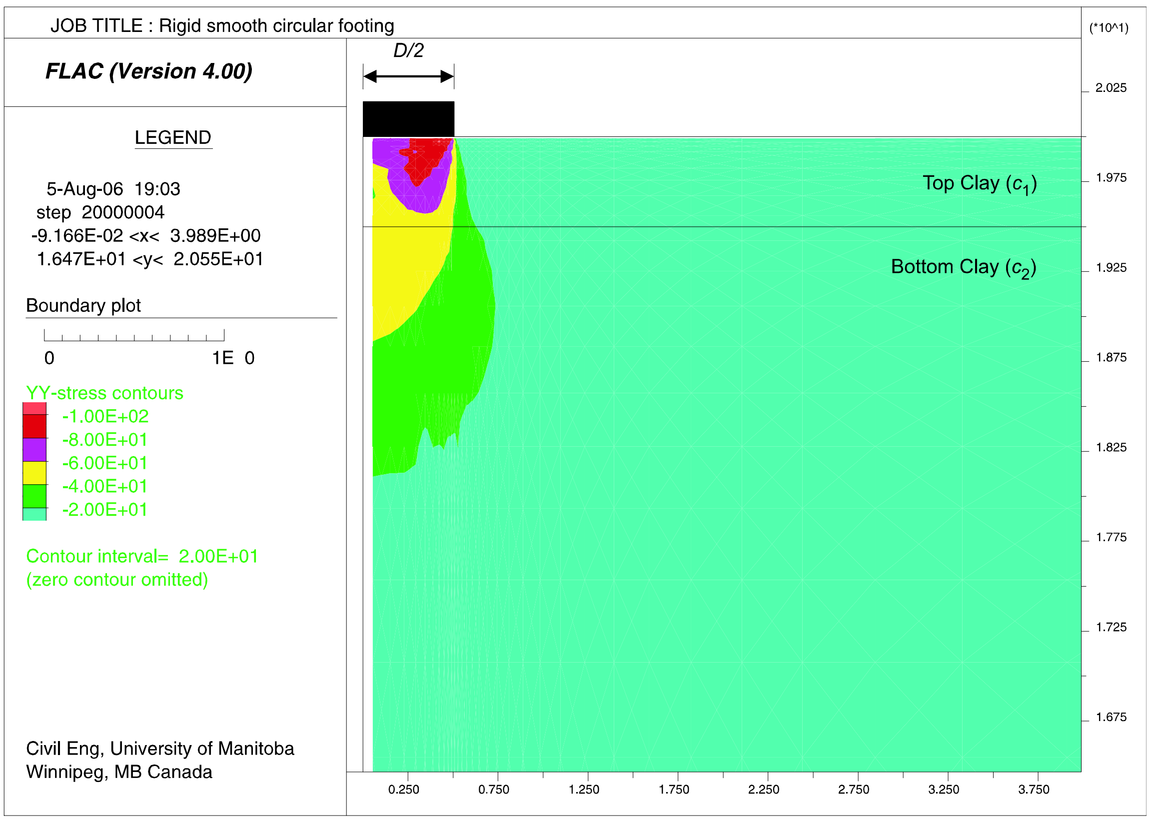

Figure A.311: Vertical stress (σ_{yy}) contours for a rigid smooth circular footing on strong clay over soft clay for 40×30 grid model, $H/D = 0.5$, $c_2/c_1 = 1/3$.

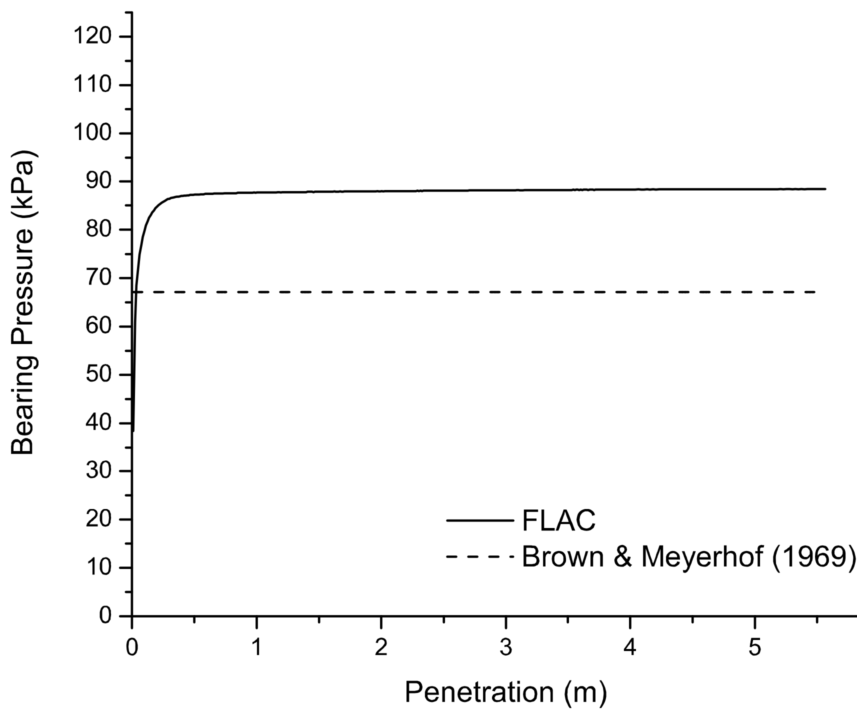

Figure A.312: Bearing pressure versus penetration curve for a rigid smooth circular footing on strong clay over soft clay for 40×30 grid model, $H/D = 0.5$, $c_2/c_1 = 1/3$.

Case 6: $c_2/c_1 = 0.2$ - Small Deformation Analysis

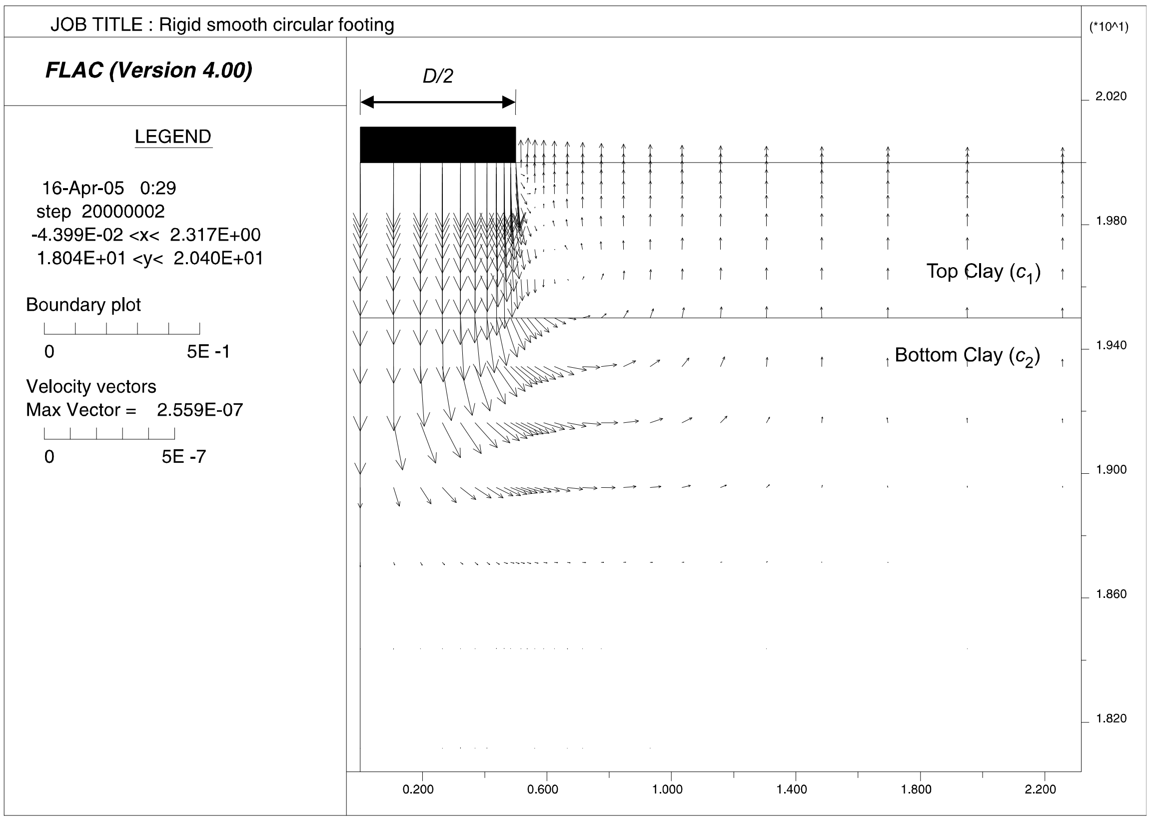

Figure A.313: Velocity vectors for a rigid smooth circular footing on strong clay over soft clay for 40×30 grid model, $H/D = 0.5$, $c_2/c_1 = 0.2$.

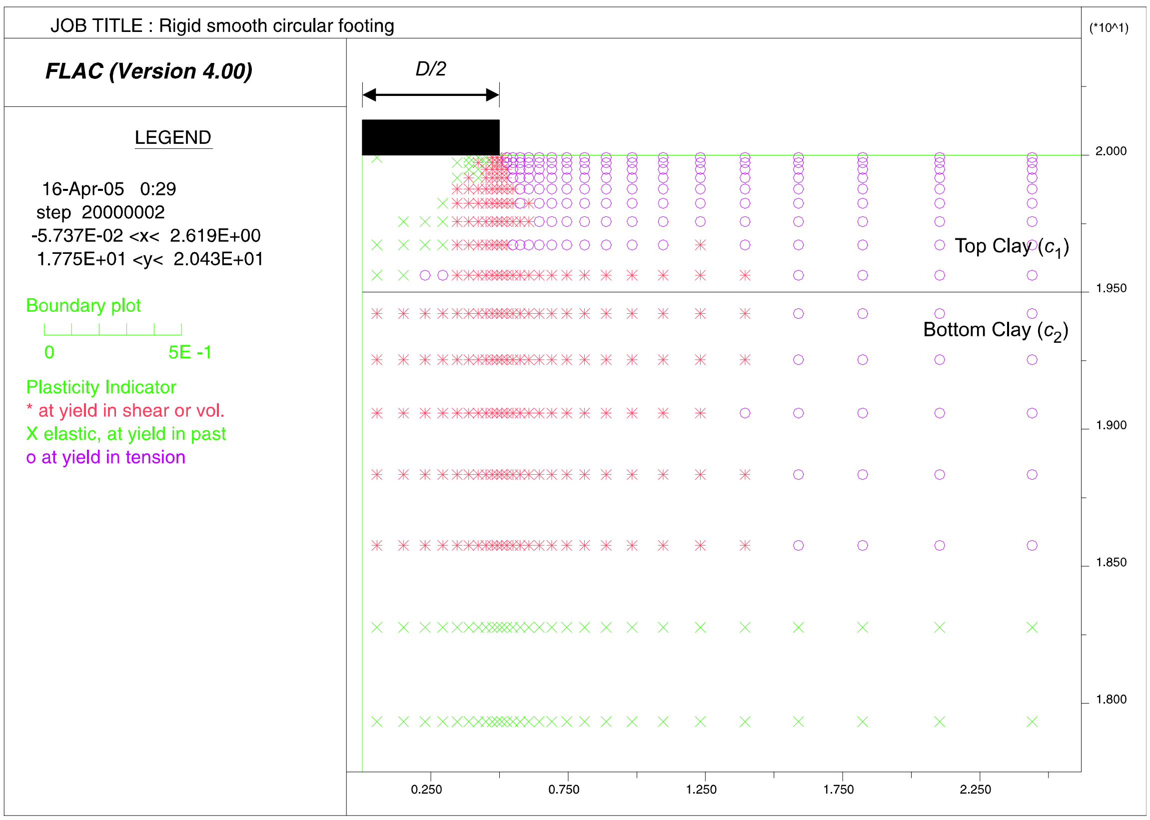

Figure A.314: Plasticity state indicators for a rigid smooth circular footing on strong clay over soft clay for 40 × 30 grid model, $H/D = 0.5$, $c_2/c_1 = 0.2$.

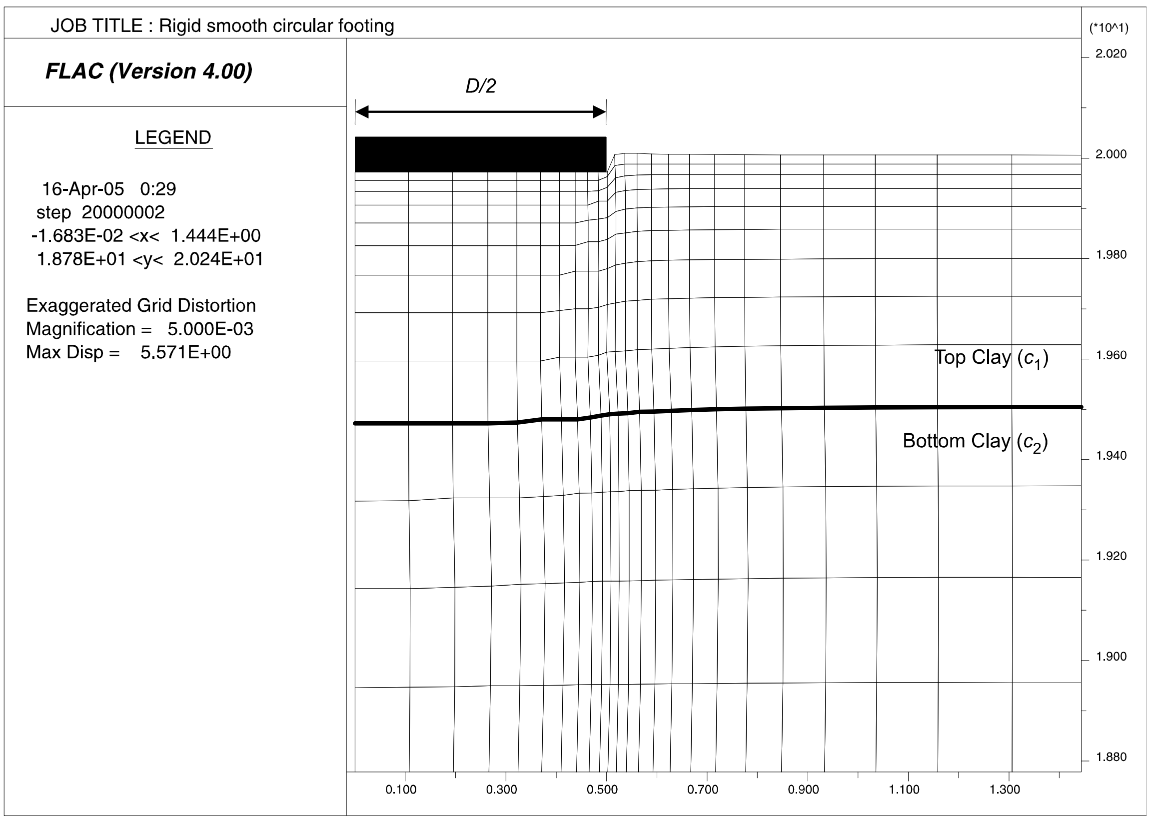

Figure A.315: Magnified grid for a rigid smooth circular footing on strong clay over soft clay for 40×30 grid model, $H/D = 0.5$, $c_2/c_1 = 0.2$.

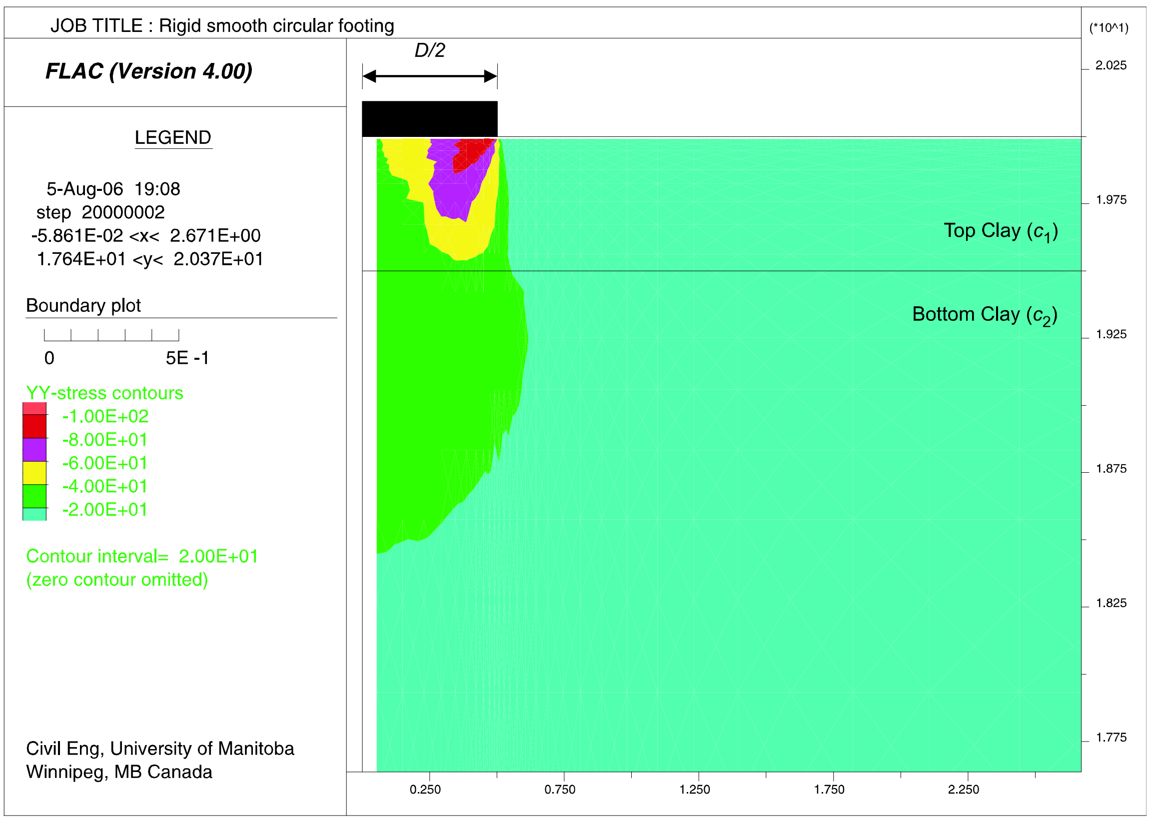

Figure A.316: Vertical stress (σ_{yy}) contours for a rigid smooth circular footing on strong clay over soft clay for 40×30 grid model, $H/D = 0.5$, $c_2/c_1 = 0.2$.

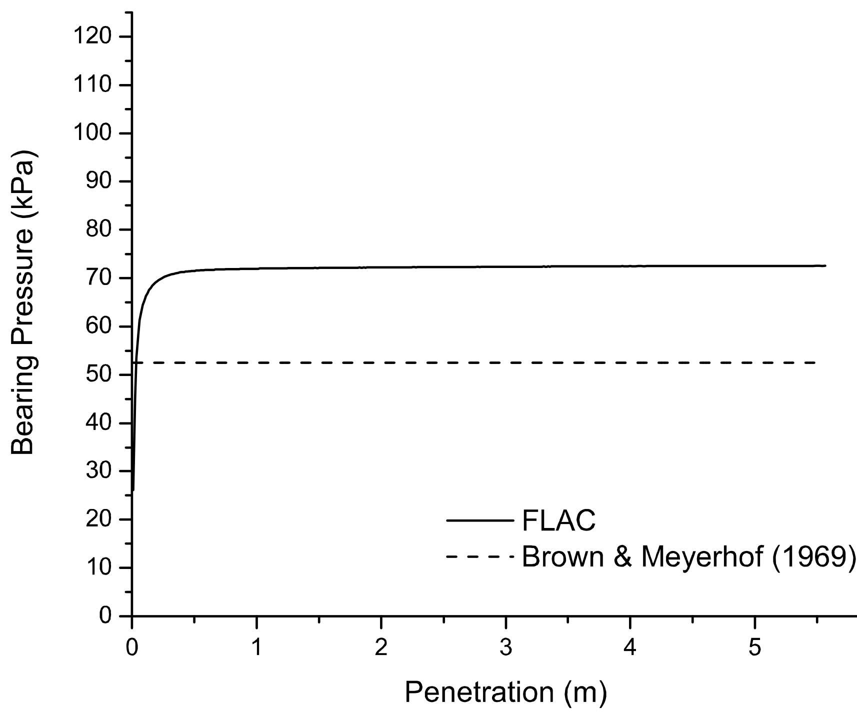

Figure A.317: Bearing pressure versus penetration curve for a rigid circular smooth footing on strong clay over soft clay for 40 × 30 grid model, $H/D = 0.5$, $c_2/c_1 = 0.2$.

Case 7: $c_2/c_1 = 0.1$ - Small Deformation Analysis

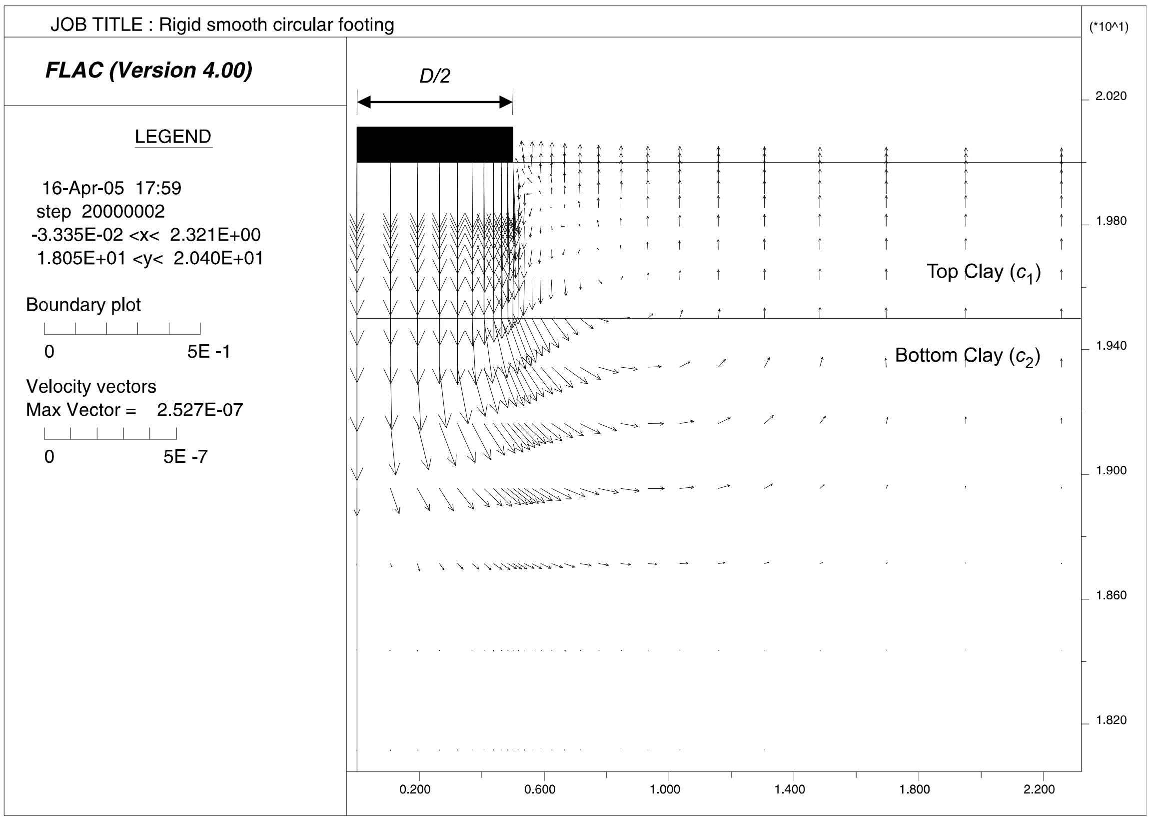

Figure A.318: Velocity vectors for a rigid smooth circular footing on strong clay over soft clay for 40×30 grid model, $H/D = 0.5$, $c_2/c_1 = 0.1$.

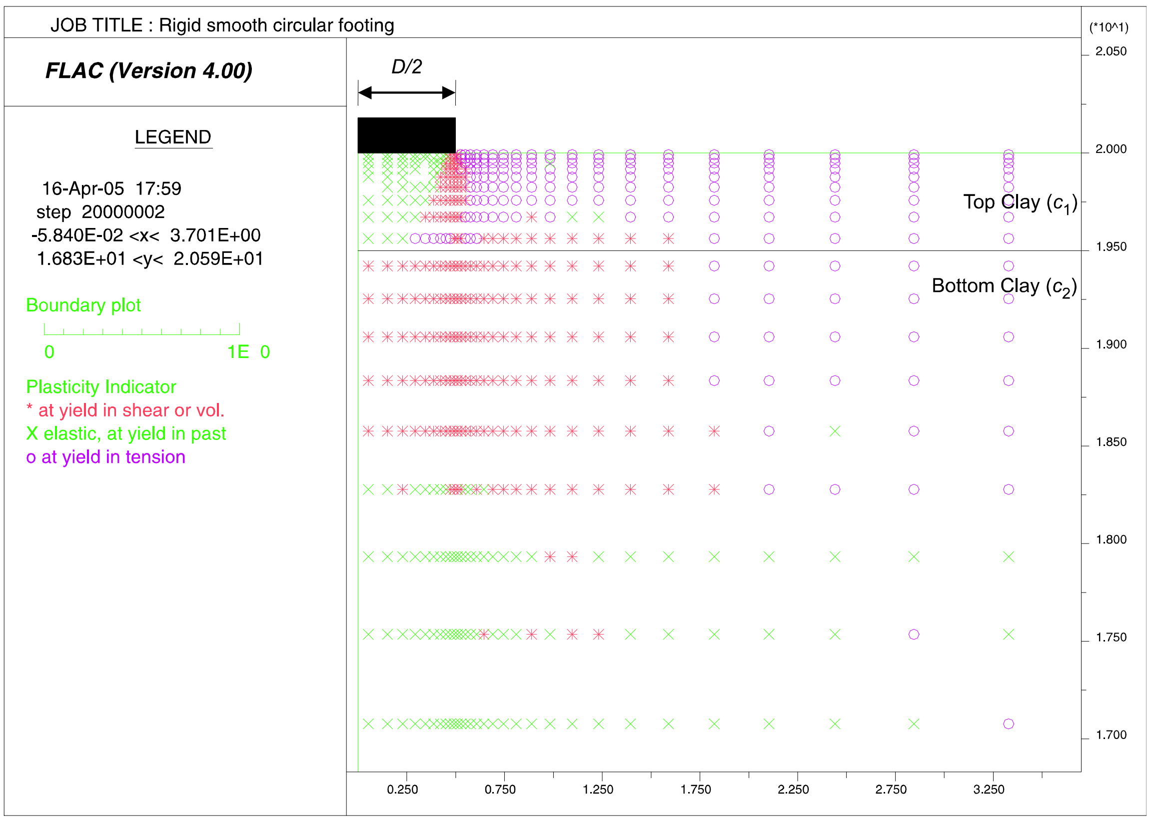

Figure A.319: Plasticity state indicators for a rigid smooth circular footing on strong clay over soft clay for 40 × 30 grid model, $H/D = 0.5$, $c_2/c_1 = 0.1$.

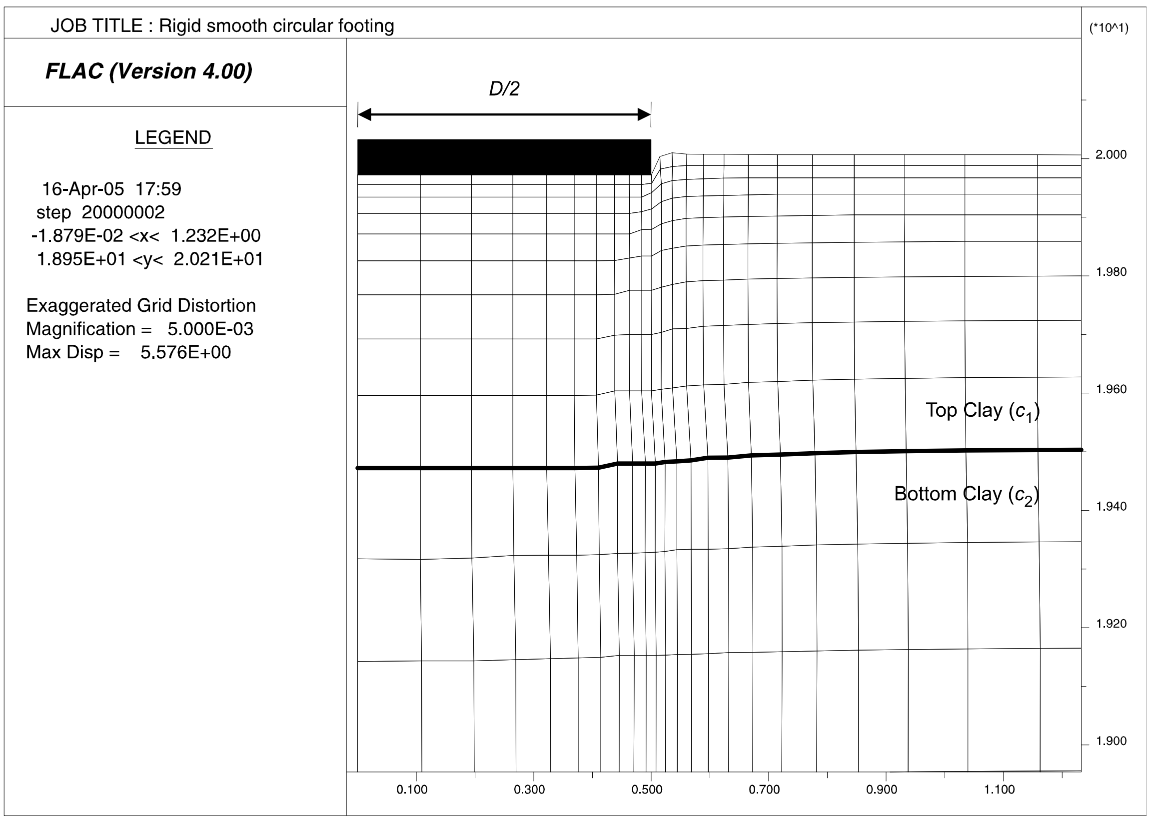

Figure A.320: Magnified grid for a rigid smooth circular footing on strong clay over soft clay for 40×30 grid model, $H/D = 0.5$, $c_2/c_1 = 0.1$.

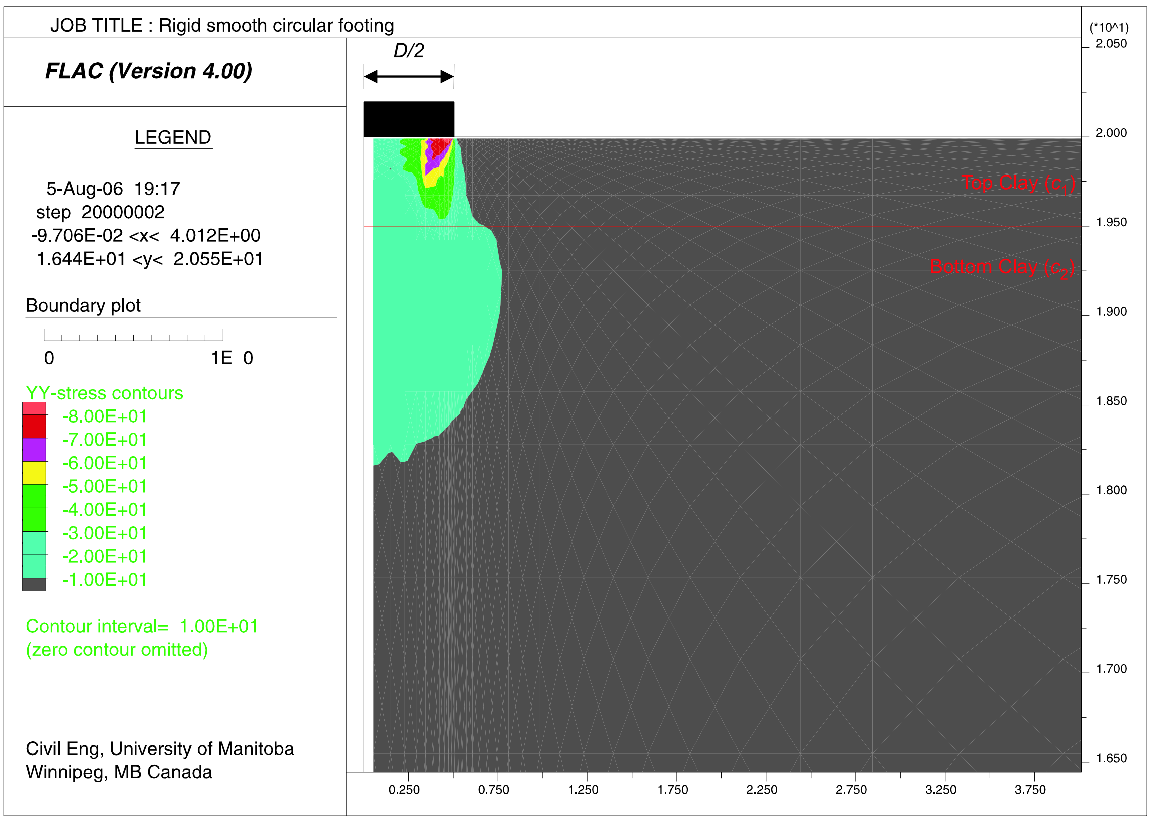

Figure A.321: Vertical stress (σ_{yy}) contours for a rigid circular smooth footing on strong clay over soft clay for 40 × 30 grid model, $H/D = 0.5$, $c_2/c_1 = 0.1$.

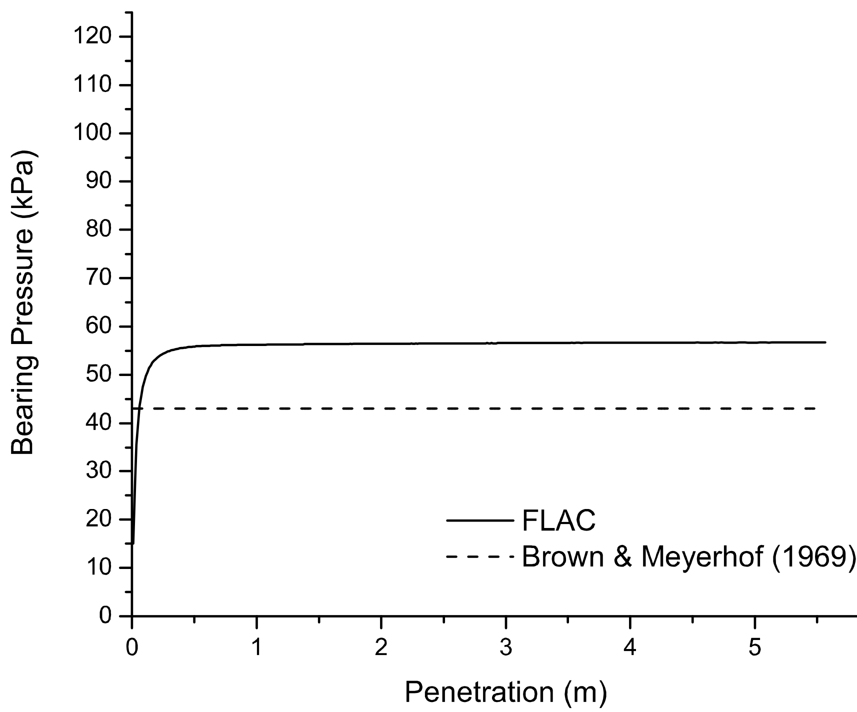

Figure A.322: Bearing pressure versus penetration curve for a rigid smooth circular footing on strong clay over soft clay for 40 × 30 grid model, $H/D = 0.5$, $c_2/c_1 = 0.1$.

A.3.5 Rigid Smooth Circular Footing on Strong over Soft Clay ($H/D = 0.25$)

Case 2: $c_2/c_1 = 0.8$ **- Small Deformation Analysis**

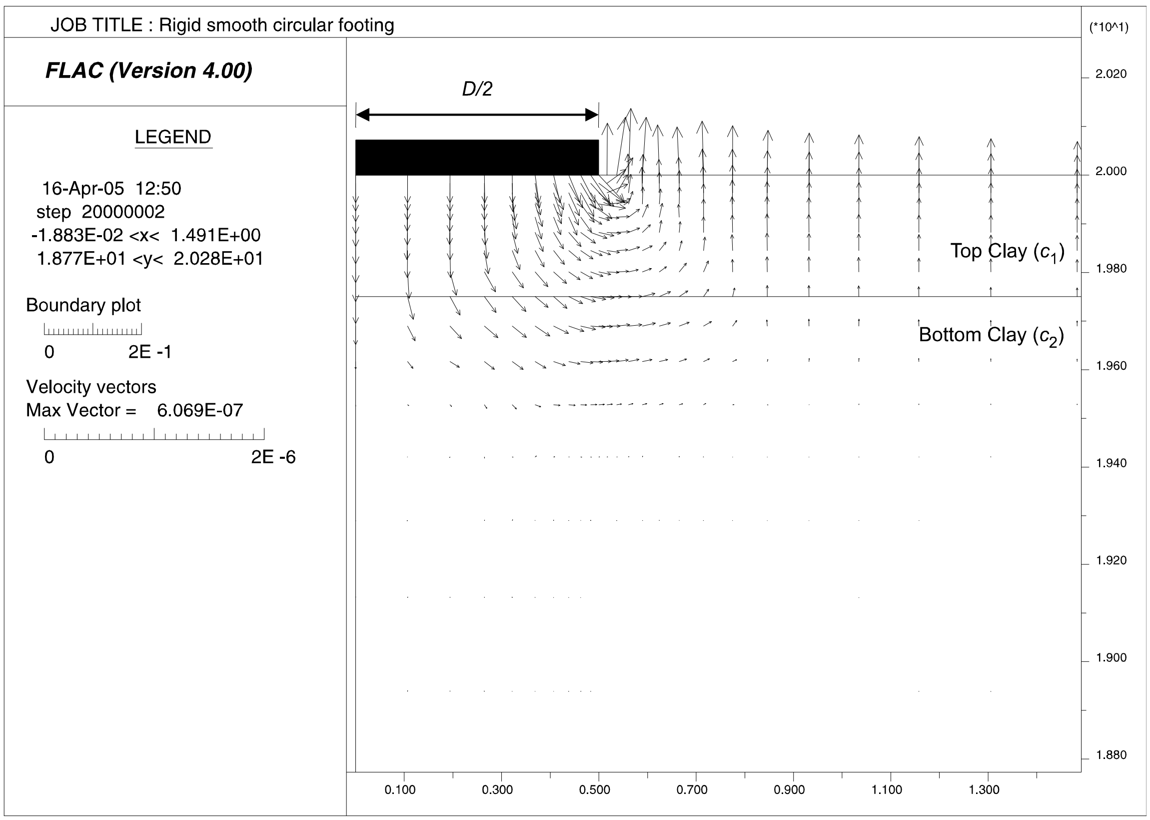

Figure A.323: Velocity vectors for a rigid circular footing on strong over soft clay for 40×30 grid model, $H/D = 0.25$, $c_2/c_1 = 0.8$.

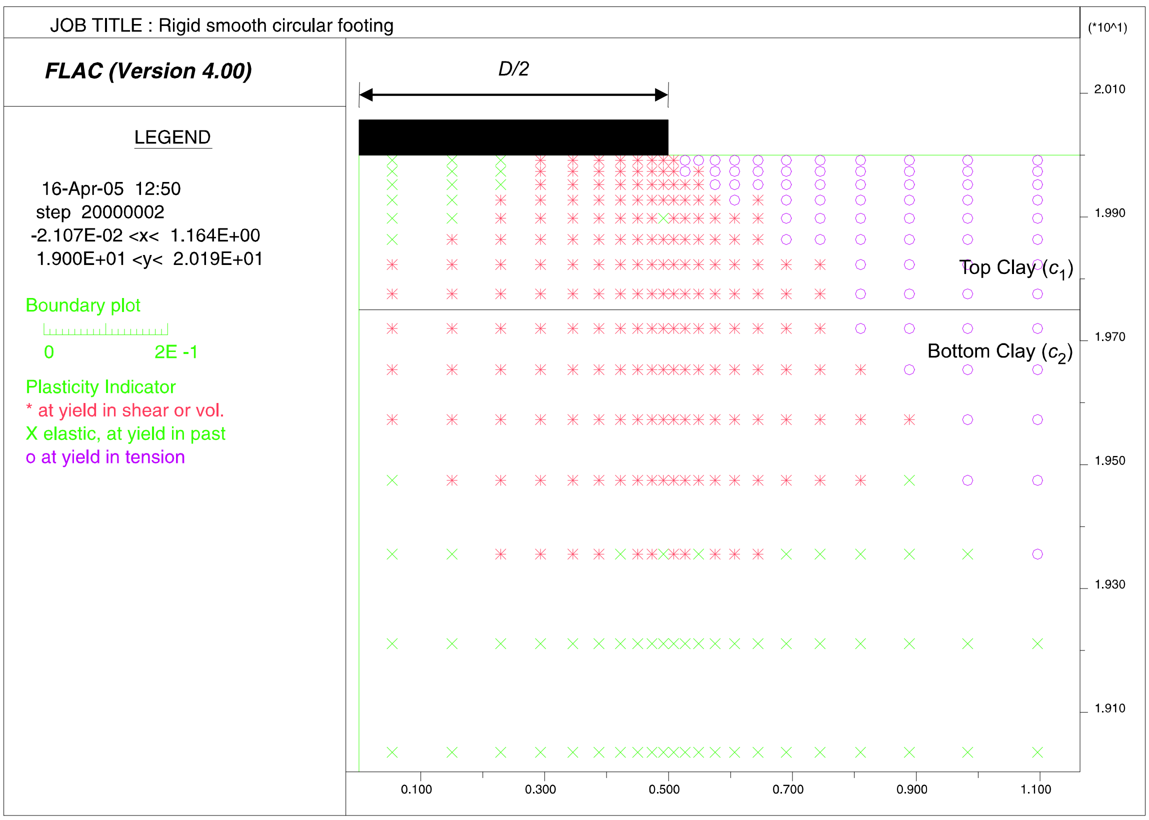

Figure A.324: Plasticity indicators for a rigid smooth circular footing on strong over soft clay for 40 × 30 grid model, $H/D = 0.25$, $c_2/c_1 = 0.8$.

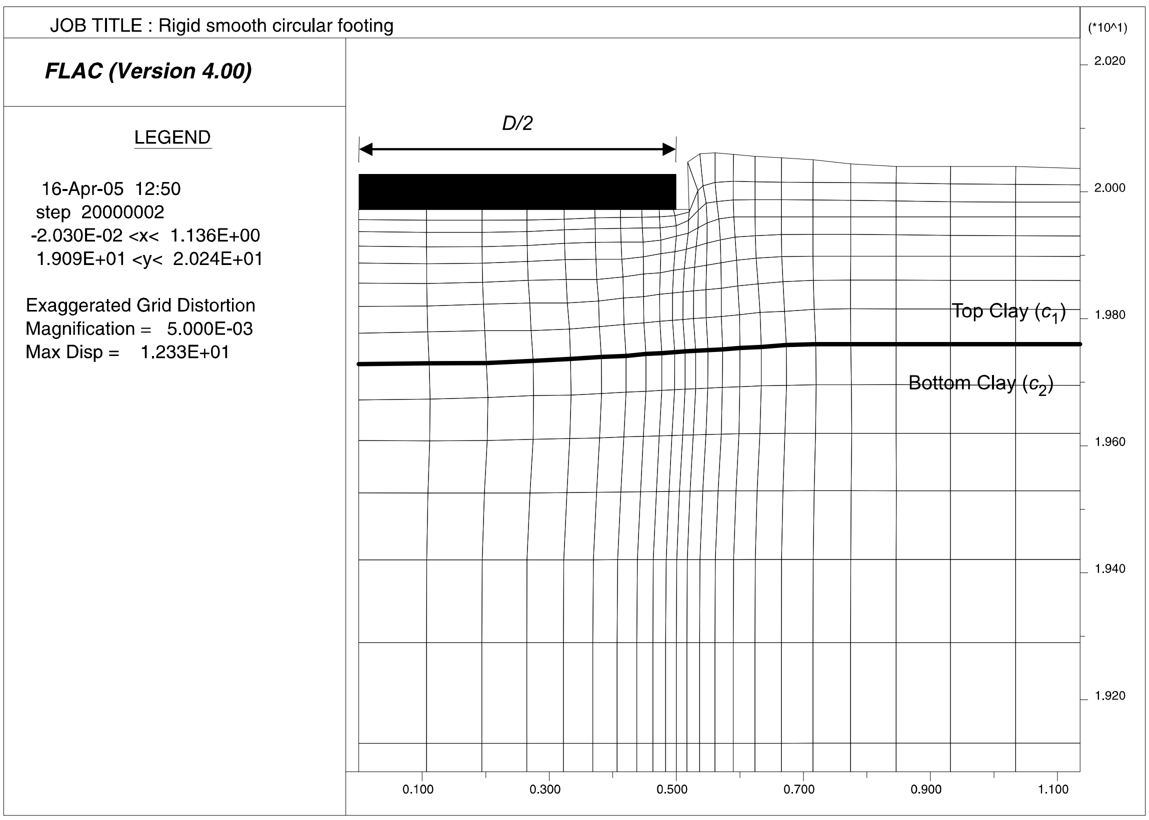

Figure A.325: Magnified grid for a rigid smooth circular footing on strong over soft clay for 40×30 grid model, $H/D = 0.25$, $c_2/c_1 = 0.8$.

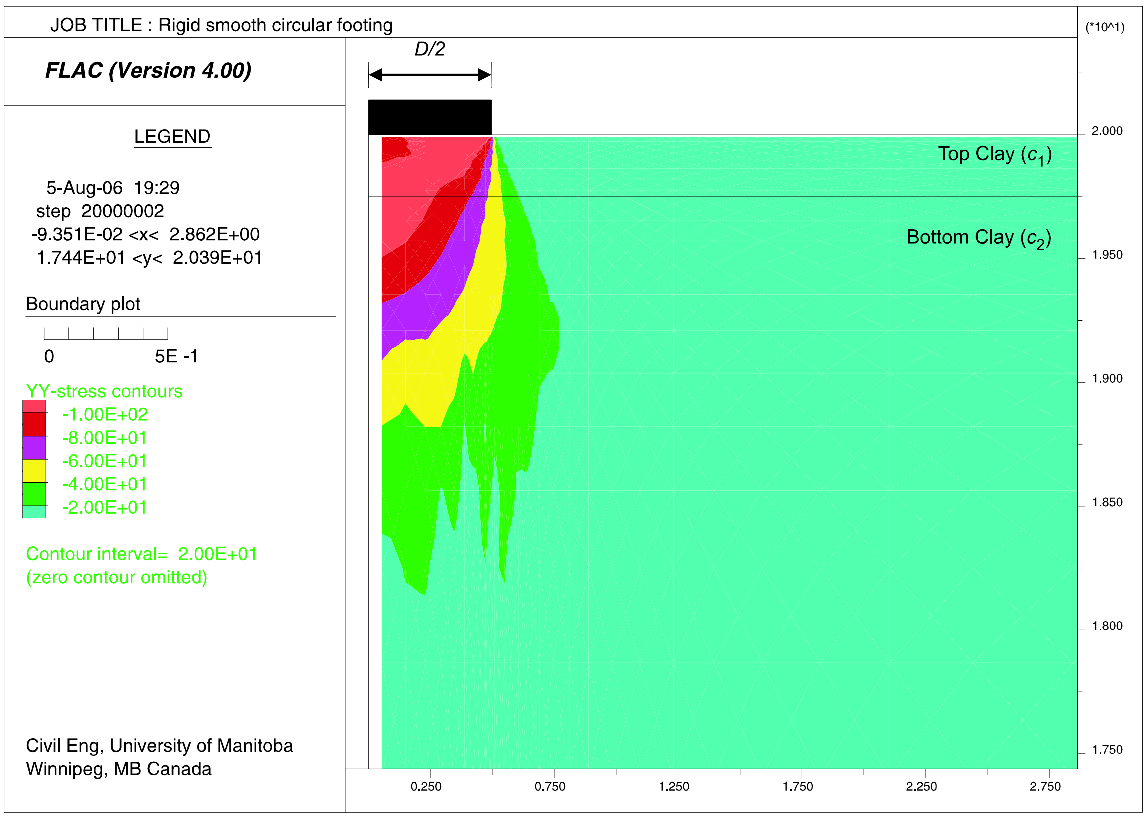

Figure A.326: Vertical stress (σ_{yy}) contours for a rigid smooth circular footing on strong over soft clay for 40 × 30 grid model, $H/D = 0.25$, $c_2/c_1 = 0.8$.

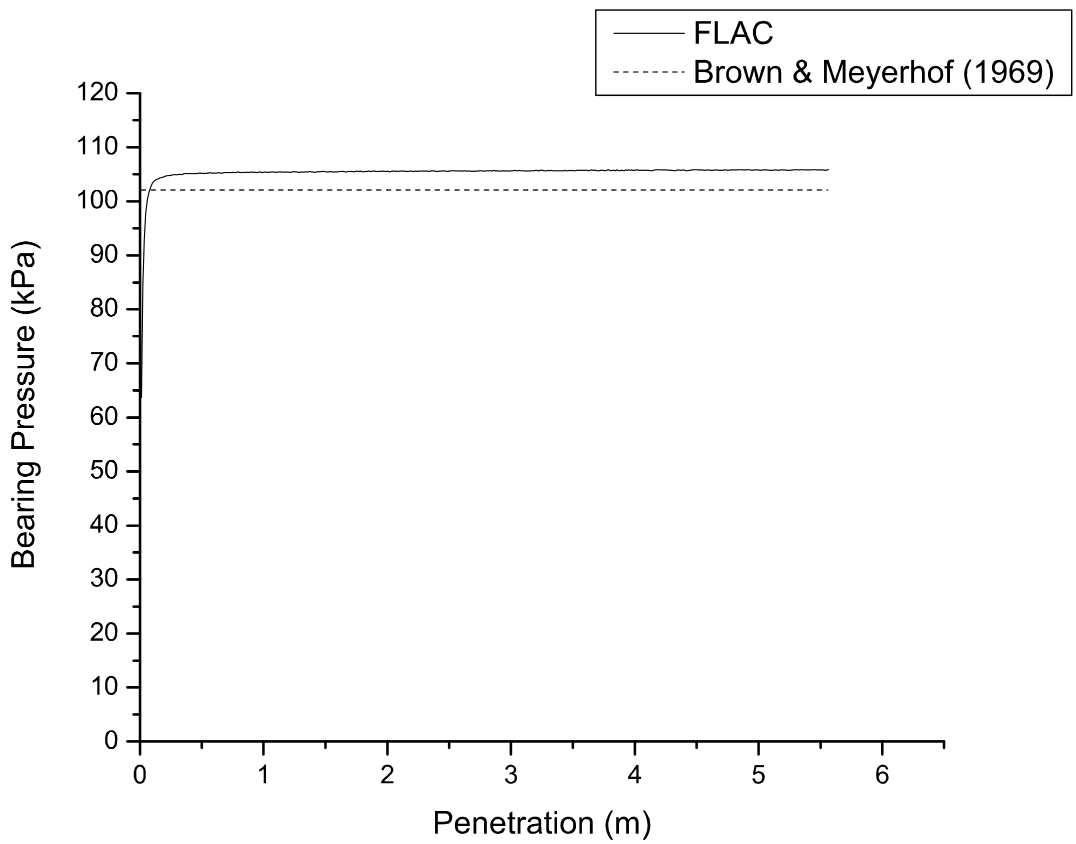

Figure A.327: Bearing pressure versus penetration curve for a rigid smooth circular footing on strong over soft clay for 40 × 30 grid model, $H/D = 0.25$, $c_2/c_1 = 0.8$.

Case 3: $c_2/c_1 = 2/3$ - Small Deformation Analysis

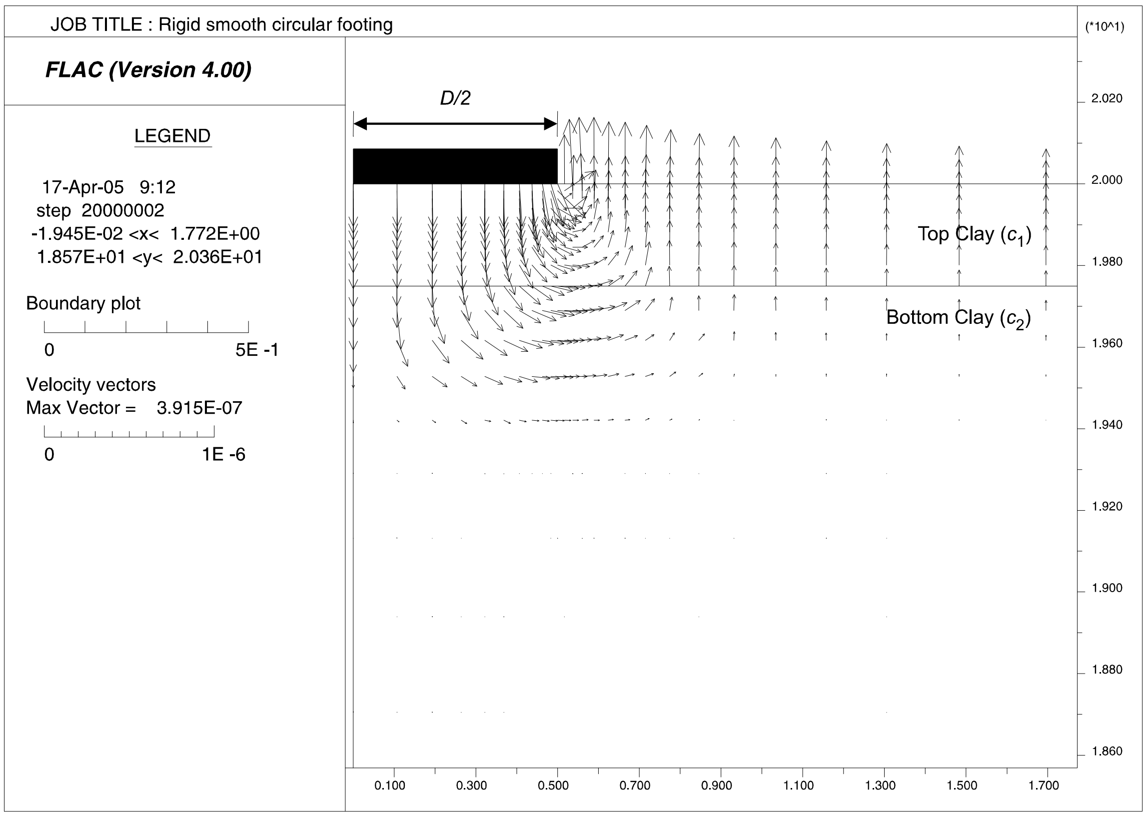

Figure A.328: Velocity vectors for a rigid smooth circular footing on strong over soft clay for 40×30 grid model, $H/D = 0.25$, $c_2/c_1 = 2/3$.

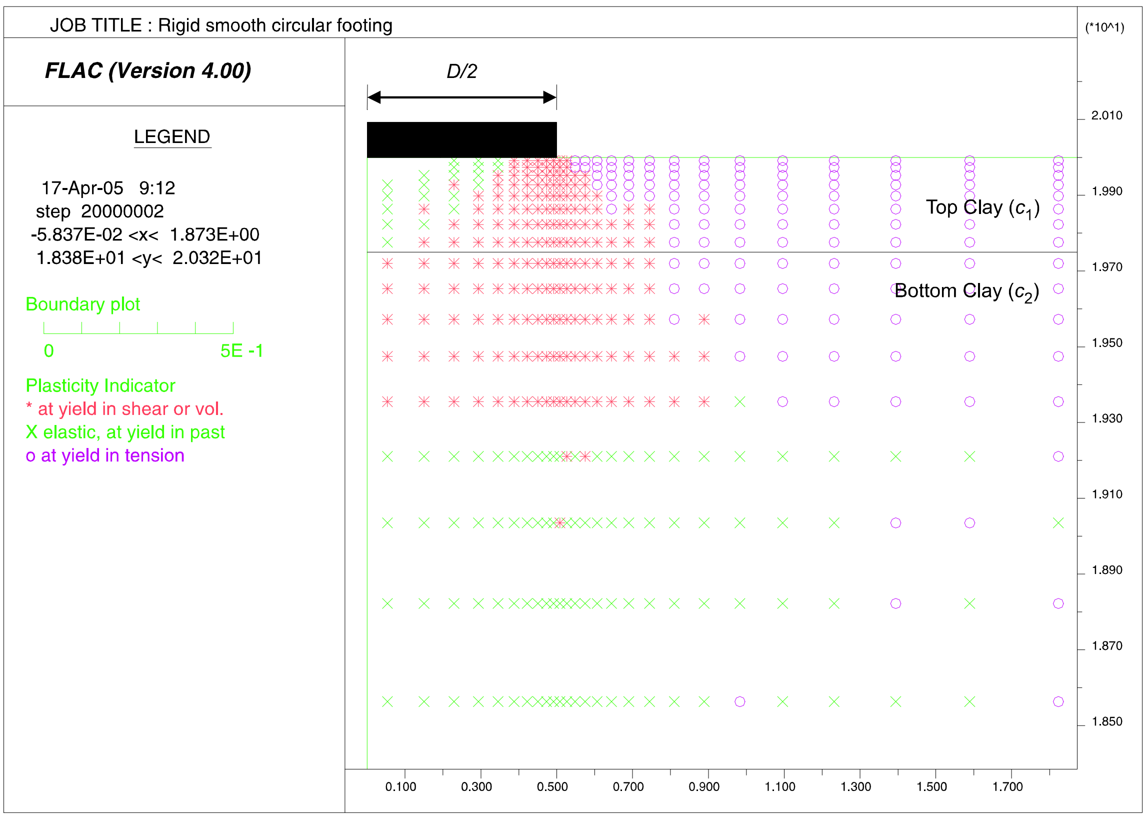

Figure A.329: Plasticity state indicators for a rigid smooth circular footing on strong over soft clay for 40 × 30 grid model, $H/D = 0.25$, $c_2/c_1 = 2/3$.

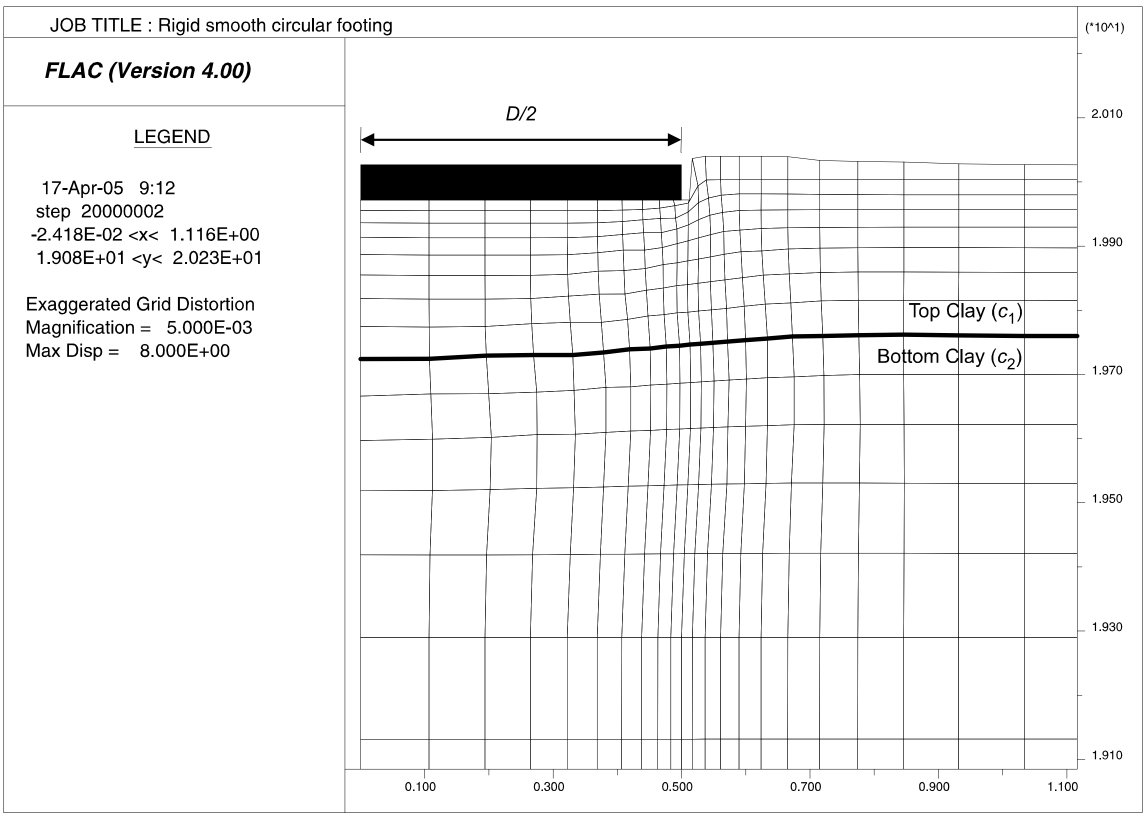

Figure A.330: Magnified grid for a rigid smooth circular footing on strong over soft clay for 40 × 30 grid model, $H/D = 0.25$, $c_2/c_1 = 2/3$.

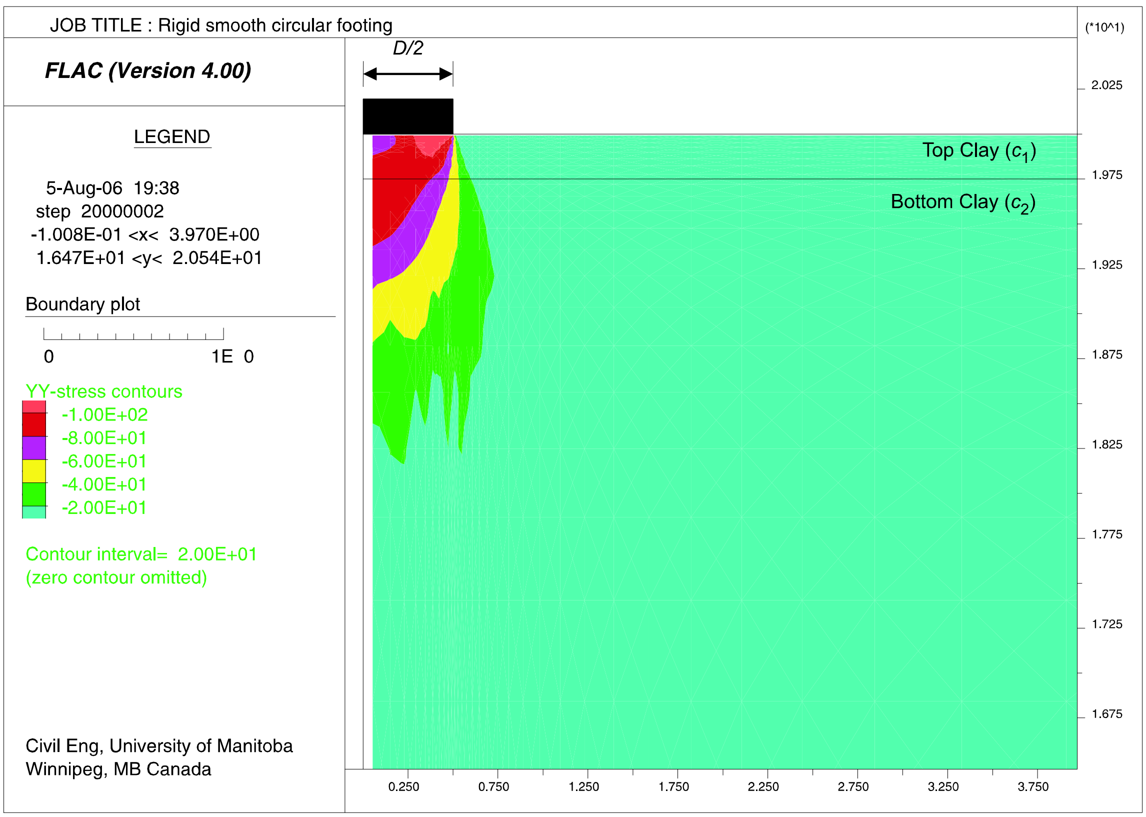

Figure A.331: Vertical stress (σ_{yy}) contours for a rigid smooth circular footing on strong over soft clay for 40 × 30 grid model, $H/D = 0.25$, $c_2/c_1 = 2/3$.

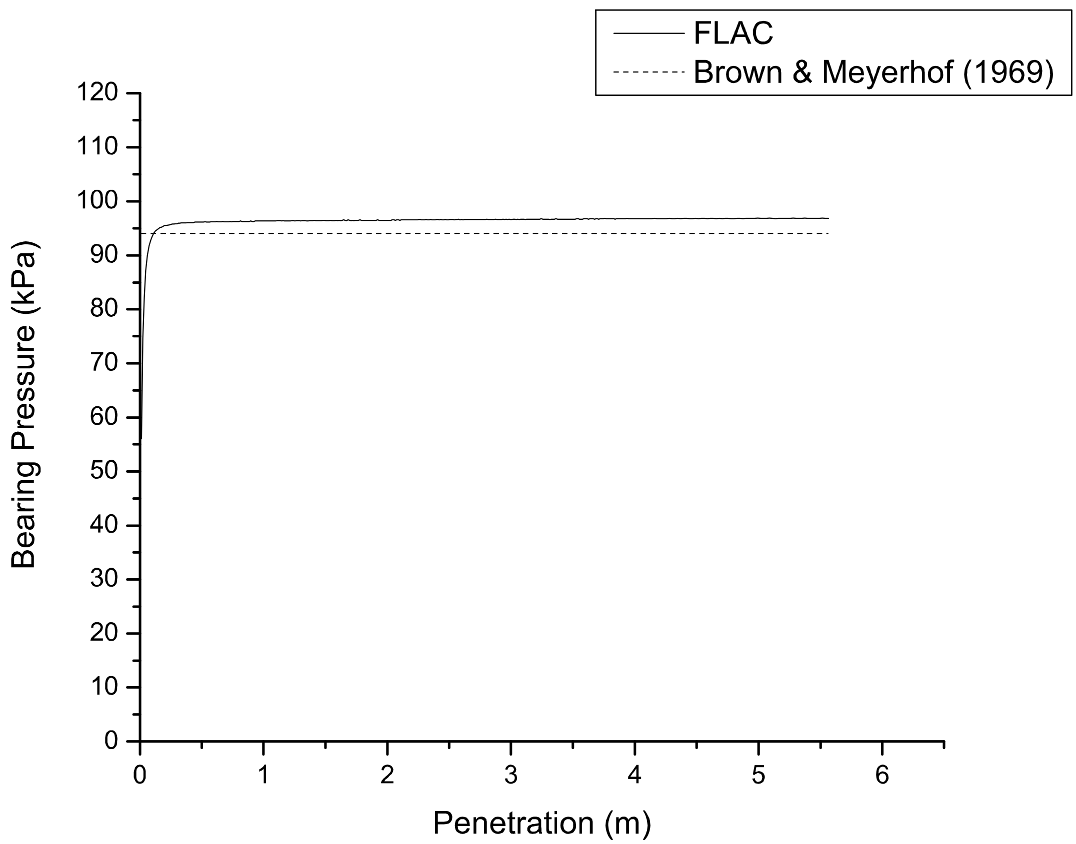

Figure A.332: Bearing pressure versus penetration curve for a rigid smooth circular footing on strong over soft clay for 40 × 30 grid model, $H/D = 0.25$, $c_2/c_1 = 2/3$.

Case 4: $c_2/c_1 = 0.5$ - Small Deformation Analysis

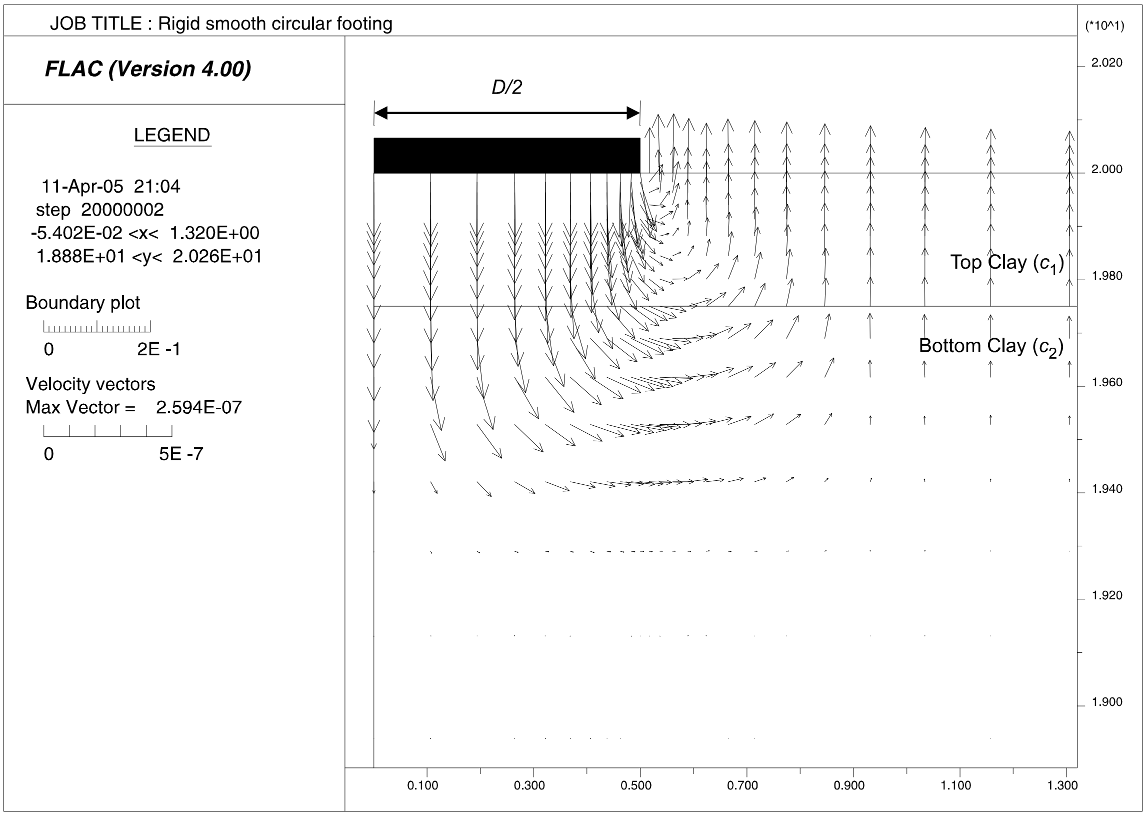

Figure A.333: Velocity vectors for a rigid smooth circular footing on strong clay over soft clay for 40×30 grid model, $H/D = 0.25$, $c_2/c_1 = 0.5$.

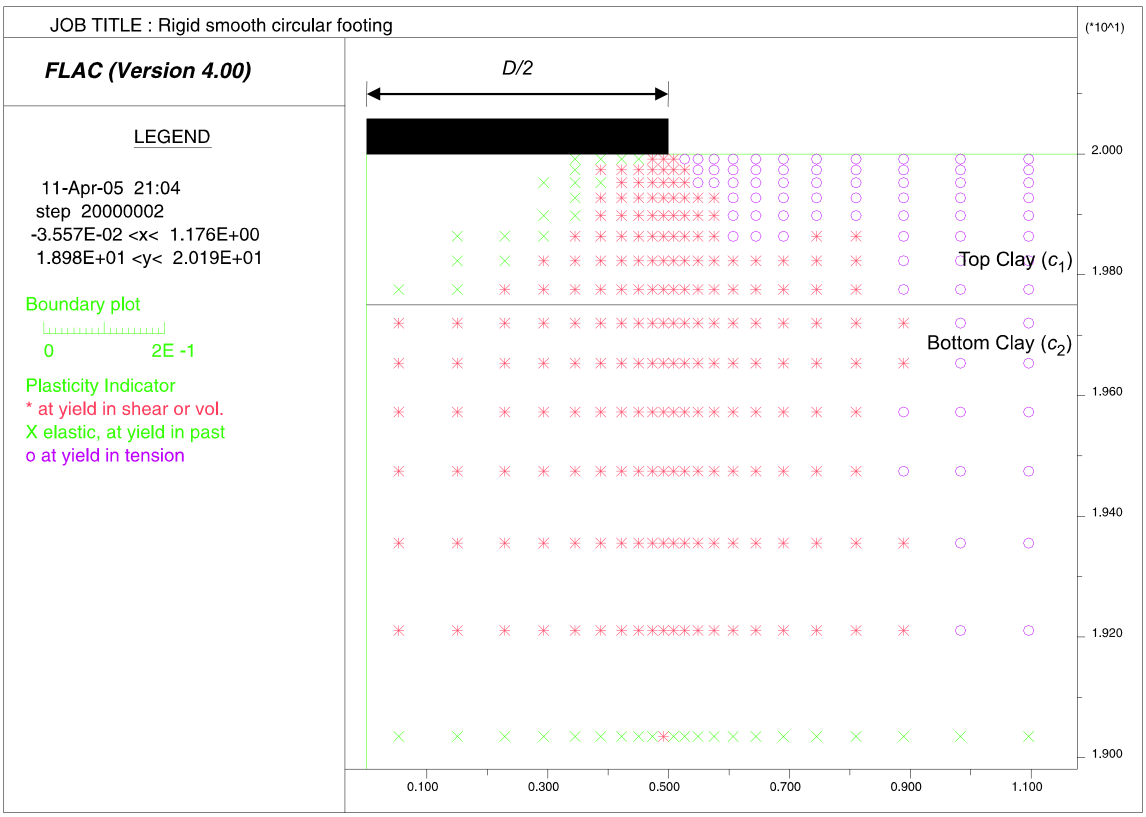

Figure A.334: Plasticity state indicators for a rigid smooth circular footing on strong clay over soft clay for 40 × 30 grid model, $H/D = 0.25$, $c_2/c_1 = 0.5$.

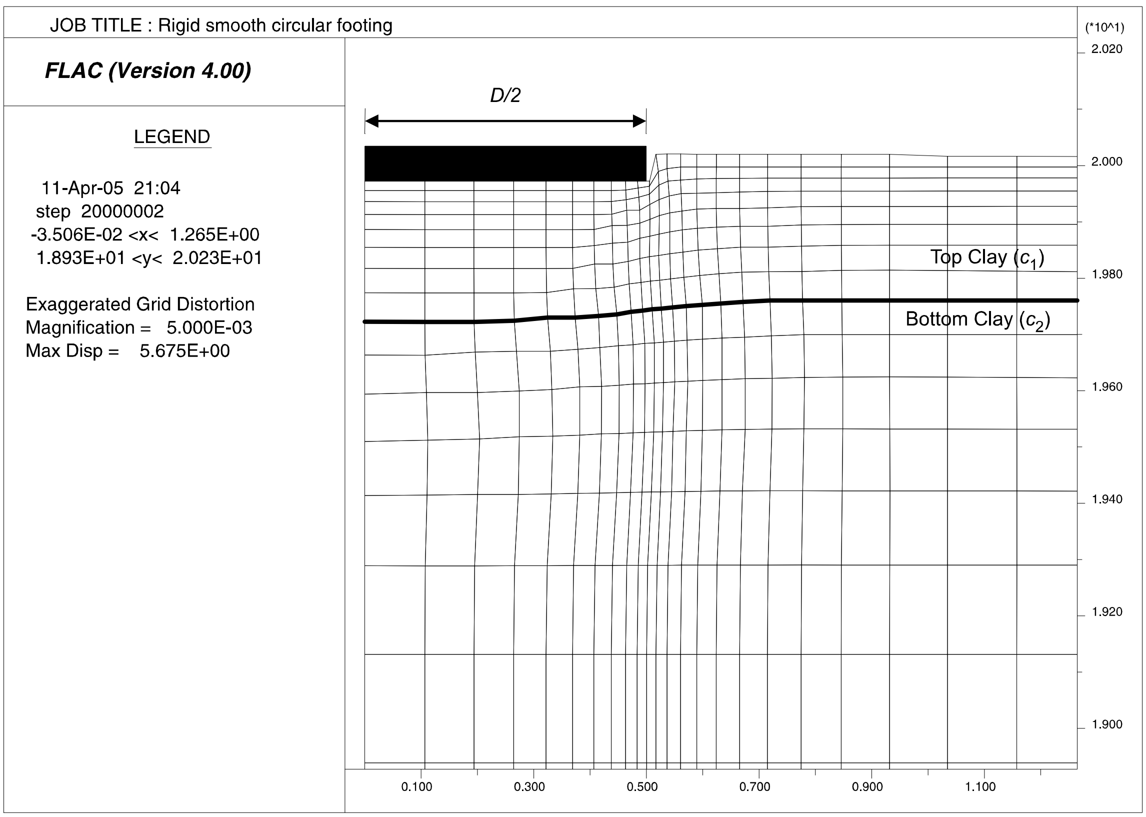

Figure A.335: Magnified grid for a rigid smooth circular footing on strong clay over soft clay for 40×30 grid model, $H/D = 0.25$, $c_2/c_1 = 0.5$.

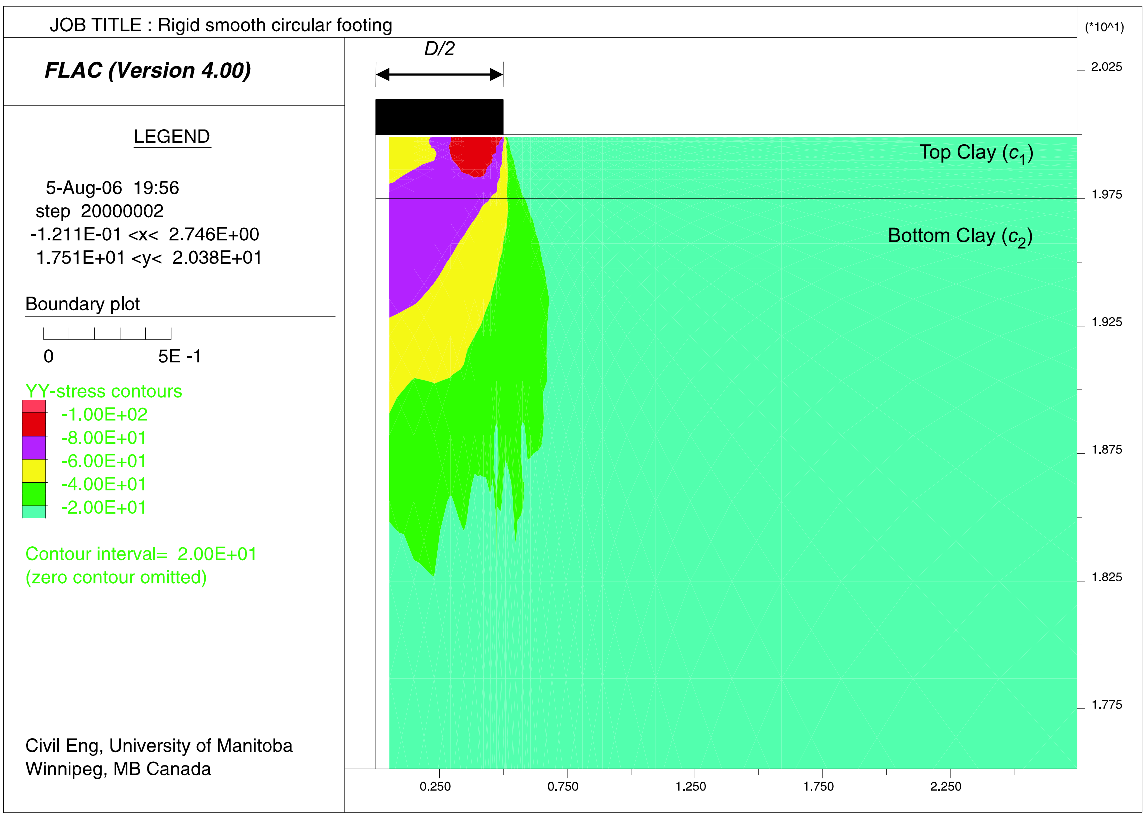

Figure A.336: Vertical stress (σ_{yy}) contours for a rigid smooth circular footing on strong clay over soft clay for 40 × 30 grid model, $H/D = 0.25$, $c_2/c_1 = 0.5$.

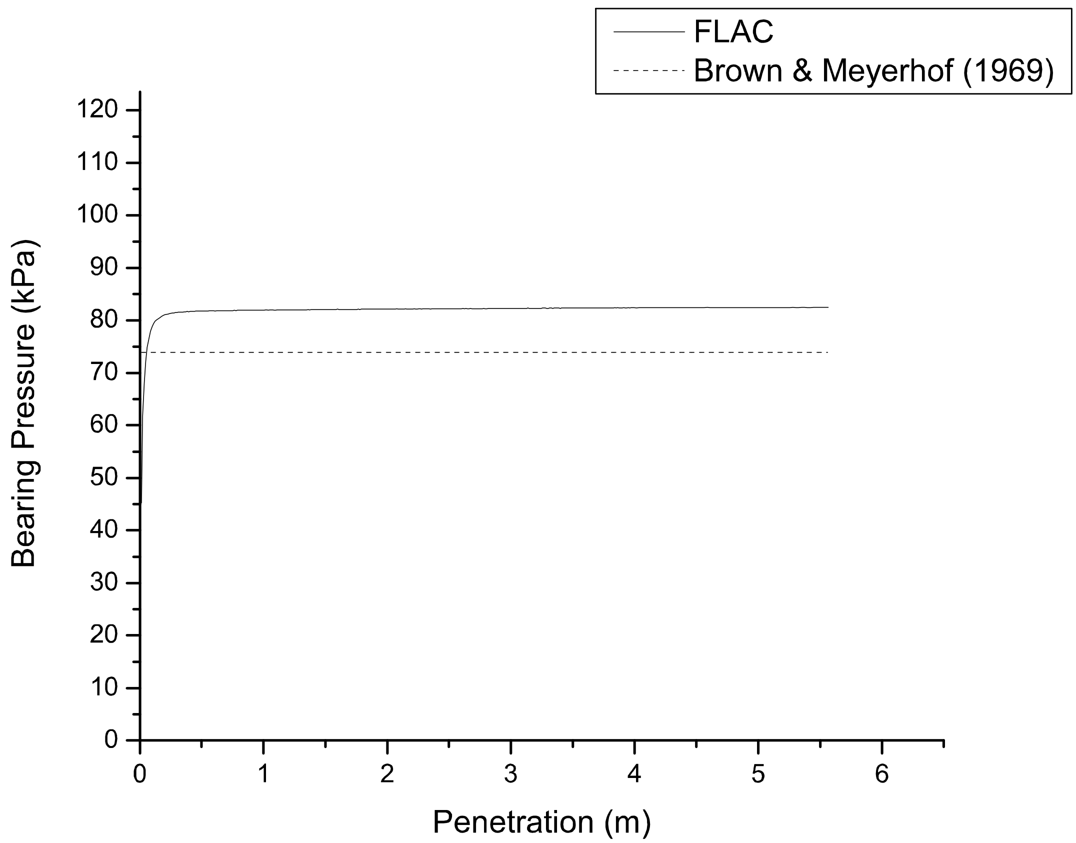

Figure A.337: Bearing pressure versus penetration curve for a rigid smooth circular footing on strong clay over soft clay for 40×30 grid model, $H/D = 0.25$, $c_2/c_1 = 0.5$.

Case 5: $c_2/c_1 = 1/3$ - Small Deformation Analysis

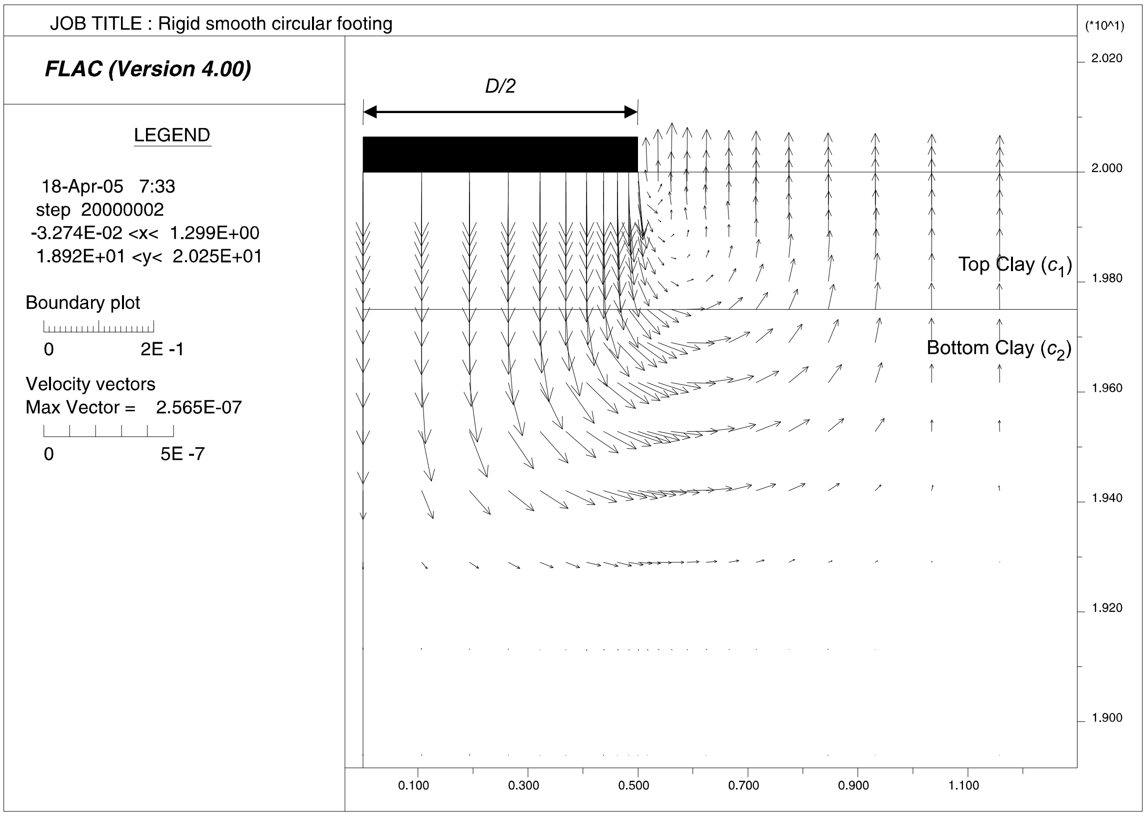

Figure A.338: Velocity vectors for a rigid smooth circular footing on strong clay over soft clay for 40×30 grid model, $H/D = 0.25$, $c_2/c_1 = 1/3$.

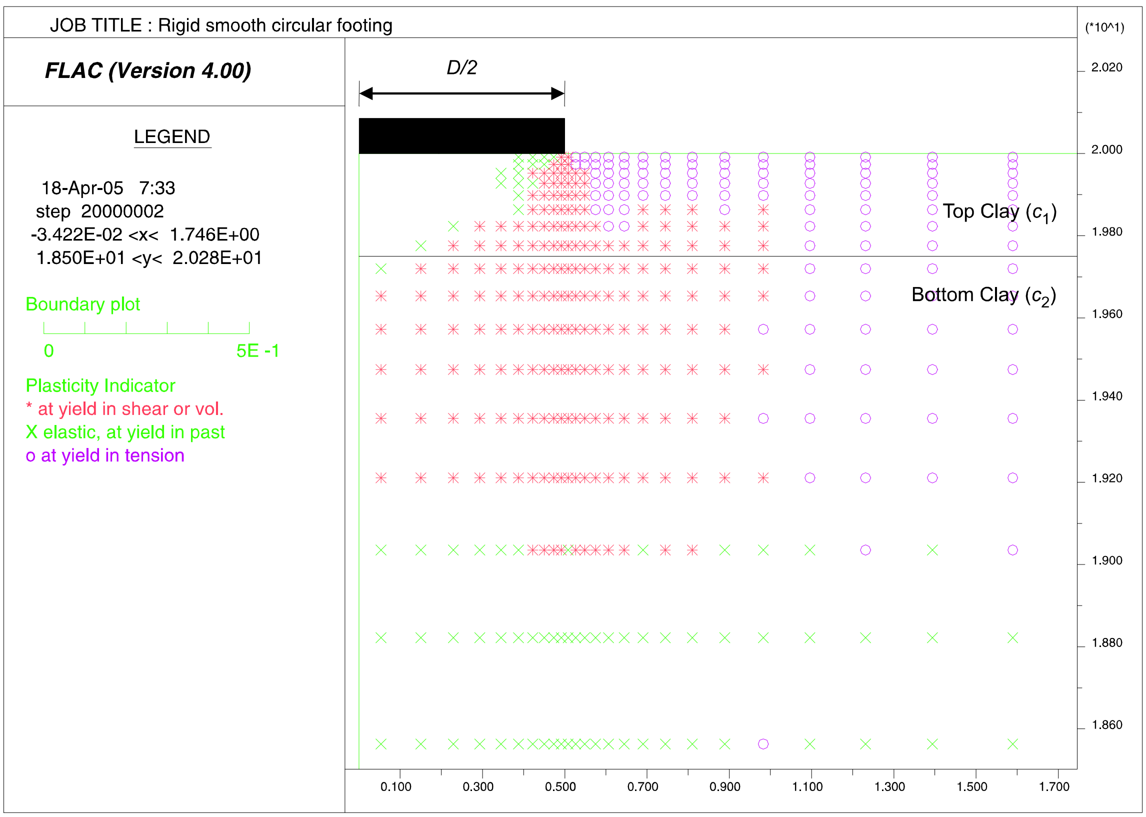

Figure A.339: Plasticity state indicators for a rigid smooth circular footing on strong clay over soft clay for 40 × 30 grid model, $H/D = 0.25$, $c_2/c_1 = 1/3$.

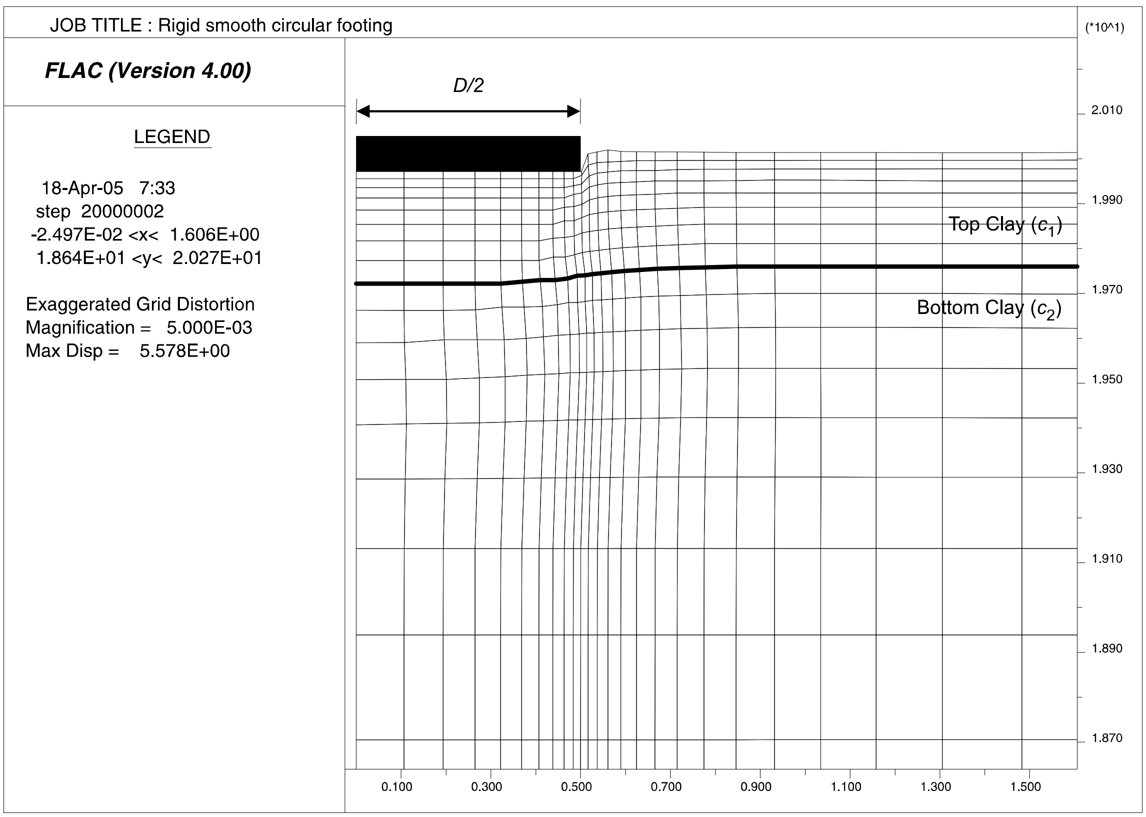

Figure A.340: Magnified grid for a rigid smooth circular footing on strong clay over soft clay for 40×30 grid model, $H/D = 0.25$, $c_2/c_1 = 1/3$.

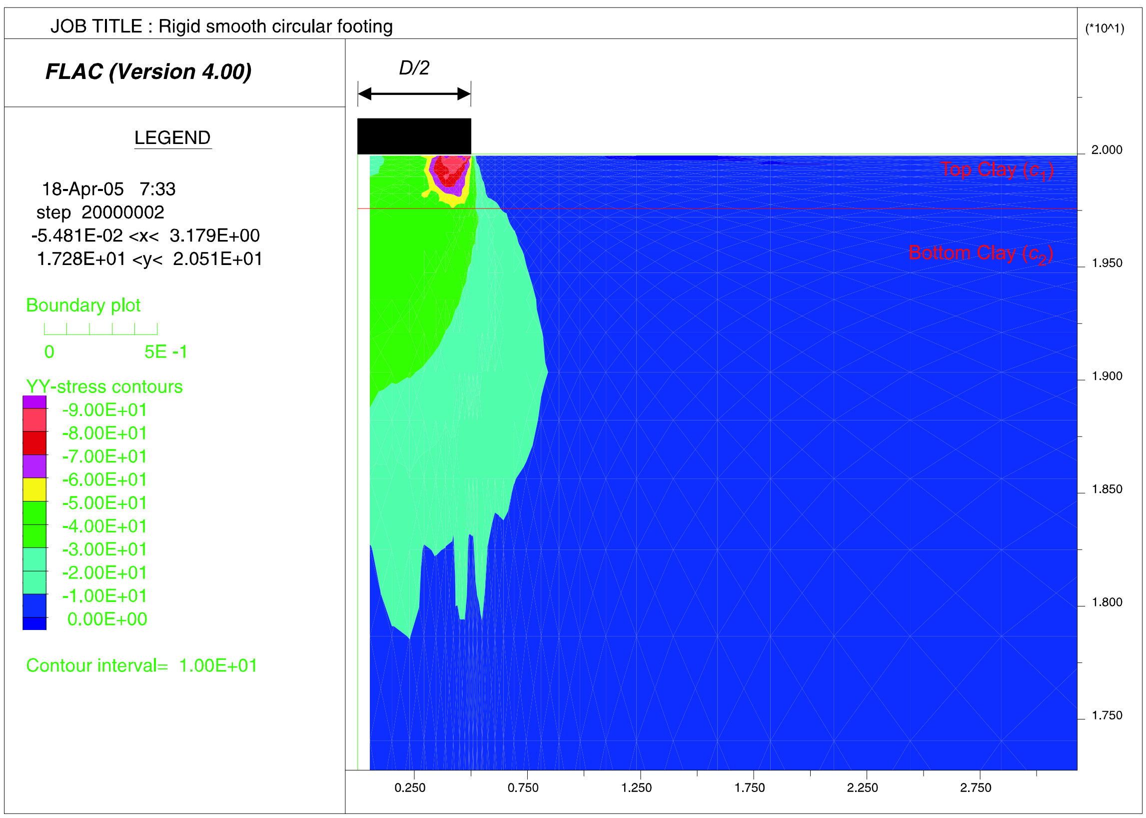

Figure A.341: Vertical stress (σ_{yy}) contours for a rigid smooth circular footing on strong clay over soft clay for 40×30 grid model, $H/D = 0.25$, $c_2/c_1 = 1/3$.

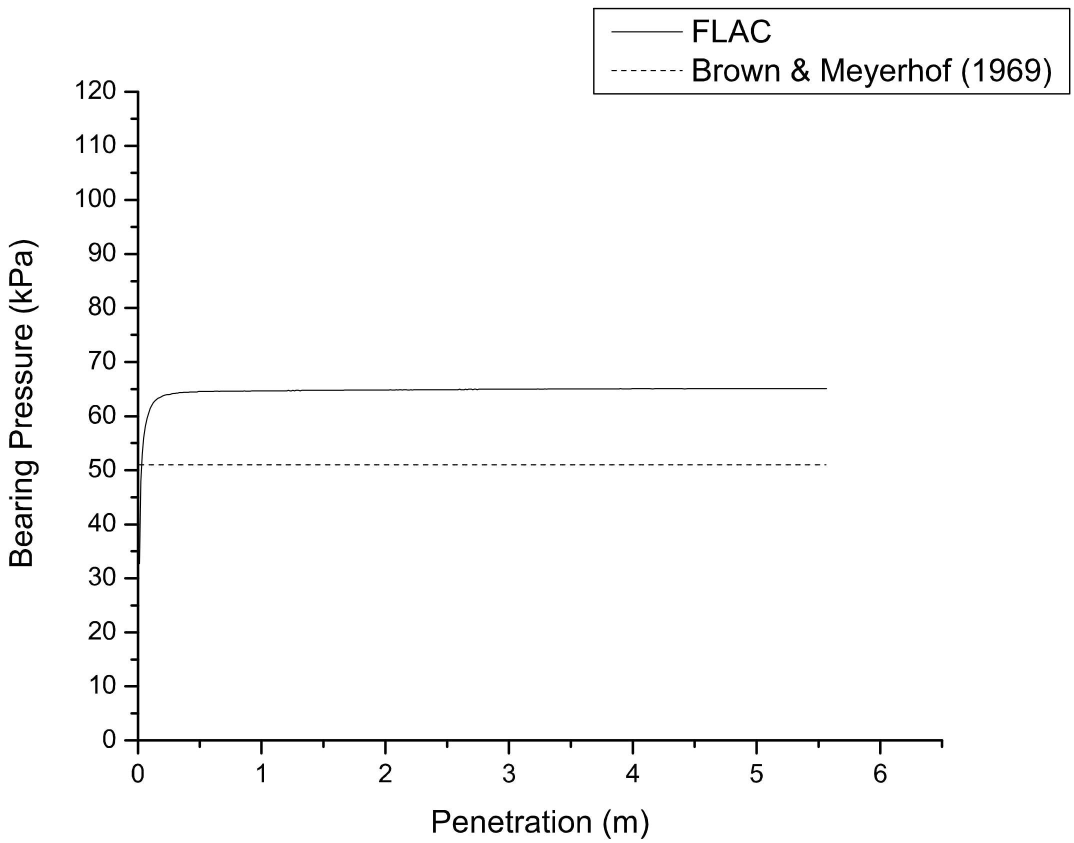

Figure A.342: Bearing pressure versus penetration curve for a rigid smooth circular footing on strong clay over soft clay for 40×30 grid model, $H/D = 0.25$, $c_2/c_1 = 1/3$.

Case 6: $c_2/c_1 = 0.2$ **- Small Deformation Analysis**

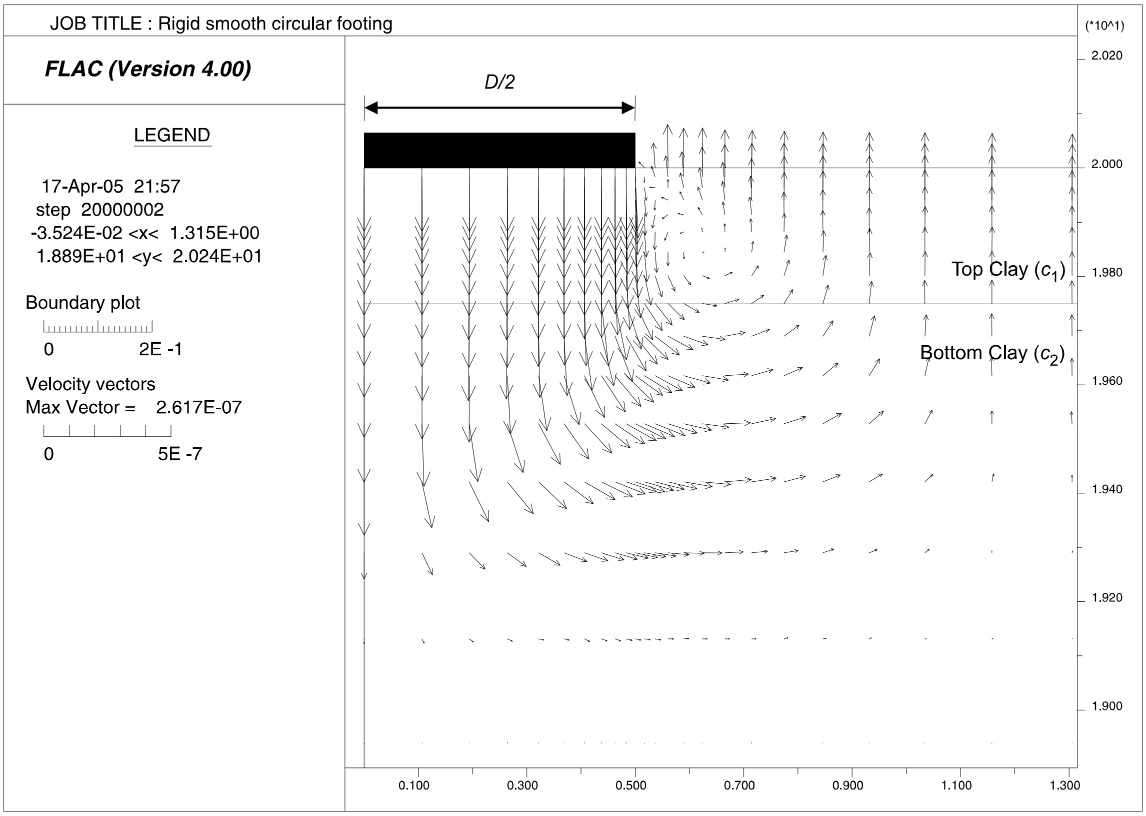

Figure A.343: Velocity vectors for a rigid smooth circular footing on strong clay over soft clay for 40×30 grid model, $H/D = 0.25$, $c_2/c_1 = 0.2$.

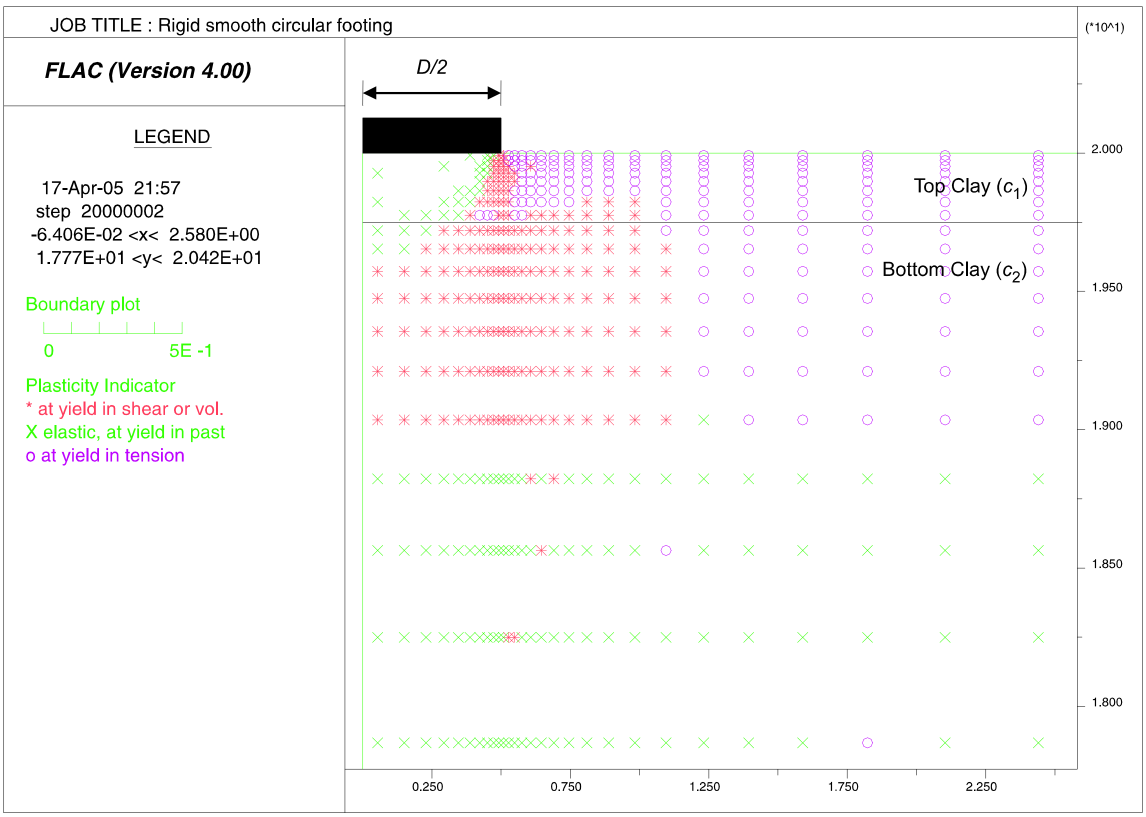

Figure A.344: Plasticity state indicators for a rigid smooth circular footing on strong clay over soft clay for 40 × 30 grid model, $H/D = 0.25$, $c_2/c_1 = 0.2$.

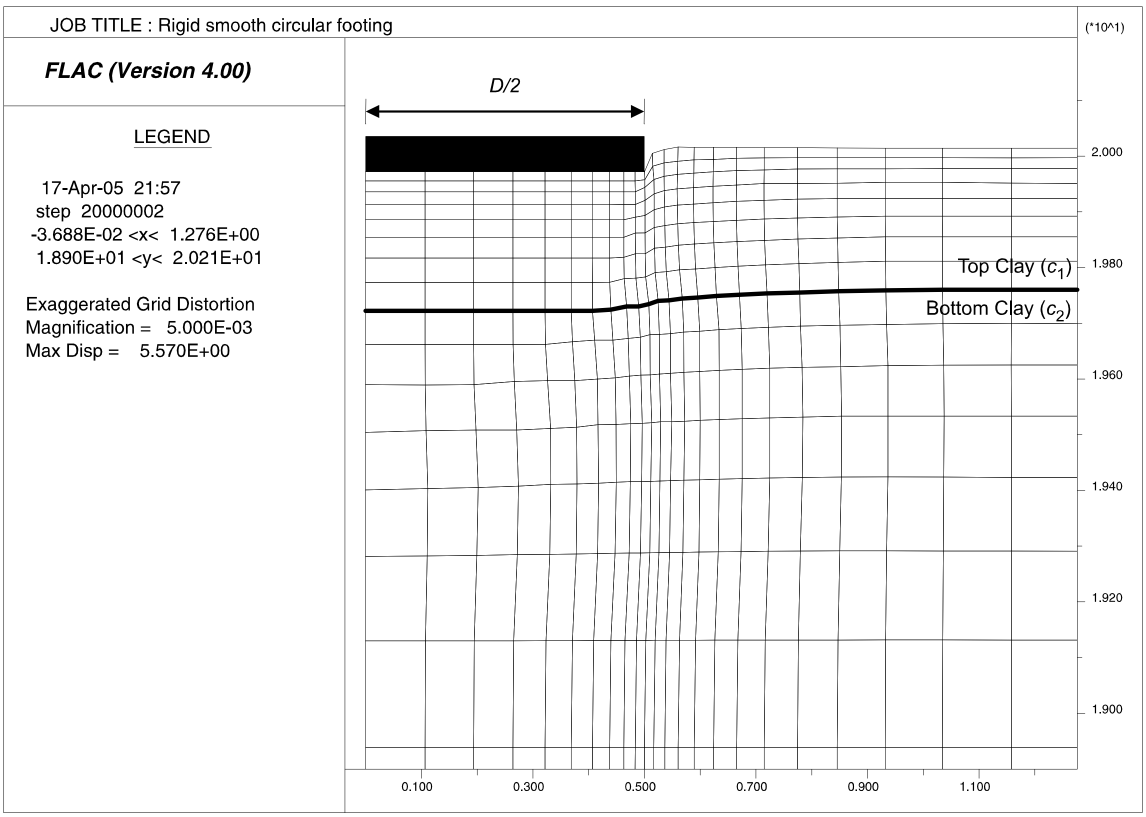

Figure A.345: Magnified grid for a rigid smooth circular footing on strong clay over soft clay for 40 × 30 grid model, $H/D = 0.25$, $c_2/c_1 = 0.2$.

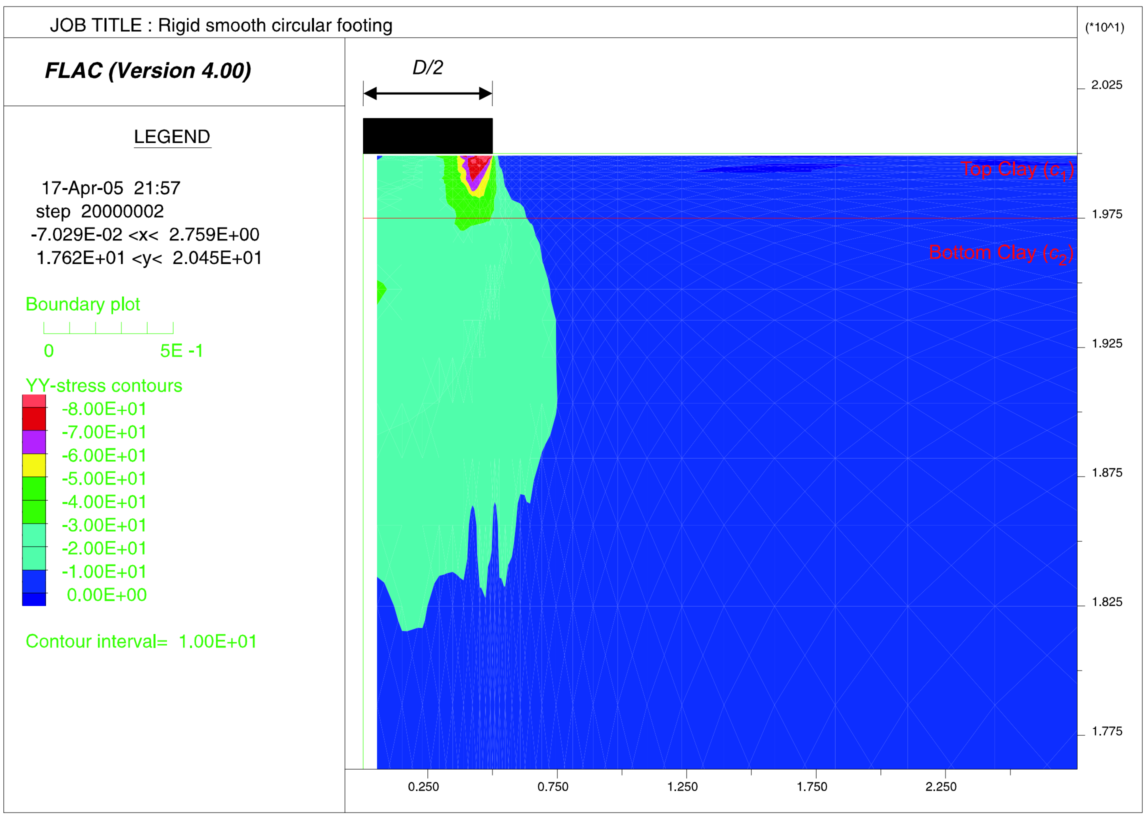

Figure A.346: Vertical stress (σ_{yy}) contours for a rigid smooth circular footing on strong clay over soft clay for 40 × 30 grid model, $H/D = 0.25$, $c_2/c_1 = 0.2$.

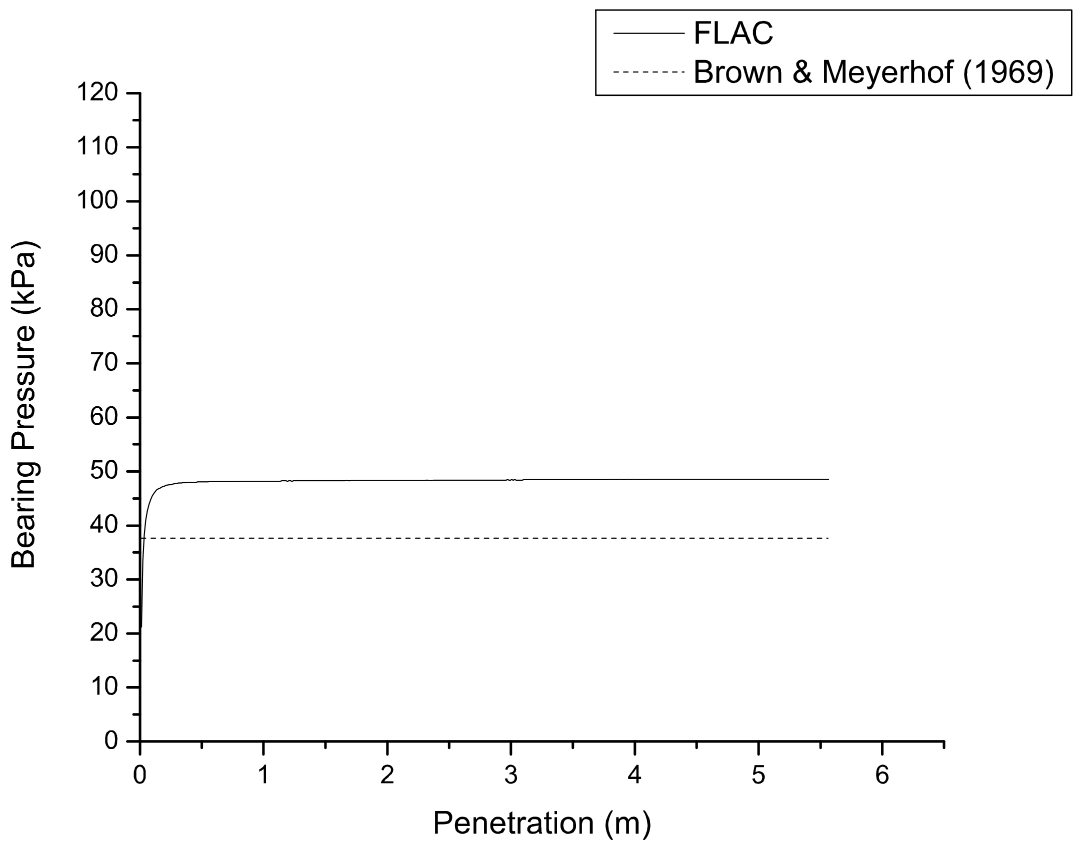

Figure A.347: Bearing pressure versus penetration curve for a rigid smooth circular footing on strong clay over soft clay for 40×30 grid model, $H/D = 0.25$, $c_2/c_1 = 0.2$.

Case 7: $c_2/c_1 = 0.1$ **- Small Deformation Analysis**

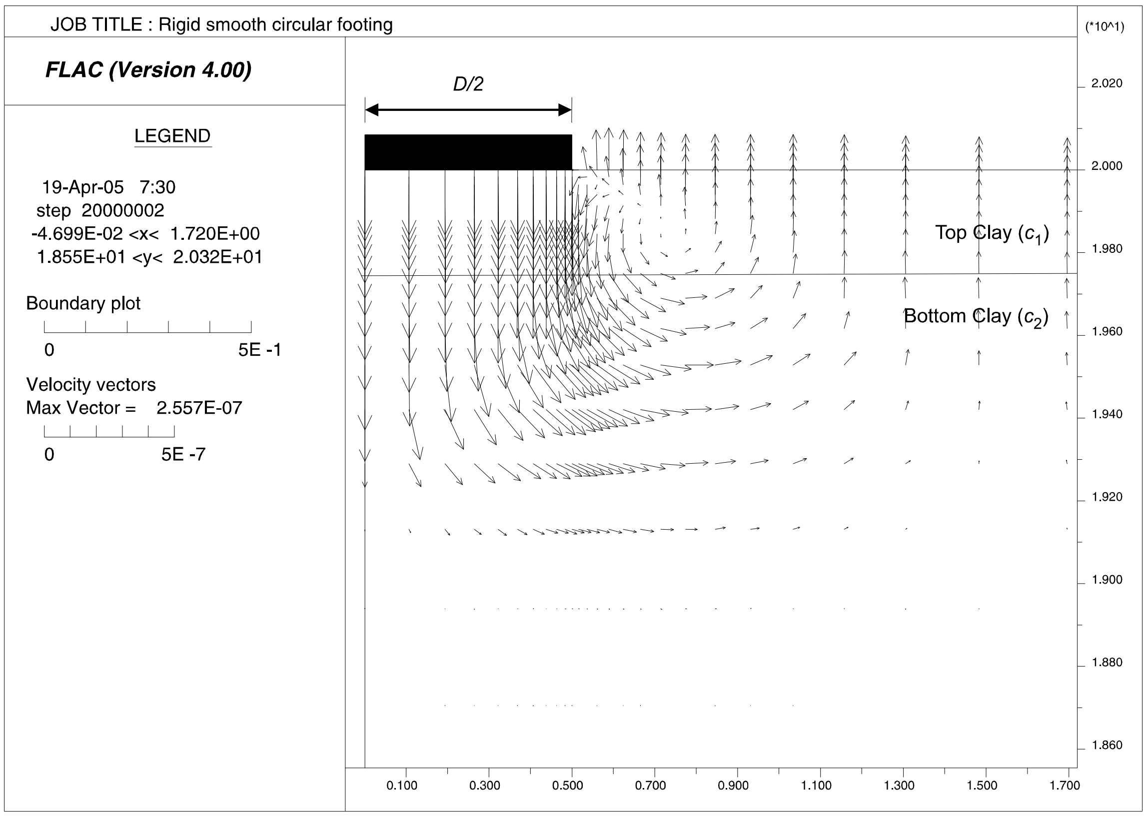

Figure A.348: Velocity vectors for a rigid smooth circular footing on strong clay over soft clay for 40×30 grid model, $H/D = 0.25$, $c_2/c_1 = 0.1$.

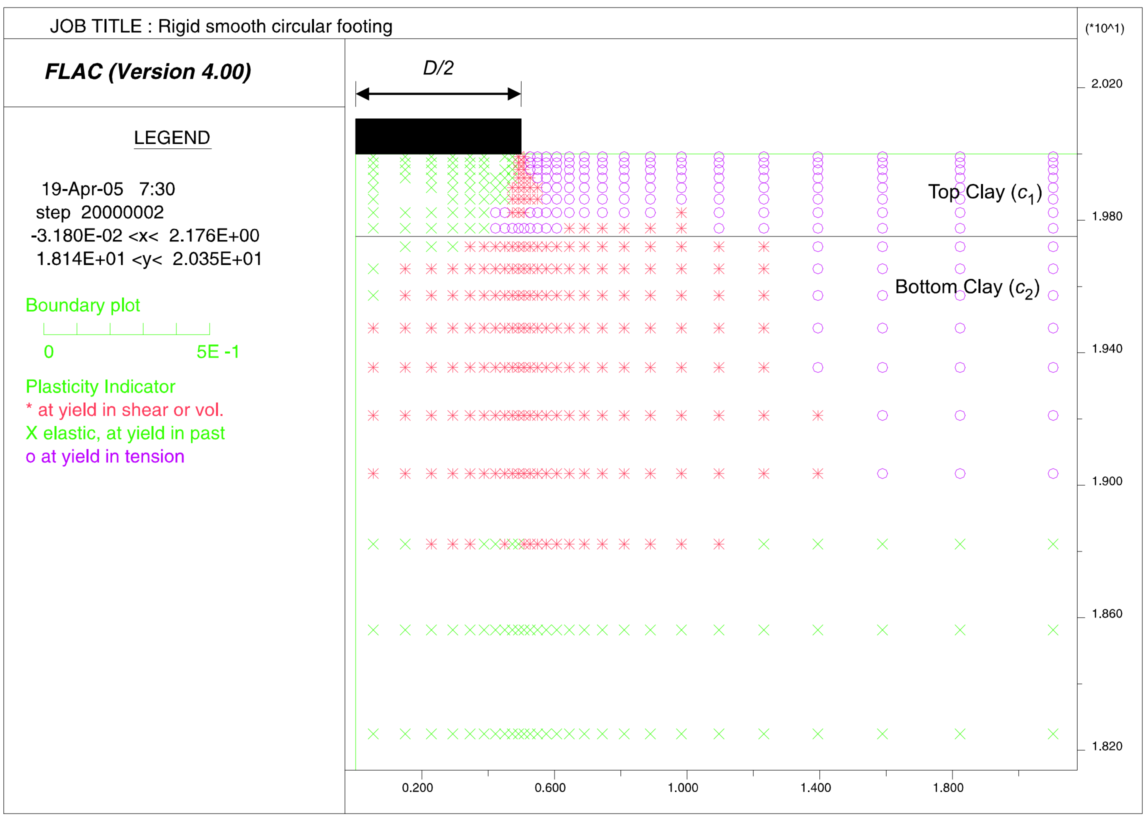

Figure A.349: Plasticity state indicators for a rigid smooth circular footing on strong clay over soft clay for 40 × 30 grid model, $H/D = 0.25$, $c_2/c_1 = 0.1$.

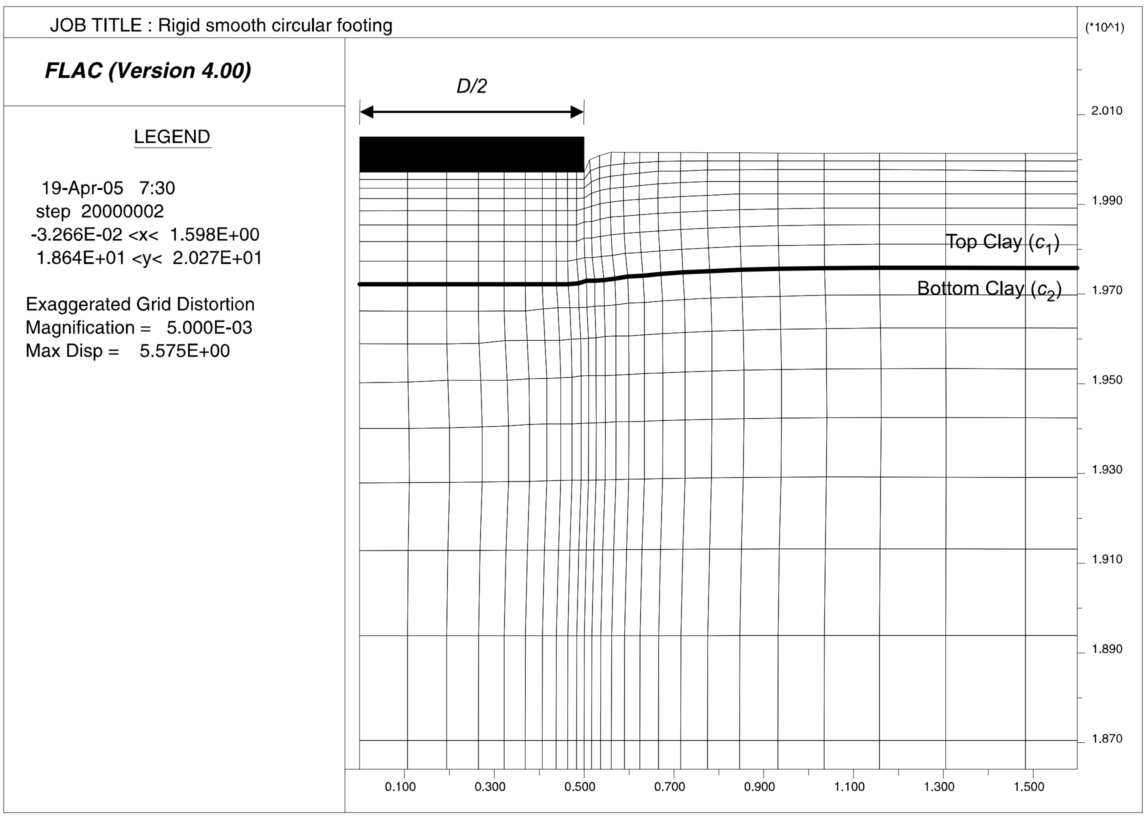

Figure A.350: Magnified grid for a rigid smooth circular footing on strong clay over soft clay for 40×30 grid model, $H/D = 0.25$, $c_2/c_1 = 0.1$.

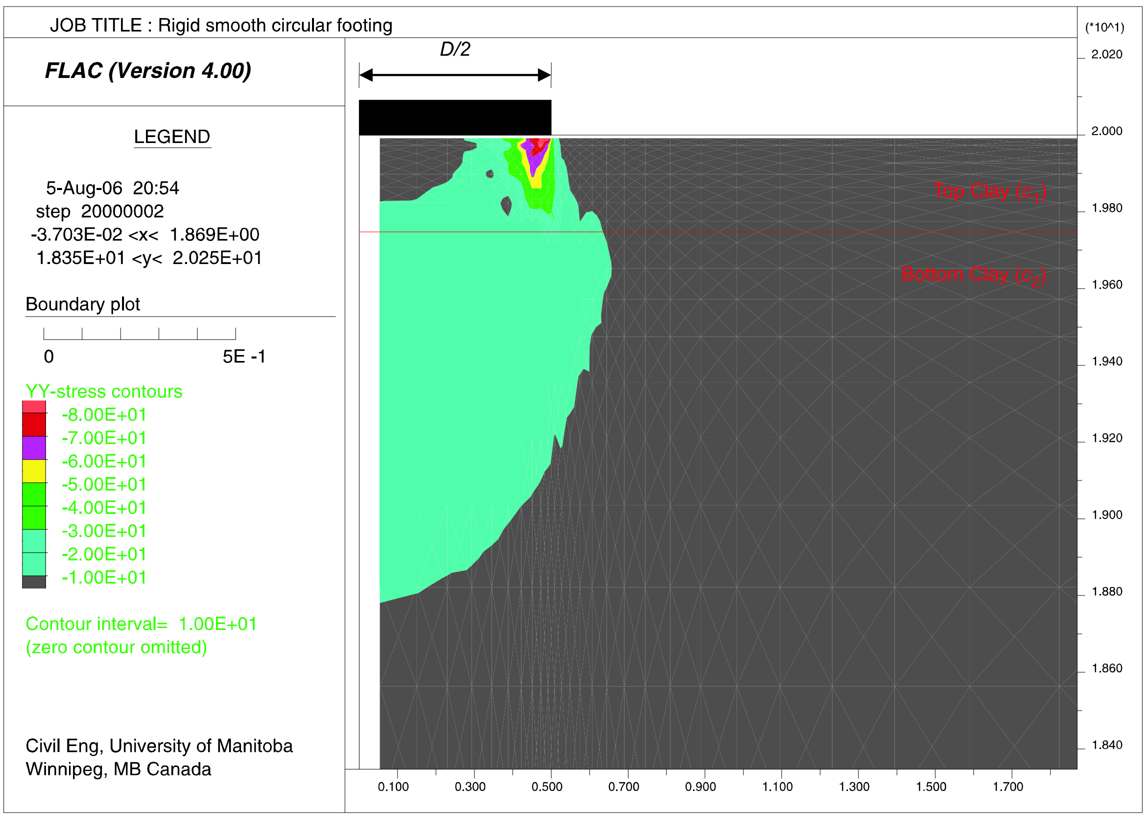

Figure A.351: Vertical stress (σ_{yy}) contours for a rigid smooth circular footing on strong clay over soft clay for 40×30 grid model, $H/D = 0.25$, $c_2/c_1 = 0.1$.

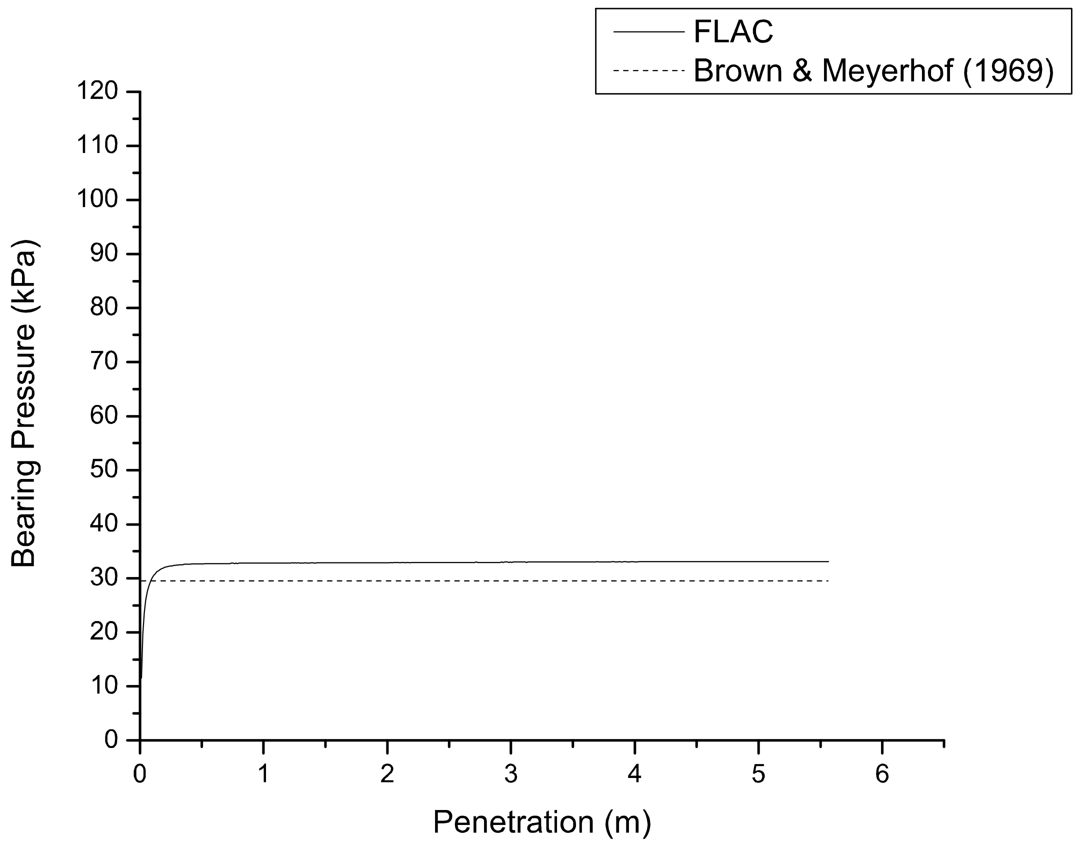

Figure A.352: Bearing pressure versus penetration curve for a rigid smooth circular footing on strong clay over soft clay for 40×30 grid model, $H/D = 0.25$, $c_2/c_1 = 0.1$.

A.4 Circular Footing on Soft Clay Overlying Strong Clay

This situation may occur where soft glacial lake clay overlies stiff till deposits. An axisymmetric analyses of the circular footing resting on the ground surface of soft clay overlying a stiff clay was investigated in this section:

Model Geometry A 40×30 elements grid similar to that in A.3 is adopted for this analysis. The model geometry is same as shown in A.239.

A.4.1 Rigid Smooth Circular Footing on Soft over Strong Clay ($H/D = 1$)

Case 2: $c_1/c_2 = 0.8$ **or** $c_2/c_1 = 1.25$ **- Small Deformation Analysis**

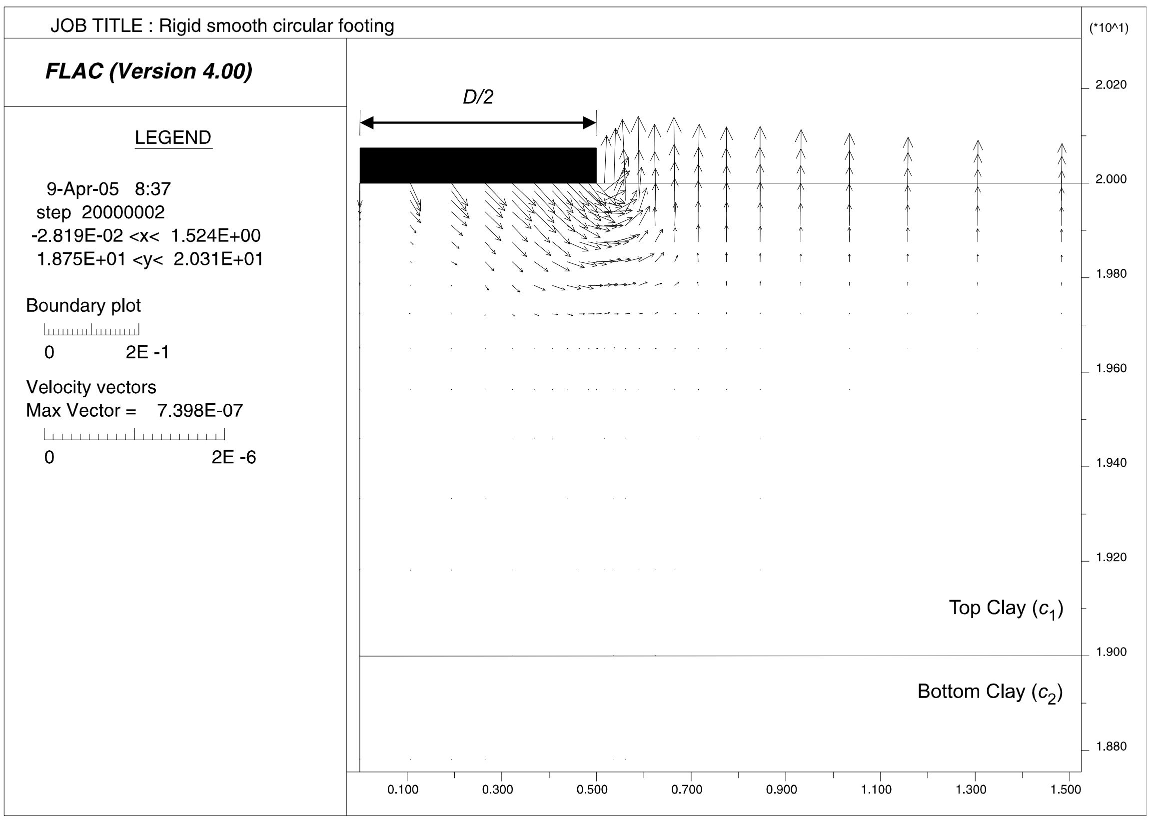

Figure A.353: Velocity vectors for a rigid circular footing on soft clay over strong clay for 40 × 30 grid model, $H/D = 1$, $c_1/c_2 = 0.8$.

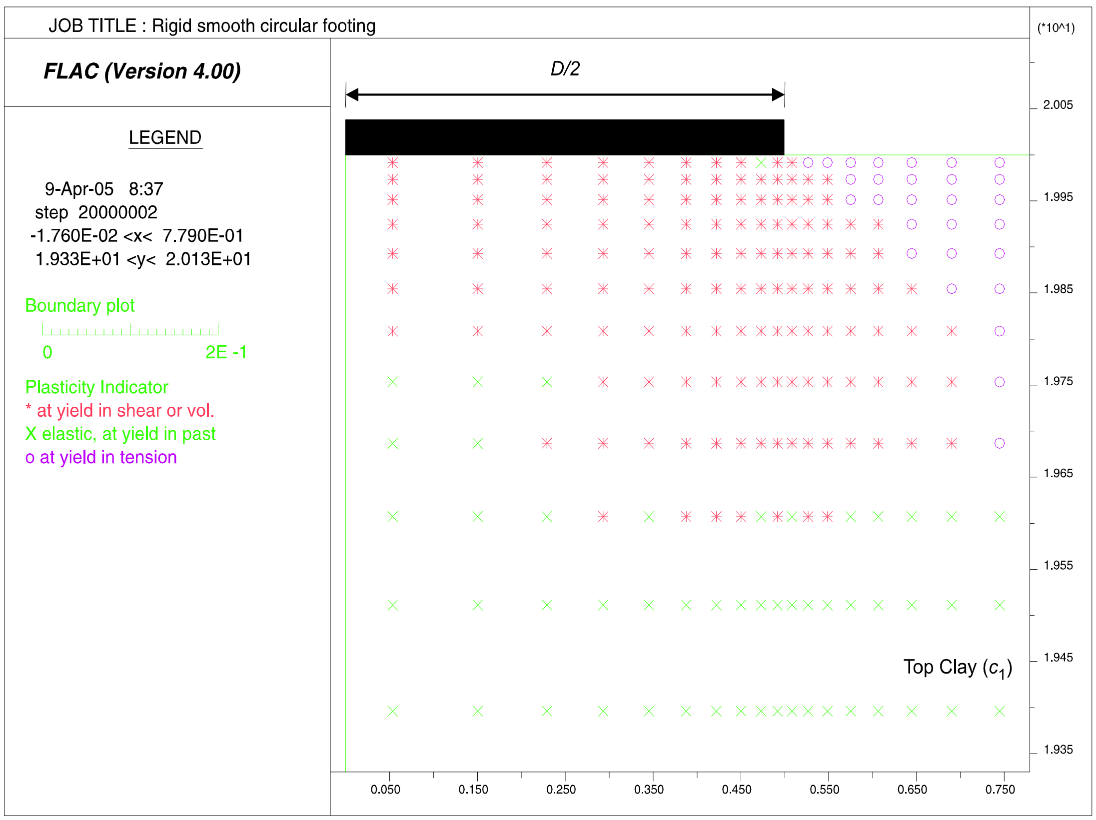

Figure A.354: Plasticity indicators for a rigid smooth circular footing on soft over strong clay for 40×30 grid model, $H/D = 1$, $c_1/c_2 = 0.8$.

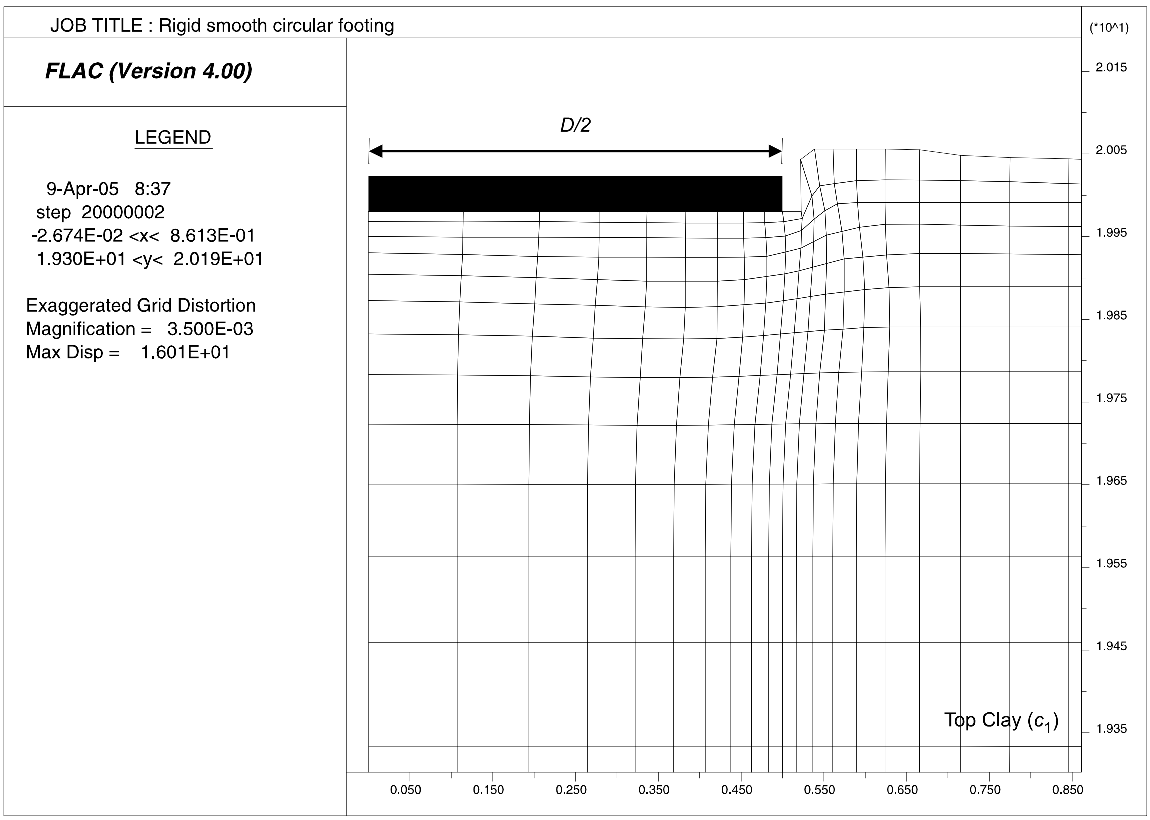

Figure A.355: Magnified grid for a rigid smooth circular footing on soft over strong clay for 40 × 30 grid model, $H/D = 1$, $c_1/c_2 = 0.8$.

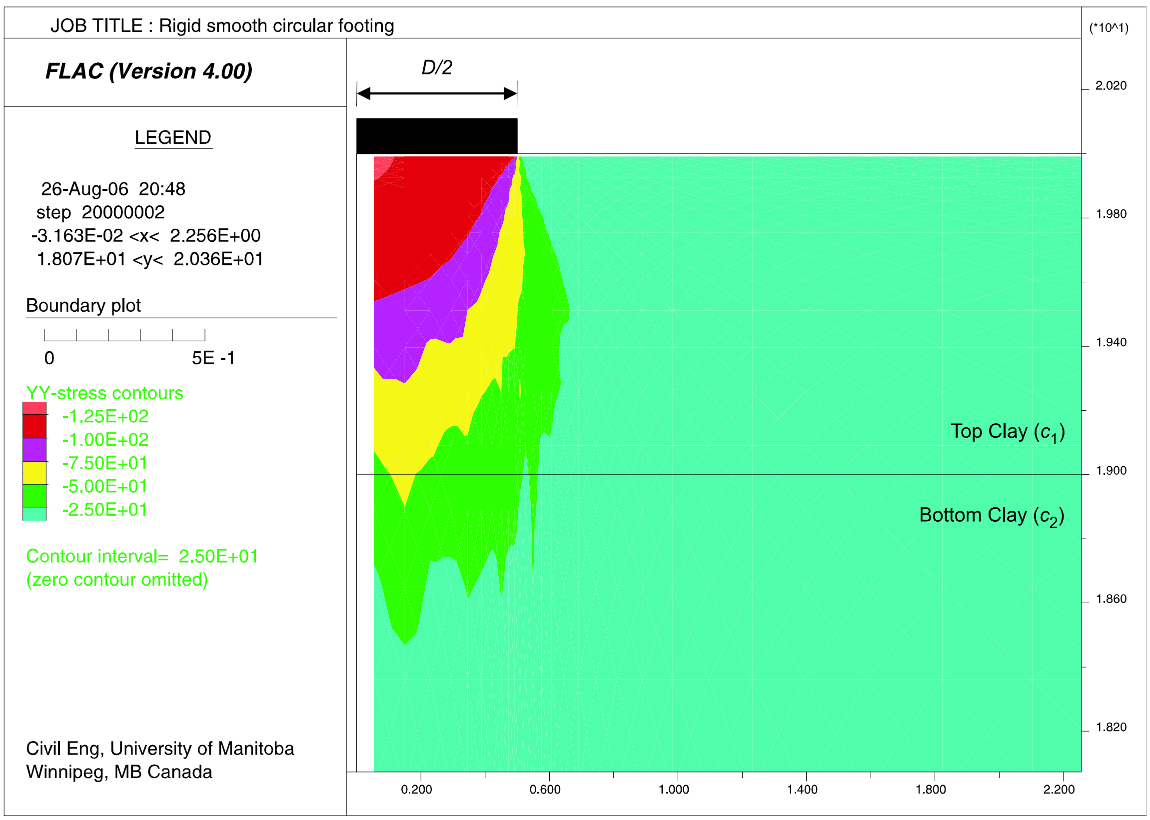

Figure A.356: Vertical stress (σ_{yy}) contours for a rigid smooth circular footing on soft over strong clay for 40 × 30 grid model, $H/D = 1$, $c_1/c_2 = 0.8$.

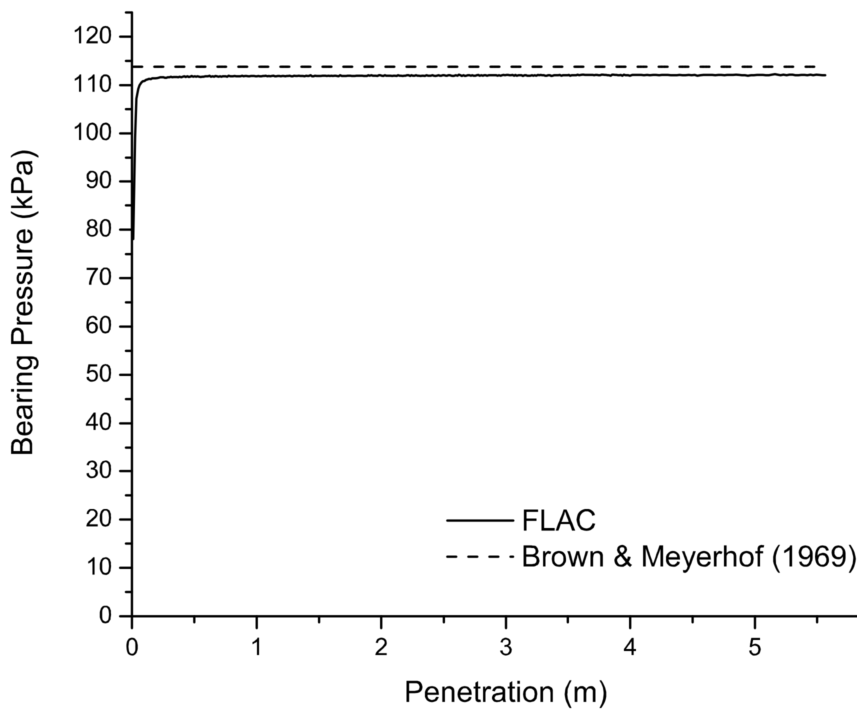

Figure A.357: Bearing pressure versus penetration curve for a rigid smooth circular footing on soft over strong clay for 40×30 grid model, $H/D = 1$, $c_1/c_2 = 0.8$.

Case 3: $c_1/c_2 = 2/3$ or $c_2/c_1 = 1.5$ - Small Deformation Analysis

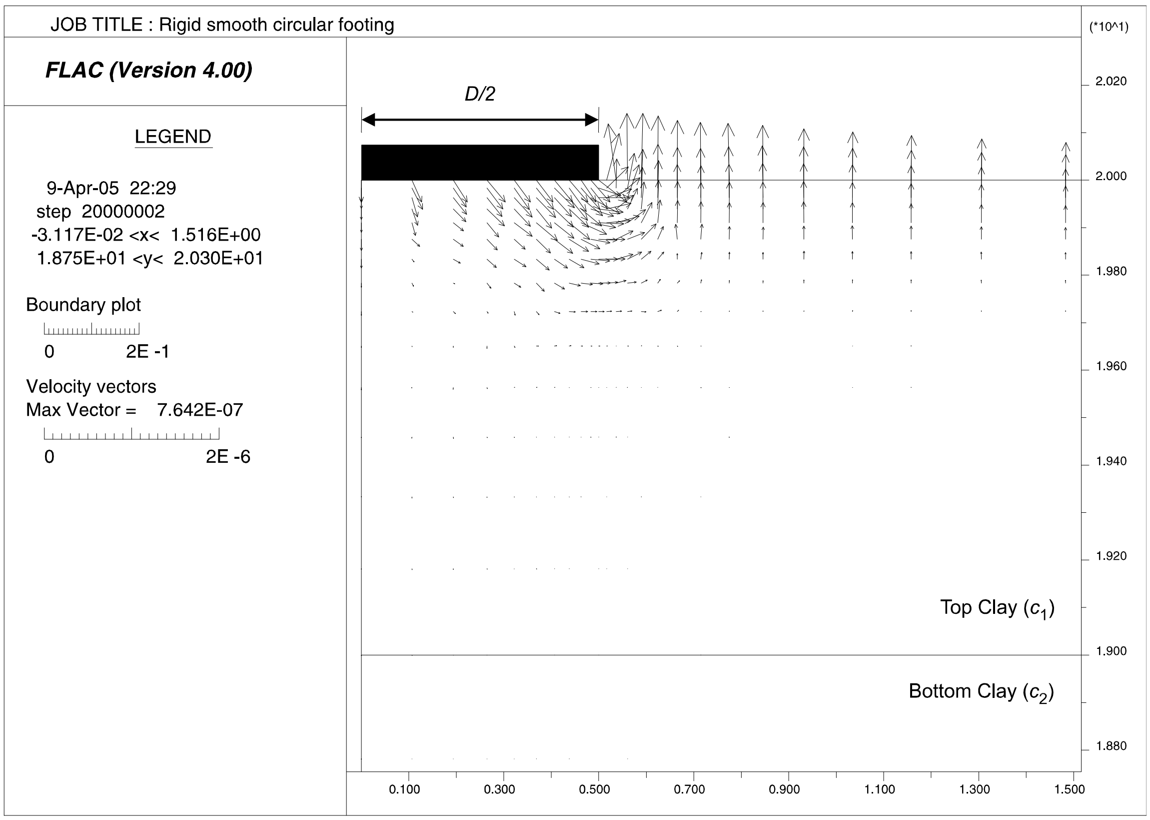

Figure A.358: Velocity vectors for a rigid smooth circular footing on soft over strong clay for 40×30 grid model, $H/D = 1$, $c_1/c_2 = 2/3$.

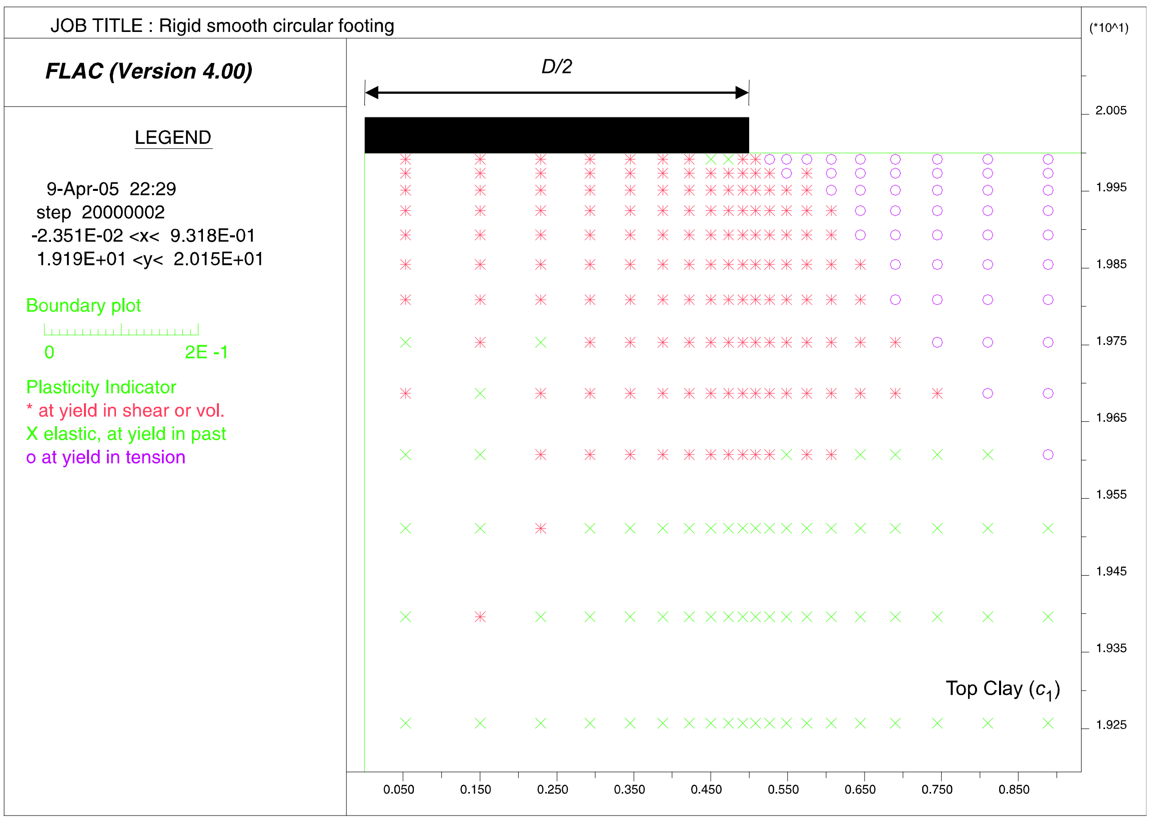

Figure A.359: Plasticity state indicators for a rigid smooth circular footing on soft over strong clay for 40 × 30 grid model, $H/D = 1$, $c_1/c_2 = 2/3$.

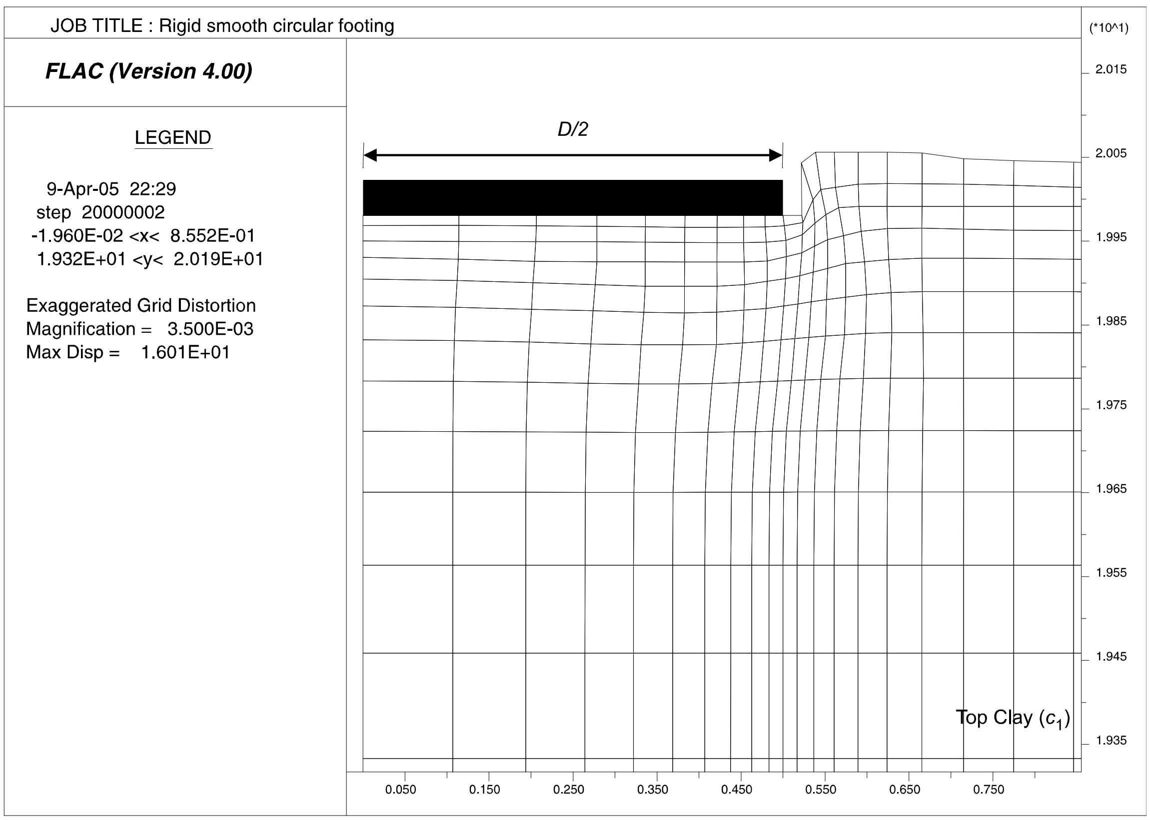

Figure A.360: Magnified grid for a rigid smooth circular footing on soft over strong clay for 40×30 grid model, $H/D = 1$, $c_1/c_2 = 2/3$.

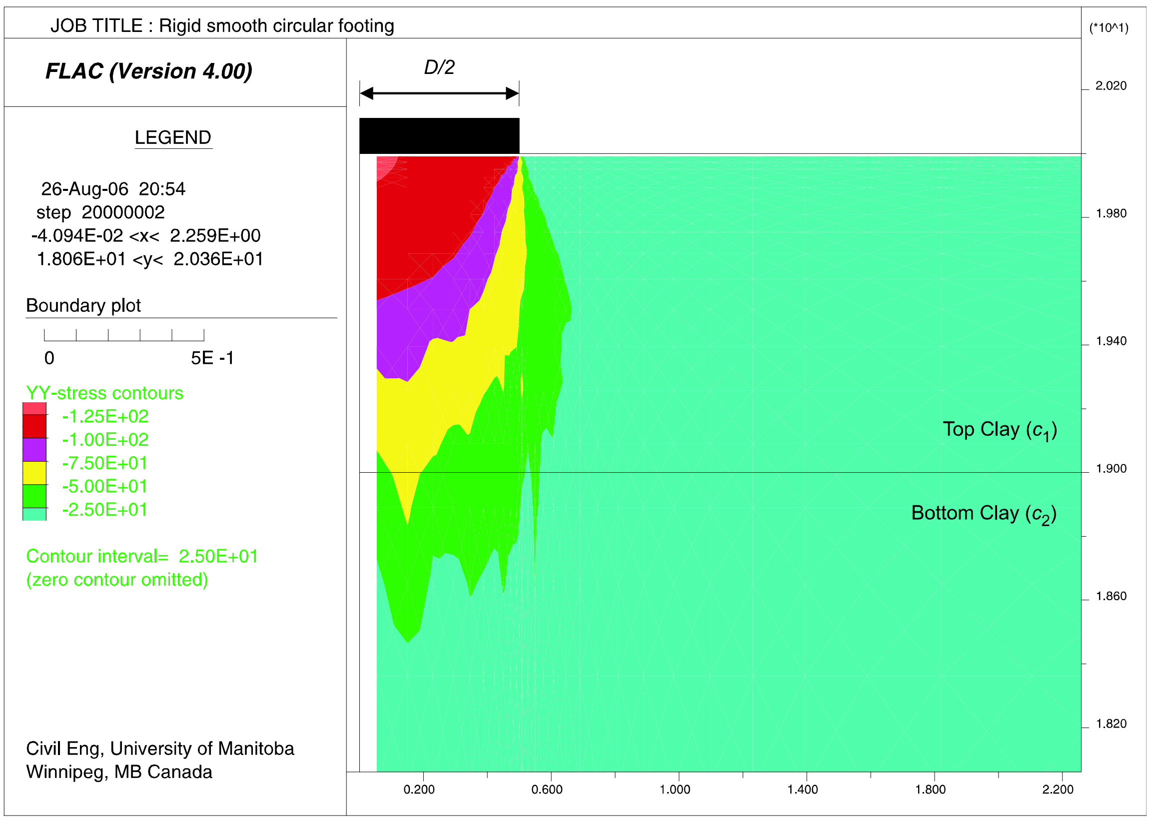

Figure A.361: Vertical stress (σ_{yy}) contours for a rigid smooth circular footing on soft over strong clay for 40×30 grid model, $H/D = 1$, $c_1/c_2 = 2/3$.

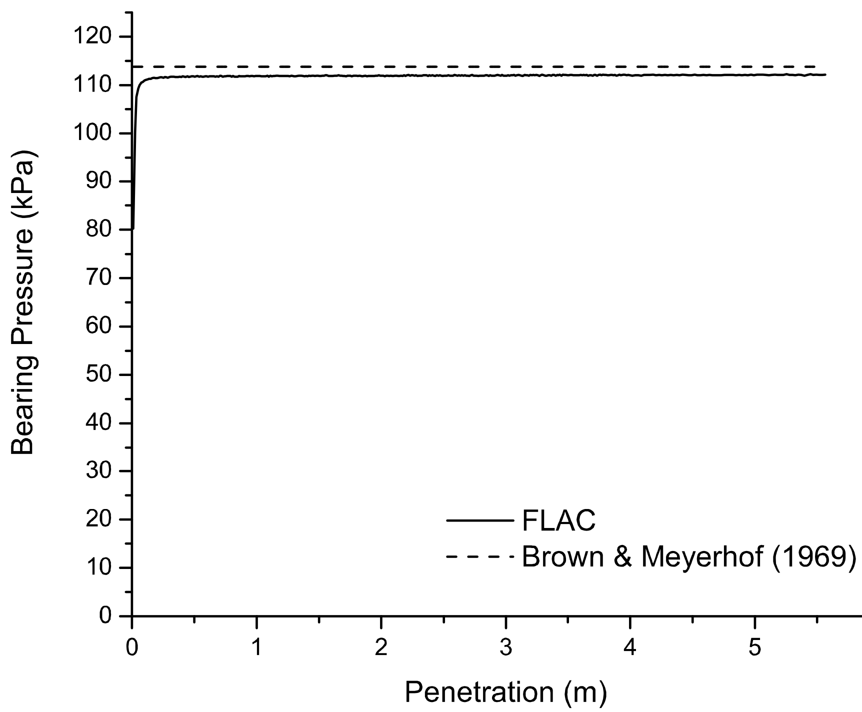

Figure A.362: Bearing pressure versus penetration curve for a rigid smooth circular footing on soft over strong clay for 40 × 30 grid model, $H/D = 1$, $c_1/c_2 = 2/3$.

Case 4: $c_1/c_2 = 0.5$ or $c_2/c_1 = 2$ - Small Deformation Analysis

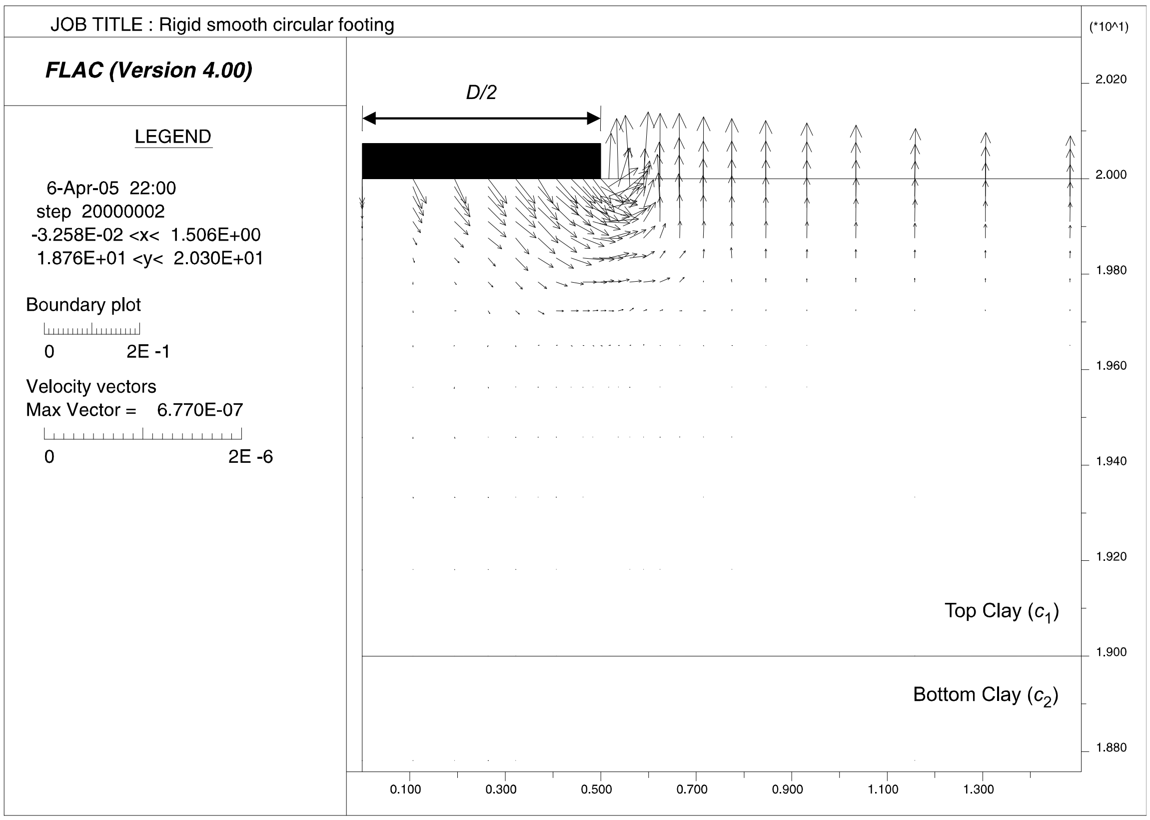

Figure A.363: Velocity vectors for a rigid smooth circular footing on soft over strong clay for 40 × 30 grid model, $H/D = 1$, $c_1/c_2 = 0.5$.

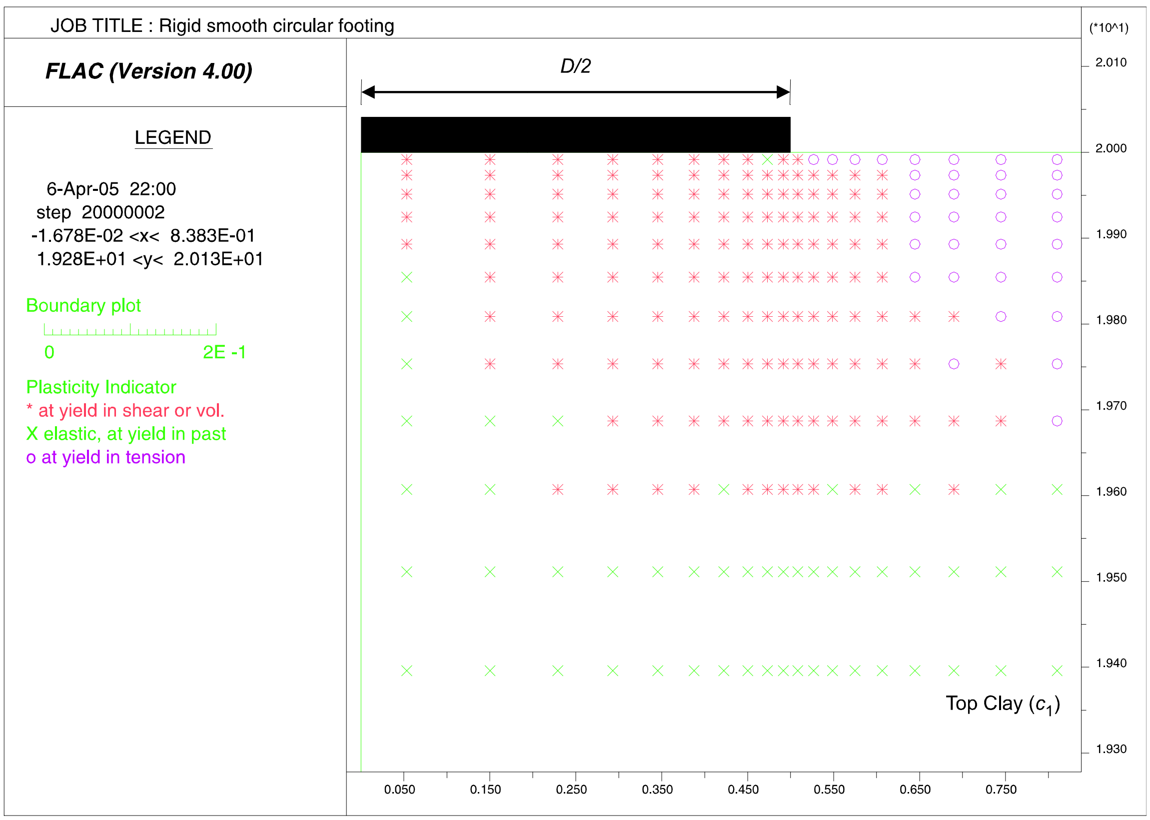

Figure A.364: Plasticity state indicators for a rigid smooth circular footing on soft over strong clay for 40×30 grid model, $H/D = 1$, $c_1/c_2 = 0.5$.

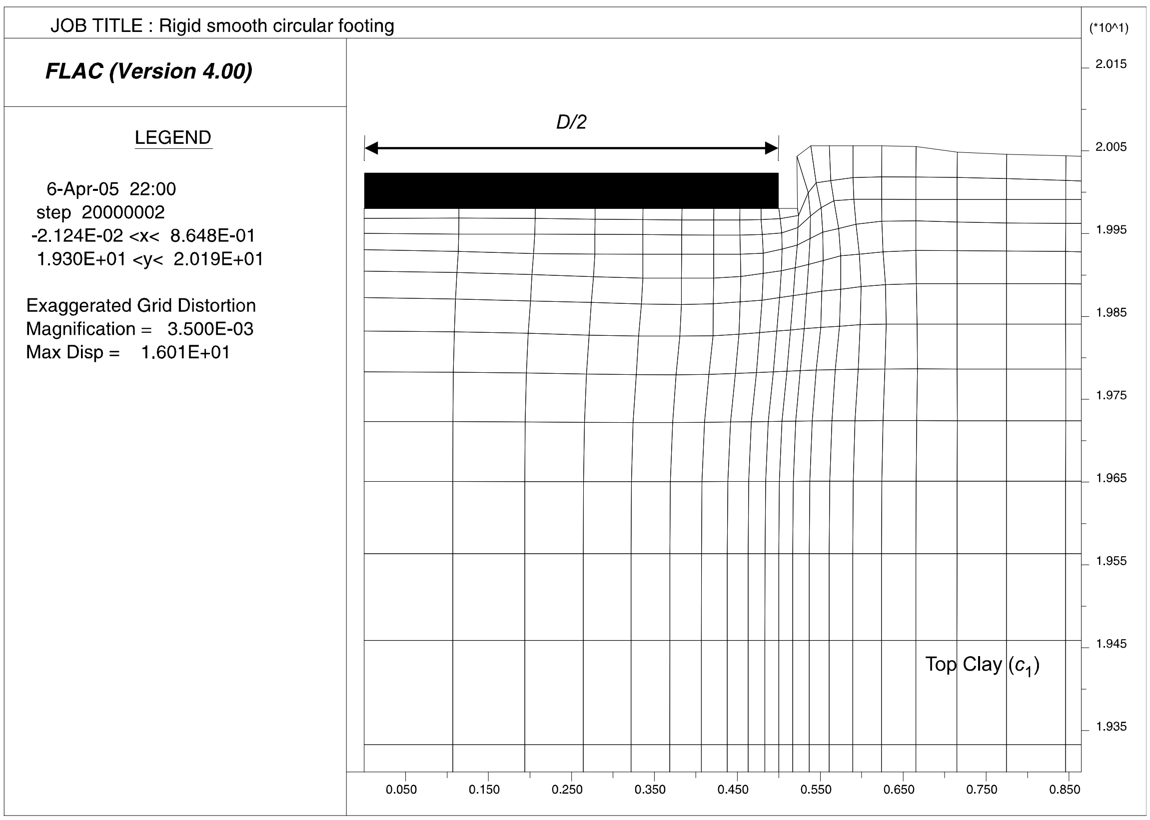

Figure A.365: Magnified grid for a rigid smooth circular footing on soft over strong clay for 40 × 30 grid model, $H/D = 1$, $c_1/c_2 = 0.5$.

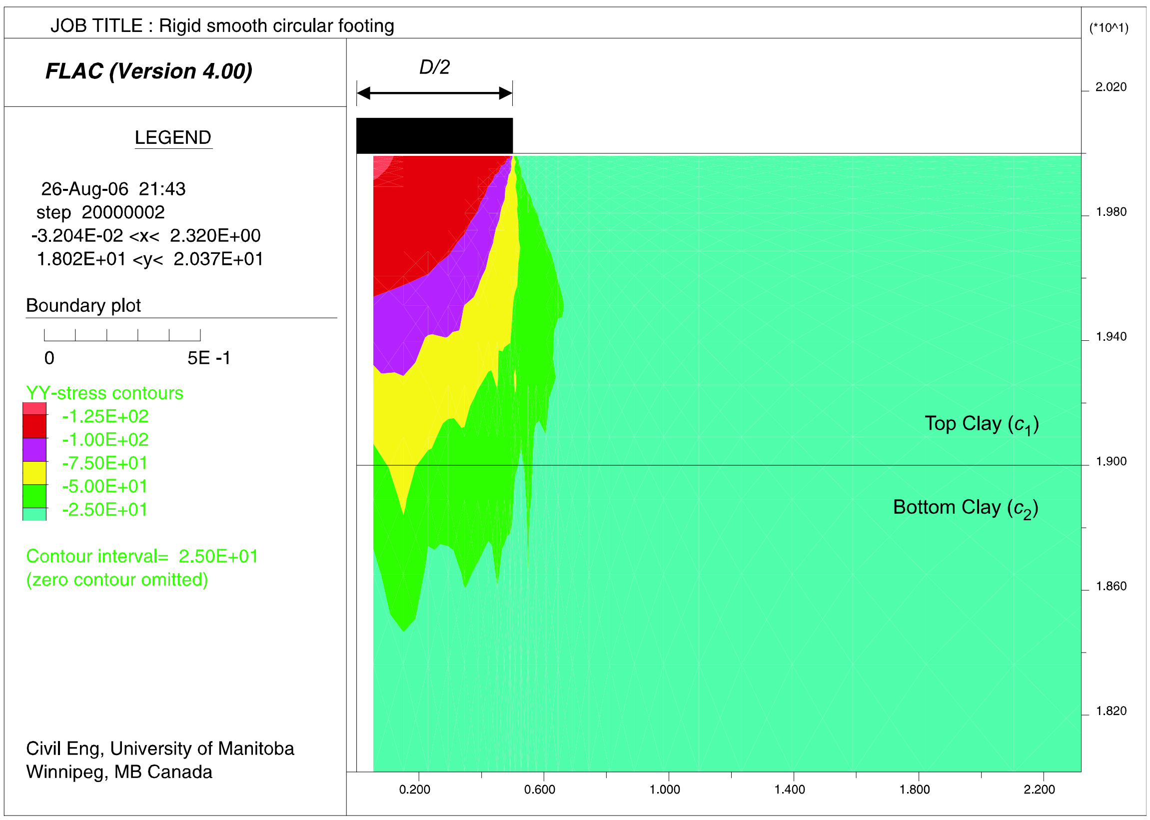

Figure A.366: Vertical stress (σ_{yy}) contours for a rigid smooth circular footing on soft over strong clay for 40×30 grid model, $H/D = 1$, $c_1/c_2 = 0.5$.

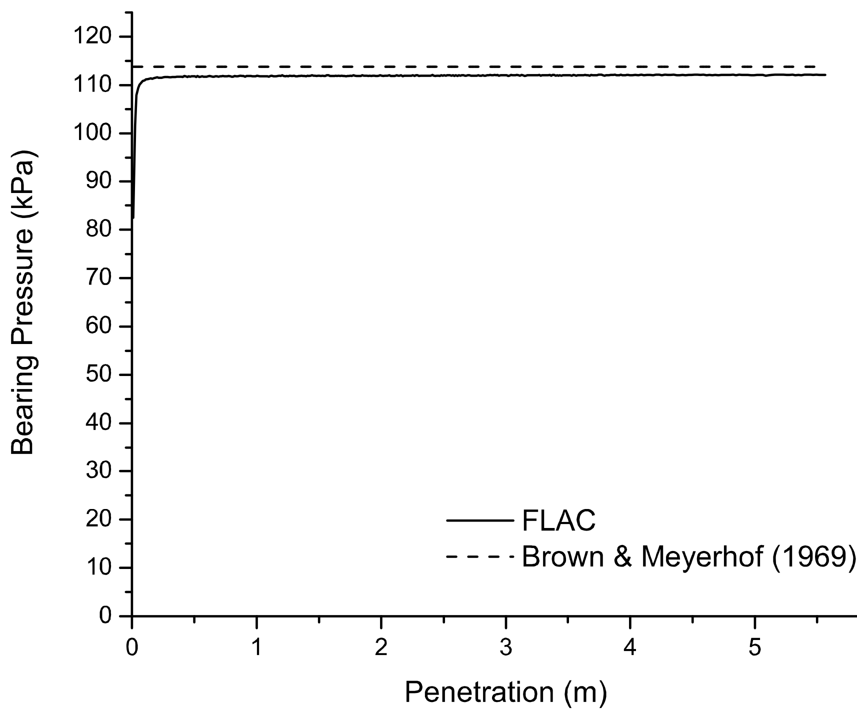

Figure A.367: Bearing pressure versus penetration curve for a rigid smooth circular footing on soft over strong clay for 40×30 grid model, $H/D = 1$, $c_1/c_2 = 0.5$.

Case 5: $c_1/c_2 = 1/3$ or $c_2/c_1 = 3$ - Small Deformation Analysis

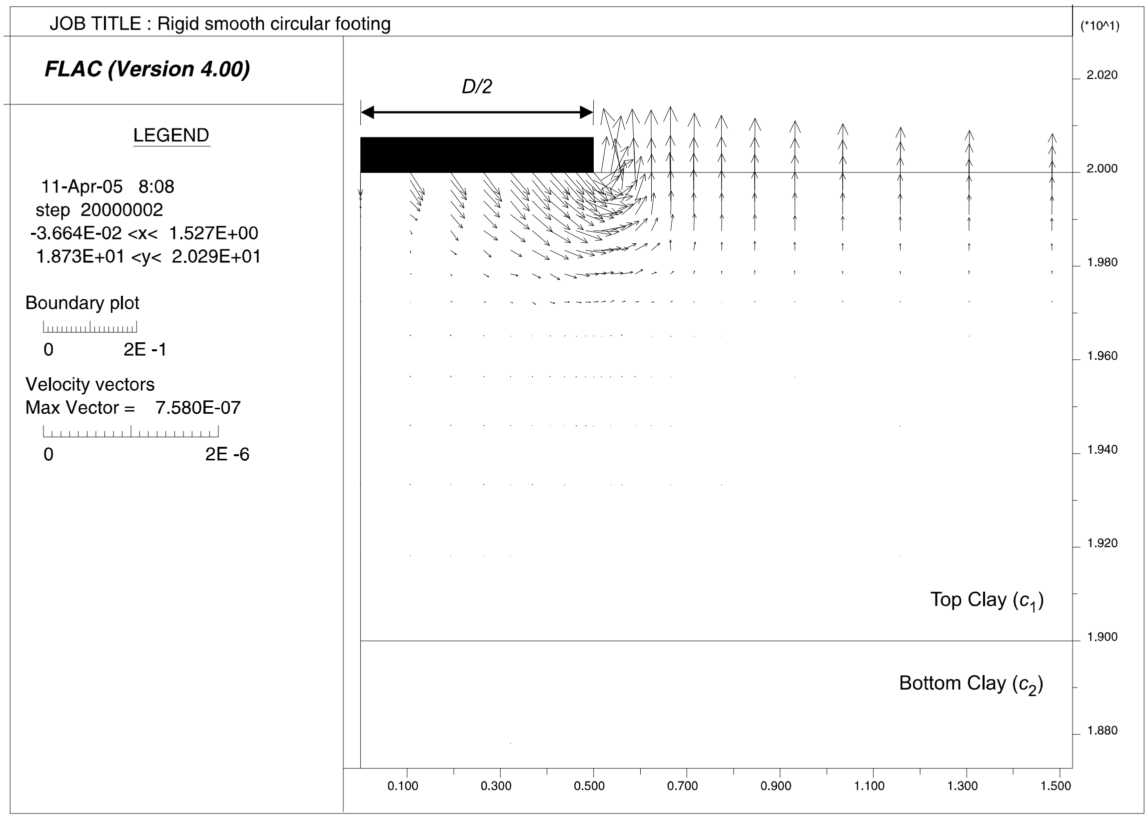

Figure A.368: Velocity vectors for a rigid smooth circular footing on soft over strong clay for 40×30 grid model, $H/D = 1$, $c_1/c_2 = 1/3$.

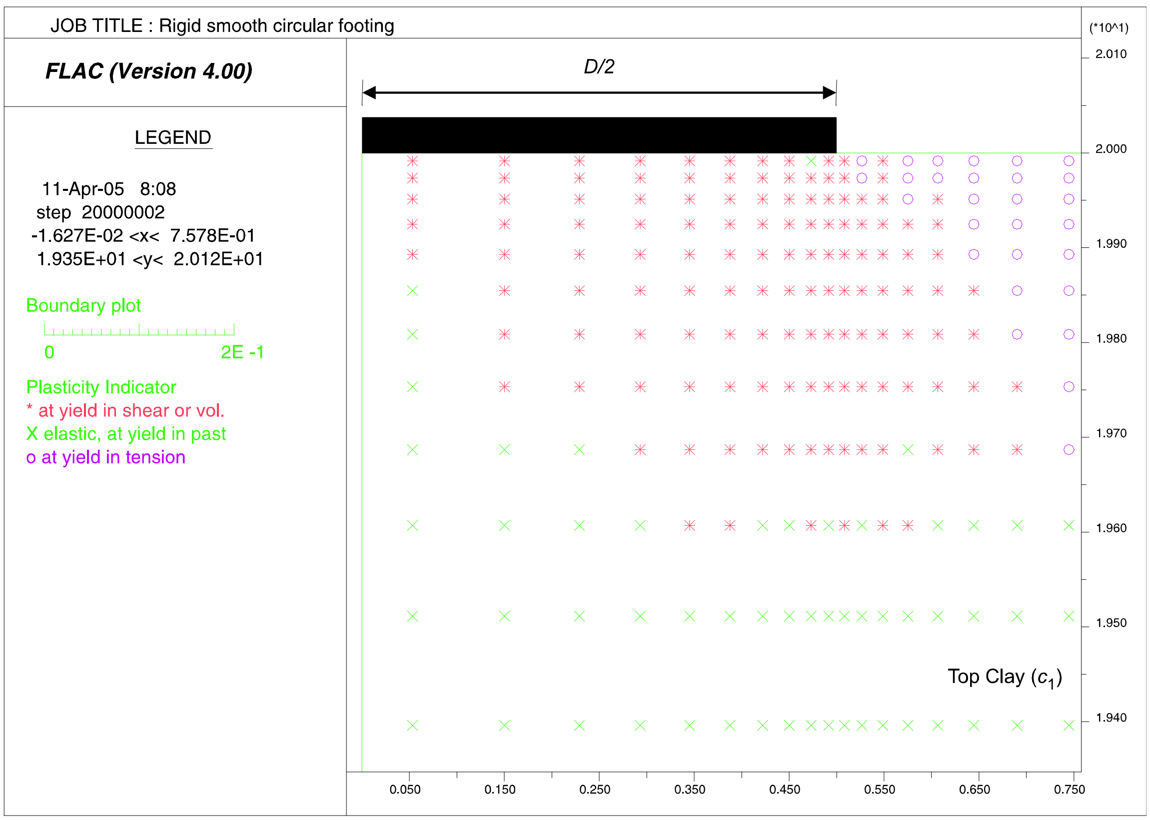

Figure A.369: Plasticity state indicators for a rigid smooth circular footing on soft over strong clay for 40×30 grid model, $H/D = 1$, $c_1/c_2 = 1/3$.

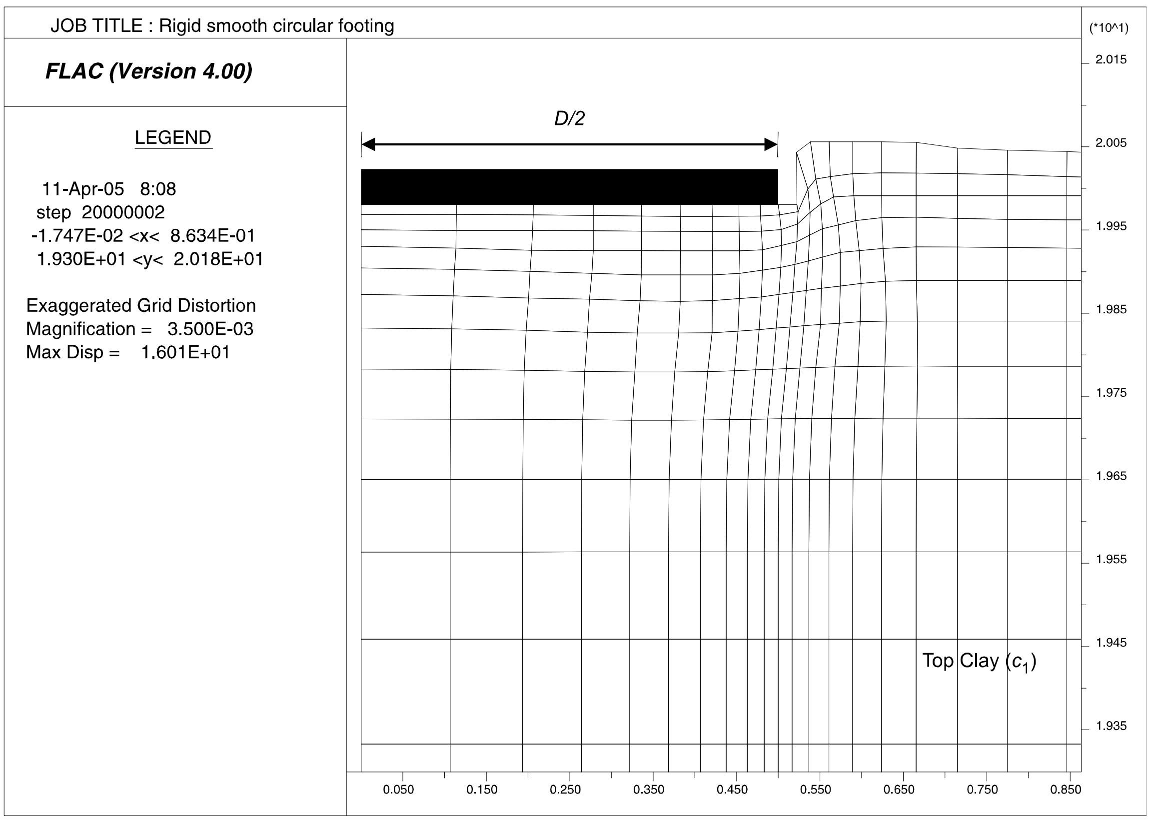

Figure A.370: Magnified grid for a rigid smooth circular footing on soft over strong clay for 40 × 30 grid model, $H/D = 1$, $c_1/c_2 = 1/3$.

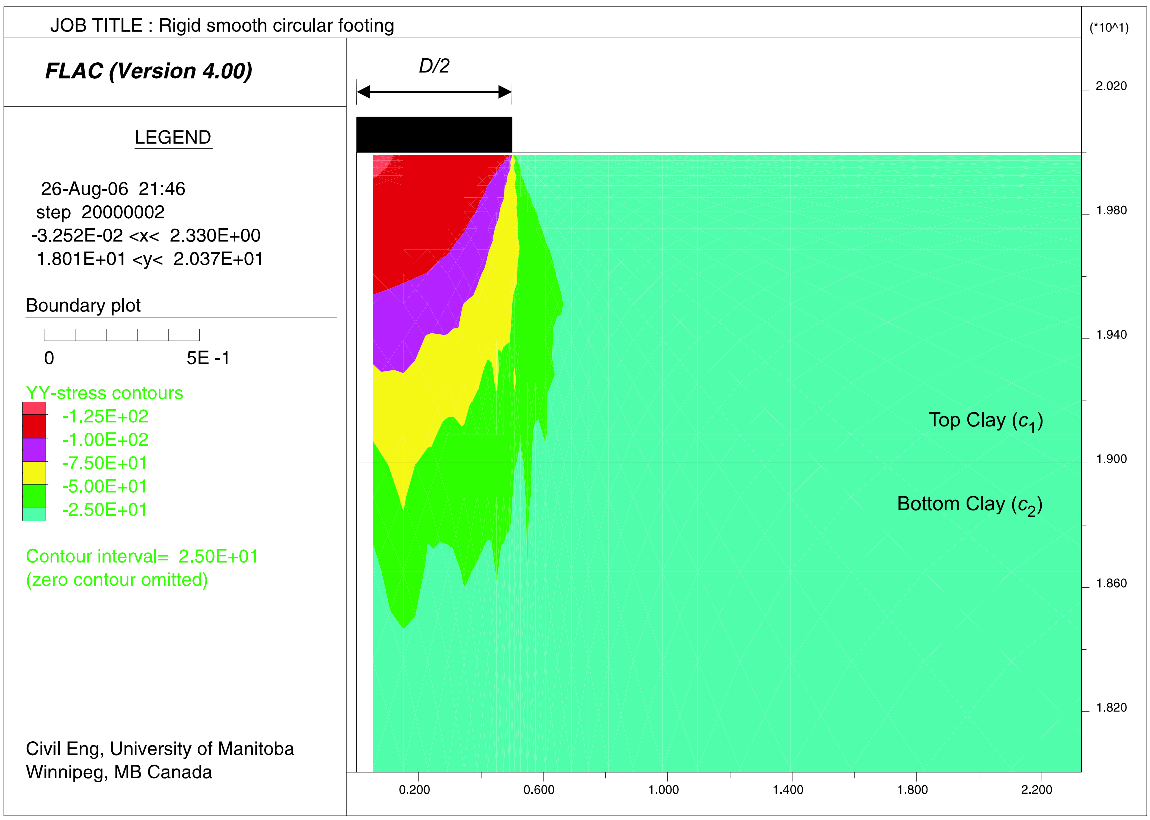

Figure A.371: Vertical stress (σ_{yy}) contours for a rigid smooth circular footing on soft over strong clay for 40×30 grid model, $H/D = 1$, $c_1/c_2 = 1/3$.

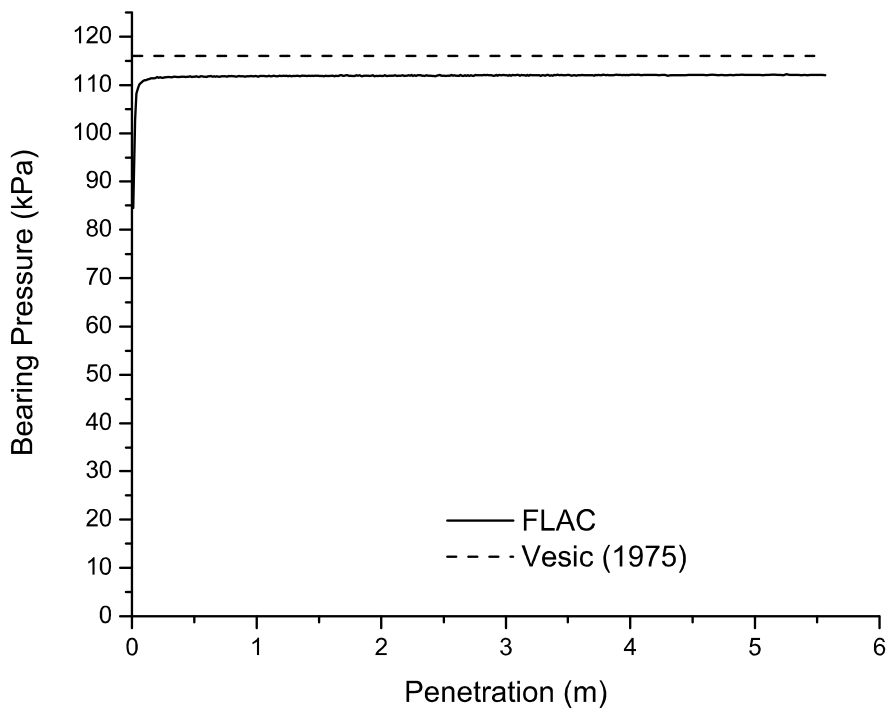

Figure A.372: Bearing pressure versus penetration curve for a rigid smooth circular footing on soft over strong clay for 40×30 grid model, $H/D = 1$, $c_1/c_2 = 1/3$.

Case 6: $c_1/c_2 = 0.2$ or $c_2/c_1 = 5$ - Small Deformation Analysis

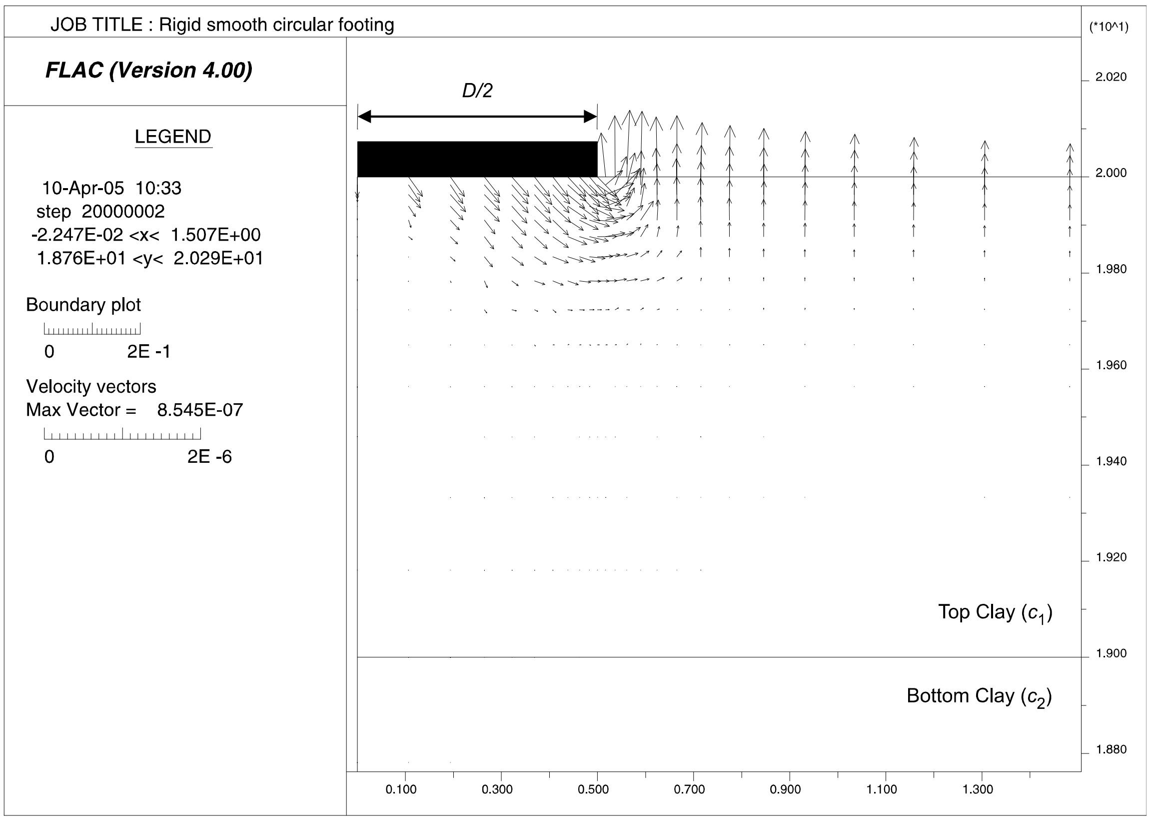

Figure A.373: Velocity vectors for a rigid smooth circular footing on soft over strong clay for 40×30 grid model, $H/D = 1$, $c_1/c_2 = 0.2$.

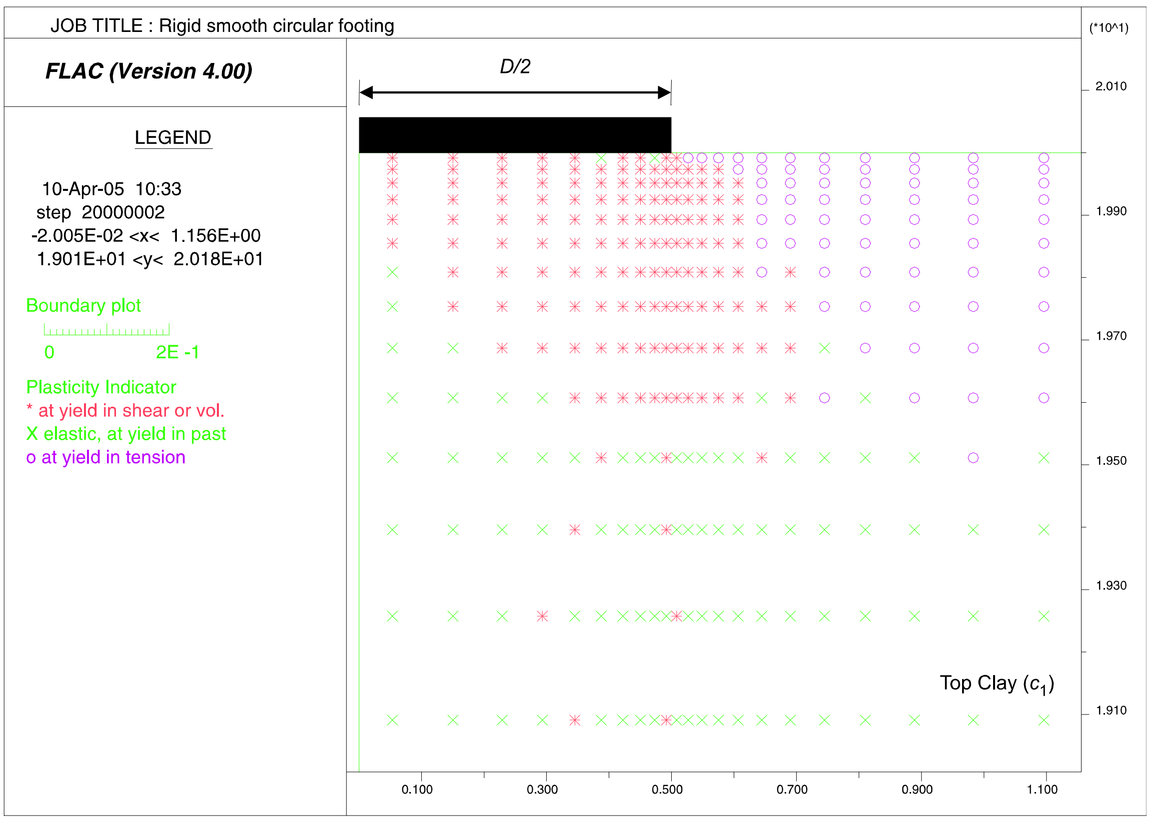

Figure A.374: Plasticity state indicators for a rigid smooth circular footing on soft over strong clay for 40 × 30 grid model, $H/D = 1$, $c_1/c_2 = 0.2$.

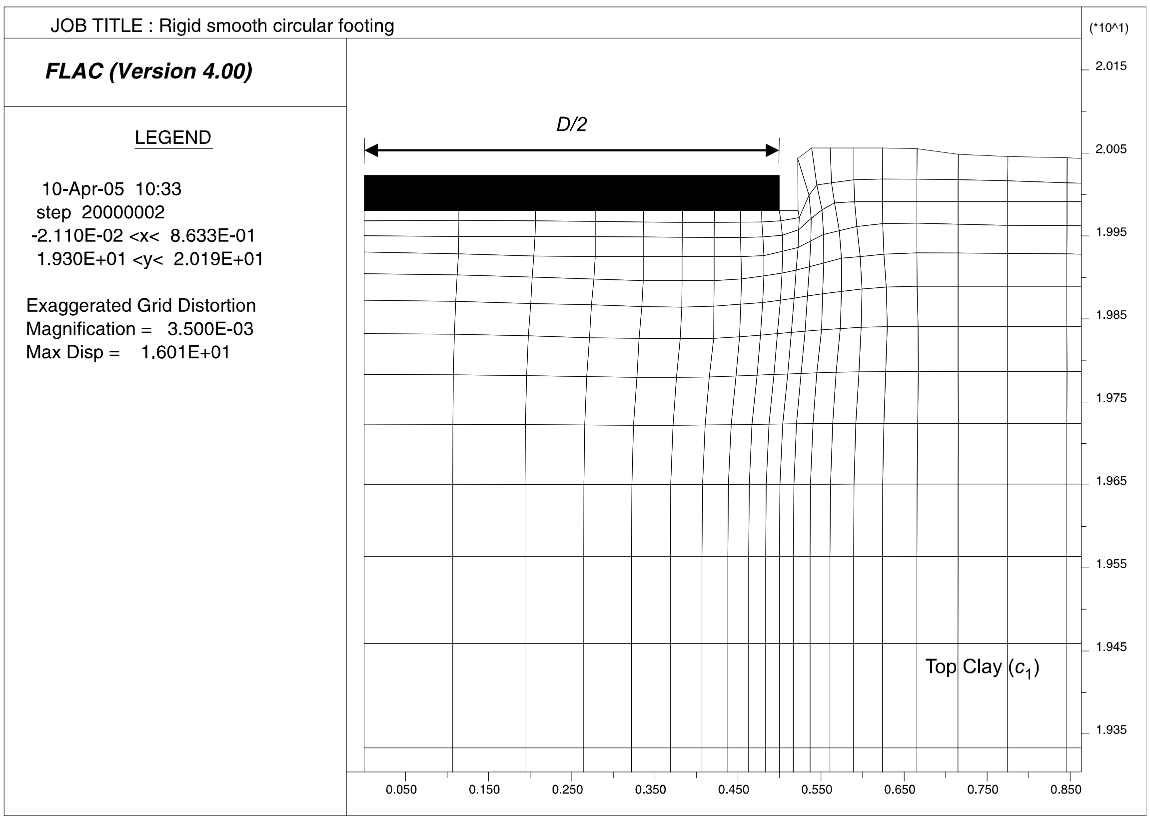

Figure A.375: Magnified grid for a rigid smooth circular footing on soft over strong clay for 40 × 30 grid model, $H/D = 1$, $c_1/c_2 = 0.2$.

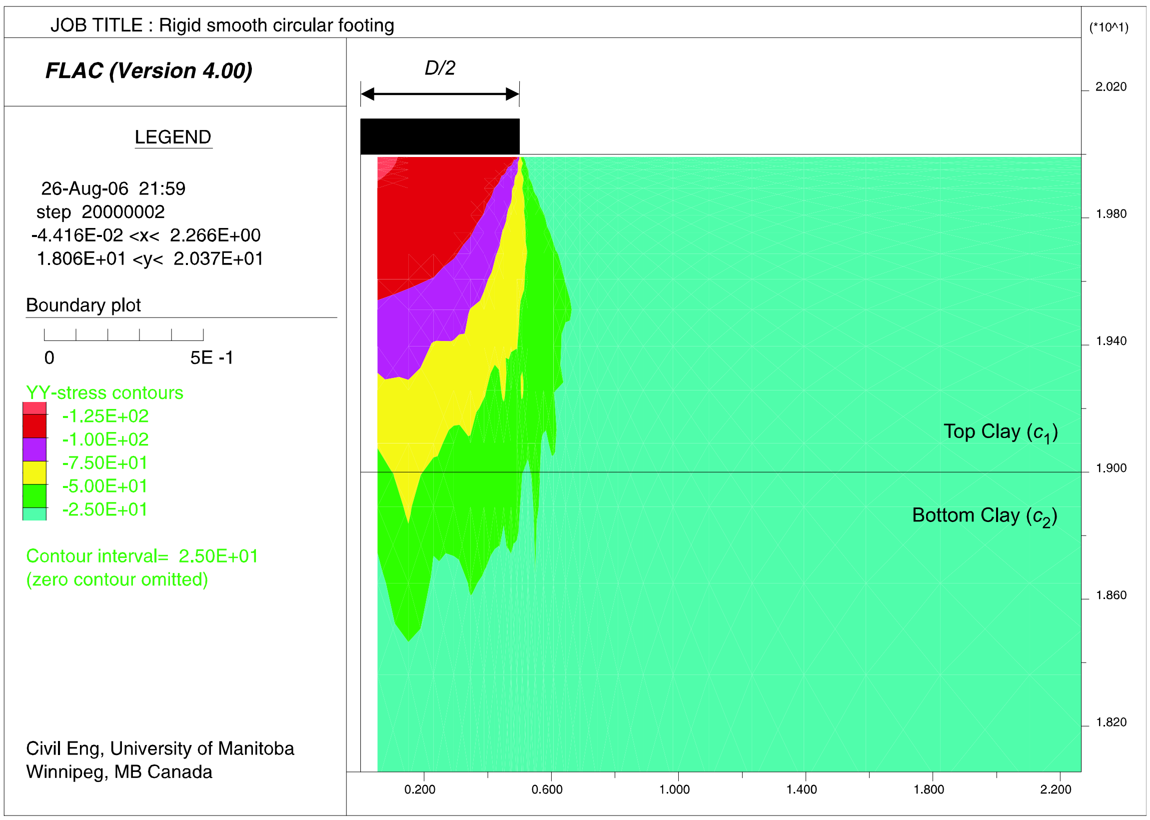

Figure A.376: Vertical stress (σ_{yy}) contours for a rigid smooth circular footing on soft over strong clay for 40×30 grid model, $H/D = 1$, $c_1/c_2 = 0.2$.

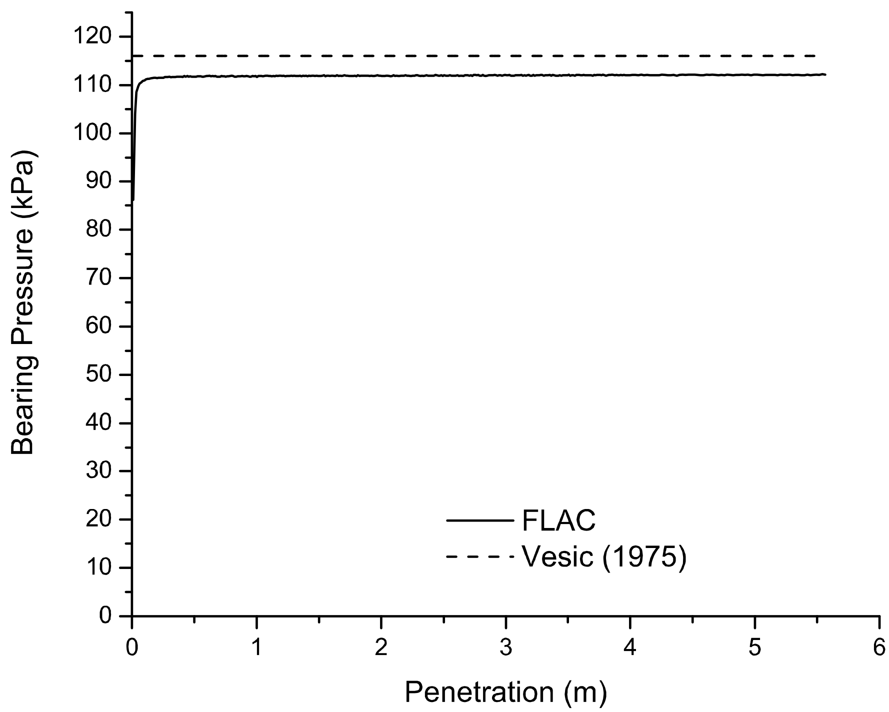

Figure A.377: Bearing pressure versus penetration curve for a rigid smooth circular footing on soft over strong clay for 40×30 grid model, $H/D = 1$, $c_1/c_2 = 0.2$.

Case 7: $c_1/c_2 = 0.1$ or $c_2/c_1 = 10$ - Small Deformation Analysis

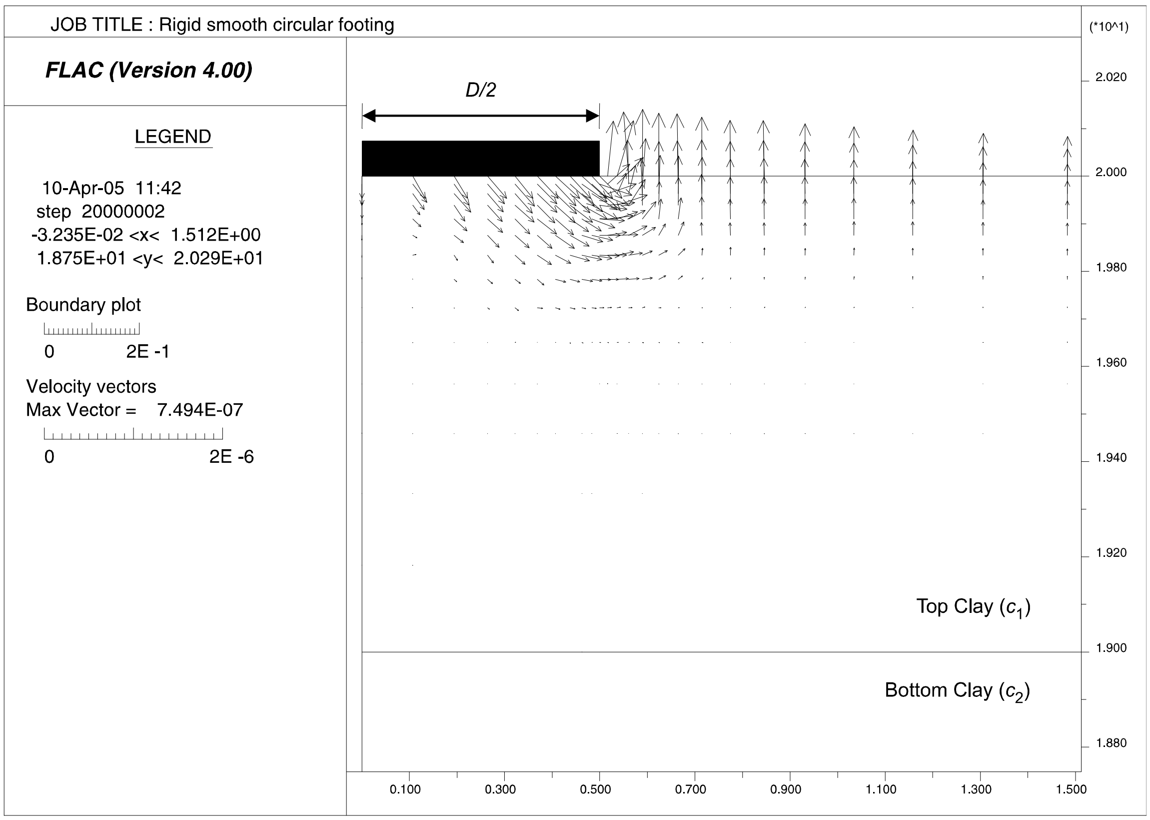

Figure A.378: Velocity vectors for a rigid smooth circular footing on soft over strong clay for 40×30 grid model, $H/D = 1$, $c_1/c_2 = 0.1$.

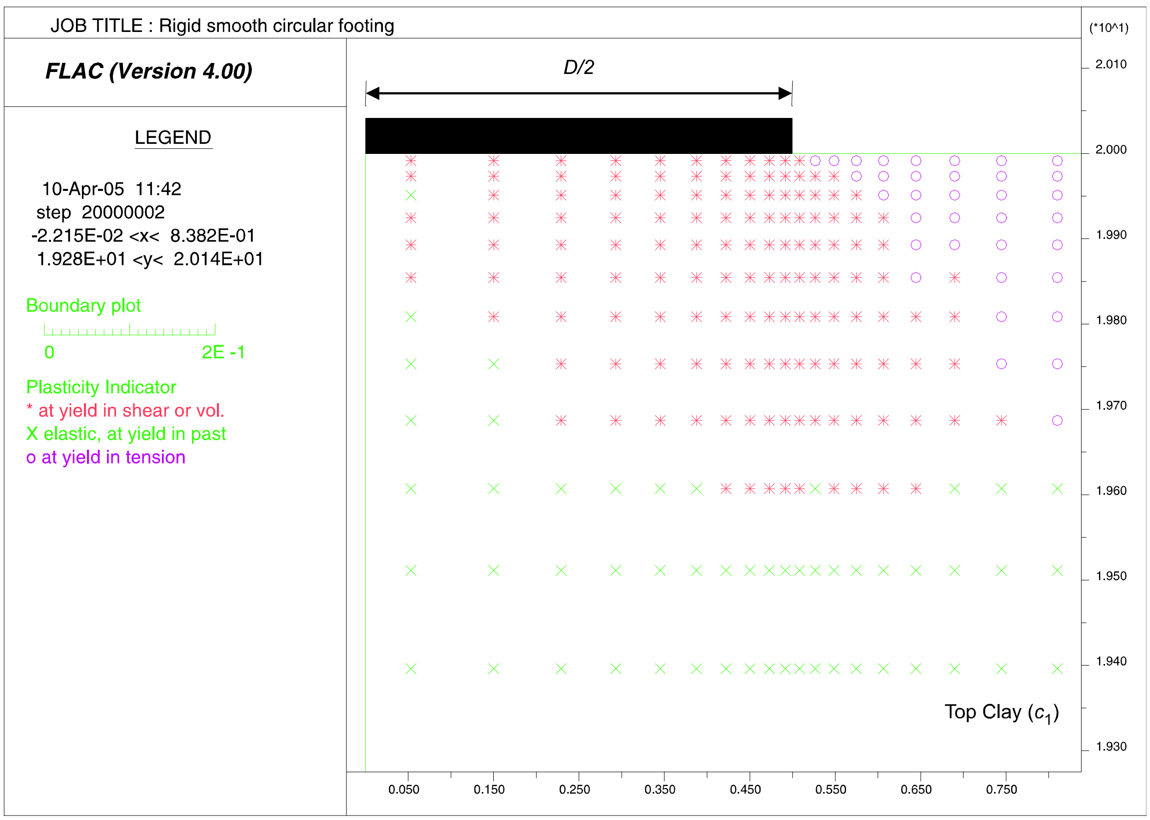

Figure A.379: Plasticity state indicators for a rigid smooth circular footing on soft over strong clay for 40 × 30 grid model, $H/D = 1$, $c_1/c_2 = 0.1$.

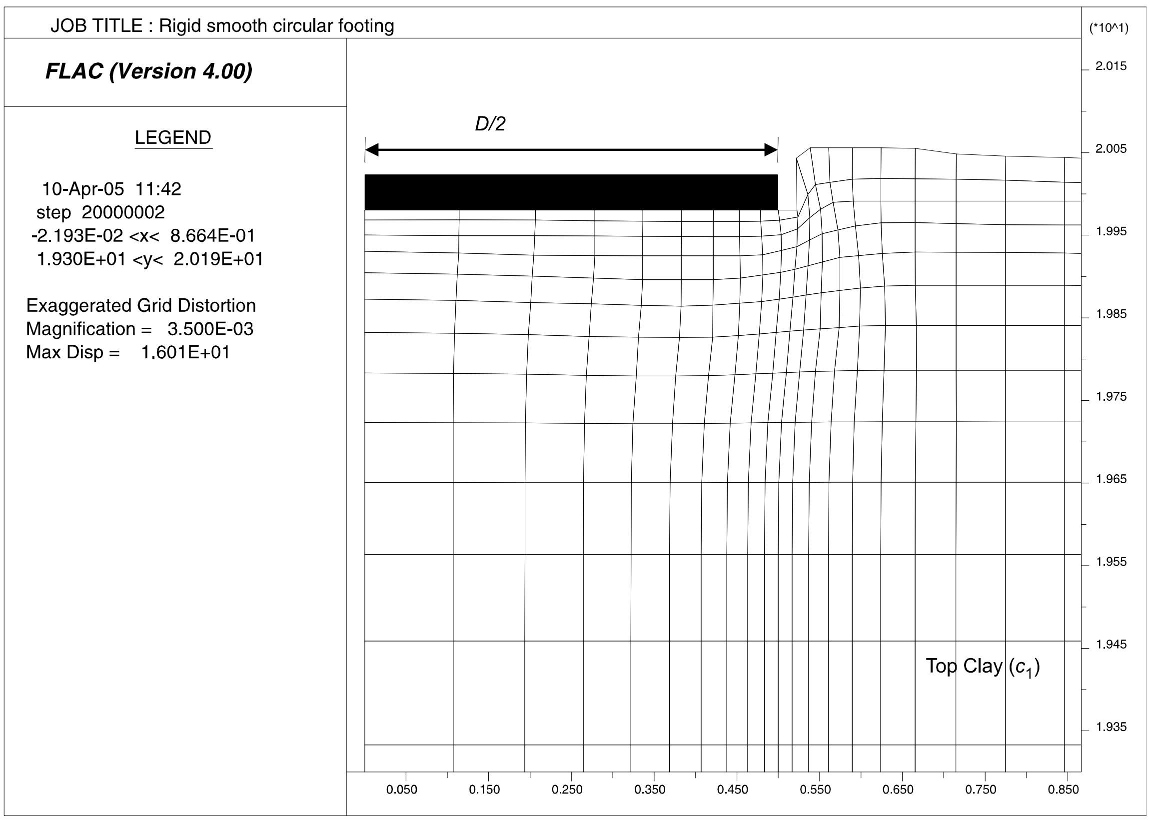

Figure A.380: Magnified grid for a rigid smooth circular footing on soft over strong clay for 40 × 30 grid model, $H/D = 1$, $c_1/c_2 = 0.1$.

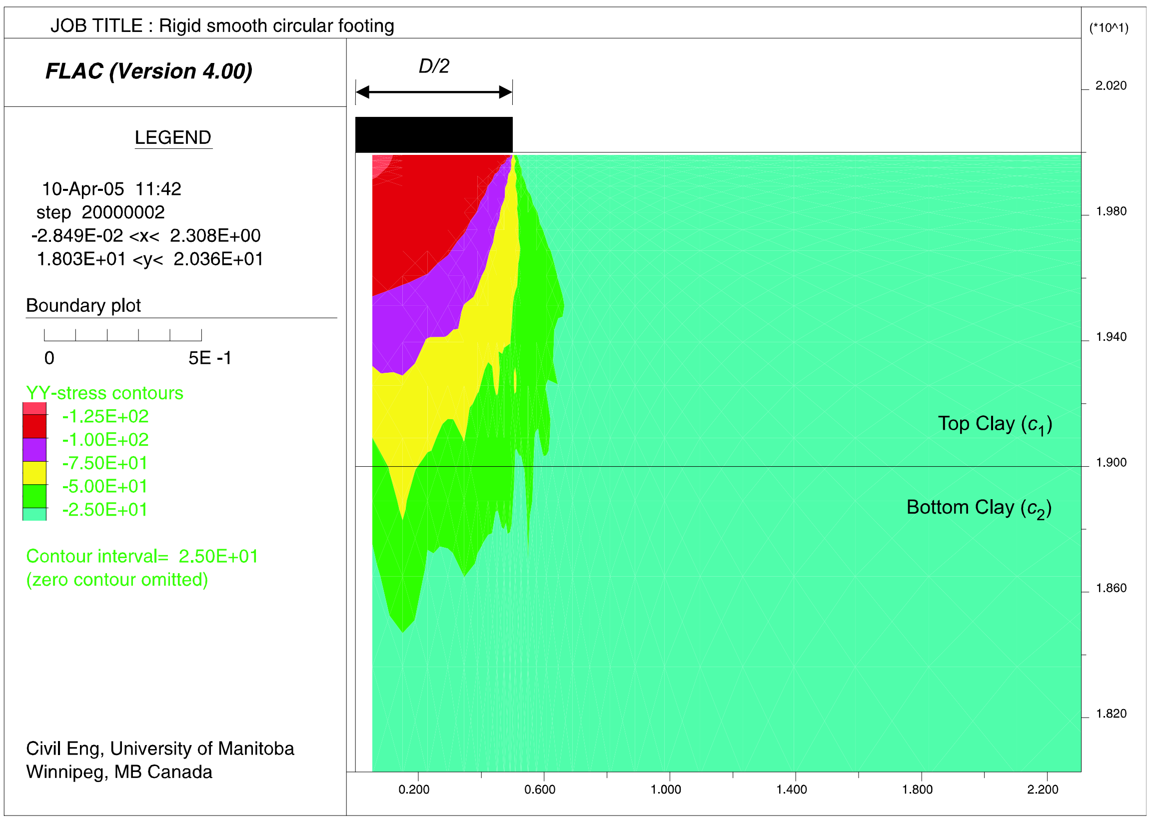

Figure A.381: Vertical stress (σ_{yy}) contours for a rigid smooth circular footing on soft over strong clay for 40×30 grid model, $H/D = 1$, $c_1/c_2 = 0.1$.

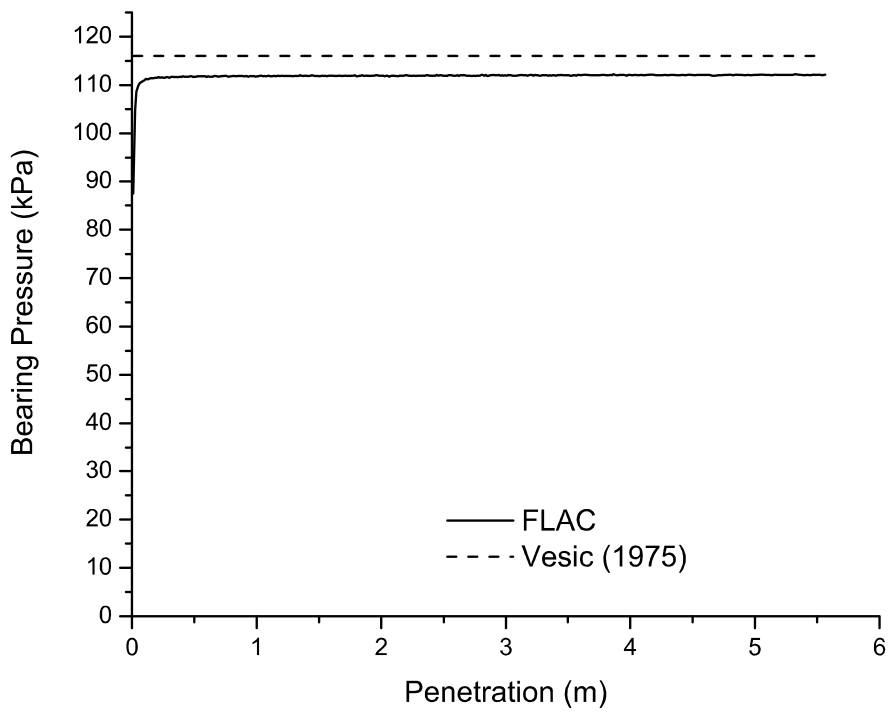

Figure A.382: Bearing pressure versus penetration curve for a rigid smooth circular footing on soft over strong clay for 40 × 30 grid model, $H/D = 1$, $c_1/c_2 = 0.1$.

A.4.2 Rigid Smooth Circular Footing on Soft over Strong Clay ($H/D = 0.5$)

Case 2: $c_1/c_2 = 0.8$ or $c_2/c_1 = 1.25$ - Small Deformation Analysis

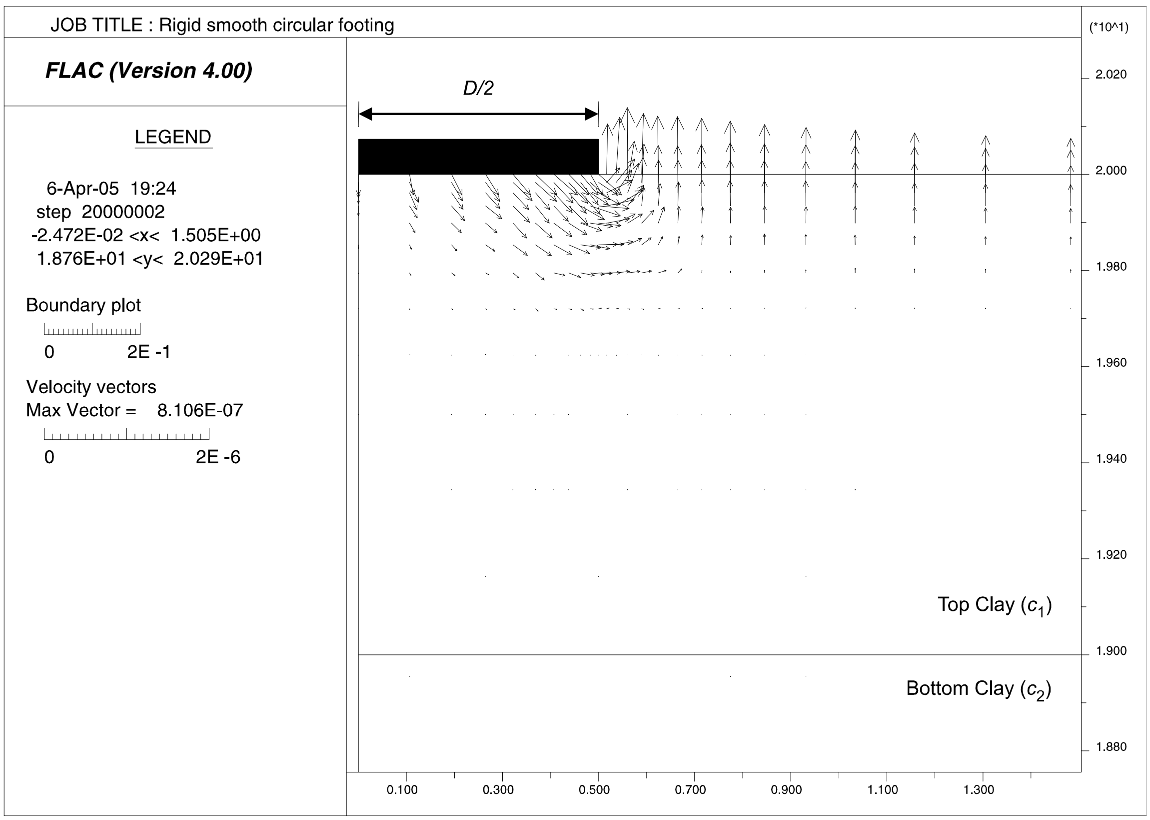

Figure A.383: Velocity vectors for a rigid circular footing on soft over strong clay for 40×30 grid model, $H/D = 0.5$, $c_1/c_2 = 0.8$.

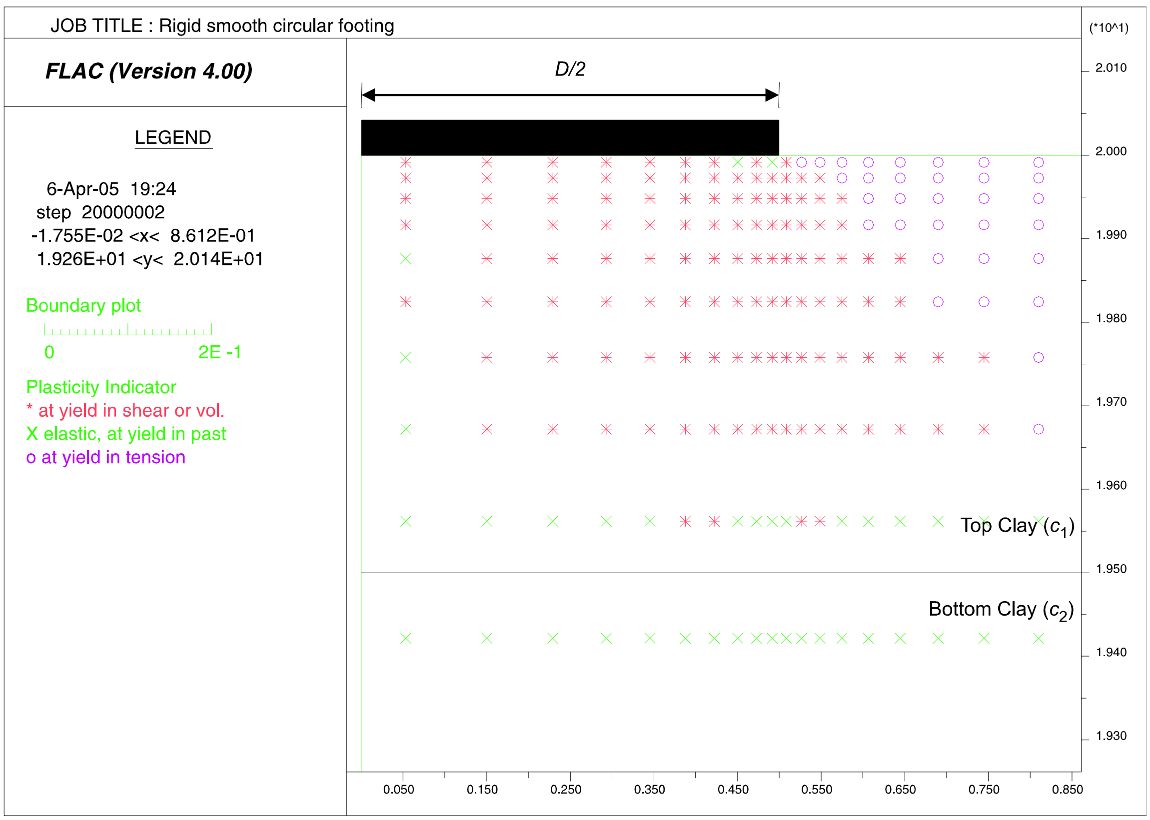

Figure A.384: Plasticity indicators for a rigid smooth circular footing on soft over strong clay for 40 × 30 grid model, $H/D = 0.5$, $c_1/c_2 = 0.8$.

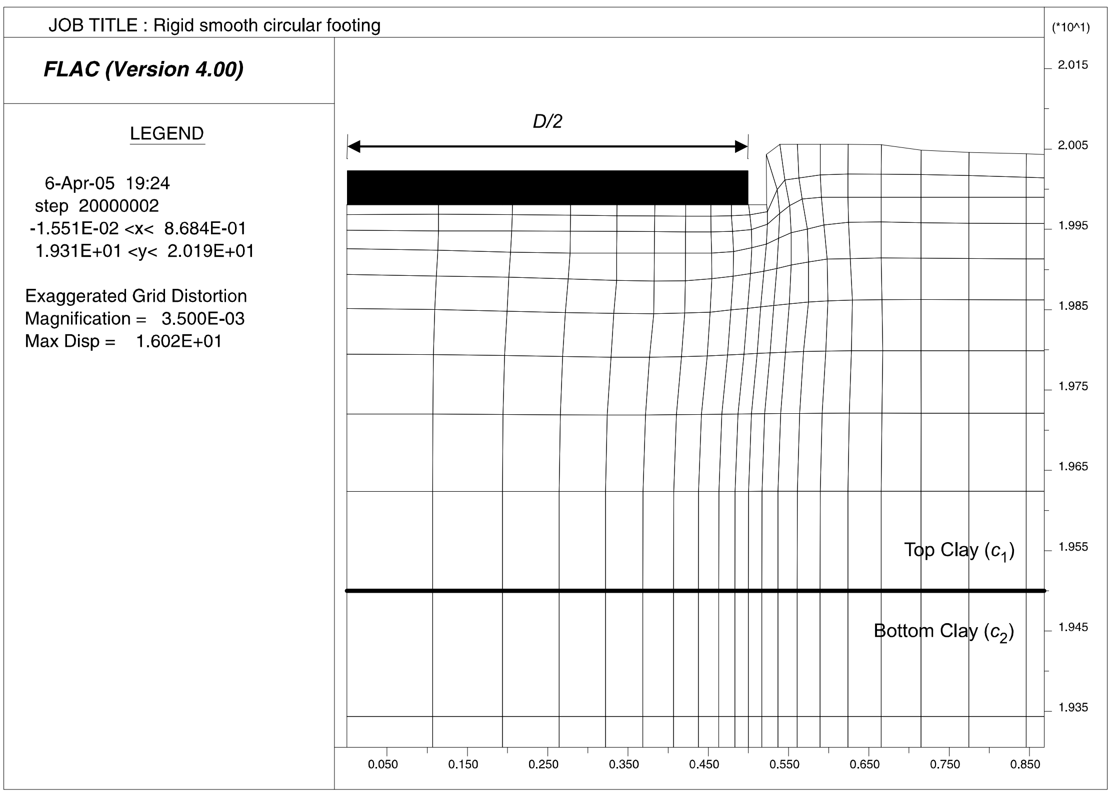

Figure A.385: Magnified grid for a rigid smooth circular footing on soft over strong clay for 40×30 grid model, $H/D = 0.5$, $c_1/c_2 = 0.8$.

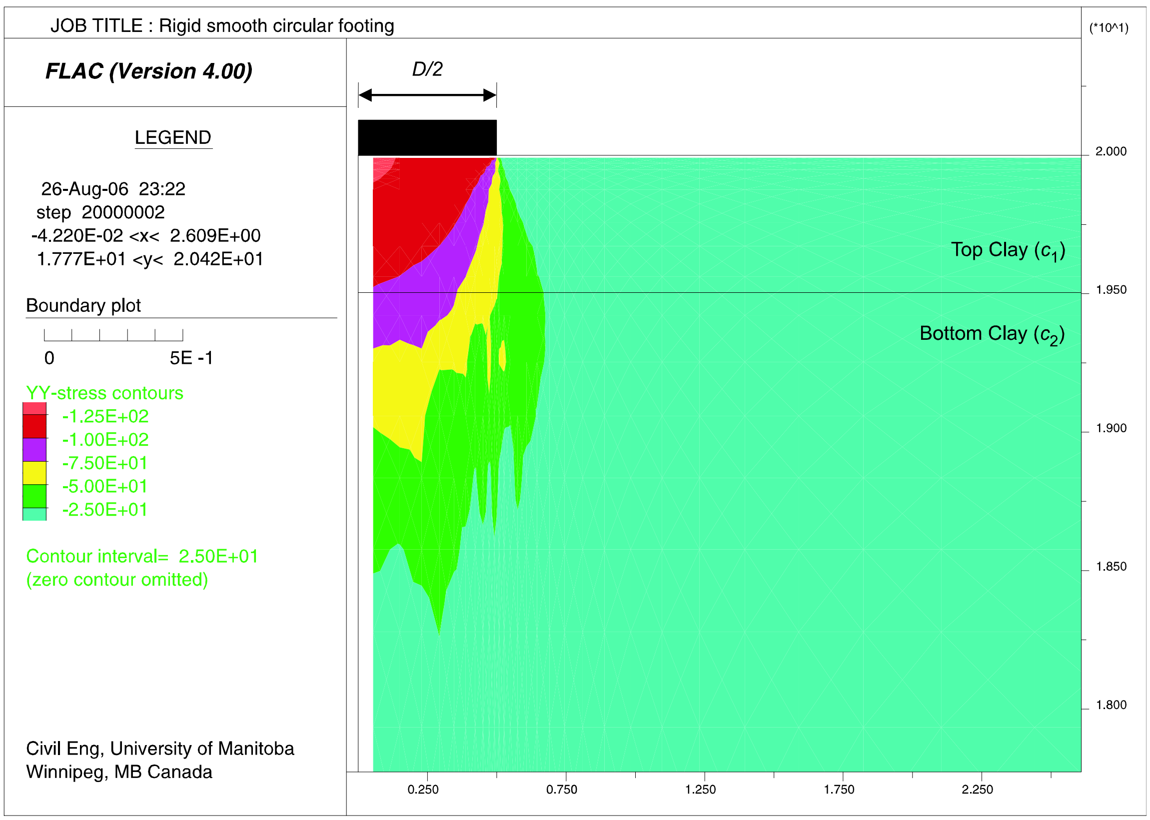

Figure A.386: Vertical stress (σ_{yy}) contours for a rigid smooth circular footing on soft over strong clay for 40×30 grid model, $H/D = 0.5$, $c_1/c_2 = 0.8$.

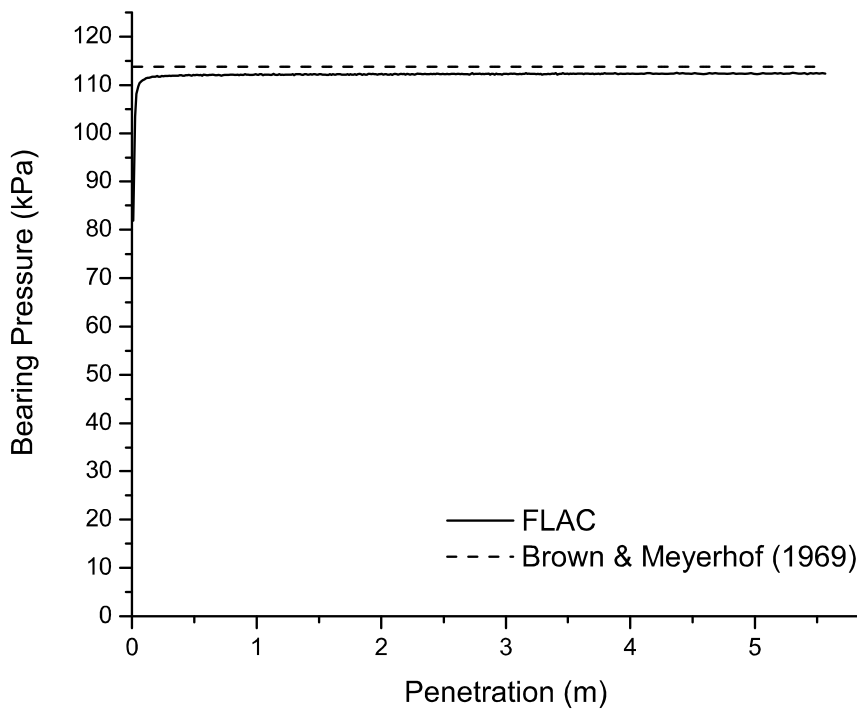

Figure A.387: Bearing pressure versus penetration curve for a rigid smooth circular footing on soft over strong clay for 40 × 30 grid model, $H/D = 0.5$, $c_1/c_2 = 0.8$.

Case 3: $c_1/c_2 = 2/3$ or $c_2/c_1 = 1.5$ - Small Deformation Analysis

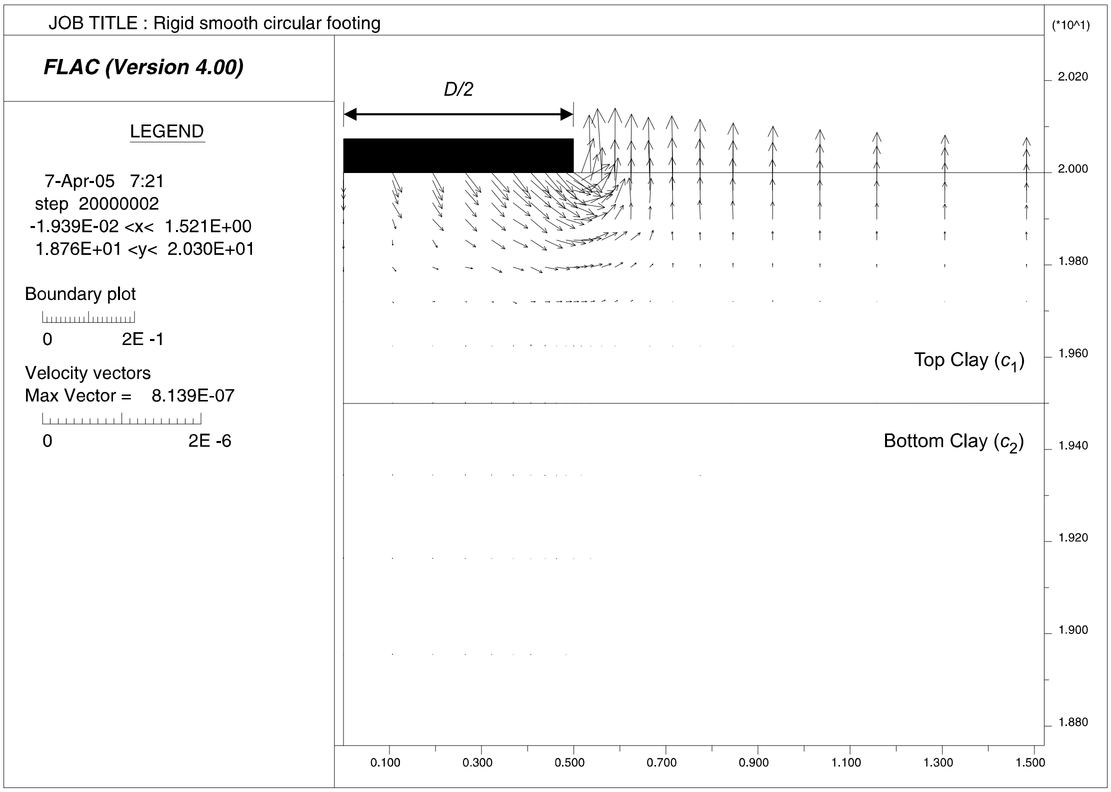

Figure A.388: Velocity vectors for a rigid smooth circular footing on soft over strong clay for 40×30 grid model, $H/D = 0.5$, $c_1/c_2 = 2/3$.

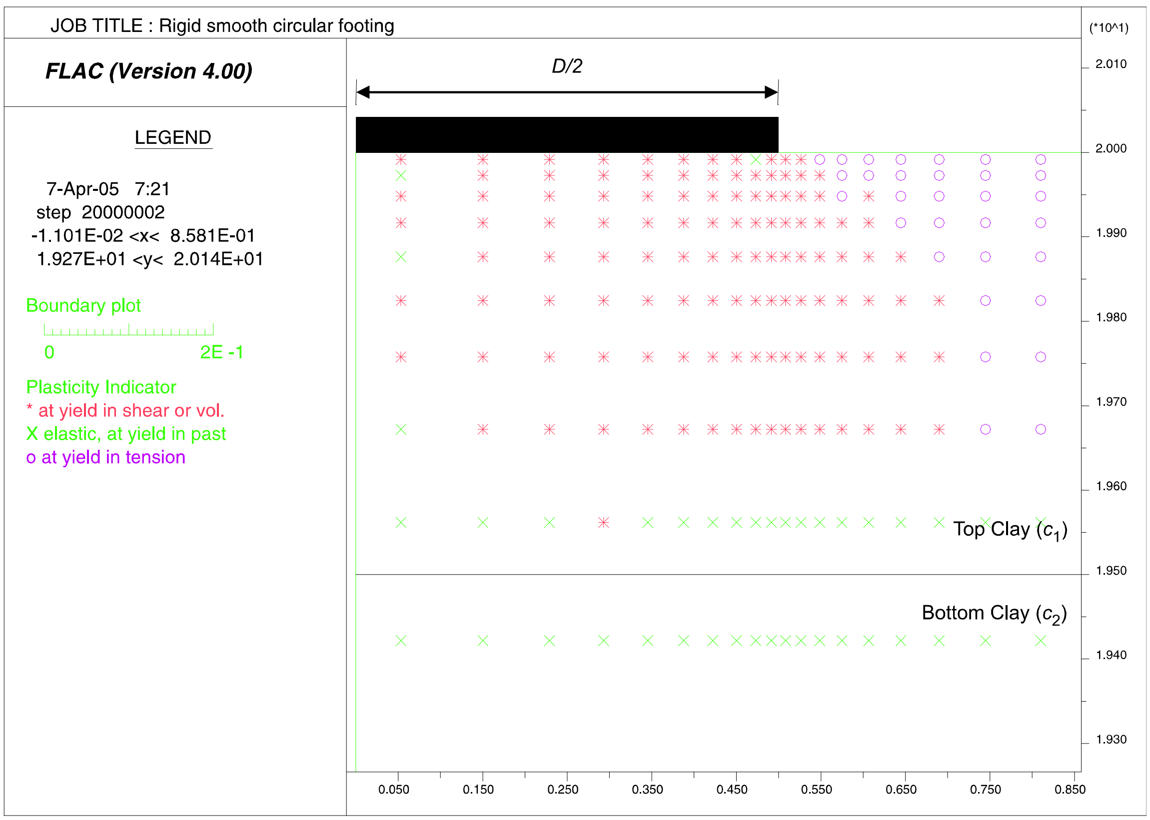

Figure A.389: Plasticity state indicators for a rigid smooth circular footing on soft over strong clay for 40 × 30 grid model, $H/D = 0.5$, $c_1/c_2 = 2/3$.

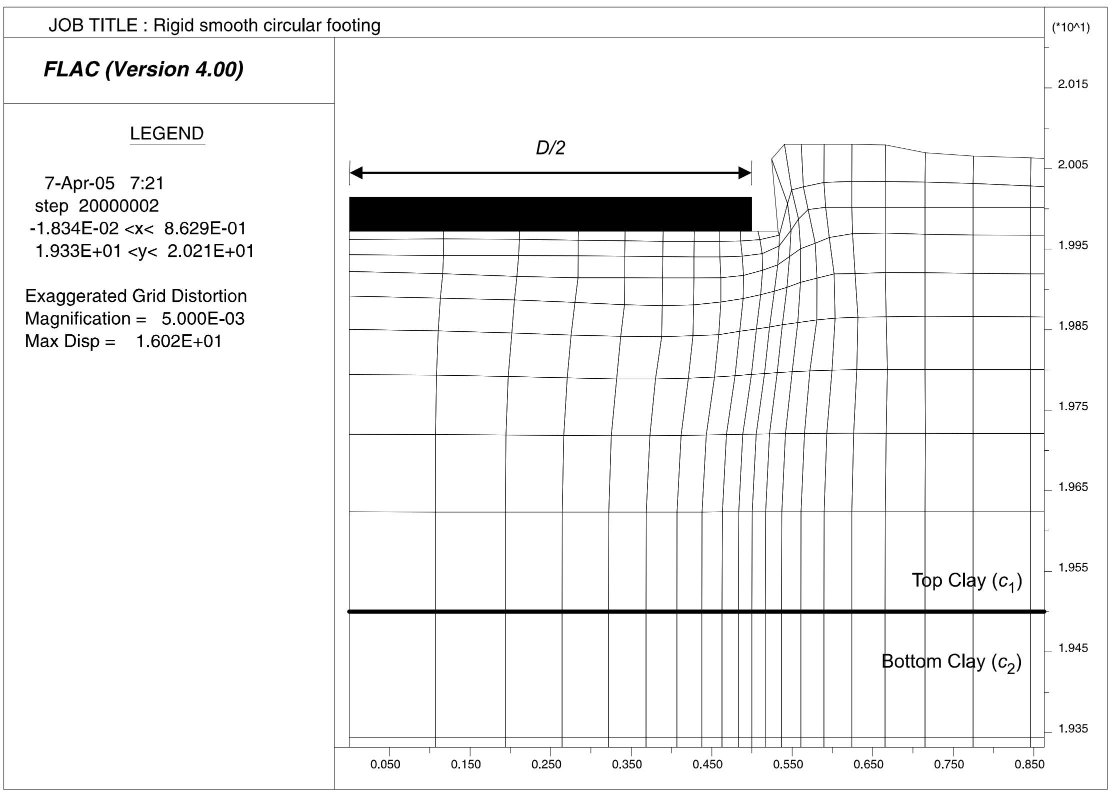

Figure A.390: Magnified grid for a rigid smooth circular footing on soft over strong clay for 40×30 grid model, $H/D = 0.5$, $c_1/c_2 = 2/3$.

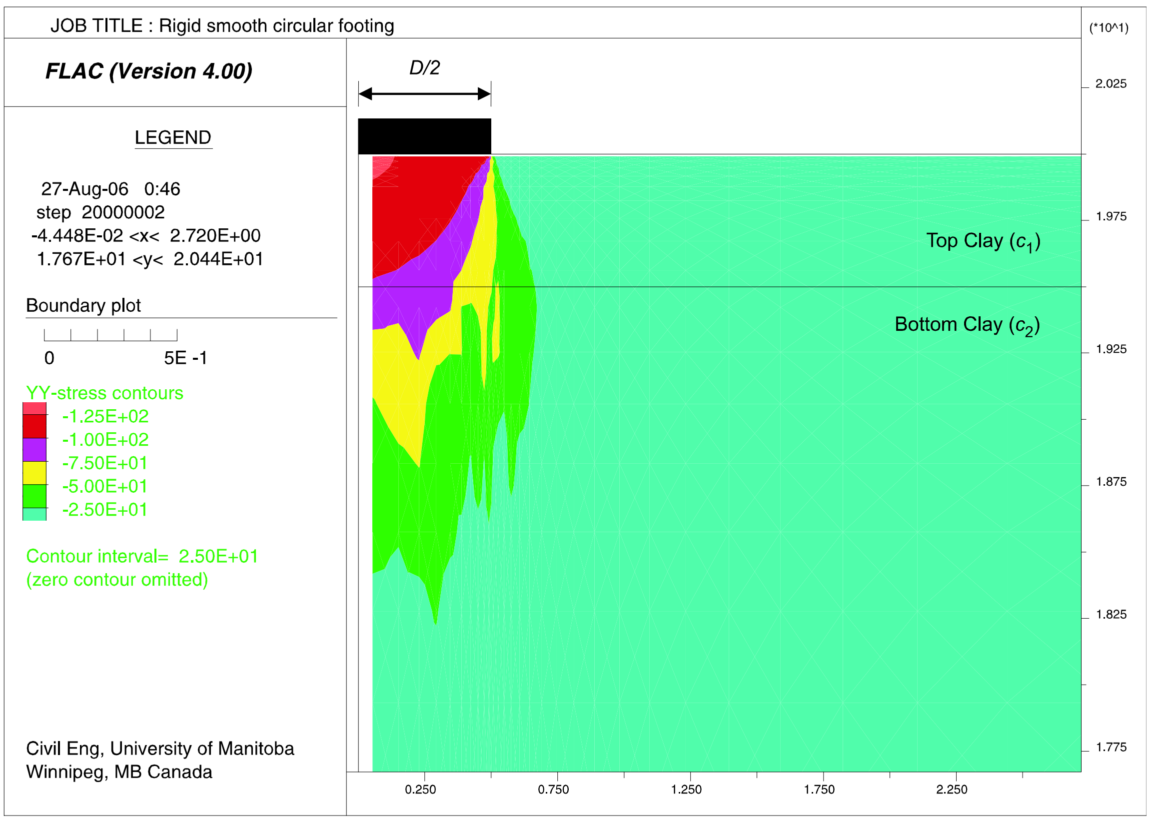

Figure A.391: Vertical stress (σ_{yy}) contours for a rigid smooth circular footing on soft over strong clay for 40×30 grid model, $H/D = 0.5$, $c_1/c_2 = 2/3$.

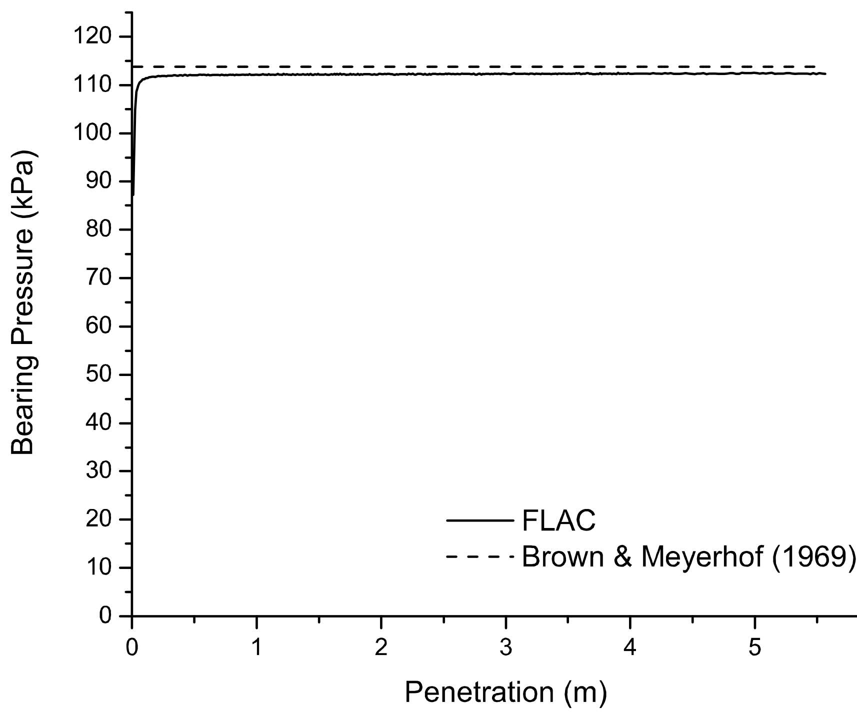

Figure A.392: Bearing pressure versus penetration curve for a rigid smooth circular footing on soft over strong clay for 40 × 30 grid model, $H/D = 0.5$, $c_1/c_2 = 2/3$.

Case 4: $c_1/c_2 = 0.5$ or $c_2/c_1 = 2$ - Small Deformation Analysis

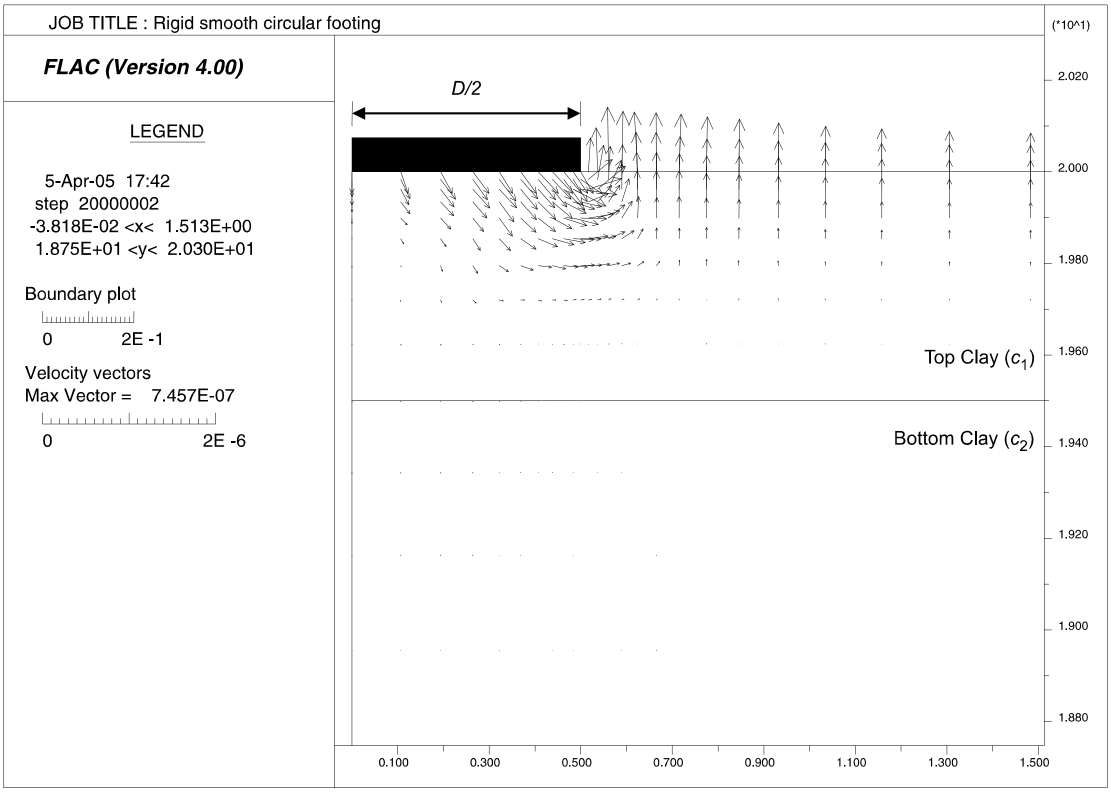

Figure A.393: Velocity vectors for a rigid smooth circular footing on soft clay over strong clay for 40×30 grid model, $H/D = 0.5$, $c_1/c_2 = 0.5$.

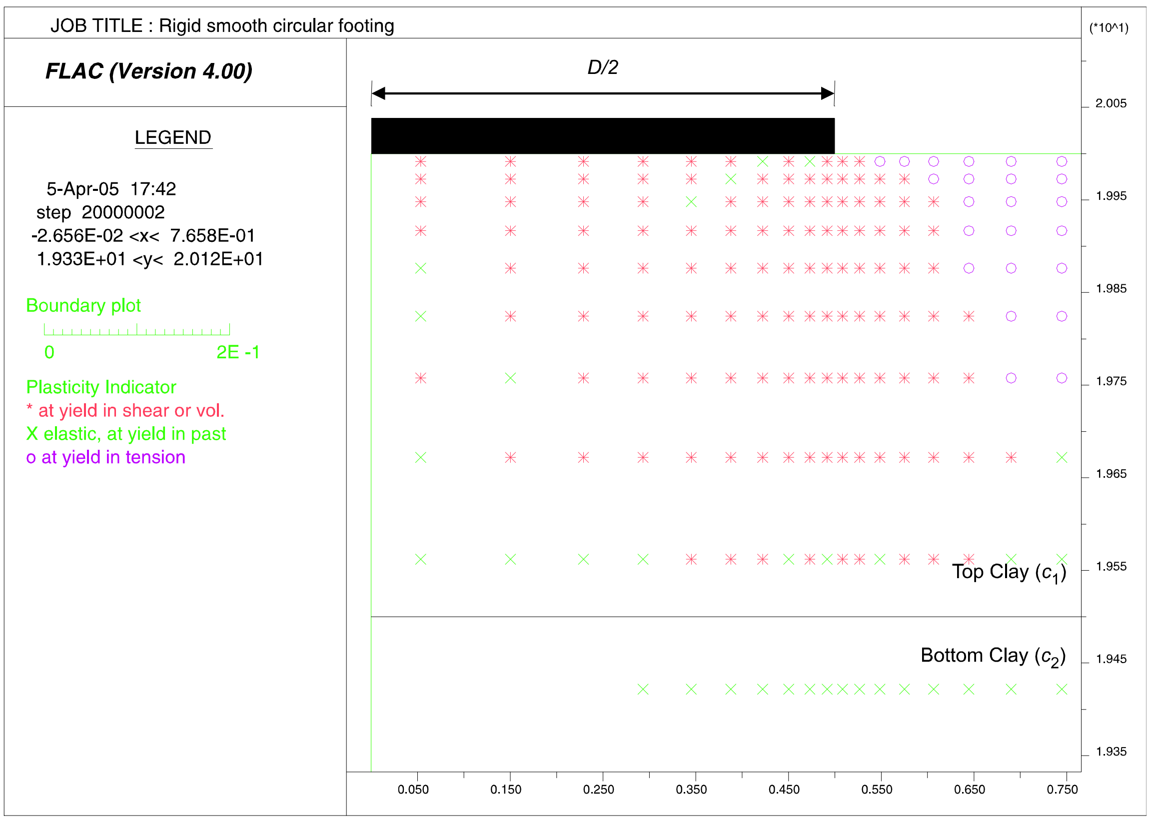

Figure A.394: Plasticity state indicators for a rigid smooth circular footing on soft clay over strong clay for 40 × 30 grid model, $H/D = 0.5$, $c_1/c_2 = 0.5$.

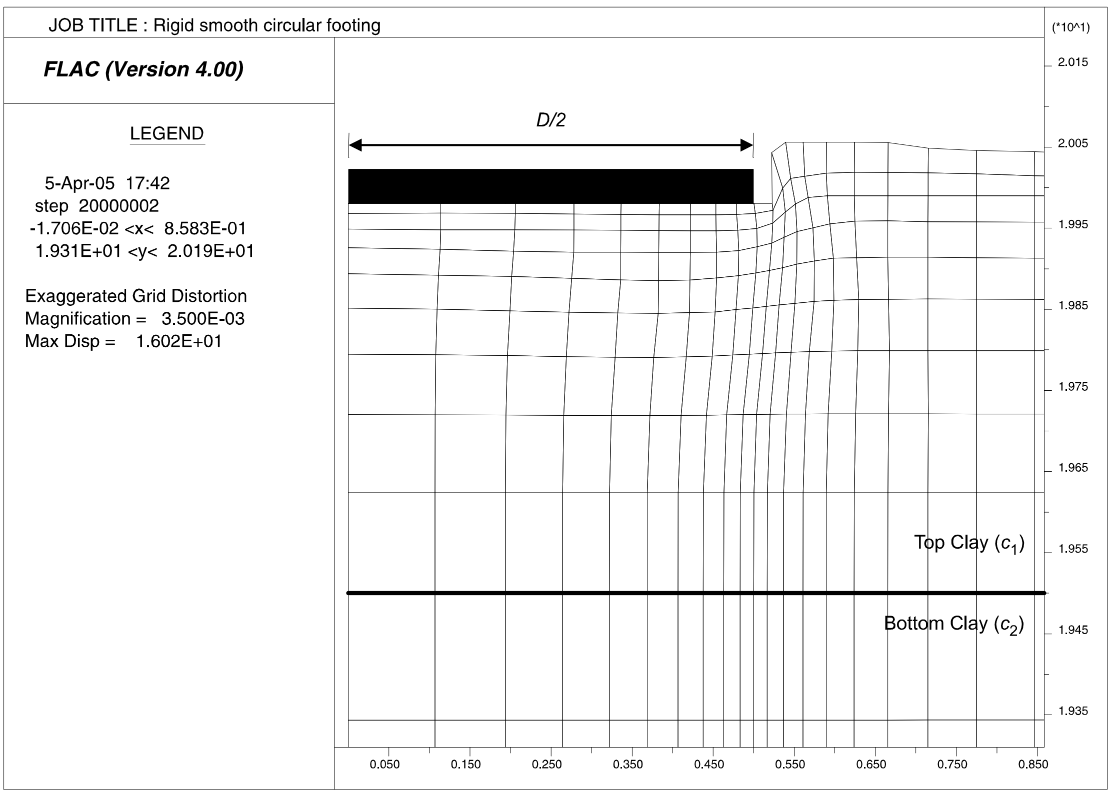

Figure A.395: Magnified grid for a rigid smooth circular footing on soft clay over strong clay for 40 × 30 grid model, $H/D = 0.5$, $c_1/c_2 = 0.5$.

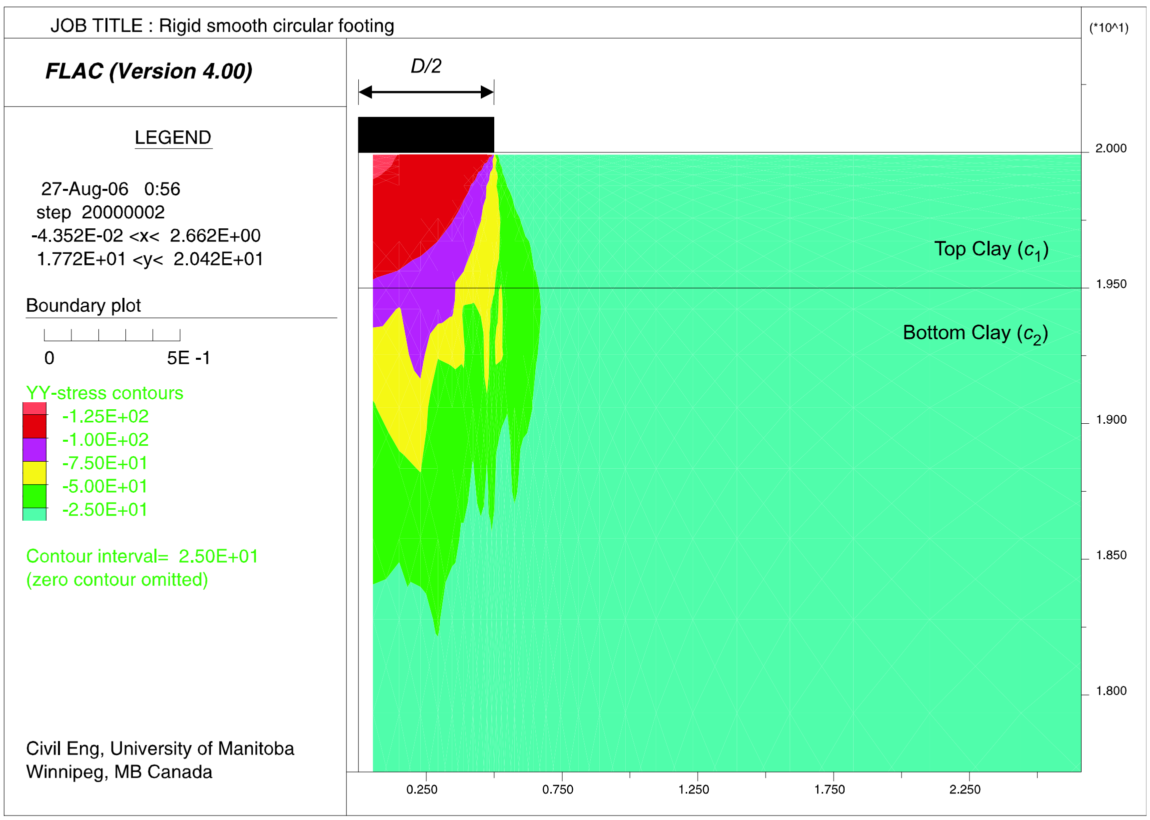

Figure A.396: Vertical stress (σ_{yy}) contours for a rigid smooth circular footing on soft clay over strong clay for 40 × 30 grid model, $H/D = 0.5$, $c_1/c_2 = 0.5$.

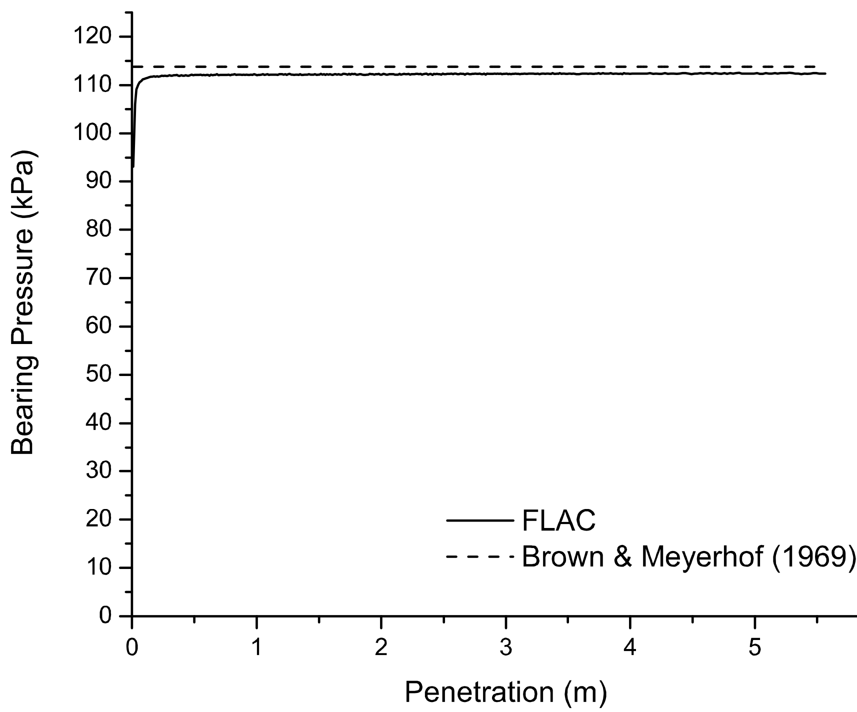

Figure A.397: Bearing pressure versus penetration curve for a rigid smooth circular footing on soft clay over strong clay for 40 × 30 grid model, $H/D = 0.5$, $c_1/c_2 = 0.5$.

Case 5: $c_1/c_2 = 1/3$ or $c_2/c_1 = 3$ - Small Deformation Analysis

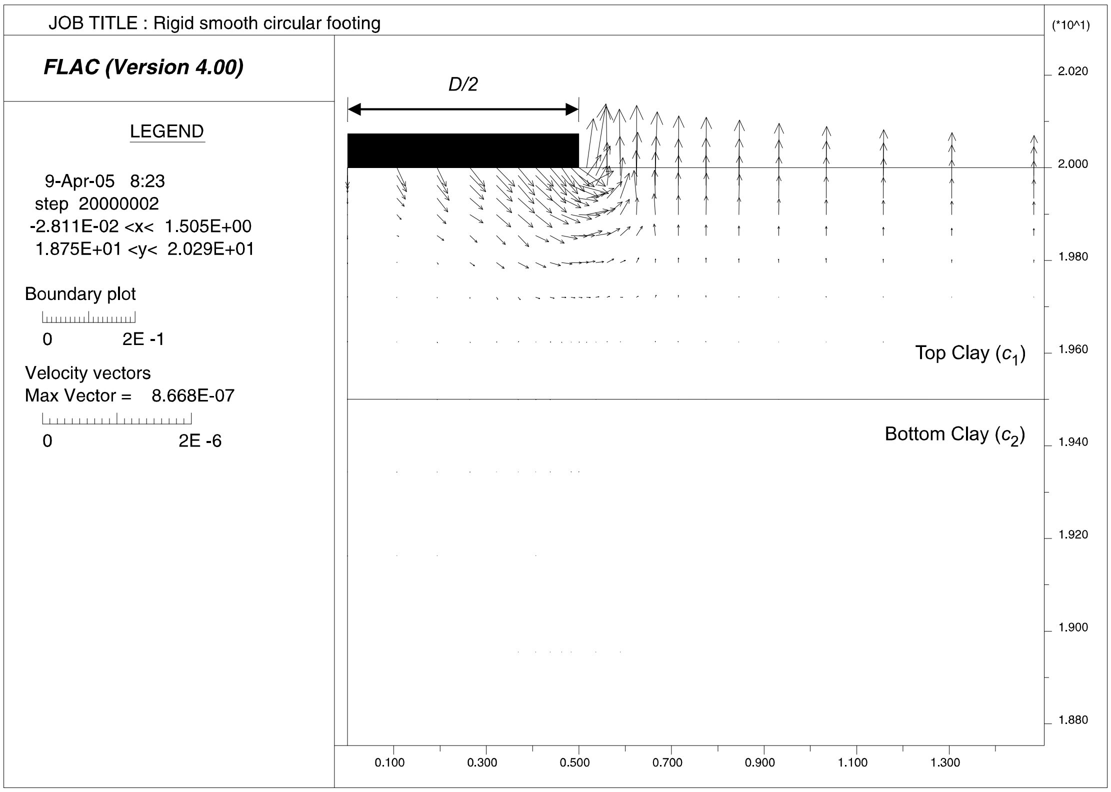

Figure A.398: Velocity vectors for a rigid smooth circular footing soft clay over strong clay for 40×30 grid model, $H/D = 0.5$, $c_1/c_2 = 1/3$.

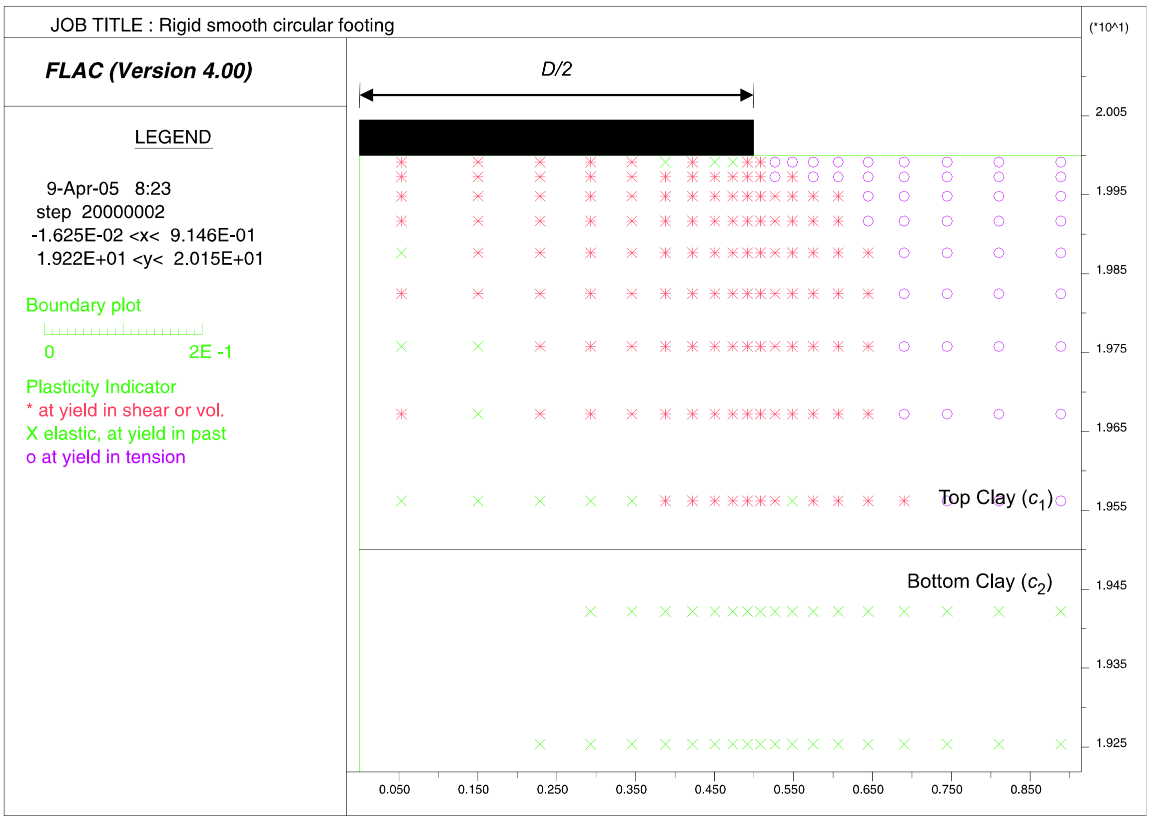

Figure A.399: Plasticity state indicators for a rigid smooth circular footing on soft clay over strong clay for 40×30 grid model, $H/D = 0.5$, $c_1/c_2 = 1/3$.

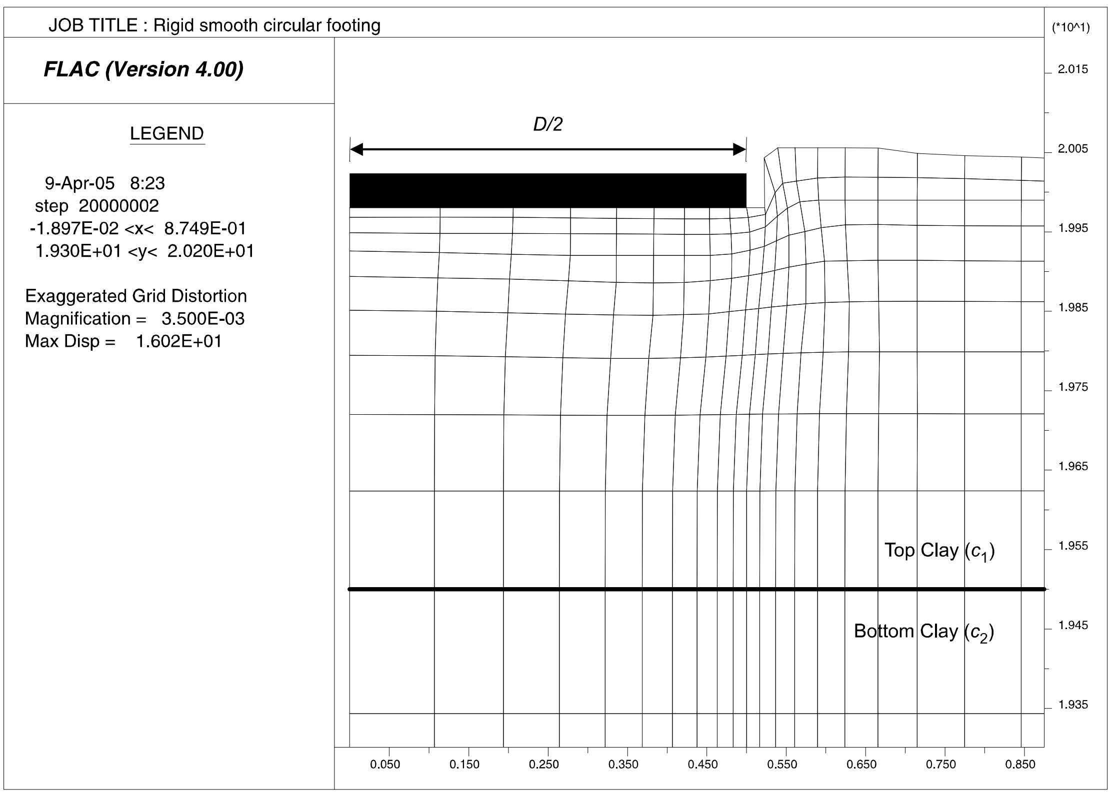

Figure A.400: Magnified grid for a rigid smooth circular footing on soft clay over strong clay for 40×30 grid model, $H/D = 0.5$, $c_1/c_2 = 1/3$.

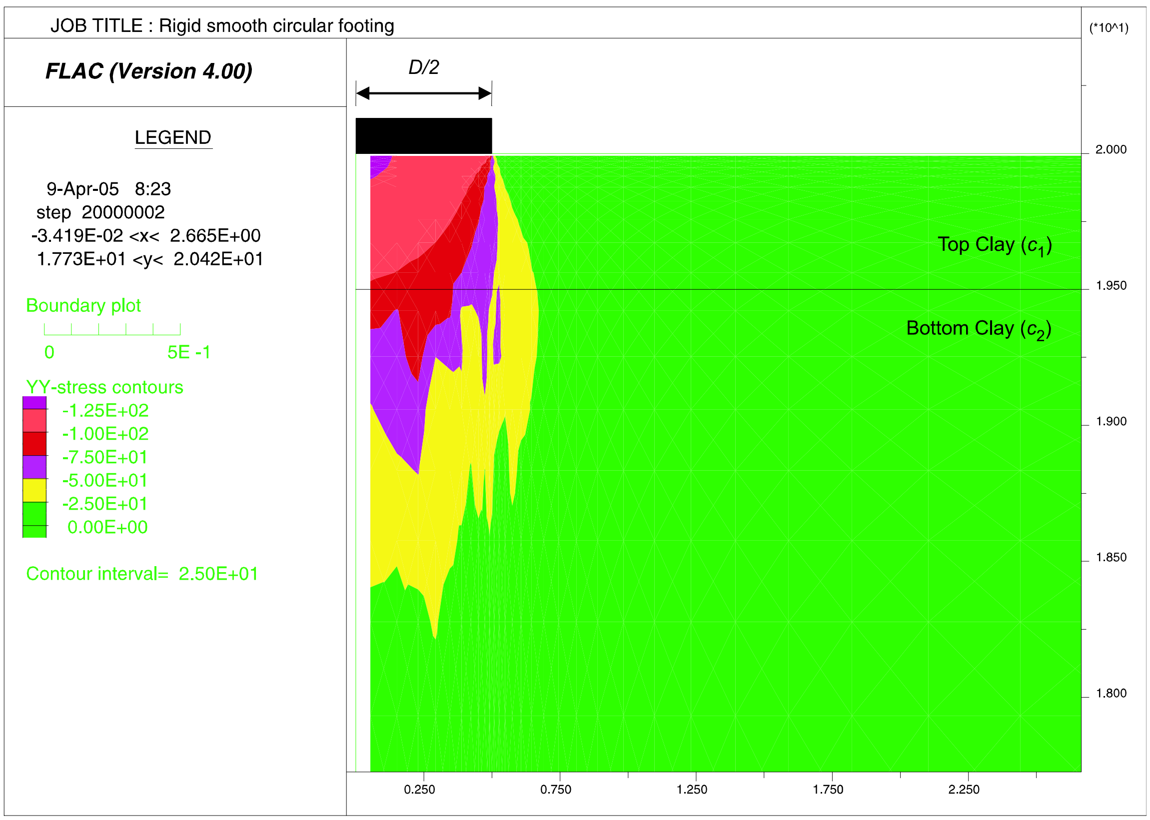

Figure A.401: Vertical stress (σ_{yy}) contours for a rigid smooth circular footing on soft clay over strong clay for 40 × 30 grid model, $H/D = 0.5$, $c_1/c_2 = 1/3$.

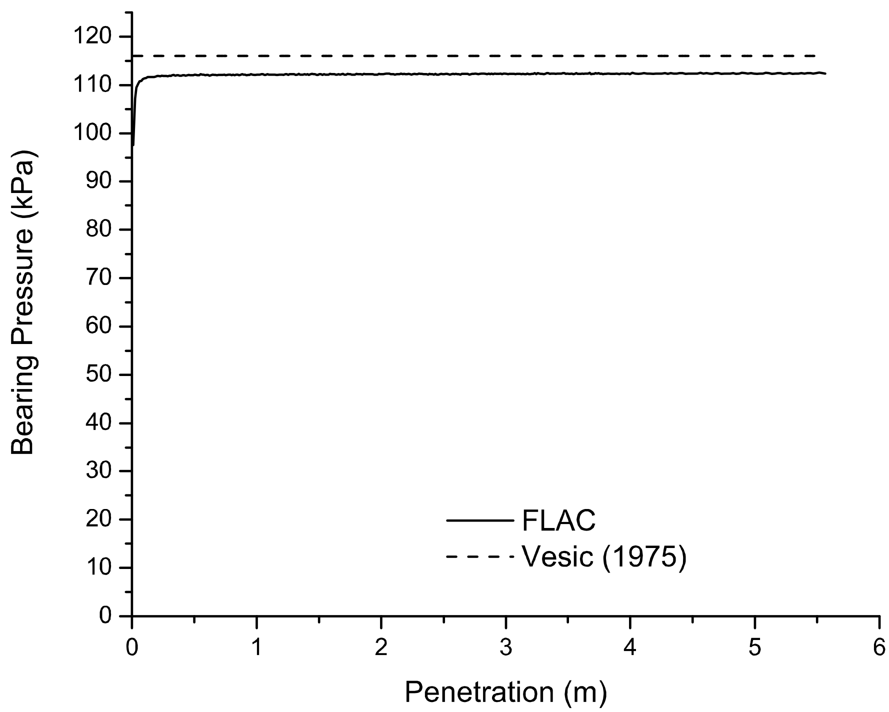

Figure A.402: Bearing pressure versus penetration curve for a rigid smooth circular footing on soft clay over strong clay for 40×30 grid model, $H/D = 0.5$, $c_1/c_2 = 1/3$.

Case 6: $c_1/c_2 = 0.2$ or $c_2/c_1 = 5$ - Small Deformation Analysis

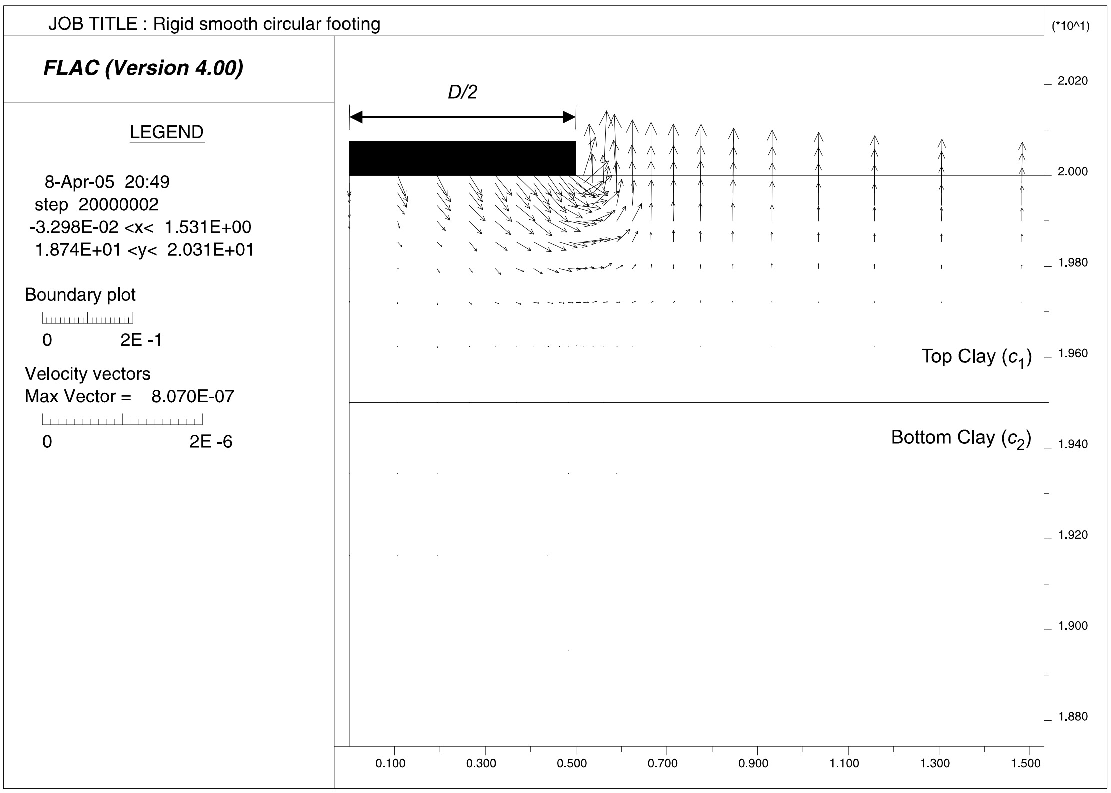

Figure A.403: Velocity vectors for a rigid smooth circular footing on soft clay over strong clay for 40×30 grid model, $H/D = 0.5$, $c_1/c_2 = 0.2$.

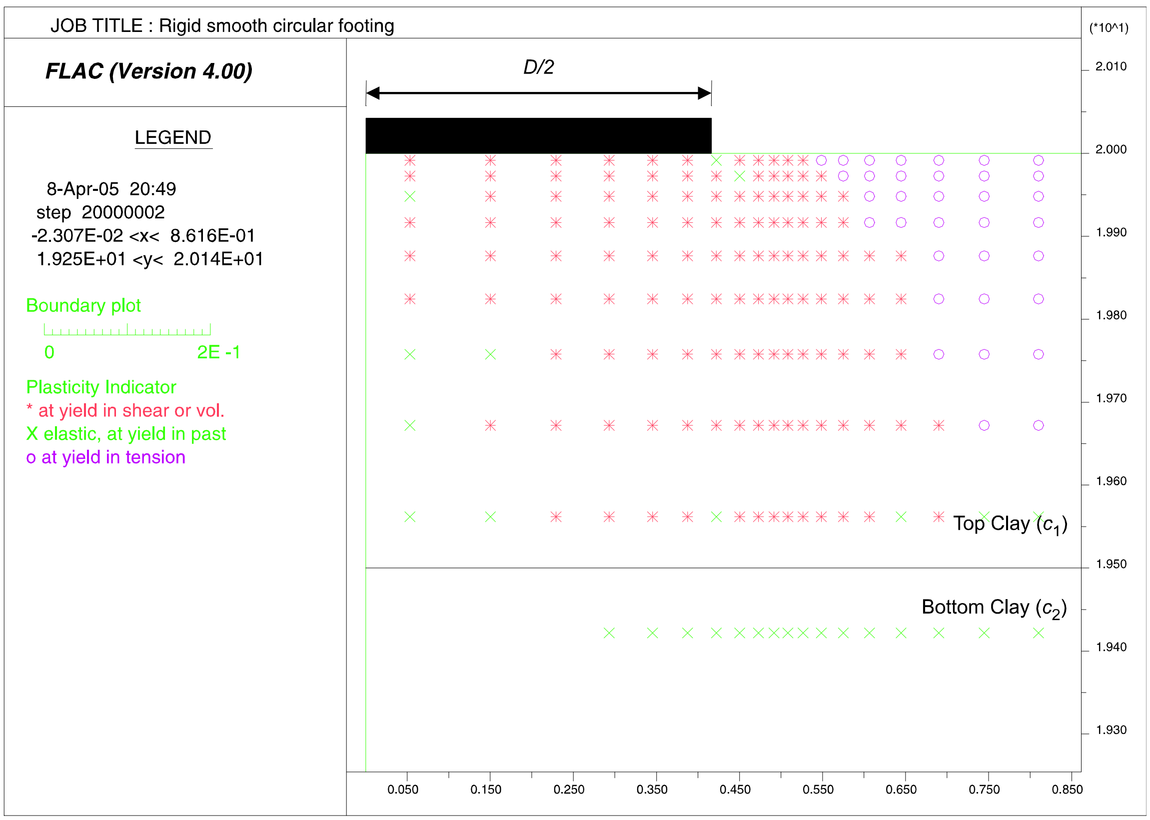

Figure A.404: Plasticity state indicators for a rigid smooth circular footing on soft clay over strong clay for 40 × 30 grid model, $H/D = 0.5$, $c_1/c_2 = 0.2$.

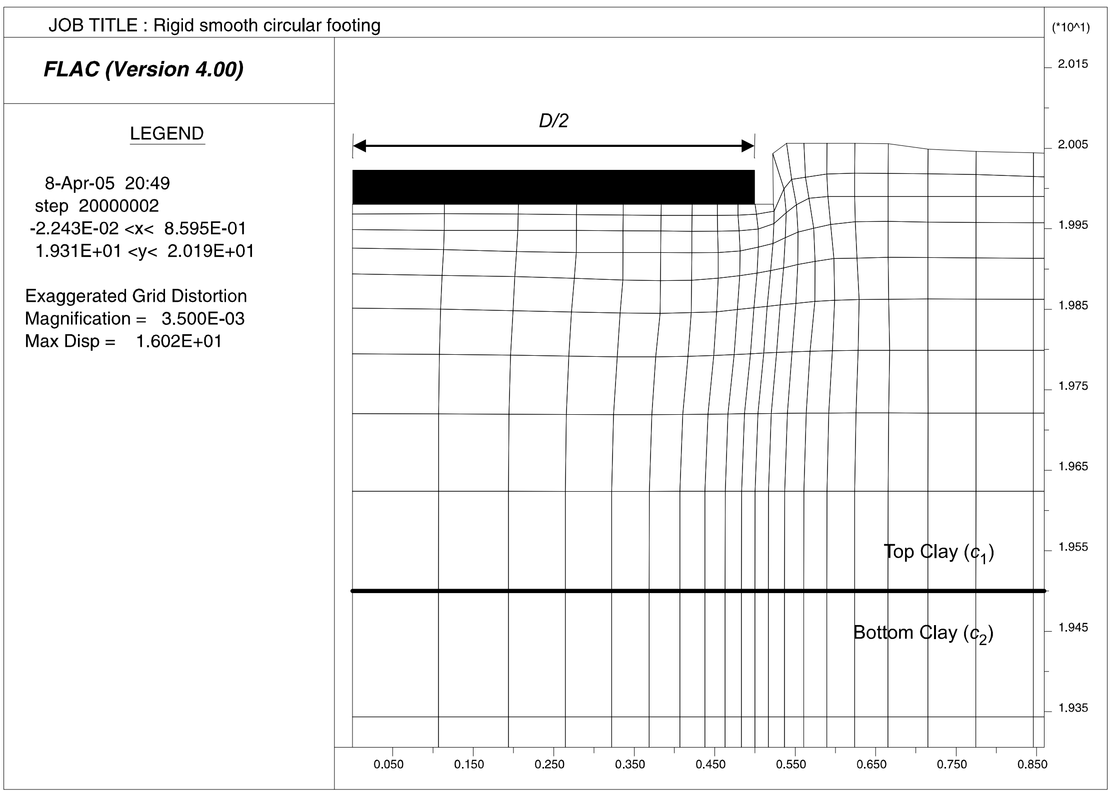

Figure A.405: Magnified grid for a rigid smooth circular footing on soft clay over strong clay for 40×30 grid model, $H/D = 0.5$, $c_1/c_2 = 0.2$.

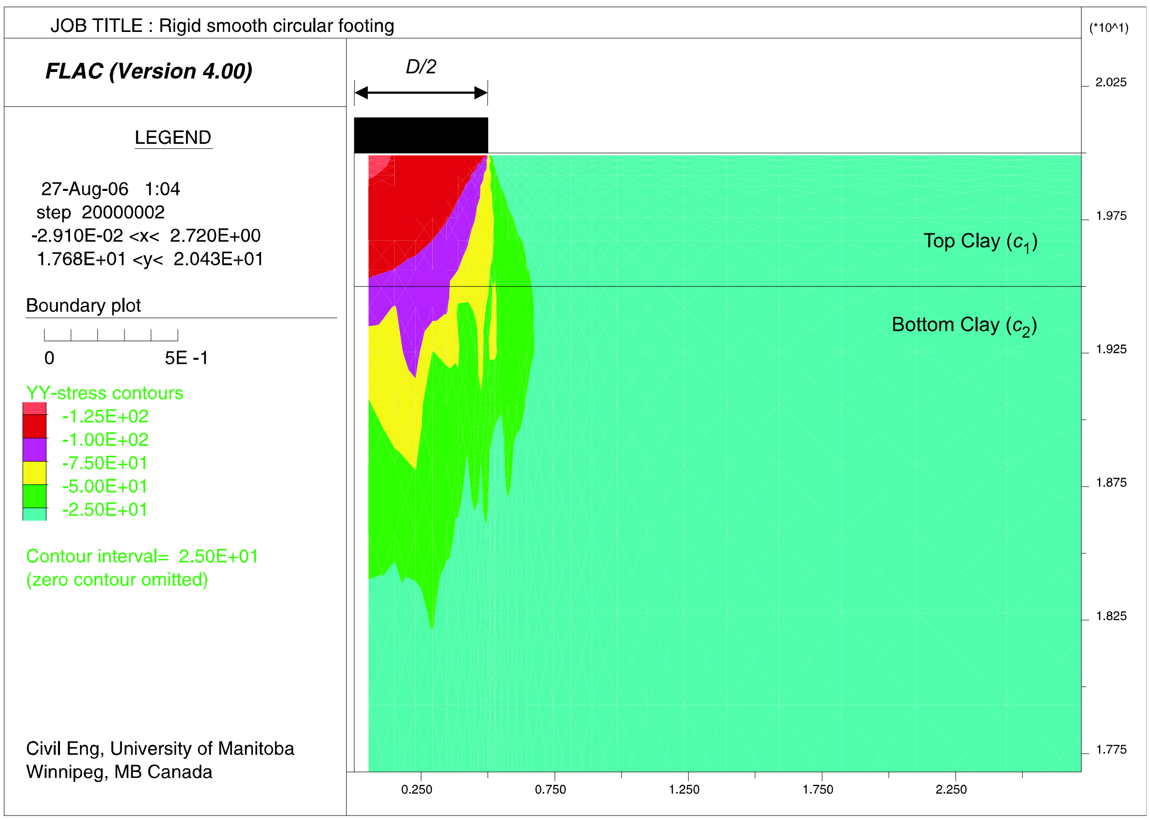

Figure A.406: Vertical stress (σ_{yy}) contours for a rigid smooth circular footing on soft clay over strong clay for 40 × 30 grid model, $H/D = 0.5$, $c_1/c_2 = 0.2$.

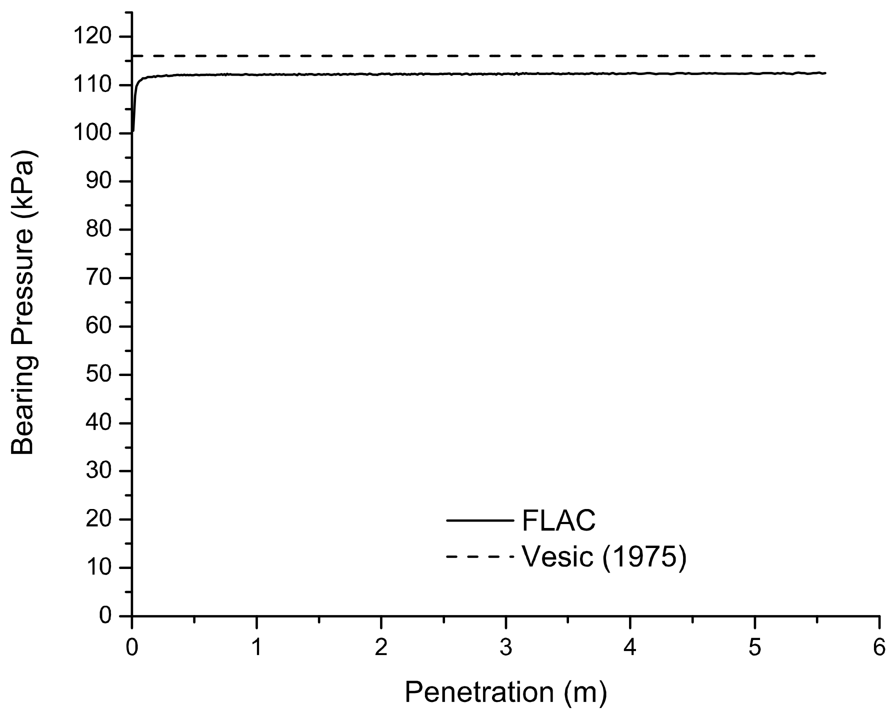

Figure A.407: Bearing pressure versus penetration curve for a rigid smooth circular footing on soft clay over strong clay for 40×30 grid model, $H/D = 0.5$, $c_1/c_2 = 0.2$.

Case 7: $c_1/c_2 = 0.1$ or $c_2/c_1 = 10$ - Small Deformation Analysis

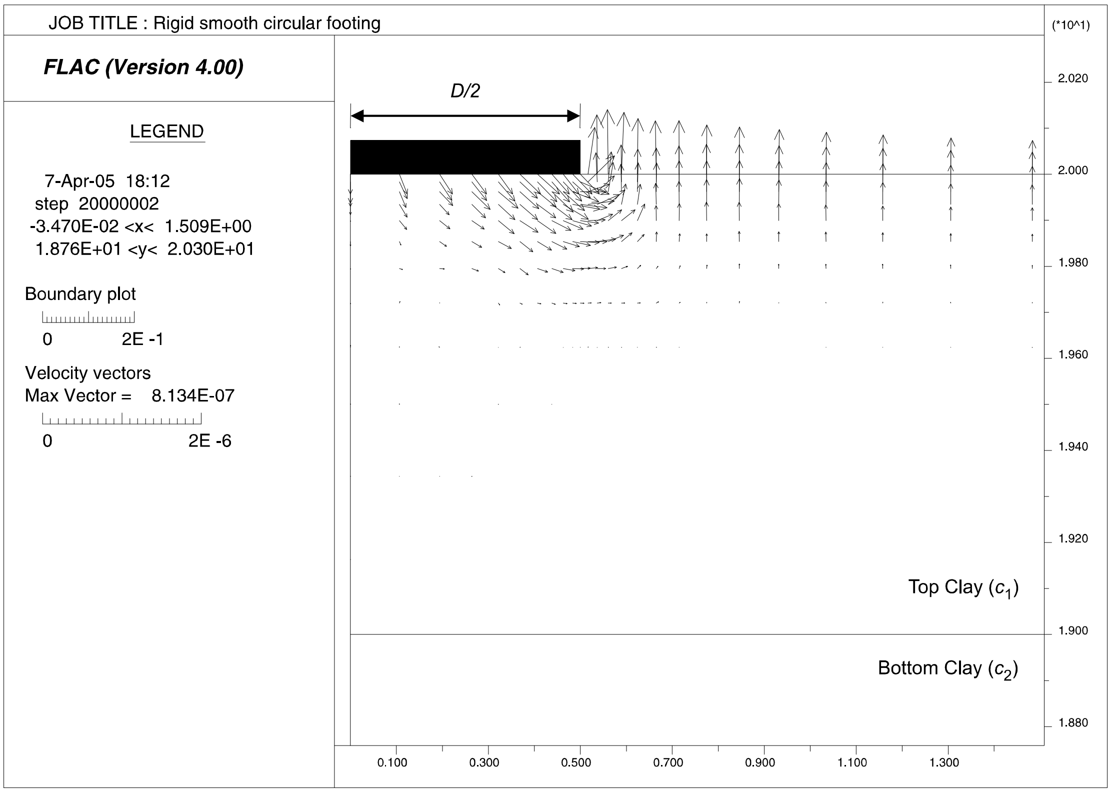

Figure A.408: Velocity vectors for a rigid smooth circular footing on soft clay over strong clay for 40×30 grid model, $H/D = 0.5$, $c_1/c_2 = 0.1$.

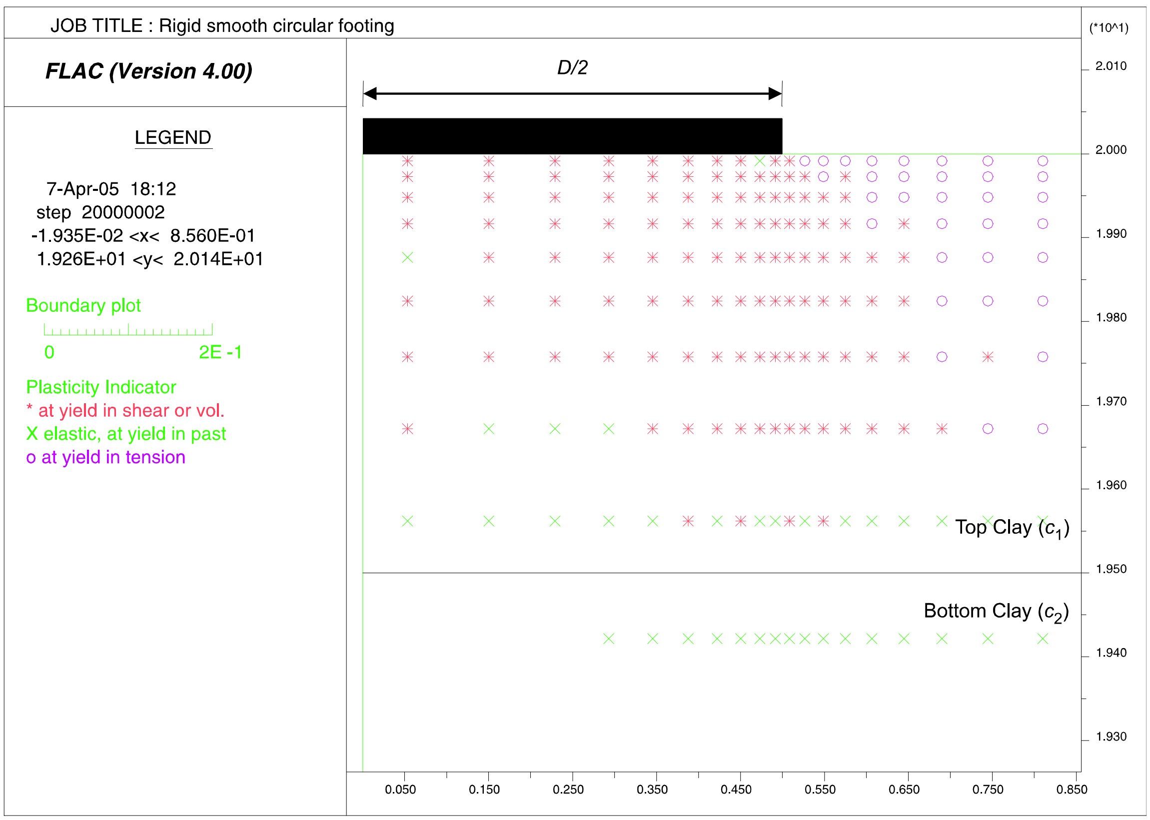

Figure A.409: Plasticity state indicators for a rigid smooth circular footing on soft clay over strong clay for 40 × 30 grid model, $H/D = 0.5$, $c_1/c_2 = 0.1$.

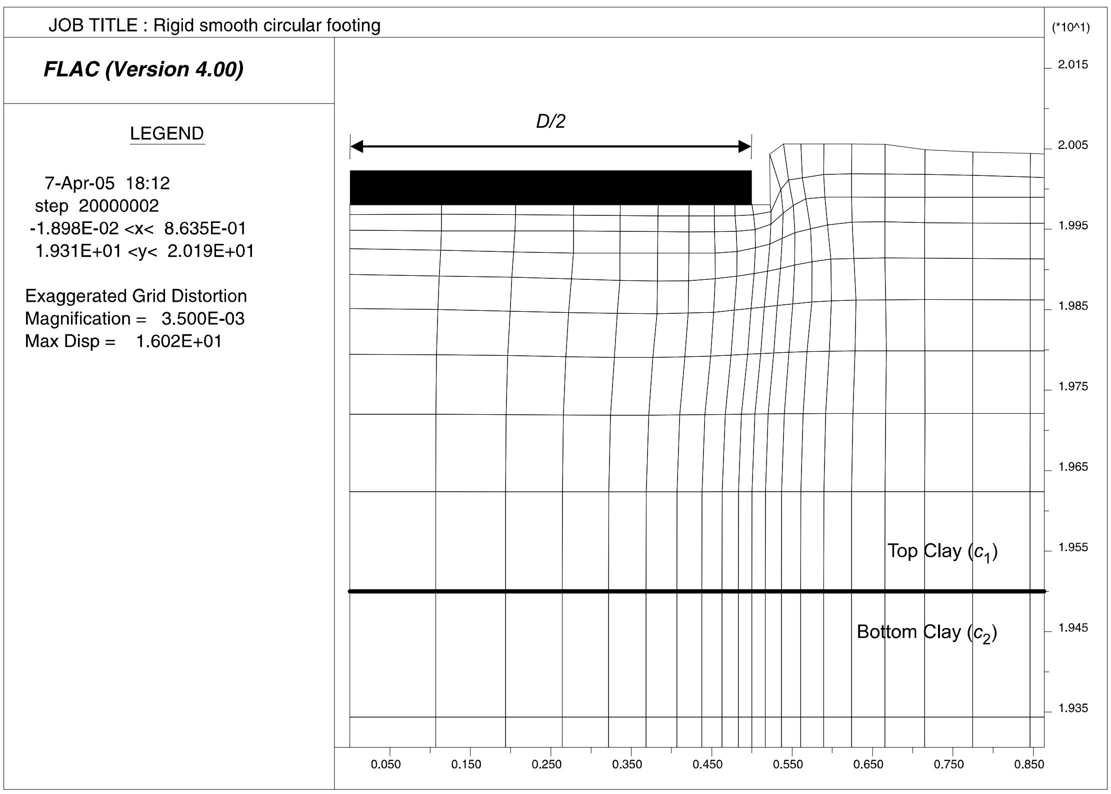

Figure A.410: Magnified grid for a rigid smooth circular footing on soft clay over strong clay for 40 × 30 grid model, $H/D = 0.5$, $c_1/c_2 = 0.1$.

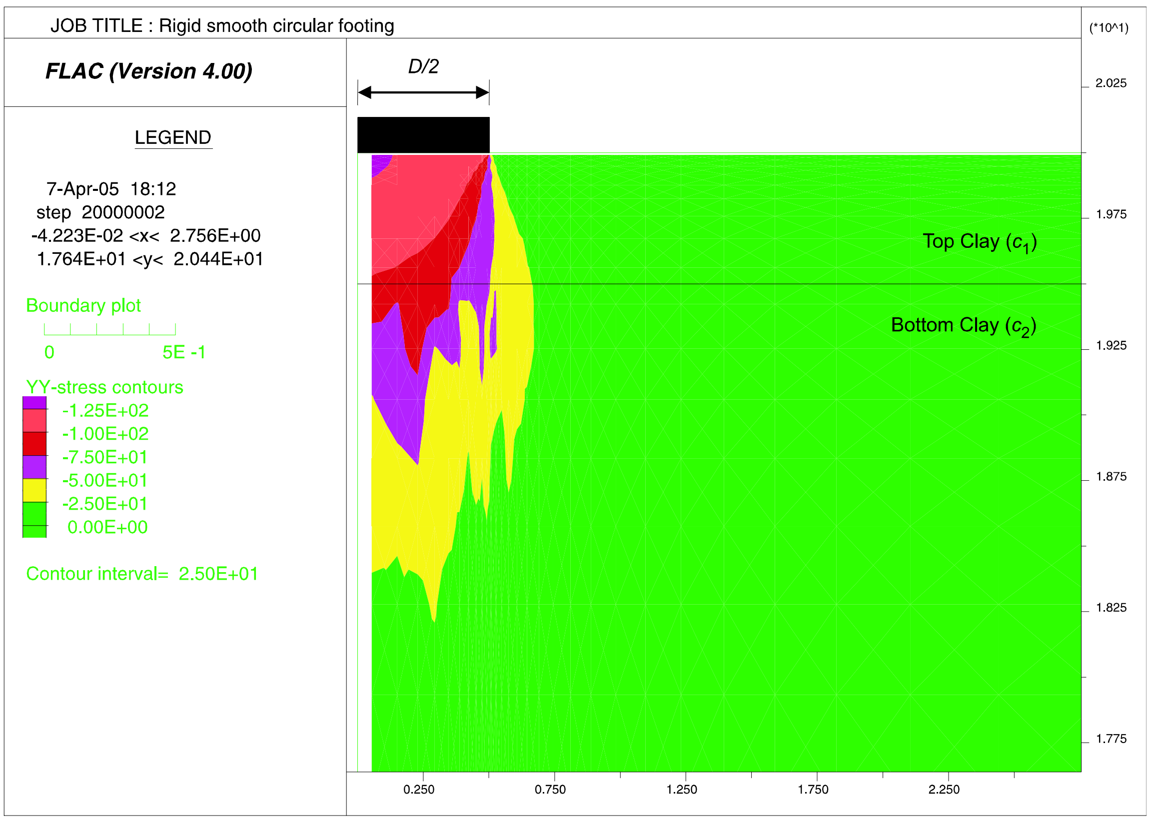

Figure A.411: Vertical stress (σ_{yy}) contours for a rigid smooth circular footing on soft clay over strong clay for 40×30 grid model, $H/D = 0.5$, $c_1/c_2 = 0.1$.

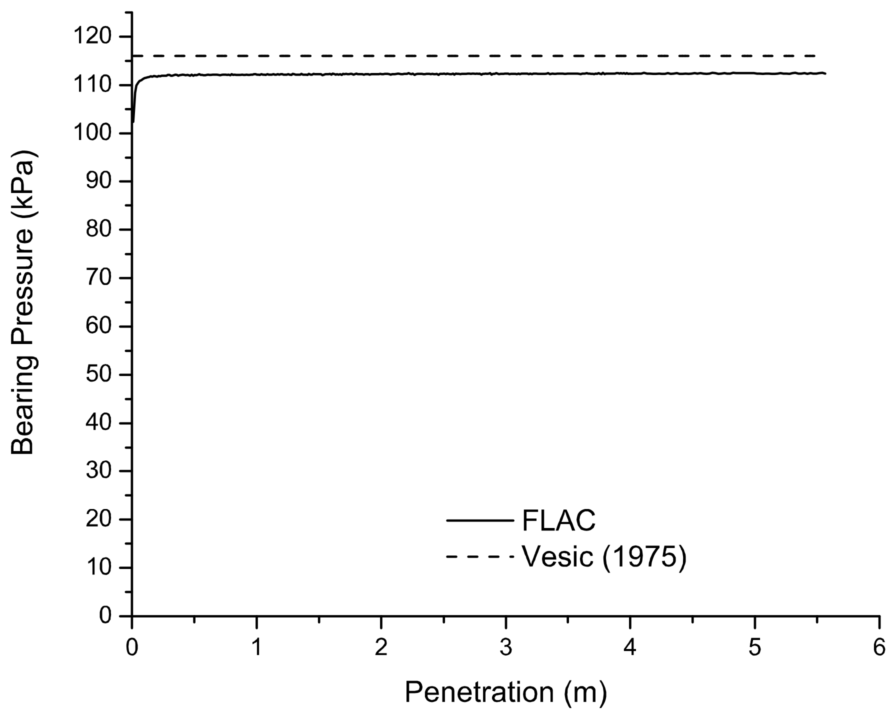

Figure A.412: Bearing pressure versus penetration curve for a rigid smooth circular footing on soft clay over strong clay for 40 × 30 grid model, $H/D = 0.5$, $c_1/c_2 = 0.1$.

A.4.3 Rigid Smooth Circular Footing on Soft over Strong Clay ($H/D = 0.25$)

Case 2: $c_1/c_2 = 0.8$ or $c_2/c_1 = 1.25$ - Small Deformation Analysis

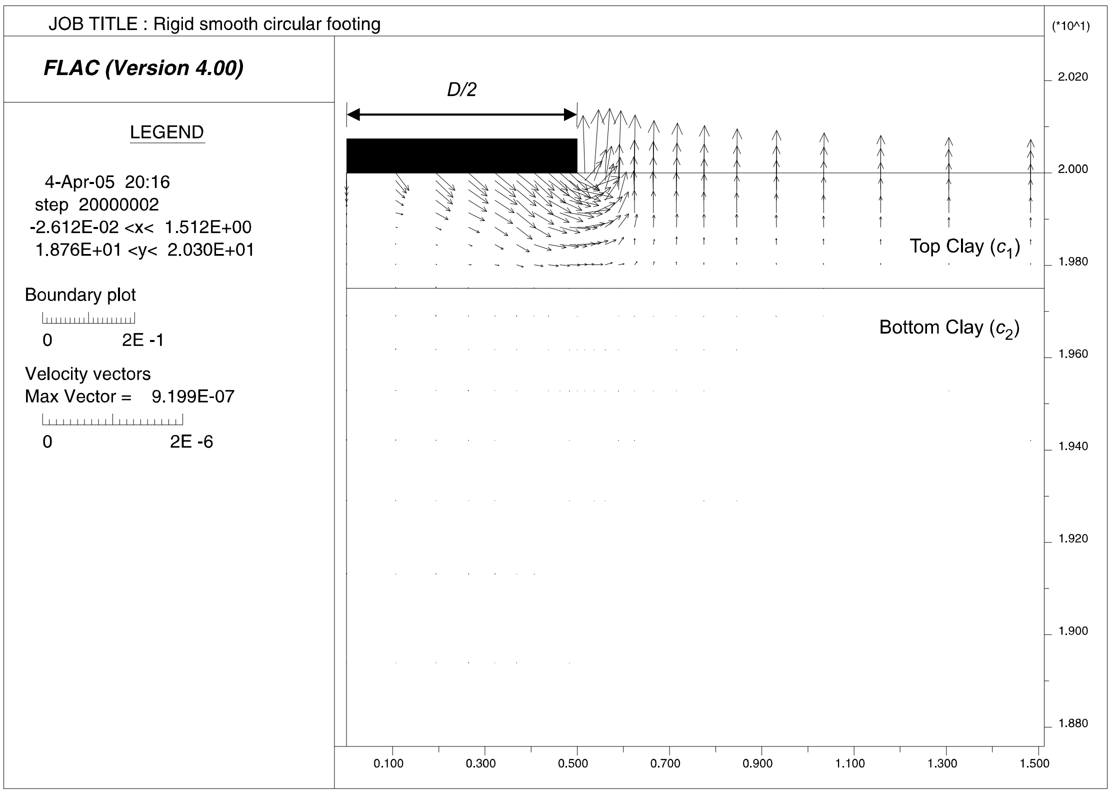

Figure A.413: Velocity vectors for a rigid smooth circular footing on soft over strong clay for 40×30 grid model, $H/D = 0.25$, $c_1/c_2 = 0.8$.

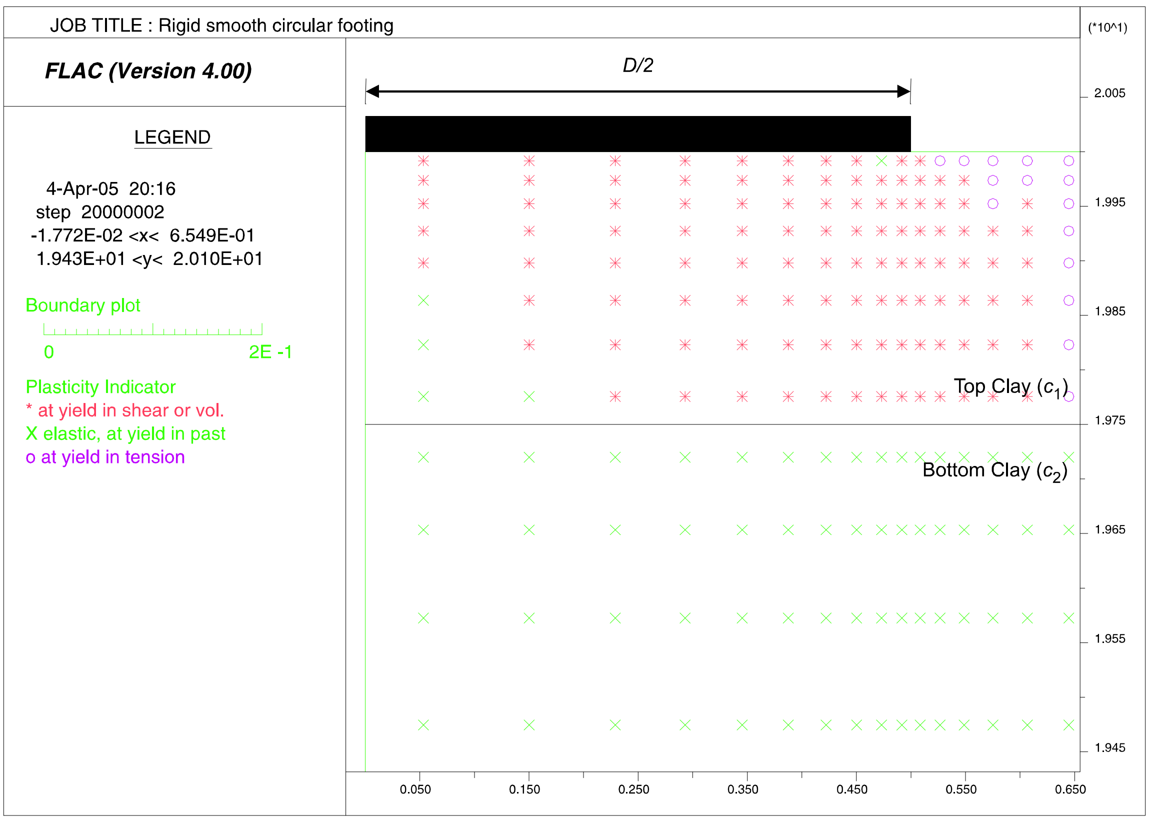

Figure A.414: Plasticity indicators for a rigid smooth circular footing on soft over strong clay for 40×30 grid model, $H/D = 0.25$, $c_1/c_2 = 0.8$.

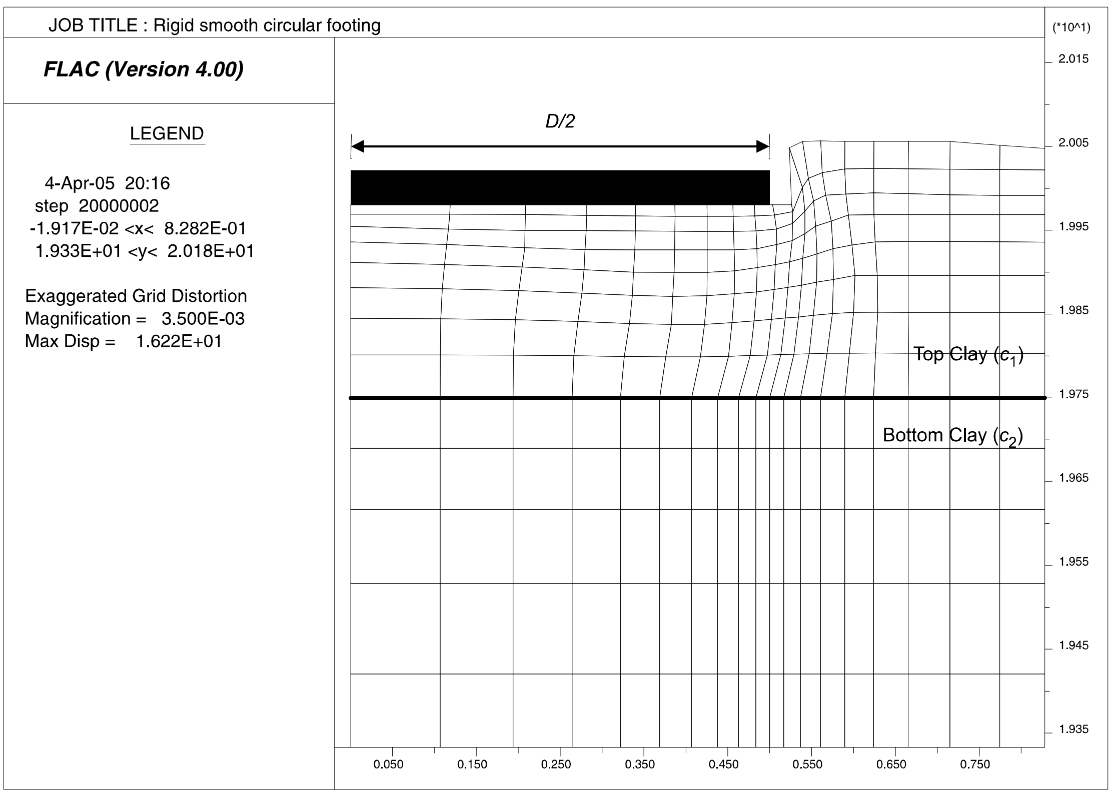

Figure A.415: Magnified grid for a rigid smooth circular footing on soft over strong clay for 40 × 30 grid model, $H/D = 0.25$, $c_1/c_2 = 0.8$.

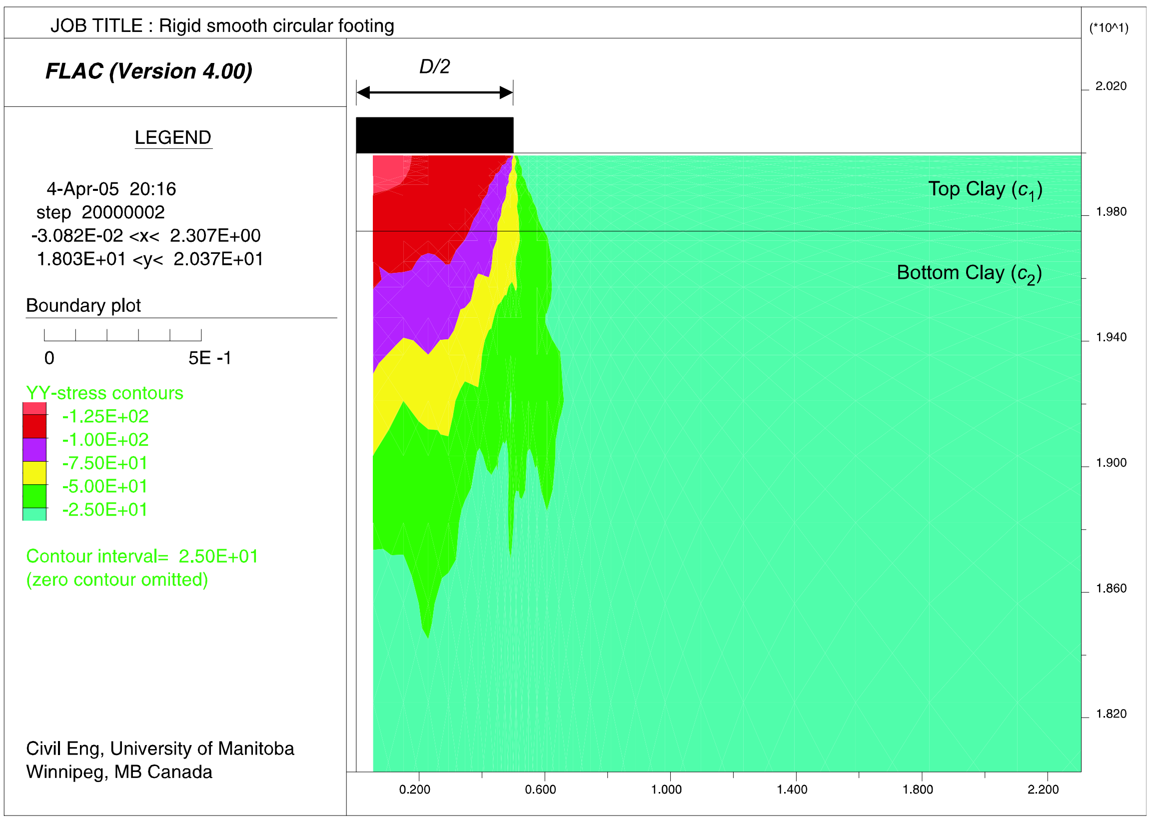

Figure A.416: Vertical stress (σ_{yy}) contours for a rigid smooth circular footing on soft over strong clay for 40×30 grid model, $H/D = 0.25$, $c_1/c_2 = 0.8$.

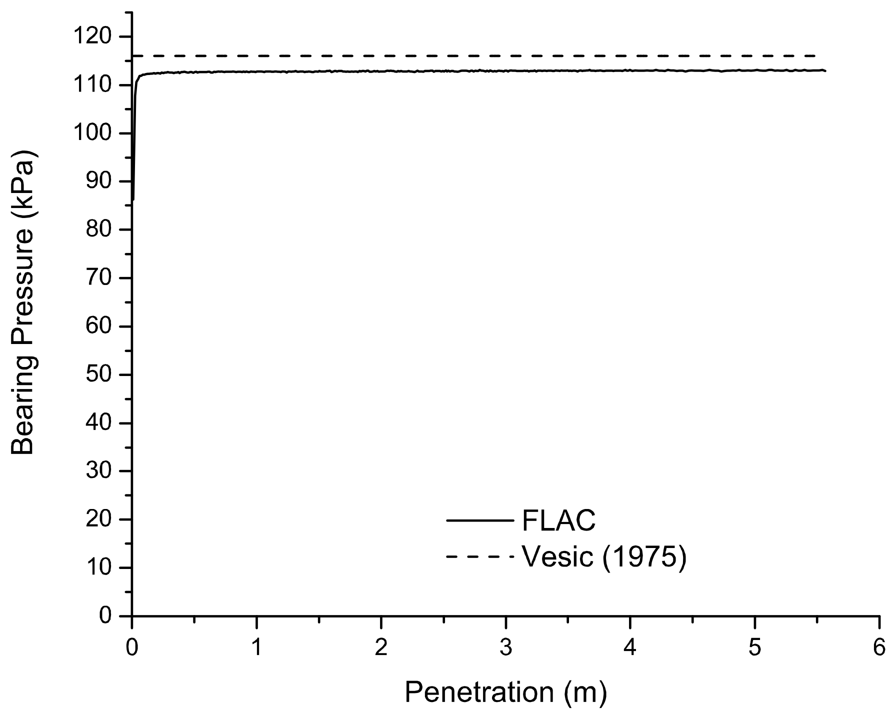

Figure A.417: Bearing pressure versus penetration curve for a rigid smooth circular footing on soft over strong clay for 40×30 grid model, $H/D = 0.25$, $c_1/c_2 = 0.8$.

Case 3: $c_1/c_2 = 2/3$ or $c_2/c_1 = 1.5$ - Small Deformation Analysis

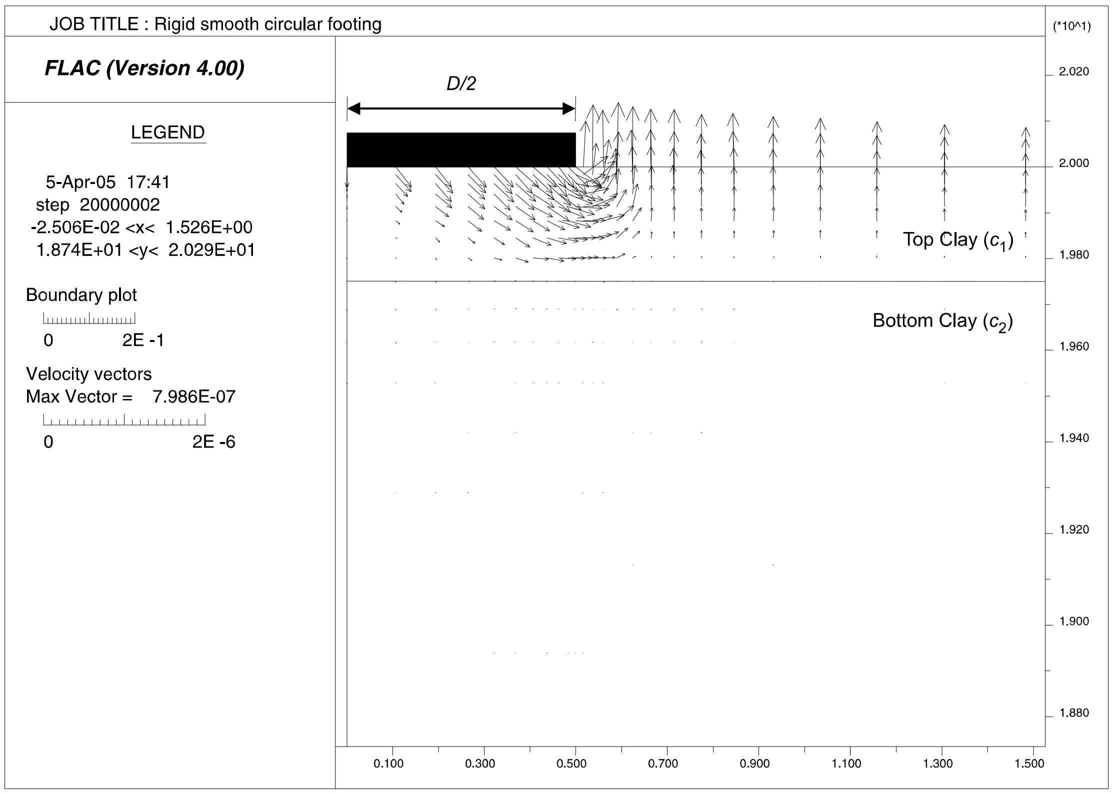

Figure A.418: Velocity vectors for a rigid smooth circular footing on soft over strong clay for 40×30 grid model, $H/D = 0.25$, $c_1/c_2 = 2/3$.

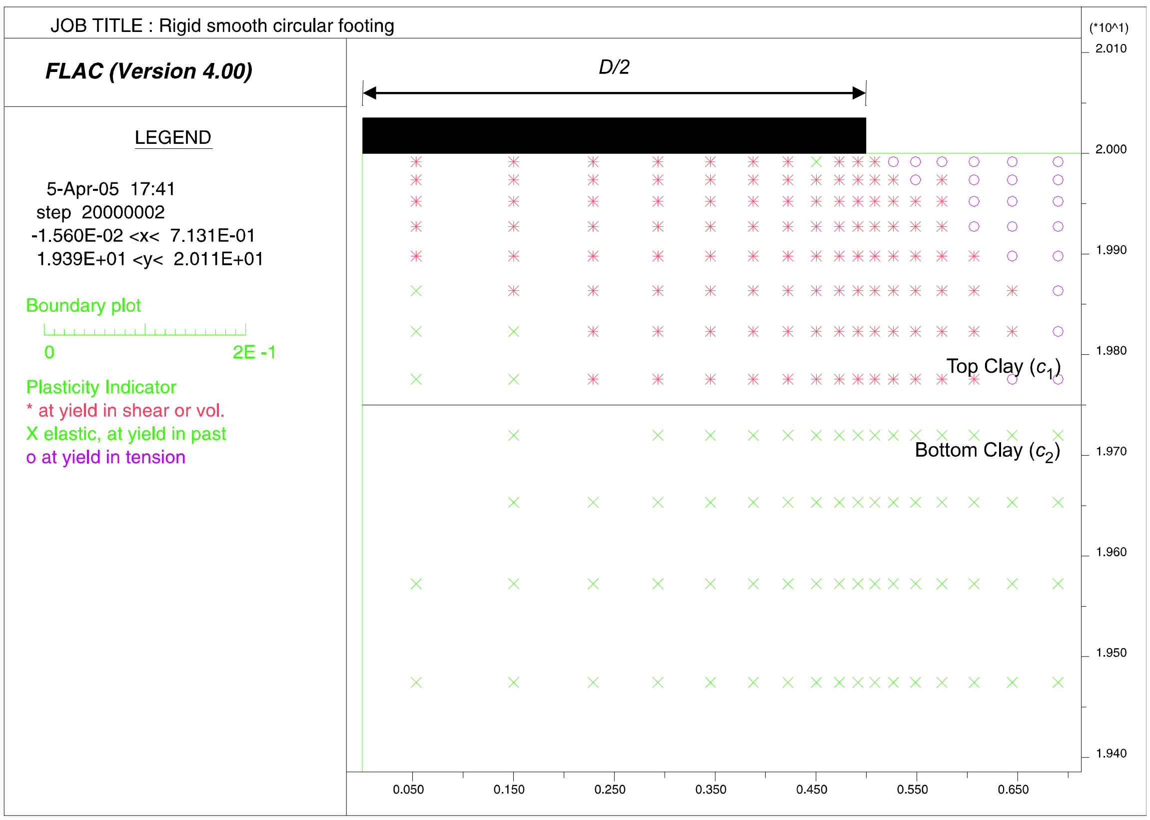

Figure A.419: Plasticity state indicators for a rigid smooth circular footing on soft over strong clay for 40 × 30 grid model, $H/D = 0.25$, $c_1/c_2 = 2/3$.

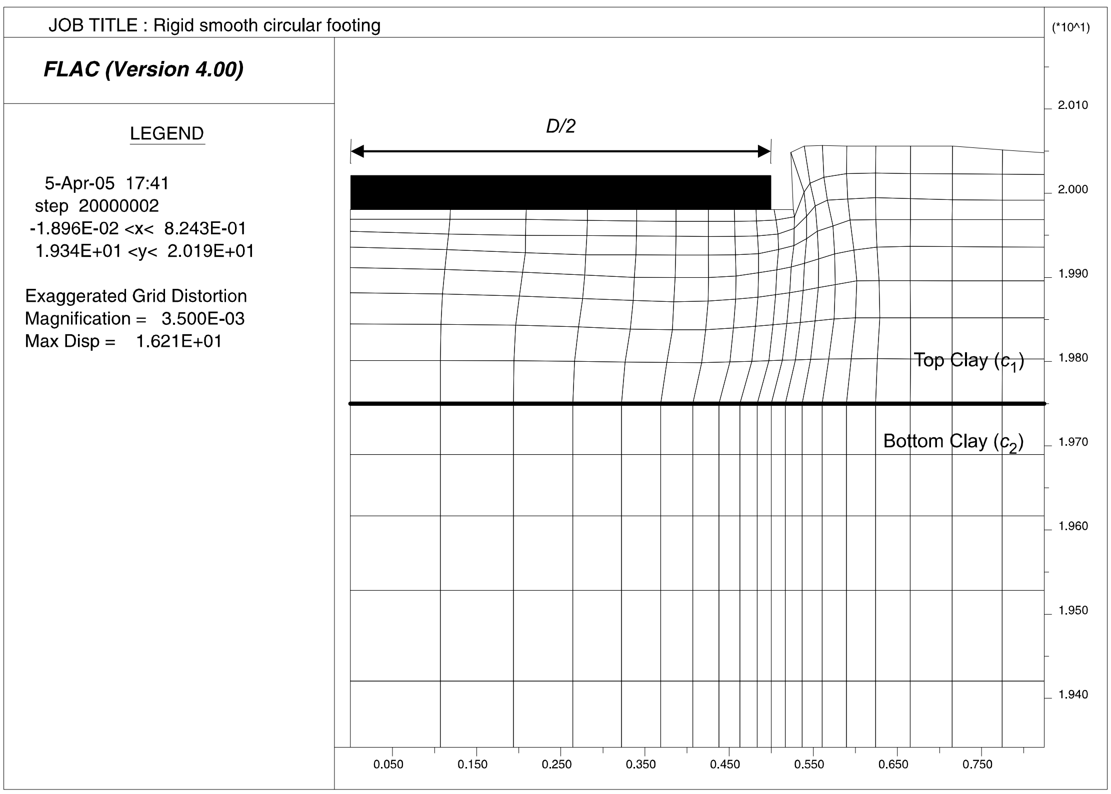

Figure A.420: Magnified grid for a rigid smooth circular footing on soft over strong clay for 40×30 grid model, $H/D = 0.25$, $c_1/c_2 = 2/3$.

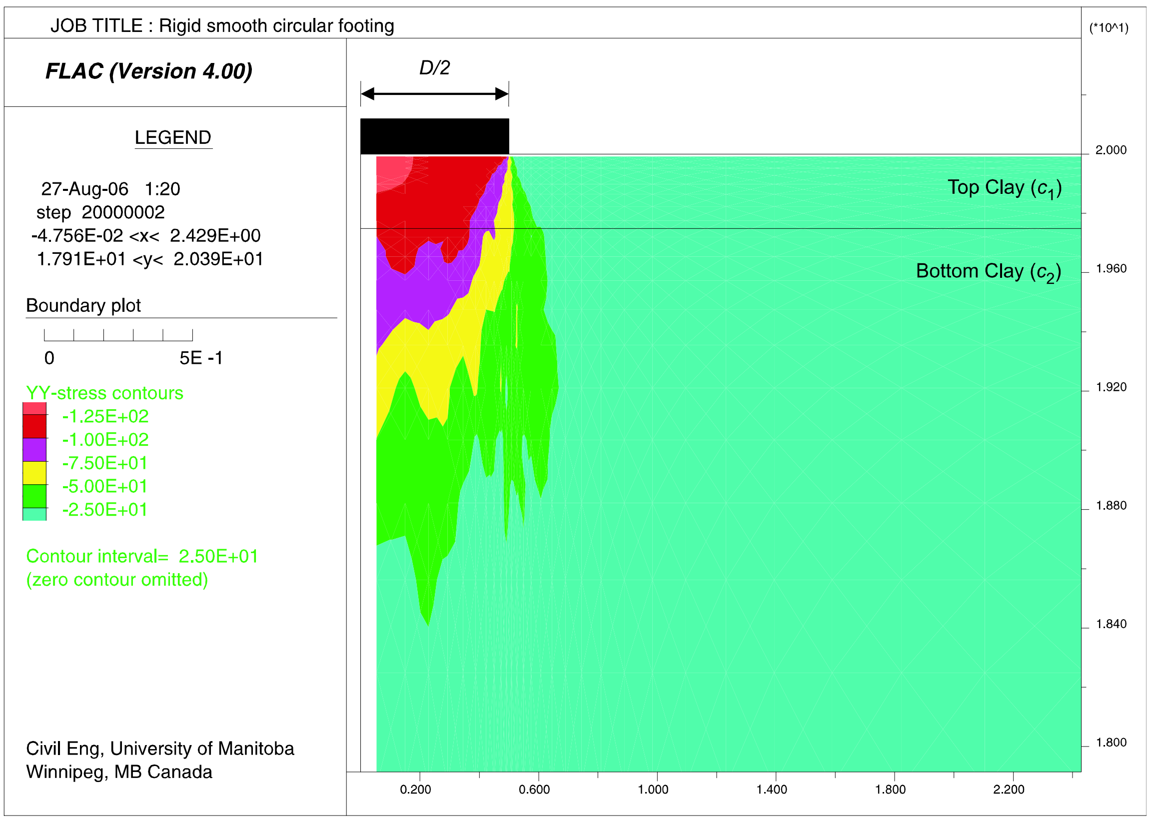

Figure A.421: Vertical stress (σ_{yy}) contours for a rigid smooth circular footing on soft over strong clay for 40×30 grid model, $H/D = 0.25$, $c_1/c_2 = 2/3$.

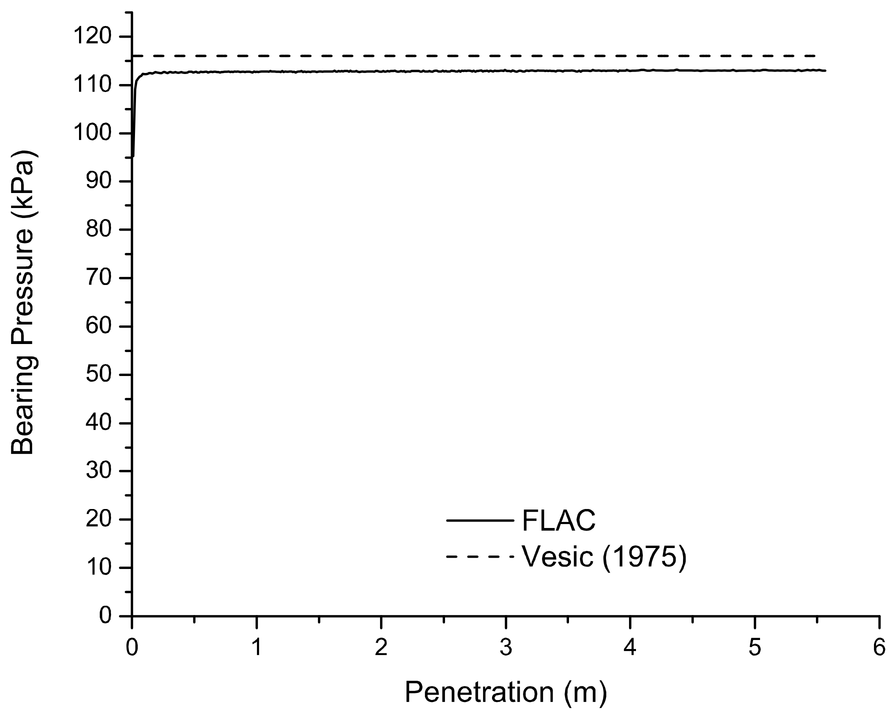

Figure A.422: Bearing pressure versus penetration curve for a rigid smooth circular footing on soft over strong clay for 40 × 30 grid model, $H/D = 0.25$, $c_1/c_2 = 2/3$.

Case 4: $c_1/c_2 = 0.5$ or $c_2/c_1 = 2$ - Small Deformation Analysis

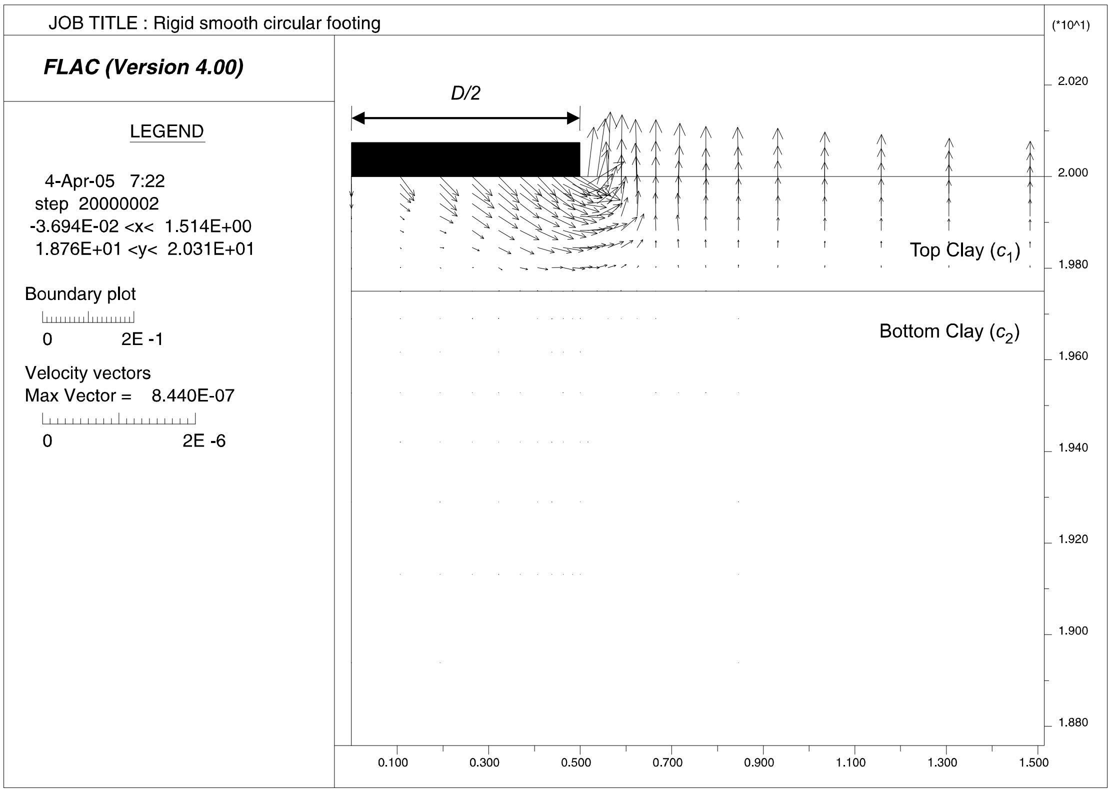

Figure A.423: Velocity vectors for a rigid smooth circular footing on soft clay over strong clay for 40×30 grid model, $H/D = 0.25$, $c_1/c_2 = 0.5$.

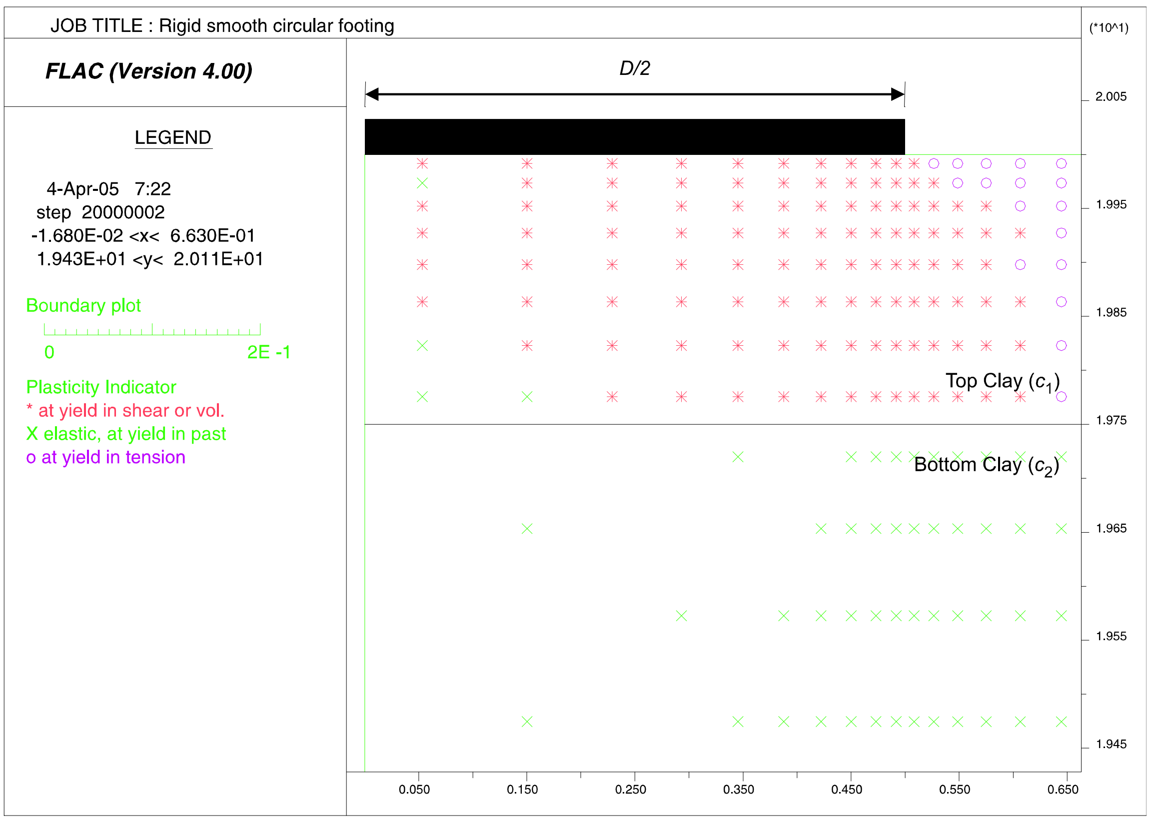

Figure A.424: Plasticity state indicators for a rigid smooth circular footing on soft clay over strong clay for 40 × 30 grid model, $H/D = 0.25$, $c_1/c_2 = 0.5$.

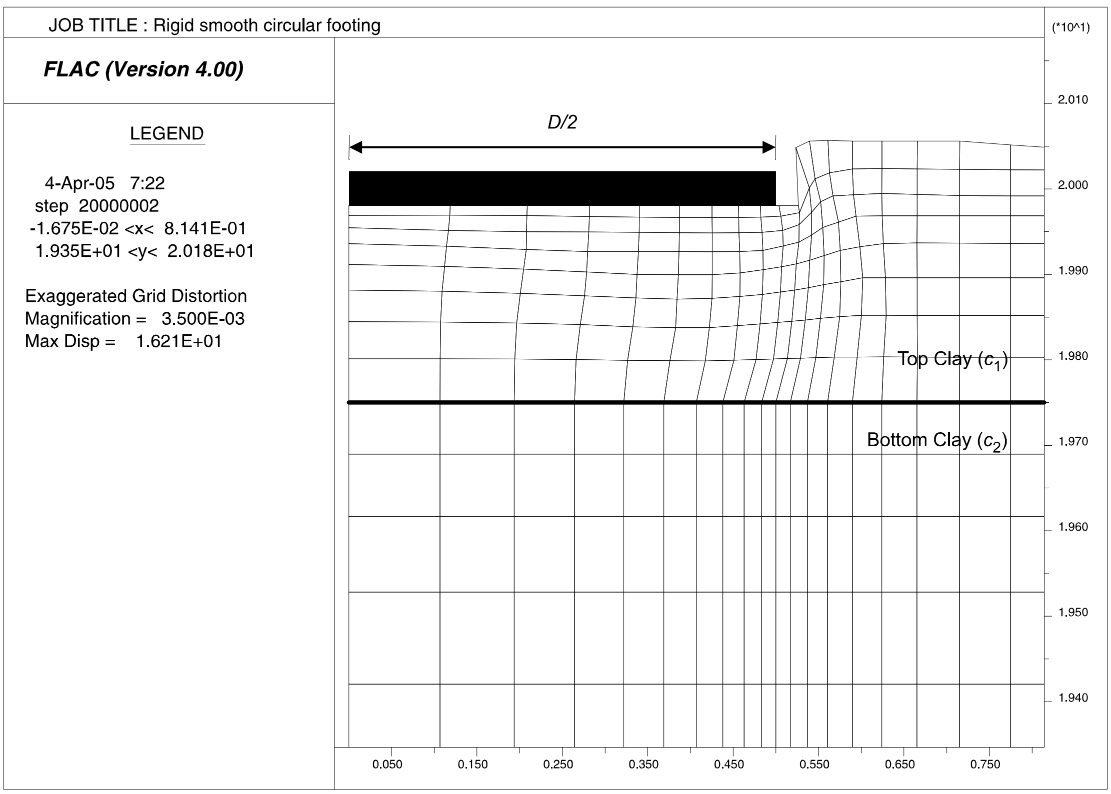

Figure A.425: Magnified grid for a rigid smooth circular footing on soft clay over strong clay for 40×30 grid model, $H/D = 0.25$, $c_2/c_1 = 0.5$.

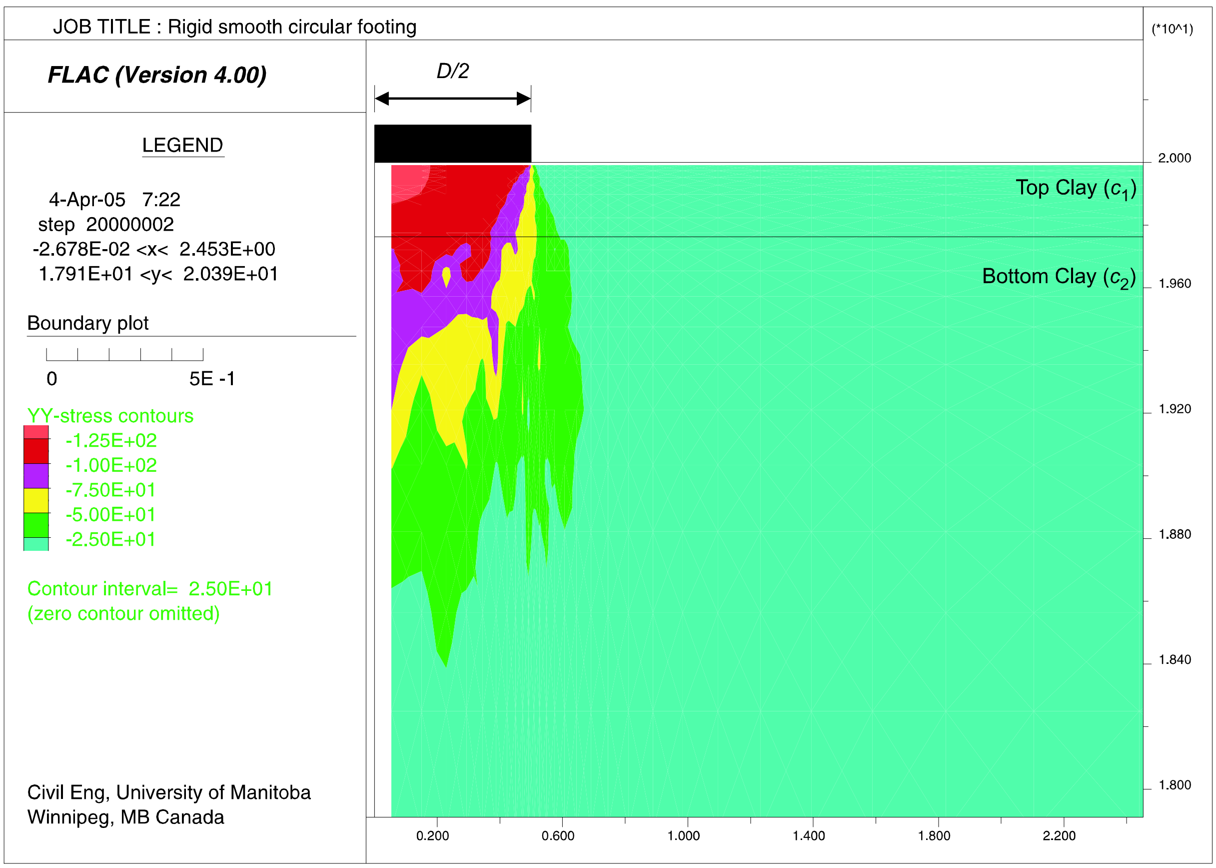

Figure A.426: Vertical stress (σ_{yy}) contours for a rigid smooth circular footing on soft clay over strong clay for 40×30 grid model, $H/D = 0.5$, $c_1/c_2 = 0.25$.

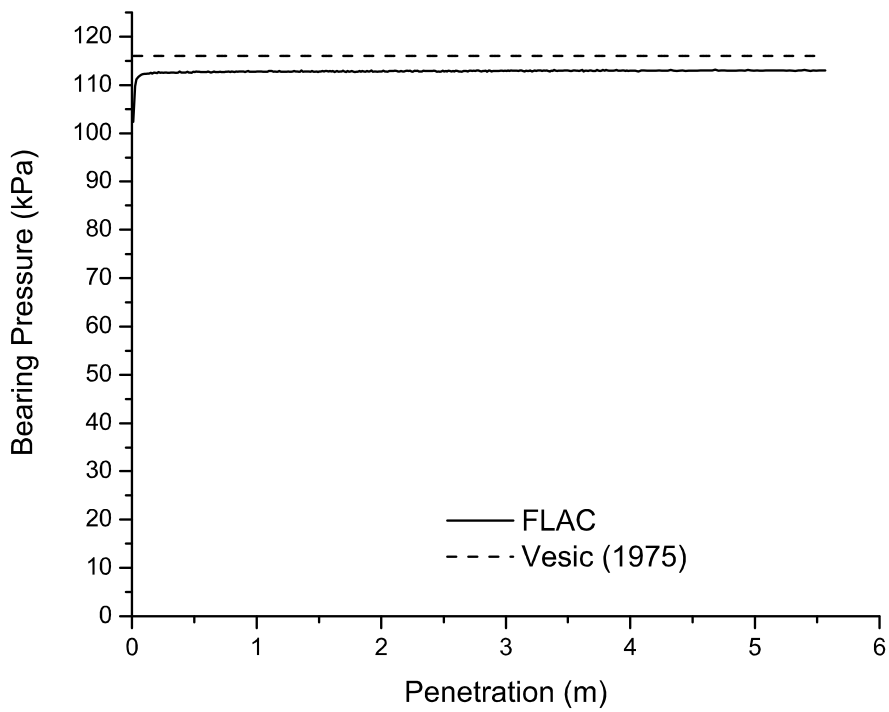

Figure A.427: Bearing pressure versus penetration curve for a rigid smooth circular footing on soft clay over strong clay for 40×30 grid model, $H/D = 0.5$, $c_1/c_2 = 0.25$.

Case 5: $c_1/c_2 = 1/3$ or $c_2/c_1 = 3$ - Small Deformation Analysis

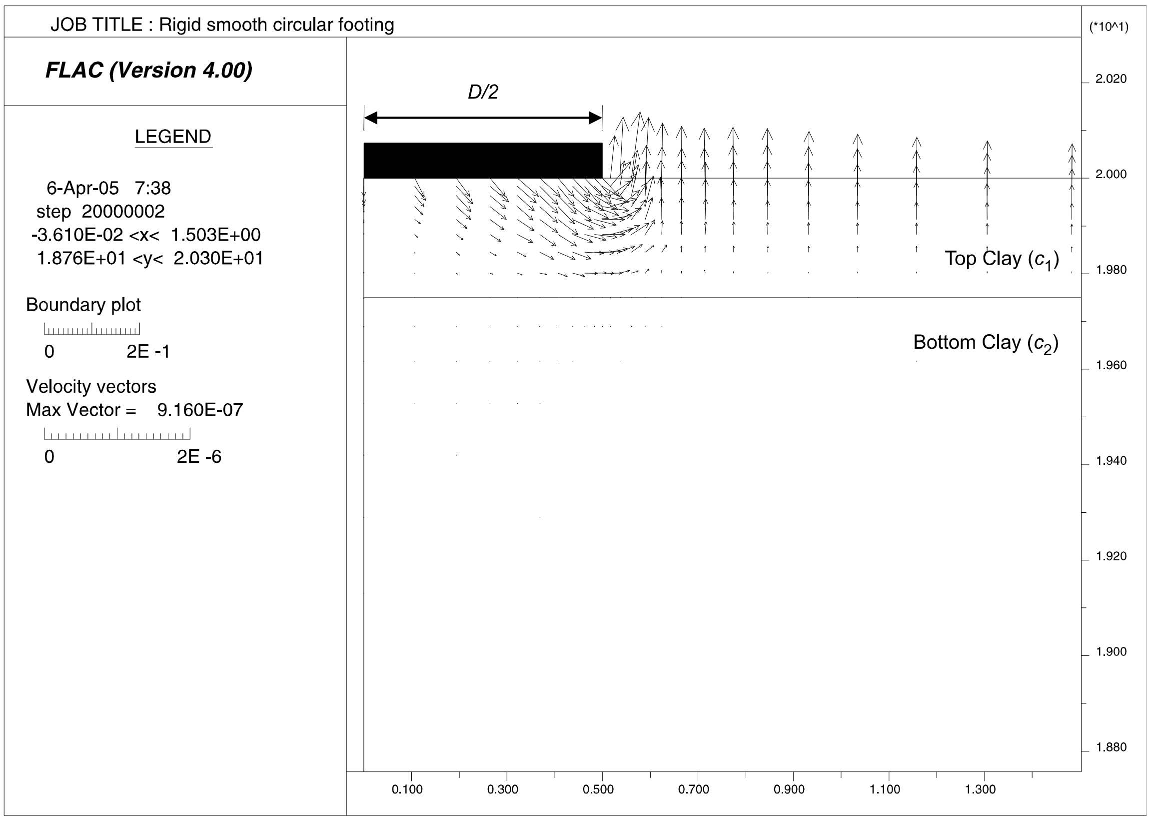

Figure A.428: Velocity vectors for a rigid smooth circular footing soft clay over strong clay for 40×30 grid model, $H/D = 0.25$, $c_1/c_2 = 1/3$.

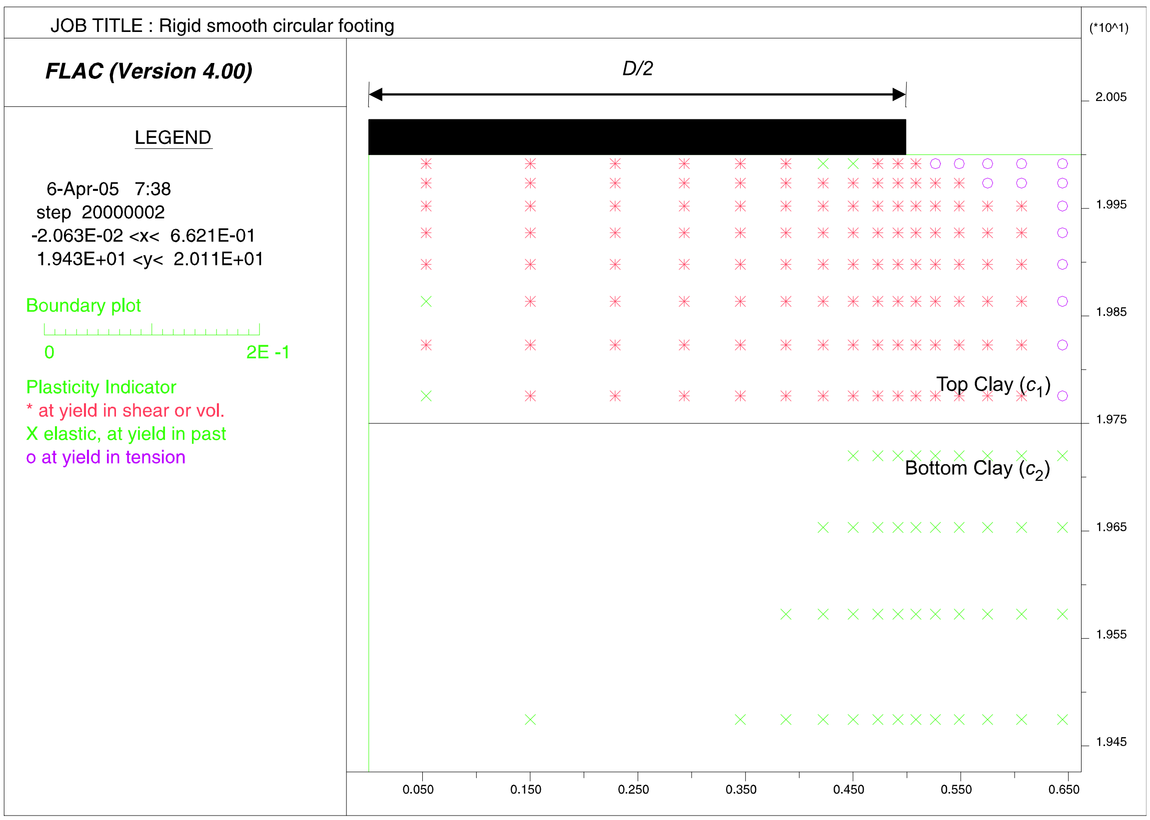

Figure A.429: Plasticity state indicators for a rigid smooth circular footing on soft clay over strong clay for 40 × 30 grid model, $H/D = 0.25$, $c_1/c_2 = 1/3$.

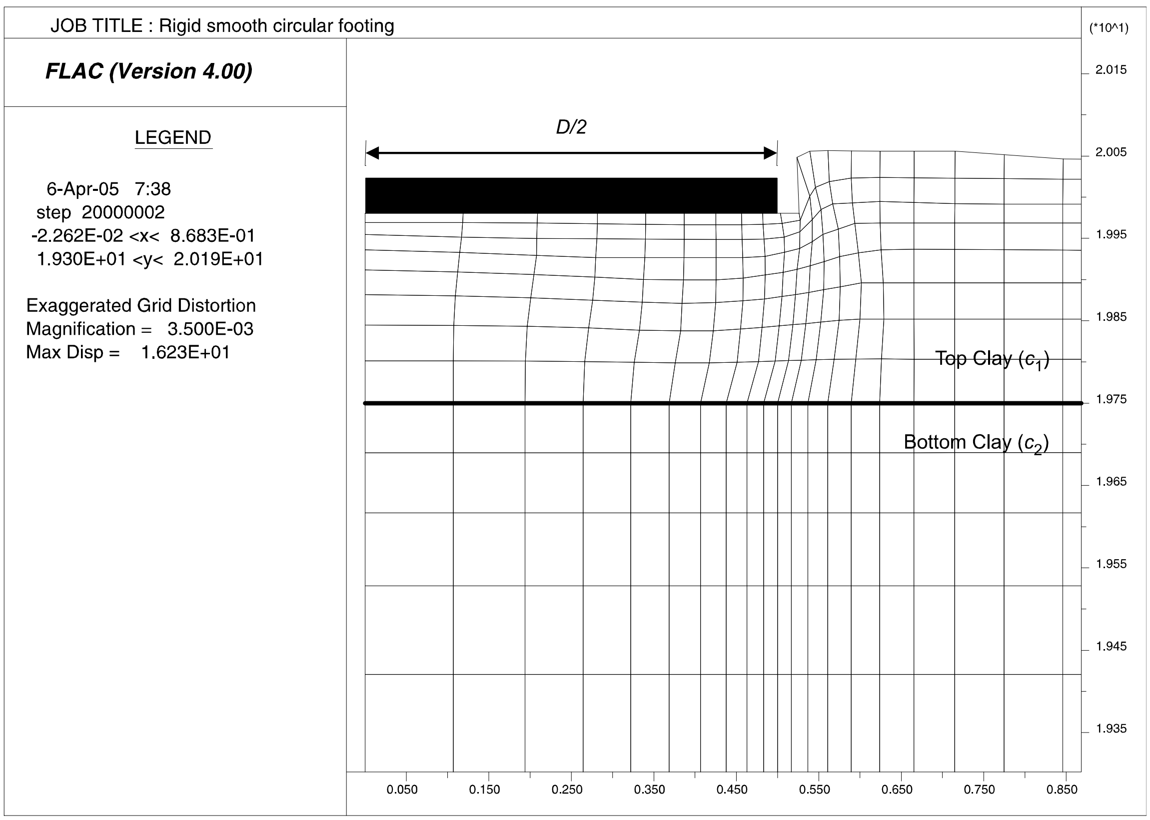

Figure A.430: Magnified grid for a rigid smooth circular footing on soft clay over strong clay for 40 × 30 grid model, $H/D = 0.25$, $c_1/c_2 = 1/3$.

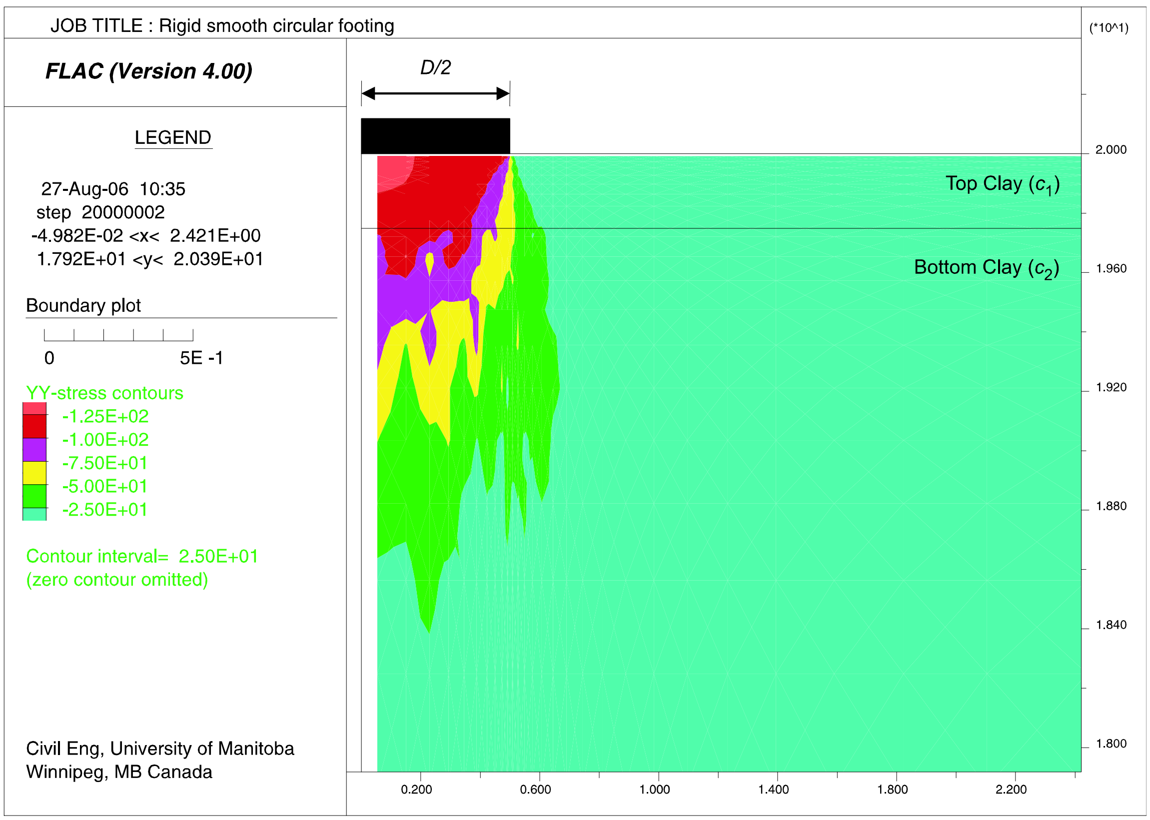

Figure A.431: Vertical stress (σ_{yy}) contours for a rigid smooth circular footing on soft clay over strong clay for 40 × 30 grid model, $H/D = 0.25$, $c_1/c_2 = 1/3$.

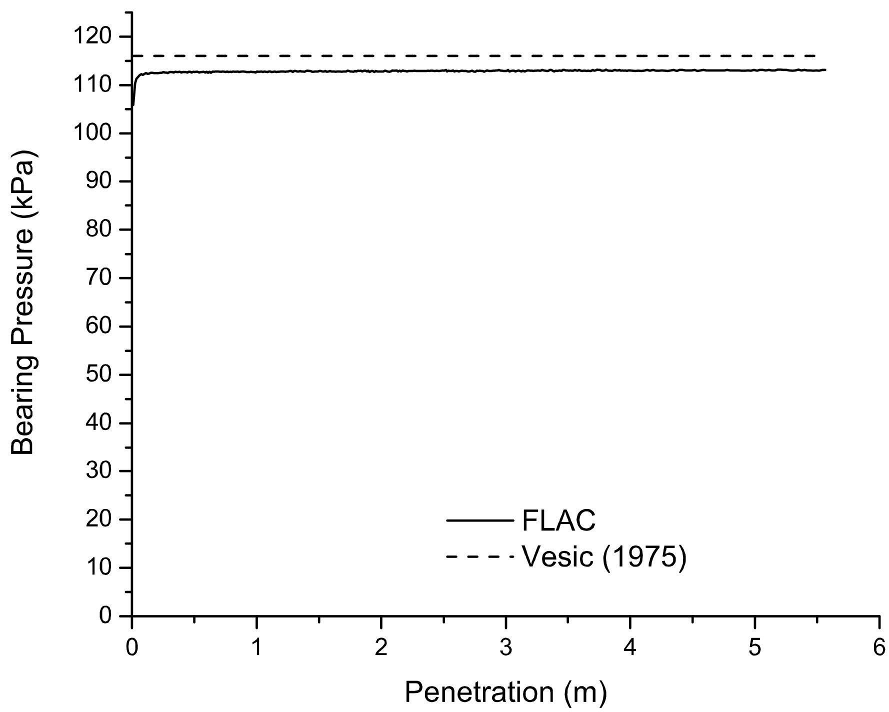

Figure A.432: Bearing pressure versus penetration curve for a rigid smooth circular footing on soft clay over strong clay for 40×30 grid model, $H/D = 0.25$, $c_1/c_2 = 1/3$.

Case 6: $c_1/c_2 = 0.2$ or $c_2/c_1 = 5$ - Small Deformation Analysis

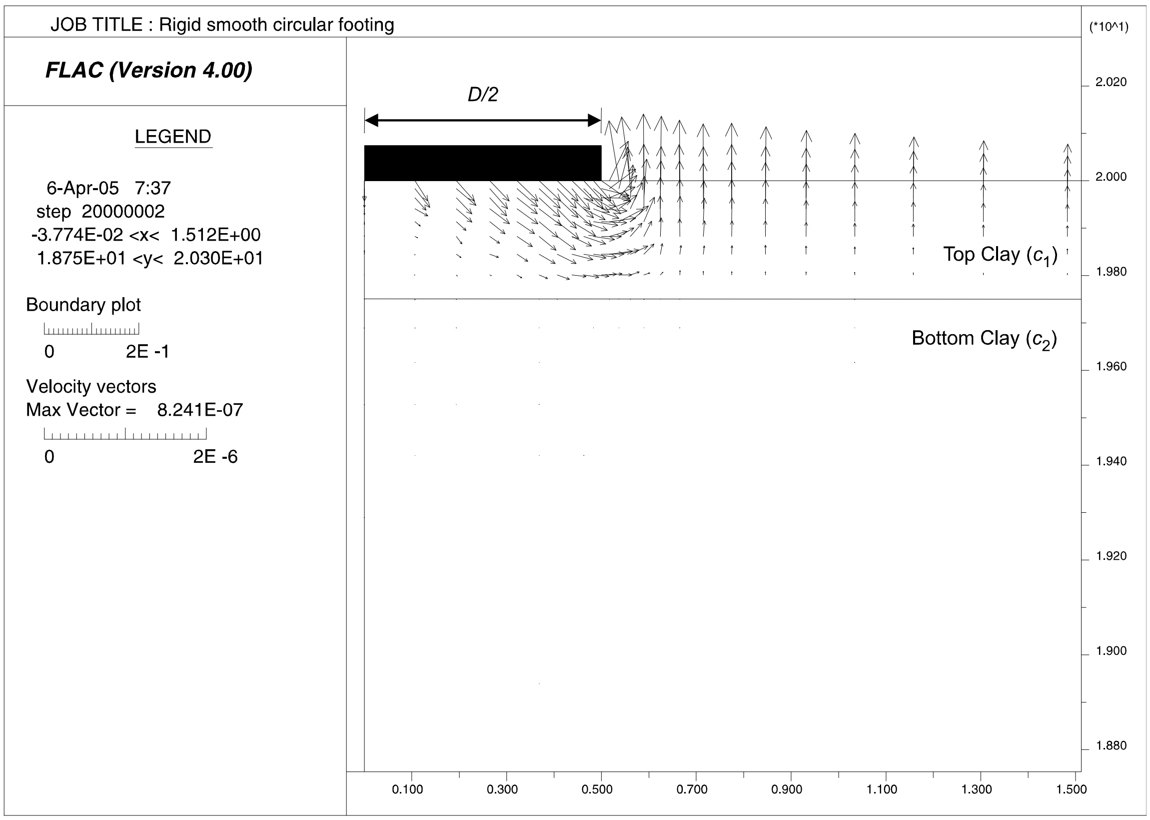

Figure A.433: Velocity vectors for a rigid smooth circular footing on soft clay over strong clay for 40×30 grid model, $H/D = 0.25$, $c_1/c_2 = 0.2$.

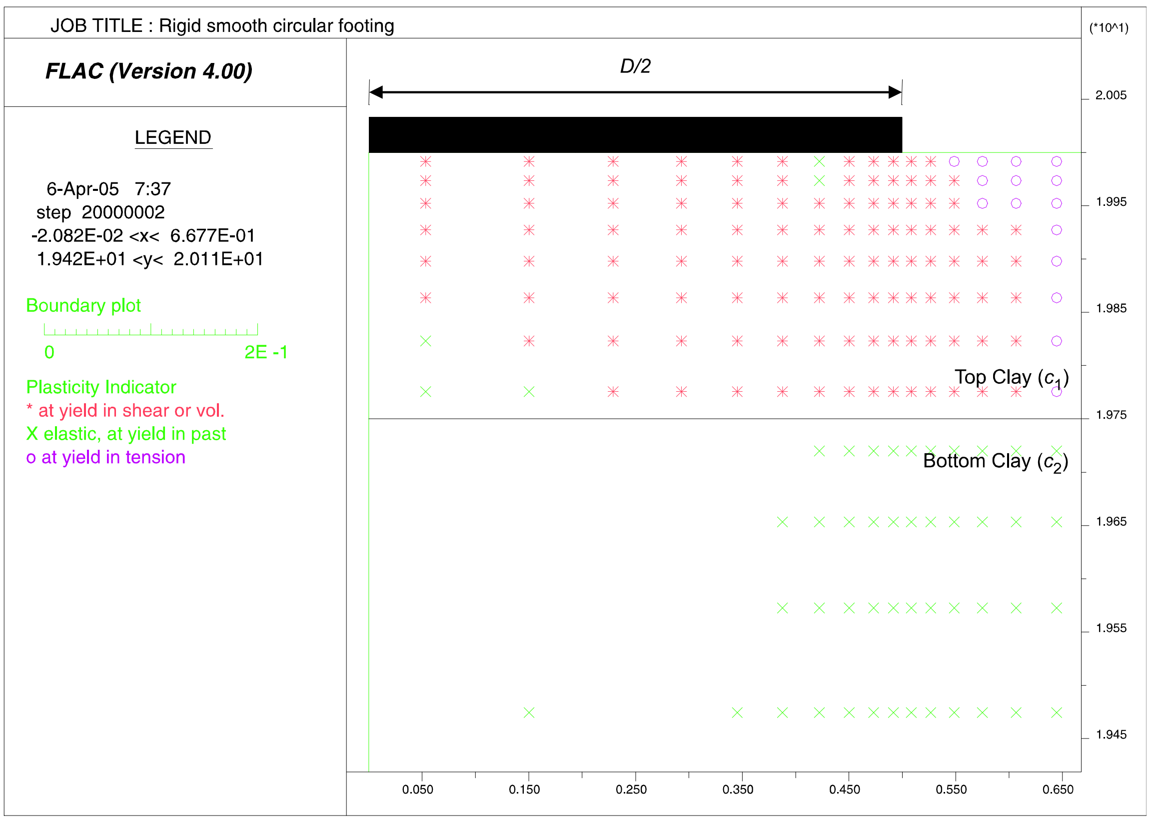

Figure A.434: Plasticity state indicators for a rigid smooth circular footing on soft clay over strong clay for 40×30 grid model, $H/D = 0.25$, $c_1/c_2 = 0.2$.

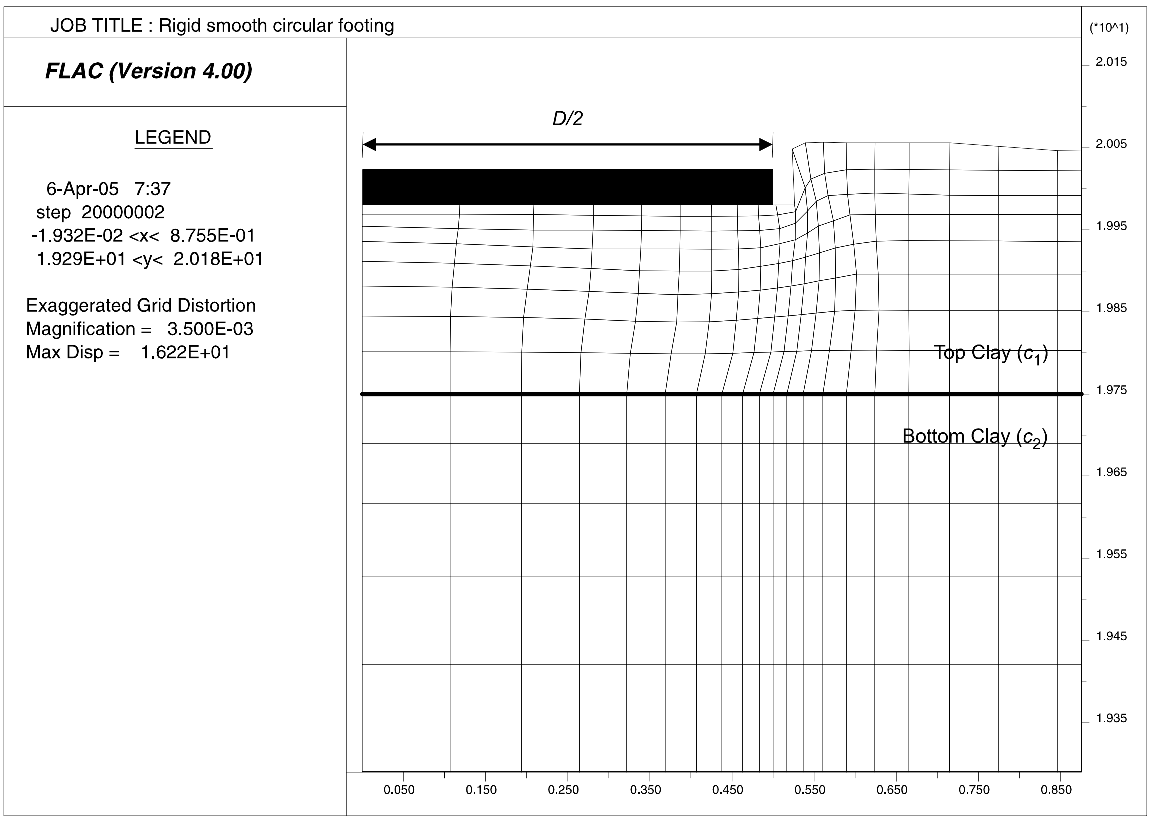

Figure A.435: Magnified grid for a rigid smooth circular footing on soft clay over strong clay for 40 × 30 grid model, $H/D = 0.25$, $c_1/c_2 = 0.2$.

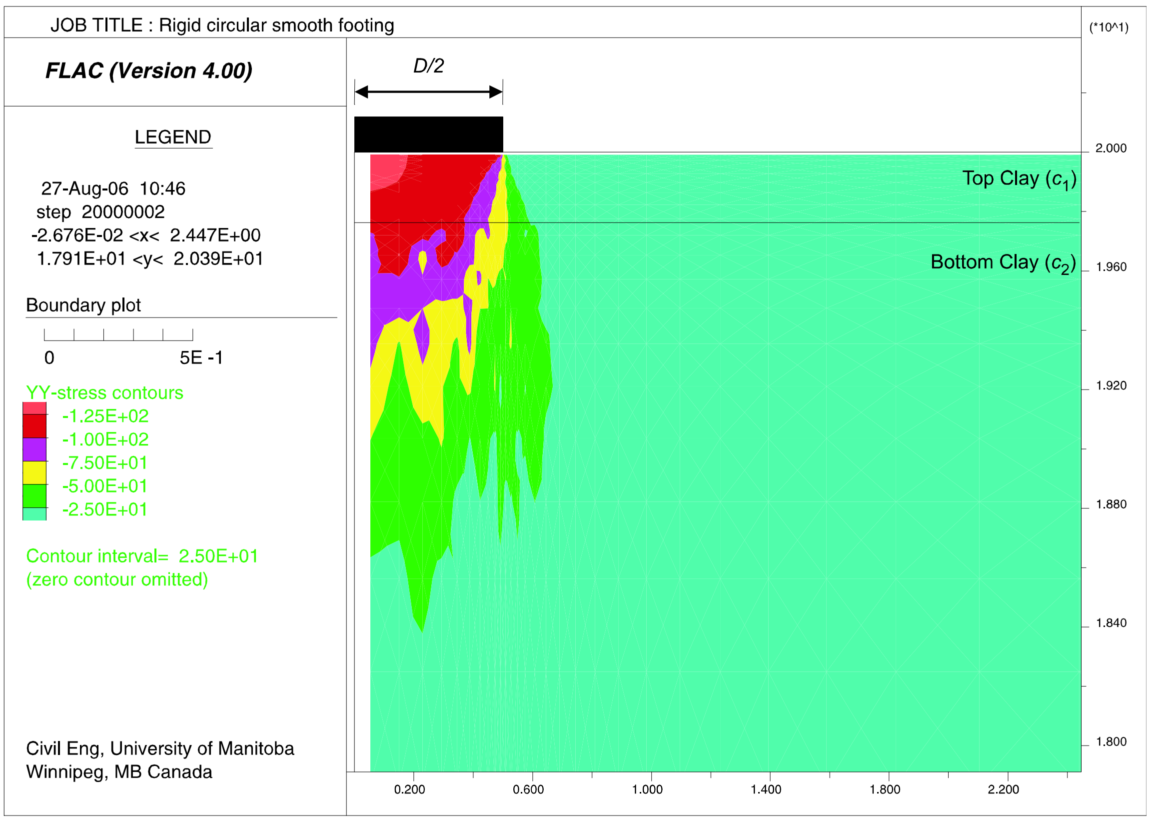

Figure A.436: Vertical stress (σ_{yy}) contours for a rigid smooth circular footing on soft clay over strong clay for 40×30 grid model, $H/D = 0.25$, $c_1/c_2 = 0.2$.

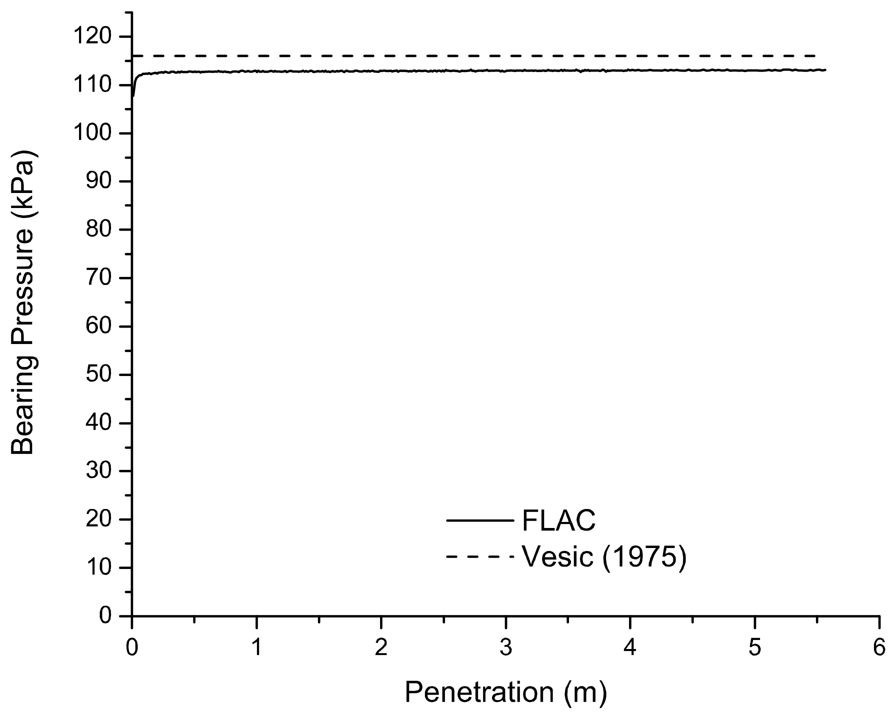

Figure A.437: Bearing pressure versus penetration curve for a rigid smooth circular footing on soft clay over strong clay for 40×30 grid model, $H/D = 0.25$, $c_1/c_2 = 0.2$.

Case 7: $c_1/c_2 = 0.1$ or $c_2/c_1 = 10$ - Small Deformation Analysis

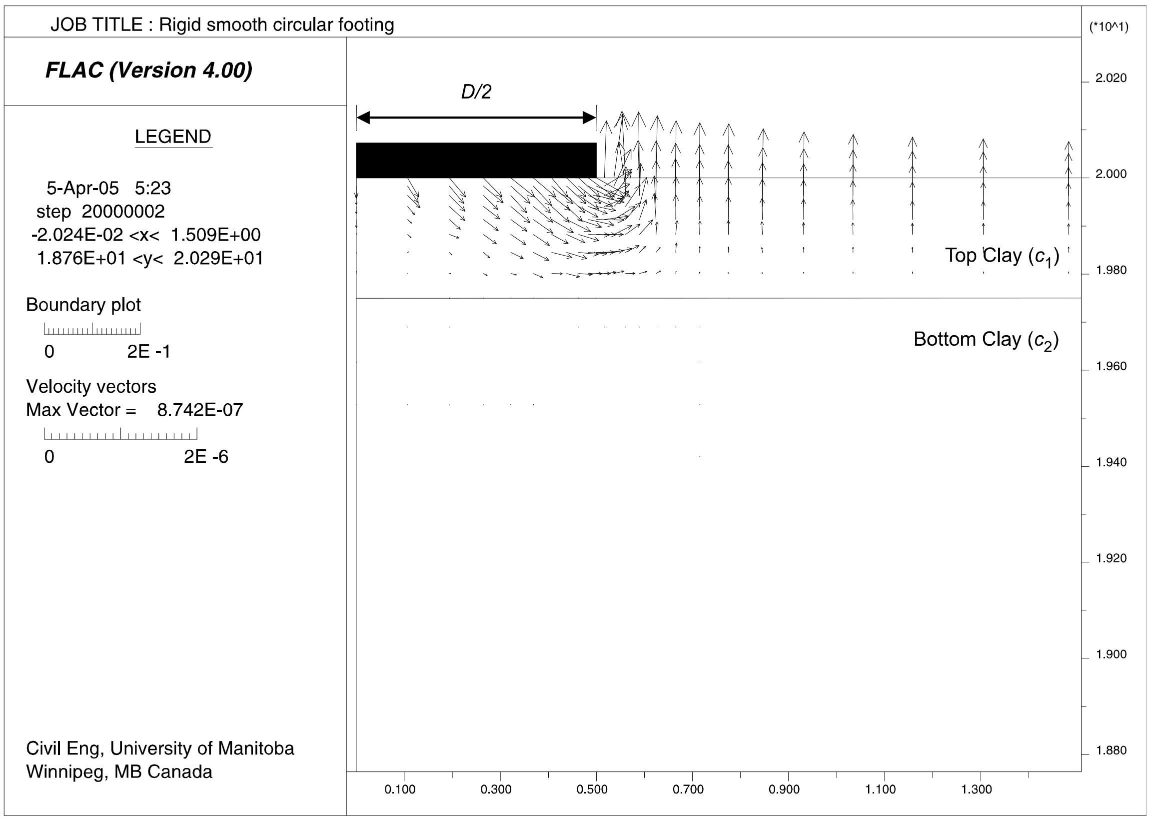

Figure A.438: Velocity vectors for a rigid smooth circular footing on soft clay over strong clay for 40×30 grid model, $H/D = 0.25$, $c_1/c_2 = 0.1$.

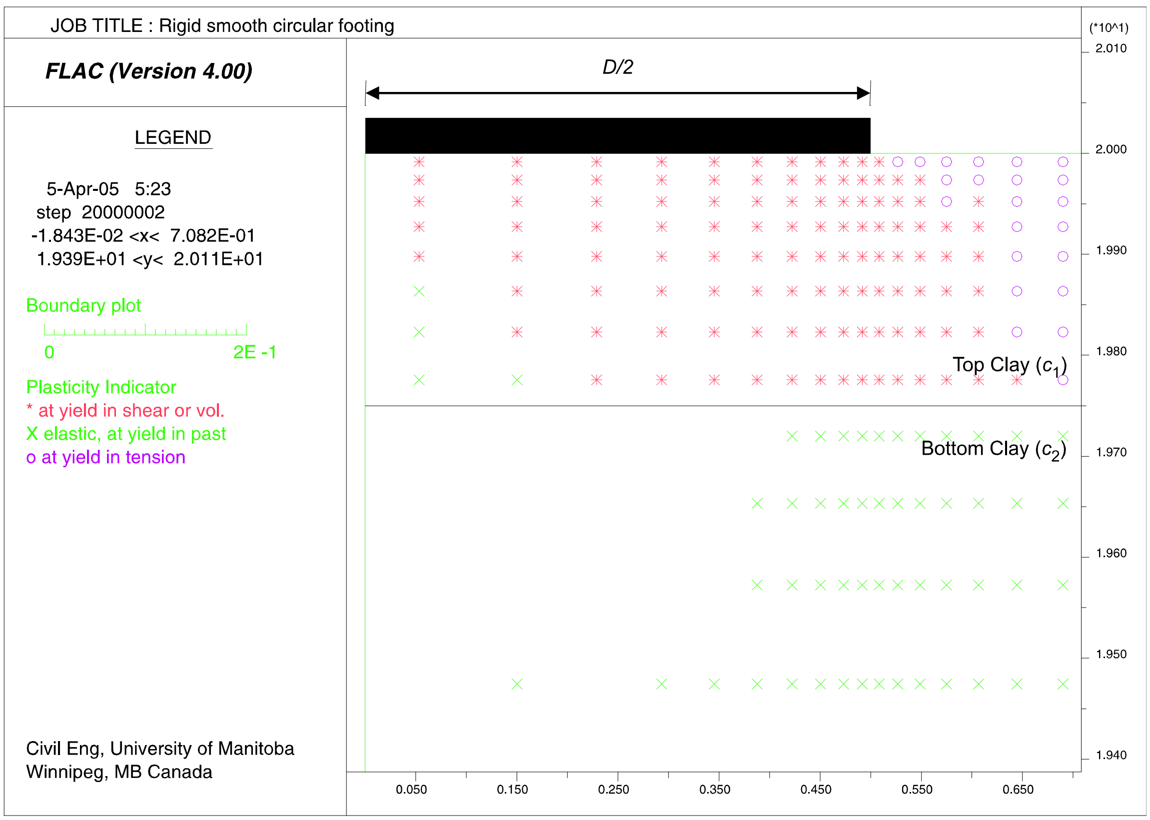

Figure A.439: Plasticity state indicators for a rigid smooth circular footing on soft clay over strong clay for 40×30 grid model, $H/D = 0.25$, $c_1/c_2 = 0.1$.

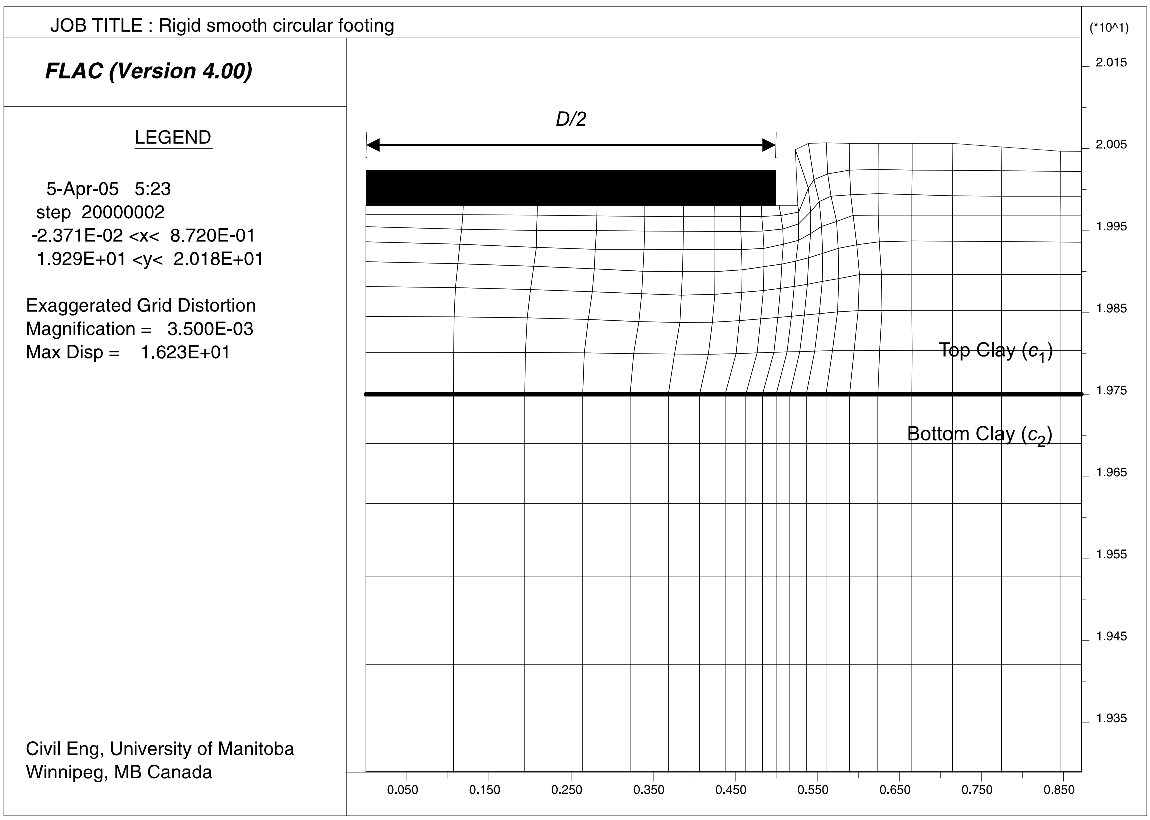

Figure A.440: Magnified grid for a rigid smooth circular footing on soft clay over strong clay for 40×30 grid model, $H/D = 0.25$, $c_1/c_2 = 0.1$.

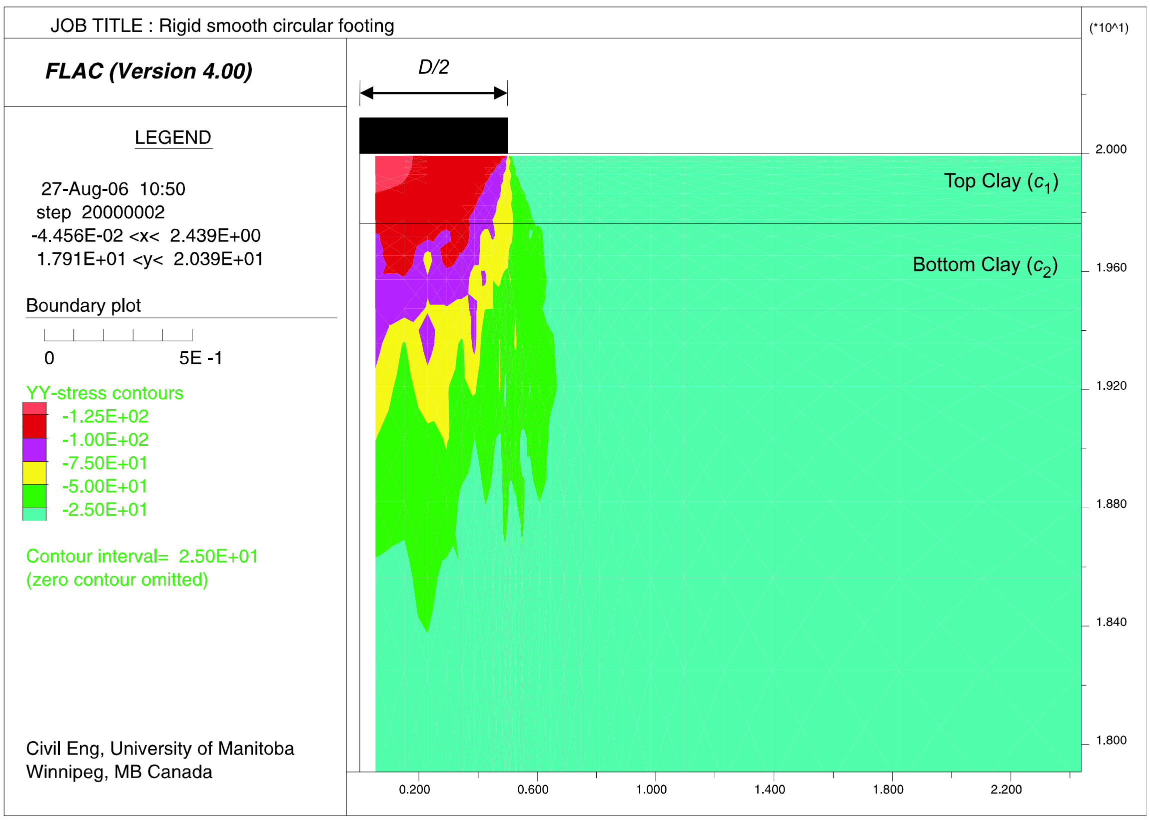

Figure A.441: Vertical stress (σ_{yy}) contours for a rigid smooth circular footing on soft clay over strong clay for 40 × 30 grid model, $H/D = 0.25$, $c_1/c_2 = 0.1$.

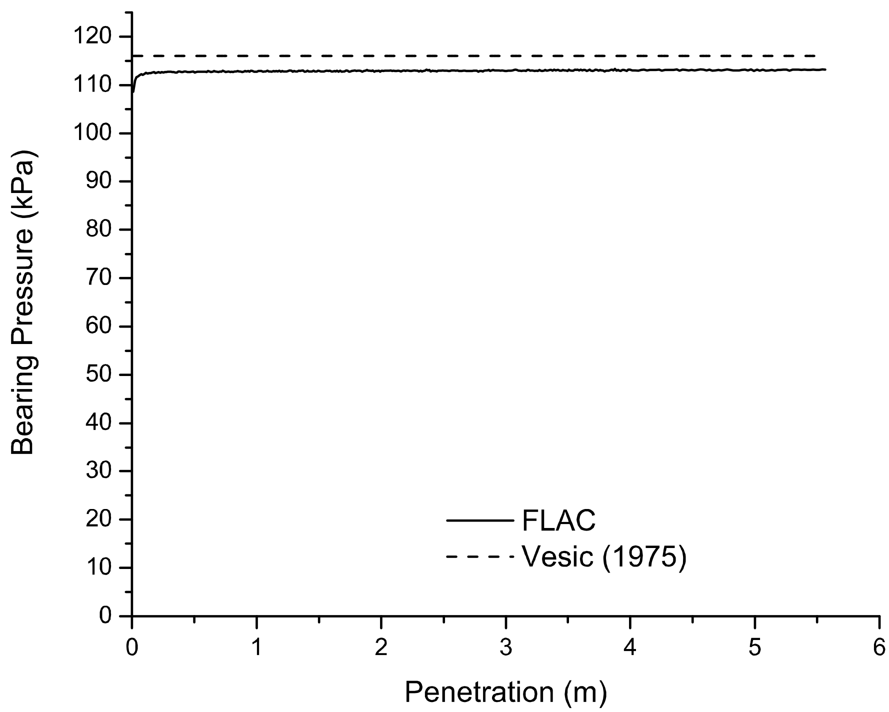

Figure A.442: Bearing pressure versus penetration curve for a rigid smooth circular footing on soft clay over strong clay for 40×30 grid model, $H/D = 0.25$, $c_1/c_2 = 0.1$.

A.5 Strip Footing on Stiff Clay Overlying Soft Clay - Large Deformation Analysis

A.5.1 Rigid Smooth Strip Footing on Strong over Soft Clay ($H/B = 1$)

Only two cases of undrained shear strength ratios $c_2/\ c_1 = 1$ and 0.1 are considered in this analysis to study the effectiveness of FLAC in large deformation analysis.

Case 1: $c_2/c_1 = 1$ **(Homogeneous clay) - Large Deformation Analysis**

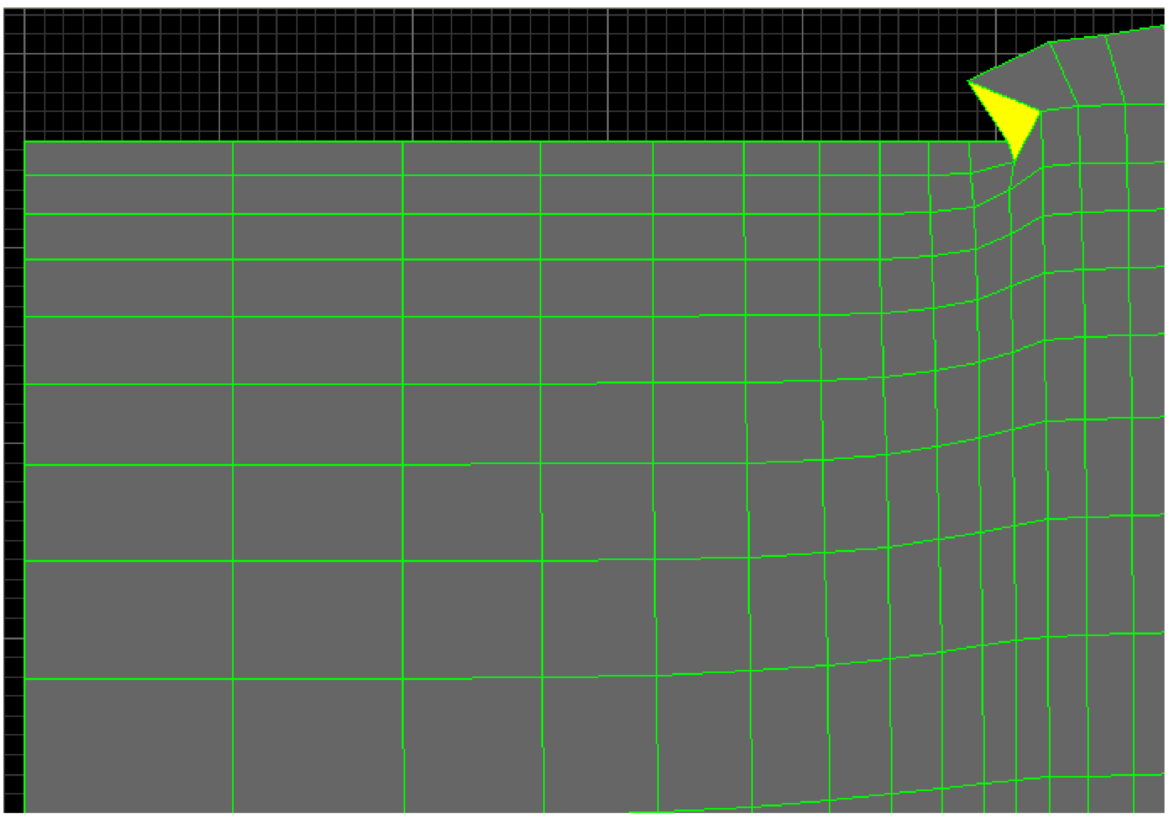

Figure A.443: Distorted zone ($i = 11, j = 31$) to show Bad Geometry error state for large deformation analysis for a rigid smooth strip footing on strong over soft clay ($H/B = 1$, $c_2/c_1 = 1$)

Test 1: Large Strain Analysis

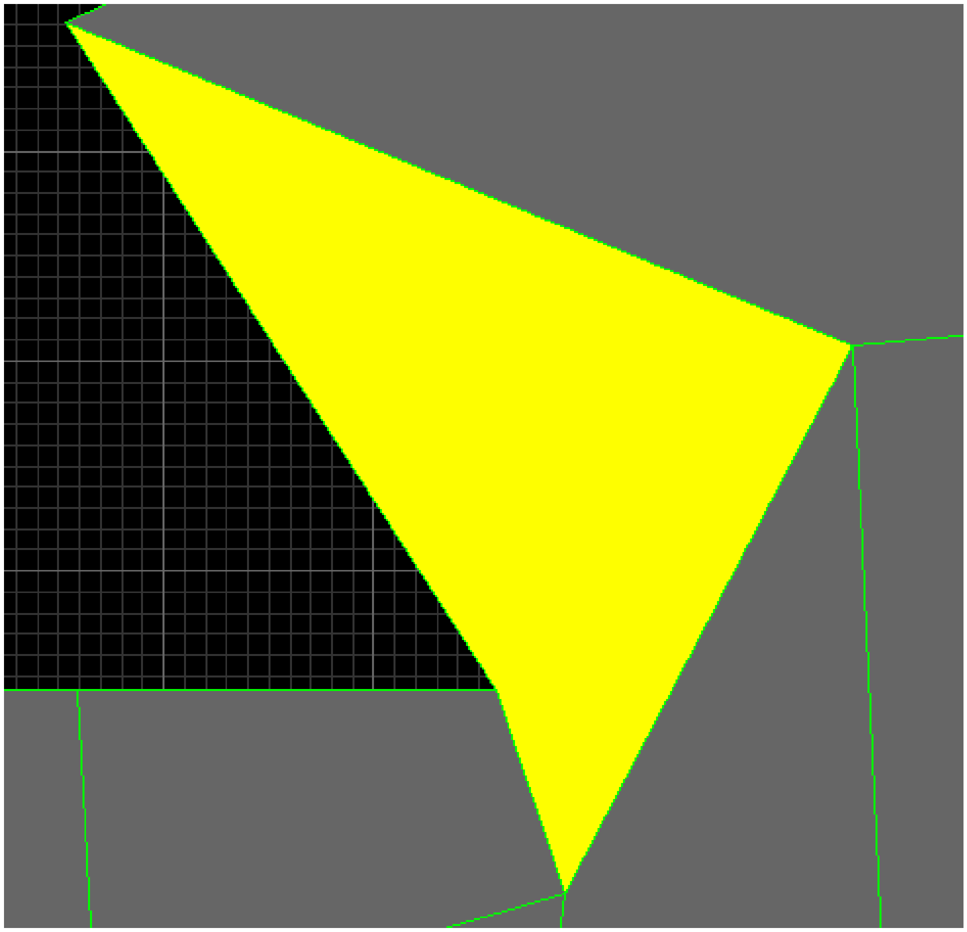

Figure A.444: Distorted zone ($i = 11, j = 31$) zoomed to show Bad Geometry error state for large deformation analysis for a rigid smooth strip footing on strong over soft clay ($H/B = 1$, $c_2/c_1 = 1$)

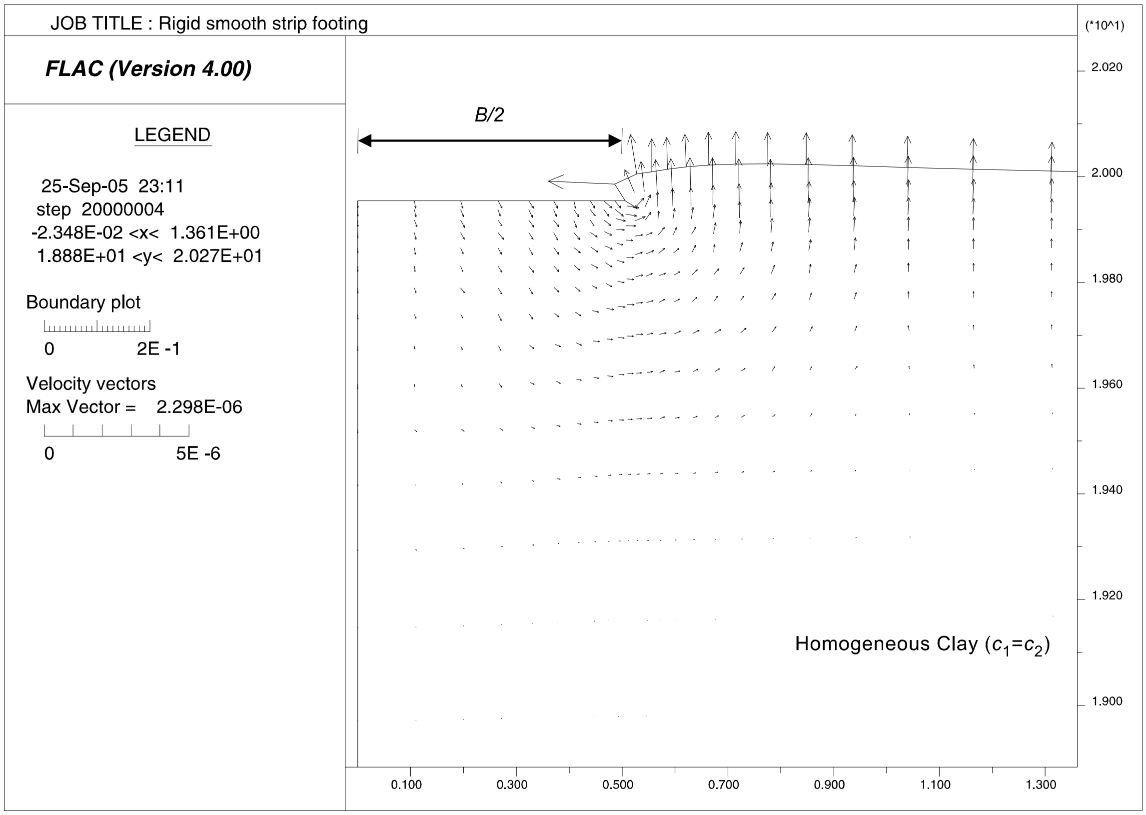

Figure A.445: Velocity vectors for combined large strain - small strain analysis of a rigid smooth strip footing on strong clay over soft clay for 40×30 grid model, $H/B = 1$, $c_2/c_1 = 1$.

Test 2: Combined Large Strain and Small Strain Analysis

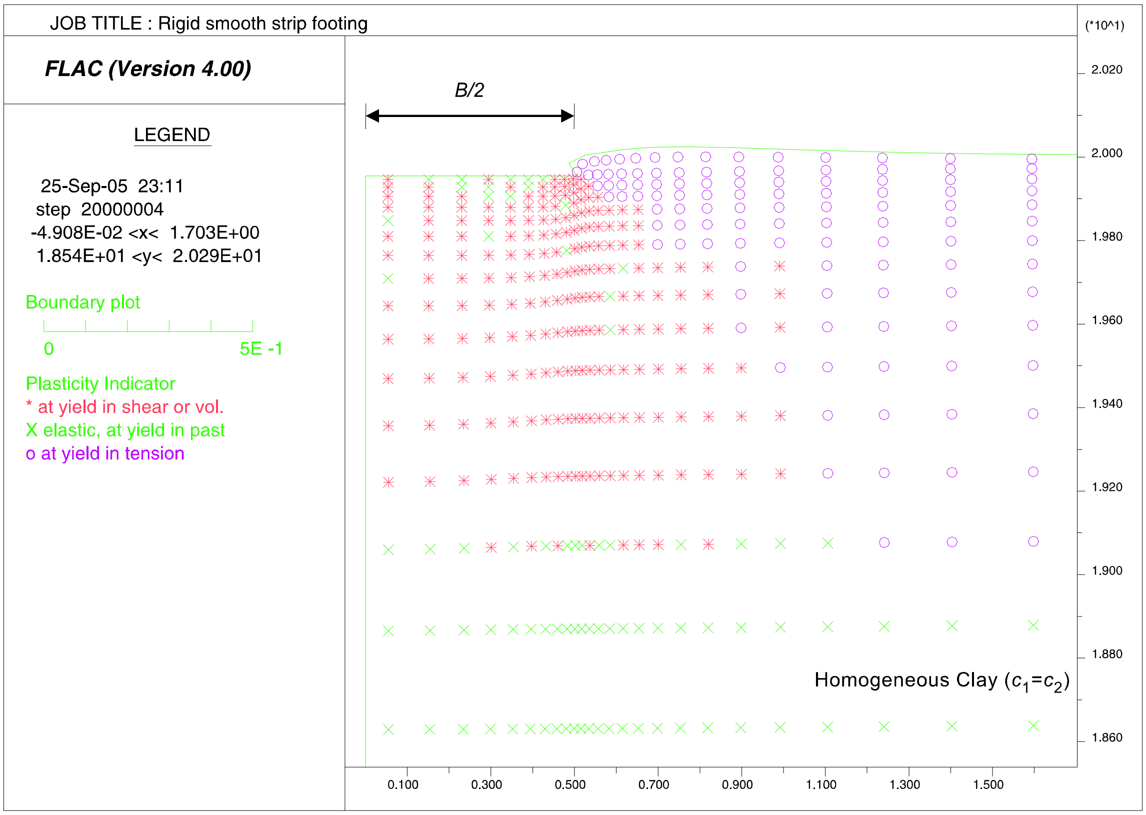

Figure A.446: Plasticity state indicators for combined large strain - small strain analysis of a rigid smooth strip footing on strong clay over soft clay for 40 × 30 grid model, $H/B = 1$, $c_2/c_1 = 1$.

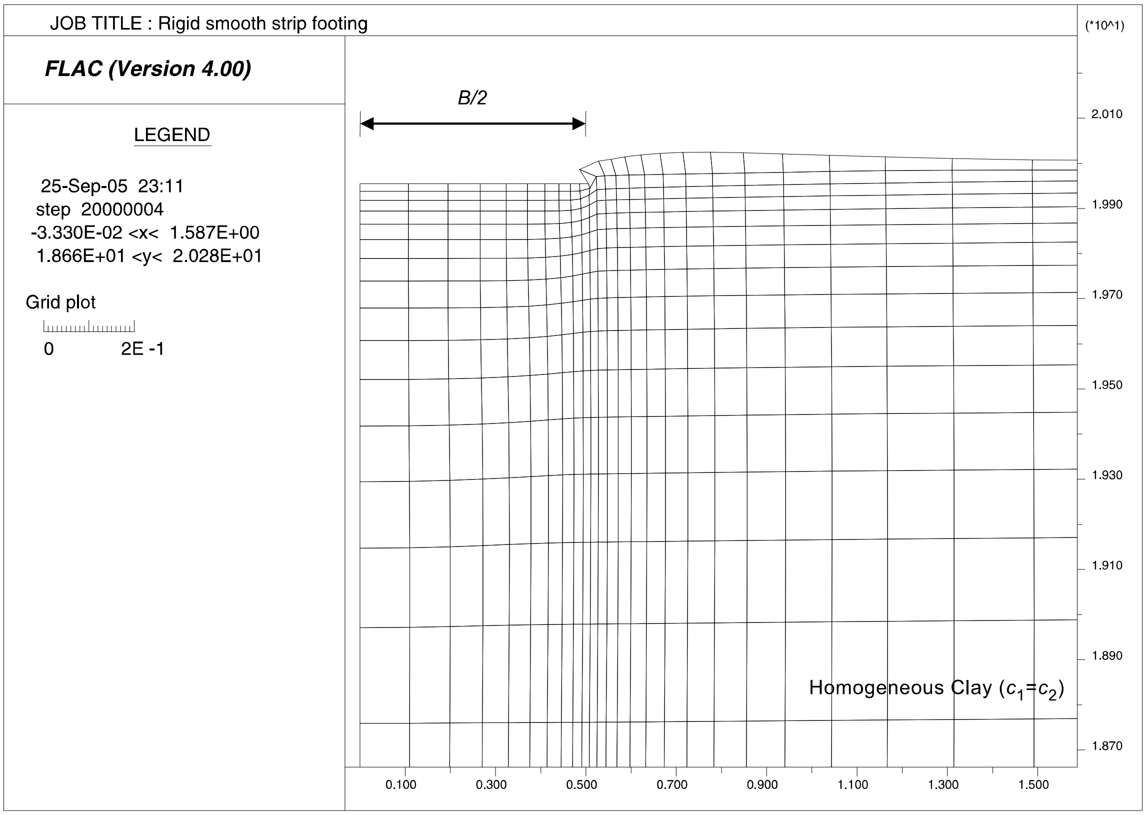

Figure A.447: Grid for a rigid smooth strip footing on strong clay over soft clay for 40×30 grid model, $H/B = 1$, $c_2/c_1 = 1$.

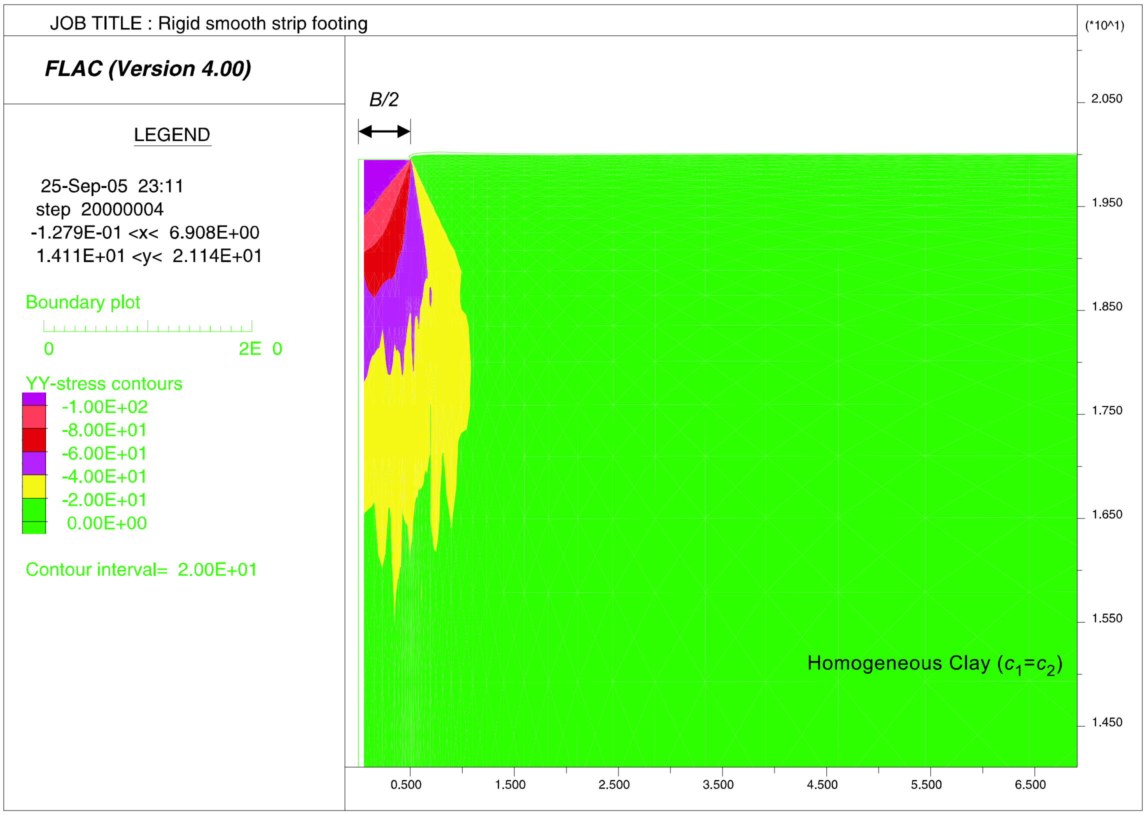

Figure A.448: Vertical stress (σ_{yy}) contours for combined large strain - small strain analysis of a rigid smooth strip footing on strong clay over soft clay for 40×30 grid model, $H/B = 1$, $c_2/c_1 = 1$.

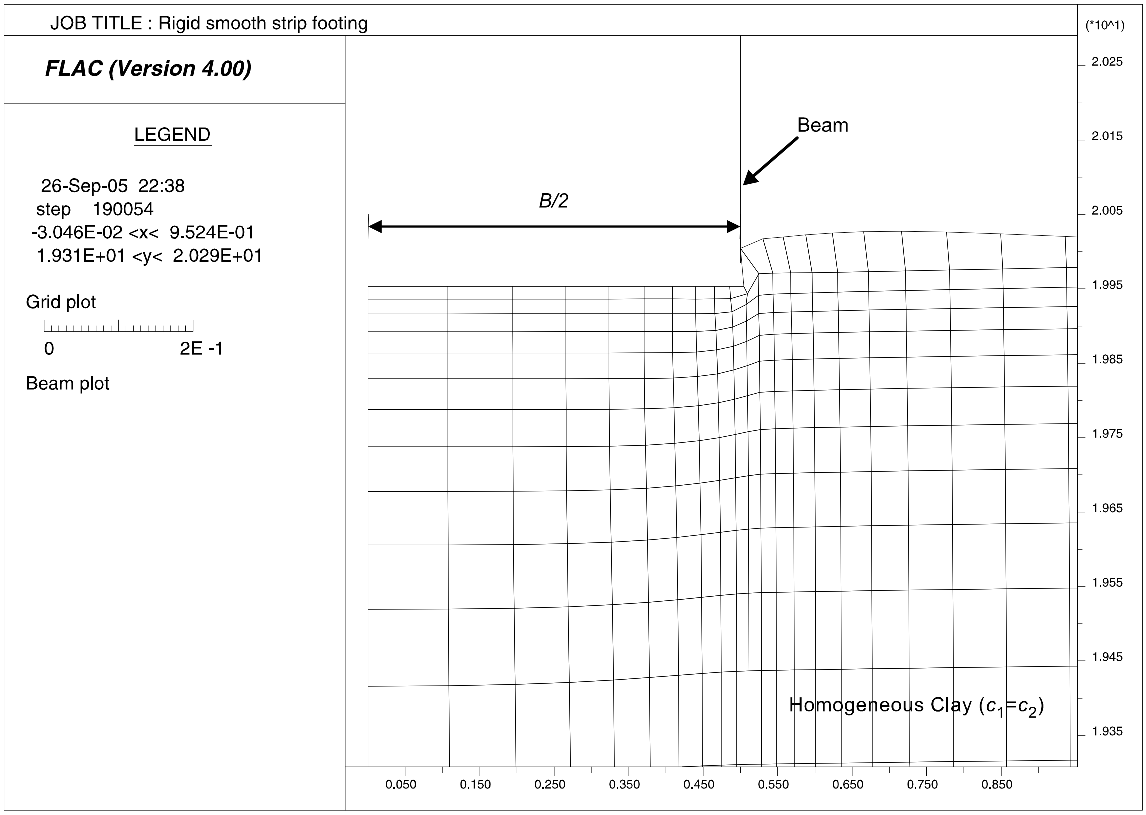

Figure A.449: Zoomed grid with beam for stopping soil spill on footing for combined large strain - small strain analysis of a rigid smooth strip footing on strong clay over soft clay for 40 × 30 grid model, $H/B = 1$, $c_2/c_1 = 1$.

Test 3: Combined Large Strain and Small Strain Analysis - Soil Restrained from Flowing over Footing

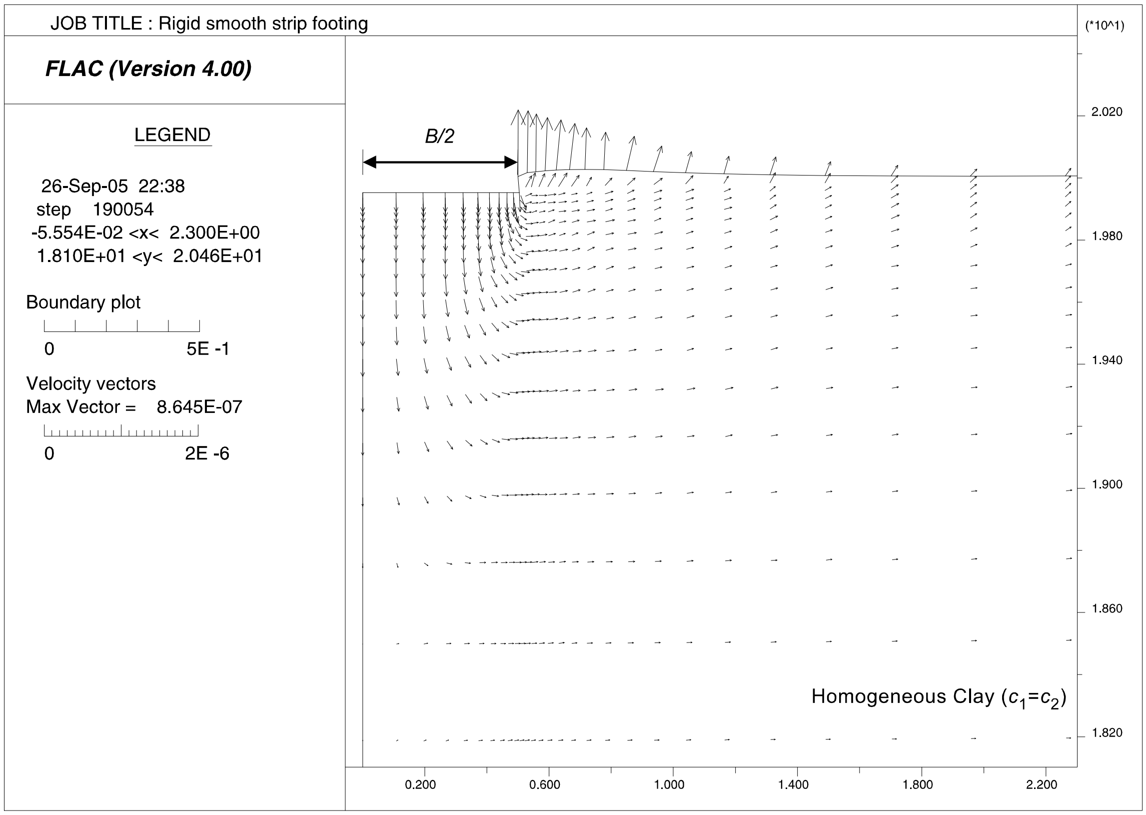

Figure A.450: Velocity vectors for combined large strain - small strain analysis of a rigid smooth strip footing on strong clay over soft clay with soil stopped spilling on footing for 40×30 grid model, $H/B = 1$, $c_2/c_1 = 1$.

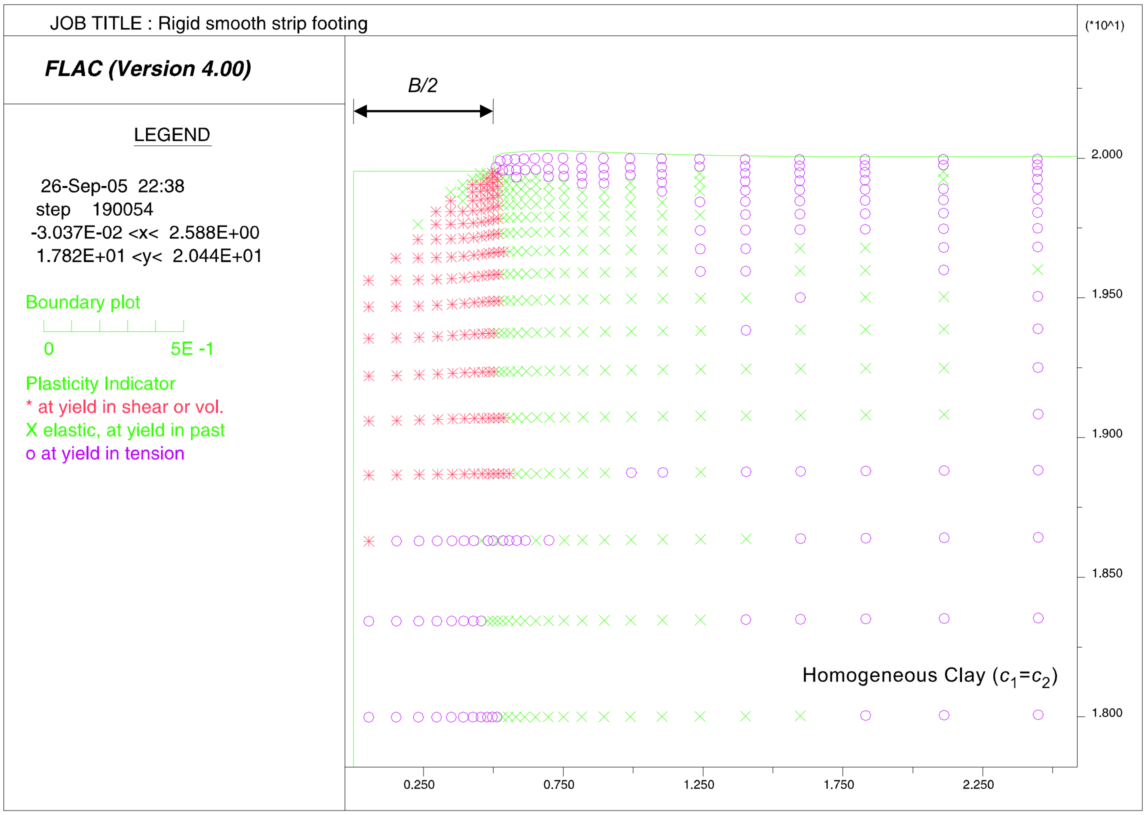

Figure A.451: Plasticity state indicators for combined large strain - small strain analysis of a rigid smooth strip footing on strong clay over soft clay with soil stopped spilling on footing for 40 × 30 grid model, $H/B = 1$, $c_2/c_1 = 1$.

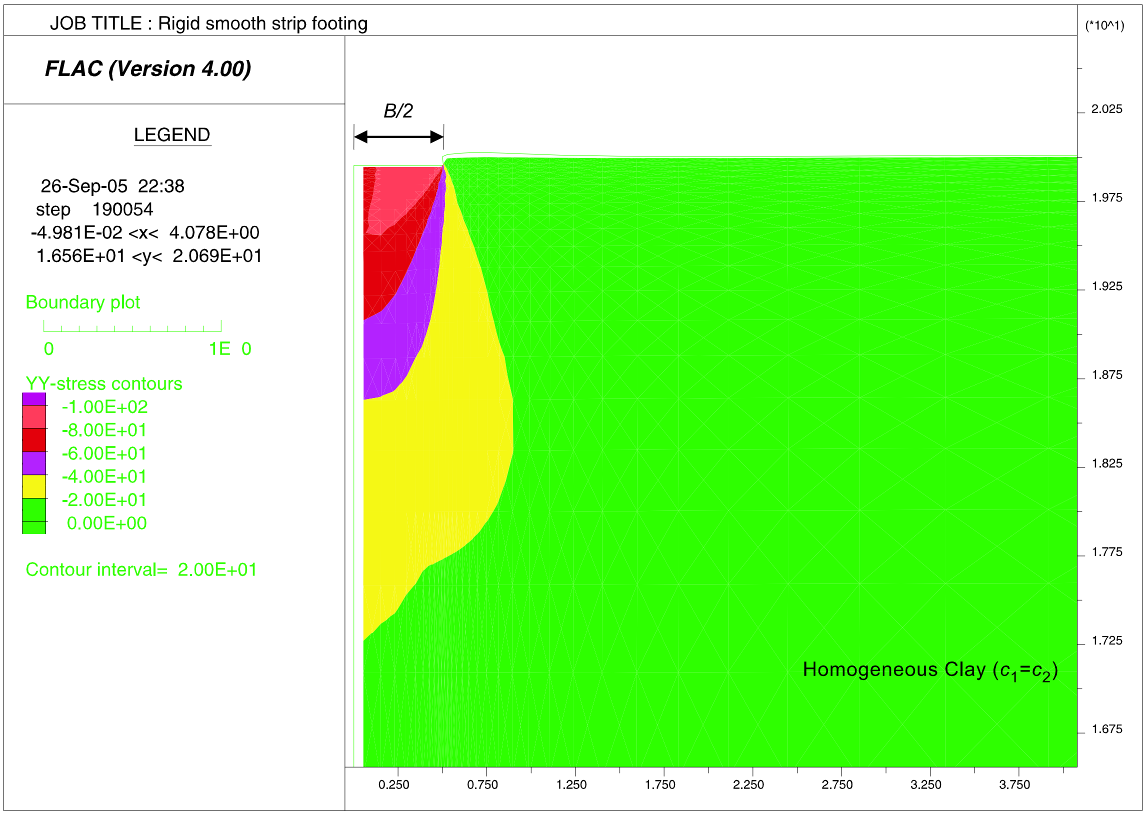

Figure A.452: Vertical stress (σ_{yy}) contours for combined large strain - small strain analysis of a rigid smooth strip footing on strong clay over soft clay with soil stopped spilling on footing for 40×30 grid model, $H/B = 1$, $c_2/c_1 = 1$.

Case 2: $c_2/c_1 = 0.1$ **(Homogeneous clay) - Large Deformation Analysis**

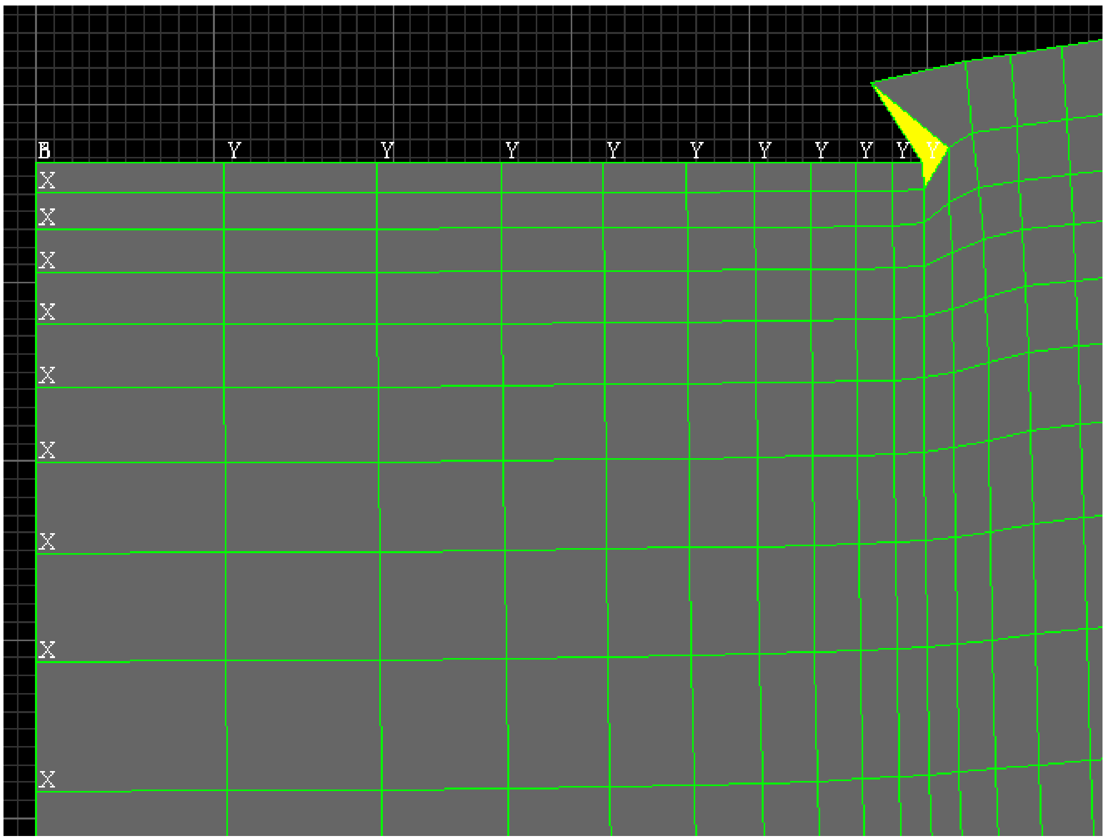

Figure A.453: Distorted zone ($i = 11, j = 31$) at Bad Geometry error state for large deformation analysis for a rigid smooth strip footing on strong over soft clay ($H/B = 1$, $c_2/c_1 = 0.1$)

Test 1: Large Strain Analysis

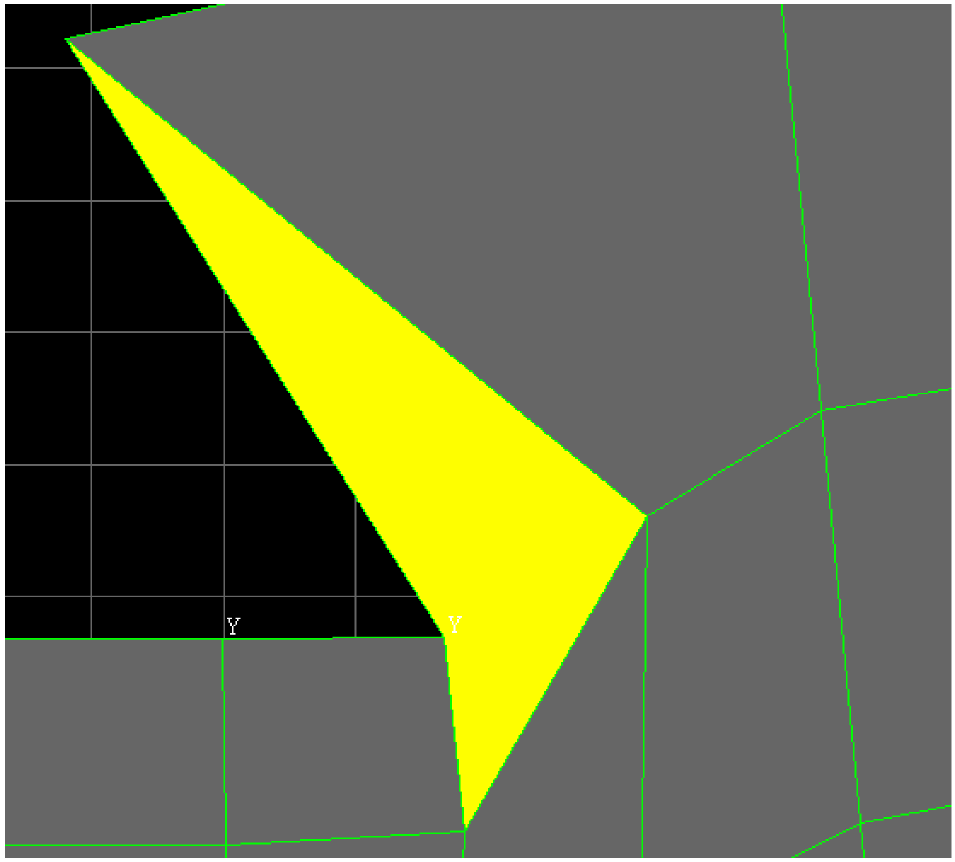

Figure A.454: Distorted zone ($i = 11, j = 31$) zoomed at Bad Geometry error state for large deformation analysis for rigid smooth strip footing on strong over soft clay ($H/B = 1$, $c_2/c_1 = 1$)

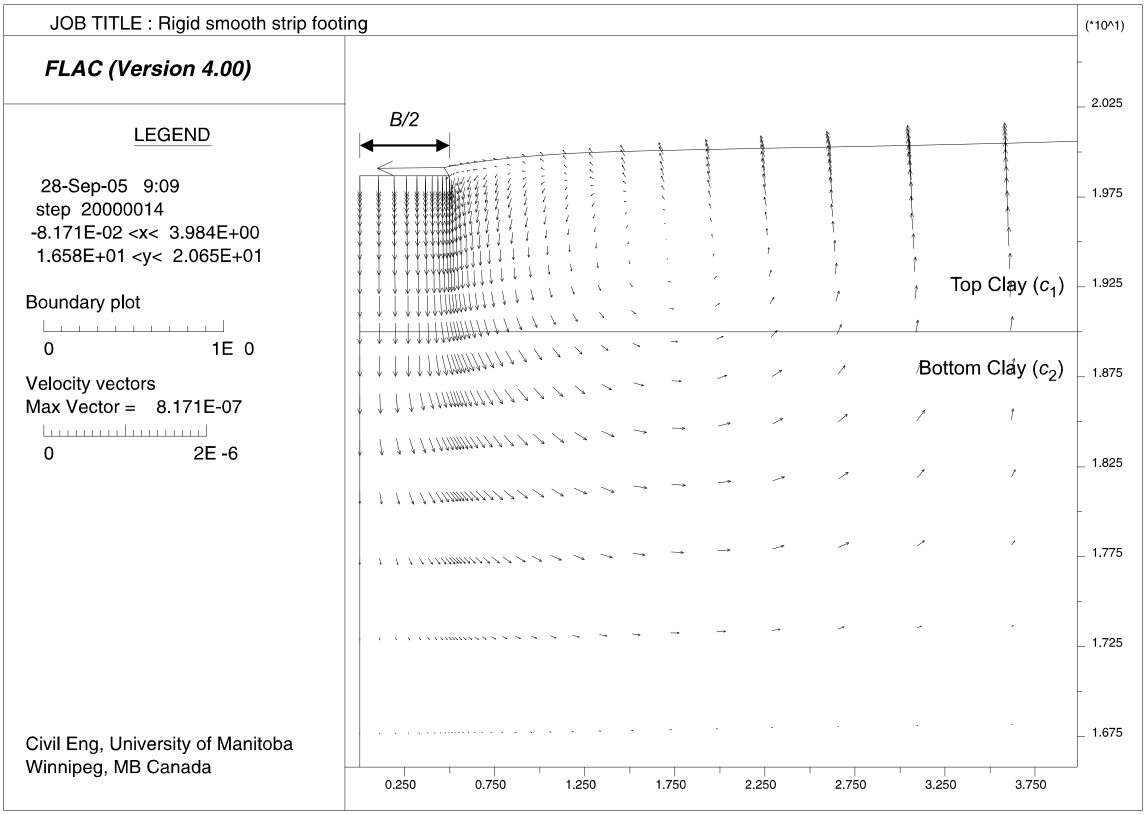

Figure A.455: Velocity vectors for combined large strain - small strain analysis of a rigid smooth strip footing on strong clay over soft clay for 40 × 30 grid model, $H/B = 1$, $c_2/c_1 = 0.1$.

Test 2: Combined Large Strain and Small Strain Analysis

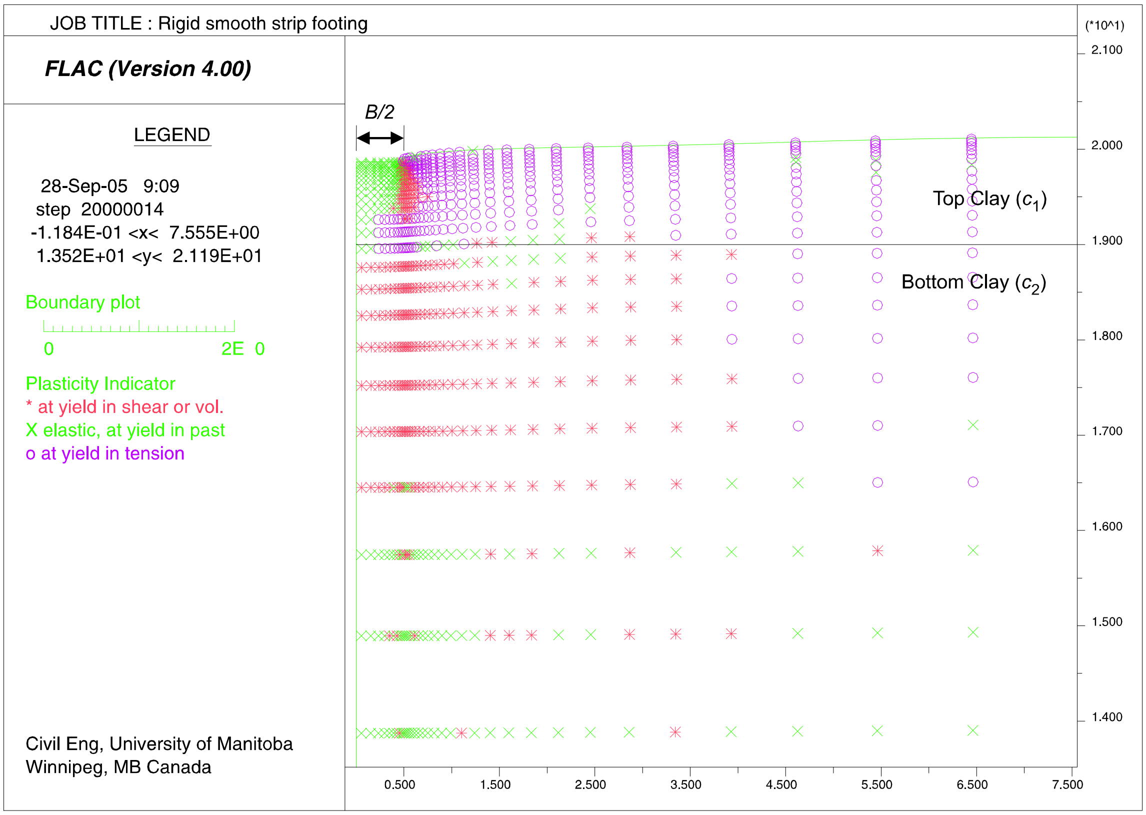

Figure A.456: Plasticity state indicators for combined large strain - small strain analysis of a rigid smooth strip footing on strong clay over soft clay for 40 × 30 grid model, $H/B = 1$, $c_2/c_1 = 0.1$.

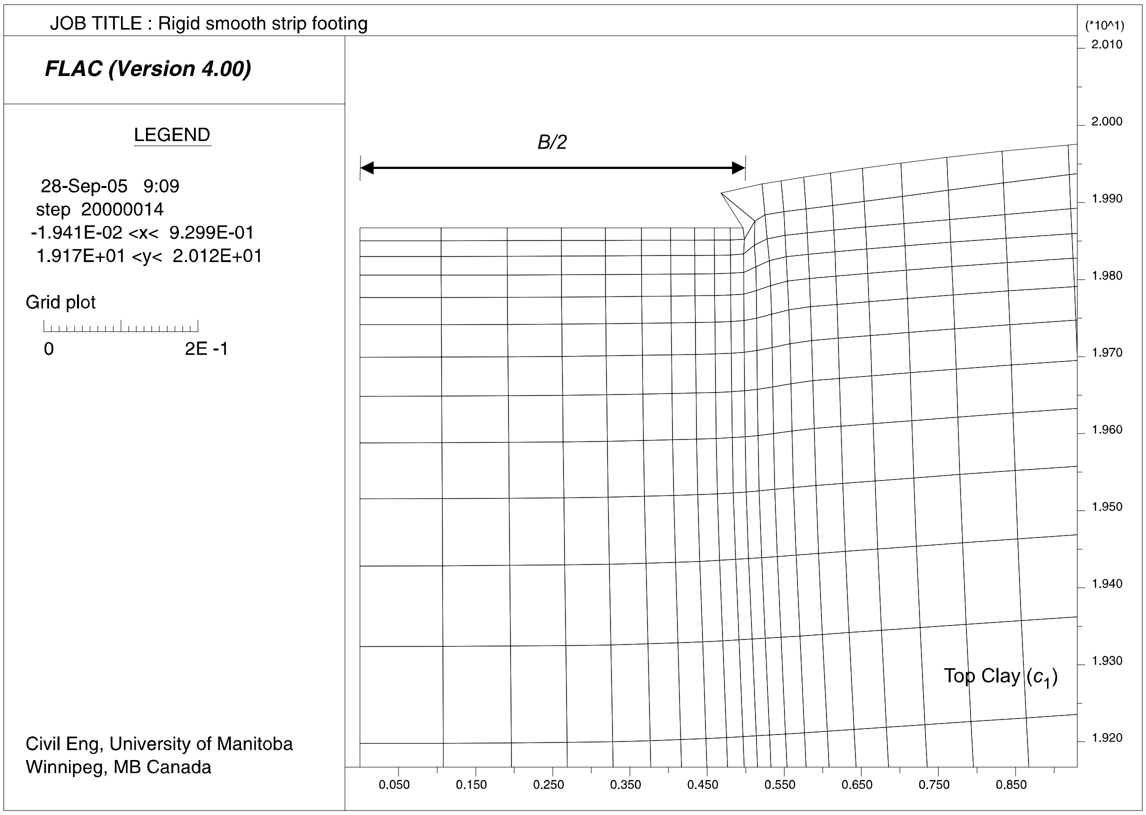

Figure A.457: Grid for rigid smooth strip footing on strong clay over soft clay for 40×30 grid model, $H/B = 1$, $c_2/c_1 = 0.1$.

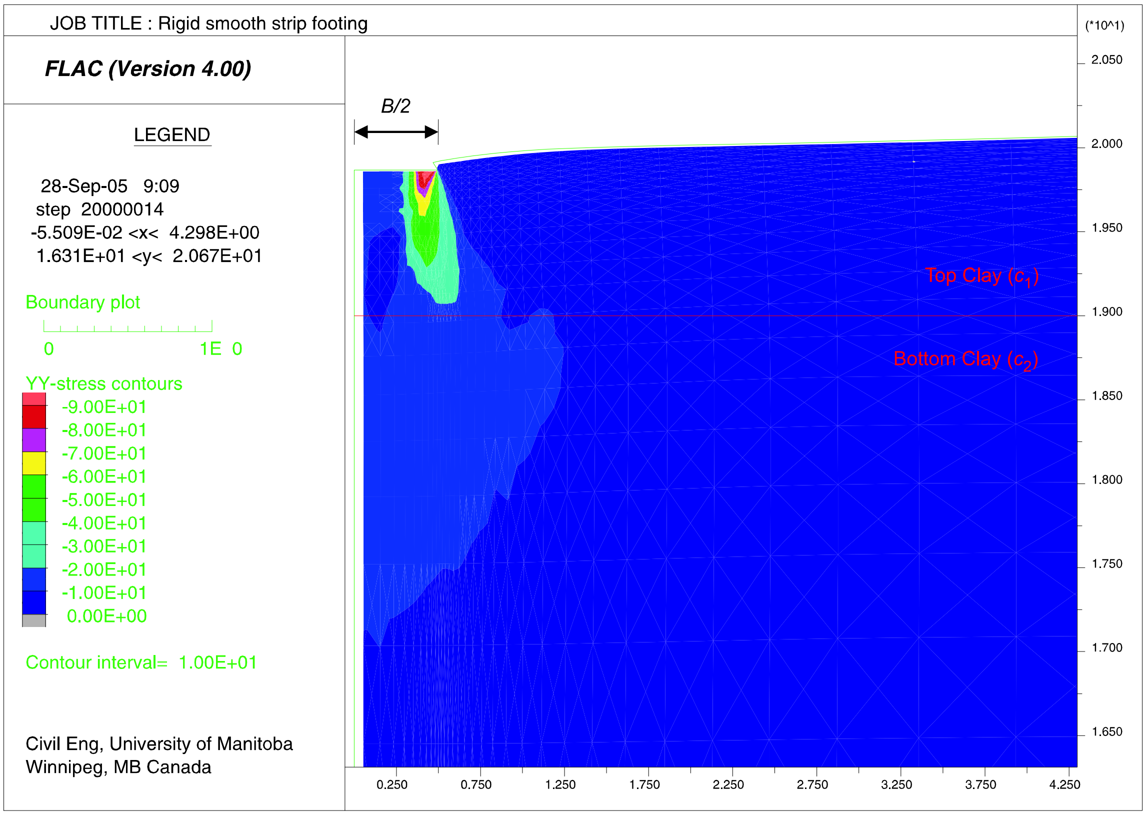

Figure A.458: Vertical stress (σ_{yy}) contours for combined large strain - small strain analysis of a rigid smooth strip footing on strong clay over soft clay for 40×30 grid model, $H/B = 1$, $c_2/c_1 = 0.1$.

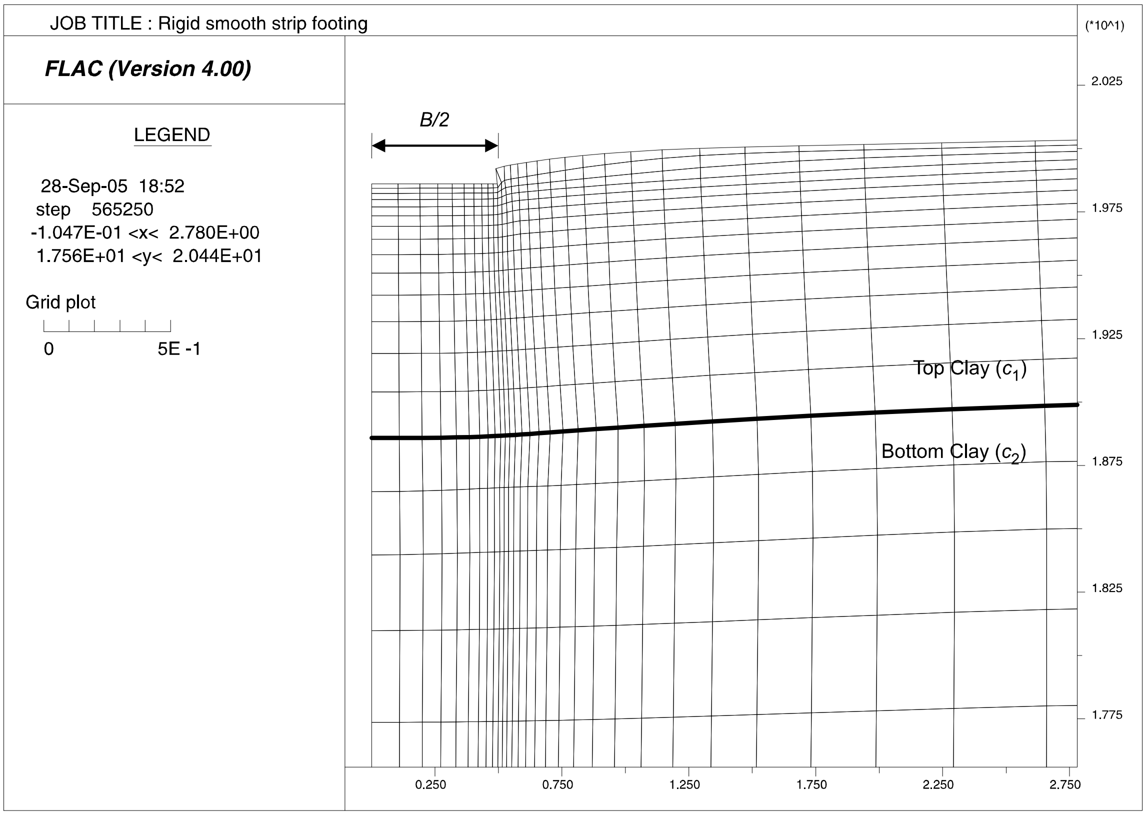

Figure A.459: Zoomed grid with beam for stopping soil spill on footing for combined large strain - small strain analysis of a rigid smooth strip footing on strong clay over soft clay for 40×30 grid model, $H/B = 1$, $c_2/c_1 = 0.1$.

Test 3: Combined Large Strain and Small Strain Analysis - Soil Restrained from Flowing over Footing

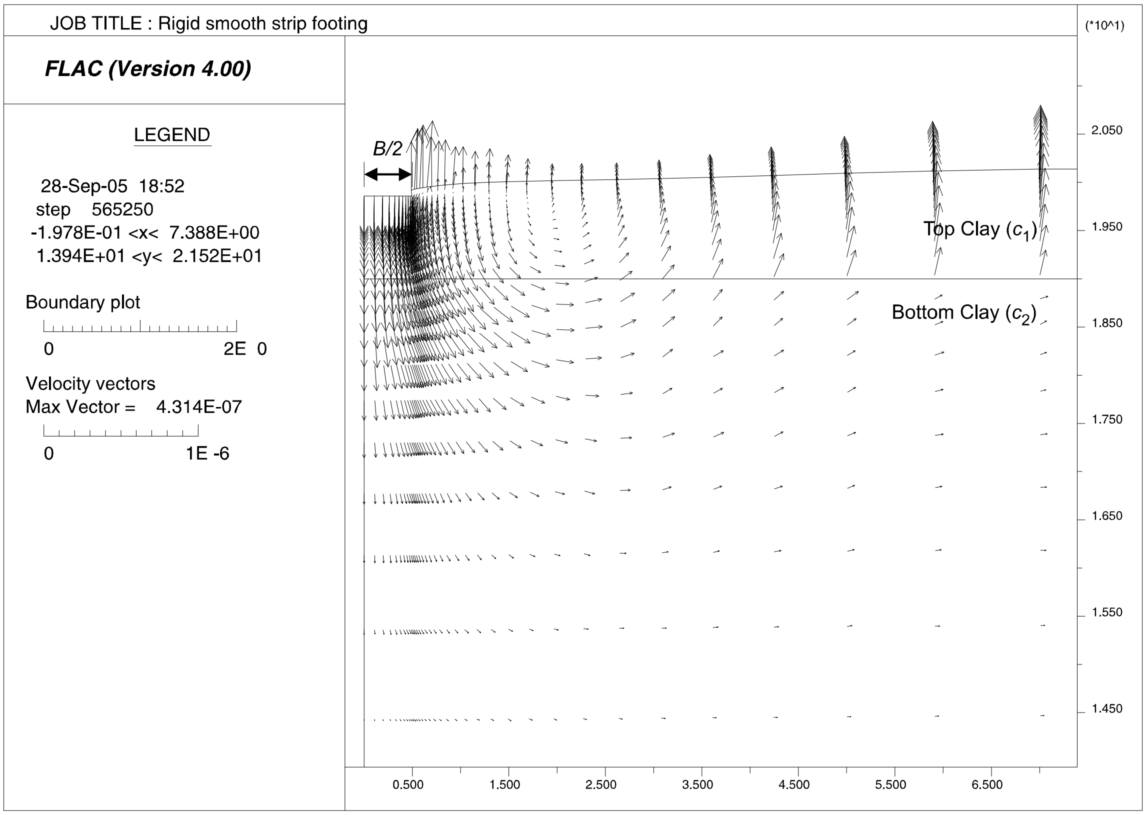

Figure A.460: Velocity vectors for combined large strain - small strain analysis of a rigid smooth strip footing on strong clay over soft clay with soil stopped from spilling over the footing for 40×30 grid model, $H/B = 1$, $c_2/c_1 = 0.1$.

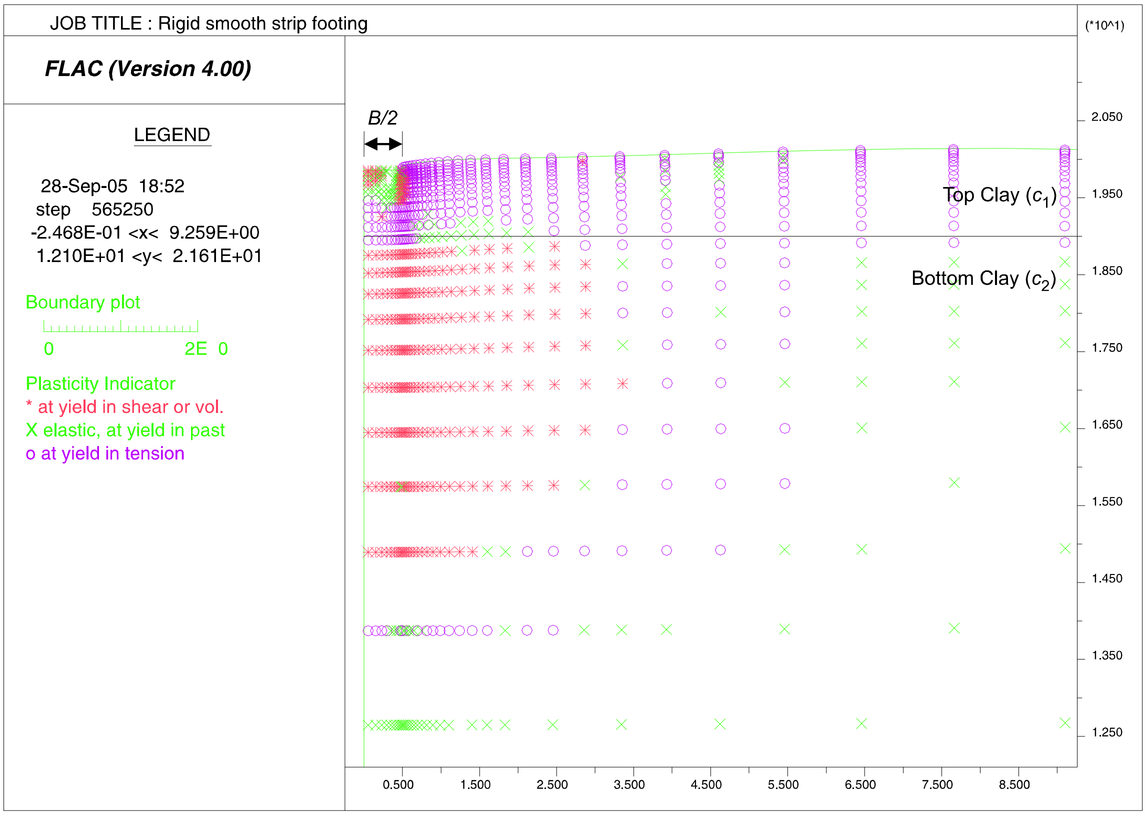

Figure A.461: Plasticity state indicators for combined large strain - small strain analysis of a rigid smooth strip footing on strong clay over soft clay with soil stopped spilling on footing for 40 × 30 grid model, $H/B = 1$, $c_2/c_1 = 0.1$.

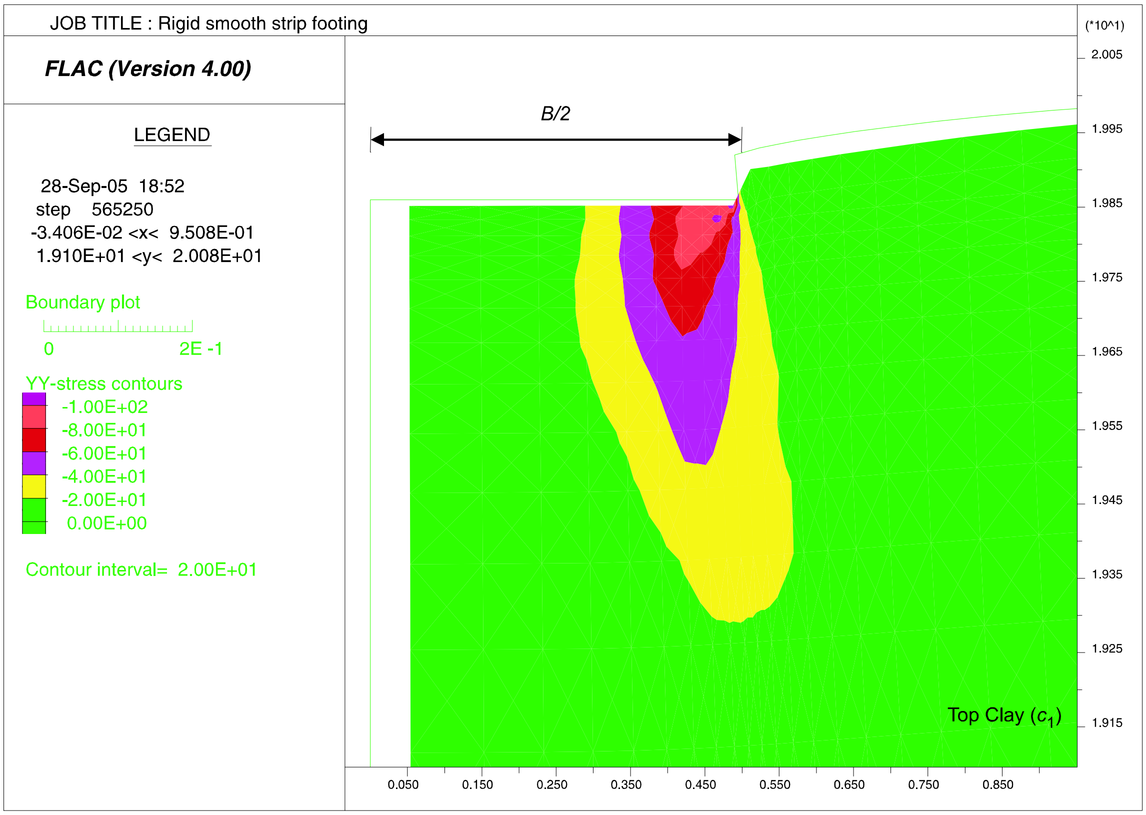

Figure A.462: Vertical stress (σ_{yy}) contours for combined large strain - small strain analysis of a rigid smooth strip footing on strong clay over soft clay with soil stopped spilling on footing for 40×30 grid model, $H/B = 1$, $c_2/c_1 = 0.1$.